



ISSN

Period.

VOL. 506 MAY 11, 1990

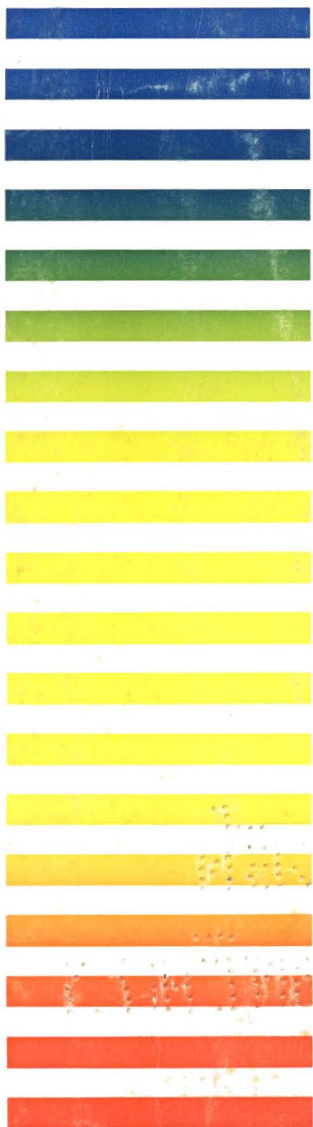
COMPLETE IN ONE ISSUE

**13th International Symposium
on Column Liquid Chromatography
Stockholm, June 25-30, 1989
Part I**

OF

CHROMATOGRAPHY

INTERNATIONAL JOURNAL ON CHROMATOGRAPHY, ELECTROPHORESIS AND RELATED METHODS



SYMPOSIUM VOLUMES

EDITOR, E. Heftmann (Orinda, CA)

EDITORIAL BOARD

S. C. Churms (Rondebosch)

E. H. Cooper (Leeds)

R. Croteau (Pullman, WA)

D. H. Dolphin (Vancouver)

J. S. Fritz (Ames, IA)

K. J. Irgolic (College Station, TX)

C. F. Poole (Detroit, MI)

R. Teranishi (Berkeley, CA)

H. F. Walton (Boulder, CO)

C. T. Wehr (Foster City, CA)

ELSEVIER

Scope. The *Journal of Chromatography* publishes papers on all aspects of chromatography, electrophoresis and related methods. Contributions consist mainly of research papers dealing with chromatographic theory, instrumental development and their applications. The section *Biomedical Applications*, which is under separate editorship, deals with the following aspects: developments in and applications of chromatographic and electrophoretic techniques related to clinical diagnosis or alterations during medical treatment; screening and profiling of body fluids or tissues with special reference to metabolic disorders; results from basic medical research with direct consequences in clinical practice; drug level monitoring and pharmacokinetic studies; clinical toxicology; analytical studies in occupational medicine.

Submission of Papers. Papers in English, French and German may be submitted, in three copies. Manuscripts should be submitted to: The Editor of *Journal of Chromatography*, P.O. Box 681, 1000 AR Amsterdam, The Netherlands, or to: The Editor of *Journal of Chromatography, Biomedical Applications*, P.O. Box 681, 1000 AR Amsterdam, The Netherlands. Review articles are invited or proposed by letter to the Editors. An outline of the proposed review should first be forwarded to the Editors for preliminary discussion prior to preparation. Submission of an article is understood to imply that the article is original and unpublished and is not being considered for publication elsewhere. For copyright regulations, see below.

Subscription Orders. Subscription orders should be sent to: Elsevier Science Publishers B.V., P.O. Box 211, 1000 AE Amsterdam, The Netherlands, Tel. 5803 911, Telex 18582 ESPA NL. The *Journal of Chromatography* and the *Biomedical Applications* section can be subscribed to separately.

Publication. The *Journal of Chromatography* (incl. *Biomedical Applications*) has 37 volumes in 1990. The subscription prices for 1990 are:

J. Chromatogr. (incl. *Cum. Indexes, Vols. 451-500*) + *Biomed. Appl.* (Vols. 498-534):

Dfl. 6734.00 plus Dfl. 1036.00 (p.p.h.) (total ca. US\$ 3885.00)

J. Chromatogr. (incl. *Cum. Indexes, Vols. 451-500*) only (Vols. 498-524):

Dfl. 5616.00 plus Dfl. 756.00 (p.p.h.) (total ca. US\$ 3186.00)

Biomed. Appl. only (Vols. 525-534):

Dfl. 2080.00 plus Dfl. 280.00 (p.p.h.) (total ca. US\$ 1180.00).

Our p.p.h. (postage, package and handling) charge includes surface delivery of all issues, except to subscribers in Argentina, Australia, Brasil, Canada, China, Hong Kong, India, Israel, Malaysia, Mexico, New Zealand, Pakistan, Singapore, South Africa, South Korea, Taiwan, Thailand and the U.S.A. who receive all issues by air delivery (S.A.L. — Surface Air Lifted) at no extra cost. For Japan, air delivery requires 50% additional charge; for all other countries airmail and S.A.L. charges are available upon request. Back volumes of the *Journal of Chromatography* (Vols. 1-497) are available at Dfl. 195.00 (plus postage). Claims for missing issues will be honoured, free of charge, within three months after publication of the issue. Customers in the U.S.A. and Canada wishing information on this and other Elsevier journals, please contact Journal Information Center, Elsevier Science Publishing Co. Inc., 655 Avenue of the Americas, New York, NY 10010. Tel. (212) 633-3750.

Abstracts/Contents Lists published in Analytical Abstracts, ASCA, Biochemical Abstracts, Biological Abstracts, Chemical Abstracts, Chemical Titles, Chromatography Abstracts, Clinical Chemistry Lookout, Current Contents/Physical, Chemical & Earth Sciences, Current Contents/Life Sciences, Deep-Sea Research/Part B: Oceanographic Literature Review, Excerpta Medica, Index Medicus, Mass Spectrometry Bulletin, PASCAL-CNRS, Pharmaceutical Abstracts, Referativnyi Zhurnal, Science Citation Index and Trends in Biotechnology.

See inside back cover for Publication Schedule, Information for Authors and information on Advertisements.

All rights reserved. No part of this publication may be reproduced, stored in a retrieval system or transmitted in any form or by any means, electronic, mechanical, photocopying, recording or otherwise, without the prior written permission of the publisher, Elsevier Science Publishers B.V., P.O. Box 330, 1000 AH Amsterdam, The Netherlands.

Upon acceptance of an article by the journal, the author(s) will be asked to transfer copyright of the article to the publisher. The transfer will ensure the widest possible dissemination of information.

Submission of an article for publication entails the authors' irrevocable and exclusive authorization of the publisher to collect any sums or considerations for copying or reproduction payable by third parties (as mentioned in article 17 paragraph 2 of the Dutch Copyright Act of 1912 and the Royal Decree of June 20, 1974 (S. 351) pursuant to article 16 b of the Dutch Copyright Act of 1912) and/or to act in or out of Court in connection therewith.

Special regulations for readers in the U.S.A. This journal has been registered with the Copyright Clearance Center, Inc. Consent is given for copying of articles for personal or internal use, or for the personal use of specific clients. This consent is given on the condition that the copier pays through the Center the per-copy fee stated in the code on the first page of each article for copying beyond that permitted by Sections 107 or 108 of the U.S. Copyright Law. The appropriate fee should be forwarded with a copy of the first page of the article to the Copyright Clearance Center, Inc., 27 Congress Street, Salem, MA 01970, U.S.A. If no code appears in an article, the author has not given broad consent to copy and permission to copy must be obtained directly from the author. All articles published prior to 1982 may be copied for a per-copy fee of US\$ 2.25, also payable through the Center. This consent does not extend to other kinds of copying, such as for general distribution, resale, advertising and promotion purposes, or for creating new collective works. Special written permission must be obtained from the publisher for such copying.

No responsibility is assumed by the Publisher for any injury and/or damage to persons or property as a matter of products liability, negligence or otherwise, or from any use or operation of any methods, products, instructions or ideas contained in the materials herein. Because of rapid advances in the medical sciences, the Publisher recommends that independent verification of diagnoses and drug dosages should be made.

Although all advertising material is expected to conform to ethical (medical) standards, inclusion in this publication does not constitute a guarantee or endorsement of the quality or value of such product or of the claims made of it by its manufacturer.

This issue is printed on acid-free paper.

**FOR ADVERTISING
INFORMATION
PLEASE CONTACT
OUR
ADVERTISING
REPRESENTATIVES**

GREAT BRITAIN

T.G. Scott & Son Ltd.

Mr. M. White or Mrs. A. Curtis
30-32 Southampton Street
LONDON WC2E 7HR
Tel: (01) 240 2032
Telex: 299181 adsale/g
Fax: (01) 379 7155

JAPAN

ESP - Tokyo Branch

Mr H. Ogura
28-1 Yushima, 3-chome, Bunkyo-Ku
TOKYO 113
Tel: (03) 836 0810
Telex: 02657617, Fax (03) 836 0204

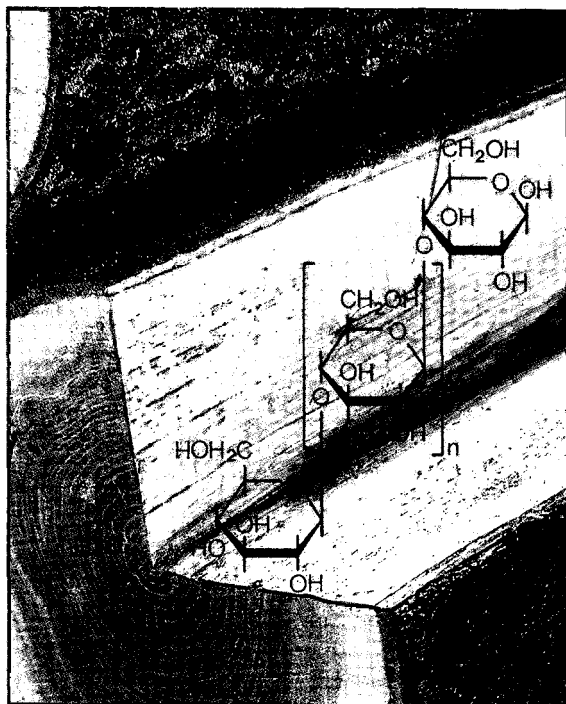
REST OF WORLD

**ELSEVIER
SCIENCE
PUBLISHERS**

Ms W. van Cattenburch
P.O. Box 211
1000 AE AMSTERDAM
The Netherlands
Tel: (20) 5803.714/715/721
Telex: 18582 espa/nl
Fax: (20) 5803.769

**Cellodextrins –
pure and economical**

**We make it easier for you to understand
nature better**



Our water soluble Cello-dextrins with a high degree of purity are excellent model compounds for mechanistic studies of enzymatic cellulose breakdown and also serve as comparative substances in HPLC or DC product analysis.

Currently available: Cello-triose, Cello-tetraose, Cello-pentaose, Cellohexaose, Celloheptaose as well as corresponding low-glucose Cellodextrin mixtures at a very economical price.

Request detailed information today, or just give us a call: 0 6151/72-3593.

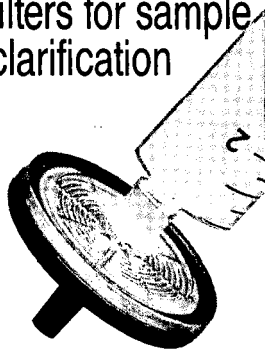
E. Merck
Frankfurter Strasse 250
D-6100 Darmstadt 1

MERCK

Sample preparation

CHROMAfil®

Disposable
filters for sample
clarification



- Prevents dirtying of sensitive instrumentation and chromatographic columns
- Types for purely aqueous, organic or organic/aqueous solutions
- Filter diameters 3, 15 and 25 mm
- Pore diameters 0.2 and 0.45 μm

Please ask
for further information



MACHEREY-NAGEL GmbH & Co. KG
P. O. Box 10 13 52 · D-5160 Düren
W. Germany · Tel. (0 24 21) 6 98-0
Telex 8 33 893 mana d · Telefax (0 24 21) 6 20 54

Switzerland: MACHEREY-NAGEL AG
P. O. Box 224 · CH-4702 Oensingen
Tel. (0 62) 76 20 66 · Telex 9 82 908 mnag ch
Telefax (0 62) 76 28 64



PLEASE
MENTION
THIS
JOURNAL
WHEN
ANSWERING
ADVER-
TISEMENTS



Frost & Sullivan

The Leading International Supplier of Business Information

Announcing the latest market research and technology
impact reports in the chemical industry.

Market Research Reports

- E1116 The European market for Pharmaceutical Intermediates.
- E1173 The European market for Disinfectants and Sanitisers.
- E1344 The European market for High Value Added Organics.
- A2141 The U.S. market for Disinfectants and Sanitisers.

PLUS many more titles for Europe and the United States.

Each report looks at how the industry will meet increasingly sophisticated end-user requirements in a highly competitive environment and provides:

- Detailed analysis and forecasts for each of the product categories in the sector covered, given in both volume and \$ value.
- Forecasts by country for a five year period.
- Appraisal of technological developments and applications.
- Detailed profiles of the leading suppliers.

Technology Impact Reports

- T021 Advanced Separation Technology.
- T033 Protein Design.
- T013 Diamond Films.

Each report studies a leading-edge technology. Emphasis is placed on the future impact of the technology on relevant industry sectors.

For further information on these reports please contact:-

Mr. Ken Levy
Frost & Sullivan Ltd
Sullivan House
4 Grosvenor Gardens
London SW1W 0DH

UNITED KINGDOM
Tel: 071-730 3438

Frau. Susanne Wicht
Frost & Sullivan
Willheim - Leuschnerstr 10
D - 6000 Frankfurt/Main 1

WEST GERMANY
Tel: 069-235057



Mme. Negrier
8 rue de l'Arcade
75008 Paris

FRANCE
Tel: (1) 4742 9127

Dr. G. Binetti
Informazioni e Strategie SRL
Via Amedeo d'Aosta 5
20129 Milano

ITALY
Tel: 02-2841941

Determination of Beta-Blockers in Biological Material

edited by **V. Marko**, *Institute of Experimental Pharmacology, Centre of Physiological Sciences, Slovak Academy of Sciences, Bratislava, Czechoslovakia*

(Techniques and Instrumentation in Analytical Chemistry, 4C)

This is the third volume of a sub-series entitled *Evaluation of Analytical Methods in Biological Systems*. (The first two were *Analysis of Biogenic Amines* edited by G.B. Baker and R.T. Coutts and *Hazardous Metals in Human Toxicology* edited by A. Vercruyssen). This new volume addresses beta-blockers - an area of research for which a Nobel Prize in Medicine was awarded in 1988. It provides an up-to-date and comprehensive coverage of the theory and practice of the determination of beta-blockers in biological material. Two main fields of research are dealt with in this book: analytical chemistry and pharmacology, and, as it deals with drugs used in clinical practice, it is also related to a third area: therapy. Thus, it offers relevant information to workers in all three fields.

Some 50 beta-blockers and nine methods of analysis are discussed. The methods are divided into three groups: optical, chromatographic, and saturation methods. In addition to the analytical methods themselves, sample handling problems are also covered in detail, as is the information content of the analytical results obtained. Special chapters are directed to those working in pharmacology and pharmacokinetics. Finally, as recent evidence points to the increased importance of distinguishing optical isomers of drugs, a chapter on the determination of optical isomers of beta-blockers in biological material is also included. An extensive subject index and two

supplements giving retention indices and structures of beta-blockers complete the book.

This is the first book to treat beta-blockers from the point of view of their determination and to discuss in detail the use of analytical methods for beta-blockers. It will thus appeal to a wide-ranging readership.

CONTENTS: Introduction (*V. Marko*). 1. Recent Developments in Clinical Pharmacology of Beta-Blockers (*M.A. Peat*). 2. Clinical Pharmacokinetics of Beta-Blockers (*T. Trnovec, Z. Kállay*). 3. Sample Pretreatment in the Determination of Beta-Blockers in Biological Fluids (*V. Marko*). 4. Determination of Beta-Blockers by Optical Methods (*W.-R. Stenzel, V. Marko*). 5. Determination of Beta-Blockers by Chromatographic Methods. GLC of Beta-Blockers (*M. Ahnoff*). HPLC Determination of Beta-Adrenergic Blockers in Biological Fluids (*J.G. Barnhill, D.J. Greenblatt*). TLC (*M. Schäfer-Korting, E. Mutschler*). 6. Determination of Beta-Blockers by Saturation Methods. Immunological Methods for the Determination of Beta-Blockers (*K. Kawashima*). Radioreceptor Assay of Beta-Blockers (RRA) (*A. Wellstein*). 7. Determination of Optical Isomers of Beta-Blockers (*T. Walle, U.K. Walle*). Subject Index. Supplements: Retention Indices of Beta-Blockers. Structures of Beta-Blockers.

1989 xiv + 334 pages
US\$ 152.75 / Dfl. 290.00
ISBN 0-444-87305-8



ELSEVIER SCIENCE PUBLISHERS

P.O. Box 211, 1000 AE Amsterdam, The Netherlands
P.O. Box 882, Madison Square Station, New York, NY 10159, USA

THE STANDARD TEXT ON THE SUBJECT...

Chemometrics: a textbook

D.L. Massart, *Vrije Universiteit Brussel, Belgium*,
B.G.M. Vandeginste, *Katholieke Universiteit Nijmegen, The Netherlands*,
S.N. Deming, *Dept. of Chemistry, University of Houston, TX, USA*,
Y. Michotte and L. Kaufman, *Vrije Universiteit Brussel, Belgium*

(Data Handling in Science and Technology, 2)

Most chemists, whether they are biochemists, organic, analytical, pharmaceutical or clinical chemists and many pharmacists and biologists need to perform chemical analyses. Consequently, they are not only confronted with carrying out the actual analysis, but also with problems such as method selection, experimental design, optimization, calibration, data acquisition and handling, and statistics in order to obtain maximum relevant chemical information. In other words: they are confronted with chemometrics.

This book, written by some of the leaders in the field, aims to provide a thorough, up-to-date introduction to this subject. The reader is given the opportunity to acquaint himself with the tools used in this discipline and the way in which they are applied. Some practical examples are given and the reader is shown how to select the appropriate tools in a given situation. The book thus provides the means to approach and solve analytical problems strategically and systematically, without the need for the reader to become a fully-fledged chemometrician.

Contents: Chapter 1. Chemometrics and the Analytical Process. 2. Precision and Accuracy. 3. Evaluation of Precision and Accuracy. Comparison of Two Procedures. 4. Evaluation of Sources of Variation in Data. Analysis of Variance. 5. Calibration. 6. Reliability and Drift. 7. Sensitivity and Limit of Detection. 8. Selectivity and Specificity. 9. Information. 10. Costs. 11. The Time Constant. 12. Signals and Data. 13. Regression Methods. 14. Correlation Methods. 15. Signal Processing. 16. Response Surfaces and Models. 17. Exploration of Response Surfaces. 18. Optimization of Analytical Chemical Methods. 19. Optimization of Chromatographic Methods. 20. The Multivariate Approach. 21. Principal Components and Factor Analysis. 22. Clustering Techniques. 23. Supervised Pattern Recognition. 24. Decisions in the Analytical Laboratory. 25. Operations Research. 26. Decision Making. 27. Process Control. Appendix. Subject Index.

"The many examples, the eye-pleasing presentation, and the references to other texts and articles make the book useful as a teaching tool. Beginners and those more familiar with the field will find the book a great benefit because of that breadth, and especially because of the clarity and relative uniformity of presentation... this book will be the standard text on the subject for some time." (Journal of Chemometrics)

1988 485 pages US\$ 92.00 / Dfl. 175.00 ISBN 0-444-42660-4

ELSEVIER SCIENCE PUBLISHERS

P.O. Box 211, 1000 AE Amsterdam, The Netherlands

P.O. Box 882, Madison Square Station, New York, NY 101593, USA

AQUEOUS SIZE-EXCLUSION CHROMATOGRAPHY

edited by P.L. DUBIN, *Indiana-Purdue University*

(*Journal of Chromatography Library*, 40)

The rapid development of new packings for aqueous size-exclusion chromatography has revolutionized this field. High resolution non-adsorptive columns now make possible the efficient separation of proteins and the rapid and precise determination of the molecular weight distribution of synthetic polymers. This technology is also being applied to the separation of small ions, the characterization of associating systems, and the measurement of branching. At the same time, fundamental studies are elucidating the mechanisms of the various chromatographic processes.

These developments in principles and applications are assembled for the first time in this book.

- Fundamental issues are dealt with: the roles of pore structure and macromolecular dimensions, hydrophobic and electrostatic effects, and the determination and control of column efficiency.
- High-performance packings based on derivatized silica are reviewed in detail.
- Special techniques are thoroughly described, including SEC/LALLS, inverse exclusion chromatography, and frontal zone chromatography.
- Attention is focussed on special applications of size-exclusion methods, such as

the characterization of micelles, separations of inorganic ions, and Hummel-Dreyer and related methods for equilibrium systems.

- Protein chromatography is dealt with in both dedicated sections and throughout the book as a whole.

This is a particularly comprehensive and authoritative work - all the contributions review broad topics of general significance and the authors are of high repute.

The material will be of special value for the characterization of synthetic water-soluble polymers, especially polyelectrolytes. Biochemists will find fundamental and practical guidance on protein separations. Researchers confronted with solutes that exhibit complex chromatographic behavior, such as humic acids, aggregating proteins, and micelles should find the contents of this volume illuminating.

Contents: Part I. Separation Mechanisms. Part II. Characterization of Stationary Phases. Part III. New Packings. Part IV. Biopolymers. Part V. Associating Systems. Subject Index.

1988 xviii + 454 pages
US\$ 144.75 / Dfl. 275.00
ISBN 0-444-42957-3



ELSEVIER SCIENCE PUBLISHERS

P.O. Box 211, 1000 AE Amsterdam, The Netherlands
P.O. Box 1663, Grand Central Station, New York, NY 10163, USA

JOURNAL OF CHROMATOGRAPHY

VOL. 506 (1990)

JOURNAL *of* CHROMATOGRAPHY

INTERNATIONAL JOURNAL ON CHROMATOGRAPHY,
ELECTROPHORESIS AND RELATED METHODS

SYMPOSIUM VOLUMES

EDITOR
E. HEFTMANN (Orinda, CA)

EDITORIAL BOARD
S. C. Churms (Rondebosch), E. H. Cooper (Leeds), R. Croteau (Pullman, WA), D. H. Dolphin (Vancouver), J. S. Fritz (Ames, IA), K. J. Irgolic (College Station, TX), C. F. Poole (Detroit, MI), R. Teranishi (Berkeley, CA), H. F. Walton (Boulder, CO), C. T. Wehr (Foster City, CA)



ELSEVIER
AMSTERDAM — OXFORD — NEW YORK — TOKYO

J. Chromatogr., Vol. 506 (1990)

Southern Parts of Stockholm and the "Old Town" around 1790. The five churches seen on the painting are from the left: "Sofia Kyrka, Maria kyrka, Tyska (German) kyrkan, Riddarholmskyrkan and Slottskyrkan". Stockholm castle is situated to the far right.
(From Aguila's *Histoire de Règne de Gustave III.*)

© ELSEVIER SCIENCE PUBLISHERS B.V. — 1990

0021-9673/90/\$03.50

All rights reserved. No part of this publication may be reproduced, stored in a retrieval system or transmitted in any form or by any means, electronic, mechanical, photocopying, recording or otherwise, without the prior written permission of the publisher, Elsevier Science Publishers B.V., P.O. Box 330, 1000 AH Amsterdam, The Netherlands.

Upon acceptance of an article by the journal, the author(s) will be asked to transfer copyright of the article to the publisher. The transfer will ensure the widest possible dissemination of information.

Submission of an article for publication entails the authors' irrevocable and exclusive authorization of the publisher to collect any sums or considerations for copying or reproduction payable by third parties (as mentioned in article 17 paragraph 2 of the Dutch Copyright Act of 1912 and the Royal Decree of June 20, 1974 (S. 351) pursuant to article 16 b of the Dutch Copyright Act of 1912) and/or to act in or out of Court in connection therewith.

Special regulations for readers in the U.S.A. This journal has been registered with the Copyright Clearance Center, Inc. Consent is given for copying of articles for personal or internal use, or for the personal use of specific clients. This consent is given on the condition that the copier pays through the Center the per-copy fee stated in the code on the first page of each article for copying beyond that permitted by Sections 107 or 108 of the U.S. Copyright Law. The appropriate fee should be forwarded with a copy of the first page of the article to the Copyright Clearance Center, Inc., 27 Congress Street, Salem, MA 01970, U.S.A. If no code appears in an article, the author has not given broad consent to copy and permission to copy must be obtained directly from the author. All articles published prior to 1980 may be copied for a per-copy fee of US\$ 2.25, also payable through the Center. This consent does not extend to other kinds of copying, such as for general distribution, resale, advertising and promotion purposes, or for creating new collective works. Special written permission must be obtained from the publisher for such copying.

No responsibility is assumed by the Publisher for any injury and/or damage to persons or property as a matter of products liability, negligence or otherwise, or from any use or operation of any methods, products, instructions or ideas contained in the materials herein. Because of rapid advances in the medical sciences, the Publisher recommends that independent verification of diagnoses and drug dosages should be made.

Although all advertising material is expected to conform to ethical (medical) standards, inclusion in this publication does not constitute a guarantee or endorsement of the quality or value of such product or of the claims made of it by its manufacturer.

This issue is printed on acid-free paper.

Printed in The Netherlands

SYMPOSIUM VOLUME



**THIRTEENTH INTERNATIONAL SYMPOSIUM
ON
COLUMN LIQUID CHROMATOGRAPHY**

PART I

Stockholm, June 25–30, 1989

Guest Editor

B. D. WESTERLUND

(Uppsala)

The proceedings of the *Thirteenth International Symposium on Column Liquid Chromatography, Stockholm, June 25–30, 1989*, are published in two consecutive volumes of the *Journal of Chromatography*: Vols. 506 and 507. A foreword to the complete proceedings only appears in Vol. 506.

CONTENTS

13TH INTERNATIONAL SYMPOSIUM ON COLUMN LIQUID CHROMATOGRAPHY, STOCKHOLM, JUNE 25-30, 1990, PART I

Foreword by D. Westerlund	1
<i>THEORY</i>	
<i>Retention mechanisms</i>	
Correlation between chemical structure of non-congeneric solutes and their retention on polybutadiene-coated alumina by R. Kaliszan and K. Ósmiałowski (Gdańsk, Poland)	3
High-performance liquid chromatography of amino acids, peptides and proteins. XCVII. The influence of the gradient elution mode and displacer salt type on the retention properties of closely related protein variants separated by high-performance anion-exchange chromatography by A. N. Hodder, M. I. Aguilar and M. T. W. Hearn (Clayton, Australia)	17
Application of chromatographic retention data in an investigation of a quantitative structure-nucleotide incorporation rate relationship by K. Valkó, T. Cserháti, I. Fellegvári, J. Sági and S. Szemző (Budapest, Hungary)	35
Secondary equilibria and their interaction with chromatographic transport by H. Poppe (Amsterdam, The Netherlands)	45
Studies on system peaks in ion-pair adsorption chromatography. III. Regulation of system peak gradient retention for obtaining analyte peak compression by T. Fornstedt, D. Westerlund and A. Sokolowski (Uppsala, Sweden)	61
Multiple peak formation in reversed-phase liquid chromatography of ramipril and ramiprilate by S. Gustafsson, B.-M. Eriksson and I. Nilsson (Mölndal, Sweden)	75
Extension of the electrostatic retention model of reversed-phase ion-pair chromatography to include the simultaneous effects of the organic modifier and the pairing ion by A. Bartha and Gy. Vigh (College Station, TX, U.S.A.) and J. Ståhlberg (Sjödertälje, Sweden)	85
Silanol effects in reversed-phase liquid chromatography by T. Welsch and H. Frank (Leipzig, G.D.R.) and Gy. Vigh (College Station, TX, U.S.A.)	97
Reversed-phase high-performance liquid chromatography in the investigation of the hydrophobicity of selected ketones by A. Siwek and J. Śliwiok (Katowice, Poland)	109
Partition coefficients and capacity factors of some nucleoside analogues by A. P. Cheung and D. Kenney (Menlo Park, CA, U.S.A.)	119
Application of a computer-assisted high-performance liquid chromatographic multi-wavelength ultraviolet detection system to simultaneous toxicological drug analyses by M. Hayashida, M. Nihira and T. Watanabe (Tokyo, Japan) and K. Jinno (Toyohashi, Japan)	133
Chromatographic characteristics of nucleic acid components on vinyl alcohol copolymer gel columns by K. Noguchi, Y. Yanagihara, M. Kasai and N. Hirata (Kawasaki, Japan)	145
Retention behaviour of mono- and dicarboxylic acids, carbohydrates and alcohols in ion-exclusion chromatography by E. Papp (Veszprém, Hungary) and P. Keresztes (Budapest, Hungary)	157

Chemometrics and chromatography

Optimization of chromatographic methods by a combination of optimization software and expert systems by P. J. Schoenmakers (Eindhoven, The Netherlands), A. Peeters (Brussels, Belgium) and R. J. Lynch (Cambridge, U. K.)	169
Theoretical optimization of open-tubular columns for liquid chromatography with respect to mass loadability by P. P. H. Tock, P. P. E. Duijsters, J. C. Kraak and H. Poppe (Amsterdam, The Netherlands)	185
Selective determination of trace levels of phenol in river water using electrochemical concentration modulation correlation chromatography by M. Engelsma, W. Th. Kok and H. C. Smit (Amsterdam, The Netherlands)	201
Validation of an expert system for the selection of initial high-performance liquid chromatographic conditions for the analysis of basic drugs by F. Maris, R. Hindriks and J. Vink (Oss, The Netherlands) and A. Peeters, N. Vanden Driessche and L. Massart (Brussels, Belgium)	211
Resolution of unresolved peaks containing unknown components by high-performance liquid chromatography with multi-wavelength detection by I. Sakuma (Saitama, Japan), N. Takai and T. Dohi (Tokyo, Japan), Y. Fukui (Saitama, Japan) and A. Ohkuho (Tokyo, Japan)	223
Optimization of mobile phase composition for high-performance liquid chromatographic separation by means of the overlapping resolution mapping scheme by S. F. Y. Li, H. K. Lee and C. P. Ong (Singapore, Singapore)	245
Regulation of peak compression effects for substituted benzamides in reversed-phase liquid chromatography by L. B. Nilsson (Södertälje, Sweden)	253
Towards a chromatographic quantitor by P. A. Bristow (Macclesfield, U.K.)	265
High-performance liquid chromatographic determination of guanidino compounds by automated pre-column fluorescence derivatization by V. K. Boppana and G. R. Rhodes (King of Prussia, PA, U.S.A.)	279
Multiple absorbance ratio correlation—a new approach for assessing peak purity in liquid chromatography by J. G. D. Marr, G. G. R. Seaton, B. J. Clark and A. F. Fell (Bradford, U.K.)	289

TECHNIQUES*Stationary phases*

Aligned fiber columns for size-exclusion chromatography by M. Czok and G. Guiochon (Knoxville and Oak Ridge, TN, U.S.A.)	303
High-performance liquid chromatography of transfer ribonucleic acids on spherical hydroxyapatite beads by Y. Yamakawa, K. Miyasaka and T. Ishikawa (Tokyo, Japan), Y. Yamada (Tochigi, Japan) and T. Okuyama (Tokyo, Japan)	319
Peptide behaviour and analysis on a chemically stable C ₁₈ -bonded vinyl alcohol copolymer column with alkaline and acidic eluents by T. Uchida, T. Ohtani, M. Kasai, Y. Yanagihara and K. Noguchi (Kawasaki, Japan) and H. Izu and S. Hara (Osaka, Japan)	327
Retention times and heats of adsorption of aromatic compounds on carbon adsorbents by S. A. Eltekova (Moscow, U.S.S.R.)	335

Investigations by ^{29}Si cross-polarization magic angle spinning NMR spectroscopy of reaction pathways of silica gel polyfunctional modification by B. Pfeleiderer, K. Albert and E. Bayer (Tübingen, F.R.G.)	343
Novel, highly deactivated reversed-phase for basic compounds by T. L. Ascah and B. Feibush (Bellefonte, PA, U.S.A.)	357
Development and use of carbon adsorbents in the liquid chromatographic separation of isomers by F. Belliardo and O. Chiantore (Turin, Italy), D. Berek and I. Novák (Bratislava, Czechoslovakia) and C. Lucarelli (Rome, Italy)	371
Lipid-vesicle-surface chromatography by Q. Yang, M. Wallstén and P. Lundahl (Uppsala, Sweden)	379
Effect of polystyrene coating on pore, structural and chromatographic properties of silica packings by A. Kurganov, O. Kuzmenko and V. A. Davankov (Moscow, U.S.S.R.) and B. Eray, K. K. Unger and U. Trüdinger (Mainz, F.R.G.)	391
<i>Methods</i>	
Indirect fluorometric detection in open-tubular capillary column chromatography by W. D. Pfeffer and E. S. Yeung (Ames, IA, U.S.A.)	401
Application of low-angle laser light scattering detection in the field of biochemistry. Review of recent progress by T. Takagi (Osaka, Japan)	409
Determination of amoxicillin in plasma by high-performance liquid chromatography with fluorescence detection after on-line oxidation by H. Mascher and C. Kikuta (Vienna, Austria)	417
Selective post-column liquid chromatographic determination of sugars in spent sulphite liquor with two enzymatic electrochemical detectors in parallel by G. Marko-Varga (Lund, Sweden), E. Dominguez (Madrid, Spain) and B. Hahn-Hägerdal and L. Gorton (Lund, Sweden)	423
Coupling of microcolumn high-performance liquid chromatography with Fourier transform infrared spectrometry by K. Jinno and C. Fujimoto (Toyohashi, Japan)	443
<i>In vivo</i> microdialysis sampling coupled to liquid chromatography for the study of acetaminophen metabolism by D. O. Scott, L. R. Sorensen and C. E. Lunte (Lawrence, KS, U.S.A.)	461
Determination of water-soluble vitamins in blood and plasma by coupled-column liquid chromatography by K. Johansen and P. O. Edlund (Solna, Sweden)	471
Displacement chromatography on cyclodextrin-silicas. III. Enantiomer separations by Gy. Vigh, G. Quintero and Gy. Farkas (College Station, TX, U.S.A.)	481
Solutions of the equilibrium and semi-equilibrium models of chromatography by S. Golshan-Shirazi and G. Guiochon (Knoxville, TN, U.S.A.)	495
Hydrodynamic chromatography of macromolecules on small spherical non-porous silica particles by G. Stegeman, R. Oostervink, J. C. Kraak and H. Poppe (Amsterdam, The Netherlands) and K. K. Unger (Mainz, F.R.G.)	547
Comparison of stationary phases for packed-column supercritical fluid chromatography by P. J. Schoenmakers, L. G. M. Uunk and H.-G. Janssen (Eindhoven, The Netherlands)	563

Chiral separations

Chiral separations of atropine and homatropine on an α_1 -acid glycoprotein-bonded stationary phase by E. Arvidsson and S. O. Jansson (Mölnadal, Sweden) and G. Schill (Uppsala, Sweden)	579
Chiral chloroformates as transparent reagents for the resolution of metoprolol enantiomers by re- versed-phase liquid chromatography by M. Ahnoff, S. Chen, A. Green and I. Grundevik (Mölnadal, Sweden)	593
Direct high-performance liquid chromatographic determination of the enantiomers of alfuzosin in plasma on a second-generation of α_1 -acid glycoprotein chiral stationary phase by A. Rouchouse, M. Manoha, A. Durand and J. P. Thenot (Paris, France)	601
Separation of the enantiomeric intermediates of some platelet-activating factor analogues on a naph- thylalanine-type Pirkle column by P. L. Camacho, E. Geiger and Gy. Vigh (College Station, TX, U.S.A.) and R. Webster and D. H. Thompson (Beaverton, OR, U.S.A.)	611
High-performance liquid chromatographic resolution of racemic 1,4-benzodiazepin-2-ones by means of a β -cyclodextrin silica bonded chiral stationary phase by C. Bertucci, E. Domenici, G. Uccello-Barretta and P. Salvadori (Pisa, Italy)	617
Direct high-performance liquid chromatographic separation of (+)- and (-)-medetomidine hydro- chloride with an α_1 -acid glycoprotein chiral column by G. Örn, K. Lahtonen and H. Jalonen (Turku, Finland)	627
<i>Author Index</i>	637

 *
 * In articles with more than one author, the name of the author to whom correspondence should be addressed is indicated in the
 * article heading by a printed asterisk (*)
 *

FOREWORD

The *13th International Symposium on Column Liquid Chromatography* (CLC '89) was held from June 25th to 30th, 1989, in Stockholm, Sweden. Over 1050 participants from 30 countries (Sweden 35%, U.S.A. 13%, F.R.G. 8%, The Netherlands 6% and Eastern Europe 5%) enjoyed a warm and fortunately almost rain-free week of both scientific and social activities. Close to 100 lectures, over 350 posters and 11 discussion sessions embodied the programme. Hence, the scientific activities were at a quantitative level similar to those in the two previous symposia in the series, Washington (1988) and Amsterdam (1987). The most abundant subjects were separations of macromolecules, preparative and chiral separations and biomedical applications. The instrument exhibition, involving 58 companies, was also an essential part of the programme. The high level of scientific activities at the symposium is certainly a very strong indicator of the need for this kind of broad programme meeting within the field of separation sciences.

The planning and accomplishment of an international symposium of this size cannot be successful without the cooperation and teamwork of many individuals. I would like especially to express my gratitude to my scientist colleagues on the organizing committee: Professors Stellan Hjertén, Björn Josefsson and Jan-Christer Janson; Drs. Bengt-Arne Persson and Jörgen Sjödah; to Dr. Anders Cronlund, of the Swedish Academy of Pharmaceutical Sciences; and to the team from the Stockholm Convention Bureau (SCB), Helena Stark, Mariana Hammarskiöld and Mikaela Johansson. I am also very grateful to my colleagues on the permanent scientific committee of this symposium series for providing advice on the scientific programme after studies of the more than 400 preliminary abstracts that were submitted to CLC '89. A special acknowledgement also goes to the two Chairmen of the two preceding symposia in the series, Professors Georges Guiochon and Hans Poppe, who assisted with much useful advice in the planning of the present symposium. I am also grateful to the Ph.D. students from the university departments, and the personnel from SCB, who assisted in such a way that all practical details functioned smoothly during the symposium. Finally, I would like to thank the staff from Elsevier, Drs. Erich Heftmann and Marc Atkins, for a pleasant and efficient collaboration in the production of these proceedings.

In January 1989, the chromatographic world untimely and most unfortunately lost one of its best known and prominent scientists, Professor Roland W. Frei, who was a good friend, colleague and mentor to numerous chromatographers around the world, and also a member of the permanent scientific committee of this symposium series. The participants of CLC '89, stood in silence to honour his memory during the Introduction, and it was emphasized that it was the aim of the symposium to proceed in his spirit, providing a suitable blend of scientific and social activities in order to stimulate the participants to interact in a pleasant atmosphere. It is my impression that we succeeded in fulfilling this goal in a way that Roland would have approved of, if he had still been among us.

The banquet was held at the Grand Hotel in Stockholm, and for those of you who enjoyed the female singing group ("Growing Girls") appearing there, I can tell that they some months later became world champions in barbershop singing at a contest held in Florida!

It is time to look forward to coming exciting symposia and I hope to see all of you in Boston in May, this year, when Professor Barry L. Karger as the Chairman responsible will no doubt arrange an attractive programme for HPLC '90.

Uppsala (Sweden)

DOUGLAS WESTERLUND

CHROMSYMP. 1711

Correlation between chemical structure of non-congeneric solutes and their retention on polybutadiene-coated alumina

ROMAN KALISZAN*

Department of Biopharmaceutics and Pharmacodynamics, Medical Academy, K. Marksa 107, 80-416 Gdańsk (Poland)

and

KRZYSZTOF OŚMIAŁOWSKI

Department of Inorganic Chemistry, Medical Academy, K. Marksa 107, 80-416 Gdańsk (Poland)

SUMMARY

The high-performance liquid chromatographic capacity factors extrapolated to pure water were determined on a polybutadiene-coated alumina (PBCA) stationary phase for a selected set of non-congeneric solutes. The structures of the test solutes were characterized by means of calculated hydrophobicity parameters and several non-empirical molecular descriptors, including topological indices, information content indices and quantum chemical indices. Unique properties of PBCA for the chromatographic determination of the hydrophobicity of diverse compounds were demonstrated. Quantitative structure–retention relationship (QSRR) studies employing non-empirical structural descriptors showed that the mechanism of retention on PBCA was similar to that on ODS phases. For a quantitative description of retention, structural parameters reflecting the bulkiness of solutes (positive input) and their polarity (negative input) predominated. Principal component analysis of structural descriptors most often used in QSRR studies allowed the extraction of two principal factors that describe retention more adequately than the individual descriptors studied. Informative values of non-empirical structural indices for the evaluation of retention were compared.

INTRODUCTION

Quantitative structure–retention relationships (QSRR) can be exploited for the prediction of retention, the determination of the structural properties of solutes and obtaining some insight into the molecular mechanism of chromatographic separations.

A reliable and precise prediction of retention in a given chromatographic system is possible for closely related, congeneric solutes only. More chemically meaningful seem to be the two remaining applications of QSRR. Bearing in mind the second aim of QSRR, *i.e.*, the determination of structural properties of solutes, we recently

turned our attention to the new generation of high-performance liquid chromatographic (HPLC) stationary phases, such as the polymer-coated reversed-phase materials introduced by Schomburg and co-workers^{1,2}. Using polybutadiene-coated alumina (PBCA) as an HPLC stationary phase, we previously proposed a method for the quantitative characterization of the hydrophobicity of diverse sets of solutes including neutral, weakly basic and weakly acidic compounds³. The uniqueness of the approach consists in its applicability to organic bases, which can be chromatographed in undissociated form. In contrast to silica-based hydrocarbonaceous stationary phases, commonly used for hydrophobicity determinations by HPLC, PBCA can be operated over a wide range of pH, including alkaline environments. The other advantage of PBCA is the lack of free silanol sites, which are responsible for undesirable specific interactions of chemically bonded silicas with polar solutes.

It seemed of interest to undertake QSRR studies of the data derived on PBCA aimed at the analysis of the mechanism of retention at the molecular level. The results of QSRR studies could be compared with those obtained previously by standard reversed-phase HPLC employing ODS materials^{4,5}. Comparison with the QSRR derived for the porous graphitic carbon–heptane normal-phase system also appeared interesting⁶.

In designing the experiment, we took the following into consideration: the solutes selected for studies should be non-congeneric and include basic, neutral and acidic compounds, the number of solutes should be sufficient for meaningful statistics but manageable for retention measurements and structural analysis and the test solutes should be stable conformationally, planar if possible and their geometry should be well established. The last condition is important for obtaining unequivocal results for structural and especially quantum chemical calculations.

Most QSRR reported in the chromatographic literature were derived by means of multiple regression analysis. The dependent variable formed a set of retention data, whereas various empirical, semi empirical and non-empirical structural parameters were assumed as independent (explanatory) variables. Unfortunately, the explanatory variables applied were often mutually interrelated by simple or multiple correlations. Moreover, it happened regularly that too many explanatory variables (including their various transformations such as squares, reciprocals and exponentials) were surveyed to describe too few retention data by multiple regression, which led to chance correlations. All this means that a number of QSRR regression equations reported in the analytical literature are without physical relevance.

Intercorrelated chemical data sets, which are unsuitable for multiple regression, can be subjected to multivariate analysis with factorial methods. Factor analysis has been applied to chromatographic data since the early 1970s, but only occasionally. The analysis reported were carried out in order to predict changes in the retention of a given set of solutes accompanying the changes in mobile–stationary phase systems^{7–10}. Wold and co-workers^{11,12} applied multivariate statistics to extract structural properties of amino acids from their various retention data.

There are numerous structural descriptors of solutes used in QSRR studies¹³. Unfortunately, significant intercorrelation among them limits the applicability of multiple regression in QSRR. On the other hand, according to the present chemometric theory, as many relevant data as possible should be considered in structure–property relationship studies because this increases the probability of good character-

ization of solutes¹². The large data tables resulting from such an assumption can be analysed by multivariate methods to extract the systematic information contained in the data. A small set of abstract principal factors extracted from a large set of various structural descriptors of the solutes should be sufficient for the description of their HPLC data expressed as logarithms of capacity factors. Based on the above assumption, we have recently been able to describe the retention of a set of variously substituted benzene derivatives on porous graphitic carbon with *n*-heptane eluent by means of two principal components extracted from a set of 18 non-empirical structural descriptors of 20 solutes¹⁴.

The experiments described in this paper were designed to obtain some insight into the molecular mechanism of retention on PBCA under reversed-phase conditions, to evaluate the informative value of non-empirical structural descriptors most often used in QSRR studies and to compare the quality of QSRR derived by means of multiple regression and of multivariate analysis.

EXPERIMENTAL

Materials

The test solutes were selected to include various structures (Fig. 1). The set of 21 solutes is diverse enough to avoid congenericity and includes aromatic hydrocarbons, substituted benzene derivatives and heteroaromatic compounds. Bearing in mind the limitations of quantum chemical method of calculation of structural indices, the solutes chosen for the study had conformations that can be unequivocally defined. The selection of rigid structures eliminates the possibility that the conformation of a solute interacting with the components of chromatographic phases differs from the conformation for which structural descriptors are determined. By choosing planar test solutes, we had in mind the feasibility of the numerical characterization of molecular shape.

The solutes chromatographed were of the highest available purity and originated from various sources.

Determination of retention parameters

The chromatographic system consisted of a single-piston reciprocating pump and a UV detector operating at 254 nm. A Rheodyne injection valve fitted with a 10- μ l sample loop was used. The HPLC column used was kindly supplied by Prof. R. A. Hartwick (Department of Chemistry, Rutgers University, Piscataway, NJ, U.S.A.). A stainless-steel column (150 \times 4.6 mm I.D.), was slurry packed with polybutadiene-coated Spherisorb A5Y using isopropanol as the slurry solvent and methanol as the packing solvent. The stationary phase was prepared according to the procedure of Schomburg and co-workers^{1,2}. Polybutadiene was immobilized on the alumina support with the help of a cross-linking reaction involving radical formation.

The mobile phase consisted of analytical-reagent grade methanol and a Britton-Robinson universal buffer prepared at pH 2.62 and 11.15. To provide a pH of 2.62, 150 ml of 0.2 *M* NaOH were added to 1000 ml of solution of 0.04 *M* CH₃COOH, 0.04 *M* H₃PO₄ and 0.04 *M* H₃BO₃. Buffer of pH 11.15 was prepared analogously by adding 825 ml of 0.2 *M* NaOH to 1000 ml of acid solution. The ionic strength of the buffers was adjusted to 0.2 by adding NaNO₃. The following metha-

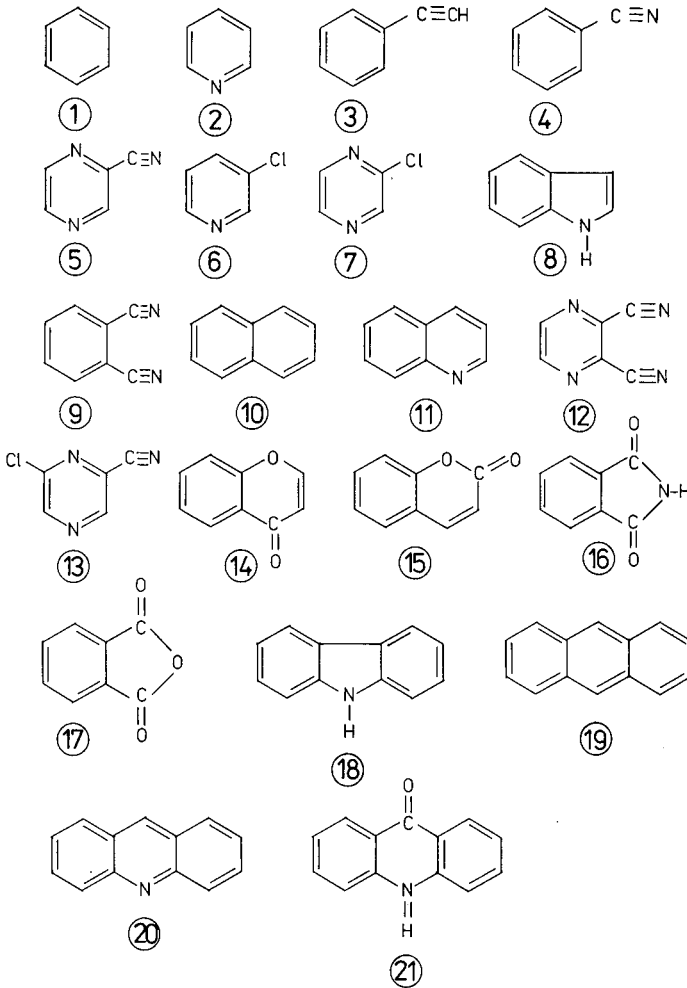


Fig. 1. Structural formulae of test solutes.

sol–buffer mixtures were used as mobile phases: 80:20, 50:50, 35:65, 20:80 and 0:100 (v/v). Before use, the eluents were filtered through 0.45- μ m nylon-66 filters. Alkaline buffer added to methanol in the proportion 20:80 (v/v) caused precipitation and this phase was discarded. Analytical-reagent grade chemicals were used.

The flow-rate was 1 ml/min. To calculate the capacity factors, k' , the solvent disturbance peak was used as a reference, observing specific precautions¹⁵.

For each solute the HPLC measurements were carried out in duplicate at both acidic and alkaline pH. Next, the $\log k'$ data were plotted against the volume fraction of methanol in the mobile phase for both pH values (see Fig. 2 for illustration). The linear part of the graph was extrapolated to zero content of methanol, yielding the value of capacity factor corresponding to pure water as the eluent, $\log k'_w$. Most of

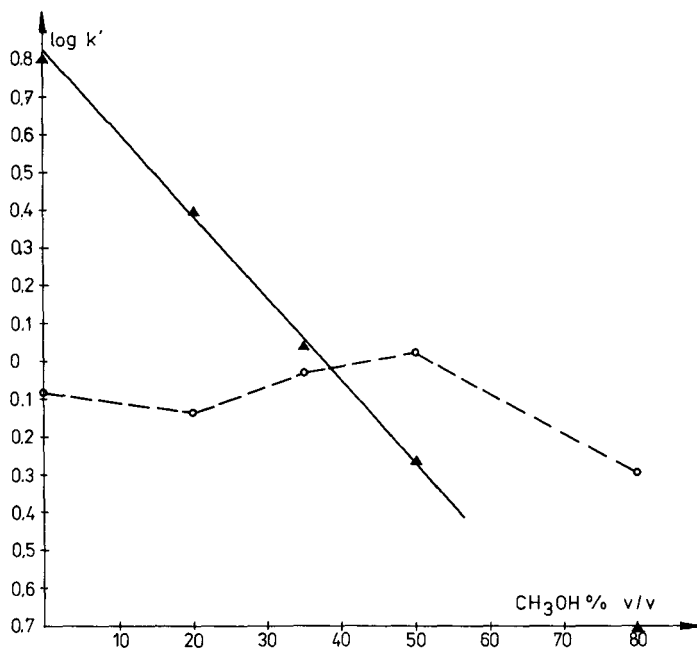


Fig. 2. Change in capacity factor with decreasing volume content of buffer in the eluent for quinoline. Solid line, best fit for the non-ionized solute (basic pH); broken line, retention of quinoline observed in the acidic eluent.

the compounds studied yielded measurable capacity factor data over a wide range of eluent compositions. In some instances, however, it was only possible to extrapolate linearly the retention observed for the two higher buffer contents studied. A similar approach has been applied by other workers¹⁶. Numerical values of $\log k'$ for non-ionized solutes extrapolated to pure aqueous eluent are given in Table I.

Structural descriptors

The HPLC system studied yields retention data reflecting the hydrophobicity of solutes. The reference scale for measurements of hydrophobicity, $\log P$, is provided by the *n*-octanol-water partitioning system. Experimentally determined $\log P$ data for 14 of 21 solutes studied were taken from ref. 17. For the full set of 21 compounds, the calculated $\log P$ data were obtained by applying the fragmental method of Hansch and Leo¹⁷. Calculated data were in good agreement with the data observed experimentally. The $\log P$ values are collected in Table I.

$\log P$ reflects ability of a compound to participate in the so-called hydrophobic interactions. Hydrophobic interactions are a complex net result of fundamental intermolecular interactions such as dispersive, inductive and dipole-dipole interactions. Thus, $\log P$ may be considered as a phenomenological structural parameter. The interpretation of empirical retention parameters in terms of other empirical or semi empirical parameters, such as $\log P$ data, is not very informative from the point of view of fundamental intermolecular interactions. More informative seem to be the

TABLE I

CAPACITY FACTORS EXTRAPOLATED TO PURE WATER, $\log k'_w$ AND STRUCTURAL DESCRIPTORS OF THE SOLUTES NUMBERED AS IN FIG. 1

For explanation of the symbols of structural descriptors see text.

Solute No.	$\log k'_w$	ind	$\log P_{(eada)}$	$\log P_{(eate)}$	molwt	bondrefr	etotal	ehomo	elumino
1	1.0750	0	2.14	2.13	78.11	26.184	-47.0940	-0.5100	0.1463
2	-0.3400	1	0.65	0.65	79.10	24.464	-50.8780	-0.4655	0.1278
3	1.8600	0	2.53	2.53	102.14	33.350	-61.0640	-0.4760	0.1258
4	0.4324	0	1.56	1.56	103.12	30.624	-64.8855	-0.4899	0.1080
5	-0.3575	1		-0.68	105.09	27.180	-72.4109	-0.4653	0.0827
6	0.2197	1	1.38	1.36	113.55	29.296	-64.5365	-0.4333	0.1093
7	-0.1656	1		0.25	114.54	27.574	-70.0568	-0.4651	0.0816
8	1.0800	1	2.13	2.14	117.15	36.460	-73.7969	-0.4118	0.1180
9	0.2043	0		1.08	128.13	35.064	-82.6595	-0.4730	0.0958
10	2.5800	0	3.35	3.28	128.17	42.976	-74.5485	-0.4097	0.1127
11	0.8170	1	2.04	2.02	129.16	41.254	-80.8656	-0.4602	0.0688
12	-0.1504	1		-0.71	130.11	31.620	-90.1945	-0.4640	0.0768
13	-0.0220	1		0.04	139.54	32.014	-87.8378	-0.4726	0.0630
14	0.4608	0		1.10	146.13	39.346	-105.2470	-0.4168	0.0618
15	0.5210	0	1.39	1.40	146.15	39.266	-105.2660	-0.4204	0.0488
16	0.2410	0	1.15	0.97	147.13	36.964	-104.8130	-0.4339	0.0687
17	0.1640	0	-0.62	-0.72	148.12	34.984	-114.9990	-0.4909	0.0477
18	2.7550	1	3.59	3.52	167.21	53.252	-100.1160	-0.3572	0.0510
19	3.8500	0	4.45	4.44	178.23	59.768	-107.0620	-0.3684	0.0383
20	1.8500	1	3.40	3.40	179.22	58.046	-107.0290	-0.3584	0.0483
21	1.5150	1		2.99	195.22	56.476	-129.2860	-0.3924	0.0761

non-empirical structural descriptors. Under the term non-empirical we understand here the molecular parameters that can be calculated exclusively on the basis of the structural formula of a solute. To calculate the following structural descriptors considered in this paper and given in Table I, only the structural formula of a solute is required.

Molecular weight is denoted here as molwt. Molecular refractivity (bondrefr) is calculated as the sum of the bond refractivities for all pairs of connected atoms according to Vogel *et al.*¹⁸. Thus, the refractivity increment for a C-H fragment is 1.676, for C-C 1.296, for C=C 4.17, for C-Cl 6.51, etc. A list of individual bond increments can be found in ref. 13 (p. 96). In fact, the bondrefr parameter is semi-empirical in nature but, in contrast to $\log P$, its calculation and interpretation cause no ambiguities.

The following molecular topological indices were considered here: Wiener index, W (wiener)¹⁹, generalized molecular connectivity indices of first and second order, ${}^1\chi^v$ and ${}^2\chi^v$, (χ_{1v} and χ_{2v}) according to Kier and Hall²⁰, and indices of molecular shape of first and second order, κ^1 and κ^2 (κ_{1v} and κ_{2v}), proposed by Kier²¹. Certainly there are other empirically modified topological indices designed for heteroatom-containing compounds, but strong intercorrelations among the exist-

<i>dipolem</i>	<i>delta</i>	<i>wiener</i>	<i>chi1v</i>	<i>chi2v</i>	<i>ic0</i>	<i>ic1</i>	<i>ic2</i>	<i>kappal</i>	<i>kappa2</i>	<i>shape</i>
0.00	0.0115	27	2.0000	1.1547	1.0000	1.0000	1.0000	3.4116	1.6058	1.294
2.06	0.2467	27	1.8497	1.0246	1.3486	1.9717	2.8454	3.3442	1.5526	1.199
0.32	0.1752	64	2.4494	1.4880	0.9852	1.8703	2.4953	4.9275	2.1818	1.481
3.28	0.2490	64	2.3843	1.4778	1.2957	1.9143	2.2878	4.8590	2.1309	1.400
3.16	0.2545	64	2.0938	1.2025	1.5395	2.6635	2.8454	4.7222	2.0300	1.526
2.21	0.3485	42	1.9494	1.1712	1.6767	2.5503	3.0958	1.5953	1.9374	1.273
2.12	0.3011	42	1.8092	1.0281	1.8464	2.4464	2.8464	4.5270	1.8880	1.373
1.92	0.2485	79	2.8880	2.0649	1.2718	2.3050	3.1494	4.6211	1.6217	1.200
5.81	0.4025	117	2.7746	1.7692	1.3788	2.2359	2.5216	6.3120	2.6602	1.092
0.00	0.0605	109	3.4047	2.3472	0.9911	1.3921	1.8366	5.4822	2.1431	1.235
2.20	0.2713	109	3.2645	2.1961	1.2533	2.0192	2.7778	9.6300	4.4962	1.333
5.61	0.3306	117	2.4942	1.4772	1.4591	2.5850	2.5850	6.1840	2.5619	1.162
2.73	0.2902	88	2.2036	1.3388	1.7899	3.0581	3.2776	5.8102	2.3000	1.492
3.37	0.5837	140	3.3433	2.2810	1.3793	2.4922	3.2869	7.6943	2.3247	1.333
5.02	0.7228	145	3.3504	2.2923	1.3793	2.2628	3.0575	6.3098	2.3247	1.265
2.08	0.7716	139	3.2356	2.3288	1.6492	2.6250	2.2750	6.0949	1.9153	1.197
4.55	0.6440	139	3.1438	2.2226	1.4566	2.4402	2.7069	6.2443	2.0003	1.092
1.73	0.3839	220	4.4047	3.2162	1.2072	2.0958	2.6412	4.9873	1.6948	1.481
0.01	0.0447	280	4.8094	3.5465	0.9799	1.4834	2.1174	7.5714	2.8451	1.559
2.20	0.3752	280	4.6793	3.3738	1.1916	1.9558	2.5557	5.7595	2.8080	1.527
4.43	0.5495	335	4.4588	3.5453	1.3918	2.4183	3.1887	8.3842	3.0367	1.473

ing topological indices (and also molecular weight) are observed and some indices just duplicate others. The topological indices selected here are those most often applied for QSRP.

A separate group of structural indices form information indices of neighbourhood symmetry of zeroth order, ic_0 , first order, ic_1 , and second order, ic_2 ²². These information content indices were calculated from probabilities of finding equivalent atoms or patterns of atoms in a given structural formula.

The molecular shape of the planar solutes studied was described by the parameter of shape, defined as the ratio of the longer to the shorter side of the rectangle of minimum area enveloping the structure drawn assuming standard van der Waals atomic radii²³.

A large group of non-empirical structural descriptors formed quantum chemical indices. Molecular parameters of orbitals were calculated with complete neglect of differential overlap, CNDO/2 method, using a standard program²⁴. The geometry assumed for calculation was based on standard crystallographic data. The following indices were calculated: total energy (etotal), energy of the highest occupied molecular orbital (ehomo), energy of the lowest unoccupied molecular orbital (elumo), dipole moment (dipolem) and electron excess charges on individual atoms. Energies

are given in Table I in electronvolts, dipole moments in debyes and excess charges in electrons. Based on charge distribution, the submolecular polarity parameter, Δ (delta), was determined as the maximal difference of electron excess charge for two atoms in the molecule⁴.

To differentiate between aromatic hydrocarbon derivatives and heterocyclic compounds, an indicator variable, *ind*, was introduced for which a value 1 was assigned in the case of benzene derivative and 0 for the remaining solutes.

Statistical analysis

Regression analysis was applied to relate retention data to calculated $\log P$ data.

Multiple regression was performed using non-empirical structural descriptors as explanatory variables and $\log k'_w$ as the dependent variable.

Principal component analysis (PCA) was carried out on a set of 16 non-empirical structural descriptors of 21 solutes. The calculation scheme proposed by Schaper and Kaliszan²⁵ was followed. The resulting principal component scores for individual solutes were related to the retention parameters by means of multiple regression analysis.

RESULTS AND DISCUSSION

The relationship between $\log k'_w$ extrapolated to pure water as eluent and $\log P$ calculated by the fragmental method is illustrated in Fig. 3. The relationship presented in Fig. 3 is described by the following regression equation:

$$\log k'_w = -0.052 + 0.208 (\log P)^2 \quad (1)$$

$$n = 21, s = 0.279, R = 0.9711, F = 314$$

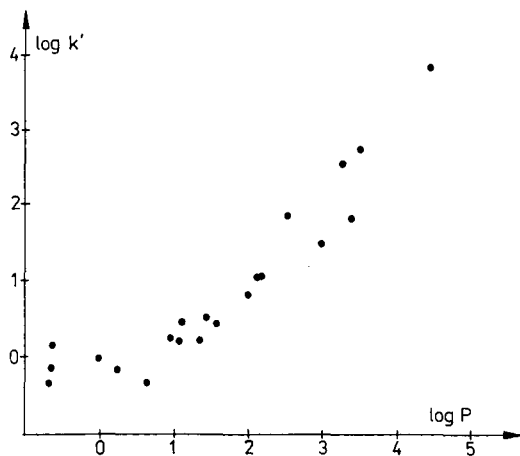


Fig. 3. Relationship between logarithms of capacity factors extrapolated to pure water as a mobile phase, $\log k'_w$, and logarithms of *n*-octanol-water partition coefficients calculated by the fragmental method of Hansch and Leo¹⁸, $\log P$.

where n is the number of compounds used for deriving the regression equation, s is the standard error of the estimate, R is the correlation coefficient and F is the value of the F -test. The statistical evaluation of eqn. 1 is satisfactory, especially as it includes a wide diversity of structures. The curvature of the $\log k'_w$ vs. $\log P$ plot is especially pronounced for highly hydrophilic solutes. The experimentally observed curvature of the relationship may be artificial to some extent. The retention of hydrophilic solutes on the relatively short column used is too low to obtain precise $\log k'_w$ data. The HPLC system applied was designed to prove the general validity of the approach and the differences in hydrophobicities of individual test solutes exceeded five $\log P$ units. When dealing with a set of less hydrophobic solutes, one can apply longer columns and/or a PBCA material of higher polymer coating. Nevertheless, the HPLC procedure applied here employing a 15-cm column packed with PBCA may be recommended for the evaluation of the hydrophobicity of compounds with $\log P$ above 0.5. The observation^{26,27} that in certain instances the calculated hydrophobicity parameters are more trustworthy than those derived experimentally by HPLC is also valid for PBCA when dealing with hydrophilic solutes.

Similar curvilinear relationships as expressed by eqn. 1 have been reported on ODS phases for barbiturates²⁸ and diols²⁹. The striking difference between PBCA and ODS is that on the former a single correlation between $\log k'_w$ and $\log P$ is obtained for a variety of solutes whereas on ODS separate relationships are reported for individual classes of compounds^{26,30,31}. Two correlation lines (for hydroxylated and non-hydroxylated solutes) were also reported on styrene-divinylbenzene copolymer stationary phase¹⁶.

The single $\log k'_w$ vs. $\log P$ relationship may be due to insignificant interactions of solutes with the alumina support in the case of PBCA as opposed to relatively stronger interactions with silanol sites in the case of ODS. The present results support our previous observations of the unique properties of PBCA as a reversed-phase material for hydrophobicity determinations.

We also attempted to relate the determined capacity factors to non-empirical molecular structural descriptors of solutes. There are several reports on the importance of molecular size for the retention of congeneric solutes on ODS^{28,32-34}. Previously, we succeeded in obtaining retention data of benzene derivatives from reversed-phase HPLC on ODS by means of size-related and a polarity-related structural descriptors^{4,5}. In a two-parameter regression equation, the size-related descriptor was the quantum chemically calculated total energy (etotal), whereas polarity was quantified by the maximum difference of electron excess charges (δ).

Here we performed the multiple regression analysis of $\log k'_w$ data using the non-empirical structural descriptors given in Table I. The most meaningful regression equation found was

$$\log k'_w = -1.618 + 0.089 \text{ bondrefr} - 2.505 \delta \quad (2)$$

$$n = 21, s = 0.500, R = 0.9090, F = 42.8$$

The term bondrefr is significant at the level of at least 0.001 and δ at the level of 0.002. An equation of similar statistical value was obtained when using the molecular connectivity indices chi1v or chi2v instead of bondrefr. No statistically valid improve-

ment of eqn. 2 was obtained by introducing of additional structural descriptors considered. Only when an indicator variable, ind, was introduced did the quality of correlation increase (eqn. 3). The indicator variable was assigned a value of 1 for benzene derivatives and 0 for heterocyclic solutes.

$$\log k'_w = -1.272 + 0.089 \text{ bondrefr} - 2.648 \text{ delta} - 0.598 \text{ ind} \quad (3)$$

$$n = 21, s = 0.394, R = 0.9476, F = 49.8$$

Intercorrelations found among structural parameters limit the applicability of multiple regression analysis in QSRR studies. Such intercorrelated data, however, can be analysed by multivariate statistical methods. The set of structural data considered here consisted of the last 16 columns in Table I, *i.e.*, excluding $\log P$ and ind.

Two principal factors extracted from the structural data set appeared meaningful for the description of the retention of the solutes. The first factor accounted for 48.6% of the variance in structural data considered and the second factor for 25.2%.

Subsequently, the loadings (eigenvectors) of the two principal components extracted were calculated. The loadings were subjected to VARIMAX rotation to maximize the variance of squared loadings and thus facilitate interpretation of meaning of individual principal components. In Fig. 4 the loadings of the two principal compo-

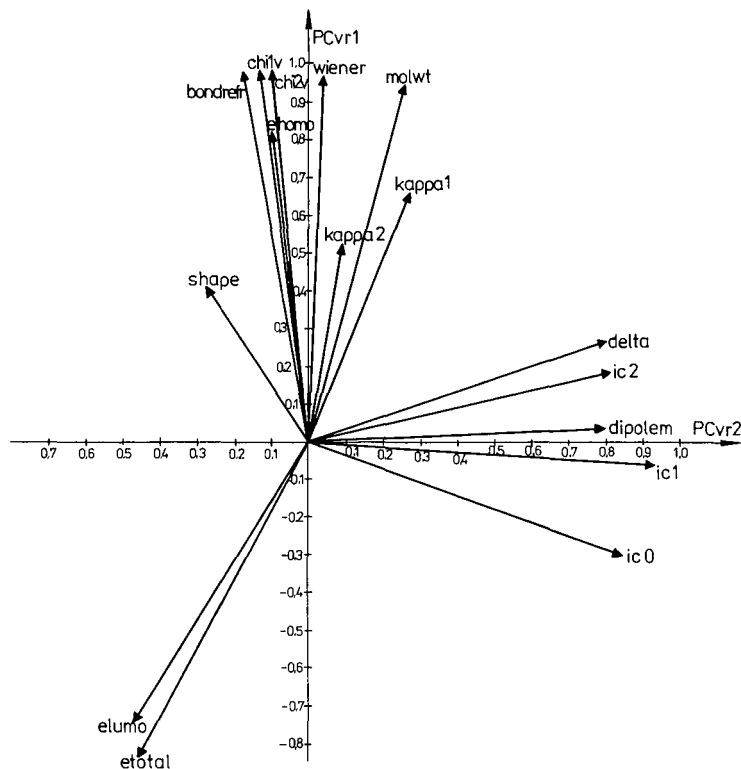


Fig. 4. VARIMAX-rotated loadings of two first principal components by individual structural descriptors denoted as in Table I.

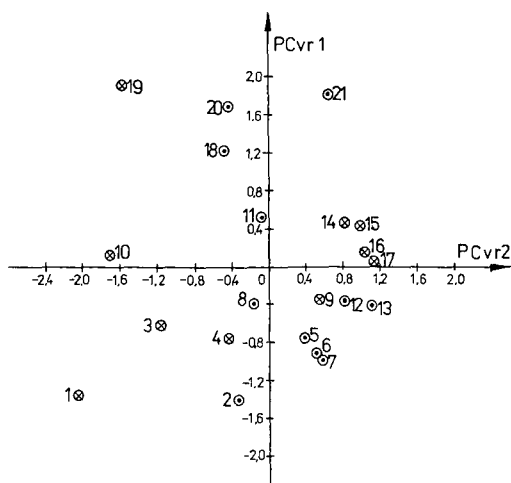


Fig. 5. Principal component scores after VARIMAX rotation for the solutes numbered as in Fig. 1.

nents by individual structural descriptors are depicted. The principal component scores for the set of 21 solutes studied, scaled to a variance of 1, obtained after VARIMAX rotation are presented in Fig. 5.

As shown in Fig. 4 the first principal component, PCvr1, is loaded mostly by such structural descriptors as *chl*v, *bondrefr*, *chi2v*, *wiener*, *molwt* and *etotal*. All these structural descriptors reflect basically the size (bulkiness) of solutes. In such a situation PCvr1 condenses information on molecular size.

The second principal component, PCvr2, is loaded predominantly by the structural descriptors *ic0*, *ic1*, *ic2*, *delta* and *dipolem*. Hence it can be concluded that PCvr2 concentrates structural information related to the so-called molecular polarity. The polar properties of chemical compounds are a function of the electron distribution within a molecule. Such properties determine the ability of a solute to participate in intermolecular interactions with the stationary and/or mobile phase of the dipole-dipole, dipole-induced dipole and electron pair donor-acceptor type.

A separate discussion should be devoted to the high loadings of PCvr2 by the information content indices *ic0*, *ic1* and *ic2*. These indices reflect the diversity in the atom composition of molecules. This is connected with specific, polar properties of solutes. In studies on structural descriptors of benzene derivatives we also observed a high loading by information content indices of the principal component reflecting the molecular polarity of solutes.

It seemed of interest to apply the structural information condensed in two principal components to correlation studies with liquid chromatographic data derived on PCBA. Eqn. 4 describes $\log k'_w$ in terms of non-rotated principal component scores scaled to a variance of 1, *i.e.*, PC1 and PC2:

$$\log k'_w = 0.8852 + 0.5942 \text{ PC1} - 0.9016 \text{ PC2} \quad (4)$$

$$n = 21, s = 0.380, R = 0.9485, F = 80.6$$

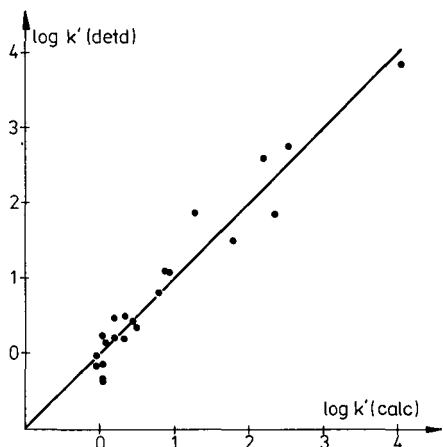


Fig. 6. Relationship between $\log k'$ (extrapolated to pure water) determined experimentally and calculated by eqn. 4.

Both the PC1 and PC2 terms are significant at at least the 0.001 significance level. The relationship between experimental $\log k'$ data and those calculated by eqn. 4 is illustrated in Fig. 6.

The statistical characteristics of eqn. 4 are better than those of eqn. 2, as indicated by the standard error, correlation coefficient and F -test. Qualitatively both equations are similar in that increasing solute bulkiness enhances retention whereas increasing polarity has the opposite effect. Eqn. 4 demonstrates that the correlation represented by eqn. 2 is not fortuitous.

Structural information extracted by principal component analysis of molecular descriptors appeared to be more precise and reliable than the respective information provided by individual structural parameters. Comparison of eqns. 4 and 3 suggests that the principal components extracted from the set of sixteen molecular descriptors contain information that allows the differentiation of benzene and heterocyclic derivatives. In other words, these factors contain information expressed explicitly by the indicator variable, *ind*, which was not included in multivariate analysis.

Analysing eqns. 2 and 4 from the point of view of the mechanism of reversed-phase HPLC on PBCA, one can conclude that non-specific, dispersive interactions of solutes with the stationary phase prevail over the analogous interactions with the mobile phase. This is indicated by the positive increment to eqns. 2 and 4 by structural parameters reflecting the ability of solutes to participate in dispersive (London-type) intermolecular interactions. On the other hand, the negative increment to eqns. 2 and 4 of the molecular parameters reflecting the ability of solutes to participate in specific, polar intermolecular interactions demonstrates that polar solute–mobile phase interactions are stronger than analogous solute–stationary phase interactions. Hence the mechanism of retention on PBCA is closely similar to that on ODS^{4,5} but basically different from that postulated for normal-phase HPLC on porous graphitic carbon^{6,14}.

The structural descriptors considered in this work can be conveniently determined by simple calculation procedures for any given structural formula. The ques-

tion is how much information about the properties of chemical compounds they contain. Principal component analysis of sixteen quantum chemical, information content and topological indices, together with molecular weight, molecular refractivity and molecular shape descriptors, allows the extraction of information useful for the determination of physico-chemical properties. Analysing loadings of principal components by individual structural descriptors (Fig. 4), one can conclude that total energy (etotal) and topological indices (wiener, chi1v and chi2v) provide information on the bulkiness of the solutes and have no advantages over established bulk measures such as molecular weight and refractivity.

Electron charge distribution calculated by standard CNDO/2 calculations provides information on the polar properties of solutes. Again, the submolecular polarity measure δ appeared to be a more appropriate descriptor of polar properties of solutes than the total dipole moment.

The CNDO/2 method is reliable as far as charge distribution is concerned but less reliable for orbital energy calculations. In such a situation, it is difficult to determine whether the chomo and elumo descriptors fail to account for the ability of the solutes to participate in electron pair donor-acceptor interactions, or whether these interactions are of little importance for retention.

Further studies are required to explain the physical meaning of information content indices.

Neither the Kier indices of shape, kappa1 and kappa2, nor the shape parameter previously proposed in this laboratory, shape, appeared meaningful for the description of retention. Probably retention differences caused by differences in molecular shape are too subtle to be detectable for such a diverse set of solutes. Hence the question remains open of whether the shape parameters considered differentiate molecular properties or just structural formulae.

REFERENCES

- 1 U. Bien-Vogelsang, A. Deege, H. Figge, J. Kohler and G. Schomburg, *Chromatographia*, 19 (1984) 170.
- 2 G. Heinemann, J. Kohler and G. Schomburg, *Chromatographia*, 23 (1987) 435.
- 3 R. Kaliszan, R. W. Blain and R. A. Hartwick, *Chromatographia*, 25 (1988) 5.
- 4 R. Kaliszan, K. Ośmiałowski, S. A. Tomellini, S.-H. Hsu, S. D. Fazio and R. A. Hartwick, *Chromatographia*, 20 (1985) 705.
- 5 R. Kaliszan, K. Ośmiałowski, S. A. Tomellini, S.-H. Hsu, S. D. Fazio and R. A. Hartwick, *J. Chromatogr.*, 352 (1986) 141.
- 6 B. J. Bassler, R. Kaliszan and R. A. Hartwick, *J. Chromatogr.*, 461 (1989) 139.
- 7 J. F. K. Huber, C. A. M. Meijers and J. A. R. J. Hulsman, *Anal. Chem.*, 44 (1972) 111.
- 8 R. F. Hirsch, R. J. Gaydos and J. R. Chretien, *Anal. Chem.*, 52 (1980) 723.
- 9 M. N. Hasan and P. C. Jurs, *Anal. Chem.*, 55 (1983) 263.
- 10 G. Gullner, T. Cserháti, B. Bordás and M. Szógyi, *J. Liq. Chromatogr.*, 9 (1986) 1919.
- 11 S. Wold, L. Eriksson, S. Hellberg, J. Jonsson, M. Sjöström, B. Skageberg and C. Wikström, *Can. J. Chem.*, 65 (1987) 1814.
- 12 L. Eriksson, J. Jonsson, M. Sjöström and S. Wold, *Quant. Struct.-Act. Relat.*, 7 (1988) 144.
- 13 R. Kaliszan, *Quantitative Structure-Chromatographic Retention Relationships*, Wiley, New York, 1987.
- 14 R. Kaliszan, K. Ośmiałowski, B. J. Bassler and R. A. Hartwick, *J. Chromatogr.*, 499 (1989) 333.
- 15 J. H. Knox and R. Kaliszan, *J. Chromatogr.*, 349 (1985) 211.
- 16 S. Bitteur and R. Rosset, *J. Chromatogr.*, 394 (1987) 279.
- 17 C. Hansch and A. Leo, *Substituent Constants for Correlation Analysis in Chemistry and Biology*, Wiley, New York, 1979.
- 18 A. I. Vogel, W. T. Cresswell, G. H. Jeffery and J. Leicester, *J. Chem. Soc.*, (1952) 514.

- 19 H. Wiener, *J. Phys. Chem.*, 52 (1948) 1082.
- 20 L. B. Kier and L. H. Hall, *J. Pharm. Sci.*, 65 (1976) 1806.
- 21 L. B. Kier, *Acta Pharm. Jugosl.*, 36 (1986) 171.
- 22 R. Sarkar, A. B. Roy and P. K. Sarkar, *Math. Biosci.*, 39 (1978) 299.
- 23 R. Kaliszan, H. Lamparczyk and A. Radecki, *Biochem. Pharmacol.*, 28 (1979) 123.
- 24 P. A. Dobosh, *QCPE*, 11 (1969) 141.
- 25 K. -J. Schaper and R. Kaliszan, in E. Mutschler and E. Winterfeldt (Editors), *Trends in Medicinal Chemistry*, VCH, Weinheim, Berlin, 1989, pp. 125–139.
- 26 C. V. Eadsforth, *Pestic. Sci.*, 17 (1986) 311.
- 27 A. J. Leo, *J. Pharm. Sci.*, 76 (1987) 166.
- 28 M. J. M. Wells, C. R. Clark and R. M. Patterson, *J. Chromatogr. Sci.*, 19 (1981) 573.
- 29 D. Noël and P. Vangheluwe, *J. Chromatogr.*, 388 (1987) 75.
- 30 J. J. Sabatka, D. J. Minick, T. K. Schumaker, G. L. Hodgson, Jr., and D. A. Brent, *J. Chromatogr.*, 384 (1987) 349.
- 31 K. Miyake, N. Mizuno and H. Terada, *J. Chromatogr.*, 439 (1988) 227.
- 32 M. J. M. Wells, C. R. Clark and R. M. Patterson, *Anal. Chem.*, 58 (1986) 1625.
- 33 R. H. Rohrbaugh and P. C. Jurs, *Anal. Chem.*, 59 (1987) 1048.
- 34 E. J. Tierney, J. M. Bellama, G. Eng, F. E. Brinckman and R. B. Johannesen, *J. Chromatogr.*, 441 (1988) 229.

CHROMSYM. 1706

High-performance liquid chromatography of amino acids, peptides and proteins

XCVII^a. The influence of the gradient elution mode and displacer salt type on the retention properties of closely related protein variants separated by high-performance anion-exchange chromatography

A.N. HODDER, M.I. AGUILAR and M.T.W. HEARN*

Department of Biochemistry, Monash University, Clayton, Victoria 3168 (Australia)

SUMMARY

The influence of different elution modes, gradient times and flow-rates on the relative retention of closely related variants of carbonic anhydrase and ovalbumin has been investigated using high-performance ion-exchange chromatography. Three isoform species of carbonic anhydrase and four isoforms related to ovalbumin eluted by anion-exchange chromatography were characterised by isoelectric focusing and sodium dodecylsulphate–polyacrylamide electrophoresis. Gradient retention data were collected using several different alkali metal halides as the displacer salt, in order to systematically evaluate the effect on selectivity of different anions and cations in the series F^- , Cl^- and Br^- , and Li^+ , Na^+ and K^+ . While the selectivity between the different ovalbumin isoform species remained essentially constant with each displacer salt, solute Z_c -values [*J. Chromatogr.*, 458 (1988) 27] varied with the type of salt. In contrast, non-parallel retention plots were obtained for the carbonic anhydrase isoforms with the Z_c values different for each isoform. Furthermore, significant differences in chromatographic behaviour for these proteins were observed between experiments carried out under gradient elution conditions with either varied gradient time and constant flow-rates or fixed gradient time and varied flow-rates. These results are discussed in terms of the influence of column residence time and protein-salt interactions of the solute's interactive ionotope and the concomitant effects these structural perturbations may have on chromatographic behaviour.

INTRODUCTION

During the past decade, high-performance liquid chromatography (HPLC) has developed into a powerful technique for the analysis of complex mixtures of biological

^a For Part XCVI, see ref. 17.

macromolecules¹⁻³. The advent of protein engineering, cell culture technologies and new methods for rapid peptide synthesis has necessitated the development of very sensitive and reliable separation strategies for the purification of target peptides and proteins from crude feedstock solutions contaminated with other structural or charged variant species. Production of polypeptides and proteins by recombinant DNA or chemical synthesis methods often result in a higher incidence rate of variant species than normally found in natural systems³, arising from expression errors, post-translational processing or incomplete peptide syntheses. In the fields of medicine and veterinary science, the removal of these variants is paramount if the target protein or peptide is intended for therapeutic use.

Removal of contaminating protein variants using the various modes of adsorption chromatography available today will only be successful if subtle differences exist between the stationary phase binding site on the contaminants and on the target protein. The further development of strategies for the separation of very closely related protein solutes requires an understanding of the relationship between chromatographic behaviour and solute structure. At the present time, the extent to which various chromatographic systems can probe and detect changes in the microstructure of protein binding sites has not been fully elucidated. In this study the influence of experimental conditions on the chromatographic behaviour of the closely related structural variants of bovine carbonic anhydrase and ovalbumin has been investigated. Retention data were used to obtain protein Z_c values^{1,2}, as a measure of the average number of electrostatic interactions occurring between the solute and stationary phase surfaces. Perturbations in the microstructure of the protein binding site were monitored by changes in Z_c with systematic changes in the displacer salt type and the buffer concentration.

MATERIALS AND METHODS

Chromatographic procedures

All chromatographic procedures were performed with a Pharmacia (Uppsala, Sweden) fast protein liquid chromatography (FPLC) system. The source of chemicals and reagents, the purity of the proteins and methods used for the numerical analysis of chromatographic retention and bandwidth data have been described in detail elsewhere^{1,4}.

Isoelectric focusing and sodium dodecylsulphate electrophoresis

Acrylamide and sodium dodecylsulphate (SDS) were of electrophoresis grade from BDH (Clayton, Australia). Ampholines (pH ranges: 3.5-10, 5-7, 4-6 and 9-11) and standard proteins of known isoelectric points (pI) were obtained in kit form from Pharmacia. All other chemicals were of analytical grade or better. Isoelectric focusing (IEF) was carried out using a Bio-Rad (Richmond, CA, U.S.A.) Bio-phoresis horizontal electrophoresis cell powered by a LKB (Bromma, Sweden) 2297 Macrodrive 5 constant-power supply. The horizontal bed was cooled to 4°C. Gel dimensions were 230 mm × 115 mm × 1 mm. SDS-polyacrylamide gel electrophoresis (PAGE) was performed using slab gels (200 mm × 170 mm × 1 mm) and an "in house" built vertical gel apparatus. Protein samples collected from Mono-Q column experiments were desalted in the following manner. A 200- μ l aliquot of sample was diluted up to

2 ml total volume by addition of the desalting buffer (20 mM Tris · HCl, 0.02% Brij-35, pH 7.4). Protein samples were then concentrated and desalted in Centricon-10 microconcentrators (Amicon, Danvers, MA, U.S.A.) by centrifuging at 2800 g for 60 min using a Sorvall RC-5B centrifuge fitted with a SS-34 head (Dupont, Wilmington, DE, U.S.A.) or until approximately 200 μ l of sample remained. The remaining sample was then dialysed for 15 h in a solution of 0.02% Brij-35 using Spectrapore (Spectrum Medical Industries, Los Angeles, CA, U.S.A.; 600–8000 molecular weight cut off) dialysis tubing.

RESULTS AND DISCUSSION

The separation and characterisation of isoforms for carbonic anhydrase and ovalbumin

Chromatographic elution profiles for many commercially available proteins, as well as proteins isolated in the research laboratory, often show multiple peaks corresponding to the existence of several structurally related species. If these proteins are isoforms of the mature, expressed form of the protein, *e.g.* if they are functionally related proteins of very similar sequence and composition arising from minor genomic or post-translational modifications in overall charge and/or hydrophobicity, then such isoform mixtures can conveniently be used to examine the chromatographic behaviour of related protein variants in terms of structure–retention dependencies. Typical of such chromatographic behaviour are the high-performance ion-exchange chromatography (HPIEC) elution profiles for bovine carbonic anhydrase and ovalbumin shown in Fig. 1, which reveal the presence of multiple peaks for each protein. The bovine carbonic anhydrase sample used in this study is known from other studies to contain at least two charged variant species which gave rise to peaks 1 to 3. These species can be readily distinguished on the basis of their *pI* values and are referred to as carbonic anhydrase II, *pI* 5.4 (CA-II_{5.4}) and carbonic anhydrase II, *pI* 5.9 (CA-II_{5.9}). Furthermore, comparative studies⁵ on the CA-II_{5.4} and CA-II_{5.9} isoforms have shown that they are genetic variants where, in the latter case, an Arg residue is replaced in the primary sequence structure by a Gln residue at position 56.

Chromatographic analysis of high-quality commercial preparations of ovalbumin by other workers⁶ has indicated that the preparations are homogeneous in

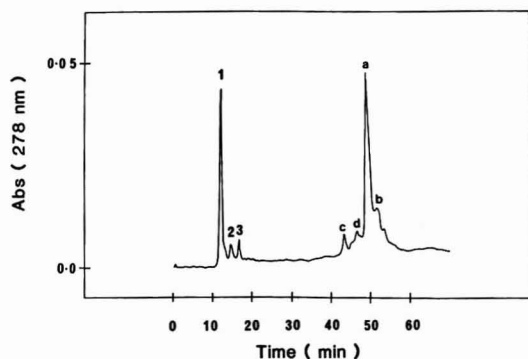


Fig. 1. Chromatogram demonstrating the presence of three bovine carbonic anhydrase isoforms (peaks 1–3) and four ovalbumin isoforms (peaks a–d), eluted with lithium chloride as the displacer salt and gradient time of 85.7 min at a flow-rate of 1 ml/min.

terms of molecular weight as determined by gel filtration. However, several chromatographic zones are also observed by ion-exchange techniques which suggests that proteins associated with these peaks could be charge or structural isoforms of ovalbumin. In order to further confirm the molecular characteristics of isoforms for carbonic anhydrase and ovalbumin with the preparations used in the present studies, samples recovered from the chromatographic studies (Fig. 1) were characterised using IEF and SDS-PAGE.

A comparison of the SDS-PAGE and IEF behaviour for the bovine carbonic anhydrase sample in peaks 1 to 3 to that for highly purified samples of CA-II_{5,4} and

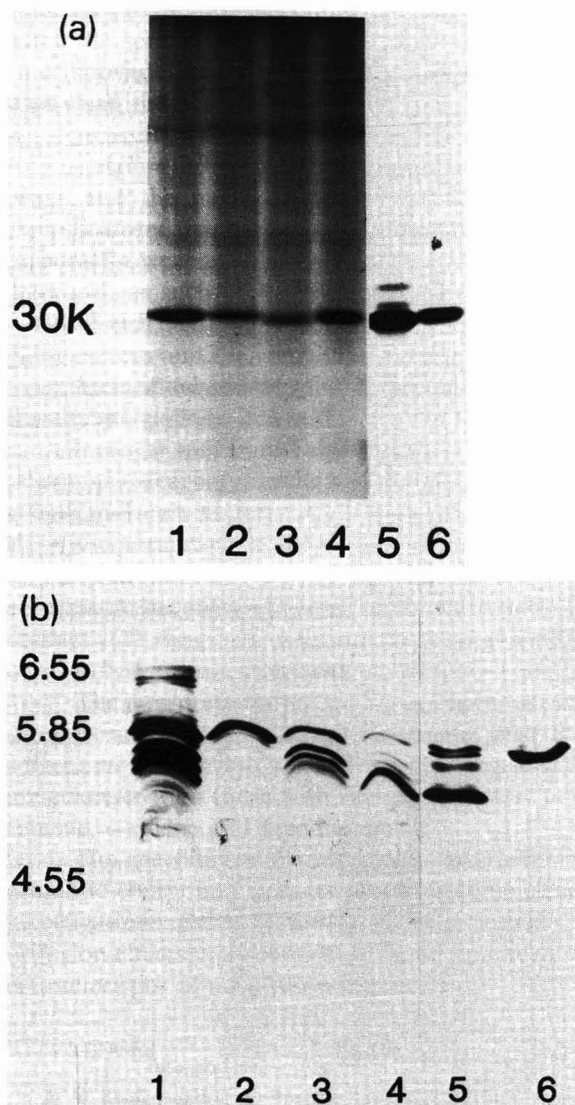


Fig. 2. Electrophoretic analysis of bovine carbonic anhydrase by (a) SDS-PAGE and (b) IEF. Samples: 1 = commercial sample; 2 = CA-1; 3 = CA-2; 4 = CA-3; 5 = CA-II_{5,4}; 6 = CA-II_{5,9}. See Materials and Methods for other details.

CA-II_{5,9} is shown in Fig. 2a and b. SDS-PAGE shows three bands of identical molecular weight. However, IEF indicates the existence of the various charged isoforms. Peak 1 (CA-1), the major species corresponds to CA-II_{5,9}, while peak 3 (CA-3) can be attributed to CA-II_{5,4}. Two additional protein species with isoelectric points at *pI* 5.60 and 5.70 were found in fractions taken from peak 2 and were identified as CA-2_{5,6} and CA-2_{5,7}. The structural origin of these latter two protein isoforms is currently under investigation.

Fig. 3a and b shows the SDS-PAGE and IEF gels for all the ovalbumin fractions collected after ion-exchange chromatography and an unchromatographed ovalbumin

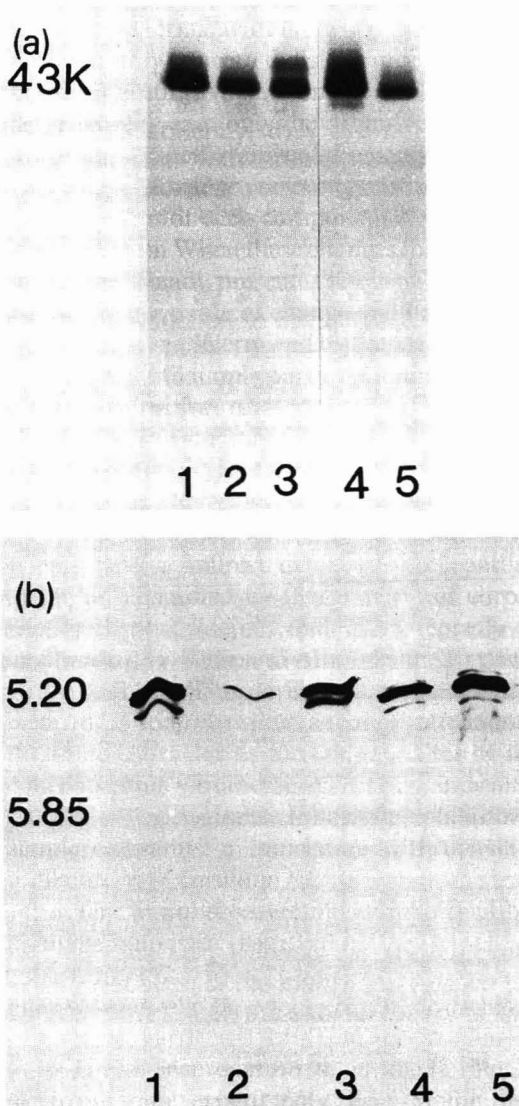


Fig. 3. Electrophoretic analysis of ovalbumin by (a) SDS-PAGE and (b) IEF. Samples: 1 = Commercial sample; 2 = Ov-c; 3 = Ov-d; 4 = Ov-a; 5 = Ov-b. K = Kilodaltons.

sample. The ovalbumin preparation was resolved into the four chromatographic peaks shown in Fig. 1, with the isoforms termed Ov-c, Ov-d, Ov-a and Ov-b, respectively, where Ov-a represents the major species of ovalbumin. The SDS-PAGE and analytical IEF results (Fig. 3) indicate that the ovalbumin species corresponding to each of the four chromatographic peaks have similar molecular weights and charge distributions. The protein species contributing to the HPIEC profile of ovalbumin therefore do not represent nett charge variants of the dominant form. Structural heterogeneity with ovalbumin is known to arise from the type or number of neutral sugars attached to the peptide chain^{7,8}. In addition, the formation of different conformational species, with different interactive properties under the chromatographic conditions used, would also give rise to a complex, multi-peak elution profile. These structural variations are not detected by methods such as IEF or chromatofocusing which separate according to nett charge or SDS-PAGE unless substantial differences in molecular mass existed between the isoforms. The existence of similar structural variants as revealed by HPIEC has been documented with other glycoproteins and is believed to be responsible for the complex elution profiles observed for electrophoretically pure samples of, for example, thyroid stimulating hormone⁹.

The effect of displacer salt type and varied gradient (VG) times on isoform $Z_{c,VG}$ values

Protein isoforms will only be separated by a particular mode of adsorption chromatography if the binding surfaces of each protein species involved in the retention process differ from each other. Furthermore, the number of functional groups at the surface of the protein which interact with the sorbent will be dependent upon the mode of elution. For example, resolution of variant proteins by immunoaffinity chromatography will only be achieved when there are differences in highly specific areas on the protein surface associated with the epitope (antigenic determinant) and these differences directly contribute to the binding process with the immobilised antibody. For other modes of adsorption chromatography such as reversed-phase, hydrophobic-interaction or ion-exchange systems, the binding site on the protein may not be as structurally specific and could occur over a much larger region of the surface area of the solute molecule or alternatively involve multisite regions of interaction. Therefore, structural changes over a far greater portion of the protein that may be invisible to immunoaffinity methods, can be detected by these chemical ligands in adsorptive chromatographic methods.

The ability of the chromatographic systems with immobilised chemical ligands to detect and anticipate small compositional or structural changes in the binding regions of proteins has not been comprehensively investigated in a systematic manner in terms of structure-retention dependencies, although the application literature on protein purification abounds with anecdotal examples of the resolution of charge and structural variations of the same protein. However, recent studies¹⁰⁻¹⁴ on the HPIEC and hydrophobic-interaction chromatographic properties of lysozyme indicate that the correlation of the three-dimensional protein structure and chromatographic properties can be used to provide significant insight into the structural factors including subtle changes in the topographic features of proteins which control or influence the selectivity of chromatographic systems. To further investigate the potential of HPIEC as a functional molecular probe for determining subtle charge variations in protein structure, the binding behaviour of the variants of bovine

carbonic anhydrase and ovalbumin was investigated as a function of the mobile phase composition, the gradient time, t_G and eluent flow-rate. The chromatographic data were analysed in terms of the Chained Pek-n-ese programme², which integrates relative retention and peak width in the gradient mode (\bar{k} , $\bar{\sigma}_v$) with the chromatographic variables, t_G , flow-rate (F), Δc , etc. The HPIEC data were then displayed as plots of $\log \bar{k}$ versus $\log 1/\bar{c}$ where \bar{k} and \bar{c} are the median capacity factor and the concentration of the displacing salt respectively.

Fig. 4a–h shows the retention plots of $\log \bar{k}$ versus $\log 1/\bar{c}$ for the isoforms of bovine carbonic anhydrase and ovalbumin eluted with a variety of alkali metal halide salts. Retention data were obtained by varying the gradient time between 8.6 and 171.1 min at a constant flow-rate of 1 ml/min with the buffer pH 9.6. The retention maps illustrate that mobile phase composition can be used to optimise the selectivity of the HPIEC separation of these isoform species. For example, Fig. 4d and g shows that the selectivity between the various bovine carbonic anhydrase variants was maintained while their elution volumes were reduced with a change in salt type from lithium chloride to potassium bromide. Other salts such as sodium chloride or sodium bromide (Fig. 4b and c) were found to decrease the selectivity between the isoforms as the gradient time was reduced. Evidently, these latter sodium salts increase the resolution of the separate isoforms of carbonic anhydrase when longer gradient times are used.

Tables I and II show the $Z_{c,vG}$ values for varied gradient time (± 1 S.D.) and coefficients of determination (r^2) in parentheses obtained from the retention data in Fig. 4a–h for bovine carbonic anhydrase and ovalbumin respectively. The $Z_{c,vG}$ values were obtained by regression analysis of linear regions of plots for $\log \bar{k}$ versus $\log 1/\bar{c}$. According to the stoichiometric displacement model¹⁵, Z_c values are a quantitative measure of the number of electrostatic interactions occurring between the solute and stationary phase medium. If the salt species in the eluent has no influence on the distribution or orientation of interactive charges on the protein surface, experimental $Z_{c,vG}$ values will be independent of the displacer ions used. However, Tables I and II show that protein $Z_{c,vG}$ values are not constant over the range of the elution conditions employed and vary significantly with the type of displacer salt used. Furthermore, the effect of individual chaotropic (water structure breaking) and kosmotropic (water structure making) displacer anions and cations on the $Z_{c,vG}$ values of both the bovine carbonic anhydrase and ovalbumin isoforms follow similar trends in the magnitude of $Z_{c,vG}$ as previously observed for other proteins¹². These results thus provide additional support for the following generalisations pertinent to the selection of displacer salts in HPIEC, namely: (1) $Z_{c,vG}$ values increase as both the anion and cation of the displacer salt becomes more chaotropic in nature. (2) $Z_{c,vG}$ values increase as both the anion and cation became more kosmotropic in nature. (3) $Z_{c,vG}$ values decrease when the displacer salt contains a combination of a chaotropic and kosmotropic ion.

The results in Tables I and II can be further used to evaluate the effect of the salt type on the ionotopic microstructure (coulombic binding site) of related variant species. Significant variations in the $Z_{c,vG}$ value indicate a change in the number of electrostatic interactions occurring between the protein and stationary phase. Under these circumstances, the most likely cause of changes in $Z_{c,vG}$ values are through salt-induced perturbations in the ionotopic structure. For example, the $Z_{c,vG}$ values for Ov-a, Ov-c and Ov-d varied with changes in the displacer salt which suggests that

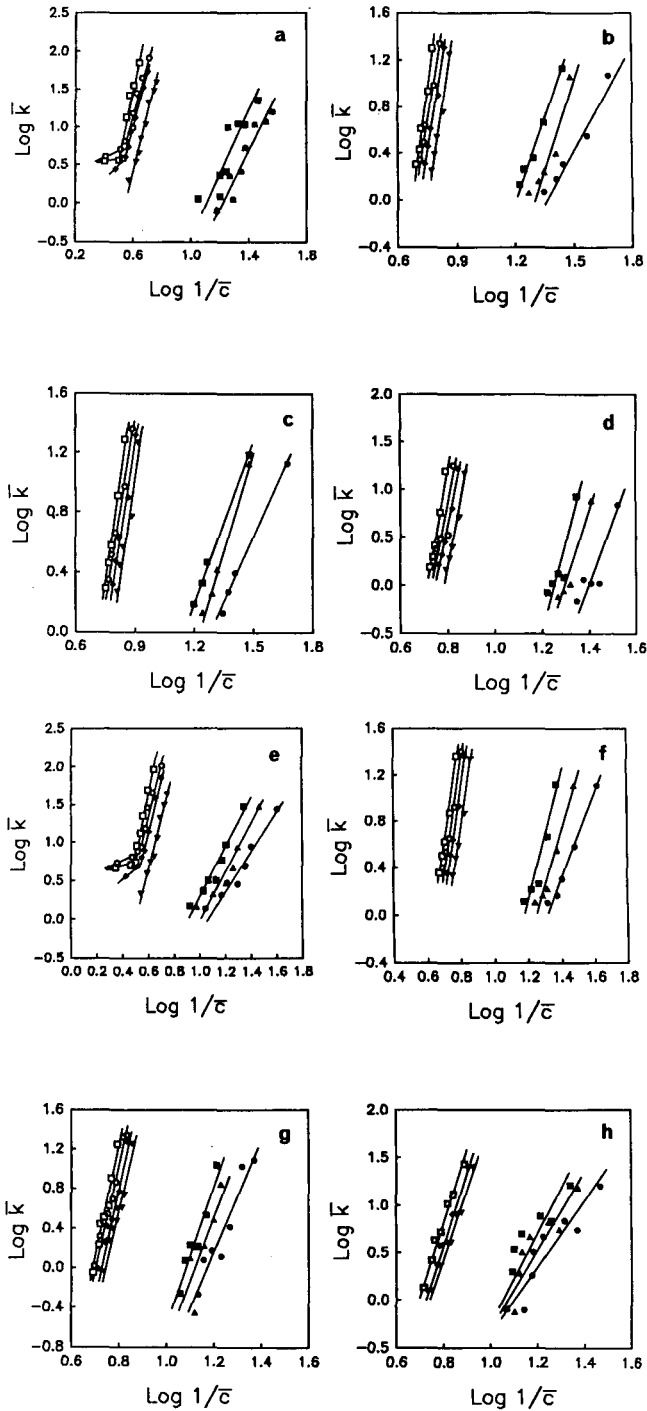


Fig. 4. Plots of $\log \bar{k}$ versus $\log 1/\bar{c}$ for bovine carbonic anhydrase isoforms 1, 2 and 3 and ovalbumin isoforms a, b, c and d. The plots were derived from gradient elution data at pH 9.6, a flow-rate of 1 ml/min with gradient times between 8.6 and 171.1 min for (a) NaF, (b) NaCl, (c) NaBr, (d) LiCl, (e) KF, (f) KCl, (g) KBr and (h) LiBr. Isoforms: ● = CA-1; ▲ = CA-2; ■ = CA-3; ▼ = Ov-c; ◆ = Ov-d; ○ = Ov-a; □ = Ov-b.

TABLE I

Z_c VALUES FOR CARBONIC ANHYDRASE VARIANTS OBTAINED BY LINEAR REGRESSION OF VARIED GRADIENT TIME EXPERIMENTS

Coefficients of determination are given in parentheses.

Salt	Protein		
	CA-1	CA-2	CA-3
LiF	Not done	Not done	Not done
LiCl	5.60 ± 2.12 (0.78)	7.44 ± 1.24 (0.95)	7.62 ± 1.98 (0.83)
LiBr	3.14 ± 0.71 (0.80)	3.67 ± 0.87 (0.78)	3.81 ± 0.86 (0.80)
NaF	3.55 ± 0.45 (0.91)	3.55 ± 0.45 (0.92)	3.52 ± 0.69 (0.81)
NaCl	3.07 ± 0.21 (0.99)	5.40 ± 1.18 (0.91)	4.46 ± 0.28 (0.99)
NaBr	2.92 ± 0.17 (0.99)	4.31 ± 0.22 (1.00)	3.55 ± 0.13 (1.00)
KF	2.37 ± 0.25 (0.95)	2.64 ± 0.36 (0.92)	3.15 ± 0.36 (0.94)
KCl	3.84 ± 0.05 (1.00)	5.10 ± 0.28 (0.99)	5.09 ± 0.92 (0.91)
KBr	5.60 ± 0.75 (0.92)	7.11 ± 2.43 (0.68)	7.33 ± 1.02 (0.92)
LiF	Not done	Not done	Not done
NaF	3.55 ± 0.45 (0.80)	3.55 ± 0.45 (0.92)	3.52 ± 0.69 (0.81)
KF	2.37 ± 0.25 (0.95)	2.64 ± 0.36 (0.92)	3.15 ± 0.36 (0.94)
LiCl	5.60 ± 2.12 (0.78)	7.44 ± 1.24 (0.95)	7.62 ± 1.98 (0.80)
NaCl	3.07 ± 0.21 (0.99)	5.40 ± 1.18 (0.91)	4.46 ± 0.28 (0.99)
KCl	3.84 ± 0.05 (1.09)	5.10 ± 0.28 (0.99)	5.09 ± 0.92 (0.91)
LiBr	3.14 ± 0.71 (0.80)	3.67 ± 0.87 (0.78)	3.81 ± 0.86 (0.80)
NaBr	2.92 ± 0.17 (0.99)	4.31 ± 0.22 (1.00)	3.55 ± 0.13 (1.00)
KBr	5.60 ± 0.75 (0.92)	7.11 ± 2.43 (0.68)	7.33 ± 1.02 (0.92)

the size of the ionotopic region is strongly influenced by the nature of the eluting salt. The $Z_{c, VG}$ values for the three variants, however, did not differ significantly within a particular salt system. For example, elution with potassium chloride and potassium fluoride gave the following results: *i.e.*, for KCl: $Z_{c, VG}$ (Ov-a) = 8.40 ± 0.76 , $Z_{c, VG}$ (Ov-c) = 8.50 ± 0.71 , $Z_{c, VG}$ (Ov-d) = 8.70 ± 0.55 and with KF, $Z_{c, VG}$ (Ov-a) = 6.37 ± 0.57 , $Z_{c, VG}$ (Ov-c) = 7.05 ± 0.48 , $Z_{c, VG}$ (Ov-d) = 6.70 ± 0.57 . This observation further indicates that the interactive behaviour of the ionotopes of the ovalbumin variants is influenced in a similar manner on exposure to various salts. The essentially constant $Z_{c, VG}$ values for Ov-a, Ov-c and Ov-d indicate the existence of ionotopes with equivalent charge densities, and for proteins with closely related structures these ionotopes are likely to be located in identical areas of the three-dimensional structure of the protein. Parallel, yet non-superimposable, plots of $\log \bar{k}$ versus $\log 1/\bar{c}$ for these protein variants further clearly indicate that these ionotopes differ, however, in their affinity for the support surface. The variation in affinities for the stationary phase can be attributed to unique structural differences within each glycoprotein isoform which may be a result of variations in conformation and/or compositional heterogeneity of the carbohydrate moiety. As such, the chromatographic data derived from the interaction of an immobilised chemical ligand, *e.g.* a quaternary ammonium group, with a protein as evidenced in HPIEC (or other

TABLE II

$Z_{c,VG}$ VALUES FOR OVALBUMIN VARIANTS OBTAINED BY LINEAR REGRESSION OF VARIED GRADIENT TIME EXPERIMENTS

Coefficients of determination are given in parentheses.

Salt	Protein			
	Ov-a	Ov-b	Ov-c	Ov-d
LiF	Not done	Not done	Not done	Not done
LiCl	9.92 ± 2.90 (0.80)	15.34 ± 1.01 (0.99)	12.41 ± 1.08 (0.98)	12.26 ± 0.87 (0.99)
LiBr	7.30 ± 0.46 (0.98)	7.30 ± 0.46 (0.98)	6.91 ± 0.54 (0.97)	7.17 ± 0.57 (0.97)
NaF	6.56 ± 0.71 (0.95)	11.21 ± 1.78 (0.91)	7.72 ± 0.45 (0.98)	7.55 ± 0.41 (0.99)
NaCl	9.40 ± 0.50 (0.99)	11.71 ± 0.93 (0.98)	10.31 ± 1.05 (0.97)	9.74 ± 0.55 (0.99)
NaBr	7.83 ± 0.48 (0.99)	10.01 ± 0.23 (1.00)	8.23 ± 1.02 (0.96)	7.95 ± 0.52 (0.99)
KF	6.37 ± 0.57 (0.97)	7.69 ± 0.64 (0.97)	7.05 ± 0.48 (0.98)	6.70 ± 0.40 (0.99)
KCl	8.40 ± 0.76 (0.98)	9.48 ± 0.74 (0.98)	8.50 ± 0.71 (0.98)	8.69 ± 0.55 (0.99)
KBr	9.48 ± 0.69 (0.97)	11.94 ± 1.05 (0.96)	9.81 ± 1.06 (0.95)	9.94 ± 1.00 (0.95)
LiF	Not done	Not done	Not done	Not done
NaF	6.56 ± 0.71 (0.95)	11.21 ± 1.78 (0.91)	7.72 ± 0.45 (0.98)	7.55 ± 0.41 (0.99)
KF	6.37 ± 0.57 (0.97)	7.69 ± 0.64 (0.97)	7.05 ± 0.48 (0.98)	6.70 ± 0.40 (0.99)
LiCl	9.92 ± 2.90 (0.80)	15.34 ± 1.01 (0.99)	12.41 ± 1.08 (0.98)	12.26 ± 0.87 (0.99)
NaCl	9.40 ± 0.50 (0.99)	11.71 ± 0.93 (0.98)	10.31 ± 1.05 (0.97)	9.74 ± 0.55 (0.99)
KCl	8.40 ± 0.76 (0.98)	9.48 ± 0.74 (0.98)	8.50 ± 0.71 (0.98)	8.69 ± 0.55 (0.99)
LiBr	7.30 ± 0.46 (0.98)	7.30 ± 0.46 (0.98)	6.91 ± 0.54 (0.97)	7.17 ± 0.57 (0.97)
NaBr	7.82 ± 0.48 (0.99)	10.01 ± 0.23 (1.00)	8.23 ± 1.02 (0.96)	7.95 ± 0.52 (0.99)
KBr	9.48 ± 0.69 (0.97)	11.94 ± 1.05 (0.96)	9.81 ± 1.06 (0.95)	9.94 ± 1.00 (0.95)

adsorptive modes) have formal similarities to the competitive binding observed with biological affinate–ligand interactions in solution or as solid phase assays.

The electrophoretic data shown in Fig. 3 suggest that Ov-b has similar molecular size and charge distribution to Ov-a, Ov-c and Ov-d. However, the $Z_{c,VG}$ values (Table II) indicate that the HPIEC binding site for Ov-b differs significantly from those of the other isoforms under the studied elution conditions. This variant generally exhibited larger $Z_{c,VG}$ values than those observed for the other ovalbumin isoforms. The larger $Z_{c,VG}$ values suggest that an increased number of electrostatic interactions were involved in the sorption of Ov-b to the stationary phase surface. Again, variations in conformation or in the composition of the carbohydrate moiety of Ov-b, undetectable by IEF methods, are likely causes for the increase in $Z_{c,VG}$.

For the bovine carbonic anhydrase isoforms denoted CA-1, CA-2 and CA-3, electrophoretic data indicate that they are charged variants. Inspection of the data in Table I shows their $Z_{c,VG}$ values varied with the type of displacer salt. Furthermore, the $Z_{c,VG}$ values for both CA-2 and CA-3 were found to be similar in most salt systems. These results indicate that the interactive ionotopes on CA-2 and CA-3 were responding in a similar manner to changes in the type of displacer salt and that these two isoforms interact with the sorbent through areas of similar charge density and topography. However, the parallel, but non-superimposable, retention plots of log

\bar{k} versus $\log 1/\bar{c}$ shown for CA-2 and CA-3 in Fig. 4a–h, indicate that the ionotopes of these isoforms differ in their relative affinity for the stationary phase. The $Z_{c,VG}$ values for major isoform species CA-1 were found to be similar to those for CA-2 and CA-3 in four of the displacer salts investigated, *i.e.*, LiCl, LiBr, NaF and KBr. This observation reveals that the interactive ionotope for CA-1 has similar charge features to those present on CA-2 and CA-3. The $Z_{c,VG}$ values for CA-1, however, were typically smaller than those for CA-2 and CA-3 when NaCl, NaBr, KF, or KCl were used as displacer salts. The relative changes in $Z_{c,VG}$ between these charge variants appears to result from specific salt effects on the protein hierarchical structure influencing the electrostatic potential of the ionotopes.

The effect of salt type and varied flow (VF) gradient elution conditions on isoform $Z_{c,VF}$ values

The plots of $\log \bar{k}$ versus $\log 1/\bar{c}$, (Fig. 5a–h) show the effect of salt type and flow-rate on the gradient retention behaviour for the various isoforms of carbonic anhydrase and ovalbumin. Flow-rates were varied between 0.1 and 2.0 ml/min, while the gradient time, t_G , was held constant at 17.1 min. At lower flow-rates many of the retention plots for the related isoforms were found to converge as selectivity, α , between the different species approached unity. Hence, the purification of protein isoforms is best accomplished at high flow-rates *e.g.* > 1 ml/min if a small gradient time, t_G is used in conjunction with the other chromatographic conditions of this study.

Tables III and IV shows the $Z_{c,VF}$ values (± 1 S.D.) and the coefficients of determination (r^2) obtained from the regression analyses of the varied flow retention data shown in Fig. 5a–h for carbonic anhydrase and ovalbumin respectively. As is evident from Table III, the $Z_{c,VF}$ values for the carbonic anhydrase isoforms, CA-2 and CA-3 differed from the $Z_{c,VF}$ value for the major isoform CA-1. Furthermore, $Z_{c,VF}$ for CA-2 and CA-3 were similar only for the NaBr, KF or KBr salt systems. This result differs to that found under conditions of fixed flow-rate and varied gradient time where equivalent $Z_{c,VG}$ values for all three isoforms were obtained for the majority of displacer salts investigated. These data reveal that under conditions of varied flow, the ionotopes of CA-2 and CA-3 exhibit similar charge densities and topographic locations when eluted with either NaBr, KF or KBr. The remaining five salts in the series have therefore changed relative charge densities of the binding domains of these isoforms through specific ion-binding effects or have altered the displacement mechanism of these charged variants.

The trends in the relative magnitudes of the $Z_{c,VF}$ values (Table IV) for the ovalbumin variants were found to differ from the patterns observed with the $Z_{c,VG}$ values (Table II). For example, the isoforms Ov-a, Ov-c and Ov-d were observed under varied gradient time conditions (Table II) to have similar $Z_{c,VG}$ values when eluted with each type of displacer salt. Inspection of the data for varied flow-rate conditions (Table IV) shows that equivalent $Z_{c,VF}$ values were only obtained for the Ov-a, Ov-c and Ov-d proteins when eluted with LiCl, NaF, KCl or KBr. These results suggest that the isoforms Ov-a, Ov-c and Ov-d appear to interact through ionotopes of similar charge density with differing affinities for the sorbent. However, their $Z_{c,VF}$ values for Ov-a, Ov-c and Ov-d became significantly different in the presence of LiBr, NaCl, NaBr or KF, presumably as a result of specific salt effects which perturb the interactive ionotopes of these three protein variants. Alternatively, these three ovalbumin

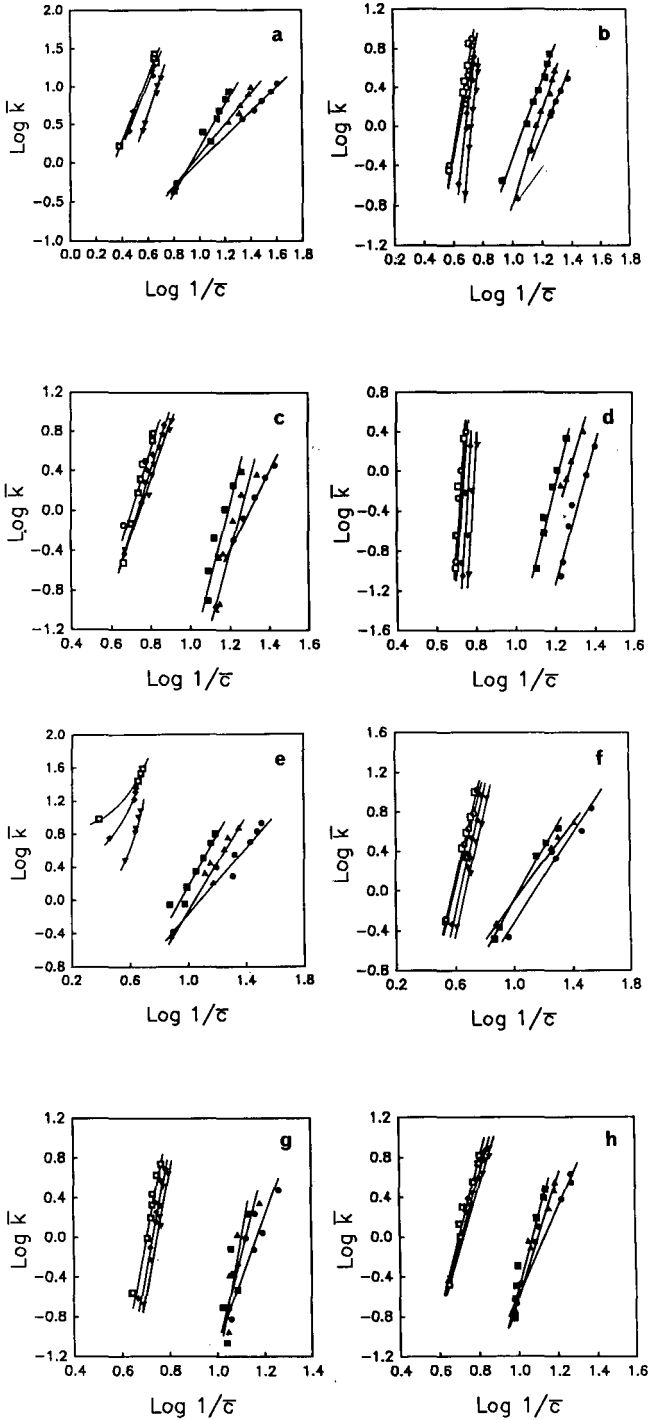


Fig. 5. Plots of $\log \bar{k}$ versus $\log 1/\bar{\epsilon}$ for bovine carbonic anhydrase isoforms 1, 2 and 3 and ovalbumin isoforms a, b, c and d. The plots were derived from gradient elution data at pH 9.6, gradient time of 17.1 min and flow-rate varying between 0.2 and 2.0 ml/min for (a) NaF, (b) NaCl, (c) NaBr, (d) LiCl, (e) KF, (f) KCl, (g) KBr and (h) LiBr. See legend to Fig. 4 for other details.

TABLE III

Z_c VALUES FOR CARBONIC ANHYDRASE VARIANTS OBTAINED BY LINEAR REGRESSION OF VARIED FLOW-RATE EXPERIMENTS

Coefficients of determination are given in parentheses.

Salt	Protein		
	CA-1	CA-2	CA-3
LiF	Not done	Not done	Not done
LiCl	6.76 ± 0.80 (0.95)	4.74 ± 0.49 (0.98)	8.10 ± 0.73 (0.97)
LiBr	4.16 ± 0.40 (0.96)	5.56 ± 0.57 (0.95)	6.77 ± 0.75 (0.94)
NaF	1.57 ± 0.07 (0.99)	2.12 ± 0.10 (0.99)	2.93 ± 0.29 (0.95)
NaCl	3.31 ± 0.16 (0.99)	4.76 ± 0.22 (0.99)	3.83 ± 0.18 (0.99)
NaBr	4.53 ± 0.53 (0.95)	6.87 ± 0.99 (0.91)	6.90 ± 0.97 (0.91)
KF	2.01 ± 0.22 (0.95)	2.81 ± 0.30 (0.95)	2.90 ± 0.35 (0.93)
KCl	2.17 ± 0.24 (0.97)	2.01 ± 0.07 (1.00)	2.60 ± 0.13 (0.99)
KBr	5.95 ± 1.19 (0.83)	7.82 ± 2.23 (0.71)	9.53 ± 3.22 (0.64)
LiF	Not done	Not done	Not done
NaF	1.57 ± 0.07 (0.07)	2.12 ± 0.10 (0.99)	2.93 ± 0.29 (0.95)
KF	2.01 ± 0.22 (0.95)	2.81 ± 0.30 (0.95)	2.90 ± 0.35 (0.99)
LiCl	6.76 ± 0.80 (0.95)	4.74 ± 0.49 (0.98)	8.10 ± 0.73 (0.97)
NaCl	2.94 ± 0.13 (0.99)	4.76 ± 0.22 (0.99)	3.83 ± 0.18 (0.99)
KCl	2.17 ± 0.24 (0.97)	2.01 ± 0.07 (1.00)	2.60 ± 0.13 (0.99)
LiBr	4.16 ± 0.40 (0.96)	5.56 ± 0.57 (0.95)	6.77 ± 0.75 (0.94)
NaBr	3.59 ± 0.18 (0.99)	6.87 ± 0.99 (0.91)	6.90 ± 0.97 (0.91)
KBr	5.95 ± 1.19 (0.83)	7.82 ± 2.23 (0.71)	9.53 ± 3.22 (0.64)

isoforms may interact through identical ionotopes but are eluted via different displacement mechanisms.

The relationship between Z_c values for Ov-a and Ov-b eluted under varied flow-rate experiments was also different to that found under conditions of varied gradient time. Similar $Z_{c,VF}$ values were obtained for both variants in the different salt systems. Furthermore, the use of LiBr, NaF, KF or KBr as displacer salts resulted in both isoforms eluting as a single peak under conditions of varied flow-rate. The ramifications of these observations are that if a matrix of displacing salts is used, then selectivity optimisation of the IEC of proteins can be rationally achieved under conditions of varied gradient time or flow-rate.

These results also indicate that subtly different modes of gradient elution can be employed to influence the electrostatic interactive surface of proteins, presumably as a consequence of the contact or residency requirements once the protein has been adsorbed. Previous studies^{12,13} have shown that both the type of salt and the column residence time can influence the Z_c value of proteins in HPIEC. This observation suggests that changes in the physicochemical basis of the sorption and desorption process can be induced by experimental factors which are commonly used to manipulate the elution time. Column residence time is one factor which differentiates the sorption conditions in varied gradient time and varied flow-rate experiments. As

TABLE IV

Z_c VALUES FOR OVALBUMIN VARIANTS OBTAINED BY LINEAR REGRESSION OF VARIED FLOW-RATE EXPERIMENTS

Coefficients of determination are given in parentheses.

Salt	Protein			
	<i>Ov-a</i>	<i>Ov-b</i>	<i>Ov-c</i>	<i>Ov-d</i>
LiF	Not done	Not done	Not done	Not done
LiCl	20.40 ± 3.57 (0.92)	24.73 ± 6.59 (0.88)	21.56 ± 6.75 (0.84)	24.28 ± 6.61 (0.87)
LiBr	7.45 ± 0.68 (0.96)	7.45 ± 0.68 (0.96)	5.95 ± 0.32 (0.99)	6.49 ± 0.42 (0.98)
NaF	4.09 ± 0.36 (0.99)	4.09 ± 0.36 (0.99)	4.81 ± 0.27 (0.99)	3.98 ± 0.41 (0.97)
NaCl	7.42 ± 0.79 (0.95)	8.09 ± 1.40 (0.89)	12.42 ± 0.56 (0.99)	10.97 ± 0.56 (0.99)
NaBr	8.05 ± 0.36 (0.99)	8.22 ± 0.47 (0.98)	5.48 ± 0.32 (0.98)	6.29 ± 0.34 (0.99)
KF	4.43 ± 0.21 (1.00)	4.43 ± 0.21 (1.00)	6.70 ± 0.69 (0.98)	9.09 ± 0.91 (0.99)
KCl	5.65 ± 0.63 (0.95)	5.97 ± 0.88 (0.92)	5.98 ± 0.44 (0.98)	6.04 ± 0.51 (0.97)
KBr	10.92 ± 0.88 (0.97)	10.92 ± 0.88 (0.97)	12.49 ± 1.17 (0.96)	11.56 ± 1.08 (0.96)
LiF	Not done	Not done	Not done	Not done
NaF	4.09 ± 0.36 (0.99)	4.09 ± 0.36 (0.99)	4.81 ± 0.27 (0.99)	3.98 ± 0.41 (0.97)
KF	4.43 ± 0.21 (1.00)	4.43 ± 0.21 (1.00)	6.70 ± 0.69 (0.98)	9.09 ± 0.91 (0.99)
LiCl	20.40 ± 3.57 (0.92)	24.73 ± 6.59 (0.88)	21.56 ± 6.75 (0.84)	24.28 ± 6.61 (0.87)
NaCl	7.42 ± 0.79 (0.95)	8.09 ± 1.40 (0.89)	12.42 ± 0.56 (0.99)	10.97 ± 0.56 (0.99)
KCl	5.65 ± 0.63 (0.95)	5.97 ± 0.88 (0.92)	5.98 ± 0.44 (0.98)	6.04 ± 0.51 (0.97)
LiBr	7.45 ± 0.45 (0.96)	7.45 ± 0.68 (0.96)	5.95 ± 0.32 (0.99)	6.49 ± 0.42 (0.98)
NaBr	8.05 ± 0.36 (0.99)	8.22 ± 0.47 (0.98)	5.48 ± 0.32 (0.98)	6.29 ± 0.34 (0.99)
KBr	10.92 ± 0.88 (0.97)	10.92 ± 0.88 (0.97)	12.49 ± 1.17 (0.96)	11.56 ± 1.08 (0.96)

the gradient time is increased protein solutes will progressively experience longer column residence times under chromatographic conditions of fixed flow-rate as well as being exposed, with long gradients, to very low rates of change in the displacer salt concentration. Under conditions of relatively long gradient time and very shallow gradients approaching isocratic conditions, there is sufficient time for the solute molecules to orientate themselves at the solute-stationary phase surface. This continuous "docking/re-docking" process will thus be very responsive to secondary equilibrium reactions that occur during or following sorption. Such dynamic interactive processes will have several consequences. Firstly, the equilibrium association constant may increase with time. Secondly, the Z_c value is anticipated to be influenced by the choice of t_G much more than by the choice of flow-rate condition. Thirdly, the increase in Z_c values or equilibrium binding constants observed as a protein unfolds with coulombic sorbents would also be consistent with these processes. Similar mechanisms may also contribute to the changes in the adsorption capacity observed with bath (batch) adsorption/desorption of proteins with preparative IEC and biomimetic affinity sorbents¹⁶. Under adsorption/desorption conditions where the three-dimensional shape of the protein, and more importantly the shape of the ionotope, is constant the magnitude of the Z_c values obtained for solutes eluted in this manner will reflect the maximum number of charged amino acid residue side

chains that contribute to the binding site on the molecule. Conversely, when the three-dimensional geometry of the protein's ionotope changes due to conformational transitions or salt-bridge perturbations then the magnitude of the Z_c values will vary depending on the salt type or column residence time. On this basis, related isoforms which are dynamically equivalent at the sorbent surface are unlikely to exhibit Z_c values which vary with a particular salt system. Similarly, when the protein isoforms are not dynamically equivalent, as may be revealed, for example, through differences in Z_c values obtained under constant and varied flow-rate conditions but with different salt systems, then the chromatographic ligand is effectively probing an ionotope of different molecular dimensions and/or charge density.

The effect of piperazine buffer concentration and varied gradient time on isoform Z_c values

Recent studies¹ have shown that changes in the eluent buffer concentration can also significantly influence solute retention in gradient HPIEC systems. Because of its buffer capacity over a wide pH range, piperazine has found numerous applications in IEC separation of proteins, particularly with eluents of basic pH value. In associated studies¹, piperazine concentrations of 40 mM or greater were found to significantly change the interactive properties of the CA-II_{5,9} isoform in anion HPIEC under gradient elution conditions. To further investigate which factors influence protein binding sites in HPIEC, the effect of piperazine concentration on the retention of structural variants of the other bovine carbonic anhydrase isoforms and ovalbumin was investigated. The $Z_{c, VG}$ values corresponding to different piperazine conditions were obtained from regression analysis of plots for $\log \bar{k}$ versus $\log 1/\bar{c}$ for these proteins eluted under gradient conditions. Solute species were eluted from a Mono-Q strong-anion-exchange column using a sodium chloride gradient increasing linearly between 0 and 300 mM. Piperazine concentrations of 0, 5, 10, 20, 30, 40 and 80 mM were selected for use in this study. At each buffer concentration, solute retention data were obtained for four different gradient times, *i.e.*, $t_G = 17.1, 34.3, 60$ and 100 min. The Z_c values obtained for each isoform are shown in Tables V and VI and are plotted against the piperazine concentration in Fig. 6a and b.

TABLE V

Z_c VALUES FOR CARBONIC ANHYDRASE VARIANTS OBTAINED BY LINEAR REGRESSION OF VARIED BUFFER EXPERIMENTS

Coefficients of determination are given in parentheses.

Piperazine (mM)	Protein		
	CA-1	CA-2	CA-3
80	1.00 ± 0.11 (0.98)	1.28 ± 0.07 (0.99)	1.54 ± 0.06 (1.00)
40	1.96 ± 0.51 (0.88)	2.49 ± 1.02 (0.75)	2.56 ± 0.61 (0.90)
30	4.20 ± 0.53 (0.97)	5.36 ± 0.07 (1.00)	3.77 ± 0.96 (0.89)
20	4.09 ± 0.28 (0.99)	4.56 ± 0.65 (0.96)	5.21 ± 0.30 (0.99)
10	4.09 ± 0.40 (0.98)	5.71 ± 0.34 (0.99)	5.58 ± 0.16 (1.00)
5	4.36 ± 0.81 (0.94)	6.66 ± 0.61 (0.99)	6.24 ± 0.66 (0.98)
0	4.04 ± 1.51 (0.78)	6.00 ± 2.07 (0.89)	6.47 ± 1.57 (0.94)

TABLE VI

Z_c VALUES FOR OVALBUMIN VARIANTS OBTAINED BY LINEAR REGRESSION OF VARIED BUFFER EXPERIMENTS

Coefficients of determination are given in parentheses.

Piperazine (mM)	Protein			
	Ov-a	Ov-b	Ov-c	Ov-d
80	6.63 ± 0.57 (0.99)	8.40 ± 0.19 (1.00)	6.77 ± 0.27 (1.00)	6.58 ± 0.21 (1.00)
40	6.31 ± 0.80 (0.97)	7.12 ± 0.99 (0.96)	6.14 ± 0.71 (0.97)	6.27 ± 0.76 (0.97)
30	9.42 ± 0.57 (0.99)	12.08 ± 0.64 (0.99)	9.71 ± 0.48 (1.00)	9.53 ± 0.19 (1.00)
20	9.00 ± 0.42 (1.00)	10.56 ± 0.50 (1.00)	9.04 ± 0.29 (1.00)	9.20 ± 0.53 (0.99)
10	9.29 ± 0.32 (1.00)	10.52 ± 0.29 (1.00)	9.42 ± 0.33 (1.00)	9.51 ± 0.29 (1.00)
5	9.73 ± 0.06 (1.00)	11.70 ± 0.77 (0.99)	9.76 ± 0.43 (1.00)	10.14 ± 0.27 (1.00)
0	12.20 ± 4.64 (0.87)	13.97 ± 2.66 (0.97)	40.33 ± 18.42 (0.83)	23.27 ± 4.38 (0.97)

Examination of the data shown in Table V and Fig. 6a reveals that the effects of the piperazine concentration on the Z_c values for CA-1 differed to those for CA-2 and CA-3. Between 0 and 30 mM piperazine, the Z_c values for CA-1 remained constant and independent of the buffer concentration. At piperazine concentrations > 30 mM the amount of positively charged piperazine buffer complexing onto the surface of the protein and sorbent was sufficient to induce a change in the protein-sorbent interactive properties, causing significant decreases in $Z_{c,VG}$. In contrast CA-2 and CA-3 had similar $Z_{c,VG}$ values at each buffer concentration which progressively decreased over

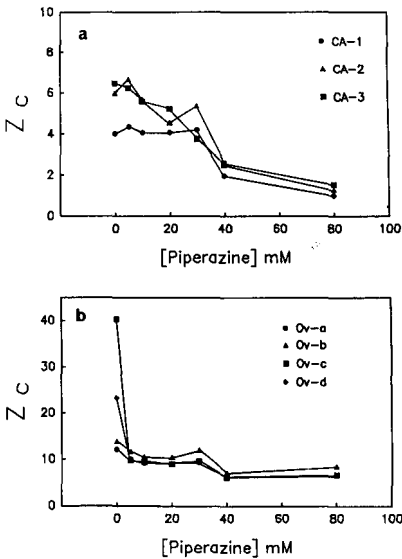


Fig. 6. Plots of Z_c versus the concentration of piperazine buffer under conditions of gradient elution with gradient times between 17.1 and 100 min and flow-rate of 1 ml/min for (a) carbonic anhydrase isoforms 1, 2 and 3 and (b) ovalbumin isoforms a, b, c and d.

the range 0 to 80 mM piperazine. Overall, these results indicate that the ionotopes of CA-2 and CA-3, although similar in charge density, were susceptible to changes in piperazine concentration. In the absence of buffer, the $Z_{c,vG}$ values for each of the carbonic anhydrase variants represent the maximum number of electrostatic interactions that can occur between each charge variant and the stationary phase in an aqueous environment at high pH.

Inspection of the data in Table VI and Fig. 6b reveals that the $Z_{c,vG}$ values for Ov-a, Ov-c and Ov-d did not vary significantly between concentrations of 10 to 80 mM piperazine. The complexation of both uni- and bivalent positively charged piperazine ions onto the surface of these proteins, above a critical buffer concentration of *ca.* 10 mM, appears to generate a coulombic binding surface on these isoforms of similar size. As the buffer concentration approaches zero, *i.e.*, below 10 mM, the $Z_{c,vG}$ values for the two isoforms Ov-c and Ov-d increase significantly. In the absence of buffer, more negatively charged sites on Ov-a, Ov-c and Ov-d become accessible for interaction with the stationary phase surface. The $Z_{c,vG}$ values obtained at 0 mM piperazine thus represent an estimate of the maximum number of electrostatic interactions that can occur between the solute and stationary phase in an aqueous environment at pH 9.6. The decrease in $Z_{c,vG}$ values observed with increasing buffer concentration over the range 0–10 mM is consistent with the stoichiometric displacement model^{14,15}. These dramatic changes in the magnitude of $Z_{c,vG}$ provide further support for the conclusion that over the range 0–10 mM piperazine Ov-a and Ov-b have similar, if not identical, ionotopic areas whilst in comparison, significantly different ionotopic areas are manifested by Ov-c and Ov-d at 0 mM piperazine. Such large differences seen in the Z_c values of protein isoforms as the buffer concentration is decreased may be a result of conformational changes. The protein isoform that is least conformationally stable under conditions of very low ionic strength will unfold to the greatest extent, and additionally accessible amino acid residues will contribute to further electrostatic interactions. This behaviour will be manifested as a large increase in Z_c at a particular buffer concentration. Such behaviour has already been proposed for subtilisin variants¹³, lysozymes^{11,14,18} and myoglobins¹⁸. If a similar phenomenon is occurring with the ovalbumin isoforms then on the basis of the changes in Z_c values observed for the above elution conditions, the relative conformational stability of the three isoforms in the absence of piperazine buffer follows the order Ov-a > Ov-d > Ov-c.

CONCLUSION

In this study the ability of HPIEC systems to probe subtle changes in the tertiary structure of several protein variants has been investigated. The use of structural variants of proteins permits the existence of different ionotopes on protein surfaces to be clearly delineated. These results further contribute towards an understanding of the factors which influence the electrostatic interactions occurring between the charged surfaces of the protein and the sorbent. This information can also be used to selectively manipulate the interactive properties of proteins for the purpose of improving resolution in chromatographic separations. For example, changes in the piperazine buffer concentration were found to influence the interactive behaviour of protein variants. Manipulation of the buffer concentration provides one additional avenue to regulate protein binding behaviour during the optimisation of chromatographic

separations where very high resolution is required *e.g.* with protein variants. These studies also clearly demonstrate that specific manipulation of displacing salt conditions in terms of salt type or rate of change of salt concentration can significantly enhance the selectivity of closely-related protein molecules.

The results presented here have important implications in studies on protein microheterogeneity and demonstrate the utility of HPIEC to complement other techniques such as IEF and chromatofocusing for the characterisation of microheterogeneous proteins derived from natural or recombinant DNA sources. Associated investigations underway in this laboratory will further characterise the influence of changes in the ionotopic structure of proteins and peptides as the biosolute approaches the stationary phase surface, through correlation of the chromatographic behaviour of several proteins with their three-dimensional structures determined by X-ray crystallographic and nuclear overhauser NMR spectroscopic procedures.

ACKNOWLEDGEMENTS

Research grants to M.T.W.H. from the National Health and Medical Research Council of Australia, the Australian Research Council and the Monash University Research Fund Committee are gratefully acknowledged. M.I.A. is a Monash University Postdoctoral Fellow and A.N.H. is a Monash University Postgraduate Scholar.

REFERENCES

- 1 A. N. Hodder, M. T. W. Hearn and M. I. Aguilar, *J. Chromatogr.*, 458 (1988) 27.
- 2 M. T. W. Hearn, A. N. Hodder and M. I. Aguilar, *J. Chromatogr.*, 458 (1988) 45.
- 3 F. E. Regnier, *Science (Washington, D.C.)*, 238 (1987) 319.
- 4 M. T. W. Hearn, A. N. Hodder and M. I. Aguilar, *J. Chromatogr.*, 443 (1988) 97.
- 5 J.-M. Gulian, N. Limozin, B. Mallet, J. DiCostanzo and M. Charrel, *Biochimie*, 59 (1977) 293.
- 6 Y. Kato, K. Komiya and T. Hoshimoto, *J. Chromatogr.*, 246 (1982) 13.
- 7 W. F. Blum and D. Gupta, in B. A. Keel and H. E. Grotjan, Jr. (Editors), *Microheterogeneity of Glycoprotein Hormones*, CRC Press, Boca Raton, FL, 1989, p. 127.
- 8 F. W. Putnam and N. Takahashi, *J. Chromatogr.*, 443 (1988) 267.
- 9 R. C. Johnston, P. G. Stanton, D. M. Robertson and M. T. W. Hearn, *J. Chromatogr.*, 397 (1987) 389.
- 10 J. Fausnaugh-Pollitt, G. Thevenon, L. Janis and F. E. Regnier, *J. Chromatogr.*, 443 (1988) 221.
- 11 A. N. Hodder, K. Machin, M. I. Aguilar and M. T. W. Hearn, *J. Chromatogr.*, submitted for publication.
- 12 A. N. Hodder, M. I. Aguilar and M. T. W. Hearn, *J. Chromatogr.*, 476 (1989) 391.
- 13 R. M. Chicz and F. E. Regnier, *J. Chromatogr.*, 443 (1988) 193.
- 14 R. R. Drager and F. E. Regnier, *J. Chromatogr.*, 359 (1986) 147.
- 15 W. Kopaciewicz, M. A. Rounds and F. E. Regnier, *J. Chromatogr.*, 266 (1983) 3.
- 16 F. B. Anspach, A. Johnston, H. J. Wirth, K. K. Unger and M. T. W. Hearn, *J. Chromatogr.*, 476 (1989) 205.
- 17 K. D. Lork, K. K. Unger, H. Bruckner and M. T. W. Hearn, *J. Chromatogr.*, 476 (1989) 135.
- 18 M. T. W. Hearn, A. N. Hodder and M. I. Aguilar, *J. Chromatogr.*, 507 (1990) 33.

Application of chromatographic retention data in an investigation of a quantitative structure–nucleotide incorporation rate relationship

K. VALKÓ*, T. CSERHÁTI, I. FELLEGVÁRI, J. SÁGI and A. SZEMZŐ

Central Research Institute for Chemistry, Hungarian Academy of Sciences, P.O. Box 17, H-1525 Budapest (Hungary)

SUMMARY

A series of 5-alkyl-, 5-alkenyl- and 5-alkynyl-substituted deoxyuridines and their triphosphate derivatives were synthesized and studied in DNA polymerase reactions. The initial rate of incorporation of the derivatives catalysed by Klenow fragment DNA polymerase enzyme (*E. coli*) was measured. Calf thymus DNA and synthetic poly (dA–dT) served as templates. The rate values were expressed as a percentage relative to the incorporation rate of natural substrate dTTP.

The high-performance liquid chromatographic (HPLC) retention behaviours of the nucleoside derivatives were investigated on silica and reversed-phase stationary phases using various mixtures of ethyl acetate–methanol and methanol–water, as respectively, mobile phases. According to the results of principal component analysis, the HPLC retention data describe the hydrophobic properties of the compounds. The inclusion complex stability constants of the derivatives with cyclodextrins determined by reversed-phase thin-layer chromatography served as a measure of the steric properties of the substituents. The electronic properties of the 5-substituents were characterized by the Swain–Lupton inductive and resonance parameters.

The results of the stepwise linear regression analysis of the nucleotide incorporation rate data and the above-mentioned physico-chemical data revealed the importance of the electronic, steric and hydrophobic properties of the substituents in the DNA polymerase reactions. The importance of the steric parameter was more significant when the poly (dA–dT) template was used instead of the random base sequence template (calf thymus DNA).

INTRODUCTION

Nucleotides as the building blocks of the DNA chain play an essential role in life-functions. The possible incorporation of nucleotide analogues into DNA can have crucial effects on its capacity to transmit genetic information. A great number of nucleoside derivatives have already been synthesized and tested as potential antiviral

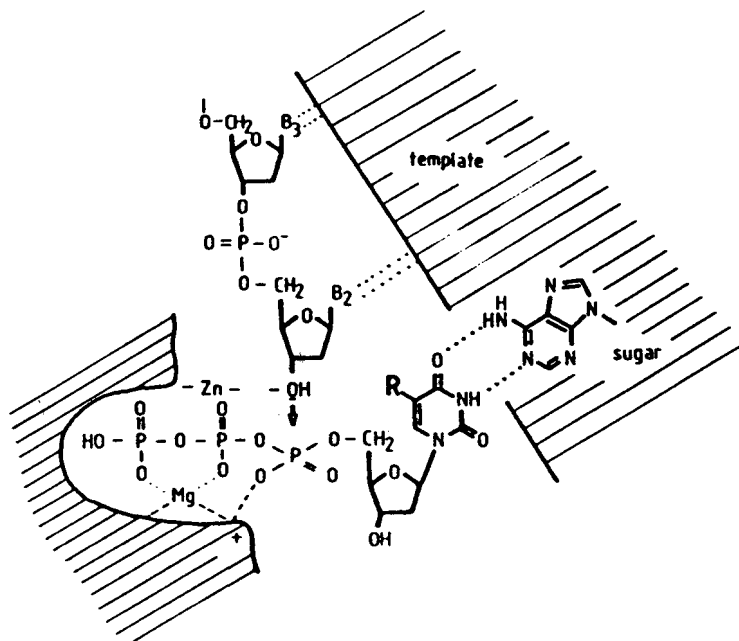


Fig. 1. Model of the nucleotide incorporation reaction.

and antitumour agents, as reviewed by De Clercq¹. Their activity can be related to their ability to incorporate into DNA or to influence the biosynthesis of DNA.

A series of 5-substituted 2'-deoxyridine-5'-triphosphates have synthesized and their initial incorporation rates into DNA have been measured. A non-linear relationship between the chain length of the 5-substituents and the incorporation rate was observed²⁻⁴. The effect of chain branching was more significant when the synthetic poly(dA-dT) template was used⁴.

To reveal the molecular parameters involved in DNA replication reactions catalysed by DNA polymerase enzyme (Fig. 1) the physico-chemical properties (hydrophobic, steric and electronic parameters according to Hansch⁵) of the corresponding nucleosides were characterized by their chromatographic retention data.

Reversed-phase high-performance liquid chromatographic (HPLC) retention data were used as a measure of hydrophobicity⁶; retention data on silica stationary phase have already been used as a measure of the adsorption properties⁷ of triazine derivatives. The importance of the steric parameters in the nucleotide incorporation reactions was established in a previous study⁸. The molar refractivities (*MR*) are not sensitive to the chain branching of the substituents, although they may influence significantly the incorporation rate. We assumed that cyclodextrin inclusion complex stability data can give information not only about the volume but also the shape of the substituents, and therefore the possible use of complex stability constants was also investigated in this study.

Principal component analysis and stepwise regression analysis were applied for selecting the most important physico-chemical properties of the derivatives that play an important role in DNA replication reactions.

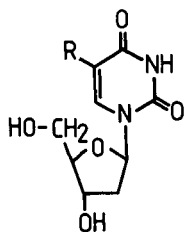


Fig. 2. Structures of the deoxyuridine derivatives investigated.

EXPERIMENTAL

The structures of the investigated compounds are shown in Fig. 2. The syntheses of the compounds have been described elsewhere^{2-4,9}. The compounds were chromatographically pure. Conditions for the measurement of the relative initial incorporation rates of the derivatives into calf thymus DNA (RATE%) and poly (dA-dT) (dAdT%) have already been published²⁻⁴. The structures of the derivatives investigated in this study, their incorporation rate data (RATE and dAdT%) and their physico-chemical parameters obtained from the Hansch-Leo compilation¹⁰ are listed in Table I. The hydrophobic substituent constant (π) defined by Hansch and

TABLE I

INVESTIGATED NUCLEOTIDE DERIVATIVES, THEIR INITIAL INCORPORATION RATES INTO CALF THYMUS DNA (RATE%) AND INTO POLY(dA-dT) (dAdT%) AND THEIR PHYSICO-CHEMICAL PARAMETERS OBTAINED FROM THE LITERATURE^{2-4,10}

No.	R	RATE%	dAdT%	π	MR	\mathcal{F}^a	\mathcal{R}^a
1	H	41	97	0.00	1.03	0.00	0.00
2	Ethyl	18	59	1.02	10.30	0.00	-0.10
3	Isopropyl	6	1	1.53	14.96	-0.05	-0.10
4	sec.-Butyl	8	21	2.07	19.61	-0.06	-0.12
5	tert.-Butyl	6	3	1.98	19.63	-0.07	-0.13
6	Pentyl	6	19	2.67	24.26	-0.06 ^b	-0.08 ^b
7	Hexyl	4	2	3.21	28.91	-0.06 ^b	-0.08 ^b
8	Vinyl	89	96	0.82	10.99	0.07	-0.08
9	(E)-Butynyl	68	80	1.90	20.29	0.03	-0.08
10	(E)-Pentynyl	37	50	2.44	24.94	0.03 ^b	-0.08 ^b
11	(E)-Hexynyl	26	43	2.99	29.59	0.03 ^b	-0.08 ^b
12	(E)-Heptynyl	19	2	3.53	34.24	0.03 ^b	-0.08 ^b
13	(E)-Octenyl	12	0.2	4.07	38.89	0.03 ^b	-0.08 ^b
14	Propynyl	99	69	0.94	14.20	0.15	-0.08
15	Butynyl	74	65	1.48	18.85	0.15 ^b	-0.08 ^b
16	Hexynyl	26	53	2.56	28.15	0.15 ^b	-0.08 ^b
17	Heptynyl	21	52	3.10	32.80	0.15 ^b	-0.08 ^b
18	Octynyl	13	8	3.64	37.45	0.15 ^b	-0.08 ^b

^a \mathcal{F} and \mathcal{R} are the Swain-Lupton type¹⁰ inductive and resonance effects, respectively.

^bEstimated data from values of propyl, propenyl, propynyl.

Leo¹⁰ and the molar refractivities of the 5-substituents with longer chain lengths were calculated on the basis of the additivity rule¹⁰.

The HPLC measurements were carried out with a Liquopump M312 pump, a variable-wavelength UV detector (Labor-MIM, Budapest, Hungary) and a Rheodyne (Cotati, CA, U.S.A.) injector (20- μ l loop). Retention time measurements were made with a Waters 740 Data Module (Millipore-Waters, Milford, MA, U.S.A.). Compounds were dissolved in methanol at a 0.1 mg/ml concentration.

Reversed-phase chromatographic conditions

An RP-8 (5- μ m) column (150 \times 4.6 mm I.D.) (Perkin-Elmer, Norwalk, CT, U.S.A.) was used with methanol-water mixtures as the mobile phase. The methanol concentration ranged from 40 to 60% (v/v) in 5% steps. A flow-rate of 1.00 ml/min was applied. Peaks were detected at 260 nm. The dead time was determined by injection of 1% sodium nitrate solution.

Normal-phase chromatographic conditions

LiChrosorb Si 60 (5 μ m) (Merck, Darmstadt, F.R.G.) material was packed into a 250 \times 4.6 mm I.D. stainless-steel column by Bioseparation Techniques (Budapest, Hungary). The mobile phase composition ranged from 10 to 25% (v/v) methanol in ethyl acetate in 5% steps. Detection was effected at 260 nm.

The logarithmic values of the capacity factors ($\log k'$) of the compounds mea-

TABLE II

INTERCEPT AND SLOPE VALUES OBTAINED BY HPLC SILICA (*SII*, *SIS*) AND REVERSED-PHASE (*RPI*, *RPS*) METHODS, THE CORRESPONDING CORRELATION COEFFICIENTS, *r*, THE INCLUSION COMPLEX STABILITY CONSTANTS DETERMINED BY RP-TLC (*K*) AND THE FIRST PRINCIPAL COMPONENTS OBTAINED FROM THE CHROMATOGRAPHIC RETENTION DATA (*PC1*) FOR THE INVESTIGATED NUCLEOSIDE DERIVATIVES.

<i>R</i>	<i>SII</i>	<i>SIS</i> $\times 10^{-2}$	<i>r</i>	<i>RPI</i>	<i>RPS</i> $\times 10^{-2}$	<i>r</i>	<i>K</i>	<i>PC1</i>
H	0.329	-2.37	0.99	0.424	-2.65	0.99	0	2.36
Ethyl	0.246	-3.35	0.99	0.590	-2.39	0.96	0	2.85
Isopropyl	0.015	-2.32	0.99	0.724	-2.39	0.98	0	1.70
<i>sec.</i> -Butyl	-0.416	-0.89	0.99	1.299	-2.82	0.98	0	-0.51
<i>tert.</i> -Butyl	-0.372	-1.12	0.99	1.301	-2.80	0.99	1.03 \pm 0.31	-0.27
Pentyl	-0.459	-0.88	0.99	2.041	-3.53	0.99	2.74 \pm 0.25	-0.52
Hexyl	-0.439	-1.20	0.99	3.001	-4.90	0.99	3.12 \pm 0.24	-2.24
Vinyl	-0.013	-2.52	0.99	0.613	-2.44	0.99	1.40 \pm 0.27	1.81
(<i>E</i>)-Butenyl	-0.394	-1.23	0.99	0.755	-1.56	0.99	1.87 \pm 0.28	0.64
(<i>E</i>)-Pentenyl	-0.405	-1.47	0.99	1.676	-2.87	0.99	0.67 \pm 0.11	-0.35
(<i>E</i>)-Hexenyl	-0.417	-1.46	0.99	2.224	-3.30	0.99	1.83 \pm 0.31	-0.87
(<i>E</i>)-Heptenyl	-0.414	-1.45	0.99	2.953	-4.09	0.99	3.40 \pm 0.26	-1.62
(<i>E</i>)-Octenyl	-0.349	-1.85	0.99	3.434	-4.45	0.99	4.60 \pm 0.24	-1.67
Propynyl	-0.042	-2.31	0.99	0.699	-2.69	0.98	0.27 \pm 0.07	1.61
Butynyl	0.063	-3.15	0.99	0.704	-2.15	0.99	0.66 \pm 0.18	2.43
Hexynyl	-0.453	-1.09	0.99	2.287	-4.02	0.99	0.70 \pm 0.14	-1.55
Heptynyl	-0.399	-1.54	0.99	2.297	-4.70	0.99	1.60 \pm 0.29	-1.84
Octynyl	-0.393	-1.57	0.99	3.268	-4.72	0.99	2.77 \pm 0.19	-1.98

sured in reversed-phase chromatographic systems were plotted against the methanol concentrations in the mobile phase. Similar plots were constructed for the $\log k'$ values obtained in the normal chromatographic mode against methanol concentration. For each compound a straight line could be fitted to at least four data points. The correlation coefficients were always higher than 0.97. The slope and the intercept values for the straight lines obtained in both the reversed-phase (*RPS*, *RPI*) and normal-phase modes (*SIS*, *SII*) were calculated and are given in Table II.

Inclusion complex stability measurements

Reversed-phase thin-layer chromatography (TLC) was used to study the inclusion complexes formed by the nucleoside derivatives with β -cyclodextrins. The determinations of the stability constants are based on the difference in lipophilicity between the complexed and free forms of the compounds¹¹.

Silufol UV254 plates (Kavalier, Sklárny, Czechoslovakia) were impregnated with paraffin oil as described elsewhere¹². The nucleoside derivatives were dissolved in methanol at a concentration of 3 mg/ml; 2 μ l of each solution were spotted on the plates separately. The mobile phase contained ethanol in the concentration range 0–15% (v/v) in steps of 5%, as it is miscible with water and forms only a weak inclusion complex with β -cyclodextrin^{13,14}. β -Cyclodextrin was obtained from Chinoïn (Budapest, Hungary) and was added to the eluent at the concentration of 15 mM. Cyclodextrin-free eluents served as controls. After chromatographic development, the plates were dried at 105°C and the nucleoside spots were detected under UV light. For each experiment four replicate determinations were carried out. The inclusion complex stability constants (*K*) were calculated as described elsewhere¹⁵ and are given in Table II.

Principal component analysis¹⁶ was applied in order to find similarities and dissimilarities between the biological, physico-chemical and chromatographic parameters, taking into consideration all compounds simultaneously. For a better understanding of the results of the principal component analysis, the non-linear map of the principal component loadings and variables was also calculated¹⁷. The calculation was run to 99.9% variance explained (*i.e.*, as many principal components were calculated as needed to explain more than 99.9% of the inherent variance of the original data matrix). Stepwise linear regression analyses of the data obtained were carried out on a IBM AT compatible personal computer using Labsware program package (Compudrug, Budapest, Hungary).

RESULTS AND DISCUSSION

The inclusion complex stability constants of the derivatives show an interesting dependence on the 5-substituents, *i.e.*, the longer the chain length, the higher is the complex stability. Double and triple bonds in the side-chain decrease the inclusion complex stability constants. As the inner side of the cyclodextrin ring is non-polar, it can be assumed that the side-chain of the derivatives (they are also non-polar) protrudes into the ring as shown schematically in Fig. 3.

Principal component analysis was carried out using the variables listed in Table I and Table II. The eighteen deoxyuridine derivatives were used as the observations. The non-linear map of the variables obtained is shown in Fig. 4. The variables describ-

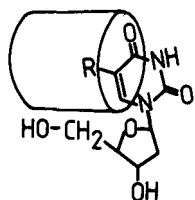


Fig. 3. Possible inclusion complex formation of the deoxynucleosides with β -cyclodextrin.

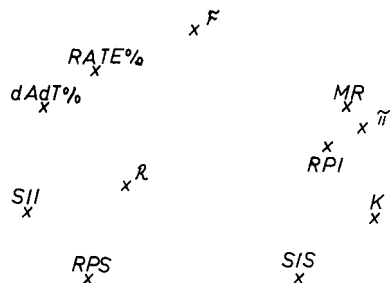


Fig. 4. Non-linear map of the principal component loadings of the incorporation rate, physico-chemical, chromatographic retention and inclusion complex stability parameters. Number of iterations, 74; maximum error, 0.031.

ing similar properties of the compounds are near to each other and the variables describing dissimilar properties are widely separated on the non-linear map of principal component loadings. As it can be seen in Fig. 4, the incorporation rate data are close to each other, and the molar refractivity (MR), π and RPI are close to each other as a measure of the hydrophobicity of the compounds⁸. The electronic parameters (\mathcal{F} , \mathcal{R}), silica retention parameters and reversed-phase slope (RPS) parameter form distinct variables. The inclusion complex stability constant (K) is relatively close to the hydrophobic parameters. The non-linear map of the compounds is shown in Fig. 5. The compounds having alkyl, alkenyl and alkynyl substituents are situated in one direction, and compounds with longer chain lengths are situated in a diagonal direction.

Another principal component analysis was carried out using only the four HPLC retention parameters (RPI , RPS , SII and SIS). Fig. 6 shows the non-linear map so obtained of the principal component loadings. When there is a double or triple bond in the 5-substituent, the nucleosides form a group with the compound having an alkyl substituent with one more CH_2 group, as can be observed in Fig. 6. The first principal component (PC1) of the chromatographic parameters describes the 74% variance of the four variables, and together with the second one more than 93%

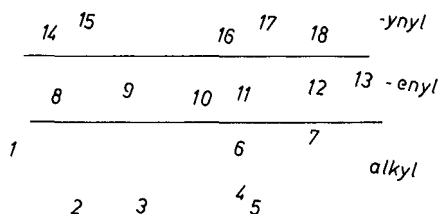


Fig. 5. Non-linear map of the principal components of the compounds of all the variables. The numbers represent the compounds listed in Table I. Number of iterations, 80; maximum error, 0.020.

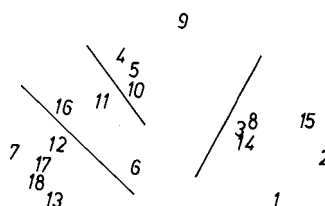


Fig. 6. Non-linear map of the principal components taking into consideration only the HPLC retention parameters (SII , SIS , RPI , RPS). The numbers represent the compounds listed in Table I. Number of iterations, 98; maximum error, 0.0057.

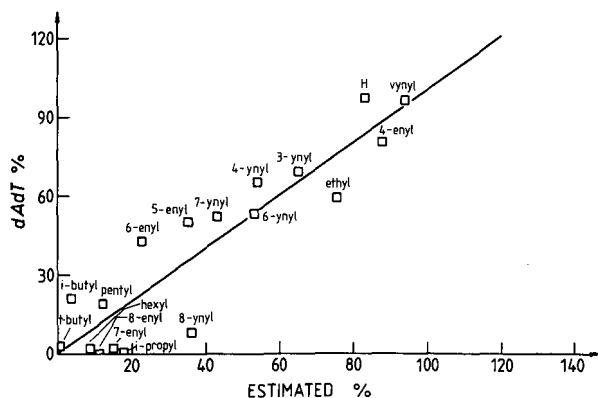


Fig. 7. Plot of the measured and estimated dAdT% values according to eqn. 1.

of the variance is explained. The PC1 variable was also used as a possible independent variable in the stepwise linear regression analysis.

In order to reveal the most important properties of the compounds which are involved in the nucleotide incorporation rate, stepwise regression analysis was carried out using the RATE% and dAdT% parameters as dependent variables. The possible independent variables were the π , MR , \mathcal{F} , \mathcal{R} , SII , SIS , RPI , RPS , K , $\log K$, PC1 variables. As was found previously⁸, the electronic (\mathcal{F}), steric (MR) and hydrophobic (RPS and RPI) parameters are all important.

The best correlation regarding dAdT% as the dependent variable is described by

$$\text{dAdT}\% = 154(\pm 41) \mathcal{F} - 28.8(\pm 3.6) \log K + 25.7 \quad (1)$$

$$n = 18; r = 0.92; s = 14.4; F = 39.2$$

where n = number of compounds, r = multiple correlation coefficient, s = standard error of the the estimate and F = the Fischer-test value. Eqn. 1 means that the higher

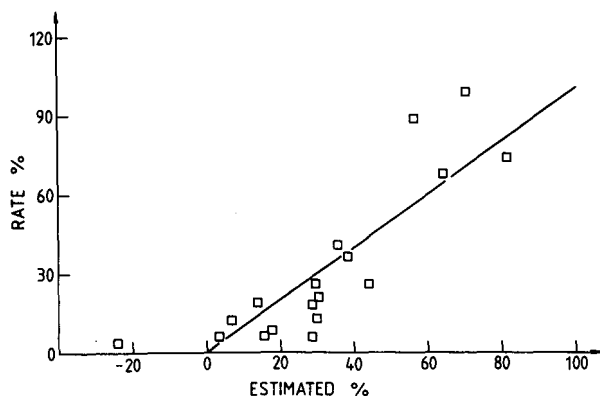


Fig. 8. Plot of the measured and estimated RATE% values according to eqn. 2.

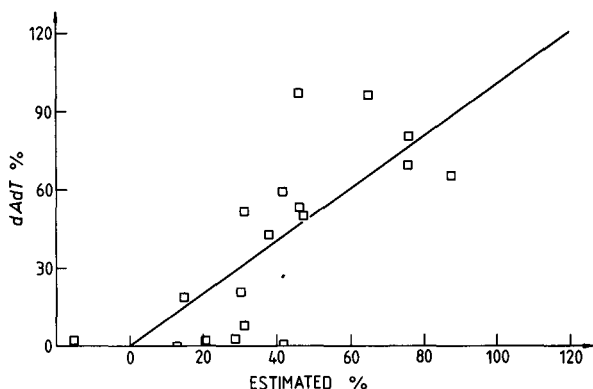


Fig. 9. Plot of the measured and estimated dAdT% values according to the equation $dAdT\% = 2189(\pm 589)RPS + 203(\pm 70)\mathcal{F} + 104$ ($r=0.75$; $s=24$; $F=9.3$).

is the inductive effect of the 5-substituent and the smaller is the stability of the inclusion complex with cyclodextrin, the higher is the percentage incorporation rate measured with poly(dA-dT) as template. A plot of the measured and estimated dAdT% values by eqn. 1 is shown in Fig. 7.

When the random sequence template (calf thymus DNA) (RATE%) is considered, the best correlation using only two independent variables is described by

$$RATE\% = 2006(\pm 417)RPS + 241(\pm 50)\mathcal{F} + 88.7 \quad (2)$$

$$n = 18; r = 0.85; s = 17.0; F = 19.5$$

A plot of the measured and estimated RATE% values according to eqn. 2 is shown in Fig. 8. The RPS variable reveals the sensitivity of the retention change caused by increasing methanol concentration and it can be regarded as a measure of the contact

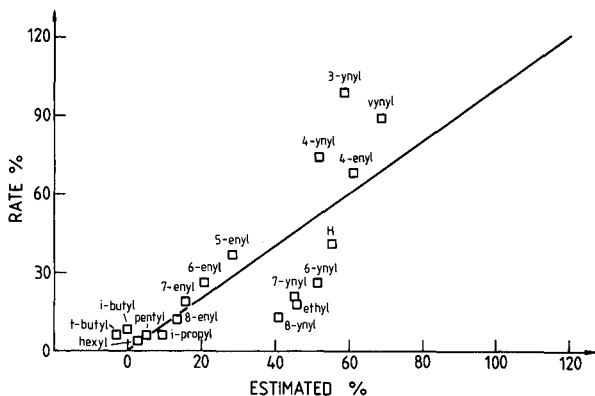


Fig. 10. Plot of the measured and estimated RATE% values according to the equation $RATE\% = 196(\pm 56)\mathcal{F} - 18(\pm 5)\log K + 19$ ($r=0.79$; $s=20$; $F=13$).

TABLE III
CORRELATION MATRIX OF VARIABLES LISTED IN TABLES I AND II

	RATE%	dAdT%	π	MR	\mathcal{F}	SII	SIS	RPI	RPS	Log K	PCI
RATE%	1.00	0.78	-0.56	-0.44	0.54	0.44	-0.46	-0.55	0.54	-0.58	0.56
dAdT%	0.78	1.00	-0.71	-0.63	0.38	0.55	-0.46	-0.63	0.55	-0.83	0.62
π	-0.56	-0.71	1.00	0.98	0.09	-0.82	0.58	0.95	-0.79	0.76	-0.91
MR	-0.44	-0.63	0.98	1.00	0.26	-0.81	0.53	0.93	-0.78	0.75	-0.89
\mathcal{F}	0.54	0.38	0.09	0.26	1.00	0.02	-0.20	0.17	-0.19	0.00	-0.08
SII	0.44	0.55	-0.82	-0.81	0.02	1.00	-0.89	0.55	-0.57	-0.66	0.89
SIS	-0.46	-0.46	0.58	0.53	-0.20	-0.89	1.00	0.53	-0.43	0.53	-0.79
RPI	-0.55	-0.63	0.95	0.93	0.17	0.55	0.53	1.00	-0.94	0.71	-0.93
RPS	0.54	0.55	-0.79	-0.78	-0.19	-0.57	-0.43	-0.94	1.00	-0.64	0.85
Log K	-0.58	-0.83	0.76	0.75	0.00	-0.66	0.53	0.71	-0.64	1.00	-0.73
PCI	0.56	0.62	-0.91	-0.89	-0.08	0.89	-0.79	-0.93	0.85	-0.73	1.00

hydrophobic surface area¹⁸ of the compounds. The slight difference between the two equations reveals the greater significance of the steric parameter when the template has a strictly alternating base sequence.

When the independent variables are exchanged in the two equations they are also significant in the correlations, but the mathematical statistical characteristics of the equations obtained are worse. The multiple correlation coefficient of eqn. 1 when RPS and \mathcal{F} are the independent variables is 0.75, and the standard error of the estimate is increased to 24. A plot of the measured and estimated dAdT% values is shown in Fig. 9.

Using $\log K$ and \mathcal{F} as independent variables in eqn. 2 resulted in a multiple correlation coefficient of 0.79 and a standard error of the estimate of 20. A plot of the measured and estimated RATE% values shown in Fig. 10 and indicates that five compounds (deoxyuridine and ethyl-, hexynyl-, heptynyl- and octynyldeoxyuridine) form another straight line. For these compounds the estimated RATE% values are higher than the measured values.

The correlation coefficients between each of the variables used in the linear regression analysis are summarized in Table III. It is noticeable that π , MR , RPI and PCI parameters show a high intercorrelation as all of them are proportional to the hydrophobicity of the molecules.

We conclude from our calculations that the physico-chemical properties of nucleoside derivatives measured by various chromatographic methods serve as a valuable aid in revealing the most important parameters which are involved in the nucleotide incorporation reactions in the Klenow DNA polymerase system. To obtain a high rate of incorporation of a nucleotide analogue into a DNA, the 5-substituent of the deoxynucleosides should have a high electron-withdrawing character and small hydrophobic surface area and should be sterically small.

REFERENCES

- 1 E. De Clercq, *Methods Findings Exp. Clin. Pharmacol.*, 2 (1980) 253.
- 2 J. T. Sági, A. Szabolcs, A. Szemző and L. Ötvös, *Nucleic Acid Res.*, 4 (1977) 2767.
- 3 L. Ötvös, J. Sági, T. Kovács and R. T. Walker, *Nucleic Acid Res.*, 15 (1987) 1763.
- 4 L. Ötvös, J. Szécsi, J. Sági and T. Kovács, *Nucleic Acids Res. Symp. Ser.*, 18 (1987) 125.
- 5 C. Hansch and T. Fujita, *J. Am. Chem. Soc.*, 86 (1964) 1616.
- 6 K. Valkó, *J. Liq. Chromatogr.*, 7 (1984) 1405.
- 7 K. Valkó, I. Fellegvári, A. Katti and L. Ötvös, *J. Liq. Chromatogr.*, 11 (1988) 833.
- 8 K. Valkó, I. Fellegvári, J. Sági, A. Szemző, *J. Liq. Chromatogr.*, 12 (1989) 2103.
- 9 A. Szabolcs, J. Sági and L. Ötvös, *J. Carbohydr. Nucleosides Nucleotides*, 2 (1975) 197.
- 10 C. Hansch and A. Leo, *Substituent Constants for Correlation Analysis in Chemistry and Biology*, Wiley, New York, 1989.
- 11 T. Cserháti, E. Fenyvesi and J. Szejtli, *Acta Biochem. Biophys. Acad. Sci. Hung.*, 18 (1983) 60.
- 12 T. Cserháti, B. Bordás, E. Fenyvesi and J. Szejtli, *J. Chromatogr.*, 259 (1983) 107.
- 13 A. Búvári, J. Szejtli and L. Barcza, *J. Inclus. Phenom.*, 1 (1983/84) 151.
- 14 A. Harada and S. Takahashi, *Chem. Lett.*, (1984) 2089.
- 15 T. Cserháti and M. Szögy, *J. Biochem. Biophys. Methods*, 14 (1987) 101.
- 16 K. V. Mardia, J. T. Kent and J. M. Bibby, *Multivariate Analysis*, Academic press, London, 1979.
- 17 W. Sammon, Jr., *IEEE Trans. Comput.*, C18 (1969) 401.
- 18 K. Valkó, *J. Liq. Chromatogr.*, 10 (1987) 1663.

CHROMSYMP. 1709

Secondary equilibria and their interaction with chromatographic transport

H. POPPE

Laboratory for Analytical Chemistry, University of Amsterdam, Nieuwe Achtergracht 166, 1018 WV Amsterdam (The Netherlands)

SUMMARY

The existence of “eigenpeaks” and the possibility of indirect detection in high-performance liquid chromatography and capillary zone electrophoresis can be understood with the same mathematical treatment. The coupled transport equations, when suitably linearized for small disturbances, can be treated as a linear eigenvalue problem. The solution predicts, in accordance with earlier results obtained by other workers, the existence of N eigenpeaks in a chromatographic or electrophoretic system, where N is the number of degrees of freedom in the description of the composition of the solution involved. Each eigenpeak corresponds to a capacity factor or mobility and is associated with an eigenvector that describes the relative intensities of the disturbances in all compounds that occur in the solution. An important experimental facility offered by these phenomena is indirect detection. A few general conclusions pertaining to this technique, invented before these phenomena were fully understood, are drawn.

INTRODUCTION

Usually in high-performance liquid chromatography (HPLC) and capillary zone electrophoresis (CZE), the distribution and transport of the various components in the column are considered separately; it is assumed that a solute can be transported without affecting the transport of another. This assumption is in sharp contrast with the basic facts about chromatographic and electrophoretic mechanisms. For instance, in adsorption chromatography (including reversed-phase chromatography), it is known that the adsorption of one component is associated with the desorption of another (displacement), the complete opposite of the above assumption! More incidental examples of mutual interactions are those brought about by so-called secondary equilibria, *e.g.*, acid–base reactions, ion-pair formation and van de Waals or covalent complexation.

Similarly, in free solution zone electrophoresis, the migration rate of an ion depends in general on the presence of other ions, because these determine the conductivity and with that the local electric field. In more particular cases, the effective

mobility of the ion considered depends on the various reactions (see above) that may alter its charge, size, etc. Therefore, here also causes for mutual interactions are abundant.

How could the theories based on such unrealistic assumptions be so successful in describing and predicting the multitude of phenomena, with respect to peak positions and peak widths, that occur in columns? The main reason is not that the sample constituents are eventually separated: first, one would still expect malfunctioning of the theory due to the interaction in the first part of the column; second, we know that independent behaviour is still a good description even if compounds coelute, *i.e.*, have been in each other's presence during their whole column history, the observed signal being simply the sum of that of the two components.

The success of the linear theory is rather due to the effective experimental techniques we use to make the behaviour of solutes adhere to idealized laws. Mostly, this can be described as buffering of conditions. Thus (a historically important example)¹, the activity of an adsorbent may be buffered by the addition of a moderator; when protolytic equilibria of the solutes occur, we intuitively choose a pH-buffered mobile phase; in CZE^{2,3}, the same is done, but the added salts also serve the purpose of buffering the electrical conductivity of the column.

Under such buffered conditions, the equations describing the transport of the solute species are linear in species concentration. This linearization can be described for chromatography as follows.

A general formulation of the transport equation is

$$\frac{\partial \tilde{c}_k}{\partial t} = \frac{\partial}{\partial z} \left(v R_k \tilde{c}_k + D_k \frac{\partial \tilde{c}_k}{\partial z} \right) \quad \text{all } 1 \leq k \leq N \quad (1)$$

where

z = the coordinate in the length direction;

t = time;

v = cross-section-averaged velocity of the mobile phase;

\tilde{c}_k = total concentration, averaged over the cross-section and both phases + possibly present support;

c_k = mobile phase concentration on the same volume basis;

D_k = a dispersion coefficient, describing, *e.g.*, lateral diffusion, non-equilibrium and flow irregularities (see below);

R_k = retardation factor, the fraction of solute in the mobile phase = c_k/\tilde{c}_k .

Some further comments should be made on eqn. 1. First, Riedo and Kováts⁴ demonstrated that one cannot generally consider v as a constant, and that in an N -component mixture in LC there are only $N - 1$ degrees of freedom, and only $N - 1$ equations of the type of eqn. 1 should be considered. We work ourselves around this complication by assuming that v is constant, either because the $N - 1$ other volume fractions are small, or because all partial molar volumes are constants. Also, one component is considered as an inert diluent and left out from the calculations. Second, the D_k values are not equal to the commonly used dispersion coefficients, as a result of using \tilde{c} rather than c . However, they may include diffusion in the stationary phase⁵.

Third, it is assumed that diffusion, convective mixing and resistance to mass transfer can be lumped into one parameter D_k . This is asymptotically true for linear cases⁶, and there is strong evidence⁷ that it is also a good approximation for non-linear cases.

In the general case, R_k (and D_k and possibly v) depend on all the concentrations of $j = 1$ up to N . The resulting set of coupled, non-linear equations presents a virtually unsurmountable mathematical problem; even with the D_k terms cancelled and only one or two components, considerable effort is needed to obtain an insight into the system⁸⁻¹⁰.

However, with a low c_k and other \tilde{c}_i s ($i \neq k$) buffered to almost constant values, R_k , v and D_k become virtually constant. The result is

$$\frac{\partial \tilde{c}_k}{\partial t} = v R_k \cdot \frac{\partial c_k}{\partial z} + D_k \cdot \frac{\partial^2 c_k}{\partial z^2} \quad (2)$$

an equation that can easily be solved. The well known result (see, *e.g.*, ref. 11) leads to the familiar Gaussian curve, when the input function is a sharp spike, of the shape

$$\tilde{c}_k = \frac{Q_k}{A \sqrt{2\pi\sigma_{z,k}}} \cdot \exp\left[-\frac{1}{2}\left(\frac{z - u_k t}{\sigma_{z,k}}\right)^2\right] \quad (3)$$

where

$$\begin{aligned} Q_k &= \text{amount injected;} \\ A &= \text{column cross-section;} \\ u_k &= \frac{R_k v}{}; \\ \sigma_{z,k} &= \sqrt{2D_k t}. \end{aligned}$$

while the response to a composite input can be obtained by convoluting eqn. 3 with that input¹².

In capillary electrophoresis, a similar situation exists. A general equation in that case is

$$\frac{\partial \tilde{c}_k}{\partial t} = -\frac{\partial J_k}{\partial z} = +\frac{\partial}{\partial z}\left(\frac{I}{\kappa} \cdot \mu_{\text{eff},k} c_k + D_k \cdot \frac{\partial^2 \tilde{c}_k}{\partial z^2}\right) \quad (4)$$

where

$$\begin{aligned} I &= \text{current density, which is a constant when the tube diameter is uniform;} \\ \kappa &= \text{conductivity of the solution, equal to Faraday's constant times the sum} \\ &\quad \sum_k \tilde{c}_k \mu_k z_k \text{ for all ionic species } k; \\ \mu_{\text{eff},k} &= \text{effective mobility of species } k, \text{ a signed quantity;} \\ z_k &= \text{charge of species } k. \end{aligned}$$

A few comments should be made on eqn. 4. First, space charges, which would invalidate the relationship for the local field, $E = I/\kappa$, are neglected. This is common in electrophoretic theories. Second, in that case, it is best to take N as one less than the number of independent ionic species, and the last concentration follows from the electroneutrality condition.

The values of $\mu_{\text{eff},k}$ may be variable, *e.g.*, owing to changes in ionic strength and reactions such as protolysis undergone by k . The value of κ is also variable in principle, because it is (to a good approximation) an additive function in all conductivities. As in chromatography, the usual experimental practice is to add such large concentrations of "indifferent" ions and reagents (such as H^+) that κ , $\mu_{\text{eff},k}$ and D_k are constants. Again, then, the equation is solved by a Gaussian function (or its convolution with any input function) and that is the usual peak shape we observe under such conditions.

It is interesting, and the main purpose of this paper, to investigate the disturbances in the mobile phase or carrier constituents (being at non-infinite dilution) brought about by the phase migration of solutes which are at high dilution. Thus, *e.g.*, in normal-phase adsorption chromatography with dichloromethane (DCM) as moderator in hexane as the mobile phase and ethyl acetate (EA) as the solute, with adsorption taking place at the front edge of the peak, EA adsorbs on the surface, inevitably displacing DCM. This means that the conditions at the very position of the peak are likely to be different from our set values. Similarly, when benzylamine (BA) is a solute in an electrophoretic experiment in an electrolyte buffered near to the $\text{p}K_a$ value of BA, its transport is bound to disturb the buffer solution; only the protonated species migrate through the solution, but on entering an "empty" part of the liquid, however, it has to be partly deprotonated in order to re-establish the protolytic equilibrium. Thereby the pH value will be disturbed, again at the very position where we want it to be constant.

LINEARIZATION

The fully linear model is insufficiently detailed to investigate these effects. On the other hand, considering the general transport equations, which in principle is preferable, leads, as indicated, to a kind of mathematical complexity that precludes finding a solution in all but the simplest of cases, and puts very high demands on the mathematical ability of the investigator. However, one can go part way along this path: the dependence of the migration rate parameters on the concentrations can be simplified in such a way that the resulting set of equations is still linear, while preserving the mutual influence of the constituents.

We first demonstrate this for liquid chromatography. First, the diffusion terms in the set of eqn. 1 are dropped; they play no essential role in the problem and can be re-inserted afterwards. The R_k factors (equal to the R_F value in thin-layer chromatography) depend on all concentrations. However, close to the mobile phase composition for all reasonably behaving systems one can describe R_k as a linear function of the concentrations \tilde{c}_j (j from 1 to N), as for all analytical experiments the deviation from the starting values will be small. Hence,

$$R_k = R_k^\circ + A'_{k,1}\Delta c_1 + A'_{k,2}\Delta c_2 + \dots + A'_{k,N}\Delta c_N \quad 1 \leq k \leq N \quad (5)$$

where

R_k° is the R value for k at exactly the mobile phase composition;
 $\Delta c_1 \dots \Delta c_N$ are the deviations in the concentrations from that composition;
 $A'_{k,1}$ are constants, to be found from an explicit expression $R_k = R_k(c_1 \dots c_N)$ as

$$A'_{ki} = \left(\frac{\partial R_k}{\partial \tilde{c}_i} \right)_{c_j \neq i}$$

As $R_k = c_k/\tilde{c}_k$, it follows that

$$A'_{ki} \ (i \neq k) = \frac{1}{\tilde{c}_k} \cdot \frac{\partial c_k}{\partial \tilde{c}_i}$$

$$A'_{kk} = \frac{1}{\tilde{c}_k} \cdot \frac{\partial c_k}{\partial \tilde{c}_k} - \frac{1}{\tilde{c}_k} \cdot R_k$$

Insertion into eqn. 5 leads to

$$\frac{\partial \tilde{c}_k}{\partial t} = -v \left(\sum_{i=1}^N A_{k,i} \cdot \frac{\partial \tilde{c}_i}{\partial z} \right) \quad 1 \leq k \leq N \quad (6)$$

where $A_{k,i} = \partial c_k / \partial \tilde{c}_i$.

Two comments should be made. First, the use of the total concentration \tilde{c} as the basic variables is unconventional, and leads to arithmic difficulties, *e.g.*, when applying a Langmuir isotherm. For chromatography it can be avoided by starting from the equation

$$\frac{\partial \tilde{c}_k}{\partial t} = -v \cdot \frac{\partial c_k}{\partial z}$$

and expanding \tilde{c}_k in terms of c_i rather than c_k (or R_k) in terms of \tilde{c}_i . However, the unconventional scheme was adopted here in order to demonstrate the analogy to electrophoresis. Second, eqn. 6 can be derived more directly by using

$$\frac{\partial \tilde{c}_k}{\partial t} = -v \cdot \frac{\partial c_k}{\partial z}$$

and expanding c_k in terms of \tilde{c}_i .

Returning to the set of eqns. 6, we note that it is linear. This leads to a drastic mathematical simplification. Most important are two facts: if a solution has been found, multiplication of this with a constant gives another solution; and any linear combination of solutions is also a solution.

The set of eqns. 6, as noted by numerous workers⁴, constitutes an eigenvalue problem. There are N solutions E_p ($p = 1 \dots N$) of the form

$$c_{k,p} = e_{k,p} F(z - \lambda_p t) \quad (7)$$

where

λ_p is one of the set of N eigenvalues of the matrix $\| A_{k,i} \|$;
 $e_{k,p}$ is the series of constants $k = 1 \dots N$ that is indicated as the eigenvector $|e_p|$;
 F is an arbitrary function; the dependence of F on $(z - \lambda_p t)$ indicates that a

translation along the z -axis with velocity λ_p occurs, while the shape of the disturbance is constant (*i.e.*, as long as the D s are zero).

Insertion of eqn. 7 in the set of differential eqns. 6 reveals that in matrix notation, $\| \cdot \|$ indicating a vector and $\| \cdot \|$ a matrix:

$$\lambda_p \|e_p\| = -v \|A\| \cdot \|e_p\|$$

the standard eigenvalue problem.

It should be noted that, as a result of the chosen formalism, the eigenvalues emerge as velocities and, when v is divided out, as R_F values. Other formalisms, which are fully equivalent but do not have the close resemblance to the treatment of CZE, would lead to eigenvalues in terms of capacity factors, inverse velocities, etc. All these different treatments would be equivalent.

The same approach can be used for electrophoresis: expand $\mu_{\text{eff},k}/\kappa$ in terms of the c_i s. It follows again that

$$\frac{\partial c_k}{\partial t} = -I \sum_{i=1}^{N-1} A_{k,i} \cdot \frac{\partial c_i}{\partial z} \quad (k = 1 \dots N-1) \quad (8)$$

where

$$A_{k,i} = \frac{\partial \left(\frac{\mu_{\text{eff},k}}{\kappa} \right)}{\partial c_i}$$

The same mathematical treatment as given above for HPLC would then lead to the appearance of eigenvalues that are, in fact, the mobilities of "concerted" disturbances.

In zone electrophoresis there is one important favourable condition: with reasonable accuracy the differential quotients $A_{k,i}$ can be predicted, because κ is equal to

$$\kappa = F \sum_{\text{all ions}} c_i \mu_i z_i$$

where F is the Faraday, while the effective mobilities $\mu_{\text{eff},k}$ can be readily calculated when species mobilities and pK_a values are known. Therefore, all values A_{ki} can be found from first principles and physical constants that are tabulated for common ions. This is in sharp contrast to the situation in chromatography, where such calculations are normally impossible. Here one has to resort to some more or less arbitrary model, or to the experimental determination of the distribution isotherms. This is already a lot of work for a single component. When composite isotherms are to be determined, the work becomes very complex. The amount of data needed merely to describe such a system grows with $z^N(N)$, where z is the number of grid points in one concentration axis (*e.g.*, studying one component with 20 grid points leads to 20 data pairs, studying four components with mutual interactions leads to $20^4 \cdot 4 = 640\,000$ data). It is therefore not surprising that simultaneous isotherm data are scarce, and limited to two interrelated components.

“Eigenpeaks”

The mathematics predict that N velocities occur, each with an associated eigenvector. This means that disturbances travel with fixed ratios of the intensities of the disturbances in the various concentrations. These disturbances can be indicated as “concerted”¹³ or as “eigenpeaks”, while the situation is also referred to as that of “coherence”¹⁰.

Why should these disturbances be so rigidly interrelated? Let us return to the normal-phase chromatography of EA with DCM as the moderator. In a diagram such as Fig. 1 we can represent the mobile phase composition, each point corresponding to a composition. Point M represents the mobile phase. Eigenvectors are represented by arrows, emanating from M . There are two of them, e_1 and e_2 . In this case (where $c_{EA} = 0$, for the eluent), the e_1 vector tells us that at the position of a positive deviation in EA (that is, in the commonly observed EA peak) there is a negative deviation in the DCM concentration, of a proportional intensity. Such a “concerted” disturbance travels with velocity λ_p . What if, by some peculiar history, the starting condition were to be different; let us assume that instead of a composition neatly in the direction of e_1 or e_2 one starts with a region of the column having composition “ Q ”.

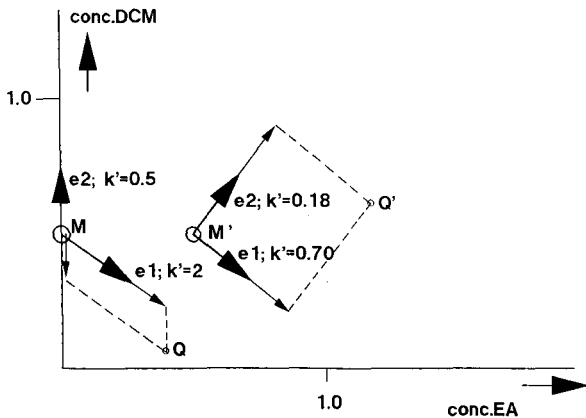


Fig. 1. Eigenvectors in a two-component system with dichloromethane (DCM) as the moderator and ethyl acetate (EA) as the solute (letters without primes) and with both components present in the mobile phase (primed letters). M, M' , mobile phase compositions; Q, Q' , compositions of injected solutions. The graph has been calculated assuming Langmuir adsorption with the expression $c_{i,s} = K_i c_{i,m} / (1 + K_{EA} c_{EA,m} + K_{DCM} c_{DCM,m})$ with $K_{EA} = 4$ and $K_{DCM} = 2$.

From Fig. 1, it is easy to see that the vector \overline{MQ} can be described as the sum of vectors e_1 and e_2 , each multiplied with a suitable constant. These would each start to travel with velocities λ_1 and λ_2 , respectively, leading to a “separation”. That means the vectors behave as if they were separate compounds in a classical chromatographic experiment.

This state of affairs becomes even more clear if we add some BA to the mobile phase, leading to mobile phase composition M' in Fig. 1, and study the profiles of BA and DCM after the application of some arbitrary injection, let us say of composition Q' . We obtain two peaks, with (in general) different velocities, but in each of the peaks

BA varies in addition to DCM. In this instance there is no “peak” identification”, and one cannot say that one peak “belongs” to BA or DCM. What occurs would be described as the separation of mathematical vectors or, physically, only if the disturbances in DCM and EA are in the right proportions to each other can they move together; if not, the disturbance as a whole will be split into two sets of disturbances that do fulfil this requirement.

Indirect detection

An experimentally important aspect of the concerted disturbances is the possibility of indirect detection. This method has been studied by numerous workers. After the series of papers by Crommen and co-workers¹³⁻¹⁵, the debate on the “mechanism” appears to have more or less terminated. In fact, it may be clear from their work and from this paper that there is no special physical mechanism involved; it is not necessary to assume special distribution phenomena such as two-site adsorption. Any transport mechanism with mutual interaction of constituents will lead to system peaks and the potential of indirect detection. This was well illustrated by the exploration of the method in capillary zone electrophoresis by two groups^{16,17}.

Indirect detection can be illustrated by the example given above. EA, if not detectable as such, can be detected via the disturbance in DCM, if that compound could be detected. The method is quantitatively reliable, because the nature of the phase system and the compounds and not, *e.g.*, the dispersion processes, govern the magnitude of the response.

The detailed calculation of Crommen and co-workers, *e.g.*, for the Langmuir isotherm case reveals that when $c_{EA} = 0$ the DCM response is proportional to $(k'_s/k'_{EA} - 1)^{-1}$, in which k'_{EA} and k'_s are the capacity factors for EA and the DCM system peak, respectively. This means first that the response changes sign when the k'_{EA} value passes that of the system peak, and second that when k_{EA} approaches k'_s , the response (*e.g.*, effective molar absorptivity) tends to infinity. The responses may look as in Fig. 2, and these were observed experimentally even before the explanation could be given. Of course, the exact equality of both k values would lead to peak overlap and

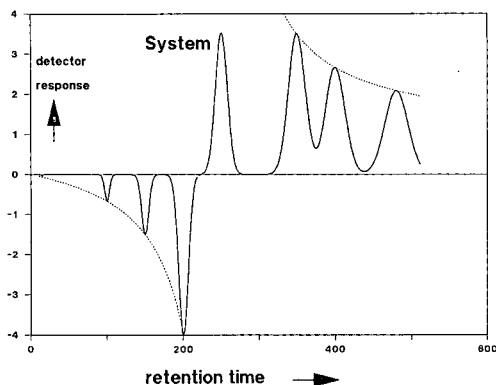


Fig. 2. Responses in indirect detection as a function of capacity factor of the solute, with analyte peaks and system peak, showing the increase in response when k'_A approaches k'_s and the sign reversal in the response when the analyte peak moves across the position of the system peak. The dashed line describes the hyperbolic curve, with a dependence like $k'_i/(k'_i - k'_s)$ on the capacity factor of the solute k_i .

the impossibility of quantification. An example may serve to illustrate the profound difficulty in the understanding of these phenomena. Experimentalists such as chromatographers are used to considering cause-effect relationships, *e.g.*, the fact that a displacement mechanism is at work, suggests at first (but false) sight that a positive EA peak would be accompanied by a positive DCM peak, because the addition of EA to a phase system with DCM would always release DCM from the stationary phase, no matter what the ratio of the k'_s values is. More detailed treatments show this view to be entirely wrong; the slot machine of mathematics delivers another result, that described above, in which the sign changes with change in capacity factor.

There seems to be no way to explain the behaviour of such systems, even in quantitative terms, without using complex mathematics. We simply have to accept as facts that only concerted disturbances can move as identities through the column and that the quantitative relationships, such as peak positions (and relative magnitudes of disturbances) can only be found as eigenvalues and eigenvectors, respectively. However, the perseverance of eigenpeaks in the column may become more familiar with the following reasoning. In every column slice, the change in the total concentration of each component is determined by the local gradient in the mobile concentration. When these changes for all components are exactly in proportion to the deviations already present, these new deviations will still have the same ratios. In this way the relative rate of change and hence the speed is the same for every component. The changes are determined by the prevailing concentrations and the transport matrix. That explains that only particular combinations of deviations can travel without being fragmented (in fact resolved in the chromatographic sense) into disturbances moving with different velocities.

Relationship with theories from preparative chromatography

It is important to stress that the close relationship between the phenomenon of system peaks, indirect detection, etc., and those observed in heavily overloaded columns, as studied by the pioneers of chromatography in the 1940s, reviewed by Helfferich and Klein¹⁰ and more recently by Rouchon *et al.*⁹, and in chemical engineering by Rhee and Amundson⁷. In these discussions the concept of "paths"¹⁰, Γ^7 or hodograph⁹ is developed. These are lines in the composition space formed by using the N concentrations as coordinate axes. A disturbance following such a path has the same character as the concerted set of minor disturbances described above: all concentration variations are rigidly interrelated. Also, the transport through the column of a disturbance following a path does not split and is described by relatively simple equations: a translation with constant velocity λ [a function $F(z - \lambda t)$] or a dilatation [a function $F(z/t)$].

The linear eigenvectors described above are the tangents to the N paths in composition space (Fig. 3).

EIGENPEAKS IN CZE

It has been demonstrated above that the same phenomena have to occur in electrophoretic experiments. Eqn. 9, for the simpler case of simple ions with no reaction such as protolysis, can be written as

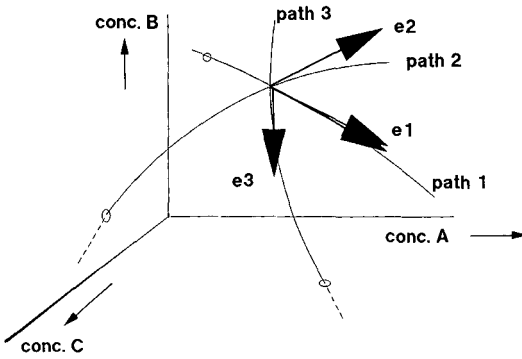


Fig. 3. The "paths" according to Helfferich and Klein¹⁰ in coherent boundaries and the eigenvectors for minor disturbances. The latter are the tangents to the former.

$$\frac{\partial c_k}{\partial t} = \mu_k I \cdot \frac{\partial}{\partial z} \left(\frac{c_i}{\kappa} \right) \quad \text{all } 1 < i < N \quad (10)$$

where $\kappa = \sum_i \mu_i c_i z_i F$

where F is Faraday's constant and the z values are the ionic charges. Thus:

$$\frac{\partial c_k}{\partial t} = \frac{I}{F} \cdot \frac{\partial}{\partial z} \left(\frac{c_k}{\sum_j \mu_j c_j z_j} \right)$$

The expression in parentheses can be expanded as a linear function of the c values. In so doing, as indicated, one should consider $N - 1$ ions, leaving the concentration of the N th ion to be determined afterwards from the electroneutrality condition. Rather than going through this exercise in general equations, we shall do it for a particular example, which demonstrates the essential features. Suppose a Li^+ ion is electrophoresed at low concentration in a carrier of KBr . Take Br^- as the indifferent ion, and set I/F to unity, as this is just a constant. We then have (with a negative μ_{Br} value)

$$\kappa = c_{\text{Li}}(\mu_{\text{Li}} - \mu_{\text{Br}}) + c_{\text{K}}(\mu_{\text{K}} - \mu_{\text{Br}})$$

$$\frac{\partial c_{\text{Li}}}{\partial t} = \frac{\partial}{\partial z} \left[\frac{\mu_{\text{Li}} c_{\text{Li}}}{c_{\text{Li}}(\mu_{\text{Li}} - \mu_{\text{Br}}) + c_{\text{K}}(\mu_{\text{K}} - \mu_{\text{Br}})} \right]$$

$$\frac{\partial c_{\text{K}}}{\partial t} = \frac{\partial}{\partial z} \left[\frac{\mu_{\text{K}} c_{\text{K}}}{c_{\text{K}}(\mu_{\text{K}} - \mu_{\text{Br}}) + c_{\text{Li}}(\mu_{\text{Li}} - \mu_{\text{Br}})} \right]$$

Expansion in Δc values of the factors in parentheses gives

$$\frac{\partial \Delta c_{\text{Li}}}{\partial t} = A_{\text{Li,Li}} \cdot \frac{\partial \Delta c_{\text{Li}}}{\partial z} + A_{\text{Li,K}} \cdot \frac{\partial \Delta c_{\text{K}}}{\partial z}$$

$$\frac{\partial \Delta c_{\text{K}}}{\partial t} = A_{\text{K,Li}} \cdot \frac{\partial \Delta c_{\text{Li}}}{\partial z} + A_{\text{K,K}} \cdot \frac{\partial \Delta c_{\text{K}}}{\partial z}$$

with

$$A_{\text{Li,Li}} = \frac{\mu_{\text{Li}}}{\kappa} - \frac{\mu_{\text{Li}} c_{\text{Li}} (\mu_{\text{Li}} - \mu_{\text{Br}})}{\kappa^2} = \frac{\mu_{\text{Li}}^a}{\kappa}$$

$$A_{\text{Li,K}} = - \frac{\mu_{\text{Li}} c_{\text{Li}} (\mu_{\text{K}} - \mu_{\text{Br}})}{\kappa^2} = 0^a$$

$$A_{\text{K,Li}} = - \frac{\mu_{\text{K}} c_{\text{K}} (\mu_{\text{Li}} - \mu_{\text{Br}})}{\kappa^2} = \frac{\mu_{\text{K}} c_{\text{K}} (\mu_{\text{Li}} - \mu_{\text{Br}})}{\kappa^2}$$

$$A_{\text{K,K}} = \frac{\mu_{\text{K}}}{\kappa} - \frac{\mu_{\text{K}} c_{\text{K}} (\mu_{\text{K}} - \mu_{\text{Br}})}{\kappa^2} = 0^a$$

The eigenvector problem is therefore

$$\begin{pmatrix} \frac{\mu_{\text{Li}}}{\kappa} & 0 \\ - \frac{\mu_{\text{K}} c_{\text{K}} (\mu_{\text{Li}} - \mu_{\text{Br}})}{\kappa^2} & 0 \end{pmatrix} \begin{pmatrix} e_{\text{Li}} \\ e_{\text{K}} \end{pmatrix} = \begin{pmatrix} \lambda e_{\text{Li}} \\ \lambda e_{\text{K}} \end{pmatrix}$$

In this case, it is easy to find the two solutions:

$$\begin{aligned} \lambda_1 = \mu_{\text{Li}}/\kappa, \quad e_{\text{K}}:e_{\text{Li}} &= - \frac{\mu_{\text{K}} c_{\text{K}} (\mu_{\text{Li}} - \mu_{\text{Br}})}{\kappa \mu_{\text{Li}}} \\ &= - \frac{\mu_{\text{K}} c_{\text{K}} (\mu_{\text{Li}} - \mu_{\text{Br}})}{c_{\text{K}} (\mu_{\text{K}} - \mu_{\text{Br}}) \mu_{\text{Li}}} \\ &= - \frac{\mu_{\text{K}} \cdot (\mu_{\text{Li}} - \mu_{\text{Br}})}{\mu_{\text{Li}} (\mu_{\text{K}} - \mu_{\text{Br}})} \\ \lambda_2 = 0, \quad e_{\text{Li}}:e_{\text{K}} &= 0 \end{aligned}$$

The first solution corresponds to the normal electrophoresis of Li^+ (the factor $1/\kappa$ in λ_1 occurs because I/κ was set to 1). The K disturbance accompanying Li^+ is related to this by the factor $\mu_{\text{K}}(\mu_{\text{Li}} - \mu_{\text{Br}})/[\mu_{\text{Li}}(\mu_{\text{K}} - \mu_{\text{Br}})]$. The disturbance in Br^- can be calculated from the electroneutrality, $e_{\text{Br}} = e_{\text{Li}} + e_{\text{K}}$:

^a Equal to these terms as $c_{\text{Li}} \approx 0$ and $\kappa \approx c_{\text{K}}(\mu_{\text{K}} - \mu_{\text{Br}})$.

$$e_{\text{Br}}:e_{\text{Li}} = 1 - \frac{\mu_{\text{K}}(\mu_{\text{Li}} - \mu_{\text{Br}})}{\mu_{\text{Li}}(\mu_{\text{K}} - \mu_{\text{Br}})} = - \frac{\mu_{\text{Br}}(\mu_{\text{Li}} - \mu_{\text{K}})}{\mu_{\text{Li}}(\mu_{\text{K}} - \mu_{\text{Br}})}$$

We note in passing that the expressions for e_{Br} and e_{K} can be obtained from each other by interchanging the indices K and Br, which indicates that the same solution would be found if K had been chosen as the N th ion.

The above shows that (a) The indirect detection of K cannot be described as a direct consequence of electroneutrality. This would give $e_{\text{K}} = -e_{\text{Li}}$, with $e_{\text{Br}} = 0$. Thus, as in Langmuir chromatography, the direct application of intuitive notions leads to an erroneous result. (b) K^+ as well as Br^- , *i.e.*, ions of both charges, could be used as a marker ion. (c) Only when $\mu_{\text{Li}} = \mu_{\text{K}}$, a situation realized, *e.g.*, when using isotopically marked K^+ as the solute, is the intuitive result $e_{\text{K}} = -e_{\text{Li}}$, $e_{\text{Br}} = 0$ correct. This is what is to be expected physically; in that case, the Cl^- ions are “decoupled” from the transport, as they would not “see” the substitution of K^+ by Li^+ .

The second solution has velocity zero, a stagnant disturbance, with identical variation in c_{K} and c_{Br} , while Li is not involved. This means that a disturbance in the carrier electrolyte concentration does not move (relative to the liquid; of course, the osmotic flow will make it move). This is a well known fact in electrophoresis; it can be derived directly from the requirement that Kohlrausch’s regulating function (KRF) is constant in time:

$$KRF = \sum \frac{c_i z_i}{\mu_i}$$

where z_i is the charge of the ion i . As $\Delta c_{\text{Li}} = 0$, it follows, from electroneutrality, that

$$\Delta KRF = \frac{\Delta c_{\text{K}}}{\mu_{\text{K}}} + \frac{\Delta c_{\text{Br}}}{\mu_{\text{Br}}} = \Delta c_{\text{K}} \left(\frac{1}{\mu_{\text{K}}} - \frac{1}{\mu_{\text{Br}}} \right)$$

which indicates that Δc_{K} does not change with time, *i.e.*, the disturbance does not move.

It should be noted that the K^+ and Br^- disturbances travelling with Li^+ can also be derived directly from KRF ; two equations are needed to relate e_{K} and e_{Br} to e_{Li} : one is the constancy of KRF , the other the electroneutrality. However, for more complicated systems one needs the eigenvector treatment.

Effect of a given injection composition

The “composition” of peaks, *i.e.*, the relative intensities in the various component disturbances, are now described in the $|e_{\text{p}}|$ vectors. However, another problem is to describe the intensities of the various peaks that result from a given injection. In Fig. 1 it was already indicated how the vector V_{inj} of the injection disturbance has to be decomposed into the vectors, e_{p} , corresponding to the various “eigenvelocities”. However, the graphical tool will not be of much help when three or more components are relevant (see Fig. 4); in that case, one needs a numerical treatment.

The decomposition of $|c_{\text{inj}}|$ into the $|e_{\text{p}}|$ is a straightforward example of linear

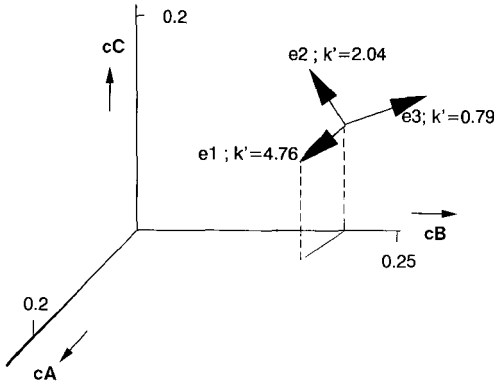


Fig. 4. Eigenvectors in a three-component system, containing A, B and C in the mobile phase. Vectors e_2 and e_3 are in the back-plane ($c_A = 0$); e_1 protrudes out of this plane and corresponds to the elution of compound A that does not occur in the mobile phase. The graph has been calculated assuming Langmuir adsorption with an expression $c_{i,s} = K_i c_{i,m} / (1 + K_A c_{A,m} + K_B c_{B,m} + K_C c_C)$ with $K_A = 10$, $K_B = 3.0$ and $K_C = 5.0$.

algebra. The $e_{p,i}$ matrix (all eigenvectors assembled to form a square matrix), indicated by $\|E\|$, is bound to have an inverse, because the e_p s are independent. The result $\|R\| = \|E\|^{-1}$ is also equal to the set of left-eigenvectors of the transport matrix $\|A\|$ (left and right eigenvectors have the same set of eigenvalues). Once $\|R\|$ is known, the intensities of the various peaks, denoted by P_p , are given by $|P| = \|R\| \cdot |c_{inj}|$. The electrophoretic example with Li^+ in KBr may illustrate this:

$$\|E\| = \begin{vmatrix} 1 & 0 \\ -\alpha & 1 \end{vmatrix}$$

where $\alpha = + \mu_K(\mu_{Li} - \mu_{Br}) / \mu_{Li}(\mu_K - \mu_{Br})$. It follows that

$$\|R\| = \begin{vmatrix} 1 & 0 \\ \alpha & 1 \end{vmatrix}$$

Case 1. Injection solution deviates from carrier by $0.0001 M Li^+$ and $0.0001 M K^+$ (i.e., the Cl^- concentration is the same).

$$P_1 = 1 \cdot 0.0001 M + 0 \cdot 0.0001 M = 0.0001 M$$

$$P_2 = \alpha \cdot 0.0001 M + 1 \cdot 0.0001 M$$

The first peak has intensity $0.0001 M$ in Li and $-\alpha$ times this value in K^+ . The second peak (stagnant) has intensity $0.0001 M(1 + \alpha)$ in K^+ . Note that the K^+ sum over both peaks (and that of Li^+) equals the injected concentration.

Case 2. Injection of Li , $0.0001 M$, "on top of" the base composition KBr , i.e., $V_{inj,Br}$ is also $0.0001 M$. This yields

$$P_1 = 1 \cdot 0.0001 M + 0 \cdot 0 = 0.0001$$

$$P_2 = \alpha \cdot 0.0001 M + 1 \cdot 0 = \alpha \cdot 0.0001$$

The first peak again has intensity $0.0001 M$ in Li^+ , of course, and $-\alpha \cdot 0.0001 M$ in K^+ . The second, stagnant, peak has $\alpha \cdot 0.0001 M$ in K^+ . The sum of the K^+ responses is zero, as it should be.

Case 3. Only by exactly “tuning” the injection of K^+ to *e.g.*, $0.0001 M$ Li and $-\alpha \cdot 0.0001 M$ K^+ can one avoid the “excitation” of the second peak:

$$P_2 = \alpha \cdot 0.0001 M + 1(-\alpha \cdot 0.0001 M) = 0.$$

Similar calculations are possible for liquid chromatography although, instead of using first principles to describe the non-linearities, one has to either use experimental composite isotherms (which are scarce), or rely on a model for the distribution behaviour such as the Langmuir composite isotherms. When suitably programmed, the arithmetic does not cause any problems.

DYNAMIC RANGE OF INDIRECT DETECTION

In both separation techniques the buffering of conditions is not perfect; it can be exhausted when high concentrations of solutes are present. When increasing these concentrations or (which amounts to the same) increasing the mass load while not changing the injection volume, inevitably at some point the non-linear behaviour will be visible again. Usually peaks then start to develop a triangular shape. This is the result of the fact that high concentrations travel [*i.e.*, the velocity “of a concentration” is $(dz/dt)_{c_i}$] at a different velocity than do low concentrations. Such effects have been described in HPLC^{18,19} as “mass overload”, “concentration overload” or “thermodynamic broadening”, which are good descriptors. Unfortunately, in CZE the term “electromigration dispersion” has found acceptance. In fact, there is no dispersion at work or anything that can be described formally as such. This is clear from the fact that the same effects can lead to zone narrowing, *e.g.*, occurring in isotachopheresis. It is proposed here to retain a more neutral term, such as “concentration overload”, in order to indicate this type of extra zone broadening.

Differences in the velocities of high and low concentrations will become visible in the electropherogram or chromatogram as soon as they are larger than the “natural” uncertainty in the velocity connected with peak dispersion. When the latter is expressed as standard deviation and taking relative to the peak position, it equals $1/\sqrt{N}$. It follows that relative variations in migration rates should exceed this value; this is more critical for CZE with 100 000–300 000 plates than for HPLC where plate counts often do not exceed 10 000. How strongly the migration rate varies with the concentration of i depends very much, of course, on the particular type of solute and system. However, when indirect detection is used, for detecting a solute i with a marker M , the marker concentration c_M is necessarily coupled to c_i , otherwise no response would be obtained. If the marker M is involved in the migration of i , it can be assumed that the migration of i is also influenced by the concentration c_M . Indeed, carrying out various numerical experiments, *e.g.*, with Langmuirian adsorption in HPLC, or for

CZE systems, shows that the marker concentration always, under conditions where indirect detection works, has a strong influence on the migration rate of i , 1% in c_M leading to variations of the order of 1%.

As the migration rate has to be kept constant within a factor of $1 \pm 1/\sqrt{N}$, as a general rule of thumb it can be stated that the marker concentration is to be held constant within the same factor. Thus, only a fraction of $1/\sqrt{N}$ of the detection range offered by the detected marker at its given concentration can be exploited; when a 1:1 response is obtained, the solute concentration has to be kept below c_M/\sqrt{N} , in order to avoid peak deformations. As, on the other hand, c_M cannot be chosen to be indefinitely high (e.g., a UV detector would not work at absorbances of 3 or higher), the indirect detection principle can in general be expected to have a negative effect on the loadability and dynamic range of the system. The problem may turn out to be more severe in CZE than in HPLC, as the plate numbers are larger and the detectors work under less favourable conditions.

This reasoning, crude as it is, obviously is strongly connected with the necessity, most explicitly formulated by Kuhr and Yeung¹⁶, to use instrumentation with a "high dynamic reserve", i.e., a capability of detecting small relative changes in the concentration of the marker.

CONCLUSION

It has been shown that system peaks and indirect detection can be treated mathematically from one viewpoint. The quantitative relationships follow readily from straightforward mathematics and can be obtained, once the distribution or transport behaviour is known, by programs that are straightforward but may sometimes be fairly complicated.

Unfortunately, it remains difficult to develop an intuitive direct understanding of the phenomena. It has been shown here that it is even risky to rely on such intuitive notions, as they tend to lead to wrong conclusions.

The common basis of indirect detection in HPLC and CZE has been elucidated. These possibilities do not depend on particular physical conditions, such as displacement in the distribution process or the concept of electroneutrality, but are always present when for some reason or another (displacement, mutual reactions, coupled protolysis) compounds influence each other in their transport behaviour.

ACKNOWLEDGEMENTS

This work was supported partly by Applied Biosystems, San Jose Operations, San Jose, CA, U.S.A. Programs for CZE calculations are obtainable from this source and those for HPLC calculations from the author.

REFERENCES

- 1 L. R. Snyder, *J. Chromatogr.*, 5 (1961) 468.
- 2 F. E. P. Mikkers, F. M. Everaerts and Th. P. E. M. Verheggen, *J. Chromatogr.*, 169 (1979) 11.
- 3 J. W. Jorgenson and K. D. Lucacs, *J. Chromatogr.*, 218 (1981) 209.
- 4 F. Riedo and E.sz. Kováts, *J. Chromatogr.*, 239 (1982) 1.
- 5 J. H. Knox and H. P. Scott, *J. Chromatogr.*, 282 (1983) 297.

- 6 L. Lapidus and N. R. Amundson, *J. Phys. Chem.*, 56 (1952) 984.
- 7 H. K. Rhee and N. R. Amundson, *Chem. Eng. Sci.*, 27 (1972) 199.
- 8 J. C. Smit, H. C. Smit and E. M. de Jager, *Anal. Chim. Acta*, 122 (1988) 1.
- 9 P. Rouchon, M. Schonauer, P. Valentin and G. Guiochon, *Sep. Sci. Technol.*, 22 (1987) 1793.
- 10 F. Helfferich and G. Klein, *Multicomponent Chromatography*, Marcel Dekker, New York, 1970.
- 11 J. C. Giddings, *Dynamics of Chromatography*, Marcel Dekker, New York, 1965.
- 12 J. C. Sternberg, *Adv. Chromatogr.*, 2 (1966) 205.
- 13 J. Crommen, G. Schill, D. Westerlund and L. Hackzell, *Chromatographia*, 24 (1987) 252.
- 14 E. Arvidsson, J. Crommen, G. Schill and D. Westerlund, *Chromatographia*, 24 (1987) 460.
- 15 J. Crommen, G. Schill and P. Herné, *Chromatographia*, 25 (1988) 397.
- 16 W. G. Kuhr and E. S. Yeung, *Anal. Chem.*, 60 (1988) 2642.
- 17 F. Foret, S. Fanati, L. Oscini and P. Bocek, *J. Chromatogr.*, 470 (1989) 299.
- 18 H. Poppe and J. C. Kraak, *J. Chromatogr.*, 255 (1983) 395.
- 19 J. A. Eble, R. L. Grob, P. E. Antle and L. R. Snyder, *J. Chromatogr.*, 384 (1987) 25.

CHROMSYM. 1791

Studies on system peaks in ion-pair adsorption chromatography

III. Regulation of system peak gradient retention for obtaining analyte peak compression

T. FORNSTEDT* and D. WESTERLUND

Department of Analytical Pharmaceutical Chemistry, Biomedical Centre, University of Uppsala, P.O. Box 574, S-751 23 Uppsala (Sweden)

and

A. SOKOLOWSKI

Pharmacia LKB Biotechnology, Chemical Production, 751 82 Uppsala (Sweden)

SUMMARY

Peak compression can be obtained when an analyte is eluted in the co-ion gradient in a large system peak. Matching of the analyte retention with this gradient was investigated. The chromatographic system was based on silanized silica and an acidic eluent, containing acetonitrile and a probe, which was an UV-detectable hydrophobic amine, protriptyline. Large system peaks, or zones, containing probe deficiencies were induced by injecting high concentrations of a hydrophobic organic anion together with cationic analytes. The back part of these system zones consisted of a steep gradient of increasing probe (co-ion) concentration, giving strongly compressed peaks when low analyte amounts were also eluted with this back-gradient. It was found that variation of the probe concentration was an efficient way of matching the retention of the system peak with analytes of widely varying retentions.

INTRODUCTION

When a solution deviating in composition from the eluent is injected into a chromatographic system, the established equilibria between the solid phase and the mobile phase are disturbed. This results in migrating zones of each eluent component participating in an interaction common with a component in the injected sample. These migrating zones, so-called system zones, can only be visualized if at least one of the equilibrated eluent components can be detected¹. The direction of the system peak will be positive or negative, depending on the charge and retention volume of the sample component relative to the corresponding eluent component^{2,3}.

When a reversed-phase ion-pair adsorption chromatographic system is equilibrated with an organic eluent cation, large system peaks can be induced by the injection of high concentrations of an organic anion. The back part of these negative system peaks consists of a steep gradient of increasing cation concentration. Co-elution of cationic analytes with this system peak gradient (co-ion) resulted in extremely narrow analyte peaks^{4,5}. When an analyte had other positions within the system zone, peak deformations were obtained instead⁵.

Both peak compression and deformation effects were previously investigated in a reversed-phase ion-pair liquid chromatographic (LC) system, but no systematic changes of the probe concentration in the eluent were performed⁵. The parameters governing the retention volumes of co-ion gradient and analyte have also been investigated^{5,6}. When the analyte and the system zone were eluted close to each other, fine adjustments of the retention volumes were made by changing the concentration of the anion in the injection solution in order to obtain peak compression.

The aim of this study was to investigate the effect of different probe concentrations for matching system zone and analyte retention volumes, in order to obtain peak compression for analytes with widely different retention volumes. For this purpose, it was important to investigate carefully the parameters determining the retention of the gradient in the back part of the large system zone or peak.

THEORETICAL

The retention equations used are based on the stoichiometric ion-pair adsorption model⁶⁻¹⁰. Retentions of both the analytes and the eluent component (system peak) are described by the partial derivative of the adsorption isotherm⁶. However, different retention equations will result, owing to the different starting conditions. At the start of elution, the analyte concentration is zero, whereas the concentration of the eluent component is finite.

Eqns. 1-3 describe the net retention volume of a cationic analyte, HA^+ , an anionic analyte, Z^- , and the organic eluent component, the probe Q^+ . In order to simplify the discussion, the solid phase is assumed to contain only one type of adsorption site. X^- is a buffer component present in the eluent. The subscript m means mobile phase and the concentration unit is molarity.

$$V_{N,HA} = \frac{W_s K_0 K_{HAX} [X^-]_m}{1 + K_{QX} [Q^+]_m [X^-]_m} \quad (1)$$

$$V_{N,Z} = \frac{W_s K_0 K_{QZ} [Q^+]_m}{1 + K_{QX} [Q^+]_m [X^-]_m} \quad (2)$$

$$V_{N,Q} = W_s \cdot \frac{C_{Q,s}}{C_{Q,m}} = \frac{W_s K_0 K_{QX} [X^-]_m}{(1 + K_{QX} [Q^+]_m [X^-]_m)^2} \quad (3)$$

K_0 gives the total adsorption capacity of the solid phase, and K_{HAX} , K_{QX} and K_{QZ} are the adsorption constants. The analyte equations assume symmetrical peaks. For high analyte concentrations, which affect both retention and peak shape, no

quantitative equation is yet available. However, equations containing an additional term in the denominator, including the analyte concentration, can be used for qualitative discussions^{6,7}. Eqn. 2, corresponding to the anion Z^- , will then also contain a term in both the numerator and the denominator involving the ion-pair distribution with the cationic buffer component.

The retention equation for the system peak is valid for only infinitesimal changes of the eluent component. In this study, large system peaks or zones were created. The retentions of these large disturbances can only be discussed qualitatively with support of eqn. 3.

At high concentrations all zones affect each other when they initially migrate together at the top of the column. The equations discussed assume that these effects are negligible, *i.e.*, the situation when the migrating zones have separated from each other.

EXPERIMENTAL

Apparatus, chromatographic technique and preparation of the eluent

These were as described previously^{6,7}. For all injections a 100- μ l loop was used.

Chemicals

Analytical-reagent grade chemicals were used unless indicated otherwise.

Acetonitrile (LiChrosolv) and dichloromethane were obtained from Merck (Darmstadt, F.R.G.) and protriptyline (PT) from Merck, Sharp and Dohme (Haarlem, The Netherlands). Sodium octanesulphonate and octylsulphate were obtained from Eastman-Kodak (Rochester, NY, U.S.A.), sodium nonyl- and decylsulphate from Merck and sodium nonane- and decanesulphonate from Fluka (Buchs, Switzerland). Phosphoric acid (99% crystalline) and 1 M sodium hydroxide solution (Titrisol) were obtained from Merck.

Desipramine and imipramine hydrochloride used as analytes were obtained from Ciba-Geigy (Basle, Switzerland). The substituted benzamides also used as analytes are denoted FLA combined with a number (*cf.*, ref. 6). They were synthesized at CNS Research and Development, Astra Research Centre (Södertälje, Sweden).

Detection technique

The detection technique has been described previously^{5,7}. When the analyte was a benzamide, its signal was measured at a wavelength where only this compound absorbed⁶. For desipramine or imipramine as analytes, their signals were recorded at 252 nm, where PT also absorbs. To compensate for the PT absorbance, 322 nm was used as a reference, as the PT absorbance at 322 nm equals that at 252 nm. The PT signal was recorded at a wavelength where only PT absorbed.

The compensating technique was used only when an analyte was present. In the other chromatographic runs only the PT signal was recorded. At the lowest PT concentration used in the eluent, the PT signal was recorded at the wavelength maximum at 291 nm. With increasing PT concentrations longer wavelengths were chosen, *viz.*, 320, 330 and 337 nm, respectively, resulting in lower absorbances. The reason for this was that the detector used did not measure negative peaks with lower relative absorbance than -0.1 a.u.f.s.

Retention volume and asymmetry factor (*asf*)

These were determined as described previously⁵.

Four different concentrations of the secondary amine protriptyline (PT; the probe) as additive were used in the reversed-phase ion-pair LC system in this study.

Determination of negative zone parameters

Very large negative system peaks had a zone shape (see Fig. 1). The depth of the negative system peak or zone is given in concentration units and is represented as ΔC . The change in PT concentration in the zone relative to the bulk concentration, C_b , was then obtained by taking the ratio $\Delta C/C_b$. This value was used as a measure of the magnitude of the probe equilibrium disturbance and is < 1 only for system peaks, not zones. The width of the zone, $w_{b,z}$, was determined at half-depth of the negative zone as described in Fig. 1.

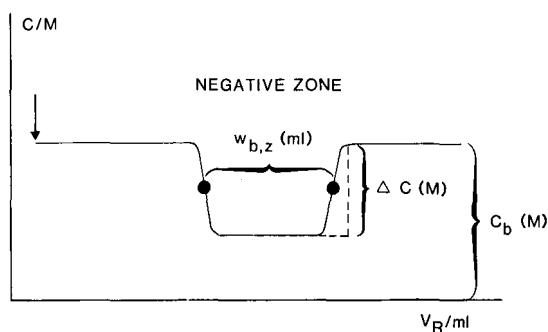


Fig. 1. Principle of measurement of parameters in a negative system zone. C_b (M) is the bulk concentration of probe in the eluent; ΔC (M) is the depth of the zone; the ratio $\Delta C/C_b$ will be the degree of the equilibrium disturbance; $w_{b,z}$ (ml) is the zone width.

RESULTS AND DISCUSSION

Solid phases consisting of silanized silica have often been found to contain two different kinds of adsorption sites with different capacities and affinities^{6,7,10,11}. In previous work, the adsorption of PT on Nucleosil C₁₈ was studied, indicating a two-site adsorption behaviour of the Langmuir type⁶. According to this, the strong site was covered to 3, 12, 41 and 78%, respectively, at the four different PT concentrations used in this work. At the two highest PT concentrations, the weak site was covered to 5 and 22%, respectively. The adsorption isotherm is assumed to be linear when less than 10% of the adsorption sites are covered with the compound of interest^{6,7,10,12}. The two lower PT concentrations used then corresponded fairly closely to the linear part of the adsorption isotherm, whereas the higher PT concentrations corresponded to the non-linear part.

Substituted benzamides⁶, desipramine and imipramine were used as cationic analytes.

In reversed phase ion-pair chromatography, equilibrium disturbances are easily obtained by the injection of an organic ion into the system. This results in migrating

zones of the different eluent components that are involved in the disturbances. If at least one of the eluent components is detectable, these zones will appear as positive or negative system peaks¹⁻³.

In this study, the equilibria of PT were disturbed by injecting a large amount of an organic anion (sulphonate or sulphate) with a retention higher than that of the probe. The injection of such an organic anion increases the distribution of the cationic probe to the solid phase. The anion is eluted together with the excess of the probe (a positive probe peak) (see Fig. 2). The compensating deficiency was visualized as a negative probe peak (the system peak) with lower retention. When larger amounts of the anion were injected, the probe deficiencies in the eluate appeared as negative zones. The depth of the zone, ΔC , approached the level of the probe concentration in the eluent, C_b . At such a large equilibrium disturbance with the ratio $\Delta C/C_b$ close to 1.0, the probe concentration in the zone was close to zero and in the back part of the system zone the probe concentration increased steeply. The retention of this gradient, $V_{R,G}$, was determined according to Fig. 2.

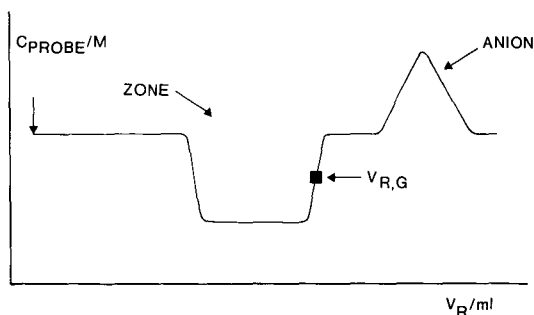


Fig. 2. Schematic representation of the probe signal after the injection of a high concentration of a hydrophobic anion. The gradient retention volume, $V_{R,G}$ (ml), is measured at half-depth of the negative zone.

Peak compression was obtained when a cationic analyte was injected together with a large amount of an organic anion and was eluted together with the back part of the negative probe system zone^{4,5}. In this situation the analyte retention volume is greater than that in the isocratic experiment, *i.e.*, analyte injected without organic anion in the injection solution⁵.

Retention regulation

The most useful peak compressions occur when the analyte peak is eluted with the gradient of the back part of the system zone or peak. The parameters determining the retention volume of this gradient and the analyte were therefore carefully studied. In this work, the emphasis was on the effects of the probe concentration in the eluent, which was systematically varied. The ionic strength and pH were kept constant.

The regulation of the analyte retention has been described elsewhere^{5-7,10,11}. The retention volume of the cationic analyte decreased with increasing concentration of PT, the latter then acting as a co-ion (*cf.*, eqn. 1). If the cationic analyte was injected together with an organic anion, the analyte retention volume increased⁵.

TABLE I

RETENTION VOLUMES AND ASYMMETRY FACTORS OF CATIONIC ANALYTES WHEN INJECTED INTO THE SYSTEM EQUILIBRATED WITH ELUENT LACKING A PROBE

Injected sample: $1.0 \cdot 10^{-5}$ M analyte in phosphate buffer (pH 2.0). Eluent: phosphate buffer (pH 2.0)-acetonitrile (3:1).

Analyte	V_R (ml)	asf	asf ^a
FLA 870	12.0	2.3	1.6
FLA 965	16.0	2.7	
FLA 659	19.5	2.4	1.2
Desipramine	19.9	2.3	1.1
Imipramine	22.5	2.6	1.1
Protriptyline (PT) (probe)	21.8	2.2	

^a Eluent contained $9.5 \cdot 10^{-4}$ M protriptyline.

The retention volumes of the analytes, including PT, injected as an analyte, when the system was equilibrated with eluent without probe, are given in Table I. The analyte retention volume decreased and the peak symmetry was improved with increasing probe concentration in the eluent.

Elution of imipramine and desipramine at a high PT concentration ($9.5 \cdot 10^{-4}$ M) resulted in very symmetrical analyte peaks; the asf value was 1.1 (*cf.*, Table I). The structural similarity between the probe (also a tricyclic antidepressant amine) and these analytes indicates similar affinities for the strong site¹⁰. At this high probe concentration, the strong sites, probably responsible for the analyte peak asymmetry, were covered to 78%⁶.

When the organic anion was injected into the system, the probe acted as a counter ion (*cf.*, eqn. 2)^{5,6,9,11}. Hence the anion retention volume increased with increasing probe concentration in the eluent⁶. As mentioned, the buffer ions are also of importance for the retention of an organic ion⁷.

The anions were injected in order to obtain large negative system zones or peaks of the probe, thus giving the probe gradient. For this purpose, it is necessary that the anion has a larger retention volume than the probe gradient of interest. The system peak retention volume decreases with increasing probe concentration (*cf.*, eqn. 3). With a low probe concentration in the eluent, it was necessary to inject hydrophobic anions, such as decylsulphate, nonylsulphate or decanesulphonate, in order to obtain separation between the system zone and the anion.

At the two higher probe concentrations, $1.9 \cdot 10^{-4}$ and $9.5 \cdot 10^{-4}$ M, the less hydrophobic anions, nonanesulphonate and octylsulphate, could also be utilized, because at these probe concentrations the anions had larger retention volumes than the system peak gradient (see Table II). The hydrophobic anions used at the two lowest probe concentrations could also be used at the higher probe concentrations. However, their retention volumes were then very large (*cf.*, Table II).

Large system peak retention

The validity of the system peak equation has been investigated in a previous study⁶. However, the equation is valid only for infinitesimal changes in the probe

TABLE II

RETENTION VOLUMES OF ORGANIC ANIONS WHEN INJECTED INTO THE SYSTEM EQUILIBRATED WITH A HIGH PROBE CONCENTRATION IN THE ELUENT

Injected sample: $5.0 \cdot 10^{-3} M$ organic anion in phosphate buffer (pH 2.0). Eluent: $1.9 \cdot 10^{-4} M$ protriptyline in phosphate buffer (pH 2.0)-acetonitrile (3:1).

Anion	V_R (ml) ^a
Nonanesulphonate	22.0
Octylsulphate	24.8
Decanesulphonate	43.5
Nonylsulphate	> 50
Decylsulphate	> 84

^a System zone back part gradient ($V_{R,G}$) = 13.4–17.2 ml.

equilibrium, *i.e.*, very small system peaks with $\Delta C/C_b$ ratios close to zero. For large system peaks the retention equation can be used only qualitatively and at least two additional effects must be taken into consideration. One of them is that large negative system peaks have higher retention volumes than large positive system peaks, owing to the non-linear adsorption isotherm⁶. The system peak retention volume will further be affected by the organic anion injected, its retention volume increasing with increasing anion hydrophobicity⁶.

The decanesulphonate anion was more retained than the probe. It was injected at $5.0 \cdot 10^{-3} M$ concentration into systems equilibrated with eluents of different probe concentrations. The retention volumes for half the downslope of the front part and half the upslope of the back part, $V_{R,G}$, of the negative system zone or peak for different eluent concentrations of the probe are shown in Fig. 3. With increasing probe concentration, the retention volumes of both the front and the back parts of the system zone decreased. However, the retention volume of the back-part gradient decreased more than the front part, resulting in a decreased zone width. At the two lower probe

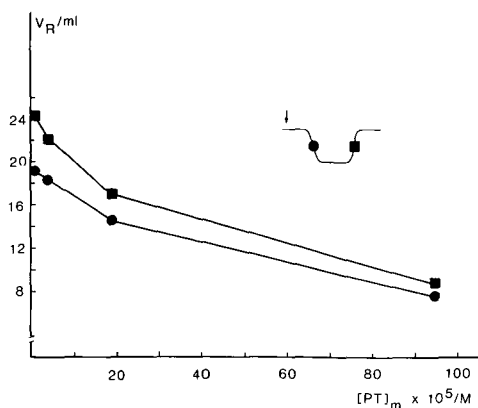


Fig. 3. Retention volumes of the front (●) and back (■) parts of the negative zone or peak, created by the injection of decanesulphonate, versus the probe concentration. Sample, $5.0 \cdot 10^{-3} M$ anion in phosphate buffer (pH 2.0); eluent, protriptyline in phosphate buffer (pH 2.0)-acetonitrile (3:1).

concentrations, *i.e.*, $7.6 \cdot 10^{-6}$ and $3.8 \cdot 10^{-5}$ M, large negative system zones were obtained (*cf.*, Fig. 2), with the ratio $\Delta C/C_b = 1.0$ (see Table III). At the two highest probe concentrations used, large negative system peaks were obtained instead of zones, the $\Delta C/C_b$ ratio being 0.67 and 0.37, respectively. The results indicate that the ability of a certain anion to disturb the probe equilibrium by the magnitude required for a zone to appear instead of a peak decreases at high probe concentrations corresponding to the non-linear part of the adsorption isotherm.

TABLE III

PARAMETERS FOR THE NEGATIVE SYSTEM ZONE OR PEAK OBTAINED BY THE INJECTION OF DECANESULPHONATE INTO THE SYSTEM EQUILIBRATED WITH ELUENTS OF DIFFERENT PROBE CONCENTRATIONS

Injected sample and eluent as in Fig. 3.

$PT (M)$	$\Delta C (M)$	$\Delta C/C_b$	$\frac{V_{R,anion}}{V_{R,G}}$	$\Delta C w_{b,z}$ (mol PT adsorbed)
$7.6 \cdot 10^{-6}$	$7.6 \cdot 10^{-6}$	1.0	1.2	$0.4 \cdot 10^{-7}$
$3.8 \cdot 10^{-5}$	$3.8 \cdot 10^{-5}$	1.0	1.4	$1.4 \cdot 10^{-7}$
$1.9 \cdot 10^{-4}$	$1.3 \cdot 10^{-4}$	0.67	2.6	$3.4 \cdot 10^{-7}$
$9.5 \cdot 10^{-4}$	$3.5 \cdot 10^{-4}$	0.37	10.3	$4.1 \cdot 10^{-7}$

The depth of the negative system peak, ΔC , increased with increasing eluent probe concentration (Table III)⁶. The product of depth and the width of the zone ($\Delta C w_{b,z}$) reflects the extra amount of probe (in moles) adsorbed due to the injection of the anion. This value also increased (Table III) with increasing eluent probe concentration; however, at high probe concentrations the increase was relatively smaller.

The smaller amount of PT adsorbed relative to the eluent concentration at high probe concentrations and the smaller equilibrium disturbances are probably due to both the existence of a non-linear adsorption isotherm and increased competition between the anion and the phosphate ion as counter ions to PT (see Theoretical). However, at low probe eluent concentrations, competition is also low, and the anion injections result in ion-pair adsorption of more or less all the content of the probe in a certain region of the eluent.

The separation between the anion and the back gradient increased with increasing probe concentration (see Table III). This is a result both of the increased anion retention volume and the decreased system peak retention volume.

A comparison was made between large system zones or peaks induced by injections of anions of different hydrophobicity. The anions injected were, in order of increasing hydrophobicity (based on retention volumes in the same eluent), decanesulphonate, nonylsulphate and decylsulphate (*cf.*, Table II). The anion concentration was $5.0 \cdot 10^{-3}$ M and injections were made at different eluent probe concentrations (see Table IV).

For all three anions, the injections resulted in the appearance of zones at the two lowest probe concentrations. However, at the higher probe concentration, the

TABLE IV

PARAMETERS OF THE NEGATIVE SYSTEM ZONE OR PEAK OBTAINED BY INJECTION OF ANIONS OF DIFFERENT HYDROPHOBICITY

Injected sample and eluent as in Fig. 3. A = Decanesulphonate; B = nonylsulphate; C = decylsulphate.

Zones or peaks	PT (M)	V _{R,G} (ml)			w _{b,z} (ml)		
		A	B	C	A	B	C
Zones	7.6 · 10 ⁻⁶	24.5	25.6	27.6	5.0	5.6	6.3
	3.8 · 10 ⁻⁵	22.2	23.0	23.8	~4	~4	~4
Peaks	1.9 · 10 ⁻⁴	16.9	16.9	17.2	~2.5	~2.5	~2.5
		(0.7) ^a	(0.7) ^a	(0.6) ^a			

^a ΔC/C_b values for the peaks.

disturbances on the probe equilibrium were smaller, and so peaks appeared instead. The retention volumes of the zone or peak, especially that of the back-part gradient, increased with increasing anion hydrophobicity, the effect being largest at the lowest probe concentrations (Table IV). At the high probe concentration, 1.9 · 10⁻⁴ M, corresponding to the non-linear part of the adsorption isotherm, the gradient retention volumes were similar, despite the different anion hydrophobicities. However, the extents of probe equilibrium disturbances were also of the same magnitude.

At the lowest probe concentration the zone width increased with increasing hydrophobicity of the injected anion, while the zone widths were approximately the same at the higher probe eluent concentrations for all anions injected (*cf.*, Table IV). This was probably due to the increased competition at high probe concentrations. Effects of anion hydrophobicity when injecting anion concentrations higher than 5.0 · 10⁻³ M were not studied.

When nonylsulphate was injected in increasing concentrations at a probe concentration of 1.5 · 10⁻⁵ M, an increasingly deeper negative system peak appeared and the retention of the back part increased⁵. However, at a certain anion concentration, the back-part retention began to decrease with a further increase in the anion concentration, probably an effect of the closely eluted anion.

At the two lowest probe concentrations used in this study, similar results were obtained with injections of the hydrophobic anions decanesulphonate and nonylsulphate. At these probe concentrations the more hydrophobic anion, decylsulphate, did not show the tendency for decreasing back-part retention when the anion concentration injected was increased to 5.0 · 10⁻³ M. The retention volume of decylsulphate was larger than those for the other two anions (*cf.*, Table II), resulting in an improved anion separation from the system zone gradient.

With the higher probe concentration, 1.9 · 10⁻⁴ M, the separation between decanesulphonate and the back-gradient was improved (*cf.*, Table III). Injections of decanesulphonate at concentrations up to 0.01 M did result in continuously increasing back-part retention volumes (Fig. 4). However, a zone was never developed, and the gradient retention increase was accompanied by an increase in the equilibrium disturbances, *i.e.*, larger ΔC/C_b values. At this probe concentration the decrease in the back-part system peak retention volumes induced by the octylsulphate anion began at

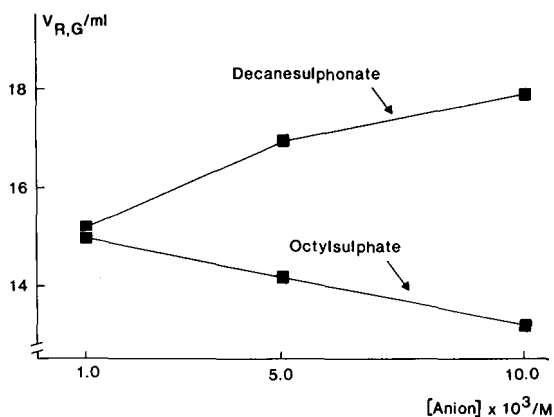


Fig. 4. Back gradient retention volumes, $V_{R,G}$, of system peaks induced by decanesulphonate and octylsulphate at high probe concentration, *versus* the injected anion concentration. Sample, anion in phosphate buffer (pH 2.0); eluent, $1.9 \cdot 10^{-4} M$ protriptyline in phosphate buffer (pH 2.0)–acetonitrile (3:1).

the low anion concentration of $1.0 \cdot 10^{-3} M$ (Fig. 4). This was also the case for nonanesulphonate, which is similar to octylsulphate in hydrophobicity (*cf.*, Table II). These decreases in gradient retention volume were accompanied by distortions of the system peak shapes (see below). However, when the probe concentration was increased to $9.5 \cdot 10^{-4} M$, the nonanesulphonate concentration could be increased to $0.01 M$ before the decrease in the back-part retention volume started.

The results shown above indicate that it is possible to increase the gradient retention by increasing the anion concentration at different probe eluent concentrations. However, a prerequisite is an adequate anion separation from the gradient, especially when injecting high concentrations of less hydrophobic anions at high probe concentration in the eluent.

It may be assumed that the increase in the gradient retention volume with increasing anion concentration was due mainly to the increased ion-pair distribution with the anion in the start zone at low probe concentration. At high-probe concentrations the increased gradient retention volume may be a consequence of non-linear adsorption behaviour and thus be due mainly to the low concentration of probe in the system peak. In that event, however, it is assumed that the anion concentrations do not reach the levels resulting in distortion of the system peak (see below).

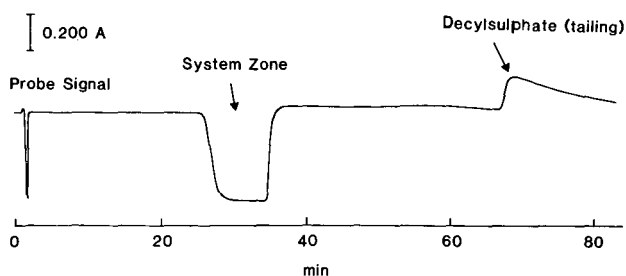
Distortion of anion and system peak

Odd-shaped anion peaks, showing diffuse and deformed front parts, appeared at high anion concentrations injected at all probe concentrations. A prerequisite for this kind of distortion to occur was that the indirectly detected anion peak was eluted after the system peak. At high probe concentrations, the injections of high concentrations of less hydrophobic anions also resulted in odd-shaped system peaks. Unusually shaped large sample and system peaks have also been described by Golshan-Shirazi and Guiochon^{13,14}.

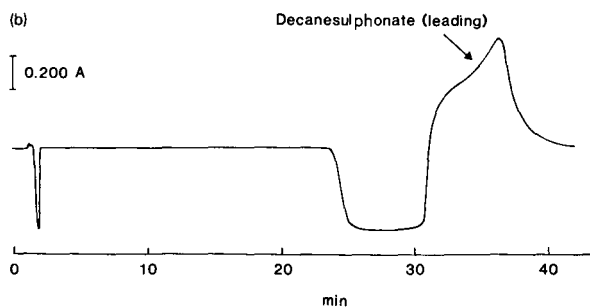
When a high concentration of the hydrophobic anion decylsulphate was injected

at low probe concentration, the system zone was well shaped and the late-eluted anion peak was tailing (Fig. 5a). When the same concentration of the less hydrophobic decanesulphonate was injected, the anion peak, which eluted very close to the system zone gradient, showed a leading effect, *i.e.*, a diffuse front side and a sharper back side (Fig. 5b). This effect decreased when the probe concentration was increased, and at an adequately high probe concentration the separation was further improved and the decanesulphonate peak showed tailing. If, on the other hand, lower decanesulphonate concentrations were injected, the anion peaks showed tailing. The less hydrophobic anions nonanesulphonate and octylsulphate resulted in very broad and diffuse front parts of the anion peaks when injected at higher probe concentrations in the eluent, $1.9 \cdot 10^{-4} M$ (see Fig. 5c). The diffuse front part of the anion peak was extremely broad

(a)



(b)



(c)

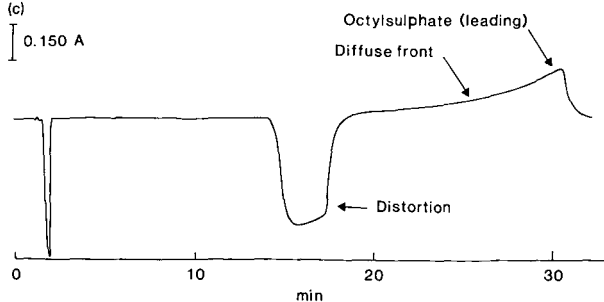


Fig. 5. Shapes of negative system zones and positive anion peaks with injected hydrophobic anions. Sample, $5.0 \cdot 10^{-3} M$ anion in phosphate buffer (pH 2.0); eluent, protriptyline in phosphate buffer (pH 2.0)–acetonitrile (3:1). (a) Anion, decylsulphate; PT concentration, $7.6 \cdot 10^{-6} M$. (b) Anion, decanesulphonate; PT concentration, $7.6 \cdot 10^{-6} M$. (c) Anion, octylsulphate; PT concentration, $1.9 \cdot 10^{-4} M$.

and partly overlapped the system peak, also being distorted. A distortion of the system peak is always seen when the diffuse front of the anion peak partly overlaps the back part of the system zone.

Hence for a certain anion injected the deformation of its front decreased with increasing probe concentration. This was probably due to the improved anion separation from the system zone gradient. On the other hand, the high probe concentration increased the risk of deformation for a poorly separated anion. The distortions may be a result of the initial co-migration of the anion zone with the system zone gradient. The probe deficiency in the system zone then gives a lowering of the retention volume of the anion front, resulting in a diffuse front part of the eluted peak (*cf.*, eqn. 2).

Comparison of large and small system peak retentions

Injections of very low analyte concentrations into the system resulted in small system peaks, owing to the low degree of equilibrium disturbances. The retention equation (eqn. 3) is quantitatively valid for these so-called infinitesimal system peaks. The back-part gradient retention volumes of the system zones or peaks, induced by injections of $5.0 \cdot 10^{-3} M$ decanesulphonate, were plotted together with the retention volumes of the corresponding infinitesimal system peaks at the different probe concentrations (Fig. 6). In line with eqn. 3, both the gradient retention volume and the infinitesimal system peak retention volume decreased with increasing probe concentration. However, the gradient retention volumes were larger at all probe concentrations. This is partly due to the fact that the retention volumes for the small system peaks were measured at the peak minimum (see ref. 5).

The larger retention volumes for the large system peaks or zones in comparison with the small ones may be explained in the following way. The retention volume of the gradient (large negative system zone or peak) is determined qualitatively by eqn. 3 in combination with the presence of the hydrophobic anion and a low concentration of

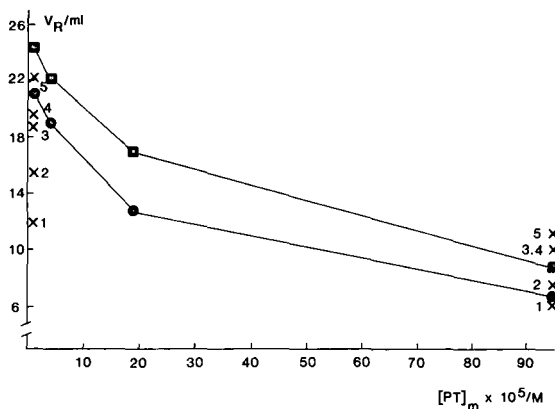


Fig. 6. Gradient retention volumes (■) (zone created by decanesulphonate, see Fig. 3) and retention volumes of infinitesimal system peaks (●) *versus* the probe concentration in the eluent. Retention volumes of some analytes at lowest and highest probe concentrations are also plotted. 1 = FLA 870; 2 = FLA 965; 3 = FLA 659; 4 = desipramine; 5 = imipramine.

probe in the system peak. When the bulk concentration is low, being on the more or less linear part of the adsorption isotherm, the gradient retention volume is mainly determined by the adsorption of PT as an ion pair with the anion. At these probe concentrations, zones were developed and an increased hydrophobicity or concentration of the injected anion resulted in increased adsorption of PT from the bulk and, therefore, a larger gradient retention volume. For a qualitative description, eqn. 3 might than be modified as below, containing an additional term (corresponding to the hydrophobic anion) in the numerator and with the denominator simplified to 1:

$$V_{N,Q} = W_s K_0 (K_{QX}[X^-]_m + K_{QZ}[Z^-]_m)$$

At high probe bulk concentrations, being on the non-linear part of the adsorption isotherm, the increased gradient retention volume is due to the lower concentration of probe in the system peak. At these high probe concentrations, the contribution from the anion to the gradient retention volume is low. Predictions of gradient retention volumes by use of the unmodified eqn. 3 will then be more adequate.

Matching

To obtain peak compression it is necessary that the analyte and the gradient be eluted together. In this situation the analyte retention is larger than in the isocratic experiment. A prerequisite is that the isocratic retention volume of the analyte peak must be lower than the retention volume of the gradient. As a consequence, it was not possible to compress the imipramine peak in this system (*cf.*, Table I). The isocratic retention volumes of different analytes are given at the lowest and highest probe eluent concentrations (Fig. 6). The analyte retention volumes decreased less than the gradient retention volumes when the probe concentration was increased (*cf.*, eqns. 1 and 3). Hence the gradient was eluted later than all analytes at the lowest probe concentration but was eluted only after two of the analytes at the highest probe concentration (*cf.*, Fig. 6). This resulted in peak compression for more hydrophobic analytes at low probe

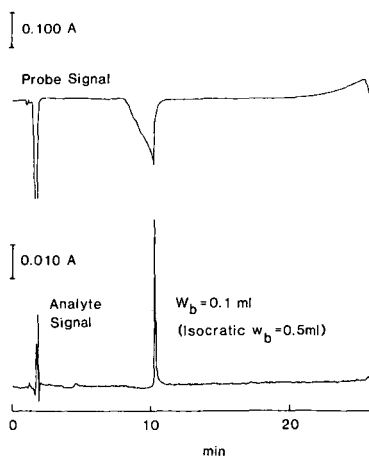


Fig. 7. Peak compression of FLA 870 at high probe concentration in the eluent. The peak width, w_b (ml), is measured at the baseline. Sample, $1.0 \cdot 10^{-5} M$ FLA 870 and $5.0 \cdot 10^{-3} M$ octanesulphonate in phosphate buffer (pH 2.0); eluent, $9.5 \cdot 10^{-4} M$ protriptyline in phosphate buffer (pH 2.0)-acetonitrile (3:1).

concentrations, whereas less hydrophobic analytes were compressed at high probe concentrations. When a poorly retarded analyte, FLA 870, was injected with a large amount of an organic anion at low probe concentration, the analyte peak was deformed and was eluted with the front part of the zone (ref. 6, Fig. 13a). However, at the highest probe concentration, FLA 870 was eluted with the gradient and was compressed (see Fig. 7). At this probe concentration analytes more hydrophobic than FLA 965 were eluted after the gradient.

CONCLUSIONS

The retention of the back-part gradient in a system peak or zone can be regulated by both the probe and the injected anion concentrations. When anion regulation is used, at low probe concentrations the gradient retention is influenced by a linear ion-pair distribution behaviour with the anion in starting and unresolved zones. The gradient retention can then also be regulated by the anion hydrophobicity. At high probe concentrations the retention is mainly influenced by the non-linear adsorption behaviour.

An adequate separation between the anion and the gradient is necessary primarily to avoid distortions of the shape of the back-part gradient, but also in order to allow regulation of the retention of the gradient by use of the anion concentration. Such conditions can be achieved by using an adequately high probe concentration.

Changing the probe concentration is an efficient way of obtaining elution of the analyte with the gradient and thus to achieve analyte peak compression. The less hydrophobic the analyte, the higher is the necessary probe concentration.

ACKNOWLEDGEMENTS

We thank the Department of CNS Research and Development, Astra Research Centre, for making substituted benzamides available. We are also grateful for grants given by the Swedish Academy of Pharmaceutical Sciences (T.F.) and from the I.F. Foundation of Pharmaceutical Research (A.S.). This project has been financially supported by Pharmacia and the Swedish Natural Science Research Council (NFR).

REFERENCES

- 1 M. Denkert, L. Hackzell, G. Schill and E. Sjögren, *J. Chromatogr.*, 218 (1981) 31.
- 2 L. Hackzell and G. Schill, *Chromatographia*, 15 (1982) 437.
- 3 G. Schill and J. Crommen, *Trends Anal. Chem.*, 6 (1987) 111.
- 4 L. B. Nilsson and D. Westerlund, *Anal. Chem.*, 57 (1985) 1835.
- 5 T. Fornstedt, D. Westerlund and A. Sokolowski, *J. Liq. Chromatogr.*, 11(13) (1988) 2645.
- 6 A. Sokolowski, T. Fornstedt and D. Westerlund, *J. Liq. Chromatogr.*, 10 (1987) 1629.
- 7 A. Sokolowski, *Chromatographia*, 22 (1986) 168.
- 8 A. Sokolowski, *Chromatographia*, 22 (1986) 177.
- 9 A. Tilly-Melin, Y. Askemark, K.-G. Wahlund and G. Schill, *Anal. Chem.*, 51 (1979) 976.
- 10 A. Sokolowski and K.-G. Wahlund, *J. Chromatogr.*, 189 (1980) 299.
- 11 A. Tilly-Melin, M. Ljungqrantz and G. Schill, *J. Chromatogr.*, 185 (1979) 225.
- 12 L. R. Snyder, *Anal. Chem.*, 39 (1967) 698.
- 13 S. Golshan-Shirazi and G. Guiochon, *J. Chromatogr.*, 461 (1989) 1.
- 14 S. Golshan-Shirazi and G. Guiochon, *J. Chromatogr.*, 461 (1989) 19.

CHROMSYMP. 1661

Multiple peak formation in reversed-phase liquid chromatography of ramipril and ramiprilate

STINA GUSTAFSSON* and BRITT-MARIE ERIKSSON

Bioanalytical Chemistry, AB Hässle, S-431 83 Mölndal (Sweden)

and

INGEMAR NILSSON

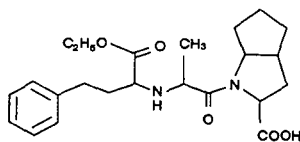
Organic Chemistry, AB Hässle, S-431 83 Mölndal (Sweden)

SUMMARY

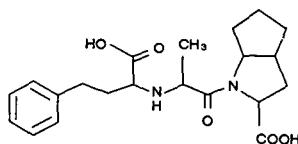
The chromatographic performance of ramipril, an angiotensin-converting enzyme inhibitor, and ramiprilate, its active metabolite, was studied on an octadecyl-bonded silica stationary phase and with aqueous eluents. The substances are peptide-related with a proline residue, a group of compounds known to exist as a mixture of two conformers in aqueous solution. The influence of column temperature, flow-rate, pH, organic modifier and stationary phase was investigated, and the *cis* and *trans* isomers of ramiprilate were assigned by nuclear magnetic resonance studies. Multiple and irregularly shaped chromatographic peaks were obtained, but by choosing appropriate conditions the compounds were eluted as single, symmetric peaks, or the two isomers of each compound could be separated.

INTRODUCTION

Multiple peak formation in reversed-phase liquid chromatography (RP-LC) of two peptide-related drugs, captopril¹ and enalapril², used as angiotensin-converting enzyme (ACE) inhibitors, and a tridecapeptide³, all containing a proline residue, have been observed. Horváth and co-workers^{4,5} reported that dipeptides containing L-proline may show peak splitting in RP-LC, owing to slow *cis-trans* isomerization. This is caused by hindered rotation around the N-substituted peptide bond. Similar observations in RP-LC have also been made for a new ACE inhibitor, ramipril (a drug developed by Hoechst), and its active metabolite ramiprilate⁶.



ramipril



ramiprilate

In this work, we studied the influence of various operating conditions on the retention, peak splitting and band broadening of ramipril and ramiprilate. The *cis* and *trans* isomers of ramiprilate were assigned by nuclear magnetic resonance (NMR) studies. Eluate fractions containing each of the chromatographically resolved isomers of ramiprilate were subjected to enzyme kinetic studies. These, and extended NMR studies, will be reported elsewhere.

EXPERIMENTAL

Chromatography

The liquid chromatograph consisted of a Model 2150 pump (LKB, Bromma, Sweden), an ISS-100 automatic injector (Perkin-Elmer, Überlingen, F.R.G.), a Model 4270 integrator (Spectra-Physics, San Jose, CA, U.S.A.) and a Spectraflow 783 UV detector (Kratos, Ramsey, NJ, U.S.A.). Ramipril and ramiprilate were kindly supplied by Hoechst (Frankfurt am Main, F.R.G.). Buffer substances and acids of analytical-reagent grade were purchased from E. Merck (Darmstadt, F.R.G.) and organic solvents of HPLC grade from Rathburn (Walkerburn, U.K.).

A Nucleosil C₁₈ (3 μ m) column (100 \times 4.6 mm I.D.) (Macherey, Nagel & Co., Düren, F.R.G.) was used and the mobile phase was, unless stated otherwise, phosphate buffer of pH 2.0 (*I*=0.10) containing various amounts of acetonitrile, tetrahydrofuran (THF) or methanol as organic modifier. Column temperatures above 25°C were controlled with a Model LC-22A column oven (Bioanalytical Systems, West Lafayette, IN, U.S.A.), and for temperatures below 25°C a thermostated water-jacket was used. A 50- μ l volume of a sample solution, 150–300 μ mol/l in phosphate buffer of pH 2.0, was injected, and the column effluent was monitored at 220 nm.

NMR

The NMR spectra were recorded on a Bruker AM 500 spectrometer. The measurements were performed at ambient temperature both in deuterated dimethyl sulphoxide ([²H₆]DMSO), in order to make a comparison with investigations on related compounds⁷, and in [²H₂]water–[²H₃]acetonitrile (80:20), a solution similar to the mobile phase in the chromatographic studies. High-temperature measurements (95°C) were performed in 10 mmol/l phosphate buffer (pH 7.3). The samples were 10 mmol/l with respect to ramiprilate. Two-dimensional (2D) ¹H–¹H and ¹H–¹³C NMR studies were also undertaken to aid in the assignments.

RESULTS AND DISCUSSION

Chromatographic studies

Column temperature. Chromatograms of ramipril and ramiprilate obtained at different column temperatures, with a mobile phase containing 30% acetonitrile, are shown in Fig. 1. With increasing temperature the conversions between the two rotamers accelerate and single peaks were obtained, at a lower temperature for ramipril than for ramiprilate. Similar effects have been reported in the RP-LC of other proline-containing substances^{3–5,8}. The influence of temperature on retention was small for both compounds.

Flow-rate. The influence of the residence time in the column on the peak shape

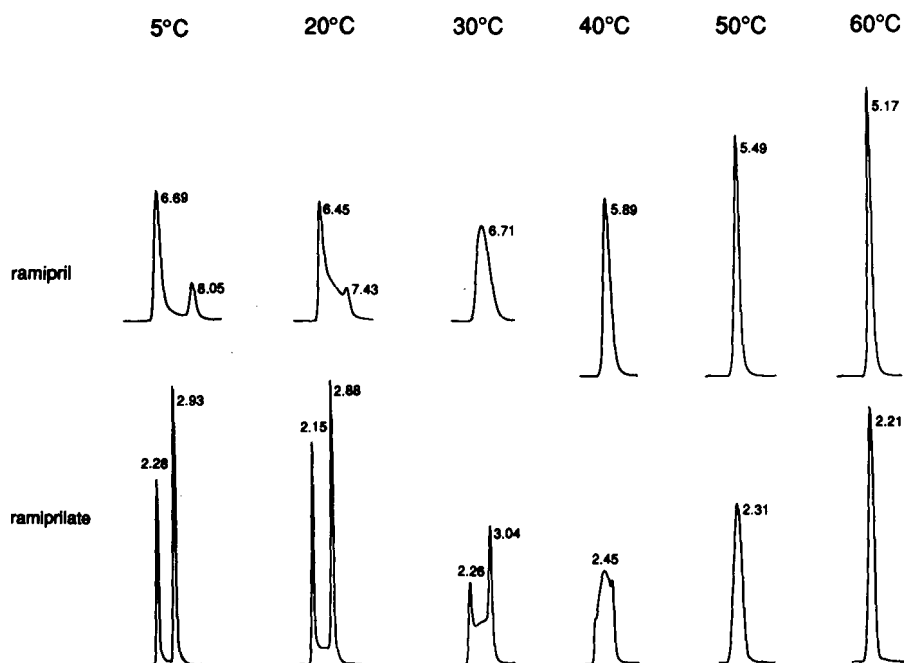


Fig. 1. Effect of column temperature on the chromatographic performance of ramipril and ramiprilate. Stationary phase, Nucleosil C_{18} , $3 \mu\text{m}$ ($100 \times 4.6 \text{ mm I.D.}$). Mobile phase, 30% acetonitrile in phosphate buffer (pH 2.0). Flow-rate, 1.0 ml/min. The retention times of the peaks are indicated.

is illustrated in Fig. 2 for ramiprilate, eluted at a flow-rate of 1.0, 0.5 or 0.3 ml/min. A mobile phase containing 30% acetonitrile was used and the column temperature was 30°C . With decreasing flow-rate a more monodisperse peak was obtained. This was also seen for ramipril (not shown here) and has been reported by Horváth and co-

1.0 ml/min 0.5 ml/min 0.3 ml/min

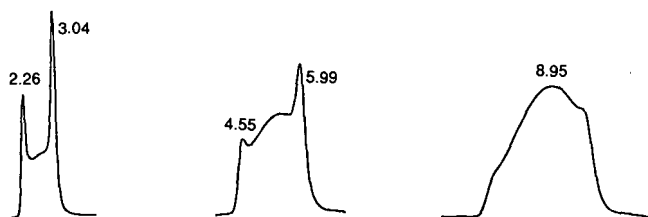


Fig. 2. Effect of flow-rate on the peak shape of ramiprilate. Flow-rate, 1.0, 0.5 or 0.3 ml/min. Column temperature, 30°C . Other conditions as in Fig. 1.

workers^{4,5} for proline-containing peptides having relaxation times of *cis-trans* isomerization commensurate with their retention times.

Influence of pH. The pH of the mobile phase had a considerable effect on the chromatographic performance of both ramipril and ramiprilate. The chromatographic peaks obtained at pH 2.0 and 6.0 are shown in Fig. 3. The mobile phase was phosphate buffer containing 25% acetonitrile and 5% THF, and the column temperature was 15°C. The flow-rate at pH 6.0 was 0.5 ml/min in order to give retention times comparable to those at pH 2.0 (1.0 ml/min). The peak shape of ramipril was improved when the pH was decreased, whereas the opposite was found for ramiprilate. A low pH was used to obtain acceptable peak shapes for captopril¹ and enalapril², both structurally related to ramipril. For alanylproline a similar effect with decrease in pH was explained by a higher isomerization rate⁴.

The influence of pH on the capacity factors (k') of ramipril and ramiprilate is shown in Fig. 4. The mobile phase was phosphate buffer (pH 2 or 3) or acetate buffer (pH 4, 5 or 6) with 20% acetonitrile and 5% THF. A column temperature of 60°C was used to obtain single peaks for both compounds. Ramipril, having acid dissociation

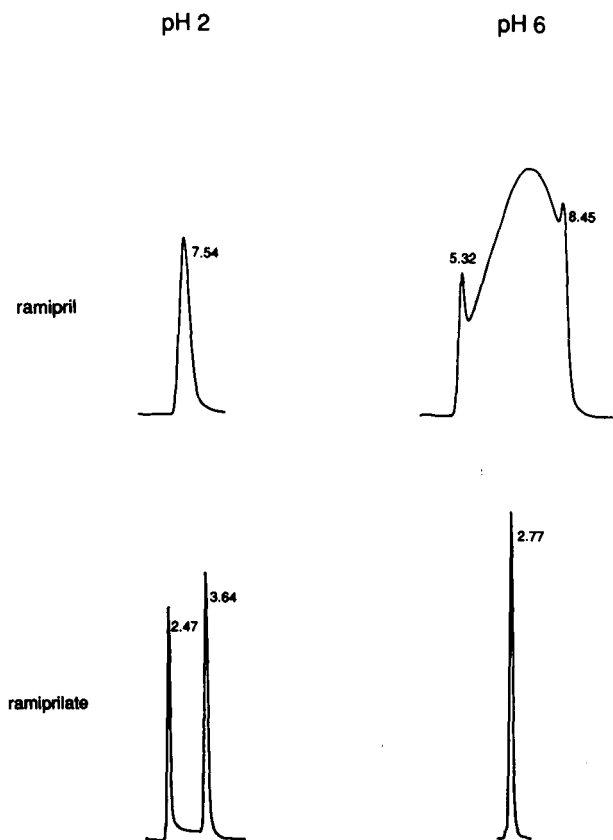


Fig. 3. Effect of pH on the peak shapes of ramipril and ramiprilate. Mobile phase, 25% acetonitrile and 5% THF in phosphate buffer (pH 2.0 or 6.0). Flow-rate, 1.0 ml/min (pH 2) or 0.5 ml/min (pH 6). Column temperature, 15°C. Stationary phase as in Fig. 1.

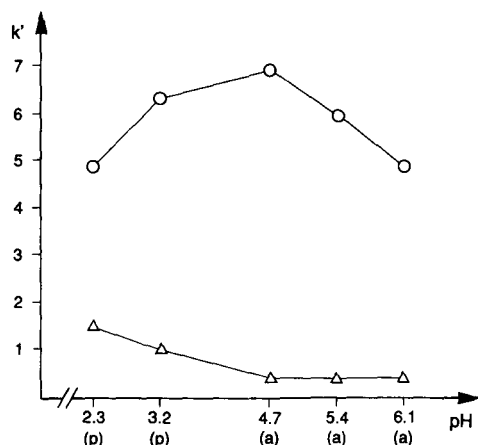


Fig. 4. Influence of pH on the capacity factors (k') of (○) ramipril and (△) ramiprilate. Mobile phase, 20% acetonitrile and 5% THF in (p) phosphate or (a) acetate buffer ($I=0.10$). Column temperature, 60°C. Stationary phase and flow-rate as in Fig. 1.

constants (pK_a) of about 3 and 5.5⁶, is zwitterionic with maximum retention in the pH region between the pK_a values. For ramiprilate, having a lowest pK_a of about 1.5 (ref. 6), no retention maximum was obtained under the chromatographic conditions used.

Organic modifier. The nature of the organic modifier in the mobile phase greatly affected the chromatographic performance of ramipril. This is shown in Fig. 5, where

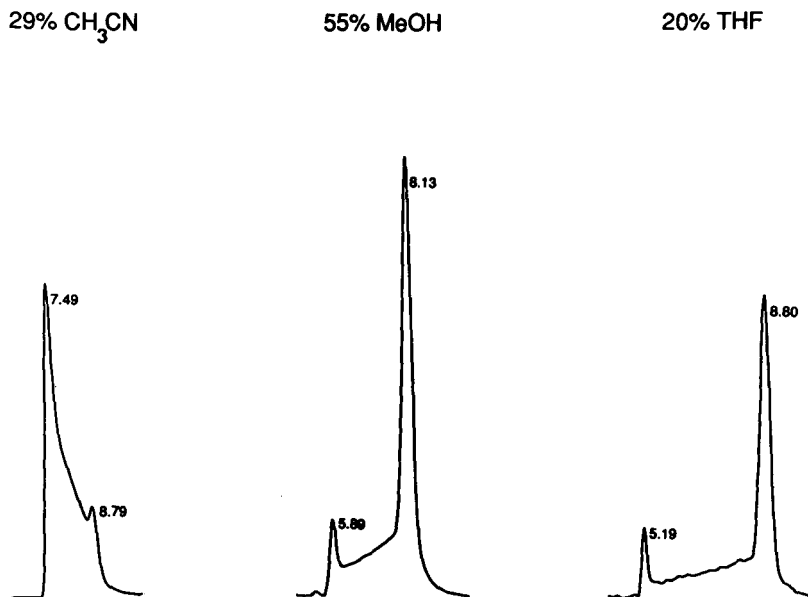


Fig. 5. Effect of organic modifier on the chromatography of ramipril. Mobile phase containing 29% acetonitrile, 55% methanol or 20% THF. Column temperature, 20°C. Other conditions as in Fig. 1. MeOH = Methanol.

acetonitrile, methanol or THF was used as a modifier in aqueous phosphate buffer. The column temperature was 20°C. Different amounts of the modifiers were added to the various systems in order to give comparable retention times. The elution order of the isomers was inverted in the chromatographic systems containing methanol and THF compared with the acetonitrile-containing system. This was verified by collecting fractions of the eluate containing the isomers of ramipril from the acetonitrile system and reinjecting them into the methanol and THF systems. The column was refrigerated at 2°C to give good resolution between the two peaks and the eluate fractions were immediately frozen to prevent transformations between the two conformers.

An improvement in the chromatography of ramipril was obtained by the addition of THF or methanol to a mobile phase containing acetonitrile. Ramipril eluted

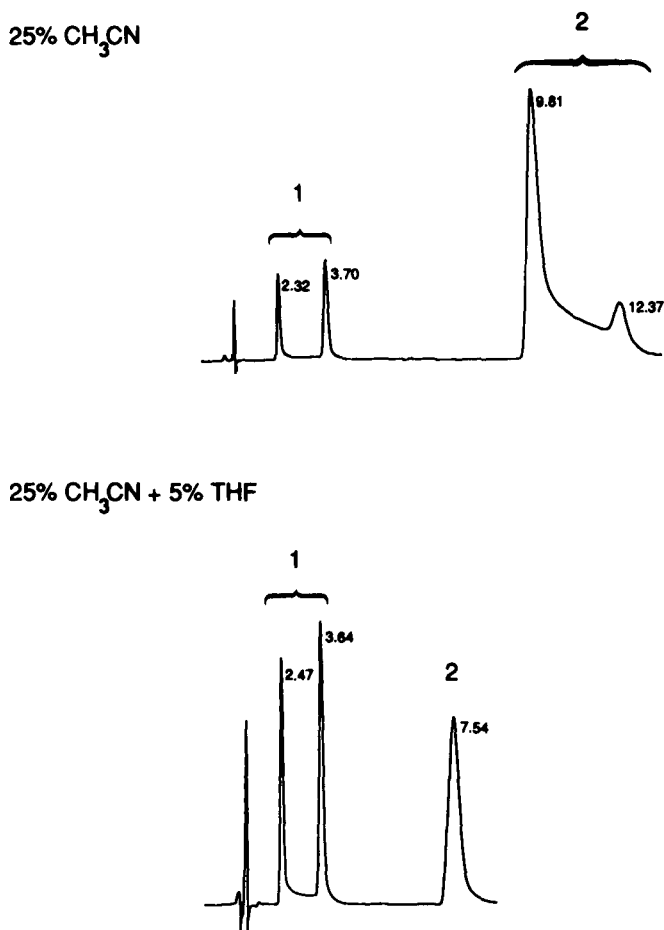


Fig. 6. Effect of addition of THF to an acetonitrile-containing system on the peak shapes of (1) ramiprilate and (2) ramipril. Mobile phase, 25% acetonitrile or 25% acetonitrile and 5% THF in phosphate buffer (pH 2.0) with a flow-rate of 1.5 or 1.0 ml/min, respectively. Column temperature, 15°C. Different attenuations were used.

as a single peak at 15°C when 5% THF was added to a mobile phase containing 25% acetonitrile, as illustrated in Fig. 6, which also shows a chromatogram obtained without THF. Ramiprilate was only slightly affected and eluted as a well resolved doublet in both systems.

Stationary phase. Chromatograms from a cation-exchange column (Nucleosil 5SA, 100 × 4.6 mm I.D.) and a C₁₈ column (see Experimental) obtained at 30 and 60°C are shown in Fig. 7. The mobile phase in both chromatographic systems was phosphate buffer (pH 2.0) with 30% acetonitrile. The numbers of theoretical plates (*N*) for the peaks obtained at 60°C are shown. The C₁₈ column was more efficient than the cation exchanger for ramipril, whereas ramiprilate showed the best performance on the cation-exchange column. The elution of ramipril as a bimodal, broad peak on the cation-exchange column at 30°C may be due to a difference in acidity for the *cis* and *trans* rotamers. Such a difference would affect the chromatography on the

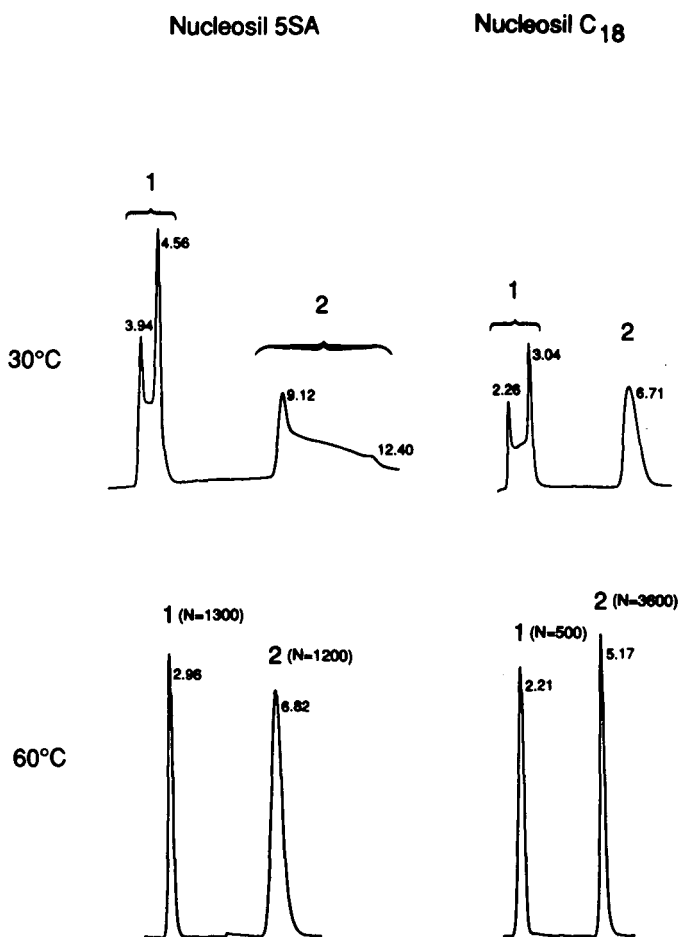


Fig. 7. Chromatograms of (1) ramiprilate and (2) ramipril from a cation-exchange column (Nucleosil 5SA, 100 × 4.6 mm I.D.) and a C₁₈ column (the same as in Fig. 1). Column temperature, 30 or 60°C. Other conditions as in Fig. 1. The numbers of theoretical plates (*N*) at 60°C are shown.

cation exchanger more than it would on the C_{18} column, from which a single peak was obtained. Different pK_a values for the isomers of some proline- and sarcosine-containing peptides have been determined by NMR^{9,10}. The results indicated intramolecular hydrogen bonding, which stabilizes the protonated *trans* isomer and decreases its acidity.

NMR studies

In Fig. 8, the ^1H NMR spectrum of ramiprilate in $[\text{}^2\text{H}_6]\text{DMSO}$ is shown. In the chemical shift range 3–4.6 ppm the spectrum exhibits two distinct sets of signals for each proton, which reveals the existence of two contributing conformers. These rotamers are assigned to the *cis-trans* equilibrium of the rotation around the amide bond. No assignment was made of signals in the region 1–3 ppm owing to difficulties with overlapping. 2D NMR studies clearly showed, however, that more than a single set of resonances contribute to the spectrum. The rotamer ratio in DMSO was integrated to be 65:35, which is similar to the ratio of the areas of the two peaks obtained after

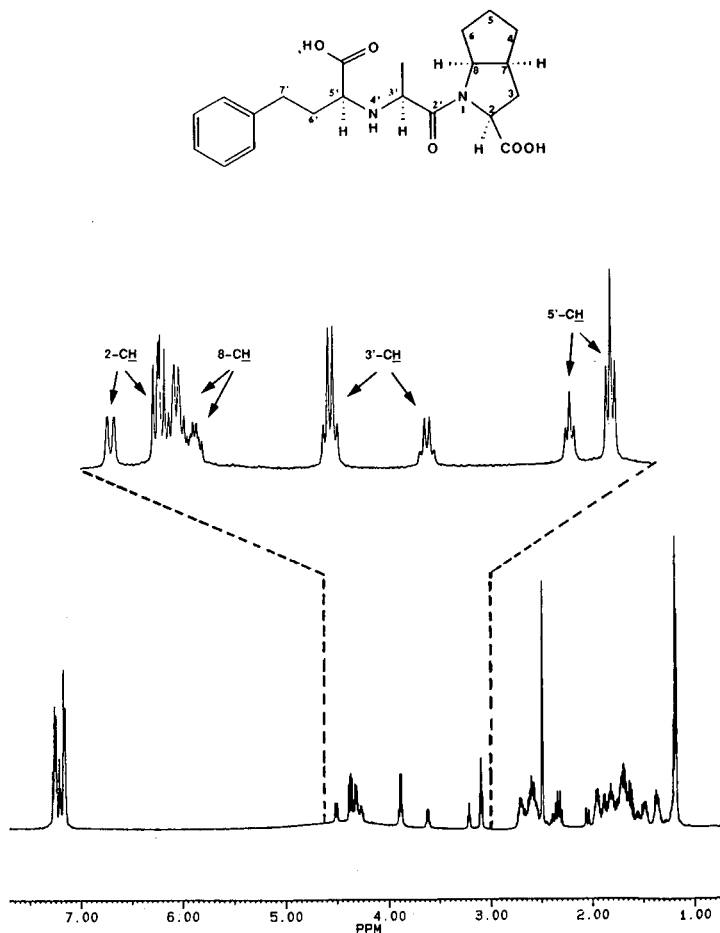


Fig. 8. ^1H NMR spectrum of ramiprilate (5 mg in 0.6 ml) in $[\text{}^2\text{H}_6]\text{DMSO}$.

injection of ramiprilate in DMSO into the refrigerated chromatographic system containing acetonitrile. In [$^2\text{H}_2$]water- $[\text{}^2\text{H}_3]$ acetonitrile the ratio was integrated to be 53:47, also in good agreement with chromatographic results. This confirms that the ratio of the two conformers, chromatographed on a cooled column, is entirely dependent on the sample conditions prior to injection. Based on the 2D NMR studies and on comparison with studies on related compounds⁷, the major rotamer was assigned to the *trans* form. At high temperature (95°C) the NMR spectra exhibited unambiguous exchange broadening. Line-shape analysis according to McConnell¹¹ gave a barrier for *trans* to *cis* rotation of 85 kJ/mol, which is of a magnitude that explains the peak splitting and band broadening seen in the chromatographic studies.

CONCLUSION

Various operating conditions greatly affected the anomalous chromatographic behaviour of the proline-containing substances ramipril and ramiprilate. The compounds eluted as increasingly monodisperse peaks with decreasing flow-rate, and with increasing column temperature single peaks were obtained. The peak shape of ramiprilate was improved when the pH was increased or if the reversed-phase column was replaced by a cation exchanger, while the opposite was found for ramipril. The elution order and the appearance of the isomers of ramipril were dependent on the nature of the organic modifier. By choosing appropriate conditions, the compounds were either eluted as single peaks or the isomers of each compound could be separated. The first-eluting isomer of ramiprilate in the chromatographic system containing acetonitrile was characterized by NMR studies as the *trans* rotamer.

ACKNOWLEDGEMENT

We are very grateful to Dr. Bengt-Arne Persson for his kind interest in this work and for valuable discussions on the manuscript.

REFERENCES

- 1 D. Perrett and P. L. Drury, *J. Liq. Chromatogr.*, 5 (1982) 97.
- 2 T. Kato, *Anal. Chim. Acta*, 175 (1985) 339.
- 3 L. Rusconi, G. Perseo, L. Franzoi and P. C. Montecucchi, *J. Chromatogr.*, 349 (1985) 117.
- 4 W. R. Melander, J. Jacobson and Cs. Horváth, *J. Chromatogr.*, 234 (1982) 269.
- 5 J. Jacobson, W. Melander, G. Vaisnys and Cs. Horváth, *J. Phys. Chem.*, 88 (1984) 4536.
- 6 T. Kuriki, H. Möller and V. Teetz (Hoechst), personal communication.
- 7 N. Platzer, J. P. Bouchet and J. P. Volland, *Magn. Reson. Chem.*, 26 (1988) 296.
- 8 S. Perlman and J. Kirschbaum, *J. Chromatogr.*, 206 (1981) 311.
- 9 C. A. Evans and D. L. Rabenstein, *J. Am. Chem. Soc.*, 96 (1974) 7312.
- 10 D. L. Rabenstein and A. A. Isab, *Anal. Chem.*, 54 (1982) 526.
- 11 H. M. McConnell, *J. Chem. Phys.*, 28 (1958) 430.

CHROMSYMP. 1747

Extension of the electrostatic retention model of reversed-phase ion-pair chromatography to include the simultaneous effects of the organic modifier and the pairing ion

AKOS BARTHA^a and GYULA VIGH*

Chemistry Department, Texas A&M University, College Station, TX 77843-3255 (U.S.A.)

and

JAN STÅHLBERG^b

Astra Pharmaceutical Production AB, Södertälje (Sweden)

SUMMARY

The electrostatic retention model of reversed-phase ion-pair chromatography is extended to include the simultaneous effects of the organic modifier and the pairing ion on both the adsorption of the pairing ion and the retention of charged solutes. A linear relationship is obtained between solute retention and the concentration of both the organic modifier and the pairing ion. Both the intercept and the slope values of the extended retention equation increase for the oppositely charged and decrease for the similarly charged solutes when a pairing ion is added to the eluent. The slope reflects the reversed-phase chromatographic retention of the solute and the solvent dependence of the adsorption term of the pairing ion. The intercept depends on the type of the organic modifier and both the concentration and hydrophobicity of the pairing ion. Qualitative and quantitative predictions made by the extended model agree well with the experimental results obtained with binary mixtures of aqueous buffers and three common organic modifiers, methanol, acetonitrile and tetrahydrofuran.

INTRODUCTION

In reversed-phase chromatography (RPC), the logarithm of the capacity factor (k') of non-ionic solutes is often described as a linear function of the concentration (φ) of the organic modifier in the eluent^{1,2}:

$$\ln k'(\varphi) = \ln k'_{wB} - S\varphi \quad (1)$$

where k'_{wB} is the capacity factor of solute B in water and S is a constant for a given

^a On leave from the University of Chemical Engineering, Veszprem, Hungary.

^b Affiliated to the Institute of Physical Chemistry, University of Uppsala, Uppsala, Sweden.

solute–solvent combination. Extensive retention data sets are available and have been analysed to determine the effects of type and/or strength of the organic solvent. Differences in the slopes (S) of the $\ln k'_{\text{vs.}} \varphi$ plots of closely related solutes have been utilized to optimize their separation.

In reversed-phase ion-pair chromatography (RP-IPC), mixtures of non-ionic, ionic and/or ionizable components are usually separated by varying the pH and/or the concentration of the pairing ion, while the concentration of the organic modifier is used only to control the solvent strength of the eluent. However, mixtures of ionic solutes with similar charge and structure often cannot be separated adequately without at least exploiting^{3–6} or, better, optimizing^{7–10} the selectivity-modifying effects of organic solvents.

In RP-IPC, the organic modifiers decrease the retention of ionic solutes through at least two effects, via the decreased hydrophobic adsorption of the solutes and the decreased surface concentration of the adsorbed ion-pairing reagent¹. As a result, in the presence of a pairing ion, the retention of ionic solutes varies more rapidly with φ than that of the uncharged solutes^{3,12}. Owing to the paucity of relevant data, the effects of the type and concentration of the organic modifier on the retention and selectivity changes of charged solutes have not yet been evaluated systematically in RP-IPC, and the current retention models of RP-IPC could not include the simultaneous effects of the pairing ion and the organic modifier.

Stahlberg and co-workers, using the Gouy–Chapman theory, developed an electrostatic model^{13–18} to describe both the adsorption isotherms of the pairing ions and the retention of ionic solutes as functions of the mobile phase concentration of the pairing ion. This model is extended in this paper to incorporate the effects of the type and concentration of the organic modifier into the adsorption isotherm equations of the pairing ions and the retention equations of charged solutes. Predictions made by the model are compared with experimental data obtained using methanol, acetonitrile and tetrahydrofuran as organic modifiers and sodium octylsulfonate and decylsulfonate as ion-pairing reagents.

THEORY

According to the electrostatic model of RP-IPC^{13–15}, the adsorbed hydrophobic pairing ions and their counter ions form an electrical double layer at the surface of the stationary phase and create a surface potential (ψ_0) between the surface of the stationary phase and the bulk of the mobile phase. The retention of ionic solutes depends both on their hydrophobicity and ψ_0 . The capacity factor (k'_{cB}) of ionic solute B of charge z_{B} is

$$k'_{\text{cB}} = k'_{\text{oB}} \exp(-z_{\text{B}} F\psi_0/RT) \quad (2)$$

where k'_{oB} is the capacity factor of solute B in the absence of a hydrophobic pairing ion, F is the Faraday constant, R is the gas constant and T is the absolute temperature.

When an organic modifier of concentration φ is added to the eluent, both k'_{oB} and ψ_0 change. In the absence of pairing ions, k'_{oB} varies with φ as

$$k'_{\text{oB}}(\varphi) = \Phi \exp[-\Delta G_{\text{B}}^0(\varphi)/RT] \quad (3)$$

where Φ is the phase ratio and ΔG_B^0 is the free energy of adsorption of solute B.

ψ_0 is related to the surface concentration, n_A , of the adsorbing hydrophobic pairing ion according to eqn. 4, obtained by solving the linearized Poisson–Boltzman equation for cylindrical surfaces (*i.e.*, idealized porous particles)^{14,15}:

$$\psi_0 = (z_A n_A F I_0) / (\kappa \epsilon_0 D_e I_1) \quad (4)$$

where z_A is the charge of pairing ion A, κ is the reciprocal Debye length, I_0 and I_1 are the modified Bessel functions of the first kind of order zero and one, respectively, ϵ_0 is the permittivity of vacuum and D_e is the dielectric constant of the eluent. When n_A is much lower than the monolayer capacity of the stationary phase, n_0 , the surface potential-modified adsorption isotherm of the pairing ion becomes

$$n_A = n_0 K_{As} c_A \exp(-z_A F \psi_0 / RT) \quad (5)$$

where K_{As} is the adsorption constant and c_A is the mobile phase concentration of the pairing ion. K_{As} depends on the type and concentration of the organic modifier:

$$K_{As} = \exp[-\Delta G_A^0(\varphi) / RT] \quad (6)$$

where $\Delta G_A^0(\varphi)$ is the free energy of adsorption of the pairing ion. With this, k'_{CB} as a function of c_A becomes

$$\frac{z_A}{z_B} \ln \left(\frac{k'_{CB}}{k'_{OB}} \right) + \ln \left[-\frac{RT}{z_A z_B F} \ln \left(\frac{k'_{CB}}{k'_{OB}} \right) \right] = \ln \left[\frac{I_0 F}{I_1 \kappa \epsilon_0 D_e} c_A \right] + \ln(n_0 K_{As}) \quad (7)$$

This expression is valid only for non-zero pairing ion concentrations.

In order to include the concentration of the organic modifier in eqn. 7, let us approximate the second term on the left-hand side as

$$\ln [\ln(k'_{CB}/k'_{OB})] \approx \ln(k'_{CB}/k'_{OB}) - 1 \quad (8)$$

The relative error of this approximation is less than 25% when $1.6 < k'_{CB}/k'_{OB} < 6$. A relative retention change of this magnitude corresponds to a pairing ion surface concentration change of 10–100 $\mu\text{mol/g}^{16}$, meaning that the expressions derived here are valid only at non-zero mobile phase concentrations and low surface concentrations of the pairing ion, and for a 2–6-fold relative change in solute retention. As such, they are considered first-order approximations which, nevertheless, reveal the relative significance of the different parameters in the control of solute retention and separation selectivity in RP-IPC.

For the sake of clarity, separate expressions are obtained for the oppositely charged ($k'_{CB} > k'_{OB}$) and the similarly charged ($k'_{CB} < k'_{OB}$) ionic solutes. When there is a unit charge of identical sign on both the pairing ion and the solute ion (*i.e.*, $z_A = z_B = \pm 1$), eqn. 7 can be rewritten (for $c_A > 0$) as

$$\ln k'_{CB} = \ln k'_{OB} - \frac{1}{2} \ln \left[\frac{I_0 F^2 \exp(1)}{I_1 \kappa \epsilon_0 D_e RT} c_A \right] - \frac{1}{2} \ln(n_0 K_{As}) \quad (9)$$

When there is a unit charge of opposite sign on both the pairing ion and the solute ion ($z_A = -z_B = \pm 1$), eqn. 7 can be rewritten (for $c_A > 0$) as

$$\ln k'_{cB} = \ln k'_{0B} + \frac{1}{2} \ln \left[\frac{I_0 F^2 \exp(1)}{I_1 \kappa \epsilon_0 D_c RT} c_A \right] - \frac{1}{2} \ln (n_0 K_{As}) \quad (10)$$

Both equations consist of three terms, the sum of which gives the retention of an ionic solute as a function of the mobile phase concentrations of both the pairing ion and the organic modifier. "Regular" RPC solute retention is decreased (eqn. 9) or increased (eqn. 10) by the addition of a pairing ion (second and third terms).

In order to evaluate eqns. 9 and 10, the dependence of their terms on the type and concentration of the organic modifier and the concentration of the pairing ion was studied. As the ionic strength of the mobile phase influences the coefficient of c_A in the second term, its value was kept constant throughout this study.

EXPERIMENTAL

The test solutes were obtained from Janssen (Beerse, Belgium). Sodium octylsulfonate (OctSO₃) and decylsulfonate (DecSO₃) were purchased from Merck (Darmstadt, F.R.G.). Distilled, deionized water, HPLC-grade organic solvents methanol (CH₃OH), acetonitrile (ACN), tetrahydrofuran (THF) and analytical-reagent grade buffer components were used for eluent preparation. The mobile phase concentration of the organic solvent was varied in the ranges 0–40% (v/v) for methanol, 0–28% (v/v) for ACN and 0–25% (v/v) for THF. The aqueous buffer (pH 2.1) contained 25 mM H₃PO₄, 25 mM NaH₂PO₄ and various concentrations of sodium bromide and sodium octylsulfonate (ion-pairing reagent). The inorganic counter ion (sodium) concentration was kept constant at 175 mM by varying the concentration ratio of sodium bromide and the pairing ion. ODS-Hypersil (5 μm) stationary phase (Shandon, Runcorn, U.K.) with a BET surface area of 173 m²/g (according to the manufacturer), was slurry packed into 120 × 4.6 mm I.D. stainless-steel columns. An LC 5560 liquid chromatograph, equipped with UV (254 nm) and refractive index (RI) detectors (all from Varian, Walnut Creek, CA, U.S.A.) and two Model 7010 six-port injection valves (Rheodyne, Cotati, CA, U.S.A.), was used. Columns were thermostated at 25°C. Both the breakthrough curves of the pairing ions (in order to determine their excess surface concentrations) and the capacity factors of the solutes could be determined by this system¹¹.

RESULTS AND DISCUSSION

Effects of the type and concentration of the organic modifier on the adsorption of the pairing ion

In Fig. 1, the surface concentration (n_A) of sodium octylsulfonate is plotted against the concentration of (a) methanol (0–40%), (b) ACN (0–28%) and (c) THF (0–25%) at constant eluent concentrations of the pairing ion ($c_A = 1, 2, \dots, 70$ mM). The plots are similar to those for tetrabutylammonium bromide¹¹: at a given c_A value, n_A decreases as the polarity of the solvent decreases (CH₃OH > ACN > THF).

In order to determine the value of the $n_0 K_{As}$ [(μmol/g)/mM] parameter of the

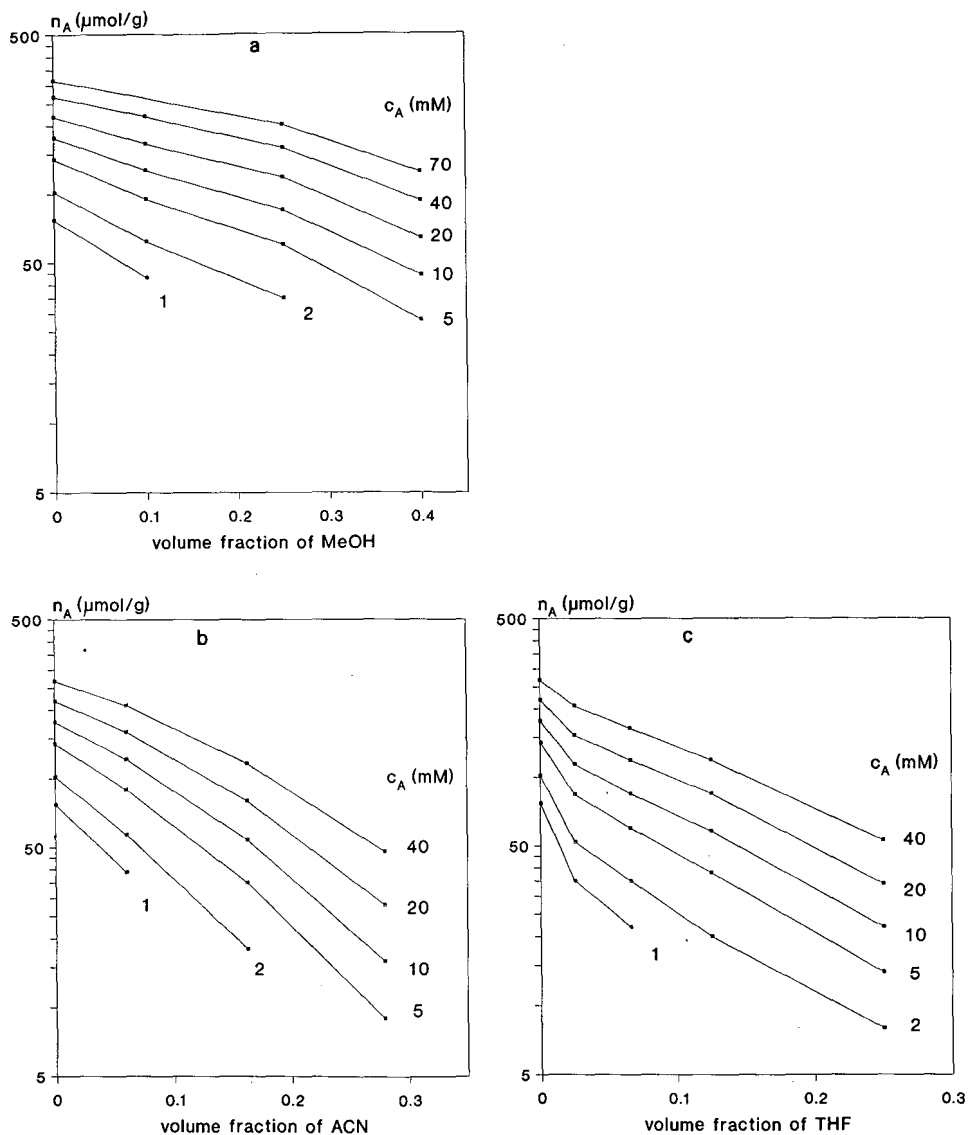


Fig. 1. Surface concentration (n_A , $\mu\text{mol/g}$) of sodium octylsulfonate as a function of the concentration of (a) methanol, (b) acetonitrile and (c) tetrahydrofuran at different eluent concentrations (c_A , mM) of the pairing ion. Aqueous buffer: pH 2.1, 25 mM H_3PO_4 , 25 mM NaH_2PO_4 , 150 mM constant ionic strength (maintained with NaBr). Stationary phase: ODS-Hypersil (5 μm). Column temperature: 25°C. MeOH = Methanol.

adsorption isotherm of sodium octylsulfonate (eqn. 5), the surface potential values were calculated from experimental retention data of ionic solutes as described in refs. 13–18. For improved precision, an average ψ_0 value, obtained with a positively and a negatively charged solute, was used in the calculations. The $\ln(n_0 K_{As})$ values

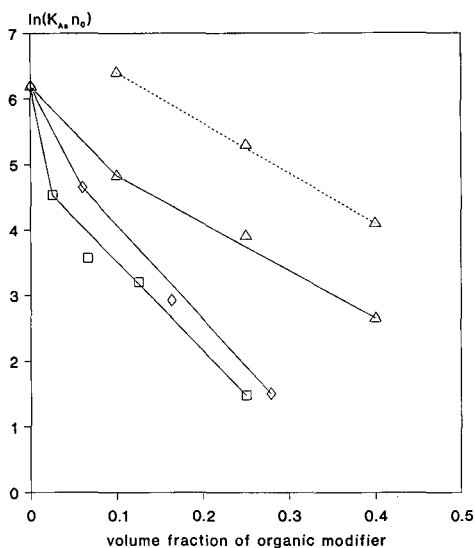


Fig. 2. The adsorption term $[\ln(n_0K_{As})]$ of sodium octyl- (solid lines) and decylsulfonate (dashed line) as a function of the (Δ) methanol, (\diamond) acetonitrile and (\square) tetrahydrofuran concentrations in the eluent. Conditions as in Fig. 1.

calculated from Fig. 1a–c and the ψ_0 values of octylsulfonate are plotted in Fig. 2 against φ for methanol, ACN and THF as organic modifier. Fig. 2 also contains data for sodium decylsulfonate as ion pairing reagent and methanol as modifier. The octyl- and decylsulfonate plots differ only in their intercepts, but not in their slopes.

After an initial, steep decrease in water-rich eluents, $\ln(n_0K_{As})$ decreases almost linearly with φ (over a limited concentration range), permitting the use of the following approximation (for $n_0K_{As} > 0$):

$$\ln(n_0K_{As}) = C - D\varphi \quad (11)$$

where C and D are constants for a given pairing ion–organic modifier combination. Coefficients C and D , calculated by linear regression from Fig. 2, are listed in Table I.

TABLE I

SLOPE (D) AND INTERCEPT (C) VALUES AND CORRELATION COEFFICIENTS (r) OF THE $\ln(n_0K_{As})$ vs. φ RELATIONSHIP FOR SODIUM OCTYLSULFONATE (OctSO₃) AND DECYLSULFONATE (DecSO₃) WITH METHANOL, ACN AND THF AS ORGANIC MODIFIERS

Modifier	φ	Pairing ion	C	D	r
CH ₃ OH	0.1–0.4	OctSO ₃	5.61	–7.26	0.996
CH ₃ OH	0.1–0.4	DecSO ₃	7.18	–7.66	0.999
ACN	0.06–0.28	OctSO ₃	5.42	–14.33	0.995
THF	0.02–0.13	OctSO ₃	4.69	–12.8	0.937

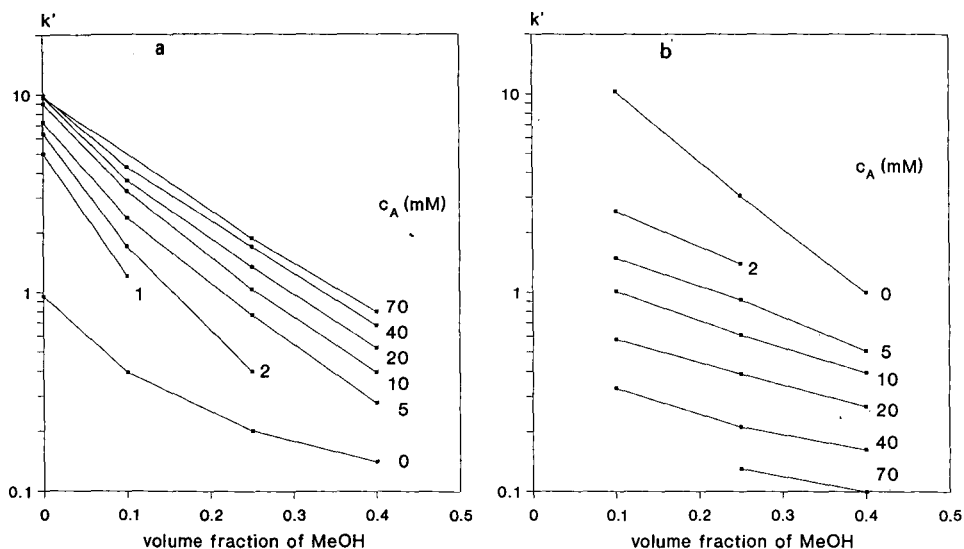


Fig. 3. Retention of the (a) octopamine and (b) 2-naphthalenesulfonate ions as a function of the methanol concentration of the eluent at $c_A = 0, 1, 2, \dots, 70$ mM concentration of sodium octylsulfonate.

Effects of the concentration of the organic modifier on the retention of charged solutes

In Fig. 3, the k' vs. φ data for the positively charged octopamine and negatively charged 2-naphthalenesulfonate ions are shown for octylsulfonate as pairing ion at $c_A = 0, 1, \dots, 70$ mM and methanol as organic modifier. Octopamine becomes more retained and 2-naphthalenesulfonate less retained in the presence of the pairing ion. The retention shifts are larger ($\Delta \ln k' \approx 1$) at low φ ($0 < \varphi < 0.1$), and smaller ($\Delta \ln k' \approx 0.6$) at larger φ ($0.1 < \varphi < 0.4$).

According to the electrostatic model of RP-IPC, these retention differences are related to the surface potential. ψ_0 , in turn, depends on both n_A and D_e (eqn. 4). As the organic modifier affects n_A , κ and D_e , and through them ψ_0 , plotting $\ln k'$ from Fig. 3 as a function of φ at constant n_A (determined from the adsorption isotherms in Fig. 1a-c) should reveal the relative roles of n_A and D_e . The retention plots shown in Fig. 4 are almost parallel, suggesting that solute retention depends primarily on the surface concentration of the hydrophobic pairing ion. The dielectric constant-related variations of k' , predicted by eqn. 4 (through κ and D_e), more or less compensate each other. Analysis of the analogous retention plots obtained with acetonitrile and tetrahydrofuran gave similar results.

Simultaneous effects of the pairing ion and the organic modifier on the retention of ionic solutes

The concentration of the organic modifier can be introduced into eqns. 9 and 10 as an explicit variable by noting that $\ln k'_{OB}$ is a linear function of φ (eqn. 1), $\ln(n_0 K_{AS})$ is a linear function of φ (eqn. 11) and the dielectric constant-related effects of the eluent largely cancel each other (Fig. 4), *i.e.*, the coefficient of c_A in eqns. 9 and 10 is constant (K_1).

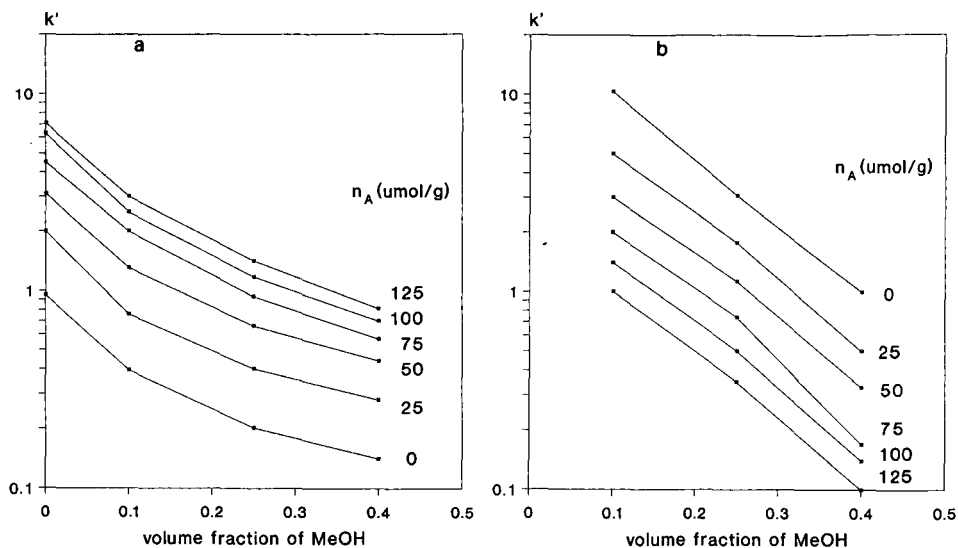


Fig. 4. Retention of (a) octopamine and (b) 2-naphthalenesulfonic acid as a function of the methanol concentration of the eluent at zero and constant ($n_A = 25, 50, \dots, 125 \mu\text{mol/g}$) stationary phase concentrations of sodium octylsulfonate.

Substitution of eqns. 1 and 11 into eqns. 9 and 10 results in

$$\ln k'_{cB} = (\ln k'_{wB} - S\varphi) - 1/2 \ln (K_1 c_A) - 1/2 (C - D\varphi) \quad (12)$$

for solutes and pairing ions with a unit charge of identical sign and

$$\ln k'_{cB} = (\ln k'_{wB} - S\varphi) + 1/2 \ln (K_1 c_A) + 1/2 (C - D\varphi) \quad (13)$$

for solutes and pairing ions with a unit charge of opposite sign. After rearrangement:

$$\ln k'_{cB} = \ln k'_{wB} - 1/2 \ln K_1 - 1/2 \ln [\exp(C)] - 1/2 \ln c_A - (S - 1/2 D)\varphi \quad (14)$$

when $z_A = z_B = \pm 1$, and

$$\ln k'_{cB} = \ln k'_{wB} + 1/2 \ln K_1 + 1/2 \ln [\exp(C)] + 1/2 \ln c_A + (S + 1/2 D)\varphi \quad (15)$$

when $z_A = -z_B = \pm 1$.

Obviously, eqns. 14 and 15 apply only for $c_A > 0$. When there is no pairing ion present, eqn. 1 must be used instead of eqns. 14 and 15. In agreement with experimental data⁸, both the intercept (first four terms) and slope (fifth term) of the $\ln k'$ vs. φ function decrease (for $z_A = z_B = \pm 1$) or increase (for $z_A = -z_B = \pm 1$) as pairing ion is added to the eluent.

The slope is independent of the concentration, but not of the hydrophobicity of the pairing ion. It is smaller by $1/2 D$ than the "regular" RPC slope (Eqn. 1) for $z_A = z_B$ and larger by $1/2 D$ for $z_A = -z_B$. The predicted slope values are compared with the

TABLE II
COMPARISON OF THE EXPERIMENTAL AND THE PREDICTED SLOPE VALUES OF THE $\ln k'$ VS. φ RELATIONSHIP FOR NEGATIVELY CHARGED, POSITIVELY CHARGED AND UNCHARGED SOLUTES

Eluents: 0 and 5 mM sodium octylsulfonate, $0.1 < \varphi_{\text{CH}_3\text{OH}} < 0.4$ ($D = -7.2$), $0.06 < \varphi_{\text{ACN}} < 0.28$ ($D = -14.4$), $0.02 < \varphi_{\text{THF}} < 0.13$ ($D = -12.8$).

Solute	$0.1 < \varphi_{\text{CH}_3\text{OH}} < 0.4$				$0.06 < \varphi_{\text{ACN}} < 0.28$				$0.02 < \varphi_{\text{THF}} < 0.13$			
	$c_A = 0 \text{ mM}$		$c_A = 5 \text{ mM}$		$c_A = 0 \text{ mM}$		$c_A = 5 \text{ mM}$		$c_A = 0 \text{ mM}$		$c_A = 5 \text{ mM}$	
	$-S_{\text{RP}}$	$-S_{\text{IPC}}$	Rel. difference (%)	Exp. Calc.	$-S_{\text{RP}}$	$-S_{\text{IPC}}$	Rel. difference (%)	Exp. Calc.	$-S_{\text{RP}}$	$-S_{\text{IPC}}$	Rel. difference (%)	Exp. Calc.
Phenol	4.6	4.5	-	-	6.8	6.3	-	-	2.3	2.2	-	-
2-Naphthalene-sulfonic acid	7.3	3.5	3.7	+ 6	14.6	8.1	7.4	- 9	12.5	6.7	6.1	- 10
Phenylalanine	6.1	10	9.7	- 3	12.9	18.5	20.1	+ 9	9.4	15.4	15.8	+ 3
Octopamine	4.7	8.2	8.3	+ 1	9.3	13.7	16.5	+ 20	6.7	11.3	13.1	+ 16
Tyrosine	6.7	10.2	10.3	+ 1	16.4	22.9	23.6	+ 3	17.9	22.6	24.3	+ 8
Norephedrine	4.9	10	8.5	- 15	8.2	15.9	15.4	- 3	-	-	-	-
Tryptophan	7.6	11.7	11.2	- 4	11.4	17.2	18.6	+ 7	-	-	-	-
Morphine	7.8	10.5	11.4	+ 9	-	-	-	-	-	-	-	-
Dopamine					15.1	19.6	22.3	+ 10	10.6	15.9	17	+ 7
Isoprenol									13.5	17	19.9	+ 17

TABLE III

D VALUES CALCULATED FROM THE RETENTION DATA FOR FIVE POSITIVELY CHARGED SOLUTES WHICH WERE OBTAINED WITHOUT AND WITH 1 mM SODIUM DECYLSULFONATE AS PAIRING ION IN $0.1 < \varphi_{\text{CH}_3\text{OH}} < 0.4$ AQUEOUS BUFFER ELUENTS (pH 2.1)

<i>Solute</i>	$c_A = 0 \text{ mM}$ – S_{RP}	$c_A = 1 \text{ mM}$ – S_{IPC}	<i>D</i>
<i>o</i> -Cresol	6.0	5.2	–
3,4-Dihydroxyphenylalanine	7.2	10.4	–6.4
Tyrosine	6.7	10.7	–8
Adrenaline	4.4	8.4	–8
Dopamine	5.6	10	–8.8
Phenylalanine	6.1	10.7	–9.2
Average			–8.1

experimental values in Table II for uncharged, positively charged and negatively charged solutes, with octylsulfonate as the pairing ion and methanol, ACN and THF as organic modifiers. The relative error between the predicted and experimental slope values varies between ± 1 and 20%, indicating that secondary effects (*e.g.*, changes in the nature of the octadecylsilica surface due to adsorption of the pairing ion) can also contribute significantly to solute retention.

Eqn. 14 or 15 can also be used to determine the value of *D* from solute retention data obtained in the absence and presence of pairing ions. The $\ln k'$ vs. $\varphi_{\text{CH}_3\text{OH}}$ values of five positively charged solutes obtained with and without decylsulfonate pairing ions were used to calculate the slope and *D* values listed in Table III. The average *D* value is –8.1, which agrees within 6% with *D* (–7.66) calculated from the adsorption data (Fig. 2).

It was reported¹⁹ that there are no large selectivity differences for closely related solutes when a pairing ion is replaced with a homologous one (*e.g.*, alkylsulfonates). This observation can be rationalized by Fig. 2 and eqns. 14 and 15: only coefficient *C*, but not coefficient *D* in eqn. 10 is changed when a pairing ion is replaced by a more hydrophobic member of the same homologous series (*D* = –7.26 for octylsulfonate and *D* = –7.66 for decylsulfonate).

According to eqns. 14 and 15, the intercept is a sum of four terms. The first, $\ln k'_{\text{wb}}$, depends only on the solute, the second, $\ln(K_1)$, depends only on the eluent, the third, $\ln[\exp(C)]$, depends on the type, but not the concentration of the pairing ion, and the fourth depends linearly on $\ln c_A$. Therefore the $\ln k'$ vs. $\ln c_A$ plots of a charged solute obtained with two different pairing ions (1 and 2) are parallel with a retention shift of

$$\Delta \ln k'_B(\varphi) = 1/2 (C_2 - C_1) + 1/2 (D_2 - D_1)\varphi \quad (16)$$

The shift is negative for $z_A = z_B = \pm 1$ and positive for $z_A = -z_B = \pm 1$.

These predictions are substantiated by the $\ln k'$ vs. c_A plots of the positively charged norephedrine and the negatively charged cresol red ions in Fig. 5 with octyl- and decylsulfonate as pairing ions and methanol as organic modifier ($\varphi_{\text{CH}_3\text{OH}} = 0.4$).

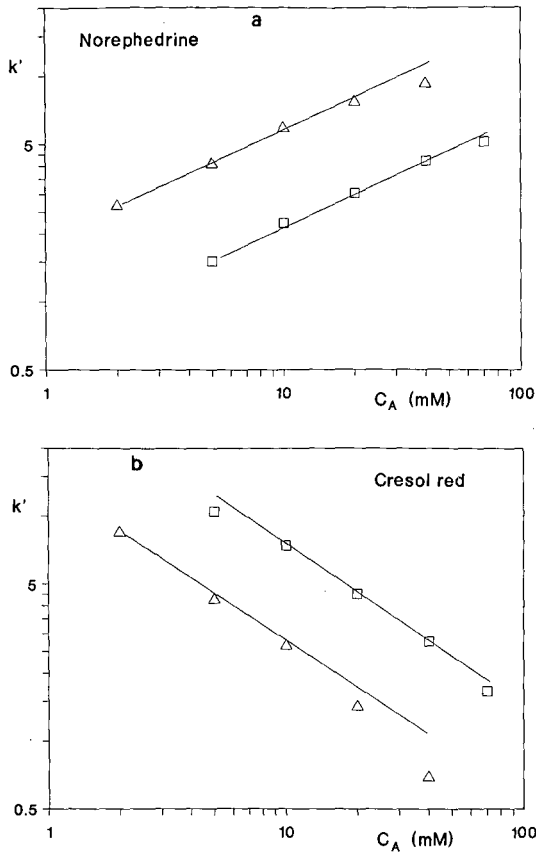


Fig. 5. Retention of (a) norephedrine and (b) cresol red as a function of the mobile phase concentration of the (\square) octylsulfonate and (Δ) decylsulfonate pairing ions in 40% methanol-aqueous phosphate buffer (pH 2.1) eluents.

These solutes were not included in the previous calculations of coefficients \hat{C} and D for the two pairing ions. The slope values are 0.45 for norephedrine and -0.65 for cresol red, both slightly different from the theoretical value of 0.5. The experimental $\Delta \ln k'$ is 0.97 for norephedrine and -1.02 for cresol red, again both slightly different from the theoretical value of 0.89 (calculated from Table I and eqn. 16). The deviations are believed to stem from the linearization of the rigorously non-linear equations, as discussed in ref. 14.

CONCLUSIONS

The electrostatic retention model of RP-IPC has been extended to account for the simultaneous effects of the pairing ion and the organic modifier on the retention of ionic solutes. Retention equations were derived assuming that the relative retention changes do not exceed the 2–6-fold range (*i.e.*, the surface concentration of the pairing ion is between 10 and 100 $\mu\text{mol/g}$), there is a linear relationship between $\ln k'$ of the

solute and the concentration of the organic modifier (for $\varphi < 0.4$) in the "regular" reversed-phase mode, there is a linear relationship between the adsorption term of the pairing ion and the concentration of the organic modifier (for $\varphi < 0.4$) and changes in the dielectric constant of the eluent do not influence the surface potential significantly.

According to the extended retention equation, both the slope and the intercept of the $\ln k'$ vs. φ relationship increase for oppositely charged solutes and decrease for similarly charged solutes when a pairing ion is added to the eluent. The slope depends on the original (reversed-phase) retention behavior of the solute and the organic solvent dependence of the adsorption term of the pairing ion. The intercept depends on the original (reversed-phase) retention of the solute in water, the type of the organic modifier and the hydrophobicity and the mobile phase concentration of the pairing ion. Predictions made by the extended equations agree well, both qualitatively and quantitatively, with experimental data observed with methanol, acetonitrile and tetrahydrofuran as organic modifiers and alkylsulfonates as pairing ions.

The extended retention model indicates that solvent strength effects depend not only on the organic modifier, but also on the charge type of the solutes and the adsorption characteristics of the pairing ion. The new retention equations can be used to determine the initial conditions of eluent optimization in reversed-phase ion-pair chromatography, provided that the charge-type and the "regular" reversed-phase retention behavior of the solutes are known.

ACKNOWLEDGEMENTS

Financial support by the Texas Coordinating Board of Higher Education TATR Program (Grant Number 3376) and the Office of International Coordination of Texas A and M University (International Enhancement Grant is) acknowledged.

REFERENCES

- 1 M. A. Quarry, R. L. Grob, L. R. Snyder, J. W. Dolan and M. P. Rigney, *J. Chromatogr.*, 384 (1987) 163.
- 2 L. R. Snyder, M. A. Quarry and J. L. Glajch, *Chromatographia*, 24 (1987) 33.
- 3 B. L. Karger, J. N. LePage and N. Tanaka, in Cs. Horvath (Editor), *High Performance Liquid Chromatography*, Vol. 1, Academic Press, New York, 1980, p. 185.
- 4 E. Tomlinson and C. E. Riley, in M. T. W. Hearn (Editor), *Ion-Pair Chromatography (Chromatographic Science Series, Vol. 31)*, Marcel Dekker, New York, 1984, pp. 101-111.
- 5 D. L. Reynolds, C. M. Riley, L. A. Sterson and A.J. Repta, *J. Pharm. Biomed. Anal.*, 1 (1983) 347.
- 6 R. B. Taylor, R. Reid and C. T. Hung, *J. Chromatogr.*, 316 (1984) 279.
- 7 A. P. Goldberg, E. Nowakowska, P. E. Antle and L. R. Snyder, *J. Chromatogr.*, 316 (1984) 241.
- 8 W. Lindberg, E. Johansson and K. Johansson, *J. Chromatogr.*, 211 (1981) 201.
- 9 B. Sachok, J. J. Stranahan and S. N. Deming, *Anal. Chem.*, 53 (1981) 70.
- 10 P. M. J. Coenegracht, N. V. Tuyen, H. J. Metting and P. M. J. Coenegracht-Lamers, *J. Chromatogr.*, 389 (1987) 351.
- 11 A. Bartha and Gy. Vigh, *J. Chromatogr.*, 260 (1983) 337.
- 12 A. Bartha and Gy. Vigh, *J. Chromatogr.*, 265 (1983) 171.
- 13 J. Stahlberg, *J. Chromatogr.*, 356 (1986) 231.
- 14 J. Stahlberg and A. Furangen, *Chromatographia*, 24 (1987) 783.
- 15 J. Stahlberg, *Chromatographia*, 24 (1987) 820.
- 16 J. Stahlberg and A. Bartha, *J. Chromatogr.*, 456 (1988) 253.
- 17 J. Stahlberg and I. Hagglund, *Anal. Chem.*, 60 (1988) 1958.
- 18 A. Bartha, Gy. Vigh and J. Stahlberg, *J. Chromatogr.*, 485 (1989) 403.
- 19 A. Bartha, Gy. Vigh, H. A. H. Billiet and L. de Galan, *J. Chromatogr.*, 303 (1984) 29.

Silanol effects in reversed-phase liquid chromatography

THOMAS WELSCH* and HARALD FRANK

Department of Chemistry, Analytical Centre, Karl Marx University, Talstrasse 35, Leipzig 7010 (G.D.R.)
and

GYULA VIGH

Chemistry Department, Texas A & M University, College Station, TX 77843 (U.S.A.)

SUMMARY

A large number of butyl-, hexyl-, octyl- and octadecylsilica stationary phases were synthesized by the usual low-temperature and also novel high-temperature silylation methods. The phases were characterized by measuring their silanol concentrations, organic functional group concentrations and wettabilities and, additionally, by reversed-phase liquid chromatographic retention measurements. Unusual retention data, not expected on the basis of the solvophobic retention theory, were observed and are explained. Separation selectivity and peak asymmetry are interpreted by taking into account the surface concentrations of both the silanol groups and the organic functional groups. The peak shape is better, but the separation selectivity is lower, when access to all silanol groups of a stationary phase is equally easy or equally difficult.

INTRODUCTION

Silica-based reversed-phase materials are the most frequently used high-performance liquid chromatographic (HPLC) stationary phases today. The reproducible production of reversed-phase silicas is still a challenge owing to our incomplete understanding of the relationships between the properties of the parent silica, the type and conditions of the derivatization reaction, the type and characteristics of the resulting surface and its chromatographic behaviour^{1–3}. As surface derivatization is never complete, one always has to consider the effects of the underivatized silanol groups, particularly their undesirable characteristics such as unpredictable retention order changes, tailing of certain polar solutes and low recovery rates of basic solutes^{1–5}.

It has been observed that end-capping with small silane reagents can eliminate some of the problems commonly attributed to the underivatized (or “residual”) silanol groups. For most reversed-phase silicas the true surface concentration of the unreacted silanol groups is unknown, and it is assumed to be equal to the difference between the original silanol concentration and the surface concentration of the bonded alkyl

groups. Often, in studies dealing with the effects of the residual silanol groups and seeking a correlation with the observed chromatographic behaviour the conclusions are based mainly on the surface concentration of the organic functional groups. Also, fairly often, end-capped and non-end-capped materials are compared directly⁶⁻¹⁰, resulting in limited, qualitative conclusions.

We have developed a high-temperature silylation process that allowed us to prepare reversed-phase materials on which the surface concentration of the organic functional groups is high and that of the residual silanol groups is low^{11,12}. Using both this and the "regular" low-temperature silylation method¹³, we were able to produce a large number of reversed-phase packing materials with different residual silanol group and organic functional group concentrations^{11,12,14}. These materials were used in this study, in which the influence of the silanol group concentration on solute retention, selectivity and peak shape were investigated for polar test solutes using methanol-water eluents. These studies complement our previous investigations of the same stationary phases with *n*-heptane as eluent¹⁵.

EXPERIMENTAL

Physico-chemical characterization of the silicas

The silica starting material and the reversed-phase packings synthesized from it were characterized by nitrogen adsorption (BET) surface area measurements (S_{BET}). Pore-size distribution and pore-volume data were derived from the S_{BET} values^{12,14}. Elemental analysis was used to determine the surface concentration of the organic functional groups (A_{C}). The reaction of methylolithium with silica¹⁶ was used to determine the surface concentration of the silanol groups (A_{OH})^{11,14,17}. As discussed previously¹⁷, the relative standard deviation of this method is 7% for Si 100 silica and 5% for RP-10 silica (five measurements).

Preparation of the stationary phases

The principles and reaction conditions of the high-temperature silylation method used for the preparation of some of the materials studied here are described elsewhere^{11,12,14}. All stationary phases were synthesized from a single batch of LiChrosorb Si 100 silica (Merck, Darmstadt, F.R.G.). This silica was selected because the pH of its aqueous slurry is nearly neutral^{18,19} and its surface is fully hydroxylated (see below).

To characterize the silica batch, its pH was measured by suspending 10 mg of silica in a mixture of 0.5 g of isopropanol and 0.5 g of 0.2 *M* aqueous potassium nitrate. The pH of the slurry¹¹ was 5.67. The specific surface area, S_{BET} , of the silica batch was 257 m²/g, and its pore volume, V_{p} , was 1.31 ml/g. Prior to silylation, LiChrosorb Si 100 was vacuum dried (0.2 Torr) at 180°C for 2 h to remove the physisorbed water. The silanol content of the dried material, A_{OH} , was determined to be 2250 $\mu\text{mol/g}$, which corresponds to a surface silanol concentration of 8.7 $\mu\text{mol/m}^2$, which agrees very well with results given in the literature for fully hydroxylated silicas^{13,20}.

The silylating reagents di-*n*-hexyltetramethyldisilazane (DHTMDS) and di-*n*-octadecyltetramethyldisilazane (DOTMDS) were synthesized in our laboratory^{11,14}. Their structure and purity were characterized by gas chromatography-mass spectrometry and NMR spectroscopy. The reagents contained a total of *ca.* 10% of the

corresponding silylamines and disiloxanes as by-products. Hexamethyldisilazane (HMDS) was obtained from Fluka (Buchs, Switzerland), and used as received. All other solutes and solvents were of analytical-reagent grade or better and were obtained locally from a number of sources. They were dried prior to use.

The preparation methods and some of the main characteristics of the reversed-phase materials studied are listed in Table I. RP silicas RP-6 I–III and RP-18 I–III were prepared by reacting the silica at room temperature with a *m*-xylene solution of the respective disilazane for 4–120 min. For 1 g of LiChrosorb Si 100, 40 ml of a 0.2 *M* solution of the disilazanes in *m*-xylene were applied. RP-6 IV and RP-18 IV were prepared by refluxing 5 g of LiChrosorb Si 100 in 200 ml of a 0.25 *M* disilazane solution in *m*-xylene for 12 h.

To achieve a very weak end-capping effect, materials RP-6 IV and RP-18 IV were allowed to stand at room temperature in HMDS solution (40 ml of 0.2 *M* HMDS in *m*-xylene for 1 g of RP silica) for 1 h, yielding materials RP-6 V and RP-18 V. The same procedure was applied overnight to RP-6 IV, resulting in material RP-6 VI.

To achieve more complete end-capping, RP-6 IV and RP-18 IV were refluxed at 139°C for 8 h in the HMDS solution, yielding materials RP-6 VII and RP-18 VII.

Materials RP-6 VIII–X and RP-18 VIII and IX were prepared by high-temperature silylation^{11,12,14}. These reactions were carried out in a thick-walled glass ampoule (15 cm × 2 cm I.D.). Disilazane (0.01 mol) was added to the tube and a filter-funnel holding 1 g silica was placed into the ampoule. The ampoule, cooled in dry-ice–acetone and kept in a vertical position, was flushed with dry nitrogen and flame-sealed. The ampoule was then placed vertically in a gas chromatographic oven and heated at a rate of 4°C/min to the final temperature and held there for 12–15 h. The final temperatures were 220°C for RP-6 VIII, 270°C for RP-6 IX, 320°C for RP-6 X and RP-18 X and 360°C for RP-6 XI and RP-18 XI. The ampoules were then slowly cooled to ambient temperature and opened.

All materials were washed by the same procedure, consisting of two rinses with 30 ml each of toluene, dichloromethane and acetone per gram of silica. Finally, the materials were dried under vacuum at 80°C for 4 h.

Wettability tests

The wettability of the reversed-phase materials in methanol–water mixtures was determined according to Engelhardt and Mathes²¹. A 100-mg amount of the stationary phase was mixed with 25 ml of water in an erlenmeyer flask. While shaking the flask, methanol was added dropwise to the slurry until the modified silica particles that floated on the surface had sunk to the bottom. At this point the surface tension of the liquid, σ_l , and the critical surface energy of the reversed-phase silica, σ_s , were considered to be equal. Based on experimental data²², a relationship was obtained between the composition of the liquid and its surface tension as:

$$\log \sigma_s = \log 166.3 - 0.406 \log [\% (v/v) \text{ methanol}] \quad (1)$$

where σ_s is in mN/m and the methanol concentration can vary between 15 and 85% (v/v). Although the critical surface energy values thus obtained may be subjectively biased, they nevertheless permit a reasonable comparison of the synthesized phases.

TABLE I
PREPARATION CONDITIONS AND MAIN CHARACTERISTICS OF THE REVERSED-PHASE MATERIALS USED

Phase symbol	Reaction conditions	RP-6			RP-18		
		α_c ($\mu\text{mol/g}$)	α_{OH} ($\mu\text{mol/g}$)	Wettability ^a	α_c ($\mu\text{mol/g}$)	α_{OH} ($\mu\text{mol/g}$)	Wettability ^a
I	Room temp., 4 min shaking	278	1784	25	126	1865	25
II	Room temp., 60 min shaking	305	1692	25	229	1722	25
III	Room temp., 120 min shaking	339	1463	41	277	1654	29
IV	Reflux in <i>m</i> -xylene, 12 h	790	1040	51	756	949	56
V	End-capping IV with HMDS at room temp., 1 h	714	989	48	764	826	57
VI	End-capping IV with HMDS at room temp., overnight	673	798	52	NP ^b	NP	NP
VII	End-capping IV with HMDS by refluxing at 139°C, 8 h	622	482	53	743	528	59
VIII	High-temp. silylation at 220°C	971	421	53	NP	NP	NP
IX	High-temp. silylation at 270°C	995	264	57	NP	NP	NP
X	High-temp. silylation at 320°C	830	190	57	582	377	64
XI	High-temp. silylation at 360°C	1013	155	59	512	275	63

^a Wettability: methanol (% v/v) in aqueous eluent required to wet the phase.

^b NP = Not produced.

Chromatographic measurements

The reversed-phase materials were slurry packed into 4 and 1.2 mm I.D. stainless-steel columns of different lengths²³. Most of the measurements were carried out with a liquid chromatograph assembled from commercially available parts: an L5000 gradient unit, an L655A12 pump, an L655A22 UV detector and D2000 integrator (all from Merck-Hitachi, Darmstadt, F.R.G.). Capacity factor measurements were made in the elution mode using 50 nM sample solutions. All columns were carefully thermostated²³ at 23°C. The retention data used here are the averages of several duplicate determinations (minimum five). Only retention data with less than a 1% relative standard deviation are used throughout the paper. The column dead volume was determined with deuterium oxide. Peak asymmetries were calculated from peak-width measurements at 15% of the peak height using the equation

$$As = 100 b_{15}/a_{15} \quad (2)$$

where a_{15} and b_{15} are the distances between the peak apex and the ascending and descending parts of the peak, respectively.

RESULTS AND DISCUSSION

Retention vs. surface composition relationships

Two RP-6 stationary phases, RP-6 IV and RP-6 X, which have nearly identical organic group concentrations but very different unreacted silanol concentrations (see Table I), were selected for the retention studies. The capacity factors of benzene, phenol and hydroquinone as a function of the methanol concentration of the eluent are shown in Fig. 1. The capacity factors of two crown ethers, 18-crown-6 and 12-crown-4, are shown in Fig. 2.

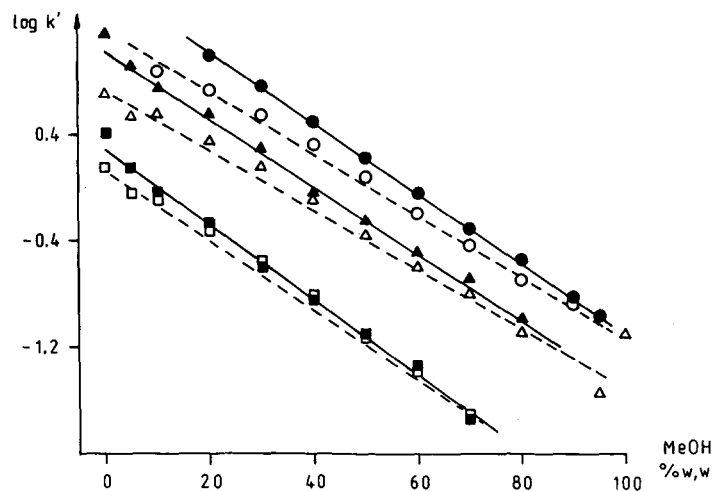


Fig. 1. Log k' as a function of the eluent composition on RP-6 reversed-phase silicas. Open symbols, $A_C = 790 \mu\text{mol/g}$, $A_{OH} = 1040 \mu\text{mol/g}$; full symbols, $A_C = 830 \mu\text{mol/g}$, $A_{OH} = 190 \mu\text{mol/g}$. \circ , \bullet = Benzene; \triangle , \blacktriangle = phenol; \square , \blacksquare = hydroquinone. MeOH = Methanol.

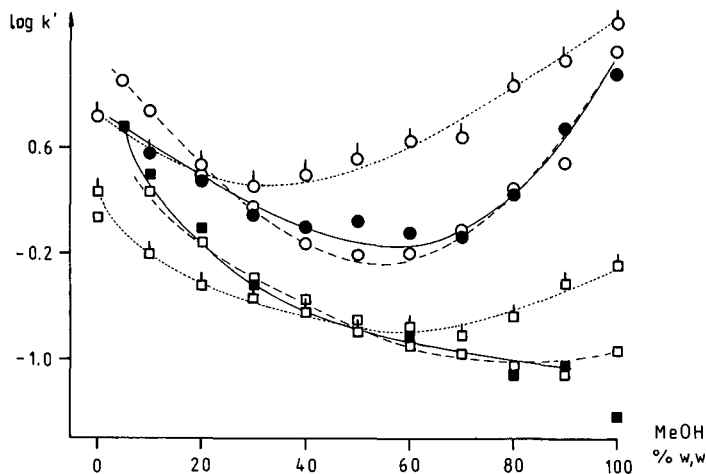


Fig. 2. $\log k'$ as a function of the eluent composition for (○, ●) 18-crown-6 and (□, ■) 12-crown-4. Dotted lines, parent silica; broken lines, RP-6 IV; full lines, RP-6 X.

The two classes of solutes show very different retention behaviours. In Fig. 1 the $\log k'$ values of all solutes decrease linearly with increasing methanol concentration in the eluent. As the polarity and water solubility of the solutes decrease from that of hydroquinone to benzene, the solute retention increases. The slope of the lines is slightly lower for the silanol-rich material. This behaviour is adequately explained by the simple solvophobic retention theory of Horváth *et al.*²⁴.

However, the $\log k'$ vs. methanol concentration curves shown in Fig. 2 are non-linear. To account for such a behaviour, Horváth and co-workers^{5,25} introduced the "dual retention mechanism" concept. The measured k' values, which passed through a minimum as a function of the water concentration of the eluent, were perceived to represent the sum of the hydrophobic capacity factor contribution and the hydrophilic capacity factor contribution.

The $\log k'$ of 18-crown-6 has an unequivocal minimum point, whereas the $\log k'$ vs. methanol concentration relationship for 12-crown-4 is merely curved. It is interesting that the retention curves are nearly identical on both the silanol-rich and the silanol-poor reversed-phase materials. The small retention differences cannot be explained solely by Horváth and co-workers' dual retention mechanism model, because the silanol concentrations (A_{OH} values) are very different, being 1040 and 190 $\mu\text{mol/g}$, respectively. This means that the crown ethers also behave as do the weakly polar solutes shown in Fig. 1, and cannot very well sense the large differences in the silanol concentration of the surface.

The non-linear retention behaviour must be caused by at least one other effect, such as the solvation (and conformational) changes of the crown ethers in the liquid phase that are induced by changes in the methanol concentration. This hypothesis may perhaps be substantiated by the observed proton NMR shifts of crown ethers in deuterium oxide-perdeuterated methanol mixtures. The chemical shift of the proton signal of 18-crown-6 varies almost linearly with the methanol concentration; it moves from 3.55 ppm in pure perdeuterated methanol to 3.97 ppm in pure deuterium oxide.

These shifts indicate that indeed there is a conformational change. This conformational change in turn might affect the retention of these solutes, and explain the observed retention curves.

In a previous paper¹¹ we described the irregular retention behaviour of aniline and pyridine on two RP-6 stationary phases with different silanol group concentrations. Maximum curves were observed for the basic solutes. In order to discuss here these effects in detail, the k' values of aniline, pyridine and benzene are plotted as a function of the methanol concentration in Fig. 3. The $\log k'$ values of all three solutes decrease with increasing methanol concentration. However, reproducible retention irregularities can be observed in the 50–80% methanol concentration range for pyridine and aniline. These irregularities cannot be explained by the current forms of either the solvophobic retention theory²⁴ or the dual retention mechanism model^{5,25}. On the silanol-rich RP-6 IV material ($A_{OH} = 1040 \mu\text{mol/g}$) pyridine shows two local maxima, the first centred around 55% and the second around 68% methanol. These maxima are slightly shifted towards higher methanol concentrations on the RP-6 X material, which has a lower silanol concentration ($A_{OH} = 190 \mu\text{mol/g}$).

Our explanation for this irregular retention behaviour is based on the dynamic surface models^{26–29}, especially on that of Nikolov²⁹. These models stipulate that the surface of the reversed-phase material is not wetted when the water concentration of the eluent is high. The bonded organic groups “fold up” in these eluents and form a dense layer which is more or less impenetrable to the eluent constituents and the solutes. The hydrophobic-dispersive interactions between the solutes and the stationary phase occur at the surface of this folded ligand layer. As the methanol concentration is increased, the surface becomes wetted. Once wetted, both the solvent and the solute molecules can penetrate the ligand layer and interact with the bulk of the organic groups. Simultaneously, the previously shielded silanol groups become

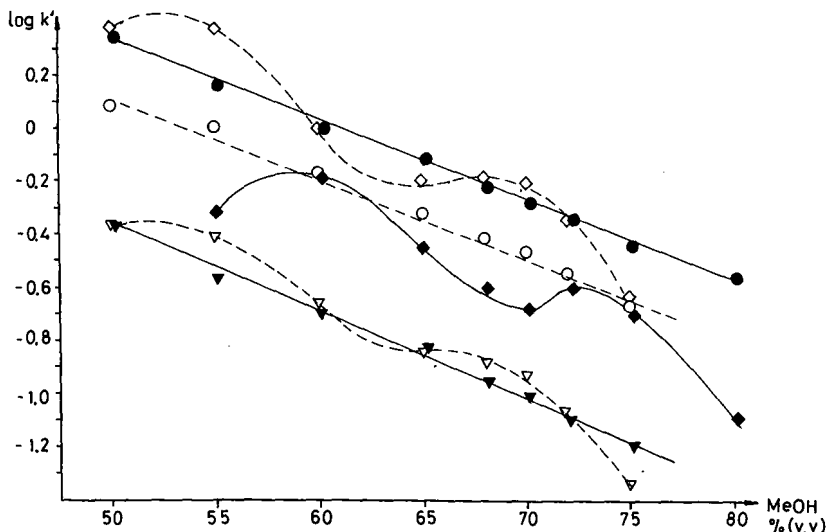


Fig. 3. $\log k'$ as a function of the eluent composition for (○, ●) benzene, (◇, ◆) pyridine and (▽, ▼) aniline. Broken lines, RP-6 IV; full lines, RP-6 X.

accessible and begin to contribute to the retention of the basic solutes, but not to the retention of benzene. As the methanol concentration is increased even further, a point is reached where all ligands become fully solvated, allowing full interaction with the silanol groups.

In order to support this interpretation of the experimental results, the wettabilities of the reversed-phase materials were determined. RP-6 IV, which has a high silanol concentration, is wetted by 51% methanol, whereas RP-6 X, which has a low silanol concentration, is wetted only at the 57% methanol concentration level (Table I). These values agree well with the points where k' begins to increase towards the first maximum shown in Fig. 3. Obviously, on the silanol-rich material the critical surface energy and the surface tension of the solvent mixture become numerically equal at lower methanol concentrations. This also explains why the position of the first k' maximum of pyridine is shifted towards higher methanol concentrations on the RP-6 X material: this phase contains fewer silanol groups and only eluents with higher methanol concentrations will wet it. The retention changes are so large that they result in retention order reversals for the benzene-pyridine peak pair. This observation is in agreement with the results of Engelhardt *et al.*³⁰, who reported that separation selectivities for the amines in general change strikingly when the composition of the eluent becomes equal to the composition of the methanol-water mixture which wets the reversed-phase material. The wettability data in Table I indicate that although the surface concentrations of the organic functional groups are similar on two reversed-phase materials, their wettabilities and hydrophobicities vary greatly with their actual silanol concentrations. When both the silanol and the organic functional group concentrations are comparable, the longer chains (C_{18}) require a higher methanol concentration for proper wetting.

Following Fowkes' treatment³¹, the surface energy of solids can be split into dispersive and polar parts:

$$\sigma_s = \sigma_s^d + \sigma_s^p \quad (3)$$

where σ_s is obtained from the wettability test and eqn. 1. The σ_s^d values can be approximated by the tabulated surface tension values of the analogous n -alkanes²², then the polar part, σ_s^p , can be calculated by eqn. 3. The calculated σ_s^d and σ_s^p values for the RP-6 IV and RP-18 IV phases are given in Table II. The polar part is much lower for the RP-18 IV phase, indicating that the longer chains have stronger shielding effects and that the influence of silanols is more pronounced when the stationary phase contains a shorter alkyl group. The apparent contradiction, which arises from the fact

TABLE II

SURFACE ENERGIES (mN/m) OF AN RP-6 AND AN RP-18 SILICA

Total surface energy, σ_s , of RP-6 and RP-18 silica divided into dispersive, σ_s^d and polar, σ_s^p parts.

Material	σ_s	σ_s^d	σ_s^p
RP-6	33	20	13
RP-18	32	28	4

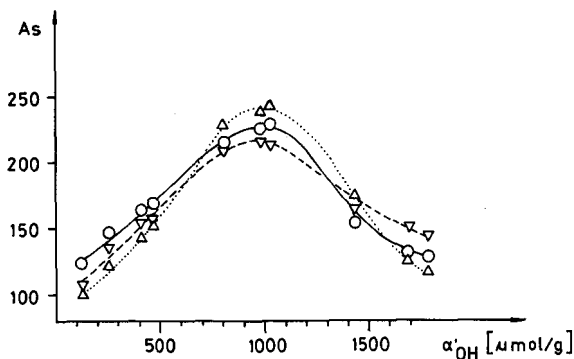


Fig. 4. Peak asymmetry as a function of the surface concentration of the silanol groups, A_{OH} , on RP-6 materials. For phase designations see Experimental. \circ = Benzyl alcohol; ∇ = phenol; \triangle = aniline. Mobile phase: methanol-water (65:35, w/w).

that in *n*-heptane eluents the shielding effect does not become stronger as the length of the alkyl chain is increased past the butyl group, can be resolved by noting that in *n*-alkane solvents the long alkyl chains are completely solvated and can move more freely.

Peak shape vs. surface composition of the alkylsilica stationary phase

As the unreacted silanol groups have been blamed for most of the undesirable effects on reversed-phase silicas, several attempts were made to eliminate them either by the use of special silane reagents², by end-capping with trimethylchlorosilane and/or HMDS or, occasionally, by adding polar masking agent to the eluent. However, a correct interpretation of the results was hampered by the fact that in most instances the actual silanol concentration of the phase was not known and quantitative correlations could not be obtained.

As we always determined the actual silanol concentration of each stationary phase by the methyllithium method (see Experimental), the peak shape and peak asymmetry data could be quantitatively correlated with the surface composition data. The asymmetry factors for the RP-6 and RP-18 phases are shown in Figs. 4 and 5,

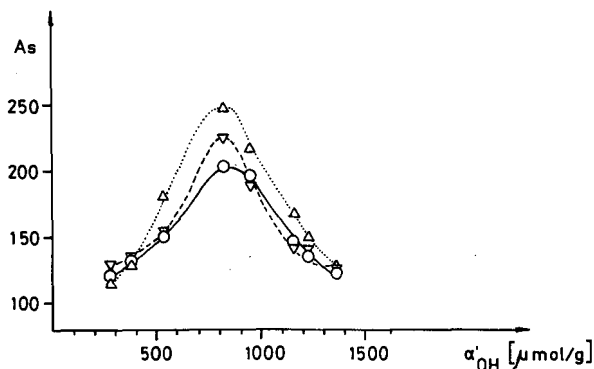


Fig. 5. Peak asymmetry as a function of the surface concentration of the silanol groups, A_{OH} , on RP-18 materials. For phase designation see Experimental. Symbols and mobile phase as in Fig. 4.

respectively. It is obvious that contrary to widely held beliefs, the asymmetry curves show a maximum when the silanol concentrations of the stationary phases are in the intermediate range (700–1100 $\mu\text{mol/g}$). These intermediate silanol concentrations are typical of the RP silicas that are produced under conditions widely accepted as optimum¹³.

As the alkyl group is changed from butyl to octadecyl, the maximum curve becomes sharper (it is spread over a narrower A_{OH} range)³². This explains why end-capping has such a large influence on the peak shape on octadecylsilicas without affecting appreciably the carbon content of the phase^{6–10}. It can be seen from Fig. 5 that the peak shape is excellent when the reversed-phase silica is deliberately incompletely derivatized (type I and II phases), a phenomenon noted, although quantitatively not explained, by Bidlingmeyer *et al.*³³ and Miller *et al.*³⁴. The peak asymmetry is worse on the regularly silylated RP-18 silicas that have a higher percentage of their silanol groups derivatized (type IV phases). Asymmetry, ironically, deteriorates even further as the material is treated with HMDS (type V material). Only when the silanol concentration is greatly reduced by drastic end-capping (type VII material) does the peak shape improve.

Very low silanol concentrations (type IX–XI materials) can only be achieved by high-temperature silylation^{11–13}. The peak asymmetries observed on these materials are as good as those on the silanol-rich materials. These findings imply that if one uses the dense monolayer-covered, commercially available RP-18 silicas, one must be willing to accept more or less severe peak asymmetry, which can be decreased only when appropriate masking agents are added to the eluents.

These findings also support the idea that it is not the absolute concentration of the silanol groups but rather their partially hindered accessibility that leads to, and controls, peak asymmetry².

Separation selectivity vs. surface composition of the alkylsilica stationary phase

The surface silanol groups of the alkylsilica stationary phases can, on the other hand, play a useful role as far as separation selectivity is concerned. In order to elucidate these effects, the relative retention values, r , with respect to benzene, of a number of polar solutes were determined on the different RP-6 phases. The representative results obtained with simple, strongly polar functional groups are shown in Fig. 6. Both the A_{OH} and the A_{C} values of the phases are shown on the horizontal axis. It can be seen that the most rapid change in selectivity occurs at intermediate silanol concentrations, in the 600–1000 $\mu\text{mol/g}$ range. (In the low to moderate silanol group concentration range, benzonitrile is an especially sensitive probe towards small changes in the silanol group concentration.)

Owing to the presence of fundamentally similar adsorption sites on the very hydrophobic stationary phases, the selectivity effects that are related to the polar functional groups of the solutes are mostly lost. On the silanol-rich materials the retention of all kinds of solutes is low. Only appropriate chemical modification of the surface, resulting in the presence of more than one type of adsorption site, can change both the topology and the adsorption energy distribution of the surface^{35–37} and result in a large polar separation selectivity. This, unfortunately, will also effect the peak asymmetry values.

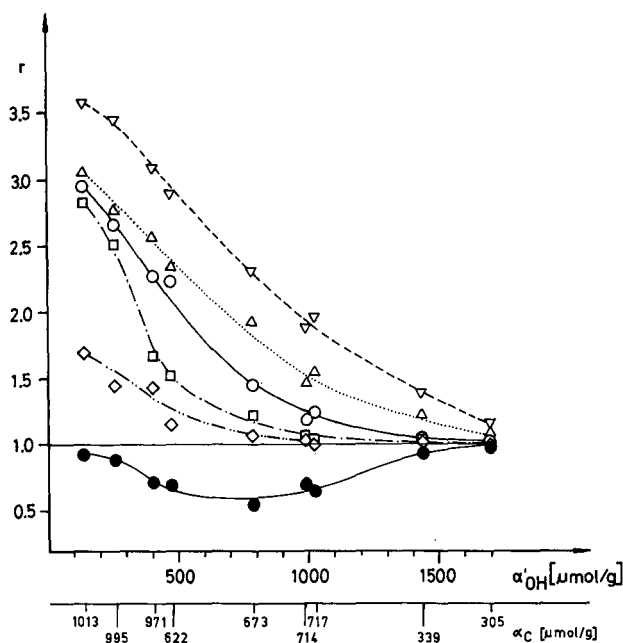


Fig. 6. Relative solute retention with respect to benzene as a function of A_{OH} and A_C . ∇ = Aniline; Δ = phenol; \circ = benzyl alcohol; \square = benzonitrile; \diamond = nitrobenzene; \bullet = butyrophenone. Mobile phase: methanol-water (65:35, w/w).

CONCLUSIONS

Unusual solute retention, peak asymmetry and separation selectivity were correlated with the silanol and organic functional group concentrations of a series of reversed-phase silicas produced by both the usual and high-temperature silylation methods. It was shown that single parameters, such as the concentration of either the organic functional groups or the silanol groups of the silica, are insufficient to account for most of the trends. Compositional and dynamic factors both have to be considered simultaneously if a more complete understanding of the nature of reversed-phase silicas is desired, as subtle interactions between solutes and eluents, such as with crown ethers, might significantly influence the observed chromatographic behaviour.

ACKNOWLEDGEMENTS

Financial support by the Texas Coordination Board of Higher Education TATR Program (Grant Number 3376) is acknowledged. The authors are grateful to E. Merck (Darmstadt, F.R.G.) for the loan of the liquid chromatograph used in part of this study.

REFERENCES

- 1 L. C. Sander and S. A. Wise, *J. Chromatogr.*, 316 (1984) 163; and references cited therein.
- 2 J. Nawrocki and B. Buszewski, *J. Chromatogr.*, 449 (1988) 25; and references cited therein.
- 3 L. C. Sander, *J. Chromatogr. Sci.*, 26 (1988) 318; and references cited therein.
- 4 N. H. C. Cooke and K. Olsen, *J. Chromatogr. Sci.*, 18 (1980) 512.
- 5 K. E. Bij, Cs. Horváth, W. R. Melander and A. Nahum, *J. Chromatogr.*, 203 (1981) 53.
- 6 N. Tanaka, H. Goodell and B. L. Karger, *J. Chromatogr.*, 158 (1978) 233.
- 7 C. Dewaele, P. Mussche and M. Verzele, *J. High Resolut. Chromatogr. Chromatogr. Commun.*, 5 (1982) 616.
- 8 M. Zakaria and P. R. Brown, *J. Chromatogr.*, 255 (1983) 151.
- 9 W. Cheng and M. McCown, *J. Chromatogr.*, 318 (1985) 173.
- 10 J. Yamaguchi, T. Hanai and H. Cai, *J. Chromatogr.*, 441 (1988) 183.
- 11 T. Welsch and H. Frank, *J. Chromatogr.*, 267 (1983) 39.
- 12 T. Welsch and H. Frank, *J. High Resolut. Chromatogr. Chromatogr. Commun.*, 8 (1985) 709.
- 13 K. K. Unger, *Porous Silica*, Elsevier, Amsterdam, 1979.
- 14 H. Frank, *Ph.D. Thesis*, Karl Marx University, Leipzig, 1985.
- 15 T. Welsch, H. Frank, H. Zwanziger, S. Liebisch and W. Engewald, *Chromatographia*, 19 (1984) 457.
- 16 K. K. Unger and E. Gallei, *Kolloid-Z. Z. Polym.*, 237 (1970) 358.
- 17 T. Welsch and H. Frank, *J. Prakt. Chem.*, 325 (1983) 325.
- 18 H. Engelhardt and H. Muller, *J. Chromatogr.*, 218 (1981) 395.
- 19 S. H. Hansen, P. Helboe and M. Thomsen, *J. Chromatogr.*, 368 (1986) 39.
- 20 Gy. Foti and E. sz. Kováts, *Langmuir*, 5 (1989) 232; and references cited therein.
- 21 H. Engelhardt and D. Mathes, *J. Chromatogr.*, 142 (1977) 311.
- 22 *Landolt-Bornstein, Zahlenwerte aus Physik, Chemie, Astronomie, Geophysik und Technik*, Vol. 2, Part 3, Springer, Berlin, Göttingen, Heidelberg, 1964, p. 421.
- 23 H. Frank and T. Welsch, *Wiss. Z. Karl-Marx-Univ. Leipzig, Math. Naturwiss. Reihe*, 35 (1986) 39.
- 24 Cs. Horváth, W. Melander and I. Molnar, *J. Chromatogr.*, 125 (1976) 129.
- 25 A. Nahum and Cs. Horváth, *J. Chromatogr.*, 203 (1981) 65.
- 26 R. K. Gilpin and J. A. Squires, *J. Chromatogr. Sci.*, 19 (1981) 195.
- 27 L. C. Sander, J. B. Callis and L. R. Field, *Anal. Chem.*, 55 (1983) 1068.
- 28 S. S. Yang and R. K. Gilpin, *J. Chromatogr.*, 394 (1987) 295.
- 29 R. N. Nikolov, *J. Chromatogr.*, 286 (1984) 147.
- 30 H. Engelhardt, B. Dreyer and H. Schmidt, *Chromatographia*, 16 (1983) 11.
- 31 F. M. Fowkes, in S. Ross (Editor), *Chemistry and Physics of Interfaces*, American Chemical Society, Washington, DC, 1971, pp. 96-132.
- 32 H. Frank and T. Welsch, unpublished results.
- 33 B. A. Bidlingmeyer, J. K. Del Rios and J. Korpi, *Anal. Chem.*, 55 (1983) 1344.
- 34 M. L. Miller, R. W. Linton, S. G. Bush and J. W. Jorgenson, *Anal. Chem.*, 56 (1984) 2204.
- 35 C. J. Giddings, *Anal. Chem.*, 35 (1963) 1999.
- 36 R. Leboda, A. Waksmundzki and S. Sokolowski, *J. Chromatogr.*, 124 (1976) 60.
- 37 R. Leboda, *Chem. Anal. (Warsaw)*, 26 (1981) 999.

Reversed-phase high-performance liquid chromatography in the investigation of the hydrophobicity of selected ketones

ANDRZEJ SIWEK and JÓZEF ŚLIWIOK*

Institute of Chemistry, Silesian University, Szkolna 9, 40-006 Katowice (Poland)

SUMMARY

Reversed-phase high-performance liquid chromatography was used to compare the hydrophobicities of ketones, the capacity factor, which was determined by extrapolation to 100% water in the mobile phase, being applied as the hydrophobic parameter. Different methods (linear, quadratic and exponential) of performing the extrapolation were compared. The chromatographic data obtained were compared with the solubilities in water, the topological indexes, the partition coefficients calculated on the basis of Rekker fragmentary constants and the electron density, which was calculated by quantum-mechanical methods

INTRODUCTION

In studies of the hydrophobicity of organic compounds^{1,2} the logarithm of the capacity factor ($\log k'_w$) extrapolated to 100% water as the eluent is widely used. In a previous study³, $\log k'_w$ values were utilized for the determination of the hydrophobicities of isomeric methylquinolines. Attention was paid to the deviations from the linear relationship between $\log k'$ and the mobile phase composition.

According to Snyder *et al.*⁴, in most instances there is a determined field of the mobile phase composition in which the following equation is valid:

$$\log k' = a\varphi + b \quad (1)$$

where φ is the volumetric fraction of the organic modifier in the mobile phase.

The utilization of the solubility parameter concept by Schoenmakers *et al.*^{5,6} resulted in the quadratic equations

$$\log k' = a\varphi^2 + b\varphi + c \quad (2)$$

$$\log k' = a\varphi^2 + b\varphi + c + e\sqrt{\varphi} \quad (3)$$

Taking into account the double mechanism of retention⁷, the following relationship has been introduced:

$$k' = a \exp(b\varphi) + (c + d\varphi)^{-1} \quad (4)$$

Many other relationships between the capacity factor and the composition of the mobile phase have been established^{8,9}.

Deviations from linearity are mainly caused by the double mechanism of retention^{7,10} or by intermolecular interactions^{11,12} and in most instances they decrease with increase in the mobile phase polarity.

In this work, an attempt was made to determine the range of mobile phase compositions in which linear extrapolations could be carried out with the required accuracy.

EXPERIMENTAL

The investigated ketones were of analytical-reagent grade from E. Merck (Darmstadt, F.R.G.), Fluka (Buchs, Switzerland) and Koch-Light Labs. (Colnbrook, U.K.). Mobile phases were prepared from analytical-reagent grade methanol and redistilled water in different volume proportions. The chemically bonded stationary phases were used, one with an irregular particle shape and a carbon content of 17.5% (Separon SIX C₁₈) and the other with spherical particles and a carbon content of 18.0% (Separon SGX C₁₈), both from Laboratorní přístroje (Prague, Czechoslovakia). The columns were 150 mm × 3.3 mm I.D. and the particle diameter was *ca.* 5 μm. A liquid chromatograph produced by Laboratorní přístroje with a UV detector set at 254 nm was used. The column void volume was determined by the injection of sodium nitrite dissolved in methanol. The mobile phase flow-rate was 0.7 ml/min. The results obtained represent the means of five measurements.

In order to determine the solubility, saturated solutions of the ketones in water were prepared. After shaking the ketones with water in test-tubes for 5 min, the test-tubes were left for 24 h at 20°C for equilibration. A series of standard ketone solutions in water was prepared and the calibration graph at maximum absorption was constructed. Next, a specified volume of the saturated aqueous solution was taken and its ketone content was determined by spectrophotometry.

RESULTS AND DISCUSSION

The capacity factors were determined for methanol–water volume fractions from 1.0:0 to 0.4:0.6. The investigations were carried out with a series of fifteen ketones, including five isomeric ketone pairs on two stationary phases. The relationship between $\log k'$ and mobile phase composition for the five selected ketones is presented in Fig. 1.

The lines in Fig. 1 intersect, so that a change of selectivity is observed while changing the mobile phase composition. The data in Table I for $\log k'_w$ extrapolated from the various mobile phase composition ranges depend on the range considered and on the nature of the stationary phase used. It was our aim to extrapolate reliably the $\log k'$ values for solutes chromatographed in pure water.

Trials were made to solve this problem with two models, as follows.

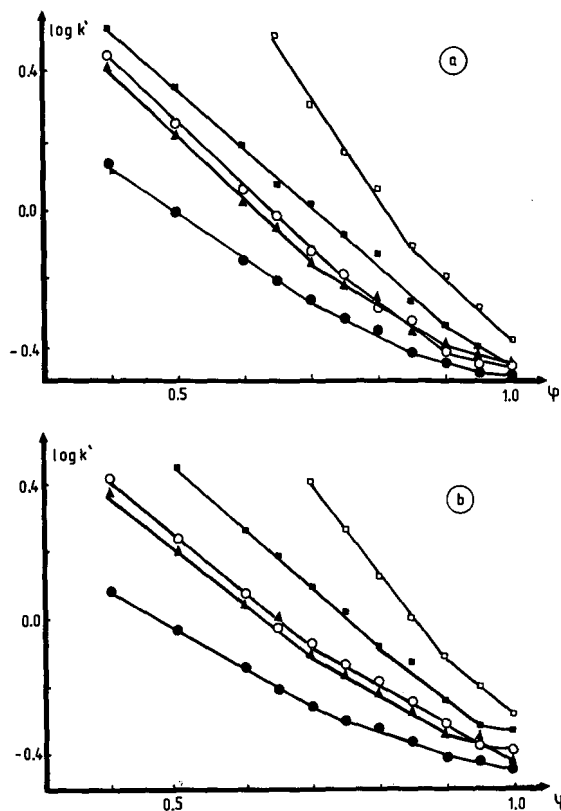


Fig. 1. Log k' vs. volumetric fraction of methanol in water, on (a) Separon SIX C_{18} and (b) Separon SGX C_{18} . ● = Ethyl methyl ketone; ○ = diethyl ketone; ▲ = isopropyl methyl ketone; ■ = isobutyl methyl ketone; □ = phenyl isobutyl ketone.

TABLE I

VALUES OF LOG k'_w OBTAINED FROM THE STRAIGHT-LINE EXTRAPOLATION IN THE VARIOUS RANGES OF THE MOBILE PHASE COMPOSITION FOR THE SELECTED PAIR OF ISOMERS

Range of the mobile phase composition (volume fraction of methanol)	Log k'_w			
	Separon SIX C_{18}		Separon SGX C_{18}	
	Diethyl ketone	Isopropyl methyl ketone	Diethyl ketone	Isopropyl methyl ketone
1.00-0.80	0.413	0.499	0.645	0.589
0.85-0.65	0.977	0.882	0.737	0.785
0.70-0.40	1.040	0.992	1.060	0.998

Model I

According to the assumption made, the value of the capacity factor is influenced, apart from by incidental factors, also by the systematic factor caused by interactions as described above. The result is a deviation of the experimental points from simple regression. These deviations are minor for the polar mobile phase but they rise following an increase in the methanol content. Consequently, the points corresponding to the mobile phase compositions with high organic modifier contents lie beyond those confidence curves which are calculated for the chosen field of probability. The rejection of those points results in abandoning the systematic error and shifting towards the mobile phase with a greater polarity.

The regression line

$$\log k' = \alpha\varphi + \beta \quad (5)$$

was determined and then the confidence interval for $\log k'$ according to published equations¹³. The value of the Student's variable t_y was taken from tables for the confidence coefficient $1 - \gamma = 95\%$ and for $n - 2$ degrees of freedom. Calculations were made according to the algorithm in Fig. 2. The highest value of the volumetric fraction of methanol in the mobile phase φ_i , at which the $\log k'_i$ lies inside the error channel, and the value of $\log k'_w = \beta$ were determined. β is the value of the intersection of the regression line in the interval $\langle \varphi_1, \varphi_i \rangle$; in our case $\varphi_1 = 0.4$. The values of φ_i and the extrapolated value of β are given in Table II.

A trial to correlate the φ_i value with the partition coefficients calculated on the basis of Rekker fragmentary constants¹⁴, $\log P_{\text{Rek.}}$, was made. For the results achieved using the Separon SIX C₁₈ column, the following relationship was obtained:

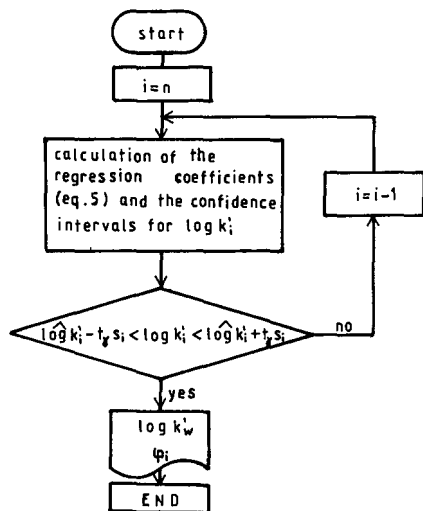


Fig. 2. Algorithm for estimation of the mobile phase composition φ_i for which the corresponding $\log k'_i$ value appears within the confidence interval; $\varphi_n = 1.0$; step = 0.05; $\log k'$ is the value determined from the regression eqn. 5.

TABLE II

CALCULATED CORRELATION PARAMETERS FOR EQN. 5 FROM MODEL I AND FOR EQNS. 1, 2 AND 11 FROM MODEL II ON TWO STATIONARY PHASES

Substance	Stationary phase ^a	Model I		Model II		
		φ_i	Eqn. 5: β	Eqn. 1: b	Eqn. 2: c	Eqn. 11: $a' + c'$
Diethyl ketone	1	0.80	1.04	0.92	1.32	1.26
	2	0.75	1.04	0.88	1.32	1.24
Isopropyl methyl ketone	1	0.85	0.96	0.87	1.24	1.18
	2	0.90	0.92	0.86	1.23	1.16
Ethyl propyl ketone	1	0.90	1.31	1.24	1.54	1.49
	2	0.95	1.27	1.23	1.52	1.48
Isobutyl methyl ketone	1	0.95	1.22	1.18	1.43	1.38
	2	0.95	1.21	1.23	1.55	1.43
Dipropyl ketone	1	0.90	1.98	1.90	2.48	2.36
	2	0.95	1.96	1.91	2.67	2.52
Methyl pentyl ketone	1	0.85	2.18	2.01	2.80	2.65
	2	0.95	2.02	1.96	2.68	2.58
Phenyl ethyl ketone	1	0.90	1.90	1.80	3.33	2.99
	2	0.90	1.91	1.81	2.50	2.37
Benzyl methyl ketone	1	0.85	1.66	1.37	2.83	2.54
	2	0.85	1.62	1.55	2.20	2.10
Phenyl isobutyl ketone	1	0.90	2.38	2.17	3.89	3.52
	2	0.95	2.36	2.26	4.29	3.84
Benzyl ethyl ketone	1	0.90	1.99	1.80	3.44	3.08
	2	0.95	1.92	1.72	3.03	2.97
Ethyl methyl ketone	1	0.75	0.53	0.42	1.12	0.96
	2	0.70	0.54	0.39	0.82	0.71
Cyclohexanone	1	0.80	0.83	0.51	1.61	1.48
	2	0.85	0.81	0.47	1.13	1.01
Diisobutyl ketone	1	1.00	2.36	2.36	3.71	3.37
	2	1.00	2.50	2.50	3.23	3.04
Cyclopropyl methyl ketone	1	0.80	0.74	0.54	1.35	1.16
	2	0.85	0.59	0.49	1.00	0.87
Phenyl cyclobutyl ketone	1	1.00	2.43	2.43	3.79	3.40
	2	0.95	2.41	2.35	2.94	2.80
Average correlation coefficient (r)		—	0.991	0.934	0.988	0.997

^a 1 = Separon SIX C₁₈; 2 = Separon SGX C₁₈.

$$\begin{aligned} \varphi_i &= 0.070 \log P_{\text{Rek.}} + 0.77 \\ n &= 15, \quad r = 0.810 \end{aligned} \quad (6)$$

and for the Separon SGX C₁₈ column:

$$\begin{aligned} \varphi_i &= 0.072 \log P_{\text{Rek.}} + 0.79 \\ n &= 15, \quad r = 0.788 \end{aligned} \quad (7)$$

These equations allow the prediction of the composition of the mobile phase for which the dependence of $\log k'$ vs. φ is rectilinear. This refers to any substance. Moreover, minor difference in the composition of the stationary phases do not have much importance as regards the results achieved. There are similar coefficients in eqns. 6 and 7.

The procedure described above can be regarded as a model for the approximate determination of the lower limit of the mobile phase composition from which linear extrapolation can be carried out.

Model II

The relationship $\log k' = f(\varphi)$ is parabolic, with a minimum for high concentrations of methanol in the mobile phase. The relationship is well depicted in this field by eqn. 2; with an increase in the polarity of the mobile phase, the linear eqn. 1 becomes valid. If the coefficients in eqn. 2 are changed and the equation is presented in the form

$$\log k' = \frac{a'}{2} \varphi^2 + (a' + b')\varphi + (a' + c') \quad (8)$$

then

$$\log k' = a' \left(1 + \varphi + \frac{\varphi^2}{2} \right) + b'\varphi + c' \quad (9)$$

in which the expression

$$1 + \varphi + \frac{\varphi^2}{2} \quad (10)$$

is an approximate development of the $\exp(\varphi)$ function into a Taylor series. As φ takes its values from the $\langle 0,1 \rangle$ interval, this approximation can be applied successfully, and then eqn. 9 takes the form

$$\log k' = a' \exp(\varphi) + b'\varphi + c' \quad (11)$$

Eqn. 11 is a good approximation of a straight line for low values (it has its oblique asymptote at $\varphi \rightarrow -\infty$); at higher values it is a good approximation of a parabola, especially for $\varphi \approx 1$.

In Table II the $\log k'_w$ values have been presented, with the following terms: the coefficient b from eqn. 1, the coefficient c from eqn. 2 and the sum of the coefficients $a' + c'$ from eqn. 11. In this instance the $\log k'_w$ values are higher than those calculated on the basis of eqn. 1 and lower than those calculated from eqn. 2. It can be seen from the comparisons of the correlation coefficients that the best estimation of the $\log k'$ vs. φ relationship was obtained by applying eqn. 11. However, the $\log k'_w$ hydrophobic

TABLE III
DIFFERENT PHYSICO-CHEMICAL PARAMETERS USEFUL IN A COMPARISON OF HYDROPHOBICITY

Substance	Log P_{rel}	Log c_M	Wiener's index, W	Connectivity index, χ	Balaban's index, IB	Net charge on carbonyl carbon atom, q_C	Net charge on oxygen atom, q_O	Difference of net charges on the carbonyl atoms, $q_C - q_O$
Diethyl ketone	0.768	-0.194	27.8	2.53	3.04	0.261	-0.280	0.0658
Isopropyl methyl ketone	0.652	-0.110	25.8	2.35	3.32	0.250	-0.263	0.0731
Ethyl propyl ketone	1.290	-0.703	46.1	3.03	3.04	0.268	-0.284	0.0650
Isobutyl methyl ketone	1.180	-0.640	44.1	2.82	3.16	0.247	-0.264	0.0761
Dipropyl ketone	1.880	-1.428	70.5	3.53	3.09	0.250	-0.269	0.0646
Methyl pentyl ketone	1.880	-1.558	74.5	3.47	2.85	0.244	-0.264	0.0647
Phenyl ethyl ketone	2.130	-1.438	94.8	4.58	2.86	0.265	-0.269	0.0612
Benzyl methyl ketone	1.430	-1.335	99.8	4.48	2.67	0.237	-0.258	0.0713
Phenyl isobutyl ketone	2.540	-1.946	127.3	4.97	2.86	0.258	-0.271	0.0668
Benzyl ethyl ketone	1.960	-1.728	140.3	5.04	2.58	0.254	-0.263	0.0699

parameters obtained by extrapolation according to eqn. 2 and likewise eqn. 11 result in excessive and divergent values compared with the two stationary phases being investigated. The best conformity of the results was obtained when applying a linear extrapolation in the range of mobile phase compositions determined according to model I. This means that in order to obtain better hydrophobic data in terms of quantity, the linear extrapolation must be carried out in an interval of $\log k'$ vs. φ relationship such that deviations of the points can only be the result of incidental errors.

In Table III, $\log P_{\text{Rek.}}$ and values of the Wiener topological index¹⁵, Balaban's index¹⁶, the connectivity index χ^{17} and the solubilities in water, $\log c_M$ (c_M is the molar concentration of the saturated ketone in water), are given. The q_C , q_O and $q_{CO} = q_C - q_O$ values are also given, where q_C is the net charge on the carbon atom of the carbonyl group, q_O is the net charge on the oxygen atom and q_{CO} is the difference of net charges on the carbonyl C and O atoms.

The net charges were calculated following the CNDO/2 method. The parametric characteristic was drawn up on data taken from the literature¹⁸. Of the net charges on various atoms, the value of q_{CO} showed the greatest conformity with the hydrophobicity sequence for isomer pairs.

The following equations express the relationships between $\log k'_w$ determined according to model I on the Separon SIX C₁₈ phase and the data in Table III:

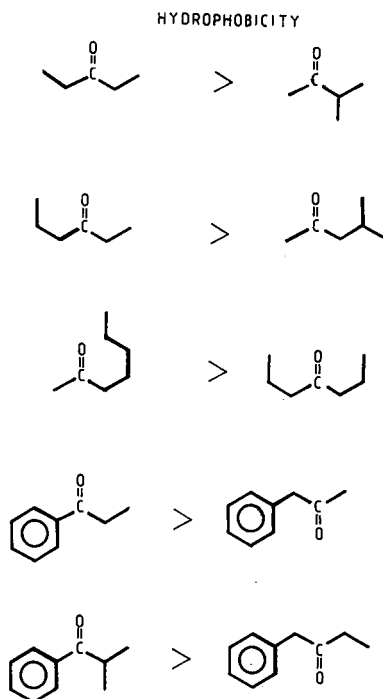


Fig. 3. Schematic comparison of hydrophobicities of the investigated isomers.

$$\log k'_w = 1.18 \log P_{\text{Rek.}} - 0.38; \quad r = 0.959 \quad (12a)$$

$$\log k'_w = -1.13 \log c_M + 0.84; \quad r = 0.966 \quad (12b)$$

$$\log k'_w = 0.015 W + 0.50; \quad r = 0.804 \quad (12c)$$

$$\log k'_w = -1.62 \chi + 1.0; \quad r = 0.787 \quad (12d)$$

$$\log k'_w = -0.28 IB + 3.41; \quad r = 0.616 \quad (12e)$$

$$\log k'_w = -49 q_{\text{CO}} + 5.03; \quad r = 0.454 \quad (12f)$$

The comparisons that were carried out showed that the chromatographic data produced gave good correlations in terms of quantity with such hydrophobic parameters as solubility in water and the partition coefficient between *n*-octanol and water. Topological indices and quantum-mechanical data do not result in good correlations with $\log k'_w$ for a whole group of compounds. They can, however, be used successfully for qualitative comparisons of hydrophobicity within the field of isomer pairs.

From the comparisons of the results obtained, it can be concluded (Fig. 3) that the hydrophobicity of organic compounds is smaller for isomers with branched hydrocarbon chains and greater for those isomers which have only one, but a considerably longer, hydrocarbon chain, *e.g.*, see methyl pentyl ketone and dipropyl ketone. The hydrophobicity is also smaller for those molecules in which diffusion of the electron charge due to inductive or resonance effects occurs.

REFERENCES

- 1 T. Braumann, *J. Chromatogr.*, 373 (1986) 191.
- 2 A. Hulshoff and J. H. Perrin, *J. Chromatogr.*, 129 (1976) 263.
- 3 A. Siwek and J. Śliwiok, *Chromatographia*, 25 (1988) 797.
- 4 L. R. Snyder, J. W. Dolan and J. R. Gant, *J. Chromatogr.*, 165 (1979) 3.
- 5 P. J. Schoenmakers, H. A. H. Billiet and L. de Galan, *J. Chromatogr.*, 185 (1979) 179.
- 6 P. J. Schoenmakers, H. A. H. Billiet and L. de Galan, *J. Chromatogr.*, 285 (1983) 107.
- 7 A. Nahum and Cs. Horváth, *J. Chromatogr.*, 203 (1981) 53.
- 8 W. R. Melander and Cs. Horváth, *Chromatographia*, 18 (1984) 353.
- 9 P.-C. Lu and X.-M. Lu, *J. Chromatogr.*, 292 (1984) 169.
- 10 R. N. Nikolov, *J. Chromatogr.*, 286 (1984) 147.
- 11 H. Colin, A. Krstulovic, G. Guiochon and Z. Yun, *J. Chromatogr.*, 255 (1983) 295.
- 12 W. R. Melander, A. Nahum and Cs. Horváth, *J. Chromatogr.*, 185 (1979) 129.
- 13 M. Dwass, *Probability and Statistics*, Benjamin, New York, 1970, p. 575.
- 14 R. F. Rekker, *The Hydrophobic Fragmental Constant*, Elsevier, Amsterdam, 1977.
- 15 H. Wiener, *J. Chem. Phys.*, 52 (1948) 1082.
- 16 A. T. Balaban, *Chem. Phys. Lett.*, 89 (1982) 399.
- 17 M. Randić, *J. Am. Chem. Soc.*, 97 (1975) 6609.
- 18 R. C. Bingham and H. J. Dewar, *J. Am. Chem. Soc.*, 97 (1975) 1302.

CHROMSYMP. 1760

Partition coefficients and capacity factors of some nucleoside analogues

ANDREW P. CHEUNG* and DEBORAH KENNEY

Life Sciences Division, SRI International, Menlo Park, CA 94025 (U.S.A.)

SUMMARY

The AIDS epidemic has brought into focus the development of antiviral agents, of which nucleoside analogues are an important class. The single most important physico-chemical property of a chemotherapeutic agent is its hydrophobicity. This paper reports the hydrophobicity, determined as log partition coefficient (P) by the shake-flask method, of 25 nucleoside analogues. The capacity factors (k') of these analogues were also obtained by reversed-phase liquid chromatography. There is a very strong linear correlation between the log P and the log k' values of all the nucleoside analogues, indicating that hydrophobicity of nucleosides can be determined by liquid chromatography.

Examination of the P data indicates that an empirical mathematical relationship exists between the partition coefficient value and the molecular structure of the nucleoside analogues. A table of constants and an equation is proposed to estimate the P of nucleoside analogues.

INTRODUCTION

The AIDS (Acquired-Immune-Deficiency Syndrome) epidemic has brought into focus the development of antiviral agents. Analogues of nucleosides represent an important class of antiviral agents. For a chemotherapeutic agent to be effective, among other properties, it has to be able to be adsorbed and distributed to the target organ or tissue. This ability is dictated by the hydrophobicity of the drug. Hydrophobicity is one of the most important physico-chemical properties affecting the drug's biological activity. It is commonly expressed as the logarithm of the partition coefficient (log p) of the chemical between 1-octanol and water. This property is usually determined by the traditional shake-flask method.

The shake-flask method has many disadvantages. It is laborious and requires that pure chemicals be used. As alternatives to this shake-flask method, several investigators^{1–3} have proposed the use of chromatography to determine the hydrophobicity of a chemical. Particularly, the logarithm of the capacity factor (log k') obtained from reversed-phase liquid chromatography (LC) has been shown to have good correlation to the log P for several classes of chemicals^{4,5}. The LC method

offers many advantages over the traditional shake-flask method. Among them, LC requires only a small amount of the chemical. Presence of impurities in the chemical does not interfere with the determination. Proper measurement of concentration is not required. LC gives better results when the solubility of the chemical in one phase is much lower than in the other phase. According to Henry *et al.*⁶ and Baker *et al.*⁷, chromatographic methods are more similar to the *in vivo* process than the shake-flask method.

Determination of hydrophobicity using LC is not free of limitations. The $\log k'$ values of the chemical and several model compounds are usually determined by LC with a single mobile phase—water or buffer with organic modifier. The $\log P$ value of the chemical is then extrapolated from linear regression analysis of the Collander equation⁸ for the model compounds.

$$\log k' = a \log p + b \quad (1)$$

This monocratic approach requires model compounds of known $\log P$. The major weakness of the method is that the Collander relationship has been shown valid for congeners only. Haky and Young⁹ determined $\log k'$ for 68 compounds using a commercial ODS column and 55% methanol in aqueous buffer. They found good linear correlation ($r=0.966$) according to eqn. 1 between $\log P$ and $\log k'$ values. They found the correlation improved if they separated the compounds into congener classes. The hydrogen bonding of the residual silanol in the ODS column to different classes of compound interferes with the partition process differently. As a result, slopes (a) and intercepts (b) of eqn. 1 for different classes of compounds may be different. Miyake *et al.*¹⁰ and Biasi and Lough¹¹ used polymer-based reversed-phase columns and obtained similar results—linear correlation between $\log P$ and $\log k'$ exists only among congeners. Several investigators^{1,12-16} bypassed the congener restriction with a polycratic approach to determine hydrophobicity by LC. In this approach, the $\log k'_x$ of the chemical is determined with several mobile phases containing different % (x) methanol in water. They found that the $\log k'_0$, the $\log k'$ when the mobile phase is 100% aqueous, follows the relationship of eqn. 2, if x is between 20 and 80.

$$\log k'_x = \log k'_0 - S x \quad (2)$$

Garst and Wilson^{13,14} and Minick *et al.*¹⁵ reported that the $\log k'_0$ thus obtained correlates linearly with the binding activity as well as $\log P$. This polycratic approach offers several advantages over the monocratic one. In the monocratic approach, the $\log k'$ of the chemical and model compounds have to be simultaneously determined under a single LC condition. This is not so required for the polycratic approach. In addition, if $\log k'_0$ is accepted as an independent hydrophobicity scale, even model compounds are not needed.

Because of the current interest in anti-AIDS agents, many derivatives of nucleosides have been synthesized as potential antiviral agents. The hydrophobicity of these chemicals would be of interest. The purpose of this paper is to report $\log P$ of 25 nucleosides and analogues determined by the shake-flask method and their $\log k'$ obtained by the monocratic LC approach. A discussion of the partition coefficients,

capacity factors and the correlation between the two is presented, and an empirical equation and a table of constants to calculate *P* of nucleoside analogues is proposed. The names and structures of these 25 chemicals are listed below and depicted in Fig. 1.

<i>Compound</i>	<i>Chemical name</i>	<i>Abbreviation</i>
1	Cytidine	C
2	2'-Deoxycytidine	DC
3	2',3'-Dideoxycytidine	DDC
4	2',3'-Dideoxycytidine-2'-ene	DDCene
5	Cytarabine	AraC
6	5-Fluoro-2',3'-dideoxycytidine	5FDDC
7	5-Bromo-2',3'-dideoxycytidine	5BDDC
8	2',3'-Dideoxy-3'-azidocytidine	AZC
9	Carbocytidine	CarboC
10	Uridine	U
11	2',3'-Dideoxy-3'-azidouridine	AZU
12	Thymidine	T
13	3'-Deoxythymidine	DDT
14	3'-Deoxythymidine-2'-ene	DDTene
15	3'-Deoxy-3'-azidothymidine	AZT
16	Adenosine	A
17	2'-Deoxyadenosine	DA
18	2',3'-Dideoxyadenosine	DDA
19	2',3'-Dideoxyadenosine-2'-ene	DDAene
20	2'-Fluoro-2',3'-dideoxyadenosine	2'FDDA
21	Adeninearaboside	AraA
22	Neplanosine	CarboA
23	Inosine	I
24	2',3'-Dideoxyinosine	DDI
25	2',3'-Dideoxyguanosine	DDG

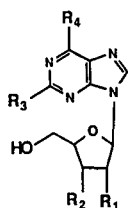
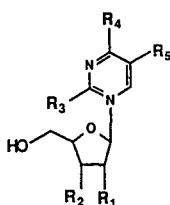
EXPERIMENTAL

Reagents and materials

The nucleosides were received from the National Cancer Institute, National Institutes of Health. Their identities were confirmed by UV and mass spectra. The purities were checked by UV and LC. Due to their high purity, >98%, they were used without further purification. Buffers were prepared from KH_2PO_4 (Mallinckrodt, analytical-reagent grade) with Milli-Q quality water and the pH adjusted with dilute KOH or H_3PO_4 . 1-Octanol (Aldrich) was HPLC grade. The buffer and 1-octanol were presaturated with each other before use.

Determination of partition coefficients (P)

Accurately weighed portions (0.2, 0.5, 1 and 1.5 mg) of each nucleoside were individually dissolved in 10.0 ml of pH 7.0, 0.05 M phosphate buffer in volumetric flasks. The UV of each solution was recorded from 300 to 200 nm with a Uvikon 810 UV-VIS spectrophotometer (Kontron, Switzerland). The absorbances of these solutions at the absorption maximum were plotted against their concentrations. If linear relationship was not obtained from the plot, the experiment was repeated with pro-



	R1	R2	R3	R4	R5		R1	R2	R3	R4
1.	OH	OH	OH	NH ₂	H	16.	OH	OH	H	NH ₂
2.	H	OH	OH	NH ₂	H	17.	H	OH	H	NH ₂
3.	H	H	OH	NH ₂	H	18.	H	H	H	NH ₂
6.	H	H	OH	NH ₂	F	20.	F	H	H	NH ₂
7.	H	H	OH	NH ₂	B _r	23.	OH	OH	H	OH
8.	H	N ₃	OH	NH ₂	H	24.	H	H	H	OH
10.	OH	OH	OH	OH	H	25.	H	H	NH ₂	OH
11.	H	N ₃	OH	OH	H					
12.	H	OH	OH	OH	CH ₃					
13.	H	H	OH	OH	CH ₃					
15.	H	N ₃	OH	OH	CH ₃					

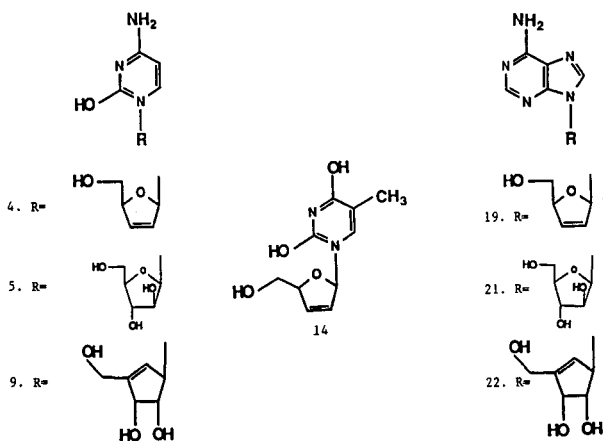


Fig. 1. Structural formula of the nucleoside analogues.

gressively more dilute solutions. This ensured that the molar absorptivity at the maximum (ϵ_{\max}) was obtained from complete solutions and that the UV follows Beer's Law. The ϵ_{\max} of each nucleoside at about 260 nm was calculated. Similarly, the ϵ_{\max} of the nucleoside in 1-octanol was determined. Because some of the nucleosides have very low solubility in 1-octanol, they were first dissolved in 1 ml ethanol before diluting to mark with octanol.

From the freshly prepared buffer solutions which gave linear response of absorbance vs. concentration, 5.00 ml each were transferred to individual centrifuge cones (glass equipped with stopper). To each cone were added 5.00 ml octanol and the cone was stoppered. The mixtures were shaken 80 times followed by centrifugation at 1000 g for 1–2 h. The aqueous and the organic phases were separated and the UV of

each recorded. The nucleoside concentration in each phase was calculated from its respective absorbance. The *P* value of the nucleoside was determined by the following expression:

$$P = [c]_o / [c]_a$$

where $[c]$ = nucleoside concentration, o = octanol phase and a = aqueous phase.

Determination of capacity factor (*k'*)

The *k'* values were determined isocratically (3% acetonitrile in pH 7.0, 0.05 M phosphate buffer, 1.0 ml/min) on a Chemcosorb-5-C₁₈-H bonded phase, 250 × 4.6 mm I.D. column (DyChrom, Sunnyvale, CA, U.S.A.) using a Model 600 solvent delivery system (Waters Assoc., Milford, MA, U.S.A.), a Model 712WISP Autosampler (Waters) and a Model 481 LC spectrophotometer (Waters). A Maxima 820 integration system (Dynamic Solution, Ventura, CA, U.S.A.) was used to collect chromatographic and retention data.

The *k'* value of each nucleoside was calculated as $(t_i - t_0) / t_0$, where t_i is the retention time of the nucleoside and t_0 is the retention time of an unretained compound. The unretained peak was determined by an injection of methanol. The *t* values of the nucleosides (except compounds, **10**, **12**, **21** and **25**) were obtained from one chromatogram. The *t* values for compounds **10**, **12**, **21** and **25** were extrapolated from a second chromatogram.

RESULTS AND DISCUSSION

Nucleosides are ionizable in aqueous solutions. In order to determine the hydrophobicity of their neutral species the experimental condition should suppress the ionization of the nucleosides to the minimum. The 25 chemicals studies are analogues of four classes of nucleosides: cytidines (**1–9**), uridines (**10–15**), adenosines (**16–22**), and inosines (**23–25**). They contain the pyrimidine and purine bases as their ionizable moiety. Their ionization constants and charge sites are depicted in Fig. 2. The basic

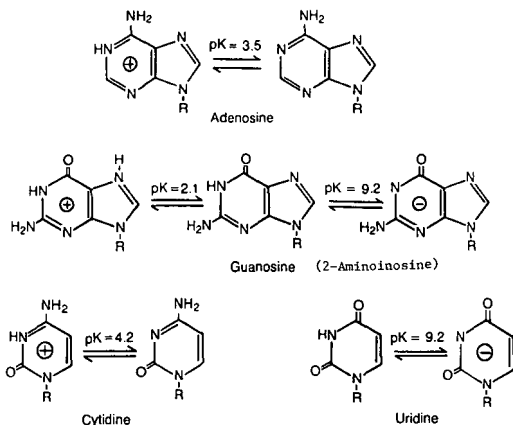


Fig. 2. Sites and p*K* values for protonation and ionization of representative nucleosides.

TABLE I

P VALUES OF DDA AND DDC BETWEEN 1-OCTANOL AND PHOSPHATE BUFFERS

The buffers were prepared from 0.05 M KH_2PO_4 . The pH was adjusted with dilute KOH or H_3PO_4 . *P* values were determined by the traditional shake-flask method.

<i>pH</i> of buffer	<i>P</i> of DDA	<i>P</i> of DDC
5	0.57	0.043
6	0.58	0.050
7	0.60	0.054
8	0.60	0.051

$\text{p}K_a$ values are 4 or lower and the acidic $\text{p}K_a$ values are about 9, therefore, a pH 6–7 buffer solution would keep the nucleosides in their unionized forms. Table I presents the *P* values of DDC (3) and DDA (18) determined between 1-octanol and pH 5, 6, 7 and 8 buffers. For DDC which has both basic and acidic $\text{p}K_a$ values, *P* decreases on both sides of pH 7 due to ionization of the basic or acidic function. For DDA which has only the basic function, *P* decreases at pH less than 7. Based on this result, *P* values of the rest of the chemicals were determined with the 1-octanol–pH 7.0 phosphate buffer system. Several investigators^{1,12–15} emphasized the advantages of extrapolating $\log k'_0$ for each chemical with the polycratic solvent approach. They also pointed out that the extrapolation is valid only when the organic modifier (methanol) in the mobile phase is within a limited range (20 to 80%). For their model compounds with large (0–8) $\log P$ values, the polycratic solvent approach is applicable. For nucleosides, the $\log P$ values of which are often small (<0), the amount of organic modifier in the mobile phase is usually less than 10%. Because of this limitation, the $\log k'$ values of the nucleosides were obtained monocratically, using a 3% acetonitrile in pH 7.0 phosphate buffer. The buffer in the mobile phase ensured that the ionization of the nucleosides were suppressed to a minimum. The organic modifier in the mobile phase was kept to a deliberately small amount (3% acetonitrile) in order to keep the LC system as similar as possible to the octanol-buffer partition system. Table II lists the determined *P* and k' values and their log values of these nucleosides and analogues.

In order to see if the nucleosides' hydrophobicity can be predicted from the k' values obtained with LC, the linear plots and linear regression analyses between the $\log P$ and $\log k'$ values in Table II were performed. Results of the linear regression analysis are summarized in Table III. The linear plots are presented in Figs. 3–5. Except for the inosines (23–25), the $\log P$ vs. $\log k'$ plot of the remaining 22 nucleoside gives a straight line joining 9 and 15 (Fig. 3). The linear correlation coefficient (*r*) for these 22 compounds is 0.991. Fig. 4 is a $\log P$ vs. $\log k'$ plot of the 25 compounds after they are separated into the pyrimidine and purine nucleoside series. Both the pyrimidines (1–15) and the purines (16–25) give straight lines with *r* of 0.994 and 0.958, respectively. Fig. 5 is the $\log P$ vs. $\log k'$ plot of the nucleosides after they are further separated as cytidines (1–9), uridines (10–15), adenosines (16–22), and inosines (23–25). The *r* of the cytidines, the uridines, the adenosines and the inosines are respectively 0.991, 0.996, 0.981 and 1.000. Even when all twenty 25 nucleosides are considered as a whole, *r* between $\log P$ and $\log k'$ of these 25 compounds is still a respectable

TABLE II

PARTITION COEFFICIENTS AND CAPACITY FACTORS OF NUCLEOSIDE ANALOGUES

P Values were determined by the traditional shake-flask method; *k'* values were determined by LC (see text for details).

Compound	<i>P</i> ± S.D.	log <i>P</i>	<i>k'</i>	log <i>k'</i>	<i>n</i>
1	0.008 ± 0.001	-2.097	0.79	-0.102	4
2	0.013 ± 0.001	-1.886	1.87	0.272	3
3	0.055 ± 0.003	-1.260	4.49	0.652	4
4	0.028 ± 0.002	-1.553	2.53	0.402	4
5	0.008 ± 0.001	-2.097	1.28	0.107	4
6	0.090 ± 0.003	-1.046	6.47	0.811	3
7	0.320 ± 0.007	-0.495	20.49	1.312	3
8	0.208 ± 0.008	-0.682	16.14	1.208	4
9	0.005 ± 0.001	-2.301	0.73	-0.136	3
10	0.013 ± 0.001	-1.886	2.02	0.306	4
11	0.465 ± 0.006	-0.333	28.81	1.460	3
12	0.079 ± 0.002	-1.102	7.68	0.885	4
13	0.264 ± 0.012	-0.578	20.82	1.303	7
14	0.193 ± 0.011	-0.714	13.83	1.141	4
15	1.091 ± 0.002	0.038	73.37	1.866	3
16	0.105 ± 0.003	-0.979	13.33	1.125	4
17	0.245 ± 0.002	-0.611	16.14	1.208	4
18	0.602 ± 0.017	-0.220	38.90	1.590	5
19	0.311 ± 0.008	-0.507	24.22	1.384	3
20	0.801 ± 0.002	-0.096	42.31	1.626	4
21	0.111 ± 0.004	-0.955	9.63	0.984	3
22	0.050 ± 0.003	-1.301	6.47	0.811	4
23	0.010 ± 0.001	-2.000	3.60	0.556	3
24	0.068 ± 0.005	-1.167	13.33	1.125	4
25	0.085 ± 0.002	-1.071	15.24	1.183	4

TABLE III

LINEAR REGRESSION ANALYSIS OF LOG *P* VS. LOG *k'*

log *P* = *S* log *k'* + *I*; *S* = slope; *I* = intercept; S.D. = standard deviation; *r* = correlation coefficient.

Data base ^a	<i>S</i> ± S.D.	<i>I</i> ± S.D.	<i>r</i>	<i>n</i>
Compounds 1-25 (all)	1.203 ± 0.064	-2.187 ± 0.170	0.969	25
Compounds 1-15 (pyrimidines)	1.198 ± 0.038	-2.116 ± 0.086	0.994	15
Compounds 16-25 (purines)	1.631 ± 0.172	-2.782 ± 0.170	0.958	10
Compounds 1-9 (cytidines)	1.224 ± 0.062	-2.106 ± 0.092	0.991	9
Compounds 10-15 (uridines)	1.254 ± 0.057	-2.217 ± 0.067	0.996	6
Compounds 16-22 (adenosines)	1.401 ± 0.124	-2.414 ± 0.093	0.981	7
Compounds 23-25 (inosines)	1.476 ± 0.016	-1.822 ± 0.008	1.000	3
Compounds 1-22 (all except inosines)	1.199 ± 0.035	-2.132 ± 0.093	0.991	22

^a From Table II.

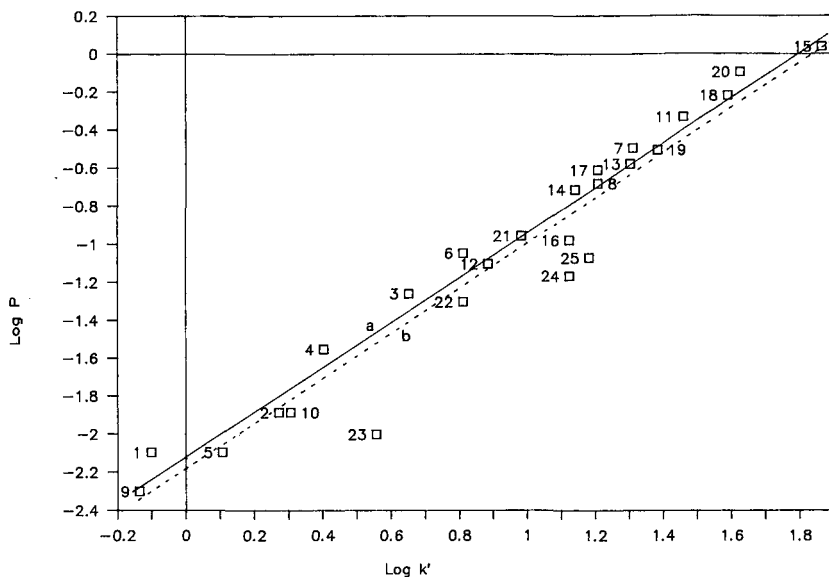


Fig. 3. Linear plot of $\log P$ vs. $\log k'$ (pH 7) of all analogues. The solid line is for compounds 1–22 (all nucleosides minus the inosines). It fits the linear equation of $\log P = 1.199 \log k' - 2.132$. The dotted line is for all 25 compounds. It fits the linear equation of $\log P = 1.203 \log k' - 2.187$.

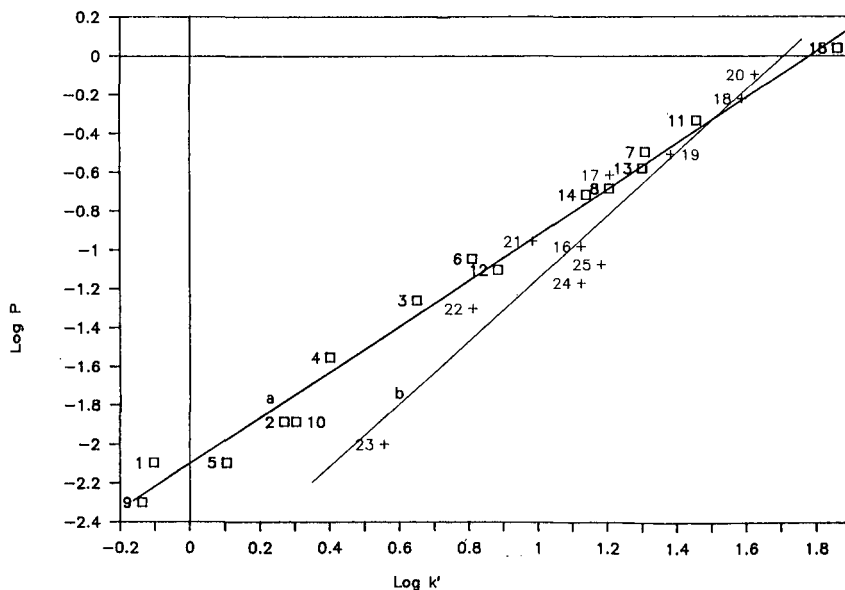


Fig. 4. Linear plot of $\log P$ vs. $\log k'$ (pH 7) of the analogues according to pyrimidine or purine derivatives. The pyrimidine (1–15) line (\square , a) fits the equation of $\log P = 1.198 \log k' - 2.116$. The purine (16–25) line ($+$, b) is represented by the equation of $\log P = 1.631 \log k' - 2.782$.

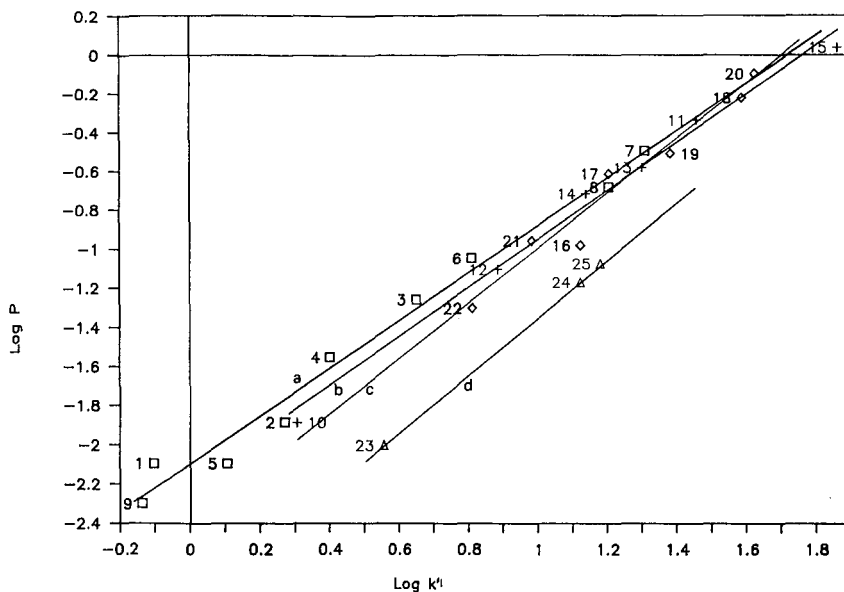


Fig. 5. Linear plot of $\log P$ vs. $\log k'$ (at pH 7) of the analogues according to cytidine, uridine, adenosine and inosine classes. Line a (\square) for the cytidines (1-9) has an equation of $\log P = 1.224 \log k' - 2.106$. Line b (+) for the uridines (10-15) has an equation of $\log P = 1.254 \log k' - 2.217$. Line c (\diamond) for the adenosines (16-22) has an equation of $\log P = 1.401 \log k' - 2.414$. Line d (\triangle) for the inosines (23-25) has an equation of $\log P = 1.476 \log k' - 2.822$.

0.969. These results are much better than those recently published by Balzarini *et al.*¹⁷ These data indicate¹⁷ that the linear correlation between $\log P$ and retention time (t_R) is good ($r \geq 0.96$) only among nucleosides having the identical base. When all of the fifteen purine derivatives are considered as one class, r is a fair 0.956. But when all fifteen pyrimidine derivatives are considered together, r is a disappointing 0.266^a. R is only 0.713 when all thirty nucleoside derivatives are considered together^b. Several factors may have contributed to this lack of linear correlation between the $\log P$ and t_R data in the paper by Balzarini *et al.*¹⁷. (a) The $\log P$ data in ref. 17 were obtained with an octanol-pH 7.5 buffer system. Under this condition the ionization of both the basic ($-\text{NH}_2$, $\text{p}K_a \leq 4$) and the acidic moiety (phenol, $\text{p}K_a \geq 9$) of the nucleosides were suppressed. The t_R data, on the other hand, were obtained from a pH 3.2 buffer environment. In this case, the $-\text{NH}_2$ group in the nucleoside bases would be partially ionized. For the $-\text{NH}_2$ -containing nucleosides (cytidines, adenosines, guanosines and diaminopurines), the $\log P$ values were obtained from neutral species, but the t_R values were obtained from partially ionized species. For nucleosides without an $-\text{NH}_2$ group (uridines and thymidines), both the $\log P$ and t_R values were derived from neutral species. Therefore, the $\log P$ and t_R obtained by Balzarini *et al.*¹⁷ would not correlate linearly among all nucleosides. (b) In ref. 17, the t_R values were obtained with a gradient mobile phase in which the acetonitrile concentration increased from 4

^a Calculated from values in Table 1 in ref. 17.

^b Calculated from values in Tables 1 and 2 in ref. 17.

to 25%, non-linearly. For compounds of different polarity, the effect of changing mobile phase on t_R would be quite different. Minick and co-workers^{15,16} observed that the effect on LC retention time due to changes in acetonitrile concentration in the mobile phase was independent of chemical structures. Thus, the use of gradient mobile phase in LC may have contributed to the poor linear correlation of Balzarini *et al.*'s data between the log P and t_R of the entire nucleoside derivatives.

It is evident from our data presented in Table III and Figs. 3–5 that there is a strong linear correlation between log P and log k' values of diversified nucleoside analogues and that hydrophobicity of nucleoside analogues can be estimated by their log k' values. The LC system, however, should closely resemble the octanol–aqueous partition system and the analytes should be kept in the neutral form.

Examination of Figs. 4 and 5 reveals that the slopes for the cytidines and the uridines are identical ($S=1.23$) but are smaller than those of the adenosines and inosines ($S=1.45$). In LC, where the C_{18} stationary phase is coated on a solid support, the size of the nucleoside base rings probably contributed more to the nucleosides' affinity to the lipophilic phase than is in the case of the shake-flask method. Since the pyrimidine ring is smaller than the purine ring, similar structural modification in the pyrimidines will have larger impact than the purines on their k' values. In the shake-flask method P is less affected by the molecular size than by the polarity of the compound, similar structural change would have similar impact on the P value of both the purine and the pyrimidine analogues. It appears that different impact of the molecular size on the k' and P of the nucleosides resulted in different slopes for the log k' vs. log P plot.

Table II shows that the P values of the uridines (10, 11), thymidines (12–15), adenosines (16–19, 21, 22) and inosines (23 and 24) are, respectively, about 2, 4, 10 and 1.2 times those of the corresponding cytidines (1–5, 8, 9). Substituting the 5-H of the pyrimidine base with F, CH_3 or Br increases its hydrophobicity by 1.6, 2 or 5 times, respectively. This substitution effect on P is in line with that observed by Garst¹⁴. Variations in the sugar moiety also have consistent effects on the hydrophobicity of the chemicals. The effect appears to be independent of the base moiety. Comparing the P values with those of the corresponding ribosides (1, 10, 12, 16, 23), the P values of the arabinosides (5, 21) are identical. The 2'-deoxyribosides (2, 17) are 2 times and the 2',3'-dideoxyribosides (3, 13, 18, 24) are 6 times more hydrophobic than the ribosides. Creation of a 2'-vinyl bond in the 2',3'-dideoxyribosides reduces their hydrophobicity by half (4, 14, 19 vs. 3, 13, 18) while insertion of a 3-azido in the dideoxyribosides increases their P values by 4 times (8, 15 vs. 3, 13). The P values of the carbo analogues (9, 22) are about half those of the corresponding ribosides (1, 16). The above observation is expected. While the spatial orientation of the $-OH$ would have no significant effect, removal of $-OH$ groups and introduction of lipophilic groups would enhance the hydrophobicity of a chemical. These changes are consistent with the atomic hydrophobicity contribution of Ghose and Crippen¹⁸. Balzarini *et al.*¹⁷ also observed similar correlation between the P values and the structural differences of their nucleoside derivatives.

In an effort to see if any empirical relationship exists between the P values and structural modifications on the nucleosides, we pooled our P data and those of Balzarini *et al.* together. We studied the combined P data from 48 nucleoside derivatives and found an empirical mathematical relationship existed between the P data and the

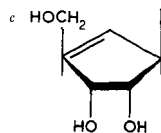
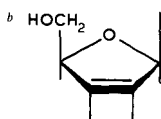
TABLE IV

EFFECT OF STRUCTURAL CHANGE ON THE *P* OF 2',3'-DIDEOXYADENOSINE (DDA)

F_i values were derived by two-dimensional correlation between the combined *P* values from Table II of this paper and Tables 1 and 2 of ref. 17 and the chemical structures.

Factors	F_i	Structural modification from DDA
F_1	0.08	Adenine changed to cytosine
F_2	0.19	Adenine changed to uracil
F_3	0.10	Adenine changed to hypoxanthine
F_4	0.18	Adenine changed to guanine
F_5	0.75	Aryl H substituted by $-NH_2$
F_6	2.05	Aryl H substituted by $-CH_3$
F_7	1.73	Aryl H substituted by F
F_8	2.38	Aryl H substituted by Cl
F_9	4.13	Aryl H substituted by Br
F_{10}	6.61	Aryl H substituted by I
F_{11}	0.15	Sugar ^a changed to ribose or arabinose
F_{12}	0.35	Sugar ^a changed to 2'-deoxyribose
F_{13}	0.66	Sugar ^a changed to 2',3'-dideoxy-2'-vinylribose ^b
F_{14}	1.17	2'-H substituted by F
F_{15}	2.21	3'-H substituted by F
F_{16}	4.33	3'-H substituted by $-N_3$
F_{17}	0.09	Sugar ^a changed to carbovinyl derivative ^c

^a 2',3'-Dideoxyribose.



structural differences of the nucleosides when they are considered as analogues of 2',3'-dideoxyadenosine (DDA). Each structural modification from DDA appears to affect the *P* of DDA (0.60) by a constant factor (F_i). These factors ($F_{i,j,k,\dots}$), derived from the combined *P* data of Balzarini *et al.* and ours, are listed in Table IV. Most of the factors are derived from four or more data points. We also discovered that there is an empirical mathematical relationship between *P* of a nucleoside analogue (P_N) and that of DDA (P_A). That relationship can be expressed as eqn. 3, where P_A is taken as 0.6^a and the *F* values are those listed in Table IV.

$$P_N = P_A F_i F_j F_k^* \dots \quad (3)$$

^a Average of 0.602 (this paper) and 0.605 (reference 16).

TABLE V
 COMPARISON OF CALCULATED (EQN. 3) AND ACTUAL *P* OF NUCLEOSIDE ANALOGUES

<i>Compound</i>	<i>P</i> <i>calculated</i>	<i>P actual</i>	
		<i>This paper</i>	<i>Ref. 17</i>
1	0.007	0.008	
2	0.017	0.013	0.017
3	0.048	0.055	0.050
4	0.032	0.028	0.038
5	0.007	0.008	
6	0.083	0.090	
3'-Fluoro-2',3'-dideoxycytidine	0.106		1.121
7	0.198	0.320	
8	0.208	0.208	0.231
9	0.004	0.005	
10	0.017	0.013	
2'-Deoxyuridine	0.040		0.031
5-Chloro-2'-deoxyuridine	0.095		0.078
5-Bromo-2'-deoxyuridine (SBDU)	0.165		0.102
5-Iodo-2'-deoxyuridine	0.264		0.244
2',3'-Dideoxyuridine	0.114		0.129
3'-Fluoro-2',3'-dideoxyuridine	0.252		0.303
3'-Fluoro-5-chloro-2',3'-dideoxyuridine	0.600		0.678
3'-Fluoro-5-bromo-2',3'-dideoxyuridine	1.041		0.903
3'-Fluoro-5-iodo-2',3'-dideoxyuridine	1.665		1.620
2,3'-Deoxy-2'-vinyluridine	0.075		0.085
11	0.494	0.465	0.480
12	0.082	0.079	0.067
3'-Fluoro-3'-deoxythymidine	0.516		0.529
13	0.234	0.264	0.233
14	0.154	0.193	0.154
15	1.012	1.091	0.964
16	0.090	0.105	
17	0.210	0.245	0.283
2-Amino-2'-deoxyadenosine (2ADA)	0.157		0.300
18	0.600	0.602	0.605
2-Amino-2',3'-dideoxyadenosine (2ADDA)	0.450		0.344
3'-Fluoro-2-amino-2',3'-dideoxyadenosine	0.994		1.128
3'-Fluoro-2',3'-dideoxyadenosine	1.326		1.207
19	0.396	0.311	0.440
20	1.038	0.801	
Azidoadenosine	2.598		2.249
2-Amino-azidoadenosine	1.949		1.725
21	0.090	0.111	
22	0.054	0.050	
23	0.009	0.010	
24	0.060	0.068	
2'-Fluoro-2',3'-dideoxyinosine	0.070	0.069 ^a	
2'-Deoxyguanosine	0.038		0.050
25	0.108	0.085	0.098
3'-Fluoro-2',3'-dideoxyguanosine	0.239		0.220
2',3'-Dideoxy-2'-vinylguanosine	0.070		0.061
Azidoguanosine	0.468		0.472

^a Ref. 19.

Thus, the *P* of AZT (15) is calculated to be $0.6 \cdot 0.19 \cdot 2.05 \cdot 4.33 = 1.012$. Table V compares the *P* values of the nucleoside analogues calculated according to eqn. 3 and to those determined by the shake-flask method. Except for 5BDDC, 5BDU, 2 ADA and 2ADDA, there is good agreement between the calculated and the actual *P* values.

Eqn. 3 and the factors *F* in Table IV are derived from experimentally determined *P* values of 48 nucleoside analogues. The data base is still relatively limited. However, it appears that the *P* or hydrophobicity of a nucleoside analogue can be calculated with eqn. 3 in conjunction with the factors in Table IV. As more data become available, the *F* values will be improved and refined and the validity of eqn. 3 will be further tested.

ACKNOWLEDGEMENTS

We wish to thank Mr. James Berg for technical assistance in obtaining data for four of the compounds, Ms. Gwen Wilkins for typing the manuscript and Dr. Karl Flora of the National Cancer Institute for encouragement in this work. This work is supported by the National Cancer Institute, NIH, PHS, under contract No. N01-CM-67864.

REFERENCES

- 1 N. Funasaki, S. Hada and S. Neya, *J. Chromatogr.*, 361 (1986) 33.
- 2 O. Papp, K. Volko, G. Szasz, I. Hermezc, J. Vamos, K. Hanko and Z. Ignath-Halasz, *J. Chromatogr.*, 252 (1982) 67.
- 3 N. El Tayer, H. van de Waterbeemd and B. Testa, *J. Chromatogr.*, 320 (1985) 305.
- 4 A. Negro, R. Mendez and F. Salto, *J. Liq. Chromatogr.*, 10 (1987) 2789.
- 5 A. Opperhuizen, *Toxicol. Environ. Chem.*, 15 (1987) 249.
- 6 D. Henry, J. H. Bock, J. L. Anderson and G. R. Carlson, *J. Med. Chem.*, 19 (1976) 619.
- 7 J. K. Baker, D. O. Rauls and R. F. Borne, *J. Med. Chem.*, 22 (1979) 1301.
- 8 R. Collander, *Acta Chem. Scand.*, 5 (1951) 774.
- 9 J. E. Haky and A. M. Young, *J. Liq. Chromatogr.*, 7 (1984) 675.
- 10 K. Miyake, F. Kitawa, N. Mizuno and H. Terada, *Chem. Pharm. Bull.*, 35 (1987) 377.
- 11 V. D. Biasi and W. J. Lough, *J. Chromatogr.*, 353 (1986) 279.
- 12 K. Valko, *J. Liq. Chromatogr.*, 7 (1984) 1405.
- 13 J. E. Garst and W. C. Wilson, *J. Pharm. Sci.*, 73 (1984) 1616.
- 14 J. E. Garst, *J. Pharm. Sci.*, 73 (1984) 1623.
- 15 D. J. Minick, J. J. Sabatka and D. A. Brent, *J. Med. Chem.*, 30 (1987) 2565.
- 16 D. J. Minick, J. H. Frenz, M. A. Patrick and D. A. Brent, *J. Med. Chem.*, 31 (1988) 1923.
- 17 J. Balzarini, M. Cools and E. De Clercq, *Biochem. Biophys. Res. Commun.*, 158 (1989) 413.
- 18 A. K. Ghose and G. M. Crippen, *J. Computational Chem.*, 7 (1986) 565.
- 19 A. P. Cheung, unpublished results.

CHROMSYMP. 1688

Application of a computer-assisted high-performance liquid chromatographic multi-wavelength ultraviolet detection system to simultaneous toxicological drug analyses

MAKIKO HAYASHIDA*, MAKOTO NIHIRA and TOKINORI WATANABE

Department of Legal Medicine, Nippon Medical School, Tokyo (Japan)

and

KIYOKATSU JINNO

School of Material Science, Toyohashi University of Technology, Toyohashi (Japan)

SUMMARY

An emergency drug screening system for the separation and identification of toxic drugs, MULTI-HPLC, is presented. Chromatographic peaks, which were impossible to identify with a conventional high-performance liquid chromatographic UV detection system, became distinguishable by the spectral search and retention prediction of the data-processing program MCASYST. Sixty-five toxic drugs, frequently identified in drug poisonings in Japan, were selected as references in the drug library. Retention time, optimum detection wavelength, detection limit and recoveries from serum and urine were listed. Possible applications of the system are demonstrated, using gastric contents, sera and urines in cases of multiple drug ingestion. Quantitative analysis was sufficiently sensitive and precise to permit clinical diagnosis with increased accuracy.

INTRODUCTION

The rapid and accurate analysis of the cause of a poisoning case is difficult and requires a competent, intensive investigator, especially in cases of multiple drug ingestion^{1,2}. However, recent progress in liquid chromatography may permit the automation of a systematic procedure^{3–5}. We report here a newly developed, sophisticated drug-screening system, MULTI-HPLC, a reversed-phase high-performance liquid chromatographic (HPLC) assay for toxic drugs in biological samples by multi-wavelength UV detection and an automated identification system, and its clinical applications.

Sixty-five toxic drugs, frequently identified in drug poisoning cases in Japan⁶, were selected as reference drugs; these should cover *ca.* 95% of drug poisoning cases. According to their pharmacological effect, they were classified as antipsychoactive, antianxiety, anticonvulsant and antidepressant drugs. They were also classified accor-

ding to their structures as barbiturates, benzodiazepines, butyrophenones and phenothiazines. In the MULTI-HPLC system these drugs, which have various physico-chemical properties, can be analysed simultaneously with a single sample injection.

EXPERIMENTAL

Liquid chromatography

The HPLC system consisted of a Model 880-PU pump and a Multi-320 multi-channel UV detector (Jasco, Tokyo, Japan). The column was a Jasco FineSil C₁₈S (250 mm × 4.6 mm I.D.) maintained at 50°C. The mobile phases were mixtures of 10 mM perchloric acid, 10 mM sodium perchlorate and acetonitrile and the flow-rate was 1 ml/min.

The data handling was performed with a NEC9801Vm₂ personal computer and data processor (DP-L320, Jasco), whose functions include data acquisition by the multi-channel UV detector, data processing, generation of three-dimensional chromatograms and contour chromatograms and peak deconvolution. A microcomputer-assisted separation system (MCASYST) was also used with the MULTI-HPLC system. The components of MCASYST are illustrated schematically in Fig. 1.

Spectrum search function. The multi-wavelength UV detector yields a specific absorption spectrum for each drug. Even when some drugs show similar or identical retention times, comparison of spectra with reference spectra, provided by a stored database drug library, helps to identify the compounds.

Retention prediction program. This is based on the statistically and experimentally determined equation

$$\log k' = (-0.0178X + 1.2003)\log P_e - (0.0034X + 0.4562)$$

where X is the volume fraction of the organic solvent, k' is the capacity factor of the solute, and P_e is a physico-chemical parameter of the solute. If X and $\log k'$ are

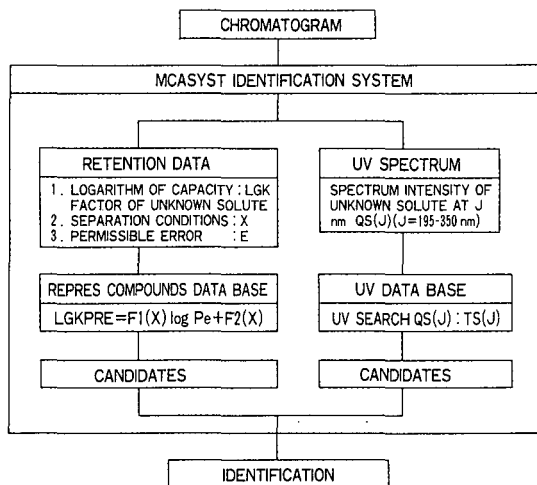


Fig. 1. Algorithm of automated identification in MCASYST.

determined, then $\log P_e$ for a toxic substance can be predicted and its identity searched for in the stored data file⁵.

Materials

All pure drugs used were kindly donated by Shionogi (Osaka, Japan), Fujisawa (Osaka, Japan), Sankyo (Tokyo, Japan), Roche (Tokyo, Japan), Upjohn (Tokyo, Japan), Takeda (Osaka, Japan) and Yoshitomi (Osaka, Japan). The standard samples were dissolved in acetonitrile at a concentration of 100 $\mu\text{g/ml}$.

Human body fluids, such as gastric contents, sera and urines from poisoned patients, were collected at the Critical Care Medical Centre (CCMC), Nippon Medical School, Tokyo, Japan. Volumes of 100 μl of biological samples and 200 μl of acetonitrile were shaken and then centrifuged at 9600 g for 20 min. After centrifugation, the extracts were passed through an Ekikurodisk cartridge (Gelman Science, Tokyo, Japan).

RESULTS AND DISCUSSION

Recovery

To test the efficiency and reproducibility of the extraction procedure, absolute recoveries from plasma and urine samples were determined. The recoveries of the 65 drugs registered in the standard drug library are listed in Table I. Drugs, that have a low solubility in acetonitrile could not be quantitatively recovered from serum.

Optimum detection wavelength

The spectra of the 65 drugs obtained with the multi-wavelength UV detector were similar to those measured by a double-beam UV spectrometer. The optimum detection wavelength was at the maximum UV absorption of the spectrum of each drug.

Linearity

A linear response with the multi-wavelength UV detector at the optimum detection wavelength of each drug was obtained except some poorly soluble drugs. The relationship between concentration and peak area was linear up to 500 $\mu\text{g/ml}$ for the 65 standard drugs.

Detection limit

The detection limit was dependent on the quality and age of the column used. Limits of detection based on a signal-to-noise ratio of 3:1 and using new, high-quality columns are listed in Table I.

Clinical applications

Possible applications of the system to gastric contents, sera and urines in drug poisoning cases were demonstrated. In drug poisoning cases the patients had sustained depression or schizophrenia and received psychiatric treatment. In suicidal attempts the patients had ingested large amounts of prescribed drugs. No information about the toxic compounds taken by the patients was available at the time of the HPLC analysis, because the patients were often in a comatose state on arrival at the CCMC.

TABLE I
LIST OF SUBSTANCES REGISTERED IN STANDARD DRUG LIBRARY

The 65 toxic drugs most frequently encountered in Japan are listed. Approximately 95% of drug poisoning cases should be covered.

Common name	Retention time (min)	k'	Log k'	Log P_e	Maximum detection wavelength (nm)	Detection limit (ng)	Recovery (%)	
							Urine	Serum
Acetaminophen	2.49	0.556	-0.255	0.480	245	2.81	142	100
Caffeine	2.87	0.794	-0.100	0.713	210	1.48	176	100
Barbital	2.91	0.819	-0.087	0.734	210	3.95	135	100
Sulpiride	2.87	0.794	-0.100	0.713	215	1.84	98	100
Acetylsalicylic acid	4.14	1.588	0.201	1.168	230	4.59	31	33
Phenobarbital	4.57	1.856	0.269	1.271	210	3.21	76	76
Bromvalerylurea	4.71	1.944	0.289	1.301	210	7.63	92	96
Ethenzamide	5.02	2.138	0.330	1.364	210	1.39	107	101
Bromazepam	4.61	1.881	0.274	1.280	235	4.50	113	101
Phenacetin	5.45	2.406	0.381	1.442	245	3.41	82	82
Cloxacolam	4.79	1.994	0.300	1.318	240	3.52	77	40
Oxazolam	5.14	2.213	0.345	1.386	240	4.02	95	63
Chlormezanone	6.41	3.006	0.478	1.588	230	4.89	49	52
Chlordiazepoxide	5.72	2.575	0.411	1.486	245	3.52	101	101
Pentobarbital	7.22	3.513	0.546	1.690	210	11.25	90	76
Nitrazepam	7.03	3.394	0.531	1.667	275	5.36	89	105
Amobarbital	7.45	3.656	0.563	1.716	210	8.49	91	91
Phenytoin	7.45	3.656	0.563	1.716	210	4.79	57	56
Secobarbital	8.91	4.569	0.660	1.863	210	13.64	91	150
Carbamazepine	8.76	4.475	0.651	1.849	215	3.31	103	116
Glutethimide	8.99	4.619	0.665	1.870	210	4.89	96	96
Oxazepam	8.45	4.906	0.691	1.909	230	5.36	102	99
Nimetazepam	11.34	6.088	0.784	2.051	265	9.00	98	87
Estazolam	11.33	6.081	0.784	2.050	225	10.23	80	90
Diazepam	11.92	6.450	0.810	2.089	240	52.63	110	110
Flumitrazepam	14.11	7.819	0.893	2.215	220	11.54	131	133
Flurazepam	13.06	7.163	0.855	2.158	230	11.84	98	96
Alprazolam	15.02	8.388	0.924	2.261	225	72.00	83	83
Medazepam	12.56	6.850	0.836	2.129	255	8.65	84	88

Haloperidol	14.95	8.344	0.921	2.258	210	14.52	96
Proprietaryzine	14.69	8.181	0.913	2.245	270	10.00	106
Triazolam	19.67	11.294	1.053	2.457	220	8.33	83
Bromperidol	16.91	9.569	0.981	2.348	210	20.45	68
Promethazine	16.37	9.231	0.965	2.324	250	9.68	44
Desipramine	17.64	10.025	1.001	2.379	210	9.78	96
Carpipramine	13.84	7.650	0.884	2.201	210	25.71	114
Miaprotlyline	21.14	12.213	1.087	2.508	210	11.84	91
Nortriptyline	20.91	12.069	1.082	2.500	210	6.92	95
Hydroxyzine	20.80	12.000	1.079	2.497	210	21.43	80
Imipramine	20.64	11.900	1.076	2.491	210	15.00	100
Trihexyphenidyl	22.49	13.056	1.116	2.552	210	50.00	93
Amitriptyline	24.90	14.563	1.163	2.624	210	21.43	103
Trimipramine	27.30	16.063	1.206	2.688	210	26.87	105
Levomopromazine	26.11	15.319	1.185	2.657	250	21.43	107
Clocapramine	24.88	14.550	1.163	2.623	210	40.00	109
Chlorpromazine	32.76	19.475	1.289	2.815	255	22.50	9
Clomipramine	38.26	22.913	1.360	2.921	210	40.00	94
Primidone	3.25	1.031	0.013	0.885	210	3.69	80
Trimethadione	3.64	1.275	0.106	1.025	210	23.08	80
Haloxazolam	4.49	1.806	0.257	1.253	245	3.88	72
Metharbital	4.57	1.856	0.269	1.271	220	7.14	82
Mephobarbital	7.95	3.969	0.599	1.770	210	6.52	115
Clofedanol	9.18	4.738	0.676	1.886	210	7.50	95
Acetylpheneturide	10.72	5.700	0.756	2.008	210	9.00	40
Clonazepam	11.14	5.963	0.775	2.037	210	5.23	113
Fludiazepam	19.61	11.256	1.051	2.455	235	10.23	121
Zotepine	37.69	22.556	1.353	2.911	215	19.15	139
Mianserine	11.49	6.181	0.791	2.061	210	6.92	118
Clotiazepam	12.56	6.850	0.836	2.129	215	9.78	97
Perphenazine	17.02	9.638	0.984	2.353	255	23.08	100
Timiperone	9.33	4.831	0.684	1.899	245	3.85	91
Etizolam	20.02	11.513	1.061	2.469	210	10.98	96
Biperiden	18.26	10.413	1.018	2.403	210	31.58	96
Bromocriptine	29.41	17.381	1.240	2.740	210	46.15	74
Indomethacin	52.72	31.950	1.504	3.140	210	27.69	86

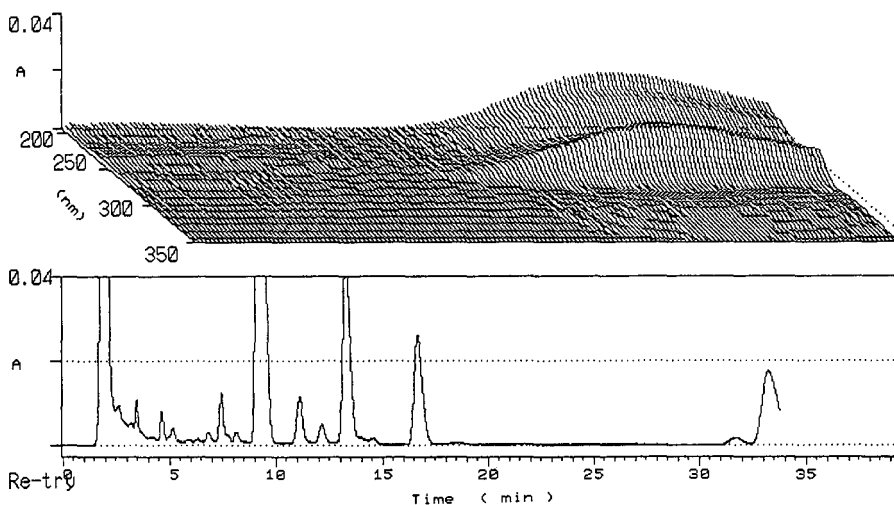


Fig. 2. Real-time display in case 1.

Using the functions of the MCASYST, the analytical procedures for identifying the unknown peaks in a sample chromatogram were the same as described previously⁷. The chromatogram of the extract of gastric contents in case 1 is shown in Figs. 2 and 3. Fig. 2 shows a real-time display during MULTI-HPLC analysis. The analyst can obtain a three-dimensional chromatogram of the unknown sample at the time of the analysis. Fig. 3A is a three-dimensional chromatogram, Fig. 3B is a contour map and Fig. 3C is a conventional chromatogram, obtained at 225 nm. Fig. 4 shows the printed output for peak 6 (at 16.71 min) in case 1. The UV search assigned it to promethazine with a coefficient of 0.99 (the definition is given in previous papers^{3,4}). Fig. 5 shows the UV spectra for peak 6. The upper spectrum in the measured one and the lower spectrum that of the promethazine standard in the UV spectral database. The retention search also indicated this compound as the first candidate with a coefficient⁵ of 0.837. The final result from both searches in the system shown in Table II indicated that promethazine was the best candidate.

The results from the MCASYST system, including coefficients for retention prediction (RPC) and spectral search (SSC), concentrations, and the lists of drugs prescribed, are shown in Tables II–IV for cases 1–3, respectively. In cases 1–3, more than six drugs in gastric contents were identified by the MCASYST system.

The results for serum and urine in case 3 are also shown in Table IV. Possible applications of the MCASYST system were obtained using biological samples. Gastric samples are most useful in determining the kind of drugs that have been taken by a patient. It is difficult to distinguish the compounds in the spectral search of serum and urine samples, as they may have been metabolized. However, there appears to be no interference with peak identification from common serum or urine components.

Recently, cases of “polydrug overdose” or “multiple drug ingestion” have increased^{8,9}. We have been making strong efforts to analyse these cases by conventional HPLC–UV systems, whereas rapid and accurate analysis by the MULTI-HPLC system is useful for “first-aid” treatment of poisoning in emergencies. However, in-

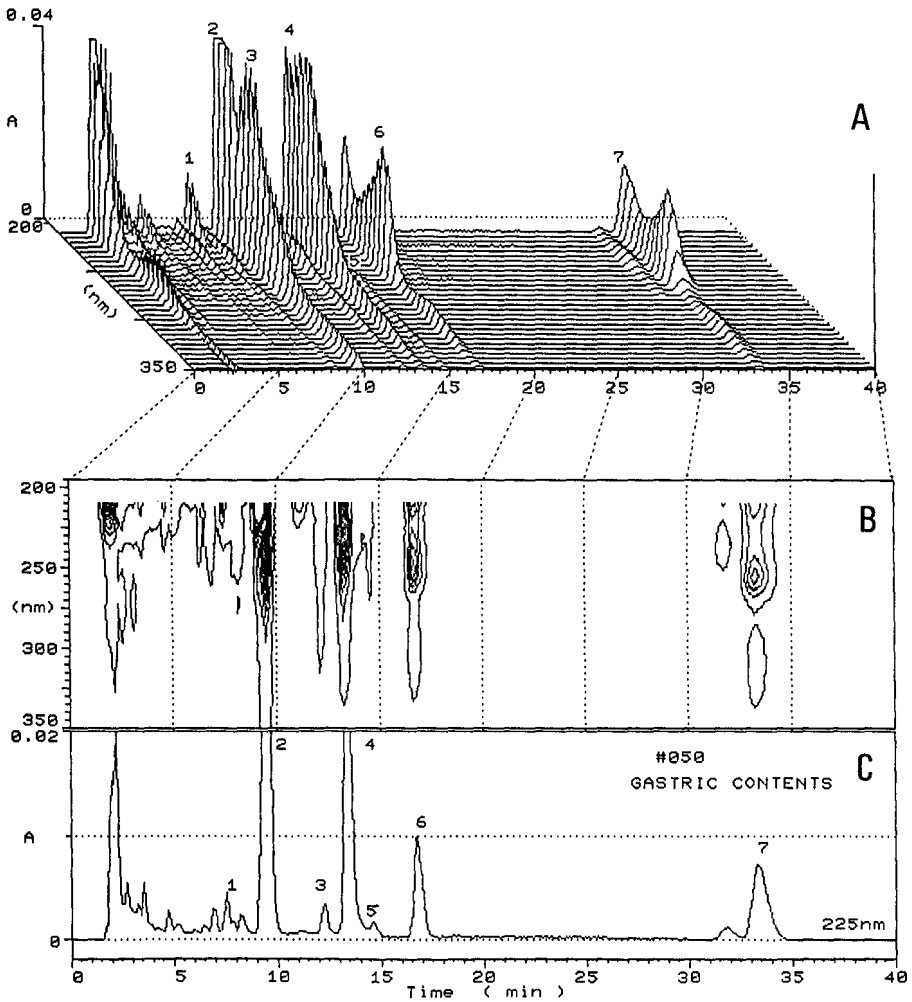


Fig. 3. (A) Three-dimensional chromatogram, (B) contour plot map chromatogram and (C) chromatogram at 225 nm for case 1. Peaks: 1=pentobarbital; 2=glutethimide; 3=diazepam; 4=flurazepam; 5=flunitrazepam; 6=promethazine; 7=chlorpromazine.

formation that was obtained from the patients about toxic compounds after their recovery from a comatose state was dubious in the most poisoning cases. The patients often said that they had injected "the prescribed drugs", which were not known in detail. Not only the number but also the name of the tablets taken remained uncertain. In clinical scenes, it should not be necessary for information obtained from patients to be required for scientific confirmation, and indeed it would be dangerous. In the cases examined here the results are different from the lists of prescribed drugs, which means that other drugs must have been taken in addition to the prescribed drugs. In some cases the patient must have ingested a few kinds of drugs and not all the drugs that had been prescribed. The possibility that the drugs ingested by the

UV SPECTRAL SEARCH		RETENTION SEARCH (ERROR<20%)	
No.	COMPOUND	log Pe	CORRELATION
1	PROMETHAZINE	2.324	0.837
2	ACETAMINOPHEN	2.261	0.688
3	PHENACETIN	2.258	0.663
4	LEVOMEPRIMAZINE	2.348	0.647
5	HALOXAZOLAM	2.354	0.595

SYSTEM OUTPUT		CORRELATION	BARGRAPH
1	PROMETHAZINE	0.913	*****

Fig. 4. MCASYS output of spectral search and retention prediction for peak 6 in case 1.

patients are different from those prescribed is demonstrated in the text. The results by the MULTI-HPLC system were also confirmed by thin-layer chromatography in each case.

Although the MULTI-HPLC system in its present form leaves many problems to be solved in practice, the concept has opened up a new dimension in emergency toxicology.

TABLE II

RESULTS OF PEAK IDENTIFICATION AND QUANTITATIVE ANALYSIS OF GASTRIC CONTENTS IN CASE 1

Case 1 = 55-year-old female, schizophrenia. RPC = retention prediction coefficient; SSC = spectral search coefficient.

Drugs prescribed	Drug measured	RPC	SSC	Concentration ($\mu\text{g/ml}$)
Lofepamine	Pentobarbital	0.992	0.99	70.62
Maprotyline	Glutethimide	0.974	0.99	820.63
Haloperidol	Diazepam	0.880	0.99	11.55
Cloxacolam	Flunitrazepam	0.896	0.98	6.23
Biperiden	Flurazepam	0.818	0.99	216.33
Haloxazolam	Promethazine	0.837	0.99	256.26
Flurazepam	Chlorpromazine	0.770	0.99	159.89
Pentobarbital				
Glutethimide				
Chlorpromazine				
Promethazine				

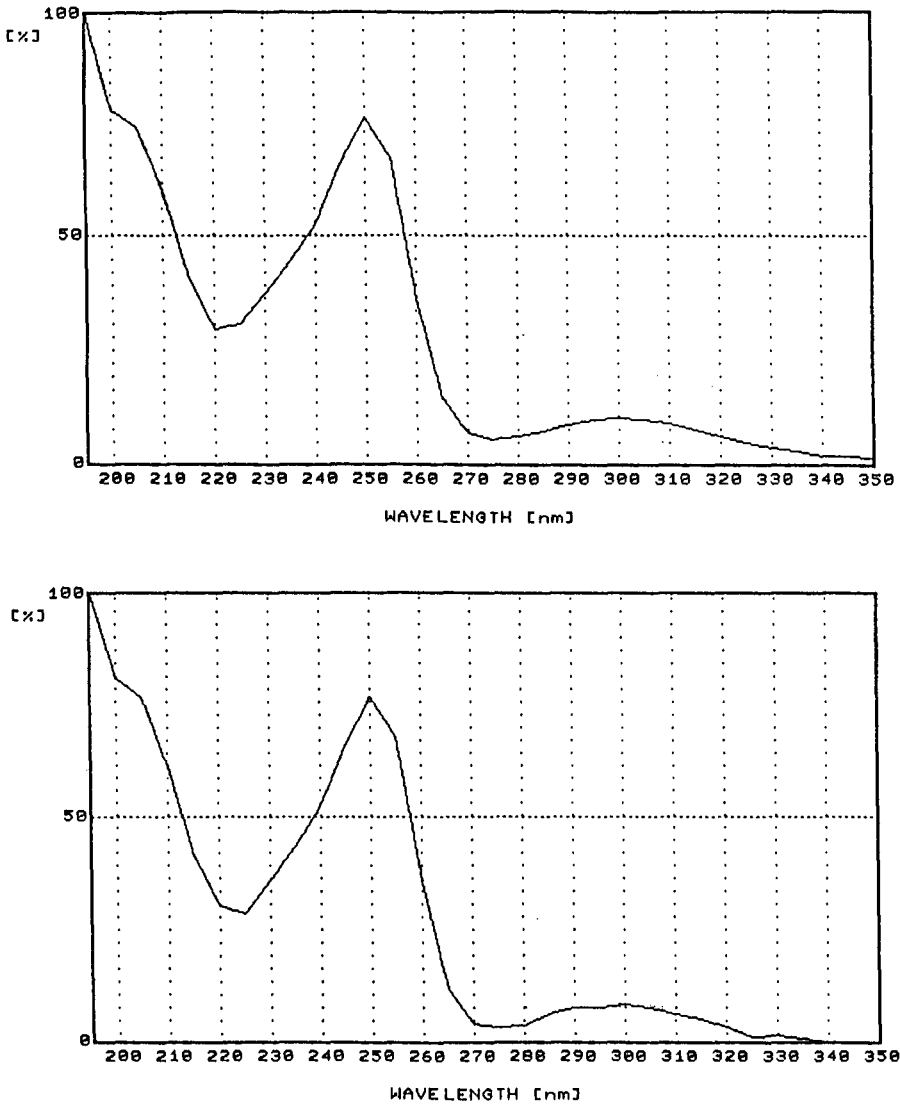


Fig. 5. (Top) spectrum of the compound in peak 6 and (bottom) spectrum of promethazine in the spectral library.

CONCLUSIONS

The computer-assisted MULTI-HPLC drug-screening system with simultaneous, multi-wavelength UV detection was developed for automated identification of toxic drugs. Chromatographic peaks that were impossible to identify by conventional HPLC became distinguishable by the spectral analysis and retention prediction of the data-processing program MCASYST and the accuracy of identification was satis-

TABLE III

RESULTS OF PEAK IDENTIFICATION AND QUANTITATIVE ANALYSIS OF GASTRIC CONTENTS IN CASE 2

Case 2 = 34-year-old male, depression. RPC = retention prediction coefficient; SSC = spectral search coefficient.

<i>Drugs prescribed</i>	<i>Drugs measured</i>	<i>RPC</i>	<i>SSC</i>	<i>Concentration ($\mu\text{g/ml}$)</i>
Sulpiride	Acetylsalicylic acid	0.840	0.96	345.76
Clozapolam	Phenobarbital	0.738	0.99	1549.78
Trihexyphenidyl	Ethenzamide	0.997	0.95	893.62
Diazepam	Diazepam	0.932	0.99	217.42
Phenobarbital	Promethazine	0.837	0.99	797.84
Promethazine	Hydroxyzine	0.914	0.95	34.38
Chlorpromazine	Chlorpromazine	0.827	0.99	754.65
Estazolam				
Haloxazolam				

TABLE IV

RESULTS OF PEAK IDENTIFICATION AND QUANTITATIVE ANALYSIS OF GASTRIC CONTENTS, SERUM AND URINE IN CASE 3

Case 3 = 57-year-old male, depression. RPC = retention prediction coefficient; SSC = spectral search coefficient.

<i>Drugs prescribed</i>	<i>Drugs measured</i>	<i>RPC</i>	<i>SSC</i>	<i>Concentration ($\mu\text{g/ml}$)</i>
Ergotamine tartrate	<i>Gastric contents</i>			
Phenobarbital	Phenobarbital	0.629	0.99	19.10
Estazolam	Nitrazepam	0.644	0.99	246.7
Hydrochlorothiazide	Amitriptyline	0.730	0.99	296.9
Dipyridamol	<i>Serum</i>			
	Phenobarbital	0.843	0.99	11.15
	Nitrazepam	0.857	—	1.08
	<i>Urine</i>			
	Phenobarbital	0.911	0.99	21.13
	Nitrazepam	0.912	0.91	0.21
	Amitriptyline	0.927	—	1.48

factory. Using the computerized procedure, analysis is speedy and almost automatically processed, avoiding "trial-and-error" condition searches. The samples can be analysed after a single injection into the MULTI-HPLC system. Quantitative analysis proved to be very sensitive and precise, permitting clinical diagnosis with increased accuracy. The MULTI-HPLC drug screening system is considered to be clinically practical and beneficial.

ACKNOWLEDGEMENTS

The authors thank Drs. S. Suzaki and Y. Yamamoto of the Critical Care Medical Centre, Nippon Medical School, Tokyo, Japan, for their collaboration in furnis-

hing the samples. This work was financially supported by a Grant-in-Aid for Developmental Scientific Research (Grant No. 61870114) from the Ministry of Education of Japan.

REFERENCES

- 1 D. W. H. Hill and K. J. Langer, *J. Liq. Chromatogr.*, 10 (1987) 377.
- 2 M. Hayashida, M. Nihira, S. Suzaki and Y. Yamamoto, *Jpn. J. Toxicol.*, 2 (1988) 49.
- 3 T. Hoshino, M. Senda, T. Hondo, M. Saito and S. Tohei, *J. Chromatogr.*, 316 (1984) 473.
- 4 T. Hoshino, M. Senda, T. Hondo, M. Saito and S. Tohei, *J. Chromatogr.*, 332 (1985) 139.
- 5 K. Jinno, M. Kuwajima, M. Hayashida, T. Watanabe and T. Hondo, *J. Chromatogr.*, 436 (1988) 11.
- 6 Y. Yamamoto, S. Ukai, Y. Okada, R. Chizuka, K. Yamashita and T. Yoshioka, *Jpn. J. Toxicol.*, 2 (1988) 193.
- 7 K. Jinno and M. Kuwajima, *J. Chromatogr. Sci.*, 27 (1989) 57.
- 8 N. K. Mello, *Jpn. J. Alcohol Drug Dependence*, 22 (1987) 84.
- 9 M. Nihira, M. Hayashida and T. Watanabe, *Jpn. J. Legal Med.*, 42 (1988) 59.

CHROMSYMP. 1657

Chromatographic characteristics of nucleic acid components on vinyl alcohol copolymer gel columns

KOHI NOGUCHI*, YUZO YANAGIHARA, MASAO KASAI and NORIKO HIRATA
Gel Separation Development Department, Asahi Chemical Industry Co., Ltd., 1-3-2 Yakoo, Kawasaki-ku, Kawasaki-shi, 210 (Japan)

SUMMARY

The chromatographic characteristics of nucleic acid components on an Asahi-pak GS-320 vinyl alcohol copolymer gel column were investigated in comparison with those on an ODS column. On both columns the order of elution within each class (nucleotide, nucleoside or nucleic acid base) was generally pyrimidine compounds followed by purine compounds, the only exception being the late elution of thymine from the GS-320 and, particularly, from the ODS column.

Between the three classes of nucleic acid components, the two columns exhibited different elution orders. On the GS-320 column, the order was consistently nucleotide, nucleoside and base, *i.e.*, in order of increasing water solubility, with a consistent correlation between capacity factors (k') and Hansch's $\log P$ values, showing that hydrophobic adsorption between the gel and the base group is the predominant separation mechanism for both the nucleosides and the bases. In the separation of nucleotides on the GS-320 column, an ion-repulsion interaction appeared to be predominant, as the k' values were negative and the retention volumes were increased by methylation of the carboxylic groups in the gel but unaffected by addition of acetonitrile to the mobile phase. On the strongly hydrophobic ODS column, nucleoside elution occurred after nucleotide and base elution and more complex correlations were observed, suggesting hydrophobic interaction of the octadecyl group of the gel with the sugar group and also with the base group, particularly for the nucleosides. This inference was supported by an observed increase in the capacity factor of ribose in the presence of antichaotropic sodium chloride on the ODS but not on the GS-320 column.

The utility of the GS-320 column for the separation of nucleic acid components was also investigated. Nucleotides, nucleosides and bases were consistently separated, apparently by a hydrophobic adsorption mechanism, permitting the simple, efficient analysis of mixtures of these substances by isocratic elution.

INTRODUCTION

The Asahipak GS-320 vinyl alcohol copolymer gel column, is a multi-purpose column for high-performance liquid chromatography (HPLC), which can be utilized for gel chromatography, reversed-phase partition or multi-mode chromatography, depending on the properties of the sample and the mobile phase¹⁻⁴. Preliminary investigations of its suitability for the analysis of nucleic acid components showed their elution order to be nucleotides, nucleosides and nucleic acid bases, unlike that exhibited on the widely used ODS column, and led to the present investigation of the chromatographic characteristics of various nucleic acid components on a GS-320 column.

EXPERIMENTAL

Chromatography was performed with a Hitachi-638 chromatograph (Hitachi Seisakusho, Tokyo, Japan), equipped with a Uvidec spectrophotometer (JASCO, Tokyo, Japan), operated at 260 nm.

The following columns were used: Asahipak GS-320 (500 mm × 7.6 mm I.D.) and GS-320H (250 mm × 7.6 mm I.D.) HPLC columns (Asahi Chemical Industries, Tokyo, Japan), packed with vinyl alcohol copolymer gel, having a mean particle diameter of 9.0 μm and an exclusion limit of 40 000 Da; YMC PACK AQ-312 or AM-312 (both 150 mm × 6.0 mm I.D.; Yamamura Kagaku, Kyoto, Japan) HPLC columns packed with ODS gel; and methylated Asahipak GS-320 gel columns (250 mm × 7.6 mm I.D.).

The methylated gel was obtained by stirring Asahipak GS-320 gel and 14% boron trifluoride-methanol in a three-necked flask, equipped with stirrer and thermometer, for 16 h at room temperature⁵. Nucleotides, nucleosides and their bases were purchased from Wako (Osaka, Japan).

RESULTS AND DISCUSSION

In general terms, the chromatographic characteristics of the bases, nucleosides and nucleotides (structures and pK_a values are given in Table I) on the GS-320 column were found to be similar to those on the ODS column, but with significantly smaller retention volumes, particularly for nucleosides, and some differences in elution order. The overall results for both columns are shown in terms of the capacity factors at pH 6.0 in Table II, the relationship between mobile phase pH and retention volume in Figs. 1-3 and the elution orders in Table III.

Nucleic acid bases

The relationship between base retention volume and eluent pH on the GS-320 column is similar to that on the ODS column, as shown in Fig. 1. The pH-retention volume profiles, showing weak retention of the bases at ionizing pH levels, suggest analogous elution mechanisms for the two columns. On both columns, the order of elution was generally pyrimidine compounds, followed by purine compounds. The exception was thymine, which was eluted after hypoxanthine from the GS-320 column and after guanine from the ODS column. It appears that the elution of thymine,

TABLE I
ABBREVIATIONS AND pK_a VALUES OF NUCLEIC ACID COMPONENTS

<i>Substance</i>	<i>Abbreviation</i>	<i>pK_a</i>
Cytosine	C	4.5, 12.2
Uracil	U	9.5
Thymine	T	9.9
Adenine	A	4.15, 9.8
Guanine	G	3.2, 9.6, 12.4
Hypoxanthine	Hx	2.00, 8.90
Cytidine	CYD	4.15, 12.5
Uridine	URD	9.2, 12.5
Thymidine	THD	9.8
Adenosine	ADO	3.5, 12.5
Guanosine	GUO	1.6, 9.2, 12.4
Inosine	INO	1.2, 8.8, 12.3
Cytidine monophosphate	CMP	4.5, 6.3
Uridine monophosphate	UMP	6.4, 9.5
Thymidine monophosphate	TMP	10.0
Adenosine monophosphate	AMP	3.7, 6.1
Guanosine monophosphate	GMP	2.5, 6.1, 9.4
Inosine monophosphate	IMP	6.0, 8.9

TABLE II
CAPACITY FACTORS (k')

Determined at 30°C with a mobile phase of 10 mM sodium hydrogenphosphate (pH 6.0) on Asahipak GS-320 and YMC PACK AQ-312 columns at flow-rates of 1.0 and 0.6 ml/min, respectively.

<i>Sample</i>	<i>Log P</i>	<i>k'</i>	
		<i>GS-320</i>	<i>AQ-312</i>
AMP	—	—0.10	6.17
GMP	—	—0.14	2.05
IMP	—	—0.21	2.31
TMP	—	—0.19	5.17
UMP	—	—0.23	1.00
CMP	—	—0.23	0.62
Adenosine	—0.18	2.15	52.99
Guanosine	—0.92	1.08	17.22
Inosine	—0.92	0.49	15.04
Thymidine	—	0.78	26.89
Uridine	—0.92	0.35	5.30
Cytidine	—0.97	0.27	3.16
Adenine	0.33	2.86	10.79
Guanine	—0.35	1.53	4.03
Hypoxanthine	—0.27	0.80	3.92
Thymine	0.05	0.85	6.29
Uracil	—0.40	0.48	1.78
Cytosine	—0.68	0.35	1.02

TABLE III
ELUTION ORDER

Columns and conditions as in Table II.

Compound	Elution order		Compound	Elution order		Compound	Elution order	
	GS-320	AQ-312		GS-320	AQ-312		GS-320	AQ-312
Cytosine	1	1	Cytidine	1	1	CMP	1	1
Uracil	2	2	Uridine	2	2	UMP	1	2
Thymine	4	5	Thymidine	4	5	TMP	4	5
Hypoxanthine	3	3	Inosine	3	3	IMP	3	4
Guanine	5	4	Guanosine	5	4	GMP	5	3
Adenine	6	6	Adenosine	6	6	AMP	6	6

which is the only one of the six bases that contains a methyl group, is strongly retarded on the ODS column as a result of strong enhancement of the hydrophobic interaction with its long alkyl group by the methyl group, whereas on the GS-320 column, which does not have a long alkyl group, the enhancement and hence the retardation effect are far smaller.

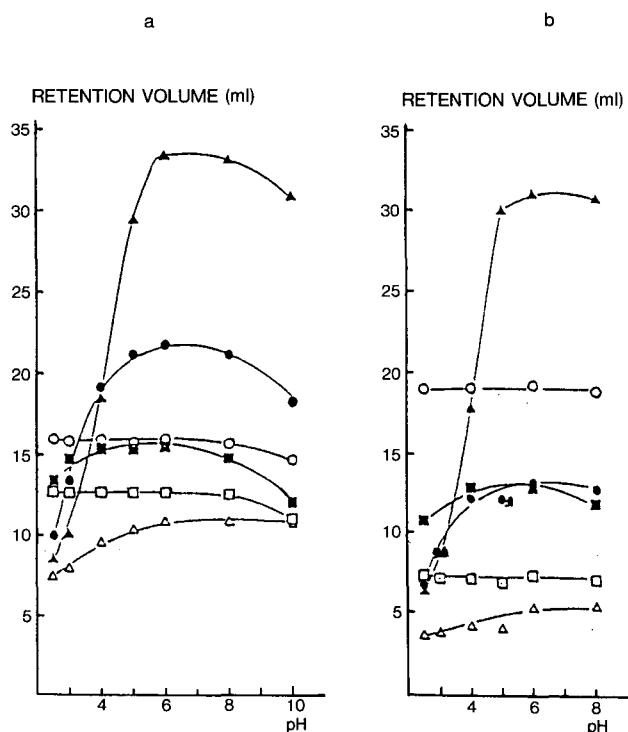


Fig. 1. Nucleic acid base retention volumes *versus* eluent pH. Columns: (a) Asahipak GS-320H; (b) YMC PACK AQ-312. Samples: 0.1 mg/ml solution, 10 μ l for (a) and 6 μ l for (b). \blacktriangle = Adenine; \bullet = guanine; \blacksquare = hypoxanthine; \circ = thymine; \square = uracil; \triangle = cytosine. Mobile phase: 10 mM sodium phosphate. Flow-rates: (a) 1.0; (b) 0.6 ml/min. Temperature, 30°C; detection at 260 nm (0.64 a.u.f.s.).

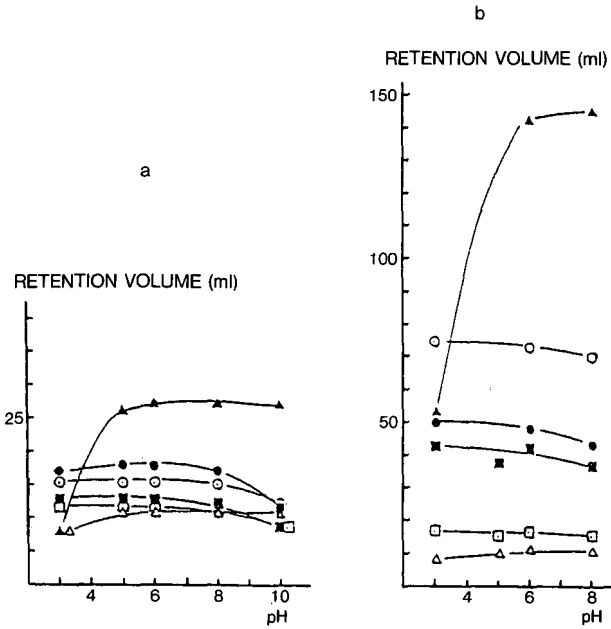


Fig. 2. Nucleoside retention volumes *versus* eluent pH. Samples: ▲ = adenosine; ● = guanosine; ■ = inosine; ○ = thymidine; □ = uridine; △ = cytidine. Detection at 260 nm (0.32 a.u.f.s.); other conditions and columns as in Fig. 1.

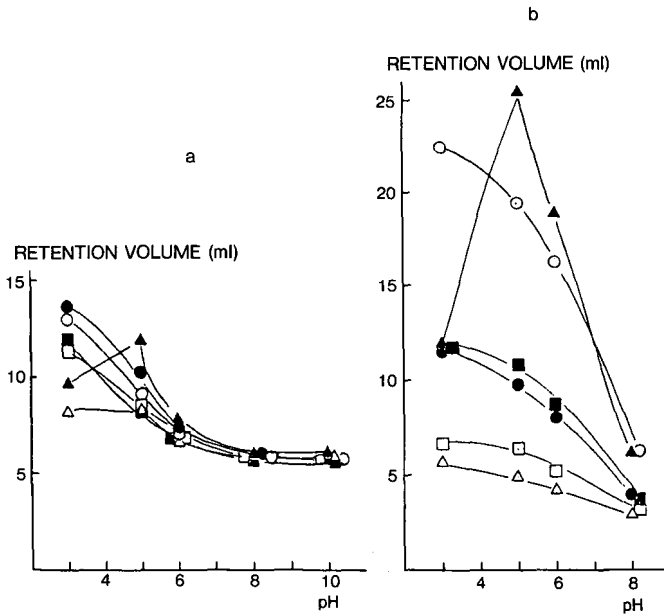


Fig. 3. Nucleotide retention volumes *versus* eluent pH. Samples: ▲ = AMP; ● = GMP; ■ = IMP; ○ = TMP; □ = UMP; △ = CMP. Columns and conditions as in Fig. 2.

A clear decrease in retention volume was observed for both columns when acetonitrile was present in the mobile phase, as shown in Fig. 4. For both columns, a positive slope was found in the plots showing the relationship between k' and Hansch's $\log P$ values⁶, an index of the hydrophobicity of nucleic acid components.

All of the above results indicate that the chromatographic mechanism for nucleic acid bases on both columns is reversed-phase partition, based on hydrophobic interaction between base and gel.

Nucleosides

For nucleosides on both columns, the pH-retention volume profile (Fig. 2), the elution order (Table III) and the effect of acetonitrile concentration in the mobile phase (Fig. 5) were all similar to those obtained for the nucleic acid bases. The k' values for nucleosides on the GS-320 column were all far smaller than those found for the ODS column. The elution mechanism is discussed below.

Nucleotides

Negative k' values were obtained on the GS-320 column, in contrast to the positive k' values obtained on the ODS column (Table II). As shown in Fig. 6, the k' values on the GS-320 column were apparently unaffected by the presence of acetonitrile in the eluent, whereas those on the ODS column were decreased sharply by the

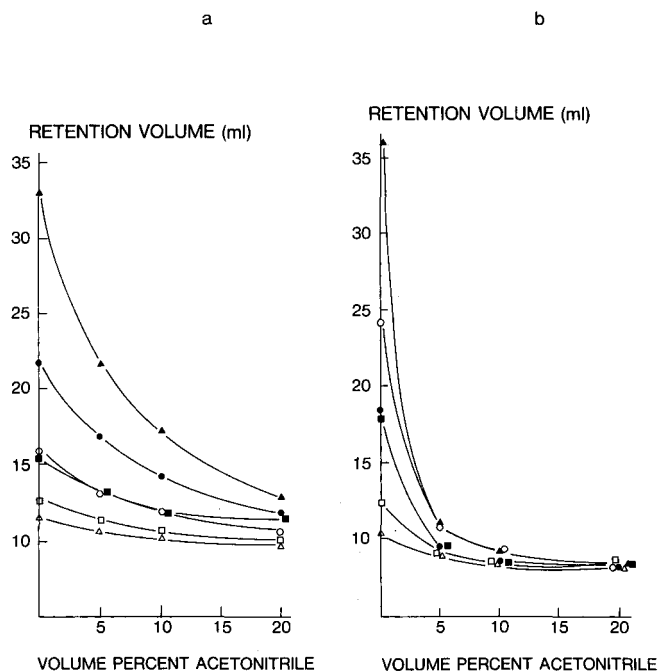


Fig. 4. Nucleic acid base retention volumes *versus* mobile phase acetonitrile content. Base designations as shown in Table I. Samples: 0.1 mg/ml solution, 20 μ l for (a) and 6 μ l for (b). \blacktriangle = Adenine; \bullet = guanine; \blacksquare = hypoxanthine; \circ = thymine; \square = uracil; \triangle = cytosine. Mobile phases: 10 mM sodium hydrogen-phosphate (pH 6.0)-acetonitrile as indicated. Columns and other conditions as in Fig. 2.

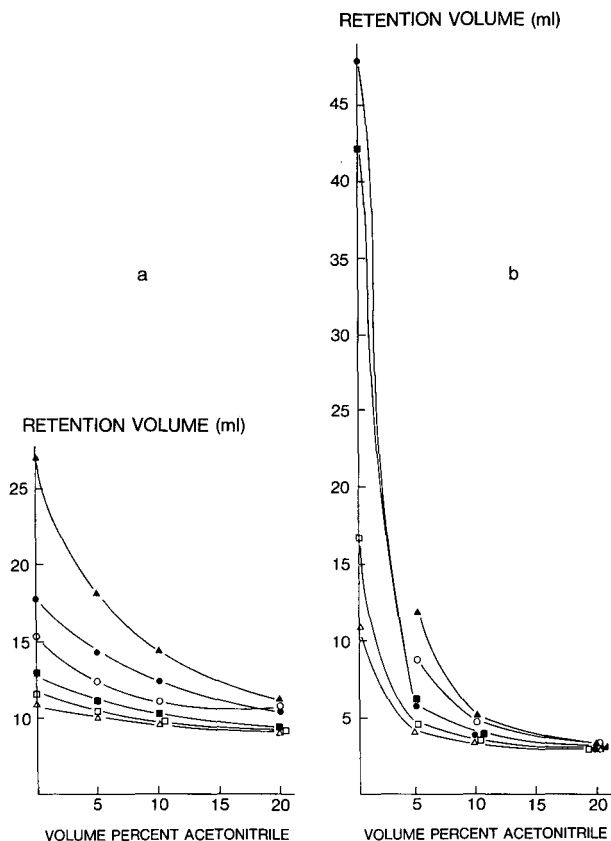


Fig. 5. Nucleoside retention volumes *versus* mobile phase acetonitrile content. Samples: \blacktriangle = adenosine; \bullet = guanosine; \blacksquare = inosine; \circ = thymidine; \square = uridine; \triangle = cytidine. Columns and conditions as in Fig. 4.

presence of as little as 5% of acetonitrile. Methylation of the GS-320 gel, which inherently contains a small amount of carboxyl groups, was found to result in larger retention volumes for nucleotides. For bases and nucleosides, on the other hand, no difference in retention volume was observed between the GS-320 and the methylated GS-320 gel columns. Overall, these results indicate that the elution mechanism for nucleotides was mainly ion repulsion on the GS-320 column and, as expected, reversed-phase partition on the ODS column.

Selectivity between a base and its derivatives

Between the three classes of nucleic acids (nucleotide, nucleoside and nucleic acid base), the two columns exhibited significantly different elution orders. On the GS-320 column, the order was consistently nucleotide, nucleoside and base, whereas on the ODS column, it was nucleotide, base and nucleoside. The reasons for this difference may be of particular interest, and were therefore investigated further.

In plots of the relationship between the capacity factors (k') and Hansch's $\log P$

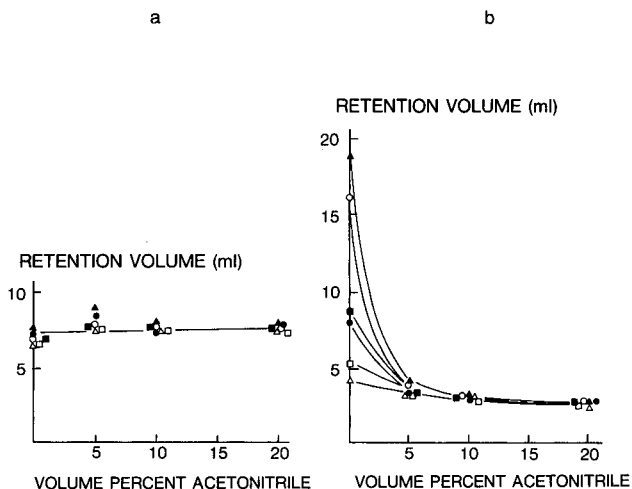


Fig. 6. Nucleotide retention volumes *versus* mobile phase acetonitrile content. Samples: ▲ = AMP; ● = GMP; ■ = IMP; ○ = TMP; □ = UMP; △ = CMP. Columns and conditions as in Fig. 4.

values of nucleosides and bases, one correlation curve was found to apply to both nucleosides and bases on the GS-320 column, but two separate correlation curves were found for the ODS column as a result of the high capacity factors of nucleosides on this column.

Linear van 't Hoff plots were obtained for both columns, as shown in Fig. 7, indicating that the nucleoside and base elutions involved reversed-phase partition, based on hydrophobic interaction, but that this interaction is remarkably strong for nucleosides on the ODS column.

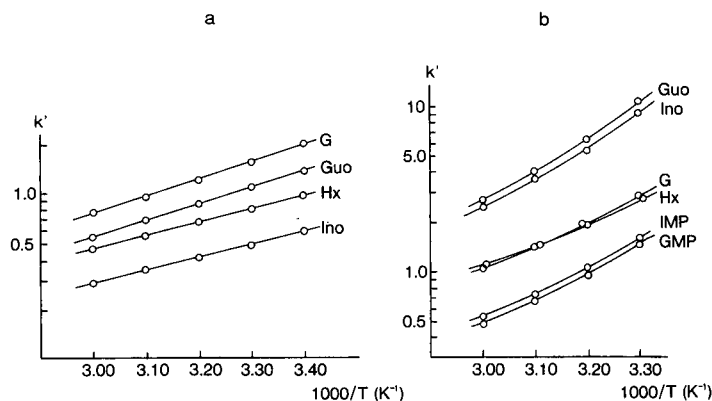


Fig. 7. Capacity factors as a function of absolute temperature. Columns: (a) Asahipak GS-320H; (b) YMC PACK AQ-312. Samples: (a) 20 μ l of 0.1 mg/ml solution of guanine, guanosine, hypoxanthine or inosine; (b) 6 μ l of 0.1 mg/ml solution of guanosine, inosine, guanine, hypoxanthine, IMP or GMP. Mobile phase, 10 mM sodium hydrogenphosphate (pH 6.0); flow-rate, (a) 1.0 ml/min, (b) 0.6 ml/min; temperature, 30°C; detector, 260 nm (0.32 a.u.f.s.).

We further found that the order of elution nucleotide, base and nucleoside observed here for the ODS column was also exhibited on the Asahipak ODP-50 column, which is packed with a gel containing C_{18} groups on a vinyl alcohol copolymer (results not shown). This suggests that the strong retention of nucleosides on the ODS column results from the strong hydrophobic character of its C_{18} group and not from its silanol group.

In a previous report, we described the retention behaviour of non-ionic surfactants, represented by the series $C_9H_{19}-C_6H_4(p)-(OCH_2CH_2)_nOH$, on an Asahipak GS-310 vinyl alcohol copolymer gel column, in comparison with that on an ODS column⁷. The GS-310 column, which is a hydrophobic polymer gel column without C_{18} groups, apparently interacted hydrophobically only with the alkylaryl groups at temperatures of $\leq 30^\circ C$ in a mobile phase of aqueous acetonitrile at low to medium concentration, whereas the strongly hydrophobic ODS column apparently interacted hydrophobically with both the alkylaryl and the polyoxyethylene groups under the same conditions.

This suggests that an analogous interaction, involving the ribose groups of the nucleosides, might occur on the ODS gel. To explore this possibility for both the ODS and GS-320 gels, we investigated the effect of mobile phase NaCl and NaSCN contents on the retention of ribose alone by both columns, and on their retention of guanosine and inosine. As shown in Table IV, the capacity factor of ribose alone with a mobile phase containing no NaCl or NaSCN was nearly zero on the GS-320 column, indicating little or no hydrophobic interaction, and 0.34 on the ODS column. The addition of NaCl, an antichaotropic agent generally known to enhance hydrophobic interaction, effected no change in the ribose capacity factor on the GS-320 column, but substantially increased that on the ODS column. The addition of NaSCN, a chaotropic agent known to inhibit hydrophobic interaction, had no significant effect on ribose elution from either the GS-320 or the ODS column. These results are in accord with the assumption of hydrophobic interaction of nucleosides with both column gels. Although the results for ribose are not definitive, particularly because of the absence of a decrease in k' in the presence of NaSCN, they suggest that

TABLE IV

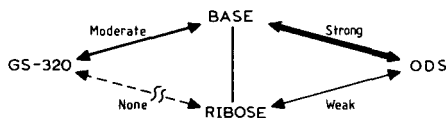
CAPACITY FACTORS (k')

Determined at $30^\circ C$ with a mobile phase of pH 6.0 and indicated content on Asahipak GS-320H and, in this experiment only, YMC PACK AM-312 columns, at flow-rates of 1.0 and 0.6 ml/min, respectively.

Column	Mobile phase	k'		
		Ribose	Guanosine	Inosine
GS-320H	10 mM sodium hydrogen-phosphate	0.02	1.10	0.49
	2 M sodium chloride	0.02	1.42	0.61
	2 M sodium thiocyanate	-0.03	0.32	0.05
AM-312	10 mM sodium hydrogen-phosphate	0.34	10.85	9.33
	2 M sodium chloride	0.41	18.71	14.86
	2 M sodium thiocyanate	0.33	4.23	3.22

a weak hydrophobic interaction also occurs between the ribose group of nucleosides and the ODS gel, but not the GS-320 gel.

The effects of organic solvent and antichaotropic salt additions to the mobile phase, the correlations between Hansch's $\log P$ and $\log k'$ and the linearity of the Van 't Hoff plots are in accord with the following scheme of hydrophobic interactions:



Hydrophobic interactions occur on the weakly hydrophobic GS-320 gel, but are relatively weak and are limited to a nucleic acid base, as it occurs alone or as part of its derivative. On the strongly hydrophobic ODS gel, on the other hand, hydrophobic interactions are strong with all three classes of nucleic acid components, and appear to occur with both the ribose group as well as the base group, particularly in nucleosides.

This gel-ribose interaction would account for the particularly high k' values of nucleosides on the ODS column, and hence for the difference in the order of elution of nucleic acid components between the ODS and GS-320 columns.

Utility of weakly hydrophobic GS-320

Isocratic analyses were performed on the GS-320 column, based on the above indications of its weakly hydrophobic effect and in particular its apparent freedom from pronounced nucleoside retention. Efficient separation of nucleic acid components was observed, as shown in the chromatograms in Fig. 8.

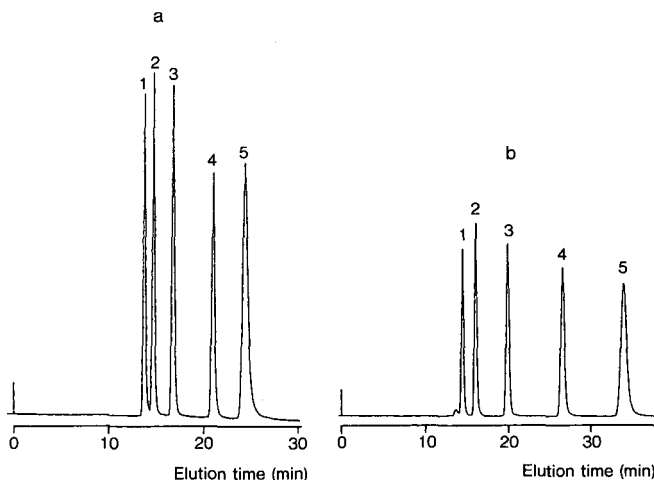


Fig. 8. Analysis of nucleic acid component mixtures. Column, Asahipak GS-320 (500 × 7.6 mm I.D.). Samples: (a) 15 μ l of (1) ATP (23 μ g/ml), (2) ADP (26 μ g/ml), (3) AMP (22 μ g/ml), (4) adenosine (22 μ g/ml) and (5) adenine (8 μ g/ml); (b) 15 μ l of (1) GTP (23 μ g/ml), (2) GDP (23 μ g/ml), (3) GMP (20 μ g/ml), (4) guanosine (21 μ g/ml) and (5) guanine (12 μ g/ml). Mobile phase, 200 mM phosphoric acid (pH 3.0); flow-rate, 1.0 ml/min; temperature, 30°C; detector, 260 nm (0.08 a.u.f.s.).

CONCLUSION

The results show that the elution of nucleic acid components on the GS-320 is effected primarily by hydrophobic interaction, similarly to that on the ODS column but substantially weaker and also differing in the following important respects.

(1) Within each class (nucleotide, nucleoside or base) a general tendency for elution of pyrimidines other than thymine before purines; elution of thymine after hypoxanthine from the GS-320 column, but after guanine from the ODS column, apparently because of interaction between the methyl group of thymine and the long alkyl group of the ODS gel.

(2) Between each base and its derivatives, elution in the order nucleotide, nucleoside and base from the GS-320 column but nucleotide, base and nucleoside from the ODS column; the difference in order is presumably attributable to restriction of interaction to the base group of nucleosides on the GS-320 column, and interaction with both the ribose as well as the base group of nucleosides on the ODS column.

(3) Elution of nucleotides before ethylene glycol, which is the non-retained solute, from the GS-320 column but after ethylene glycol from the ODS column, increased k' values for nucleotides on methylated GS-320 gel and the absence of any apparent effect by mobile phase acetonitrile on the k' values for nucleotides on the GS-320; all suggesting interaction dominated by ion repulsion between the phosphoric group of the nucleotide and the small number of carboxylic groups present in the GS-320 gel, in contrast to a predominant hydrophobic interaction between the octadecyl group of the ODS gel and the base group in the nucleotide.

The weakly hydrophobic polymeric structure of the GS-320 gel, and the resulting differences between its elution characteristics and those of the ODS column, permit highly practical, efficient analyses of complex molecules, based on the hydrophobicity of their components, as shown here for nucleic acid components by the chromatograms of component mixtures.

REFERENCES

- 1 H. Wada, K. Makino and T. Takeuchi, *J. Chromatogr.*, 320 (1985) 369.
- 2 K. Makino, H. Wada, H. Ozaki, T. Takeuchi, H. Hatano, T. Fukui, K. Noguchi and Y. Yanagihara, *Chromatographia*, 20 (1985) 713.
- 3 K. Yasukawa, M. Kasai, Y. Yanagihara and K. Noguchi, *J. Chromatogr.*, 332 (1985) 287.
- 4 N. Hirata, M. Kasai, Y. Yanagihara and K. Noguchi, *J. Chromatogr.*, 434 (1988) 71.
- 5 H. Sunaga and K. T. Suzuki, *J. Liq. Chromatogr.*, 11 (1988) 701.
- 6 C. Hansch and A. J. Leo, *Substituent Constants for Analysis in Chemistry and Biology*, Wiley, New York, 1979, pp. 182-258.
- 7 K. Noguchi, Y. Yanagihara, M. Kasai and B. Katayama, *J. Chromatogr.*, 488 (1989) 365.

Retention behaviour of mono- and dicarboxylic acids, carbohydrates and alcohols in ion-exclusion chromatography

ELIZABETH PAPP*

Research Group for Analytical Chemistry of the Hungarian Academy of Sciences, P.O. Box 158, H-8201 Veszprém (Hungary)

and

PETER KERESZTES

Bio Separation Technologies, P.O. Box 1, H-1775 Budapest (Hungary)

SUMMARY

The retention behaviour of mono- (C_1 – C_5) and dicarboxylic acids (C_2 – C_8), alcohols (C_1 – C_4) and carbohydrates (sucrose, α -D- and β -D-glucose, L-sorbose, D-xylose, D-mannose, D-galactose, D-fucose, D-lyxose, L- and D-arabinose, D-fucose and D-ribose) was studied using a poly(styrene-divinylbenzene) sulphonate (H^+) cation-exchange resin (Catex-H). The effects of the concentration of sulphuric acid and acetonitrile in the eluent and the column temperature (20–35°C) on the retention of compounds and on the number of the theoretical plates were investigated. For detection, UV and refractive index detectors connected in series were used.

INTRODUCTION

In an other paper¹, the separation of different short alkyl chain mono- and dicarboxylic acids was studied by reversed-phase high-performance liquid chromatography (RP-HPLC) and reversed-phase ion-pair HPLC (RP-IP-HPLC). A wide scope of these methods was achieved by the application of two stationary phases with different polarities (octylsilica and PRP-1), by adding methanol to the mobile phase, by changing the concentrations of the salt and the phosphoric acid and by the application of an ion-pair forming reagent (tetrabutylammonium hydrogensulphate, TBAHSO₄). Despite the advantage of the RP-HPLC and RP-IP-HPLC methods, the separation of hydrophilic carboxylic acids of low molar mass is difficult.

A versatile approach is ion-exclusion chromatography (IEC), in which hydrophilic weak acids, alcohols and carbohydrates^{2–16} are separated on a cation-exchange resin in the H^+ form, using an acidic eluent. In IEC strong acids, being highly ionized, pass quickly through the column. They are excluded from the negatively charged resin phase according to the Donnan membrane equilibrium principle and elute at the dead volume of the column. Non-ionic compounds (undissociated acids, alcohols and carbohydrates) can enter the resin network. Acids of intermediate strength such as

most carboxylic acids are partially ionized, depending on the pH of the medium. They generally eluted in order of their pK_a values¹⁷. In the separation of weak acids ($2.5 < pK_a < 6.0$) by IEC, other mechanisms also play a role, such as adsorption (partition) on the surface of the matrix of the cation-exchange resin.

Long alkyl chain carboxylic acids in the molecular form are retained on the stationary phase usually by a combination of ion exclusion, size exclusion and hydrophobic interaction.

In this work, a poly(styrene-divinylbenzene) sulphonate (H^+) cation-exchange resin (Catex-H) was applied to elucidate the retention mechanism by studying the effect of the experimental conditions on the retention of various solutes.

EXPERIMENTAL

The laboratory-made instrument used consisted of a pump (Model 6000 A, Waters Assoc.), variable-wavelength UV detector (Model OE-308, Labor MIM), an injector valve (Model 7125, Rheodyne) with a 10- μ l loop, a differential refractometer detector (LC 4010, Varian) and two recorders [Model 4225 (1 V), Knauer, and Model 9176 (1 mV), Varian].

The analytical column was Catex-H, 8% cross-linked (exchange capacity 4.0 mequiv./g, 250×4.0 mm I.D., 6 μ m) (Bio-Separation-Technologies, Budapest, Hungary). The column temperature was maintained by means of a water-bath and a water-jacket.

The eluents were dilute sulphuric acid of different concentrations at a flow-rate of 0.2 ml/min. Standard solutions of compounds were prepared from analytical-reagent grade chemicals without further purification.

RESULTS AND DISCUSSION

Changes in the retention of the compounds were studied as a function of the concentration of the sulphuric acid eluent between $5 \cdot 10^{-4}$ and $3 \cdot 10^{-3}$ M. The retention of the carbohydrates was found to be constant. The retention of the mono- and dicarboxylic acids was determined by their ionization ability, while the retention of the alcohols decreased as the concentration of sulphuric acid in the eluent increased. Fig. 1 shows the $\log k'$ (capacity factor) vs. $\log c_{H_2SO_4}$ (sulphuric acid concentration) functions obtained for the alcohols. The dead volume (v_0) data required for the calculation of the capacity factor, k' , were obtained by injection of strong acid samples (nitric, hydrochloric and sulphuric) ($v_0 = 1.15$ ml).

As can be seen, the decrease in retention is accompanied by a change in selectivity. With 10^{-3} M sulphuric acid eluent, *n*- and isopropanol, *n*- and isobutanol (Fig. 2) and *tert.*-, *sec.*- and *n*-butanol ($k' = 2.13, 2.94$ and 4.03) can be well separated. In $2 \cdot 10^{-3}$ M eluent, however, the *n*- and iso-alcohols cannot be separated.

The retention behaviour of the carboxylic acids is related to the difference in the pH of the eluent and the pK_a value of the acids. Retention of the acids, occurring in fully or partially ionized form with variation in the pH of the eluent, decreases as the

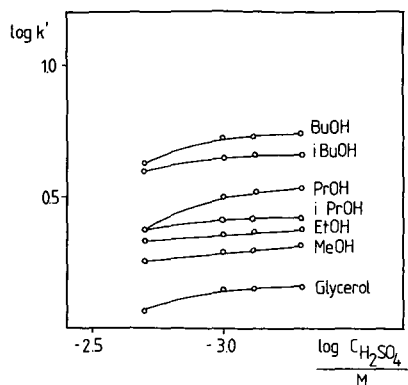


Fig. 1. Retention of alcohols as a function of sulphuric acid concentration in the eluent at 25°C. Me = Methyl; Et = ethyl; iPr = isopropyl; Pr = propyl; iBu = isobutyl; Bu = butyl.

hydrogen-ion concentration decreases. The capacity factor and the hydrogen-ion concentration of the eluent are interrelated by the following equation¹⁸:

$$k' = \frac{a}{1 + \frac{K_a}{[H^+]}} \quad (1)$$

where a is a constant in the partition coefficient. This equation was applied to some partially ionized dicarboxylic acids in the $1 \cdot 10^{-3}$ – $6 \cdot 10^{-3}$ M hydrogen ion concentration range. Fig. 3 shows the results for maleic ($pK_{a1} = 1.8$), citraconic ($pK_{a1} = 2.42$) and fumaric ($pK_{a1} = 3.0$) acids. The slopes of the straight lines are 0.732, 0.766 and 0.949, respectively. Similar results were obtained by Walser¹⁰ for maleic, fumaric and pyruvic acids on a PRP-X300 medium-capacity cation-exchange resin column.

Comparing the straight lines obtained with the PRP-X300 (0.17 mequiv./g)¹⁰ and Catex-H (4.0 mequiv./g) resins, it can be seen that the retention values are signif-

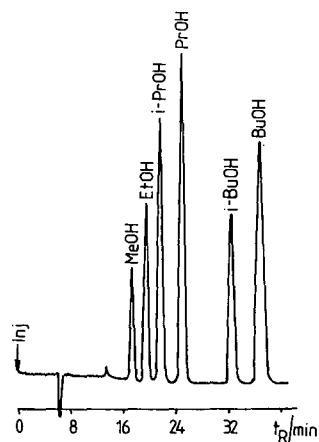


Fig. 2. Chromatogram of alcohols using 10^{-3} M sulphuric acid eluent at 35°C. Refractive index detector. t_R = Retention time.

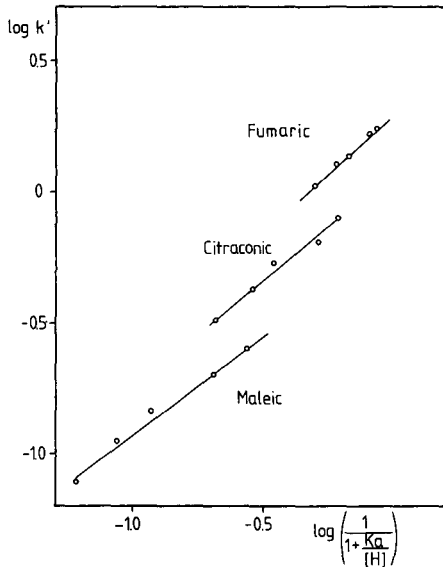


Fig. 3. Variation of retention of relatively strong dicarboxylic acids as a function of H^+ concentration in the eluent.

icantly higher for maleic and fumaric acids on the lower capacity PRP-X300 cation exchanger.

The retention of the weaker ($pK_a > 3.5$) mono- and dicarboxylic acids did not change appreciably in the pH range 2.2–3.0. The relationship between the logarithm of the capacity factor of the various carboxylic acids and their pK_a values (pK_{a1} for dicarboxylic acids) was also studied. The $\log k'$ values obtained with $10^{-3} M$ sulphuric acid eluent are plotted as a function of the pK_a of the carboxylic acid in Fig. 4.

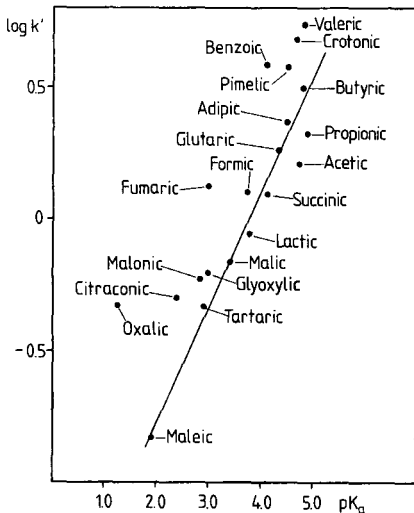


Fig. 4. Relationship between the retention of acids and their pK_a values. Eluent, $10^{-3} M$ sulphuric acid; 25°C.

Most of the acids are eluted in order of their pK_a values. A straight line can be fitted to the points obtained. For some acids the points do not be on the straight line. The deviation is most significant for oxalic acid ($pK_a = 1.23, 3.80$), whose degree of ionization is the highest at the pH of the eluent. The deviation is also significant for fumaric and citraconic acids. Both acids have a higher retention than could be expected on the basis of their pK_{a1} values.

The retention of the mono- ($n_C > 3$) and dicarboxylic acids with longer carbon chains ($n_C > 5$) and that of the unsaturated crotonic acid is again higher than could be predicted by considering the pK_a values. This indicates that in these instances the retention deviation can be interpreted on the basis of a hydrophobic-type reversed-phase mechanism on the surface of the (apolar) cation-exchange stationary phase. This is corroborated by the results shown in Fig. 5, where the $\log k'$ values of the mono- and dicarboxylic acids are plotted against their carbon atom number. Similarly to the linear $\log k' - n_C$ relationships known in reversed-phase liquid chromatography, a straight line is obtained but only for higher carbon atom number carboxylic acids on the strong acid cation-exchange resin. The deviating retention values obtained for the C_4 and C_5 dicarboxylic acids can presumably be understood by assuming a mixed retention mechanism (ion exclusion + hydrophobic interaction).

The effect of the concentration of sulphuric acid on the theoretical plate number (N) was also studied. It was found that the plate number calculated from the alcohol peaks does not change as the concentration of sulphuric acid increases. The plate numbers calculated from the carbohydrate peaks almost doubled when the acid concentration of the eluent was increased from $5 \cdot 10^{-4}$ to $2 \cdot 10^{-3}$ M, e.g., from 1300 to 2790 for D-galactose and from 1370 to 2430 for D-mannose. The plate number changed in a different way for the carboxylic acids. Some typical data are given in Table I. As can be seen, the plate number is highly influenced by the degree of ionization of the acid. For the relatively strong carboxylic acids which are partially

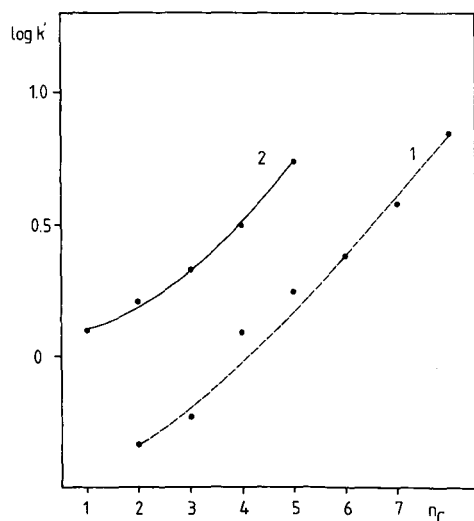


Fig. 5. Dependence of k' on the number of carbon atoms (n_C) of acids: 1, dicarboxylic acids; 2, monocarboxylic acids. Eluent; 10^{-3} M sulphuric acid; 25°C.

TABLE I
COMPARISON OF THE COLUMN EFFICIENCIES

Variation of number of theoretical plates (N) calculated from the peaks of acids with different sulphuric acid concentrations ($5 \cdot 10^{-4}$ – $3 \cdot 10^{-3}$ M) in the eluent at 25°C.

Acid	N /column			
	Sulphuric acid concentration			
	$5 \cdot 10^{-4}$ M	$1 \cdot 10^{-3}$ M	$2 \cdot 10^{-3}$ M	$3 \cdot 10^{-3}$ M
Oxalic	75	130	220	220
Citric	280	1000	1000	1000
Fumaric	1880	2980	3050	5120
Itaconic	3060	3670	5940	9780
Formic	3940	4800	12140	15000
Acetic	4160	4600	16500	16500
Crotonic	7400	8650	11600	11900

ionized at the pH of the eluent (oxalic, maleic and tartaric acids), the N values are low. For the acids with higher pK_a values, higher N values were obtained. As the concentration of sulphuric acid was increased the theoretical plate number increased for all the carboxylic acids studied. Using various acid eluents, Tanaka and Fritz⁵

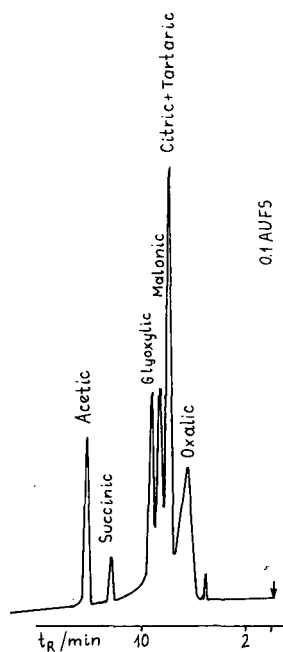


Fig. 6. Chromatogram of a synthetic mixture of acids. Eluent, $2 \cdot 10^{-3}$ M sulphuric acid; UV detection, 0.1 a.u.f.s., 220 nm; 10 μ l of 10^{-3} – 10^{-4} M carboxylic acids.

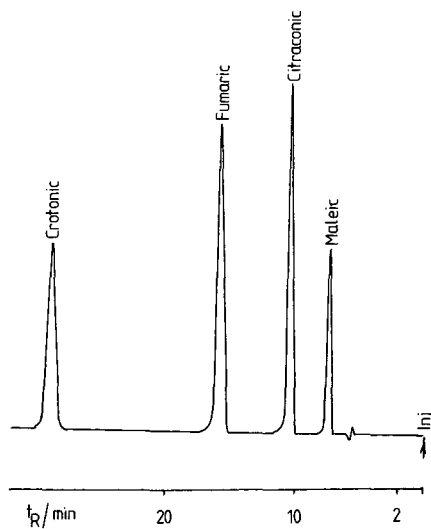


Fig. 7. Chromatogram of a synthetic mixture of acids. Eluent, $3 \cdot 10^{-3}$ M sulphuric acid; UV detection, 0.1 a.u.f.s., 220 nm; 10 μ l of 10^{-4} – 10^{-5} M dicarboxylic acids.

found that the N values obtained from the formic acid peaks were different. With water it was 130, in carbonic acid–water eluent 320 and in other acidic eluents (sulphuric, phosphoric, benzoic and salicylic acids) >2300 .

Figs. 6 and 7 show the chromatograms of two synthetic acid mixtures. The eluents were $2 \cdot 10^{-3}$ and $3 \cdot 10^{-3}$ M sulphuric acid, respectively. The chromatograms of two different carbohydrate mixtures are shown in Fig. 8, obtained with $2 \cdot 10^{-3}$ M sulphuric acid as the eluent.

The retention of the compounds was also studied as a function of the column temperature at a constant 10^{-3} M acid concentration of the eluent. Similar experiments were made by Pecina *et al.*² with alcohols, aldehydes, ketons and carboxylic acids on an HPX-87H column in the range 40–80°C. The same type of column was used by Chiu⁶ to study the change in retention of the various mono- and dicarboxylic acids in the range 20–60°C. Results obtained on the Catex-H column are similar to their results. The curves for some carboxylic acids indicate that only the retention of crotonic acid decreases slightly with increasing temperature (Fig. 9). No change was experienced in the retention of the carbohydrates. The plate number, however, calculated from the peak width increases slightly with increasing column temperature. Pecina *et al.*² observed a small increase in the retention of carbohydrates at higher temperatures.

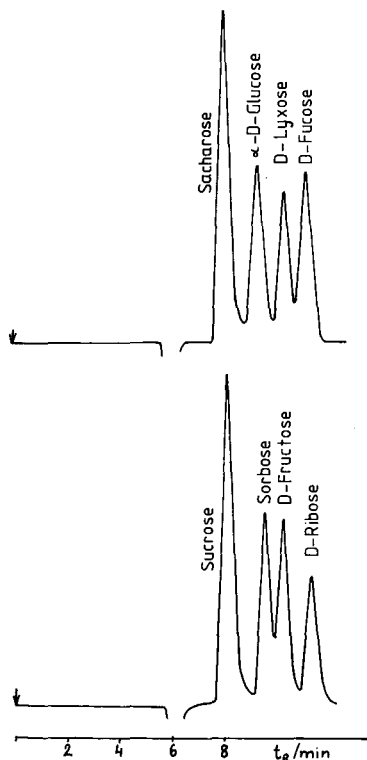


Fig. 8. Chromatograms of carbohydrates. Eluent, $2 \cdot 10^{-3}$ M sulphuric acid; refractive index detection, 4×10^{-5} refractive index units full-scale; $10 \mu\text{l}$ of $3 \cdot 10^{-3}$ M each carbohydrate.

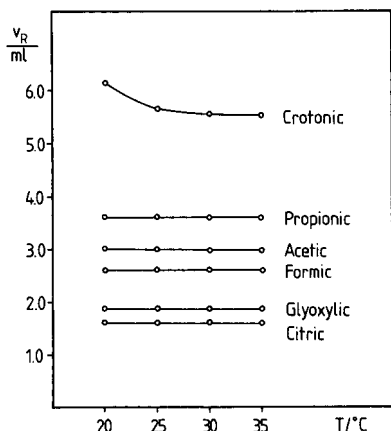


Fig. 9. Variation of retention volume (V_R) of carboxylic acids with column temperature (T). Eluent, 10^{-3} M sulphuric acid.

The retention of the alcohols increases in the range 20–35°C (Fig. 10). This change was not accompanied by a change in selectivity. Curves of various shapes were obtained by Pecina *et al.*² for the alcohols at higher temperatures, but the changes were not significant. In order to decrease the retention of strongly adsorbed compounds methanol⁵ and acetonitrile^{5,19} are used as organic modifiers in the IEC technique. The effect of the acetonitrile concentration in the eluent was also investigated for the three types of compounds studied. In an eluent containing 10^{-3} M sulphuric acid the concentration of the acetonitrile was varied between 0 and 10% (v/v). As the curves in Figs. 11 and 12 indicate, the changes are different for the various acids. The most significant decrease in retention was observed with crotonic acid. The same phenomena was observed by Kazuyoshi *et al.*¹⁹ using a TSK gel SCX column. The decrease in retention clearly indicates that the crotonic acid is retained on the matrix of the cation-exchange resin by a hydrophobic interaction mechanism. The retention volume (V_R) curves exhibit a maximum at *ca.* 2.5% acetonitrile concentration for the

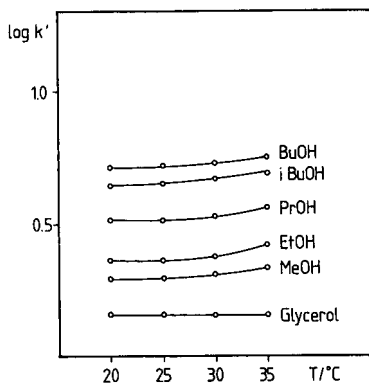


Fig. 10. Capacity factor of alcohols as a function of column temperature. Eluent, 10^{-3} M sulphuric acid.

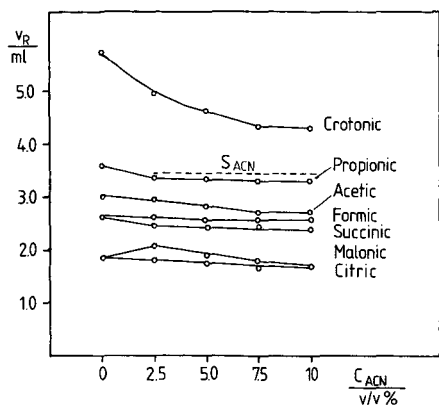


Fig. 11. Retention volume of carboxylic acids as a function of acetonitrile (ACN) concentration in the eluent. Eluent, 10^{-3} M sulphuric acid + 0–10% ACN.

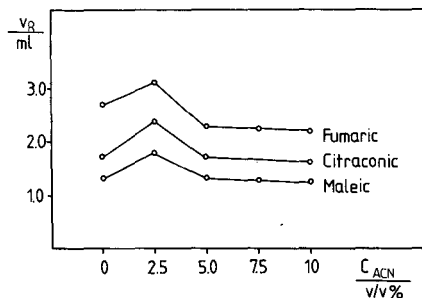


Fig. 12. Retention volume of relatively strong dicarboxylic acids as a function of acetonitrile (ACN) concentration in the eluent.

partially ionized carboxylic acids (fumaric, citraconic, maleic, malonic; Figs. 11 and 12). The retention enhancement observed at low acetonitrile concentration can be interpreted by the change in the ionization of the acid. A further increase in the acetonitrile concentration does not affect substantially the degree of ionization and the retention is not changed as can be seen from the curves in Fig. 12. An increase in the acetonitrile concentration strongly decreases the retention of the alcohols, as shown in Fig. 13. This indicates a partial hydrophobic retention mechanism for the longer carbon chain alcohols. The retention of the carbohydrates was found to be hardly influenced by the addition of acetonitrile to the eluent.

On the chromatograms of the alcohols and acids a disturbing system peak appears if the eluent contains acetonitrile and the injected samples are aqueous solutions (Figs. 14 and 15). The position of the system peak (S_{ACN}) does not change but its height is proportional to the ACN concentration of the eluent. The system peak may

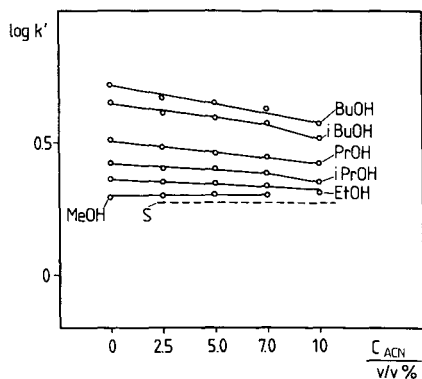


Fig. 13. Variation of capacity factor of alcohols with acetonitrile (ACN) concentration in the eluent.

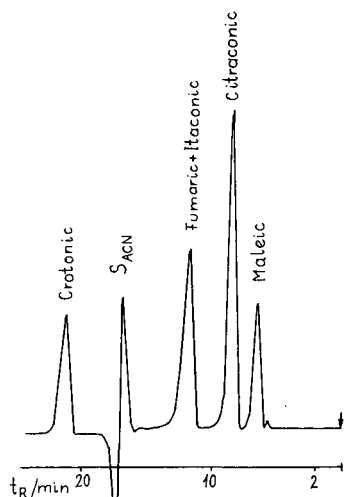


Fig. 14. Chromatogram of acids with an acetonitrile (ACN)-containing eluent. Eluent, 10^{-3} M sulphuric acid + 10% ACN; UV detection, 0.05 a.u.f.s., 220 nm; $10 \mu\text{l}$ of 10^{-4} – 10^{-5} M acids; 25°C .

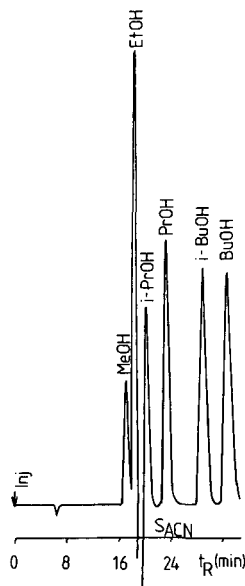


Fig. 15. Chromatogram of alcohols in acetonitrile (ACN)-containing eluent. Eluent, 10^{-3} M sulphuric acid + 2.5% ACN; refractive index detection; 25°C .

disturb the evaluation of the chromatograms. As can be seen in Fig. 15, the determination of ethanol is not possible.

The column efficiency for the acids is strongly affected by the presence of acetonitrile in the eluent. Table II gives the calculated N values for eluents containing 2.5 and 10% acetonitrile. The plate numbers, however, did not change significantly for the carbohydrates and alcohols.

TABLE II
COMPARISON OF COLUMN EFFICIENCIES

Variation of number of theoretical plates (N) calculated from the peaks of acids with different acetonitrile concentrations (2.5 and 10%) in the eluent.

Acid	N /column	
	Acetonitrile concentration	
	2.5%	10%
Citric	1650	740
Tartaric	1250	720
Maleic	1460	610
Fumaric	3460	1310
Acetic	4100	2500
Formic	4700	2900
Crotonic	6800	4100

CONCLUSION

It may be concluded that the retention behaviour of the acids corresponds to the ion exclusion theory but some acids (oxalic, citraconic and fumaric) show significant deviations in the pK_a and $\log k'$ relationship. Above three carbon atoms in the monobasic acids and above five carbon atoms at the dibasic acids the hydrophobic interaction effect between the solute and stationary phase prevails (*i.e.*, the $\log k'$ vs. n_C curves are linear). The number of theoretical plates of the column is strongly related to the ionization state of the solute.

The system peak (S_{ACN}) observed on the chromatograms (obtained with organic modifier-containing eluents) made possible a study of the retention mechanism in those system where the water concentration of the sample was higher than that of the eluent. The water peak of the sample appears at an eluent volume corresponding to the full permeability of the column ($v_{S_{ACN}}$). Three regions can therefore be identified on the chromatogram. The first region extends from the injection point to the totally excluded volume (the small peak in front of the maleic acid in Fig. 14). The second region is from the totally excluded volume up to the totally permeated volume; the retentions of the solutes eluted in this region are governed by the Donnan and steric exclusion (*e.g.*, maleic, fumaric, acetic and propionic acid). When the retention volume of the solute is higher than the totally permeated volume, then the retention is dominated by the hydrophobic interaction between the solute and the stationary phase (*e.g.*, crotonic acid, monobasic acids with $n_C > 3$ and dibasic acids with $n_C > 5$).

For the separation of the *n*- and iso-alcohols the selectivity is increased on decreasing the sulphuric acid concentration of the eluent. The retention of alcohols can be decreased by the use of acetonitrile as modifier but the appearance of the system peak must be taken into consideration.

The retention behaviour of the carbohydrates proved to be almost independent of changes in the concentration of sulphuric acid, acetonitrile and column temperature in the ranges investigated.

REFERENCES

- 1 E. Papp, *J. Chromatogr.*, submitted for publication.
- 2 R. Pecina, G. Bonn, E. Burtsher and O. Bobleter, *J. Chromatogr.*, 287 (1984) 245.
- 3 R. D. Rocklin, R. W. Slingsby and C. A. Pohl, *J. Liq. Chromatogr.*, 9 (1986) 757.
- 4 B. K. Glod and W. Kemula *J. Chromatogr.*, 366 (1986) 39.
- 5 K. Tanaka and J. S. Fritz, *J. Chromatogr.*, 361 (1986) 151.
- 6 G. Chiu, *J. High. Resolut. Chromatogr. Chromatogr. Commun.*, 9 (1986) 57.
- 7 P. R. Haddad, P. W. Alexander, M. Y. Croft and D. F. Hilton, *Chromatographia*, 24 (1987) 487.
- 8 J. Haginaka, J. Wakai and H. Yashuda, T. Nomura, *J. Chromatogr.*, 447 (1988) 373.
- 9 T. Murayama, T. Kubota, Y. Hanaoka, S. Rokushika, K. Kihara and H. Hatano, *J. Chromatogr.*, 435 (1988) 417.
- 10 P. Walser, *J. Chromatogr.*, 439 (1988) 71.
- 11 D. P. Lee and A. D. Lord, *LC · GC, Mag. Liq. Gas Chromatogr.*, 5 (1987) 261.
- 12 P. R. Haddad and P. E. Jackson, *J. Chromatogr.*, 447 (1988) 155.
- 13 T. Okada, *Anal. Chem.*, 60 (1988) 1336.
- 14 T. Okada, *Anal. Chem.*, 60 (1988) 1666.
- 15 T. Okada, and P. K. Dasgupta, *Anal. Chem.*, 61 (1989) 548.
- 16 K. B. Hicks and A. T. Hotchkiss, *J. Chromatogr.*, 441 (1988) 382.
- 17 K. Tanaka, T. Ishizuka and H. Sunahara, *J. Chromatogr.*, 174 (1979) 153.
- 18 D. J. Pietrzyk, E. P. Kroeff and T. D. Rotsch, *Anal. Chem.*, 50 (1978) 497.
- 19 F. M. Kazuyoshi and T. Masahiko, *Bunseki Kagaku*, 37 (1988) 553.

CHROMOSYMP. 1790

Optimization of chromatographic methods by a combination of optimization software and expert systems

PETER J. SCHOENMAKERS*

Philips Research Laboratories, P.O. Box 80000, 5600 JA Eindhoven (The Netherlands)

ANNE PEETERS

Pharmaceutisch Instituut, Vrije Universiteit Brussel, Laarbeeklaan 103, B-1090 Brussels (Belgium)

and

RODERICK J. LYNCH

Philips Scientific, York Street, Cambridge CB1 2PX (U.K.)

SUMMARY

Expert systems and other sophisticated computer programs can be of great benefit for the optimization of chromatographic separations. However, two factors have seriously hindered their proliferation. First, the area of method development for chromatography encompasses such a great variety and such a large amount of knowledge and expertise that it is not realistic to try and cover the entire area with a single program. Second, computer programs may be very complex to use, so that only experts can apply them. Steps towards the solution of both problems are described. Three different computer programs, two of which are expert systems, are used coherently for method optimization. Each system can assist the chromatographer in performing a certain well-defined task. The selectivity-optimization system (Diamond) is a package of conventional computer programs. Therefore, we refrain from calling it an expert system. One expert system is specifically applied to reduce the level of expertise required for applying this package. The most difficult decision that a Diamond user needs to make is the selection of the most appropriate optimization criterion. This decision can be made with the help of the expert system for CRITERION SELECTION (CRISE). The second expert system (System-Optimization System, SOS) is used to transform the chromatogram with optimum selectivity that results from Diamond into the optimum overall method by establishing the best column dimensions, flow-rate, instrumentation, injected amount, *etc.* An example is presented to demonstrate that the coherent use of several sophisticated computer programs can make method development in chromatography both better and easier.

INTRODUCTION

The major steps in developing a chromatographic method can be identified as

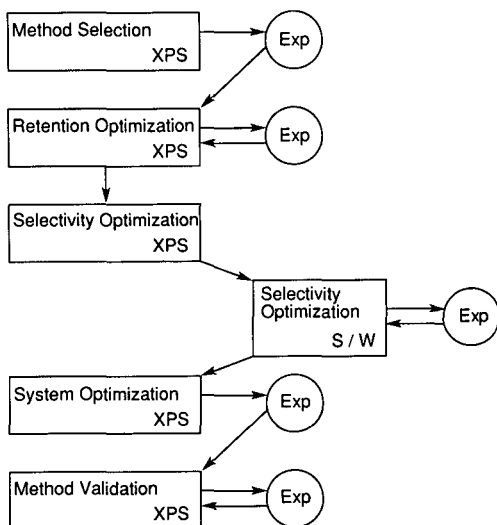


Fig. 1. Major steps in developing a chromatographic method. Boxes represent software (S/W) and circles represent chromatographic experiments (Exp). XPS denotes expert system.

follows^{1,2} (Fig. 1): (i) method selection; (ii) retention optimization; (iii) selectivity optimization; (iv) system optimization; and (v) method validation.

Method selection is the process of selecting the appropriate chromatographic method [e.g., gas chromatography (GC) or liquid chromatography (LC); normal-phase or reversed-phase LC; ion-exchange or ion-pairing LC, etc.] and the appropriate conditions (temperature, mobile-phase composition, pH, etc.) to elute the sample components as (reasonably) sharp, (reasonably) symmetrical peaks. Method selection is based on an understanding of the different chromatographic techniques and, most of all, on knowledge about the sample and its components. The goal of the method-selection step is to obtain chromatographic peaks for all the sample components of interest. It is important that none of these compounds remains on the column. Therefore, it is better at this stage when retention is too low than when it is too high. A typical chromatogram that may be obtained is the top one in Fig. 2.

In the *retention-optimization* step, the peaks obtained in the chromatogram after the method selection will be moved into the optimum range of capacity factors, usually by varying the composition of the mobile phase. It may be possible to predict the conditions for optimum retention based on a knowledge of the chromatographic process and the initial chromatogram. It may be necessary to improve this prediction after a second chromatogram has been obtained. The resulting chromatogram may typically be the second one in Fig. 2. In this chromatogram, all peaks are eluted in the optimum retention range, but not all of them are separated.

If the retention times of all peaks are in the optimum range, but the separation is not satisfactory, there are two possible solutions, selectivity optimization and system optimization.

*Selectivity optimization*³ is the process that aims at improving the separation by altering the retention of the individual sample components relative to each other. To

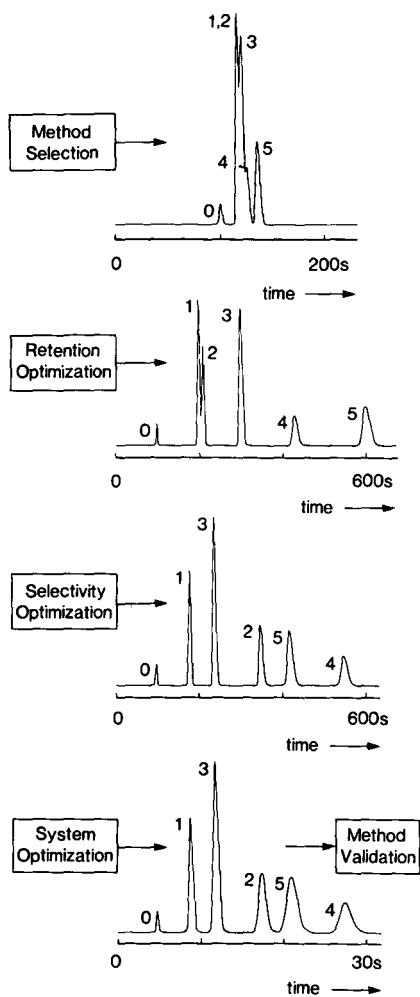


Fig. 2. Schematic illustration of a series of chromatograms that may be obtained during the development of a chromatographic method.

change the selectivity, either the stationary phase (GC or LC) or the mobile phase (LC) will usually be changed. Selectivity optimization is not usually a predictable process. Therefore, a number of sophisticated experimental optimization procedures have been applied to or developed for chromatography³⁻⁵. The desired result of the selectivity-optimization process is a chromatogram in which the peaks are more evenly distributed, as is illustrated in Fig. 2.

System optimization can be used either if the resolution is higher than required or if the separation is not good enough. In the first instance it may lead to a considerable reduction in the analysis time and in the second case it may be used to increase the resolution. Improving the sensitivity (signal-to-noise ratio) of the method may also be one of the goals of the system-optimization process. Parameters considered during this process may typically be the dimensions of the column, the flow-rate,

sample volume, etc. The effects of these parameters are to a large extent predictable, so that much of the system optimization can be based on calculations^{6,7} or computer simulations⁸. An example of a result of a system-optimization step is shown in Fig. 2.

The final step in the method-development process is the *method validation*. It will always be necessary to demonstrate the applicability of the proposed method for the intended purpose. This very purpose will determine the extent to which a method will need to be validated. Generally, the more often a method is intended to be applied, the more different people will be using it and the greater the consequences of the results obtained by the method, the more extensive will be the testing¹. Method validation will typically involve setting up systematic test programmes, performing series of experiments and evaluating the results. Experimental designs and statistics are important aspects of this process.

In recent years, there has been much interest in the use of computer programs to assist the chromatographer in developing chromatographic methods (see, *e.g.*, refs. 3, 4 and 9). An ideal situation may be one in which the user (chromatographer) can consult a single computer program, through which he or she can direct the method-development process, control the instrument, collect the data and evaluate the results. Within such a computer program a number of modules may exist to assist the user in the different steps of the method-development process. In other words, all the boxes in Fig. 1 may be called upon by the computer program. At present, such an ideal situation cannot yet be approached. In this paper, a step is made towards such an ideal situation by looking at the coherent application of several sophisticated software programs for optimizing liquid-chromatographic separations. The three programs that have been used in the present work are the following (Fig. 3): an expert system for the selection of the most suitable criterion for selectivity optimization¹⁰; a program for the optimization of selectivity by varying the composition of the mobile phase¹¹; and an expert system for optimizing the column, operating conditions and instrumentation¹².

Expert system for criterion selection

The expert system for criterion selection represents one of the aspects of selectivity optimization, as is illustrated in Fig. 4. In order for an experimental selectivity-

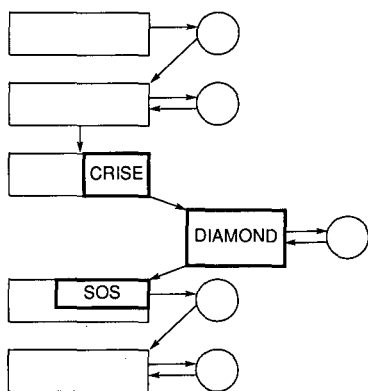


Fig. 3. Three computer programs studied in this work in relation to the scheme in Fig. 1.

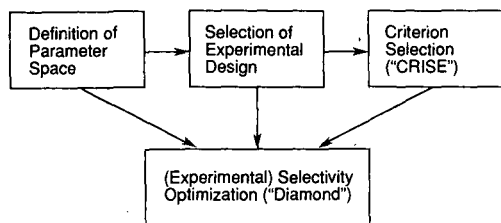


Fig. 4. Major aspects of selectivity optimization in chromatography.

optimization procedure (bottom) to be performed, decisions are needed on (i) the parameter space, *i.e.*, the parameters (variables) that will be considered together with their minimum and maximum values (limits); (ii) the experimental design, *i.e.*, the pattern according to which the necessary experiments will be performed; and (iii) the optimization criterion, *i.e.*, the parameter that will be used to judge the quality of the chromatogram. The goal of the selectivity-optimization process is to find the set of conditions (within the parameter space) that results in the best possible value for the optimization criterion. This set of conditions is referred to as the optimum.

There is not a single optimization criterion that is always the best one to use. Which criterion should be used will depend on the method to be developed, the optimization procedure to be used, the characteristics of the sample and the possibilities of the user. The expert system for CRITERION SELECTION (CRISE) has been described in detail elsewhere¹⁰. It assists the user in selecting the most appropriate optimization criterion.

Selectivity optimization

The selectivity-optimization procedure used has been described elsewhere^{11,13}. The Diamond package features an interpretive optimization procedure, including (i) the definition of an (approximately) isoelutropic triangle, with binary mixtures of, *e.g.*, methanol–water, acetonitrile–water and tetrahydrofuran–water at the corners, ternary mixtures along the sides and quaternary mixtures in the middle; (ii) the recording of ten three-dimensional (3-D) diode-array chromatograms equally distributed throughout the triangle; (iii) the labelling of the peaks in the 3-D chromatograms to determine the retention times of each individual solute at each composition; (iv) the modelling of the retention surfaces for all individual solutes; and (v) the calculation of the response surface (optimization criterion *vs.* composition) for the entire chromatogram.

System optimization

The expert system for system optimization has been described in detail^{12,14}. The mobile and stationary phase are not altered in this process, but the column dimensions, flow-rate, etc., may be changed. Based on an initial chromatogram and a set of initial conditions, the program selects the best possible column from a column database created by the user and combines this with the best possible detector (cell) from the detector database and with the best possible time constant from a list of possible values. The optimum result is defined as (i) the resolution for all relevant pairs of peaks must exceed a minimum value specified by the user; (ii) the signal-to-

noise ratio for the smallest relevant peak must exceed a minimum value specified by the user; and (iii) the required analysis time should be as short as possible. Together with the optimum column, detector cell and time constant, the system recommends the optimum flow-rate and sample size and predicts the required analysis time, the "critical resolution" (*i.e.*, the lowest value observed for the resolution between a relevant pair of peaks) and the pressure drop over the column. It also provides an explanation of its reasoning in the form of a bar chart and some additional advice to the user¹⁴.

EXPERIMENTAL

The expert system for criterion selection (CRISE) was implemented in the commercially available expert-system shell KES (Knowledge Engineering System; Software Architecture and Engineering, Arlington, VA, U.S.A.; release 2.4). The expert system runs on an Apollo workstation and on an IBM PC.

A prototype version of the Philips Scientific (Cambridge, UK) Diamond package for the selectivity optimization in high-performance liquid chromatography was run on a Philips 3202 personal computer (IBM/AT compatible). Data acquisition was performed using a Philips Scientific 4120 diode-array detector and the PU 6003 diode-array datastation running on the 3202 computer. Three-dimensional chromatograms were recorded at ten points in the isoeluotropic solvent triangle and peak labelling could be performed using the routines available within the Diamond package¹¹.

The version of the system-optimization expert system used was written in Pascal for a MicroVAX workstation (Digital Equipment, Maynard, MA, U.S.A.). An extensive description of this system has been given elsewhere¹⁴. An IBM-PC version of this system is now commercially available through Philips Scientific.

The practical example considered in this study concerns the separation of ten phenolic priority pollutants: phenol, 4-nitrophenol, 2,4-dinitrophenol, 2-chlorophenol, 2-nitrophenol, 2,4-dimethylphenol, 2-methyl-4,6-dinitrophenol, 4-chloro-3-methylphenol, 2,4-dichlorophenol and 2,4,6-trichlorophenol. The column used was a Dynamax axially compressed RP-18 column from Raynin (Emeryville, CA, U.S.A.). Further details on the experimental procedures can be found elsewhere¹⁵.

RESULTS AND DISCUSSION

Expert system for criterion selection

The CRISE expert system is thought to be applicable to a wide variety of optimization procedures in which non-programmed (*e.g.*, isocratic) separations are being optimized. It is difficult to test the usefulness of the system with only one particular optimization strategy. Therefore, we have validated the expert system by applying it to a selection of ten literature reports, which were selected so as to represent as good a selection of different selectivity-optimization procedures as possible. This selection is summarized in Table I. Although most of the applications deal with LC, one of them (Val8) deals with selectivity optimization in GC and one (Val10) with supercritical-fluid chromatography (SFC).

From all ten reports, the information relevant for selecting the optimization

TABLE I

SUMMARY OF THE TEN APPROACHES TO SELECTIVITY OPTIMIZATION SELECTED FROM THE LITERATURE

No.	Authors	Ref.	Method description
Val1	Eppert <i>et al.</i>	16	Two-dimensional window diagrams
Val2	Cooper and Hurtubise	17	Window diagrams
Val3	Billiet <i>et al.</i>	18	Iterative optimization
Val4	Goldberg <i>et al.</i>	19	Sentinel ^a
Val5	Berridge and Morrissey	20	Simplex optimization
Val6	Conlon	21	Pesos
Val7	Haddad and Sekulic	22	Optimization with tailed peaks ^a
Val8	Hinshaw and Ettore	23	Selectivity tuning ^a (GC)
Val9	Naish <i>et al.</i>	11	Diamond
Val10	Schoenmakers	24	Interpretive optimization ^a (SFC)

^a Tested with or without allowing system (column) optimization to take place after selectivity optimization.

criteria was selected and presented to both the human expert (P.J.S.) and the expert system. In some instances more than one possible answer was considered to certain questions asked by the expert system. This led for some of the test cases to more than one consultation. The resulting advice from the expert system is summarized in Table II.

The elementary criterion selected was either the resolution (R_s), the separation factor (S), the separation factor corrected for variations in the plate count between different solutes or between different experiments (S_N) or the peak-valley ratio (P). The expert system will recommend whether or not it is advisable to correct the elementary criterion for large variations in peak heights between different peaks or for peak asymmetry²⁵. Also, it reveals whether or not the use of weighting factors (preferably 0 for irrelevant peaks and 1 for all relevant peaks) is recommended.

After selecting the most appropriate elementary criterion, the expert system will select the global optimization criterion, *i.e.*, the criterion that can be used to characterize the quality of the separation in the entire chromatogram. A fixed-threshold criterion implies that the analysis time is minimized, while the lowest value for the elementary criterion observed in the chromatogram does not fall below a specified value. For example, a minimum resolution of 1.5 may be specified. Two-criterion optimization²⁶ involves the simultaneous optimization of retention and resolution, then finding the proper trade-off between these two parameters at the end of the optimization process.

When the system-optimization system is available for further improving the results of the selectivity-optimization process, this can be taken into account during the selection of the criterion. It can be specified at this stage whether or not columns of different length and/or particle size will be considered in the system-optimization step. By taking the possibilities of the system-optimization into account at this stage, a better overall optimum may be found in the end²⁴.

The best possible distribution of all peaks over the chromatogram may be selected as the global optimization criterion, if the analysis time does not vary greatly

TABLE II

SUMMARY OF THE ADVICE PRESENTED BY THE EXPERT SYSTEM FOR CRITERION SELECTION (CRISE) FOR A TOTAL OF NINETEEN RUNS IN RELATION TO THE TEN DIFFERENT APPROACHES TO SELECTIVITY OPTIMIZATION LISTED IN TABLE I

WF indicates whether or not the use of weighting factors (0 and 1) is recommended. R_s denotes the resolution, S the separation factor, S_N the separation factor corrected for variations in the plate count and P the peak-valley ratio¹⁰. L is the column length and d_p the particle size.

No.	Runs	Recommendations of CRISE		Corr. ^a	WF
		Elementary criterion	Global criterion		
Val1	2	S_N	Fixed threshold	PHR	No
			or ^b : two-criterion optimization	PHR	No
Val2	4	S_N or ^c : S	Fixed threshold	PHR	No
			or ^d : best distribution	PHR	No
Val3	2	R_s	Fixed threshold	PAS	Yes
			or ^b : two-criterion optimization	PAS	Yes
Val4	2	S_N	Fixed threshold	None	No
			or ^e : minimum analysis time (L variable)	None	No
Val5	1	P	Fixed threshold	N/A	No
Val6	1	P	Fixed threshold	N/A	No
Val7	2	R_s	Fixed threshold	PAS	No
			or ^e : minimum analysis time (L variable)	PAS	No
Val8	1	S_N	Minimum analysis time (L variable)	PHR	No
Val9	2	R_s	Best distribution	PAS	Yes
			or ^f : minimum analysis time (L and d_p variable)	PAS	Yes
Val10	2	S	Fixed threshold	None	No
			or ^e : Best distribution in \sim minimum time (L variable)	None	No

^a Recommended corrections: PHR = peak-height ratio, PAS = peak asymmetry.

^b When no *a priori* decision on a threshold value can be made.

^c Depending on whether or not the plate count can be measured for one peak.

^d Depending on whether minimum analysis time or best distribution of peaks is desired.

^e Depending on whether system (column) optimization is allowed after selectivity optimization.

^f Depending on whether the best distribution of peaks on a given column or the shortest analysis time on a column of optimum length and with optimum particle size is desired.

with variations of the conditions (within the parameter space). A good distribution of peaks may also be considered as a sort of secondary criterion, while emphasis is put on the shortest possible analysis time (see Val10 in Table II).

The main conclusions of the validation of the expert system for criterion selection were that (i) the expert system provided clear and unambiguous answers for each consultation and (ii) the expert system and the human expert provided the same

answers for all ten cases (nineteen consultations) considered during the validation. These conclusions imply that the expert system performs as intended. It does not imply that the expert system always provides the correct advice, because the correctness of the knowledge supplied to the expert system by the human expert has not been rigorously validated.

For a full explanation of optimization criteria, the reader is referred to refs. 3, 10 and 24.

Selectivity optimization

In this study we focused on the optimization part of the Diamond package. Establishing the elution order (and the retention times) of the ten individual solutes from the ten three-dimensional chromatograms will not be discussed in this paper. Based on the correct assignment of all the solutes, the retention surfaces for each solute can be calculated using piecewise-quadratic interpolation between the ten experimental data points¹¹. Once the retention times of each solute can be calculated at each composition, a response surface can be calculated. Such a surface shows the variation of the overall optimization criterion with the mobile phase composition. An example is shown in Fig. 5. In this example, the minimum value for the separation factor [$S = (k_2 - k_1)/(2 + k_1 + k_2)$] is used as the optimization criterion. Response surfaces can be presented as quasi-three-dimensional plots (Fig. 5a) or as contour plots. In the latter instance, the total range of criterion values is divided in a number of equal sub-ranges, each of which is displayed in a certain shade of grey (as in Fig. 5b) or, preferably, in a different colour. In Fig. 5b the highest point on the surface is indicated by the cursor.

At the bottom of Fig. 5b a so-called stick chromatogram is displayed. This gives the position of all the peaks in the chromatogram on a $\ln(1 + k)$ scale. On this scale all peaks are of equal width (if the plate count N is constant throughout the chromatogram). Hence the stick diagram provides an illustration of the expected separation at the position of the cursor, which can be anywhere in the triangle.

A number of different optimization criteria can be applied within the present prototype version of Diamond. A list of these is presented in Table III, together with a short description of each of the optimization criteria.

Within the Diamond system the optimization of the mobile-phase composition takes place in a so-called isoelutropic plane. This implies that the (binary) compositions at the vertices have been selected such that the analysis time (retention time of the last peak, t_w) is roughly constant (typically within a factor of 2–3). This will then also apply for all other (ternary and quaternary) compositions that can be formed by blending the three binary mixtures in different ratios. In the present example t_w varies from about 15 to about 44 min, *i.e.* by about a factor of three.

One of the possible recommendations of the CRISE system is to use a threshold criterion, which implies that the retention time is minimized in the range of compositions for which S_{\min} exceeds a certain minimum (“threshold”) value. In Diamond, a slightly different criterion is implemented, which yields similar results. This is the STMIN criterion in Table III, which equals S_{\min}/t_w . This criterion locates the optimum at an S_{\min} value close to the maximum value. This can be understood as follows.

The minimum value for the separation factor observed in the chromatogram varies from 0 (when two solutes “cross over”) to about 0.04 if all peaks are considered

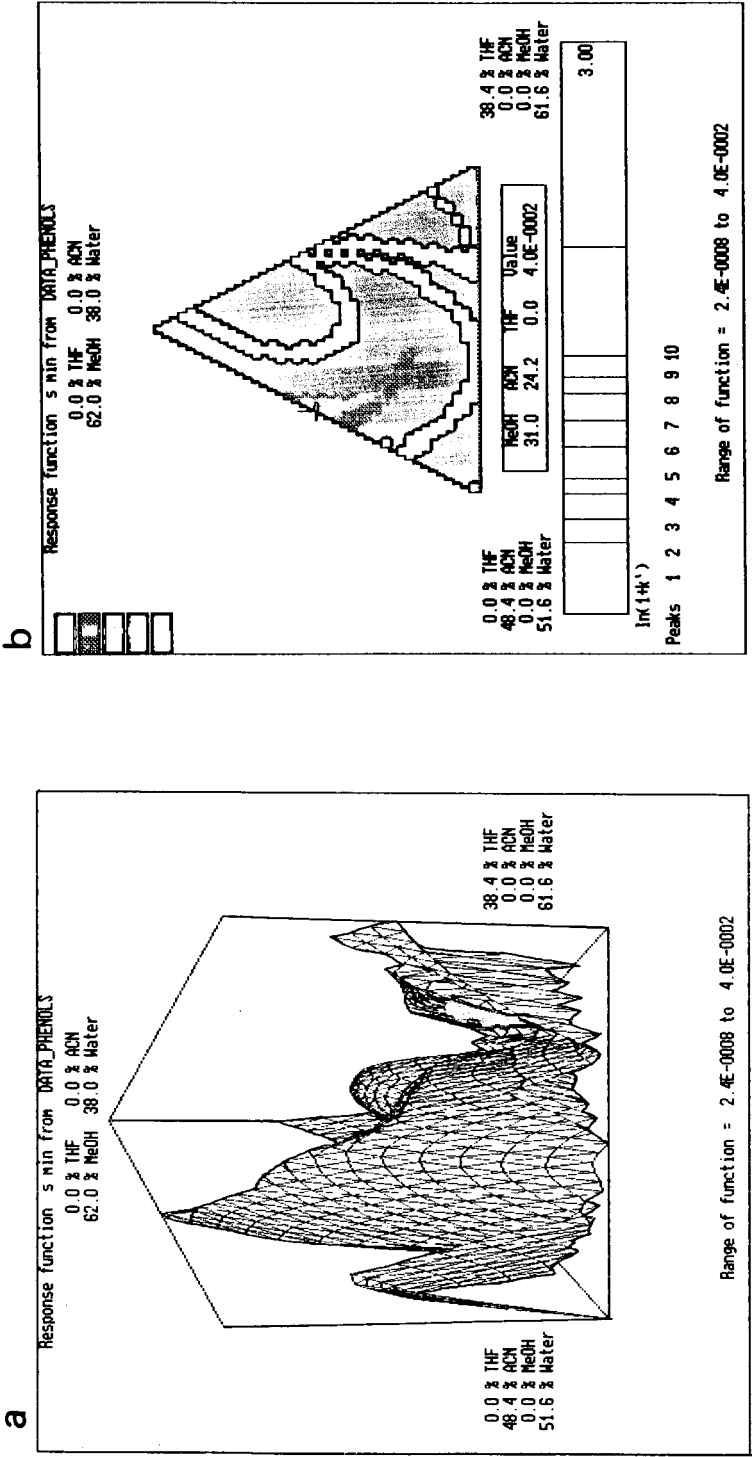


Fig. 5. Example of a response surface for the phenol sample. Criterion: S_{min} ; relevant peaks: all. (a) Pseudo-three-dimensional plot; (b) contour plot. In (b) the range of S_{min} values from 0.00 to 0.04 has been divided into equal sub-ranges. The highest point on the contour is indicated by the cursor. The white areas are lowest. Below the triangle is a stick chromatogram on a $\ln(1+k')$ scale (explained in text). ACN = Acetonitrile; MeOH = methanol; THF = tetrahydrofuran.

TABLE III

DESCRIPTION OF THE OPTIMIZATION CRITERIA USED IN THE SELECTIVITY-OPTIMIZATION PROGRAM DIAMOND

For a detailed explanation of all criteria, see refs. 3, 10 and 24.

Abbreviation	Criterion	Description
TNE	$[t_{ne}]_{r,d}$	Minimum required analysis time, allowing the column length to vary (with the flow-rate and particle size constant) during a subsequent system-optimization step
RSTAR	r^*	Best (most equal) distribution of all relevant peaks over the chromatogram
SMIN	S_{\min}	Lowest value for the separation factor (proportional to resolution) between a relevant pair of peaks in the chromatogram
STMIN	S_{\min}/t_{ω}	Corresponds to S_{\min} divided by the required analysis time. This criterion approximates a "fixed-threshold" one, <i>i.e.</i> , to reach a required (resolution) target in the shortest possible time
RNT	$[r^*]_{nt}$	As TNE, but also paying some attention to the best possible distribution of peaks

to be relevant, and from 0 to about 0.07 if only components 7, 8 and 9 are relevant. Because t_{ω} varies by no more than a factor of three, the retention time can compensate for no more than a factor of three variation in S_{\min} . Hence the criterion STMIN will locate the optimum at a composition where S_{\min} is at least 35% of its highest value. At the predicted optimum composition, S_{\min} will be higher than about 0.014 if all peaks are considered (> 0.025 for components 7, 8 and 9 only). The criterion STMIN thus behaves similarly to a fixed-threshold criterion, in which the optimum is located at the composition where S_{\min} exceeds a certain minimum value and t_{ω} is as small as possible.

The other four criteria can potentially be selected by the expert system as the most appropriate optimization criterion for an interpretive method, such as that employed in Diamond. The expert system distinguishes between two different situations for applying the system-optimization system (SOS) after the selectivity-optimization step. A different criterion may be used depending on whether the column length or both the column length and the particle size will be allowed to vary within SOS. The criteria currently incorporated in Diamond correspond to the former situation.

Table IV shows some of the optima predicted by the Diamond system for the sample of ten phenolic solutes. If all ten solutes are considered to be relevant, four out of five criteria yield the same optimum composition, whereas the fifth criterion locates the optimum in the same area. For complex samples this is likely to be the case, because there will not be many regions in the triangle in which all peaks can be separated. The optimum predicted with the majority of the optimization criteria is illustrated by the chromatogram in Fig. 6a. All ten solutes are seen to be separated in about 20 min using the same column, flow-rate, etc., as were used to record the ten initial 3-D chromatograms.

If not all ten solutes are considered to be relevant and if changes in the elution order occur when the composition is varied, the selection of different criteria may well lead to the prediction of different optimum compositions. This is illustrated in Table

TABLE IV

SUMMARY OF OPTIMA FOUND FOR THE SEPARATION OF TEN PHENOLIC SOLUTES

Optimum No.	Relevant peaks	Criteria	Composition (%)		
			CH ₃ OH	ACN ^a	THF ^b
1	All	TNE, SMIN, STMIN, RNT	31.0	24.2	0.0
2	All	RSTAR	26.3	26.6	1.0
3	7,8,9	TNE, RNT	7.7	15.7	21.1
4	7,8,9	RSTAR	1.6	46.0	1.0
5	7,8,9	SMIN	17.0	1.2	1.0
6	7,8,9	STMIN	7.7	41.1	1.0

^a Acetonitrile.^b Tetrahydrofuran.

IV for the example in which only components 7, 8 and 9 are considered to be relevant. In this instance the criteria TNE and RNT yield the same optimum composition, but in all other instances the predicted optima are located at significantly different positions in the triangle. The location of the different optima is illustrated in Fig. 7.

Fig. 8a illustrates that if only three peaks are considered to be relevant (optimum No. 3 in Table IV), the program (correctly) ignores the quality of the separation between irrelevant peaks. Notably, peaks 3, 4 and 5 are all poorly resolved at the optimum composition. However, the resolution of the relevant peaks 7, 8 and 9 and the resolution between these peaks and all the irrelevant peaks is very good.

System optimization

When the system-optimization system SOS is consulted for the predicted optimum chromatograms, it suggests that much can still be gained in terms of the required analysis time. The system was consulted for all six optima listed in Table IV. A

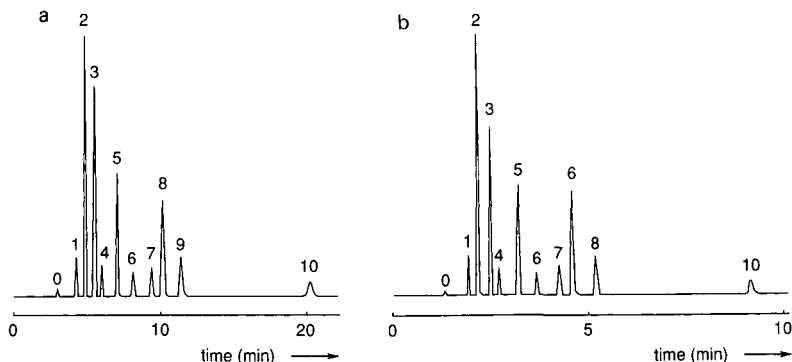


Fig. 6. Predicted optimum chromatograms for the separation of all ten phenolic solutes. For the mobile-phase composition and the criteria used see Table IV. (a) Optimum predicted by the Diamond system on the column used to record the ten 3-D chromatograms. (b) Optimum predicted by the SOS system using the optimum column (see Table V).

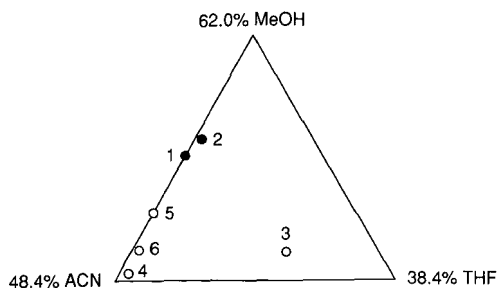


Fig. 7. Location of the different optima listed in Table IV in the isoeuotropic triangle. Closed circles correspond to situations in which all solutes are considered to be relevant. For the open circles only components 7, 8 and 9 were relevant.

minimum resolution of 2 and a required signal-to-noise ratio of 200 were specified for all situations. Three "standard" detector cells (8, 2.4 and 1.2 μl , as Nos. 1, 2 and 3, respectively) were included in the detector database and time constants of 50, 100, 200 and 500 ms were allowed. The maximum distortion factors for extra-column dispersion in the time and volume domains^{12,14} were allowed to be the 0.5 and 0.2, respectively. The overall minimum and maximum values for the flow-rate were 0.02 and 10 ml/min, respectively. The overall pressure limits were 10 and 250 bar. A

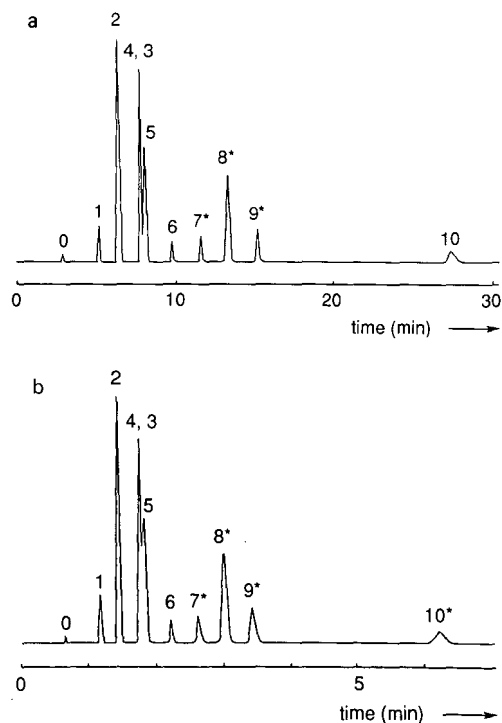


Fig. 8. As Fig. 6, but now only solutes 7, 8 and 9 (indicated by asterisks) are considered to be relevant.

TABLE V

SUMMARY OF THE CONSULTATION OF THE "SOS" SYSTEM FOR THE PREDICTED OPTIMA LISTED IN TABLE IV

Top: summary of the column database. Bottom: results for each of the optima. t_D is the required analysis time for the column and conditions used in the Diamond system (*i.e.*, before SOS); t_S is the required analysis time for the optimum predicted by the SOS system.

Column No.	Length (cm)	I.D. (mm)	Particle size (μm)			
1	30	4.6	10			
2	25	4.6	8			
3	25	4.6	5			
4	15	4.6	5			
5	10	4.6	3			
6	25	2	8			
7	25	1	8			

Optimum No. (Table IV)	t_D (s)	Optimum column				
		Column No. (above)	Detector cell	Time constant	Flow-rate (ml/min)	t_S (s)
1	1208	5	3	200	0.61	551
2	1229	3	2	500	0.89	1036
3	1645	4	2	500	1.92	373
4	990	5	3	200	0.76	362
5	2240	4	2	500	2.18	448
6	1060	5	3	200	1.02	228

maximum amount of 20 μl of sample (20 times the initial amount) was allowed. The column database is summarized in Table V (top). Column 1 was the column used to record the 3-D chromatograms for the Diamond program and the initial plate count was taken as 10 000.

The resulting optimum separations predicted by the SOS system are summarized in Table V (bottom). In all situations it can be seen that the predicted analysis time after system optimization is (much) lower than before. When all peaks need to be separated, the required number of plates is fairly large, but the analysis time can still be reduced by about a factor of two. When only peaks 7, 8 and 9 are relevant, the initial number of plates is higher than needed and the analysis time can be reduced by factors of 3–5 for the different optima. The initial column was never suggested to be the optimum choice by the SOS system. The system lists the best possible results that can be obtained on all (valid) columns. For example, if column 1 were to be selected, the analysis time at optimum conditions for a minimum resolution of 2 between relevant peaks would be 1652, 2073, 746, 1085, 833 and 809 for the six different optima. A comparison of these values with the numbers listed in the last column in Table V (bottom) illustrates the benefits of the SOS system.

The predicted optimum separations corresponding to the chromatograms in Figs. 6a and 8a (and to the optima Nos. 1 and 3 in Tables IV and V) are shown in Figs. 6b and 8b. The selectivity does not change on going from Fig. 6a to 6b or from

Fig. 8a to 8b, *i.e.*, the relative retention times are constant. However, the absolute retention times are reduced considerably.

CONCLUSIONS

We have tried to demonstrate that different computer programs can be used coherently for developing chromatographic methods. We have described some careful steps on the road towards an integrated system for method development in chromatography. In this work, different software programs were used as such, while no attempts were made to actually integrate the software into one program or even one computer. In fact, the three different programs used required three different computers. Integrating several expert systems into one system is one of the goals of the "Expert Systems for Chemical Analysis" project². One of the laboratories involved in this work (Vrije Universiteit Brussel) is currently trying to develop a connection between different programs for performing the tasks of method development and method optimization, including the optimization of retention, selectivity and the chromatographic system. The overall system will appear to the user as a single computer program.

In this work we have demonstrated the value of using a combination of different computer programs. An expert system was used to select the most appropriate selectivity-optimization criterion. This system yielded the same advice as the human expert. A systematic procedure for optimizing the mobile-phase composition in reversed-phase LC was used in combination with several different optimization criteria. In some instances, the optimum composition can vary greatly once a different optimization criterion has been selected. The resulting optimum chromatogram can be subjected to an expert system for system optimization. This system predicts the best possible column, instrumentation and operating conditions based on the optimum chromatogram found during the selectivity optimization.

The use of these three systems together offers great advantages to the user. The selection of the most appropriate optimization criterion is difficult and only a few specialists are thought to master this area. Without the best optimization criterion, systematic selectivity-optimization procedures will not be used correctly and will not produce the best possible results. The expert system for criterion selection can thus make selectivity-optimization procedures easier to use and make them yield better results.

Likewise, the results of the selectivity-optimization process can be much improved by consulting the system-optimization system afterwards. This may result in much shorter analysis times and a much better sensitivity for the proposed method. The best results can be obtained if the possibilities of the system-optimization system are borne in mind during the selection of the optimization criterion, illustrating how the different systems interact together. The system-optimization system may also be consulted to decide on whether or not selectivity optimization is required. It can be rapidly consulted to see what kind of separation may be achieved without selectivity optimization. If this is thought to be adequate, the selectivity optimization can be forfeited.

There is much work to be done in demonstrating the applicability of the software programs discussed in this work, in verifying the correctness of the advice

offered by the expert system and in experimentally validating the methods proposed by systematic procedures such as ours. For example, the effect of the variability of retention and selectivity between different column materials will need to be considered. A good deal of work is in progress at the moment, but with the increasing availability of expert systems for chromatographers we feel that both research and applications in the area will blossom in the near future.

ACKNOWLEDGEMENTS

Part of this research was supported by the European Commission within ESPRIT Project 1570, "Expert Systems for Chemical Analysis". We acknowledge the valuable contributions of many members of the ESCA project team to the ideas formulated in this paper. The phenols data set was recorded by Nigel Warren (Philips Scientific). The peak labelling was performed by Pam Chamberlain, using the Diamond package. The assistance of Anita van Berkel in maintaining the system-optimization expert system at Philips Research, Eindhoven, is appreciated.

REFERENCES

- 1 P. J. Schoenmakers and M. Mulholland, *Chromatographia*, 25 (1988) 737.
- 2 D. Goulder, T. Blaffert, A. Blokland, L. Buydens, A. Chhabra, A. Cleland, N. Dunand, H. Hindriks, G. Kateman, H. van Leeuwen, D. Massart, M. Mulholland, G. Musch, P. Naish, A. Peeters, G. Postma, P. Schoenmakers, M. de Smet, B. Vandeginste and J. Vink, *Chromatographia*, 26 (1988) 237.
- 3 P. J. Schoenmakers, *Optimization of Chromatographic Selectivity - A Guide to Method Development*, Elsevier, Amsterdam, 1986.
- 4 J. C. Berridge, *Techniques for the Automated Optimization of HPLC Separations*, Wiley, Chichester, 1985.
- 5 J. C. Berridge, *Chemometr. Intell. Lab. Syst.*, 3 (1988) 175.
- 6 G. Guiochon, in Cs. Horváth (Editor) *High-Performance Liquid Chromatography*, Vol. 2, Academic Press, New York, 1980, pp. 1-56.
- 7 R. P. W. Scott, *J. Chromatogr.*, 468 (1989) 99.
- 8 J. W. Dolan, L. R. Snyder and M. A. Quarry, *Chromatographia*, 24 (1987) 261.
- 9 L. R. Snyder, J. L. Glajch and J. J. Kirkland, *Practical HPLC Method Development*, Wiley, New York, 1989.
- 10 A. Peeters, L. Buydens, D. L. Massart and P. J. Schoenmakers, *Chromatographia*, 26 (1988) 101.
- 11 P. J. Naish, R. J. Lynch and T. Blaffert, *Chromatographia*, 27 (1989) 343.
- 12 P. J. Schoenmakers, N. Dunand, A. C. Cleland, G. Musch and T. Blaffert, *Chromatographia*, 26 (1988) 37.
- 13 P. J. Naish and R. J. Lynch, *Chromatographia*, 29 (1990) 79.
- 14 P. J. Schoenmakers and N. Dunand, *J. Chromatogr.*, 485 (1989) 219.
- 15 N. R. Warren and J. T. Hann, *13th International Symposium on Column Liquid Chromatography, Stockholm, June 25-30, 1989*, Poster No. 86.
- 16 G. Eppert, G. Liebsche, M. Ihrke and G. Arendt, *J. Chromatogr.*, 350 (1985) 471.
- 17 H. A. Cooper and R. J. Hurtubise, *J. Chromatogr.*, 328 (1985) 81.
- 18 H. A. H. Billiet, A. C. J. H. Drouen and L. de Galan, *J. Chromatogr.*, 316 (1984) 231.
- 19 A. P. Goldberg, E. Nowakowska, P. E. Antle and L. R. Snyder, *J. Chromatogr.*, 316 (1984) 241.
- 20 J. C. Berridge and E. G. Morrissey, *J. Chromatogr.*, 316 (1984) 69.
- 21 R. D. Conlon, *Instrum. Res.*, 1 (1985) 74.
- 22 P. R. Haddad and S. Sekulic, *J. Chromatogr.*, 459 (1984) 79.
- 23 J. V. Hinshaw, Jr. and L. S. Ettre, *Chromatographia*, 21 (1986) 561.
- 24 P. J. Schoenmakers, *J. Liq. Chromatogr.*, 10 (1987) 1865.
- 25 P. J. Schoenmakers, J. K. Strasters and Á. Bartha, *J. Chromatogr.*, 458 (1987) 355.
- 26 A. K. Smilde, A. Knevelman and D. A. Doornbos, *J. Chromatogr.*, 369 (1986) 1.

CHROMSYMP. 1782

Theoretical optimization of open-tubular columns for liquid chromatography with respect to mass loadability

P. P. H. TOCK*, P. P. E. DUIJSTERS, J. C. KRAAK and H. POPPE

Laboratory of Analytical Chemistry, University of Amsterdam, Nieuwe Achtergracht 166, 1018 WV Amsterdam (The Netherlands)

SUMMARY

A procedure is described for designing open-tubular liquid chromatographic (LC) columns with high resolving power, optimized for mass loadability. Large film thicknesses improve the loadability, but decrease the efficiency owing to the increased mass-transfer term. Normally an arbitrary upper limit of the magnitude of the contribution of the stationary phase mass-transfer term to the overall plate-height equation of about 20% is accepted. The present approach allows the real optimum value of the contribution of the stationary phase mass-transfer term to be calculated. The optimum was found to occur at about 50% in most instance. This corresponds to a plate height equation $h = 2/v + 0.12v$ for $k' = 3$ instead of the expression for very thin films $h = 2/v + 0.08v$ as advocated by Knox and Gilbert (h = reduced plate height, v = reduced velocity; k' = capacity factor). The maximum column length is about 5 m for all phase systems with $3 \cdot 10^5$ theoretical plates, dead time of mobile phase 1000 s and 20 MPa pressure drop along the column. The mass loadability of an open-tubular LC column and a 21- μm micropacked capillary were compared and were found to be in the same range. The optimization procedure uses known and established relationships, describing speed, efficiency and mass loadability in chromatographic systems. The calculations were carried out with a spreadsheet computer program.

INTRODUCTION

Optimum resolving power and speed for open-tubular liquid chromatographic (LC) columns has been predicted for columns of I.D. 1–5 μm ^{1,2}. It has been shown that the theoretical predicted optimum resolving power can be realized in practice^{3–14}. Various stationary layers or films can now be coated successfully in 5- μm (and larger) fused-silica capillaries with near to the theoretical performance^{6–12}. The excellent performance can only be realized by keeping the external band broadening in these systems below 1 nl. The requirements on the external band broadening can be achieved by applying on-column detection^{4,5} and split-injection techniques^{3,11}. However, these required extremely small volumes, implying a dramatic decrease in concentration detectability of the solutes, which limits the dynamic range of the system. Improve-

ments in this respect can be achieved by increasing the mass loadability of open-tubular LC columns. This can be achieved by using larger inner diameters, which would be putting the cart before the horse in view of the increase in the transverse molecular diffusion term in the Golay equation¹⁵, and by using thicker stationary phases. The latter also can only be increased to a certain limit, because of the accompanying increase in the stationary mass-transfer term in the Golay equation. Normally an arbitrary upper limit (*e.g.*, 20%) to the magnitude of the contribution of the stationary phase mass-transfer term relative to the overall plate height equation is accepted. However, whether this percentage represents the correct, *i.e.*, optimum, value is unknown. Therefore, it is of importance to develop an optimization strategy procedure in order to design columns with a high resolving power in a reasonable analysis time with high sample capacity.

We believe that columns optimized from this point of view offers more prospects in the near future. The better efficiency of open-tubular LC columns compared with packed columns has been proved, but for more practical use of open-tubular LC in the future, *e.g.*, outside research and university laboratories, it is necessary to demonstrate its real power with practical applications. In view of the large differences in concentrations that occur in such applications, a high dynamic range, and therefore a high column loadability, are essential. The present procedure gives the chromatographer an easy guideline to design such columns.

Many papers^{16,17} have discussed the influence of various column parameters on loadability, efficiency and speed. Noy *et al.*¹⁸ derived some equations which show the effect of column dimensions on the minimum detectable amount (for a mass flow-sensitive detector) and the minimum analyte concentration (for a concentration-sensitive detector).

Recently, Ghijsen and Poppe¹⁹ reported an optimization procedure for designing capillary gas chromatographic (GC) columns with maximum loadability at a given performance in terms of efficiency and speed of separation and compared these columns with packed GC columns. They used a procedure based on known and established relationships describing plate height (Golay–Giddings)²⁰, speed (t_m according to Knox and Saleem)² and an estimate of mass loadability, M_{pl} , which is equal to the amount of stationary phase in one plate²¹. The calculations were carried out with a spreadsheet computer program, which ensured the user a large flexibility for selecting different specifications. Especially the flexibility attracted us to use this procedure to propose a new design of open-tubular LC columns.

The optimization procedure was carried out for three phase systems, the usefulness of which has been demonstrated in open-tubular LC: a porous silica layer with a liquid–liquid phase system^{10–12}, a cross-linked silicone phase system^{6–10} and an adsorption system on a flat wall, which will henceforth be termed as liquid–liquid system, silicone system and monolayer system, respectively.

PROCEDURE

The optimization procedure was carried out following the flow chart in Fig. 1 (symbols are defined at the end of the paper). It starts with the input of the specifications (t_m , ΔP , N) and the experimental constant (φ , η) to calculate h , using eqn. 1, which is a rearranged form of the well known equation of Knox and Saleem². Once

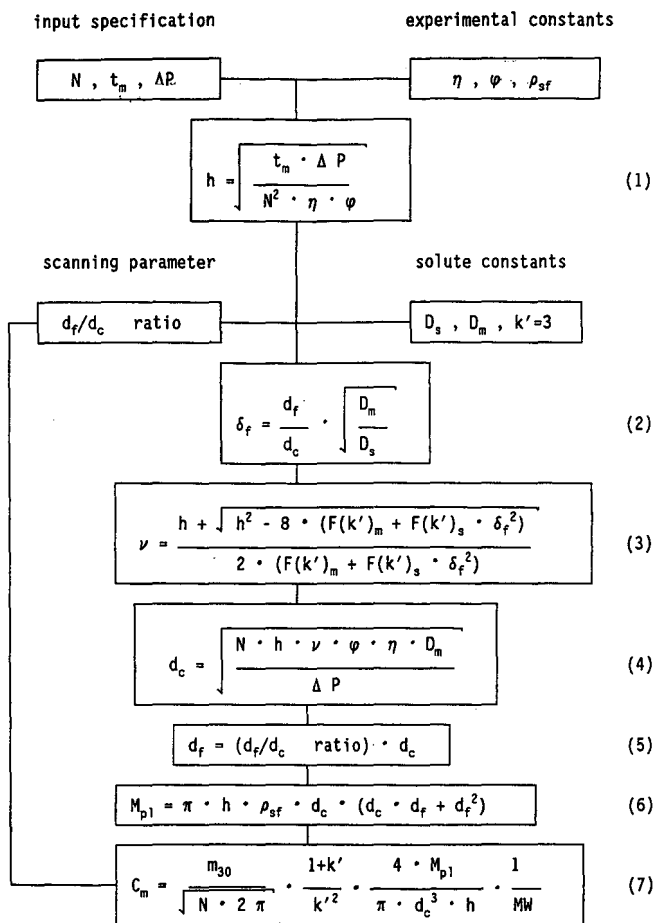


Fig. 1. Flow chart for the optimization procedure.

h is known, the value of ν , and with that the whole set of conditions, would be accessible, provided that the h - ν curve is available. Each value of the d_f/d_c ratio (the scanning parameter) corresponds to one particular h - ν plot, $h = 2/\nu + C\nu$, where $C = F(k')_m + F(k')_s \delta_f^2$ and δ_f is the reduced film thickness²²:

$$F(k')_m = \frac{(1 + 6k' + 11k'^2)}{96(1 + k')^2}$$

$$F(k')_s = \frac{2k'}{3(1 + k')^2}$$

Scanning the value of d_f/d_c yields a set of solutions to the problem. The derivation of the h - ν curve in each instance proceeds via δ_f , calculated with eqn. 2 substituting D_s , D_m , $k' = 3$ and the ratio d_f/d_c . The definition of d_f and d_c can be seen in Fig. 2. The

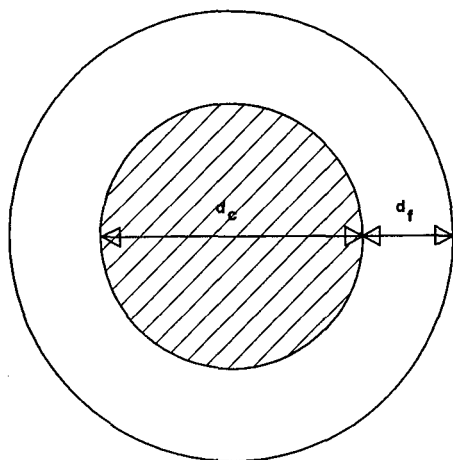


Fig. 2. Definition of the inner diameter and film thickness as used in the optimization procedure.

value of δ_f was then substituted in the rearranged dimensionless Golay–Giddings equation²⁰ (eqn. 3), to obtain the h – v function and v (taking the larger root). Next d_c was calculated with eqn. 4, the Poiseuille equation.

Once a whole set of columns, each with a δ_f value, but all of them satisfying the speed and efficiency requirements, have been found, the one with the highest mass loadability, M_{pl} , can be selected. As a criterion to do that, the amount of stationary phase (either surface area or volume/mass) was used, in accordance with the theoretical²¹ and the experimental evidence^{23,24}, showing that this is a good measure of loadability. Finally, d_f , M_{pl} and C_m , the eluting concentration which is the outlet concentration of the solute in the mobile phase, were calculated using eqns. 5, 6 and 7, respectively.

The d_f/d_c ratio was varied from 0 to 3 in steps of 0.05 for the liquid–liquid system and from 0 to 0.3 in steps of 0.005 for the silicone system. The obtained values of M_{pl} , d_c , d_f , $d_c + 2d_f$, L and C_m were plotted against the d_f/d_c ratio for different specifications, *e.g.*, varying one specification while the others remained fixed.

RESULTS AND DISCUSSION

The optimization procedure in Fig. 1 was applied to the liquid–liquid system and the silicone system. The d_f/d_c ratio was used as the scanning parameter and the fixed input specifications were $N = 3 \cdot 10^5$, $t_m = 1000$ s and $\Delta P = 20$ MPa. For the monolayer system, where the d_f/d_c ratio cannot be used, ΔP was used as the scanning parameter. The optimization procedure for the different specifications, different phase systems and the corresponding figures are summarized in Table I.

In the figures some d_f/d_c ratios have been marked with an asterisk; for these points the specifications can only be realized in the minimum of the h – v curve. Larger d_f/d_c ratios are inaccessible, because v cannot be calculated in eqn. 3 (Fig. 1) with the input specifications; the determinant of this equation is negative. The explanation of this fact is that for the d_f/d_c ratios marked with an asterisk h_{\min} of the corresponding

TABLE I
CHARACTERISTICS OF THE OPTIMIZATION

Phase system ^a	$N \cdot 10^5$	t_m (s)	ΔP (MPa)	Fig.	Remarks
LL	3	1000	Variable	3a	$M_{pi}-d_t/d_c$ ratio
LL	3	Variable	20	3b	$M_{pi}-d_t/d_c$ ratio
LL	Variable	1000	20	3c	$M_{pi}-d_t/d_c$ ratio
S	3	1000	Variable	4	$M_{pi}-d_t/d_c$ ratio
M	3	Variable	x-axis	5	$M_{pi}-\Delta P$
LL	3	1000	20	6a	Column dimensions
S	3	1000	20	6b	Column dimensions
LL	Variable	1000	20	7a	C_m-d_t/d_c ratio
S	Variable	1000	20	7b	C_m-d_t/d_c ratio
LL/S	x-axis	1000	20	8	Maximum $M_{pi}-N$
LL/S	x-axis	1000	20	9	$C_m^{opt}-N$

^a LL = Liquid-liquid system, $D_s = 5 \cdot 10^{-10}$ m²/s; S = silicone system, $D_s = 7 \cdot 10^{-12}$ m²/s; M = monolayer system.

$h-v$ curve is equal to the defined h , calculated with eqn. 1 (Fig. 1). For a larger d_t/d_c ratio, h_{min} of the corresponding $h-v$ curve increases, *e.g.*, h_{min} is larger than the specified h , and therefore no v can be found on the $h-v$ curve for the specified h . Inaccessible points are indicated with an asterisk in all figures.

Liquid-liquid system

In Fig. 3a, the calculations were made for various pressure drops in the range 2–100 MPa. It can be seen that the d_t/d_c ratio for the maximum M_{pi} decreases with increasing ΔP , but for $\Delta P = 40$ MPa or higher the optimum d_t/d_c ratio approaches a value $d_t/d_c = 0.485$. For the fixed input specifications the plate-height equation is $h = 2/v + 0.133v$; there is an increase in C of *ca.* 60% compared with columns with a very thin film. The column dimensions for the maximum M_{pi} at 20 and 40 MPa are listed in Table II. From these data it can be seen that doubling ΔP from 20 to 40 MPa hardly changes the column dimensions, but M_{pi} increase 1.4-fold. At high allowed pressure drops, *i.e.*, when a sizeable film thickness is possible, the loadability is indeed in general proportional to the square root of the inlet pressure.

In Fig. 3b, the calculations were made for various t_m values and it can be seen that the d_t/d_c ratio for maximum M_{pi} again increases to 0.485 with increasing t_m . The value of M_{pi} increases by a factor of 4 on doubling t_m , whereas the column dimensions show an increase of d_c , d_t , $d_c + 2d_t$ and L (Table II).

In Fig. 3c, the calculations were made for various N values and it can be seen that the d_t/d_c ratio for maximum M_{pi} increases only from 0.475 for $N = 3 \cdot 10^5$ to 0.495 for $N = 1 \cdot 10^5$. In this instance M_{pi} increases 16.5-fold, whereas d_c and L increase by the square root of 3 and d_t increases 1.8-fold (Table II).

As an example, these calculations show that when a plate number of $3 \cdot 10^5$ is needed, a pressure drop of 20 MPa can be allowed in combination with a dead time of 1000 s (an analysis time of 4000 s), and with maximum loadability this will result in the following column system: coat a $3.9 \text{ m} \times 9.6 \mu\text{m}$ I.D. capillary with a porous support

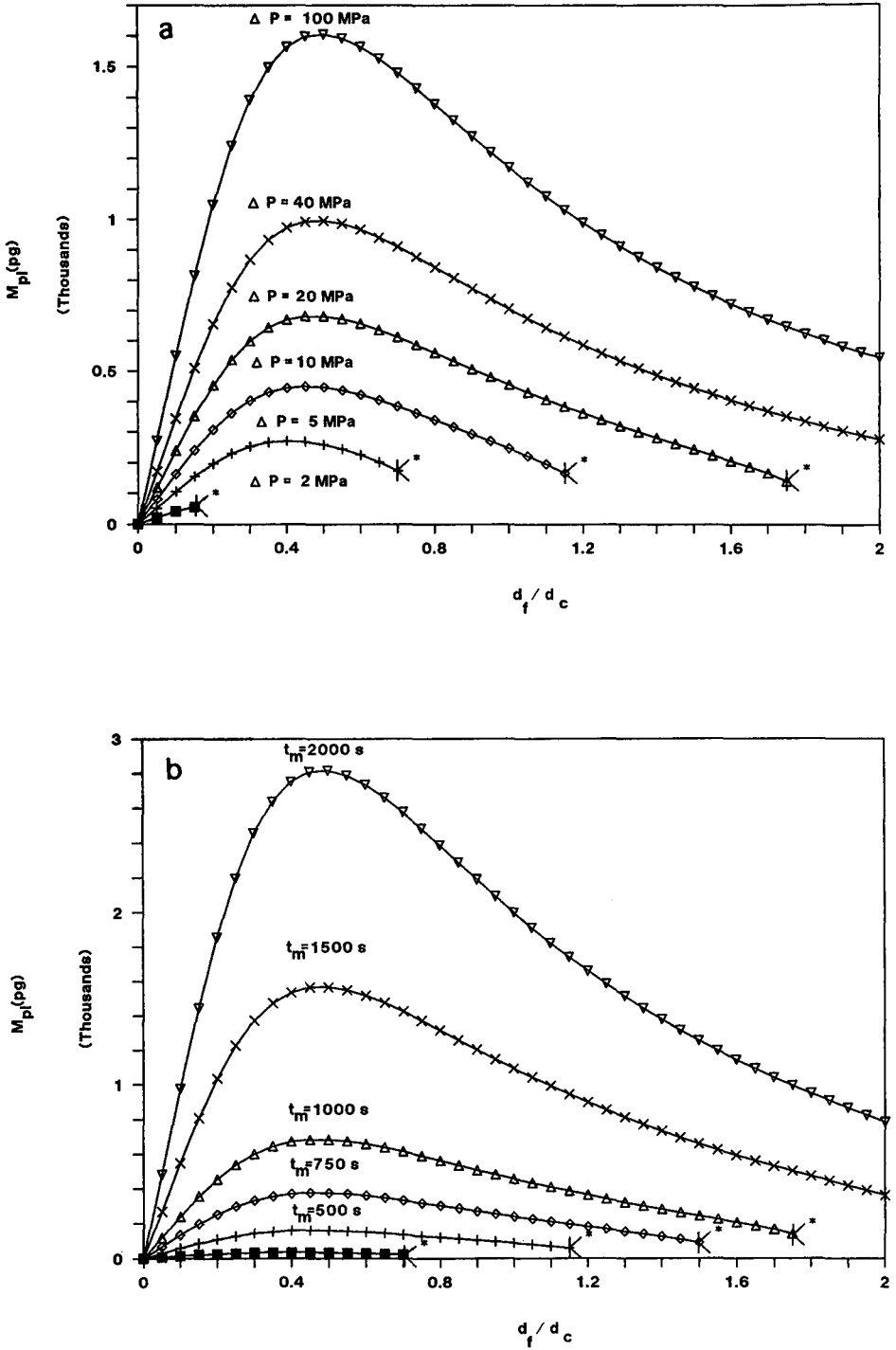


Fig. 3.

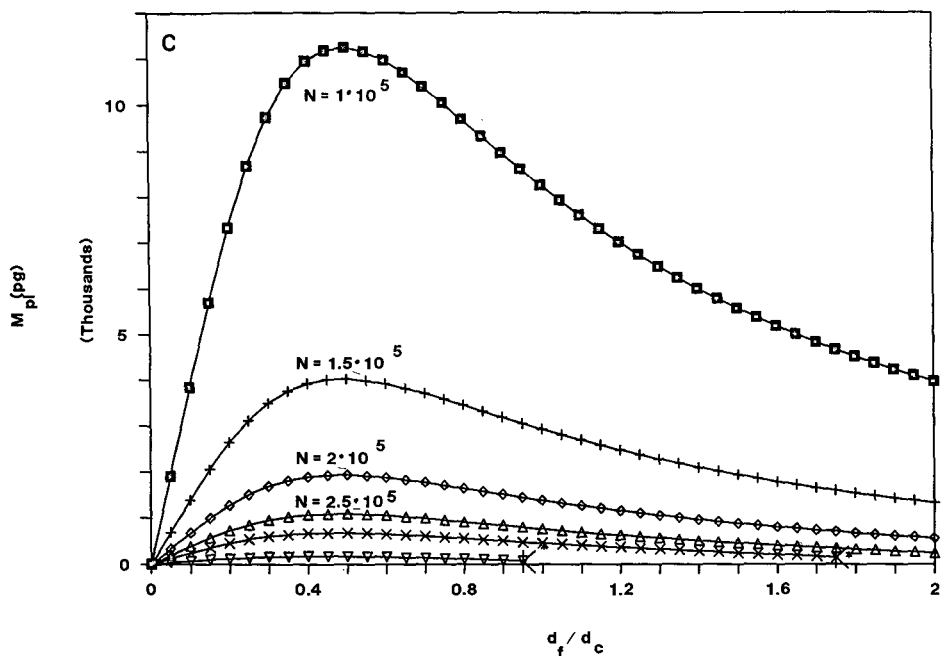


Fig. 3. Mass loadability M_{pl} (pg) versus d_f/d_c ratio for the liquid-liquid system. (a) $N = 3 \cdot 10^5$, $t_m = 1000$ s and various ΔP values: $\blacksquare = 2$; $+$ = 5; $\diamond = 10$; $\triangle = 20$; $\times = 40$; $\nabla = 100$ MPa. (b) $N = 3 \cdot 10^5$, $\Delta P = 20$ MPa and various t_m values: $\blacksquare = 250$; $+$ = 500; $\diamond = 750$; $\triangle = 1000$; $\times = 1500$; $\nabla = 2000$ s. (c) $t_m = 1000$ s, $\Delta P = 20$ MPa and various N values: $\blacksquare = 1 \cdot 10^5$; $+$ = $1.5 \cdot 10^5$; $\diamond = 2 \cdot 10^5$; $\triangle = 2.5 \cdot 10^5$; $\times = 3 \cdot 10^5$; $\nabla = 5 \cdot 10^5$.

layer and generate on this column a liquid-liquid system with a film thickness of 2.3 μm . The maximum loadability will be 680 pg of a solute with $k' = 3$. From Fig. 3a-c for the liquid-liquid system the following conclusions can be drawn: changes in N and t_m have a very strong and strong influence, respectively, on M_{pl} ; changes in ΔP has a weak influence on M_{pl} , approximately by $\sqrt{\Delta P}$; the arbitrary upper limit of a 20% increase in C is an acceptable limit, but at maximum M_{pl} for the liquid-liquid system a 60% contribution of the mass-transfer term gives a better compromise; the plate height equation for the liquid-liquid system is $h = 2/\nu + 0.133\nu$; and M_{pl} increases, as expected, with a decrease in efficiency or with an increase in analysis time or pressure drop.

Silicone system

The optimization procedure was also carried out with the silicone system. The resulting plots were similar to those for the liquid-liquid system. The dependences of M_{pl} on N , t_m and ΔP are identical for both phase systems, only the d_f/d_c ratio and the obtained M_{pl} values being different. In Fig. 4, which can be compared with Fig. 3a, it can be seen that M_{pl} and the d_f/d_c ratios are about ten times smaller for the silicone system than for the liquid-liquid system. This can be explained by the difference in the diffusion coefficients in the stationary phase for the two phase systems; in eqn. 2 (Fig. 1), δ_f depends on the square root of the diffusion coefficients. In Table II the column

TABLE II
COLUMN DIMENSIONS AT MAXIMUM LOADABILITY

Phase system ^a	Input specifications			Column dimensions							Fig.	
	$N \cdot 10^5$	t_m (s)	ΔP (MPa)	d_f/d_c	C	d_c (μm)	d_f (μm)	d_b^b (μm)	L (m)	M_{pl} (pg)		C_m (mmol/l)
LL	3	1000	40	0.485	0.136	4.91	2.38	9.67	5.49	1000	9.33	3a
LL	3	1000	20	0.475	0.133	4.90	2.33	9.56	3.87	680	9.07	3a
LL	3	2000	20	0.485	0.136	6.94	3.37	13.67	7.76	2820	9.33	3b
LL	1	1000	20	0.495	0.138	8.49	4.20	16.90	6.71	11 000	15.7	3c
S	3	1000	40	0.0475	0.117	5.29	0.25	5.79	5.91	86	0.64	4
S	3	1000	20	0.0465	0.115	5.28	0.25	5.77	4.17	59	0.63	4
S	3	2000	20	0.0475	0.117	7.48	0.36	8.19	8.36	244	0.64	—
S	1	1000	20	0.0480	0.118	9.19	0.44	10.07	7.27	970	1.13	—
M	3	1000	20	0	0.08	6.51	0	6.51	5.15	0.3 fg	—	5
M	3	2000	20	0	0.08	9.26	0	9.26	10.36	0.8 fg	—	5

^a LL = Liquid-liquid system; S = silicone system; M = monolayer system.

^b $d_b = d_c + 2d_f$.

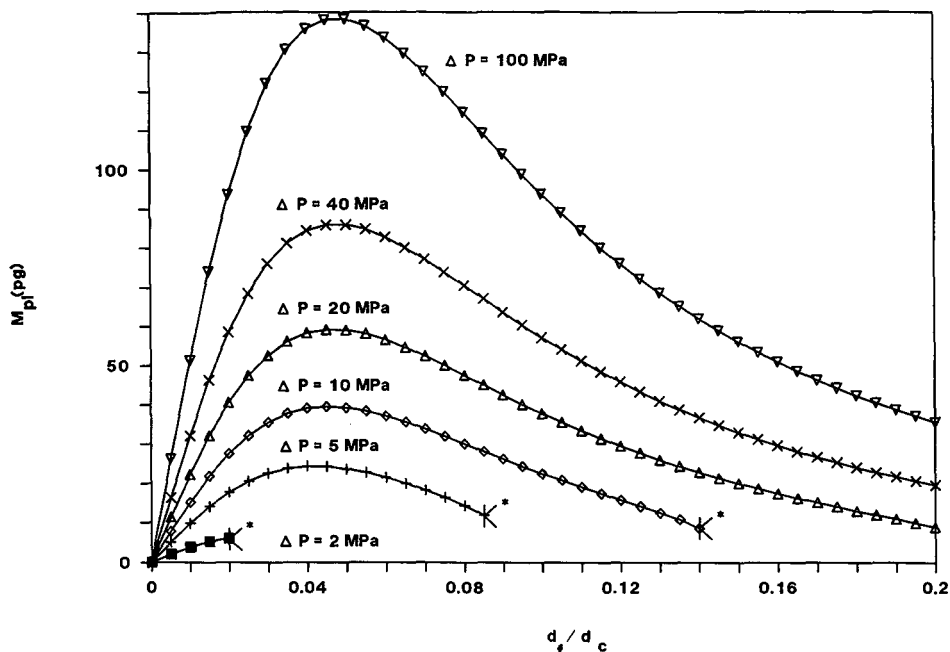


Fig. 4. Mass loadability M_{pi} (pg) versus d_f/d_c ratio for the silicone system with $N = 3 \cdot 10^5$, $t_m = 1000$ s and various ΔP values: $\blacksquare = 2$; $+$ = 5; $\diamond = 10$; $\triangle = 20$; $\times = 40$; $\nabla = 100$ MPa.

dimensions for the maximum M_{pi} are listed and it can be seen that the main differences between the two phase systems are found in d_f and $d_c + 2d_f$, which amount to a factor of 10 and 1.7, respectively. The other column dimensions are almost the same. The plate-height equation for $\Delta P = 20$ MPa is $h = 2/v + 0.115v$, which is an increase in C of about 50%.

From Fig. 4, it can be concluded that: the use of a phase system with a very small diffusion coefficient in the stationary phase is, as expected, unfavourable with respect to mass loadability, roughly in proportion to the expression $\sqrt{(D_{s1}/D_{s2})}$, and the dependence of N , t_m and ΔP on M_{pi} is identical with that for the liquid-liquid system.

Monolayer system

The optimization procedure shown in Fig. 1 cannot be used for mass-loadability optimization for the monolayer system. The flow chart had to be changed, because the thickness of the monolayer cannot be varied and there is one degree of freedom less. The pressure drop ΔP was chosen as the scanning parameter with various t_m values and $N = 3 \cdot 10^5$. M_{pi} was calculated using the equation

$$M_{pi} = \pi h d_c^2 M W \alpha_{OH(s)} \quad (8)$$

In Fig. 5 it can be seen that (i) M_{pi} is about $2 \cdot 10^6$ and $2 \cdot 10^5$ times smaller than in the liquid-liquid system and the silicone system, respectively, (ii) M_{pi} increases continuously with increasing ΔP and (iii) doubling t_m increases M_{pi} 2.7-fold (Table II). In Table II, the column dimensions for $\Delta P = 20$ MPa and $t_m = 1000$ and 2000 s are

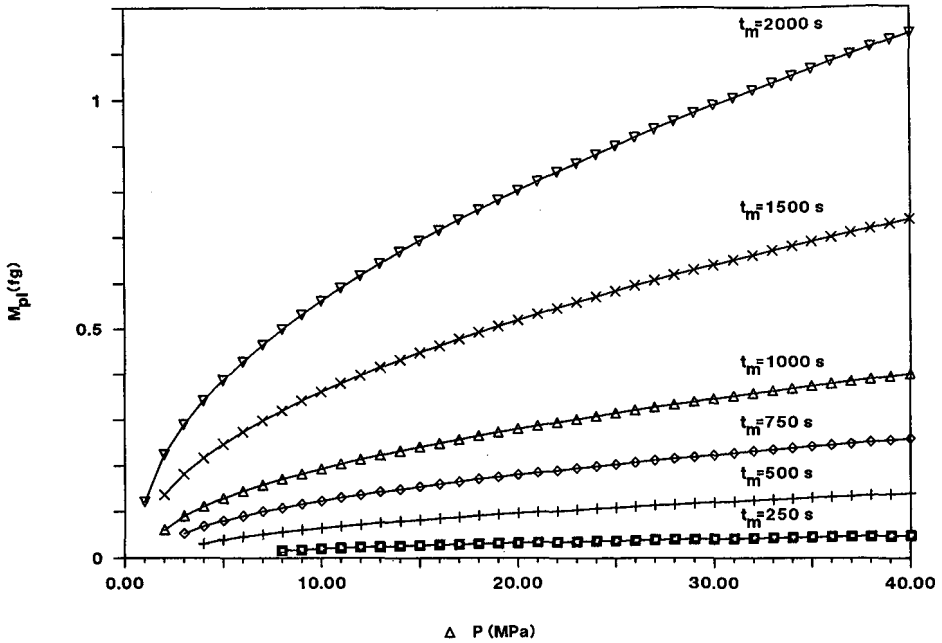


Fig. 5. Mass loadability M_{pi} (fg) versus ΔP for the monolayer system with $N = 3 \cdot 10^5$ and for various t_m : \blacksquare = 250; + = 500; \diamond = 750; \triangle = 1000; \times = 1500; ∇ = 2000 s.

listed. L and d_c increase by the same factor on doubling t_m and are hardly different compared with the other phase systems. Finally, it can be noted that M_{pi} increases enormously if a stationary layer or film is applied in the capillary and therefore in our opinion columns should be prepared with stationary phases with suitable thickness.

Column dimensions

In Fig. 6a and b, the column dimensions for the liquid-liquid and silicone systems, respectively, are shown. It can be seen that the plots of L and d_c are almost identical for the two systems (except for the differing horizontal scales), whereas for d_f and $d_c + 2d_f$ a large difference is observed. The maximum length of the columns is about 5 m for the fixed input specifications. For the liquid-liquid system $d_c + 2d_f$ has a maximum at $d_f/d_c = 0.55$ and the maximum for d_f is at $d_f/d_c = 1.2$; for the silicone system these maxima are at $d_f/d_c = 0.01$ and 0.145, respectively.

Eluting concentration

In Fig. 1, C_m can be calculated with eqn. 7 and in Fig. 7a and b C_m is shown for the liquid-liquid and silicone system, respectively. The results of our calculations show that C_m can be influenced only by N and the d_f/d_c ratio, and not by ΔP and t_m . This can be explained by eqn. 7, in which C_m depends only on the reciprocal square root of N and the phase ratio, and the latter can be expressed as a function of d_f/d_c . The value of C_m varies in proportion to the reciprocal of the square root of N , and C_m increases continuously with increasing d_f/d_c . In Table II, C_m is listed at maximum M_{pi} and it can be seen that C_m is 14.4 times smaller for the silicone system than the liquid-liquid

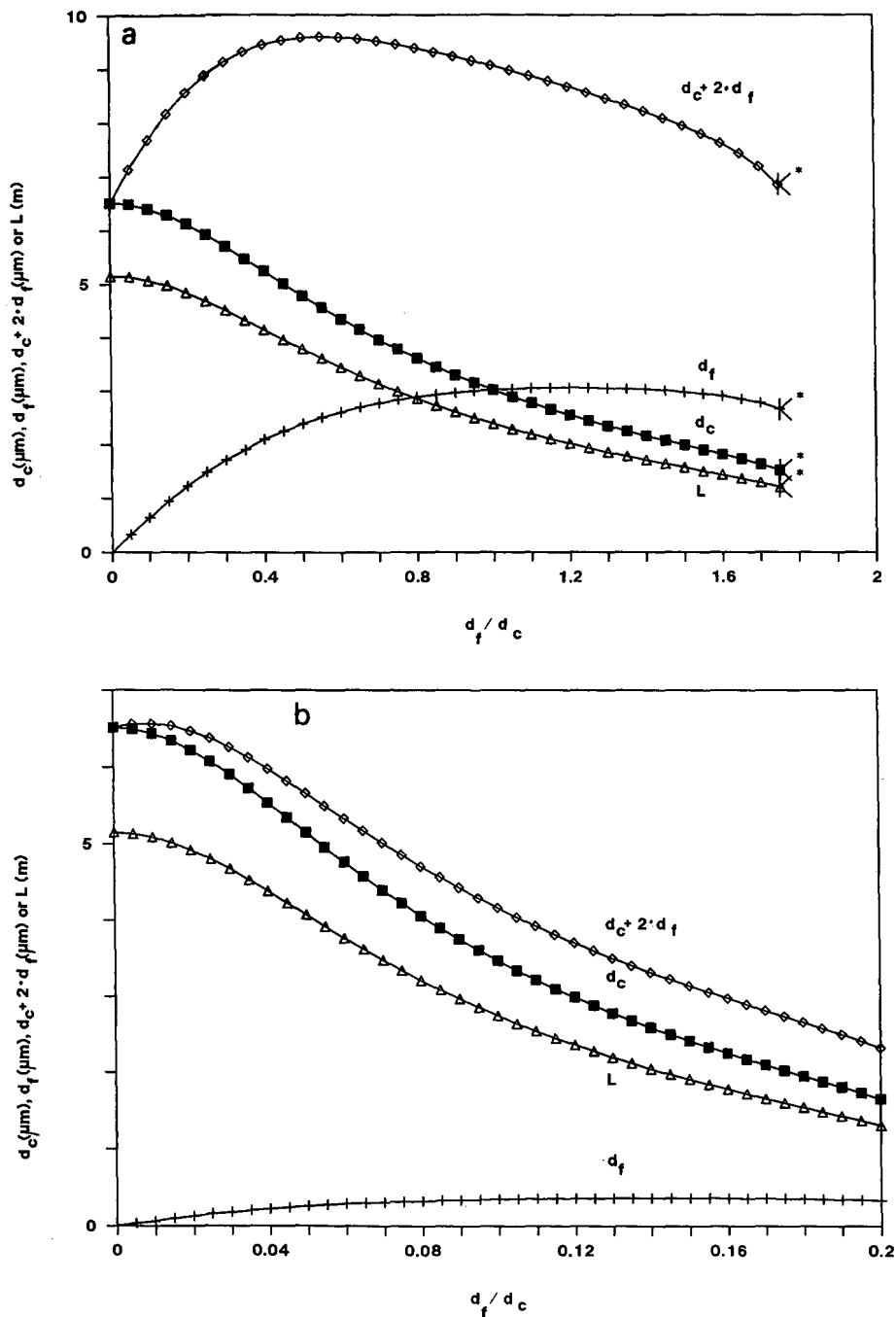


Fig. 6. Column dimensions versus d_f/d_c ratio. (a) For the liquid-liquid system with $N = 3 \cdot 10^5$, $t_m = 1000$ s and $\Delta P = 20$ MPa. $\blacksquare = d_c$ (μm); $+$ = d_f (μm); $\diamond = d_c + 2d_f$ (μm); $\triangle = L$ (m). (b) For the silicene system with $N = 3 \cdot 10^5$, $t_m = 1000$ s and $\Delta P = 20$ MPa. $\blacksquare = d_c$ (μm); $+$ = d_f (μm); $\diamond = d_c + 2d_f$ (μm); $\triangle = L$ (m).

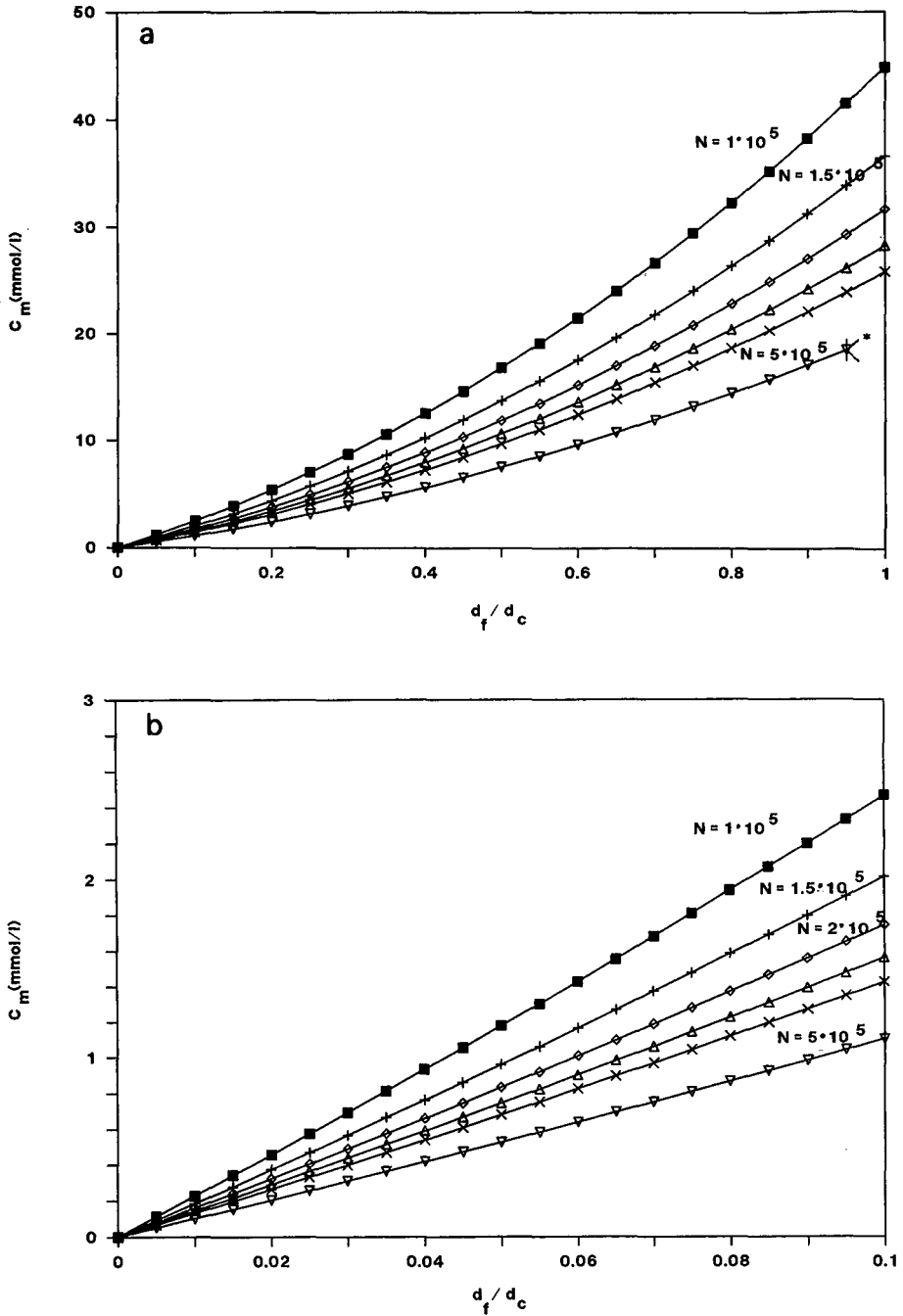


Fig. 7. Eluting concentration C_m (mmol/l) versus d_f/d_c ratio. (a) For the liquid-liquid system with $t_m = 1000$ s, $\Delta P = 20$ MPa and various N values: $\blacksquare = 1 \cdot 10^5$; $+$ $= 1.5 \cdot 10^5$; $\diamond = 2 \cdot 10^5$; $\triangle = 2.5 \cdot 10^5$; $\times = 3 \cdot 10^5$; $\nabla = 5 \cdot 10^5$. (b) For the silicone system with $t_m = 1000$ s, $\Delta P = 20$ MPa and various N values: $\blacksquare = 1 \cdot 10^5$; $+$ $= 1.5 \cdot 10^5$; $\diamond = 2 \cdot 10^5$; $\triangle = 2.5 \cdot 10^5$; $\times = 3 \cdot 10^5$; $\nabla = 5 \cdot 10^5$.

system. This demonstrates again the importance of having a high diffusion coefficient in the stationary layer. In Fig. 7a the curve of C_m is linear from $d_t/d_c = 0$ to 0.1, and in this region the phase ratio can be approximated by 4 times the d_t/d_c ratio, but for larger d_t/d_c ratios the phase ratio had to be calculated with 4 times $d_t/d_c + (d_t/d_c)^2$. For the liquid-liquid system only the latter equation for the phase ratio had to be used.

Dependence of C_m and the maximum M_{pl} on the efficiency

As mentioned above, C_m and the maximum M_{pl} depend very strongly on the efficiency. The maximum M_{pl} and subsequently C_m were calculated for the liquid-liquid system and the silicone system for $N = 1 \cdot 10^4 - 1 \cdot 10^6$. In Fig. 8 it can be seen that the two curves are identical for both systems, but M_{pl} for the liquid-liquid system is about ten times larger than that for the silicone system. In this plot it is obvious that the loadability is extremely sensitive to the number of plates needed in the chromatographic system. Increasing N means a decrease in M_{pl} ; an increase in N of one order of magnitude gives a decrease in M_{pl} of three orders of magnitude.

In Fig. 9 it can be seen that for C_m , at maximum M_{pl} , the same conclusion as mentioned above can be drawn, except that C_m for the liquid-liquid system is about 15 times larger than that for the silicone system. An increase in N by a factor of 10 decreases C_m by a factor of the square root of 10.

Packed capillaries versus open-tubular columns

It is interesting to compare the loadabilities obtained with those obtained with the so-called micro-packed capillaries. Such columns, as studied by Novotny and

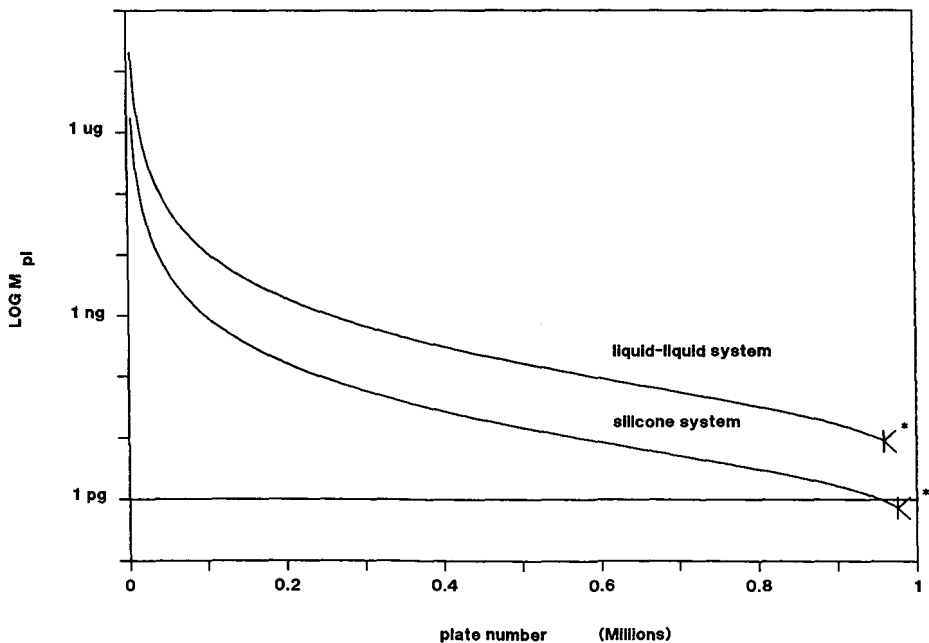


Fig. 8. Maximum mass loadability M_{pl} (pg) on a log scale versus N for the liquid-liquid system and the silicone system, with $t_m = 1000$ s and $\Delta P = 20$ MPa.

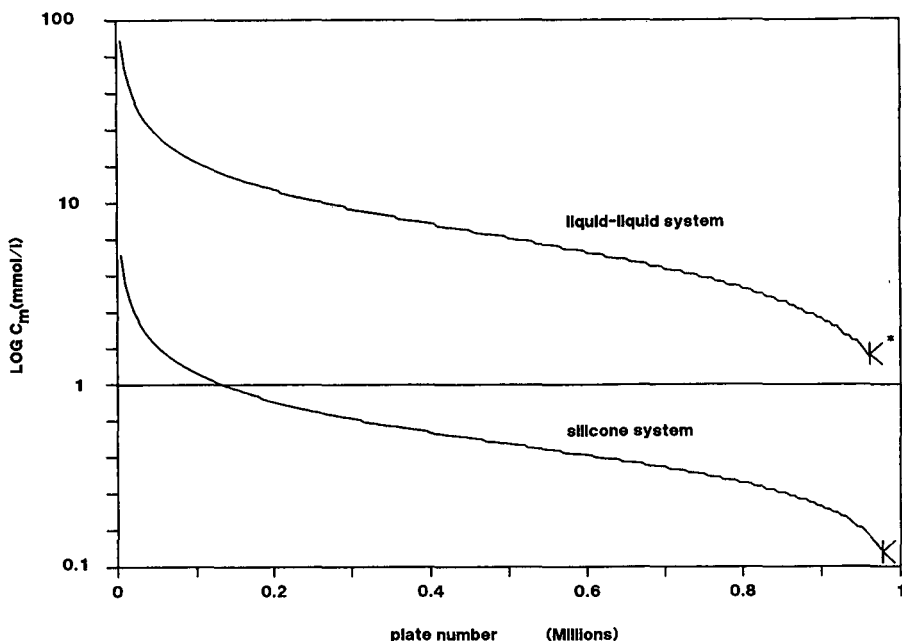


Fig. 9. Eluting concentration C_m (mmol/l), at maximum loadability, on a log scale versus N for the liquid-liquid system and the silicone system, with $t_m = 1000$ s and $\Delta P = 20$ MPa.

co-workers²⁵⁻²⁷ and more recently by Kennedy and Jorgenson²⁸, aim at the realization of higher speeds and accessible plate counts by exploiting the smaller packing density and associated better permeabilities and separation impedances. The value of the latter may also be significantly improved by the smaller h values [down to 1 (ref. 28)], giving an additional improvement of a factor of 4. Altogether, separation impedances $E = h^2\phi$ as low as 500 have been observed^{28,29}. The open-tubular columns found in this work to be optimum have E values (e.g., the second entry in Table II) of $32 \cdot h^2 = 220$, i.e., in the same range.

The mentioned kinetic performance of micro-packed capillary columns can only be realized if the ratio of the particle to the tube diameter is very low, of the order of 5. As particle sizes of about $5 \mu\text{m}$ are indicated, a tube diameter of $25 \mu\text{m}$ is a good average if E values of 500 are to be obtained. The sample capacity is therefore also very low and it will be compared with our results.

The first point is to find the operating point generating $3 \cdot 10^5$ plates in 1000 s (t_m). With $d_p = 5 \mu\text{m}$ and $D_m = 10^{-9} \text{ m}^2/\text{s}$, this condition indicates that $H/v = 0.0033 \text{ s} = d_p^2/D_m \cdot h/v$, i.e., $h/v = 0.132$. Taking one of Kennedy and Jorgenson's columns (Fig. 3a in ref. 28), one can intersect the $h = 0.132 v$ line with the observed $h-v$ dependence. One then finds $h_{\text{oper}} \approx 1.3$, $v_{\text{oper}} = 10$ ($21\text{-}\mu\text{m}$ d_c column). In such a column, having the required kinetic performance, the volume of porous silica in one plate is

$$\pi/4 \cdot d_c^2 H \varepsilon_{\text{SiO}_2} = \pi/4 \cdot d_c^2 h d_p \varepsilon_{\text{SiO}_2} = 1.4 \cdot 10^{-15} \text{ m}^3$$

(with $d_c = 21 \mu\text{m}$, $d_p = 5 \mu\text{m}$ and $\varepsilon_{\text{SiO}_2} = 0.6$).

In the open-tubular LC column, the second entry in Table II, we have a volume of porous silica in one plate of

$$\pi/4(d_b^2 - d_c^2)H = 6.9 \cdot 10^{-16} \text{ m}^3$$

(with $H = 12.9 \mu\text{m}$, $d_b = 9.56 \mu\text{m}$ and $d_c = 4.90 \mu\text{m}$).

It follows that the mass loadability when the surface areas in both types of silica are the same differ by only a factor of two. The conclusion is that the range of application, detection and injection problems, etc., will be virtually the same for both types of chromatography. A similar conclusion was also drawn by Guiochon³⁰. However, open-tubular LC columns have much greater potential for further kinetic improvements on further miniaturization. On the other hand, it has to be admitted that Kennedy and Jorgenson²⁸ demonstrated their type of columns experimentally, while the thick-film 5- μm open tube, entry 2 in Table II, has not yet been realized.

CONCLUSIONS

Changes in N have a very strong influence on M_{pl} , whereas changes in t_m and ΔP have a strong and a weak influence, respectively, on M_{pl} . A 10-fold increase in N means a decrease of a factor of 1000 in M_{pl} .

The maximum column length for the fixed input specifications is about 5 m for all the mentioned phase systems.

The d_t/d_c ratio at maximum loadability for the liquid-liquid system is 10 times larger than for the silicone system, which can be explained by the expression $\sqrt{(D_{s1}/D_{s2})}$. The use of a phase system with a very small diffusion coefficient in the stationary phase is unfavourable with respect to mass loadability.

The plate-height equation for the liquid-liquid system at maximum M_{pl} is $h = 2/v + 0.133v$ and for the silicone system $h = 2/v + 0.115v$. This is an increase in C of 60% (the liquid-liquid system) and 50% (the silicone system) compared with C for very thin films ($h = 2/v + 0.08v$).

The monolayer system has a M_{pl} which is about $2 \cdot 10^6$ smaller than that for the liquid-liquid system.

C_m can only be influenced by the d_t/d_c ratio and N . For the liquid-liquid system C_m is about 15 times larger than for the silicone system.

The calculated M_{pl} of a 21- μm I.D. micro-packed capillary column and an open-tubular LC column (second entry in Table II) are in the same range. However, it should be pointed out that the thick-film 5- μm open-tubular LC column has not yet been realized.

SYMBOLS

D_m	diffusion coefficient in the mobile phase ($D_m = 1 \cdot 10^{-9} \text{ m}^2/\text{s}$)
D_s	diffusion coefficient in the stationary phase (liquid-liquid system, $D_s = 5 \cdot 10^{-10} \text{ m}^2/\text{s}$; silicone system, $D_s = 7 \cdot 10^{-12} \text{ m}^2/\text{s}$)
d_c	diameter of the cross-section of the mobile phase in the column (μm)
d_t	film thickness of the stationary phase (μm)
h	reduced plate height

k'	capacity factor ($k' = 3$)
L	column length (m)
M_{pl}	mass loadability in one plate, equal to the amount of stationary phase in one plate (pg)
N	number of theoretical plates
ΔP	pressure drop across the column (MPa)
v	reduced velocity
η	viscosity of the mobile phase ($\eta = 1 \cdot 10^{-3}$ Pa s)
φ	pressure resistance factor (open tube: $\varphi = 32$)
δ_f	reduced film thickness
ρ_{sf}	density of stationary phase ($\rho_{\text{sf}} = 1 \cdot 10^6$ g/m ³)
t_m	dead time of the mobile phase (s)
C_m	eluting concentration (mmol/l)
MW	molecular weight of solute (MW = 200 g/mol)
m_{30}	reduced load that corresponds to a 30% increase in peak width ($m_{30} = 2$)
$\alpha_{\text{OH(s)}}$	surface concentration of the accessible silanols (4 $\mu\text{mol/m}^2$)
$F(k')_m, F(k')_s$	functions of k'

REFERENCES

- 1 J. H. Knox and M. T. Gilbert, *J. Chromatogr.*, 186 (1979) 405.
- 2 J. H. Knox and M. Saleem, *J. Chromatogr. Sci.*, 7 (1969) 614.
- 3 J. Jorgenson and E. J. Guthrie, *J. Chromatogr.*, 255 (1983) 335.
- 4 H. P. M. van Vliet and H. Poppe, *J. Chromatogr.*, 346 (1985) 149.
- 5 L. A. Knecht, E. J. Guthrie and J. Jorgenson, *Anal. Chem.*, 56 (1984) 479.
- 6 S. Folestad, B. Josefsson and M. Larsson, *J. Chromatogr.*, 391 (1987) 347.
- 7 O. van Berkel, J. C. Kraak and H. Poppe, *Chromatographia*, 24 (1987) 739.
- 8 P. R. Dluznieski and J. W. Jorgenson, *J. High Resolut. Chromatogr. Chromatogr. Commun.*, 11 (1988) 332.
- 9 O. van Berkel-Geldof, J. C. Kraak and H. Poppe, *J. Chromatogr.*, 499 (1990) 345.
- 10 H. Poppe, J. C. Kraak, O. van Berkel-Geldof and P. P. H. Tock, in P. Sandra (Editor), *Proceedings of Ninth Congress on Capillary Chromatography, Monterey, 1988*, Hüthig, Heidelberg, p. 345.
- 11 P. P. H. Tock, G. Stegeman, R. Peerboom, H. Poppe, J. C. Kraak and K. K. Unger, *Chromatographia*, 24 (1987) 617.
- 12 P. P. H. Tock, C. Boshoven, H. Poppe, J. C. Kraak and K. K. Unger, *J. Chromatogr.*, 477 (1989) 95.
- 13 M. D. Oates and J. W. Jorgenson, *Anal. Chem.*, 61 (1989) 432.
- 14 R. T. Kennedy and J. W. Jorgenson, *Anal. Chem.*, 61 (1989) 436.
- 15 M. J. E. Golay, in H. Desty (Editor), *Gas Chromatography 1958*, Butterworths, London, 1958, pp. 36–55.
- 16 L. S. Ettre, *Chromatographia*, 17 (1983) 553.
- 17 C. A. Cramers, *J. High Resolut. Chromatogr. Chromatogr. Commun.*, 9 (1986) 676.
- 18 Th. Noy, J. Curvers and C. Cramers, *J. High Resolut. Chromatogr. Chromatogr. Commun.*, 9 (1986) 753.
- 19 R. T. Ghijsen and H. Poppe, *J. High Resolut. Chromatogr. Chromatogr. Commun.*, 11 (1988) 271.
- 20 J. C. Giddings, S. L. Seager, L. R. Stucki and G. H. Stewart, *Anal. Chem.*, 32 (1960) 867.
- 21 H. Poppe and J. C. Kraak, *J. Chromatogr.*, 255 (1983) 395.
- 22 P. J. Schoenmakers, *J. High Resolut. Chromatogr. Chromatogr. Commun.*, 11 (1988) 271.
- 23 J. E. Eble, R. L. Grob, P. E. Antle and L. R. Snyder, *J. Chromatogr.*, 384 (1987) 25.
- 24 R. T. Ghijsen, H. Poppe, J. C. Kraak and P. P. E. Duysters, *Chromatographia*, 27 (1989) 60.
- 25 T. Tsuda and M. Novotny, *Anal. Chem.*, 50 (1978) 271.
- 26 V. L. McGuffin and M. Novotny, *J. Chromatogr.*, 255 (1983) 381.
- 27 K. E. Karlsson and M. Novotny, *Anal. Chem.*, 60 (1988) 1662.
- 28 R. T. Kennedy and J. W. Jorgenson, *Anal. Chem.*, 61 (1989) 1128.
- 29 C. Borra, M. Soon and M. Novotny, *J. Chromatogr.*, 385 (1987) 75.
- 30 G. Guiochon, *Anal. Chem.*, 53 (1981) 1318.

CHROMSYMP. 1763

Selective determination of trace levels of phenol in river water using electrochemical concentration modulation correlation chromatography

M. ENGELSMA, W. Th. KOK and H. C. SMIT*

University of Amsterdam, Laboratory for Analytical Chemistry, Nieuwe Achtergracht 166, 1018 WV Amsterdam (The Netherlands)

SUMMARY

Electrochemical concentration modulation (ECM) was used as a sample introduction technique in the correlation chromatographic (CC) trace determination of phenol in water. The linearity and sensitivity of the method were tested and detection limits were calculated. The selectivity of the technique was confirmed by comparison with loop injection experiments using several detection methods. In preliminary experiments it was found that ECM–CC, in combination with fluorescence detection, is selective and sensitive enough to be used for the monitoring of the phenol concentration in river water at the draining points for drinking water production.

INTRODUCTION

Water from polluted rivers, such as the Rhine, is used to feed buffer reservoirs as a first step in the production of drinking water. As the quality of river water is not constant, continuous monitoring at the draining point is necessary to maintain an acceptable initial purity. Phenols are important pollutants of river water, being degradation products of many organic compounds, such as pesticides used in agriculture, and waste products from a variety of chemical industries¹

A large number of high-performance liquid chromatographic methods for the determination of phenols have been reported. However, most of them circumvent phenol itself and otherwise detection limits for phenol are relatively high. In general, this is caused by the inability to effect a satisfactory preconcentration of the polar phenol on apolar materials. Additionally, the fast-eluting phenol will often coelute with other polar compounds. EEC regulations² require phenol concentrations in water intended for human consumption to be less than $5.3 \cdot 10^{-9}$ mol/l. A method for phenol monitoring at the draining point in a river should therefore have a sufficiently low detection limit in addition to allowing continuous analysis. Because of the complexity of environmental water samples it should also be selective.

Nielen *et al.*³ reported a sophisticated method involving two successive preconcentration and clean-up steps on a large hydrophobic precolumn and an ion-

exchange column, after which the actual separation took place on a reversed-phase column employing fluorescence detection. The limit of detection (LOD) for phenol was $1.1 \cdot 10^{-10}$ mol/l. Although the experimental setup used was fairly complicated (two pumps, three electrically actuated valves, three precolumns, a switching unit, a programmer), it was fully automated and reasonably selective. Laeven *et al.*⁴ reported a correlation chromatographic method using fluorescence detection for the determination of phenol, achieving an LOD of $3.2 \cdot 10^{-11}$ mol/l in a 80-min experiment. The equipment was not very suitable for routine analysis, however, and the selectivity was only determined by the fluorescence detector.

Rennie and Mitchell⁵ proposed an elegant method involving dual-electrode electrochemical detection without preconcentration, with a detection limit of $3.6 \cdot 10^{-10}$ mol/l for phenol. Here the detection method provides the selectivity and the method can be automated. Borra *et al.*⁶ combined preconcentration on a graphitized carbon black cartridge column and not very selective UV detection at 280 nm, which produced an LOD for phenol of $2.7 \cdot 10^{-9}$ mol/l. Bigley and Grob¹ used a selective post-column reaction with 4-aminoantipyrine with UV detection at 509 nm and reported an LOD of $5.3 \cdot 10^{-6}$ mol/l without preconcentration. Another reaction-detection method was proposed by de Ruiter and co-workers^{7,8}, involving off-line dansylation, post-column photolysis and fluorescence detection of the reaction products, which gave a 10-fold gain in fluorescence intensity compared with phenol itself. However, the method is difficult to automate.

This paper describes a method that can be used for the continuous selective monitoring of phenol in river water. A relatively simple experimental set-up is needed and the method has sufficient sensitivity and high selectivity compared with the methods mentioned above. Further, the method can be automated without much effort.

Electrochemical concentration modulation

The principle of electrochemical concentration modulation (ECM) correlation chromatography (CC) was described previously^{9,10}. A coulometric cell is placed in front of the separation column (Fig. 1). Using computer control, an alternating potential is applied to the working electrode while the sample-eluent mixture flows through the system continuously. When the upper and the lower potential are chosen to be above and below, respectively, the half-wave potential of the compound of interest, sample introduction takes place when the electrode potential is at the lower level, whereas the compound is completely oxidized at the upper level. The resulting detector signal will be a superposition of a number of chromatograms shifted in time. As the method is basically a correlation chromatographic method¹¹, the potential is modulated according to a pseudo-random binary sequence. In that case the detector signal can be deconvoluted by cross-correlating with the modulation pattern. The resulting correlogram resembles the corresponding chromatogram but will have a better signal-to-noise ratio because of the multiplex advantage^{12,13}. The selectivity, however, is also enhanced as only compounds having half-wave potentials in the modulation region will appear in the correlogram. So far the selectivity of the method is the same as that of a dual-electrode determination. However, an additional selectivity dimension is provided by the detector. The only constraint is the detectability of the compound of interest or of an electrochemical reaction product. Amperometric and fluorescence detection were compared in this work.

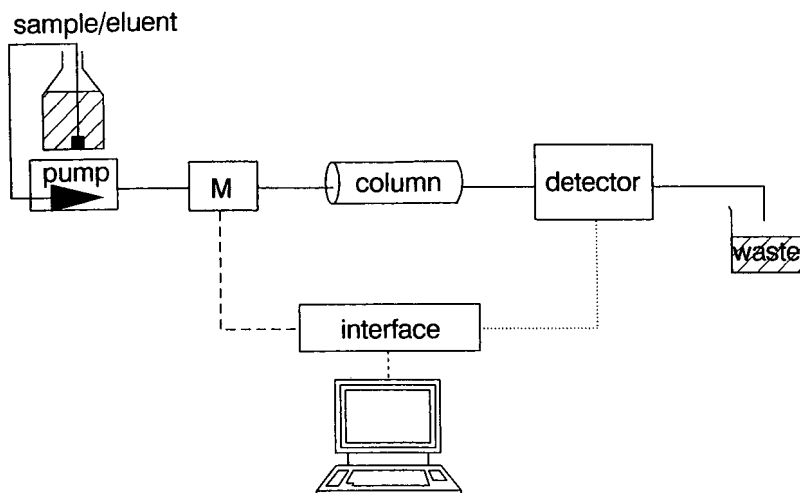


Fig. 1. Experimental set-up for ECM-CC. The eluent contains the sample. M is the modulator-potentiostat combination.

EXPERIMENTAL

Modulation CC

An ESA Model 5021 conditioning cell, capable of withstanding 80 bar back-pressure, was used as the modulator cell. A potentiostat (Princeton Applied Research, Model 174A) supplied the potential to the porous graphite working electrode. The potentiostat was externally controlled by an intelligent ADC/DAC interface (Cambridge Electronic Design, Model 1401) connected to a microcomputer (Acorn, Model BBC Master). The detector signal was sampled synchronously with the same interface. The control software was developed in our laboratory. Cross-correlations were performed off-line on a Hewlett Packard HP 9000 Model 300 computer.

Injection sequences consisting of 63 or 511 clock periods (cp) of 10 s each were used to modulate the electrode potential. The modulation interval was selected by monitoring the fluorescence intensity as a function of the modulator cell working electrode potential after 20- μ l loop injections of 10^{-6} mol/l phenol dissolved in the eluent. The fluorescence intensity decreased to half its original value when the electrode potential was 0.4 V with respect to the reference electrode of the modulator cell. A modulation interval of -0.1 to 0.9 V was used although a smaller interval was equally applicable.

Chromatography

An Applied Biosystems Model SF400 pump equipped with a liquid pulse damper delivered a constant eluent/sample flow of 0.60 ml/min. A Rheodyne injection valve with a 60- μ l loop was used for the loop injection experiments. A 0.2- μ m carbon filter (ESA) and a 0.5- μ m metal in-line filter (Upchurch Scientific) preceded the modulator cell to prevent clogging of the porous working electrode. The metal frit

was placed between the carbon filter and the cell because the carbon filter was found to release small particles of carbon in an eluent containing acetonitrile.

A 100 mm × 4.6 mm I.D. stainless-steel column was used, filled with Hypersil ODS (5 μm) particles. The plate number was *ca.* 2000.

Chemicals and solutions

Analytical-reagent grade chemicals were used unless indicated otherwise.

The eluent was acetonitrile (Rathburn, HPLC-S grade)–aqueous buffer (pH 4) (30:70, v/v). The buffer solution contained 0.05 mol/l acetic acid (Merck), adjusted to pH 4 with concentrated sodium hydroxide solution (Baker, Analyzed Reagent), and 0.05 mol/l potassium nitrate (Janssen Chimica). Acetonitrile was filtered before mixing with the buffer using a 0.5-μm PTFE membrane filter (Millipore, type FH). The buffer solution was filtered over a 0.2-μm membrane filter (Sartorius, cellulose acetate, type 11107).

Canal water, obtained from the Nieuwe Achtergracht in Amsterdam, was filtered over a 0.5-μm membrane filter (Millipore type AA), acidified with glacial acetic acid up to 0.05 mol/l and adjusted to pH 4.0 by addition of concentrated sodium hydroxide solution. Potassium nitrate was dissolved (0.05 mol/l) and the solution was filtered a second time using the 0.22-μm cellulose acetate filter. For the recovery experiment the canal water was spiked with phenol up to a concentration of $1.38 \cdot 10^{-8}$ mol/l. Stock solutions for the calibration experiments were made starting from a 10^{-3} mol/l phenol solution in acetonitrile. Subsequent diluted solutions were made using the standard eluent.

Detection

A Perking Elmer LS-4 fluorescence detector, equipped with a 3-μl flow cell, operating at an excitation wavelength of 270 nm and an emission wavelength of 299 nm with 10-nm slits, was used. Optimum excitation and emission wavelengths were obtained by measuring the excitation and emission spectra of a 10^{-6} mol/l phenol solution in the eluent.

Electrochemical detection was performed using a cell (Bioanalytical Systems) equipped with a glassy carbon working electrode and an Ag/AgCl reference electrode. The detection potential of 1.1 V was applied by a potentiostat (Bioanalytical Systems, Model LC-4). The optimum detection potential was obtained by measurement of a hydrodynamic voltammogram. The electrochemical detector was equilibrated overnight at the detection potential, allowing for the background current to settle. The UV detector (Waters Assoc., Model 441) used during the loop injection experiments was operated at 254 nm.

RESULTS AND DISCUSSION

Time constant and ghost peak

In a previous paper it was reported that the use of a chemical concentration modulator in CC can result in the appearance of ghost peaks in the correlogram¹⁰. Theoretically, ghost peaks are caused by reproducible injection errors resulting in erroneous injection patterns decomposable into shifted and/or inverted versions of the ideal injection pattern¹⁴. Physico-chemically the origin lies in the symbiotic action

of the time constant of the modulator and the position and size of the modulation interval relative to the response of a particular compound as a function of the modulation force.

In ECM-CC, the RC circuit constructed by the double-layer capacitance at the surface of the working electrode and the residual resistance between the working electrode and the reference electrode are responsible for the time constant of the modulator cell. The relative position of the half-wave potential of the analyte in the potential interval used is the other part of the potential ghost peak generator.

This problem can be solved in a number of ways¹⁵. In this work we used a fast modulator cell and favourable eluent conditions such as a low viscosity (acetonitrile as modifier), a substantial salt concentration (0.1 mol/l) and a background electrolyte consisting of ions with a high mobility (potassium nitrate).

In the ESA Model 5021 conditioning cell, counter and reference electrodes are placed on both sides of the porous graphite electrode, which results not only in a more homogeneous working electrode potential but also in a smaller residual resistance. This should lead to an appreciable decrease in the time constant of the cell relative to the ESA Model 5020 guard cell used in the previous investigation, where the counter and reference electrodes are positioned on the upstream side of the working electrode.

In our previous work, the best fit to the decay rate of the current response after the application of a potential step was accomplished using the sum of two exponentials as a fit function. Although the physical meaning of the two associated time constants is not clear, their values can be used as a measure of the speed of the modulator cell.

The time constants for both cells were determined using the same experimental conditions. We found for the conditioning cell values of 0.11 and 0.98 s and for the guard cell 0.16 and 3.9 s. The weight factors of the corresponding exponentials were almost the same for both cells. The lowest time constants are probably limited to some extent by the electronic circuits used in collecting the data. It is clear that the conditioning cell is considerably faster. Fig. 2 shows the charging currents for both cells as a function of time after the potential step. In the correlogram only a tiny, so-called λ_3 ghost peak could be detected at a "retention time" of 170 s when a 63-unit injection sequence was used. This type of ghost peak disappears after subtraction of a correlogram originating from the inverted (high-level potential becomes low-level potential and *vice versa*) modulation pattern. This is shown in Fig. 3. Fine tuning of the modulation interval would also result in the disappearance of this ghost peak¹⁰. The standard modulation pattern results in a negative phenol peak because a high electrode potential corresponds to a negative injection.

Sensitivity

Calibration graphs were recorded for loop injection and ECM-CC experiments using both electrochemical and fluorescence detection. The standard deviation of the baseline noise in the resulting chromatograms and correlograms was used as a measure of the uncertainty in the determinations. The calibration graphs are shown in Fig. 4. The dashed lines represent three times the standard deviation (3σ) of the baseline noise. The crossings of the dashed and solid lines are a measure of the detection limit according to the 3σ criterion.

All points on the calibration graph for the ECM-CC experiment with electro-

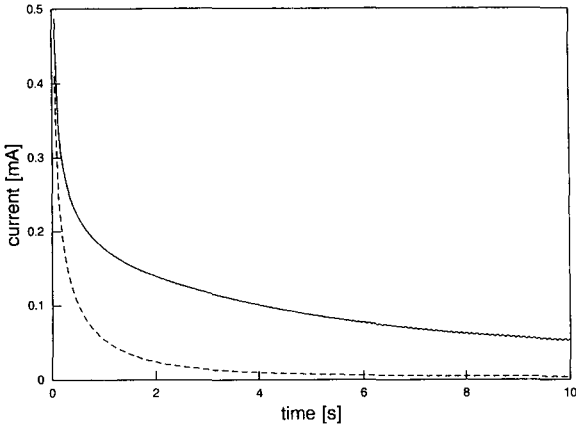


Fig. 2. Decay curves of the charging current after the application of a -0.2 to 0.8 V potential step to the Model 5020 guard cell (solid line) and the Model 5021 conditioning cell (dashed line). Experimental conditions as described.

chemical detection in Fig. 4c result from a 63 cp injection sequence. Each injection period lasts 10 s. The result for the standard solution containing the highest phenol concentration ($8.48 \cdot 10^{-6}$ mol/l) is not plotted on the calibration graph because during the measurement the surface of the glassy carbon working electrode became

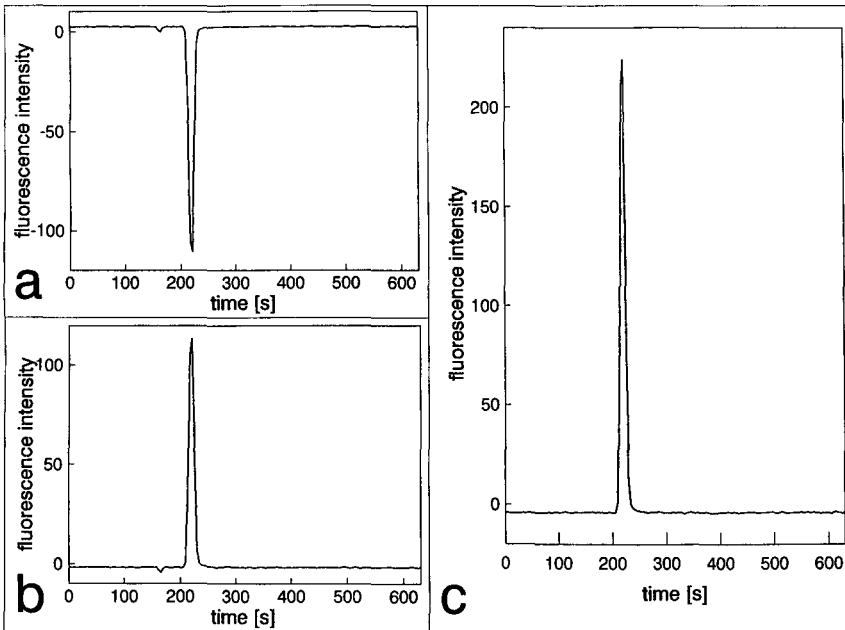


Fig. 3. Correlograms for a $4.2 \cdot 10^{-6}$ mol/l phenol solution in the eluent. The small peak at 170 s in the λ_3 ghost peak. Correlograms were obtained using (a) the standard modulation pattern and (b) the inverted modulation pattern. (c) Subtraction of (a) from (b); the ghost peak disappeared.

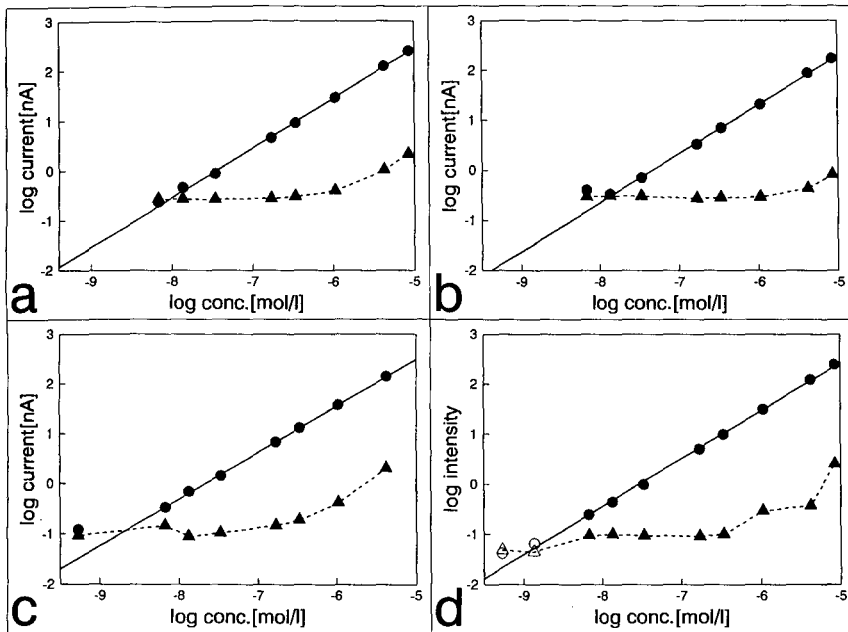


Fig. 4. Log-log calibration graphs using (a) loop injection and electrochemical detection; (b) loop injection and fluorescence detection; (c) ECM-CC and electrochemical detection; (d) ECM-CC and fluorescence detection. Solid lines are the calibration graphs. Dashed lines are $3\sigma_{\text{baseline noise}}$ curves. Solid symbols in the ECM-CC experiments were from 63 cp injection sequences (11 min); open symbols from 511 cp sequences (80 min). Statistical data are given in Table I.

covered with a polymeric phenol film, causing a rapid decrease in sensitivity. The polymeric film had to be removed by polishing the surface with a diamond powder slurry.

The points denoted by the open circles on the calibration graph for the ECM-CC experiments with fluorescence detection were measured using a 511 cp injection sequence to lower the detection limits. For higher concentrations it is not necessary to use long injection sequences and for the highest concentrations loop injections will do as well in terms of signal-to-noise ratio. The points with the solid symbols were recorded using a 63 cp injection sequence.

ECM-CC results were normalized to give peak heights comparable to those in loop injection experiments; only the noise is significantly reduced, as can be seen from the figures.

Table I lists the statistical data for the calibration graphs shown. The calibration graph obtained for the ECM-CC experiment using electrochemical detection is reasonably straight over three orders of magnitude. With fluorescence detection the linear range spans four orders of magnitude. Table II lists the detection limits for ECM-CC and loop injection experiments. Also, a factor describing the measured and theoretical values for the gain in signal-to-noise ratio at phenol concentrations near the detection limit is given for the correlation experiments with respect to the corresponding loop injection experiment.

TABLE I
STATISTICAL DATA ON LOG-LOG CALIBRATION GRAPHS

Regression analysis	Experiment ^a			
	L/EC	L/FI	CC/EC	CC/FI
Lowest concentration (mol/l)	$1.4 \cdot 10^{-8}$	$1.4 \cdot 10^{-8}$	$6.8 \cdot 10^{-9}$	$1.4 \cdot 10^{-9}$
Highest concentration (mol/l)	$8.5 \cdot 10^{-6}$	$8.5 \cdot 10^{-6}$	$4.2 \cdot 10^{-6}$	$8.5 \cdot 10^{-6}$
Number of points	7	7	7	9
Intercept	7.41	7.18	7.14	7.20
Slope	0.99	0.98	0.93	0.96
Coefficient of determination	0.999	0.999	0.999	0.998
Standard error of <i>y</i> estimate	0.04	0.03	0.02	0.05
Standard error of slope	0.02	0.01	0.01	0.01

^a L = loop injection; CC = correlation chromatography; EC = electrochemical detection; FI = fluorescence detection.

As the long-term baseline stability of the fluorescence detector was much better than that for the electrochemical detector, the former was chosen for the 511 cp ECM-CC experiment. As can be seen in Table II, an 80-min ECM-CC experiment with fluorescence detection results in a lowering of the detection limit by a factor 11, which is in agreement with the theoretical value.

The detection limit achieved is sufficient for the desired determination of phenol in river water. It is striking that the noise in both the loop injections experiments and the ECM-CC experiments increases when higher concentrations of phenol are used. This means that the signal-to-noise ratio becomes constant at higher phenol concentrations.

TABLE II
ESTIMATED DETECTION LIMITS^a AND SIGNAL-TO-NOISE GAIN FACTORS^b

Experiment ^c	Sequence length (cp)	No. of injections	LOD ^d (mol/l)	Gain factor	
				Experimental	Theoretical
L/EC	—	1	$1.0 \cdot 10^{-8}$	—	—
L/FI	—	1	$1.4 \cdot 10^{-8}$	—	—
CC/EC	63	32	$2.3 \cdot 10^{-8}$	4	4
CC/FI	63	32	$3.2 \cdot 10^{-9}$	4	4
CC/FI	511	256	$1.2 \cdot 10^{-9}$	11	11

^a Three times the standard deviation of the baseline noise, calculated over 300 points.

^b Ratio of estimated detection limits of loop injection experiments and corresponding CC experimental values. Theoretical values are calculated using signal-to-noise gain = $\frac{1}{2}\sqrt{n}$, where *n* = sequence length¹⁶.

^c See Table I.

^d Concentrations in the eluent.

Selectivity

The selectivity enhancement achieved when using ECM for sample introduction was tested using ECM-CC with fluorescence detection and comparing the results obtained for canal water with those obtained by loop injection using various detectors. As the canal water contained a trace of phenol there was no need to spike the sample solution at this point. Fig. 5a-c show the chromatograms after injection of 60 μ l of filtered canal water prepared as described under Experimental, using (a) UV detection (b), electrochemical detection and (c) fluorescence detection. The last method is obviously the most selective but not the most sensitive. Fig. 5d shows a correlogram of the same sample-eluent solution, obtained using ECM-CC with fluorescence detection. Clearly the phenol peak at 225 s is enhanced with respect to the signal at 70 s when the intensities are compared with the chromatogram in Fig. 5c. Further, the decrease in baseline noise is clear.

Phenol in canal water

As was observed previously, the canal water contained a trace amount of phenol. To check for the losses during the filtration steps, the canal water was spiked with phenol such that the additional concentration became $1.38 \cdot 10^{-8}$ mol/l. After the correlation experiments the difference between the peak heights of the unspiked and the spiked correlograms was used to calculate the phenol recovered. The recovery was 78% (single experiment). The phenol concentration in the sample-eluent when corrected for the recovery was $2.1 \cdot 10^{-8}$ mol/l. As only 70% of the eluent consisted of

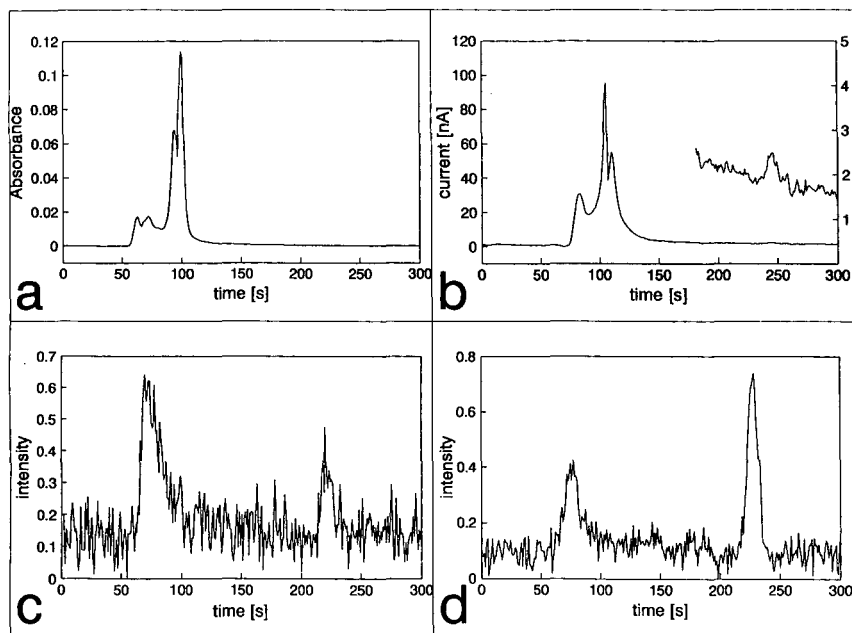


Fig. 5. (a-c) Chromatograms and (d) a correlogram for a canal water sample. Phenol elutes at 230-240 s. The selectivity increases in the order (a) UV detection, (b) electrochemical detection, (c) fluorescence detection and (d) ECM-CC with fluorescence detection.

canal water, the phenol concentration in the pure canal water sample was calculated to be $3.0 \cdot 10^{-8}$ mol/l.

CONCLUSION

The selectivity of the method compares well with those of the methods mentioned in the Introduction. The sensitivity is sufficient but certainly not the best. The reason for this is partly that almost no optimization was attempted. The column used was not very efficient (2000 plates), the excitation source of the fluorescence detector was old and noisy and the electrochemical detector used was not very sophisticated. A coulometric detector would be preferable in phenol determinations because of the formation of a polymeric layer on the electrode surface. However, in comparison with the loop injection experiments the gain in signal-to-noise ratio is according to the theory in most instances, so the use of more sensitive detectors may lower the detection limits even more. Although the ECM-CC technique was used here to determine only phenol, it can also be used for substituted phenols provided that their half-wave potentials are compatible with the modulation interval used.

REFERENCES

- 1 F. P. Bigley and R. L. Grob, *J. Chromatogr.*, 350 (1985) 407.
- 2 Council Directive on the Quality of Water Intended for Human Consumption, *Off. J. Eur. Commun.*, August 1980, No. L229/11(80/778/EEC).
- 3 M. W. F. Nielen, J. de Jong, R. W. Frei and U. A. Th. Brinkman, *Int. J. Environ. Anal. Chem.*, 25 (1986) 37.
- 4 J. M. Laeven, H. C. Smit and J. C. Kraak, *Anal. Chim. Acta*, 150 (1983) 253.
- 5 P. J. Rennie and S. F. Mitchell, *Chromatographia*, 24 (1987) 319.
- 6 C. Borra, A. Di Corcia, M. Marchetti and R. Samperi, *Anal. Chem.*, 58 (1986) 2048.
- 7 C. de Ruiter, J. F. Bohle, G. J. de Jong, U. A. Th. Brinkman and R. W. Frei, *Anal. Chem.*, 60 (1988) 666.
- 8 C. de Ruiter, R. R. Otten, U. A. Th. Brinkman and R. W. Frei, *J. Chromatogr.*, 436 (1988) 429.
- 9 D. P. Carney and J. B. Phillips, *Anal. Chem.*, 58 (1986) 1251.
- 10 M. Engelsma, D. J. Louwerse, H. F. M. Boelens, W. Th. Kok and H. C. Smit, *Anal. Chim. Acta*, submitted for publication.
- 11 H. C. Smit, *Trends Anal. Chem.*, 2 (1983) 1.
- 12 H. C. Smit, *Chromatographia*, 3 (1970) 515.
- 13 M. Kaljurand and E. Küllik, *Computerized Multiple Input Chromatography*, Wiley, New York, 1989.
- 14 R. Mulder, P. J. Hoogerbrugge, H. C. Smit, *Chemomet. Intell. Lab. Syst.*, 1 (1987) 243.
- 15 M. Engelsma, D. J. Louwerse, W. Th. Kok and H. C. Smit, in preparation.
- 16 M. Kaljurand and E. Küllik, *J. Chromatogr.*, 186 (1979) 145.

CHROMSYM. 1772

Validation of an expert system for the selection of initial high-performance liquid chromatographic conditions for the analysis of basic drugs

FRANS MARIS*, RIK HINDRIKS and JAN VINK

Akzo Pharma Division, Organon International BV, Analytical R&D Laboratories, P.O. Box 20, 5340 BH Oss (The Netherlands)

and

ANNE PEETERS, NADINE VANDEN DRIESSCHE and LUC MASSART

Farmaceutisch Instituut VUB, Laarbeeklaan 103, B-1090 Brussels (Belgium)

SUMMARY

A prototype expert system was built which gives advice on the liquid chromatographic conditions for the analysis of basic compounds. In the validation process, the correct implementation of the knowledge and the advice of the expert system on real samples has been checked. For more than 50 compounds, the consultation of the expert system resulted in 75% correct proposals. Rules have been implemented to guide the operator in case the first proposal results in retention times that are not in the desired range.

INTRODUCTION

Several groups are working on the applicability of expert systems in (liquid) chromatography^{1–7}, which indicates a broad interest both from industry and universities in these types of computer systems. Within ESPRIT (European Strategic Programme for Research and Development in Information Technology), a programme supported by the EEC, a group of scientists is working on a joint project, “Application of Expert Systems in Chemical Analysis” (ESCA)⁸. The aim of this project is to demonstrate the applicability of expert systems in high-performance liquid chromatography (HPLC), particularly applied to pharmaceutical analysis. This project covers the whole field of method development. The scheme shown in Fig. 1 became the basis of our work within ESCA. Based on this scheme, four different stand-alone expert systems were developed^{9–12}.

The selection of the initial HPLC conditions, which is the first step in method development (Fig. 1), requires specific knowledge and expertise. For example, several studies¹³ are directed at finding the relationship between chemical structure and chromatographic retention. Further, the chromatographic behaviour of basic pharmaceutical substances in HPLC is strongly influenced by the type of column packing, the

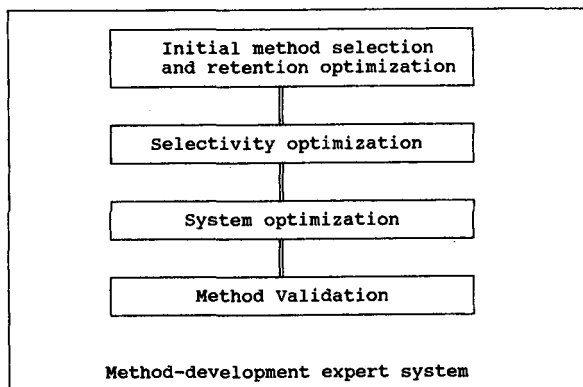


Fig. 1. Outline of an integral expert system for method development in HPLC. This paper concerns the initial method selection and retention optimization.

pH of the mobile phase and the concentration and type of buffer ions. This results in many choices to be made by the chromatographer.

In order to assist the chromatographer, an expert system has been developed for the selection of initial HPLC conditions¹¹. On the basis of HPLC data for about 600 different Organon compounds and literature data, rules were defined and a knowledge base was built. The knowledge was implemented in KES (Knowledge Engineering System; Software A&E Architecture), a mid-sized expert system shell which runs on an IBM-PC.

In this paper we present details on the implementation of chemical knowledge and the validation of the expert system. Attention is also focused on the necessity to expand the chemical knowledge. This will be required when this expert system has to be combined with the expert systems on selectivity and system optimization to form a single, integrated expert system for method selection.

DESCRIPTION OF THE EXPERT SYSTEM

The present expert system, also called DASH (Drug Analysis System in HPLC) was originally developed as a first-guess system for method selection and retention optimization of basic drugs. The system is used in the purity control of drugs, synthesized within Organon, and predicts conditions for isocratic elution only.

In the first step of drug development, a large number of compounds are synthesized. Before these compounds are screened in pharmacological tests, they are subjected to HPLC analysis to check their purity. As most of these compounds are submitted for analysis only once, optimization of either the selectivity or the analysis time is not required. However, the "first-guess" HPLC conditions should preferably result in capacity factors (k') between 3 and 10 in order to obtain optimum resolution in an acceptable time.

In a previous paper¹¹, data-flow diagrams are shown outlining the reasoning process of this expert system. In the expert system rules are implemented on the selection of the column dimensions, flow-rate, pH and detection wavelengths. Another important part of the chemical knowledge is the calculation of the percentage of

methanol in the mobile phase in order to obtain a k' of about 5. To do so, the chemical structure of a compound has to be broken down into structural elements. Each element is linked to a percentage of methanol which can be positive or negative and which can be pH dependent. The proposed mobile phase composition is based on the calculation of the polarity of structural fragments that are not affected by the pH and of fragments for which the polarity depends strongly on pH, *viz.*, N-containing groups. The final percentage of methanol is calculated by summing all contributions which correspond with the structural elements. In order to prevent the expert system from suggesting unrealistic percentages of methanol, constraining rules are also implemented.

IMPLEMENTATION, PROBLEMS AND SOLUTIONS

DASH is implemented in the expert system shell KES (Knowledge Engineering System, Software A&E Architecture, release 2.4). The knowledge base operates on an IBM PS/2 computer. No major difficulties were met in the implementation of the knowledge of DASH.

However, some problems were observed in the use of the tool KES. Most of the attention was focused on building classes, each with the appropriate variables, resulting in a clear, frame-like structure. KES does not really allow splitting up the rule base into different parts. By using clearly arranged classes and by defining the class to which each rule applies, a splitting up of the rules has been achieved to a certain extent.

The major difficulty is to provide a good user interface. Some questions, automatically introduced by KES, may result in some confusion for the user. It is not possible to avoid this and the only way to make the output as clear as possible is to choose understandable variable names.

Another disadvantage is that an answer given by the user cannot easily be changed afterwards. When mistakes have been entered, the user has to stop the consultation and to start it all over again. He can only change/correct previous answers when he knows the attribute names of the variables. In situations in which this is really necessary, some actions can be defined so that control of the answers is performed and questions can be reanswered. It is not a feature provided by KES, but it must be built-in by the knowledge engineer.

TEST PROCEDURE

The advice of the expert system concerns the following items: column type, column size (conventional or microbore), mobile phase (type and composition), flow-rate and detector. Ideally, the system should respond in such a way that a capacity factor in the range 3–10 is obtained for the compound.

In order to consult the expert system, the following input is required: (i) character of the main component (*e.g.*, quaternary N compound, salt), UV activity of the counter ion; (ii) polarity of the (main) component; this information is obtained by the expert system through a list of structural elements, which together comprise the molecule; (iii) impurities present (if applicable); this information can be obtained either from the chemist or from an analysis with other techniques, *e.g.*, NMR; (iv) availability of detector types.

The following features are tested: (i) completeness, applicability and robustness of the system (capability of handling incomplete or poor-quality data); (ii) quality and consistency of the expert system advice; (iii) accuracy of the chemical knowledge for the analysis of specific basic compounds in the estimation of the percentage of methanol.

VALIDATION PROCESS

Approach

The validation procedure consisted of two processes: (i) validating the software, *i.e.*, the completeness and the robustness of the system, and (ii) validation of the chemical knowledge by following the advice of the expert system for a large number of CNS-active drugs. An expert system which is only suitable for specific Organon compounds is limited. Therefore, in a later stage, during the evaluation process, the suitability of the expert system for a broader range of compounds, *viz.*, compounds with pK_a values between 3 and 10 (measured for the protonated compound), will be tested.

The expert system was initially tested by the consultation of the system with twenty reference compounds. It was verified whether the system gave the same advice as the expert intended it to. In other words, the correct implementation of all the rules and the correct functioning of the inference engine is controlled. The expert system has been validated further by the analysis of more than 50 basic compounds. These compounds are mainly CNS-active drugs and varied in pK_a value from 5 to 9. Also, some compounds were tested for which the chemical knowledge in DASH was expected to be inadequate to give a correct first guess. The compounds were analysed on a Nova-Pak C_{18} or a μ Bondapak C_{18} column at both pH 7.4 and 4.0. The buffer consisted of a 0.05 M tetramethylammonium hydroxide buffer solution acidified with concentrated phosphoric acid to pH 7.4 or 4.0. In order to obtain more analytical information, the compounds were analysed preferably at three methanol percentages. In this way, plots of $\log k'$ versus percentage of methanol could be drawn for all compounds.

Pass/fail criteria

The system is considered to fail if: (1) no answer is obtained (software/hardware failure); (2) a clearly incorrect answer is obtained, *e.g.*, percentage of methanol out of range; (3) the experimentally obtained capacity factor is outside the range $3 \leq k' \leq 10$.

In the first instance, the reason for the failure should be identified. If it is the software, it should be identified whether it is due to a bug or to incorrect or missing knowledge. In the second and third instances incorrect and/or missing knowledge should also be identified. If possible, the system should be modified and, eventually, rules should be altered and/or added.

RESULTS AND DISCUSSION

Validation of the implementation.

The correct implementation of all the rules was tested in DASH (version 1.1) by

checking all the possibilities suggested by the expert system and by entering wrong and/or incomplete data. A few reasoning mistakes were found and, therefore, some rules were changed. A general problem remains that when a wrong answer is entered, the complete consultation has to be carried out again.

The consistency of the advice of the expert system was found to be good. In order to improve the clarity of the advice, extra text was added in two parts of the output. For example, when the user has only a refractive index detector available, a suggestion is added on the necessary sample concentration.

Calculation of the percentage of modifier

The rules for calculating the percentage of methanol were implemented correctly. This was checked by consulting the expert system for twenty nitrogen-containing compounds, the structures of which varied considerably. We found that when an LC expert, who is not familiar with organic chemical structures, consulted the system, more than 50% of the structures were incorrectly translated into the structural elements. Three suggestions were made which have already been implemented: (1) after entering the structural elements, the total number of N, C, O, S and Cl atoms is shown on the screen; the number of H atoms will not be shown, because this cannot be calculated; (2) if the user notices that a mistake has been made, *e.g.*, when the chemical formula is not correct (see 1), then it must be possible to reintroduce the structural elements; (3) a concise user manual is necessary, in which it is explained how a structure can be translated into the structural elements.

The number of structural elements is still the subject of discussion. On the one hand, it was found that some structural elements or groups were missing, *e.g.*, F, Br and C=S. Moreover, there is also the need for more structural elements to express differences in types of nitrogen-containing moieties (see below). On the other hand, the system should remain practical. This means that all structural elements must preferably be shown on one screen and the user should not become confused by too many choices. In conclusion, the number of structural elements must be restricted to (i) the possible atoms, (ii) regularly appearing small groups and (iii) small groups which strongly influence the polarity of a compound.

The best alternative would be to use a system by which the complete chemical structure can be entered. We are now studying the use of DARC, a computer program for the storage and retrieval of chemical structures developed by Télésystème (Paris, France). A small additional program was written for DARC, in which the available structural elements are defined. The link between DARC and DASH is now off-line, *i.e.*, the DARC system only generates a list of structural elements, and not yet on-line. Using a DARC-DASH coupling there is no obvious limitation to the available number of structural elements while the user-friendliness is clearly improved.

Accuracy of the chemical knowledge

The accuracy of the chemical knowledge for calculating the percentage of methanol was investigated by analysing more than 50 compounds synthesized at Organon (most of them both at pH 7.4 and 4.0). The compounds were all analysed at least at two different percentages of methanol, so that two or more data points were obtained with k' values larger than 3. The percentage of correct answers, the average difference in the percentage of methanol found experimentally for $k'=5$ and the percentage

suggested by the expert system, and the slope of $\log k'$ versus percentage of methanol are shown in Table I.

Most of the compounds studied were analogues of the compounds shown in Fig. 2A. For these types of compounds a good score of more than 75% was obtained in all instances. Generally, the results were slightly better at pH 7.4 than at pH 4.0. Also, compounds were analysed with structural moieties such as those shown in Fig. 2B. For these types of compounds additional nitrogen-containing structural elements have to be defined in order to improve the accuracy of the expert system advice, especially at pH 4.0.

More meaningful are the data on the differences between the experimental percentages of methanol and the results of DASH. The average difference can, if necessary, be reduced by changing the starting level ("zero level") of the methanol percentage. The standard deviation on the average difference illustrates the accuracy of the expert system. These data can also be translated into selectivity (α) values. Using the average slope of the $\log k'$ versus methanol percentage curve for a Nova-Pak C₁₈ column at pH 7.4, an average k' of 5.2 is calculated. Further, it can be calculated that the criterion $3 \leq k' \leq 10$ corresponds to an allowable variation in the percentage of methanol of +5 and -7%.

Limitations to the accuracy of retention optimization

Although this is not really part of the validation process, it is important to describe the expected accuracy of the system. There are some factors which cause small changes in retention behaviour, such as (i) column-to-column reproducibility, (ii) changes in the pH of a solution when methanol is added and (iii) shifts in pK_a values of compounds with variation in the percentage of methanol. However, these factors can usually be kept under control in practice.

More serious problems are encountered with isomers, *e.g.*, *cis-trans* isomers.

TABLE I

VALIDATION OF THE CHEMICAL KNOWLEDGE FOR THE CALCULATION OF THE PERCENTAGE OF METHANOL (%M) IN THE MOBILE PHASE

Column	No. of compounds	% good score ($3 \leq k' \leq 10$)	% M exp. - DASH \pm S.D. ^c	Slope of $\log k'$ vs. %M \pm R.S.D. ^c
Nova-Pak C ₁₈				
pH 7.4	24	87	0.5 \pm 4.3	-0.044 \pm 12%
pH 4.0	23	78	1.6 \pm 4.8	-0.041 \pm 18%
μ Bondapak C ₁₈				
pH 7.4	17	88	0.3 \pm 4.7	-0.036 \pm 10%
pH 4.0	17	76	0.3 \pm 8.6	-0.030 \pm 11%
pH 4.0	15 ^a	87	-2.1 \pm 4.8	
Nova-Pak C ₁₈				
pH 7.4	12 ^b	75	-0.5 \pm 5.1	-0.044 \pm 16%
pH 4.0	5 ^b	40	9.2 \pm 8.5	

^a Deleting two outliers from the previous result.

^b Miscellaneous drugs with N-containing moieties as shown in Fig. 2B.

^c S.D. = Standard deviation; R.S.D. = relative standard deviation; %M exp. - DASH = difference in %M found experimentally for $k' = 5$ and suggested by the expert system.

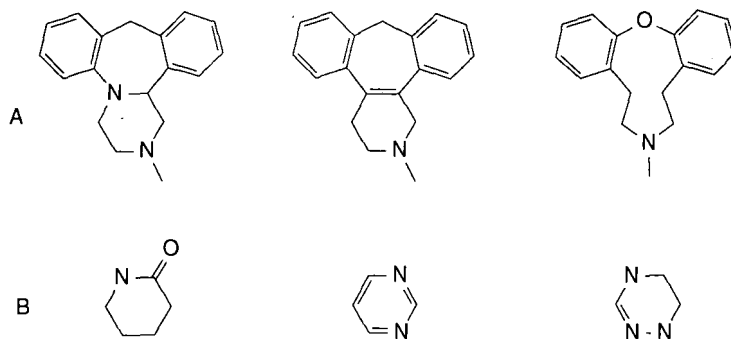


Fig. 2. Chemical structures of (A) three Organon compounds and (B) three structural elements.

The expert system does not take stereochemical effects into account, although differences in the required methanol percentages can easily amount to 5% for *cis-trans* isomers.

A second limitation is inherent in the method chosen for calculating the percentage of methanol. When, for example, a chlorine atom is added to an aromatic ring of a molecule, the influence of the chlorine on the overall polarity will depend on the polarity of that molecule. This effect is not considered by the expert system. For both polar and non-polar compounds, the advice is obtained to increase the percentage of methanol by 7%.

During the development of the expert system, several compounds which differed only in one atom were analysed. These "pairs" of compounds were analysed at pH 7.4, 6.0 and 4.0. The variation in pH results in a variation of the polarity and, therefore, of the retention behaviour. To compensate for this the percentage of methanol has to be changed. The results are given in Table II. It can be seen that the largest contribution of an atom that reduces the polarity, such as chlorine, is at a low pH. For an atom that increases the polarity, such as oxygen, the effect is largest at a high pH.

For calculating the percentages of methanol, DASH uses the average contributions listed in Table II. However, this will generally result in a predicted percentage of methanol that is too high for very non-polar compounds and too low for very polar compounds. If necessary, a rule can be formulated to correct for this effect.

TABLE II

CONTRIBUTION OF SOME STRUCTURAL ELEMENTS AT DIFFERENT pH VALUES EXPRESSED AS A PERCENTAGE OF METHANOL AT $k' = 5$

Moiety	No. of "pairs"	pH 7.4	pH 6.0	pH 4.0
Cl on aromatic group	7	5	5	9
O in ether; positioned between two aromatic groups	3	-8	-8	-3
S atom; positioned between two aromatic groups	2	1	1	4
CH ₃	3	5	5	7

The third, and most important, limitation is the exact pK_a value of a compound. The pK_a value determines the degree of protonation at a certain pH. In turn, the degree of protonation strongly influences the polarity of a compound. A separate expert system would be necessary to calculate or estimate the pK_a value. Even when this would be possible, it remains questionable whether it is possible to translate the pK_a value into the percentage of methanol needed in the mobile phase. Therefore, in our opinion, it is more straightforward to define additional types of nitrogen-containing moieties in order to enhance the applicability of the expert system to other classes of drugs.

Generally, it can be concluded that most of the emphasis must be directed at avoiding serious mistakes in the calculation of the percentage of methanol and not at improving the accuracy further within the range of $3 \leq k' \leq 10$. For instance, great improvements can be obtained for the two outliers in Table I, for which the "error" of DASH in calculating the percentages of methanol was 11 and 22%.

Limitation of stationary phases

In most instances, the expert system suggests the use of either a Nova-Pak or a μ Bondapak C_{18} column. However, several other C_{18} phases are also available for the analysis of basic substances. From the literature¹⁴ rules can be derived, *e.g.*, using data on the loading of C_{18} phases and the silanol activity of the stationary phases, by which the percentages of methanol can be roughly translated from one column to another.

Expected impurities

When impurities are expected, there is one variable available in DASH to influence the separation, *viz.*, the pH of the mobile phase. When the user has to separate *cis-trans* isomers, the expert system recommends the use of a pH of 7.4. When other impurities are expected, the reasoning is that when the impurity is slightly more polar the best separation can be obtained at a pH where the major compound is not protonated and, therefore, relatively non-polar. For basic compounds this can be achieved at a high pH. When the impurity is much more polar than the major compound, the resolution should not become too large and, therefore, a low pH is recommended. The opposite reasoning process is followed when the impurity is slightly or much less polar than the compound of interest.

A limiting factor is that the user has to decide on the differences in polarity. As an alternative, the expert system can calculate the differences in polarity. The expert system must then be able to judge, based on additional rules, which pH should be preferred. Especially for structurally related compounds, this option can be very powerful. When at both pH values the differences in polarity (methanol percentage) are too large, gradient elution can be suggested.

Retention optimization: DASH'

During the validation of DASH, it was found that in more than 75% of the consultations a correct advice was given by the expert system. However, we expect that the results will be less satisfactory when the range of compounds is enlarged during the evaluation. Therefore, an extension of the expert system is desirable, so that a bad first guess can easily be transformed into a good second guess. This exten-

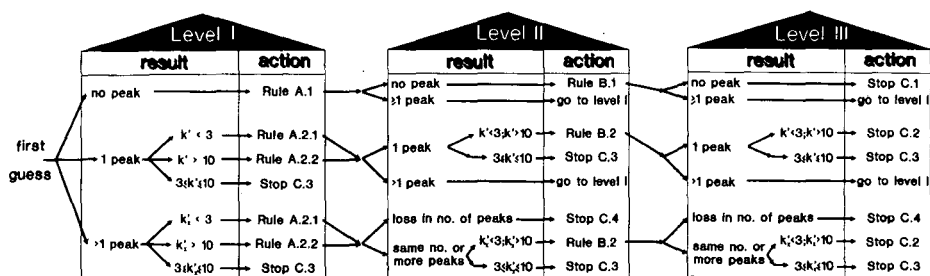


Fig. 3. The decision process in DASH' for a next guess. The rules for a next experiment (A and B) and to stop (C) are given in Table III. For further information, see text.

sion of DASH, specifically meant for retention optimization, is called DASH'.

A flow diagram of DASH' and the rules implemented in DASH' are shown in Fig. 3 and Table III, respectively. A consultation of DASH can yield up to a maximum of six guesses. This does not seem to be very effective, but the maximum number will only be reached in exceptional cases. In principle DASH' can also be consulted when a reversed-phase LC first-guess method taken from the literature failed.

TABLE III
RULES FOR THE CALCULATION OF A NEXT GUESS

A. After first guess:

1. No peak is recorded; increase % methanol by an absolute amount of 20%.
2. The compound of interest has:
 - 2.1. $k' < 3$; decrease % methanol with an absolute amount of $10 \times (5 - k')$ %
 - 2.2. $k' > 10$;

Nova-Pak C_{18} ; pH 7.4 and pH 4.0: calculate % methanol for $k' = 5$ from the curve obtained by the first-guess data point (% methanol, k') and the fact that the slope of the % methanol-log k' curve is expected to be -0.044 (pH 7.4) and -0.041 (pH 4.0).

μ Bondapak C_{18} ; pH 7.4 and pH 4.0: calculate % methanol for $k' = 5$ from the curve obtained by the first-guess data point (% methanol, k') and the fact that the slope of the % methanol-log k' curve is expected to be -0.036 (pH 7.4) and -0.030 (pH 4.0).

- 2.3. $3 \leq k' \leq 10$; retention optimization is finished.

B. After second, third, etc., guess:

1. Still no peak is recorded; increase sample amount by a factor of 10.
2. The compound of interest had $k' < 3$ or > 10 :
 - 2.1. If during first guess no peak was recorded, then go to A.2.
 - 2.2. Use both data points and fit a linear curve through the % methanol-log k' points; calculate % methanol for $k' = 5$.

C. Rules to stop:

1. If after third guess still no peak is recorded, then the method is not suitable for this compound. When only a UV detector was used, the expert system will suggest the use of a refractive index detector, a sample concentration of > 5 mg/ml and the first-guess conditions.
2. If three successive guesses result in $k' < 3$ or > 10 , then the method is not suitable for this compound. An alternative method can be suggested, e.g., when $k' < 3$, use a PIC reagent.
3. When $3 \leq k' \leq 10$, the retention optimization is finished. If two or more peaks are observed, then calculate the resolution.

Knowledge on the average slope of the log k' versus percentage of methanol lines is important for obtaining an accurate second guess. The slopes listed in Table I are used in DASH' (rules A.2.2 in Table III). Another option is that the user can ask for a certain k' , and DASH' will calculate the percentage of methanol. Because generally log k' versus percentage of methanol curves are only linear for k' values higher than 2 or 3, the calculation can only be expected to be accurate for k' values of 2 and higher.

CONCLUSIONS

From this validation, it can be concluded that the knowledge base is correctly implemented in the expert system. Improvements made in DASH, partly as a result of the validation, are (i) the presentation of a formula for the chemical composition combined with a possibility of correcting the answers and (ii) a system for further retention optimization when the first guess is not successful. This second extension called DASH, will also give the user the possibility to obtain capacity factors other than 5.

A problem was observed with the currently available structural elements. In order to keep the expert system practical, the number of structural elements is limited in the present set-up of the consultation. Investigations are in progress to combine DASH with a system in which the total chemical structure can be entered.

The accuracy of the advice based on the chemical knowledge for the method selection of the tested compounds is acceptable. Improvements can be obtained for compounds with other types of nitrogen-containing groups, the retention of which cannot be predicted accurately by the present system.

One of the problems with DASH, when it is to be combined with the expert systems for system optimization and selectivity optimization, is that DASH in principle only calculates the best LC conditions for one compound at a time. Probably some kind of repetitive consultation with a possibility of comparing the results will lead to a system which can also predict the initial LC conditions for a mixture of compounds.

ACKNOWLEDGEMENT

This research is supported by the European Commission as part of ESPRIT Project 1570 (ESCA).

REFERENCES

- 1 S. S. Williams, J.-L. Excoffier and S. Abbott, *Pittsburgh Conference on Analytical Chemistry and Applied Spectroscopy, Atlanta, GA, 1989*, abstract No. 1162.
- 2 M. A. Tischler and E. A. Fox, *Comput. Chem.*, 11 (1987) 235.
- 3 A. F. Fell, T. P. Bridge and M. H. Williams, *J. Pharm. Biomed. Anal.*, 6 (1988) 555.
- 4 J. W. Dolan and L. R. Snyder, *Pittsburgh Conference on Analytical Chemistry and Applied Spectroscopy, Atlanta, GA, 1989*, Abstract No. 1160.
- 5 J. J. Kirkland, J. L. Glajch, S. W. Rementer, T. G. Jones and L. R. Snyder, *Pittsburgh Conference on Analytical Chemistry and Applied Spectroscopy, Atlanta, GA, 1989*, Abstract No. 1161.
- 6 R. S. Hodges, J. M. R. Parker and C. T. Mant, *Pittsburgh Conference on Analytical Chemistry and Applied Spectroscopy, Atlanta, GA, 1989*, Abstract No. 1163.

- 7 M. De Smet, A. Peeters, L. Buydens and D. L. Massart, *J. Chromatogr.*, 457 (1988) 25.
- 8 D. Goulder, T. Blattert, A. Blokland, L. Buydens, A. Chhabra, A. Cleland, N. Dunand, H. Hindriks, G. Kateman, H. van Leeuwen, D. Massart, M. Mulholland, G. Musch, P. Naish, A. Peeters, G. Postma, P. Schoenmakers, M. De Smet, B. Vandeginste and J. Vink, *Chromatographia*, 26 (1988) 237.
- 9 A. Peeters, L. Buydens, D. L. Massart and P. J. Schoenmakers, *Chromatographia*, 26 (1988) 101.
- 10 P. J. Schoenmakers, N. Dunand, A. Cleland, G. Musch and Th. Blaffert, *Chromatographia*, 26 (1988) 37.
- 11 H. v. Leeuwen, B. Vandeginste, M. Mulholland and G. Kateman, *Anal. Chim. Acta*, submitted for publication.
- 12 R. Hindriks, F. Maris, J. Vink, A. Peeters, M. De Smet, D. L. Massart and L. Buydens, *J. Chromatogr.*, 485 (1989) 255.
- 13 R. R. Kaliszan, *Quantitative Structure-Chromatographic Retention Relationships*, Ellis Horwood, Chichester, 1987.
- 14 M. A. Stadialus, J. S. Berus and L. R. Snyder, *LC-GC, Mag. Liq. Gas Chromatogr.*, 6 (1988) 494.

CHROMSYMP. 1741

Resolution of unresolved peaks containing unknown components by high-performance liquid chromatography with multi-wavelength detection

ICHIRO SAKUMA*

Faculty of Science and Engineering, Tokyo Denki University, Hatoyama, Hiki-gun, Saitama 350-03 (Japan)

NOBUHARU TAKAI

Institute of Industrial Science, University of Tokyo, 22-1 Roppongi, 7-chome, Minato-ku, Tokyo 106 (Japan)

TAKEYOSHI DOHI

Faculty of Engineering, University of Tokyo, 7-3-1, Hongo, Bunkyo-ku, Tokyo 113 (Japan)

YASUHIRO FUKUI

Faculty of Science and Engineering, Tokyo Denki University, Hatoyama, Hiki-gun, Saitama 350-03 (Japan)
and

AKIYUKI OHKUBO

Faculty of Medicine, University of Tokyo, 7-3-1, Hongo, Bunkyo-ku, Tokyo 113 (Japan)

SUMMARY

A method for the resolution of unresolved peaks obtained by high-performance liquid chromatography with multi-wavelength detection was developed. The method estimates the elution profiles and absorption spectrum of a component eluting at the rising edge or trailing edge of the unresolved peak and estimates the relative intensity of the derived three-dimensional chromatogram of one component by rank annihilation.

Artificial unresolved peaks and actual unresolved three-component peaks were resolved by the developed method. The results showed that the method can estimate peak area with errors of less than about 10% when the resolution R_s of the components is greater than about 0.4. The accuracy of estimation is considered to be superior to that of the method based on principal component analysis followed by multiple regression analysis, especially if the elution profiles of components are distorted from a Gaussian shape such as with tailing, where the estimation of elution profiles by principal components analysis seems erroneous.

INTRODUCTION

Several methods that resolve unresolved peaks in chromatograms only by data analysis of three-dimensional chromatograms obtained by high performance liquid chromatography (HPLC) with multi-wavelength detection such as with diode-array

detectors have been reported. In these methods, the multivariate analysis technique is applied to the analysis of an unresolved peak in a three-dimensional chromatogram¹⁻⁷. In one of these methods, the spectrum of a component that elutes at the rising edge of an unresolved peak and that of a component at the trailing edge are estimated by extrapolation of observed spectra, and the elution profiles of two components are estimated by means of multiple regression analysis (curve fitting)⁴. However, the application of this method is limited to the resolution of two-component unresolved peaks.

For the resolution of unresolved peaks containing more than three components, principal component analysis (factor analysis) is used, where the data matrices obtained are decomposed into the orthonormal vectors calculated by principal component analysis, and the elution profile or spectrum of each component present is estimated as a linear combination of these orthonormal vectors (the first step). Generally, only the elution profile or absorption spectrum is estimated. Thereafter, the remaining spectra or elution profiles are estimated by curve fitting of the estimated value to the observed data matrix (the second step)^{1-3,6,7}. However, in these methods, errors in the first estimation step have direct influences on the estimation results of the second step. Consequently, the precision of the qualitative and quantitative estimation of each component's spectrum and elution profile may deteriorate.

In this study, a new method was developed that estimates both the elution profile and the absorption spectrum of each component in an unresolved peak and estimates the shapes and intensities of the three-dimensional chromatograms of components in the unresolved peak. The performance of the developed method in unresolved peak resolution was evaluated and compared with that of the conventional peak resolution method.

EXPERIMENTAL

Estimation of elution profile

Details of the theoretical aspects of the estimation method using principal component analysis are available in several references⁸⁻¹⁰. A brief description of algorithm is presented here. A multi-wavelength absorption detector can simultaneously monitor several chromatograms at N different wavelengths λ_i ($i = 1, 2, \dots, N$). Let d_{ij} be the measured absorbance of an unresolved peak at wavelength λ_i and time t_j ($j = 1, 2, \dots, M$); three-dimensional chromatographic data can be expressed as an $N \times M$ matrix as follows:

$$D = \begin{pmatrix} d_{11} & d_{12} & \dots & d_{1M} \\ d_{21} & d_{22} & \dots & d_{2M} \\ \vdots & \vdots & \dots & \vdots \\ d_{N1} & d_{N2} & \dots & d_{NM} \end{pmatrix} \quad (1)$$

The i th-row vector is an observed chromatogram at wavelength λ_i and the j th-column vector is an observed spectrum at time t_j .

Here we assume that an unresolved peak consists of L components, and the

spectrum S_k and elution profile (chromatogram) C_k are expressed as the following vectors:

$$S_1 = \begin{pmatrix} s_{11} \\ s_{12} \\ \vdots \\ s_{1N} \end{pmatrix}, S_2 = \begin{pmatrix} s_{21} \\ s_{22} \\ \vdots \\ s_{2N} \end{pmatrix}, \dots, S_L = \begin{pmatrix} s_{L1} \\ s_{L2} \\ \vdots \\ s_{LN} \end{pmatrix}$$

$$C_1 = \begin{pmatrix} c_{11} \\ c_{12} \\ \vdots \\ c_{1M} \end{pmatrix}, C_2 = \begin{pmatrix} c_{21} \\ c_{22} \\ \vdots \\ c_{2M} \end{pmatrix}, \dots, C_L = \begin{pmatrix} c_{L1} \\ c_{L2} \\ \vdots \\ c_{LM} \end{pmatrix}$$

where s_{ki} is the relative intensity of the spectrum of the k th component at wavelength λ_i and c_{kj} is the relative intensity of the elution profiles of the k th component at time t_j .

If the detector output is proportional to the concentration of a sample, and the principle of superposition is valid for both the absorption spectra and elution profiles of sample mixtures, the observed data matrix D can be expressed as

$$D = \sum_{k=1}^L e_k S_k C_k^T + R \quad (4)$$

where the superscript T denotes the transposed matrix (vector), e_k is a value proportional to the concentration of the k th component and R is the noise matrix. If we neglect R , the rank of the matrix D is equal to the number of components L , as the spectra and elution profiles of different components are linearly independent. Hence the data matrix D can be decomposed by L sets of orthonormal vectors u_k and v_k ($k = 1, 2, \dots, L$) as follows:

$$D = \sum_{k=1}^L \xi_k u_k v_k^T \quad (5)$$

The ξ_k are coefficients in the linear combination. As u_k and v_k are orthonormal,

$$D v_k = \xi_k u_k \quad (6)$$

$$u_k^T D = \xi_k v_k^T$$

It follows that:

$$D^T D v_k = \xi_k^2 v_k \quad (7)$$

$$D D^T u_k = \xi_k^2 u_k$$

These relationships mean that \mathbf{u}_k and \mathbf{v}_k are the eigenvectors of second moment matrix $D^T D$ or DD^T and ξ_k^2 is its k th eigenvalue. In other words, \mathbf{u}_k and \mathbf{v}_k are principal components of multivariate data D . In a real data matrix, because of the existence of noise the rank of the data matrix D is greater than the number of components L . However, eigenvalues of the matrix $D^T D$ contain the information about the number of component in the unresolved peak. By analysing the eigenvalues, we can estimate the number of components, as described by Malinowski^{11,12}.

On the other hand, comparing eqns. 4 and 5, we can see that the elution profile and spectrum of the k th component can be expressed as a linear combination of eigenvectors \mathbf{u}_k and \mathbf{v}_k :

$$\mathbf{S}_k = \sum_{l=1}^L x_{kl} \mathbf{u}_l \quad (8)$$

$$\mathbf{C}_k = \sum_{l=1}^L y_{kl} \mathbf{v}_l \quad (9)$$

where the x_{kl} and y_{kl} ($k = 1, 2, \dots, L; l = 1, 2, \dots, L$) are the coefficients in the linear combination that must be determined for each component k .

As \mathbf{v}_k can be calculated from a given data matrix D using eqn. 7, and the elution profile of each component is expressed as eqn. 9, we can estimate the elution profile of each component by estimating the coefficients y_{kl} in eqn. 9.

In the estimation of y_{kl} , two natural constraints and one evaluation function are assumed:

(1) the elution profile of each component is not negative, which can be expressed as

$$c_{kl} \geq 0 \quad (10)$$

(2) the spectrum of each component is not negative; after estimating the elution profiles of all the components in the unresolved peak, we can estimate the spectrum (spectra multiplied by the relative concentration) of each component \mathbf{S}_k , which can be expressed as

$$s_{ki} \geq 0 \quad (11)$$

(3) under the above two constraints, the elution profiles have an ideal shape as a chromatographic peak. To express unimodality of a chromatographic peak, the area to norm ratio is generally used^{2,6}. However, in this study, to express other properties of chromatographic shape (smoothness and stability of the baseline in addition to unimodality), the following function expressing the entropy of time derivatives of elution profiles are adopted¹³⁻¹⁵:

$$H = - \sum_{l=1}^L \sum_{j=1}^M P_{lj} \log (P_{lj}) \quad (12)$$

$$P_{lj} = |c'_{lj}| / \left(\sum_{j=1}^M |c'_{lj}| \right) \tag{13}$$

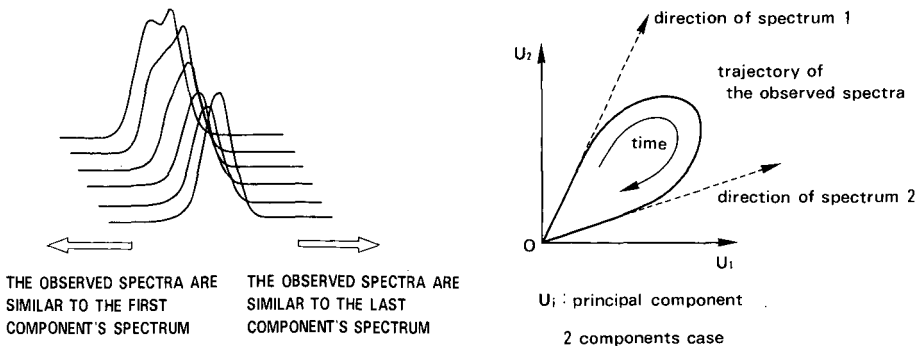
where c'_{lj} is the first or second derivative of the l th component's elution profiles at time t_j . By minimizing eqn. 12, ideal elution profiles of components are estimated under the constraints of eqns. 10 and 11. In order to avoid ambiguity in the relative intensities of the elution profiles, the area of each elution profile is set to unity in the actual estimation process.

Estimation of spectrum

By the same discussion as for the spectra, the observed spectrum at time t_j can be expressed as a linear combination of eigenvectors u_k in eqn. 7. Let d_j be the j th column vector of the data matrix expressing the spectrum at time t_j ; d_j can be also expressed as a linear combination of u_k as follows:

$$d_j = \sum_{l=1}^L w_{jl} u_l \tag{14}$$

To discuss changes in the coefficients w_{jl} as time advances, let us consider the two-component case. Fig 1a shows a schematic diagram of three-dimensional chromatogram of a two-component unresolved peak. Using eqn. 14, each observed spectrum must be located on the plane determined by two eigenvectors u_1 and u_2 . Considering eqn. 14, the coefficients w_{jl} are considered to be coordinates in the plane determined by u_1 and u_2 . They also express the direction of the observed spectrum in this plane as Fig. 1b shows. We can plot the trajectory of the observed spectra (Fig. 1b). Consider that the spectra at the rising edge of unresolved peak resemble the spectrum of the component which elutes at the rising edge; the direction determined by w_{ij} converges to the direction of the pure spectrum of the first-eluted compounds in the



(a)

(b)

Fig. 1. Estimation of a spectrum by extrapolation. (a) Three-dimensional chromatogram of two-component unresolved peak. (b) Trajectory of observed vectors in the space determined by the two principal components.

initial part of the trajectory. Thus, by extrapolating the w_{ij} in the reverse direction of time, the spectrum of the first-eluting compounds can be estimated as a convergence direction of the observed spectra in the plane determined by \mathbf{u}_1 and \mathbf{u}_2 . The convergence direction can be calculated numerically by approximating the trajectory of the tip of the observed spectrum vectors by a polynomial of parameters such as the length of the trajectory from the origin. Similar argument can be used for more than three-component cases. Hence one can at least estimate the spectrum of the component which elutes first at the rising edge of an unresolved peak and that of the component which elutes at its trailing edge.

Estimation of relative intensity of an estimated three-dimensional chromatogram

In the above methods, elution profiles C_k of all the components in an unresolved peak and spectrum S_1 of the component that elutes at the rising edge or trailing edge of the unresolved peak can be estimated. Hence we can determine the shape of the three-dimensional chromatogram P_1 of the components eluting at the rising (or trailing) edge of the unresolved peak:

$$P_1 = S_1 C_1^T \quad (15)$$

To resolve an unresolved peak into each component, the relative intensity of this three-dimensional chromatogram P_1 must be estimated. In this estimation, rank annihilation is adopted¹⁶⁻¹⁸.

Let α be the best estimate of relative intensity of P_1 . As the data matrix after subtracting the three-dimensional chromatogram of the first-eluting component contains only $L-1$ components, the degrees of freedom of the matrix $(D - \alpha P_1)$ decreases from the original number of components L to $L-1$. This condition can be expressed as

$$\text{rank} \{(D - \alpha P_1) (D - \alpha P_1)^T\} = L-1 \quad (16)$$

The analytical solution of eqn. 16 was given by Lorber¹⁹. Let U and V be matrices constructed by \mathbf{u}_k and \mathbf{v}_k in eqn. 7 as follows:

$$\begin{aligned} U &= [\mathbf{u}_1, \mathbf{u}_2, \dots, \mathbf{u}_L] \\ V &= [\mathbf{v}_1, \mathbf{v}_2, \dots, \mathbf{v}_L] \end{aligned} \quad (17)$$

Define \mathbf{a} and \mathbf{b} as

$$\begin{aligned} \mathbf{a} &= U^T S_1 \\ \mathbf{b} &= V^T C_1 \end{aligned} \quad (18)$$

Note that \mathbf{a} and \mathbf{b} are L -dimensional vectors. Let a_i and b_i be the i th element of \mathbf{a} and \mathbf{b} , then the estimated α is calculated as follows:

$$1/\alpha = \sum_{i=1}^L a_i b_i / \xi_i \quad (19)$$

Note that ξ_i is the square root of the k th eigenvalue expressed as eqn. 7.

$D - \alpha P_1$ contains only $L - 1$ components. By iterating these procedures, we can resolve an unresolved peak into three-dimensional chromatograms of existing components.

Computer program

Programs performing the above-described algorithm were developed on an NEC PC-9801 personal computer. The programs were written in C language.

A brief description of the flow of operation is as follows:

(1) Determine the area of an unresolved peak using the cursor displayed on the CRT of the computer together with the contour plot of the three-dimensional chromatogram.

(2) Calculate eigenvectors and eigenvalues of the second moment matrix $D^T D$.

(3) Determine the number of components contained in the unresolved peak by analysing the eigenvalues calculated in step 2.

(4) Estimate the elution profiles of each component by minimizing eqn. 12 under the constraints.

(5) Determine the region of the rising edge using the displayed cursors together with a three-dimensional chromatogram or contour plot of an unresolved peak displayed on the CRT of the computer. After setting the region, the computer automatically extrapolates the observed spectra and calculates the estimated spectrum of the first- (or last-) eluting component.

(6) Calculate the relative intensity α of the three-dimensional chromatogram P_1 in the given unresolved peak data using eqns. 17–19.

(7) Subtract the estimated three-dimensional chromatogram of the component eluting at the rising edge or trailing edge of the unresolved peak.

(8) If the remaining unresolved peak contains more than two components repeat steps 2–7.

In the estimation of elution profiles, non-linear programming with constraints must be performed. An augmented Lagrangian algorithm was adopted for that purpose²⁰.

Procedures

Unresolved peak data were prepared both by numerical calculation of artificial chromatograms and by the actual measurement of unresolved peaks by HPLC with multi-wavelength detection. The developed algorithm was tested in the resolution of artificial and actual unresolved peak data. In order to investigate the performance of the developed method compared with the method based on principal component analysis followed by multiple regression analysis, the same data were analysed using multiple regression analysis where the spectrum of each component was estimated by curve fitting of the estimated elution profiles by multiple regression analysis.

The artificial three-dimensional chromatograms were generated assuming that it contained two or three components, that the three components had the spectra shown in Fig. 2 and that each chromatogram was Gaussian with the same variance (peak width). Several three-dimensional chromatogram data were calculated at different resolutions, R_s , and peak-height ratios. Also, random noise of the order of 1% of the standard deviation of the chromatographic data were added to the data. The size of the

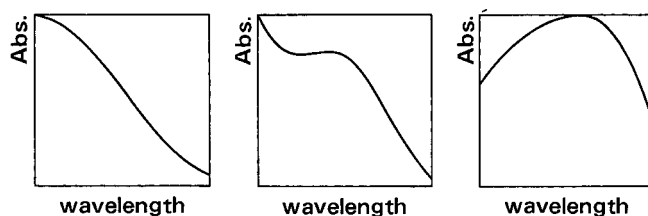


Fig. 2. Spectra of three components used in artificial unresolved peak calculation.

data matrix was 30×30 , which meant that 30 chromatograms were measured at 30 different wavelengths and the intensities (absorbances) of the chromatograms were measured at 30 different points of time.

In the experiment on unresolved peaks of actual samples, the three-components sample mixtures shown in Table I were separated by reversed-phase HPLC under the conditions shown in Table II. The areas to be analysed by the algorithms were determined by manual operation using cursors displayed on the CRT display of the computer system together with the contour plot of the three-dimensional chromatogram obtained. The data matrix size was 30×40 , which meant that the chromatograms were measured at 30 different wavelengths and at 40 different points in time. Caffeine eluted first, *N*-methylaniline second and *o*-*tert.*-butylphenol third in this separation system. The measured resolutions were as follows: (i) with 84.0%

TABLE I

SAMPLES USED IN THE EXPERIMENTS

Samples were dissolved in acetonitrile.

Sample	Caffeine concentration (wt.-%)	<i>N</i> -Methylaniline concentration (vol.-%)	<i>o</i> - <i>tert.</i> -Butylphenol concentration (vol.-%)
A	0.043	0.0033	0.033
B	0.051	0.0040	0.020
C	0.064	0.0025	0.025
D	0.073	0.0029	0.014
E	0.128	0.0000	0.000
F	0.000	0.0100	0.000
G	0.000	0.0000	0.100

TABLE II

HPLC SEPARATION CONDITIONS

Packing	Hitachi 3056 (ODS)
Column	50 mm \times 4 mm I.D.
Eluent	acetonitrile-water: (1) 84.0:16.0 (v/v); (2) 80.6:19.4 (v/v)
Flow-rate	1.0 ml/min
Injection volume	10 μ l
Detector	MCPD-350 diode-array detector (Otsuka Electronics, Osaka, Japan) with laboratory-made data acquisition system ²¹

acetonitrile as the eluent, R_s (caffeine/N-methylaniline) = 0.33 and R_s (N-methylaniline/*o*-*tert*-butylphenol) = 0.22; and (ii) with 80.6% acetonitrile as the eluent, R_s (caffeine/N-methylaniline) = 0.46 and R_s (N-methylaniline/*o*-*tert*-butylphenol) = 0.33.

The results of the unresolved peak separation were evaluated using the spectrum shape similarity, defined as the correlation coefficients between the actual spectrum and the estimated spectrum for qualitative aspects and the peak area of the estimated elution profile compared with the actual peak area for quantitative aspects.

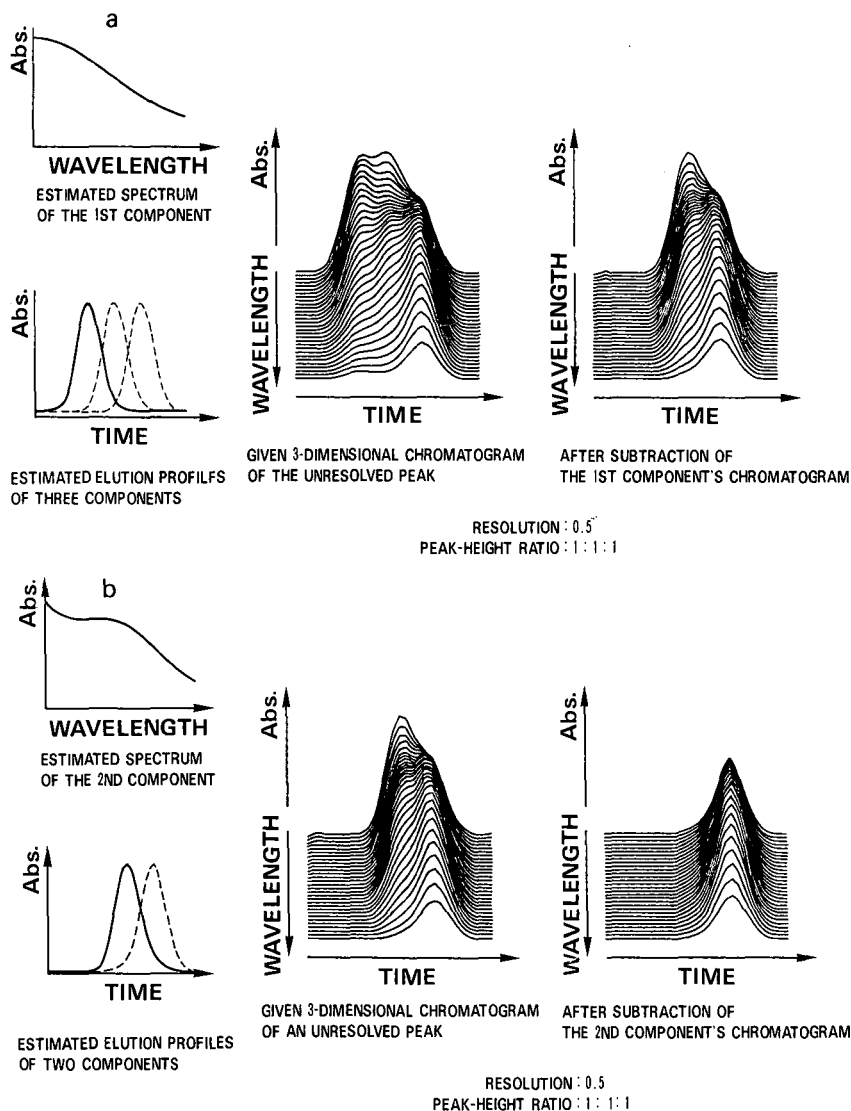


Fig. 3. Example of peak resolution of artificial three-component unresolved peak. (a) Subtraction of the first component; (b) subtraction of the second component.

RESULTS

Fig. 3 shows an example of peak resolution by the proposed method. Fig. 3a shows subtraction of the first components from the original three-dimensional chromatogram and Fig. 3b subtraction of the second components from the residual two-component three-dimensional chromatogram.

Table III shows the estimated peak area (peak volume summation of the peak area at every wavelength) of each component of a two-component unresolved peak with various resolutions. For an unresolved peak with resolution $R_s < 0.4$, the estimation errors were larger than 10% and for $R_s > 0.5$ they were less than 10%. Table IV shows the results obtained by multiple regression analysis. In the resolution of those artificial unresolved peaks with $R_s < 0.4$, the developed method was not as efficient as the method using multiple regression analysis. However, in the analysis of those artificial unresolved peaks with $R_s > 0.5$, the results obtained by the two methods did not show clear differences.

TABLE III

RESULTS OF PEAK RESOLUTION OF ARTIFICIAL TWO-COMPONENT UNRESOLVED PEAK BY THE DEVELOPED METHOD

The values in parentheses represent the actual peak volumes.

Peak-height ratio	Resolution, R_s	Component 1		Component 2	
		Total peak area	Error (%)	Total peak area	Error (%)
		(4701)		(5180)	
1:1	0.1	6889	46.5	2990	-42.3
	0.2	5340	13.6	4539	-12.4
	0.3	4014	-14.6	5866	13.2
	0.4	5311	13.0	4570	-11.8
	0.5	5059	7.6	4823	-6.9
	0.6	4935	5.4	4948	-4.5
	0.7	4991	6.2	4892	-5.6
		(4701)		(2573)	
2:1	0.1	5738	22.1	2694	-39.7
	0.2	5020	6.8	2697	-11.8
	0.3	3987	-15.2	3155	+28.4
	0.4	5171	10.0	2395	-17.6
	0.5	4962	5.6	2664	-9.4
	0.6	4892	4.1	2757	-6.7
	0.7	4842	3.0	2788	-4.9
		(7522)		(2058)	
4:1	0.1	8381	11.4	2213	-41.2
	0.2	5769	-23.3	3345	-85.8
	0.3	6647	-11.6	2363	+43.1
	0.4	7083	-5.8	2313	+22.0
	0.5	7434	-1.2	1734	5.0
	0.6	7623	1.3	2000	-4.2
	0.7	7668	1.9	1717	-6.4

TABLE IV

RESULTS OF PEAK RESOLUTION OF ARTIFICIAL TWO-COMPONENT UNRESOLVED PEAK BY THE METHOD OF PRINCIPAL COMPONENT ANALYSIS FOLLOWED BY MULTIPLE REGRESSION ANALYSIS

The values in parentheses represent the actual peak volumes.

Peak-height ratio	Resolution, R_s	Component 1		Component 2	
		Total peak area	Error (%)	Total peak area	Error (%)
		(4701)		(5180)	
1:1	0.1	4560	-3.0	5319	+2.7
	0.2	4604	-2.1	5276	+1.9
	0.3	4320	-8.1	5560	+7.3
	0.4	4980	5.7	4902	-5.4
	0.5	4608	-1.9	5274	+1.7
	0.6	4492	-4.5	5391	+4.1
	0.7	4383	-6.8	5500	+6.2
		(4701)		(2573)	
2:1	0.1	4596	-2.2	2694	+4.7
	0.2	4593	-2.3	2697	+4.8
	0.3	4135	-12.0	3155	+22.6
	0.4	4896	4.1	2395	-6.9
	0.5	4628	-1.6	2664	+3.5
	0.6	4535	-3.5	2757	+7.2
	0.7	4504	-4.2	2788	+8.4
		(7522)		(2058)	
4:1	0.1	7379	-2.0	2213	+7.5
	0.2	6247	-17.0	3345	+62.5
	0.3	7229	-3.9	2363	+14.8
	0.4	7280	-3.2	2313	+12.4
	0.5	7859	4.5	1734	-15.7
	0.6	7594	1.0	2000	-2.8
	0.7	7878	4.7	1717	-16.6

Table V shows the correlation coefficients between the estimated spectrum and actual spectrum of the first and the second components in artificial three-component unresolved chromatograms. Table VI shows the results of the estimated peak volume. As shown in the two-component case, the peak areas of the component having the highest intensity in those unresolved peaks with $R_s > 0.4$ were estimated with errors of about 10%. Table VII shows the results by multiple regression analysis on the same data and it is clear that the developed system did not show any superiority.

However, the results for the unresolved peaks of an actual three-component mixture showed differences between the proposed method and the method with multiple regression analysis. Fig. 4 shows the actual elution profiles of the three components using 84.0% and 80.6% acetonitrile as the eluent. The peaks of caffeine and *o*-*tert*-butylphenol were relatively wide and all the peaks showed tailing. Fig. 5 shows an example of the resolution of the unresolved peak of an actual sample mixture. The three-dimensional chromatogram of caffeine was subtracted from the originally observed three-dimensional chromatogram.

TABLE V

CORRELATION COEFFICIENTS BETWEEN ACTUAL SPECTRUM AND ESTIMATED SPECTRUM OF THE FIRST AND SECOND COMPONENTS FOR PEAK RESOLUTION OF ARTIFICIAL TWO-COMPONENT UNRESOLVED PEAK BY THE DEVELOPED METHOD

Resolution	Peak-height ratio	Component 1	Component 2
0.4	1:1:1	0.9996	0.9995
0.5	1:1:1	1.0000	0.9989
0.6	1:1:1	1.0000	0.9996
0.7	1:1:1	1.0000	1.0000
0.4	2:2:1	0.9999	0.9893
0.4	4:4:1	0.9999	0.9853
0.4	2:1:1	1.0000	0.9696
0.4	4:2:1	1.0000	0.9706
0.4	4:1:1	1.0000	0.9518
0.5	2:2:1	1.0000	0.9990
0.5	4:4:1	1.0000	1.0000
0.5	2:1:1	1.0000	0.9999
0.5	4:2:1	1.0000	0.9997
0.5	4:1:1	1.0000	0.9971

Figs. 6 and 7 show the results of concentration estimation by the proposed methods and Figs. 8 and 9 those obtained by multiple regression analysis. The estimated concentration was calculated from the estimated peak area of each component and the peak area of a standard one-component sample with known concentrations. Figs. 6 and Fig. 8 show the results of peak resolution where R_s (caffeine/N-methylaniline) = 0.33 and R_s (N-methylaniline/*o*-*tert*-butylphenol) = 0.22. Figs. 7 and Fig. 9 show the results of peak resolution R_s (caffeine/N-methylaniline) = 0.46 and R_s (N-methylaniline/*o*-*tert*-butylphenol) = 0.33.

For the unresolved peak resolution of actual three-component mixtures, the correlation coefficients between the estimated and actual concentrations were 0.916 and 0.976 by the proposed method and 0.803 and 0.952 by the method of principal component analysis followed by multiple regression analysis. These results showed that the proposed method was superior for the estimation of components in actual unresolved peaks.

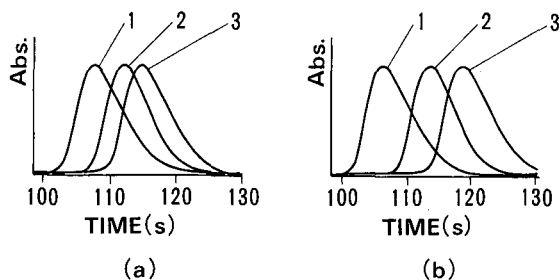


Fig. 4. Actual elution profiles of (1) caffeine, (2) N-methylaniline and (3) *o*-*tert*-butylphenol. Eluent: acetonitrile-water, (a) 84.0:16.0 (v/v) and (b) 80.6:19.4 (v/v).

TABLE VI
RESULTS OF PEAK RESOLUTION OF ARTIFICIAL THREE-COMPONENT UNRESOLVED PEAK BY THE DEVELOPED METHOD

R_s	Peak-height ratio	Component 1			Component 2			Component 3		
		Actual peak volume	Estimated peak volume	Error (%)	Actual peak volume	Estimated peak volume	Error (%)	Actual peak volume	Estimated peak volume	Error (%)
0.4	1:1:1	4701	4619	-1.7	5180	6354	22.7	6890	5878	-14.7
0.5	1:1:1	4701	4760	1.3	5180	4916	-5.1	6890	7099	3.0
0.6	1:1:1	4701	4916	4.6	5180	5240	1.2	6890	6619	-3.9
0.7	1:1:1	4701	4510	-4.1	5180	5536	6.9	6890	6728	-2.3
0.4	2:2:1	5641	5729	1.6	6216	5279	-15.1	4134	4985	20.6
0.4	4:4:1	5641	5613	-0.5	6216	5638	-9.3	2067	2674	29.4
0.4	2:1:1	5641	5666	0.4	3108	2145	-31.0	4134	5074	22.7
0.4	4:2:1	5641	5675	0.6	3108	2301	-26.0	2067	2842	37.5
0.4	4:1:1	5641	5694	0.9	1554	1167	-24.9	2067	2403	16.3
0.5	2:2:1	5641	5500	-2.5	6216	6003	-3.4	4134	3795	-8.2
0.5	4:4:1	5641	5675	0.6	6216	6470	4.1	2067	1775	-14.1
0.5	2:1:1	5641	5596	-0.8	3108	3384	8.9	4134	3904	-5.6
0.5	4:2:1	5641	5539	-1.8	3108	3532	13.6	2067	1744	-15.6
0.5	4:1:1	5641	5094	-9.7	1554	2788	79.4	2067	1382	-33.1

TABLE VII
RESULTS OF PEAK RESOLUTION OF ARTIFICIAL THREE-COMPONENT UNRESOLVED PEAK BY THE METHOD OF PRINCIPAL COMPONENT ANALYSIS FOLLOWED BY MULTIPLE REGRESSION ANALYSIS

R_s	Resolution, Peak-height ratio	Component 1			Component 2			Component 3		
		Actual peak volume	Estimated peak volume	Error (%)	Actual peak volume	Estimated peak volume	Error (%)	Actual peak volume	Estimated peak volume	Error (%)
0.4	1:1:1	4701	4761	4.2	5180	4710	9.1	6890	7302	6.0
0.5	1:1:1	4701	4726	0.5	5180	5224	0.8	6890	6824	-0.9
0.6	1:1:1	4701	4667	-0.7	5180	4981	-3.8	6890	7127	3.5
0.7	1:1:1	4701	4368	-7.0	5180	4954	-4.4	6890	7453	8.2
0.4	2:2:1	5641	5881	4.3	6216	6402	3.0	4134	3709	-10.3
0.4	4:4:1	5641	5608	-0.6	6216	5427	-12.7	2067	2890	39.8
0.4	2:1:1	5641	5573	-1.2	3108	3378	8.7	4134	3934	-4.8
0.4	4:2:1	5641	5542	-1.8	3108	3240	4.2	2067	2035	-1.5
0.4	4:1:1	5641	5603	-0.7	1554	1827	17.6	2067	1833	-11.3
0.5	2:2:1	5641	4853	-14.0	6216	7404	19.1	4134	3737	-9.6
0.5	4:4:1	5641	5476	-2.9	6216	6096	-1.9	2067	2353	13.8
0.5	2:1:1	5641	5638	-0.1	3108	3283	5.6	4134	3965	-4.1
0.5	4:2:1	5641	5749	1.9	3108	3044	-2.1	2067	2025	-2.0
0.5	4:1:1	5641	5028	-10.9	1554	2100	35.1	2067	2135	3.3

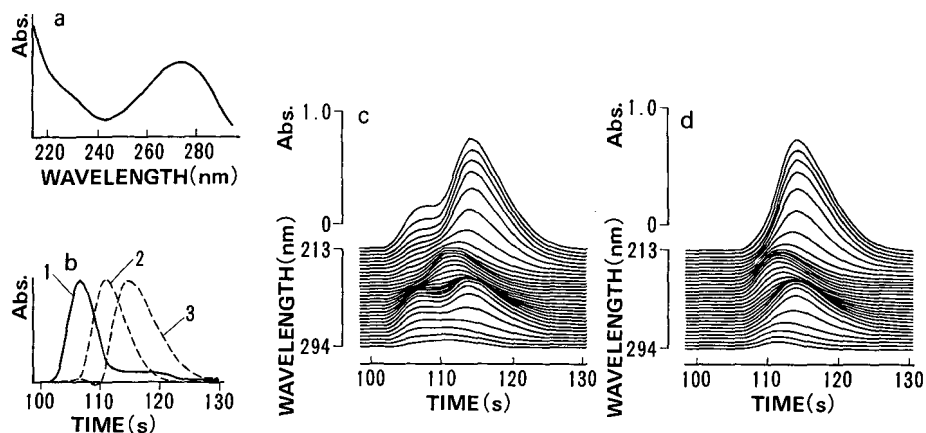


Fig. 5. Example of peak resolution of actual three-component unresolved peak to illustrate elution profile estimation and observed spectra extrapolation followed by rank annihilation. (a) Estimated spectrum of caffeine. (b) Estimated elution profiles of (1) caffeine, (2) N-methylaniline and (3) *o*-tert.-butylphenol. (c) Three-dimensional chromatogram of caffeine, N-methylaniline and *o*-tert.-butylphenol. (d) Three-dimensional chromatogram after subtraction of caffeine. Sample: 0.043% (w/w) caffeine, 0.033% (v/v) N-methylaniline and 0.033% (v/v) *o*-tert.-butylphenol (10 μ l). Eluent: acetonitrile-water (84.0:16.0, v/v). Resolution: R_s (caffeine/N-methylaniline) = 0.33; R_s (N-methylaniline/*o*-tert.-butylphenol) = 0.22.

DISCUSSION

Effects of peak resolution on the estimated results

The results of the resolution of unresolved peaks on both artificial unresolved chromatograms and actual chromatograms showed that when $R_s >$ than 0.4, the dominant component in the unresolved peak can be determined with a maximum error of about 10% by the developed method. Computer simulations were performed for the two-component case where unresolved peaks with $R_s <$ 0.3 were resolved. The estimation errors were larger for an unresolved peak with $R_s <$ 0.4.

The results for the actual unresolved peaks also showed that the peak areas of three components could be estimated with a correlation coefficient of 0.976 when $R_s =$ 0.46 and 0.33. On the other hand, when $R_s =$ 0.22 and 0.33, the correlation coefficient between the estimated peak areas and the actual peak areas decreased to 0.916. These results also showed that the developed method could separate unresolved peaks with $R_s \geq$ 0.4. These results coincided with those for the artificial unresolved peaks. Hence it is considered that $R_s =$ 0.4 is a certain criterion that determines the limits of the ability of the developed peak resolution method. The main factor determining this limitation is considered to be errors in spectrum estimation. The results of the experiments on peak resolution by multiple regression analysis showed that the elution profiles were well estimated, so that the estimation errors under the condition of small R_s were relatively small, as shown in Table IV. It is considered that the errors in estimation using the developed method mainly came from errors in spectrum estimation in the experiments on the artificial unresolved peaks. It is difficult to extrapolate the observed spectra only by curve fitting to a polynomial in the case of small resolutions because the observed spectra suffer from distortion by several

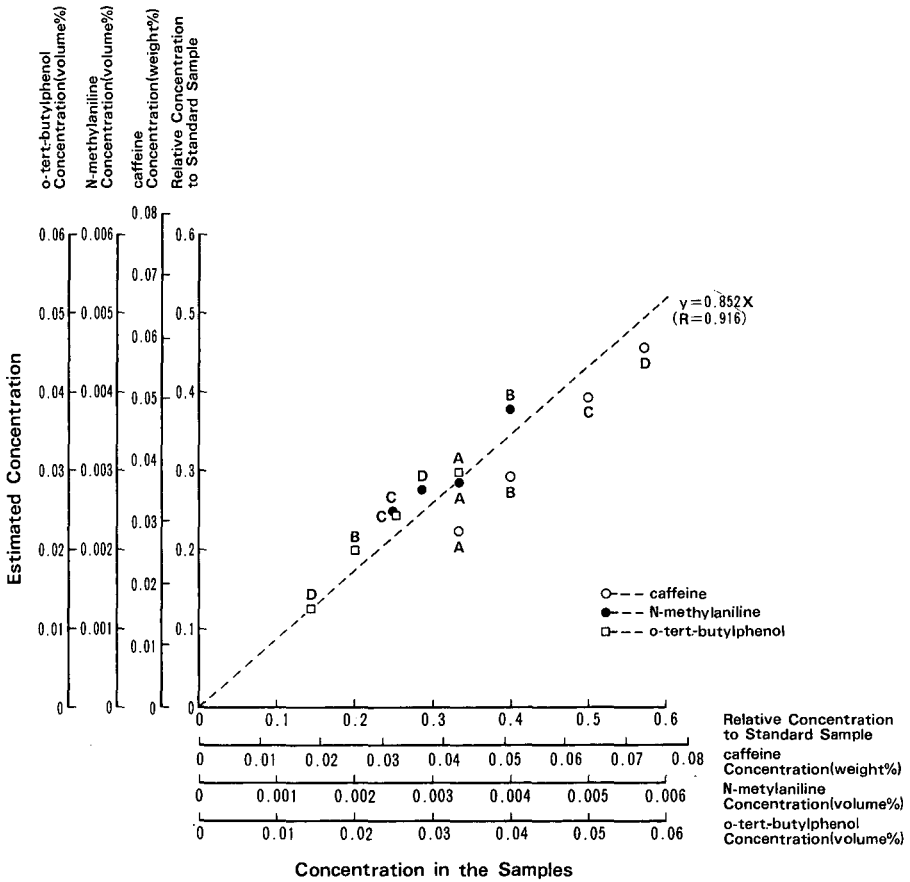


Fig. 6. Results of quantitative analysis by the developed method. Eluent: acetonitrile-water (84.0:16.0, v/v). Resolution: R_s (caffeine/N-methylaniline) = 0.33; R_s (N-methylaniline/o-tert-butylphenol) = 0.22. Quantitation: (○) caffeine, peak area at 262 nm; (●) N-methylaniline, peak area at 246 nm; (□) o-tert-butylphenol, peak area at 227 nm. A, B, C and D correspond to the sample shown in Table I.

co-eluting components. Hence it is considered that the present method was not suitable for the resolution of strongly overlapped peaks with small resolutions.

Effects of peak-height ratio on the estimated results

The results of computer simulation on the artificial unresolved peaks showed that if the peak height of one component is much smaller than those of co-eluting components, the errors in its area estimation were relatively large in comparison with those for the dominant component in the unresolved peak. However, those components which had the largest intensities in a unresolved peak could be well determined with small errors when there were large differences in peak height between the co-eluting compounds. Hence it is considered that the developed method can be applied to the quantitative analysis of the main component's peak area in an unresolved peak with estimation errors < 10% provided that $R_s \geq 0.4$.

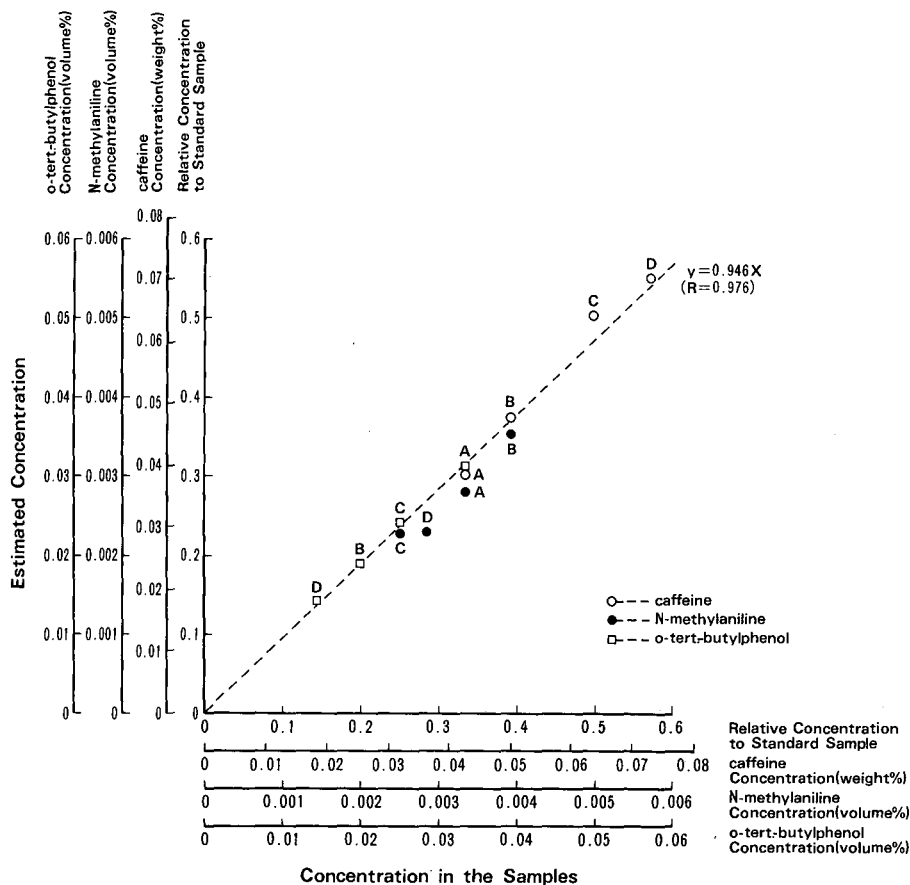


Fig. 7. Results of quantitative analysis by the developed method. Eluent: acetonitrile–water (80.6:19.4, v/v). Resolution: R_s (caffeine/N-methylaniline) = 0.46; R_s (N-methylaniline/*o*-tert.-butyl phenol) = 0.33. Quantitation as in Fig. 6. A, B, C and D correspond to the samples shown in Table I.

Comparison of the developed peak resolution method and the conventional method based on principal component analysis and multiple regression analysis

In this work, the two methods for unresolved peak resolution were compared by resolving the same unresolved peak data obtained through computer simulations and HPLC separations of actual three-component mixtures.

One method was the developed method where elution profile estimation based on principal component analysis, spectrum estimation by extrapolating the observed spectra and rank annihilation to estimate the amount of a component were performed (method 1). The other was the conventional method where elution profile estimation based on principal component analysis followed by multiple regression analysis was performed (method 2).

The results for the artificial unresolved peaks showed that the performance of method 1 was almost the same in the two-component case and slightly poorer in the three-component case compared with that of method 2. In the computer simulation of

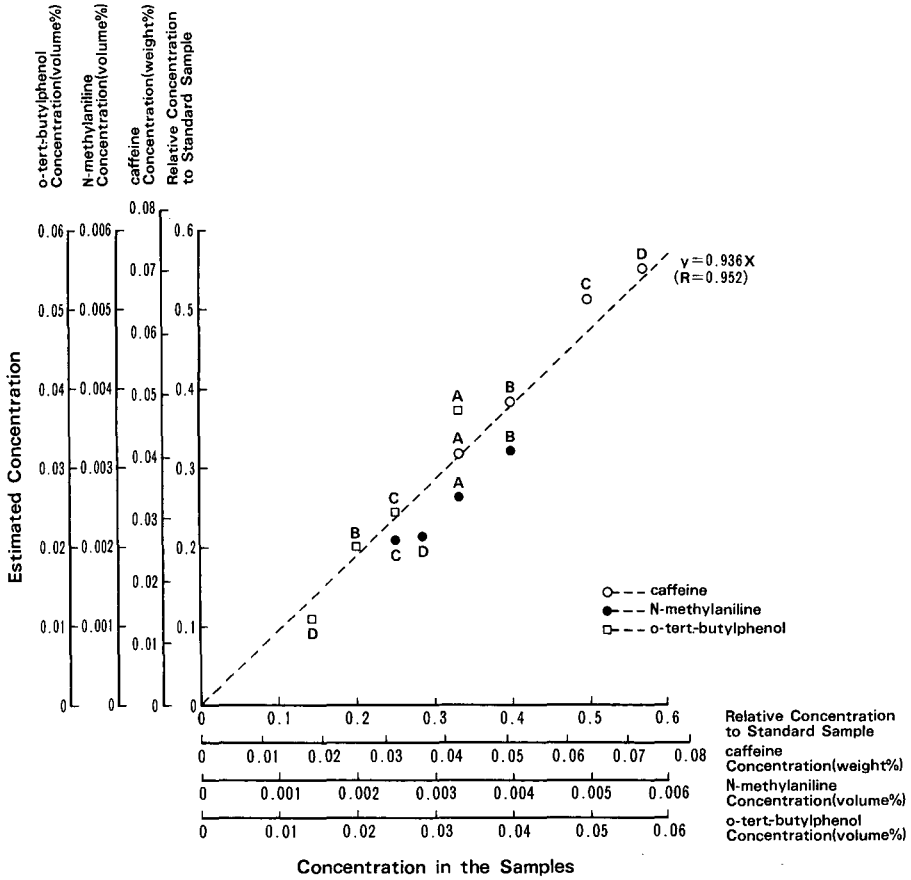


Fig. 9. Results of quantitative analysis by the method of principal component analysis followed by multiple regression analysis. Eluent: acetonitrile-water (80.6:19.4, v/v). Resolution: R_s (caffeine/N-methylaniline) = 0.46; R_s (N-methylaniline/o-tert.-butylphenol) = 0.33. Quantitation as in Fig. 6. A, B, C and D correspond to the samples shown in Table I.

estimation errors in the three-component case. As a result, we could not estimate the peak areas of each component by method 1 with smaller errors than by method 2.

On the other hand, in HPLC separations of actual samples, the elution profiles of caffeine, N-methylaniline and o-tert.-butylphenol showed extensive tailing and the shapes of the elution profiles differed from each other, as shown in Fig. 4. They differed from the ideal elution profiles such as Gaussian. Minimization of eqn. 12 leads to localization (sharpening) of the elution profiles. In these situations, the method overestimates the elution profiles. The band width of the estimated elution profile of caffeine in Fig. 5 was narrower than that of the actual elution profile in Fig. 4. To express the tailing of real data, unrealistic peak tailings appeared in the estimation result. This result showed the problems that arise in elution profile estimation based on principal component analysis. In that method, a function expressing the ideal characteristics of elution profiles was introduced to estimate the elution profiles of

components. However, in the actual HPLC separation, the elution profiles sometimes differ from the ideal elution profiles. In this situation, the estimation method is not consistent with the actual elution profiles. Hence errors in the elution profile estimation directly affect the spectrum estimation in method 2, as it uses estimated elution profiles in the subsequent multiple regression analysis for spectrum estimation.

On the other hand, in method 1, the elution profiles and spectra are estimated independently. Even if the result of elution profile estimation is erroneous, this error will not directly affect the results of spectrum estimation. If the spectrum of the component in the unresolved peak is well estimated, the errors in quantitative estimation mainly come from the elution profile estimation. For actual sample mixtures, the elution profile estimation was not so good because of the existence of tailing, but the spectrum estimation was considered to have only small errors. Consequently, it is considered that the errors in the total estimation were smaller than those by method 2. Even when $R_s = 0.46$ and 0.33 and the elution profiles were estimated with smaller errors, the results showed an improvement in the accuracy of estimation by the developed method, as shown in Figs. 7 and 9.

When elution profile distortion such as peak tailing is observed, where the elution profile estimation by principal components analysis might be erroneous, the proposed method is considered to be superior to conventional methods.

An additional advantage of the developed method over the conventional method is that we can easily take the spectrum information into consideration when the absorption spectra of components in an unresolved peak are available before peak resolution. Although the elution profile stability is not so good in HPLC, as the elution profiles differ slightly in each separation and are affected by deterioration of the analytical column, it is often capable of obtaining reliable spectrum information about components in unresolved peaks. If we can obtain a standard spectrum of a component in an unresolved peak beforehand, we can utilize it immediately by the proposed method.

Feasible application area of the developed method compared with the experimental method for optimization of HPLC separations

Generally, optimization of HPLC separations by experimental approaches such as selection of columns and eluents and adjustment of flow-rate and gradient sequences are performed in order to obtain good chromatographic separations. We must first try these experimental methods before using the developed peak resolution method. There is no need to resort to the chemometric approach when we obtain good data by actual experiments. Chemometric approaches such as the developed method are only useful when these experimental approaches are impossible or very difficult to use. It is considered that this condition is often encountered in the analysis of biological fluids. In the HPLC separation of biological fluid samples such as urine and serum, there are many co-eluting compounds together with the compound of interest. The amounts of the co-eluting compounds fluctuates widely from sample to sample, or different kinds of co-eluting compounds may be present in different samples. The degrees of overlap may differ from sample to sample. As a result, even if one can find appropriate separation conditions for the analysis of a certain sample, these conditions may not be optimum for another sample. Under these conditions, the developed peak resolution method is useful for compensating for the low separation capability of the actual HPLC system.

CONCLUSION

A method for the resolution of unresolved peaks obtained by HPLC with multi-wavelength detection was developed. The method estimates the elution profiles and absorption spectrum of a component eluting at the rising edge or trailing edge of the unresolved peak and estimates the relative intensity of the derived three-dimensional chromatogram of one component by rank annihilation. The method can estimate peak areas with errors $\leq 10\%$ when $R_s \geq 0.4$. In comparison with the method based on principal component analysis followed by multiple regression analysis, the estimation accuracy was considered to be superior, especially when the elution profiles of the components are distorted from Gaussian, such as when tailing occurs, where the elution profile estimation by principal components analysis seems erroneous.

REFERENCES

- 1 D. W. Osten and B. Kowalski, *Anal. Chem.*, 56 (1984) 991.
- 2 B. Vandeginste, R. Essers, T. Bosman, J. Reijnen and G. Kateman, *Anal. Chem.*, 57 (1985) 971.
- 3 B. G. M. Vandeginste, F. Leyten, M. Gerritsen, J. W. Noor and G. Kateman, *J. Chemometr.*, 1 (1987) 57.
- 4 W. Lindberg, J. Oehman and S. Wold, *Anal. Chem.*, 58 (1986) 1415.
- 5 D. H. Burns, J. B. Callis and G. D. Christian, *Anal. Chem.*, 58 (1986) 1415.
- 6 P. J. Gemperline, *Anal. Chem.*, 58 (1986) 2656.
- 7 J. K. Strasters, H. A. H. Billet, L. de Galan, B. G. M. Vandeginste and G. Kateman, *Anal. Chem.*, 60 (1988) 2745.
- 8 W. H. Lawton and E. A. Sylvestre, *Technometrics*, 13 (1971) 617.
- 9 E. A. Sylvestre, W. H. Lawton and M. S. Maggio, *Technometrics*, 16 (1974) 353.
- 10 W. P. Carery, K. R. Beebe, E. Sanchez, P. Geladi and B. R. Kowalski, *Sensors Actuators*, 9 (1986) 223.
- 11 E. R. Malinowski, *Anal. Chem.*, 49 (1977) 606.
- 12 E. R. Malinowski, *Anal. Chem.*, 49 (1977) 612.
- 13 K. Sasaki, S. Kawata and S. Minami, *Appl. Opt.*, 22 (1983) 3599.
- 14 K. Sasaki, S. Kawata and S. Minami, *Appl. Opt.*, 23 (1984) 1955.
- 15 S. Kawata, H. Komeda, K. Sasaki and S. Minami, *Appl. Spectrosc.*, 39 (1985) 610.
- 16 C. N. Ho, G. D. Christian and E. R. Davidson, *Anal. Chem.*, 50 (1978) 1108.
- 17 C. N. Ho, G. D. Christian and E. R. Davidson, *Anal. Chem.*, 52 (1980) 1071.
- 18 C. N. Ho, G. D. Christian and E. R. Davidson, *Anal. Chem.*, 53 (1981) 92.
- 19 A. Lorber, *Anal. Chim. Acta.* 164 (1984) 293.
- 20 E. Aiyosi and K. Shimizu, *Nonlinear Programming* (in Japanese), Nikka-Giren, Tokyo, 1978, Ch. 10, p. 237.
- 21 I. Sakuma, T. Dohi, N. Takai, H. Funakubo, Y. Okabe, T. Katoda, Y. Sekiguchi and T. Isomura, *Annual Report of Engineering Research Institute Faculty of Engineering, University of Tokyo*, University of Tokyo, Tokyo, Vol. 42, 1983, p. 53.

Optimization of mobile phase composition for high-performance liquid chromatographic separation by means of the overlapping resolution mapping scheme

S. F. Y. LI*, H. K. LEE and C. P. ONG

Department of Chemistry, National University of Singapore, 10 Kent Ridge Crescent, Singapore 0511 (Singapore)

SUMMARY

The use of the overlapping resolution mapping (ORM) scheme to predict the optimum mobile phase composition for isocratic reversed-phase separation was examined. The application of the method to the separation of a mixture of ten polycyclic aromatic hydrocarbons was demonstrated. The ORM scheme was found to be a rapid and versatile method.

INTRODUCTION

In a previous paper¹, we reported the application of the overlapping resolution mapping (ORM) scheme to the optimization of mobile phase composition for the separation of eleven priority phenols. Although high-performance liquid chromatography (HPLC) has been used extensively for the analysis of polycyclic aromatic hydrocarbons (PAHs)^{2–5}, the use of the ORM scheme for the optimization of separation of these compounds has not been examined. The ORM scheme is an interpretative optimization method in which the extent of chromatographic separation is predicted indirectly from the retention behaviour of the individual solutes⁶. For the optimization of eluent mixtures with up to quaternary compositions, only seven experiments need to be carried out according to the Snyder selectivity triangle⁷ before one can locate the optimum conditions. Computer programs have been written to assist in the computation steps and in the prediction of optimum conditions⁸.

In this paper, a procedure is described that enables optimum solvent systems to be selected by simple experimentation. The application of the procedure to the separation of ten PAHs is demonstrated.

EXPERIMENTAL

The chromatographic work was performed using a Shimadzu LC-6A isocratic instrument equipped with a Model SPD-6A variable-wavelength UV spectrophoto-

metric detector. Samples were injected with a Rheodyne 7125 injector with a 20- μ l loop. The chromatographic data were collected and analysed on a Chromatopack C-R3A data processor.

All chromatographic runs were duplicated with a reproducibility between runs of $\pm 2\%$ or better. The void volume was obtained by using methanol as the unretained component for all mobile phases. The results obtained were within 1% of each other. The amount of sample injected did not affect the retention times at the concentrations used. Two reversed-phase columns were employed for the analyses: a Whatman Partisil-5 ODS-3 column of 5- μ m particle size (100 mm \times 4.6 mm I.D.) and a Perkin-Elmer 3 \times 3 HS C₁₈ column of 3- μ m particle size (33 \times length and 4.6 mm I.D.). The wavelength of the detector was set at 254 nm. The organic modifiers used were methanol, acetonitrile and isopropanol with water as the inert carrier. A flow-rate of 0.8 ml/min was used throughout. The Perkin-Elmer column was first used to determine the optimum mobile phase composition using the ORM scheme. Once the optimum mobile phase had been established, the Whatman column was then used to test the validity of the results of the optimization procedure.

Seven of the PAHs, fluoranthene, chrysene, fluorene, benzophenanthrene, dibenz[*a,h*]anthracene, benz[*a*]anthracene and coronene, were supplied by Fluka and were of the purest grade available. The remaining three PAHs, naphthalene, pyrene and phenanthrene, were obtained from Aldrich and their purities were better than 99%. HPLC-grade acetonitrile and methanol (J. T. Baker) and analytical-reagent grade isopropanol (Aldrich) were used for the preparation of the mobile phases. The A + B (*quantum sufficit* or sufficient quantity) addition method recommended by Runser⁹ was used. According to this method, correct volumes of organic modifier were first added, followed by water which was used to make up to the required volume. All the solvents were filtered through Millipore membrane filters and degassed in an ultrasonic bath.

The PAH mixture was prepared by dissolving known amounts of individual PAHs in the minimum amount of dimethyl sulphoxide (DMSO) and then diluting with the mobile phase. This procedure was essential as many of the PAHs are not very soluble in water. However, as DMSO has a high UV cut-off (330 nm), which might interfere with the analyses, the amounts used were kept as small as possible. The concentrations of the PAHs in the standard mixture ranged between 0.33 and 27.50 ng/ μ l. Owing to the possibility of degradation or decomposition of the PAHs under light, the standard solution was protected from light and stored in a cool location. Individual PAHs were also prepared in the same manner to assist in the identification. All the samples were filtered and degassed before injection into the column.

RESULTS AND DISCUSSION

A schematic diagram of the ORM scheme is illustrated in Fig. 1. The first step in the optimization procedure was to establish the goals of the process. For HPLC separations, this task is not always straightforward as the separation is governed by many factors and parameters¹⁰. Nevertheless, two criteria were used in the investigation reported here. The first was that all the peaks in the final chromatogram (*i.e.*, the "optimized" chromatogram) should have a resolution, R_s , of at least unity between peaks. The second criterion was that all the peaks should have capacity

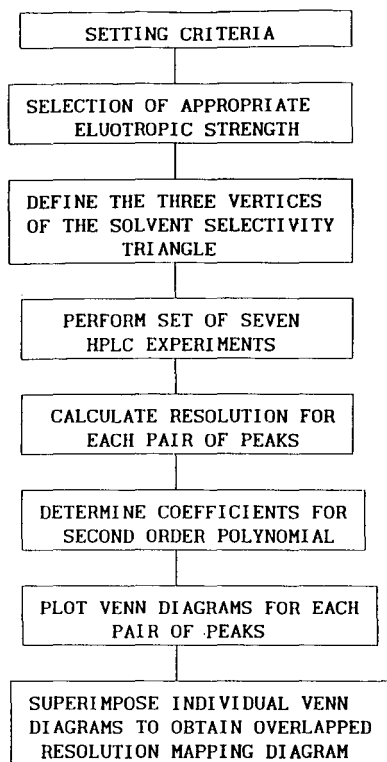


Fig. 1. Schematic diagram of the ORM scheme.

factors, k' , in the range 0–20, to ensure that the total analysis time falls within a reasonable range.

The next step was to identify the three vertices of the Snyder selectivity triangle⁷, which is illustrated in Fig. 2. The three points on the triangle (A, B and C) represent the three iso-elutropic binary mixtures (*i.e.*, organic modifier + carrier, water) of equivalent solvent strength. Before the composition of these three binary mixtures could be determined, it was first necessary to define the appropriate elutropic strength for the system. The elutropic strength was chosen so that the second criterion

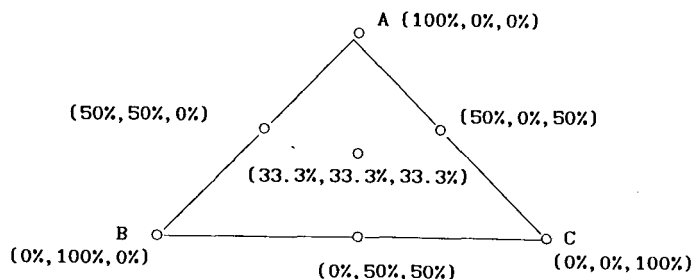


Fig. 2. Solvent selectivity triangle showing compositions (% v/v) of mobile phase consisting of mixtures of binary solvents A (methanol–water), B (acetonitrile–water) and C (isopropanol–water).

TABLE I

RESULTS OF PRELIMINARY RUNS USING ELUENT MIXTURES CONSISTING OF METHANOL AND WATER

<i>Methanol-water composition (v/v)</i>	<i>k' for last-eluting peak</i>	<i>Solvent strength</i>
60:40	26.0	1.80
70:30	22.0	2.10
72:38	19.5	2.16

TABLE II

MOBILE PHASE COMPOSITIONS IN TERMS OF VOLUME PERCENTAGES OF THE BINARY MIXTURES A (METHANOL-WATER), B (ACETONITRILE-WATER) AND C (ISOPROPANOL-WATER)

<i>Eluent mixture</i>	<i>A</i>	<i>B</i>	<i>C</i>
1	100.0	0.0	0.0
2	0.0	100.0	0.0
3	0.0	0.0	100.0
4	50.0	50.0	0.0
5	0.0	50.0	50.0
6	50.0	0.0	50.0
7	33.3	33.3	33.3

defined earlier could be satisfied. The selection was based on the suggestion by De Galan *et al.*¹¹, who recommended the use of methanol-water binary mixtures for identifying the mobile phase composition that gives k' values for all the peaks within the desired range (0–20). Consequently, three preliminary runs were carried out using methanol-water mobile phases with the compositions given in Table I. The results of these preliminary runs are also shown in Table I. The mobile phase methanol-water (72:28, v/v) gave the smallest capacity factor for the last-eluting component and

TABLE III

MOBILE PHASE COMPOSITIONS AS PERCENTAGES OF PURE SOLVENTS IN MIXTURE

<i>Eluent mixture</i>	<i>Concentration (% v/v)</i>			
	<i>Methanol</i>	<i>Acetonitrile</i>	<i>Isopropanol</i>	<i>Water</i>
1	72.0	0.0	0.0	28.0
2	0.0	70.0	0.0	30.0
3	0.0	0.0	51.6	48.4
4	36.0	35.0	0.0	29.0
5	0.0	35.0	25.8	39.2
6	36.0	0.0	25.8	38.2
7	24.0	23.3	17.2	35.5

TABLE IV

RETENTION TIMES (min) OF PAH COMPOUNDS IN EACH OF THE SEVEN ELUENT MIXTURES LISTED IN TABLE III

No.	Compound ^a	Eluent mixture						
		1	2	3	4	5	6	7
1	Cor	0.482	0.472	0.452	0.587	0.455	0.469	0.459
2	Nap ^b	2.050	0.940	1.210	1.408	1.056	1.517	1.186
3	Fl	2.697	1.260	2.041	5.782	1.517	2.685	1.828
4	Ph	2.952	1.405	2.157	2.518	1.652	2.836	1.995
5	Ft	4.280	1.783	2.679	3.484	2.080	3.820	2.649
6	Pyr	4.717	1.808	2.836	3.842	2.289	4.078	2.903
7	Benzo	6.408	2.285	3.580	4.963	4.573	5.443	3.623
8	BiB(a,h) ^b	2.230	4.332	3.582	13.822	3.115	5.518	3.766
9	Ch ^b	7.513	2.477	3.977	5.567	3.005	6.382	4.110
10	B(a)	7.798	2.542	4.196	5.783	3.135	6.724	4.268

^a (1) Cor = coronene; (2) Nap = naphthalene; (3) Fl = fluorene; (4) Ph = phenanthrene; (5) Ft = fluoranthene; (6) Pyr = pyrene; (7) Benzo = benzophenanthrene; (8) DiB(a,h) = dibenz[a,h]anthracene; (9) Ch = chrysene; (10) B(a) = benz[a]anthracene.

^b The standard mixture was spiked with this component to improve detection.

satisfied the second optimization criterion. This mobile phase was then selected as solvent A in the solvent selectivity triangle shown in Fig. 2. Subsequently, the solvent strength of this mobile phase was calculated using the following equation:

$$ST = S_a\phi_a + S_b\phi_b + \dots \quad (1)$$

where ST represents the solvent strength of the mixture, ϕ_i are the volume fractions of each component and S_i are the individual solvent strengths of the organic modifiers¹¹. After determining the solvent strength for mobile phase A, the other two iso-elutotropic

TABLE V

RESOLUTION BETWEEN ADJACENT PEAKS IN THE CHROMATOGRAMS OBTAINED USING THE SEVEN ELUENT MIXTURES LISTED IN TABLE III

Peak pair	Eluent mixture						
	1	2	3	4	5	6	7
1	4.094	4.216	4.181	4.829	4.237	4.579	3.978
2	0.636	1.981	3.890	4.933	2.573	3.877	2.748
3	1.550	0.773	0.461	3.217	0.666	0.453	0.775
4	0.702	1.622	1.968	0.630	1.909	2.512	2.956
5	3.648	0.108	0.555	1.824	0.830	0.561	0.972
6	0.991	2.344	2.446	1.132	1.568	2.826	2.055
7	2.918	0.736	0.006	0.386	0.925	0.182	0.357
8	1.670	0.247	1.254	0.003	0.375	1.481	0.836
9	0.425	4.680	0.864	11.843	0.057	0.408	0.363

mixtures B (acetonitrile–water) and C (isopropanol–water) could be calculated using eqn. 1. Four additional mobile phase compositions were then selected from the solvent selectivity triangle. The seven eluent mixtures chosen are listed in Table II and are also illustrated in Fig. 2. As the compositions shown in Table II are in terms of the binary solvents A, B and C, the actual compositions in terms of the pure solvents were recalculated and are given in Table III.

Experiments using these seven mobile phases were then performed and the results are listed in Table IV. All chromatographic results were obtained in duplicate with reproducibilities better than $\pm 2\%$. The void time for the Perkin-Elmer column was 0.38 min.

In addition to the standard mixture, individual PAHs were also analysed to assist in the identification and calculation of the resolution. From the results of the seven experiments the resolution, R_s , could be calculated using either of the following two equations:

$$R_s = \frac{1}{4} (\alpha - 1) N^{\frac{1}{2}} \left(\frac{k'}{k' + 1} \right) \quad (2)$$

$$R_s = \frac{2(t_2 - t_1)}{w_2 + w_1} \quad (3)$$

where R_s is the resolution for a pair of adjacent peaks, α is the relative retention ratio, N is the number of theoretical plates of the column, k' is the capacity factor for one of the peaks, t_i is the retention time of the i th peak and w_i is the width of the i th peak. The values of R_s calculated are listed in Table V.

Subsequently, the R_s values were fitted into a second-order polynomial:

$$R_s = a_1x_1 + a_2x_2 + a_3x_3 + a_{12}x_1x_2 + a_{23}x_2x_3 + a_{13}x_1x_3 + a_{123}x_1x_2x_3 \quad (4)$$

TABLE VI
COEFFICIENTS OF EQN. 4 FOR THE NINE PAIRS OF PEAKS

Peak pair	Coefficient						
	a_1	a_2	a_3	a_{12}	a_{23}	a_{13}	a_{123}
1	4.094	4.216	4.181	2.696	0.398	1.522	- 18.861
2	0.636	1.981	3.890	14.498	1.240	3.766	- 42.879
3	1.550	0.773	0.461	8.222	-1.358	-0.656	- 22.755
4	0.702	1.622	1.968	-2.128	2.296	2.868	32.076
5	3.648	0.108	0.555	-0.216	-5.086	0.918	0.597
6	0.991	2.344	2.446	-2.142	-0.602	1.724	6.516
7	2.918	0.736	0.006	-5.764	-2.148	-0.756	2.703
8	1.670	0.247	1.254	-3.822	-4.348	2.922	9.777
9	0.425	4.680	0.864	37.162	-2.350	9.456	-119.988

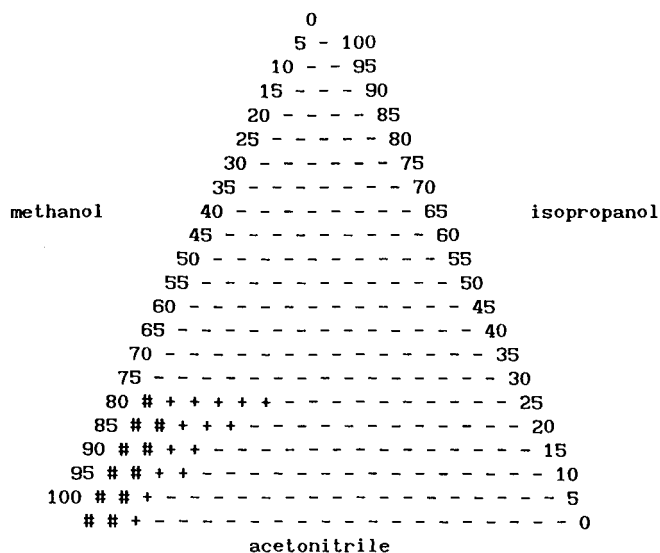


Fig. 3. Overlapping resolution diagram for the nine pairs of peaks. Symbols: --, $R \leq 0.5$; +, $0.5 < R < 1.0$; # $R \geq 1.0$.

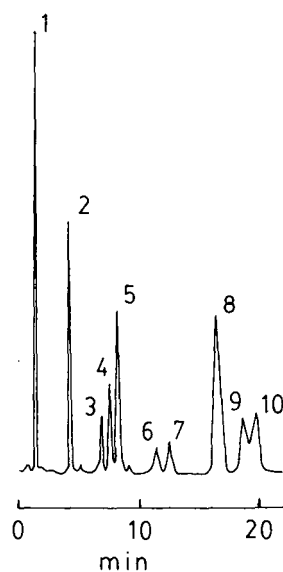
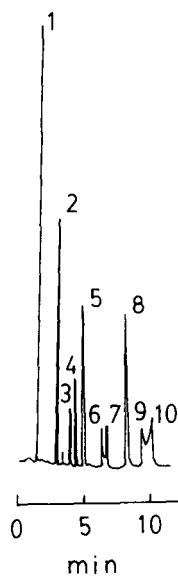


Fig. 4. Chromatogram of standard mixture of PAHs using a mobile phase consisting of methanol-acetonitrile-isopropanol-water (61.20:3.50:5.16:30.14, v/v). Column: Perkin-Elmer 3×3 HS C_{18} . Other chromatographic conditions as described in text. For peak identification, see Table IV.

Fig. 5. Chromatogram of standard mixture of PAHs using a mobile phase consisting of methanol-acetonitrile-isopropanol-water (61.20:3.50:5.16:30.14, v/v). Column: Whatman Partisil-5 ODS-3. Other chromatographic conditions as described in text. For peak identification, see Table IV.

where a_i are coefficients and x_i are the volume fractions of the mobile phases A, B and C. With the aid of a modified version of the Basic program given by Berridge⁸, the coefficients for each peak pair were determined. These coefficients are listed in Table VI. Using eqn. 4, together with the coefficients listed in Table VI, the R_s values for other mobile phase compositions within the solvent triangle could be calculated. These values were used to construct Venn diagrams or resolution plots for all the peak pairs. The individual resolution plots were then superimposed to give an overlapped resolution diagram, which is shown in Fig. 3. The area marked with # represents the optimum region where the solvent compositions would result in satisfactory separation of all the peaks (i.e., $R_s > 1$).

To confirm the results of the optimization procedure, an additional experiment using one of the mobile phase compositions in the optimum region was performed to verify that a satisfactory separation of all the peaks could be achieved. A mobile phase consisting of methanol–acetonitrile–isopropanol–water (61.20:3.50:5.16:30.14, v/v) was used for this purpose. A typical chromatogram obtained is illustrated in Fig. 4. Satisfactory separation was achieved for the ten PAHs. A further test was performed using a different column (the Whatman column). The same mobile phase was used and the chromatogram obtained is shown in Fig. 5. Complete separation was also observed. As the latter column is longer, longer retention times were observed.

The above results demonstrated that the ORM optimization scheme is a rapid and versatile method. Optimum separation can be achieved without much difficulty even when quaternary mobile phases are considered, because only seven different mobile phase systems need to be examined in order to obtain the necessary data for the resolution plots. Moreover, no re-optimization is required once the optimum mobile phases have been established. This would certainly be a useful advantage over many other optimization techniques, as a shorter column can be used first to determine the optimum mobile phase. Subsequently, a longer column can be used to improve the separation further if necessary. With such a scheme, the overall analysis time can be significantly reduced. Further, in any case of column failure during the course of the experiment, a new column with the same type of stationary phase can be used to replace the damaged column and there is no need to repeat the whole optimization procedure. This is, of course, a very useful feature of the ORM technique as it would mean that wastage of expensive solvents and analysis time can be minimized.

REFERENCES

- 1 C. P. Ong, H. K. Lee and S. F. Y. Li, *J. Chromatogr.*, 464 (1989) 405.
- 2 K. Ogan and E. Katz, *J. Chromatogr.*, 188 (1980) 115.
- 3 A. Colmjo and J. C. Maconald, *Chromatographia*, 13 (1980) 350.
- 4 M. L. Lee, D. L. Vassilaros, C. M. White and M. Novotny, *Anal. Chem.*, 51 (1979) 768.
- 5 K. Jinno, T. Hondo and M. Saito, *Chromatographia*, 20 (1985) 351.
- 6 J. L. Glajch, J. J. Kirkland, K. M. Squire and K. M. Minor, *J. Chromatogr.*, 199 (1980) 57.
- 7 L. R. Snyder, *J. Chromatogr. Sci.*, 16 (1978) 223.
- 8 J. C. Berridge, *Techniques for the Automated Optimization of HPLC Separations*, Wiley, Chichester, 1985, p. 91.
- 9 D. J. Runser, *Maintaining and Troubleshooting LC Systems, User's Guide*, Wiley, New York, 1981, p. 18.
- 10 J. P. Bounine, G. Guiochon and H. Colin, *J. Chromatogr.*, 298 (1984) 1.
- 11 L. de Galan, D. P. Herman and H. A. H. Billet, *Chromatographia*, 24 (1987) 108.

Regulation of peak compression effects for substituted benzamides in reversed-phase liquid chromatography

LARS B. NILSSON

Astra Research Centre AB, Bioanalysis, S-15185 Södertälje (Sweden)

SUMMARY

The possibilities of regulating peak compression effects, *i.e.*, of making the analyte peak coelute with the system peak, were investigated for substituted benzamides. The changes in capacity factor for the system peak relative to the retention of the analyte were studied by varying the composition of the mobile phase. The parameters useful for altering the capacity factor ratio were found to be the ionic strength of the phosphate buffer and to some extent the pH, whereas the amount of acetonitrile and the concentration of the amine modifier gave negligible effects. Variation of the amount of silanol groups on the solid phase could also be used as an efficient means for regulation of the capacity factor ratio.

INTRODUCTION

Mobile phases in reversed-phase liquid chromatography often contain additives, *e.g.*, ion-pairing reagents and competing ions, in order to change the retention and/or the selectivity or to improve the peak symmetry. When using such mobile phases, the injection of a sample not identical with the mobile phase will disturb the column equilibria and generate two kinds of peaks. The first kind is the ordinary peaks corresponding to the injected compounds. The other kind originates from the equilibrium disturbance and is called system peaks, as they reflect the concentration changes of the mobile phase components^{1–5}. A system peak is thus a zone with an excess or a deficit of a mobile phase component, eluting at a retention volume characteristic of that component. The theoretical treatment of system peaks has so far been limited to those developed by very small equilibrium disturbances (*e.g.*, ref. 6).

It has been shown that, under special circumstances, peak compression^{7–9} or peak deformation¹⁰ will occur for analytes coeluting with the system peak. The peak compression effect might give extremely narrow peaks and apparent efficiencies up to $5 \cdot 10^6$ plates/m have been observed¹¹, so this effect is of interest as a means of improving the sensitivity in liquid chromatography. One bioanalytical application has been published in which peak compression was applied to the determination of low levels of FLA 908, a minor remoxipride metabolite, in urine⁸. To be able to make

further use of the peak compression effects and to learn how to avoid peak deformation, a better understanding of these phenomena is necessary.

In earlier studies with tertiary amines as model compounds, the amine modifiers used in the mobile phase were *N,N*-dimethylalkylamines, the alkyl group varying from hexyl to dodecyl⁷⁻⁹. The system peaks for these modifiers have different capacity factors, giving retention "windows" in between. For analytes eluting in these retention windows, it has not been possible to obtain useful peak compression effects. The aim of this work was to find parameters that can be used for the fine regulation of the ratio of the system peak capacity factor to the analyte capacity factor and thereby broaden the applicability of the peak compression effect.

EXPERIMENTAL

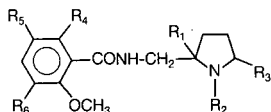
Chemicals

N,N-Dimethyloctylamine (DMOA) was obtained from ICN Pharmaceuticals (Plainview, NY, U.S.A.) and *N,N*-dimethylheptylamine (DMHA), *N,N*-dimethylnonylamine (DMNA) and *N,N*-dimethyldecylamine (DMDA) from Ames Labs. (Millford, CT, U.S.A.). Other chemicals, of HPLC or analytical-reagent grade, were obtained from the usual commercial sources and used as received.

The model compounds (Fig. 1) were substituted benzamides related to the neuroleptic compound remoxipride and synthesized at CNS Research and Development, Astra Research Centre (Södertälje, Sweden). Their syntheses have been described: compound II¹², compounds III-V¹³, compound VI¹⁴ and compound VII¹⁵.

Chromatography

Six different columns were used: a factory-packed Spherisorb ODS-1 (3 μm ; 100 \times 4.6 mm I.D.) from Phase Separations (Queensferry, U.K.), a factory-packed Nucleosil 120-3 C₁₈ (100 \times 4.6 mm I.D.) from Macherey-Nagel (Düren, F.R.G.), and four columns (100 \times 4.6 mm I.D.) with 5- μm Spherisorb ODS-1 and Spherisorb ODS-2 (Phase Separations) in different proportions (100:0, 75:25, 50:50 and 0:100). The mixed packing slurries were stirred for 1 h before the columns were packed. Methyl isobutyl ketone was used as a slurry medium and hexane as the eluent. The packing pressure was 400 bar.



	R ₁	R ₂	R ₃	R ₄	R ₅	R ₆
I (remoxipride)	H	C ₂ H ₅	2H	OCH ₃	H	Br
II	H	C ₃ H ₇	2H	OCH ₃	H	Br
III	H	C ₂ H ₅	2H	OCH ₃	Cl	Br
IV	H	C ₂ H ₅	2H	OCH ₃	Cl	Cl
V	H	C ₂ H ₅	2H	OH	Cl	Cl
VI	H	C ₂ H ₅	2H	OH	Br	OCH ₃
VII	OH	C ₂ H ₅	O	OCH ₃	H	Br

Fig. 1. Structure of model compounds.

The mobile phases were different concentrations of acetonitrile in phosphate buffers of various pH and ionic strengths, with or without the addition of amine modifiers (DMHA to DMDA). The flow-rate was 1.0 ml/min. The analytes were dissolved in phosphate buffer with the same pH and ionic strength as the mobile phase. The injection volume was 100 μ l.

The chromatographic system consisted of a Model 590 programmable pump (Waters Assoc., Milford, MA, U.S.A.), a Perkin-Elmer (Überlingen, F.R.G.) ISS-100 autosampler and a Perkin-Elmer LC-95 UV detector. The cell volume was 1.4 μ l and the detector was operated at 208 nm. A refractive index (RI) detector (Waters Model 410) was coupled in series with the UV detector and used to study the retention of the system peak. The UV detector signal was monitored with a Model SP 4270 integrator (Spectra-Physics, San Jose, CA, U.S.A.) and the RI detector signal was recorded with a Kipp & Zonen (Delft, The Netherlands) BD 41 recorder. To prolong the lifetime of the analytical column, a guard column dry-packed with Corasil (Waters Assoc.) was placed between the pump and the autosampler.

Determination of capacity factors

The column mobile phase volume, V_m , was measured by the injection of potassium nitrate. The system peak is the result of fairly large changes in the concentration of the amine modifier in the mobile phase. Being on the non-linear part of the adsorption isotherm, the retention volume for the system peak depends strongly on how it is generated. In this work, the retention volume was measured for the small positive system peak generated when phosphate buffer was injected. Effects on the peak shape can be expected when the capacity factor of this system peak is the same as the isocratic capacity factor of the analyte, *i.e.*, the ratio of these capacity factors is 1.0.

PRINCIPLE OF THE PEAK COMPRESSION EFFECT

A mobile phase with a UV-transparent cationic modifier, *e.g.*, DMNA, is used. The UV-absorbing amine analyte is injected dissolved in a solution of an organic anion, *e.g.*, nonyl sulphate, with a larger retention than the cationic modifier. This anion generates a system peak with a DMNA deficit and a nonyl sulphate peak containing the corresponding excess of DMNA. These peaks can be observed with RI detection (Fig. 2, top trace). The system peak is thus a zone of mobile phase with a lower concentration of DMNA, giving an increased retention of the amine analytes within this zone. If the analytes are injected dissolved in phosphate buffer, all three compounds show normal peaks (Fig. 2, middle trace). When the analytes are injected in a solution of a counter ion, the peak shapes for the analytes eluting before or after the system peak are hardly influenced at all, whereas the analyte coeluting with the system peak will elute in a narrow band (Fig. 2, bottom trace). This analyte will be trapped by the system peak and, owing to its higher retention within this zone of DMNA deficit, it will move more slowly than the zone until it reaches the higher DMNA concentration of the surrounding mobile phase where the analyte retention is equal to, or even higher than, the system peak retention. The result is that the analyte is concentrated in a narrow band at the back of the system peak⁷.

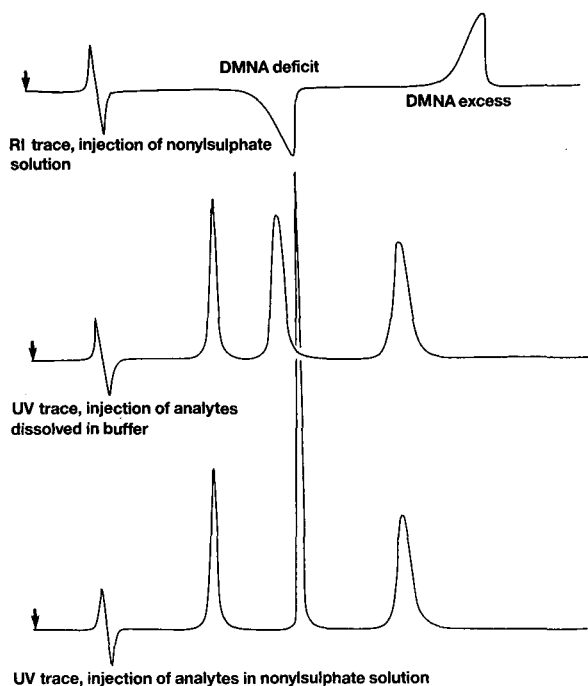


Fig. 2. Schematic representation of the peak compression effect exemplified with a mobile phase containing DMNA as the amine modifier and using nonyl sulphate in the solution injected to create the system peak.

RESULTS AND DISCUSSION

Choice of solid phases

The retention of basic compounds such as amines has been found to be correlated with the surface concentration of residual silanols¹⁶. Several simple chromatographic tests for residual silanols have been published¹⁶⁻¹⁸. In this paper, a test was performed by injecting a mixture consisting of two amines (compounds I and II, Fig. 1) with a high affinity to silanols, and a lactam (VII), a neutral compound expected not to be retained on silanols. Mobile phases with and without DMOA added to mask the residual silanols¹⁹ were used, and the influence of the DMOA addition on the retention of these three analytes was studied.

Two octadecylsilica columns with different specifications were initially compared: Spherisorb ODS-1, a low-carbon-content (7%) support with a large number of residual silanol groups, and Nucleosil 120-3 C₁₈, with a higher carbon-content (11%). On the latter (Table I) the amines elute earlier than the lactam for both mobile phases and the addition of DMOA does not change either the retention or the peak efficiency and symmetry. Hence, this batch of the support can be regarded as fully end-capped.

The results for Spherisorb ODS-1 (5- μ m) are completely different (Table I). The retention of the amines is high without DMOA, but decreases drastically when DMOA is added. Simultaneously, the peak efficiency and symmetry are improved. The retention, efficiency and symmetry of the lactam peak are not influenced by the

TABLE I

INFLUENCE OF AMINE MODIFIER ON CAPACITY FACTORS FOR TWO DIFFERENT OCTADECYLSILICA COLUMNS

Mobile phase: acetonitrile-phosphate buffer (pH 2.00, $I = 0.05$) (28:72, v/v) without or with 0.4 mM DMOA.

Compound	Column			
	Nucleosil 120-3 C ₁₈		Spherisorb ODS-1 (5 μ m)	
	Without DMOA	With DMOA	Without DMOA	With DMOA
I	0.78	0.72	9.26	2.01
II	1.37	1.25	18.9	3.95
VII	2.02	1.91	1.64	1.59

addition of DMOA. These results were as expected for the Spherisorb ODS-1 supports and indicate a high number of residual silanols. The results (not shown) for the 3- μ m Spherisorb ODS-1 gave an almost identical pattern but slightly shorter retention and higher efficiency.

For the study of peak compression effects, it is essential to use a support where the addition of an amine modifier, responsible for the system peak, has a pronounced effect on the retention of the analyte amines. Hence there should be a large difference in retention for an amine analyte within the system peak compared with outside. A support with a high number of residual silanols is, therefore, expected to give the strongest compression effects and the Spherisorb support was chosen for the peak compression studies.

Variation of the lipophilicity of the amine modifier

In order to obtain peak compression effects for a specific analyte, an amine modifier giving a system peak with a retention close to that of the analyte must be chosen. The retention of the system peak and the retention of the analytes using mobile phases with amine modifiers of different lipophilicity were studied (Table II). With

TABLE II

CAPACITY FACTORS WITH AMINE MODIFIERS OF DIFFERENT LIPOPHILICITY

Mobile phase: acetonitrile-phosphate buffer (pH 2.00, $I = 0.05$) (26:74, v/v) with 0.5 mM amine modifier. Spherisorb ODS-1 (5 μ m) was used.

Amine modifier	Compound				
	I	VII	II	III	System peak
DMHA	3.40	2.18	6.40	7.82	1.81
DMOA	2.21	2.21	4.19	5.31	2.50
DMNA	1.49	2.20	2.80	3.45	3.54
DMDA	0.87	2.14	1.69	2.26	5.15

increasing lipophilicity of the amine modifier, the system peak retention increases, whereas the amine analyte retention decreases. The lactam retention was constant, however. These results were as expected, but of more importance for the purpose of peak compression was the change in retention for the system peak relative to the analyte. This change is best illustrated by plotting the ratio of the capacity factor for the system peak to that of the analyte (Fig. 3). Peak compression effects, as mentioned above, can be expected when the ratio is about 1.0. Under these conditions, DMNA seemed to be a perfect choice if a peak compression effect was required for III, and DMOA might be useful for I. For II, DMNA gave too high a capacity factor ratio whereas the ratio using DMOA was too low. To be able to obtain peak compression effects also for II, a change of amine modifier is obviously not a suitable approach, and alternative means of regulating the capacity factor ratio must be found.

The compounds giving the system peak and the analytes are all tertiary amines, and changes in the mobile phase composition might be expected to have a similar influence on the retention of both kinds of peaks. However, amines might have different retentions as solutes and as mobile phase components, reflected in the different expressions for their capacity factors⁴. Further, in the present system an amine is added to the mobile phase to mask residual silanols and therefore the silanophilic part of the retention is probably much greater for the amine modifier, giving the system peak, than for the analytes. The influence of the mobile phase components on the retention for both kinds of peaks was studied to see if these assumed differences in retention mechanism could be useful for changing the capacity factor ratio and, thus, regulating the peak compression effects.

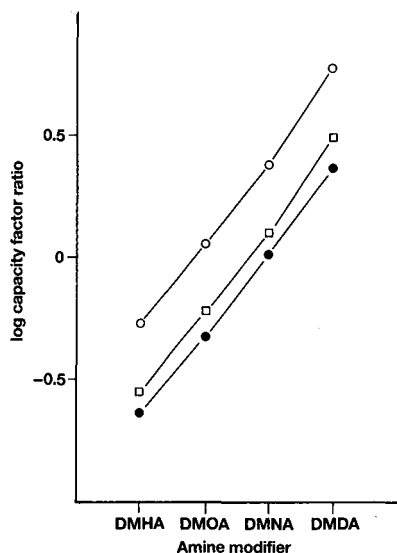


Fig. 3. Influence of the lipophilicity of the amine modifier on the capacity factor ratio. Spherisorb ODS-1 was used and the mobile phase was acetonitrile-phosphate buffer (pH 2, $I = 0.05$) (26:74, v/v) with 0.5 mM amine modifier. ○ = k' (system peak)/ k' (I); □ = k' (system peak)/ k' (II); ● = k' (system peak)/ k' (III).

TABLE III

INFLUENCE OF THE ACETONITRILE CONCENTRATION IN THE MOBILE PHASE ON THE CAPACITY FACTOR RATIO

Mobile phase: acetonitrile-phosphate buffer (pH 2.00, $I = 0.05$) (28:72, v/v) with 0.6 mM DMOA. Spherisorb ODS-1 (5 μm) was used.

Acetonitrile concentration (%)	Compound		
	I	II	III
23	1.13	0.58	0.44
25.5	1.10	0.57	0.45
28	1.08	0.55	0.45
30.5	1.05	0.52	0.44
33	1.01	0.52	0.45

Variation of the acetonitrile and amine modifier concentrations

With DMOA as the amine modifier, the acetonitrile concentration of the mobile phase was varied from 23 to 33%, giving a 2-fold decrease in the capacity factors for both the system peak and the analytes. For I, with about the same capacity factor as the system peak, and also for II there was an insignificant decrease in capacity factor ratio with increasing acetonitrile concentration, whereas for III the ratio was constant (Table III).

Changing the amine modifier concentration from 0.4 to 1.2 mM gave a more than 2-fold decrease in all capacity factors, but the ratios were constant (Table IV). Variation of the acetonitrile or amine modifier concentration is therefore not useful for changing the capacity factor ratio. In a study by Fornstedt *et al.*^{20,21}, using protriptyline as the amine modifier, changes in the capacity factor ratios were observed when amine modifier concentrations of 0.0076, 0.20 and 0.95 mM were compared. These changes are probably a reflection of the change in coverage of the silanophilic site. The coverage was found to be 3, 41 and 78%, respectively. Peak compression effects were found only at the two highest concentrations²¹.

TABLE IV

INFLUENCE OF THE MOBILE PHASE DMOA CONCENTRATION ON THE CAPACITY FACTOR RATIO

Mobile phase: acetonitrile-phosphate buffer (pH 2.00, $I = 0.05$) (28:72, v/v) with DMOA. Spherisorb ODS-1 (3 μm) was used.

DMOA concentration (mM)	Compound		
	I	II	III
0.4	1.26	0.71	0.57
0.6	1.22	0.70	0.54
0.8	1.21	0.70	0.54
1.0	1.18	0.68	0.51
1.2	1.20	0.70	0.52

Variation of the pH and ionic strength of the phosphate buffer in the mobile phase

The ionic strength of the phosphate buffer was varied from 0.02 to 0.20 at pH 2.00, 2.50 and 3.50. Five amine model compounds and the lactam were injected. The capacity factor of the lactam was the same for all mobile phases. The plots of $\log k'$ against ionic strength at pH 2.00 show a small decrease in the capacity factor for the amine compounds when the ionic strength increases, but on the other hand the capacity factor for the system peak increases (Fig. 4). The plots for the analytes are parallel, except for a slight decrease in retention when the analyte elutes close to the system peak. A probable explanation is that the system peak resulting from an injection of buffer is a zone with an excess of DMNA, thus giving coeluting analytes a shorter retention. At pH 2.50 (not shown), the results were very similar to those at pH 2.00, whereas at pH 3.50 the decrease in retention for the analytes and the increase in retention for the system peak were more pronounced than at pH 2.00 (Fig. 5).

The capacity factor ratio plots (pH 2.00 in Fig. 6 and pH 3.50 in Fig. 7) illustrate the rapidly decreasing ratios at ionic strengths below 0.1. At pH 3.50, it is possible to obtain an almost 3-fold change in ratio. A probable explanation for the opposite behaviour of the system peak and the amine analytes is a more extensive distribution of the amine modifier to the solid phase with increasing ionic strength. The amine analytes will then experience an increasing competition for the sites and the retention will decrease. It should be noted that at pH 3.50, using the same amine modifier, it is possible to obtain peak compression effects for four of the five analytes by using buffers with different ionic strengths. For V, a more lipophilic amine modifier must be used.

The influence of pH on the capacity factor ratio at low ionic strength is shown in Table V. The ratios are the same at pH 2.00 and 2.50 but decreases at pH 3.50. At higher ionic strengths, the ratios are independent of pH.

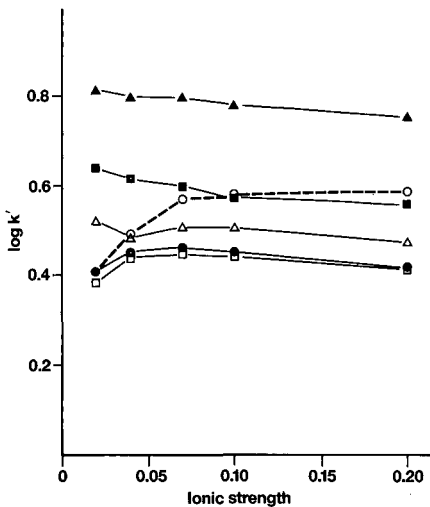


Fig. 4. Influence of ionic strength on the capacity factor at pH 2.00. The column was Spherisorb ODS-1 and the mobile phase was acetonitrile-phosphate buffer (pH 2, $I = 0.02-0.20$) (30:70, v/v) with 0.5 mM DMNA. ○ = System peak (broken line); □ = II; △ = III; ● = IV; ■ = VI; ▲ = V.

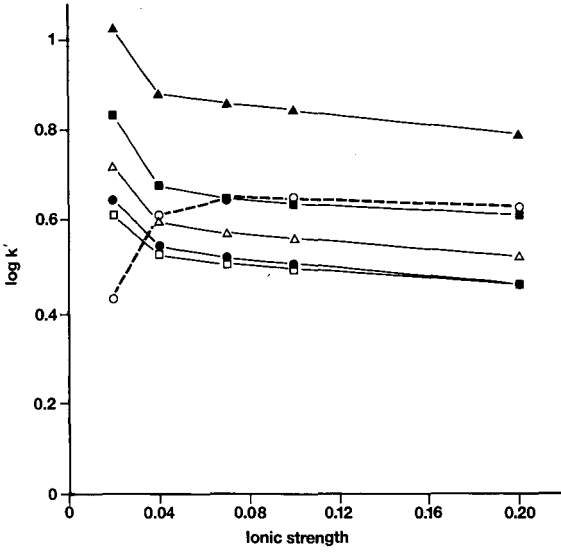


Fig. 5. Influence of ionic strength on the capacity factor at pH 3.50. Conditions and symbols as in Fig. 4.

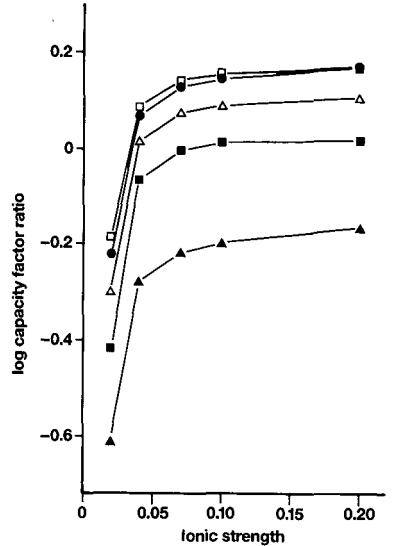
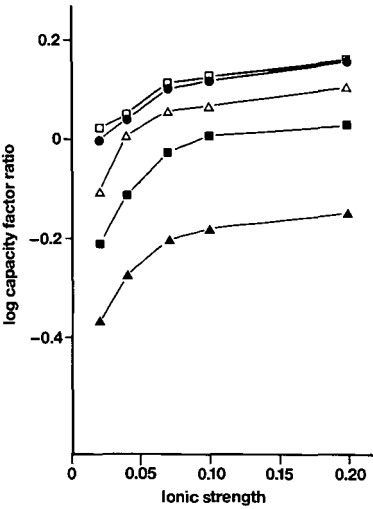


Fig. 6. Influence of ionic strength on the capacity factor ratio at pH 2.00. Conditions as in Fig. 4. $\square = k'$ (system peak)/ k' (II); $\Delta = k'$ (system peak)/ k' (III); $\bullet = k'$ (system peak)/ k' (IV); $\blacksquare = k'$ (system peak)/ k' (VI); $\blacktriangle = k'$ (system peak)/ k' (V).

Fig. 7. Influence of ionic strength on the capacity factor ratio at pH 3.50. Conditions as in Fig. 4 and symbols as in Fig. 6.

TABLE V
INFLUENCE OF pH ON THE CAPACITY FACTOR RATIO

Mobile phase: acetonitrile–phosphate buffer (pH 2.00–3.50, $I = 0.02$) (30:70, v/v) with 0.5 mM DMNA. Spherisorb ODS-1 (5 μm) was used.

pH	Compound				
	II	IV	III	VI	V
2.00	1.06	1.00	0.77	0.58	0.39
2.50	1.06	1.00	0.76	0.58	0.38
3.50	0.66	0.61	0.51	0.39	0.25

Varying the ionic strength, and at low ionic strengths also varying the pH, can thus be useful for the fine regulation of the peak compression effect. However, it is not the ideal tool as very small variations in the ionic strength can have a drastic effect on the capacity factor ratio. An extremely careful preparation of the buffer is necessary.

Influence of the support

As the amount of silanols is very important for the retention of amines, experiments were designed in which the amount of silanols in the column was varied. This was done by packing columns where Spherisorb ODS-1 was mixed with Spherisorb ODS-2. According to the manufacturer's specification, ODS-2 is "fully capped" with a bonded phase loading of 0.5 mmol/g (12%), whereas ODS-1, as mentioned above, is "partially capped" with a loading of 0.3 mmol/g (7%). Four columns were packed, with ODS-1 to ODS-2 ratios of 100:0, 75:25, 50:50 and 0:100. All four columns gave excellent efficiency (60 000–80 000 plates/m, calculated using the peak width at half-height) for the neutral compound VII, which is not sensitive to the presence of silanols. As expected for amines retained mainly on the residual silanols, the capacity factors decreased with increasing amounts of ODS-2 (see Table VI). The efficiency of the amine peaks decreased with an increasing amount of

TABLE VI
INFLUENCE OF THE SUPPORT ON THE CAPACITY FACTORS

Column 1, 100% ODS-1; column 2, ODS-1–ODS-2 (75:25); column 3, ODS-1–ODS-2 (50:50); column 4, 100% ODS-2. Mobile phase: acetonitrile–phosphate buffer (pH 2.00, $I = 0.05$) (28:72, v/v) without or with 0.5 mM DMNA.

Compound	Column 1		Column 2		Column 3		Column 4	
	Without DMOA	With DMOA	Without DMOA	With DMOA	Without DMOA	With DMOA	Without DMOA	With DMOA
VII	1.87	1.83	1.71	1.64	1.58	1.49	1.37	1.33
I	17.0	1.83	10.5	1.15	8.38	0.97	3.80	0.67
II	33.5	3.49	21.2	2.30	16.8	1.98	6.87	1.45
System peak	—	3.54	—	3.08	—	3.00	—	2.92

ODS-2, from about 30 000 plates/m for 100% ODS-1 to about 4000 plates/m for 100% ODS-2.

The addition of DMNA to the mobile phase gave drastically reduced capacity factors for the amines on all four columns (Table VI). The decrease in capacity factor with increasing amount of ODS-2 still occurred, but to a smaller extent. The efficiency for the lactam peak was not changed whereas an improvement was seen for the amines, giving about 80 000 plates/m for 100% ODS-1 and 50 000 plates/m for 100% ODS-2. The retention of the system peak decreased only slightly with an increasing percentage of ODS-2, resulting in an increase in capacity factor ratio (Fig. 8). The use of mixed supports is obviously an interesting means of regulating peak compression effects as a more than 2-fold change in capacity factor ratio occurred. The manipulation of the amount of silanols on the column gives the possibility of optimizing peak compression effects also at high ionic strength. As small changes in the ionic strength of the phosphate buffer then will not affect the capacity factor ratio, this should give more robust systems.

For the ODS-2 column, it can also be noted that the drastic decrease in retention for amines on adding DMNA to the mobile phase, and also the inferior peak shape and efficiency without DMNA, indicate a considerable amount of residual silanols also on this "fully capped" support.

CONCLUSION

There are several ways of regulating peak compression effects. First, the proper amine modifier is chosen. Fine regulation can then be achieved by selecting a column with a suitable amount of silanols and by adjusting the ionic strength and the pH of the

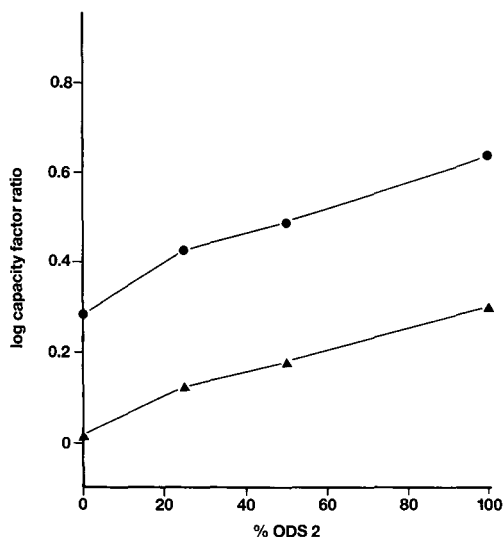


Fig. 8. Influence of the support on the capacity factor ratio. The columns were packed with mixed supports: column 1, 100% Spherisorb ODS-1; column 2, ODS-1-ODS-2 (75:25); column 3, ODS-1-ODS-2 (50:50); column 4, 100% ODS-2. The mobile phase was acetonitrile-phosphate buffer (pH 2, $I = 0.05$) (28:72, v/v) with 0.5 mM DMNA. ● = k' (system peak)/ k' (I); ▲ = k' (system peak)/ k' (II).

mobile phase. Using these methods, it seems possible to obtain peak compression effects for all amine analytes within the studied capacity factor range. Work is in progress to demonstrate how these findings can be used in practical work.

ACKNOWLEDGEMENTS

The author thanks Prof. Douglas Westerlund and Dr. Thomas Nordgren for valuable comments on the manuscript.

REFERENCES

- 1 M. Denkert, L. Hackzell, G. Schill and E. Sjögren, *J. Chromatogr.*, 218 (1981) 31.
- 2 L. Hackzell and G. Schill, *Chromatographia*, 15 (1982) 437.
- 3 G. Schill and J. Crommen, *Trends Anal. Chem.*, 6 (1987) 111.
- 4 J. Crommen, L. Hackzell, G. Schill and D. Westerlund, *Chromatographia*, 24 (1987) 252.
- 5 S. Levin and E. Grushka, *Anal. Chem.*, 59 (1987) 1157.
- 6 J. Crommen, G. Schill and P. Herne, *Chromatographia*, 25 (1988) 397.
- 7 L. B. Nilsson and D. Westerlund, *Anal. Chem.*, 57 (1985) 1835.
- 8 L. B. Nilsson, M. Widman, B. Bryske and D. Westerlund, *Chromatographia*, 22 (1986) 283.
- 9 M. Johansson and D. Westerlund, *J. Chromatogr.*, 452 (1988) 241.
- 10 T. Fornstedt, D. Westerlund and A. Sokolowski, *J. Liq. Chromatogr.*, 11 (1988) 2645.
- 11 L. B. Nilsson, unpublished results.
- 12 T. de Paulis, Y. Kumar, L. Johansson, S. Råmsby, L. Florvall, H. Hall, K. Ängeby-Möller and S.-O. Ögren, *J. Med. Chem.*, 28 (1985) 1263.
- 13 T. de Paulis, Y. Kumar, L. Johansson, S. Råmsby, H. Hall, M. Sällemark, K. Ängeby-Möller and S.-O. Ögren, *J. Med. Chem.*, 29 (1986) 61.
- 14 T. Högberg, S. Bengtsson, T. de Paulis, L. Johansson, P. Ström, H. Hall and S.-O. Ögren, *J. Med. Chem.*, 33 (1990) 1155.
- 15 L. Gawell, C.-E. Hagberg, T. Högberg and M. Widman, *Acta Chem. Scand.*, 43 (1989) 476.
- 16 L. Nondek, B. Buszewski and D. Berek, *J. Chromatogr.*, 360 (1986) 241.
- 17 P. C. Sadek and P. W. Carr, *J. Chromatogr. Sci.*, 21 (1983) 314.
- 18 L. C. Sander, *J. Chromatogr. Sci.*, 26 (1986) 380.
- 19 A. Sokolowski and K.-G. Wahlund, *J. Chromatogr.*, 189 (1980) 299.
- 20 T. Fornstedt, D. Westerlund and A. Sokolowski, *J. Chromatogr.*, 506 (1990) 61.
- 21 T. Fornstedt, personal communication.

CHROMSYMP. 1691

Towards a chromatographic quantitor

PAUL A. BRISTOW

Imperial Chemical Industries plc, Pharmaceutical Department, Hurdsfield Industrial Estate, Macclesfield, Cheshire SK10 2NA (U.K.)

SUMMARY

A specification is outlined for a quantitation system which takes chromatographic signals from one or more single or multichannel detectors, records more than one chromatogram, and uses objective chromatographic information provided by the operator. This information will help estimate the comparative concentration, and its uncertainty of selected components. The advantages of this approach are compared to the limitations of conventional integration of single chromatograms. Some tentative suggestions for implementation are given.

INTRODUCTION

Chromatography is the source of many quantitative analytical results and the quantitation of chromatograms is a vital part of an analyst's professional tools. Analytical results are almost always referenced to *some* standard material: whether it is yesterday's batch or National Bureau of Standards certified Standardised Reference Material, the answers are relative. Current commercial systems concentrate on integration of individual chromatograms. They fail to meet the two real needs of analysts: the comparison of unknown and standard samples yielding an estimate of comparative concentrations of components, and an estimate of their uncertainty.

These simply stated requirements are not met by any commercial systems, nor described in the chromatographic literature. The history of quantitative chromatography is refinement of single chromatogram integration, a difficult task constrained by very wide dynamic range signals, and until recently, too little storage space to keep even one whole chromatogram in fast access memory. The hardware no longer constrains us. This paper proposes a new approach to the whole problem and outlines a specification. Its objective is to encourage discussion and refinement of the specification by analysts, and commercial implementation. Some research, and considerable development, will be needed to implement systems of this sort. They will be large software systems requiring professional production tools such as high level languages of certified compliance to international standards. They should be independently validated to public standards. For brevity a system of this class will be called a chromatographic quantitor. (It is worth noting that the historical record in

the chromatographic literature¹⁻¹⁴ is sparse compared to the proprietary information guarded by integrator vendors, and in contrast to the importance of these unpublished algorithms to analysts using them. With so much secrecy, thorough validation is impossible.)

SCOPE

The scope of the quantitator concept is all separation systems using elution from a column with serial detectors, for example gas and liquid chromatography, ion chromatography, amino acid analysers with all detectors, and detectors scanning a sorbent like thin-layer chromatography. The quantitator software might be built into a chromatograph, perhaps in ROM (Read Only Memory firmware), externally as part of a data system, or a combination. The principles apply whether the detector(s) is (are) single- or multi-channel though the implementation problems are quite different if more than a few channels are involved. The UV diode-array detector is the most important multi-channel detector. It is suggested that all implementations cater for at least two channels, and solve the problem of synchronisation of detectors in series when one will lag by a constant time. Beyond a few channels, different computational techniques will be needed^{15,16}. In the following discussion it is assumed that the quantitator has some control over the chromatograph. If automatic control is not implemented, this may require the analyst to alter settings manually.

WHY DO INTEGRATORS FAIL TO QUANTITATE RELIABLY?

There can be few users of chromatography who have not seen integrations which even novice chromatographers can dismiss as nonsense. Worse still is that integrators rarely warn when results are unreliable, even when this is obvious to the human eye. I submit that this is because the chromatographer has information which has not been given to the integrator, and without which integrators are doomed to unreliability. Moreover, until algorithms for processing digitised analog voltages are given, and can accept, all the available information, they can never produce the best possible estimates of quantities, nor useful estimates of uncertainty. Even if information can be inferred from closer examination of the data, reliability and credibility will be improved if it can be checked against operator input information. For example, it may be possible to deduce the unretained peak time from a chromatogram, but it is still worth checking that this agrees with an operator input value and thus compute confidence limits for this time. It will probably be more accurate to use a column bore input by an operator, but useful to cross check that this information is not grossly wrong, for example 0.46 instead of 4.6 mm. Apart from some assumptions, usually rather weak, about peak shape made by integration algorithms, the only other source of information is the so-called integration parameters.

INTEGRATION PARAMETERS

Chester and Cram¹ in 1971 showed that "...the limits of integration have an astounding effect on the accuracy...". Many current problems with reliability of integration are still rooted in the need for integration parameters from the operator. It

is undesirable that the adjustment of integration parameters provides the user with a way of manipulating the results and not consistent with Good Laboratory Practice or quality standards like ISO 9000. Integration parameters are idiosyncratic and not portable.

Of course, the integrator needs to have any information that cannot be inferred from the chromatogram, such as whether isothermal or isocratic conditions apply, or whether any switching takes place, and when negative peaks are reasonable. For example, when a quantitor has assessed sample chromatogram(s), it should be much better than the operator at assessing the effect of different analog to digital sampling rates. If the sampling rate is controlled by hardware, a change in rate might necessitate reinjection of some or all samples.

Although many commercial systems have progressed in reducing the number of integration parameters required from the operator, a quantitor must not require, nor even permit, any at all. The input must be objective, observable and thus portable between systems, for example column length or flow-rate.

INFORMATION AVAILABLE TO A QUANTITATOR

To quantitate, information can be obtained from the operator, calculated from the basic theories of chromatography, deduced from the analog signal, extrapolated from previous chromatograms using the same column or previous injections of the same and other samples, and confirmed from expectations of results.

(1) The operator might tell, for example, the column size, flow-rate, isocratic or gradient elution, size and type of packing material.

(2) From chromatographic theory for liquid chromatography the algorithm might calculate, for example, the elution volume of unretained substances and the monotonic change in peak width under isocratic elution. Appropriate theory for the type of chromatography, gas or liquid, eluted or developed like thin layer chromatography, must be used of course.

(3) From the analog signal the algorithm might deduce, for example, the character of detector noise and analog-to-digital quantisation¹⁷ and the effect this will have on peak start and end detection and thus the uncertainty of peak area measurement¹⁸⁻²². Because of the changing nature of noise and the large number of measurements needed to determine noise, it is impractical to ask the operator to estimate this information. However, it would be useful to ask for an expectation, perhaps from the instrument specification or previous performance, to allow a check for satisfactory operation, for example checking that the deuterium lamp does not need replacing.

(4) Previous injections will hold information about the actual peak shape for this column, and previous chromatograms of the same sample will allow extrapolation to predict the peak shape expected for a particular component for future injections. Peaks with un-chromatographic shape, for example, with a flat top (not detected at all by integrators), must have a very high uncertainty.

Pattern matching by using peak shape must surely be the most sensitive and reliable method²³⁻²⁵.

(5) Informed expectations, for example that the sample will be 0.95 to 1.05 times the standard, are an important and underused source of information.

ANALOG SIGNALS

The obvious input to a quantitator is the raw analog detector signal. This must be converted to digital form either by sampling very frequently using an auto-ranging high-speed analog-to-digital converter (typically sampled at line frequency or integrated by counting pulses from a voltage-to-pulse converter less frequently, clearing at each time slice).

Because analog signals are degraded the longer the transmission distances, it is almost certainly best to place the analog-to-digital converter inside the chromatograph. (It can never be best, as many diode detectors are linked at present, to convert to a digital signal and then back to an analog signal which is fed to an analog-to-digital converter in the integrator.) Whatever the mechanism, these data must be transferred to the quantitator automatically (and error free). Data compression algorithms can be used to reduce the volume without any information loss, that is the original data can be obtained exactly by expanding the compressed data. Digital filtering can also reduce the data volume, with negligible loss of information if applied correctly. Combining too many adjacent time slices, for example, would materially reduce the chromatographic information.

There is a continuous spectrum of rawness of data from 100 μ s analog-to-digital samples at line frequency, through integrated time slices of about a second, up to the final peak areas and uncertainties. The only information output really required is component concentrations and their uncertainty²⁰. Only when a quantitator is proven can we safely regard this information as the rawest data that need to be stored permanently to conform to "good laboratory practice". This validation will not be a trivial task. Meanwhile the arid debates on "what are raw data?" will no doubt continue.

Comparison with a modern balance may be helpful. After a sample is placed on the pan and released, weights are taken many times per second. Only when the variance of weight reaches a target value (usually implicitly plus or minus about the least significant digit) is a weight actually recorded, for example in a laboratory information management system (LIMS). Because the algorithm for weighing is simple, and can be tested simply by placing known weights on the balance, we regard it as well-proven (perhaps naively). We would not consider storing all the weighings taken: nor should we need to for chromatography.

IMPLEMENTATION

The implementation problem of how to get and store this information will not be discussed further, except to note that it would be too tedious if the operator had to answer questions on all the conceivable conditions for every chromatogram. A store of data will be needed, filled initially with suitable default values, for example with 4.6 mm bore for liquid chromatography but 0.25 mm for capillary gas chromatography. It must be possible to notify a quantitator of changes, in the flow-rate, for example, perhaps automatically if the quantitator can communicate with the pump. As other information becomes relevant, a quantitator must be able to ask for it, and to resolve conflicts between information supplied and that deduced from the analog record. Implementors will have ample chance to show their user-friendliness, but automatic interrogation of the hardware will be even more friendly and reliable.

It is not yet clear how much information should be input (and output) interactively with the operator, and how transfers to and from any LIMS should be done. For example, final results need to be stored in a LIMS, methods loaded from LIMS, and sample sequence information sent to a quantitator. It may prove impractical or undesirable to store standard chromatograms and extensive history of results in a quantitator (it might imply disc storage) but it is essential to implement a portable interface between LIMS and quantitator so that the quantitator can ask LIMS to store or provide data. When results validation is considered there are some tests that quantitator cannot reasonably perform. For example, checking against an expected value, and upper and lower limits should be carried out by quantitator but assessing the rate of product degradation can only reasonably be carried out by a LIMS. Uncertainty estimates will surely be stored with each result.

PORTABILITY

An important implementation objective is that the information, and thus the method of analysis, shall be portable. This means that if the same input data, for example both digitised analog data and chromatographic data like flow-rate, are fed to more than one quantitator, the results should not differ more than the (un)certainty or confidence limits. (This does not mean that one quantitator cannot be better than another in being able to justify smaller uncertainty estimates, perhaps at the expense of computation time or memory size).

At present, if an analysis is carried out by using one chromatography data system, we cannot be confident that the same results will be obtained from another type of data system, even after choosing integration parameters to suit the new system. In practice, the work involved in re-validating the method is so great that it is skimped. Because standards may change, for example over the decades of life of a pharmaceutical compound, even if all the validation work is repeated, comparisons are not without risk. Without uncertainty estimates, the comparison of results from different systems always carries some risk.

SAMPLES AND THE INFORMATION THEY MAY YIELD

It may be helpful to classify, at least roughly, samples which may be available, and the information a quantitator may derive from them.

Reference samples

These are often the purest available, with information on purity, and impurities if known from other analytical methods, and an uncertainty estimate for this additional information. Classification as reference or standard is, of course, an arbitrary decision made by the analyst.

Typical samples

These will contain more than one component, but not contain more impurities than most of the samples to be analysed.

Control samples

These are synthetic mixtures of standards and the matrix. They should reveal the effect of the matrix on the analysis.

Atypical samples

These will contain unusual concentrations of components. For example, the liquor after crystallisation will often contain much of the impurities in the purified sample and these may be the purest sample of the impurities that can be obtained. The retention time, and perhaps spectrum or relative response in ultraviolet and refractive index detection, can be best assessed from these type of sample. This information can be used to estimate how well they can be measured in more typical samples.

Pure samples of impurities

Sometimes quite pure samples of some impurities are available. Occasionally, chemists can be persuaded to synthesise these specially!

Internal standards

These may show the effect of sample preparation and variation in injection volume. They may also provide useful markers for retention times.

Blanks

Samples in which some standard(s) have zero concentration.

REPLICATE RESULTS

In estimating uncertainty, the number of replicates of integrations of injections are usually too few (often two or three) to be statistically interesting compared to the peaks measured with hundreds of rather precise digitised voltages (better than 12 bit or 1 in 4096 relative to a nearby reading). [Manufacturers' claims of over 20 bits refer more to the range of voltages that can be measured and obscure the precision and/or accuracy with which any particular voltage can be measured, usually between 12 bits (1 in 4096) and 16 bits (1 in 65538)]. Digitisation can cause computational noise¹⁷.

Results from replicate injections also contain the confounding influence of the many operating conditions that will vary between injections.

EXPECTED RESULTS

The quantitator might be able to use any prior knowledge about expected results. For example, if we are measuring the degradation of a batch of material then any significant increase in the concentration of the main component is not plausible. We can extrapolate from measurements on previous batches of the same material, and measurements on this batch at earlier times to give an expected degradation (and an uncertainty estimate). Armed with the data from previous analyses, a quantitator could assess the significance of differences between expectations and result, and determine the number of replications necessary to achieve a arbitrary level of confidence, or advise the level of confidence as a function of the number of replicates. This would follow the current practice of repeating suspect results without sinking to repeating the analysis until the expected result is obtained!

UNEXPECTED RESULTS

A quantitor might also respond specially to results outside expected limits, for example outside 95 to 105% of a nominally pure standard. The principle proposed is that the risk of accepting a result is lower the more nearly it meets expectations.

UNCERTAINTY ESTIMATES

Errors can be absolute inaccuracy of concentration if standards containing known concentration (and known inaccuracy of concentration) are available. If standards are not available, then uncertainty must be expressed as precision of peak area, in, say, $mV \cdot s$. For this reason the term "uncertainty estimate" is used in this paper. As usual, the error will vary with concentration or peak size, height and/or area, and only variation of the concentration of component(s) in standard chromatogram(s) will allow this to be explored in detail^{26,27}.

CONFIDENCE

An indicator of the confidence we can place in the uncertainty estimate would also be useful. The simplest is the number of measurements, related to degrees of freedom in the jargon of statistics, but it might be helpful in view of the complexity of combined uncertainty estimation to compute an explicit estimate of the uncertainty in the uncertainty estimate—"a variance of the variance". If it is based on only a few chromatograms this value will be rather rough, but for hundreds of samples both the uncertainty estimate and its variance will become quite well defined, correctly reflecting the real situation. Confidence could also be expressed by upper and lower confidence limits with some arbitrary probability.

POSSIBLE METHODS OF PEAK AREA UNCERTAINTY ESTIMATION

Detector noise and pump flow-rate variation can probably be considered separately. Liquid flow-rate imprecision has always been impossible to measure well enough at high enough speed. Retention time is a highly integrated value and its variation only places very wide limits on the short-term variations. The detector noise is easier to tackle, and may well dominate errors. The most serious uncertainties in peak area assessment arise from uncertainties about peak start and stop points, especially on long tails, of course. For many chromatograms (especially isothermal and isocratic) the noise on the baseline can be studied in detail and its frequency distribution¹⁸ assessed quite well, if necessary, by monitoring for quite long periods without injection. There are usually some quiet sections of undoubted baseline before injection or during chromatograms, for example before the first peak is eluted.

A naive method of establishing error limits would be to establish a point at which the peak-start criterion is not yet met, and another at which the peak has undoubtedly started, the peak-start point normally used lying somewhere midway. Similarly peak-end limits could be calculated (and would usually be wider apart because of tailing). The peak noise might be added to or subtracted from the observed reading to estimate these points. The baseline and peak area could then be calculated assuming

the first start and last end point, and then the last start and first end, and thus the uncertainty estimated from their differences from the most probable estimate from midway start and end points. For groups of peaks, the computations are more complex, but in principle the valley positions suffer a similar uncertainty.

More sophisticated curve fitting and deconvolution methods^{23,25,28-51} might well lead to better estimates. Deconvolution would achieve more acceptance by users if they knew how reliable its results were. Estimation of uncertainty must correctly reflect the reality that measurement of small peaks before large ones is much better than measuring on the tail of the large peak. This has important advantages in the use of the uncertainty as a criterion for optimisation⁵².

PEAK HOMOGENEITY

The reliability, or accuracy, of chromatography is most seriously compromised when a peak represents more than one component and this is not sensed.

Our most precise detectors, the flame-ionisation detector and the single-wavelength ultraviolet detector, are non-identifying⁵³. They provide no information about peak homogeneity, apart from peak shape. Only by *comparison* of chromatograms can we assess the limits on homogeneity. As more chromatograms are compared, a better assessment can be made. For example, if a series of samples, perhaps interposed with standards, are being run and the column performance is steadily being degraded by sample debris or column decay, it is possible to predict the most likely and worst likely peak shape for the next sample. If the next sample produces a wider peak, then we must suspect a hidden peak. A quantitator algorithm would probably request a standard chromatogram or two which would confirm or deny the diagnosis: rejection of the sample result might be premature.

Detectors combining techniques (so-called hyphenated) are usually much less reliable than chromatography (the liquid branch of which has an unenviable reputation itself) but they, and all multichannel detection, dramatically improve the chance of sensing hidden peaks.

During the next half decade, the diode array detector will gain enough computer power to give useful information on peak non-homogeneity⁵⁴, but this will compound the quantitation problem because the area (or volume) integrating role will become embedded into the factor analysing function. It alone promises to be no less reliable than current single-wavelength detectors.

TARGET UNCERTAINTY

Many chromatographic values can change: baseline, retention time, peak shape. The key criterion for whether these changes are important is whether they increase the uncertainty of the result too much. For example, in estimating a main component we often require an accuracy, relative to a "standard", of a few percents or better, whereas for impurities we may be unconcerned at tens of percent relative imprecision. To judge whether a chromatogram is acceptable, we clearly need an estimate of uncertainty and the quantitation process must provide this. The quantitator will advise for all items quantified, if appropriate or requested, the estimates of uncertainty and an indicator of confidence in the uncertainty estimates, and minimum detectable

quantities^{18,20,23,55-71}. After one or more chromatograms have been run, the analyst will be able to set target uncertainties for all peaks detected. These may range from infinity (for peaks which are of no interest) downwards. The units may be absolute weights, or concentration, or relative to other components. By comparing the estimated uncertainty with the analyst's target, the chromatograms can be judged acceptable or not. If unacceptable, more injections may be needed, or more drastic action such as instrument repair or method change. If replication is indicated, then it should be possible to predict how certainty will improve as more injections are made.

Target uncertainty is the only input to a quantitor which may be arbitrary and not objective (though of course target uncertainty should be the analyst's objective). It makes a real "system suitability test" possible, rather than indirect ones, for example plate height or resolution targets, used at present. Even more important, the target uncertainty provides an ideal criterion for optimisation of chromatographic conditions⁷². It allows the user to specify in non-chromatographic measurement terms what he wants from the analytical procedure. If other constraints need also to be imposed, for example, maximum time, a quantitor should be able to predict uncertainties. (Most separation quality measures used by optimisation methods, for example resolution, are only one of many factors controlling the uncertainty of measurement).

Finally, because an estimate of uncertainty is available, the result (and the uncertainty estimate, of course) are suitable for storage automatically in a LIMS as raw data.

EXAMPLE OF AN APPLICATION OF A QUANTITATOR

In the analysis of pure chemicals, such as an active drug, a quantitor might guide the operator in the following sequence of measurements on various samples.

Preliminary method development is usually based on known chemical data and this is used to select gradient conditions for scouting chromatograms. At first a quantitor has little additional information apart from the column size and which theory applies. However, it can make estimates of the uncertainty in area measurement from possible baseline and separation degree, and assess the errors caused by sampling rates. As more chromatograms are run, expected peak shapes become more defined.

These experiments should establish chromatographic conditions, perhaps now isocratic, that elute the main component with reasonable retention and specificity. Chromatograms are run for the quantitor until the confidence in uncertainties estimated is high enough. Chromatographic conditions may need altering. The number and retention, and uncertainty estimates, of impurities can now be assessed in more detail, especially by running atypical sample(s). These will need to be analysed more than once, and with standards interposed to compensate for drift of retention. Chromatographic conditions may need refining to improve separation.

When the typical sample(s) are run, the impurities in atypical samples (and standards too, for single peak chromatograms are virtually unknown) can be identified by retention time and peak shape, and perhaps confirmed by other techniques. Initial estimates of uncertainty can be refined. Some strongly overlapped components may be revealed: it will also be possible to estimate from the number and density of impurity peaks, the risks or probability that other underlying peaks will be undetected⁷³⁻⁷⁵.

For example, in a complex and variable matrix like urine, there is a high risk that

a change in diet or metabolism will lead to a new peak overlapping that from an analyte under study. In a pure chemical the risk is statistically much lower. Although the variance of risk calculations is high, it can be used to refine the uncertainty estimate and suggest when more resolution (which only gives a modest improvement to risk) or multichannel detection (which has generally better specificity) is needed to give credible results, for example for forensic evidence.

As more typical samples are analysed, interspersed with standards at intervals determined dynamically by the quantitator, the uncertainty estimates will be continuously refined, in particular, the distribution of errors. A Gaussian distribution is abnormal in analytical chemistry⁷⁶. Baseline noise and drift, and retention drift norms will also be established.

OPTIMISATION

A method of quantitation is now quite well defined. At this point, if not before, optimisation of chromatographic conditions may be appropriate. An important objective of optimisation is to ensure robustness⁷⁷ so that small changes in conditions do not lead to sharp increases in uncertainty. For example, does a likely change in column temperature or solvent composition change uncertainty significantly?

Of course repetition of all the previous experiments to establish the change in uncertainty estimates is hardly necessary. The quantitator might also guide the user in the number of analyses required to achieve an arbitrary level of confidence and indicate the predicted confidence for a given number of analyses. (To have confidence in standard deviations within 20% needs about 50 replicate observations, 10% needs 250, 5% needs 1000 and 1% needs 20 000^{78,79}.)

Finally, in routine use analysing many typical samples a quantitator should continue to refine the uncertainty estimates showing this through an increased confidence. The distribution of errors will become more defined. This might be used to reject certain results. For example, some instrumental feature, like air bubbles, might cause some results to be more often in error in one direction giving a bimodal error distribution. If analyses are done in triplicate and two results are close and the third is different by the observed bimodal difference, it might be more reasonable to ignore the third result and return the mean of the other two as the best answer. (The third result could still be used to refine the bimodal error distribution.)

The quantitator should advise the error distribution, and any sudden changes to it, as an aid to instrument fault diagnosis and maintenance⁸⁰. For example, the appearance of a bimodal error distribution might signal a leaking injection valve. The Kalman filter, recently reviewed by Brown⁸¹, has been shown useful in this situation⁸²⁻⁸⁶.

METHOD VALIDATION

It follows that the validation of a method, now established by a limited number of initial experiments, should be continuously refined⁸⁷⁻⁹³, narrowing if possible the uncertainty estimate, as more standards and samples are measured. This should lead to best use of the data, neither overoptimistic neglecting, for example, degradation of the column with many chromatograms, nor pessimistic because too few samples are

analysed exploring too many variables. In principle, all previous chromatograms have some relevance to any particular chromatogram, but in practice only a few will prove relevant enough to be considered individually (though the quantitator must be able to incorporate a summary of information from previous chromatograms, for example using the Kalman filter concept).

Many methods are used to analyse hundreds of similar samples. In this case it should be possible to deduce quite a lot about the distribution of errors, especially if replicates are done. For example, do air bubbles in an injection loop cause the largest errors always to be in one direction giving a biased error distribution rather than Gaussian? This would not be obvious from a dozen chromatograms run for uncertainty estimation. Could the risk of outliers from abnormal factors be quantified well enough to justify reducing the replication and thus reduce the cost?

If the column performance declines as more samples are done, an objective, and cheapest, decision to replace it with a new one can be taken if the uncertainty estimate becomes worse than the target uncertainty. The quality of the data is much better assured, and costs should be less than replacing the column after an arbitrary number of analyses.

POTENTIAL BENEFITS FROM USING A CHROMATOGRAPHIC QUANTITATOR

- (1) Removal of arbitrary "integration parameters".
- (2) Ideal specification of analytical performance for legal, regulatory and commercial purposes because only the target uncertainty need be specified.
- (3) Improvement in reliability of results, and an estimate of the reliability achieved.
- (4) Direct estimate of uncertainty on each peak.
- (5) Explicit determination of the error caused by interfering substances.
- (6) Less risk of undetected peaks hidden under others.
- (7) Meeting uncertainty targets is the ideal criterion for optimisation of chromatographic conditions.
- (8) Placing entire responsibility for the estimation of uncertainty in quantitation on the manufacturer, who cannot claim that user has selected wrong integration parameters.
- (9) Easier validation of the quantitation system with real samples rather than artificial tests or inspection of program code.
- (10) Elimination of much unnecessary column testing and unnecessary control of column parameters. A system is suitable if the uncertainty estimates are better than specified limits.
- (11) Elimination of the need to check chromatograms by eye and the cost of hardware and software to aid this.
- (12) Reduced volume of raw data which must be stored.
- (13) Far greater tolerance to retention drift and peak shape change.
- (14) Reduction in analysis time and solvent use by reducing unnecessary resolution.
- (15) Reduction in number of replicates required (or warning that more replicates are required to achieve the target uncertainty).
- (16) Less injections of standards without reducing confidence.

- (17) Increased column lifetime by only replacing when error rises too high.
- (18) Better diagnostic information reducing instrument down time.
- (19) Using computing (which is getting cheaper) instead of using chromatography (which is getting more expensive). Helping development of better chromatography which can solve more difficult analytical problems.

ACKNOWLEDGEMENTS

I thank many colleagues in Imperial Chemical Industries plc, who have improved these ideas by their criticisms and encouraged me by their scepticism that such software is feasible.

REFERENCES

- 1 S. N. Chesler and S. P. Cram, *Anal. Chem.*, 43 (1971) 1922.
- 2 P. C. Kelly and W. E. Harris, *Anal. Chem.*, 43 (1971) 1184.
- 3 P. C. Kelly and W. E. Harris, *Anal. Chem.*, 43 (1971) 1170.
- 4 H. D. Metzger and K. G. Radszuweit, *Chromatographia*, 5 (1972) 186.
- 5 S. N. Chesler and S. P. Cram, *Anal. Chem.*, 44 (1972) 2240.
- 6 S. R. Abbott, J. R. Berg, P. Achener, R. L. Stevenson, *J. Chromatogr.*, 126 (1976) 421.
- 7 G. M. Bobba and L. F. Donaghey, *J. Chromatogr. Sci.*, 15 (1977) 47.
- 8 L. Andersson, *J. Chromatogr.*, 216 (1981) 35.
- 9 R. P. W. Scott and C. E. Reese, *J. Chromatogr.*, 138 (1977) 283.
- 10 R. L. Aiken, G. T. Fritz, D. M. Marion, K. H. Michel and T. Wolf, *J. Chromatogr. Sci.*, 19 (1981) 338-348.
- 11 S. R. Bakalyar and R. A. Henry, *J. Chromatogr.*, 126 (1976) 327-345.
- 12 L. M. McDowell, W. E. Barber and P. W. Carr, *Anal. Chem.*, 53 (1981) 1373-1376.
- 13 R. W. McCoy, R. L. Aiken, R. E. Pauls, E. R. Ziegel, T. Wolf, G. T. Fritz and D. M. Marmion, *J. Chromatogr. Sci.*, 22 (1984) 425.
- 14 E. F. G. Woerlee and J. J. Mol, *J. Chromatogr. Sci.*, 18 (1980) 258.
- 15 P. Geladi and B. Kowalski, *Anal. Chim. Acta*, 185 (1986) 1.
- 16 S. Ebel and W. Muck, *Fresenius Z. Anal. Chem.*, 331 (1988) 359-366.
- 17 G. Horlick, *Anal. Chem.*, 47 (1974) 352-354.
- 18 C. N. Renn and R. E. Synovec, *Anal. Chem.*, 60 (1988) 1829-1832.
- 19 D. T. Rossi, *J. Chromatogr. Sci.*, 26 (1988) 101-105.
- 20 H. C. Smit and E. J. van den Heuvel, *Topics Curr. Chem.*, 141 (1987) 64-89.
- 21 M. S. Jeansone and J. P. Foley, *J. Chromatogr.*, 461 (1989) 149-163.
- 22 D. I. Eikens and P. W. Carr, *Anal. Chem.*, 61 (1989) 1058-1062.
- 23 R. E. Synovec and E. S. Yeung, *Anal. Chem.*, 58 (1986) 2093-2095.
- 24 G. Reich, *Anal. Chim. Acta*, 201 (1987) 153-170, 171-183.
- 25 G. Reich, *Chromatographia*, 24 (1987) 659-665.
- 26 H. N. J. Poullisse and P. Engelen, *Anal. Lett.*, 13 (A14) (1980) 1211-1234.
- 27 L. M. Schwartz, *Anal. Chem.*, 52 (1980) 1141-1147.
- 28 R. A. Moore, *Analyst (London)*, 104 (1979) 71-777.
- 29 S. T. Baile, *Quantitative Column Liquid Chromatography*, Elsevier, Amsterdam, 1984, Ch. 6.
- 30 B. G. M. Vandeginste and L. de Galan, *Anal. Chem.*, 47 (1975) 2124-2132.
- 31 M. Rosenbaum, V. Hancii and R. Komers, *J. Chromatogr.*, 246 (1982) 1-11.
- 32 R. A. Carana, R. B. Searle, T. Heller and S. I. Shupack, *Anal. Chem.*, 58 (1986) 1162-1167.
- 33 J. Debets, *J. Liq. Chromatogr.*, 8 (1985) 2725-2780.
- 34 R. A. Vaidya and R. D. Hester, *J. Chromatogr.*, 287 (1984) 231-244.
- 35 R. Cela and J. A. Perez-Bustamante, *Comput. Appl. Lab.*, 1 (1983) 137-144.
- 36 F. Dondi and F. Pulidori, *J. Chromatogr.*, 284 (1984) 293-301.
- 37 F. Dondi and M. Remelli, *J. Chromatogr.*, 315 (1984) 67-73.
- 38 F. Dondi, A. Betti, G. Bio and C. Bighi, *Anal. Chem.*, 53 (1981) 496-504.

- 39 O. Grubner, *Anal. Chem.*, 43 (1971) 1934–1937.
- 40 S. Frazer and M. F. Burke, *Anal. Chim. Acta*, 177 (1985) 15–22.
- 41 C. H. Lochmuller and M. Sumner, *J. Chromatogr. Sci.*, 18 (1980) 159–165.
- 42 J. K. Kauppinen, D. J. Moffatt, H. H. Mantsch and D. G. Cameron, *Anal. Chem.*, 53 (1981) 1454–1457.
- 43 R. Delly, *Anal. Chem.*, 57 (1985) 388, 58 (1985) 2344–2346.
- 44 J. P. Foley and J. G. Dorsey, *J. Chromatogr. Sci.*, 22 (1984) 40–46.
- 45 J. P. Foley and J. G. Dorsey, *Anal. Chem.*, 55 (1983) 730–737.
- 46 H. C. Smit, J. C. Smit and E. M. de Jager, *Chromatographia*, 22 (1986) 123–131.
- 47 J. Grimalt, H. Iturriaga and X. Tomas, *Anal. Chim. Acta*, 139 (1982) 155–166.
- 48 R. G. Brownlee and J. W. Higgins, *Chromatographia*, 11 (1978) 567–572.
- 49 W. W. Yau, *Anal. Chem.*, 49 (1977) 395–398.
- 50 C. Vidal-Madjar and G. Guiochon, *J. Chromatogr.*, 142 (1977) 61–86.
- 51 J. Olive, J. O. Grimalt and H. Iturriaga, *Anal. Chim. Acta*, 219 (1989) 257–272.
- 52 P. R. Haddad and S. Sekulic, *J. Chromatogr.*, 459 (1988) 79–90.
- 53 P. J. Naish and S. Hartwell, *Chromatographia*, 26 (1988) 285–296.
- 54 T. P. Bridge, M. H. Williams and A. F. Fell, *J. Chromatogr.*, 465 (1989) 59–67.
- 55 C. E. Reese, *J. Chromatogr. Sci.*, 18 (1980) 249.
- 56 Z. Hippe, A. Bierowska and T. Pietryga, *Anal. Chim. Acta*, 122 (1980) 279.
- 57 J. M. Laeven and H. C. Smit, *Anal. Chim. Acta*, 176 (1985) 77–104.
- 58 P. J. H. Scheeren, P. Barna and H. C. Smit, *Anal. Chim. Acta*, 167 (1985) 65–80.
- 59 J. P. Foley and J. G. Dorsey, *Chromatographia*, 18 (1984) 503.
- 60 J. E. Knoll, *J. Chromatogr. Sci.*, 13 (1985) 422.
- 61 H. C. Smit and H. L. Walg, *Chromatographia*, 8 (1975) 311.
- 62 R. E. Synovec and E. S. Yeung, *Anal. Chem.*, 57 (1985) 2162.
- 63 J. B. Phillips, *Anal. Chem.*, 58 (1986) 2091.
- 64 C. A. Clayton, J. W. Hines and P. D. Elkins, *Anal. Chem.*, 59 (1987) 2506–2514.
- 65 P. J. Naish, R. J. Dolphin and D. P. Goulder, *J. Chromatogr.*, 395 (1987) 55–71.
- 66 R. L. Watters, R. J. Carroll and C. H. Spiegelman, *Anal. Chem.*, 59 (1987) 1639–1643.
- 67 S. Ebel, H. Kuhnert and W. Muck, *Chromatographia*, 23 (1987) 934–938.
- 68 W. L. Creten and L. J. Nagels, *Anal. Chem.*, 59 (1987) 822–826.
- 69 P. E. Poston and J. M. Harris, *Anal. Chem.*, 59 (1987) 1620–1626.
- 70 Y. Hayashi, T. Shibazaki, R. Matsuda and M. Uchiyama, *Anal. Chim. Acta*, 202 (1987) 187–197.
- 71 Y. Hayashi, T. Shibazaki, R. Matsuda and M. Uchiyama, *J. Chromatogr.*, 407 (1987) 59–64.
- 72 P. J. Schoenmakers, N. Dunand, A. Clenad, G. Musch and T. Blaffert, *Chromatographia*, 26 (1988) 37–44.
- 73 J. M. Davis and J. C. Giddings, *Anal. Chem.*, 57 (1985) 2166–2177.
- 74 M. Martin, D. P. Herman and G. Guiochon, *Anal. Chem.*, 58 (1985) 2200–2207.
- 75 J. M. Davis, *J. Chromatogr.*, 449 (1988) 41–52.
- 76 G. R. Phillips and E. M. Eyring, *Anal. Chem.*, 55 (1983) 1134.
- 77 M. Mulholland and J. Waterhouse, *Chromatographia*, 25 (1988) 769.
- 78 H. C. Hamaker, *J. Assoc. Off. Anal. Chem.*, 69 (1986) 417–436.
- 79 L. D. Fields and S. J. Hawkes, *Anal. Chem.*, 58 (1986) 1593–1595.
- 80 L. A. Rusinov and V. V. Kurkina, *J. Chromatogr.*, 365 (1986) 367–374.
- 81 S. D. Brown, *Anal. Chim. Acta*, 181 (1986) 1–26.
- 82 P. C. Thijssen, S. M. Wolfrum, G. Kateman and H. C. Smit, *Anal. Chim. Acta*, 156 (1984) 87–101.
- 83 P. C. Thijssen, *Anal. Chim. Acta*, 162 (1984) 253–262.
- 84 P. C. Thijssen, G. Kateman and H. C. Smit, *Anal. Chim. Acta*, 173 (1985) 265–272.
- 85 P. C. Thijssen, H. H. M. de Jong, G. Kateman and H. C. Smit, *Anal. Chim. Acta*, 170 (1985) 265–278.
- 86 P. C. Thijssen, N. J. M. L. Janssen, G. Kateman and H. C. Smit, *Anal. Chim. Acta*, 177 (1985) 457–469.
- 87 L. M. Schwartz, *Anal. Chim. Acta*, 178 (1985) 355–359.
- 88 L. M. Schwartz, *Anal. Chem.*, 58 (1986) 246–251.
- 89 J. E. Haky and E. A. Domonkos, *J. Chromatogr. Sci.*, 23 (1985) 364–369.
- 90 M. J. Cardone, *Anal. Chem.*, 58 (1986) 438–445, 445–448.
- 91 P. W. Carr, *Anal. Chem.*, 52 (1980) 1746–1750.
- 92 G. J. Kemp, *Anal. Chim. Acta*, 176 (1985) 229–247.
- 93 E. L. Inman, J. K. Fischman, P. J. Jimenez, G. D. Winkel, M. L. Persinger and B. S. Rutherford, *J. Chromatogr. Sci.*, 25 (1987) 252.

CHROMSYMPO. 1716

High-performance liquid chromatographic determination of guanidino compounds by automated pre-column fluorescence derivatization

VENKATA K. BOPANA and GERALD R. RHODES*

Department of Drug Metabolism, Smith Kline & French Laboratories, P.O. Box 1539, King of Prussia, PA 19406 (U.S.A.)

SUMMARY

An automated pre-column derivatization approach was used to develop a high-performance liquid chromatographic method for the determination of endogenous guanidino compounds. A commercially available autoinjector which was capable of adding and mixing reagent solutions and timing the reaction prior to injection was used to generate a fluorescent product by reaction of guanidino compounds with alkaline ninhydrin. The fluorescent products were separated by reversed-phase chromatography and detected with a fluorometer. Optimization of the pre-column reaction conditions resulted in a simple, highly sensitive and specific analytical method for the determination of guanidino compounds with excellent reproducibility and linearity. Application of this methodology to the determination of methylguanidine in human plasma samples resulted in a limit of quantification of 1 ng/ml (13.7 pmol/ml). The method was successfully employed for the quantification of circulating levels of methylguanidine in normal human subjects and uremic patients. The methodology should be generally applicable to the detection of other guanidino compounds in biological fluids.

INTRODUCTION

Pre-column derivatization methods are often preferred over post-column reaction methods in high-performance liquid chromatography (HPLC) because the chromatographic system is less complex and higher sensitivity may be achieved due to the elimination of peak broadening, baseline noise and dilution effects resulting from the addition of post-column reagents and the volume of the reaction coil. Manual pre-column derivatization methods, however, also suffer from certain disadvantages such as requirements for precise control and reproducibility of reaction conditions and the generation, in most cases, of a single, stable reaction product. For example, several fluorescence reagents are difficult to utilize in a pre-column derivatization method since the reaction product has only limited stability. However, automation of this

process so that pre-column derivatization occurs just prior to chromatographic analysis can eliminate these drawbacks. In the present paper, we describe such an automated pre-column derivatization approach for the fluorescence determination of several endogenous guanidino compounds.

Guanidino compounds, including methylguanidine, have been shown to be elevated substantially in the plasma of uremic patients compared to normal subjects¹⁻⁵ and are suspected renal toxins whose measurement provides an indication of renal status. These guanidino compounds react with ninhydrin under strongly alkaline conditions to generate a highly fluorescent, but unstable product and, consequently, a previously reported method utilized a combination of HPLC and post-column fluorescence derivatization⁶ for the measurement of guanidino compounds. In our approach, guanidino compounds are reacted with ninhydrin just prior to HPLC analysis, by a commercially available autoinjector with sophisticated pre-column derivatization capabilities, and the derivatized products were analyzed by reversed-phase HPLC with fluorescence detection. Using this methodology, we developed a substantially simplified, specific and highly sensitive (1 ng/ml) analytical method for the measurement of methylguanidine in human plasma samples. This methodology has been shown to be suitable for the measurement of methylguanidine plasma levels in normal human subjects and those with renal insufficiency.

EXPERIMENTAL

Chemicals

L-Arginine (ARG) hydrochloride, guanidine (G) hydrochloride, guanidinoacetic acid (GAA), guanidinosuccinic acid (GSA), β -guanidinopropionic acid (GPA), γ -guanidinobutyric acid (GBA), methylguanidine (MG) hydrochloride and ethylguanidine (EG) hydrochloride were obtained from Sigma (St. Louis, MO, U.S.A.). Ninhydrin and trifluoroacetic acid (TFA) were obtained from Pierce (Rockford, IL, U.S.A.). HPLC-grade methanol and sodium acetate were purchased from J. T. Baker (Philipsburg, NJ, U.S.A.). Weak cation-exchange (carboxymethylhydrogen form, CBA) solid phase extraction columns (1 ml) and the Vac-Elut manifold were purchased from Analytichem (Harbor City, CA, U.S.A.). All other chemicals were reagent grade and obtained from local sources.

Sample preparation

A CBA solid phase extraction column was conditioned by successive washings with 1 ml of 1% TFA in methanol, 1 ml of methanol and 2 ml of water. An aliquot of plasma (1 ml) was mixed in a 75 \times 10 mm borosilicate tube with 50 μ l of internal standard solution (ethylguanidine, 10 μ g/ml). The pH of the plasma was adjusted to 11 by adding 26 μ l of 1.0 M sodium hydroxide solution. The plasma sample was vortex mixed and the sample was then poured onto the CBA column and vacuum was applied. The column was washed with 3 ml of water and then with 1 ml of methanol. The sample was then eluted from the column with 2 ml of 1% TFA in methanol and the eluents were collected into a 100 \times 75 mm borosilicate tube. The methanol was evaporated under a gentle stream of nitrogen at 40°C and the residue reconstituted in 200 μ l of 20% aqueous methanol.

HPLC

The HPLC system consisted of a Hitachi 665A-12 high-pressure gradient solvent delivery system (EM Science, Cherry Hill, NJ, U.S.A.), an autoinjector with pre-column reagent addition and mixing capabilities (Varian, Model 9090, Sunnyvale, CA, U.S.A.) and an Hitachi F-1000 fluorescence detector (EM Science). Chromatographic separation of methylguanidine and other endogenous guanidino compounds was achieved on a 22 cm \times 4.6 mm I.D., 5- μ m octadecyl silica column (Pierce) connected in-line with a 5 cm \times 4.6 mm I.D. octyl silica guard column at a mobile phase flow-rate of 1 ml/min. The mobile phase consisted of 0.05 M sodium acetate buffer (pH 6) and methanol as the organic modifier. The mobile phase solvents were degassed by filtering through a 0.2- μ m Nylon-66 filter before use. Following chromatographic separation, fluorescence detection of derivatized guanidino compounds was accomplished using excitation at 390 nm while monitoring the fluorescence emission with a 470-nm cut-off filter. The chromatographic data were collected with a computer automated laboratory system (CIS-Beckman, Berkely, CA, U.S.A.).

Automated pre-column derivatization

A portion (30 μ l) of the sample extract or a standard solution was transferred to an autoinjector vial and loaded on the autoinjector. Sodium hydroxide solution (25 μ l) was added and the resultant solution was mixed by syringe filling and expulsion (three cycles). Ninhydrin reagent solution (5 μ l) was then added to the sample vial, mixed as above, allowed to react at room temperature for 5 min and then a portion of the final solution (20 μ l) was injected for HPLC analysis. Low volumes of sodium hydroxide and ninhydrin reagent solutions were chosen to perform the pre-column derivatization in order to minimize dilution effects and thus maximize the overall sensitivity.

Optimization of the pre-column reaction proceeded from the initial conditions described above using a standard mixture of several endogenous guanidino compounds (containing GSA, GAA, GPA, ARG, GBA, G, MG and EG; 300 pmol per component). This standard mixture was repetitively derivatized using systematic alterations in the reagent concentrations and reaction time prior to HPLC separation and analysis. The fluorescence intensity for each component was monitored by measuring the resultant chromatographic peak height while keeping the HPLC conditions constant. Using this approach optimal conditions were determined to maximize the fluorescence intensity obtained following pre-column derivatization.

Standard curves for methylguanidine assay

To establish calibration curves, a series of methylguanidine standard solutions, containing 0, 1, 2, 5, 10, 20, 50, 100, 200, 500 and 1000 ng/ml, were prepared in plasma and 1 ml samples were processed by the extraction procedure described above. The peak height ratios of methylguanidine to internal standard were weighted by $1/y$ (based on analysis of residuals) and plotted against the concentrations of methylguanidine. Linear regression analysis gave a calibration line that was used to calculate the concentration of methylguanidine in unknown samples and seeded control samples.

RESULTS AND DISCUSSION

As mentioned earlier, several chromatographic methods using post-column fluorescence derivatization have been described for the determination of guanidino compounds in biological fluids⁷⁻¹¹. Only one previous pre-column derivatization method has been described using the reaction of benzoin with guanidino compounds to generate a fluorescence product suitable for HPLC analysis^{12,13}. However, this manual pre-column method suffers from several disadvantages including benzoin's lack of aqueous solubility, a complex number of reagent addition steps to perform the reaction and stabilize the resultant product and variability in the reaction time. In order to develop simplified methodology for the determination of guanidino compounds, we explored fluorescence derivatization methods for their applicability for automated pre-column derivatization. We found that ninhydrin was the reagent of choice due to its stability and solubility in aqueous solutions, low background fluorescence and the ability to carry out the reaction at room temperature in a period of time consistent with that for chromatographic analysis (< 15 min). The use of automated pre-column derivatization resolves the problem associated with the stability of the fluorescent product formed in the reaction of ninhydrin with guanidino compounds.

Optimization of the ninhydrin pre-column derivatization conditions was accomplished as described in the experimental section of the text and based upon measurement of chromatographic peak height. The derivatized guanidino compounds from the standard mixture were separated by gradient elution HPLC using an initial mobile phase composition of 0.05 *M* sodium acetate (pH 6)-methanol (80:20). Following the injection, the methanol concentration was held at 20% for 5 min, increased to 30% over 5 min, held at 30% for 5 min and then cycled back to the initial conditions in 2 min.

The effect of the reagent concentration on the fluorescence intensity observed following ninhydrin pre-column derivatization was examined by successively varying the base and ninhydrin concentrations to establish optimal concentrations for each reagent. Initially, the concentration of sodium hydroxide was varied from 0.1 to 1.0 *M* while maintaining the ninhydrin concentration at 0.6% (w/v) (Fig. 1). As can be observed from Fig. 1, the base concentration has a significant and similar effect on the fluorescence intensity observed with all the endogenous guanidino compounds examined here. Based on these results, a sodium hydroxide concentration of 0.8 *M* was determined to be optimal for routine use. Subsequently, the concentration of ninhydrin was varied from 0.05 to 1.0% (w/v) while maintaining the base concentration at 0.8 *M* (Fig. 2). As can be seen from Fig. 2, maximum fluorescence intensity was observed for all the guanidino compounds, with the exception of GSA, at a ninhydrin concentration of 0.8% (w/v).

Using the optimal reagent concentrations established above, the effect of the pre-column reaction time was examined by allowing the reaction to proceed for times ranging from 1 to 14 min. The results of this experiment are shown in Fig. 3. In order to optimize the fluorescence intensity for all the guanidino compounds examined, a reaction time of 10 min was chosen for the pre-column derivatization. At reaction times longer than 12 min, a loss of fluorescence intensity was routinely observed due to instability of the fluorescent product formed in the reaction.

Thus the optimal sodium hydroxide and ninhydrin concentrations and reaction

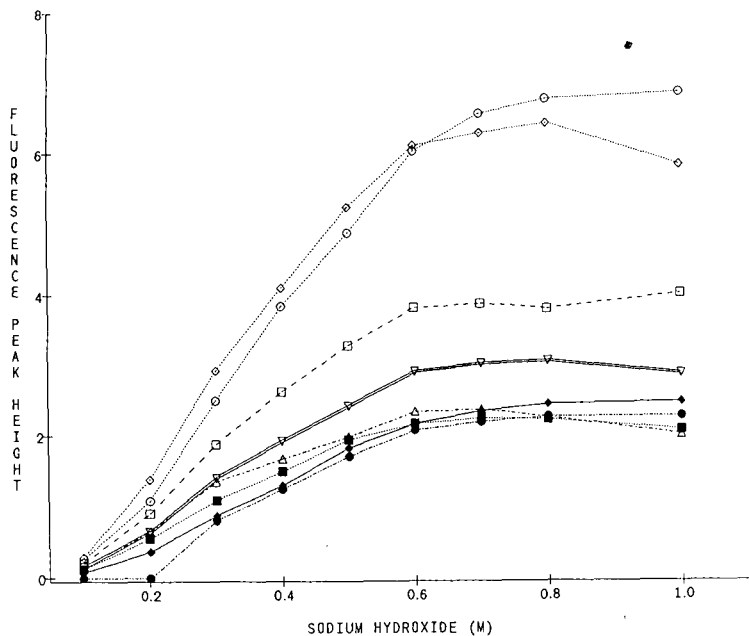


Fig. 1. Effect of sodium hydroxide concentration on the pre-column derivatization of guanidino compounds. The conditions are described in the text. Curves: ○ = GSA; ◇ = GAA; □ = GPA; △ = ARG; ▽ = GBA; ● = G; ◆ = MG; ■ = EG.

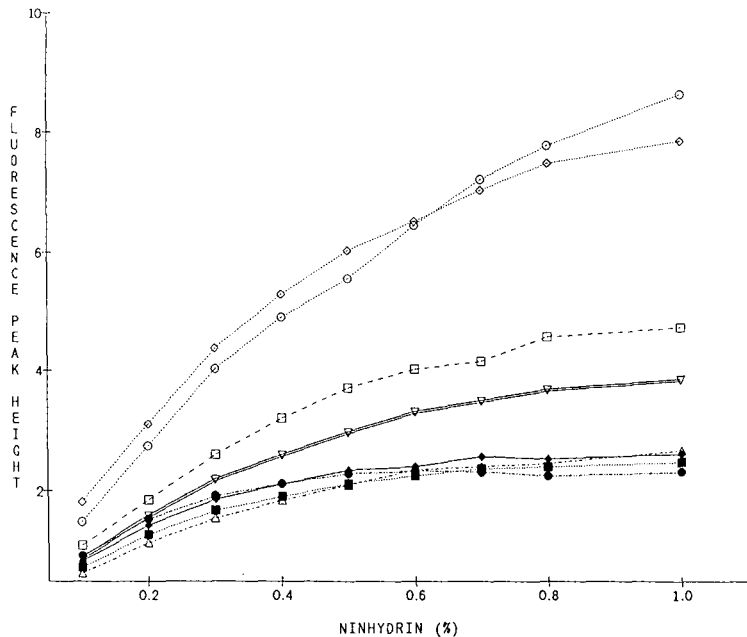


Fig. 2. Effect of ninhydrin concentration on the pre-column derivatization of guanidino compounds. The conditions are described in the text. See Fig. 1 for identification of curves.

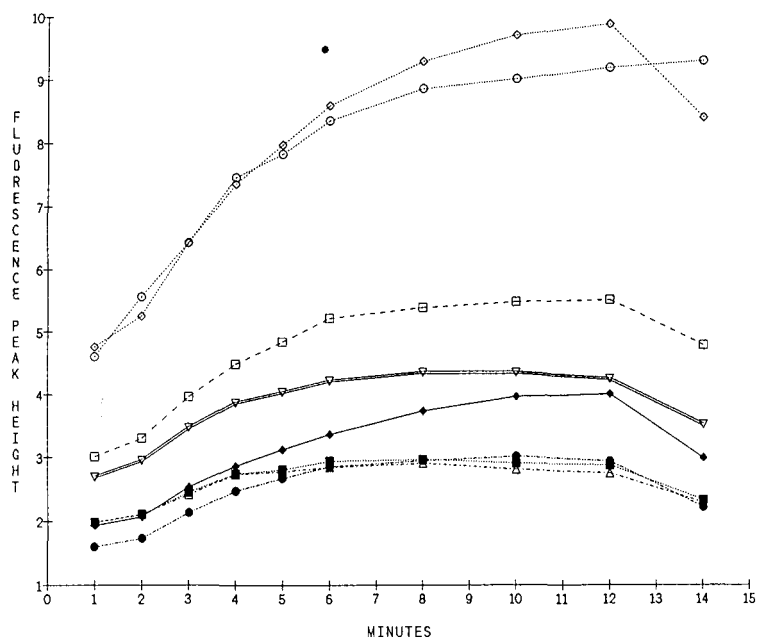


Fig. 3. Effect of reaction time on the pre-column derivatization of guanidino compounds. The conditions are described in the text. See Fig. 1 for identification of curves.

time for the pre-column derivatization of guanidino compounds with ninhydrin were determined to be 0.8 *M*, 0.8% (w/v) and 10 min, respectively. These conditions were used to obtain the remainder of the results described in this paper. Fig. 4 shows a chromatogram obtained from the analysis of a standard solution of eight guanidino compounds separated using the gradient elution conditions described above. As can be observed, separation of the guanidino compounds was achieved in less than 20 min.

In order to determine the applicability of this approach for routine quantification of guanidino compounds, the linearity and precision of the ninhydrin pre-column derivatization method were examined. The linearity was evaluated over the range from 9 to 3000 pmol by analysis of a series of standard solutions prepared by serial dilution of a guanidino stock standard solution (100 μ mol per component). As shown in Fig. 5, the methodology demonstrated excellent linearity yielding linear responses for all guanidino compounds examined over the range of 9 to 3000 pmol. The curves were highly reproducible and correlation coefficients were typically greater than 0.999 for all guanidino components. The precision of the pre-column derivatization method was determined by repetitive analysis of a guanidino standard solution (containing 300 pmol per component) with measurement of the resultant chromatographic peak heights. The method displayed excellent chromatographic peak height reproducibility, yielding a coefficient of variation (C.V.) ranging from 0.8 to 4.2% for the guanidino compounds examined (Table I). The lower limit of detection (signal-to-noise ratio = 3) ranged from 1 to 8 pmol for the guanidino compounds examined. These results provide the necessary dynamic range for guanidino compounds in physiological samples.

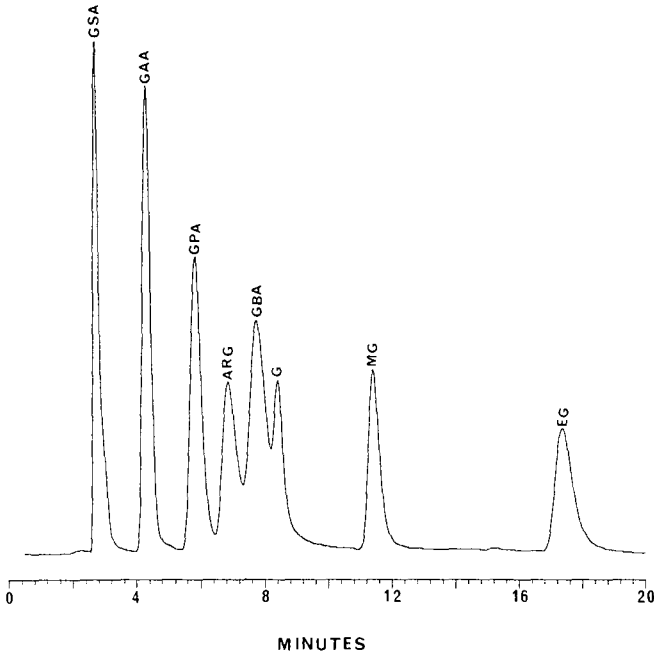


Fig. 4. Chromatogram of an aqueous standard solution of endogenous guanidino compounds separated by gradient elution. The chromatographic conditions are described in the text.

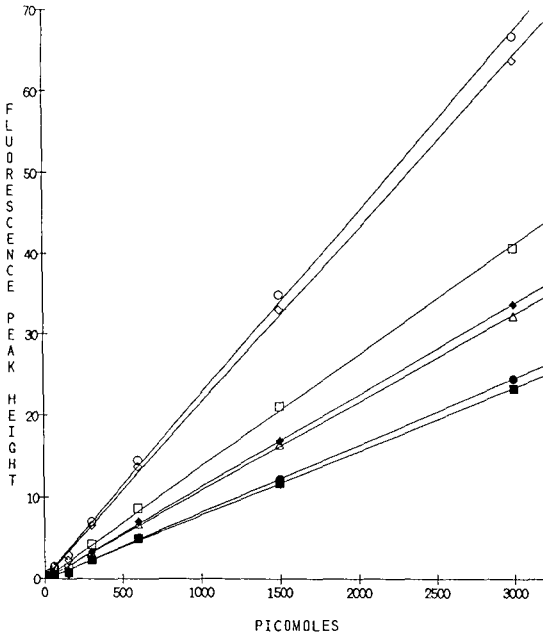


Fig. 5. Linearity of the pre-column derivatization HPLC method for the measurement of guanidino compounds. The conditions are described in the text. See Fig. 1 for identification of curves.

TABLE I
REPRODUCIBILITY OF THE PRE-COLUMN DERIVATIZATION HPLC METHOD

Injection number ^a	Fluorescence intensity of guanidino compounds (peak heights)							
	GSA	GAA	GPA	ARG	GBA	GUA	MG	EG
1	6.72	6.14	3.85	2.20	2.99	2.21	2.34	1.61
2	6.98	6.20	3.83	2.32	3.00	2.23	2.35	1.60
3	6.99	6.32	3.88	2.39	3.11	2.25	2.28	1.70
4	6.87	6.30	3.85	2.28	3.02	2.22	2.37	1.69
5	6.80	6.42	3.94	2.32	3.06	2.26	2.38	1.69
6	6.81	6.36	3.95	2.36	3.08	2.22	2.37	1.73
7	6.87	6.39	3.94	2.37	3.09	2.24	2.43	1.71
8	6.74	6.39	3.87	2.36	3.11	2.21	2.66	1.65
9	6.86	6.55	4.03	2.44	3.19	2.21	2.40	1.71
10	7.03	6.59	3.92	2.34	3.11	2.21	2.39	1.69
Mean	6.87	6.37	3.91	2.34	3.08	2.23	2.40	1.68
S.D.	0.11	0.14	0.06	0.07	0.06	0.02	0.10	0.04
C.V. (%)	1.54	2.18	1.57	2.79	1.98	0.83	4.20	2.66

^a An aliquot (30 μ l) of standard solution containing 300 pmol of each guanidino compound was repetitively analyzed using the methods described in the text and their fluorescence was measured.

The sensitivity, specificity, linearity and precision of the ninhydrin pre-column derivatization approach described here for the determination of guanidino compounds was clearly suitable for their quantitative analysis in biological fluids. In addition, this approach was equally sensitive to other methods utilizing post-column derivatization of guanidino compounds. Based upon these results, we applied this methodology to the development of a highly sensitive and specific HPLC method for the measurement of methylguanidine in human plasma samples. The method involves isolation of methylguanidine and an internal standard (ethylguanidine) from plasma by solid phase extraction prior to analysis by the combined pre-column derivatization and HPLC methodology described here. In order to optimize for the separation and measurement of methylguanidine, isocratic mobile phase conditions were employed. The isocratic mobile phase composition used was 0.05 M sodium acetate buffer (pH 6)–methanol (75:25, v/v), at a flow-rate of 1 ml/min. These conditions provided highly reproducible chromatographic analysis providing the retention times of 10.3 and 20.2 min for methylguanidine and the internal standard, respectively. In addition, using these chromatographic conditions, methylguanidine and the internal standard were fully separated from other endogenous guanidino compounds. Typical chromatograms of plasma extracts obtained from a normal subject and a patient with renal insufficiency are shown in Fig. 6 A and B, respectively. Using this method, the limit of detection for methylguanidine in plasma samples was 1 ng/ml (signal-to-noise ratio = 3). Extraction recovery of methylguanidine and internal standard was determined by comparing the peak heights of the standards injected directly on the column with the response to standards extracted from plasma. The recoveries for methylguanidine and internal standard were quantitative. Calibration curves obtained for methylguanidine were linear with concentration from 1 to 1000 ng/ml in plasma samples. Correlation coefficients exceeded 0.999 for all plasma standard curves. The accuracy

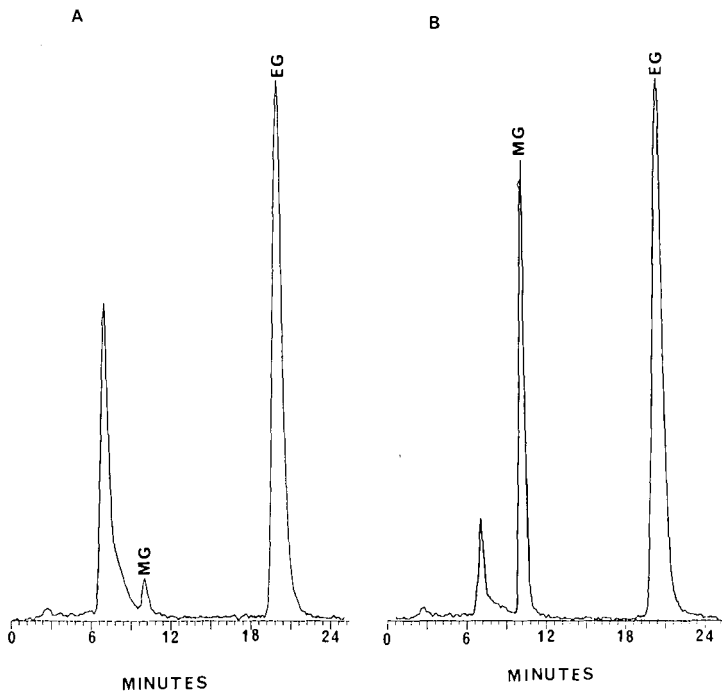


Fig. 6. Chromatograms of plasma extracts from a normal subject (A) and a subject with renal insufficiency (B). The conditions are described in the text. The concentrations of methylguanidine (MG) are 10.3 ng/ml in (A) and 186.6 ng/ml in (B), respectively. EG = Ethylguanidine.

and precision of the methylguanidine assay were within 11% across the calibration range. Table II summarizes the results of a three-day assay validation study in which six replicate seeded standards at three concentrations, 10, 100 and 1000 ng/ml were analyzed each day by this methodology. Clearly, the assay developed here for the measurement of methylguanidine in plasma samples was sufficiently accurate and precise for routine analysis of clinical samples.

TABLE II

ACCURACY AND PRECISION DATA FOR METHYLGUANIDINE IN PLASMA

Theoretical concentration (ng/ml)	Assay concentration ^a (Mean ± S.D.) (ng/ml) (n = 6)	Coefficient of variation (%)		Accuracy (%) ^d
		Intra-assay ^b (n = 6)	Inter-assay ^c (n = 18)	
10	9.27 ± 0.78	8.29	10.71	99.7
100	105.46 ± 2.08	1.97	6.74	99.5
1000	1014.60 ± 40.50	3.99	7.02	98.4

^a Mean value on a single day.

^b (S.D./mean) · 100 in same assay.

^c (S.D./mean) · 100 in three different assays.

^d Percent ratio of actual to theoretical concentration.

In conclusion, the methodology described here was simple, highly sensitive, specific and routinely useful for the quantification of methylguanidine in normal and uremic subjects. This automated pre-column derivatization methodology offers convenience and can be readily incorporated into existing laboratory HPLC systems. Moreover, this method offers a simple alternative for post-column reaction systems for the measurement of guanidino compounds without compromising the sensitivity and selectivity offered by such systems.

REFERENCES

- 1 H. Yatzidis, D. Oreopoulos, N. Tsaparas, S. Voudiceari, A. Stavroulakis and S. Zestaanakakis, *Nature (London)*, 212 (1966) 1498.
- 2 S. Giovannetti, M. Biagni, P. L. Balestri, R. Navalesi, P. Giagnoni, A. de Matteis, P. Ferro-Milone and C. Perfetti, *Clin. Sci.*, 36 (1969) 445.
- 3 S. Giovannetti, P. L. Balestri and G. Barsotti, *Arch. Intern. Med.*, 131 (1973) 709.
- 4 G. Barsotti, G. Bevilacqua, E. Morelli, P. Cappelli, P. L. Balestri and S. Giovannetti, *Kidney Int. Suppl.*, 7 (1975) S-299.
- 5 S. Giovannetti, M. Biagini and L. Cioni, *Experientia*, 24 (1968) 341.
- 6 Y. Hiraga and T. Kinoshita, *J. Chromatogr.*, 226 (1981) 43.
- 7 Y. Yamamoto, A. Saito, T. Manji, K. Maeda and K. Ohta, *J. Chromatogr.*, 162 (1979) 23.
- 8 Y. Yamamoto, T. Manji, A. Saito, K. Maeda and K. Ohta, *J. Chromatogr.*, 162 (1979) 327.
- 9 M. D. Baker, H. Y. Mohammed and H. Veening, *Anal Chem.*, 53 (1981) 1658.
- 10 Y.-L. Hung, M. Kai, H. Nohta and Y. Ohkura, *J. Chromatogr.*, 305 (1984) 281.
- 11 Y. Kobayashi, H. Kubo and T. Kinoshita, *Anal. Biochem.*, 160 (1987) 392.
- 12 M. Kai, T. Miyazaki, M. Yamaguchi and Y. Ohkura, *J. Chromatogr.*, 268 (1983) 417.
- 13 M. Kai, T. Miyazaki and Y. Ohkura, *J. Chromatogr.*, 311 (1984) 257.

CHROMSYM. 1712

Multiple absorbance ratio correlation — a new approach for assessing peak purity in liquid chromatography

J. G. D. MARR^{a,*}, G. G. R. SEATON, B. J. CLARK and A. F. FELL

Pharmaceutical Chemistry, School of Pharmacy, University of Bradford, Bradford BD1 7DP (U.K.)

SUMMARY

The theory of multiple absorbance ratio correlation (MARC), a novel method for examining chromatographic peaks, is presented. The MARC hypothesis provides a method for examining chromatographic peaks for homogeneity, identity and purity, operating on multi-wavelength data sets which do not contain full spectra. Paraxanthine (PX) is an endogenous caffeine metabolite which is spectrally similar ($r > 0.99$) to theophylline (TH) and which often coelutes with it. Multi-wavelength data, collected using an HP1040A diode-array detector, for a series of binary mixtures of TH and PX ($0.7 < R_s < 2.9$; 0–50% PX), was analysed using MARC. The algorithm calculates a correlation factor between an internal (for homogeneity) or an external (for identity) reference 5-point vector and a similar 5-point vector acquired at sequential time intervals throughout the peak being investigated. For samples where the binary peak was homogeneous, limits of detection for PX of 1% (w/w) were obtained. This compared with limits of 5–10% (w/w) for the standard absorbance ratio (AR) method. MARC was found to be less sensitive to wavelength choice than AR. The sensitivity of MARC was independent of the chromatographic resolution.

INTRODUCTION

One of the main problems associated with chromatographic method development is the determination of the purity or homogeneity of the analyte peaks. With the advent of computer-aided UV–VIS detection methods, notably in the form of diode-array detection (DAD), chemometric methods have been developed which enable the analyst to verify the homogeneity and/or identity of peaks by manipulating the spectrochromatographic data set^{1–4}. However, these methods are very computer intensive and confidence in the results is governed by the operators appreciation of the limitations of the algorithms employed^{5,6}.

The potential for using UV-absorbance data, at a defined number of wavelengths, for peak deconvolution and solute identification was first recognised in a theoretical analysis by Ostojic⁷. Due to a lack of suitable detector technology, initial

^a Present address: Control Development, Upjohn Ltd., Fleming Way, Crawley RH10 2NJ, U.K.

application of the theory required repeated analysis, two detectors in series or stop-flow conditions⁸⁻¹⁰. However, the advent of multi-wavelength detectors permitted the necessary data to be collected simultaneously in one analysis^{11,12}. Subsequently, various workers have investigated the limitations of the theory of absorbance ratioing as it is applied in the chromatographic environment^{13,14}. In order to overcome the constraints imposed by the choice and number of wavelengths used without resorting to the use of computer-intensive chemometric methods, White^{15,16} has proposed the use of three or more absorbance ratio values to characterise a compound. A slightly different approach has been proposed as a general screening method by Poile and Conlon¹⁷ who utilised data extracted at nine pre-defined wavelengths from the apical spectrum as a measure of 'peak purity'. The algorithm employed by Alfredson and Sheehan¹⁸ also utilises data collected from pre-defined areas of the apical and inflection point spectra as a means of evaluating the 'purity' and identity of the chromatographic peak. If the identity of at least one of the eluting components is known then spectral suppression, using two discrete wavelengths¹⁹⁻²¹, may be used. In the more general application of this principle, where N ($N \geq 2$) components overlap, it is appropriate to operate on an over-determined data set, *i.e.* one in which $N + 1$ wavelengths are used. This has been demonstrated using the multiple spectral suppression algorithm, where data sets incorporating up to eight discrete wavelengths can be used^{22,23}.

Provided there is an adequate data sampling rate, the correlation between adjacent time-point spectra collected in DAD should always be 1²⁴. Any deviation from unity is indicative of a change in the retention characteristics of spectrally-dissimilar co-eluting components. Consequently, if a known spectrum is used as the correlation template, then variations in the resulting correlation coefficient, with time across the peak, will provide an indication of peak homogeneity. This approach forms the basis of the multiple absorbance ratio correlation (MARC) algorithm. If the apical spectrum is used as the reference spectrum the process is said to be internally referenced and is referred to as IMARC. However, if a spectrum of known purity and identity *e.g.* from a spectral library, is used the results from this externally referenced application (EMARC) will not only provide the analyst with an estimation of peak homogeneity but also of possible identity. As data from more than two independent domains are being examined and the results compared to those for a reference of known quality^{24,25}, the EMARC results will give an estimation of both the homogeneity and purity of the peak.

In order to test this hypothesis it was necessary to modify the practical application of the theory, outlined above. The memory capacity of the computer controller for DAD was not sufficient to permit whole spectra to be used in each time-point calculation. Consequently, the data used to represent the reference and test spectra had to be reduced. As the probability of five or more components co-eluting in practice is low^{26,27}, monitoring simultaneously at six independent wavelengths will produce an over-determined data set sufficient for most applications. This modification allows the reference and test spectra to be represented by reduced data set (RDS) vectors of up to six points each. The resultant multi-chromatographic data set is therefore a user-defined subset of the total spectrochromatographic data set, differing only in the number of wavelength components included.

Beer's law states that for a pure chemical species, there is a linear relationship

between concentration and absorbance at every wavelength. One of the fundamental principles of rapid scanning detectors, including DAD systems, is that the change in concentration with time is negligible compared to the time taken to scan between the various wavelengths. Consequently, the ratio of absorbances at two or more wavelengths, at any time point in a chromatogram, becomes the ratio of the extinction coefficients. As the extinction coefficient at each wavelength is an intrinsic property of a compound, the ratios will also be characteristic, especially if more than one pair of wavelengths is used^{8,13,15}. It follows, therefore, that the normalised values in the six-point RDS vector should also be distinctive. Therefore, rather than compare individual RDS vector components between the reference and unknown compound, a more rapid initial screen can be performed using the algebraic sum of the RDS vector components (SUM).

The major objectives of the work described here were to translate the MARC hypothesis into a working algorithm on a currently available DAD system and to evaluate the subsequent performance using a binary mixture of spectrally similar compounds at different chromatographic resolutions.

EXPERIMENTAL

The liquid chromatograph consisted of an LDC Constametric 3000 dual reciprocating piston pump (LDC-Milton Roy, Riviera Beach, FL, U.S.A.) and an injection valve fitted with a 50- μ l loop (Model 7125; Rheodyne, Berkeley, CA, U.S.A.) through which samples were introduced using a 100- μ l syringe (SGE, Ringwood, Australia). The 100 \times 8 mm I.D. Nova-Pak C₁₈ Radial-Pak cartridge was held in an RCM 100 module (Waters Millipore, Millford, MA, U.S.A.).

The Hewlett-Packard (HP) 1040A DAD system was set up to monitor six wavelengths simultaneously: 204, 220, 240, 250, 268 and 284 nm (all \pm 2 nm), against a common non-absorbing wavelength of 550 \pm 20 nm. The HP 1040A was controlled from an HP 85A computer through an HP-IB interface. An HP 9121 dual disk drive, an HP 2225A "think-jet" printer and an HP 7470 plotter were also connected to the computer via other HP-IB connections. The original HP 85A specifications were enhanced through the addition of read only memory modules for input/output and printer-plotter communications and available memory (expanded by 16K) (Hewlett-Packard, Waldbronn, F.R.G.).

Theophylline (1,3-dimethylxanthine, TH) and paraxanthine (1,7-dimethylxanthine, PX) were used as received (Sigma, St. Louis, MO, U.S.A.). Single-component and mixed solutions were made up in and diluted with methanol-water (20:80, v/v). The mixtures contained a constant concentration of TH (52.51 μ g ml⁻¹) and variable concentrations of PX (0.525–52.5 μ g ml⁻¹). Methanol and acetonitrile were both HPLC grade and used as received (Rathburn Chemicals, Walkerburn, U.K.).

Based on the method proposed by Butrimovitz and Raisys²⁸ three different mobile phases were developed. In each case the flow-rate was 1.5 ml min⁻¹ and the mobile phase comprised varying combinations of methanol-acetonitrile-sodium acetate (20 mM, adjusted to pH 5 with acetic acid), depending on the degree of separation required between the two analytes. The three specified values of resolution (R_s) were 0.7, 1.26 and 2.9, for which the respective mobile phase compositions were 0:10:90, 10:8:82 and 28:0:72 (all v/v/v).

RESULTS AND DISCUSSION

Between 1967 and 1987 over 860 papers on the subject of TH analysis were recorded by the *Chemical Abstracts* reference system, of which 33% were for HPLC-based analytical methods. TH is a drug with a therapeutic window of 5–20 $\mu\text{g ml}^{-1}$. The consequences to the patient of clinical concentrations outside of these limits have been widely discussed elsewhere^{29–33}. Recently, however, concern has been raised over the interference of endogenous components in the quantification of TH by the established HPLC methods. PX is a structural isomer of TH and is a metabolite of both caffeine and TH and endogenous levels of PX have been established as one of the reasons for over-estimating the concentrations of TH in blood samples^{34–38}.

The wavelengths used to test the algorithm were chosen to cover the spectral range 200–350 nm. Although some reference was made to the spectra of TH and PX (Fig. 1), the detection wavelengths were not necessarily chosen to be specific for those two compounds, apart from the criteria that there should be significant absorption at all wavelengths. Spectrally TH and PX are very similar ($r = 0.9947$). Examination of spectrochromatographic data sets indicates that, unless baseline resolution can be assured, co-elution of TH and PX could readily go undetected or be assigned as a column malfunction (Fig. 2a–c).

As with absorbance ratio plots^{14,39} it was necessary to modify the graphical scale on which the results of the MARC algorithm were viewed, in order to visually emphasize any changes in the correlation coefficient across the peak. Miller and Miller⁴⁰ suggest that a two-tailed *t*-test can be used, with $N - 2$ degrees of freedom (N = number of wavelengths monitored), to calculate a value for “*t*” below which changes in r (the correlation coefficient) are not significant. Using eqn. 1 and $N = 6$

$$t = r(N - 2)^{\frac{1}{2}}(1 - r^2)^{-\frac{1}{2}} \quad (1)$$

$t = 2.776$ when $p = 0.05$ and $t = 4.604$ when $p = 0.01$. These give limits of $r \geq 0.82$ and $r \geq 0.92$, respectively. These confines therefore provide the scale against which changes in the values of r can be assessed.

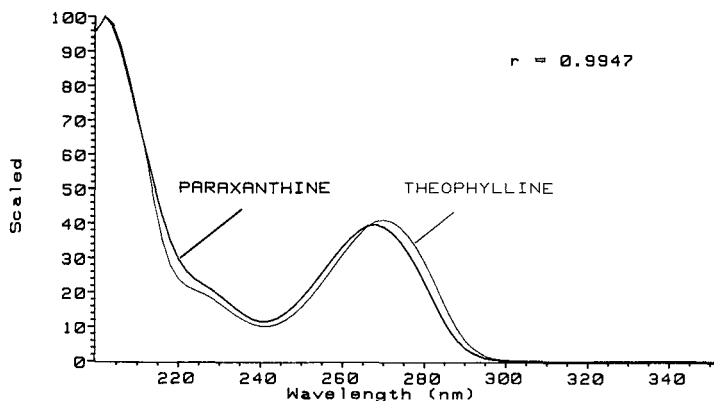


Fig. 1. Comparison of normalised theophylline and paraxanthine spectra collected on-line. See text for chromatographic conditions for $R_s = 2.9$.

Again, analogous to absorbance ratio⁴⁰, there are two significant values for the correlation coefficient: the maximum value obtained (r_{max}) and the mean value calculated across the peak (r_{mean}). Each of the two utilities provides a different amount of information about the content of the peak under investigation. When the IMARC algorithm is used the reference RDS vector will be that extracted at the apex of the peak under investigation. With the EMARC algorithm the identity of the reference RDS vector will be signified by EMARC(X), where X is the identity of the reference

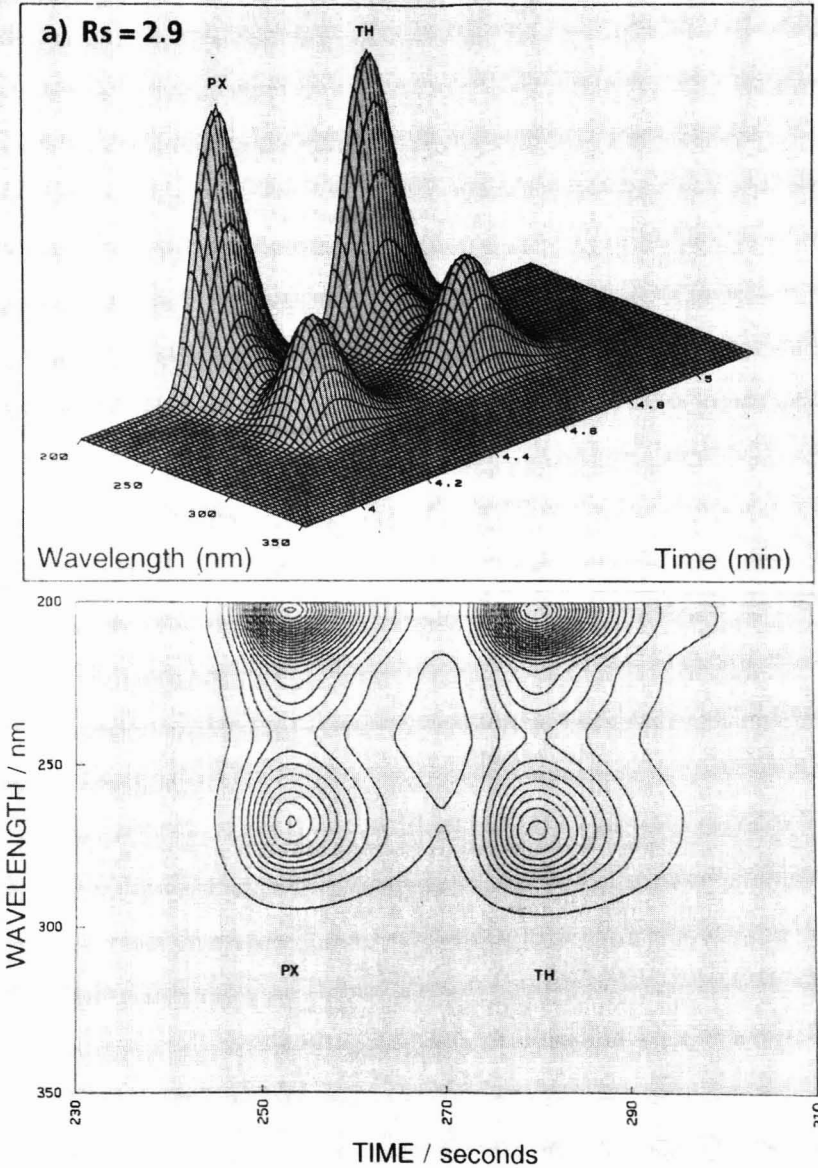


Fig. 2.

(Continued on p. 294)

compound. The IMARC and EMARC algorithms are identical in their operation apart from the source of the reference RDS vector used in the calculation.

The selectivity of the EMARC algorithm was evaluated using the binary solutions of PX and TH chromatographed under the $R_s = 2.9$ conditions described above. Application of EMARC(PX) and EMARC(TH) to the TH peak gave the results for r_{\max} shown in Fig. 3. The mean r_{\max} result which was obtained following application of EMARC(PX) was $0.9950 \pm 0.16\%$ relative standard deviation

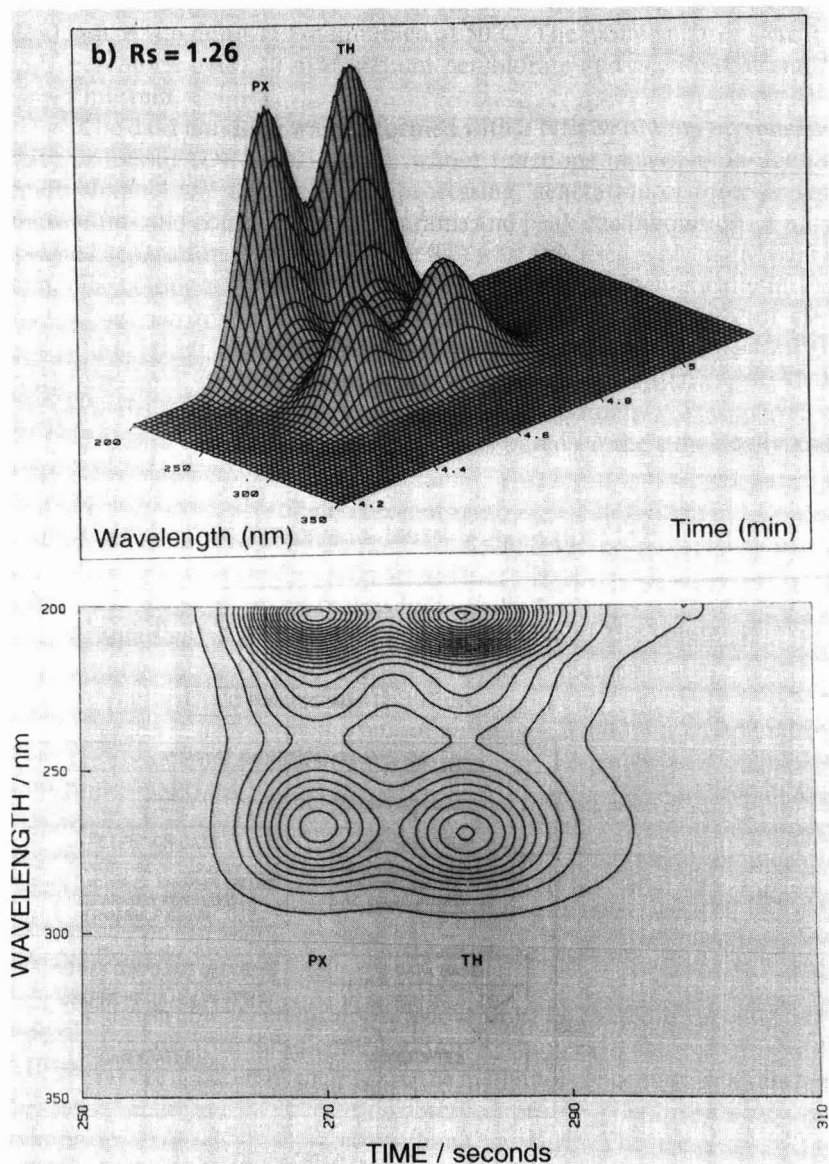


Fig. 2.

(R.S.D.), encompasses the correlation value calculated between the full spectra for TH and PX of 0.9947. This indicates that the reduction from >70 individual wavelength points in the total spectrum to the 6 points used in the practical application of the algorithm has not proved detrimental to the performance of the algorithm.

When the two components partially overlap ($R_s = 1.26$) the respective

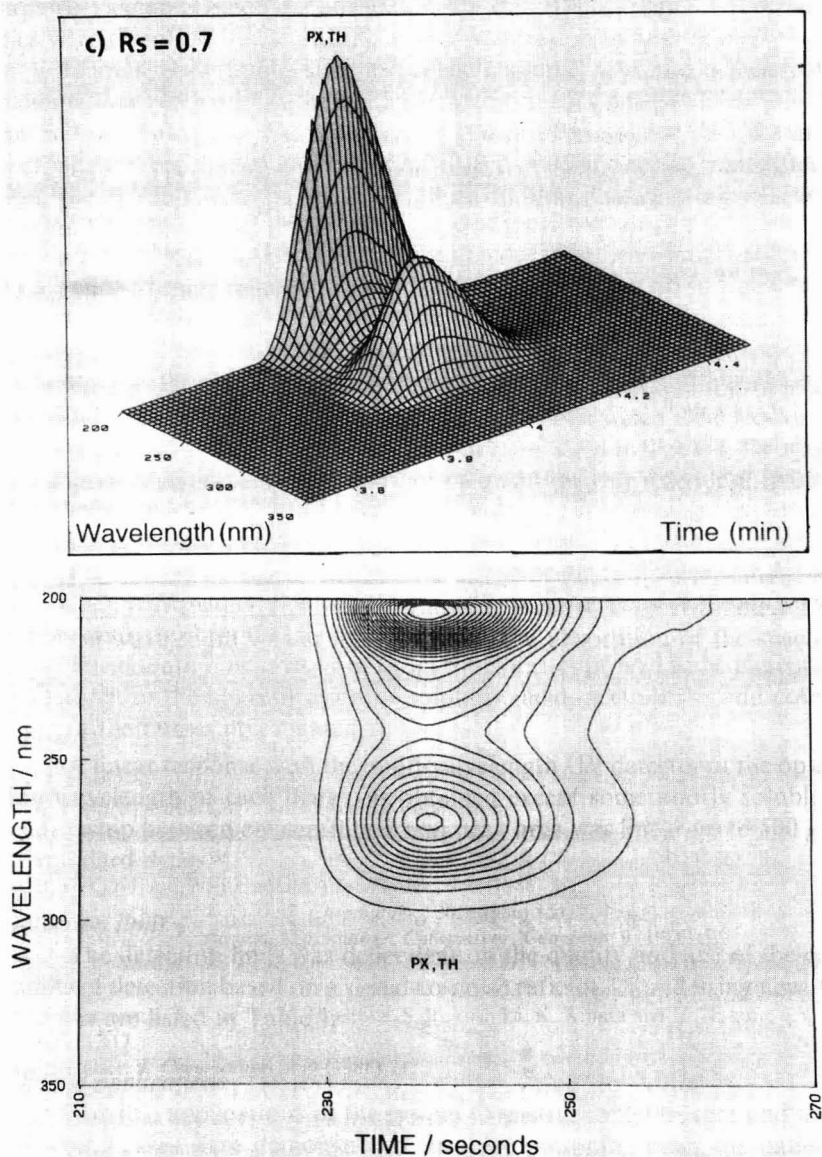


Fig. 2. Pseudo-three-dimensional and the corresponding contour plot representations of the full spectrochromatographic data sets for a mixture of theophylline (TH; $52.51 \mu\text{g ml}^{-1}$) and paraxanthine (PX; $52.5 \mu\text{g ml}^{-1}$) chromatographed under three different resolution conditions: (a) $R_s = 2.9$, (b) $R_s = 1.26$ and (c) $R_s = 0.7$. See text for chromatographic conditions.

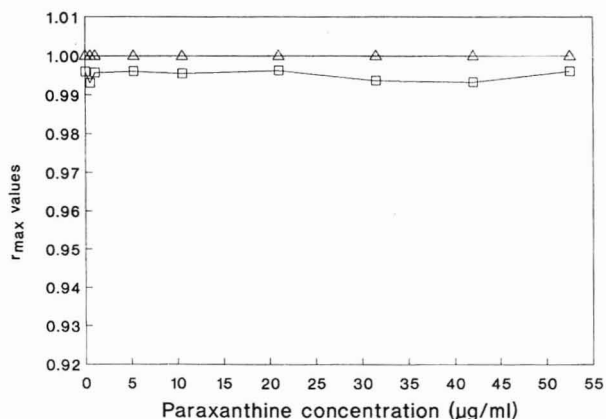


Fig. 3. The r_{max} results following application of EMARC(TH) (Δ) and EMARC(PX) (\square) to the theophylline peak. $R_s = 2.9$; see text for chromatographic conditions.

EMARC r_{mean} values reflect the relative proportions of TH and PX in the mixed peak (Fig. 4). By definition, if there is an area in the binary peak where only one component elutes, the EMARC r_{max} value for that component will be 1. As this is the case for both components, monitoring the difference between r_{max} and r_{mean} increases the apparent discrimination of the method (Fig. 5).

With minimal resolution between the two components ($R_s = 0.7$), the conclusions drawn from the basic r_{max} values are not as distinct as in the previous applications (Fig. 6). However, discernment may be improved by monitoring a linear function of the difference between the IMARC and EMARC r_{mean} values (Fig. 7). In this latter case the crossover point of the (IMARC–EMARC) graphs represents the equiabsorptive mixture, *i.e.* an equal contribution from each of the components to the total multichromatographic absorbance of the composite peak.

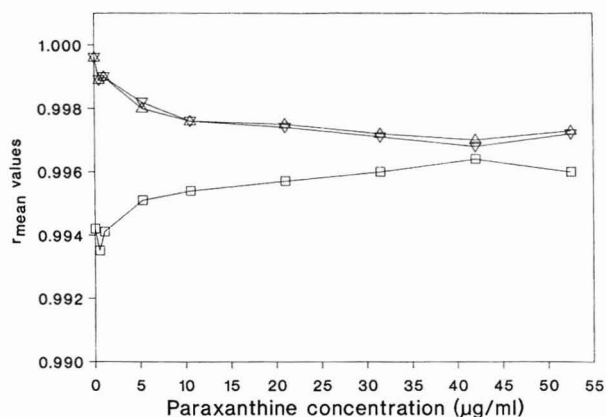


Fig. 4. The r_{mean} results following application of the MARC algorithm to binary mixtures of paraxanthine and theophylline: Δ = IMARC; ∇ = EMARC(TH); \square = EMARC(PX). $R_s = 1.26$; see text for chromatographic conditions.

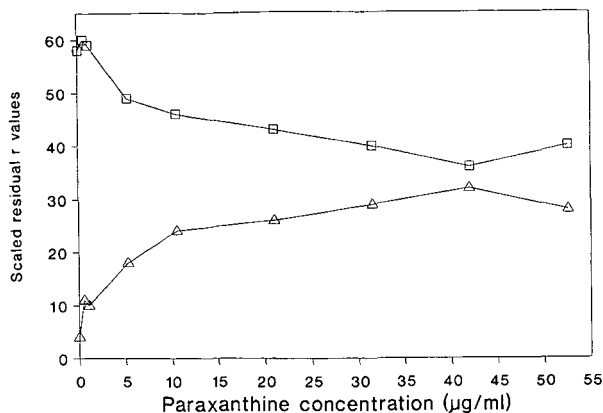


Fig. 5. Improvement in the discrimination of the EMARC(TH) (△) and the EMARC(PX) (□) obtained by monitoring the value of the difference $r_{\max} - r_{\text{mean}}$, $R_s = 1.26$; see text for chromatographic conditions.

As well as monitoring the r_{\max} and r_{mean} values it is possible to monitor the IMARC SUM values. Table I indicates that these measurements are concentration independent and analyte specific for PX and TH. Fig. 8 indicates that the IMARC SUM value is linearly proportional to the PX content of the peak, at the time point when the value is calculated. The difference in the gradients of the two graphs corresponding to the chromatographic conditions $R_s = 0.7$ and $R_s = 1.26$ is an indication of the extent to which the PX peak extends under the apex of the resultant binary peak.

Calculation of the maximum value of the absorbance ratio between the signals monitored at 220 and 268 nm (A_{220}/A_{268}) for the TH peaks ($R_s = 2.9$ and 1.26) and the fused peaks ($R_s = 0.7$) gave the results presented in Fig. 9. As the results for the TH peak under the chromatographic conditions for $R_s = 2.9$ and 1.26 were not significantly different only one set of results has been plotted. Whereas the peak

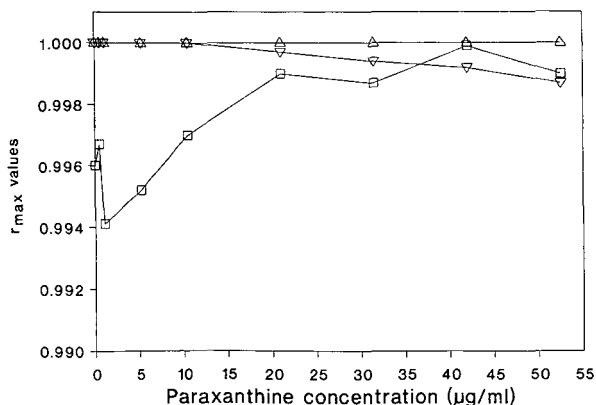


Fig. 6. The r_{\max} results following application of the MARC algorithm to binary mixtures of paraxanthine and theophylline: △ = IMARC; ▽ = EMARC(TH); □ = EMARC(PX). $R_s = 0.7$; see text for chromatographic conditions.

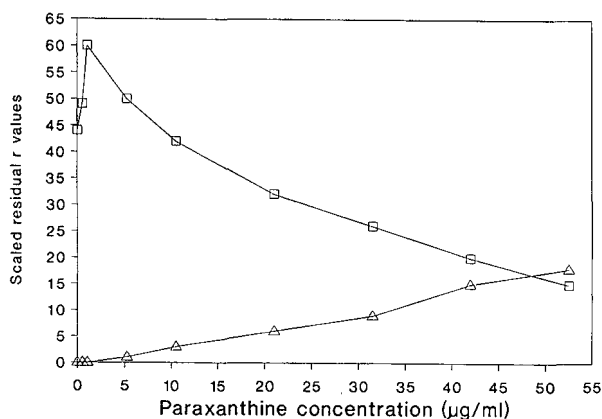


Fig. 7. Improvement in the discrimination of the MARC algorithm by monitoring the difference in the r_{mean} values obtained using IMARC and EMARC: Δ = IMARC - EMARC(TH); \square = IMARC - EMARC(PX). $R_s = 0.7$; see text for chromatographic conditions.

height measurements, at 220 nm, increased linearly in proportion to the PX concentration (in $\mu\text{g ml}^{-1}$) in the mixtures, the corresponding absorbance ratio graph is curvilinear. (The reverse situation occurs if the PX concentration is expressed as "percentage total xanthine content in the mixture".) Therefore, unlike the IMARC SUM method where the comparative graph of IMARC SUM *vs.* PX concentration ($\mu\text{g ml}^{-1}$) was linear ($R_s = 0.7$, Fig. 8), the absorbance ratio method could only be used as a relative method for determining the concentration of PX in the mixture. In the former case there was an observable change in the IMARC SUM value of the mixture containing $0.525 \mu\text{g ml}^{-1}$ compared to that for TH alone, whereas the PX concentration must be greater than $5 \mu\text{g ml}^{-1}$ before any significant change in the absorbance ratio is recorded.

TABLE I

SELECTIVITY AND STABILITY OF SUM MEASUREMENT FOR PX (5.25–52.5 $\mu\text{g/ml}$) AND TH (52.51 $\mu\text{g/ml}$)

For chromatographic conditions see text.

Sample	N	IMARC component wavelength (nm)						SUM
		204	220	240	250	268	284	
TH								
Mean	18	1.0000	0.2528	0.1070	0.1679	0.4200	0.1915	2.1391
R.S.D.	0	0	0.12	0.56	0.92	0.43	0.47	0.18
PX								
Mean	12	1.0000	0.3141	0.1214	0.1955	0.4108	0.1363	2.1780 ^a
R.S.D.	0	0	0.76	2.31	2.10	2.19	2.42	0.98

^a Mean values are significantly different; $p = 0.05$.

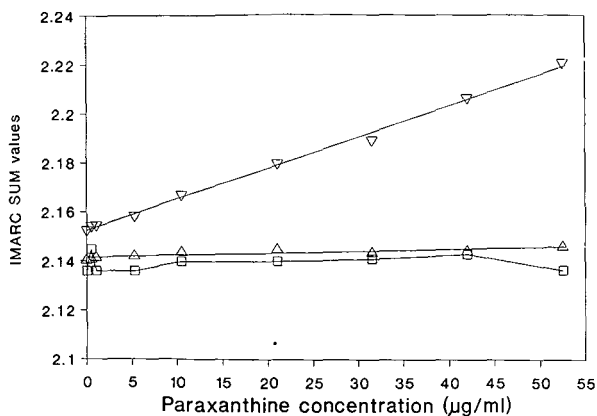


Fig. 8. Values of the IMARC SUM for the theophylline peak resolved from or coeluting with paraxanthine in a series of binary mixtures containing constant theophylline concentrations ($52.51 \mu\text{g ml}^{-1}$) and variable paraxanthine concentrations ($0\text{--}52.5 \mu\text{g ml}^{-1}$). R_s : $\square = 2.9$; $\triangle = 1.26$; $\nabla = 0.7$. See text for chromatographic conditions.

CONCLUSIONS

In conclusion, the application of EMARC(X) is specific and most sensitive when X is the minor component in the mixture. Selectivity and sensitivity may be enhanced by a judicious combination of either the IMARC and EMARC results or the r_{max} and r_{mean} results, dependent on the degree of resolution between the two components in the binary peak. The algorithm makes no assumptions about the peak shape of any of the co-eluting components. The values of r_{mean} obtained following application of either IMARC or EMARC, give an indication of the homogeneity of the peak, while the EMARC r_{max} value may be used secondarily as an indication of identity.

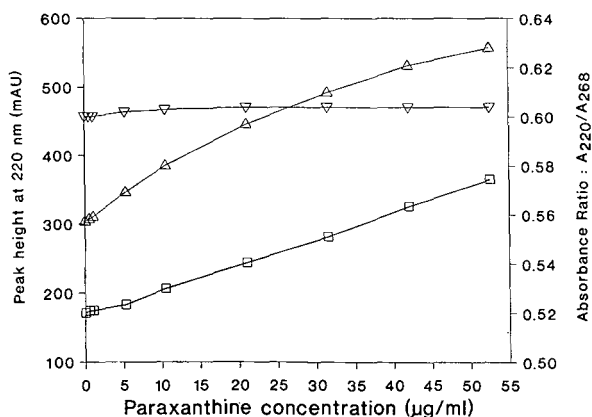


Fig. 9. Peak height at 220 nm ($R_s = 0.7$; \square) and absorbance ratio (A_{220}/A_{268}) values ($R_s = 1.26$, ∇ ; $R_s = 0.7$, \triangle) for the theophylline peak ($52.51 \mu\text{g ml}^{-1}$) in mixtures with paraxanthine ($0\text{--}52.5 \mu\text{g ml}^{-1}$). See text for chromatographic conditions.

The IMARC SUM value was found to be analyte specific and concentration independent, being dependent on the number and the uniqueness of the wavelengths used in its calculation. For a binary peak the value of the IMARC SUM was proportional to the concentration of the minor component in the mixture, with sensitivity being inversely proportional to chromatographic resolution. The limit of detection for PX in the mixture with TH was found to be 10% (w/w) using the absorbance ratio method. This compared with a 1% limit for the IMARC SUM method.

There is some indication in the results that the performance of the MARC algorithm is dependent on the number and specificity of the wavelengths used rather than on the chromatographic resolution. As the similarity of the spectra of the constituent components increases, it is expected that it may be necessary to increase the quantity and/or the selectivity of the wavelengths used in the algorithm. With the advent of more powerful computer controllers for DAD systems it should also be possible to expand the practical application of the MARC algorithm to match the original theory, *i.e.* using full spectra as the reference templates and operating on full spectrochromatographic data data sets. This would remove the need for analysts to choose "the most appropriate" wavelengths for inclusion in the algorithm. The algorithm would then become a truly operator-independent method.

ACKNOWLEDGEMENTS

The program used to produce the contour plots was a modification of the original programs written by Dr. H. P. Scott (Beecham Pharmaceuticals, Worthing, U.K.). We would also like to thank Dr. M. Seymour (Upjohn Ltd., Crawley, U.K.) for his helpful comments on the structure of this paper and Mr. T. Mettrick (School of Pharmacy, University of Bradford, Bradford, U.K.) for performing the *Chemical Abstracts* search.

REFERENCES

- 1 B. R. Kowalski, *Anal. Chem.*, 52 (1980) 112R–122R.
- 2 I. E. Frank and B. R. Kowalski, *Anal. Chem.*, 54 (1982) 232R–243R.
- 3 L. S. Ramos, K. R. Beebe, W. P. Carey, E. Sanchez M, B. C. Erickson, B. E. Wilson, L. E. Wangen and B. R. Kowalski, *Anal. Chem.*, 58 (1986) 294R–315R.
- 4 J. K. Strasters, H. A. H. Billiet, L. de Galaan, B. G. M. Vandeginste and G. Kateman, *J. Chromatogr.*, 385 (1987) 181–200.
- 5 W. H. Lawton and E. A. Sylvestre, *Technometrics*, 13 (1987) 617–633.
- 6 G. G. R. Seaton, J. G. D. Marr, B. J. Clark and A. F. Fell, *Anal. Proc.*, 23 (1986) 424–426.
- 7 N. Ostojic, *Anal. Chem.*, 46 (1974) 1653–1659.
- 8 R. Yost, J. Stoveken and W. Maclean, *J. Chromatogr.*, 134 (1977) 73–78.
- 9 A. M. Krstulovic, R. A. Hartwick, P. R. Brown and K. Lohse, *J. Chromatogr.*, 158 (1978) 365–376.
- 10 J. K. Baker, R. E. Skelton and C. Ma, *J. Chromatogr.*, 168 (1979) 417–427.
- 11 M. S. Denton, T. P. DeAngelis, A. M. Yacynych, W. R. Heineman and T. W. Gilbert, *Anal. Chem.*, 48 (1976) 20–24.
- 12 R. E. Dessey, W. D. Reynolds, W. G. Nunn, C. A. Titus and G. F. Moler, *Clin. Chem.*, 22 (1976) 1472–1482.
- 13 P. A. Webb, D. Ball and T. Thornton, *J. Chromatogr. Sci.*, 21 (1983) 447–453.
- 14 A. C. J. H. Drouen, H. A. H. Billiet and L. de Galan, *Anal. Chem.*, 56 (1984) 971–978.
- 15 P. C. White, *J. Chromatogr.*, 200 (1980) 271–276.
- 16 P. C. White and T. Catterick, *J. Chromatogr.*, 402 (1987) 135–147.
- 17 A. F. Poile and R. D. Conlon, *J. Chromatogr.*, 204 (1981) 149–152.

- 18 T. Alfredson and T. Sheehan, *J. Chromatogr. Sci.*, 24 (1986) 473–482.
- 19 G. T. Carter, R. E. Schiesswohl, H. Burke and R. Yang, *J. Pharm. Sci.*, 71 (1982) 317–321.
- 20 A. F. Fell, B. J. Clark and H. P. Scott, *J. Pharm. Biomed. Anal.*, 1 (1983) 557–572.
- 21 B. J. Clark, A. F. Fell, H. P. Scott and D. Westerlund, *J. Chromatogr.*, 286 (1984) 261–273.
- 22 P. Horvath, personal communication.
- 23 J. G. D. Marr, P. Horvath, B. J. Clark and A. F. Fell, *Anal. Proc.*, 23 (1986) 254–256.
- 24 J. Halket, *J. Chromatogr.*, 179 (1979) 229–241.
- 25 J. Van Rompay, *J. Pharm. Biomed. Anal.*, 4 (1986) 725–732.
- 26 E. Sanchez, L. S. Ramos and B. R. Kowalski, *J. Chromatogr.*, 385 (1987) 151–164.
- 27 E. Sanchez, L. S. Ramos and B. R. Kowalski, *J. Chromatogr.*, 385 (1987) 165–180.
- 28 G. P. Butrimovitz and V. A. Raisys, *Clin. Chem.*, 25 (1971) 1461–1464.
- 29 W. C. Bowman and M. J. Rand, *Textbook of Pharmacology*, Blackwell, London, 2nd ed., 1980, pp. 27.27–27.28.
- 30 T. W. Rall, in A. G. Gilman, L. S. Goodman and A. Gilman (Editors), *The Pharmacological Basis of Therapeutics*, Macmillan, New York, 6th ed., 1980, pp. 592–607.
- 31 P. W. Trembath, in P. Turner and D. Shand (Editors), *Recent Advances in Clinical Pharmacology*, No. 2, Churchill Livingstone, Edinburgh, 1980, pp. 55–71.
- 32 C. S. Frings, R. C. Keefer and J. M. Saloom, *Clin. Toxicol.*, 8 (1975) 553–561.
- 33 D. R. Jarvie, A. M. Thompson and E. H. Dyson, *Clin. Chim. Acta.*, 168 (1987) 313–322.
- 34 J. R. Miksic and B. Hodes, *Clin. Chem.*, 25 (1979) 1866–1867.
- 35 H. A. Farrish and W. A. Wargin, *Clin. Chem.*, 26 (1980) 524–525.
- 36 N. Daoud, T. Arvidsson and K. G. Wahlund, *J. Pharm. Biomed. Anal.*, 4 (1986) 253–260.
- 37 R. H. Drost, H. V. Schultz, R. A. A. Maes and J. M. van Rossum, *Clin. Toxicol.*, 25 (1987) 231–241.
- 38 C. L. Fligner and K. E. Opheim, *J. Anal. Toxicol.*, 12 (1988) 339–343.
- 39 H. Cheng and R. R. Gadde, *J. Chromatogr. Sci.*, 23 (1985) 227–230.
- 40 J. C. Miller and J. N. Miller, *Statistics for Analytical Chemistry*, Ellis Horwood, Chichester, 2nd ed., 1988, pp. 104–109.

CHROMSYMP. 1700

Aligned fiber columns for size-exclusion chromatography

MARTIN CZOK and GEORGES GUIOCHON*

*Department of Chemistry, University of Tennessee, Knoxville, TN 37996-1600, and Division of Analytical Chemistry, Oak Ridge National Laboratory, Oak Ridge, TN 37831-6120 (U.S.A.)

SUMMARY

Chromatographic columns are being developed that contain, instead of porous particles as in classical packed columns, bundles of aligned porous silica fibers of claimed diameter 18 μm and average pore size 270 \AA . From these properties, the material is comparable to conventional silica particles as a stationary phase for high-performance liquid chromatography. However, as fibers can be packed much more densely than spherical particles, the interstitial volume of the packing is significantly lower, while the pore volume can be higher. This combination of geometrical properties is important for size-exclusion chromatography. The performance of a prototype Aligned Fiber Column was tested by measuring the elution times and band broadening of polystyrene molecular weight standards with methylene chloride as the eluent. The results were compared to those found for columns packed with 10- or 3- μm silica particles. In view of possible applications for the separation of biopolymers, the surface of the column was modified by grafting alkyl diol groups in an *in situ* silanization process. The results obtained with several different proteins show a very low residual activity of the surface (only strongly basic proteins are retained), a slight decrease in the pore volume and pore diameters, with little change in the porosity ratio. As this was the first attempt at *in situ* diol bonding of any silica material, some polymerization of the silane occurred, seriously decreasing the efficiency of the column.

INTRODUCTION

In size-exclusion chromatography (SEC) the biggest molecules can move only between the particles of the packing and their elution volume is equal to the interstitial volume (V_0). For small molecules the pore volume (V_p) is also accessible and they are eluted with the mobile phase volume ($V_m = V_0 + V_p$). Hence the first peak of the chromatogram appears after V_0 and the separation takes place within the time corresponding to the elution of one pore volume. For easier comparison, the different contributions to the column volume are expressed as fractions of the empty column volume (porosities ϵ). Here we use the ratio V_p/V_0 to represent the geometrical characteristics of the column. Some workers prefer to use $(V_p + V_0)/V_0 = 1 + V_p/V_0$. The conversion is easy.

In practice, for most columns packed with microparticulate silica, the interstitial volume is about 40% of the total volume of the bed and the pore volume accounts approximately for another 40%. This means that the first half of the analysis time is spent waiting for the first peak and that the peak capacity is limited accordingly. Grushka¹ showed that the peak capacity, n , in SEC is given by

$$n = 1 + (\sqrt{N} / 4) \cdot \ln[1 + (V_p / V_0)] \quad (1)$$

The peak capacity is the number of Gaussian peaks that can be placed in the chromatogram, while maintaining a resolution of unity between them; N is the number of theoretical plates of the column. Eqn. 1 shows that, together with the column efficiency or plate number, the ratio of pore volume and interstitial volume will determine the separation power of the column as measured by the peak capacity.

Therefore, a higher pore volume and a lower interstitial volume would be desirable. For an ideal packing of spheres the volume fraction between particles can be calculated to be 26%, assuming the densest hexagonal arrangement. Slight variations in the particle size and shape, however, make it difficult to approach this theoretical limit closely. On the other hand, the pore volume cannot be increased very much without sacrificing the mechanical stability of the particles. The same is true also for packing materials based on organic polymers. The porosity ratio, V_p/V_0 , of most commercial phases for SEC is between 1.0 and 1.3. This means that the two segments of the chromatogram, from the time of injection to elution of the first peak, and from there to the elution of the last peak, are about equal. If we use an exceptionally low value of 0.35 for the interstitial porosity ε_0 (ref. 2) and assume that as much as 80% of the particle volume is accessible as pore volume, we find an upper practical limit for the porosity ratio of $V_p/V_0 = 1.5$. The upper theoretical limit would correspond to totally porous particles with $V_p/V_0 = 0.65/0.35 = 1.9$. Therefore, in practice, there is not much hope of improvement beyond this value for packings of particles.

However, when the particles are replaced with parallel porous fibers, we can expect a significantly higher packing density. From analogous geometrical considerations we find that an ideal packing of identical cylindrical fibers would fill almost 91% of the column volume, leaving an interstitial porosity of only 9%. If it is possible to manufacture porous silica fibers with a specific pore volume (ml/g) similar to that of conventional silica particles, the time range available for the actual separation would be increased with respect to the total analysis time. In practice, packings of fibers have an external porosity between 0.15 and 0.18. Again using a porous fraction for the fibers of 80%, but with $\varepsilon_0 = 0.15$, we find a porosity ratio of $V_p/V_0 = 4.5$. If a 10% interstitial porosity could be achieved, the porosity ratio would reach a value of 7.2. Hence the use of aligned fiber columns offers a large potential improvement in SEC performance.

It has been shown that a bundle of (non-porous) fibers can be regarded as a system of parallel capillaries^{3,4}. Between three neighboring fibers a flow channel is created, the cross-sectional area and flow resistance of which depend on the radii of the respective fibers. As all channels are fed with the same inlet pressure, slightly different radii will result in different flow velocities (the velocity being proportional to the square of the fiber radius). The signal of the detector is the sum of all the individual chromatograms. Hence fluctuations in the fiber radius will lead to an additional

contribution to the broadening of the chromatographic bands. Together with the dispersion in each of the capillaries, which has been shown by Golay⁵ to be large for star-shaped cross-sectional channels, this will result in excessive band broadening. Therefore, it is essential to have access to a source of fibers with an extremely homogeneous distribution of their diameters. Further, careful packing of these fibers is critical. Buckling or misalignment of a few fibers results in the formation of channels with an average velocity considerably higher than the average channel velocity, which may account for a considerable fraction of the total flow-rate. Such packing errors result in important band broadening or even in multiple bands for a single compound.

When the fibers are porous, however, crossover of solute molecules between neighboring flow channels, by diffusion through a fiber, becomes a possibility. This process will contribute to the relaxation of radial concentration gradients and to a decrease in column dispersion. Local concentration differences will be averaged out in a similar way as in packings of particles. This effect was observed in the preparation of Aligned Fiber Columns (PPG Industries, Pittsburgh, PA, U.S.A.). The efficiency of columns containing porous fibers is higher than that of columns packed with non-porous fibers⁶.

EXPERIMENTAL

The size-exclusion properties of an Aligned Fiber Column (AFC) were determined and compared with those of two conventional microparticulate silica materials. The characteristics of these columns were as follows:

PPG Industries AFC:	30 × 2.36 cm, 250 Å, 18 μm;
IMPAQ RG 2010 Si:	25 × 0.46 cm, 198 Å, 9 μm;
Vydac 101 TP B3:	5 × 0.46 cm, 300 Å, 3 μm.

From measurements described below, it was derived that the average cross-sectional areas available to the liquid flow in these columns are 2.4 cm² (AFC), 0.15 cm² (IMPAQ) and 0.12 cm² (Vydac).

The AFC was kindly supplied by PPG Industries. At present no columns of this kind are commercially available. Both the IMPAQ and the Vydac columns were packed in our laboratory from bulk material; IMPAQ, courtesy of PQ (Valley Forge, PA, U.S.A.) and Vydac, courtesy of Separations Group (Hesperia, CA, U.S.A.). The HETP values obtained for these two columns were between 60 and 70 μm for benzene in methylene chloride (1 ml/min), which is significantly higher than what could be expected from these materials if an optimized packing procedure had been used. The high-performance liquid chromatographic (HPLC) system used consisted of a Waters 510 pump (Millipore-Waters, Milford, MA, U.S.A.), a Rheodyne 7125 injection valve (Rheodyne, Cotati, CA, U.S.A.) and a Kratos Spectroflow 757 UV detector (ABI-Kratos, Ramsey, NJ, U.S.A.).

For the determination of the pore-size distribution of these packing materials, a set of thirteen polystyrene standards was used (4-5713; Supelco, Bellefonte, PA, U.S.A.), with molecular weights between 800 and 1 860 000 daltons, and benzene was used as a fully permeating substance. The individual molecular weights are given

as labels in Fig. 2 (in thousands). The polydispersities (M_w/M_n) of the polystyrene standards were given by the manufacturer as ≤ 1.06 . The samples were eluted with methylene chloride at various flow-rates (PPG, 10, 5, 2.5, 1 and 0.5 ml/min; IMPAQ, 1, 0.5, 0.1 and 0.05 ml/min; Vydac, 1 ml/min). The evaluation followed the method of Halász and Martin⁷. HETP values were determined by the graphical tangent method, equating the baseline width of the triangles to 4σ .

The *in situ* surface modification of the AFC was based on a standard method⁸, which had to be modified because of the lower reactivity of the alkoxy silane compared with chlorosilanes. The silane used was glycidoxypolytrimethoxysilane, purchased from Silar Labs. (Scotia, NY, U.S.A.).

RESULTS AND DISCUSSION

Porosities

The elution times of benzene and PS 1860 were used to calculate the total mobile phase volume (V_m), the interstitial volume (V_0), and finally their difference, the pore volume (V_p), all expressed as porosities (Table I).

TABLE I
POROSITIES OF AFC AND MICROPARTICULATE SILICAS

Material	ϵ_0	ϵ_m	ϵ_p	ϵ_p/ϵ_0	$\epsilon_p/(1-\epsilon_0)$
AFC	0.18	0.54	0.36	2.0	0.44
IMPAQ silica	0.42	0.89	0.47	1.1	0.81
VYDAC silica	0.41	0.71	0.30	0.7	0.51

The interstitial porosities of the two particulate silicas are in the usual range, slightly above 40%, and 1.5 times the theoretical value corresponding to an ideal packing of spheres. As expected, the volume between the fibers of the AFC is significantly lower. The ideal value of 9% is not reached, however, indicating some irregularity of the packing.

The pore volume of IMPAQ silica is at the upper limit for silica particles, whereas that of Vydac silica is low. The ratio between pore volume and interstitial volume of the AFC is twice that for typical silica packings. This can also be seen from the two chromatograms in Fig. 1 which are scaled to equal length to demonstrate the expanded separation period of the AFC. The porosity ratio of the AFC is still low compared with what could be expected (see Introduction).

The last column in Table I lists the porous fraction of each particle or fiber. Typically, values around 70% would be expected. The value for the IMPAQ material is above average, whereas the Vydac particles and the AFC fibers prove to be relatively compact. This result is not surprising for the AFC, in view of the procedure used to prepare the material.

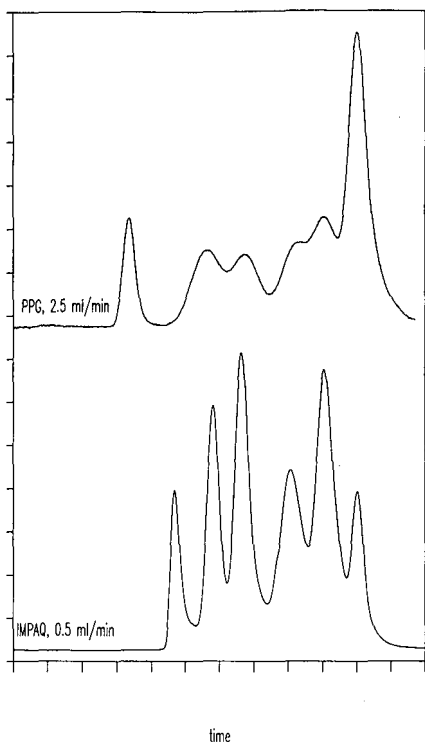


Fig. 1. Size-exclusion separation of a mixture of six polystyrene standards in methylene chloride on two columns (retention scaled to elution of last peak). Molecular weights were 1860, 47.5, 28.4, 9, 2 and 0.078 kilodaltons.

Pore size distributions

For molecular weight calibrations in SEC, the logarithms of the molecular weights are plotted against the elution times of the polystyrene standards (Fig. 2; molecular weights in thousands as labels). The elution times have been replaced by the size-exclusion distribution coefficient, $K_{\text{sec}} = (V_e - V_0)/V_p$ (where $K_{\text{sec}} = 0$ corresponds to total exclusion, $K_{\text{sec}} = 1$ to the benzene peak). For the AFC there is an approximately linear region of the calibration graph from a molecular weight of 100 000 to *ca.* 10 000 daltons, followed by a steeper region down to small molecules. This means that the best molecular weight discrimination (relative, on a logarithmic scale) is found with the molecular weights centered around 30 000 daltons, but also that in the range around 1000 daltons a rough estimate remains possible.

The calibration graphs of the two particulate silica columns, also given in Fig. 2, are more symmetrical and do not possess the sudden cut-off at the exclusion limit. Also, the molecular weight ranges are wider and therefore the selectivity between solutes in the center of the chromatogram will be lower.

For the characterization of size-exclusion packings, it is possible to convert the calibration graphs to pore size distributions following a complex procedure described by Knox and co-workers^{9,10}. For our purposes the semi-empirical method of Halász

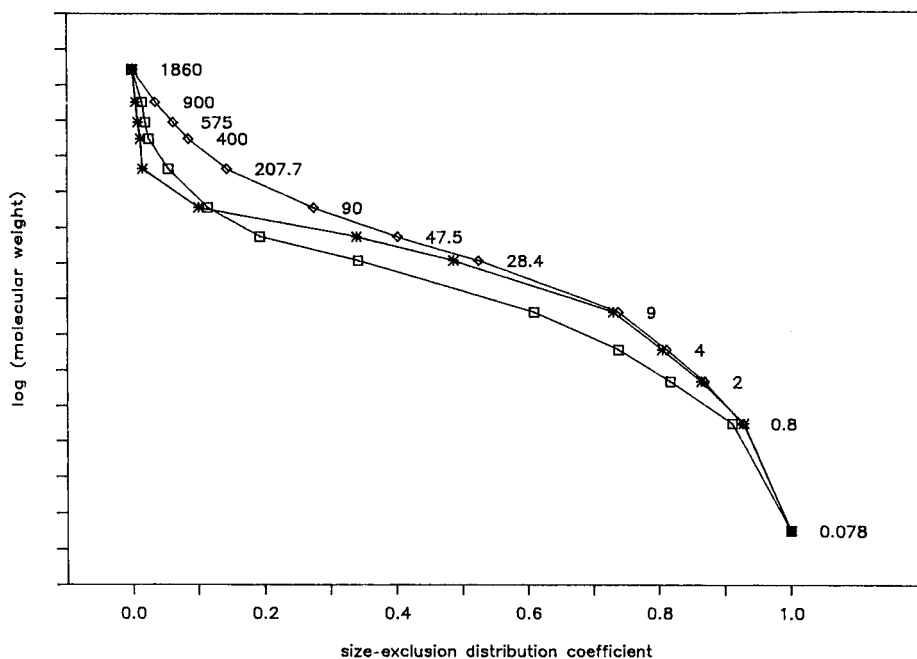


Fig. 2. Size-exclusion calibration graph for polystyrenes in methylene chloride on three different columns (labels: molecular weight in thousands). \diamond = Vydac; \square = IMPAQ; * = PPG.

and Martin⁸ was chosen. As it constitutes merely a linear transformation of the calibration graph, the resulting 'pore size distributions' are too broad and the mean pore sizes may not agree very well with those determined with other methods. However, this procedure is useful and practical for the comparison of the three columns.

From the retention times, the fraction of the pore volume that is accessible to molecules of a given molecular weight is determined. If the size of the molecules can be directly correlated with the diameter of the pores (which has been shown to be an oversimplification⁹), then we find the contribution of pores of a given size to the total pore volume. Often this experimental pore size distribution can be idealized as a log-normal curve, which is characterized by its mean value (at an accessibility of 50%) and its standard deviation.

Table II contains the mean Halász diameters and the widths of the pore size distributions (as standard deviations of the logarithms of the pore diameters).

The Halász diameters are smaller than the nominal values, which were determined by other methods, but vary in the same order. The standard deviations correspond to the range of molecular weights that can be separated on the columns. It is obvious that the AFC has a very narrow pore size distribution and therefore the separation between neighboring peaks in this range should be better than with the other two materials.

Other examples for conventional narrow pore size silicas have been given by Kirkland¹¹. The slopes of the calibration graphs given for his PSM silica correspond to molecular weight ranges spanning a factor of 90–450. The corresponding values for

TABLE II
MEAN HALÁSZ DIAMETERS AND WIDTHS OF PORE SIZE DISTRIBUTIONS

Material	Halász diameter (\AA)	σ
AFC (250 \AA)	170	0.40
IMPAQ silica (200 \AA)	150	0.48
Vydac silica (300 \AA)	240	0.54

the IMPAQ and Vydac column are 90 and 120, respectively, whereas for the AFC a value of about 40 is found.

Efficiencies, peak capacities

Due to the low diffusion coefficients of polymer molecules, it is impractical to operate SEC columns packed with conventional SEC stationary phases at the optimum eluent velocity^{12,13}. In addition, the band width of polymer peaks depends strongly on the flow-rate (Fig. 3). The HETP increases much more steeply with in-

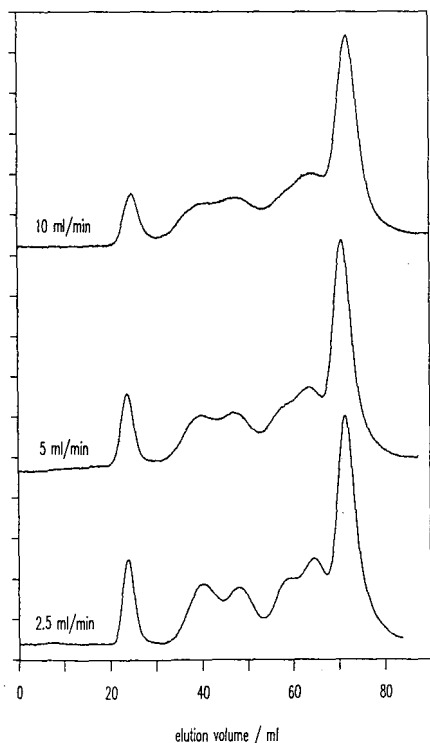


Fig. 3. Improvement in resolution by decreasing the flow-rate on the Aligned Fiber Column.

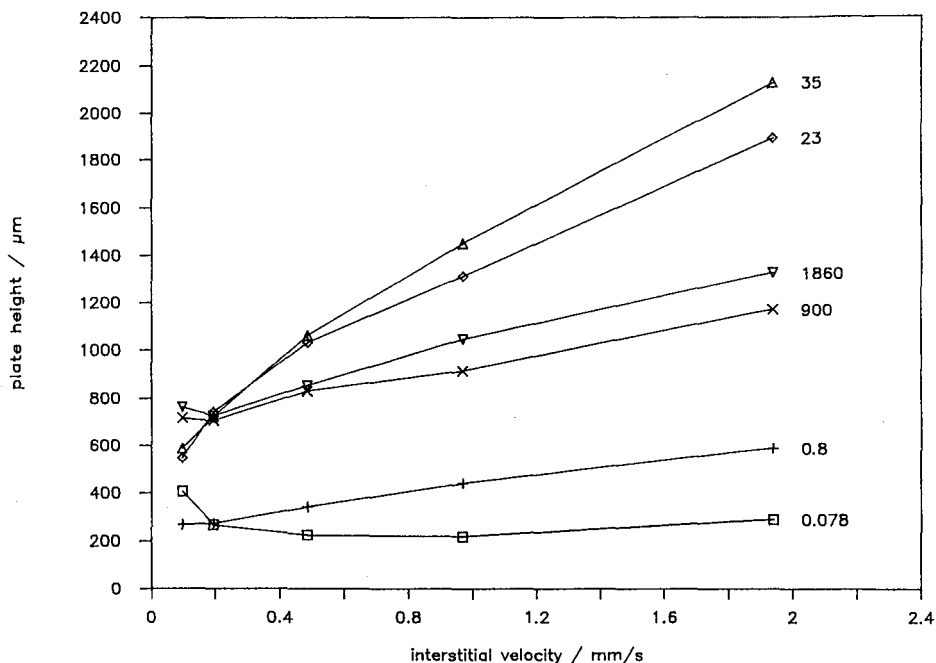


Fig. 4. HETP vs. interstitial velocity curves for some polystyrene standards (labels: molecular weight in thousands).

creasing flow-rate than it does for small molecules, *i.e.*, the C -term of the Van Deemter equation is larger for polymers. This can be seen in Fig. 4, which shows the velocity dependence of the HETP for a series of polystyrene standards. The optimum velocity is observed only for benzene (mol.wt. = 0.078 kilodaltons). For the other standards the flow-rate would have to be decreased below 0.5 ml/min and the analysis time increased beyond 3 h in order to observe the minimum value of the HETP. The lowest HETP value found for benzene is slightly above 200 μm , corresponding to about 1400 plates. This low efficiency, which is disappointing even for an 18- μm support column, indicates that the packing procedure for the fibers has not yet been optimized.

Fig. 5 shows a plot of the plate heights for all standards at all flow-rates, as a function of their position in the chromatogram, as given by K_{sec} . From benzene to polystyrene 90 000, the HETP increases owing to decreasing diffusion coefficients. Then the HETP drops suddenly, because the pores are no longer accessible and the higher molecular weight polymers experience only limited band broadening in the interstitial volume.

For the IMPAQ column, the plot of HETP *versus* the position of the band in the chromatogram is similar, the only difference being that the maximum plate height is shifted towards lower molecular weights. However, the values of the HETP measured are smaller by at least a factor of 3. For benzene, a minimum value of 70 μm is found.

The peak capacity can also be used as a measure of the column performance. It

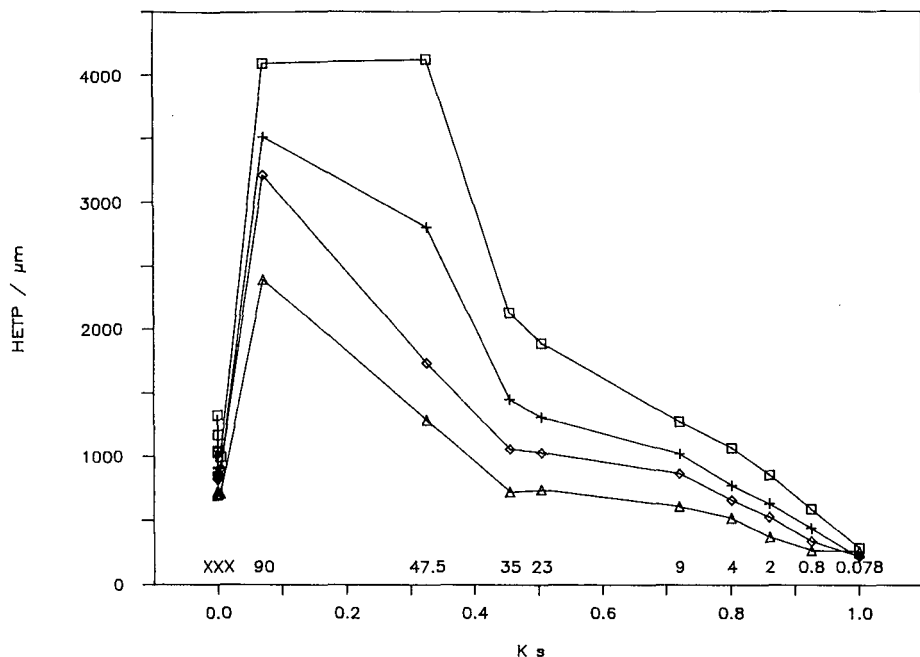


Fig. 5. HETP vs. K_{sec} of polystyrene standards at different flow-rates; □ = 10; + = 5; ◇ = 2.5; △ = 1 ml/min.

is the number of peaks that would fit into the chromatogram if all of them were separated by a resolution of 4σ . It can be calculated by dividing the duration of the chromatogram by the baseline width of one peak. To take into account the dependence of the peak width, w_b , on the retention, the peak capacity for the SEC columns studied was calculated from a summation over all standards (Δt = elution time interval between two successive peaks):

$$PC = \frac{(t_m - t_0)^2}{\Sigma(w_b \Delta t)} \quad (3)$$

The result is reported in Fig. 6 for both the AFC and the IMPAQ columns as a function of flow-rate. The peak capacity of the AFC is a steep function of the flow-rate. At extremely low velocities and with analysis times of several hours it approaches the values found with the IMPAQ column.

Hence it is possible in SEC to compensate for the poor mass transfer of the column by an exceptionally low flow-rate. More important, it is also possible to compensate for the poor efficiency by an exceptionally large porosity ratio. Higher efficiencies can be expected in the future as a result of continuing research and further optimization efforts⁶.

DIOL bonded phase

If the Aligned Fiber Column material is to be used for the size-exclusion chromatography of proteins, the silica surface has to be modified by reaction with a silane

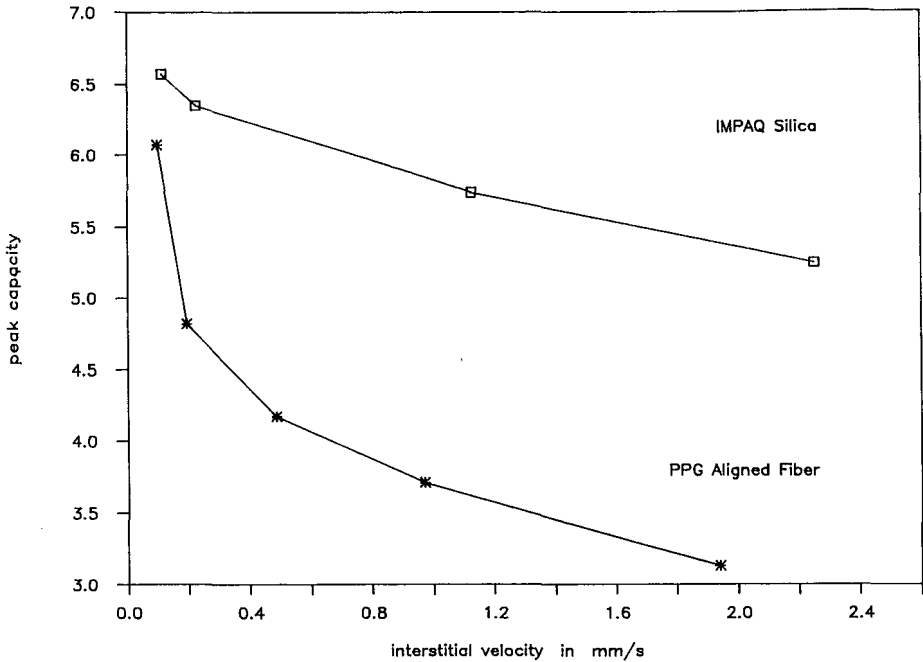


Fig. 6. Peak capacity for polystyrene standards vs. interstitial velocity.

carrying a hydrophilic group. The most widely used and most readily available of such silanes is glycidoxypropyltrimethoxysilane, which, after bonding, is hydrolyzed to give the so-called diol phase. With our one column we could not optimize the bonding procedure but had to accept the results produced in our first attempt.

For surface modification, an *in situ* bonding procedure was used⁷. Since this alkoxy silane is far less reactive than chlorosilanes, significant changes in the procedure were necessary. A 300-ml volume of a 10% solution of the diol silane in toluene was recirculated through the column for 500 min at room temperature, then the solution was left in the column overnight and washed out the next morning with methanol. After several hours of equilibration with a phosphate buffer, hydrolysis of the epoxy functional groups to the diol form was assumed to be complete. Initial tests showed that proteins could be eluted within the exclusion volume when phosphate buffer (0.2 mol/l, pH 6.8) was used as the mobile phase.

As preliminary experiments had suggested that some polymerization of the silane had occurred, we tried to use an additional heat treatment to rearrange the polysiloxane molecules adsorbed on the surface and form a more homogeneous layer. The column was dried by passing a stream of nitrogen through it, then the inlet and outlet were sealed with stainless-steel plugs and the column was 'baked' overnight in an oven at 200°C. After washing out all the material that had become dislodged, the pore size distribution of the 'baked diol' column was determined (see below). Repeating the baking procedure a second time did not produce any further significant change.

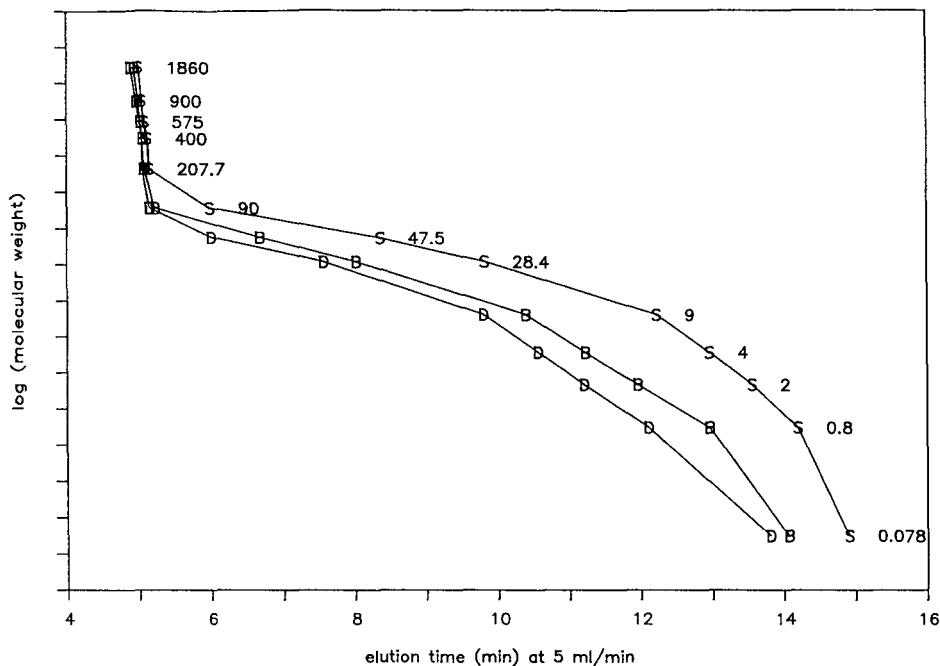


Fig. 7. Size-exclusion calibration graphs for the Aligned Fiber Column before and after silanization to the diol phase. S = Silica; B = baked diol; D = diol.

Both the freshly synthesized diol and the baked diol columns were characterized with polystyrene standards in methylene chloride at 5 ml/min (Fig. 7). The results are summarized in Table III.

After bonding, the pore volume was found to have decreased by more than 10%, whereas the interstitial porosity had hardly changed. This means that most of the silane was bound in the pores and did not affect the channels between fibers. As expected, the pore diameters also decreased, lowering the exclusion limit to a molecular weight below 90 000 daltons and the average Halász diameter to 106 Å (127 Å after heat treatment).

After silanization, the efficiency of the column had deteriorated markedly, with the formation of double peaks for small molecules such as benzene (Fig. 8). This

TABLE III
POROSITIES OF ORIGINAL AND TREATED AFC

AFC	ϵ_m	ϵ_0	ϵ_p	ϵ_p/ϵ_0
Silica	0.54	0.18	0.36	2.0
Diol	0.50	0.18	0.32	1.8
Baked diol	0.52	0.18	0.34	1.9

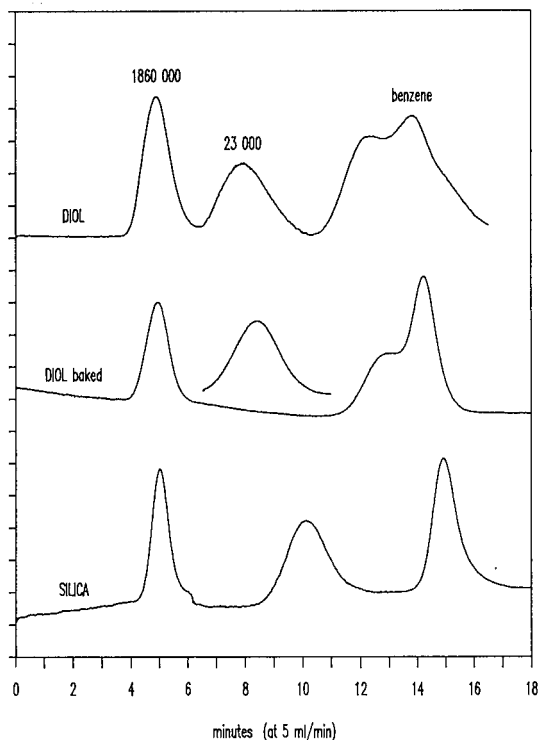


Fig. 8. Comparison of peak positions and band broadening on the diol columns.

indicates that changes in the pore structure took place that hinder diffusion. During the heat treatment, about half on the initially bound silane was removed, as indicated by the change in pore volume. At the same time the efficiency also increased. For the higher molecular weight compounds, the HETP values approached those found before silanization. Small molecules, however, were still eluted as double peaks.

The following figures show the chromatographic behavior of proteins on the diol column. A phosphate buffer at pH 6.8 with a phosphate concentration of 0.2 mol/l was chosen as the mobile phase. The ionic strength is needed to suppress ion-exchange interactions of the basic proteins with the residual silanols found even on a well deactivated modified silica surface.

The size calibration graph (Fig. 9) begins at a molecular weight of about 170 000 daltons and ends with the dead time ($K_{scc} = 1$) at 13.8 min (5 ml/min). As proteins are more tightly coiled than linear polymers, it is expected that the same retention time would be observed for proteins of higher molecular weight than the polystyrene samples. Unlike the random coils of polystyrene standards, protein molecules in their native state differ in structure, shape and compactness. For that reason, a perfectly smooth calibration graph is not to be expected under these conditions. The three proteins eluting close to or after the void volume are strongly basic ($pI > 9$) and hence are slightly retained by cation exchange.

In Fig. 10 some of the chromatograms obtained are reproduced. As the viscos-

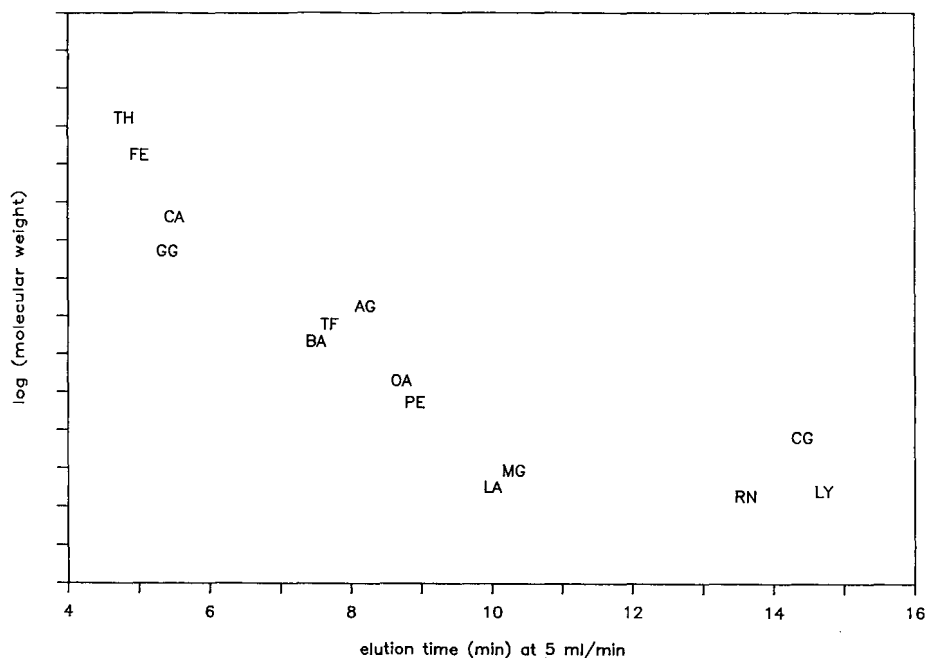


Fig. 9. Size-exclusion calibration graph for proteins on the diol Aligned Fiber Column. Mobile phase: phosphate buffer, pH 6.8, 0.2 mol/l. Proteins and approximate molecular weights (in thousands): TH = thyroglobulin (porcine), 660; FE = Ferritin (equine), 450; CA = Catalase (bovine), 240; GG = γ -globulins (bovine), 170; AG = Amyloglucosidase (*Aspergillus niger*), 97; TF = transferrin (bovine), 80; BA = serum albumin (bovine), 67; OA = ovalbumin (chicken), 45; PE = Pepsin (porcine), 36; CG = chymotrypsinogen A (bovine), 25; MG = myoglobin (equine), 17.8; LA = lactalbumin (bovine), 14.4; LY = lysozyme (chicken), 14.4; RN = ribonuclease A (bovine), 13.7.

ity of aqueous buffers is much higher than that of methylene chloride, the diffusion coefficients of proteins are correspondingly lower, and the bands are extremely broad and do not offer much potential for an actual separation. In addition, the late-eluting proteins show double peaks. A decrease in flow-rate from 5 to 0.1 ml/min results in a significant sharpening of the bands, but the separation time also increases from 15 min to 12 h, becoming prohibitively long.

Hence the diol bonding with our unoptimized method was only a partial success. The coverage is sufficiently dense for the unretained elution of most proteins, but polymerization of the silane led to excessive band broadening. Together with a higher initial efficiency of the packing and a higher pore volume, a better silanization procedure could lead to stationary phases superior to conventional size-exclusion materials.

CONCLUSIONS

Good resolution between polymer peaks in size-exclusion chromatography is favored by three factors. The length of the actual chromatogram, and with it the peak capacity, increases with the pore volume of the stationary phase. A narrow pore size

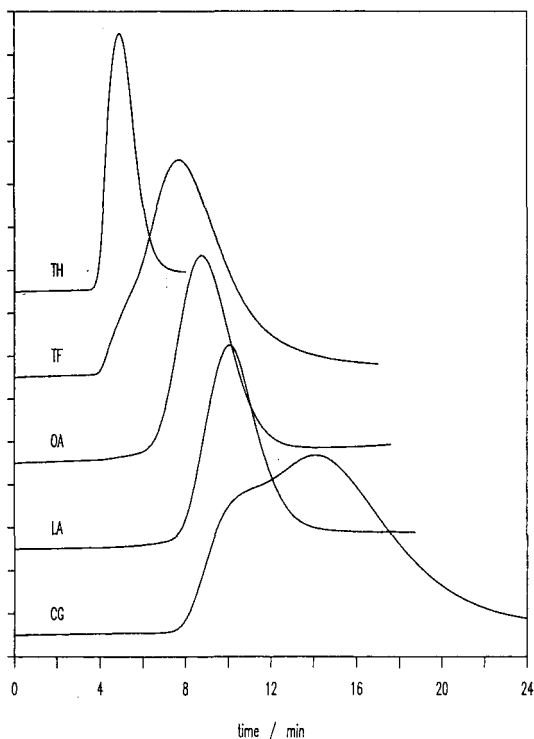


Fig. 10. Elution profiles of some proteins on the diol column. Conditions, protein abbreviations and molecular weights as in Fig. 9.

distribution causes a narrow molecular weight range to be spread over the whole length of the chromatogram. Band broadening must be kept as low as possible.

The porosity ratio of the Aligned Fiber Column excels over those of conventional silica packings. For the purification of monodisperse polymers such as proteins, the narrow pore size distribution should also be an advantage. If the material is to be used for the determination of molecular weight profiles of inhomogeneous synthetic polymers, however, a wider pore size distribution might be needed. Comparison with other silica packings indicates that the specific pore volume of this material could still be increased. According to the manufacturer, fibers with a higher porous fraction have been prepared recently, raising the ratio of pore volume to interstitial volume above 3 (ref. 6). Also, wider pore size distributions could be prepared on demand.

The HETP value for the Aligned Fiber Column tested, on the other hand, did not compare favorably with that of standard silica packings. An improved packing procedure and the future introduction of smaller fiber diameters, however, may lead to a useful alternative to conventional size-exclusion materials.

It was shown that the surface of the column can be effectively deactivated by *in situ* reaction with glycidoxypopylsilane. In the course of the reaction, however, some polymerization of the silane seems to have occurred, leading to excessive band broadening and the formation of double peaks. By partially removing the siloxane it was

possible to restore some of the previous efficiency. The structure of the packing did not seem to suffer from the silanization reaction. The deactivation procedure was not optimized. With a different modification procedure, better results can be expected.

ACKNOWLEDGEMENTS

This work was supported in part by grant 89-01382 from the National Science Foundation and by the cooperative agreement between the University of Tennessee and the Oak Ridge National Laboratory. We thank Dr. Richard Beaver (PPG Industries) for supplying the Aligned Fiber Column.

REFERENCES

- 1 E. Grushka, *Anal. Chem.*, 42 (1970) 1142.
- 2 K. K. Unger, G. Jilge, J. N. Kinkel and M. T. W. Hearn, *J. Chromatogr.*, 359 (1986) 61.
- 3 R. F. Meyer, P. B. Champlin and R. A. Hartwick, *J. Chromatogr. Sci.*, 21 (1983) 433.
- 4 R. D. Hegedus, *J. Chromatogr. Sci.*, 26 (1988) 425.
- 5 M. J. E. Golay, in D. H. Desty (Editor), *Gas Chromatography 1958*, Butterworths, London, 1958, p. 36.
- 6 R. Beaver, PPG Industries, Pittsburgh, PA, personal communications, 1988 and 1989.
- 7 R. K. Gilpin, D. J. Camillo and C. A. Janicki, *J. Chromatogr.*, 121 (1976) 13.
- 8 I. Halász and K. Martin, *Angew. Chem., Int. Ed. Engl.*, 17 (1978) 901.
- 9 J. H. Knox, H. P. Scott, *J. Chromatogr.*, 316 (1984) 311.
- 10 J. H. Knox, H. J. Ritchie, *J. Chromatogr.*, 387 (1987) 65.
- 11 J. J. Kirkland, *J. Chromatogr.*, 125 (1976) 231.
- 12 J. C. Giddings, *Adv. Chromatogr.*, 20 (1982) 217.
- 13 G. Guiochon and M. Martin, *J. Chromatogr.*, 326 (1985) 3.

CHROMSYMP. 1735

High-performance liquid chromatography of transfer ribonucleic acids on spherical hydroxyapatite beads

YOSHIO YAMAKAWA*

Department of Applied Immunology, National Institute of Health, Kamiosaki 2-10-35, Shinagawa-ku, Tokyo 141 (Japan)

KENJI MIYASAKA and TOSHIHIRO ISHIKAWA

New Venture Business Department, Toa Nenryo Kogyo Co., Hitotsubashi 1-1-1, Chiyoda-ku, Tokyo 100 (Japan)

YUKO YAMADA

Laboratory of Chemistry, Jichi Medical School, Minamikawauchi machi, Kawauchi-Gun, Tochigi 320-04 (Japan)

and

TSUNEO OKUYAMA

Department of Chemistry, Faculty of Science, Tokyo Metropolitan University, Fukazawa 2-1-1, Setagaya-ku, Tokyo 158 (Japan)

SUMMARY

High-performance liquid chromatography (HPLC) on newly developed spherical beads of hydroxyapatite was applied to the analysis of purified *E. coli* tRNAs (Val, Met, Tyr and Phe). tRNAs were eluted from the column separately with appreciable differences in retention time by a 45-min gradient of phosphate buffer (pH 6.8) of concentration from 64 to 123 mM; both the retention times and peak areas of respective tRNAs were highly reproducible. Total tRNA (tRNA^{Total}) preparations obtained from *E. coli* and *B. subtilis* were also analysed on the column. It is possible even to elute tRNA^{Total} which may, in general, contain 60 or more tRNA species with a relatively shallow gradient such as 75–132 mM. The recovery of tRNA from the column was as high as 90%. Owing to the complicated composition, the elution profile of tRNA^{Total} had a wide spread irregular shape but, with a 1-h gradient more than ten peaks were easily detected. When the amino acid-accepting activity of tRNA in the eluate of tRNA^{Total} was determined, for ten specific tRNAs, each activity peak was eluted sharply from the column. In addition, several tRNA activities were eluted in different fractions. This indicates that isoacceptors were separated by the column. The results show that HPLC on hydroxyapatite beads is useful for the purification and characterization of tRNA.

INTRODUCTION

Adsorption chromatography on hydroxyapatite (HAP), introduced by Tiselius *et al.*¹, is sometimes a very effective process for purification of biomacromolecules

such as proteins and nucleic acids. However, the method was not widely accepted because the synthesis of HAP with reproducible properties was difficult. Currently, spherical beads of HAP, a new type of ceramic which has a rigid structure and uniform quality, are being produced by several manufacturers. Basic studies on some of these new ceramic HAP beads for high-performance liquid chromatography (HPLC) have been reported by Kadoya *et al.*². We have also reported on the easy purification of mouse monoclonal antibodies, especially IgM, using HPLC on HAP beads³. The results of the various studies indicate that HPLC on HAP is a valuable method for the purification and analysis of biological polymers. We now report the application of this method to the separation of tRNAs of *E. coli* and *B. subtilis*.

EXPERIMENTAL

tRNAs

Purified *E. coli* tRNAs (Val, Lot No. 42F-05392; f-Met, Lot No. 86F-05121; Tyr, Lot No. 67F-02831; Phe, Lot No. 24F-03761) were purchased from Sigma (St. Louis, NO. U.S.A.). Total tRNAs (tRNA^{Total}) was prepared from *E. coli* K12 and *B. subtilis* W168 as described by Zubay⁴. Purified tRNA was dissolved in 5 mM phosphate buffer (pH 6.8) at about 0.5 mg/ml and was stored at 5°C. tRNA^{Total} was also dissolved in the same buffer at a concentration of about 1.5–2 mg/ml. The concentration of tRNA was determined spectrophotometrically with the use of the value $E_{1\text{cm}}^{0.1\%} = 20$ at 260 nm.

Determination of amino acid-accepting activity

The preparation of crude *E. coli* aminoacyl-tRNA synthetase and the assay of the amino acid-accepting activity of tRNA with ¹⁴C-labelled amino acids were carried out as described by Nishimura *et al.*⁵.

Columns

Packed columns (10 × 0.75 cm I.D. and 10 × 2.14 cm I.D.) of HAP were obtained from Toa Nenryo Kogyo (Tokyo, Japan). A narrow bore column packed with 2.2- μm HAP beads was used for routine analysis, whereas a large-bore column packed with 5- μm beads was used for semi-preparative purposes.

Apparatus

A Shimadzu LC-6A liquid chromatograph with a two-pump gradient system was used. Elution of nucleic acids was monitored with a SPD-6A UV detector at 260 nm and a Chromatopak C-R6A recorder. Samples were introduced into the column with either a SIL-6A automatic sample injector or a Rheodyne 7125 sample injector. The eluate was collected manually according to the recorder signal.

Elution

Elution of tRNA from the column was performed with a linear gradient of phosphate buffers (pH 6.8) of concentration between (A) 5 mM and (B) 300 mM. With a gradient from 20 to 45 B, which corresponds to phosphate concentrations from 75 to 138 mM, it was possible to elute tRNAs from the column. The analytical column was eluted with a flow-rate of 0.5 ml/min (*ca.* 20 kg/cm²) and the semi-preparative column at 4.0 ml/min (*ca.* 5 kg/cm²). Chromatography was carried out at room temperature.

RESULTS

Chromatography of E. coli tRNAs

Fig. 1 shows typical elution profiles of the purified *E. coli* tRNAs on an analytical HAP column. tRNAs were eluted from the column with different retention times by a shallow gradient (20–40% B, corresponding to 64–123 mM phosphate) of phosphate buffer (pH 6.8). It was found that tRNA^{f-Met} and tRNA^{Val} were eluted as relatively sharp peaks whereas tRNA^{Tyr} was eluted as a broad peak and tRNA^{Phe} as two distinct peaks. The phenylalanine-accepting activity in the eluate of tRNA^{Total} of *E. coli* was determined in the same manner, and showed two distinct peaks (see Fig. 6). Chromatography of an equimolar mixture of three tRNAs (f-Met, Val and Phe) was performed successfully using a similar gradient (see Fig. 2b).

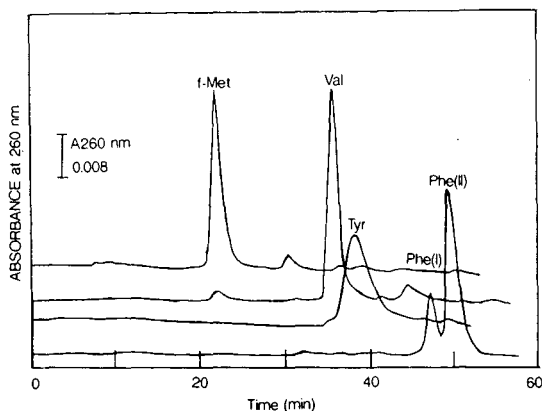


Fig. 1. Chromatography of *E. coli* tRNAs on an HAP column. Four purified tRNAs (about 4 μ g) were applied to a column (10 \times 0.75 cm I.D.) of HAP which had been equilibrated with 20% B. The column was eluted at a flow-rate of 0.5 ml/min with a 45-min linear gradient of phosphate buffer (pH 6.8) from 20 to 40% B. A, 5 mM phosphate buffer pH 6.8; B, 300 mM phosphate buffer (pH 6.8).

Reproducibility

To determine the reproducibility of the chromatography of tRNAs on the HAP column, an equimolar mixture of purified tRNAs (f-Met, Val and Phe) was analysed four times on the column. Both the retention times and peak areas of were highly reproducible (Table I).

TABLE I

REPRODUCIBILITY OF RETENTION TIMES AND PEAK AREAS OF PURIFIED *E. coli* tRNAs

tRNA	Retention time (min) ^a	Peak area (μ V) ^a
f-Met	21.89 \pm 0.3	38 650 \pm 145
Val	32.37 \pm 0.4	33 654 \pm 1053
Phe I	44.32 \pm 0.4	11 589 \pm 468
Phe II	46.01 \pm 0.3	26 574 \pm 724

^a Means of four runs \pm S.D.

Chromatography of tRNA^{Total}

Fig. 2a shows a typical elution profile of *E. coli* tRNA^{Total} on an analytical column when eluted with a 45-min gradient of phosphate buffer from 23 to 45% B. For comparison, the elution profile of a mixture of three purified tRNAs analysed under the same conditions is shown in Fig. 2b. It was possible to elute tRNAs from the column with a shallow gradient of 23–45% B because as much as 95% of the material applied to the column was recovered in the eluates. Comparing these chromatograms, it appeared that tRNA^{f-Met}, tRNA^{Val} and tRNA^{Phe} were eluted in the early, middle and late parts of the tRNA^{Total} chromatogram, respectively. The order of elution of respective tRNAs in tRNA^{Total} from the HAP column was verified by determining the amino acid-accepting activity in the eluate (see Fig. 6). The elution profile of tRNA^{Total}, recorded at 260 nm, had a widespread irregular, shape, as tRNA^{Total} usually contains about 60 species of molecules, including isoacceptors. Therefore, we tried to improve the resolution by extending the gradient time. Comparative chromatograms of *E. coli* tRNA^{Total} obtained with the extended gradient time are shown in Fig. 3. The overall elution profile is still similar but a minor improvement in the resolution was achieved.

Chromatography of *B. subtilis* tRNA^{Total} was also performed under similar conditions, as shown in Fig. 4a. Separation of peaks seemed more evident in comparison with the chromatogram of *E. coli* tRNA^{Total}. To verify the peak positions, several fractions (hatched areas in Fig. 4a) were diluted 3–5-fold with buffer A and rechromatographed under the same conditions. These results are shown in Fig. 4b. The respective fractions were eluted from the column with retention times identical with those obtained in the first chromatography.

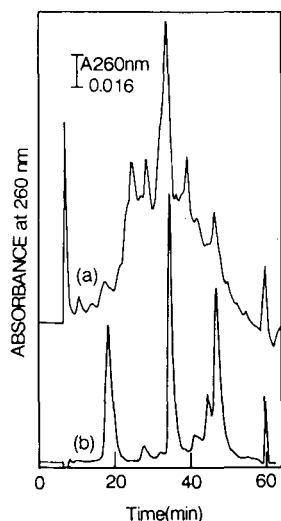


Fig. 2. Chromatography of (a) tRNA^{Total} and (b) a mixture of purified tRNAs of *E. coli* on an HAP column. (a) Total tRNA (about 40 μ g) of *E. coli* was applied to a column (10 \times 0.75 cm I.D.) of HAP which had been equilibrated with 23% B. The column was eluted at a flow-rate of 0.5 ml/min with a 60-min linear gradient of phosphate by increasing the fraction of buffer B to 43%. Buffers A and B as in Fig. 1. (b) A mixture of three purified tRNAs (f-Met, Val and Phe; 10 μ g each) was chromatographed under the same conditions as in (a).

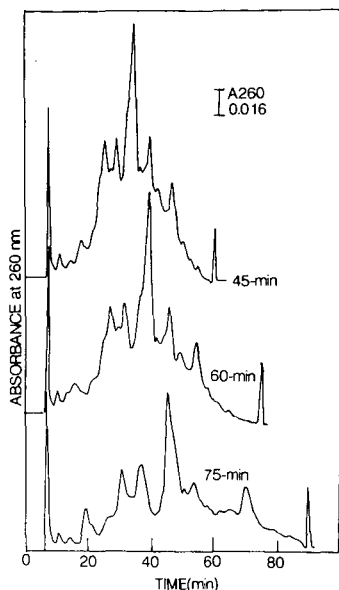


Fig. 3. Effect of extending the gradient time on the resolution of tRNA^{Total} on HAP chromatography. tRNA^{Total} of *E. coli* (about 40 μ g) was applied to a column of HAP and eluted at different gradient times as indicated. Conditions in Fig. 2 except for the gradient time.

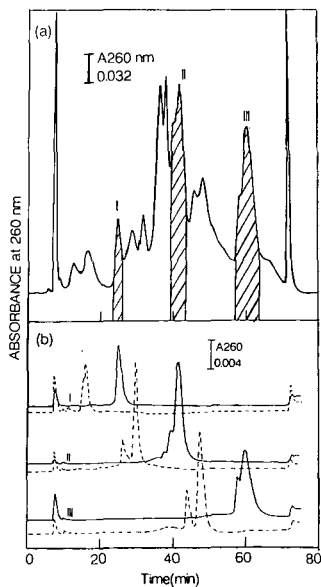


Fig. 4. (a) Chromatography of tRNA^{Total} of *B. subtilis* on an HAP column and (b) rechromatography. (a) tRNA^{Total} (80 μ g) of *B. subtilis* was applied to a column of HAP which had been equilibrated with 22% B. The column was eluted at a flow-rate of 0.5 ml/min with a 60-min linear gradient of phosphate by increasing the fraction of buffer B to 39%. Buffers A and B as in Fig. 1. (b) Each fraction [hatched in (a)] was diluted 3–5-fold with buffer A and then rechromatographed under the same conditions as in (a); the dashed lines indicate rechromatography performed using buffers containing 0.1 M sodium chloride.

Effects of sodium chloride on chromatography

Recently, Lindeberg *et al.*⁶ found that the resolution of aminoacyl-tRNAs in HAP chromatography is improved by the addition of 0.1 M sodium chloride to phosphate buffers. To confirm this, we performed rechromatography of the same fractions as used in the previous investigation with phosphate buffers including 0.1 M sodium chloride. The resulting chromatograms are shown in Fig. 4b (dashed lines). Even though the same phosphate gradient was used, sharper peaks were obtained and the resolution between the main and minor component(s) in the respective fractions was clearly improved. However, it must be emphasized that peaks were eluted at lower phosphate concentrations (about 10 mM), which may indicate that the interaction between tRNA and HAP was reduced by sodium chloride. With the expectation of an improved resolution, tRNA^{Total} of *B. subtilis* was again chromatographed in phosphate buffers containing 0.1 M sodium chloride. The chromatogram is shown in Fig. 5. Comparison with Fig. 4 indicates that the elution order of the significant peaks was not altered but the peaks became narrower on addition of sodium chloride to the phosphate buffers.

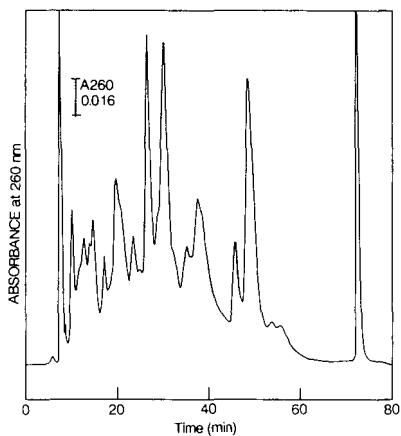


Fig. 5. Chromatography of tRNA^{Total} of *B. subtilis* in phosphate buffer containing sodium chloride. tRNA^{Total} (about 60 µg) of *B. subtilis* was applied to a column of HAP which had been equilibrated with 22% B. The column was eluted as described previously (22–39% in 60 min; flow-rate, 0.5 ml/min) with a gradient of phosphate buffer containing 0.1 M sodium chloride. A, 5 mM phosphate buffer (pH 6.8) containing 0.1 M sodium chloride; B, 300 mM phosphate buffer (pH 6.8) containing 0.1 M sodium chloride.

Amino acid-accepting activity of tRNAs after separation with the semi-preparative column

To determine the amino acid-accepting activity after separation by chromatography on HAP, 5 mg of *E. coli* tRNA^{Total} were loaded on the 2.14-cm I.D. column and the specific amino acid-accepting activity in the eluates was measured. The results are shown in Fig. 6. The resolution of tRNA^{Total} monitored at 260 nm was poor in comparison with the chromatogram from the analytical column (*cf.*, Fig. 2). However, the amino acid-accepting activity for each tRNA was eluted in a reasonably narrow peak, except for valine-accepting activity. tRNAs such as tRNA^{Met}, tRNA^{Val},

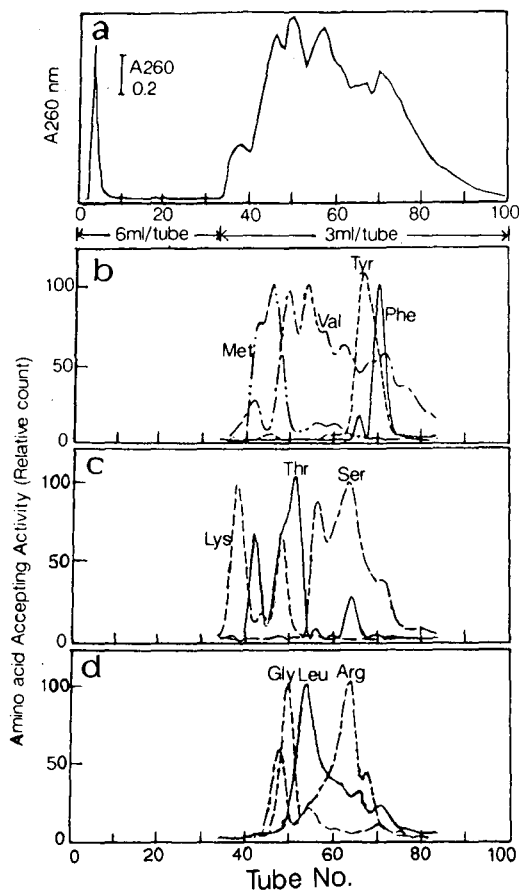


Fig. 6. Chromatography of tRNA^{Total} of *E. coli* on a semi-preparative column of HAP. tRNA^{Total} (5 mg) of *E. coli* was applied to the column of HAP (10 × 2.14 cm I.D.) which had been equilibrated with 20% B. The column was eluted with a 120-min linear gradient of phosphate by increasing the fraction of buffer B to 40%. Fractions of 6 or 3 ml were collected by a fraction collector to determine the absorbance at 260 nm and the amino acid-accepting activities. The buffers did not contain sodium chloride.

tRNA^{Tyr} and tRNA^{Phe} contained in tRNA^{Total} were eluted from the column in the order expected from the results in Fig. 1. Two or more peaks were found for each amino acid-accepting activity, which indicates that isoacceptors of tRNA were separated by the chromatography.

DISCUSSION

As tRNA^{Total} contains various tRNA molecules with physico-chemically similar properties, several chromatographic steps with various retention modes were used to purify the desired tRNA. All the results described here indicate that HPLC on spherical HAP beads is useful and effective for the purification and characterization of tRNAs. With a gradient from 75 to 140 mM phosphate buffer (pH 6.8), it was

possible to elute tRNAs from the column but fine adjustment of the gradient (only a few percent) might be necessary, depending on the the columns. tRNA^{Total} of baker's yeast was also chromatographed using the same column under similar conditions.

The resolution of tRNAs was improved by the addition of sodium chloride to the phosphate buffer. Further attempts should be made to improve the resolution. From this point of view, it would be interesting to study chromatography at different pH values or with buffers containing reagents that might cause conformational changes in tRNA molecules, such as an alcohol. With divalent cations, for example, the addition of 10 mM magnesium chloride should be avoided as the column loses its original properties, as suggested by Lindeberg *et al.*⁶. We also confirmed similar phenomena. In this connection, it is recommended that magnesium chloride, which is occasionally added for stabilization of tRNAs, be removed from the sample prior to chromatography.

REFERENCES

- 1 A. Tiselius, S. Hjertén and O. Levin, *Arch. Biochem. Biophys.*, 65 (1956) 132.
- 2 T. Kadoya, T. Isobe, M. Ebihara, T. Ogawa, M. Sumita, H. Kuwahara, A. Kobayashi, H. Ishikawa and T. Okuyama, *J. Liq. Chromatogr.*, 9 (1986) 3543.
- 3 Y. Yamakawa and J. Chiba, *J. Liq. Chromatogr.*, 11 (1988) 665.
- 4 G. Zubay, *J. Mol. Biol.*, 4 (1962) 347.
- 5 S. Nishimura, F. Harada, U. Narushima and T. Seno, *Biochim. Biophys. Acta*, 142 (1967) 133.
- 6 J. Linderberg, T. Srichaiyo and S. Hjertén, *J. Chromatogr.*, 499 (1990) 153.

CHROMSYMP. 1786

Peptide behaviour and analysis on a chemically stable C₁₈-bonded vinyl alcohol copolymer column with alkaline and acidic eluents

TAKATERU UCHIDA*, TOMOKO OHTANI, MASAO KASAI, YUZO YANAGIHARA and KOHJI NOGUCHI

Gel Separation Development Department, Asahi Chemical Industry Co., Ltd., 1-3-2 Yakoo Kawasaki-ku, Kawasaki-shi 210 (Japan)

HIROYUKI IZU

University of Osaka Prefecture, Osaka-fu (Japan)

and

SABURO HARA

Osaka University, Osaka-fu (Japan)

SUMMARY

C₁₈-bonded vinyl alcohol copolymer (ODP) gel showed no weight loss or decrease in column efficiency for alkyl alcohols after being immersed in aqueous solutions of pH 2 and 10 at 50°C for 48 h, and only a 1% weight loss and a slight decrease in alkyl alcohol retention volumes after similar immersion at pH 13.

The chemical stability of the ODP gel was further demonstrated in analyses of acidic, neutral and basic peptides on an ODP column with eluents of pH 3-10, which showed that the peptides differ considerably in the sensitivity of their retention behaviour to eluent pH, even though hydrophobic interaction invariably appeared to be the main retention mechanism.

The ODP column was therefore applied to the analysis and alignment of lysil-endopeptidase (LEP) peptides derived from reduced and S-carboxymethylated carboxyl proteinase (Rcm-P-CP) of *Pseudomonas* sp. 101. One acid-soluble and seven alkaline-soluble LEP peaks were found in analyses on the ODP column using acidic and alkaline eluents, respectively. The chymotryptic peptides of Rcm-P-CP were first separated on an ODS column with an acidic eluent, and the eight eluates which contained lysine residue, as determined by amino acid analysis, were then analysed on the ODP column with an alkaline eluent, resulting in a further separation of each into several peaks and thus in the recovery of fractions of pure peptides. The LEP peptide alignment was then determined by overlapping the sequences of the chymotryptic peptides with the C- and N-terminal regions of the LEP peptides.

INTRODUCTION

In recent years, reversed-phase chromatography has become predominant throughout high-performance liquid chromatography (HPLC) applications¹. Octadecylsilica (ODS) columns are most commonly employed because of their high efficiency in the separation of peptides and other substances of low molecular weight. Peptide separations are possible but usually less efficient on ion-exchange columns, and are generally impractical by gel permeation chromatography because of the similar molecular weights of many peptides. ODS columns nevertheless have certain disadvantages², related to the inherently poor chemical stability of ODS gels. Their service life is generally short and they are not compatible with alkaline eluents or rinses.

As an alternative to ODS columns, a number of columns packed with conventional polymer gels have been developed in the past few years. These provide excellent chemical stability, but show a far lower column efficiency.

C₁₈-bonded vinyl alcohol copolymer (ODP) gel was developed to match ODS gels in chromatographic resolution and allow the use of eluents over a wide pH range, and columns packed with the ODP gel were found to exhibit stable performance on exposure to solutions of varying pH and polarity at 30°C^{3,4}. This stability is of particular interest in the separation of peptides, because it raises the possibility of a distinction in chromatographic behaviour among acidic, neutral and basic peptides under the influence of both alkaline and acidic eluents.

Here we describe an investigation of the chemical stability of the ODP gel itself, the influence of pH on the chromatographic behaviour of peptides on the ODP column and the applicability of the ODP column to the analysis of peptides with acidic and alkaline eluents.

EXPERIMENTAL

ODP column (150 mm × 6 mm I.D.) containing Asahipak ODP-50 (Asahi Chemical, Kawasaki, Japan) ODP gel of 5.0- μ m particle diameter with a surface area of 150 m²/g and a C₁₈ group bonding density of 5 μ mol/m² was used. A commercially available YMC Pack AM-312 (Yamamura Chemical, Kyoto, Japan) ODS column (150 mm × 6 mm I.D.) was also used.

The following chromatography equipment was employed: ERC-3110 degassers (Erma Optical Works, Tokyo, Japan), LC-4A (Shimazu, Kyoto, Japan) and 880PU (Japan Spectroscopic, Tokyo, Japan) pumps, Rheodyne (Cotati, GA, U.S.A.) Model 7125 injector and Uvidec-IV ultraviolet detector (Japan Spectroscopic). Sample injection volumes were 10–100 μ l.

Chemicals and organic solvents of HPLC grade were obtained from Wako (Osaka, Japan). Peptides were obtained from the Peptide Institute (Osaka, Japan).

Carboxylproteinase was isolated from *Psuedomonas* sp. 101 as described previously⁵. Rcm-carboxyl proteinase (Rcm-P-CP) was obtained by reduction of carboxylproteinase with mercaptoethanol and alkylation with iodoacetic acid.

The Rcm-P-CP was digested with lysilendopeptidase in aqueous pyridine or with chymotrypsin in ammonium hydrogencarbonate buffer (pH 8.0) containing urea at 30°C for 6 h.

RESULTS AND DISCUSSION

Gel stability in acidic and basic solutions

Apparently complete stability in a broad pH range was observed for the ODP gel, as indicated in Fig. 1, and also on the basis of its weight and alkyl alcohol retention volumes before and after immersion of 7 g of gel in 200 ml of 50 mM sodium phosphate-acetonitrile (90:10) at pH 2, 10 or 13 for 48 h at 50°C followed by filtering and drying the constant weight. No observable weight loss or decrease in column efficiency occurred in the gels subjected to immersion at pH 2 or 10, indicating extremely high stability in this range. Even after immersion at pH 13, the gel showed a weight loss of only 1% and a very slight decrease in retention volumes, which may be attributable to a small loss of its C₁₈ groups.

Influence of pH on peptide elution

Chromatographic characteristics on the ODP column with eluents of pH 3–10 were investigated for six acidic, neutral and basic oligopeptides with the isocratic points pI^6 and hydrophobicities, as calculated by the method of Okuyama and Sasaga⁷ from Rekker's hydrophobic fragmental constants⁶ shown in Table I.

The results for the two acidic peptides are shown in Fig. 2. The increase in the Phe-Leu-Glu-Glu-Ile capacity factor (k') with decrease in pH may be attributable to a corresponding increase in its hydrophobicity. This is in accord with the known tendency for the charge carried by acidic peptides, having isoelectric points at about

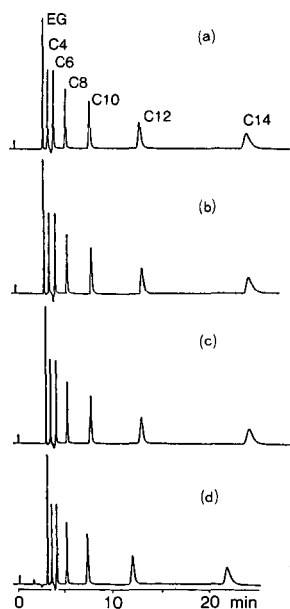


Fig. 1. Chromatograms of alkyl alcohols with columns packed with ODP gel before and after immersion in acidic and alkaline solutions. Columns packed with: (a) untreated ODP gel; (b) ODP gel after immersion in solution of pH 2; (c) ODP gel after immersion in solution of pH 10; (d) ODP gel after immersion in solution of pH 13. Eluent, methanol-water (80:20); flow-rate, 1.0 ml/min; temperature, 30°C.

TABLE I

PEPTIDES AND THEIR PARAMETERS

Type	Peptide	pI^a	$\sum f^b$
Acidic	Phe-Leu-Glu-Glu-Ile	3.12	6.08
	Glu-Gly-Phe	3.29	2.17
Neutral	Leu-Trp-Met	5.96	5.38
	Leu-enkephalin; Tyr-Gly-Gly-Phe-Leu	5.90	5.93
Basic	Leu-Trp-Met-Arg	11.05	6.08
	Des-Arg ⁹ -Bradykinin; Pro-Pro-Gly-Phe-Ser-Pro-Phe-Arg	11.05	6.08

^a Isoelectric point.

^b Sum of Rekker's hydrophobic constants.

pH 3, to decrease with increasing solution acidity, resulting in increased hydrophobicity. On the other hand, this effect was apparently not sufficient to result in observable changes in the retention of Glu-Gly-Phe, which is characterized by very low hydrophobicity, and its capacity factor was close to zero throughout the pH range 3–10.

The results for the two neutral peptides are shown in Fig. 3. For Leu-Trp-Met, the capacity factor was fairly high at pH 8 but decreased rapidly on both sides of this peak, indicating that an increasing positive or negative charge and thus decreasing hydrophobicity may be expected with any increasing departure from approximately neutral eluent pH.

For Leu-enkephalin, despite its similarity to Leu-Trp-Met in both isoelectric point and hydrophobicity, the capacity factor was nearly constant throughout the pH range 3–8, suggesting that this peptide inherently is capable of only a weak hydrophobic interaction with the octadecyl groups of the ODP gel, for reasons which remain unclear.

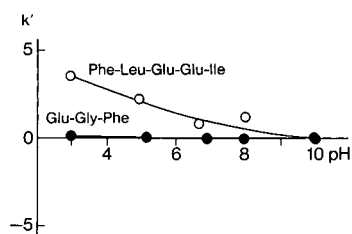


Fig. 2. Influence of pH on capacity factor (k') of acidic peptides. Samples: ○ = Phe-Leu-Glu-Glu-Ile; ● = Glu-Gly-Phe. Column, Asahipak ODP-50; Eluent, 50 mM ammonium acetate buffer-acetonitrile (85:15); flow-rate, 1.0 ml/min; temperature, 30°C.

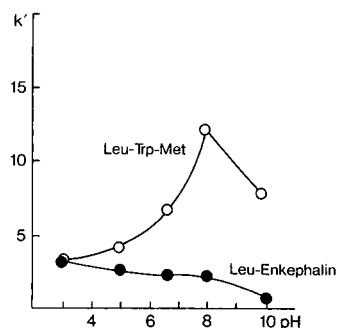


Fig. 3. Influence of pH on capacity factor (k') of neutral peptides. Samples: ○ = Leu-Trp-Met; ● = Leu-enkephalin. Column and conditions as in Fig. 2.

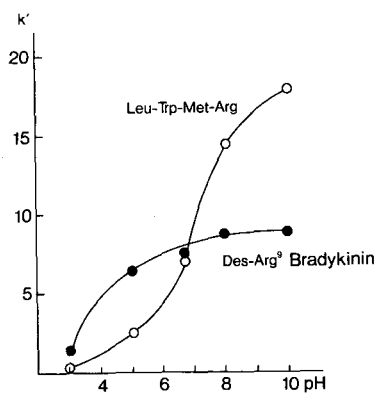


Fig. 4. Influence of pH on capacity factor (k') of basic peptides. Samples: ○ = Leu-Trp-Met-Arg; ● = Des-Arg⁹-Bradykinin. Column and conditions as in Fig. 2.

As shown in Fig. 4, the capacity factor for both basic peptides on the ODP column showed a clear tendency to increase with increasing eluent pH. This is in accord with the known tendency for the positive charge carried by basic peptides, with isoelectric points at about pH 11 to decrease with increasing solution pH, and for this decrease to result in increased hydrophobicity. On the other hand, markedly higher k' values were observed in the high pH region for Leu-Trp-Met-Arg than for Des-Arg⁹-Bradykinin, despite their similarity in both pI and hydrophobicity values. The reason remains unclear, although it is presumably related to a corresponding difference in charge-carrying capacity.

The results show distinctive differences among the six oligopeptides in the susceptibility of their chromatographic behaviour to changes in eluent pH, and thus suggest the possibility that peptides which cannot be separated with acidic eluents might be amenable to separation with neutral or alkaline eluents. The behaviours that were observed are largely in accord with the presumption of hydrophobic interaction with the ODP gel as the main separation mechanism, but other mechanisms might also be responsible.

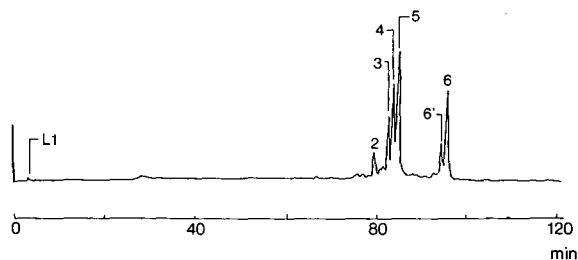


Fig. 5. Separation of ammonium hydrogencarbonate (pH 8.0)-soluble lysilendopeptidase peptides of Rcm-P-CP. Column, Asahipak ODP-50. Eluent: A, 50 mM ammonium hydrogencarbonate (pH 8.0); B, 50 mM ammonium hydrogencarbonate (pH 8.0)-acetonitrile (20:80); linear gradient from A to B in 160 min. Flow-rate, 1.0 ml/min; detection, UV at 230 nm; temperature, ambient. The amino acid composition of peak L-6' was the same as that of peak L-6 but with methionine sulphoxide in place of methionine.

L1 : Ala-Ala-Gly-Thr-Ala-Lys
 L2 : Leu-Ser-AlaAsn-Gly-Phe
 L3 : Leu-Trp-AlaGlu-Ser-Lys
 L4 : Ser-Gly-AsnIle-Ala-Lys
 L5 : Val-Ile-AsnAsp-Gly-Lys
 L6 : Gly-His-AsnVal-Ala-Lys
 L7 : Pro-Ser-TrpAsp-Val-Lys

Fig. 6. Amino acid sequence of N- and C-terminal regions of the lysilendopeptidase peptides of Rcm-P-CP, as determined by Edman degradation and carboxypeptidase digestion.

Analysis of peptides derived from carboxyl methylated proteinase of pseudomonas sp. 101

The effectiveness of the ODP column for peptide analysis with neutral or alkaline eluents was investigated by attempting its application to the determination of the amino acid sequence of carboxylproteinase of *Pseudomonas sp. 101*.

The proteinase was first reduced and S-carboxymethylated, and the resulting Rcm-P-CP was digested with lysilendopeptidase. The resulting mixture of lysilendopeptidase (LEP) peptides was freeze-dried and then placed in ammonium hydrogencarbonate (pH 8.0). The dissolved fraction was analysed on the ODP column with 50 mM ammonium hydrogencarbonate (pH 8.0)-acetonitrile as eluent, yielding the seven peaks shown in Fig. 5, representing six peptides. The precipitate was dissolved in 50% acetic acid and then analysed on the ODP column with 0.05% trifluoroacetic acid (TFA)-acetonitrile as eluent, yielding a single peak. The eluates of all seven peptides were fractionated, and the amino acid sequences of their N- and C-terminal regions were determined. As shown in Fig. 6, six of these contained a C-terminal lysine residue and one contained a C-terminal phenylalanine residue.

To permit the determination of the alignment of these LEP peptides by overlapping, Rcm-P-CP was digested with chymotrypsin and the chymotryptic peptides were analysed on an ODS column with 0.05% TFA-acetonitrile as eluent (Fig. 7). The eluates of eight peaks were determined by amino acid analysis to contain lysine residues, and were then analysed on the ODP column with ammonium hydrogencarbonate (pH 8.0)-acetonitrile. Peaks C-1 and C-2 in Fig. 7 were thus each further separated into six peaks (Fig. 8A and B, respectively). Amino acid analyses revealed that in both instances the eluate of peak f contained lysine. Each of the other seven peaks eluted from the ODS column similarly yielded several peaks on the ODP col-

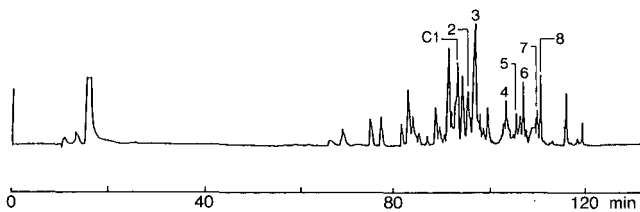


Fig. 7. Separation of chymotryptic peptides of Rcm-P-CP. Column, YMC A-324. Eluents: A, 0.05% TFA; B, 0.05% TFA-acetonitrile (20:80); linear gradient from A to B in 160 min. Flow-rate, 1.5 ml/min. Other conditions as in Fig. 5. Numbered peaks contained lysine residues.

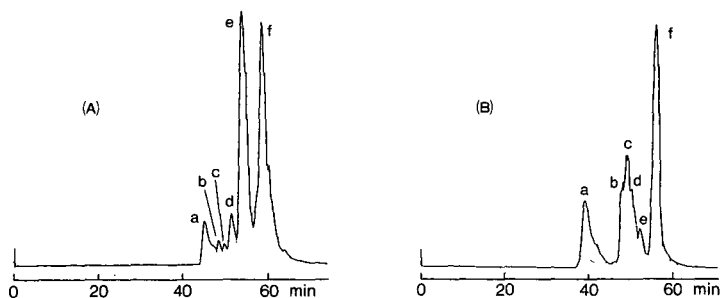


Fig. 8. Separation of two lysine-containing fractions after YMC A-324 chromatography. Column Asahipak ODP-50. Eluents: A, 50 mM ammonium hydrogencarbonate (pH 8.0); B, 50 mM ammonium hydrogencarbonate (pH 8.0)-acetonitrile (40:60); linear gradient from A to B in 60 min. Flow-rate, 0.5 ml/min. Other conditions as in Fig. 5. (A) Fraction C-1, lysine residue in peak f eluate. (B) Fraction C-2, lysine residue in peak f eluate.

umn, thus resulting in the recovery of a pure lysine-peptide fraction. The amino acid sequences of these lysine-peptides were determined by Edman degradation and carboxypeptidase digestion to be as shown in Fig. 9.

Overlapping of the sequences of the lysine-peptides and those of the C- and N-terminal regions of the LEP peptides was then performed, and indicated the alignment of the LEP peptides to be as shown in Fig. 10.

CONCLUSION

The ODP gel exhibits excellent chemical stability, making it amenable to solutions of alkaline pH and thus permitting its application with alkaline eluents to the analysis of peptides that are insoluble in acidic solvents and therefore cannot be effectively analysed on ODS columns.

Peptides, as amphoteric electrolytes, carry amounts of charge that vary with solution pH, resulting in a corresponding variation in their hydrophobic interaction with the ODP gel and thus in a chromatographic behaviour on the ODP gel which correlates with the eluent pH.

- C1 : Ser-Ala-Ile-Ser-Ser-Thr-Pro-Ser-Leu-Val-His-Asp-Val-Lys-Ser-Gly-Asn-Asn-Gly-Tyr
 C2 : Ala-Ala-Gly-Thr-Ala-Lys-Gly-His-Asn-Pro-Thr-Glu-Phe-Pro-Thr-Ile-Tyr
 C3 : Gly-Ser-Leu-Asp-Ile-Ala-Lys-Leu
 C4 : Ser-Asn-Glu-Thr-Val-Trp-Asn-Glu-Gly-Leu-Asp-Ser-Asp-Gly-Lys-Leu-Trp
 C5 : Glu-Ser-Lys-Pro-Ser-Trp-Gln-Ser-Val-
 C6 : Glu-Ser-Lys-Pro-Ser-Trp-Gln-Ser-Val-
 C7 : Asn-Gln-Ala-Val-Ser-Asp-Asn-Val-Ala-Lys-Val-Ile-Asn-Val-Ser-Leu-
 C8 : Asn-Gln-Ala-Val-Ser-Asp-Asn-Val-Ala-Lys-Val-Ile-Asn-Val-Ser-Leu-

Fig. 9. Amino acid sequence of chymotryptic peptides of Rcm-P-CP, as determined by Edman degradation and carboxypeptidase digestion.



Fig. 10. Alignment found for lysilendopeptidase peptides.

As shown here by the analysis and isolation of the peptides which facilitated alignment of the LEP peptides derived from Rcm-P-CP, efficient separation can be obtained on the ODP column using both alkaline and acidic eluents, even for mixtures that cannot be effectively separated on ODS columns because of their incompatibility with alkaline solutions.

The ODP column will provide a practical, effective tool for a widely increased range of peptides analysis.

REFERENCES

- 1 A. M. Krstulovic and P. R. Brown, *Reversed Phase High Performance Liquid Chromatography*, Wiley, New York, 1982.
- 2 N. Tanaka, *Tanpakushitsu Kakusan Koso*, 31 (1986) 66.
- 3 K. Yasukawa, Y. Tamura, T. Uchida, Y. Yanagikara and K. Noguchi, *J. Chromatogr.*, 410 (1987) 129.
- 4 Y. Yanagihara, *et al.*, *Chromatographia*, 24 (1987) 701.
- 5 K. Oda, M. Sugitani, K. Fukuhara and S. Murao, *Biochim. Biophys. Acta*, 923 (1987) 463.
- 6 T. Manabe, *Kagaku No Ryoiki*, 36 (1982) 470.
- 7 T. Okuyama and R. Sasagawa in S. Hara and T. Nakajima (Editors), *Kagaku No Ryoiki, Zokan 133, Biomedical Chromatography*, Nankodo, Tokyo, 2nd ed., 1981, p. 57.

CHROMSYMP. 1860

Retention times and heats of adsorption of aromatic compounds on carbon adsorbents

N. A. ELTEKOVA

Institute of Physical Chemistry, U.S.S.R. Academy of Sciences, Moscow (U.S.S.R.)

SUMMARY

A high-performance liquid chromatographic method was applied to the determination of the adsorption isotherms and heats of benzene, toluene, ethylbenzene, *o*-xylene, pseudocumene, *p*-diethylbenzene and anisole from *n*-heptane on carbon adsorbents. The retention times of these compounds were determined at 20, 40 and 60°C. Comparison of the results of chromatographic and static investigations allowed the character of the dynamic process to be established. The heats of adsorption of aromatic compounds on carbon and silica adsorbents were compared. The mechanism of the adsorption interaction is discussed.

INTRODUCTION

Of the various carbon adsorbents, graphitized thermal carbon black has been used with success in gas chromatography. Fundamental work carried out by Kiselev and co-workers¹⁻³ stimulated the development of a new method for the determination of molecular structure, the so-called chromatocopy². However, carbon adsorbents have not yet been applied in liquid chromatography.

Knox and Unger⁴ and Unger⁵ showed that microparticles of carbon adsorbents obtained by carbonization of polymeric materials possessed great selectivity and high capacity, and could be applied in the liquid chromatography of molecules and macromolecules.

This paper reports some results of a study of the structure and surface properties of two carbon adsorbents, Carboraffin⁶ and active carbon AU-40⁷, by HPLC and static methods. The main aim was to establish the possibility of applying HPLC for the determination of the thermodynamic characteristics of adsorption on carbon adsorbents.

EXPERIMENTAL

Adsorbates

Benzene, toluene, *o*-xylene, ethylbenzene, *p*-diethylbenzene, pseudocumene and anisole (V. O. Khimreaktiv, U.S.S.R.) were used as adsorbates. They were purified by

fractional distillation *in vacuo* or by recrystallization and their purity was controlled chromatographically.

Solvent

n-Heptane (V. O. Khimreaktiv) was used as the solvent and the eluent. It was distilled, dried and kept under NaA zeolite.

Adsorbents

Active carbon AU-40 had the following structural parameters⁷: total micropore volume, $W_0 = 0.32 \text{ cm}^3 \text{ g}^{-1}$; half-width of micropores, $x_0 = 0.6 \text{ nm}$; characteristic adsorption energy, $E_0 = 18.6 \text{ kJ mol}^{-1}$; and specific surface area, $S = 500 \text{ m}^2 \text{ g}^{-1}$. Carboraffin was kindly provided by Dr. O. Kadlec (Institute of Physical Chemistry and Electrochemistry, Prague, Czechoslovakia), and had the following structural parameters⁶: $W_0 = 0.95 \text{ cm}^3 \text{ g}^{-1}$, $x_0 = 2.2 \text{ nm}$, $E_0 = 8.9 \text{ kJ mol}^{-1}$ and $S = 940 \text{ m}^2 \text{ g}^{-1}$.

Apparatus

The investigations were conducted on a Tsvet-304 chromatograph with a UV detector ($\lambda = 254 \text{ nm}$), cell volume $7 \mu\text{l}$. An LDC (Riviera Beach, FL, U.S.A.) differential refractometer, cell volume $5 \mu\text{l}$, was also used. The chromatographic column was $10 \text{ cm} \times 0.3 \text{ cm}$ I.D., particle size of adsorbent $10 \pm 2 \mu\text{m}$ and flow-rate 1 ml min^{-1} . In static experiments the equilibrium concentrations were determined from the difference in the heights of the chromatographic peaks on a high-performance analytical column.

RESULTS AND DISCUSSION

Calculation of adsorption isotherm.

The excess adsorption value in static experiments was calculated from the equation

$$\Gamma_1^{(v)} = n\Delta x_1/mS \quad (1)$$

where n is the total number of moles of solution, Δx is the difference in concentrations before and after adsorption, m is the adsorbent mass and S is the specific surface area of the adsorbent.

The adsorption value of component 1 under conditions of equilibrium chromatography can be determined from the equation

$$\Gamma_1^{(d)} = 1/A \int_0^{c_1} V_R dc_1 \quad (2)$$

where V_R is the retention volume, A is the total surface area of the adsorbent in the column and c_1 is the concentration of component 1 in the mobile phase.

The procedure for calculating the adsorption isotherms for the aromatic compound-*n*-heptane system from the liquid adsorption chromatographic data was

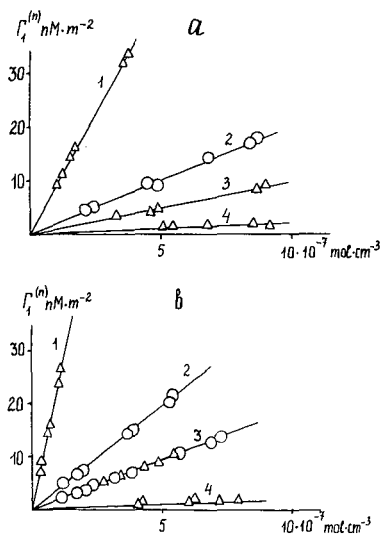


Fig. 1. Isotherms for the adsorption of (a) toluene and (b) anisole from solutions in *n*-heptane on active carbon AU-40 (1, 2), silica [$S = 80 \text{ m}^2 \text{ g}^{-1}$ (ref. 8)] (3) and graphitized carbon black [$S = 85 \text{ m}^2 \text{ g}^{-1}$ (ref. 9)] (4) at 20°C . Δ , Static measurements; \circ , chromatographic measurements.

described in detail elsewhere⁸. Fig. 1 shows thus calculated isotherms for the adsorption of (a) toluene and (b) anisole from solutions in *n*-heptane with active carbon AU-40 (1 and 2) and silica (3). Fig. 1 also shows for comparison the isotherms for the adsorption of toluene and anisole from solutions in *n*-heptane on the surface of graphitized carbon black, obtained by the static method (4). From Fig. 1, it can be seen that for toluene and anisole in the adsorption on AU-40 active carbon the static adsorption isotherm lies much higher than the adsorption isotherm calculated from the liquid adsorption chromatographic data. This non-coincidence of the adsorption isotherms obtained by different methods, as shown previously⁹, is indicative of the non-equilibration of the conditions under which the chromatographic experiment was conducted. The sharp difference between the adsorption of toluene and anisole on active carbon and on graphitized black indicates a difference in the structure of these adsorbents with a similar nature of their surface, *i.e.*, the presence of micropores in the active carbon. Micropores in the active carbon increase the adsorption potential, and so the adsorption isotherms of toluene and anisole, obtained by the static method on active carbon, lie higher than those obtained on non-porous graphitized carbon black¹⁰. It seems that not all the pores in the microporous active carbon take part in the chromatographic process, as the mass exchange in narrow micropores is strongly impeded and, as a result, the static and the chromatographic toluene and anisole adsorption isotherms do not coincide. With macroporous silica one observes complete coincidence of anisole adsorption isotherms obtained by the static and the chromatographic methods, which indicates equilibration of the chromatographic process in this instance.

Adsorption equilibrium constant

Previously an expression was proposed⁸ for the adsorption equilibrium constant in the following form:

$$K_1 = \Gamma_1^{(v)} \gamma_{a,1} / c_1 \gamma_{v,1} = \exp[(\mu_{a,1}^0 - \mu_{v,1}^0) / RT] \quad (3)$$

where $\gamma_{a,1}$ and $\gamma_{v,1}$ are the activity coefficients of component 1 in the surface and the bulk solution, respectively, and $\mu_{a,1}^0$ and $\mu_{v,1}^0$ are the standard chemical potentials of component 1 in the surface and the bulk solution, respectively. For $c_1 \rightarrow 0$, $\gamma_{v,1} \rightarrow 1$ and $\Gamma_1 \rightarrow 0$, $\gamma_{a,1} \rightarrow 1$,

$$K_1 = \lim_{c_1 \rightarrow 0} \Gamma_1 / c_1 = K_H \quad (4)$$

where K_H is Henry's constant. An infinitely dilute solution was chosen as the standard state.

From the theory of equilibrium chromatography, it follows that

$$K_H = V_{A,1} \quad (5)$$

where $V_{A,1}$ is the absolute retention volume of component 1.

To establish the reliability of the chromatographic data and equilibration, the $V_{A,1}$ values obtained from the chromatograms were compared with the K_H values calculated from static adsorption isotherms using eqn. 4 (Table I).

From Table I, it can be seen that with macroporous silica the K_H and $V_{A,1}$ values for toluene and anisole coincide, which indicates that the chromatographic process is taking place under equilibrium conditions. With the mesoporous carbon adsorbent carboraffin, the K_H and $V_{A,1}$ differ *ca.* 1.5-fold and with the microporous active carbon 5-fold. This indicates that not all the surface of microporous adsorbents takes part in the chromatographic process, but only the available surface, which can be estimated from the expression $SV_{A,1}/K_H = S_g$.

Calculation of ΔH^0 , ΔF^0 and ΔS^0

Fig. 2 shows the $\log V_{R,1}$ vs. $1/T$ dependence for the various aromatics on

TABLE I

K_H AND $V_{A,1}$ VALUES OF TOLUENE AND ANISOLE ON SILICA AND CARBON ADSORBENTS
Component 2 = *n*-heptane.

Component 1	Silica		Carboraffin		Active carbon	
	K_H ($\text{mm}^3 \text{ m}^{-2}$)	$V_{A,1}$ ($\text{mm}^3 \text{ m}^{-2}$)	K_H ($\text{mm}^3 \text{ m}^{-2}$)	$V_{A,1}$ ($\text{mm}^3 \text{ m}^{-2}$)	K_H ($\text{mm}^3 \text{ m}^{-2}$)	$V_{A,1}$ ($\text{mm}^3 \text{ m}^{-2}$)
Toluene	7.0	7.0	2.0	1.5	110	22
Anisole	15	15	20	14.5	240	40

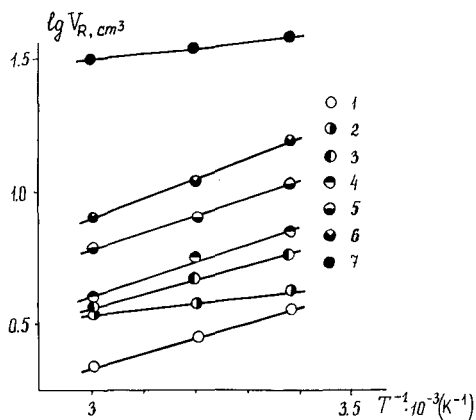


Fig. 2. $\lg V_R$ vs. $1/T$ for (1) *p*-diethylbenzene, (2) ethylbenzene, (3) benzene, (4) toluene, (5) *o*-xylene, (6) pseudocumene and (7) anisole on carboraffin.

carboraffin. The enthalpies of adsorption of these compounds on carboraffin were calculated from the slopes of the curves according to the equation

$$\Delta(\Delta H) = -RT^2 \cdot \frac{d \ln V_R/T}{dT} \quad (6)$$

The total enthalpy of the adsorption of aromatic compounds was found taking into account the net heat of adsorption of *n*-heptane according to the equation

$$-\Delta H^0 = \Delta(\Delta H) + \beta \Delta H_{C_7H_{16}} \quad (7)$$

where β is the displacement coefficient, equal to the ratio of the areas of molecules of aromatic compounds to that of *n*-heptane.

Fig. 3 shows the dependences of the enthalpies of adsorption of aromatic compounds on the molar volume \bar{V}_0 of these molecules. Linear dependences of $-\Delta H^0$ on \bar{V}_0 for adsorption on carboraffin are observed for two series of compounds: benzene, toluene, *o*-xylene and pseudocumene, and anisole, ethylbenzene and *p*-diethylbenzene.

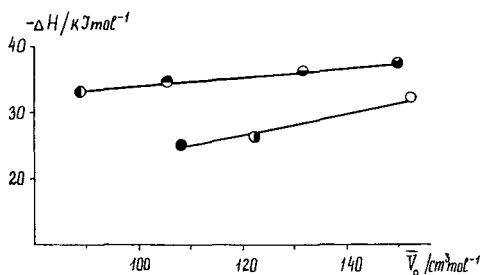


Fig. 3. $-\Delta H^0$ vs. \bar{V}_0 for aromatic compounds (numbers as in Fig. 2) on carboraffin.

TABLE II

VALUES OF ΔF^0 , ΔH^0 AND ΔS^0 FOR THE ADSORPTION OF AROMATIC COMPOUNDS ON CARBORAFFIN AND HYDROXYLATED SILICA

Substance	Carboraffin			Silica		
	$-\Delta F^0$ (kJ mol ⁻¹)	$-\Delta H^0$ (kJ mol ⁻¹)	ΔS^0 (J mol ⁻¹ K ⁻¹)	$-\Delta F^0$ (kJ mol ⁻¹)	$-\Delta H^0$ (kJ mol ⁻¹)	ΔS^0 (J mol ⁻¹ K ⁻¹)
Benzene	2.7	33	-100	5.5	24	-60
Anisole	14	25	-37	8.0	28	-65

Free-energy variations in the adsorption of aromatic compounds were calculated from the equation

$$-\Delta F^0 = 2.3 RT \log K_H \quad (8)$$

Entropy variations in the adsorption of aromatic compounds on silica and carboraffin were calculated from the equation

$$F^0 = H^0 - T\Delta S^0 \quad (9)$$

An infinitely dilute solution was taken as the standard state in the calculations. Results are given in Table II.

It can be seen from Table II that for the adsorption of benzene from solutions in *n*-heptane on carboraffin the benzene molecule loses more degrees of freedom than the anisole molecule. Owing to their great affinity, the flat benzene molecules are attached closely to the graphite-like surface of the carbon sorbent, which leads to a loss of mobility of the molecules along the surface and to a decrease in the entropy of adsorption. In contrast to benzene, the methyl group of anisole molecules hinders close contact with the graphite ring on the carbon surface and hence increases the mobility of adsorbed anisole molecules.

The interpretation of two linear dependences in the plots (Fig. 3) of $-\Delta H$ vs. \bar{V}_0 involves not only the entropy factor but also the *para*-effect. The interactions of solvent molecules with molecules such as anisole, ethylbenzene and *p*-diethylbenzene are stronger than those with shorter and more compact molecules such as benzene, toluene, *o*-xylene and pseudocumene.

The mechanism of adsorption interactions in the carbon sorbent-solvent-aromatic compound systems should become clearer with further systematic HPLC investigations. Other factors (*e.g.*, microporosity, impurities on the carbon surface, diffusion effects) may contribute to the total retention values and the thermodynamic characteristics of adsorption interactions.

REFERENCES

- 1 A. V. Kiselev and D. P. Poshkus, *Adv. Colloid Sci.*, 9 (1978) 1.
- 2 A. V. Kiselev and D. P. Poshkus, *Faraday Symp. Chem. Soc.*, 15 (1980) 15.
- 3 A. V. Kiselev, D. P. Poshkus and Ya. I. Yashin, *Molecular Fundamentals of Adsorption Chromatography*, Khimiya, Moscow, 1986, p. 65.

- 4 J. H. Knox and K. K. Unger, *J. Liq. Chromatogr.*, 6, Suppl. 1 (1983) 1.
- 5 K. K. Unger, *Anal. Chem.*, 55 (1983) 361.
- 6 M. M. Dubinin, O. Kadlec and N. S. Polyakov, *Izv. Akad. Nauk SSSR, Ser. Khim.*, 4 (1987) 719.
- 7 M. M. Dubinin, *Dokl. Akad. Nauk SSSR*, 275 (1984) 1442.
- 8 N. A. Chuduk, A. V. Kiselev and Yu. A. Eltekov, *J. Colloid Interface Sci.*, 84 (1981) 149.
- 9 N. A. Eltekova and Yu. A. Eltekov, *Zh. Fiz. Khim.*, 60 (1986) 2272.
- 10 N. A. Eltekova, *J. Chromatogr.*, 364 (1986) 425.

CHROMSYM. 1656

Investigations by ^{29}Si cross-polarization magic angle spinning NMR spectroscopy of reaction pathways of silica gel polyfunctional modification

BETTINA PFLEIDERER, KLAUS ALBERT and ERNST BAYER*

Institut für Organische Chemie, Auf der Morgenstelle 18, Universität Tübingen, D-7400 Tübingen (F.R.G.)

SUMMARY

Di- and trifunctionally modified silica gels (C_{18}) were investigated by ^{29}Si cross-polarization magic angle spinning NMR spectroscopy and the relative amounts of surface species were determined by peak deconvolution. On the basis of structure assignment and change in species decomposition with different reaction conditions, it is possible to construct a scheme for reaction pathways in polyfunctional modifications. Thus, distinct species composition can be correlated with reactions occurring at the surface.

Synthesis with and without an argon atmosphere and the use of the stationary phases in high-performance liquid chromatography (HPLC) cause dramatic changes in species composition. Derivatization in a dry argon atmosphere results in the formation of monodentate species (D_1 , D_2) (difunctionally modified) or bidentate species (T_2) (trifunctionally modified), whereas without an argon atmosphere mainly condensed species ($\text{D}_4 + \text{D}'_4$ and $\text{T}_4 + \text{T}'_4$) are formed. Disregarding the reaction procedures, modification with dichlorosilanes preferentially forms monodentate species, and trifunctional modification favours the formation of bidentates. Condensation reactions seem to play a minor role during modification. However, they are most important in the ageing process of polyfunctional modified phases, both in the dry form and during their use in HPLC.

INTRODUCTION

The chemical modification of silica surfaces by organosilanes is of increasing interest in different fields of chemistry, especially in view of their use as stationary phases in reversed-phase (RP) chromatography¹. ^{29}Si solid-state NMR magic-angle spinning (MAS), ^1H high-power decoupling² and cross-polarization (CP)³ have been used to distinguish between the different chemical species on the surface^{4–7}.

It has been shown that, with the exception of monofunctional derivatization^{4–8}, reactions used to prepare chemically modified silica do not lead to single chemical species. Many assignments^{5,6} and descriptions of the qualitative changes in species composition after solvent or heat treatment have been reported previously^{5,7,9}. How-

ever, no complete assignment and quantitative analysis of the species compositions has been performed. The composition of the surface species is essential for a comparison of the changes that occur during different modification procedures and of the changes that occur during the ageing process of stationary phases and for correlation with chromatographic performance.

Therefore, we have determined the quantitative amounts of different surface species, obtained under different conditions, in order to establish systematic correlations between species composition and preferred pathways occurring in polyfunctional modifications. Hence it should be possible to correlate a given species composition with distinct reaction pathways. The changes in surface species composition during prolonged elution with the mobile phase acetonitrile and ageing in the presence of air was also investigated.

We prepared several stationary phases with di- and trichlorosilanes under controlled reaction conditions and investigated them by ^{29}Si -CP-MAS-NMR spectroscopy, estimating the relative amounts of surface species obtained.

EXPERIMENTAL

Surface modification

Silicas were modified according to Kinkel and Unger¹⁰. Briefly, 5 g of silica were activated at 473 K and at a reduced pressure of $<10^{-3}$ mbar. After 12 h, the material was cooled to room temperature. A solution of 0.15 mol of 2,6-lutidine and of 0.12 mol of the appropriate organosilane in 30 ml of dry dichloromethane was added to the activated silica gel. The reaction mixture was stirred and heated thoroughly, washed with dichloromethane, ethanol, 50% aqueous ethanol, and diethyl ether and dried at 340 K and $<10^{-3}$ mbar for 24 h. Some operations were performed in an argon atmosphere.

Silylation reagents and the analytical techniques have been described previously¹¹. Reactions of silica with octadecylsilanes were performed on Nucleosil with a particle size of 7 μm , an average pore size of 100 Å and a surface area of 350 m^2/g (Machery, Nagel & Co, Düren, F.R.G.).

Solvent experiment

The flow experiment were performed at a flow-rate of 1 ml/min using a Bruker LC 31 HPLC instrument (Karlsruhe, F.R.G.) with stainless-steel HPLC columns (125 \times 4 mm I.D.) and acetonitrile, (HPLC grade; Merck, Darmstadt, F.R.G.) as the mobile phase for 3–4 days. The columns were stored under acetonitrile for 2 weeks and then flushed again to prevent them from drying. The whole procedure was repeated several times up to 3 months. The samples were then taken from the columns, dried and investigated by ^{29}Si solid-state NMR spectroscopy.

NMR parameters

Solid-state ^{29}Si NMR spectra were obtained on a Bruker MSL 200 Fourier transform NMR spectrometer with samples of 200–300 mg in double-bearing rotors of ZrO_2 . MAS was routinely performed at 4-kHz spinning rates. The pulse sequence of the CP-MAS experiment used has been described in detail elsewhere¹². Typically, the proton 90° pulse length was 6 μs and the repetition time 2 s.

Contact-time variation experiments of di (D) and trifunctionally (T) modified phases revealed a common CP behaviour. The optimum contact time for maximum magnetization of all D-units was obtained at 5 ms, and the optimum of the T-units at 2.5 ms, independent of the silica gel used⁹, and these contact times were employed in the following measurements. All ²⁹Si spectra were externally referenced to liquid tetramethylsilane and the chemical shifts are given in parts per million.

Peak deconvolution

Calculated deconvolutions of the experimental spectra were based on Gaussian peak shapes. We used constant chemical shifts and a constant peak width for each surface species of the D- and T-units. The width ranged from 110 ± 5 Hz (T_1, T'_1), 120 ± 5 Hz (D_3), 140 ± 5 Hz (D_1, D_2) to 210 ± 5 Hz (T_2). The $T_3 + T'_3, T_4 + T'_4$, and $D_4 + D'_4$ species, corresponding to various polymerized species, were calculated assuming variable peak width. Optimum results could be obtained by a simulation at

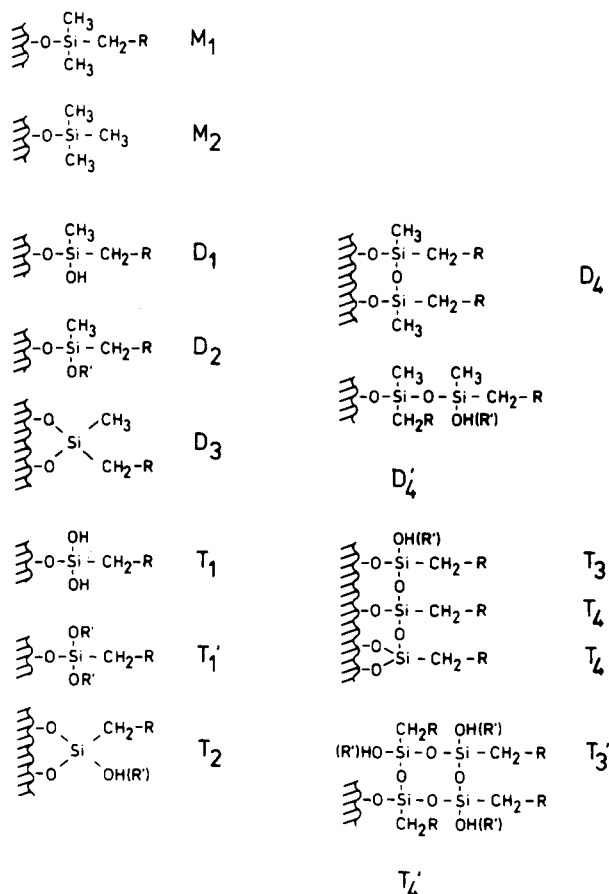


Fig. 1. Detectable surface species of a silica gel silylation with monochlorosilane (M), dichlorosilane (D) and trichlorosilane (T). R = *n*-alkyl, R' = CH₃. D₄, T₃ and T₄ are polymerized along the surface and D'₄, T'₃, and T'₄ perpendicular to the surface.

constant chemical shift and constant peak width. The deviation of the intensities of experimental and simulated spectra was 3%.

RESULTS

The surface species (Fig. 1) are described by the D, T, Q notation, which refers to the number of oxygen (di-, tri- and tetraoxo) atoms bound to the silicon atom¹³. The assignments of the different Q-, D- and T-units, which have been described earlier⁴⁻⁶, are summarized in Table I.

The spectra of derivatized silica gels show the chemical shifts of the native silica gel, geminal silanediol groups Q₂ (-91 ppm), silanol groups Q₃ (-101 ppm) and siloxane groups Q₄ (-110 ppm), in addition to the signals of the silanes. After reaction with octadecylmethylchlorosilane, we obtained signals of D₁ (-4 ppm), D₂ (-7 ppm), D₃ (-10 ppm) and of various D₄ + D'₄ species (-14 to -22 ppm) and after reaction with octadecyltrichlorosilane, resonances of T₁ (-46 ppm), T'₁ (-50 ppm), T₂ (-56 ppm), T₃ + T'₃ (-59 ppm) and T₄ + T'₄ species (-64 to -70 ppm).

The resonances obtained between -64 and -70 ppm (trifunctionally modified) or between -14 and -21 ppm (difunctionally modified) are due to D₄ or T₄ units with different extents of cyclization, which influence the chemical shift. This has been also observed in ²⁹Si liquid high-resolution NMR. For instance, resonances of the cyclic species occur at $\delta = -20$ ppm for (Me₂SiO)₄, $\delta = -22.8$ ppm for (Me₂SiO)₅ and $\delta = -23$ ppm for (Me₂SiO)₆¹³ (where Me = methyl).

In order to construct the preferred reaction pathways, phases were prepared in the presence of moisture and in a dry argon atmosphere. The influence of the different

TABLE I
CHEMICAL SHIFTS OF THE SILANE SIGNALS

For assignments, see Fig. 1. D'₄, T'₃ and T'₄ are species polymerized perpendicular to the surface; D₄, T₃ and T'₄ are polymerized along the surface. T₂ and T₃ were used to differentiate between a silicon having two (-O-Si-O)_n units as neighbours (T₂) and a silicon having one (-O-Si-O)_n unit and one (-O-Si-R-) unit as neighbours (T₃), because of different chemical shifts of the T₂ and T₃ groups due to the different chemical surroundings.

Structural type	δS^a
Q ₂	-91
Q ₃	-101
Q ₄	-110
D ₁	-4
D ₂	-7.2
D ₃	-10
D ₄ + D' ₄	-14 to -21
T ₁	-46
T' ₁	-50
T ₂	-55.5 (R ≥ CH ₃)
T ₃ + T' ₃	-59 (R ≥ CH ₃)
T ₄ + T' ₄	-64 to -70

^a Chemical shifts in ppm with respect to liquid Me₄Si.

reaction procedures on the species composition of a difunctionally modified Nucleosil is shown in Fig. 2, and the different species composition of a trifunctionally modified Nucleosil is shown in Fig. 4. To obtain quantitative data, we performed a peak deconvolution by Gaussian peak shapes of the resonance patterns of the derivatized species. An example shows the deconvolution of the D units of Fig. 2 (Fig. 3).

Modification in an argon atmosphere leads to the preferred formation of monodentate D_1 and D_2 , whereas the amount of condensed species $D_4 + D'_4$ is 37% (Table II). Derivatization in the absence of an argon atmosphere reduces the monodentate D_1 , D_2 and the bidentate D_3 species, whereas condensation to $D_4 + D'_4$ increases to 49.6%. In addition to the already assigned signals (Fig. 1), we found a signal at +1.6 ppm, amounting to 3% (Table II) and 6.2% (Table III) of the total intensity. This resonance has also been obtained for other difunctionally modified phases.

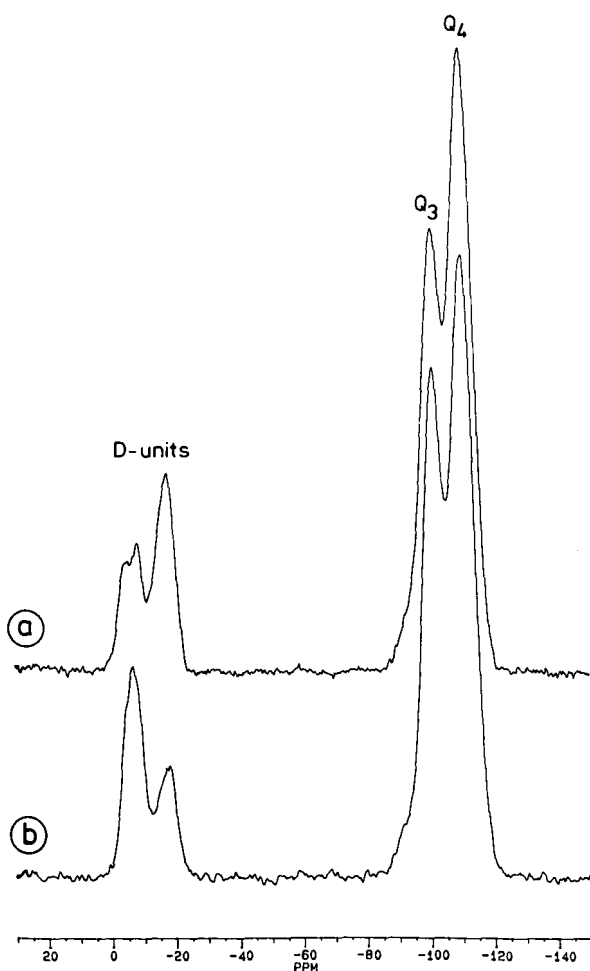


Fig. 2. ^{29}Si -CP-MAS-NMR spectrum of Nucleosil (batch 5051) silylated with octadecylmethyldichlorosilane. The contact time was 5 ms. (a) In the absence of argon; (b) in an argon atmosphere.

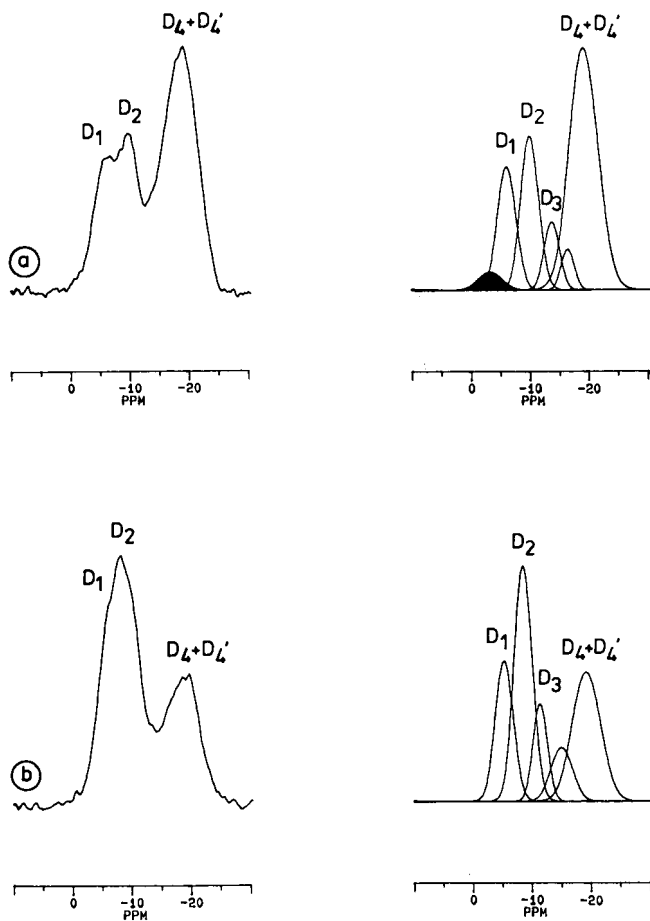


Fig. 3. Simulation of the D-units of the experimental spectrum in Fig. 2. (a) Experimental spectra and simulated species after silylation in air; (b) experimental spectra and simulated species after derivatization in an argon atmosphere. ■ = Unknown resonance.

It is interesting to note that in trifunctionally, in contrast to difunctionally, modified stationary phases, the amount of the monodentate species T_1 and T'_1 is relatively low. Their relative amounts, even for reactions in an argon atmosphere, do not exceed 10% (Table II). However, derivatization in an argon atmosphere yields mainly the bidentate species, T_2 (55.6%) and the cross-linked condensed species, $T_4 + T'_4$ (23.4%). Derivatization in the absence of an argon atmosphere leads to a reduced amount of T_2 (26.4%), whereas the amount of the condensed species, $T_4 + T'_4$, increased to 65.1% (Table II).

In order to characterize the preferred reactions of the surface after modification, especially in combination with solvent, we flushed polyfunctional modified samples in an HPLC apparatus with HPLC-grade acetonitrile for several days, stored the column in acetonitrile, and again flushed the columns every 2 weeks to prevent them from drying. We repeated this procedure for up to 3 months. The stationary phases

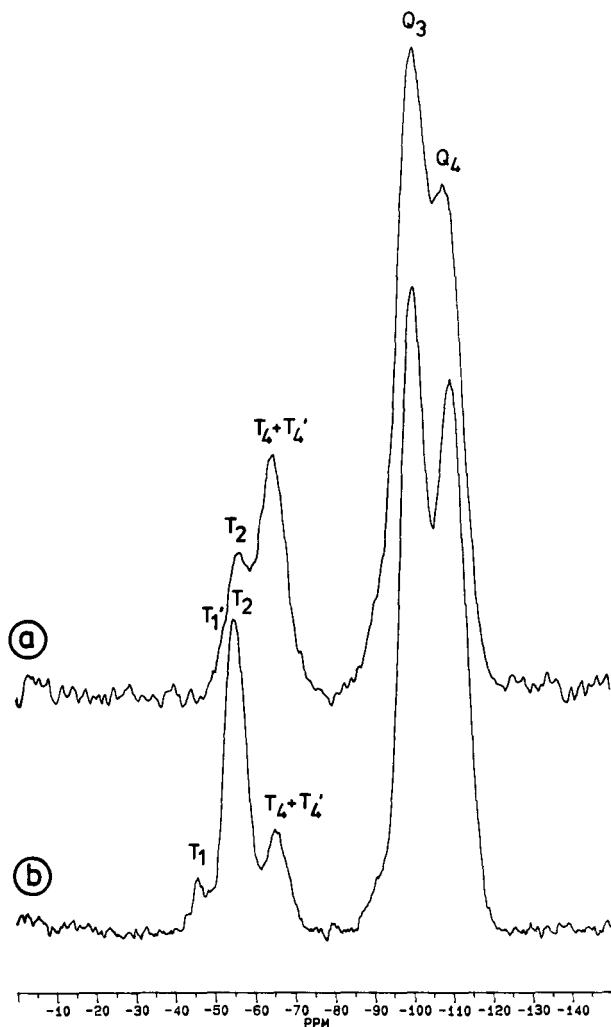


Fig. 4. ^{29}Si -CP-MAS-NMR spectrum of Nucleosil (Batch 5051), silylated with octadecyltrichlorosilane. The contact time was 2.5 ms. (a) In the absence of argon; (b) in an argon atmosphere.

were then taken from the columns, dried and investigated by ^{29}Si solid-state NMR spectroscopy. The experiments reveal a change in the variety of species. The monodentate species D_1 , D_2 , T_1 and T'_1 are reduced with a significant increase in the concentration of the condensed species D_3 , $\text{D}_4 + \text{D}'_4$, $\text{T}_3 + \text{T}'_3$ and $\text{T}_4 + \text{T}'_4$. Fig. 5 shows an example of a difunctionally modified phase. As shown in Table III, there is a 50% decrease in the amount of the monomeric species (unknown, D_1 and D_2), whereas the condensed species $\text{D}_4 + \text{D}'_4$ increase by 50%. Condensation, although slower, is also observed during ageing of dry stationary phases. The accelerated condensation in the presence of solvent is due to increased mobility and reaction ratio in the solvated form.

TABLE II

RELATIVE AMOUNTS OF MOLECULAR STRUCTURES OBTAINED AFTER TWO DIFFERENT MODIFICATION CONDITIONS OF NUCLEOSIL (BATCH 5051) WITH DICHLOROSILANE OR TRICHLOROSILANE

Modifier	Structural type	δ^a	Relative amount (%) ^b	
			No Ar	In dry Ar atmosphere
Dichlorosilane	Unknown	+ 1.6	3	—
	D ₁	-4.2	16.2	19.2
	D ₂	-7.2	19.7	32.9
	D ₃	-10.5	7.5	10.8
	D ₄ + D' ₄	-14 to -20	49.6	37
Trichlorosilane	T ₁	-46.5	—	5.7
	T' ₁	-50.0	2.9	3
	T ₂	-55.5	26.4	55.6
	T ₃ + T' ₃	-59.0	5.4	12.2
	T ₄ + T' ₄	-64 to -75	65.1	23.4

^a Chemical shifts in ppm with respect to liquid Me₄Si.

^b Error, $\pm 3\%$.

DISCUSSION

On the basis of the changes in surface species composition under various reaction conditions, it is possible to construct a scheme for the consecutive pathways in polyfunctional modifications of HPLC RP materials.

In difunctional derivatization with dichlorosilane (Fig. 6A), the first step is the formation of the monodentate I. This has also been observed by Sindorf and Maciel⁵. The intermediate is hydrolysed during washing at the end of the synthesis to the monodentates D₁ and D₂ (Fig. 6B). The amount of D₂ is therefore an indirect indication of the amount of monodentate I at the end of the reaction, as the D₂ species can only be formed from I in the washing step with ethanol. A large amount of D₂ can

TABLE III

RELATIVE AMOUNTS OF MOLECULAR STRUCTURES OF A DIFUNCTIONALLY MODIFIED NUCLEOSIL (BATCH 4111) AND AFTER FLUSHING THIS STATIONARY PHASE WITH ACETONITRILE AS SOLVENT

Structural type	δ^a	Relative amount ^b	
		Original	After solvation
Unknown	+ 1.6	6.2	—
D ₁	- 4.2	19.0	15.2
D ₂	- 7.2	35.1	17
D ₃	-10.5	12.8	12.8
D ₄ + D' ₄	-14 to -20	27.1	54.7

^a Chemical shifts in ppm with respect to liquid Me₄Si.

^b Error, $\pm 3\%$.

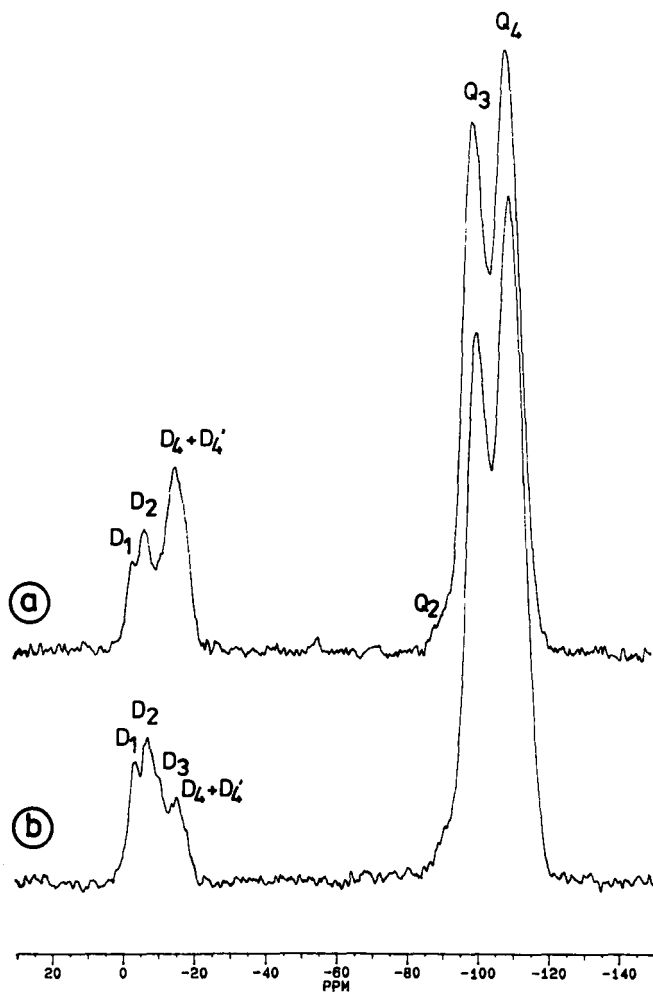
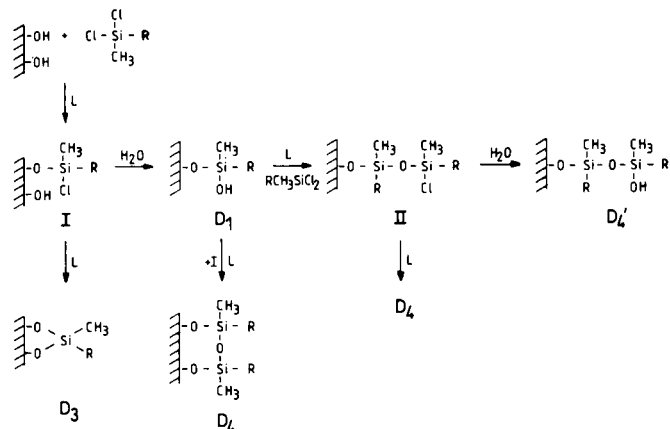


Fig. 5. ^{29}Si -CP-MAS-NMR spectrum of Nucleosil (Batch 4111) silylated with octadecylmethyldichlorosilane. The contact time was 5 ms. (a) After solvent exposure; (b) original phase.

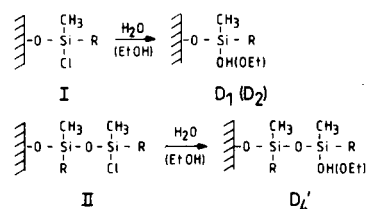
be correlated with a large amount of monodentate I. Hence the large amount of D_2 in reactions in an argon atmosphere reveal (Table II) that many of the monodentate I species neither have formed condensed species nor have reacted with the silica to form bidentate D_3 (Table III). However, the small amount of D_3 in the presence and absence of moisture clearly indicates that the bidentate D_3 formation is not favoured, but, as seen in Fig. 3, it still occurs. These findings are in contrast to those of Sindorf and Maciel⁵ and of Gilpin and Burke⁸, who described D_3 almost as hypothetical moieties. The ratio of monodentate (D_1, D_2) to bidentate (D_3) after the washing step is in our example *ca.* 5 (Table II) and never < 3 . This indicates that the formation of the monodentates D_1 and D_2 , even in the presence of moisture, is always preferred.

In the trifunctional modification with trichlorosilane (Fig. 7A) the reaction also begins with the formation of an intermediate, I^5 , which can react further via two

A. Reactions with moisture



B. Washing



C. Condensation

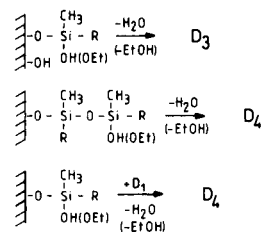


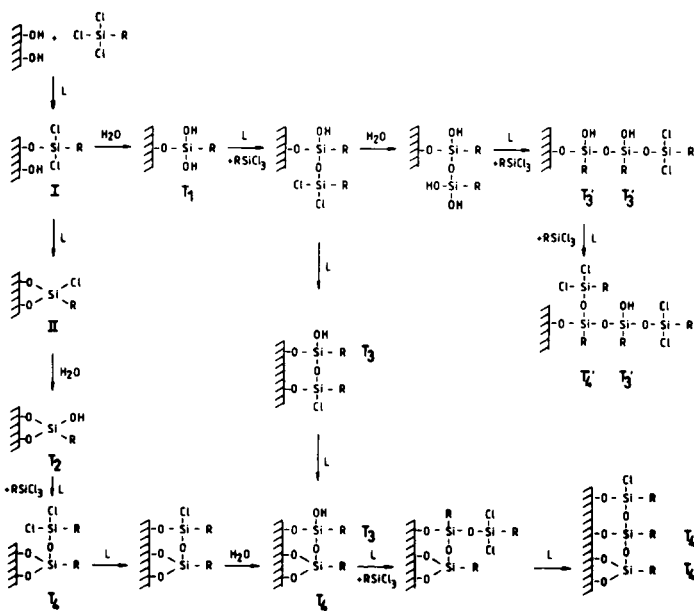
Fig. 6. Possible reaction pathways occurring after modification with octadecylmethylchlorosilanes. L = 2,6-lutidine (used as a catalyst); R = C₁₈H₃₇; Et = ethyl.

reaction pathways. One possibility is the reaction to bidentate II, which is hydrolysed during washing to bidentate T₂. The other possibility is the reaction with moisture to T₁ and further formation of cross-links (T₃ + T₃, T₄ + T₄). The monodentate I is hydrolysed during washing to monodentates T₁ and T₁' (Fig. 7B). In contrast to the difunctional modification, the formation of II is obviously preferred, as we obtained only a small amount of T₁ and T₁' after washing the samples, whereas the amount of bidentate T₂ is very high. Sindorf and Maciel⁵ also observed the most intense resonance at -53 to -55 ppm. However, they proposed for this resonance a structure resembling that of T₃ + T₃. In our opinion and that of other workers⁷, this resonance must be ascribed to a bidentate with chelate bonding (T₂). This argument is supported by the high stability of trifunctionally modified stationary phases in HPLC

because, owing to a chelate effect, a bidentate, (T_2 , D_3) should be more stable than a monodentate species¹⁴. These results agree with those of the recent investigations of Hetem *et al.*,¹⁵ who demonstrated in ageing experiments with various eluent compositions in the HPLC test that the trifunctional modified phases are the most stable.

The species T_1 , like the D_2 species, can only be formed during the washing step with ethanol, following the reaction procedure (Scheme 7B), and is therefore an indicator for the amount of intermediate I. Especially the derivatization in the presence of an argon atmosphere leads to an increase in bidentate species, T_2 (55.6%). The ratio of monodentate (T_1 , T_1) to bidentate (T_2) is 1:7 in an argon atmosphere and 1:9 in the presence of moisture (Table II). The reason for the large amount of bidentate may be that trichlorosilanes have three reactive groups, and hence a higher probability of having the appropriate steric form to react with two neighbouring surface silanols, in contrast to dichlorosilanes with only two functional groups. The

A. Reactions with moisture



B. Washing



C. Condensation



Fig. 7. Possible reaction pathways occurring after modification with octadecyltrichlorosilane. L = 2,6-lutidine (used as a catalyst); R = $C_{18}H_{37}$; Et = ethyl.

more moisture is available in the modification procedure, the more chlorine atoms of the trichlorosilanes are hydrolysed and therefore the formation of the T_2 species is not favoured, owing to the reduced amount of available reactive groups.

We believe that the concentration of the species polymerizing perpendicular to the surface (D'_4 , T'_3 and T'_4) should be relatively low, compared with the amounts of species polymerizing along the surface (D_4 , T_3 and T_4), owing to steric hindrance of the bulky octadecyl chains. Therefore, condensation of monodentates yields mainly D_4 , T_3 and T_4 species. Their amounts depend on the reaction procedure. Derivatization in the absence of an argon atmosphere causes increased condensation (Table II). The more moisture is available for the reaction, the more favoured is the competitive reaction of the monodentate I to D_1 or T_1 (Figs. 6A and 7A), which can react further with chlorosilane, catalysed by 2,6-lutidine, to form the condensation products $D_4 + D'_4$ or T_3, T'_3 and $T_4 + T'_4$. Hence the reduced amounts of D_2 or T_2 without an argon atmosphere are easily explained by assuming that most of the monodentate I has formed $D_4 + D'_4$ or $T_4 + T'_4$ before washing.

The condensation reactions (Figs. 6C and 7C) seem to play a minor role in the modification procedure. This is indicated by the relatively small amount of D_3 or $T_3 + T'_3$ in all derivatized stationary phases (Table II). However, after flushing the stationary phases and storing in contact with solvent (Fig. 5, Table III), the amount of monodentates, D_1 and D_2 is reduced by almost 50%, whereas the $D_4 + D'_4$ species are correspondingly increased. The ethoxy species, D_2 , seems to form these condensed species preferentially, whereas the amount of D_1 species is hardly affected. These findings indicate that the condensation reactions play an important role in the ageing process of stationary phases in HPLC. We observed similar, but weaker, effects for dry samples that had been stored in the presence of air for 3 months. The amount of $D_3, D_4 + D'_4, T_3 + T'_3$ and $T_4 + T'_4$ species is increased whereas that of the monodentates D_1 and D_2 or T_1 and T'_1 is decreased (not shown). The faster condensation in the presence of eluent may be due to an increased mobility of the surface groups in the solvated form.

At present, a complete assignment of all individual resonances is impossible. We are able to determine the relative amounts of the already known surface species, as a small amount of simulated intensity cannot yet be assigned. We believe that the unknown resonances of the D units at +1.6 ppm could be due to cracked silanes. Unhydrolysed chlorosilanes can be excluded, because the appropriate resonance would appear at *ca.* +9 ppm⁵.

Spectra of the modified phases (Figs. 2 and 4) indicate that silanediol groups are still present, despite the fact that they are thought to be very reactive and to react completely with the silanes¹⁶. This may be caused by a renewed hydrolysis of siloxane groups during the modification procedure.

ACKNOWLEDGEMENTS

We thank Graeme Nicholson for his help in preparing this manuscript. We gratefully acknowledge the support by Hewlett-Packard, Waldbronn, F.R.G.

REFERENCES

- 1 K. K. Unger, *Porous Silica (Journal of Chromatography Library, Vol. 16)*, Elsevier, Amsterdam, 1979.
- 2 J. Schaefer and E. O. Stejskal, *J. Am. Chem. Soc.*, 98 (1976) 1031.
- 3 A. Pines, M. Gibby and J. S. Waugh, *J. Chem. Phys.*, 59 (1973) 569.
- 4 D. W. Sindorf and G. E. Maciel, *J. Am. Chem. Soc.*, 103 (1981) 4263.
- 5 D. W. Sindorf and G. E. Maciel, *J. Am. Chem. Soc.*, 105 (1983) 3767.
- 6 E. Bayer, K. Albert, J. Reiners, M. Nieder and D. Müller, *J. Chromatogr.*, 264 (1983) 197.
- 7 J. W. de Haan and L. J. van de Ven, *J. Colloid Interface Sci.*, 110 (1986) 591.
- 8 R. K. Gilpin and M. F. Burke, *Anal. Chem.*, 45 (1973) 1383.
- 9 K. Albert, B. Pfeleiderer and E. Bayer, in D. Leyden and W. T. Collins (Editors), *Chemically Modified Surfaces 2*, Gordon and Breach, New York, 1988, p. 287.
- 10 J. N. Kinkel and K. K. Unger, *J. Chromatogr.*, 316 (1984) 193.
- 11 J. N. Kinkel, *Ph. D. Dissertation*, Johannes Gutenberg University, Mainz, F.R.G., 1984.
- 12 M. J. Sullivan and G. E. Maciel, *Anal. Chem.*, 54 (1982) 1615.
- 13 R. K. Harris, J. D. Kennedy and W. McFarlane, in R. K. Harris and B. E. Mann (Editors), *NMR and the Periodic Table*, Academic Press, New York, 1978, p. 309.
- 14 F. Bassolo and R. C. Johnson, *Coordination Chemistry*, Benjamin, New York, 1964, p. 128.
- 15 M. Hetem, L. J. van de Ven, J. W. de Haan, C. Cramers, K. Albert and E. Bayer, *J. Chromatogr.*, 479 (1989) 269.
- 16 J. Köhler, D. B. Chase, R. D. Farlee, A. J. Vega and J. J. Kirkland, *J. Chromatogr.*, 352 (1986) 275.

CHROMSYMP. 1722

Novel, highly deactivated reversed-phase for basic compounds

TRACY L. ASCAH* and BINYAMIN FEIBUSH

Research and Development, Supelco Inc., Bellefonte, PA 16823 (U.S.A.)

SUMMARY

Silica has proven invaluable as a support material for reversed-phase high-performance liquid chromatography. However, contributions of residual acidic silanols lead to poor chromatography of basic compounds. This paper demonstrates the utility of a new, highly deactivated silica-based reversed-phase packing material for the study of a series of weak and strong organic bases. Correlation between retention times on the column and octanol-water partition coefficients at pH 7.0 is demonstrated. Also shown are the results of further experiments in which we investigated the retention characteristics of basic, acidic and neutral compounds by the new deactivated phase.

INTRODUCTION

Silica-based reversed-phase high-performance liquid chromatography (RP-HPLC) has become the method of choice for a large proportion of liquid chromatographic separations. Many of the benefits of RP-HPLC can be attributed to the silica itself, which lends mechanical stability, narrow distribution of pore and particle sizes, and chemical reactivity for easy modification of the surface silanol groups. The latter characteristic of silica provides numerous possibilities for stationary phases.

Unfortunately this reactivity, although the key to the success of silica supports, is also in part the source of its limitations. Even under optimal known conditions, only partial alkylation of the silanols is accomplished, leaving an excess of unreacted groups which can strongly interact with and adsorb basic organic analytes. The kinetics of this adsorption/desorption are slow relative to the other chromatographic processes¹ and produce broad, tailing peaks which are difficult to quantify and can interfere with closely eluting compounds.

A great deal of research has gone into the quantitation of residual silanols, as witnessed by the large variety of techniques used. Methods employed for this study have included: complexation with copper-amine compounds², methane or ethane release after reaction with methyl- or ethyl-lithium compounds³, deuterium exchange⁴, surface pH^{5,6}, ²⁹Si cross-polarization magic angle spinning NMR, proton spin-counting solid-state NMR, diffuse-reflectance infrared Fourier-transform

(DRIFT), thermogravimetric and elemental analysis^{7,8}, Raman spectroscopy^{9,10}, behavior of various basic test probes¹¹⁻¹⁵, titration with sodium hydroxide¹⁶ and gas-phase titration with amines¹⁷ or diethylketone¹⁸.

In addition, it has been suggested that the silica surface has different kinds of silanol groups, *e.g.* free (isolated), associated (vicinal), geminal, etc., having different physical/chemical activities and affecting differently the chromatographic results^{3,19}.

To limit the negative effect of such groups on reversed-phase supports, special treatment of the surface before bonding and better bonding procedures were recommended. For general discussions of silanol research see Unger³, Engelhardt and Müller⁵, Nawrocki and Buszewski²⁰, Bayer and Paulus²¹ and Iler²².

The problem of reactive silanols is most apparent in the chromatography of amines, especially those which are sterically less hindered and thus are able to penetrate to the surface and interact with the silanol groups. To diminish the effect of the silanols, bulky ligands were synthesized to make the underlying silanols less accessible to basic compounds^{23,24}. Other investigators formed a protective polymer on the silica surface and showed improved chromatographic results^{25,26}. Nevertheless, even with such improvements, silanol suppression techniques such as using low pH or high ionic strength mobile phases, addition of amines, etc., are still required. In this respect, it should be mentioned that non-silica-based HPLC supports (*e.g.* cladded

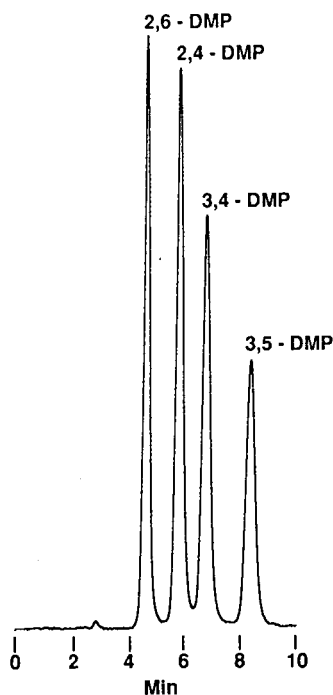


Fig. 1. Dimethylpyridine (DMP) derivatives. Column, 50 mm \times 4.6 mm Suplex pKb-100 (5- μ m packing); mobile phase, acetonitrile-25 mM aqueous potassium phosphate, pH 7.0 (2:98); detection, 254 nm UV, 0.16 a.u.f.s.; sample, 5 μ l (0.5 μ l/ml of each compound in mobile phase buffer); flow-rate, 2 ml/min; temperature, 35°C.

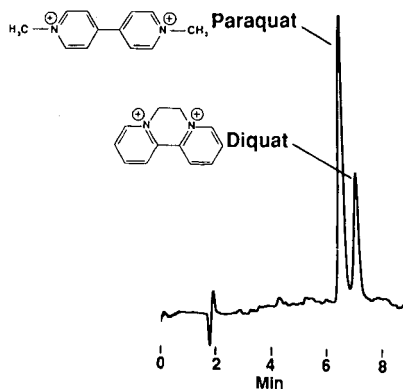


Fig. 2. Quaternary ammonium compounds paraquat and diquat. Column, 150 mm \times 4.6 mm Suplex pKb-100 (5- μ m packing); mobile phase, acetonitrile-(25 mM potassium phosphate, 5 mM decylsulfonate, pH 3.0) (30:70); detection, 254 nm UV, 0.008 a.u.f.s.; sample, 10 μ l (paraquat 4 μ g/ml, diquat 10 μ g/ml in mobile phase buffer); flow-rate, 1 ml/min; ambient temperature.

alumina, polymeric resins, and graphitized carbon) show potential but have their own limitations.

Recently^{27,28} a new HPLC material was introduced that possesses the benefits of silica-based RP but minimizes the adverse silanol reactivity by attaching chemically competing nucleophilic groups close to the silica surface. Using such a reversed-phase material, the usual chromatographic performance of non-polar analytes is extended to basic probes. The result is that analyses of bases can be performed at neutral pH, low ionic strength, and without amino modifiers. An example of the utility of the phase for the separation of dimethylpyridine (lutidine) isomers is seen in Fig. 1. Even the more potent quaternary bases such as paraquat and diquat are easily resolved (see Fig. 2).

This novel reversed-phase column, SuplexTM pKb-100, was used to study a series of predominantly monofunctional organic bases which differ in the ability of the basic nitrogen to interact with the surface silanols²⁹⁻³¹. Correlation between chromatographic retention and octanol-water partition coefficients was determined and asymmetry factors were correlated to the pK_a values of the different bases.

We also studied how the retention of these basic compounds, as well as acidic and neutral species, is affected by changes in the mobile phase conditions. Since silanols are effectively excluded from the retention process, the retention is primarily the result of altering the polar/hydrophobic nature of the sample molecule and of concurrent partitioning changes in the ligated stationary phase.

This report should serve as a demonstration of the potential use of the new deactivated reversed-phase in the study of organic bases.

EXPERIMENTAL

Chromatography

Chromatography was carried out on a Spectra-Physics (San Jose, CA, U.S.A.) liquid chromatographic system consisting of an SP8800 gradient pump, SP8780 autosampler and SP4290 integrator interfaced with LABNET/RS-232 connected to

a Kratos (Ramsey, NJ, U.S.A.) Spectroflow 757 variable-wavelength UV detector or on a Hewlett-Packard (Avondale, PA, U.S.A.) HP-1090 liquid chromatograph equipped with an HP-1040A diode array detector, autosampler, column oven, HP-85B PC system controller and an HP-3392A integrator/recorder.

The HPLC columns used were Suplex pKb-100 or Supelcosil™ LC-8-DB (both 150 × 4.6 mm, 5- μ m particles having 100-Å pores) and were obtained from Supelco, Bellefonte, PA, U.S.A. In some experiments short columns (50 × 4.6 mm) were used to reduce the run time and conserve mobile phase. Analytical columns were protected by 0.5- μ m in-line frit filters.

Analytical columns used in the deactivated column comparison study were as follows: Ultracarb ODS-20 (150 × 4.6 mm, 5 μ m, Phenomenex, Rancho Palos Verdes, CA, U.S.A.); Zorbax R_x (150 × 4.6 mm, 5 μ m, Mac-Mod Analytical, Chadds Ford, PA, U.S.A.); SynChropak SCD-100 (150 × 4.6 mm, 5 μ m, Keystone Scientific, State College, PA, U.S.A.); Capcell Pak C18-SG (250 × 4.6 mm, 5 μ m, Shiseido, Tokyo, Japan); Hibar LiChrosorb RP-Select B (250 × 4 mm, 5 μ m, E. Merck, Darmstadt, F.R.G.); Chemcosorb 5-ODS-H (150 × 4.6 mm, 5 μ m, Chemco Scientific, Osaka, Japan); Deltabond Octyl (150 × 4.6 mm, 5 μ m, Keystone Scientific); Chromega γ -C₁₈ (250 × 4.6 mm, 5 μ m, Fisher Scientific, Fair Lawn, NJ, U.S.A.) and Rexchrom ODS (150 × 4.6 mm, 5 μ m, Regis, Morton Grove, IL, U.S.A.).

All solvents were of HPLC grade and were obtained from Accusolv Anachemia (Champlain, NY, U.S.A.). Deionized water was prepared in-house on a Milli-Q system (Millipore, Milford, MA, U.S.A.). HPLC-grade potassium hydrogen phosphate and phosphoric acid were purchased from Fisher Scientific. Triethylamine (TEA) was obtained from Kodak (Rochester, NY, U.S.A.).

Samples for chromatography were obtained from Sigma (St. Louis, MO, U.S.A.) or Aldrich (Milwaukee, WI, U.S.A.). Stock solutions of standards were made in acetonitrile and were diluted in mobile phase buffer (25 mM aqueous potassium phosphate, pH 7.0) before use. Mobile phase and other chromatographic conditions appear in the figure captions.

Capacity factors (k') were measured by the equation:

$$k' = (t_R - t_0)/t_0 \quad (1)$$

where t_R is the retention time of the compound of interest and t_0 is the column void time measured using the solvent disturbance peak obtained when trace amounts of methanol were injected onto the column.

The asymmetry factor (AF_{10}) was calculated by drawing a perpendicular line from the apex of the peak to the baseline and measuring the front (A) and back (B) widths of the peak at 10% height:


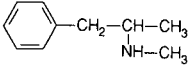
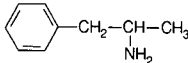
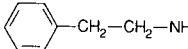
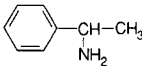
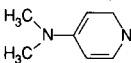
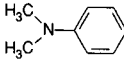
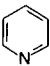
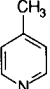
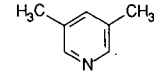
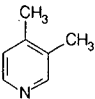
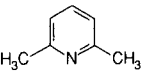
$$AF_{10} = B/A \quad (2)$$

Insight into the significance of capacity and asymmetry factors can be found in ref. 32.

The Foley-Dorsey method³³, which utilizes statistical moments, was used to measure the column efficiency since skewed peaks were often involved. The method uses the equation:

$$N = \frac{41.7 \left(\frac{t_R}{w} \right)^2}{\frac{B}{A + 1.25}} \quad (3)$$

TABLE I
STRUCTURES OF COMPOUNDS USED IN THIS STUDY

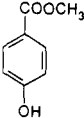
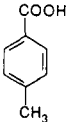
<i>Compound No.</i>	<i>Name</i>	<i>Structure</i>
1	Benzene	
2	Methamphetamine	
3	Amphetamine	
4	β -Phenethylamine	
5	α -Phenethylamine	
6	4-Dimethylaminopyridine	
7	N,N-Dimethylaniline	
8	Pyridine	
9	4-Methylpyridine	
10	3,5-Dimethylpyridine	
11	3,4-Dimethylpyridine	
12	2,6-Dimethylpyridine	

(Continued on p. 362)

TABLE I (continued)

Compound No.	Name	Structure
13	2,4-Dimethylpyridine	
14	Aniline	
15	3,5-Dimethylaniline	
16	3,4-Dimethylaniline	
17	2,6-Dimethylaniline	
18	2-Hydroxypyridine	
19	Codeine	
20	Triprolidine	

TABLE I (continued)

Compound No.	Name	Structure
21	Diphenhydramine	$\begin{array}{c} \text{C}_6\text{H}_5 \\ \diagdown \\ \text{CHOCH}_2\text{CH}_2\text{N} \\ \diagup \\ \text{C}_6\text{H}_5 \end{array} \begin{array}{c} \text{CH}_3 \\ \diagup \\ \text{N} \\ \diagdown \\ \text{CH}_3 \end{array}$
22	Methylparaben	
23	Maleic acid	$\begin{array}{c} \text{H} & & \text{H} \\ & \diagdown & / \\ & \text{C}=\text{C} \\ & / & \diagdown \\ \text{HOOC} & & \text{COOH} \end{array}$
24	Probenecid	$(\text{CH}_3\text{CH}_2\text{CH}_2)_2\text{NSO}_2-\text{C}_6\text{H}_4-\text{COOH}$
25	<i>p</i> -Toluic acid	
26	Propoxyphene	$\begin{array}{c} \text{CH}_3 \quad \text{OOCCH}_2\text{CH}_3 \\ \quad \\ (\text{CH}_3)_2\text{NCH}_2\text{CH}-\text{C}-\text{CH}_2\text{C}_6\text{H}_5 \\ \\ \text{C}_6\text{H}_5 \end{array}$

where N is the efficiency in plates per column and w is the peak width at 10% height. The efficiency values in plates per column were divided by the column length to give efficiency in plates per meter.

All values of k' , N , and AF_{10} were the means of at least two injections for which the measurements differed by less than 2%. Each experiment was repeated and the results verified on a different column run on the alternate chromatographic system. The structures of compounds used in this paper are shown in Table I.

Selected organic bases

The compounds chosen are a sampling of hindered and unhindered, primary, secondary, tertiary and heterocyclic amines. A hindered amine is one in which bulky alkyl groups are substituted near the basic nitrogen limiting its interaction with the silica surface.

TABLE II

RETENTION (k') AND ASYMMETRY (AF_{10}) VALUES FOR SOME ORGANIC BASES

Conditions: column, 50 × 4.6 mm Suplex pKb-100; mobile phase, acetonitrile-25 mM aqueous potassium phosphate, pH 7.0 (2:98); flow-rate, 2 ml/min; temperature, 35°C. n.a. = Not available.

Compound No. ^a	Name	pK_a^b	Concentration	k'	$\log P_{o/w}$	AF_{10}
1	Benzene	—	7 μ l/ml	24.3	2.10	0.97
2	Methamphetamine	10.2	50 μ g/ml	4.77	n.a.	1.72
3	Amphetamine	10.0	50 μ g/ml	3.57	1.66	1.31
4	β -Phenethylamine	10.0	50 μ g/ml	1.96	1.41	1.58
5	α -Phenethylamine	9.2	1 μ l/ml	1.95	n.a.	1.43
6	4-Dimethylaminopyridine	9.6	60 μ g/ml	0.92	1.34	3.12
7	N,N-Dimethylaniline	5.15	0.1 μ l/ml	66.2	2.36	1.05
8	Pyridine	5.25	1 μ l/ml	2.71	0.64	1.51
9	4-Methylpyridine	5.68	1 μ l/ml	7.79	1.27	1.93
10	3,5-Dimethylpyridine	6.15	0.5 μ l/ml	26.2	n.a.	1.43
11	3,4-Dimethylpyridine	n.a.	0.5 μ l/ml	20.6	n.a.	1.57
12	2,6-Dimethylpyridine	n.a.	0.5 μ l/ml	13.1	1.68	1.70
13	2,4-Dimethylpyridine	6.99	0.5 μ l/ml	17.1	n.a.	1.77
14	Aniline	4.63	1 μ l/ml	5.23	0.90	1.00
15	3,5-Dimethylaniline	n.a.	1 μ l/ml	42.8	n.a.	1.05
16	3,4-Dimethylaniline	n.a.	50 μ g/ml	37.4	n.a.	1.02
17	2,6-Dimethylaniline	3.55, 3.95	1 μ l/ml	34.3	n.a.	1.11
18	2-Hydroxypyridine	0.75	50 μ g/ml	0.81	-0.58	1.17

^a From Table I.

^b pK_a Values from refs. 31, 34 and 35.

The pK_a values reported in Table II were obtained from the literature^{31,34,35}. Some pK_a values were not available. Octanol-water partition coefficients were obtained from Hansch and Leo³⁶. Benzene was used as a non-ionic probe to obtain the AF_{10} value which excludes the silanol contribution.

Dilute solutions of each base were made in mobile phase buffer. The mobile phase used in this study was acetonitrile-25 mM aqueous potassium phosphate pH 7.0 (2:98). The very low organic concentration resulted in high k' values for some compounds, but the use of 50-mm columns kept the total analysis time low, while also reducing solvent consumption. The short columns also enabled the concurrent study of amines with drastically different k' values. The mobile phase conditions in this study (pH 7, low ionic strength, no amino additives) ensured that residual silanols are not artificially suppressed by the mobile phase, but by the bonded phase of the Suplex pKb-100. (The pK_a of the silanol group is *ca.* 4.5.)

RESULTS AND DISCUSSION

In this study, we attempted to determine the extent of suppressed activity of the silica gel matrix in the new type of reversed-phase column. We evaluated the relationship between the peak symmetry of the bases and their pK_a values, as well as the correlation between the octanol-water partition coefficient and retention time.

TABLE III

PEAK SHAPE OF CODEINE^a ON SILANOL-DEACTIVATED HPLC COLUMNS

Conditions: columns, 150 or 250 mm × 4.6 mm (5- μ m packings). Columns were further described in the Experimental section. Mobile phase: acetonitrile–25 mM aqueous potassium phosphate, pH 6.2; flow-rate, 1 or 2 ml/min; ambient temperature.

Column	k' ^b	AF_{10}	N ^c
Suplex pKb-100	2.22	1.26	11 130
LiChrosorb RP Select B	1.86	2.13	3500
SCD-100	1.84	3.00	6330
Deltabond octyl	2.37	3.93	1200
Rexchrom ODS	2.10	5.16	270
Zorbax R _x	2.58	6.0	870
Capcell Pak C18	1.62	n.m. ^d	n.m.
Chemcosorb 5 ODS H	2.44	n.m.	n.m.
Chromega γ -C ₁₈	2.29	n.m.	n.m.
Ultrasorb ODS 20	2.15	n.m.	n.m.
Supelcosil LC-18-DB	2.15	n.m.	n.m.

^a Compound 19 from Table I, $pK_a = 8.21$.

^b Acetonitrile–buffer ratio adjusted to maintain k' within a narrow range.

^c Plates/m measured by Foley–Dorsey method³³.

^d AF_{10} and N not measurable because of extremely long time for peak to return to baseline.

Finally, as no silanol suppressing additives were needed in the mobile phase, we determined how selectivity between basic, acidic, and neutral analytes was affected by altering mobile phase conditions.

In Table II there is a list of primarily organic bases, their pK_a values, capacity (k') and asymmetry factors (AF_{10}) on a Suplex pKb-100 column using acetonitrile–25 mM aqueous potassium phosphate pH 7.0 mobile phase (2:98) at 35°C. As mentioned, at this pH residual silanol groups should be fully effective.

Even though the new reversed-phase column shows a significant improvement in peak symmetry in comparison to some other commercial deactivated reversed-phases (see Table III), “silanol effects” are still observed, as indicated by peak asymmetry (see Table II). Peak asymmetry of the bases depends, in part, on their pK_a values. Compounds 10–13, for example, are dimethyl-substituted pyridine isomers. The asymmetry factors increase with pK_a values in the order 1.43, 1.57, 1.70 and 1.77 for compounds 10, 11, 12 and 13, respectively. Two of the pK_a values are not reported, but could be approximated from the inductive effect of substitution in the *ortho*-, *meta*- and *para*-positions on the basicity of the compounds. We assumed that compound 12 has a pK_a value comparable to that of compound 13, as one additional *ortho*- replaces a *para*-substituent. Compound 11, a *m,p*-isomer, should have a pK_a between 6.15 and 6.99 in comparison to an *m,m*- and *o,p*-analogue, respectively.

On the other hand, not only pK_a but also steric factors in the close vicinity of the basic nitrogen contribute to the “silanol effect”, as can be seen for compound 6 vs. compounds 2–5. Here, an unhindered, protonated planar sp^2 nitrogen is compared to a protonated sp^3 nitrogen. Compound 6, with a pK_a of 9.6, has an asymmetry factor of 3.12 vs. 1.31–1.72 for compounds 2–5 which have pK_a values between 9.2 and 10.2.

TABLE IV

EFFECT OF TRIETHYLAMINE (TEA) CONCENTRATION ON PEAK SHAPE AND RETENTION OF BASES ON DEACTIVATED PHASES

Conditions: columns, 150 × 4.6 mm, 5 μm, mobile phase for Suplex pKb-100, acetonitrile-25 mM aqueous potassium phosphate (0-0.14%, v/v, TEA), pH 6.0 (22:78); mobile phase for LC-8-DB, acetonitrile-25 mM aqueous potassium phosphate (0-0.147%, v/v, TEA), pH 3.0 (40:60); flow-rate, 2 ml/min; temperature, 35°C.

Compound	Suplex pKb-100			LC-8-DB	
	TEA (%)	AF ₁₀	k'	AF ₁₀	k'
Triprolidine (compound 20) ^a	0	1.23	3.83	8.48	5.18
	0.02	1.20	3.65	5.73	2.15
	0.08	1.24	3.61	2.93	1.61
	0.14	1.21	4.02	2.58	1.44
Diphenhydramine (compound 21) ^a	0	1.25	4.44	3.60	2.31
	0.02	1.16	4.23	3.14	2.11
	0.08	1.10	4.19	2.35	1.74
	0.14	1.19	4.62	2.30	1.65

^a From Table I.

It should be mentioned that, when working with these and other organic compounds in an aqueous mobile phase, the sample concentration must be carefully considered. A ten-fold increase in concentration of the pyridine derivatives (from 0.5 to 5 μl/ml in a 5-μl injection) caused a doubling of the asymmetry factor.

For regular organic bases, the contribution to reversed-phase retention due to "silanol effects" is negligible or small on the Suplex pKb-100 in comparison to a Supelcosil LC-8-DB column, as can be seen from Table IV. Adding TEA, a common silanol suppressor, to the mobile phase-reduced asymmetry and retention on the Supelcosil LC-8-DB column, while leaving asymmetry unaffected and retention even slightly increased on the Suplex column. A possible explanation for this increase is reduced solubility of the basic analyte in the mobile phase upon the addition of TEA.

It is of interest that hydrophobic-related retention and distribution coefficients between a water-octanol layer for the same bases are highly correlated³⁷. A plot of log *k'* vs. log *P*_{o/w}, the octanol-water partition coefficient, is described in Fig. 3. There is a good correlation between the retention time and the partition coefficient, except for compounds 3, 4 and 6. In the pH 7.0 buffered mobile phase, these three compounds are completely charged (protonated) and are driven into the polar mobile phase, while at their unbuffered pH (identical with their p*K*_a), the compounds would show a greater tendency towards the octanol phase in an octanol-water mixture. On the other hand, the p*K*_a values of the majority of the bases are similar, and at pH 7.0 all are in the free base form. Thus, for these compounds, there is good correlation between the two techniques (*r* = 0.98).

Effect of pH

A benefit of diminished silanol activity is the ability to better use pH as a tool for

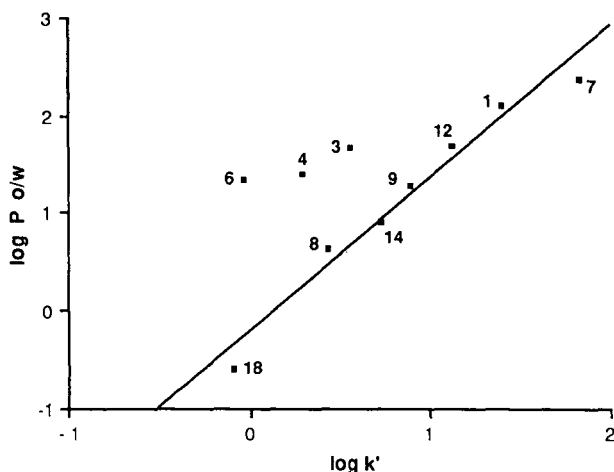


Fig. 3. Log $P_{o/w}$ (octanol-water partition coefficient) vs. log k' , retention on a Suplex pKb-100 column. Conditions and compounds as in Tables I and II.

improving resolution. Whereas in the analysis of bases on traditional RP-HPLC columns it is necessary to work at low pH to suppress silanols, the Suplex phase expands the workable pH range. For example, Table V shows the effect of pH of a 25 mM potassium phosphate buffer on retention on a Suplex pKb-100 column. Retention of amines 3, 4, 6 and 14 increases with increasing pH. The neutral compound, methylparaben, is unaffected while that of three organic acids (probenecid, maleic and *p*-toluic acids) decreases. The percent of acetonitrile was adjusted to maintain all k' values within the 0–7 range.

By increasing the pH, the extent of ionization of basic compounds is decreased, hence increasing the compound's hydrophobic character and increasing its retention

TABLE V

EFFECT OF pH OF A 25-mM POTASSIUM PHOSPHATE MOBILE PHASE ON RETENTION BY SUPLEX pKb-100

Conditions: column, 150 × 4.6 mm Suplex pKb-100; mobile phase, acetonitrile–25 mM potassium phosphate (ratio indicated in table); flow-rate, 2 ml/min; temperature, 35°C.

Compound		% CH ₃ CN	k'			
No.	Name		pH 7.01	pH 5.50	pH 3.49	pH 2.06
4	β -Phenethylamine	2	3.55	1.21	0.58	0.35
3	Amphetamine	2	6.20	2.78	1.55	0.59
14	Aniline	2	5.00	4.69	0.35	0
6	4-Dimethylaminopyridine	2	3.28	0.94	0	—
22	Methylparaben	25	2.88	3.05	2.85	2.78
23	Maleic acid	2	0.09	5.41	32.0	—
24	Probenecid	35	1.49	9.20	27.0	—
25	<i>p</i> -Toluic acid	25	0.91	9.19	14.5	—

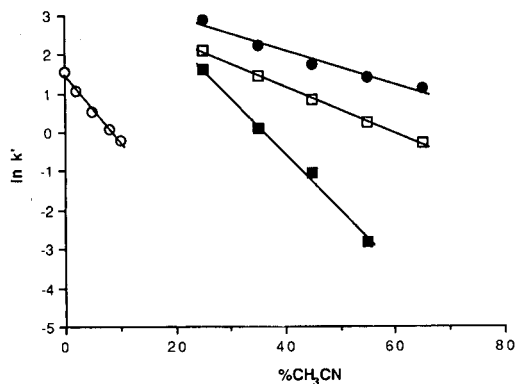


Fig. 4. Effect of acetonitrile concentration on retention of acidic, basic and neutral compounds. Column, 150 mm \times 4.6 mm Suplex pKb-100 (5- μ m packing); mobile phase, acetonitrile-25 mM potassium phosphate, pH 6.0; flow-rate, 2 ml/min; temperature, 35°C. \square = *p*-Toluic acid; \circ = amphetamine; \blacksquare = propoxyphene (pK_a 10.0); \bullet = benzene.

by a reversed-phase mechanism. The opposite effect occurs for an acid, being more hydrophobic at lower pH. Retention of a neutral species, without an ionizable moiety in this pH range, does not show a pH dependence. It is important to mention that peak shape for these compounds was not significantly affected by the pH over the investigated range.

Effect of organic modifier

Retention on the Suplex pKb-100 stationary phase (acid, base and neutral species) correlates with the organic modifier concentration of the mobile phase in a predictable manner (see Fig. 4). The excellent linearity between $\ln k'$ and acetonitrile concentration demonstrates that the column operates by a reversed-phase mechanism, even with very basic compounds.

CONCLUSION

A new silica-based RP-HPLC packing material, Suplex pKb-100, which shows a high level of silanol deactivation, was used for the study of organic bases at pH 7. The higher pH range could be essential for improving resolution of organic bases and cannot be used on conventional RP-HPLC columns due to excessive tailing. Retention times were found to correlate with lipophilic character as measured from octanol-water partition coefficients. Results of the retention study indicate that selective, predictable retention behavior of acidic and neutral species is possible as well. A reversed-phase mechanism was verified by the linear relationship between $\ln k'$ of acidic, neutral and basic species and concentration of organic modifier in the mobile phase.

REFERENCES

- 1 T. Ohkuma and S. Hara, *J. Chromatogr.*, 400 (1987) 47.
- 2 E. C. Jennings, Jr. and R. G. Brownlee, *Anal. Chem.*, 58 (1986) 2895.

- 3 K. K. Unger, *Porous Silica (Journal of Chromatography Library*, Vol. 16), Elsevier, Amsterdam, 1979.
- 4 G. Fóti, C. Martinez and E. sz. Kováts, *J. Chromatogr.*, 461 (1989) 243.
- 5 H. Engelhardt and H. Müller, *J. Chromatogr.*, 218 (1981) 395.
- 6 S. H. Hansen, P. Helboe and M. Thomsen, *J. Chromatogr.*, 368 (1986) 39.
- 7 J. Köhler and J. J. Kirkland, *J. Chromatogr.*, 385 (1987) 125.
- 8 J. Köhler, D. B. Chase, R. D. Farlee, A. J. Vega and J. J. Kirkland, *J. Chromatogr.*, 352 (1986) 275.
- 9 D. M. Krol and J. G. van Lierop, *J. Non-Cryst. Solids*, 63 (1984) 131.
- 10 D. M. Krol, C. A. M. Mulder and J. G. van Lierop, *J. Non-Cryst. Solids*, 86 (1986) 241.
- 11 C. T. Mant and R. S. Hodges, *Chromatographia*, 24 (1987) 805.
- 12 P. C. Sadek and P. W. Carr, *J. Chromatogr. Sci.*, 21 (1983) 314.
- 13 M. J. Walters, *J. Assoc. Off. Anal. Chem.*, 70 (1987) 465.
- 14 L. C. Sander, *J. Chromatogr. Sci.*, 26 (1988) 380.
- 15 P. L. Zhu, D. J. Wang, J. Q. Jin and S. L. Cao, *Chromatographia*, 25 (1988) 419.
- 16 A. L. Khurana and C.-T. Ho, *J. Liquid Chromatogr.*, 11 (1988) 3205.
- 17 J. Nawrocki, *Chromatographia*, 23 (1987) 722.
- 18 J. Nawrocki, D. L. Moir and W. Szczepaniak, *J. Chromatogr.*, 467 (1989) 31.
- 19 G. E. Maciel and D. W. Sindorf, *J. Am. Chem. Soc.*, 102 (1980) 7606.
- 20 J. Nawrocki and B. Buszewski, *J. Chromatogr.*, 449 (1988) 1.
- 21 E. Bayer and A. Paulus, *J. Chromatogr.*, 400 (1987) 1-4.
- 22 R. K. Iler, *The Chemistry of Silica*, Wiley-Interscience, New York, 1979.
- 23 J. J. Kirkland, J. L. Glajch and R. D. Farlee, *Anal. Chem.*, 61 (1989) 2.
- 24 M. A. Stadalius, J. S. Berus and L. R. Snyder, *LC · GC, Mag. Liq. Gas Chromatogr.*, 6 (1988) 494.
- 25 G. Schomburg, A. Deege, J. Köhler and U. Bien-Vogelsang, *J. Chromatogr.*, 282 (1983) 27.
- 26 P. Kolla, J. Köhler and G. Schomburg, *Chromatographia*, 23 (1987) 465.
- 27 B. Feibush, *U.S. Pat.*, Patent pending.
- 28 T. L. Ascah, B. Feibush, R. C. Ludwig and L. T. Peters, Paper No. 1450 presented at the *1989 Pittsburgh Conference and Exposition on Analytical Chemistry and Applied Spectroscopy, Atlanta, GA, March 9, 1989*.
- 29 J. S. Kiel, S. L. Morgan and R. K. Abramson, *J. Chromatogr.*, 320 (1985) 313.
- 30 D. L. Reynolds, C. M. Riley, L. A. Sternson and A. J. Repta, *J. Pharm. Biomed. Anal.*, 1 (1983) 347.
- 31 B. Law, *J. Chromatogr.*, 407 (1987) 1.
- 32 L. R. Snyder and J. J. Kirkland, *Introduction to Modern Liquid Chromatography*, Wiley-Interscience, New York, 2nd ed., 1979.
- 33 J. P. Foley and J. G. Dorsey, *Anal. Chem.*, 55 (1983) 730.
- 34 R. C. Weast (Editor), *Handbook of Chemistry and Physics*, CRC Press, Boca Raton, FL, 68th ed., 1987.
- 35 E. Papp and Gy. Vigh, *J. Chromatogr.*, 282 (1983) 59.
- 36 C. Hansch and A. Leo, *Substituent Constants for Correlation Analysis in Chemistry and Biology*, Wiley, New York, 1979.
- 37 F. Gago, J. Alvarez-Builla and J. Elguero, *J. Chromatogr.*, 449 (1988) 95.

CHROMSYMP. 1830

Development and use of carbon adsorbents in the liquid chromatographic separation of isomers

F. BELLIARDO*

Dipartimento di Scienza e Tecnologia del Farmaco, Facoltà di Farmacia, Università di Torino, cso Raffaello 31, 10125 Turin (Italy)

O. CHIANTORE^a

Dipartimento di Chimica Inorganica, Chimica Fisica e Chimica dei Materiali, Facoltà di Scienze, M.F.N., Università di Torino, Via P. Giuria 7, 10125 Turin (Italy)

D. BEREK and I. NOVÁK

Polymer Institute, Slovak Academy of Sciences, 84236 Bratislava (Czechoslovakia)
and

C. LUCARELLI

Istituto Superiore di Sanità, Viale Regina Elena 299, 00161 Rome (Italy)

SUMMARY

Porous carbonaceous sorbents, prepared by a replicate method on a silica template, were examined under the liquid chromatographic conditions. The carbons were obtained by pyrolysis of two different organic precursors (a phenol-formaldehyde resin and saccharose) at 600°C. Columns packed with 15–20- μm particles were obtained by means of high-viscosity slurry techniques. The separation of some pairs of *E/Z* diastereomers is described and discussed.

INTRODUCTION

Significant progress in the preparation of carbonaceous adsorbents as stationary phases for high-performance liquid chromatography (HPLC) has taken place in the last decade^{1–10}. Many varieties of carbonaceous materials have been developed and applied to a fair range of chemically different solutes ranging from non-polar to highly polar and ionic. However, the chromatographic behaviours of such carbonaceous stationary phases were different, owing to a variety of factors; some of them have new properties and offer a unique hydrophobic and hydrophilic selectivity which is different from that of reversed-phase alkyl-bonded silica. Unfortunately, most of the carbons produced have some but not all of the desirable requirements for good chromatographic phases, such as the correct combination of particle rigidity, high surface area, uniformity of the pore structure and uniformity of the surface composition.

^a Author deceased.

An ideal carbonaceous column packing material, showing high chemical stability over a wide pH range, adequate particle hardness to withstand high pressures, high surface area, defined functional groups homogeneously distributed on the particle surface and a mean pore size larger than 10 nm to ensure a rapid mass transfer to solutes is very difficult to obtain, and inevitably compromises will have to be made. Despite this, some good-quality carbons have recently been developed and tested¹¹. Critical reviews of the progress and problems in the field of carbonaceous adsorbents for LC have been published^{12,13}. Columns with high-efficiency carbon packings have only just become commercially available (Hypercarb; Shandon, Runcom, U.K.). The superior selectivity of the surface of some carbons towards positional isomers such as *E/Z* is one of the most impressive properties compared with conventional HPLC phases.

This paper describes the results obtained with two different carbon adsorbents in the separation of *E/Z* isomers of α -chlorochoalcone (2-chloro-1,3-diphenyl-1-propen-1-one), saffrole-(*E/Z*)-isosafrrole and -(*E/Z*)-stilbene.

EXPERIMENTAL

Materials

The LC separations were carried out with carbon CF-18 (derived from phenol-formaldehyde resin) and CF-19 (from saccharose), prepared at the Institute of Polymers of the Slovak Academy of Science (Bratislava, Czechoslovakia), using a replicate method involving the pyrolysis of precursors on a microparticulate silica matrix¹⁴⁻¹⁶.

The physical and chemical characterizations of the carbonaceous adsorbents, performed through particle-size analysis, shape determination via electron microscopy, surface area determination, thermal analysis and Fourier transform (FT) IR spectroscopy have been described previously¹⁷.

Both carbons used in this work have a sponge-like structure with good mechanical strength. Scanning electron micrographs of CF19 and CF18 are shown in Figs. 1 and 2. The determined physical characteristics of the two packing materials are summarized in Table I.

The rough materials with particle size ranging from 5 to 90 μm , were directly sieved into narrow-mesh size fractions using an ASTM-DIN 5- μm IG/1 microsieve shaker (Giuliani, Turin, Italy). The stainless-steel chromatographic columns (250 \times 4.6 mm I.D.) were packed using the slurry-packing technique. The slurry contained about 8% (w/w) of carbon adsorbent in a mixture of dibromomethane and acetonitrile. The density of the mixture was adjusted in order to avoid considerable floating and sedimentation of carbon particles. After treatment in an ultrasonic bath for 5 min, the slurry was pressed into the column with acetonitrile under a pressure of 20-30 MPa.

Equipment

The analyses were performed on a Perkin-Elmer Series 3B liquid chromatograph equipped with a Rheodyne 7125 injection valve and a Perkin-Elmer LC-100 column oven. Component elution was monitored with a Perkin-Elmer LC-75 variable-wavelength detector coupled with a Perkin-Elmer LC-75 Autocontrol.

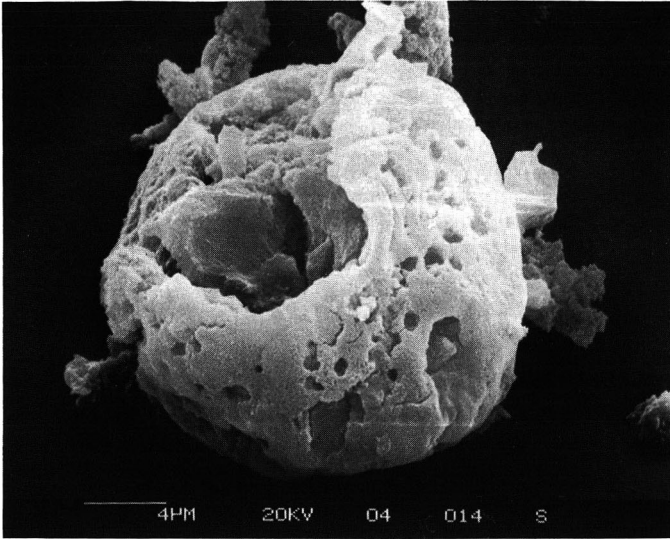


Fig. 1. Scanning electron micrograph of carbon CF18.

The separations were achieved under the following conditions. For (*E/Z*)- α -chlorochoalcone, the mobile phase was acetonitrile–water–chloroform (70:10:2), flow-rate 2 ml min^{-1} , temperature 35°C and wavelength 260 nm . For safrole–(*E/Z*)-isofafrole, the mobile phase was acetonitrile–water–chloroform (70:6:5), flow-rate 2 ml min^{-1} , temperature 35°C and wavelength 254 nm . For (*E/Z*)-stilbene, the mobile phase was acetonitrile–chloroform–2-propanol (50:40:10), flow-rate 2 ml min^{-1} , temperature 35°C and wavelength 290 nm . Peak areas were measured with a Perkin-Elmer LCI 00 laboratory computing integrator.

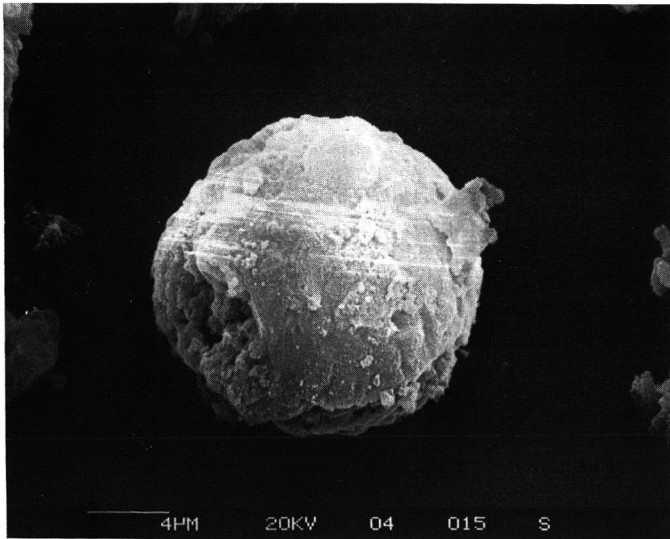


Fig. 2. Scanning electron micrograph of carbon CF19.

TABLE I

PHYSICAL CHARACTERISTICS OF THE PYROLYTIC CARBONS

d_n = number-average particle diameter; d_w = weight-average particle diameter.

Sample	Surface area (m^2/g)	Bulk density (g/cm^3)	Residual silica (%)	d_n μm	d_w μm	d_w/d_n
CF18	770	0.26	10	26.7	32.9	1.23
CF19	735	0.45	2	22.4	32.7	1.46

For peak assignments, the UV spectra of the separated *E/Z* isomers were measured in the stopped-flow mode on the LC-75 Autocontrol and compared with reference spectra.

RESULTS AND DISCUSSION

The diffuse reflectance (DR)-FT-IR spectra of the two carbons used show a number of absorptions due to the presence of several functional groups; the charring process did not reach the stage of complete destruction of the starting structure. At the temperature used in the preparation of the two carbon adsorbent samples (600°C), a carbonaceous polymer network was formed which still maintained some of the chemical features of the initial material, together with new functional groups generated in the carbonization process. The carbon obtained by pyrolysis of saccharose is different to that from phenol-formaldehyde; both types of carbons, however, show a mixed behaviour owing to the presence of polar and non-polar groups. In CF19 carbon the charring of saccharose proceeded with extensive condensation of the starting molecules and aromatization of the resulting structure; oxygen-containing groups were still substantially present either as OH residues or as ether links or as newly formed C=O groups¹⁷.

As expected, the carbonaceous packing is suitable for the separation of homologous series of compounds, which depend on hydrophobic selectivity, and for the separation of isomers which depend on stereoselective surfaces.

In preliminary experiments, chromatographic separations were achieved using a binary solvent mixture of acetonitrile and water. Although mixtures of acetonitrile and water can generally be used to obtain mobile phases with a wide range of eluotropic strength, the results were not satisfactory. By increasing the strength parameter (ϵ) by adding chloroform to the mobile phases, the efficiency and the selectivity were considerably improved.

The preliminary studies performed on CF19 confirmed that this material was more suitable than CF18 for the resolution of positional isomers, and therefore we used columns packed with the former phase in subsequent work.

Fig. 3 shows the separation of *E/Z* isomers of α -chlorochoalcone on a CF19 column. Figs. 4 and 5 illustrate the separation of safrole – (*E/Z*)-isosafrole and (*E/Z*)-stilbene in the same column.

Although the particle batches of carbon CF19 used were relatively large ($d_p > 15 \mu m$) and irregularly shaped and the size distribution was not perfectly uniform, which is generally prejudicial to efficiency, the *E/Z* isomers tested were very easily

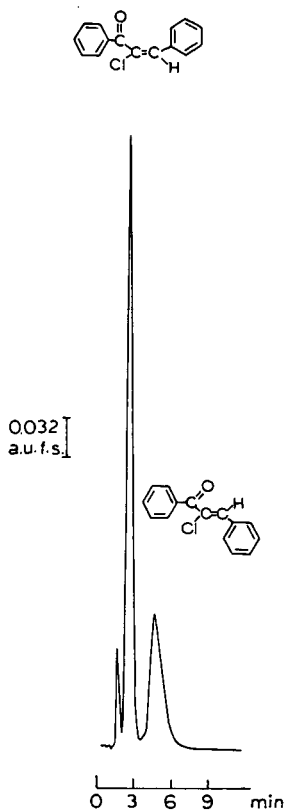


Fig. 3. Separation of (*E/Z*)- α -chlorochoalcone. The peak at a retention time of 1.77 min is an impurity. Column, CF19, 15–20 μ m (250 \times 4.6 mm I.D.); mobile phase, acetonitrile–water–chloroform (70:10:2); flow-rate, 2 ml min⁻¹; temperature, 35°C; wavelength, 260 nm.

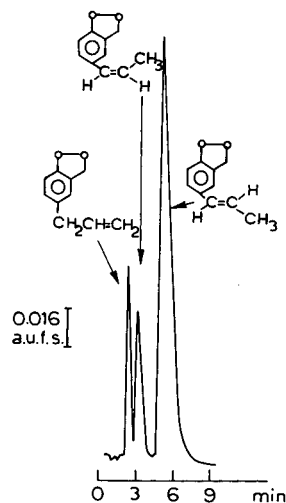


Fig. 4. Separation of safrole and (*E/Z*)-isosafole. Column, CF19, 15–20 μ m (250 \times 4.6 mm I.D.); mobile phase acetonitrile–water–chloroform (70:6:5); flow-rate, 2 ml min⁻¹; temperature, 35°C; wavelength, 254 nm.

separated and the chromatographic behaviour of the carbon column was satisfactory. The peak broadening that can be observed on the chromatograms may be due to the presence of narrow pores on the carbon particle surface (very low mass transfer in such pores), to the irregular shape and size range of the particles or to incorrect packing.

Even though in solute–sorbent interactions charge transfer (π -complexes) and polarization phenomena play an important role, the greatest contribution to absorption on the carbonaceous surface seems to be associated with dispersion forces of the sorbate molecules¹⁸. The structural effect of the sorbate molecules is non-linear and depends on the difference in the geometric structure of the molecules.

For example, in the (*E/Z*)- α -chlorochoalcon separation, the molecule of the *E*-isomer is less planar than the *Z*-isomer molecule, which has a higher contact surface area with the carbonaceous adsorbent. The *Z*-isomer, which is more planar, is therefore more strongly retained than the *E*-isomer, in which the smaller surface area of contact reduces the absorption contribution.

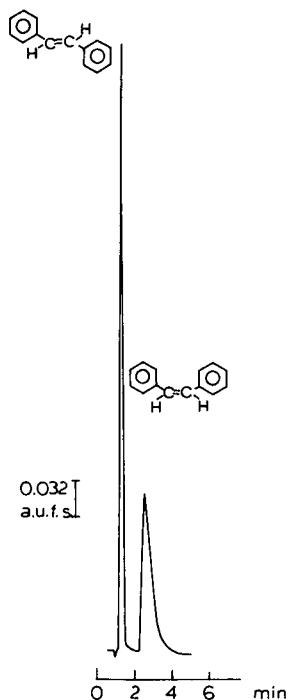


Fig. 5. Separation of (*E/Z*)-stilbene. Column, CF19, 15–20 μm (250 \times 4.6 mm I.D.); mobile phase, acetonitrile–chloroform–2-propanol (50:40:10); flow-rate, 2 ml min^{-1} ; temperature, 35°C; wavelength, 290 nm.

CONCLUSION

Despite the fact that the separation of *E/Z* isomers was performed with a medium-efficiency column, the initial results are very promising. Dispersion forces play the major role in the adsorption on the surface of the carbonaceous particles, and this is shown by stereoselectivity in the separation of positional isomers, particularly when changes in the substituent positions have a considerable effect on the space configuration of molecules having the same mass.

To conclude, the carbonaceous adsorbents tested revealed a very high resolving power for isomer separations compared with conventional packing materials such as silica and silica-bonded phases, on which the resolution of these molecules is very difficult to achieve.

ACKNOWLEDGEMENTS

We acknowledge the gift of α -chlorocholeone samples by Professor O. Caputo (Istituto di Chimica Farmaceutica Applicata, Università di Torino). We also express our gratitude to Dr. G. Artuffo for technical assistance.

REFERENCES

- 1 H. Colin, C. Eon and G. Guiochon, *J. Chromatogr.*, 119 (1976) 41.
- 2 H. Colin, C. Eon and G. Guiochon, *J. Chromatogr.*, 122 (1976) 223.
- 3 H. Colin and G. Guiochon, *J. Chromatogr.*, 126 (1976) 43.
- 4 H. Colin and G. Guiochon, *J. Chromatogr.*, 137 (1977) 19.
- 5 K. Unger, P. Roumeliotis, H. Mueller and H. Goetz, *J. Chromatogr.*, 202 (1980) 3.
- 6 J. H. Knox, B. Kaur and G. R. Millward, *J. Chromatogr.*, 352 (1986) 3.
- 7 R. Kaiser, *Chromatographia*, 3 (1970) 38.
- 8 T. Yamabe and N. Takai, *Seisan-Kenkyu*, 26 (1974) 178.
- 9 Z. Plzak, F. P. Dousek and J. Jansta, *J. Chromatogr.* 147 (1978) 137.
- 10 V. Patzelova, J. Jansta and F. P. Dousek, *J. Chromatogr.*, 148 (1978) 53.
- 11 J. H. Knox and M. T. Gilbert, *Ger. Pat.* 2 946 688-4 (1980); *Br. Pat.* 2035282 B (1978); *U.S. Pat.*, 4 263 268 (1981).
- 12 J. H. Knox, K. K. Unger and H. Mueller, *J. Liq. Chromatogr.*, 6 (1983) 1.
- 13 K. K. Unger, *Anal. Chem.*, 55 (1983) 361A.
- 14 I. Novak and D. Berek, *Czech. Pat.* CS AO 231 197.
- 15 I. Novak and D. Berek, presented at the 6th Discussion Conference, *Chromatography of Polymers and Polymers in Chromatography, Prague, 1978*, paper C27.
- 16 I. Novak and D. Berek presented at the 2nd Danube Symposium Progress in Chromatography, Carlsbad, 1979 paper C1.1.
- 17 O. Chiantore, I. Novak and D. Berek *Anal. Chem.* 60 (1988) 638.
- 18 E. Skuthanova, L. Felt, E. Smolkova-Keulemansova and J. Skuthan, *J. Chromatogr.*, 292 (1984) 233.

Lipid-vesicle-surface chromatography

QING YANG, MARIA WALLSTÉN and PER LUNDAHL*

Department of Biochemistry, Biomedical Centre, University of Uppsala, P.O. Box 576, S-751 23 Uppsala (Sweden)

SUMMARY

Egg-yolk phospholipid vesicles (liposomes) containing stearylamine cations or phosphatidylserine anions, were formed and entrapped in agarose gel beads (Sephacrose 6B) by a dialysis procedure. On a column of entrapped phospholipid–stearylamine (4:1) (cationic) vesicles, 0.36 mg of ferritin was bound per μmol lipids at 0.05 *M* ionic strength and pH 7. About 30% of the vesicle surface thus became covered with ferritin. Only 0.04 mg of citraconylated myoglobin was bound per μmol lipids, as myoglobin is much smaller than ferritin. Haeme groups were readily inserted into the lipid bilayers. An excess amount of bovine serum albumin (BSA) or ribonuclease A was applied to entrapped ionic vesicles and the bound proteins were eluted by increasing the ionic strength from 0.01 to 0.2 or 0.5 *M*. After three to five runs, 82–88% of the vesicles (the phospholipids) remained entrapped. The capacity of the cationic vesicle-column for BSA decreased more than did the amount of entrapped vesicles, which indicates a preferential loss of stearylamine. Ion-exchange experiments were done with human plasma and with BSA monomers and dimers on entrapped cationic vesicles. Plasma proteins could be separated. BSA dimers were eluted later than BSA monomers in a sodium chloride gradient and the separation was better than on DEAE-Sephacrose. The contact area between the protein and the vesicle surface is important for the binding strength. Protein–vesicle surface interactions can be studied by chromatography on entrapped vesicles.

INTRODUCTION

Immobilized artificial membrane chromatography by use of synthetic chromatographic supports composed of a membrane-forming lipid, lecithin, mimicking a cell membrane lipid monolayer, has been reported recently by Pidgeon and Venkataram¹. We have recently developed a procedure for dialysis entrapment of lipid vesicles and protein–lipid vesicles in gel beads without the use of hydrophobic ligands. Sufficiently large lipid vesicles become trapped in the gel bead pores in which they are formed². Lipid vesicles (liposomes) are composed of amphiphiles, phospholipids, forming lipid bilayers that enclose one or more aqueous compartment(s)³. The entrapment of lipid vesicles in gel beads provides a possibility for chromatography of water-soluble

proteins and hydrophilic peptides on the vesicle surfaces. This can be useful for studies of solute interactions with the lipid bilayers. The specific or non-specific interaction of biomolecules with cell membranes may afford special properties for the lipid-vesicle-surface chromatography. The main aim of this work was to show that the entrapped vesicles are accessible to proteins and are relatively stable on binding and elution of proteins with increasing ionic strength, and that chromatography is therefore possible with the vesicle surfaces as a stationary phase. Ion-exchange chromatography of plasma proteins and of BSA monomers and dimers on entrapped cationic vesicle columns was demonstrated.

EXPERIMENTAL

Materials

Sephacrose 6B, Sepharose CL-6B, Sephadex G-25 M (PD-10) columns and horse spleen ferritin (gel filtration calibration protein) were purchased from Pharmacia LKB (Uppsala, Sweden). Bovine serum albumin (BSA) (A-7030), BSA monomers (A-1900) and dimers (A-9039), ribonuclease A (bovine pancreas, type III-A, R-5125), stearylamine and bovine brain extract (80–85% phosphatidylserine, B-1627) were purchased from Sigma (St. Louis, MO, U.S.A.). Citraconic anhydride (purum) was from Fluka (Buchs, Switzerland). Dialysis tubings were of the regenerated cellulose type with a diameter of 20 mm (cut-off M_r , 12 000–14 000) from Viskasi (Chicago, IL, U.S.A.). All chemicals were of analytical-reagent grade unless stated otherwise. Human blood plasma was obtained from the blood bank at the University Hospital (Uppsala, Sweden) and was transferred to buffer A (ionic strength 0.22 M, pH 7.1; see below) by chromatography on a Sephadex G-25 column. Aliquots were stored at -70°C .

Buffers

Buffers A–D all contained the following components: 1 mM Na_2EDTA , 1 mM 2-mercaptoethanol and 0.1 mM D-glucose, combined with (A) 200 mM NaCl, 20 mM Tris–HCl (pH 7.1), (B) 20 mM NaCl, 20 mM Tris–HCl (pH 7.1), (C) 20 mM NaCl, 20 mM citric acid (pH 4) and (D) 200 mM NaCl, 20 mM citric acid (pH 4).

Lipid/cholate solutions

A 100 mM phospholipid solution was prepared by dispersing egg-yolk phospholipids (70% phosphatidylcholine, 21% phosphatidylethanolamine⁴) in 125 mM cholate, 200 mM NaCl, 2 mM dithioerythritol, 1 mM Na_2EDTA , 0.1 mM D-glucose and 20 mM Tris–HCl (pH 7.1). The suspension was stirred for 35 min at 22°C . Other procedures were as described previously⁴.

A phospholipid–stearylamine solution was prepared by mixing stearylamine, the above 100 mM phospholipid solution, 750 mM cholate and buffer A to final concentrations of 10 mM stearylamine, 40 mM lipids and 62.5 mM cholate. The pH was adjusted to 8 and the mixture was stirred under nitrogen at 22°C until the stearylamine was dissolved.

Bovine brain extract (80–85% phosphatidylserine) was dissolved with cholate to final concentrations of 40 mM lipids (ca. 33 mM phosphatidylserine) and 100 mM cholate in 5 mM Tris–HCl (pH 7.1) containing 1 mM 2-mercaptoethanol and 1 mM Na_2EDTA . This solution is denoted phosphatidylserine solution below. The corresponding vesicles are denoted phosphatidylserine vesicles (anionic vesicles).

Methods

Entrapment. Egg-yolk phospholipid vesicles were entrapped in agarose gel beads by dialysis of the lipid solution that had been mixed with the gel beads². Briefly, 3 ml of the phospholipid–stearylamine or phosphatidylserine solution (see *Materials*) was mixed with agarose gel beads by pumping the solution into a Sepharose 6B column (packed volume 2.5 ml). The gel was then transferred from the column into a dialysis cell (see Fig. 1 in ref. 2) and dialysed against 4×500 ml of buffer A (see *Materials*) for 2.5 days at 22°C. After dialysis the gel beads were washed three times with buffer A by centrifugation at 150 g for 5 min. The gel was repacked into a column and further washed by chromatography with five column volumes of buffer A. All entrapments and experiments with entrapped vesicles were done at room temperature.

Stability of entrapped vesicles. Excess amounts of BSA, 9.6 mg in 3 ml of starting buffer (10 mM Tris–HCl, pH 8.5, containing 0.1 mM Na₂EDTA and 0.2 mM 2-mercaptoethanol) were applied to a phospholipid–stearylamine (4:1) (cationic) vesicle–Sepharose 6B column (2.8 × 1 cm I.D.). This column was connected to a UV monitor (UV-2; Pharmacia LKB) and a recorder. The column was equilibrated with the starting buffer before protein application, and the bound proteins were eluted by increasing the ionic strength. This chromatographic experiment was repeated on the same column three to five times over 1.5–2 days at room temperature.

All fractions upon application, rinsing, elution and equilibration were collected in weighed tubes (to determine the fraction mass) and the amounts of the released phospholipids were determined by phosphorus analyses according to the method of Bartlett⁵. The entrapped phospholipids remaining in the column after the repeated chromatographic experiments was solubilized with 100 mM cholate for phosphorus analysis. The amount of phospholipids retained in the corresponding chromatographic run No. N , expressed as a percentage of the initial amount of entrapped lipids, was calculated as $100(E - R_{N-1})/E$, where E is the initial amount of entrapped phospholipids, which was calculated as the sum of the amounts of lipids released throughout the repeated chromatographic experiments and the amount of lipids solubilized with 100 mM cholate, and R_{N-1} is the phospholipids released in the preceding chromatographic experiment(s), $N - 1$. For entrapped phosphatidylserine (anionic) vesicles, 8 mg of ribonuclease A in starting buffer (0.01 M NaCl in 5 mM Tris–HCl, pH 7.1) were applied to the vesicle–Sepharose 6B column (2.8 × 1 cm I.D.). Other experimental conditions were the same as for the entrapped cationic vesicles.

Citraconylation of myoglobin. Horse-heart myoglobin was citraconylated by the procedure described by Lundahl⁶ using 10 mmol of citraconic anhydride per mmol of lysine or per gram of myoglobin. This procedure replaces the positive charges of the N-terminal amino group and the lysine ϵ -amino groups with carboxyl groups. The citraconylated myoglobin (CMG) was transferred to buffer B by chromatography on Sephadex G-25. In some experiments CMG was dialysed against 4×500 ml of buffer B for 2 days at 7°C. Isoelectric focusing of CMG and dialysed CMG showed 3–5 bands in the pH range 4–5.3.

Electrophoresis. Sodium dodecyl sulphate polyacrylamide gel electrophoresis (SDS-PAGE) with a linear gradient of acrylamide concentration from 8 to 25% and silver staining of the gel was done essentially as described in ref. 7. Isoelectric focusing was done on ready-made polyacrylamide gels containing carrier ampholytes with a pH range of 3–10 (LKB Ampholine PAGplates; Pharmacia LKB) at 2000 V for 3000 Vh. The focusing gel was stained with Coomassie Brilliant Blue R-250.

TABLE I

CAPACITY OF CATIONIC VESICLES FOR BINDING OF FERRITIN

16 mg of ferritin in 5 ml of buffer B (ionic strength 0.05 M, pH 7.1) were applied in buffer B to 0.5-ml tandem columns of Sepharose 6B, neutral lipid vesicle-Sepharose 6B and cationic lipid vesicle-Sepharose 6B. Elutions were done for each column separately. Flow-rate, 6 ml/h.

Column	Amount of lipids ^a (μmol)	Eluted ferritin			
		Buffer A (ionic strength 0.22 M) (mg)	100 mM cholate (mg)	Sum (mg)	$\frac{\mu\text{g protein}}{\mu\text{mol lipid}}$
Sepharose 6B	—	0.004	0.003	0.007	—
Neutral vesicle ^b -Sepharose 6B	5.9	0.01	0.005	0.015	2.5
Cationic vesicle ^c -Sepharose 6B	5.6	1.65	0.35	2.00	360

^a The amount of lipids in the entrapped cationic vesicles is expressed as the sum of the amounts of phospholipids and stearylamine. The latter amount was calculated according to the ratio of the stearylamine added to the phospholipids.

^b Egg-yolk phospholipid vesicles.

^c Egg-yolk phospholipid-stearylamine vesicles (molar ratio 4:1).

Protein amounts. Protein amounts were determined by automated total amino acid analysis with 24-h hydrolysis in 6 M hydrochloric acid.

RESULTS

Surface accessibility of entrapped vesicles

For studies of the interaction of proteins with entrapped vesicles the vesicle surfaces must be easily accessible. Protein interactions with the entrapping gel matrix should be minimal. To investigate this, we chose a large spherical protein, ferritin (M_r 440 000, K_{av} 0.33 on Sepharose CL-6B, isoelectric point 4.3–4.4⁸) and applied an excess amount of this protein at an ionic strength of 0.05 M to three tandem columns containing Sepharose 6B, egg-yolk phospholipid (neutral) vesicle-Sepharose 6B and cationic vesicle-Sepharose 6B. The ferritin passed through the first two columns and bound extensively (0.36 mg/ μmol lipid; see Table I) in the cationic vesicle-gel column, which became dark brown. Approximately 30% of the outer surfaces of the vesicles became covered with ferritin molecules, as estimated by use of the cross-sectional area of ferritin (*ca.* 11 300 \AA^2), of egg-yolk phospholipid molecules [*ca.* 70 \AA^2 (ref. 9)] and of stearylamine (*ca.* 35 \AA^2). More than 80% of the adsorbed ferritin could be released by increasing the ionic strength to 0.22 M.

Binding of a small, highly negatively charged protein to entrapped vesicles

On the application of citraconylated myoglobin (CMG) to entrapped neutral and cationic vesicle-Sepharose 6B columns, both columns became dark red. The lipids and the bound material were eluted with cholate. The eluate contained a large amount of haeme groups, as determined by measuring the absorbance of the haeme groups at

TABLE II

BINDING OF CITRACONYLATED MYOGLOBIN (CMG) AND HAEME GROUPS TO NEUTRAL AND CATIONIC LIPID VESICLE-GEL COLUMNS (1×0.7 cm I.D.) WITH AMOUNTS OF ENTRAPPED LIPIDS^a OF 5.3 AND 6.0 μmol , RESPECTIVELY

Samples A and A', 5 mg/ml of CMG in 4.5 ml and 5.5 ml of buffer B, respectively. Sample B, 3.2 mg/ml of dialysed CMG in 2.5 ml of buffer B. Flow-rate, 6 ml/h.

Sample	Column	Amount of bound CMG		Amount of bound haeme group (nmol/ μmol lipid ^d)
		$\mu\text{g}/\mu\text{mol}$ lipid ^b	nmol/ μmol lipid	
A	Neutral vesicle ^b - Sephrose 6B	5.5	0.31	7.5
A'	Cationic vesicle ^c - Sephrose 6B	9.6	0.55	14.5
B	Cationic vesicle ^c - Sephrose 6B	39	2.2	<1.5

^a Amount of entrapped lipids including stearylamine as in Table I.

^b Egg-yolk phospholipid vesicles.

^c Egg-yolk phospholipid-stearylamine vesicles (molar ratio 4:1).

412 nm, but only a small amount of protein. The amounts of haeme groups and CMG were about twice as high on the cationic as on the neutral vesicles (Table II). Haeme groups were released from the CMG and became inserted into the lipid bilayer of the entrapped vesicles on binding of the CMG to the vesicle surfaces. Dialysis removed haeme groups from the CMG solution. Accordingly, only small amounts of haeme groups became adsorbed when dialysed CMG was applied to the columns, and the cationic vesicles bound a relatively large amount of citraconylated apomyoglobin (Table II), about 0.23 mg on the 0.5-ml column. The main conclusion is that the haeme groups readily become inserted in the lipid bilayer. Their carboxyl groups decrease the vesicle charge. Therefore, CMG bound reasonably well to the cationic vesicles only when the amount of haeme groups was decreased.

Stability of entrapped vesicles

We have previously shown that entrapped vesicles are retained through several washing steps². The question posed here is whether the entrapped vesicles are stable on changes in osmotic pressure for chromatography of proteins. Fig. 1A illustrates the retention of the phospholipids of lipid vesicles entrapped in gel beads on repeated cycles of salt gradient elution. The vesicles that became too small relative to the pores in which they were entrapped were eluted in the first chromatographic run. After the first run, the retention of phospholipid vesicles in subsequent chromatographic experiments decreased only slightly. Most of the remaining vesicles were stably entrapped. In BSA chromatography on entrapped cationic vesicles the retentions of the vesicles were 88% on five repeated cycles of the chromatographic experiment and 82% on three cycles with increasing ionic strength from 0.01 to 0.21 M (\circ in Fig. 1A) and from 0.01 to 0.51 M (Δ in Fig. 1A). The retention was 88% for ribonuclease A on entrapped anionic vesicles (\square in Fig. 1A). As expected, the entrapped vesicles were

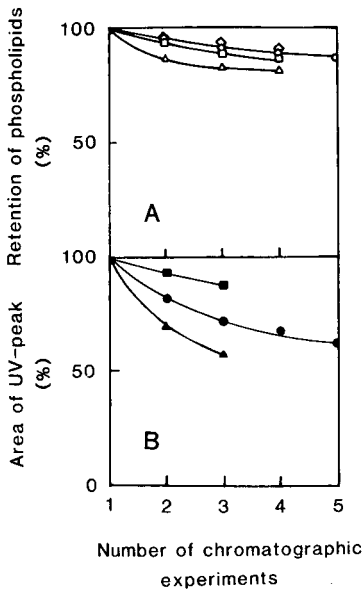


Fig. 1. (A) Stability of entrapped vesicle columns. Retention of entrapped phospholipid vesicles in consecutive chromatographic runs. Chromatography of BSA on the entrapped cationic vesicles (○, △) and of ribonuclease A on the entrapped anionic vesicles (□), or on the cationic vesicles without application of proteins (◇), NaCl gradient elutions: (○) 0–0.2 M NaCl; (△ and ◇) 0–0.5 M NaCl; (□) 0.01–0.5 M NaCl. For the experimental procedures see *Stability of entrapped vesicles*. (B) Relative area of UV peaks for protein elutions. The filled symbols correspond to the open symbols in (A). The first peak of elution before leakage of phospholipids occurred was expressed as 100% in relation to the second, the third, and so on. Each curve in (A) and (B) corresponds to experiments on a single column.

more stably confined to the pores when the salt concentration of the eluent was decreased to that at which the vesicles were formed. The effect of osmotic pressure alone (◇ in Fig. 1A) on the leakage of the entrapped vesicles was less than the combined effects of binding of protein and subsequent elution by increasing the ionic strength (○, □ and △ in Fig. 1A). This phenomenon was further studied by use of a model protein, lysozyme, for binding on the surface of entrapped phosphatidylserine vesicles¹⁰. For the entrapped anionic vesicles the decrease in the area of the UV peaks corresponding to eluted proteins was approximately in proportion to the decrease in the corresponding retention of the entrapped vesicles (□ and ■ in Fig. 1A and B, respectively). However, the area for the entrapped cationic vesicles decreased more steeply (▲ and ● in Fig. 1B) than did the corresponding retention of the vesicles (△ and ○ in Fig. 1A). It seems that stearylamine incorporated into the vesicle bilayer was released to some extent on the binding and release of BSA from the cationic vesicles, which reduced the charge density on the vesicle surface. It should be noted that the areas of the UV peaks mainly represent “protein-binding capacity”. However, the vesicles that are released during protein elutions give light scattering at 280 nm, which also shows up as an apparent absorption, particularly in the case of the first chromatographic run with a non-negligible loss of lipids.

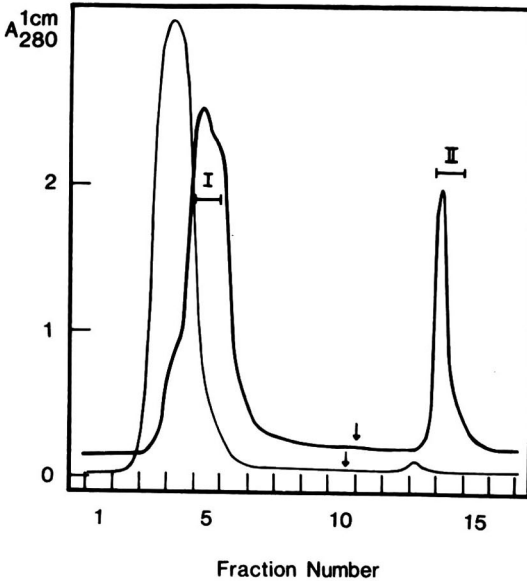


Fig. 2. Chromatography of human plasma on a Sepharose 6B column with entrapped cationic lipid vesicles (thick line) or without lipid vesicles (thin line). The column was equilibrated with buffer B (ionic strength 0.05 *M*, pH 7) before and after application, and bound proteins were eluted with buffer C (ionic strength 0.06 *M*, pH 4). The arrows indicate the start of the elution with buffer C. Sample, human blood plasma (see *Materials*) diluted 10-fold with distilled water; sample volume, 2 ml; column dimensions, 3.2 × 1 cm I.D. (bed volume 2.5 ml); flow-rate, 3 ml/h; fraction volume, 0.5 ml; amount of entrapped phospholipids in the column, 15 μ mol.

Chromatography of plasma proteins on entrapped cationic vesicles

On chromatography of human plasma proteins on an entrapped cationic vesicle–Sepharose 6B column, at ionic strength 0.05 *M* and pH 7, we found that many proteins in the M_r range from 16 000 to *ca.* 300 000, or proteins with subunits in this range, bound to the column and could be eluted (peak II, thick line, in Fig. 2; lane II in Fig. 3) at pH 4 (buffer C, ionic strength 0.06 *M*). Albumin and other proteins passed straight through the column (peak I, thick line, in Fig. 2 and lane I in Fig. 3). The leakage of phospholipids on elution with buffer C was 1%. A similar chromatographic experiment in which the bound plasma proteins were eluted by increasing the ionic strength from 0.05 to 0.24 *M* and decreasing the pH from 7 to 4 showed a chromatographic pattern (not shown) and non-bound and bound proteins (lanes a and b in Fig. 3) similar to that in Fig. 2 (thick line) and to lanes I and II in Fig. 3, respectively. The loss of the vesicles was 10% in this instance. It is clear that the entrapped cationic vesicles were more stable on protein elution with decrease in pH alone than together with increase in ionic strength. After storage of the column at 7°C for 3 days the leakage of phospholipids was 1.5% on elution with a decrease in pH alone. Chromatography of plasma after removal of the entrapped vesicles with 100 mM cholate showed mainly a single peak corresponding to non-bound materials. The peak was minimal on elution with buffer C (Fig. 2, thin line).

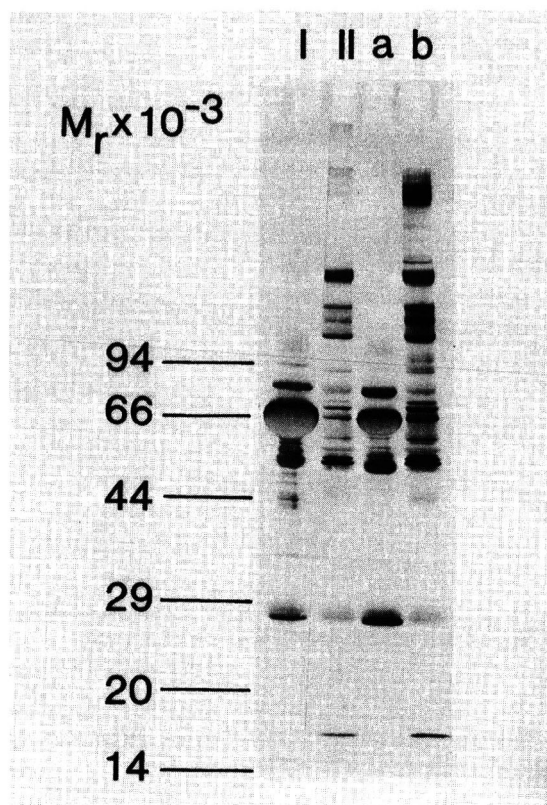


Fig. 3. SDS-PAGE of the non-bound and bound proteins. Sample volume, 35 μ l. Lanes I and II, the non-bound and bound plasma proteins indicated by bars in Fig. 2, thick line. Lanes a and b show the same non-bound and bound proteins, respectively, in another similar fractionation for which the elution was done with buffer D (ionic strength 0.24 M, pH 4).

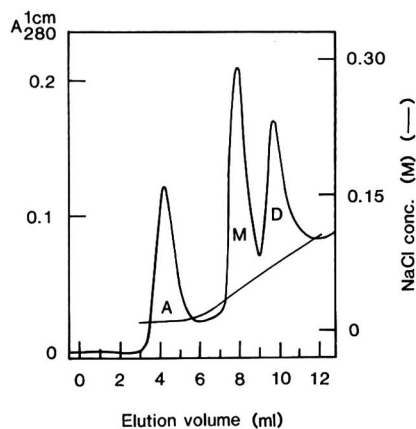


Fig. 4. Chromatography of a mixture of BSA monomers (M) and dimers (D) on a cationic vesicle-Sepharose 6B column (2.9 \times 1 cm I.D.). Sample, 0.2 mg of each component in 0.2 ml of starting buffer (10 mM Tris-HCl, pH 8.5, containing 0.1 mM EDTA and 0.2 mM mercaptoethanol). The proteins were eluted with a gradient of NaCl in the starting buffer. Flow-rate, 1 ml/h. A, Unidentified non-proteinaceous material.

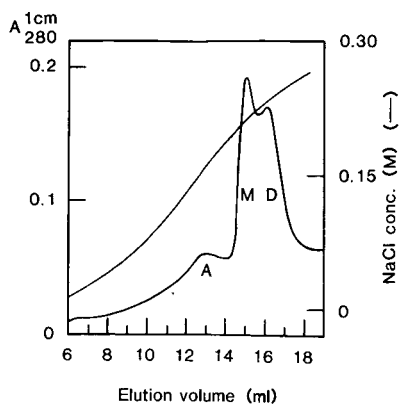


Fig. 5. Chromatography of BSA monomers and dimers on a DEAE-Sepharose 6B column (3.0×1 cm I.D.). The experiment was done as in Fig. 4. Notations as in Fig. 4.

Chromatography of bovine serum albumin on entrapped cationic vesicles

BSA monomers and dimers became well separated on entrapped cationic vesicles at the low flow-rate of 1 ml/h (Fig. 4). The identity of the components was verified by "native" electrophoresis (not shown). Separation could also be achieved at a higher flow-rate, 10 ml/h (not shown). Chromatography on DEAE-Sepharose 6B gave only a slight separation at a flow-rate of 1 ml/h (Fig. 5). At 10 ml/h the monomer and dimer did not separate (not shown). The monomer and dimer were eluted at low ionic strength (0.048 and 0.075 *M*, respectively) from entrapped cationic vesicle-Sepharose 6B. As expected, the elution of the monomer and dimer on DEAE-Sepharose 6B required a higher ionic strength (0.213 and 0.237 *M*, respectively). The fact that the binding strength of BSA monomer and dimer was much lower on the cationic vesicle-gel than on the DEAE gel is due to the two-dimensional interactions between protein molecules and the bilayer surface of entrapped vesicles, and to the relatively low charge density of the stearylamine cations on the surface. The average distance between the stearylamine molecules can be estimated as 18 Å.

DISCUSSION

The results indicate that the adsorption of proteins on the surfaces of charged entrapped vesicles is dependent on the vesicle charge density and on the protein size in addition to charge. The protein size (and shape) affects the contact area with the vesicle surface. Protein desorption from the vesicle surfaces was achieved below 0.1 *M* ionic strength. The electrostatic interactions between the charged vesicles and proteins were thus relatively weak, in agreement with results by Maretzki *et al.*¹¹ concerning the binding of proteins to membrane surfaces.

We have found that 30% of the outer surface of the entrapped cationic vesicle became covered by ferritin molecules. Ferritin is composed of several subunits with a total net negative charge of at least -130 at pH 7 (estimated from the amino acid composition). Owing to the strong electrostatic repulsion between adjacent ferritin molecules and the relative low ligand density of the stearylamine (20%) on the vesicle surfaces, close packing of the ferritin is impossible.

Citraconylation increases the number of negative charges present on the proteins at neutral pH^{12,13}. However, much smaller amounts of citraconylated myoglobin (CMG, Table II) were bound than of ferritin (Table I) on the entrapped cationic vesicles. The vesicle bilayers contained approximately one stearylamine molecule per 320 Å², which corresponds to an average distance between the cations of 18 Å [the distance between the anions of the Mono S ion exchanger is 2.3–2.5 Å (F. Regnier, personal communication)]. About four stearylamine molecules may come into contact with one myoglobin molecule, whereas approximately twice as many stearylamine molecules might interact with one ferritin molecule. For CMG the binding will therefore be less efficient than for ferritin, in agreement with our results. It is possible to obtain a more efficient binding for small proteins by use of a high ligand density of the charge groups on the vesicle surface.

Insertion of haeme groups into the vesicle bilayers on the interaction of haemoglobin with phosphatidylserine vesicles has been reported by Shviro *et al.*¹⁴. We observed a similar phenomenon on chromatography of CMG on both entrapped cationic and neutral lipid vesicles (Table II). The released haeme groups became incorporated into the lipid bilayer of the entrapped vesicles and were therefore separated from the non-bound protein. This is an experimental example of the non-specific interaction of biomolecules with lipid membranes on chromatography, as mentioned by Pidgeon and Venkataram¹.

Quantitative binding studies may be done with large, flat lipid bilayer surfaces on planar supports, as in the elegant procedures described by McConnell *et al.*¹⁵ and Tamm¹⁶. Our results confirm that the surfaces of vesicle entrapped in agarose gel beads are largely accessible to macromolecules. Therefore, entrapped vesicles can also be used for lipid bilayer–macromolecule interaction studies.

The regular two-dimensional array of charged groups on the vesicle surface and the low binding strength between proteins and the vesicle surfaces may give a high resolution with low salt gradient elution. Antibodies and other cell-specific proteins can be immobilized on the entrapped vesicle surfaces^{17,18} for affinity chromatography.

Unfortunately, there were small losses of the entrapped vesicles of *ca.* 1–15% (data from test under Results and from Fig. 1A) on the chromatography of proteins under the different experimental conditions. Obviously, this decreased the column capacity for protein binding (see Fig. 1B). It was found that protein elution with a low pH (4.0) or with a gradient of low final ionic strength decreased the loss of the entrapped vesicles. In addition, a decrease in sample load may be required as the protein binding and release also affect the leakage (see Results). Polymerized vesicles prepared by covalently cross-linking the individual phospholipid molecules¹⁹ enhance their resistance to osmotic shock²⁰, to ethanol and to sodium dodecyl sulphate²¹. Therefore, by use of such polymerized vesicles entrapped in gel beads their stability on protein chromatography may be improved.

ACKNOWLEDGEMENTS

We thank Eva Greijer for valuable assistance and Lars Andersson for comments on the manuscript. We are grateful for financial support from the Swedish Natural Science Research Council, the O. E. and Edla Johansson Science Foundation and the Swedish National Board for Technical Development (Grant No. 89-519 P).

REFERENCES

- 1 C. Pidgeon and U. V. Venkataram, *Anal. Biochem.*, 176 (1989) 36.
- 2 M. Wallstén, Q. Yang and P. Lundahl, *Biochim. Biophys. Acta*, 982 (1989) 47.
- 3 D. Lichtenberg, *Methods Biol. Anal.*, 33 (1987) 337.
- 4 M. Sandberg, P. Lundahl, E. Greijer and M. Belew, *Biochim. Biophys. Acta*, 924 (1987) 185.
- 5 G. R. Bartlett, *J. Biol. Chem.*, 234 (1959) 466.
- 6 P. Lundahl, *Biochim. Biophys. Acta*, 379 (1975) 304.
- 7 L. Andersson and P. Lundahl, *J. Biol. Chem.*, 263 (1988) 11414.
- 8 I. Urushizaki, Y. Niitsu, K. Ishitani, M. Matsuda and M. Fukuda, *Biochim. Biophys. Acta*, 243 (1971) 187.
- 9 C. Huang and J. T. Mason, *Proc. Natl. Acad. Sci. U.S.A.*, 75 (1978) 308.
- 10 O. Yang and P. Lundahl, *J. Chromatogr.*, in press.
- 11 D. Maretzki, B. Reimann and S. M. Rapoport, *Trends Biochem. Sci.*, 14 (1989) 93.
- 12 M. Z. Atassi and A. F. S. A. Habeeb, *Methods Enzymol.*, 25 (1972) 546.
- 13 R. P. Singhal and M. Z. Atassi, *Biochemistry*, 10 (1971) 1756.
- 14 Y. Shviro, I. Zilber and N. Shaklai, *Biochim. Biophys. Acta*, 687 (1982) 63.
- 15 H. M. McConnell, T. H. Watts, R. M. Weis and A. A. Brian, *Biochim. Biophys. Acta*, 864 (1986) 95.
- 16 L. K. Tamm, *Biochemistry*, 27 (1988) 1450.
- 17 V. Weissig, J. Lasch, A. L. Klibanov and V. P. Torchilin, *FEBS Lett.*, 202 (1986) 86.
- 18 A. A. Bogdanov, Jr., A. L. Klibanov and V. P. Torchilin, *FEBS Lett.*, 231 (1988) 381.
- 19 D. S. Johnston and D. Chapman, in G. Gregoriadis (Editor), *Liposome Technology*, Vol. I, CRC Press, Boca Raton, FL, 1984, pp. 123-129.
- 20 H.-H. Hub, B. Hupfer, H. Koch and H. Ringsdorf, *Angew. Chem., Int. Ed. Engl.*, 19 (1980) 938.
- 21 B. Hupfer, H. Ringsdorf and H. Schupp, *Chem. Phys. Lipids*, 33 (1983) 355.

CHROMSYMP. 1807

Effect of polystyrene coating on pore, structural and chromatographic properties of silica packings

A. KURGANOV, O. KUZMENKO and V. A. DAVANKOV

Institute of Organo-Element Compounds, Academy of Sciences of the U.S.S.R., Moscow (U.S.S.R.)
and

B. ERAY, K. K. UNGER* and U. TRÜDINGER

Institut für Anorganische Chemie und Analytische Chemie, Johannes Gutenberg-Universität, D-6500 Mainz (F.R.G.)

SUMMARY

A series of mesoporous and macroporous silicas with a mean pore diameter (PD), between 6 and 200 nm were reacted with a copolymer of styrene and vinyl-methyldiethoxysilane. The mass load of coated silicas corresponded to the monolayer capacity of the polymer calculated on the basis of the molecular cross-sectional area, except for the two mesoporous silicas of PD = 6 and 7.5 nm. Depending on the pore size, changes occurred in the specific surface area, a_s , between the native and the coated product. A comparison of the specific pore volume, v_p , of silicas before and after polymer immobilization indicated a major loss of v_p for the two mesoporous silicas whereas this effect was much less pronounced for the macroporous silicas. Surprisingly, the two macroporous silicas of PD = 50 and 100 nm exhibited a decrease in the mean pore diameter after modification, which seems to be caused by the narrowing of the pore entrances owing to polymer immobilization. The change in d_p was shown by size-exclusion separations of polystyrenes on the native and coated silica. Tests of the packings in reversed-phase chromatography with amines as solutes showed that silanophilic effects on the coated silicas were absent. It was demonstrated that the immobilization did not change the performance of the silica columns in terms of plate height and plate number.

INTRODUCTION

To overcome the intrinsic limited pH stability of bonded silica packings in high-performance liquid chromatography (HPLC), attempts have been made to coat the surface of silicas with polymers. The aim is to form a thin and homogeneous layer of polymer with desired functionalities that provides maximum coverage of the surface of the native silica support, maintains the column performance and permits the retention to be controlled and the selectivity to be adjusted. The various routes in the

synthesis of HPLC stationary phases with polymeric coatings have recently been reviewed by Schomburg¹.

Polystyrene-coated silicas for reversed-phase HPLC were first introduced by Horváth and Lipsky² using a pellicular type of support. Caude and Rosset³ prepared a polystyrene-coated silica in a two-step procedure. First, the silica was reacted with vinyltriethoxysilane and the vinyl-bonded silica was then subjected to polymerization with styrene. The unbound polystyrene was removed by extraction and the product was converted into an ion exchanger by an appropriate reaction. Quivoron⁴ prepared coated silica supports using living polystyrene made by cationic polymerization. A drastic decrease in the specific surface area of the silica support compared with the parent material was observed when increasing amounts of polystyrene were employed. More recently, Suzuki *et al.*⁵ polymerized styrene on the silica surface by adsorbing chloromethylstyrene and divinylbenzene on the silica from a solution in N,N-dimethylformamide. The excess of monomers was removed and the dry product was subjected to polymerization in an autoclave. The polystyrene-coated silica showed a 20% decrease in specific surface area, a_s , compared with the starting material. This decrease in a_s is the same as observed on silanized silicas with long-chain *n*-alkylsilanes⁶. Kurganov *et al.*⁷ developed a procedure for coating silicas with a copolymer of styrene and vinylsilane, which was employed as a precursor to synthesize a chiral packing for the resolution of racemates by ligand-exchange chromatography. The packing exhibited improved hydrolytic stability compared with other ligand-exchange types of stationary phases, and this is assumed to be caused by a multi-point bonding of the copolymer to the silica surface.

The procedure advocated by Kurganov *et al.*⁷ was used here to prepare reversed-phase and size-exclusion packings for HPLC. The aim was to assess the pore structure and chromatographic properties of the product relative to the parent material. Silicas of different origin and pore sizes were employed.

EXPERIMENTAL

Chemicals and materials

Zorbax PSM 60, PSM 500 and PSM 1000, all of particle diameter d_p 5 μm , were a gift from DuPont (Wilmington, DE, U.S.A.). Silasorb Si 300 and Si 600, d_p 5 μm , were obtained from Lachema (Prague, Czechoslovakia).

LiChrosorb Si 100, d_p 5 μm , and LiChrospher Si 500, d_p 10 μm , were purchased from Merck (Darmstadt, F.R.G.). A spherical silica of d_p 10 μm and a nominal pore diameter of PD = 200 nm was a gift from Merck.

Polymer standards of molecular weight 1400 (1.06), 4900 (1.04), 10 000 (1.05), 16 600 (1.02), 29 500 (1.03), 110 000 (1.20), 220 000 (1.05), 310 000 (1.04), 710 000 (1.05) and 1 250 000 (1.14) were supplied by Polymer Standards Service (Mainz, F.R.G.); the values in parantheses are the polydispersity, $u = M_w/M_n$, were M_w is the weight-average and M_n the number-average molecular weight.

All solvents for the syntheses were of analytical-reagent grade. HPLC-grade solvents for chromatographic measurements were obtained from Merck.

Preparation of coated silica supports

A copolymer with a molecular weight of 10 000 with a silicon content of 2.0%

(w/w) was synthesized by polymerization of styrene and vinylmethyldiethoxysilane as described elsewhere⁷. The ratio of styrene to silane units in the copolymer was calculated to be 12:1.

All silicas were coated by the following procedure described for Zorbax PSM 60. The amount of copolymer used was adjusted to the specific surface area of native silica.

Zorbax PSM 60 (45.3 g) was weighed into a three-necked flask equipped with a stirrer and Dean–Stark separator, then 200 ml of toluene were added. The suspension was heated under reflux for 1–2 h until no water was liberated from the silica, then a solution of 4.0 g of copolymer in 50 ml of toluene was added and the suspension was agitated and heated under reflux for 4 h. The hot suspension was filtered through a porous glass frit of porosity $< 2 \mu\text{m}$ and the remaining silica was washed twice with 100 ml of hot toluene. End-capping of the product was performed by heating the slurry of the coated silica with 6.0 ml of hexamethyldisilazane dissolved in 150 ml of toluene under reflux for 2 h. The silica was then filtered through a porous glass frit of porosity

TABLE I

CHARACTERISTIC PARAMETERS OF UNCOATED AND COATED SILICAS

Abbreviations: a_s = specific surface area of the native silica according to BET, using $a = 0.162 \text{ nm}^2$ per molecule; a_s^* = specific surface area of the native silica according to BET, using the weight-corrected a_s of the native silica; $a_s^{0.162}$ = specific surface area of the native silica according to BET, using $a_m = 0.162 \text{ nm}^2$ per molecule; $a_s^{0.20}$ = specific surface area of the native silica according to BET, using $a_s = 0.20 \text{ nm}^2$ per molecule; PD = nominal pore diameter of the native silica; α_{exp} = surface concentration of monomer units calculated from the carbon content.

Silica	a_s (m^2/g)	a_s^* (m^2/g)	$a_s^{0.162}$ (m^2/g)	$a_s^{0.20}$ (m^2/g)	PD (nm)	Carbon content (% w/w)		α_{exp} ($\mu\text{mol}/\text{m}^2$)
						Before end-capping	After end-capping	
Zorbax PSM 60								
Uncoated	384	—	—	—	6	—	—	—
Coated	—	334	245	301	—	10.9	13.4	3.6
Zorbax PSM 500								
Uncoated	29	—	—	—	50	—	—	—
Coated	—	28	26	32	—	2.4	2.4	9.3
Zorbax PSM 1000								
Uncoated	17	—	—	—	100	—	—	—
Coated	—	16.8	17	21	—	1.3	1.4	8.4
LiChrosorb Si 100								
Uncoated	245	—	—	—	10	—	—	—
Coated	—	209	229	282	—	14.5	14.6	7.4
LiChrospher Si 500								
Uncoated	90	—	—	—	50	—	—	—
Coated	—	81	80	98	—	10.0	10.5	12.3
Silasorb Si 600								
Uncoated	520	—	—	—	7.5	—	—	—
Coated	—	434	400	492	—	14.0	16.5	3.5
Silasorb Si 300								
Uncoated	240	—	—	—	10	—	—	—
Coated	—	184	220	271	—	15.0	16.1	8.2
Silica, PD = 200 nm								
Uncoated	17	—	—	—	200	—	—	—
Coated	—	17	17	21	—	2.7	2.7	15.5

< 2 μm , washed with hot toluene, ethanol and water and dried overnight at 100°C. The properties of the uncoated and the coated silicas are given in Table I.

Chromatographic experiments

The coated silicas were slurry-packed into columns of 250 \times 4.6 mm I.D. or 125 \times 4.6 mm I.D. (Bischoff Analysentechnik, Leonberg, F.R.G.) using a 5% (w/w) suspension of cyclohexanol-toluene (50:50, v/v). Ethanol was employed as a displacing solvent. The native silica was slurry-packed with ethanol from a 5% (w/w) suspension.

Chromatographic experiments were performed on a system consisting of a pump (Model 2200; Bischoff), UV detector with a fixed wavelength of 254 nm (Model UV III, Latek, Heidelberg, F.R.G.) or a variable-wavelength UV detector (Model BT 3030, Biotronic, Maintal, F.R.G.) and a potentiometric recorder (Model RE 541, Metrawatt, F.R.G.; or Model 2210, Pharmacia-LKB Biotechnology, Uppsala, Sweden). The column temperature was ambient. The injection volume was 10 μl .

Nitrogen sorption measurements

Nitrogen adsorption-desorption isotherms at 77 K were determined gravimetrically, using a laboratory-made device, equipped with a Sartorius vacuum microbalance (Model 4433, Sartorius-Werke, Göttingen, F.R.G.). Nitrogen was of 99.99% purity (Linde, Düsseldorf, F.R.G.). The specific surface area was calculated from nitrogen adsorption using the two-parameter BET equation⁸. The pore-size distribution was calculated from the desorption isotherm using the Kelvin equation and the method of Pierce⁸.

Mercury porosimetry

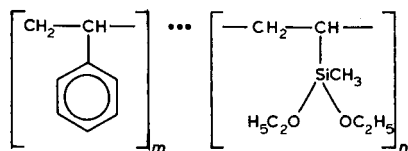
Mercury porosimetry was performed using a Carlo Erba (Milan, Italy) porosimeter with a maximum pressure of about 2500 bar. The pore-size distribution was calculated from the experimental data using the Washburn equation⁹.

All mathematical calculations of the experimental data and their presentation in graphical form were performed by using the program EQPLOT developed in this laboratory on an IBM-compatible computer.

RESULTS AND DISCUSSION

Polymer coating as a function of the mean pore diameter of the silica

The starting copolymer of $M_w = 10\,000$ has the following structure:



In the immobilization procedure, the ethoxy groups of the copolymer react with the hydroxyl groups of the silica and ethanol is evolved. In the optimum case the copolymer unit is linked by two siloxane groups to the surface. From the mean

molecular weight of the polymer using the equation¹⁰ $r = 0.0123 M^{0.588}$, the radius of a random coil polymer chain is calculated to be 1.4 nm. Using this value, a surface concentration equivalent to a monolayer of $x_m = 0.07 \mu\text{mol}/\text{m}^2$ is derived.

The mass load derived from the calculated surface concentration can now be compared with the actual mass load based on the carbon content. The carbon content represents 88% of the total mass of the polymer. For the coated macroporous Zorbax PSM 1000, the mass load equivalent to the surface concentration of a monolayer is calculated to be $(0.07 \cdot 10^{-6} \text{ mol}/\text{m}^2) \cdot (10\,000 \text{ g}/\text{mol}) \cdot (17 \text{ m}^2/\text{g}) = 11.9 \text{ mg}/\text{g}$. The experimental value is $(10.9 \text{ mg}/\text{g}) \cdot 100/88 = 12.3 \text{ mg}/\text{g}$. Hence the calculated and experimental values are in fairly good agreement assuming a dense monolayer. The same is valid for the coated Zorbax PSM 500 (calculated value 20.3 mg/g, found 27.0 mg/g).

The surface concentration of the monolayer can also be related to the bound monomer unit of copolymer and then becomes $7 \mu\text{mol}/\text{m}^2$. The experimental values for Zorbax PSM 1000 and 500 are of the same order, namely 8.4 and 9.3 $\mu\text{mol}/\text{m}^2$, respectively. The values calculated for LiChrospher Si 500 and the spherical silica of PD = 200 nm are higher than $7 \mu\text{mol}/\text{m}^2$ (12.3 and 15.5 $\mu\text{mol}/\text{m}^2$, respectively).

When the mean pore diameter of the starting silica falls into the mesopore range ($2 < \text{PD} < 50 \text{ nm}$), the polymer will have limited access to the pores in the immobilization procedure and therefore the experimental mass load should be lower than the calculated value based on a freely accessible surface. This is clearly seen with Zorbax PSM 60 and Silasorb Si 600 with mean pore diameters of 6 and 7.5 nm, respectively, where the values are calculated 238 and experimental 109 mg/g for Zorbax PSM 60 and calculated 364 and experimental 140 mg/g for Silasorb Si 600. In accord with this observation, the surface concentration per copolymer unit is lowest for these two types of all the silicas studied: Zorbax PSM 60 3.6 $\mu\text{mol}/\text{m}^2$ and Silasorb Si 600 3.5 $\mu\text{mol}/\text{m}^2$.

Further evidence that the mesopores of 6–7 nm do not remain fully accessible to the polymer is that the end-capping of the coated Zorbax PSM 60 and Silasorb Si 600 increases the carbon content by about 2–3% (w/w), whereas end-capping of the other coated silicas scarcely changes the carbon content. It is conceivable that the small hexamethyldisilazane is capable of reacting with the hydroxyl groups that were left unreacted in the polymer immobilization procedure.

Effect of coating on the specific surface area (a_s)

Changes in a_s between the native and the coated silicas can be detected by comparing the corresponding a_s values before and after coating. There are two ways to determine the specific surface area of the coated silicas. First, the actual value of a_s is measured by nitrogen adsorption applying the BET method⁸. The monolayer capacity of adsorbed nitrogen in mol/g is then obtained, and is multiplied by Avogadro's number and the molecular cross-sectional area of adsorbed nitrogen, a_m . Usually a_m is taken to be 0.162 nm² per molecule. Amat and Kováts¹¹ have pointed out, however, that silanized surfaces behave as low-energy surface systems with a lower packing density of adsorbed nitrogen. Hence the molecular cross-sectional area of nitrogen becomes 0.20 nm² per molecule compared with 0.162 nm² per molecule for hydroxylated surfaces. Treating the polymer-coated silicas as low-energy systems, their a_s values have to be multiplied by a factor of $0.20/0.162 = 1.23$. Second, neglecting the changes in the chemical composition of the surface, the a_s of a given

coated silica can be evaluated from value for the native silica by applying a correction for the weight increase, ΔG , caused by the coating⁶. The corrected specific surface area, a_s^* , of the native silica is then

$$a_s^* = a_s (1 - \Delta G)$$

The different values of a_s , viz., a_s of the native silica, using $a_m = 0.162 \text{ nm}^2$, a_s^* of the coated silica, using the weight-corrected a_s of the native silica, $a_s^{0.162}$ of the coated silica, using $a_m = 0.162 \text{ nm}^2$ and $a_s^{0.20}$ of the coated silica, using $a_m = 0.20 \text{ nm}^2$, are given in Table I. Several observations can be made. A decrease in the specific surface area of the coated silica takes place compared with that of the native material for Zorbax PSM 60 and Silasorb Si 600, taking a_s^* , $a_s^{0.162}$ and $a_s^{0.20}$ into consideration, and in these instances pore blockage seems highly probable. The simple weight correction of the native silica provides no conclusive means of judging the effect of coating on a_s : the a_s values are lower than, equal to or higher than the a_s values of the coated silicas either using $a_m = 0.162 \text{ nm}^2$ or $a_m = 0.20 \text{ nm}^2$; the a_s values with $a_m = 0.20 \text{ nm}^2$ of the coated silicas are higher than those of the native silica, using $a_m = 0.162 \text{ nm}^2$ for PSM 500, PSM 1000, LiChrosorb Si 100, LiChrospher Si 500, Silasorb Si 300 and silica, PD = 200 nm. This increase is difficult to explain, however; it might be that the polymer coating itself develops some porosity with micropores which additionally contribute to the internal surface area.

Effect of coating on the specific pore volume (SPV) and the pore-size distribution (PSD)

In order to assess the effect of polymer coating on the SPV and PSD of the silicas, the corresponding values have to be compared before and after the polymer immobilization. Significant changes are expected for the mesoporous silicas whereas the macroporous silicas should maintain their native pore structure. For the

TABLE II

SPECIFIC PORE VOLUME (SPV) OF NATIVE AND POLYSTYRENE-COATED SILICAS

SPV(G) = specific pore volume according to the Gurvitch rule estimated from the saturation uptake of adsorbed nitrogen⁸. SPV(Hg) = specific pore volume from mercury porosimetry measurements estimated from the volume of intruded mercury at maximum pressure⁸.

Silica	SPV (ml/g)
Zorbax PSM 60	
Uncoated	0.70 (G)
Coated	0.41 (G)
Zorbax PSM 500	
Uncoated	0.31 (Hg)
Coated	0.26 (Hg)
Zorbax PSM 1000	
Uncoated	0.24 (Hg)
Coated	0.23 (Hg)
Silica, PD = 200 nm	
Uncoated	0.36 (Hg)
Coated	0.36 (Hg)

mesoporous Zorbax PSM 60 the SPV was calculated from the saturation uptake of adsorbed nitrogen, n_s , according to the Gurvitch rule assuming a liquid adsorbate⁸. The SPV of the macroporous silicas was calculated from mercury porosimetry measurements as the corrected volume of intruded mercury at maximum pressure. The results are given in Table II. As expected, the SPV of Zorbax PSM 60 as an example is reduced by about 40% after immobilization. The SPV of Zorbax PSM 500 and PSM 1000 is diminished, whereas that of the silica, PD = 200 nm, remains unaffected.

The average thickness of the polymer coating calculated from the density of the polymer, the mass load and the specific surface area of the silica is about 2 nm. Hence it is conceivable that the mean pore diameter of the Zorbax PSM 60 is drastically reduced by the coating and correspondingly the SPV changes.

The PSDs of the macroporous silicas were determined by two independent methods: (i) mercury porosimetry using the Washburn equation⁹ and (ii) size-exclusion chromatography measuring the elution volumes of standard polystyrenes and using the calculation procedure advocated by Knox and co-workers^{10,12}.

Fig. 1 shows as an example the cumulative pore size distribution curve assessed by mercury porosimetry (MP) and by size-exclusion chromatography (SEC) of uncoated and coated Zorbax PSM 1000. The coating slightly diminishes the PSD derived from MP measurements. The pore-size reduction is seen to be more dramatic on comparing the curves from SEC measurements: the mean pore diameter at 50% of the cumulative pore volume is about 80 nm before and to 40 nm after the immobilization of the polymer. The discrepancy in the PSD between the two methods is not surprising because they are based on different assumptions and the samples are measured under widely different conditions. In MP, mercury is forced by pressure into the pores of the dry powder. In SEC, the particles are filled with benzene as solvent and the polymer coating is solvated and might swell. This extension in volume might lead to pore blockage and limit the access of polystyrene molecules in SEC experiments.

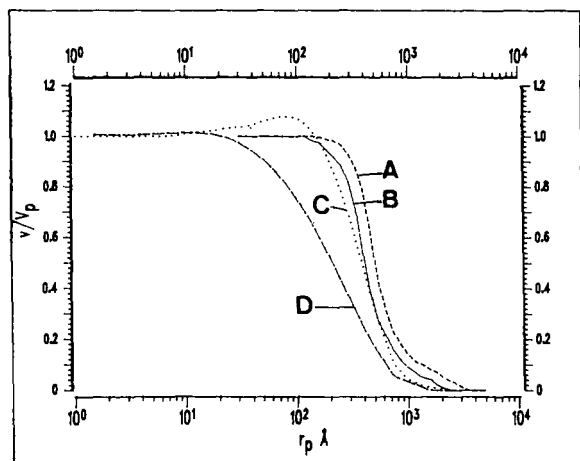


Fig. 1. Cumulative pore-size distribution of the uncoated and coated Zorbax PSM 1000. Mercury porosimetry data using a contact angle of mercury of 140° and a surface tension of 480 mN/m^2 : A = before; B = after polymer immobilization. Data from SEC using the method of Knox and co-workers; C = before; D = after polymer immobilization.

Provided that the PSD curves from SEC measurements reflect the real chromatographic situation, the fractionation range of the coated Zorbax PSM 1000 should be shifted to the low-molecular-weight range compared with the native packing. This was indeed observed (Fig. 2). The SEC results for the polystyrene standard mixture on uncoated and coated Zorbax PSM 1000 indicate that a higher resolution in the low-molecular-weight range takes place for the coated packing. A similar effect resulted for uncoated and coated Zorbax PSM 500.

Effect of coating on chromatographic properties

The performance of the polymer-coated silicas was tested by measuring the plate height of retained and unretained solutes as a function of the linear flow-rate of the eluent in the reversed-phase (RP) mode. By plotting the data as the reduced plate height h against the reduced linear velocity v , the constants A , B and C of the Knox equation were calculated by curve fitting using the equation¹³

$$h = Av^{1/3} + B/v + Cv$$

The values derived for the dimensionless constants were $A \approx 1$, $B \approx 2$ and $C \leq 0.1$. This indicates that the columns were well packed ($A \approx 1$) and the mass transfer

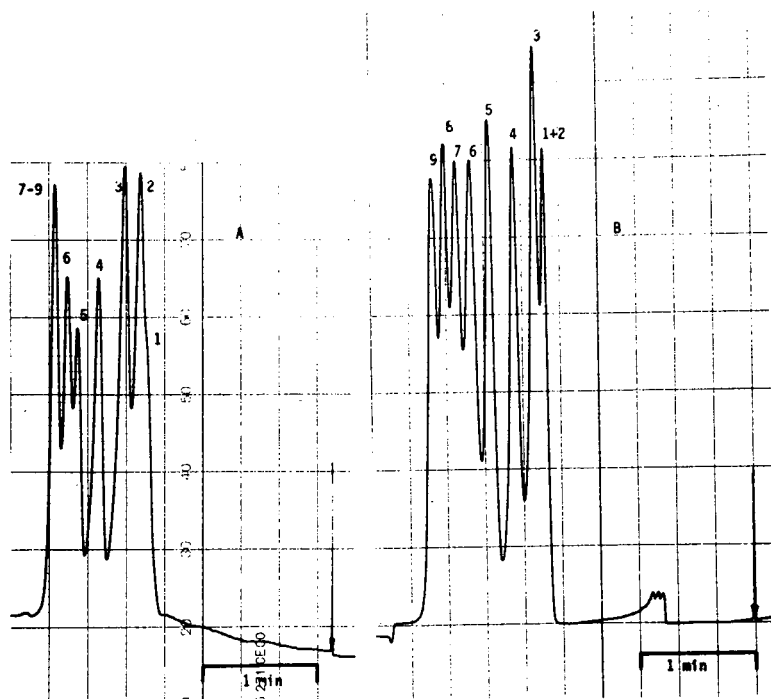


Fig. 2. Separation of a mixture of polystyrene (PS) standards on a column packed with (A) uncoated Zorbax PSM 1000 and (B) coated Zorbax PSM 1000. Column, 250 × 4.6 mm I.D.; mobile phase, tetrahydrofuran; flow-rate, 0.5 ml/min; UV detection (280 nm). Solutes: 1 = PS, M_w 1250 kDa; 2 = PS, 700 kDa; 3 = PS, 310 kDa; 4 = PS, 110 kDa; 5 = PS, 29.5 kDa; 6 = PS, 10 kDa; 7 = PS, 4050 kDa; 8 = PS, 1400 kDa; 9 = benzene.

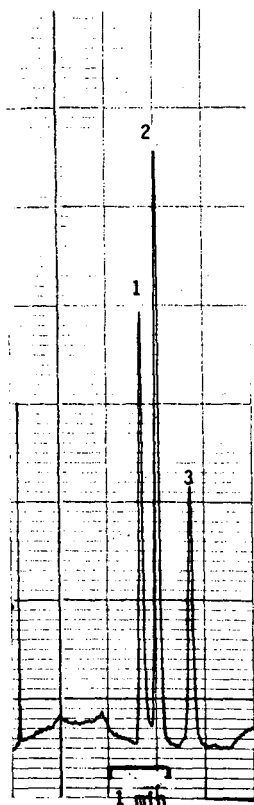


Fig. 3. Separation of a mixture of amines on a coated Zorbax PSM 500 column. Column, 250 × 4 mm I.D.; mobile phase, water-acetonitrile (40:60, v/v); flow-rate, 0.5 ml/min; UV detection (280 nm). Solutes: 1 = 2,6-dimethylpyridine; 2 = 1-naphthylamine; 3 = benzylamine.

between the mobile and the stationary phases is of the same order as in conventional RP columns ($C \leq 0.1$), *i.e.*, the polymer coating did not impair the kinetic performance of the silicas in terms of plate height and plate number¹³.

The completeness of coverage of the silica by a polymer can be checked by monitoring the retention and peak width of basic compounds under reversed-phase conditions. The chromatograms for 2,6-dimethylpyridine, 1-naphthylamine and benzylamine on the column packed with coated Zorbax PSM 500 (Fig. 3) show totally symmetrical peaks, indicating no effect of residual silanols on retention. The excellent pH stability of the coated packings under acidic conditions was demonstrated by separating peptides and proteins during several months of continuous operation of the same column under gradient elution conditions at pH 1–2.

The highly dense coverage of the surface of silica together with the multi-point attachment of the polymer also promises a high temperature stability. This favourable property can be utilized for the rapid separation of peptides at elevated temperatures. Such studies are in progress.

REFERENCES

- 1 G. Schomburg, *LC · GC, Mag. Liq. Gas Chromatogr.*, 6 (1988) 35.
- 2 Cs. Horváth and S. R. Lipsky, *Nature (London)*, 211 (1966) 748.
- 3 M. Caude and R. Rosset, *J. Chromatogr. Sci.*, 15 (1977) 540.
- 4 C. Quivoron, *J. Liq. Chromatogr.*, 1 (1978) 479.
- 5 T. Suzuki, O. Itabashi, T. Goto, T. Yokoyama and T. Kimura, *Bull. Chem. Soc. Jpn.*, 60 (1987) 2839.
- 6 K. K. Unger, N. Becker and P. Roumeliotis, *J. Chromatogr.*, 125 (1979) 115.
- 7 A. Kurganov, A. Tevlin and V. Davankov, *J. Chromatogr.*, 261 (1983) 479.
- 8 S. J. Gregg and K. S. W. Sing, *Adsorption, Surface Area and Porosity*, Academic Press, London, 1982.
- 9 E. W. Washburn, *Proc. Natl. Acad. Sci. U.S.A.*, 7 (1921) 115.
- 10 J. H. Knox and H. Scott, *J. Chromatogr.*, 316 (1984) 311.
- 11 D. Amati and E. Kováts, *Langmuir*, 3 (1987) 687.
- 12 J. H. Knox and H. J. Ritchie, *J. Chromatogr.*, 387 (1987) 66.
- 13 J. H. Knox, *High Performance Liquid Chromatography*, Edinburgh University Press, Edinburgh, 1978, pp. 10–12.

Indirect fluorometric detection in open-tubular capillary column chromatography

WILLIAM D. PFEFFER and EDWARD S. YEUNG*

Ames Laboratory-USDOE and Department of Chemistry, Iowa State University, Ames, IA 50011 (U.S.A.)

SUMMARY

Reversed-phase open-tubular capillary (OTC) columns are prepared by cross-linking vinyl silicone gums on the inside of fused-silica capillaries. These columns are then provided with a low capacity of anion-exchange sites by dynamic modification with cetyltrimethylammonium bromide. Following anion-exchange chromatography, common anions are detected by indirect fluorescence detection, using micromolar salicylate as the eluent and the visualization agent, and a UV laser as the excitation source. Unmodified reversed-phase OTC columns are used for the separation of various alcohols. These alcohols are detected by indirect fluorescence detection, using 2,7-dichlorofluorescein as the fluorescent reagent and a visible laser as the excitation source. The small dimensions (13–15 μm I.D.) of the OTC columns and good stability of the fluorescence background (dynamic reserve $\geq 10^3$) allow femtogram (attomole) amounts of both types of analytes to be detected. The detectable concentrations are in the 30-nM range.

INTRODUCTION

The method of indirect detection in liquid chromatography has received a considerable amount of attention in the past few years^{1–3}. Essentially, a detectable species is present in the eluent and produces a constant background signal at the detector. When an analyte is eluted from the column, it changes the concentration of that species at the detector and with it the background signal; hence, the analyte is detected indirectly. Schemes for the indirect detection of electrolytes⁴, non-electrolytes⁵ or both⁶ have been devised and used with considerable success. A variety of detectors have been employed, including fluorometric^{7–10}, polarimetric¹¹ and electrochemical¹², but the majority of the work has been done with photometric detectors^{4–6, 13–18}.

Another topic receiving considerable interest in chromatography is the use of microcolumns^{19,20}. The advantages of using microcolumns are their efficiency for small samples, reduced analyte dilution, reduced flow-rate and high separation efficiency. Of the four types of microcolumns being used — small-bore packed, packed capillary, semi-packed capillary and open-tubular capillary (OTC) — OTC columns

have the attraction of being able to produce high separation efficiencies in a reasonable time with superior limits of detection (LOD)²¹. Theory suggests that the internal diameter of OTC columns needs to approach that of column packing material (1–10 μm) in order to operate at maximum efficiency^{22,23}. Although once difficult to prepare, procedures in which silicone gums are used have somewhat simplified OTC column preparation^{24,25}.

The coupling of microcolumns with indirect detectors allows sensitive detection of those analytes which yield poor absorption, fluorescence, or electrochemical response. Analytes detected indirectly in microcolumn separations include anions^{7,10,13}, alcohols^{9,14}, hydrocarbons¹⁵, and ethylene glycol oligomers¹⁶. In the examples cited, the photometric detector is the most popular. Because a large, stable background signal is essential for any indirect detection method, restrictions on path length (b) and molar absorptivity (ϵ) and concentration (C_m) of the background reagent must be adhered to. For example, since absorption detectors typically have noise around 0.0001 a.u.f.s., maintaining a stability of only 1 part in 1000, the background absorbance must be at least 0.1 a.u.f.s. For columns with diameters of 10–100 μm , this fact imposes even stricter constraints on the ϵ and C_m of the background reagent. Indirect fluorometric detection should not suffer from these limitations to the same degree indirect photometric detection does. When excitation is provided by a laser, reduced b , ϵ , or C_m can largely be compensated for by increasing the power of the incident radiation to yield ample photons at the detector such that the system remains above the shot-noise limit, *i.e.*, background stability is independent of ϵ , b and C_m .

In this work, polymer-coated OTC columns of 13–15 μm I.D. were used for the separation of electrolytes and non-electrolytes. When the polymer surface is treated with a quaternary ammonium salt, the capillary effectively functions as an ion-exchange column. The untreated polymer surface allows the capillary to function as a reversed-phase column. Indirect fluorometric detection allows extremely low levels of both types of analytes to be detected.

EXPERIMENTAL

Reagents

Electrolytes. Sodium salicylate, sodium acetate, and high-performance liquid chromatography (HPLC)-grade methanol were supplied by Fisher Scientific (Fairlawn, NJ, U.S.A.). Sodium nitrite was supplied by Mallinckrodt (St. Louis, MO, U.S.A.). The eluent was prepared by dissolving sodium salicylate in water and degassing the solution in an ultrasonic bath under vacuum. Samples were dissolved in the eluent.

Non-electrolytes. The alkanols were supplied by Aldrich (Milwaukee, WI, U.S.A.), Sigma (St. Louis, MO, U.S.A.), or Eastman Kodak (Rochester, NY, U.S.A.). Solutions containing the fluorescent reagent, 2,7-dichlorofluorescein (2,7-DCF, Eastman) were prepared from a 1-mM acetic acid buffer in 0–10% acetonitrile (HPLC grade, Eastman). The pH of the final solution was adjusted to a value between 3.0 and 5.0. The eluent was degassed by sparging with nitrogen gas. Alkanol samples were prepared by mixing them with aqueous acetonitrile of the same concentration as the eluent.

In both the electrolyte and non-electrolyte experiments, the water used was purified in a Barnstead Nanopure II system (Barnstead, Division of Sybron, Boston, MA, U.S.A.). All chemicals were of reagent grade and used as supplied unless specified.

Column preparation

The columns were prepared by a procedure adapted from Farbrot *et al.*²⁴. A fused-silica capillary column (Polymicro Technologies, Phoenix, AZ, U.S.A.; 50–120 cm × 150 μm O.D. and 13–15 μm I.D.) was purged with helium for 30 min. The column was then filled with a solution of 1–2% (w/v) PS-255 or PS-265 (Petrarch Systems, Bristol, PA, U.S.A.) in pentane, in which the cross-linking agent dicumyl peroxide (Pfaltz and Bauer, Waterbury, CT, U.S.A.) was present at an amount of 1% (w/w) of the polymer. Following removal of the column from the filling device, the ends were cut off and left open. The column was then immersed in a water bath with its ends exposed to air or placed in a gas chromatography (GC) oven and the solvent was evaporated at temperatures of either 35 or 40°C. After evaporation was complete, the column was again flushed with helium for 30 min. The ends were sealed with sodium silicate, and cross-linking was carried out by using a temperature program of 15°C/min to 175°C, then 175°C for 3 min. After cross-linking was complete, the polyimide coating was burned off at one end of the column to facilitate on-column detection.

Chromatographic system

The chromatographic system employed in this work is identical to that described in ref. 10, with the exception that a microsyringe pump (ISCO, Lincoln, NE, U.S.A.; Model μLC-500) was used in the constant-flow mode to propel the eluent through the column. A split-injection ratio of 200 is used. The injector (Rheodyne, Cotati, CA, U.S.A.; model 7520) rotor volume was 0.2 μl for the electrolyte experiments and 0.5 μl in the non-electrolyte experiments. When in use, the ion-exchange column was kept in a water bath held at ambient temperature.

Dynamic modification of the column

The procedure used for dynamic modification of the capillary column is similar to that described earlier^{7,10,26}. Here, the column was equilibrated with a solution of 30 mM cetyltrimethylammonium bromide (Aldrich) in 95% aqueous methanol. Cetyltrimethylammonium bromide could be removed by washing the column with 50% aqueous methanol, thereby returning it to a reversed-phase column.

Detector

In the electrolyte experiments, 330-nm radiation from an argon-ion laser (Spectra-Physics, Mountain View, CA, U.S.A.; Model 2035) passes through a laser intensity stabilizer (Cambridge Research and Instrumentation, Cambridge, MA, U.S.A.; Model LS100, UV optics installed), where it is stabilized to a power of *ca.* 4 mW. Upon exiting the stabilizer, the radiation is focused onto the column via a 1-cm focal length fused-silica lens. The column normal is at Brewster's angle to the incident radiation. Collection of fluorescence is perpendicular to the plane of incidence and is effected by a 20 × microscope objective. The illuminated region is magnified by

approximately $60 \times$ and forms an image at a spatial filter. Fluorescence from the internal bore of the column passes through the spatial filter, through a cut-off filter (Schott Glass, Duryea, PA, U.S.A.; UV-360) and falls onto the cathode of a photomultiplier tube (Hamamatsu, Bridgewater, NJ, U.S.A.; R928).

The system used for the indirect detection of non-electrolytes is essentially the same as above but with the following exceptions: excitation is provided by the 488-nm line of an argon-ion laser (Laser Ionics, Orlando, FL, U.S.A.; Model 554A). After passing through the stabilizer, the radiation is split, and *ca.* 2 mW is focused onto the capillary by a 0.9-cm focal-length lens; background radiation is rejected via an OG-515 cut-off filter (Schott).

Data were recorded on a strip chart recorder (Houston Instruments, Austin, TX, U.S.A.; Model B5117-5I) or subjected to analog-to-digital conversion (Data Translation, Marlborough, MA, U.S.A.; Model DT2827, 2 Hz) and stored in a personal computer (IBM PC-AT). Data recorded on the strip chart could also be digitized by a video camera and a frame grabber system (Data Translation, Auxiliary Frame Processor; Model DT2858). Digitized data were later smoothed by using a moving-window average.

RESULTS AND DISCUSSION

Electrolytes

The limiting concentration (C_{lim}) of an analyte that can be detected by indirect fluorometry of photometry is generally described by

$$C_{lim} = C_m/DR \quad (1)$$

where C_m is the concentration of the background reagent, D is the dynamic reserve (ratio of the background signal to the noise on the background), and R is the displacement ratio (moles of reagent displaced by moles of analyte). Indirect detection in ion chromatography is possible because as the analyte is eluted, it displaces an equivalent amount of the reagent ion. In this case, R is generally regarded as unity as long as the analyte and reagent ions are of equal valence.

To achieve elution and detection of low concentrations of anions in single-column ion-exchange chromatography, anion-exchange columns of low capacity are required. One way to produce a low-capacity anion-exchange column effectively is by the method of dynamic modification^{7,10,26}. Column capacity can be varied by changing modifier concentration or organic content of the modifying solution. Previously, Takeuchi and Yeung⁷ modified microbore silica gel columns with quaternary ammonium salts to separate several common inorganic anions with sub-nanogram LOD, using a laser-based double-beam indirect fluorometric detector. Later, by using a similar modification and detection scheme, a reversed-phase OTC column separated anions with picogram LOD¹⁰.

The double-beam design in indirect fluorometric detection has been shown to maintain a dynamic reserve of $5 \cdot 10^3$ until the background concentration falls below $10^{-7} M$ ⁸. The dynamic reserve for indirect photometry is in excess of 10^4 but decreases proportionally with background concentration when absorption falls below 1 a.u.f.s. When capillary columns are used, the lower limit of C_m or ϵ is increased due to

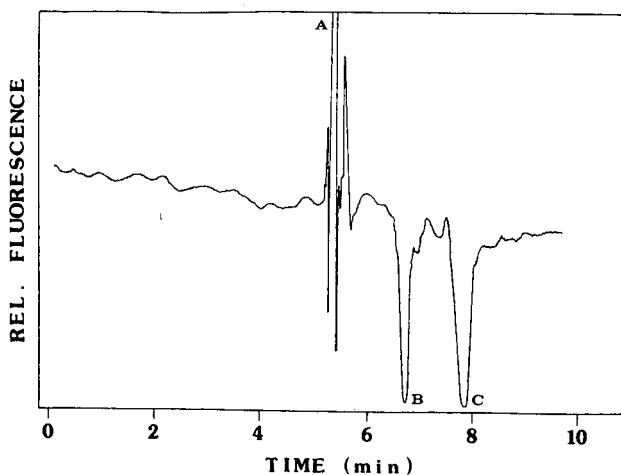


Fig. 1. Anion chromatogram with indirect fluorometric detection. (A) Salicylate (system peak); (B) acetate; and (C) nitrite. The amount of acetate and nitrite injected was 7 fmol each. Flow-rate, 35 nl/min; eluent, $2 \cdot 10^{-6}$ M sodium salicylate; column, 120 cm \times 15 μ m I.D. 2% PS-264.

reduced path-length. If C_m is raised to compensate for b , decreased detectability will result, as shown by eqn. 1.

The high dynamic reserve reported in ref. 7 is due to the use of the double-beam design in conjunction with high-frequency modulation and lock-in detection. This detection scheme is not particularly well suited for use with capillary columns, as discussed in ref. 10. Laser flicker noise, which can be as high as 1% of the total power, can be effectively reduced to levels below 0.02% by use of a laser intensity stabilizer. This approach has been used to produce stable fluorescence backgrounds for indirect fluorometric detection in capillary zone electrophoresis^{27,28}.

The chromatogram in Fig. 1 shows the separation of acetate from nitrite on a dynamically modified OTC column of 15 μ m I.D. Once the column had been modified, it could be used for several days without decrease in performance. Capacity factors for the anions are similar to those reported for a dynamically modified C_8 OTC column of 50 μ m I.D.¹⁰. The displacement ratios for the anions calculated from peak height and peak volumes were found to be 1/18 for acetate and 1/12 for nitrite. Eqn. 1 suggests lowering of C_m to decrease C_{lim} , but further reduction of C_m results in a corresponding reduction in D . Displacement ratios of < 1 have been observed before for separations in which salicylate concentrations of $< 10^{-5}$ M were used^{7,10}. These low displacement ratios can be attributed to interactions other than ion exchange, occurring at the column surface when low-capacity columns and low reagent concentrations are used.

The baseline in Fig. 1 represents a 0.93- μ A current from the phototube and is stable to 1 part in 1000. This is a direct consequence of the intensity-stabilized beam and the use of a 30-point moving-window average for the digitized data. The use of the microscope objective in conjunction with spatial and cut-off filters kept stray radiation levels to below 20% of the total signal when low concentrations of fluorophore were used. This is important, since the displacement ratio is calculated from

only that fraction of the signal due to probe fluorescence. These improvements in the design given in ref. 10 keep the baseline noise at a level of 0.93 nA, which corresponds to 15 fg or 0.3 fmol of nitrite injected. This is *ca.* 70 times less than that reported in ref. 10. Most of this improved mass detectability can be attributed to the reduced column dimensions. The remaining improvement is due to an increase in dynamic reserve and differences in displacement ratio. The concentration detectability for nitrite, which was calculated to be $2.4 \cdot 10^{-8} M$, is slightly better than that reported in ref. 10, due to the increase in dynamic reserve in the present experiments. In separate experiments using 10- μm capillaries, we have achieved baseline noise levels equivalent to 10 fg or 0.2 fmol of nitrate injected.

Non-electrolytes

As opposed to equivalent displacement of the background ions by analyte ions in ion-exchange chromatography, indirect detection of non-electrolytes in reversed-phase chromatography relies on the analyte perturbing the partitioning dynamics of the reagent, which has been equilibrated between the mobile and stationary phases. Thus, the eluted analyte zone contains either an excess or a deficit of the reagent, as compared to the unperturbed reagent concentration. In this case, R is usually $\ll 1$.

Most separations involving indirect photometric or fluorometric detection of non-electrolytes employ an ultraviolet-absorbing, non-ionic reagent^{5,9,14-16}. Separations using a reagent which absorbs in the visible region have been reported and are based on a type of complexation between the analyte and probe^{17,18}. A simple argon-ion laser, capable of emitting at 488 nm, is a popular, relatively low-cost, and reliable source with excellent beam characteristics. Fluorescent molecules, capable of absorbing at this wavelength, tend to be large, ionizable species which do not chromatograph well in the reversed-phase mode. Ion suppression, as its name implies, is a technique which can improve the chromatographic behavior of ionizable compounds by suppressing their ionization when a buffer is used to control the pH²⁹. Maintaining the pH of a 2,7-DCF solution between 3.0 and 5.0, we found that the fluorescent compound could be used as a reagent for indirect detection of non-electrolytes. Although 2,7-DCF has a reduced fluorescence yield in this pH range, its fluorescence was easily visible when micromolar solutions were excited with a 2-mW unfocused beam of 488.0 nm radiation.

The chromatogram in Fig. 2 shows the separation of various alcohols on an OTC column of 13 μm I.D. For the laser power and photomultiplier tube voltage being used, this concentration of 2,7-DCF allowed the system to remain above the shot-noise limit. Unlike ion chromatography, lowering of C_m does not give better detectability for non-electrolytes⁹. The total peak area of the positive peaks does not equal the total peak area of the negative peaks. This could be the result of the ionizable nature of the probe but this has also been observed occasionally for neutral reagents¹⁴. The hour-to-hour reproducibility of the system was good and could be maintained for several days by allowing the pump to run continuously at a reduced flow-rate. However, when the column was washed with aqueous methanol and later re-equilibrated with the eluent containing the reagent, the retention of the alcohols would remain essentially the same but the system-peak retention would be unpredictable. This suggests that the retention of 2,7-DCF is, in part, due to sites different from those responsible for alcohol retention.

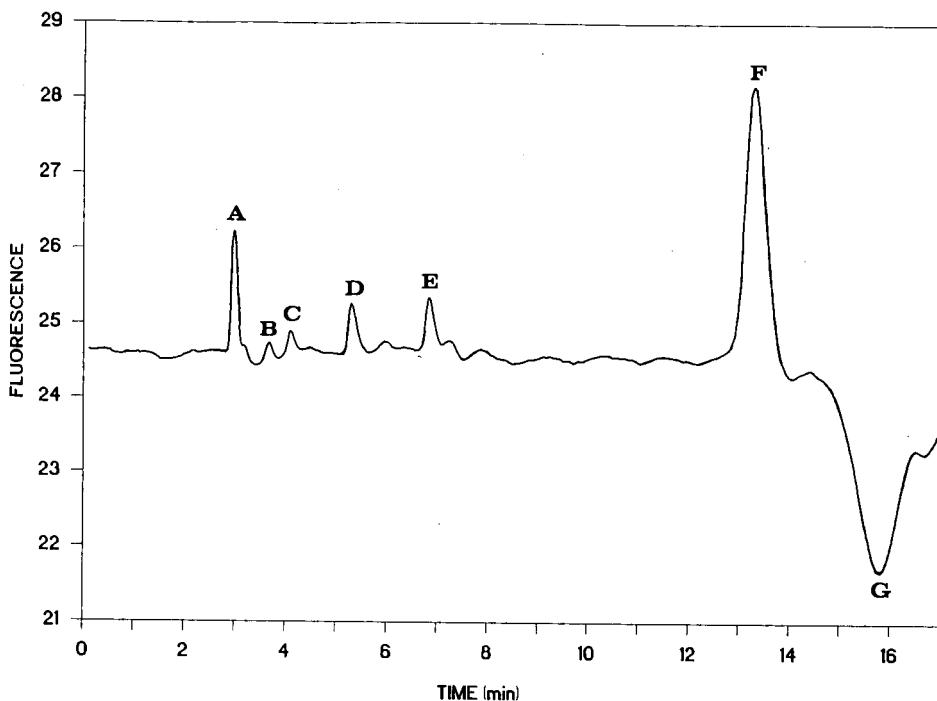


Fig. 2. Chromatogram of none-electrolytes with indirect fluorometric detection. (A) Solvent disturbance due to excess acetonitrile in sample solution; (B) 2-heptanol; (C) 1-heptanol; (D) 2-octanol; (E) 1-octanol; (F) 1-nonanol; and (G) 2,7-DCF (system peak). All alcohols were at 0.01% (v/v), except 1-nonanol which was 0.005%. Eluent, $2 \cdot 10^{-6}$ M 2,7-DCF in 5% acetonitrile containing, 10^{-3} M acetic acid (pH 4.0); flow-rate, 23 nl/min; injection volume, 230 pl; column, 50 cm \times 13 μ m I.D., 1% PS-255.

The displacement ratio for each of the alcohols in Fig. 2 was found to be: 2-heptanol, 1:3000; 1-heptanol, 1:2400; 2-octanol, 1:850; 1-octanol, 1:870; and 1-nonanol, 1:27. As with other non-electrolyte indirect detection systems, analytes eluted closer to the system peak produced more efficient displacement of the reagent⁹. These ratios are larger than those reported in ref. 9 but comparable to those in ref. 14.

The dynamic reserve in Fig. 2 is calculated to be 1500. As before, this stability is attributed to the use of a laser intensity stabilizer and a moving-window average (10-point). The limit of detection (signal-to-noise ratio, $S/N = 2$) for the early-eluted alcohols is a few picograms, and 72 fg or 0.5 fmol for 1-nonanol. This figure for 1-nonanol is about four orders of magnitude lower than that reported for 1-nonanol in ref. 14, where packed capillaries (340 μ m I.D.) and indirect photometric detection were used. Again, the majority of this improvement is due to the reduction of column dimensions, specifically the internal diameter. For the same detectable concentration, the mass involved is smaller with smaller columns. Naturally, indirect photometry is not applicable to columns with these dimensions.

It is interesting to note that the concentration detectability for 1-nonanol, $3.6 \cdot 10^{-8}$ M, and the concentration detectability of nitrite, $2.4 \cdot 10^{-8}$ M, are nearly equal. This is the result of the displacement ratio for nitrite being unusually small for ion-

exchange chromatography and the displacement ratio for 1-nonanol being unusually large for reversed-phase chromatography.

CONCLUSION

The use of silicone gums simplifies the production of OTC columns. These columns may be dynamically modified to function in the ion-exchange mode or used as they are in the reversed-phase mode. Indirect fluorometric detection of analytes in either mode with OTC columns allows extremely low mass detectability.

ACKNOWLEDGEMENTS

The authors would like to thank Lance B. Koutny for his assistance in the use of the video camera and the frame grabber. The Ames Laboratory is operated by Iowa State University for the U.S. Department of Energy. This work was supported by the Director of Energy Research, Office of Basic Energy Sciences, Division of Chemical Sciences.

REFERENCES

- 1 G. Schill and J. Crommen, *Trends Anal. Chem.*, 6 (1987) 111.
- 2 D. Ishii and T. Takeuchi, *J. Liq. Chromatogr.*, 11 (1988) 1865.
- 3 E. S. Yeung, *Acc. Chem. Res.*, 22 (1989) 125.
- 4 H. Small and T. E. Miller, *Anal. Chem.*, 54 (1982) 462.
- 5 J. E. Parkin, *J. Chromatogr.*, 287 (1984) 457.
- 6 L. Hackzell and G. Schill, *Chromatographia*, 15 (1982) 437.
- 7 T. Takeuchi and E. S. Yeung, *J. Chromatogr.*, 370 (1986) 83.
- 8 S-I. Mho and E. S. Yeung, *Anal. Chem.*, 57 (1985) 2253.
- 9 T. Takeuchi and E. S. Yeung, *J. Chromatogr.*, 366 (1986) 145.
- 10 W. D. Pfeffer, T. Takeuchi and E. S. Yeung, *Chromatographia*, 24 (1987) 123.
- 11 D. R. Bobbitt and E. S. Yeung, *Anal. Chem.*, 56 (1984) 1577.
- 12 J. Ye, R. P. Baldwin and K. Ravichandran, *Anal. Chem.*, 58 (1986) 2337.
- 13 T. Takeuchi, E. Suzuki and D. Ishii, *J. Chromatogr.*, 447 (1988) 221.
- 14 T. Takeuchi and D. Ishii, *J. Chromatogr.*, 393 (1987) 419.
- 15 T. Takeuchi and D. Ishii, *J. Chromatogr.*, 396 (1987) 149.
- 16 T. Takeuchi and D. Ishii, *J. Chromatogr.*, 403 (1987) 324.
- 17 T. Gnanasambandan and H. Freiser, *Anal. Chem.*, 54 (1982) 1282.
- 18 T. Gnanasambandan and H. Freiser, *Anal. Chem.*, 54 (1982) 2379.
- 19 P. Kucera (Editor), *Microcolumn High-Performance Liquid Chromatography*, Elsevier, Amsterdam, 1984.
- 20 F. J. Yang (Editor), *Microbore Column Chromatography: A Unified Approach to Chromatography*, Marcel Dekker, New York, 1989.
- 21 M. Novotony, *Anal. Chem.*, 60 (1988) 500A.
- 22 J. H. Knox and M. T. Gilbert, *J. Chromatogr.*, 186 (1979) 405.
- 23 J. W. Jorgenson and E. J. Guthrie, *J. Chromatogr.*, 255 (1983) 355.
- 24 A. Farbrøt, S. Folestad and M. Larsson, *J. High Resolut. Chromatogr. Chromatogr. Commun.*, 9 (1986) 117.
- 25 P. R. Dłuzneski and J. W. Jorgenson, *J. High Resolut. Chromatogr. Chromatogr. Commun.*, 11 (1988) 332.
- 26 R. M. Cassidy and S. Elchuk, *Anal. Chem.*, 54 (1982) 1558.
- 27 W. G. Kuhr and E. S. Yeung, *Anal. Chem.*, 60 (1988) 573.
- 28 W. G. Kuhr and E. S. Yeung, *Anal. Chem.*, 60 (1988) 2642.
- 29 B. A. Bidlingmeyer, *J. Chromatogr. Sci.*, 18 (1980) 525.

CHROMSYMP. 1663

Application of low-angle laser light scattering detection in the field of biochemistry

Review of recent progress

TOSHIO TAKAGI

Institute for Protein Research, Osaka University, Suita, Osaka 565 (Japan)

SUMMARY

Among various detectors now available, the low-angle laser light scattering photometer has not attracted much attention. This unique detector, however, affords invaluable information on the characterization of biopolymers with respect to their molar mass.

INTRODUCTION

Molar masses of proteins have traditionally been determined by physico-chemical techniques, such as osmometry, ultracentrifugation and light scattering. The introduction of techniques that depend on the molecular sieve effect of gels has changed the situation. Nowadays, biochemists chiefly depend on techniques such as gel permeation chromatography (GPC) and gel electrophoresis for the molar mass determination of proteins and nucleic acids. However, the size of a macromolecule is not always a unique function of its molar mass and the realization of this situation has led to reconsideration of molar mass determination through an approach with a secure physico-chemical basis.

About 10 years ago, we had the strong feeling that a convenient and reliable technique for molar mass determination was necessary other than the classical physico-chemical techniques. We became interested in the low-angle laser light scattering (LALLS) technique, developed in 1971 by Kaye *et al.*¹, as a promising candidate. When used as a detector for GPC, it was regarded as the most accurate approach for the determination of the molar mass distribution of polymers. The impact of the new technique was limited, however, and it failed to be accepted in the field of biopolymer research, owing to the absence in those days of GPC columns suitable for aqueous solvents and to the ignorance of using aqueous solvents in the construction of the initial models of commercial instruments.

We began studies on the introduction of the LALLS technique into the field of biochemistry and cooperated with Tosoh in an effort to develop a LALLS photometer

suitable for the purpose, helped considerably by the simultaneous development of GPC columns for aqueous solvents by that company. This paper reviews those efforts but avoiding overlap with a previous review².

TYPICAL EXPERIMENTAL PROCEDURE

A Model LS-8000 low-angle laser light scattering photometer (LALLS detector) from Tosoh is used in the author's laboratory. It is compact ($620 \times 310 \times 330$ mm) and weighs 37 kg. The light source is a 5-mW helium-neon laser with a wavelength of 633 nm. The flow cell with an internal volume of $30 \mu\text{l}$ ($10 \text{ mm} \times 2 \text{ mm}$ I.D.) can be thermostated by a constant-temperature water-jacket. Forward scattering from a $0.1\text{-}\mu\text{l}$ volume is collected at an angle of *ca.* 5° . With respect to sensitivity, $50 \mu\text{g}$ of bovine serum albumin with a molar mass of 66 300 gave a sufficient pen deflection. The amount of bovine serum albumin is one tenth of that required in the initial model (LS-8). The LALLS detector can accommodate a precision differential refractive index (RI) detector (Model RI-8011: light source, photodiode with an effective wavelength of 660 nm) in a single body.

Fig. 1 shows the outline of the optics of the Model LS-8000 LALLS detector. The baseline stability was significantly improved by the shift of the monitoring point of the light source from the rear side of the cell traditionally positioned there¹ to the front of the cell.

Fig. 2 shows the most refined system we are now using. The degasser (DG) is provided with a long PTFE tube surrounded by a reduced-pressure atmosphere, thus efficiently eliminating air dissolved in the solvent. Although recent models of pumping devices produce a pulseless flow, in our experience installation of a damping system consisting of a damper (Da) and a tube with a narrow orifice after the pump is necessary for extension of the life time of the usually expensive column. The columns (GC and MC), flow cell of the LALLS detector and the tubing connecting them are thermostated. The tubing was placed between a pair of plastic tubes with walls of high

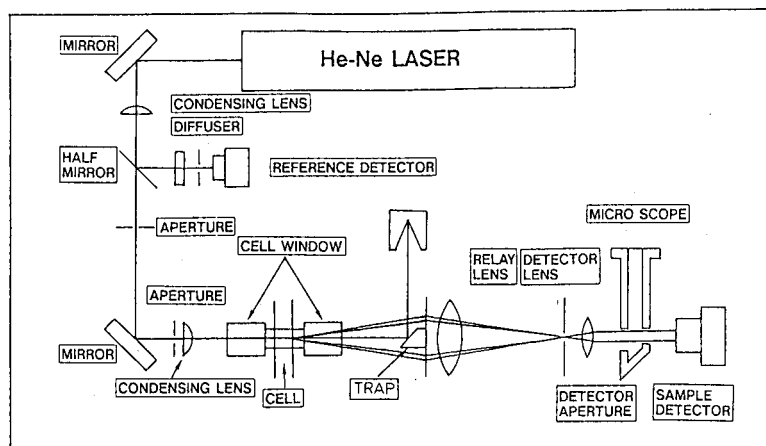


Fig. 1. Optics of the TSK Model 8000 LALLS detector.

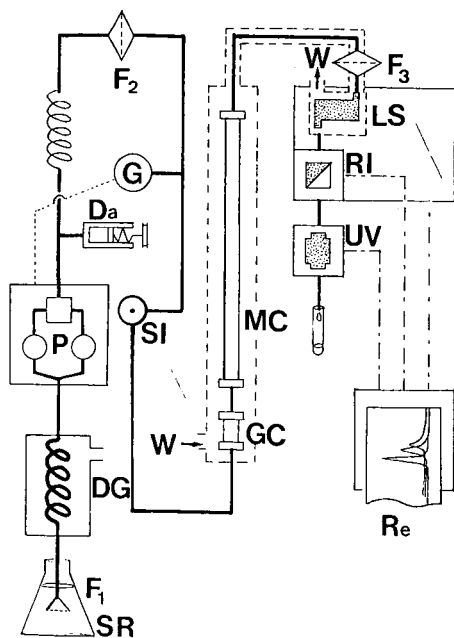


Fig. 2. Schematic diagram of the instrumentation. SR = solvent reservoir; F_1 = sintered stainless-steel filter (Umetani Seiki, Model SFY); DG = degasser (Erma Optical Works; Model ERC-3310); P = dual pump (Tosoh, CCPD); Da = bellows-type damper (Umetani Seiki, Model S-100) with a helically coiled stainless-steel tube (2 m \times 0.1 mm I.D.) on the downstream side; G = pressure gauge (Umetani Seiki) provided with a safety device to shut down the pump when the pressure exceeds the limit value for the column; F_2 = sintered stainless-steel filter (Umetani Seiki, Model SLF); SI = sample injector with a sample loop of 100- μ l internal volume; GC = guard column (Tosoh, TSK-GEL GSWXL, 4.0 cm \times 6.0 mm I.D.); MC = main column (Tosoh, TSK-GEL G3000SWXL, 30 cm \times 7.8 mm I.D.); F_3 = ultrafilter with pore size of 0.5 μ m (Millipore, type FHLP 01300); LS = LALLS detector (Tosoh, LS-8000); RI = RI detector (Tosoh, RI-8011); UV = UV detector (Tosoh, UV-8000); Re = three-pen recorder. The region enclosed by the dashed lines is thermostated by circulation of constant-temperature water.

heat conductivity and semicircular cross-section. The provision for thermostating is essential when a sample undergoes temperature-dependent association-dissociation.

Compared with the RI and UV detectors, each with a cell of internal volume 10 μ l, the LALLS detector (LS) has cell volume of 30 μ l, and hence broadening of a peak during passage through this cell is more significant than that for either of the other detector cells. When thermostating is not required, the UV detector is therefore preferably installed in advance of the LALLS detector. The RI detector should not be installed before the LALLS detector, because temperature of the RI detector cell is set about 10°C higher than room temperature for strict thermostating. Installation of the RI detector before the LALLS detector results in supplying a solution or solvent of a higher temperature to the LALLS detector, which is sensitive to temperature fluctuations. Further details of the system are described in the legend to Fig. 1.

The use of the LALLS detector requires greater care than that required in ordinary high-performance liquid chromatographic (HPLC) experiments, primarily because LALLS detector gives a signal that is proportional to the product of molar

mass and weight concentration, which implies that any dust particles will give an enormous noise, and a small air bubble will also act as a particle because of the significant difference in the refractive indices of air and the solvent. Dusts and air bubbles must be therefore removed with extreme care. The higher the molar mass of the sample, the easier is the measurement using the LALLS detector. When the molar mass of a sample is an order of 10^6 , an extremely low sample concentration is required even at the lowest sensitivity setting. In such a situation, measurements must be carried out in a well thermostated room to stabilize the RI detector, which is equipped with a thermostated cell but still requires further thermostating of the whole equipment in operation at such a high sensitivity. When these prerequisites are fulfilled, measurements can be carried out routinely using a system such as that shown in Fig. 2.

DATA HANDLING

As the result of improvements to the LALLS detector, measurements can now be carried out at a concentration low enough to make consideration of the concentration dependence unnecessary. Outputs of the three detectors, designated (LS), (RI) and (UV), respectively, are related to the molar mass of a sample according to the following equation, which is derived from the classical Rayleigh equation³:

$$M = k \cdot \frac{(\text{LS})}{(\text{dn/dc})(\text{RI})} \quad (1)$$

This expression is valid when both the protein concentration and scattering angle are low enough to allow neglect of the concentration-dependent terms in the Rayleigh light scattering equation³. Using the system shown in Fig. 2, these requirements are satisfied in most instances.

For a sample detectable by the UV detector, the value of the specific refractive increment, (dn/dc) , can be assumed to be proportional to $(\text{RI})A/(\text{UV})$, where A is molar absorptivity of the sample, Eqn. 1 can be accordingly modified to give the following equation:

$$M = k' \cdot \frac{(\text{LS})(\text{UV})}{A(\text{RI})^2} \quad (2)$$

This is the general equation applicable to most proteins. Determination of the value of A is a crucial prerequisite and requires great patience and skill. This is an unavoidable step in determination of molar mass when the particular protein cannot be assumed to be a simple protein, as in examples which will be described later.

When dn/dc is assumed to be equal for samples of unknown molar mass and for standard samples of known molar mass, eqn. 1 can be simplified to give the following equation:

$$M = k'' \cdot \frac{(\text{LS})}{(\text{RI})} \quad (3)$$

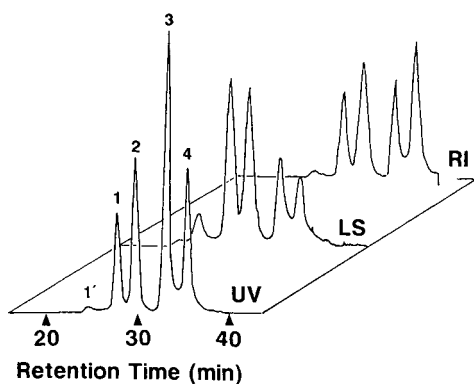


Fig. 3. Typical example of elution curves obtained with UV, LS and RI detectors. The numbers in parentheses are the amounts of the proteins applied. 1 = Bovine serum albumin (50 μg ; 1', dimer); 2 = ovalbumin (60 μg); 3 = carbonic anhydrase (75 μg); 4 = ribonuclease (100 μg).

For water-soluble globular proteins that do not contain significant amounts of non-amino acid components, the above assumption is valid as a first approximation. Furthermore, eqn. 3 can even be modified to give the following equation when only a dissociation-association phenomenon of a particular protein is involved:

$$M = k''' \cdot \frac{(\text{LS})}{(\text{UV})} \quad (4)$$

We have carried out a series of studies in which the most appropriate equation among eqns. 1-3 was utilized in each. An example is given shown below. Fig. 3 shows three elution curves obtained by the three detectors for four proteins. Another run was made with a mixture containing different set of four proteins. For these proteins, dn/dc can be safely assumed to be identical. Fig. 4 shows plot of the (LS)/(RI) ratios for the

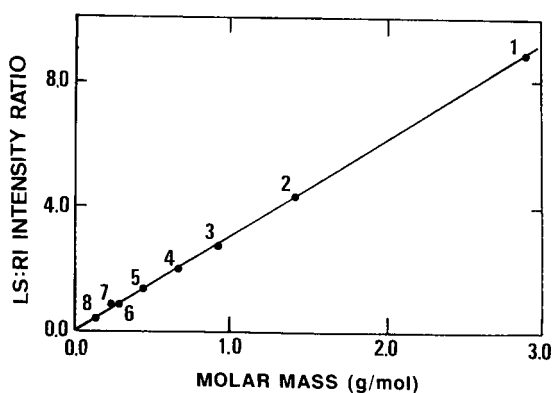


Fig. 4. Plot of the ratio of output of the LALLS detector to that of the RI detector. Proteins with molar masses in parentheses: 1 = yeast glutamate dehydrogenase (290 000); 2 = hog heart muscle acetate dehydrogenase (142 000); 3 = yeast enolase (93 345); 4 = bovine serum albumin (66 300); 5 = ovalbumin (44 000); 6 = bovine carbonic anhydrase (29 000); 7 = yeast adenylate kinase (21 500); 8 = bovine pancreatic ribonuclease (13 700).

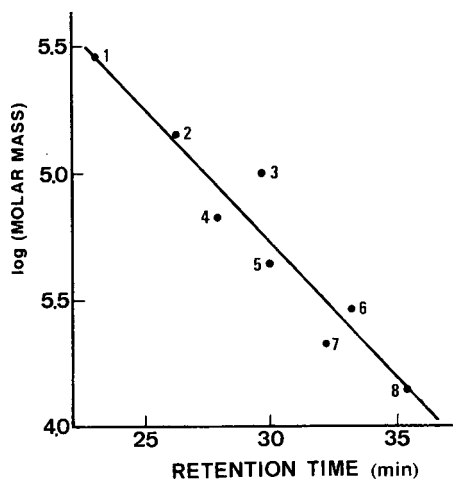


Fig. 5. Plot of logarithms of molar masses of the proteins in Fig. 4 against their retention times.

total of eight proteins against their molar mass. The linearity of the plot clearly demonstrates the efficiency of the approach in the determination of the molar mass of such proteins. Such a plot can be used as a calibration line for the determination of the molar mass of an unknown protein provided that it can be assumed to have the same value of dn/dc as the standard proteins.

A plot of \log (molar mass) against retention time gave scattered points as shown in Fig. 5. The line tentatively drawn through the points can hardly be used as a calibration line.

APPLICABILITY OF GPC-LALLS IN BIOCHEMISTRY

The result described above is only an example of the application of the GPC-LALLS system. Comparison of Figs. 4 and 5 clearly shows that the GPC-LALLS technique is far superior to the conventional approach, where molar mass is determined simply from retention time.

The molar mass determination of membrane proteins is one of the most fascinating fields of application of the technique. Confirmation of the trimeric nature of porin, an *E. coli* outer membrane protein, solubilized by either sodium dodecyl sulphate (SDS)⁴ or octaethylene glycol *n*-dodecyl ether⁵ was the initial example of the successful application in the approach. The technique was further applied to the characterization of the nature of Na^+ , K^+ -ATPase solubilized by SDS⁶ or the non-ionic surfactant described above⁷. The methodology of the application of GPC-LALLS to membrane proteins was reviewed recently⁸.

The approach was further extended recently to monitoring the molar mass of ATPase just after passing through a TSK-GEL G3000SWXL column equilibrated with a buffer containing ATP and other necessary ingredients for exerting its enzymatic activity⁹. The results thus obtained allow the examination of the correlation of the association-dissociation of the subunits with the enzymatic activity. It was found that the minimum unit of the enzyme is the protomer with the composition of $\alpha\beta$

(protomer), and the change in the affinity between a pair of the protomers is sensitive to the ionic environment and temperature. This suggests that the change is directly involved in the expression of the pumping activity of the enzyme.

With membrane proteins, surfactants or lipids are non-covalently bound to them. The technique is also efficient for determining the molar mass of a complex protein to which non-amino acid components are covalently bound. We have shown examples of successful application of the technique for several glycoproteins¹⁰.

Application of the GPC-LALLS technique is not limited to proteins, and we have determined the molar mass of micelles of octaethylene glycol *n*-dodecyl ether⁵. Recently we have applied the technique to the determination of the molar masses of human hepatitis B vaccines, which were produced by the recombinant DNA technique and are protein-lipid complexes with molar mass of several millions¹¹. With surfactant micelles, a high sensitivity was required for the LALLS detector but was not necessary for the refractometer. With the vaccine particles, a high performance is required of the refractometer. Temperature control not only of the measuring cells but also of the overall system is required. Temperature fluctuations in any part of the system lead to viscosity fluctuations and thus pressure fluctuations, giving an unstable baseline. In our experience, the measuring system can be used reliably for materials whose molar masses range between several thousands and several millions if the system is fine-tuned. Another example of the application of the GPC-LALLS technique to biological particles is the molar mass determination of protein micelles in milk^{12,13}. For flexible polymers with a molar mass comparable to those of vaccine particles and casein micelles, the reliability may be reduced, however, owing to intramolecular interference of scattered light.

Another application of the technique is the determination of the molar mass distribution of biopolymers. We have successfully determined unequivocally for the first time the molar mass distribution of amylose using this technique^{14,15}. Proteins form aggregates when they are heated. When the heating is moderate, some proteins form aggregates that can be fractionated using a GPC column with high porosity. We showed the first example of the observation of such a phenomenon with ovalbumin heated to *ca.* 80°C¹⁶.

In conclusion, we believe that the application of the GPC-LALLS technique in biochemistry has made accurate molar mass measurements of biopolymers easier and has opened up approaches leading to new concepts such as the structure-function relationship of the membrane protein.

Krull's group at Northwestern University is active in the application of GPC-LALLS to the characterization of proteins, and have applied it to detect the gradient elution of proteins from hydrophobic interaction or reverse-phase chromatographic columns¹⁷. They also showed that detection by LALLS and UV detectors is compatible with an HPLC run in the gradient elution mode. They recently published an excellent review of the application of the LALLS technique to biopolymers¹⁸.

ACKNOWLEDGEMENTS

The applications of the GPC-LALLS technique were carried out in cooperation with the following, associated with our group as graduate students (Mr. T. Nashima, Dr. J. Miyake, Mr. K. Kameyama, Dr. S. Maesawa and Mr. Y. Watanabe) or as

visiting researchers (Dr. S. Hizukuri from Kagoshima University, Dr. Y. Hayashi from Kyorin University, Dr. T. Ono from Iwate University, and Dr. Akio Kato from Yamaguchi University). Staff of the R & D Group of Tosoh responded promptly to our requests to improve their products. The contribution of these workers is appreciated. This work was supported by Scientific Research Funds (Grant Nos. 321930, 447123 and 56580110) of the Ministry of Education, Science and Culture of Japan.

REFERENCES

- 1 W. Kaye, A. J. Havlik and J. B. McDaiel, *J. Chromatogr.*, 9 (1971) 695.
- 2 T. Takagi, in H. Parvez, Y. Kato and S. Parvez (Editors), *Progress in HPLC: Gel Permeation and Ion-Exchange Chromatography of Proteins and Peptides*, Vol. 1, VNU Science, Amsterdam, 1985, Ch. 3, p. 27.
- 3 C. Tanford, *Physical Chemistry of Macromolecules*, Wiley, New York, 1961 p. 275.
- 4 K. Kameyama, T. Nakae and T. Takagi, *Biochim. Biophys. Acta*, 706 (1982) 19.
- 5 S. Maezawa, Y. Hayashi, T. Nakae, J. Ishii, K. Kameyama and T. Takagi *Biochim. Biophys. Acta*, 747 (1983) 291.
- 6 T. Takagi, S. Maezawa and Y. Hayashi, *J. Biochem.*, 101 (1987) 805.
- 7 Y. Hayashi, T. Takagi, S. Maezawa and H. Matsui, *Biochim. Biophys. Acta*, 748 (1983) 153.
- 8 Y. Hayashi, H. Matsui and T. Takagi, *Methods Enzymol.*, 172 (1989) 514.
- 9 Y. Hayashi, K. Kimura, H. Matsui and T. Takagi, *Biochim. Biophys. Acta*, 983 (1989) 217.
- 10 S. Maezawa and T. Takagi, *J. Chromatogr.*, 280 (1983) 124.
- 11 Y. Sato, N. Ishikawa and T. Takagi, *J. Chromatogr.*, 507 (1990) 25.
- 12 T. Ono and T. Takagi, *J. Dairy Res.*, 53 (1986) 547.
- 13 T. Ono, H. Kohno, S. Odagiri and T. Takagi, *J. Dairy Res.*, 56 (1989) 61.
- 14 T. Takagi and S. Hizukuri, *J. Biochem.*, 95 (1984) 1459.
- 15 S. Hizukuri and T. Takagi, *Carbohydr. Res.*, 134 (1984) 1.
- 16 A. Kato and T. Takagi, *J. Agric. Food Chem.*, 35 (1987) 633.
- 17 R. Mhatre, H. H. Stuting and I. S. Krull, *J. Chromatogr.*, submitted for publication.
- 18 H. M. Styting, I. S. Krull, R. Mhatre, S. C. Krzysko and H. G. Barth, *LC · GC, Mag. Liq. Gas Chromatogr.*, 7 (1989) 402.

CHROMSYMP. 1689

Determination of amoxicillin in plasma by high-performance liquid chromatography with fluorescence detection after on-line oxidation

H. MASCHER* and C. KIKUTA

Pharm-Analyt Lab. GmbH, Wienerstrasse 37, P.O. Box 4, A-2514 Traiskirchen/Vienna (Austria)

SUMMARY

A simplified high-performance liquid chromatographic method for the determination of amoxicillin in plasma is described. Specific and sensitive fluorescence detection was achieved by on-line post-column electrochemical oxidation, using an electrochemical detector. Owing to the high specificity of the detection system, deproteinized plasma samples could be injected directly without prior treatment. This method permits a very fast and reproducible determination of amoxicillin in plasma on a routine basis at levels, down to 50 ng/ml. The absolute detection limit is about 10 pg injected.

INTRODUCTION

Amoxicillin (α -amino-*p*-hydroxybenzylpenicillin; Fig. 1) is an orally absorbed, acid-stable, broad-spectrum antimicrobial agent. Using high-performance liquid chromatographic (HPLC) methods with UV detection at low wavelength, *e.g.*, 230 nm¹⁻³, the determination of amoxicillin in body fluids was difficult and the detection limits were *ca.* 500 ng/ml. In order to enhance the selectivity, different HPLC methods with pre-column⁴⁻⁶ or post-column⁷⁻⁹ reactions have been developed.

Derivatization of amoxicillin to a fluorescent compound in an on-line electrochemical reactor proved to be a useful approach, resulting in higher reproducibility and increased sensitivity. This paper describes a reliable HPLC method for amoxicillin especially applicable to routine work. It includes the optimization of the on-line electrochemical reaction and the development of a new HPLC separation system. In order to reduce sample manipulation, protein precipitation with perchloric acid was used.

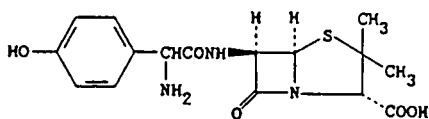


Fig. 1. Structure of amoxicillin.

EXPERIMENTAL

Materials

All reagents were of analytical-reagent grade or better and were purchased from Merck (Darmstadt, F.R.G.) or Fluka (Buchs, Switzerland). Solvents used for chromatography were obtained as HPLC far-UV grade (acetonitrile) or were purified in the laboratory (water).

An isocratic HPLC system consisting of the following components was used: a Kontron (Zürich, Switzerland) Model 420 solvent delivery pump, a Rheodyne (Cotati, CA, U.S.A.) Model 125 injection valve with a 20- μ l loop, a Merck Hitachi Model F1000 fluorimetric detector (Merck) and an LDC CI-10B chromatographic integrator (Milton-Roy, Riviera Beach, FL, U.S.A.). The post-column electrochemical reaction was monitored with a Model 5010 electrochemical detector (ESA, Bedford, MA, U.S.A.).

Methods

Amoxicillin was separated on an 80 \times 4 mm I.D. stainless-steel column packed with Nucleosil 120 3C₁₈ (SRD, Vienna, Austria) and 0.02 M methanesulphonic acid-acetonitrile (92.5:7.5, v/v) as the mobile phase. The effluent was monitored after

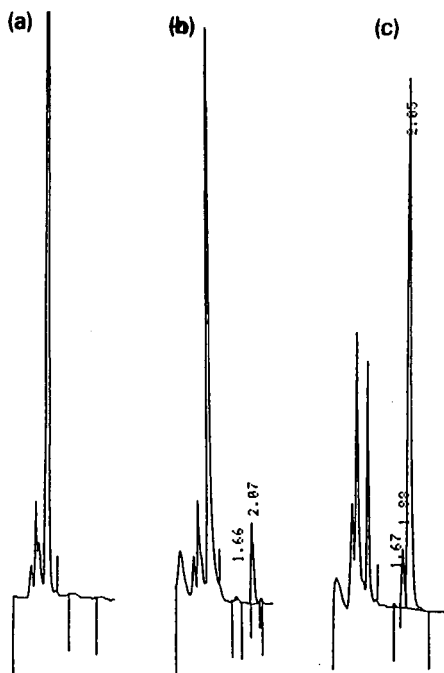


Fig. 2. Chromatograms obtained after injection of 20 μ l of deproteinized plasma: (a) pre-dose plasma; (b) plasma spiked with 0.42 μ g/ml of amoxicillin ($t_R = 2.1$ min); (c) plasma from a volunteer given a single oral dose of amoxicillin, 15 min after application, with an amoxicillin plasma level of 1.63 μ g/ml. Column, Nucleosil 3C₁₈, 80 \times 4 mm I.D.; eluent, 0.02 M methanesulphonic acid-acetonitrile (92.5:7.5, v/v); fluorimetric detection, λ_{ex} , 255 nm, λ_{em} , 400 nm, after post-column oxidation at 0.78 V. Numbers at peaks indicate retention times in min.

on-line post-column electrochemical reaction at 0.78 V at an excitation wavelength of 255 nm and an emission wavelength of 400 nm.

Plasma samples were stored at -30°C until analysis. After thawing, 1.0 ml of a plasma sample (standard or volunteer plasma) was mixed with 0.15 ml of 20% perchloric acid and centrifuged at *ca.* 2000 *g* for 4 min. Supernatants were used for further analysis. As amoxicillin is unstable in this supernatant, HPLC analysis was carried out within 15 min after protein precipitation.

Blank plasma samples were spiked with amoxicillin. These samples were analysed as described above. Finally, peak areas were plotted against concentration.

RESULTS AND DISCUSSION

Different liquid chromatographic systems were used for the determination of amoxicillin in plasma. With a C_{18} column and methanesulphonic acid-acetonitrile (92.5:7.5, v/v) as the eluent, amoxicillin is rapidly and efficiently separated from plasma matrix components (Fig. 2a and b).

Selective separation and specific fluorescence detection allow the direct injection of small volumes of plasma into the HPLC system without further purification. Fig. 2c shows a chromatogram obtained after injection of 20 μl of deproteinized plasma from a volunteer after a single oral dose of amoxicillin.

Although the assay was performed without the use of an internal standard, the day-to-day variation for the range 0.09–21.0 $\mu\text{g}/\text{ml}$ was less than 10% standard deviation (median, 3.7%) (Table I). The absolute recovery for amoxicillin from plasma was $>94\%$.

Electrochemical oxidation of amoxicillin results in the formation of two major reaction products, one with intense fluorescence ($\lambda_{\text{em.}}$ 400 nm, $\lambda_{\text{ex.}}$ 255 or 280 nm) and the other with a UV absorption maximum at 255 nm. In off-line experiments, the amoxicillin peak was eluted from the column and, after passage through the electrochemical detector cell, was collected and injected into a more selective HPLC

TABLE I

DAY-TO-DAY REPRODUCIBILITY (FOUR DIFFERENT DAYS) AND ACCURACY OF THE DETERMINATION OF AMOXICILLIN IN SPIKED HUMAN PLASMA

Fluorescence detection: excitation 255 nm, emission 400 nm.

<i>Amoxicillin added</i> ($\mu\text{g}/\text{ml}$)	<i>Amoxicillin found</i> ($\mu\text{g}/\text{ml}$) ^a	<i>Relative standard</i> <i>deviation</i> (%)	<i>Recovery</i> (%)
0.087	0.079 \pm 0.007	8.9	90.8
0.210	0.189 \pm 0.007	3.7	90.0
0.420	0.411 \pm 0.034	6.3	97.9
0.842	0.882 \pm 0.057	6.5	104.8
1.684	1.741 \pm 0.078	4.5	103.4
3.368	3.522 \pm 0.062	1.8	104.6
6.736	6.599 \pm 0.109	1.7	98.0
10.521	10.521 \pm 0.247	2.3	103.2
21.042	20.794 \pm 0.200	1.0	98.9

^a Mean \pm S.D. ($n = 4$).

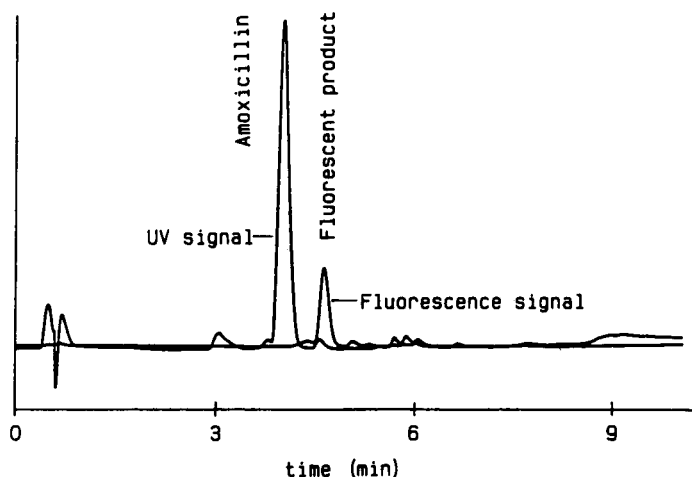


Fig. 3. Chromatogram obtained after injection of oxidized amoxicillin. Column, Nucleosil 3C₁₈, 80 × 4 mm I.D.; eluent, 0.02 M methansulphonic acid–acetonitrile (98:2, v/v). (A) Fluorimetric detection, λ_{em} . 255 nm, λ_{em} . 480 nm; (B) UV detection at 250 nm.

system [methansulphonic acid–acetonitrile (98:2, v/v)]. This system separates native amoxicillin and the major reaction products (Fig. 3).

A decrease in peak area at higher potential applied to the electrochemical detector cell could be monitored only when the excitation wavelength was set at 255 nm. Setting the excitation wavelength to 280 nm resulted in an increase in the peak area at higher potential. The increase in the peak area was limited only by the detector's ground current, caused by the mobile phase (see Fig. 4).

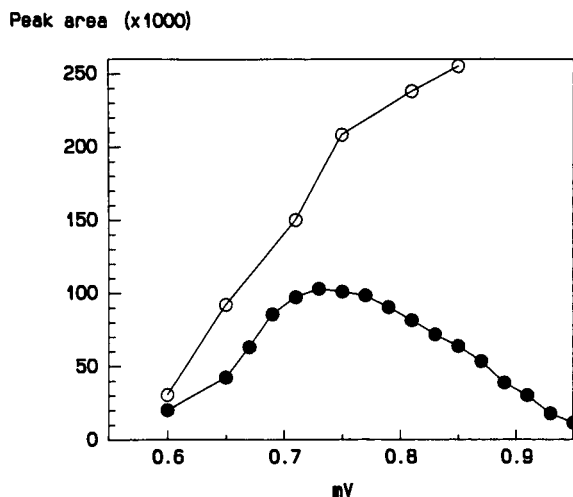


Fig. 4. Potential course of fluorescence change for one-line electrochemically oxidized amoxicillin at two excitation wavelengths: ● = 255 nm; ○ = 280 nm.

REFERENCES

- 1 T. B. Vree, Y. A. Hekster, A. M. Baars and E. van der Kleijn, *J. Chromatogr.*, 145 (1978) 496.
- 2 M. Foulstone and C. Reading, *Antimicrob. Agents Chemother.*, 22 (1982) 753.
- 3 T. L. Lee and M. A. Brooks, *J. Chromatogr.*, 306 (1984) 429.
- 4 K. Miyazaki, K. Ohtani, K. Sunada and T. Arita, *J. Chromatogr.*, 276 (1983) 478.
- 5 J. Haginaka and J. Wakai, *Analyst (London)*, 110 (1985) 1277.
- 6 T. L. Lee, L. D'Arconte and M. A. Brooks, *J. Pharm. Sci.*, 68 (1979) 454.
- 7 J. Carlqvist and D. Westerlund, *J. Chromatogr.*, 164 (1979) 373.
- 8 J. Carlqvist and D. Westerlund, *J. Chromatogr.*, 344 (1985) 285.
- 9 J. Haginaka and J. Wakai, *J. Chromatogr.*, 413 (1987) 219.

CHROMSYMP. 1708

Selective post-column liquid chromatographic determination of sugars in spent sulphite liquor with two enzymatic electrochemical detectors in parallel

G. MARKO-VARGA*

Department of Analytical Chemistry, University of Lund, P.O. Box 124, S-221 00 Lund (Sweden)

E. DOMINGUEZ

Department of Pharmacy, Food Analysis and Nutrition, University of Alcalá de Henares, Madrid (Spain)

B. HAHN-HÄGERDAL

Department of Applied Microbiology, University of Lund, P.O. Box 124, S-221 00 Lund (Sweden)

and

L. GORTON

Department of Analytical Chemistry, University of Lund, P.O. Box 124, S-221 00 Lund (Sweden)

SUMMARY

Matrix components in spent sulphite liquor interfere with the liquid chromatographic determination of sugars. High selectivity can be obtained by coupling the column with two immobilized enzyme reactors and amperometric detection. The carbohydrates eluted from the column are mixed with a make-up flow, consisting of a nicotinamide adenine dinucleotide (NAD⁺) buffer. Because the chromatographic separation of sugars in spent sulphite liquor is incomplete, the column effluent is split into two detection paths, each containing an immobilized enzyme reactor, with different selectivity, coupled on-line with amperometric flow-through cells. One reactor contains mutarotase, glucose dehydrogenase and galactose dehydrogenase and the other also contains an additional enzyme, xylose isomerase. The carbohydrates are oxidized to form an equivalent amount of reduced coenzyme (NADH), which is detected electrochemically with an electrode modified by a phenoxazine derivative.

INTRODUCTION

In recent years there has been great interest in fermenting cheap sources of carbohydrates to ethanol. Carbohydrate mixtures derived from lignocellulosic materials are such sources¹. They can be produced by either acid or enzymatic hydrolysis, usually preceded by heat treatment. Sulphite pulping of lignocellulose also gives a fermentable by-product, known as spent sulphite liquor. Typically, a lignocellulose hydrolysate may contain a mixture of D-glucose, D-mannose, D-galactose, L-arabinose and D-xylose². In addition, when a lignocellulose hydrolysate is obtained

by enzymatic hydrolysis, it will also contain D-cellobiose³. The pretreatment and hydrolysis processes create compounds such as acetic acid and furfural, which are inhibitory to the microorganisms fermenting the carbohydrates to ethanol. In this context, fermentation with a combination of ordinary baker's yeast, *Saccharomyces cerevisiae*, and the enzyme xylose isomerase (glucose isomerase) has been found to be superior to fermentation with other yeasts^{4,5}. D-Xylose is not fermentable unless isomerized to D-xylulose³. To follow the process there is a need for an analytical procedure that permits the quantification of the saccharides in the fermentor, including D-xylulose, during fermentation. In this investigation we used spent sulphite liquor, supplemented with D-xylulose and D-cellobiose, as a model fermentation substrate.

We have previously described detection systems for flow-injection analysis (FIA) and liquid chromatography (LC) for the selective determination of D-xylose and D-xylulose^{6,7}. The detection system is based on post-column immobilized enzyme reactors (IMER), which oxidize the sugars selectively to form dihydronicotinamide adenine dinucleotide, (NADH), followed by selective electrochemical detection of NADH at a chemically modified electrode (CME)^{6,7}. There has recently been great interest in utilizing CMEs as electrochemical detectors in analytical flow systems because of their unique property of enhancing sensitivity and selectivity^{8,9}. By a combination of two selective steps in the detection system, the enzymatic (IMER) and the electrochemical (CME), further selectivity can be gained, which is important in the analysis of complex samples.

This paper extends previous systems by including two post-column enzyme electrochemical detection systems working in parallel for the selective monitoring of the concentrations of sugars in spent sulphite liquor.

Owing to the difficulty of achieving the complete chromatographic separation of all monosaccharides, the effluent from the column is split into two streams of equal flow-rates, each passing through a post-column enzyme electrochemical detection system but with different selectivities. In one detection path three enzymes are immobilized: mutarotase, galactose dehydrogenase, and glucose dehydrogenase. In this reactor all saccharides, except D-xylulose, are oxidized to form NADH. In the other path, a reactor containing an additional enzyme, xylose isomerase, is co-immobilized with the other three enzymes. Thus, D-xylulose is also oxidized to form NADH in this reactor. The NADH formed in both reactors is further transported to electrochemical flow-through cells where it is selectively and catalytically oxidized at 0 mV vs. SCE at an electrode chemically modified with a phenoxazine derivative^{6,7,10,11}.

EXPERIMENTAL

Flow system

The basic components of the flow system consisted of an LC pump, Model 2150 (LKB, Bromma, Sweden), an injector, Model 7045 (Rheodyne, Cotati, CA, U.S.A.), with sample loops of 5, 10, 20, 50, 100 and 200 μ l and separation columns of the Aminex HPX 87 type (300 \times 7.8 mm I.D.), containing sulphonic groups.

Three commercially available columns were used, Aminex HPX 87P (Pb²⁺ loaded), Aminex HPX 87C (Ca²⁺ loaded) and Aminex HPX 87H (H⁺ form), all

supplied by Bio-Rad Labs., Richmond, CA, U.S.A. The HPX-87H column was used at 40°C with 5 mM sulphuric acid as the mobile phase. A K⁺ ligand-exchange column was prepared by treating an Aminex HPX 87H column with 0.1 M K₂HPO₄ (pH 7.0) for 24 h to load the sulphonate sites with K⁺, and used with the same solution as the mobile phase. Li⁺ and Mg²⁺ columns were made by treating Aminex HPX 87P columns with stock metal ion solution prepared by dissolving analytical-reagent grade metal nitrate in water to make 0.1 M solutions. The pH was adjusted to 6.5 and the solution was allowed to pass through the column for 24 h to load the polymer resin. After loading, the resin was removed from each column and dissolved in 1 M nitric acid and analysed with atomic absorption spectrometry to ensure that no traces of Pb²⁺ remained. Subsequently the columns were equilibrated with water before use. The HPX-87P and HPX-87C columns were used as received.

The mobile phase was carefully deaerated. It consisted of water in all instances, except for the H⁺ and the K⁺-loaded columns (see above). The mobile phase was prethermostated to 40°C for the column in the protonated form and otherwise to 85°C by passing the carrier through a 2-ml loop in the column oven, Model 2155 (LKB), prior to injection of sample¹². Prethermostating the mobile phase promotes separation of the saccharides.

Spent sulphite liquor was prepared as follows before samples were injected into the LC system. The liquid was neutralized by the addition of sodium hydroxide to a final pH of 7.0, filtered through 0.40- μ m membrane filters (Millex-HV; Millipore, Milford, MA, U.S.A.) to remove solid particles, and then passed through a solid-phase extraction column for sample clean-up^{12,13}. The extraction column was conditioned by passivation prior to sample passage, as described previously¹⁴. A strong anion-exchange phase was used, containing quaternary amine functional groups (SAX, volume 3 ml; Analytichem International, kindly donated by Mr. G. Oresten, Sorbent, Västra Frölunda, Sweden). The sample solution was further diluted with water before injection (see Results and Discussion). A small guard column was used when pretreated and diluted samples of spent sulphite liquor were introduced into the chromatographic system. This consisted of a stainless-steel column (2.5 cm \times 0.4 cm I.D.), filled with the same material as the Aminex HPX-87P column.

The effluent from the column was mixed with a deaerated make-up flow consisting of 0.7 M phosphate buffer (pH 7.0) containing 21 mM magnesium nitrate, 7 mM EDTA and 14 mM nicotinamide adenine dinucleotide (NAD⁺), necessary for the enzymatic reaction (see below). The EDTA was added to the make-up flow to complex metal ions leaking from the column that would otherwise poison the enzymes¹². However, EDTA alone may inactivate the enzymes, but this is counteracted by the addition of Mg²⁺ to the buffer¹². The make-up flow was delivered by a second LC pump, Model 2150 (LKB), passing through a pulse damper (Touzart Matignon, Paris, France). The combined flows passed through a 50- μ l single bead string reactor (SBSR) (100 mm \times 0.8 mm I.D.), filled with solid glass beads, diameter 0.5 mm, to promote complete mixing and counteract band-broadening effects^{12,13}.

The three-electrode amperometric flow-through cell was of the confined wall-jet type, and has been described previously¹⁵. The working electrode consisted of a polished and pretreated graphite rod¹³, RW 001 (Ringsdorf Werke, F.R.G.), the 0.0731-cm² flat surface of which was exposed to the flow. The surface of the graphite was chemically modified by introduction of a mediator to promote electrocatalytic

oxidation of NADH. This was achieved by applying a few droplets of a dissolved redox mediator (a bisphenoxazinyl derivative of terephthalic acid¹¹) in acetone and allowing the solvent to evaporate. The modifier contains an extended aromatic ring system and is strongly adsorbed on the surface of the electrode. The surface coverage of the mediator was at least $2 \cdot 10^{-9}$ mol cm⁻² (ref. 11), determined by cyclic voltammetry, before insertion of the electrode in the flow cell. Fig. 1 shows the cyclic voltammograms obtained for (a) a naked and (b) a chemically modified graphite electrode. The surface coverage of the adsorbed mediator can be evaluated by integration of the area under the waves. The formal potential of the adsorbed mediator is given by taking the mean potential of the peaks of the oxidation and reduction waves. Fig. 1c shows evidence of the electrocatalytic properties of the adsorbed mediator in the presence of NADH. Fig. 1 reveals that the catalytic reaction between NADH and the adsorbed

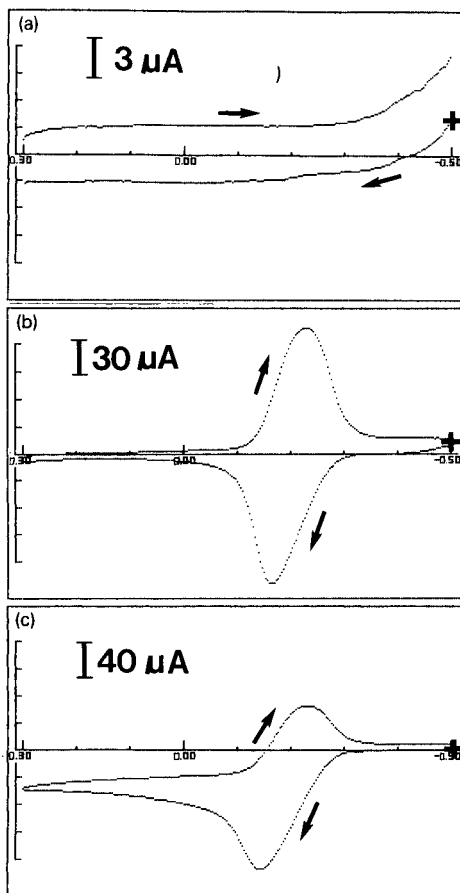


Fig. 1. Cyclic voltammograms of (a) a naked graphite electrode, (b) graphite chemically modified with a bisphenoxazinyl derivative of terephthalic acid, (c) as (b) but in the presence of 8 mM NADH. The contacting electrolyte was 0.25 M phosphate buffer (pH 7.0). Surface coverage, 7.5 nmol cm⁻²; sweep rate, 100 mV s⁻¹. +, Starting potential. The x-axis denotes the applied potential vs. a saturated calomel reference electrode.

mediator is fast and also that the catalytic reaction can occur at potentials substantially lower than 0 mV, as the anodic peak potentials of the cyclic voltammograms in Fig. 1b and c, with and without the presence of NADH, are almost identical¹⁰.

A platinum-wire counter electrode and an Ag/AgCl (0.1 M KCl) reference electrode were used. The cell was connected to a potentiostat (Zäta Elektronik, Lund, Sweden). The applied voltage was 0 mV vs. Ag/AgCl throughout all the experiments^{11,13}.

In the final flow system (Fig. 2), two identical electrochemical cells were used, each connected to one potentiostat. To split the combined flows after mixing with the make-up flow, a gradient mixer (GM), Model 2152 (LKB), was used in the backward mode and at the highest frequency to yield an optimum splitting ratio and to prevent band broadening.

In some experiments a spectrophotometric flow-through detector, Model 2151 (LKB), was used at 340 nm to determine the NADH formed in the flow system.

Enzyme reactors

The following enzyme preparations were used. Xylose isomerase (XI) (E.C. 5.3.1.5) from *Streptomyces* sp. was generously supplied by Miles Kali Chemie (Hannover, F.R.G.) as a suspension with an activity of 4.5 U mg⁻¹ protein. Mutarotase (MT) (E.C. 5.1.3.3) from porcine kidney was purchased from Sigma (St. Louis, MO, U.S.A.), cat. no. M-4007, dissolved in 3.2 M ammonium sulphate, with an activity of 5800 U mg⁻¹ protein. Glucose dehydrogenase (GDH) (E.C. 1.1.1.47) from *Bacillus megaterium* was purchased from Merck (Darmstadt, F.R.G.), cat. no. 13732,

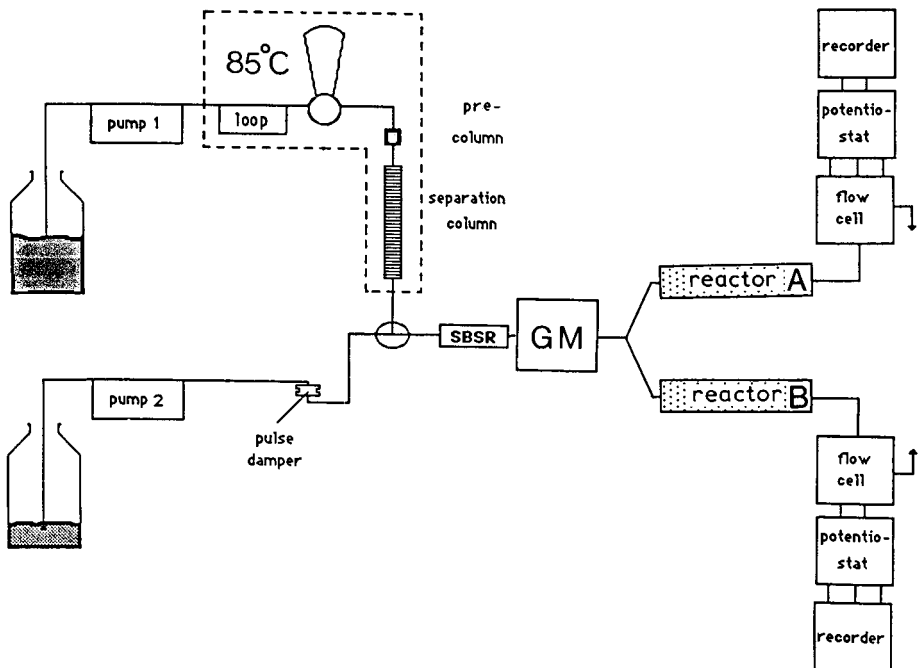


Fig. 2. Final chromatographic set-up. For details, see text.

as a lyophilized powder with an activity of 220 U mg⁻¹ protein. Based on experience, it was used as received without further treatment^{6,13}. Galactose dehydrogenase (GaDH) (E.C. 1.1.1.48) from recombinant *Escherichia coli* using *Pseudomonas fluorescens* gene, from Sigma, cat. no. G-6637, obtained as a suspension in 3.2 M ammonium sulphate with an activity of 50 U mg⁻¹ protein, was kindly donated by Mr. H. Toomson (Kebo Lab, Stockholm, Sweden).

Prior to immobilization, XI, MT and GaDH were dialysed against a large excess of 0.1 M phosphate buffer (pH 7.0) to remove the ammonia and other low-molecular-weight substances that could otherwise interfere in the immobilization reaction. The units given for XI are as described previously⁶, and those for MT, GDH and GaDH are according to the manufacturers' specifications.

Controlled-pore glass (CPG-10) from Serva, pore diameter 47 nm and particle size 37–74 µm, was washed, dried, silanized with 3-aminopropyltriethoxysilane and activated with glutaraldehyde according to previously published procedures^{16,17} before coupling of the enzymes. The Zr-silica was a zirconium-covered silica phase, LiChrospher Si-500, consisting of 10-µm spherical silica with a pore size of 500 Å, kindly donated by Mr. Gyula Szabo (Bioseparation Technologies, Budapest, Hungary). It was silanized and activated with glutaraldehyde according to the procedure outlined above for the CPG.

Enzyme reactor I. To 1 g of the activated CPG-10 support, an enzyme mixture of 746 U of XI, 17 400 U of MT, 10 000 U of GDH and 375 U of GaDH dissolved in 0.1 M phosphate buffer (pH 7.0) was added. After reducing the air pressure of the reaction mixture, the coupling was allowed to proceed overnight at 4°C. The coupling yield was determined by analysis, measuring the reaction rate of the remaining unimmobilized enzyme in the buffer solution. It was found to be 43% for XI using 500 mM D-fructose and 7.5 mM NAD⁺, 59% for GDH using 250 mM D-glucose and 2.5 mM NAD⁺ and 60% for GaDH using 250 mM D-galactose and 2.5 mM NAD⁺. The zero-order reaction conditions for evaluation were made at 25°C and in 0.1 M phosphate buffer (pH 7.0) containing 8 mM magnesium nitrate. The NADH produced was measured spectrophotometrically at 340 nm. The coupling yield for MT was not specifically evaluated^{6,13}. The enzyme-CPG was packed into a reactor having a low dead volume⁶. Throughout, a volume of 250 µl was used for this reactor.

Enzyme reactor II (denoted A in Fig. 2). To 1 g of the activated Zr-silica an enzyme mixture of 746 U of XI, 17 400 U of MT, 10 000 U of GDH and 375 U of GaDH was added.

Enzyme reactor III (denoted B in Fig. 2). To 1 g of the activated Zr-silica an enzyme mixture of 17 400 U of MT, 10 000 U of GDH and 375 U of GaDH was added. Reactors II and III were both slurry packed into 79-µl stainless-steel reactors to obtain optimum packing of the enzyme-glass using a highly viscous, 5.0 M sucrose slurry and a high-pressure pump between 0.28 and 1.12 kg m⁻². When not in use, all reactors were filled with 0.1 M phosphate buffer containing 1 M sodium chloride for stabilization of the enzymes^{12,13}.

Chemicals

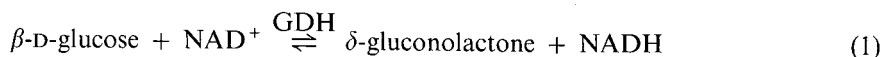
NAD⁺ and NADH were obtained from Merck (cat. no. 24542) and from Sigma (cat. no. N-8129), respectively. The sugars L-arabinose, D-xylose, D-glucose, D-cellobiose, D-galactose and D-mannose were obtained from Sigma and D-xylulose was

produced and purified in this laboratory⁷. The water used throughout was of the highest purity grade, Milli-RQ4 (Milliporé).

RESULTS AND DISCUSSION

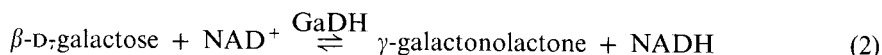
Post-column LC detection scheme

In the presence of NAD^+ , GDH catalyses the oxidation of the β -anomeric form of a series of aldoses whereby a lactone and NADH are produced. The reaction is exemplified below with the oxidation reaction of β -D-glucose:



Other carbohydrates that are oxidized according to a similar reaction scheme are D-xylose, D-mannose, D-cellobiose, D-lactose, D-ribose, D-deoxyglucose and D-glucosamine^{12,15}.

Similarly to GDH, GaDH catalyses the oxidation of the β -form of a series of carbohydrates. The best known are D-galactose and L-arabinose¹⁸:

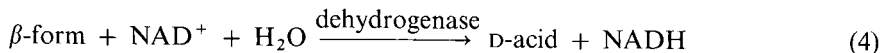


The reversibility of reactions 1 and 2 is counteracted by the irreversible addition of water to the lactone formed¹⁹:



The rate with which this addition occurs is pH dependent and is governed by a more alkaline pH, especially for the lactones produced in reaction 2²⁰.

The sum of the reactions is thus an irreversible oxidation of the β -form of the sugars:



constituting the thermodynamic driving force for the production of the NADH for which the detection system is designed (see below).

At mutarotational equilibrium, a substantial amount of each of the above-mentioned saccharides occurs in the corresponding α -anomeric form, which is not oxidizable by the dehydrogenases. To make this portion of the carbohydrates detectable and to make the detection system independent of whether mutarotational equilibrium is at hand, MT is co-immobilized with the dehydrogenases. MT catalyses the interconversion between the two anomeric forms:



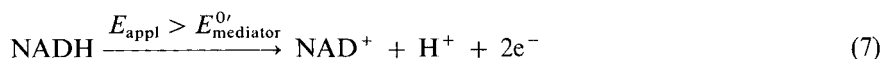
thus making the entire concentration of the saccharide detectable.

D-Xylulose is a ketose for which no commercial dehydrogenase is available for efficient oxidation and NADH production. However, D-xylulose can be isomerized to form α -D-xylose with XI:



This enzyme is best known as glucose isomerase and is commercially used for the isomerization of D-glucose to D-fructose^{21,22}. The anomeric form of the ketose taking part in reaction 6 is not fully known^{23–25}. Subsequent mutarotation of the α -D-xylose (reaction 5), and oxidation of the β -form (reaction 3), make D-xylulose detectable.

The NADH formed in the reactors is transported with the flow carrier to the electrochemical flow-through cell where it is electrochemically oxidized¹⁰. Through surface modification of the graphite electrode with an electrocatalytically active aromatic redox mediator (a bisphenoxazinyl derivative of terephthalic acid¹¹), the NADH can be selectively and rapidly oxidized at 0 mV vs. Ag/AgCl^{11,13}. The net reaction is



where E_{appl} denotes the applied potential of the modified graphite electrode and $E_{\text{mediator}}^{\text{O}}$ denotes the formal potential of the adsorbed mediator.

The modification of the electrode surface decreases the large overvoltage (*ca.* 1 V) and circumvents electrode fouling, which are serious drawbacks with the direct electrochemical oxidation of NADH^{26,27}. Most common low-molecular-weight interferents are neither oxidized nor reduced at the applied potential^{15,28}. The background current and noise levels of the graphite electrode material are also at their lowest values around 0 mV¹³. Overall, this makes the detection mode close to the optimum for the determination of NADH.

There are several aspects to be considered when making use of a sequence of enzymatic reactions in a detection system²⁹. By co-immobilizing the enzyme on the same support or in the same matrix, the reaction sites become closer and the kinetics of the reactions, converting intermediates and driving unfavourable equilibria to the product side, become more favourable than if immobilized one at a time with subsequent mixing of the different enzyme-glass portions^{29,30}. The kinetics and equilibrium of each of the different enzymatic steps in the sequence should not counteract each other and the $K_{\text{ps}}^{\text{app}}$ ($= V_{\text{max}}/K_{\text{M}}^{\text{app}}$)¹⁷ of the following enzyme in a sequence must be greater than the preceding enzyme activity²⁹.

The optimum ratio of the enzymes can be calculated on the basis of the properties of each individually immobilized enzyme. The ratio obtained when co-immobilized cannot be predicted as the kinetics, denaturation effects and overall yield of the binding reactions to the support cannot be predicted from a mixture of several enzymes. A detailed study of the optimum ratio when co-immobilizing XI, MT and GDH was made separately³¹, the influence of the thermodynamic driving force to form NADH (reaction 4) and the overall enzyme kinetics were considered. The

properties of immobilized GaDH were studied separately³². Experiments from these studies were guidelines for the enzymatic ratios used in the IMERs in this study.

Post-column parameters

pH dependence. Previous papers on reactors containing co-immobilized XI, MT and GDH have been used as parts of the detection system in both FIA^{6,31} and LC applications⁷. As an extension to our previous work, a fourth enzyme, GaDH, was co-immobilized with the other three to increase the number of detectable sugars.

To minimize band-broadening effects of the chromatographic peaks in the IMER, the volume of the reactor is necessarily small. This may result in the conversion efficiencies of some substrates being low, owing to the restricted amount(s) of immobilized enzyme(s) that can be contained within the reactor. It is therefore necessary to optimize the detection system so that the enzymes can be utilized in such a way that the highest and long-term stable response conditions prevail.

Reactor I was investigated in the FIA mode by omitting the separation column and the gradient mixer (see Fig. 2) for evaluation of the pH optimum for detection of the sugars. The substrates were injected one at a time in these experiments. Reactions 1–7 all have different pH optima. The combined effects of these reactions on the detection system are depicted in Fig. 3. The reaction rate between NADH and the adsorbed mediator on the graphite surface is governed by a more acidic pH¹⁰, which is reflected in curve b.

It was concluded from previous investigations that immobilized GDH has a broad optimum pH range^{13,15}. The responses to equal concentrations of NADH and D-glucose are almost identical at pH 6–7. At more alkaline pH, the response to D-glucose is lower than that to NADH, reflecting a decrease in the turnover rate of GDH. The addition of water to the lactone, formed in reaction 1, is governed by higher pH values which could otherwise be expected to increase the overall reaction rate (reaction 4) for NADH formation²⁰. The activity of GDH differs for the various substrates. D-Glucose (Fig. 3a) is much more efficiently oxidized than, *e.g.*, D-xylose (Fig. 3e). The effect of the addition of water to the lactone is greater for the oxidation of

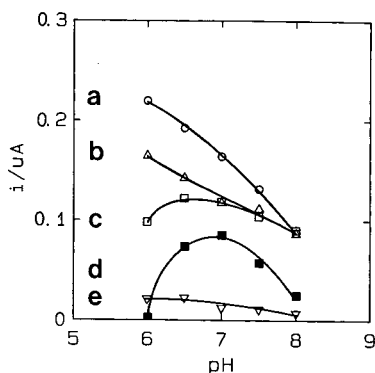


Fig. 3. Response vs. pH for 20 μ l of (a) 0.5 *M* D-glucose, (b) 0.35 *M* NADH, (c) 0.5 *M* D-galactose, (d) 9.0 *M* D-xylulose and (e) 0.15 *M* D-xylose with reactor I. The flow system was operated in the FIA mode, using 0.1 *M* phosphate buffer (pH 7.0) as the eluent (0.75 ml min⁻¹); applied potential, 0 mV vs. Ag/AgCl. For details, see text.

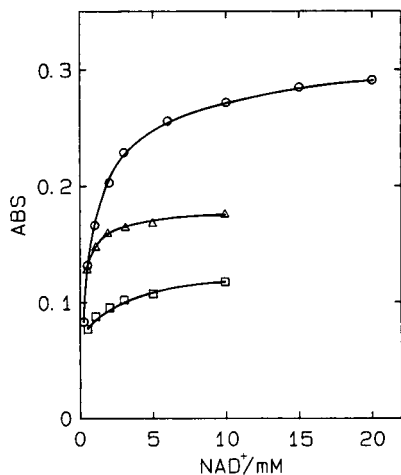


Fig. 4. Influence of the concentration of NAD^+ in the carrier flow in a flow-injection manifold on the response for (○) D-galactose (0.4 mM); (△) D-xylose (1 mM) and (□) D-xylulose (1 mM). The flow-rate through reactor I was for (○) 1.0 and for (△) and (□) 0.6 ml min^{-1} . Injection volume, 50 μl .

D-galactose (Fig. 3c), where proportionally higher response values are obtained at higher pH. The optimum response for D-xylulose is found close to pH 7, mainly reflecting the optimum activity for immobilized XI found at pH 7⁶.

The combined effects of pH on the electrocatalytic response factor, on the addition of water to the lactones and on the activities of the four co-immobilized enzymes indicate that pH 7 should be the optimum for detection, especially for the substrates with low turnover rates in the reactor, namely D-xylose and D-xylulose. This pH was therefore used throughout all the experiments described below.

NAD⁺ dependence. The dependence of the concentration of NAD^+ in the make-up flow was also investigated with the equipment used in the FIA mode and with a spectrophotometric flow-through detector, at 340 nm, for evaluation of the NADH formed. Fig. 4 shows the effect on the response for three sugars, D-galactose, D-xylose and D-xylulose, when increasing the NAD^+ concentration in the make-up flow from 0.5 to 10 mM or more. The direct influence of the NAD^+ concentration on reactions 1 and 2 is clearly depicted, in addition to the indirect influence on reactions 5 and 6 to increase the driving force for NADH production. It is also known from earlier experiments⁶ that a high concentration of NAD^+ governs the driving force for D-xylulose oxidation (reactions 5 and 6), as stated above. At a higher concentration than about 10 mM the response levels off to a constant value. Owing to the high cost of NAD^+ , a final concentration of 14 mM NAD^+ in the make-up flow was chosen, resulting in an NAD^+ concentration of 2 mM in the IMER. Response efficiencies between 72 and 90% of the maximum values at 10 mM NAD^+ in the IMER were obtained with this NAD^+ concentration for the sugars depicted in Fig. 4: D-galactose 72%, D-xylose 88% and D-xylulose 90%. These values are high enough to obtain high detection responses.

Chromatographic separation

Sugars can be separated with varying success on polymer-based ion-exchange or ligand-exchange columns. The separation is largely dependent on the cation (proton or metal ion) bound to the stationary phase and the type of sugar interacting with it³³⁻³⁵. The polymeric columns loaded with metal ions show good stabilities. Minor metal leakage may, however, occur from the resin³⁶ and may interact in a negative way when post-column immobilized enzyme reactors are used¹². The decline in performance with these columns is almost always due to the introduction of contaminants present in the sample or in the mobile phase that precipitate or clog the column. This can be overcome or at least greatly decreased by using proper sample clean-up procedures. The sugar molecules are uncomplexed in the aqueous mobile phase but are bound to the stationary phase as complexes with the metal ion. It is essential here that an aqueous mobile phase is used that is compatible with the enzyme electrochemical detection system. The dominating mechanism for separation of the sugars is mainly related to the stability constants, K_{stab} , of the complexes formed. The capacity factor, k' , can be expressed as³⁵

$$k' = V_s/V_m [M^{x+} (aq.)] K_{stab} \quad (8)$$

where V_s is the volume of the stationary phase, V_m is the volume of the mobile phase and $x+$ is the valency of the metal ion, M .

Five different metal-loaded columns and a column in the H^+ form were studied for their abilities to separate the sugars most commonly present in lignocellulose hydrolysates, *viz.*, D-glucose, D-mannose, D-galactose, L-arabinose and D-xylose. D-Xylulose and D-cellobiose were added to the mixture for reasons indicated in the Introduction. All columns used were of equal size and equal cross-linking for otherwise identical conditions when evaluating the binding interaction. Three commercially available columns were used (H^+ , Ca^{2+} and Pb^{2+}) and the other three (K^+ , Li^+ and Mg^{2+}) were prepared according to the scheme outlined under Experimental.

TABLE I

CHROMATOGRAPHIC CHARACTERISTICS OBTAINED WITH THE SIX INVESTIGATED LIGAND-EXCHANGE COLUMNS USING THE ENZYMATIC ELECTROCHEMICAL DETECTOR

Ce = D-Cellobiose, Glu = D-glucose, Xo = D-xylose, Gal = D-galactose, Ara = L-arabinose, Xy = D-xylulose, Man = D-mannose.

Ligand	Retention time (min)						
	Ce	Glu	Xo	Gal	Ara	Xy	Man
H^+	7.0	8.4	9.0	9.2	9.8	9.6	8.2
K^+	7.8	10.2	10.7	10.9	11.2	10.7	10.9
Li^+	7.6	9.2	10.3	10.4	11.8	12.0	10.8
Mg^{2+}	7.0	9.0	9.8	9.0	11.2	11.1	10.0
Ca^{2+}	8.0	10.0	10.8	11.3	13.3	13.6	11.6
Pb^{2+}	10.7	12.6	13.6	13.3	15.4	16.4	16.6

Single-line detection system

The influences of the different metal ions on the separation of the sugars present in spent sulphite liquor are shown in Table I and in Fig. 5, where the k' values are

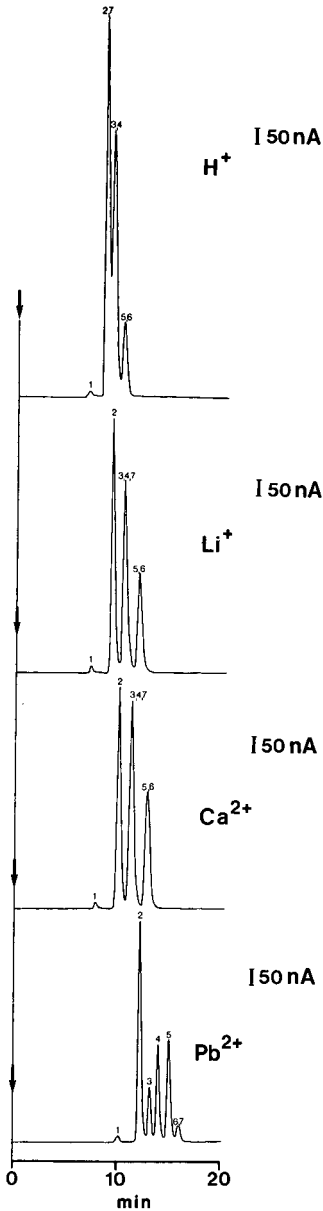


Fig. 5. Chromatograms obtained with different columns for 10 μ l of spent sulphite liquor, diluted 30-fold and spiked with D-cellobiose and D-xylulose. Column flow-rate, 0.6 ml min⁻¹; make-up, 0.1 ml min⁻¹. Concentrations of sugars: 1.5 mM D-cellobiose (peak 1), 0.7 mM D-glucose (peak 2), 1.4 mM D-xylose (peak 3), 0.4 mM D-galactose (peak 4), 0.4 mM L-arabinose (peak 5), 1.5 mM D-mannose (peak 6) and 3.6 mM D-xylulose (peak 7).

shown to increase as the stabilities of the complexes increase. Fig. 5 shows the retention patterns for some of the different columns, with increasing binding strength. Pb^{2+} has the best binding capacity for the sugar mixture. Ca^{2+} , Li^+ and Mg^{2+} have similar strengths. However, the order of retention differs for the different columns (Table I). The H^+ and K^+ columns are similar in separation capacity, having the weakest complex binders of the six types studied. The Pb^{2+} column resolves all sugars except D-mannose and D-xylulose, which elute in the same peak (6, 7 in Fig. 5). The peak is broad not only because of band broadening but also because the retention times differ but not sufficiently to result in complete separation.

The dependence of the injection volume on the resolution of these two sugars was therefore investigated to see whether a smaller injection volume could increase the resolution sufficiently to separate the two sugars. No separation between D-mannose and D-xylulose was achieved at any injection volume (data not shown). However, it can be seen from Table II, illustrating the response and band broadening at the peak half-height, $w_{\frac{1}{2}}$, that by using injection volumes larger than 100 μl a much higher response will not be obtained but rather a larger dispersion, which leads to a decrease in resolution. The choice of the injection volume will also be dependent on the concentration of the sugars in the sample. For spent sulphite liquor, a sample loop of 10 μl was chosen because it resulted in a good resolution and no substantial decrease in signal response was found compared with a 20- μl loop.

The flow-rate of the make-up and the injection volume may contribute substantially to the band broadening³⁷. It was therefore investigated whether optimizing these parameters could increase the resolution of D-mannose and D-xylulose and make their quantification possible. Fig. 6 shows the effect on the response of the flow-rate of the make-up. The optimum flow-rate yielding the highest response values was *ca.* 0.1 ml min⁻¹. In these experiments the composition of the make-up was kept constant. At lower make-up flow-rates, the sugars will be less diluted and the residence time in the IMER will be longer. These two effects will

TABLE II

INFLUENCE OF THE INJECTION VOLUME (5–200 μl) ON THE PEAK HEIGHT, AND BAND BROADENING, $w_{\frac{1}{2}}$, IN THE CHROMATOGRAMS OF 1.3 mM D-XYLOSE, 0.8 mM D-GLUCOSE, 0.5 mM D-GALACTOSE, 0.45 mM L-ARABINOSE, 30 mM D-XYLULOSE AND 2.2 mM D-CELLOBIOSE WITH REACTOR I

Flow-rate, 0.6 ml min⁻¹; make-up flow, 0.1 ml min⁻¹.

Sugar	Peak height, <i>i</i> (nA)					Peak broadening, $w_{\frac{1}{2}}$ (min)				
	Injection volume					Injection volume				
	5 μl	10 μl	50 μl	100 μl	200 μl	5 μl	10 μl	50 μl	100 μl	200 μl
D-Cellobiose	8	13	55	62	78	0.36	0.40	0.43	0.49	0.63
D-Glucose	310	505	1330	2425	3747	0.38	0.41	0.44	0.46	0.53
D-Xylose	70	105	300	550	850	0.38	0.41	0.44	0.49	0.62
D-Galactose	125	200	355	488	575	0.45	0.47	0.49	0.59	0.92
L-Arabinose	130	210	360	490	525	0.44	0.48	0.55	0.63	0.78
D-Xylulose	20	28	85	138	225	0.56	0.61	0.66	0.71	0.84

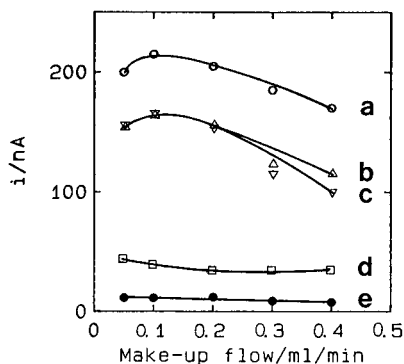


Fig. 6. Influence on the response of the make-up flow for (a) 0.7 mM D-glucose, (b) 0.7 mM D-galactose, (c) 0.73 mM L-arabinose, (d) 2.0 mM D-xylose and (e) 1.2 mM D-xylulose. Injection volume, 10 μ l; flow-rate, 0.6 ml min⁻¹.

enhance the concentration of NADH especially for the sugars that do not yield 100% conversion efficiencies to form NADH. The response of the electrochemical detector is, however, governed by a higher flow-rate. The combined effects of higher NADH concentrations at a lower flow-rate of the make-up and a higher response of the CME at a higher flow-rate of the make-up are depicted in Fig. 6. For sugars with high conversion efficiencies an increase in the flow-rate from 0.05 to 0.1 ml min⁻¹ will result in an increased response owing to a more efficient mass transport of NADH to the electrode surface. A further increase in flow-rate will only increase the band broadening of the peak and hence lower the response. For sugars with low conversion efficiencies an increase in the flow-rate from 0.05 to 0.1 ml min⁻¹ will result in a decreased response owing to a lower residence time in the IMER and hence in a lower NADH production. An optimum flow-rate of the make-up was therefore concluded to be *ca.* 0.1 ml min⁻¹ and was used for all subsequent experiments. Table III shows the response factors for the seven sugars investigated using reactor I and a flow-rate of the make-up of 0.1 ml min⁻¹. With the experimental conditions given above, the detection limits (signal-to-noise ratio 3:1) for the sugars were as follows: D-glucose 55 ng, D-galactose 81 ng, L-arabinose 80 ng, D-xylose 117 ng, D-mannose 0.79 μ g, D-xylulose 1.3 μ g and D-cellobiose 3.1 μ g.

Fig. 7 shows calibration graphs obtained under optimum conditions for D-glucose, D-galactose, L-arabinose, D-mannose and D-xylose using reactor I. As

TABLE III

EFFICIENCIES OF CONVERSION OF SUGARS TO NADH IN REACTOR I WITH THE EXPERIMENTAL PARAMETERS GIVEN IN FIG. 7

Sugar	Conversion (%)	Sugar	Conversion (%)
L-Arabinose	75	D-Mannose	5.4
D-Cellobiose	0.8	D-Xylose	14
D-Galactose	72	D-Xylulose	3.8
D-Glucose	100		

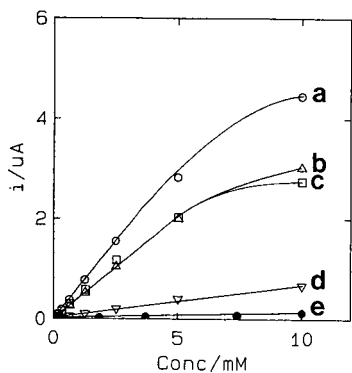


Fig. 7. Calibration graphs for (a) D-glucose, (b) D-galactose, (c) L-arabinose, (d) D-xylose and (e) D-xylulose with reactor I. Samples were prepared from reference stock solutions. Injection volume, 20 μ l; column flow-rates as in Fig. 6.

expected, rectilinear calibration graphs were obtained from the detection limit (signal-to-noise ratio 3:1) at the micromole level over more than two orders of magnitude in concentration, where the concentration of NAD^+ in the reactor, 2 mM, becomes the limiting factor^{13,15}. This makes quantification of the sugars easy. Diluting spent sulphite liquor 10–100 times prior to injection should give resulting final concentrations of sugars in the sample found within the linear response range of the detection system².

Application of the post-column set-up

A comparison is shown in Fig. 8 between the chromatograms obtained for spent

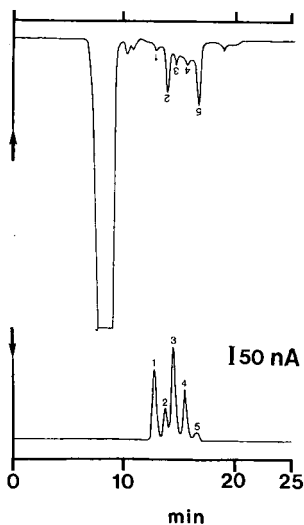


Fig. 8. Chromatograms of 20 μ l of spent sulphite liquor, diluted 100-fold, with an RI detector, attenuation 8.0 (upper), and enzyme electrochemical detector (lower). Flow-rate, 0.6 ml min^{-1} ; make-up flow, 0.1 ml min^{-1} . Concentrations found: 0.13 mM D-glucose (peak 1), 0.16 mM D-xylose (peak 2), 0.23 mM D-galactose (peak 3), 0.11 mM L-arabinose (peak 4) and 0.51 mM D-mannose (peak 5).

sulphite liquor with the enzymatic electrochemical detector and the generally used refractive index (RI) detector. The post-column detector responds selectively to the five sugars present in the sample whereas the chromatogram obtained with the RI detector shows several unidentified interfering peaks and low sensitivity and selectivity. As is clearly seen, the selectivity of the enzyme electrochemical detection makes quantitative and qualitative analysis of the contents of sugars in the sample very much easier. The main purpose of this study was to work out a sensitive and specific chromatographic system for the determination of sugars in complex biotechnical matrices, where for selectivity reasons in some instances they cannot be monitored using conventional LC detectors such as RI or UV, as shown in Fig. 8.

The inability, however, to separate D-mannose and D-xylulose is a major drawback with the system outlined above. The attempts to increase the resolution through optimization of the metal in the separation column, the injection volume and the flow-rate of the make-up flow did not solve the problem. Peak 5 in Fig. 8 may thus reflect the presence of both D-mannose and D-xylulose in the sample.

Dual-line detection system

D-Mannose is made detectable by the action of immobilized GDH (reaction 1). D-Xylulose, however, is made detectable by the subsequent action of three enzymes, XI, MT and GDH (reactions 6, 5 and 1). By omitting XI from the reactor, D-xylulose should not be detected, as GDH has no activity for D-xylulose.

The combined flow of the effluent and the make-up was therefore split into two detection streams with identical flow-rates by the use of a high-frequency gradient mixer operated in the backward mode. One of the detection streams contained a reactor with co-immobilized MT, GDH and GaDH (reactor III) and the other stream a reactor with co-immobilized XI, MT, GDH and GaDH (reactor II) (Fig. 2). As the flow is split, the resulting flow-rate will be decreased to half its value in each path. A decrease in the flow-rate may result in greater diffusion, yielding a lower resolution. However, by proper optimization of the band-broadening effects, it can be seen in Fig. 9 that this is not so.

Splitting the effluent of the column may also contribute to the band-broadening effects³⁷. To minimize this and further reduce the inherent band broadening obtained with post-column reactors, a Zr-treated silica was used as the enzyme carrier in this instance. From an earlier investigation it was found that this Zr-silica has a higher enzyme loading capacity and a higher long-term stability than CPG-10¹³. The higher loading capacity of the Zr-silica should make it possible to make smaller reactors with activity equal of that of a CPG-10 reactor. The small particle size of the Zr-silica should also be advantageous in obtaining better flow characteristics³⁷. These two Zr-silica reactors were also high-pressure packed into stainless-steel reactors (see Experimental) to obtain as uniform a packing as possible for optimum flow characteristics.

Fig. 9 shows the two chromatograms obtained for a single injection of spent sulphite liquor spiked with D-cellobiose and D-xylulose. Chromatogram B reflects the selectivity of reactor III containing co-immobilized MT, GDH and GaDH. Here all sugars except D-xylulose are selectively detected. Peak 6 therefore only reflects the concentration of D-mannose. Chromatogram A reflects the selectivity of reactor II containing co-immobilized XI, MT, GDH and GaDH. Peak 6 in this instance is the

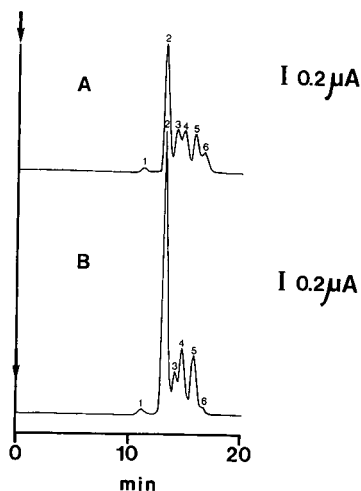


Fig. 9. Dual chromatogram for a single injection ($10 \mu\text{l}$) of spiked spent sulphite liquor diluted 10-fold, obtained with the parallel detection system of reactors II and III. Flow-rate, 0.6 ml min^{-1} ; make-up flow, 0.1 ml min^{-1} ; flow-rates through the reactors, 0.35 ml min^{-1} . Concentrations of sugars: 7.5 mM D-cellobiose (peak 1), 4.3 mM D-glucose (peak 2), 7.3 mM D-xylose (peak 3), 2.4 mM D-galactose (peak 4), 2.3 mM L-arabinose (peak 5), 4.5 mM D-mannose (peak 6 in B), 4.5 mM D-mannose and 18 mM D-xylulose (peak 6 in A).

combined response to both D-mannose and D-xylulose. By calibration of the two parallel detection paths simultaneously, the concentration of D-mannose in the sample is obtained from detector B and the concentration of D-xylulose can be calculated by subtracting the response of D-mannose from the total response current of peak 6 obtained from detector A.

TABLE IV

ANALYTICAL DATA FOR SPIKED SPENT SULPHITE LIQUOR, CHROMATOGRAPHED AND DETECTED USING THE PARALLEL DETECTION MODE DEPICTED IN FIG. 2

Reactor	Peak No. ^a	Analyte	R.S.D. (%) ($n = 10$)
II	1	D-Cellobiose	3.1
	2	D-Glucose	4.0
	3	D-Xylose	5.2
	4	D-Galactose	1.8
	5	L-Arabinose	2.2
	6	D-Xylulose/D-mannose	3.8
III	1	D-Cellobiose	5.1
	2	D-Glucose	1.7
	3	D-Xylose	2.8
	4	D-Galactose	3.7
	5	L-Arabinose	1.8
	6	D-Mannose	3.9

^a For peak identification, see Fig. 8.

The volume of reactor I is 250 μl whereas that of each of reactors II and III is only 79 μl . Even though a better support was chosen for making reactors II and III, the decrease in reactor volume to only 79 μl has the result that the conversion efficiency for none of the sugars reached 100%. The splitting of the flow after addition of the make-up will also decrease the flow-rate through each of the detection paths compared with the use of only one detection path (reactor I). Therefore, the signal responses to the sugars will decrease and the detection limits will increase compared with the single-line detection system. The repeatability, expressed as relative standard deviation (R.S.D., %), for ten injections of the spiked spent sulphite sample is given in Table IV, and was typically less than 6%.

CONCLUSIONS

The use of a selective post-column detection device based on immobilized enzymes is clearly demonstrated to be preferred to the generally used RI detector. Spent sulphite liquor constitutes a complex matrix for which an unselective detector is non-optimum. Even if separation problems have not been fully solved, the use of two enzyme-based selective detection systems working in parallel can solve a specific problem. The parallel detection system also greatly reduces the laboratory time and amount of equipment because only a single injection is required with one chromatographic system to give a true picture of the composition of the sample.

Reactor I retained 85% of its initial activity after 3–4 weeks. A faster deactivation of the IMERs was observed when the detection system was applied to the determination of sugars in spent sulphite liquor compared with standard solutions prepared in pure water. This may be due to inadequate clean-up of the spent sulphite liquor in which a large number of compounds in the complex matrix may be present which can interact with, inhibit or denature the enzymes. A more elaborate sample clean-up step including a solid-phase extraction procedure is therefore currently being studied in order to overcome this problem and also to make it possible to use this separation and detection system to follow the fermentation of spent sulphite liquor to ethanol described in the Introduction.

ACKNOWLEDGEMENTS

This investigation was financially supported by the Swedish Board for Technical Development (STU) and the National Energy Administration (STEV). E.D. was the recipient of a post-doctoral fellowship from the Spanish Ministry of Education and Science. The authors thank Dr. I. Csiky, Fermenta Products, Strängnäs, Sweden, for constructive and valuable discussions concerning this work.

The gifts of the XI preparation from Miles Kalie Chemie, the GaDH preparation from Mr. H. Toomson, Kebo Lab, the Zr-silica from Mr. Gy. Szabo, Bioseparation Technologies, and the solid-phase extraction columns from Mr. G. Oresten, Sobent, and the loan of chromatographic apparatus from Miss L. Holmertz, Pharmacia/LKB, Lund, Sweden, are all gratefully acknowledged.

REFERENCES

- 1 K. Skoog and B. Hahn-Hägerdal, *Enzyme Microb. Technol.*, 10 (1988) 66.
- 2 T. Lindén and B. Hahn-Hägerdal, *Biotechnol. Tech.*, 3 (1989) 189.
- 3 F. Tjerneld, I. Persson, P.-Å. Albertsson and B. Hahn-Hägerdal, *Biotechnol. Bioeng. Symp.*, No. 15 (1985) 419.
- 4 B. Hahn-Hägerdal, S. Berner and K. Skoog, *Appl. Microbiol. Biotechnol.*, 24 (1986) 287.
- 5 T. Lindén and B. Hahn-Hägerdal, *Enzyme Microb. Technol.*, 11 (1989) 583.
- 6 E. Dominguez, B. Hahn-Hägerdal, G. Marko-Varga and L. Gorton, *Anal. Chim. Acta*, 213 (1988) 139.
- 7 G. Marko-Varga, E. Dominguez, L. Gorton and B. Hahn-Hägerdal, *Anal. Chim. Acta*, 225 (1989) 263.
- 8 R. W. Murray, A. G. Ewing and R. A. Durst, *Anal. Chem.*, 59 (1987) 379A.
- 9 S. Dong and Y. Wang, *Electroanalysis*, 1 (1989) 99.
- 10 L. Gorton, *J. Chem. Soc., Faraday Trans. I*, 82 (1986) 1245.
- 11 L. Gorton, B. Persson, M. Polasek and G. Johansson, *Proceedings of ElectroFinnAnalysis, 1988*, Plenum Press, New York, in press.
- 12 G. Marko-Varga, *J. Chromatogr.*, 408 (1987) 157.
- 13 G. Marko-Varga, *Anal. Chem.*, 61 (1989) 831.
- 14 E. Hoffmann, G. Marko-Varga, I. Csiky and J. Å. Jönsson, *Int. J. Environ. Anal. Chem.*, 25 (1986) 161.
- 15 R. Appelqvist, G. Marko-Varga, L. Gorton, A. Torstensson and G. Johansson, *Anal. Chim. Acta*, 169 (1985) 237.
- 16 H. H. Weetal and R. A. Messing, in M. L. Hair (Editor), *The Chemistry of Biosurfaces*, Vol. II, Marcel Dekker, New York, 1972, Ch. 12.
- 17 G. Johansson, L. Ögren and B. Olsson, *Anal. Chim. Acta*, 145 (1983) 71.
- 18 T. E. Barman, *Enzyme Handbook*, Vol. I, Springer, Heidelberg, 1969, p. 72.
- 19 R. Vormbrock, in H. U. Bergmeyer (Editor), *Methods of Enzymatic Analysis*, Vol. 6, Verlag Chemie, Weinheim, 3rd ed., 1984, p. 172.
- 20 B. J. van Schie, R. J. Rouwenhorst, J. A. M. De Bont, J. P. van Dijken and J. G. Kueven, *Appl. Microbiol. Biotechnol.*, 26 (1987) 560.
- 21 W.-P. Chen, *Process Biochem.*, June/July (1980) 30.
- 22 W.-P. Chen, *Process Biochem.*, August/September (1980) 36.
- 23 K. J. Schray and I. A. Rose, *Biochemistry*, 10 (1971) 1058.
- 24 J. M. Young, K. J. Schray and A. S. Mildvan, *J. Biol. Chem.*, 250 (1975) 9021.
- 25 H. Kersters-Hilderson, M. Claeysens, C. Van Doorslaer and C. K. De Brutne, *Carbohydr. Res.*, 47 (1976) 269.
- 26 Z. Samec and P. J. Elving, *J. Electroanal. Chem.*, 144 (1983) 217.
- 27 J. Moiroux and P. J. Elving, *J. Am. Chem. Soc.*, 103 (1980) 6533.
- 28 A. Schelter-Graf, H.-L. Schmidt and H. Huck, *Anal. Chim. Acta*, 163 (1984) 299.
- 29 S. P. J. Brooks and C. H. Suelter, *Anal. Biochem.*, 176 (1989) 1.
- 30 B. Mattiasson, in T. N. S. Chang (Editor), *Biomedical Applications of Immobilized Enzymes and Proteins*, Vol. 2, Plenum Press, New York, 1977, p. 261.
- 31 E. Dominguez, G. Marko-Varga, B. Hahn-Hägerdal and L. Gorton, in preparation.
- 32 G. Marko-Varga, Lund, unpublished results, 1987.
- 33 P. Jonsson and O. Samuelsson, *Anal. Chem.*, 39 (1967) 1156.
- 34 S. J. Angyal, *Pure Appl. Chem.*, 35 (1973) 131.
- 35 R. W. Goulding, *J. Chromatogr.*, 103 (1975) 229.
- 36 P. Vrátný, U. A. Th. Brinkman and R. W. Frei, *Anal. Chem.*, 57 (1985) 224.
- 37 I. S. Krull (Editor), *Reaction Detection in Liquid Chromatography*, Marcel Dekker, New York, 1986.

CHROMSYMP. 1728

Coupling of microcolumn high-performance liquid chromatography with Fourier transform infrared spectrometry

KIYOKATSU JINNO* and CHUZO FUJIMOTO

School of Materials Science, Toyohashi University of Technology, Toyohashi 440 (Japan)

SUMMARY

The coupling of high-performance liquid chromatography with Fourier transform infrared spectrometry is discussed, with emphasis on recent work by the authors' group.

INTRODUCTION

Infrared spectrometry has several important characteristics which make it a potentially ideal detection method for chromatography¹⁻⁴. Most organic (and many inorganic) compounds have strong, relatively narrow absorption bands in the mid-infrared region that are highly specific and give detailed structural information about the compound. Even when an unequivocal identification is impossible, isomeric substitution pattern information can be obtained from the fingerprint region. Moreover, different functional groups have characteristic infrared bands, and hence the presence or absence of a class of compound can be quickly verified if the species are present in sufficient concentration. In this regard, IR spectrometry possesses many attributes expected of universal or selective detectors.

The combination of high-performance liquid chromatography (HPLC) with Fourier transform IR spectrometry (FT-IR) is not at as advanced state of development as that of gas chromatography (GC) with FT-IR. Although there are several reasons for the poor performance of these techniques, the most important is related to the IR absorbance of the mobile phase. All HPLC mobile phases absorb IR radiation at certain wavenumbers, and as the mobile phase is present at a much higher concentration than the sample components in HPLC, sample spectra can only be obtained in regions of the spectrum free from solvent absorption bands. Water and methanol, which are common polar solvents used in reversed-phase HPLC, completely obscure solute bands across the spectrum. Hence the observation and identification of trace compounds of interest in the presence of the HPLC mobile phase are major problems in using IR detection in HPLC. Therefore, two major approaches to HPLC-FT-IR has been proposed, namely flow-cell methods with using less conven-

tional solvents⁵⁻¹² as the mobile phase and the solvent-elimination technique with more conventional solvents¹³⁻²³.

FLOW-CELL APPROACH IN MICROCOLUMN HPLC-FT-IR

In spite of the mobile-phase restriction, the flow-cell method provides the simplicity of interfacing and real-time monitoring of the chromatographic effluent and universal applicability to samples. If a solvent that has favourable transparency in regions separated from most of the analyte absorptions can be selected, the method offers the potential to serve as a universal or functional group-selective detector⁵⁻¹².

Perfluorinated solvents are typically such mobile phases and can be employed for the IR detection of sample components having C-H fragments in their structures^{5,6}. Deuterated solvents are also reasonably transparent in certain narrow spectral regions, especially with very short path-length flow cells⁷⁻¹². Further, there is an even greater range of choice of polarity with the latter than the former.

Microcolumns were easily incorporated into this combined technique because, although the high cost of such solvents precludes their use as mobile phases in conventional HPLC, microcolumn HPLC does provide opportunities for their use because of the low solvent consumption. The use of microcolumns has the further advantage that the effluent concentration is much increased over that with a conventional analytical column for a constant amount of sample injected. A higher analyte concentration means that short path-length flow cells can be employed, thereby allowing for wider IR window regions or the achievement of greater detector sensitivity for a fixed cell path length.

A laboratory-constructed flow cell for microcolumn HPLC-FT-IR is shown in Fig. 1⁸. A window cut out of a silver chloride pellet was employed, which allowed us

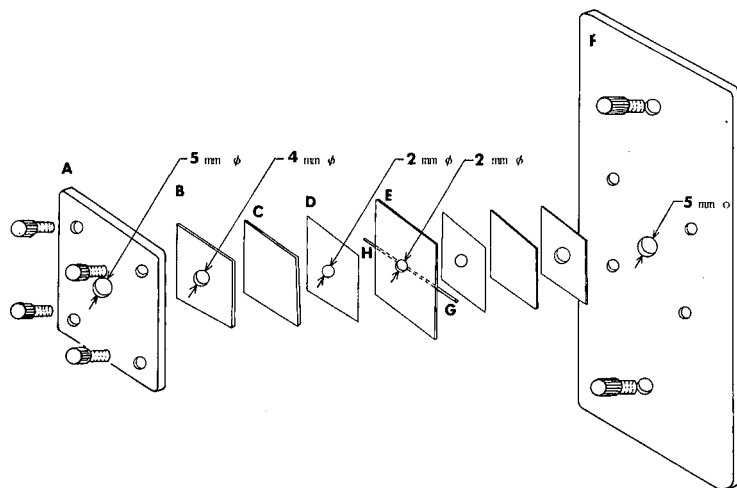


Fig. 1. Micro flow cell with minimized internal volume ($1.3 \mu\text{l}$) for microcolumn HPLC-FT-IR. A = Window holder; B = 1-mm PTFE pad; C = 0.5-mm AgCl window; D = 0.07-mm PTFE pad; E = 0.4-mm cell body; F = window holder for mounting; G = inlet tube (0.13 mm I.D.); H = outlet tube (0.31 mm I.D.). (From ref. 8 with permission.)

to observe several spectroscopically important regions, owing to its complete transparency across the entire spectrum. The assembly was mounted on the sample holder of a beam condenser in the sample compartment of a JEOL JIR 40X FT-IR spectrometer (JEOL, Tokyo, Japan). The total cell volume, including a 2-cm length of inlet tube for the cell, was estimated to be about $1.6 \mu\text{l}$; this volume is still larger than that of a UV detector used in microcolumn HPLC. The absorption of the three most commonly used solvents for reversed-phase HPLC (water, methanol and acetonitrile) is much stronger than that of any of the solvents considered below. Although the spectrum of acetonitrile is less strongly absorbing than that of methanol, the presence of even 10–20% of water will make reversed-phase HPLC-FT-IR measurements extremely difficult and very short path-length cells should be employed, as shown in Fig. 2, where IR spectra of mixtures of acetonitrile, methanol and water and their deuterated counterparts are illustrated².

In terms of solute detection (rather than solute identification), it is essential to find solvents that are transparent to IR radiation at the wavenumbers of interest. There is no doubt that deuterated solvents satisfy this requirement, as shown in Fig. 2. A comparison of the FT-IR chromatograms of phthalates, separated by reversed-phase HPLC using deuterated and non-deuterated solvents, is shown in Fig. 3. By using the deuterated solvents, the chromatographic peaks measured at 2965 cm^{-1} (C–H stretching) appeared, which were not clearly distinguished from the baseline fluctuation when the non-deuterated solvents were used as the mobile phase. Also, more sensitive detection is achieved at 1300 and 1730 cm^{-1} , corresponding to C–O and C=O stretching vibrations, respectively: it seems likely that the reduced absorbance at these wavenumbers for the deuterated solvent accounts for the results⁸.

SOLVENT-ELIMINATION APPROACH IN MICROCOLUMN HPLC-FT-IR

It should be noted that the real utility of IR spectrometry is, most often, not in the availability of the chromatogram, but in that of the spectrum of the eluate. Obviously, the only way to avoid the solvent interference problem is to eliminate the solvent prior to the IR measurements. Here all of the spectrum could be observed, not just those bands in window regions of the mobile-phase solvent spectrum, and the concentration of the analyte in the IR beam could be increased. Therefore, various solute transport designs have been proposed to improve the identification capability of HPLC-FT-IR. Because of the reduced flow-rate, microcolumn HPLC again has great promise for this type of interfacing. The "buffer-memory" technique was developed to realize this advantage in HPLC-FT-IR^{13–20}. The principle of the buffer-memory technique involves continuous deposition of the total column effluent on an IR-transparent medium such as a potassium bromide crystal plate, followed by the analysis of the eluates left on the collection medium as a function of the distance moved of the medium by transmission spectrometry. It is fairly easy to preserve a single substrate. Because the sample is left as a permanent record of the separation, more information can be effectively delivered to the analyst if the "memory" is accessed by other instrumental methods. In other words, because all information on the sample is stored in the memory, one can extract the desired information from it. In this sense, the substrate might be likened to a computer disk.

A typical example will be presented to demonstrate the potential of the proposed

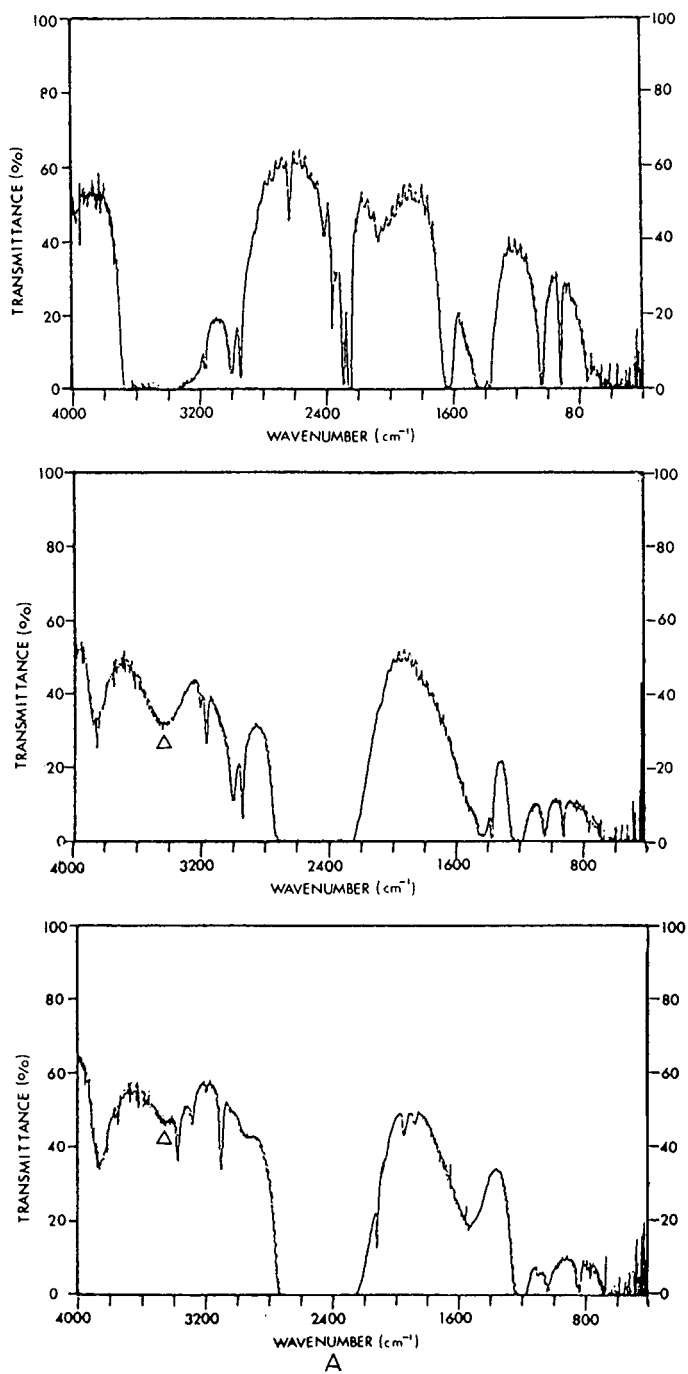


Fig. 2.

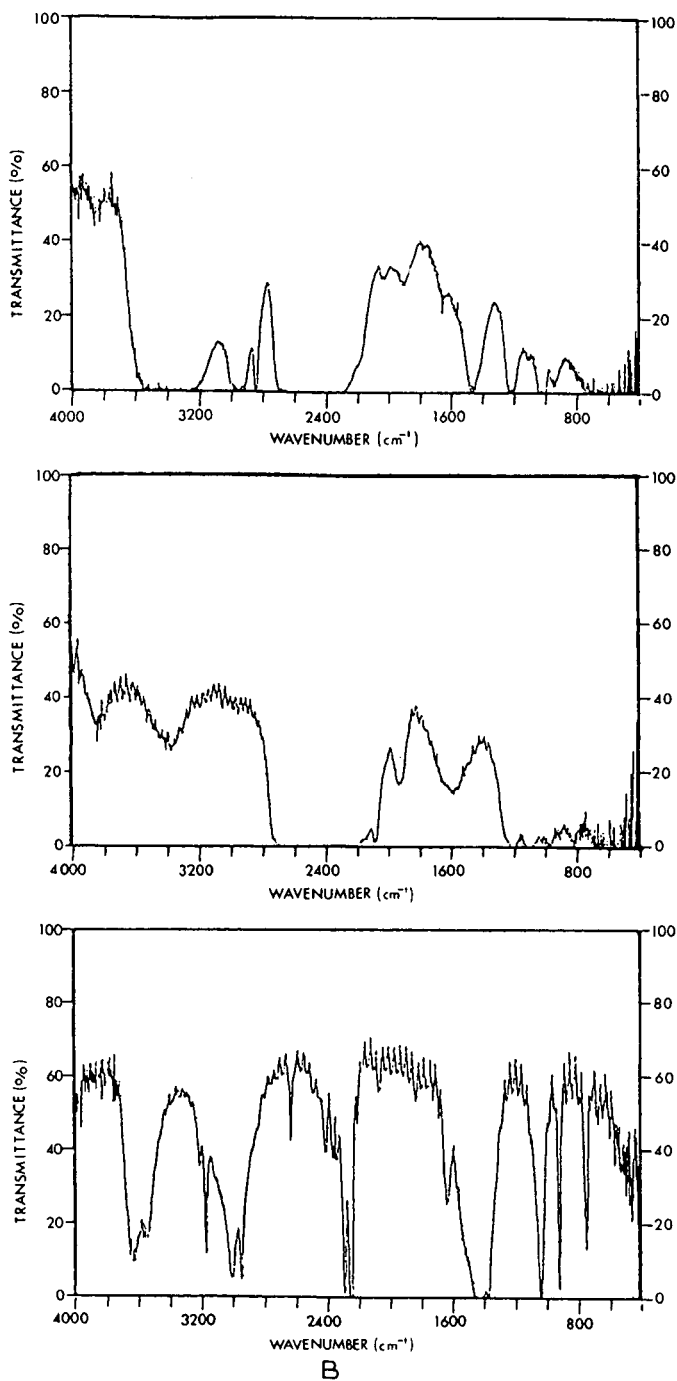


Fig. 2. IR spectra of deuterated and non-deuterated solvents used for reversed-phase chromatography. (A) Acetonitrile-water: top, CH₃CN-H₂O (90:10); middle, CH₃CN-²H₂O (50:50); bottom, C²H₃CN-²H₂O (50:50). (B) Methanol-water: top, CH₃OH-²H₂O (50:50); middle, C²H₃O²H-²H₂O (50:50); bottom, CH₃CN-H₂O (99:1). (From ref. 2 with permission.)

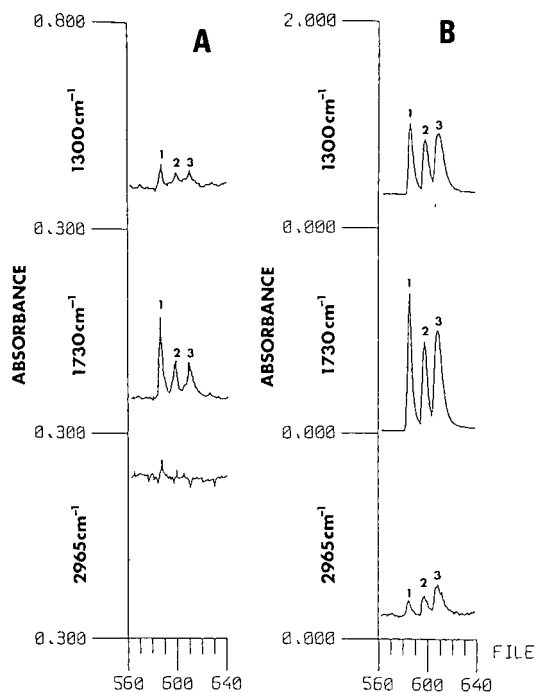


Fig. 3. Reversed-phase separation of phthalates: (A) with acetonitrile–water (90:10); (B) with the deuterated solvents ($C^2H_3CN-2H_2O$) (90:10). Column, Chemcosorb ODS-H (14 cm \times 0.5 mm I.D.); flow-rate, 4 μ l/min; FT-IR accumulation, 10 times. Solutes: 1, dimethyl phthalate (14 μ g); 2, di-*n*-butyl phthalate (13 μ g); 3, di-*n*-pentyl phthalate (17 μ g).

buffer-memory technique, which can be conveniently employed for the sequential analysis of chromatographically separated organic and organically bounded metal species by spectrometric methods. The concept includes the utilization of the proposed technique for *in situ* measurements by IR and X-ray fluorescence (XRF) spectrometry followed by mass spectrometric (MS) detection in order to elucidate the structures of unknown analytes.

To demonstrate the feasibility and usefulness of the proposed concept, a solution of metal diethyldithiocarbamate (DDTC) complexes was prepared. Three DDTC complexes, bis(diethyldithiocarbamato)copper(II), tris(diethyldithiocarbamato)chromium(III) and tris(diethyldithiocarbamato)cobalt(III), were dissolved in chloroform at concentrations of 1, 1.5 and 1.5% (w/v), respectively. Fig. 4 shows the IR transmittance chromatogram monitored at 1265 cm^{-1} after the eluent had been deposited and collected on a potassium bromide plate.

XRF spectra can then be measured without removing the HPLC peak of interest from the potassium bromide plate. The memorized plate is placed in a simple holder made of acrylic resin and moved manually through intervals as small as 1 mm in the Ge K X-ray beam to obtain the XRF spectra. The XRF spectrometer used was of the energy-dispersive type, therefore permitting simultaneous multi-element detection. One of the spectra obtained in this way is shown in Fig. 5. The fluorescence peaks of Cr,

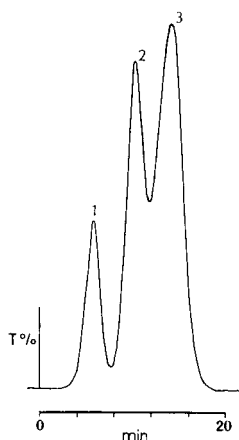


Fig. 4. IR chromatogram from a mixture of three DDTC complexes¹⁶. Mobile phase, benzene; flow-rate, 8 μ l/min. The three complexes are (1) DDTC-Cu^{II}, (2) DDTC-Cr^{III} and (3) DDTC-Co^{III} (1.0, 1.5 and 1.5%, w/w, respectively). Monitoring at 1265 cm^{-1} .

Cu, Al and K, together with the Ge scattering peak, are clearly visible. The Al peak originates from the material of beam coursing.

The peak area of each analyte fluorescence was plotted against the retention time, where normalization has been performed by using the Al peak. Fig. 6 demonstrates the resulting chromatograms for each analyte metal. Although some peak broadening can be seen, which can be mainly attributed to the use of an X-ray beam mask which was larger than the width of the aperture used in the IR experiment.

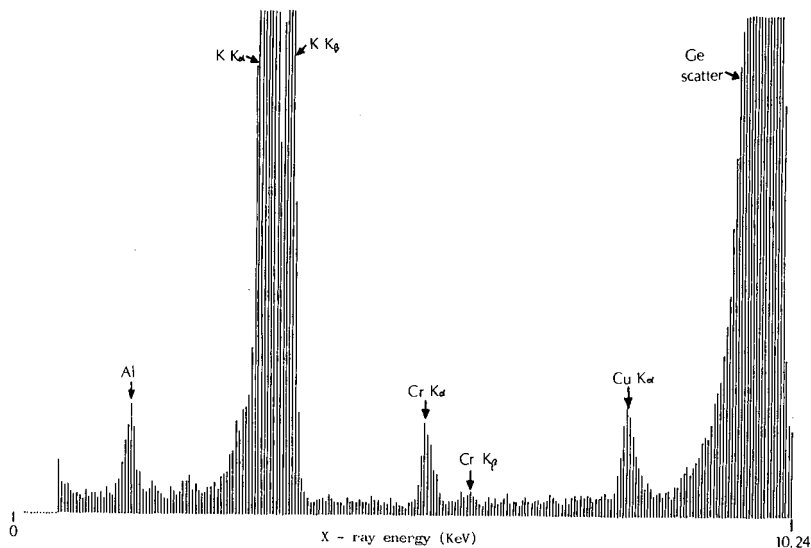


Fig. 5. XRF spectrum obtained through excitation of the species memorized on a potassium bromide plate with Ge K X-rays¹⁶. Counting time (live), 100 s.

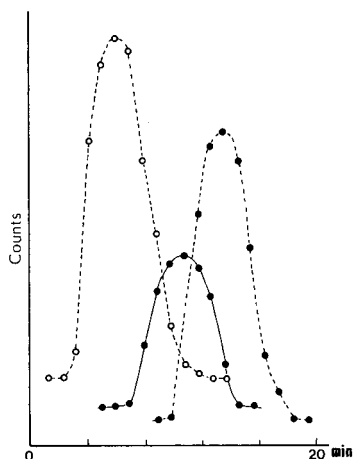


Fig. 6. Metal chromatograms obtained by XRF¹⁶. ○ = 8.05 keV; ● (solid line) = 5.42 keV; ● (dashed line) = 6.93 keV.

the peak maxima coincide in position with those of the IR chromatogram. A comparison between the two sets of chromatograms implies that the peaks labelled 1, 2 and 3 in Fig. 4 are due to copper-, chromium- and cobalt-containing species, respectively. Following the XRF measurements, the structure of the deposited components can be confirmed by mass spectrometry. The peaks were scraped off the plate with a clean blade and introduced into the ion source using a direct-insertion probe. As expected, the mass spectra were in excellent agreement with those of authentic samples.

As described above, a new dimension has been added to the spectrometric detection and identification of HPLC-separated species. The buffer-memory technique provides some benefits with respect to both IR absorption detection and metal detection. To our knowledge, such an attempt has never been made in the area of chromatography. In most instances, chromatographic effluents are discarded after detection. Alternatively, the fractions may be taken in a fraction collector and subsequently analysed by a different technique. However, the method does have limitations, for example, one will have difficulty in storing the solute-containing vials as the number of isolated fractions increases, and spectroscopic retrieval at any point of the chromatogram is, in principle, impossible. In contrast, the substrate used in the buffer-memory technique also serves as a storage device.

Although the buffer-memory technique has been demonstrated to be a powerful interfacing technique between HPLC and FT-IR, it cannot tolerate the aqueous mobile phases used in reversed-phase chromatography because they are of comparatively low volatility and readily dissolve potassium bromide. Instead of the potassium bromide plate, a stainless-steel wire net can be utilized as a buffer-memory substrate¹⁷. The effluent from a reversed-phase microcolumn is deposited on the metal wire net from which the aqueous solvent is evaporated using a heated nitrogen flow, so that the deposit is suspended between the metal meshes. The separation of three cold medicine components is shown in Fig. 7. No interference from the mobile phase solvents, water and methanol, is seen in the three-dimensional chromatogram.

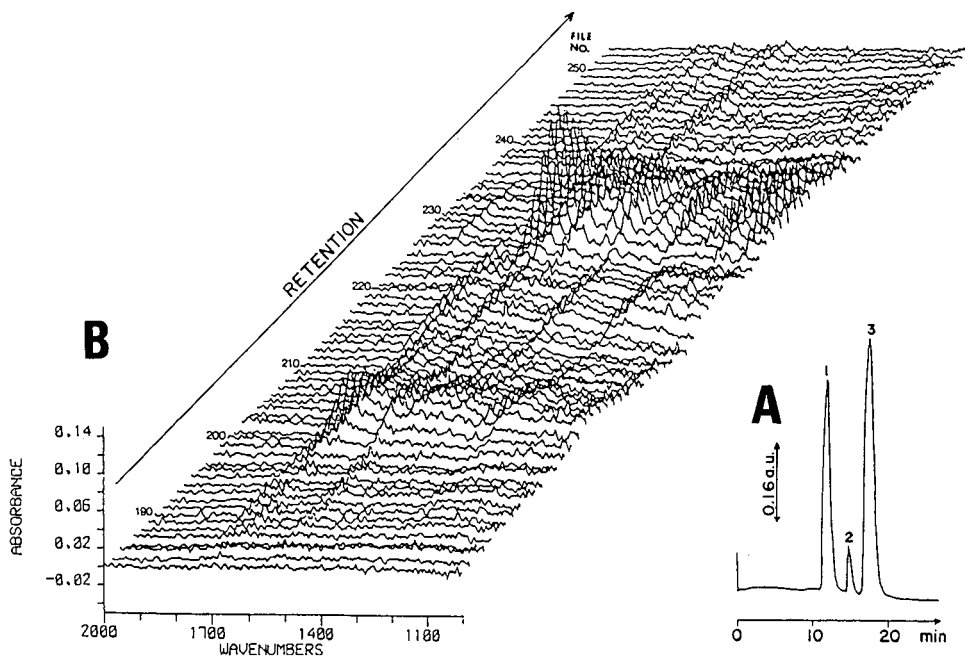


Fig. 7. Reversed-phase separation of caffeine, aspirin and phenacetin with (A) UV and (B) FT-IR detection via the buffer-memory technique¹⁷. Column, 25 cm \times 0.5 mm I.D., Develosil ODS-10; mobile phase, methanol-water (3:2); flow-rate, 4 μ l/min; accumulation, 100 times. Peaks: 1 = caffeine; 2 = aspirin; 3 = phenacetin.

The merit of the buffer-memory technique compared with several other approaches can be found in the combination of HPLC, thin-layer chromatography (TLC) and FT-IR^{18,19}. The combination of HPLC with TLC utilizes two-dimensional development and hence gives a better analytical performance. In HPLC-TLC, a sample can be subjected to two separation processes at right-angles to each other. The total column effluent from microcolumn HPLC can be deposited on the TLC plate as a continuous line, and the plate developed by the usual process. After development, one can use diffuse-reflectance IR detection to measure the IR spectra of the sample spots on the TLC plate without the need for any chemical process.

It is well known that all adsorbents used for TLC show strong absorption of IR radiation. The diffuse-reflectance IR spectra of silica gel and alumina on TLC substrates are shown in Fig. 8. It is seen that the percentage of IR radiation diffusely reflected from both adsorbents is significantly less than that from potassium bromide powder. Alumina has a wider spectral window than silica gel, which means that more spectral information can be obtained with alumina than with silica gel. It is expected that diffuse-reflectance measurements will be impossible in the frequency range below 1200 cm^{-1} because of the strong absorptivity of alumina in this region. However, an alumina TLC plate was preferred in this example, as the remainder of the spectrum is transparent enough to allow spectral measurements of compounds on the plate.

A typical eight-component separation was performed by reversed-phase microcolumn HPLC and the components deposited on the alumina TLC plate were

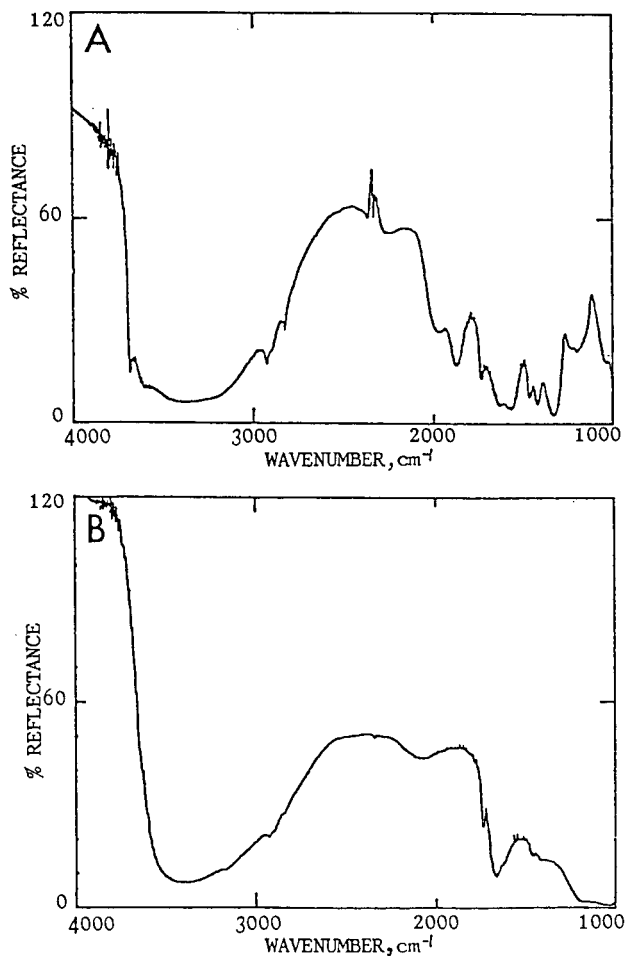


Fig. 8. Diffuse-reflectance IR spectra of (A) silica TLC plate and (B) alumina TLC plate measured by using potassium bromide powder as a reference.

subjected to diffuse-reflectance IR measurements. The collected track on the plate gave the reconstructed IR chromatogram shown in Fig. 9. As can be seen, four major peaks appear in the IR chromatogram (using UV detection, a similar chromatogram was obtained)¹⁹. By retrieving the filed spectra, one can obtain the IR spectra corresponding to the four separated peaks. One of the spectra is shown in Fig. 10, where the spectra of peak 3 in Fig. 9 were retrieved from the appropriate files. After the second development by normal-phase TLC, IR measurements were performed by scanning the plate and the reconstructed FT-IR chromatograms on the TLC plate are summarized in Fig. 11, which clearly indicates eight peaks. The spectrum of each peak can be easily called from the computer file. The spectra obtained are illustrated in Fig. 12, where identifiable spectra with even narrow wavenumber regions are seen. The spectrum of peak 8 is clearly consistent with that of peak 3 in Fig. 9. This means that

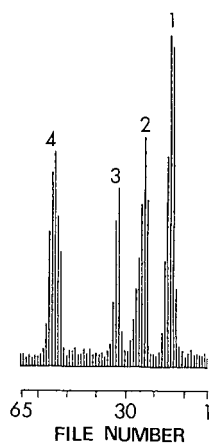
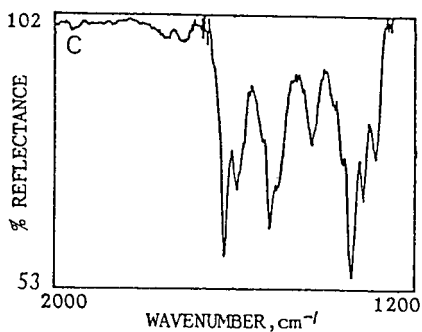
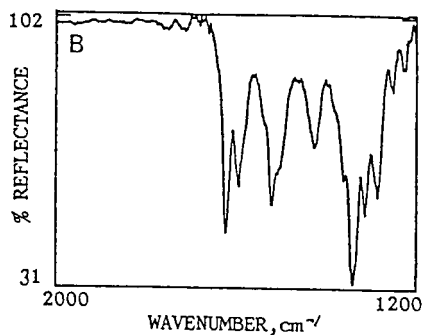
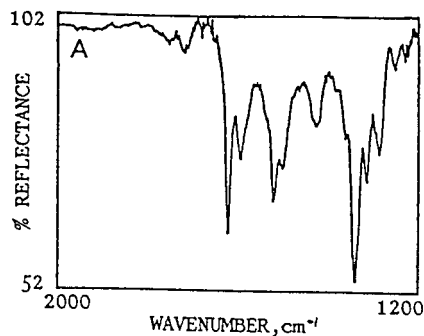


Fig. 9. FT-IR reconstructed chromatogram of the eight-component mixture after deposition of the microcolumn HPLC eluent on an alumina TLC strip at a speed of 1 mm/min. Column for HPLC: 30 cm \times 0.53 mm I.D., Vydac 201 TPB5; mobile phase, methanol-water-acetone (60:35:5); flow-rate, 2.67 μ l/min. (Reproduced from ref. 19 with permission.)

Fig. 10. File IR spectra from peak 3 in Fig. 9. (A) File No. 31; (B) file No. 32; (C) file No. 34.



TLC development did not lead to any problems in obtaining identifiable IR spectra. The detection limit of this microcolumn HPLC-TLC-FT-IR measurements has been calculated and the diffuse-reflectance IR spectrum of 50 ng of *o*-nitroaniline on an alumina TLC plate shown in Fig. 13 suggests that the limit is close to subnanogram amounts.

The buffer-memory interface has been adopted in a commercially available device (JEOL, Japan) with a rotating 50-mm diameter potassium bromide disk²⁰. Fig.

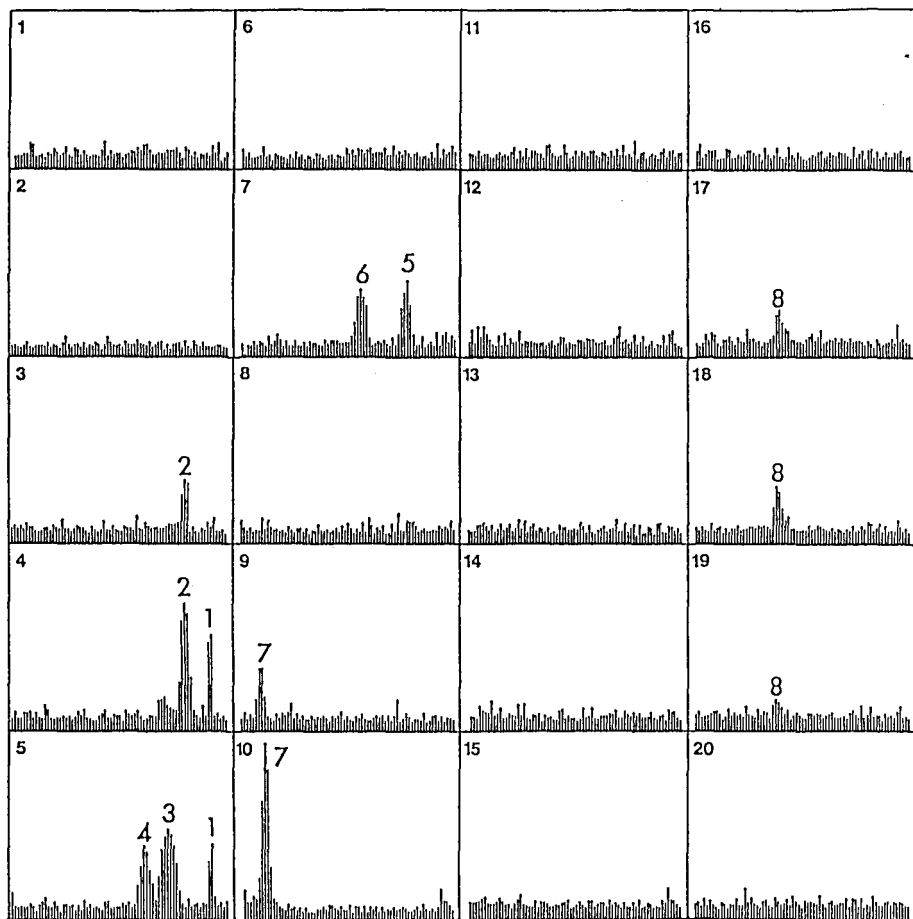


Fig. 11. FT-IR reconstructed chromatograms obtained after the HPLC deposits had been developed on the alumina TLC plate with chloroform-*n*-hexane (50:50). (From ref. 19 with permission).

14 shows the collection device. The disk is placed in a circular stainless-steel holder with a 5-mm high flange and locked by means of a constant spring at the side of the flange. The disk holder has an opening 8 mm wide, and is about 110 mm long near the edge at the base to allow an IR beam to pass through the holder with a crystal in place. The chromatographic effluent is brought onto the salt surface as the disk rotates. The turning speed of the disk can be changed between 2 and 198 min per revolution by the motor drive. After the chromatographic run, the salt disk, together with the holder, is removed from the holder mounting shaft and then transferred to a $3 \times$ beam condenser that is equipped with a disk rotary assembly whose construction is the same as that outlined above. The disk is rotated once again with the identical drive unit and spectral data are continuously obtained by using GC-FT-IR software.

To illustrate the performance of this device, a separation of polymer additives was performed on a 20 cm \times 0.53 mm I.D. fused-silica size-exclusion chromato-

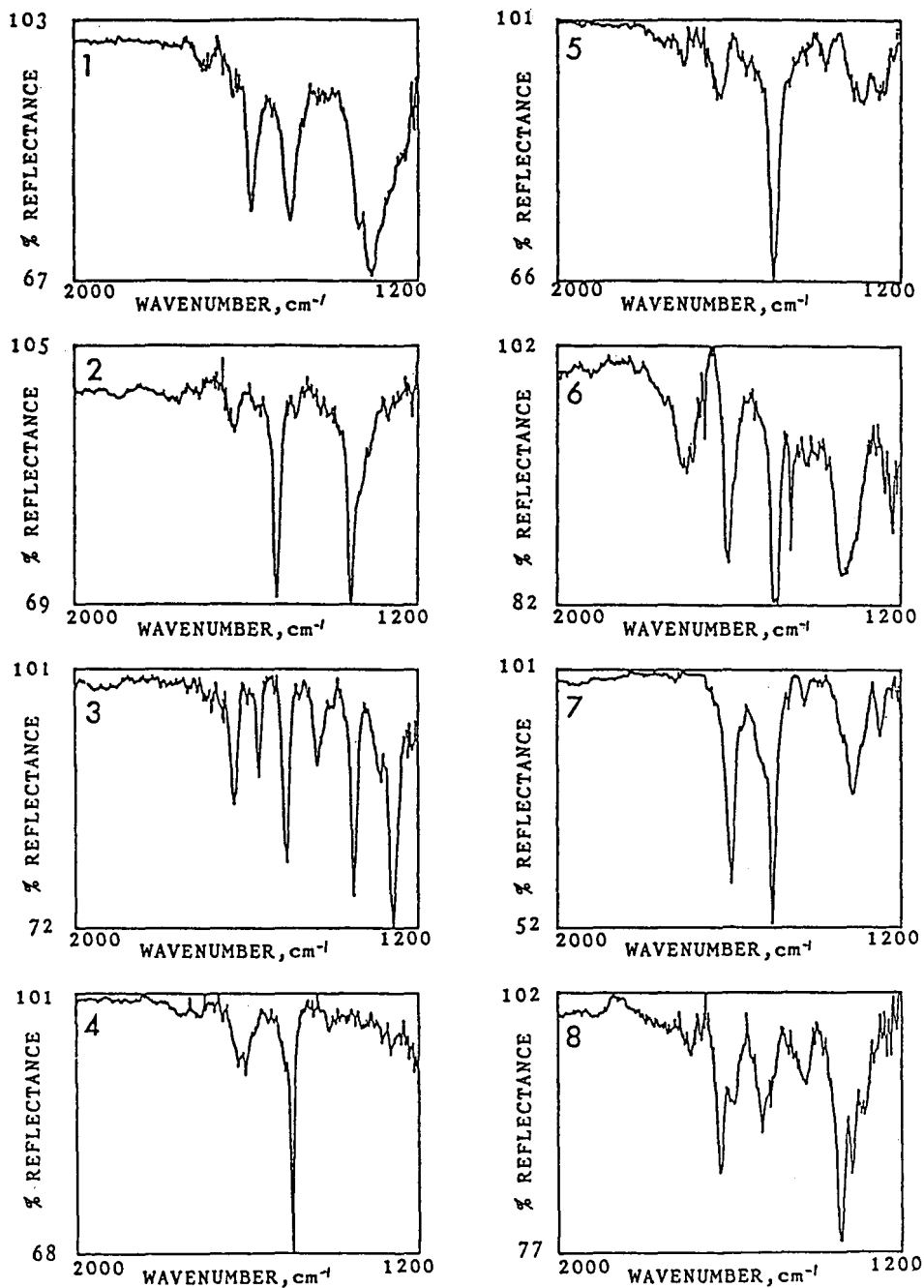


Fig. 12. Filed IR spectra of the components of the test mixture in Fig. 11. (From ref. 19 with permission.)

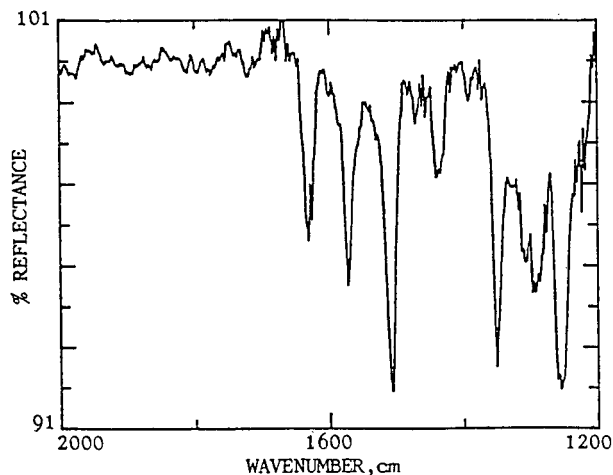


Fig. 13. Diffuse-reflectance IR spectrum of *o*-nitroaniline for a 50-ng amount collected on an alumina TLC plate.

graphic (SEC) column with tetrahydrofuran as the mobile phase²¹. The resulting Gram-Schmidt reconstructed chromatogram for 6 μ g injected is shown in Fig. 15. The high signal-to-noise ratio confirms that the detection limit by this technique will be considerably lower than the amount injected (60 ng). Representative IR spectra are shown in Fig. 16.

OTHER APPROACHES IN MICROCOLUMN HPLC-FT-IR

Various other promising approaches in microcolumn HPLC-FT-IR can be considered.

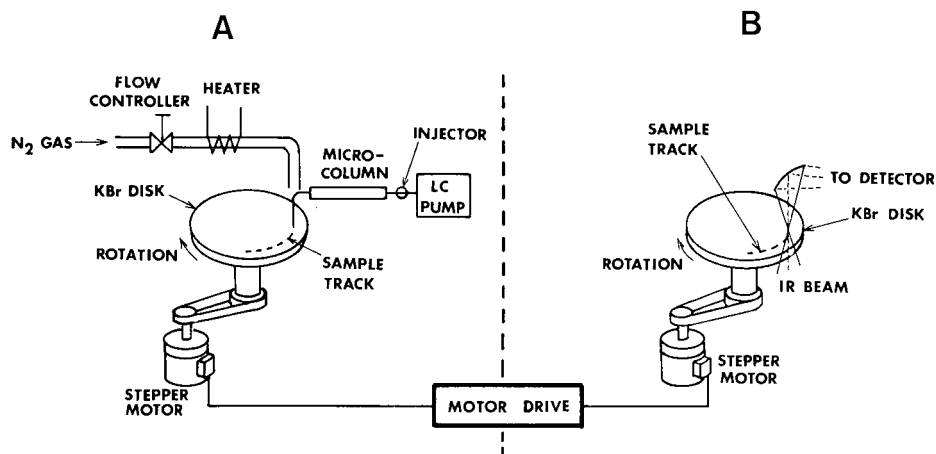


Fig. 14. Schematic diagram showing two operating modes of the interface. (A) Collection of the effluent as a continuous band on a potassium bromide disk; (B) measurements of spectral data with the device in the rear sample compartment of a JEOL FTIR spectrometer. (From ref. 20 with permission.)

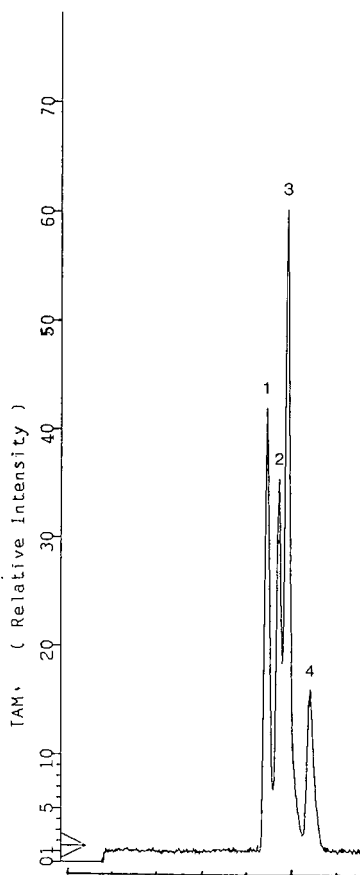


Fig. 15. Chromatogram of microcolumn HPLC-FT-IR separation of a synthetic polymer additive mixture²¹. Peaks: 1 = Irganox 1076; 2 = Santonox; 3 = Cyasorb UV-531; 4 = Cyasorb UV-9 (6 μg each). Column, 20 cm \times 0.53 mm I.D. with SEC packing; mobile phase, tetrahydrofuran; flow-rate, 2.67 $\mu\text{l}/\text{min}$. From ref. 21.

An interface designed for the measurement of diffuse-reflectance spectra of peaks eluting from microcolumns was constructed by Conroy *et al.*²². This interface was based on the principle developed previously for conventional HPLC²⁴, and consists of a carousel containing 180 small cups filled with powdered potassium chloride. The effluent from a microcolumn (0.5 and 1 mm I.D.) was dropped into the cups. A drop monitor was mounted at the end of the transfer tube, which allowed only one drop to be collected in each cup. After each drop fell, the carousel was rotated using a stepper motor so that the next cup moved into place to receive the next drop. The carousel was preheated under an IR lamp so that the solvent evaporated rapidly and the solute was deposited. After deposition, the diffuse-reflectance spectrum of each deposit was measured. A reasonably high signal-to-noise ratio spectrum was obtained for 10 ng of 4-chloronitrobenzene eluted from 50 cm \times 1 mm I.D. microcolumn packed with 10- μm silica by using 2% methanol in *n*-hexane.

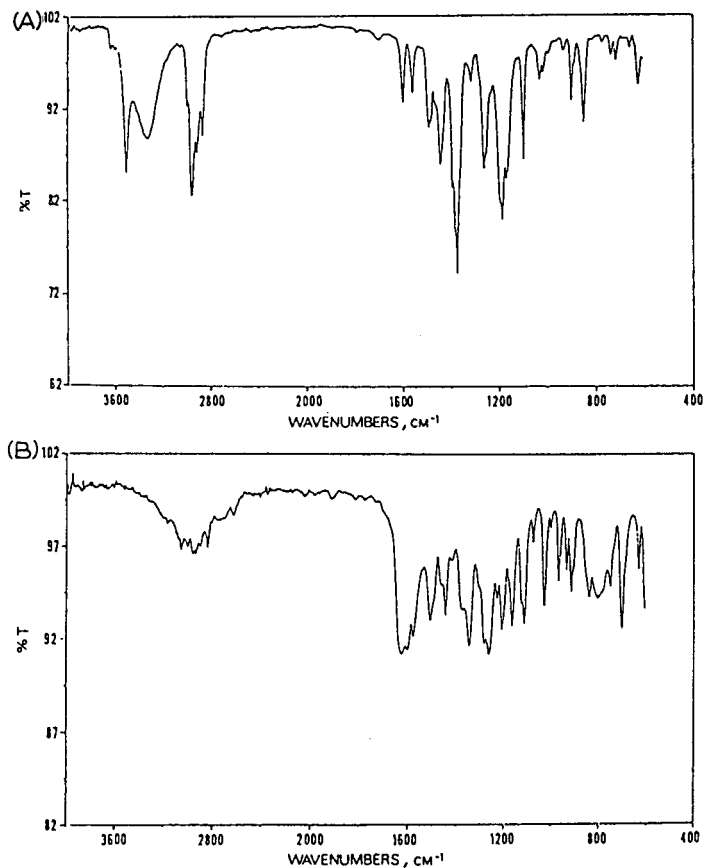


Fig. 16. IR spectra of (A) peak 2 in Fig. 15 and (B) peak 4 in Fig. 15. From ref. 21.

Kalasinsky *et al.*²³ developed an interface that incorporates a post-column reaction to obtain diffuse-reflectance spectra of aqueous reversed-phase HPLC eluates. Water was removed from aqueous solvents by an acid-catalysed reaction with 2,2-methoxypropane to produce methanol and acetone, which can be readily evaporated before deposition on powered potassium chloride. This interface worked well for mobile phases containing as much as 80% water.

Castles *et al.*²⁵ adopted an ultrasonic nebulization technique combined with a vacuum collection station as an interface between the microcolumn and the diffuse-reflectance IR spectrometer. The inherent desolvation that occurs on nebulization of the reversed-phase eluent from microcolumn HPLC, together with the vacuum collection system and the diamond powder substrate, made possible the continuous collection of the solutes on the substrate held on a linear transport device. IR spectra of the compounds separated by reversed-phase HPLC were measured after deposition. The detection limits were relatively higher, however.

More recently, Gagel and Biemann^{26,27} reported an impressive and promising

method for the continuous recording of IR spectra of components separated by microcolumn HPLC. By means of a heated gas nebulizer, the effluent from a microcolumn was sprayed onto and evaporated from a rotating aluminum disk that had a reflective surface. This is a similar concept to the thermospray interface developed for HPLC-MS interfacing. After deposition, the solutes were analysed by rotating the disk in the sample compartment of an FT-IR spectrometer, reflection-absorption spectra being continuously collected. The analysis of closely eluting isomers and the measurement of a spectrum from a 31-ng injection of phenanthroquinone separated by reversed-phase HPLC were demonstrated.

Although microcolumn HPLC separations were not tried in the interface evaluation, two promising methods in reversed-phase HPLC-FT-IR have recently been reported by Taylor and co-workers^{28,29} and Robertson *et al.*³⁰. The former used the flow-cell approach and the latter the solvent-elimination approach.

In the former approach, an interface device based on the post-column extraction of solutes into a suitable analyte fluid was constructed. Solute from reversed-phase HPLC separations are extracted into carbon tetrachloride as an IR-transparent solvent and then an FT-IR spectrometer measures the spectra in an efficient, real-time fashion. In this concept, the combined method involves solute extraction in an aqueous-organic segmented stream, separation of the aqueous and organic phases and inspection of the organic effluent through a flow-cell interface. Greater potential may be possible if this concept can be applied to a microcolumn HPLC-FT-IR interface.

MAGIC ("monodispersive aerosol generation interface combining") was originally developed by Willoughby and Browner³¹ and the interface technique has recently become commercially available for HPLC-MS interfacing. Robertson *et al.*³⁰ first reported the use of this MAGIC interface for conventional reversed-phase HPLC-FT-IR and demonstrated the potential of this technique for the further development of the HPLC-FT-IR solvent-elimination approach. If one could use microcolumn HPLC instead of conventional HPLC for this MAGIC interface evaluation, the results could be excellent.

It is interesting at this point to re-emphasize that the interface techniques which are commercially available for HPLC-MS seems to be applicable to HPLC-FT-IR, so in the future we should have a unified interface device for combined chromatography-spectrometry in a similar fashion to that proposed by Haefner *et al.*³² for combination with FT-IR.

REFERENCES

- 1 P. R. Griffiths, S. L. Pentoney, Jr., A. Giorgetti and K. H. Shafer, *Anal. Chem.*, 58 (1986) 1394A.
- 2 K. Jinno, in E. S. Yeung (Editor), *Detectors for Liquid Chromatography*, Wiley, New York, 1986, Ch. 3.
- 3 P. R. Griffiths and C. M. Conroy, *Adv. Chromatogr.*, 25 (1986) 105.
- 4 K. Jinno, *Chromatographia*, 23 (1987) 55.
- 5 C. C. Johnson and L. T. Taylor, *Anal. Chem.*, 56 (1984) 2642.
- 6 K. Jinno, C. Fujimoto and S. Nakanishi, *Chromatographia*, 20 (1985) 279.
- 7 C. Fujimoto and K. Jinno, *J. High Resolut. Chromatogr. Chromatogr. Commun.*, 6 (1983) 374.
- 8 C. Fujimoto, G. Uematsu and K. Jinno, *Chromatographia*, 20 (1985) 112.
- 9 K. Jinno, C. Fujimoto and G. Uematsu, *Am. Lab.*, 16, No. 2 (1984) 39.
- 10 K. Jinno and C. Fujimoto, *J. Liq. Chromatogr.*, 7 (1984) 2059.
- 11 C. Fujimoto and K. Jinno, *Chromatographia*, 17 (1983) 259.
- 12 L. T. Taylor, *J. Chromatogr. Sci.*, 23 (1985) 265.

- 13 K. Jinno, C. Fujimoto and Y. Hirata, *Appl. Spectrosc.*, 36 (1980) 313.
- 14 K. Jinno, C. Fujimoto and D. Ishii, *J. Chromatogr.*, 239 (1982) 625.
- 15 K. Jinno and C. Fujimoto, *J. High Resolut. Chromatogr. Chromatogr. Commun.*, 4 (1981) 532.
- 16 C. Fujimoto, K. Jinno and Y. Hirata, *J. Chromatogr.*, 258 (1983) 81.
- 17 C. Fujimoto, T. Oosuka and K. Jinno, *Anal. Chim. Acta*, 178 (1985) 159.
- 18 C. Fujimoto, T. Morita and K. Jinno, *J. Chromatogr.*, 438 (1988) 329.
- 19 C. Fujimoto, T. Morita, K. Jinno and K. Shafer, *J. High Resolut. Chromatogr. Chromatogr. Commun.*, 11 (1988) 810.
- 20 C. Fujimoto, T. Morita, K. Jinno and S. Ochiai, *Chromatographia*, 23 (1987) 512.
- 21 C. Fujimoto and K. Jinno, *Trends Anal. Chem.*, 8 (1989) 90.
- 22 C. M. Conroy, P. R. Griffiths and K. Jinno, *Anal. Chem.*, 572 (1985) 822.
- 23 K. S. Kalasinsky, J. A. S. Smith and V. F. Kalasinsky, *Anal. Chem.*, 57 (1985) 1969.
- 24 D. T. Kuehl and P. R. Griffiths, *Anal. Chem.*, 52 (1980) 1394.
- 25 M. A. Castles, L.V. Azzaraga and L. A. Carreria, *Appl. Spectrosc.*, 40 (1986) 673.
- 26 J. J. Gagel and K. Biemann, *Anal. Chem.*, 58 (1986) 2184.
- 27 J. J. Gagel and K. Biemann, *Anal. Chem.*, 59 (1987) 1266.
- 28 J. W. Hellgeth and L. T. Taylor, *Anal. Chem.*, 59 (1987) 295.
- 29 S. Shah and L. T. Taylor, *LC-GC*, 7 (1989) 340.
- 30 R. M. Robertson, J. A. deHaseth, J. D. Kirk and R. F. Browner, *Appl. Spectrosc.*, 42 (1988) 1365.
- 31 R. C. Willoughby and R. F. Browner, *Anal. Chem.*, 56 (1984) 2626.
- 32 A. M. Haefner, K. L. Norton, P. R. Griffiths, S. Bourne and R. Gurbelo, *Anal. Chem.*, 60 (1988) 2441.

CHROMSYM. 1743

***In vivo* microdialysis sampling coupled to liquid chromatography for the study of acetaminophen metabolism**

DENNIS O. SCOTT, LORI R. SORENSEN and CRAIG E. LUNTE*

Department of Chemistry, University of Kansas, Lawrence, KS 66045 (U.S.A.)

SUMMARY

In vivo microdialysis sampling coupled to liquid chromatography is a powerful tool for the study of drug metabolism. This technique is illustrated by investigating the pharmacokinetics of acetaminophen in the blood and liver of an anesthetized rat. The pharmacokinetics of the sulfate and glucuronide metabolites as well as the parent acetaminophen can be determined with high precision using microdialysis sampling. Microdialysis samples can be collected at a high rate from several sites without fluid loss with a single animal. Because the animal serves as its own control better data can be obtained. Liquid chromatography provides determination of multiple analytes per sample for metabolic profiling. This technique will provide more accurate and precise pharmacokinetic data while requiring fewer animals.

INTRODUCTION

The pharmacokinetics of a drug are typically determined by administering a known dose and withdrawing blood samples at timed intervals¹. These samples are then analyzed for the drug of interest. To study tissue levels of a drug, many animals must be dosed with the same concentration of the drug and several animals sacrificed at each desired time point. Tissue samples from each animal are analyzed for the drug and the data from all of the animals at each time point averaged to generate the pharmacokinetic curve. Using microdialysis sampling coupled to liquid chromatographic detection allows the entire pharmacokinetic curve to be obtained from a single animal at several anatomical sites. This results in data of higher precision and accuracy while using fewer animals.

Microdialysis sampling is accomplished by implanting a small probe in the tissue of interest. The probe consists of a short length of dialysis tubing through which the sampling solution is slowly perfused. Molecules of molecular weight below the cutoff of the dialysis tubing will diffuse into the probe because of the concentration differences between the tissue and the perfusion medium. The perfusion medium is collected and analyzed by liquid chromatography to determine what compounds were present in the tissue during the dialysis experiment. Because the cutoff is typically such that proteins are excluded, microdialysis samples can be injected directly into the

chromatographic system. This technique has found great utility for the *in vivo* study of neurotransmitters²⁻⁵.

This report describes the application of *in vivo* microdialysis perfusion to the determination of the pharmacokinetics of acetaminophen (APAP) in the blood and liver of an anesthetized rat. The dialysis samples were analyzed by liquid chromatography with UV absorbance detection. This allowed the detection of APAP as well as its major metabolites, the sulfate and glucuronide conjugates. Well defined pharmacokinetic curves could be constructed using a single animal while experiments on multiple animals were highly reproducible. Simultaneous sampling at different sites in the animal was accomplished by using multiple dialysis probes. The relative rates of clearance from various organs could therefore be determined.

EXPERIMENTAL

Materials

APAP, β -glucuronidase (type B-1 from bovine liver) and sulfatase (type H-1 from *Helix pomatia*) were purchased from Sigma (St. Louis, MO, U.S.A.). HPLC-grade acetonitrile was obtained from Fisher (Fair Lawn, NJ, U.S.A.). All other chemicals were reagent grade or better and were used as received.

Microdialysis apparatus

Microdialysis sampling was performed using a CMA/100 microinjection pump from Bioanalytic Systems (BAS)/Carnegie Medicin (West Lafayette, IN, U.S.A.) coupled to the dialysis probe which was implanted in the animal (Fig. 1). The perfusion medium was pumped through the probes at a flow-rate of 5 μ l/min for all experiments. This perfusion rate was chosen to provide both reasonable recoveries and sampling times. As the perfusion rate is increased, the recovery decreases as does the time needed to collect sufficient sample for chromatographic analysis. The perfusion rate used for any given experiment depends upon several factors including the type of chromatographic system (*i.e.* conventional or microbore) and sensitivity of the detector. For intravenous sampling a BAS/Carnegie Medicin dialysis probe of the "cannula" type was used (Fig. 1A). These probes have a 4-mm dialysis membrane made of polycarbonate ether with a molecular weight cutoff of 20 000. For intravenous insertion of the microdialysis probe a probe guide from BAS/Carnegie Medicin was used. For tissue sampling the probe was constructed in-house from dialysis tubing purchased from Spectrum Medical Industries (Los Angeles, CA, U.S.A.). The tubing was regenerated cellulose with an I.D. of 150 μ m, a wall thickness of 9 μ m and a molecular weight cutoff of 9000 daltons. The ends of a *ca.* 5 mm length of dialysis tubing were sealed to pieces of 26-gauge stainless steel with "hot melt" glue. "Hot melt" glue (Ridlen/AAI Adhesives, Dallas, TX, U.S.A.) is a wax-based adhesive and was found to be easy to use and provide leakproof seals. This probe design is illustrated in Fig. 1B.

Prior to use, the dialysis tubing was activated by pretreatment with sodium hydroxide. The tubing was primed with a solution of isopropyl alcohol and 20% (v/v) glycerol for 5 min. The tubing was then hydrolyzed for 2 min with 0.1 M methanolic sodium hydroxide. A neutralizing solution containing 1% (v/v) acetic acid and 20% (v/v) glycerol in isopropanol was next pumped through the probe for 5 min. The probe was finally perfused with distilled water for several hours to remove residual glycerol.

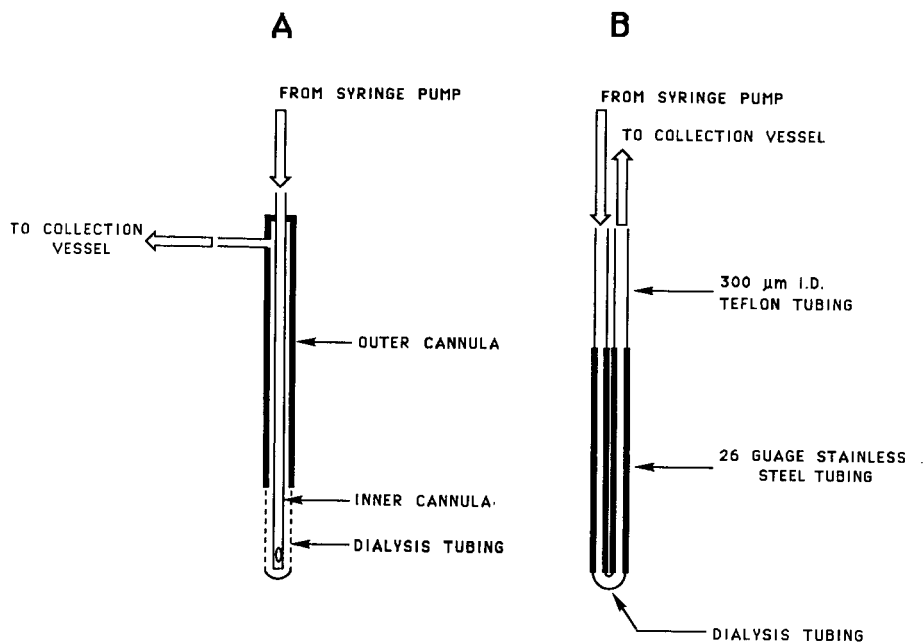


Fig. 1. Diagrams of (A) the "cannula"-type microdialysis probe and (B) the "loop"-type microdialysis probe. Dimensions are given in the text.

Chromatographic system

The liquid chromatographic system was a BAS LC-400 Chromatographic System equipped with a Shimadzu SPD-6AV variable-wavelength UV-VIS absorbance detector (Shimadzu, Columbia, MD, U.S.A.). A Hypersyl ODS 5- μm (4.6 mm \times 15 cm I.D.) column was used to achieve separation. The mobile phase was 0.05 M ammonium phosphate buffer, pH 2.7, with 10% (v/v) acetonitrile. A flow-rate of 1 ml/min and a 20- μl sample loop were used for all experiments. The UV detector was operated at 250 nm.

Microdialysis probe characterization

In order to determine the *in vivo* concentration of APAP giving rise to the concentration detected in the perfusion medium, it is necessary to know the recovery of the dialysis probe. This is typically expressed as the relative recovery, which is the ratio of the concentration in the perfusion medium to the concentration in the sample. Each probe must be calibrated individually because the recovery is different for each probe, even one of the same nominal length used at the same perfusion rate. Recovery was determined by spiking fresh rat whole blood with a known concentration of APAP. An aliquot of this spiked blood was centrifuged, filtered through a 22- μm filter and analyzed chromatographically. The rest of the spiked blood was used as a dialysis sample. The perfusion medium was a Ringer's saline solution as used for the *in vivo* experiments. Several dialysis samples were collected and analyzed chromatographically. APAP concentrations were selected to bracket the expected *in vivo* concentrations. The recovery of each dialysis probe was determined both before and

after implantation. The recovery found after the implantation was used to calculate *in vivo* concentrations although the two recoveries were never found to differ by more than 5%.

Enzymatic hydrolysis

For cleavage of conjugates by β -glucuronidase, 100 μ l of enzyme solution, 1250 U/ml in 0.1 M sodium phosphate buffer, pH 4, was added to 100 μ l of dialysate. Hydrolysis was carried out for 8 h at 40°C. Cleavage of sulfate conjugates was achieved by adding 100 μ l of enzyme solution, 200 U/ml sulfatase in 0.1 M sodium acetate, pH 5, to 100 μ l of dialysate. The sample was incubated for 5 min at 34°C. The two hydrolysis samples and an untreated dialysate were analyzed consecutively by liquid chromatography.

In vivo experiments

Four- to five-month old Spargue-Dawley rats weighing *ca* 400 g were used. Rats were anesthetized with the inhalation anesthetic isoflurane. The choice of anesthetic is critical for metabolism experiments as most anesthetics are extensively metabolized and will interfere with the metabolism of other compounds. Isoflurane is reported to be exhaled 95% unchanged with less than 0.17% being metabolized and does not effect renal or hepatic function^{6,7}. The rat's respiration was closely monitored during the entire experiment and maintained at a rate of *ca.* 50 min⁻¹. The animal's body temperature was maintained with a heating pad beneath its body and a heat lamp above.

For intravenous sampling a cannula-type probe was inserted into the jugular vein. A small incision was made in the side of the neck. The pectoral muscle was gently lifted and an intravenous probe guide inserted through the pectoral muscle into the jugular vein. The muscle closed around the probe guide and held it securely in place. The dialysis probe was inserted into the vein through the probe guide. The incision was then packed with damp gauze. There is no bleeding from around the probe if the insertion is done properly.

For implantation into the liver a "loop"-type probe was used. A small incision was made in the peritoneal cavity to expose the liver. A small incision was made into the liver and the dialysis probe carefully inserted. The skin was closed securely around the probe and the incision was packed with damp gauze. The probe cannot be held rigidly by an external clamp or it will shift in the liver during the animals breathing. If done properly, this procedure should not cause much bleeding.

Metabolism experiments were performed by perfusing the implanted probes with a Ringer's solution consisting of 155 mM NaCl, 5.5 mM KCl, and 2.3 mM CaCl₂. A perfusion rate of 5 μ l/min was used with samples being collected for 10-min intervals. Dialysis samples were diluted with Ringer's solution as needed to keep the concentration in the range of calibration. Blanks were collected for at least 1 h following insertion of the microdialysis probes. No interferences were observed in blanks from either blood or liver dialysates. The animal was then dosed intraperitoneally (i.p.) with APAP in Ringer's solution (100 mg/kg) at 37°C. Dialysis samples were collected until less than 1% of the maximum concentration of APAP remained in the blood or liver. This was typically 6–7 h after dosing. The *in vivo* APAP concentration was calculated by determining the APAP concentration in the dialysate

from a standard curve and then accounting for the recovery of the microdialysis probe. As no standards were available for either the sulfate or glucuronide conjugates, peak heights in mAU were used for these compounds. Pharmacokinetic parameters such as half-life of elimination could still be determined even without actual concentrations.

RESULTS

Intravenous microdialysis sampling

Typical chromatograms of blood dialysate obtained by *in vivo* sampling are shown in Fig. 2. *In vivo* dialysis samples were diluted ten-fold with Ringer's solution and directly injected into the chromatograph. As can be seen no interferences occur in the blank obtained prior to dosing of the animal with APAP (Fig. 2A). An advantage of microdialysis sampling is that the actual animal serves as its own control. Fig. 2B is a chromatogram of the dialysate after administration of APAP. The retention times of APAP, the sulfate and the glucuronide are 4.2, 3.2 and 2.6 min, respectively. The identities of the glucuronide and sulfate conjugates of APAP were confirmed by enzymatic hydrolysis. The chromatogram of a dialysate sample hydrolyzed with sulfatase shows that the peak tentatively identified as the sulfate conjugate is no longer present and also shows an increase in APAP (Fig. 2C). Following hydrolysis with β -glucuronidase both the peaks identified as the glucuronide and the sulfate conjugate

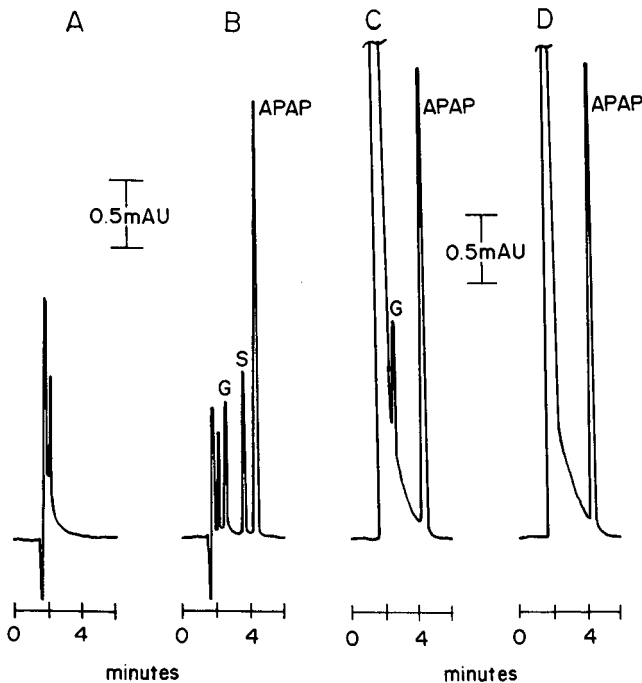


Fig. 2. Chromatograms of *in vivo* blood dialysate. (A) Blank (prior to dosing with APAP), (B) 1 h after a 100-mg/kg i.p. dose of APAP, (C) treated with sulfatase, (D) treated with β -glucuronidase. Peaks: APAP = acetaminophen; G = glucuronide conjugate; S = sulfate conjugate. Chromatographic conditions are given in the text.

are no longer present again with an increase in APAP (Fig. 2D). Commercial β -glucuronidase contains some sulfatase activity⁸ so this result is not surprising. These results provide strong evidence for the identity of the two APAP metabolites detected even though no standards are available. The glucuronide and sulfate conjugates are the two major metabolites previously found for APAP^{9,10}.

A typical pharmacokinetic curve for elimination of APAP from blood following a 100-mg/kg i.p. dose is shown in Fig. 3. APAP rapidly distributes in the blood, reaching a maximum concentration in *ca.* 60 min. The concentration then slowly decreases over several hours. The pharmacokinetics of this process can be described by an open single-compartment model which exhibits first order kinetics. From the slope of the semi-log presentation of the elimination phase, the half-life of elimination was found to be 34.1 ± 1.0 min ($n=4$). The two metabolites appear 20 min after the APAP and mirror its rise in concentration. The pharmacokinetics of both metabolites exhibit plateau regions followed by elimination (Fig. 3). The elimination phase can again be modeled by an open single-compartment model. The half-life of elimination was determined to be 37.8 ± 5.6 min ($n=3$) for the glucuronide and 51.8 ± 14.5 minutes ($n=3$) for the sulfate conjugate.

In vivo microdialysis in the liver

Typical chromatograms of liver dialysate obtained by *in vivo* sampling are shown in Fig. 4. As with the blood dialysate, the liver dialysate could be directly injected into the liquid chromatograph. The chromatogram of the blank sample prior to dosing with APAP shows no interferences. The chromatogram of a sample obtained 1 h after a 100-mg/kg i.p. dose of APAP contains APAP as well as its sulfate and glucuronide conjugates. Identities of the conjugates were again confirmed by enzymatic hydrolysis.

The pharmacokinetics of elimination of APAP from both the liver and blood following a 100-mg/kg i.p. dose of APAP are shown in Fig. 5. These data were obtained simultaneously by implanting two probes, one in the liver the other intravenous, in the same animal. Uptake of APAP into the liver is clearly slower than in the blood with the peak concentration not reached until almost 2 h after administration. However the half-life of elimination was found to be the same as from the blood, 35.1 min.

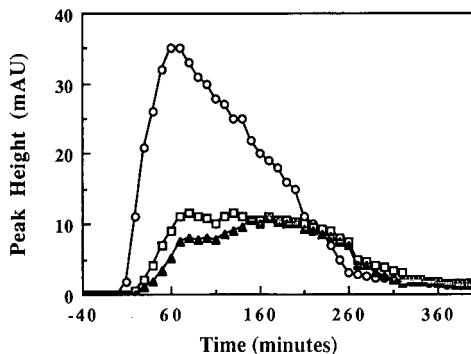


Fig. 3. Relative time course of blood concentration of APAP and its metabolites. Symbols: \circ = APAP; \square = sulfate conjugate; \blacktriangle = glucuronide conjugate.

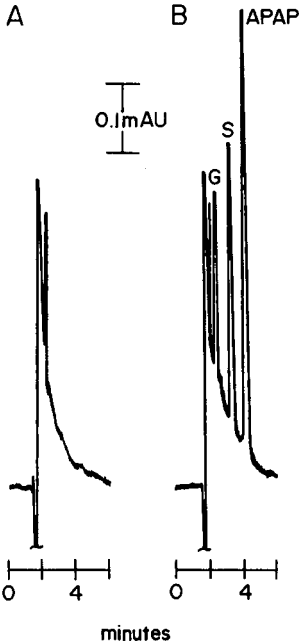


Fig. 4. Chromatograms of *in vivo* liver dialysate. (A) Blank (prior to dosing with APAP, (B) 1 h after a 100-mg/kg i.p. dose of APAP. Peaks as in Fig. 2.

The appearance of the APAP conjugates in the liver directly corresponds to the uptake of APAP (Fig. 6). The concentrations of both the glucuronide and the sulfate conjugate take longer to peak in the liver than in the blood, mirroring the behavior of APAP itself. As in the blood, a plateau region followed by elimination is observed. The half-life of elimination for both conjugates was the same as the elimination from blood, 38.4 min for the glucuronide and 52.6 min for the sulfate conjugate.

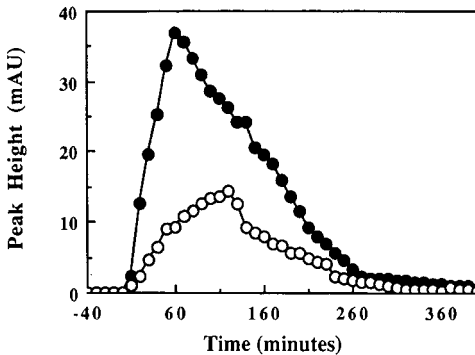


Fig. 5. Relative time course blood and liver APAP following a 100-mg/kg i.p. dose. Symbols: ● = blood concentration; ○ = liver concentration.

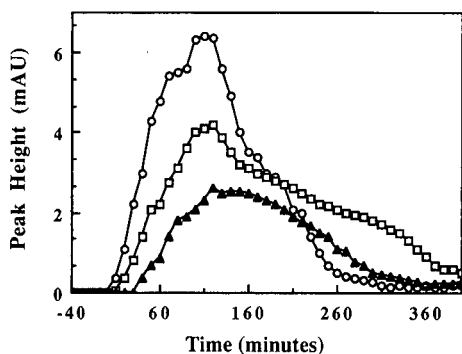


Fig. 6. Relative time course of liver concentration of APAP and its metabolites. Symbols as in Fig. 3.

CONCLUSIONS

In vivo microdialysis sampling coupled to liquid chromatography is a powerful tool for the study of the pharmacokinetics of drugs. The technique is not limited to APAP but has general applicability. A strength of the technique is that the detection method is not directly coupled to the sampling method. Indeed, it is possible to use multiple detection methods on a single sample to optimize detection of several compounds for metabolic profiling. Microdialysis offers several advantages for pharmacokinetic studies. The temporal resolution is much higher than for other methods. While 10-min intervals were used for these experiments, shorter or longer times are easily achieved. Since no blood is drawn, a large number of samples can be collected from a single animal without loss of fluid volume. Simultaneous sampling can be achieved using multiple dialysis probes. Two probes were used for these experiments, one intravenous and one in the liver, but probes can be implanted at other sites such as the kidney, brain, or in the intestine with little difficulty. The major limitation on the number of probes that can be used and the temporal resolution that can be achieved is the ability to analyze the large number of samples generated. Because complete pharmacokinetic curves can be obtained for several organs using a single experimental animal, overall fewer animals will be necessary to obtain data on a given drug.

ACKNOWLEDGEMENT

The authors wish to acknowledge Merck, Sharpe & Dohme for financial support of this work.

REFERENCES

- 1 M. Rowland and T. N. Tozer, *Clinical Pharmacokinetics: Concepts and Applications*, Lea & Febiger, Philadelphia, PA, 1989.
- 2 U. Ungerstedt, in C. A. Marsden (Editor), *Measurement of Neurotransmitter Release In Vivo*, Wiley-Interscience, Chichester, 1984, p. 81.
- 3 U. Ungerstedt, C. Forster, M. Herrera-Marschitz, I. Hoffman, U. Jungnelius, U. Tossman and T. Zetterstrom, *Neurosci. Lett. (Suppl.)*, 10 (1982) 493.

- 4 M. Sandberg and S. Lindstrom, *J. Neurosci. Methods*, 9 (1983) 65.
- 5 U. Ungerstedt and A. Hallstrom, *Life Sci.*, 41 (1987) 861.
- 6 *USP Drug Information*, United States Pharmacopeial Convention Inc., Rockville, MD, 9th, ed., 1989, p. 230.
- 7 *Drug Evaluation*, 6th ed., American Medical Association, Philadelphia, PA, 1988, p. 296.
- 8 G. F. Weirich, *Arch. Insect. Biochem. Physiol.*, 3 (1986) 109.
- 9 J. A. Hinson, L. R. Pohl, T. J. Monks and J. R. Gillette, *Life Sci.*, 29 (1981) 107.
- 10 M. Hamilton and P. T. Kissinger, *Anal. Biochem.*, 125 (1982) 143.

CHROMSYMP. 1740

Determination of water-soluble vitamins in blood and plasma by coupled-column liquid chromatography

KURT JOHANSEN and PER OLOF EDLUND*

Bioanalytical Section, R & D, Kabi Pharma, Box 1828, S-17126 Solna (Sweden)

SUMMARY

A method is described for the simultaneous determination of riboflavin and the coenzymes related to pyridoxine and thiamine. Pyridoxal-5'-phosphate (PLP) bound to proteins as a Schiff base was liberated and stabilized by reaction with semicarbazide. Blood or plasma proteins were precipitated with acid and the supernatant formed was injected into a liquid chromatographic system consisting of one precolumn and two analytical reversed-phase columns. Riboflavin was detected by its native fluorescence with a separate detector while post-column reactions based on the fluorescence of PLP semicarbazone in alkaline solution and the oxidation of thiamine to thiochrome were combined in the same reaction detector. Chromatographic separation was achieved within 7 min and normal endogenous levels were quantified with a precision of 2-5% (relative standard deviation).

INTRODUCTION

In spite of the well known biochemical functions of the common vitamins, it is still difficult to find established methods for the assessment of vitamin status in health and disease. The vitamin concentrations in plasma varies with the daily intake of nutrients and does not reflect the degree of tissue saturation. Several approaches have been suggested for overcoming this problem, usually by some method of indirect measurement of the coenzyme related to the vitamin of interest. Several review books are available on the subject¹⁻³. Vitamin B₆ status has been studied by xanthurenic acid excretion following a tryptophan load⁴, by measurement of enzyme activity without⁵ or with⁶ *in vitro* stimulation with excess pyridoxal-5'-phosphate (PLP). Measurement of the urinary excretion of 4-pyridoxic acid, the principal B₆ metabolite, has also been used⁷. There has been some debate on the subject of which parameter gives the most relevant information about vitamin B₆ status². Plasma PLP appears to be a good candidate⁸ and several chemical methods based on liquid chromatography (LC) have been described⁹⁻¹².

Brin¹³ demonstrated that erythrocyte transketolase activity is a reliable index of the availability of the coenzyme thiamine pyrophosphate (TPP) and thus correlated

with the degree of thiamine deficiency in both humans and animals. This coenzyme can also be quantified by LC¹⁴⁻¹⁶.

Plasma levels of riboflavin tend to reflect current intake and erythrocyte levels have been used more often to study riboflavin status¹. An enzymatic method based on *in vitro* stimulation of erythrocyte glutathione reductase, an enzyme containing FAD, has been used as an alternative to riboflavin levels^{1,17}.

This paper describes how coupled-column LC combined with fluorescence detection can be used for the rapid and simultaneous quantification of PLP, TPP and riboflavin, three analytes useful for the assessment of vitamin status.

EXPERIMENTAL

Chemicals and reagents

Riboflavin (R), pyridoxal-5'-phosphate (PLP), thiamine monophosphate (TMP) and thiamine pyrophosphate (TPP, cocarboxylase) were obtained from Sigma (St. Louis, MO, U.S.A.). Pyrophosphoric acid and triethylamine (TEA) were obtained from Fluka (Buchs, Switzerland) and acetonitrile and potassium hexacyanoferrate(III) from Merck (Darmstadt, F.R.G.). Sodium hexylsulphate (HeSO₄) was obtained from Kodak (Rochester, NY, U.S.A.). All other chemicals were of analytical-reagent grade. Water was purified in a Milli-Q water purification system (Millipore).

Apparatus

The liquid chromatograph consisted of three pumps (Model LC-6A), an autosampler (Model SIL-6A), two six-port valves (FCV-2AH) for chromatography, a fluorescence detector (Model RF-530) and a system controller (SCL-6A), all from Shimadzu (Kyoto, Japan). The system controller was programmed to control the column-switching valves and the detector was used for detection of TMP, TPP and PLP at excitation and emission wavelengths of 367 and 470 nm, respectively. An additional fluorescence detector (Model LS-4) from Perkin-Elmer (Norwalk, CT, U.S.A.) operated at excitation and emission wavelengths of 446 and 524 nm, respectively, was used for detection of riboflavin.

The precolumn, column 1 (15 × 3.2 mm I.D. Brownlee cartridge) contained 7- μ m polymer particles (Applied Biosystems, Santa Clara, CA, U.S.A.). The analytical column for the separation of TPP, TMP and PLP (150 × 4.6 mm I.D.), column 2, contained 5- μ m styrene-divinylbenzene copolymer particles from Polymer Labs. (Shropshire, U.K.) and the column for riboflavin (100 × 4 mm I.D.), column 3, contained 3- μ m Spherisorb ODS-silica (Phase Separations, Queensferry, U.K.). The effluent from column 2 was connected to a low-dead-volume tee (Valco) for addition of post-column reagent [200 mg/l potassium hexacyanoferrate(III) in 2 M sodium hydroxide solution], followed by a stitched PTFE capillary (3.5 m × 0.38 mm I.D.) connected to the Shimadzu detector (see Fig. 1). The PTFE capillary was stitched into a metal net with a mesh size of 1 mm. The post-column reagent was pumped from a glass bottle with aid of a static nitrogen gas pressure of 28 p.s.i., which resulted in a flow-rate of 0.25 ml/min.

The mobile phase for the precolumn (C1) was pumped by pump 1 at a flow-rate of 1 ml/min and consisted of 0.1 M NaH₂PO₄ and 10 mM pyrophosphoric acid with

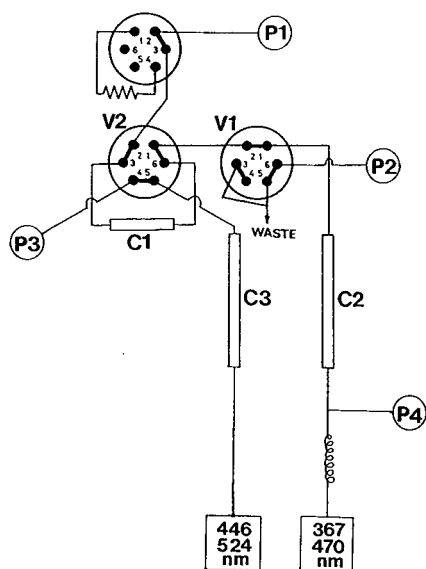


Fig. 1. Chromatographic system consisting of precolumn (C1) and polymeric column for separation of phosphates (C2) and ODS column for riboflavin (C3). V1 and V2 = six-port electric switching valves.

pH adjusted to 4 with 1 *M* sodium hydroxide solution. The mobile phase for the second column (C2) consisted of 10 *mM* triethylamine, 10 *mM* pyrophosphoric acid and 1 *mM* hexylsulphate in 0.1 *M* NaH_2PO_4 (pH 4), pumped by P2 at 1 ml/min. The mobile phase for the third column consisted of 13% acetonitrile in 0.1 *M* phosphate buffer (pH 4), pumped by P3 at 0.8 ml/min.

Sample preparation

Blood or plasma (0.5 ml) was diluted with 0.5 ml of mobile phase 2 from the chromatograph. The blood samples were mixed with 0.25 ml of 1 *M* semicarbazide, while 0.15 ml was used for plasma samples. The samples were derivatized in the dark at ambient temperature for 15 min, followed by protein precipitation with 0.4 ml of 25% (w/v) trichloroacetic acid and centrifugation for 5 min. The supernatants were filtered through cotton-wool wound around the tip of a Pasteur pipette and dispensed to autosampler vials. A volume of 80 μl was injected into the chromatograph for analysis. Calibration was performed by standard addition of TPP, PLP and riboflavin to normal blank plasma or blood to obtain a concentration of 200 ng/ml of the analytes. A duplicate of the blank standard and at least four fortified standards were extracted along with unknown samples as described above. The slope of the calibration graph of peak height *versus* concentration added was used for quantification of unknown samples.

RESULTS AND DISCUSSION

Sample preparation

PLP is bound to ϵ -amino acid residues of albumin in plasma¹⁸. The Schiff base or

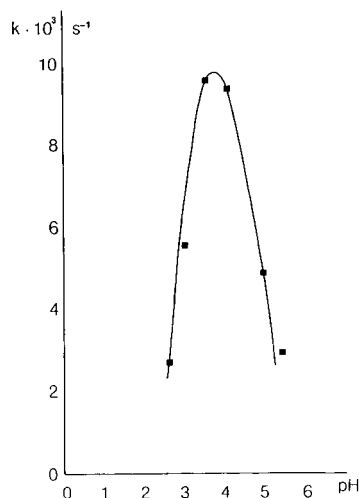


Fig. 2. Pseudo-first-order rate constants for derivatization of PLP with semicarbazide as a function of pH determined by LC at a reagent concentration of 3 mM at 26°C.

semicarbazone formation is dependent on pH with a maximum at *ca.* pH 3.5 (see Fig. 2). The most common methods for extraction of PLP from plasma involve protein precipitation with trichloroacetic⁹⁻¹¹ or perchloric acid¹², which acidifies the samples sufficiently to dissociate PLP from proteins¹⁸. Competitive reaction with excess of semicarbazide can also be used to liberate and stabilize PLP. Semicarbazone formation improves the fluorescence compared with free PLP and stabilizes the analyte towards photochemical decomposition¹⁹. Riboflavin is also sensitive to light and samples must be protected from strong daylight during handling and extraction. The extraction method with TCA described under Experimental gave recoveries close to 100% for all of the analytes studied except riboflavin in blood, where the recovery was 76% (see Table I). Riboflavin is less hydrophilic than TPP and PLP and it has not been possible

TABLE I

RECOVERY AND PRECISION

Compound	Matrix	Recovery (%)	<i>n</i>	Precision ^a (%)	Detection limit (ng/ml)
TPP	Blood	93 ± 7.8	13	1.2	2
	Plasma	85 ± 3.2	8	8.5	2
TMP	Blood	103 ± 8	13	14	1
	Plasma	104 ± 2	8	5.8	1
PLP	Blood	93 ± 2.8	13	3.6	2
	Plasma	100 ± 9.8	13	2.0	2
R	Blood	76 ± 5.6	13	9.1	1
	Plasma	94 ± 6.5	13	1.7	0.5

^a Inter-assay precision (relative standard deviation) at endogenous levels.

R	0					1 ⁺
PLP	1 ⁺	+ -	1 ⁻	2 ⁻	3 ⁻	
TPP	3 ⁺	2 ⁺	1 ⁺	+ -	1 ⁻	2 ⁻
	0	2	4	6	8	10
	pH					

Fig. 3. Estimation of the state of ionization of the analytes as a function of pH. The pK_a values were estimated from pK_a values of the vitamins in ref. 1 combined with pK_a values of pyrophosphoric acid.

to obtain a quantitative recovery of this compound without excessive dilution of the sample. FAD was strongly (covalently) bound to enzymes and recoveries were too low for meaningful quantification. Extraction under more drastic conditions, *e.g.*, heating, or the use of a stronger acid, hydrolysed FAD to FMN and riboflavin. Therefore, only riboflavin concentrations were quantified.

Chromatographic separation

The analytes studied differed widely in acid-base properties (see Fig. 3) and polarity, with TPP being the most polar with little or no retention on conventional reversed-phase columns whereas riboflavin was strongly retained. Trace enrichment procedures have been used for this compound^{20,21}. Thus gradient or coupled-column procedures must be used to elute these compounds in the same chromatographic

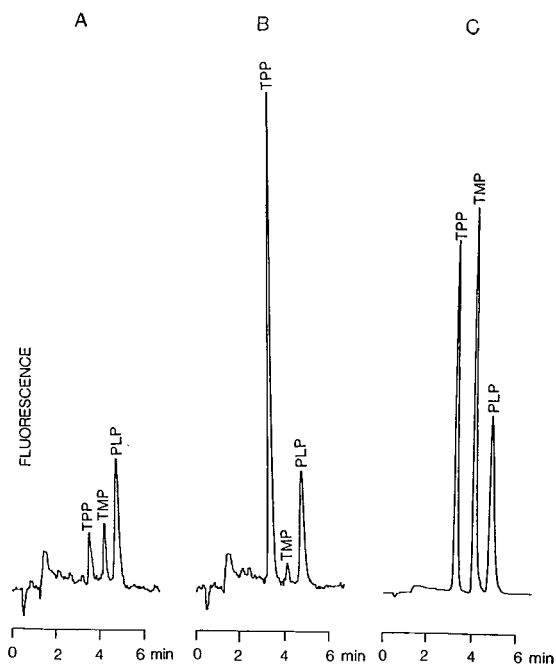


Fig. 4. Chromatograms obtained with (A) a plasma sample, (B) a blood sample and (C) a fortified blood sample. The phosphates were separated on a polymer column as described under Experimental during the experiment. The plasma concentrations were TPP 4 ng/ml, TMP 5 ng/ml and PLP 25 ng/ml. The blood concentrations were TPP 60 ng/ml, TMP 2 ng/ml and PLP 25 ng/ml.

system. We preferred the latter approach because faster separations with very short re-equilibration times can be achieved and better baseline stability is obtained for trace analysis. A small precolumn packed with polymeric reversed-phase particles was used for the separation of riboflavin from TPP, TMP and PLP. The more polar analytes were eluted from the precolumn with buffer for further separation by ion-pair chromatography with a mixture of triethylamine and hexylsulphate on a polymeric column (see Fig. 4). Riboflavin was eluted from the precolumn with a mobile phase containing 13% acetonitrile for separation on a separate column (Fig. 5). The column-switching events are summarized in Table II.

At pH 4 riboflavin was neutral whereas TPP was mostly present as a singly charged cation and PLP was present as an anion or zwitterion (see Fig. 3). Thus TPP and TMP were retained as ion pairs with hexylsulphate and PLP as an ion pair with triethylamine on polymeric reversed-phase columns and the selectivity for separation of thiamine phosphates from PLP can be controlled by the TEA- H_2SO_4 ratio (Fig. 6). The hexylsulphate concentration required to obtain suitable selectivity varied between different columns. A new column required 3 mM hexylsulphate (Fig. 6) whereas a column that had been used for 1 year required a concentration of 1 mM hexylsulphate (Fig. 4). The column packed with polymeric particles gave a much stronger retention than silica-based ODS columns and symmetrical peaks were obtained (see Fig. 4). Semicarbazide is an oxidizable compound and had to be at least partially separated from TPP to avoid quenching of the post-column reaction with

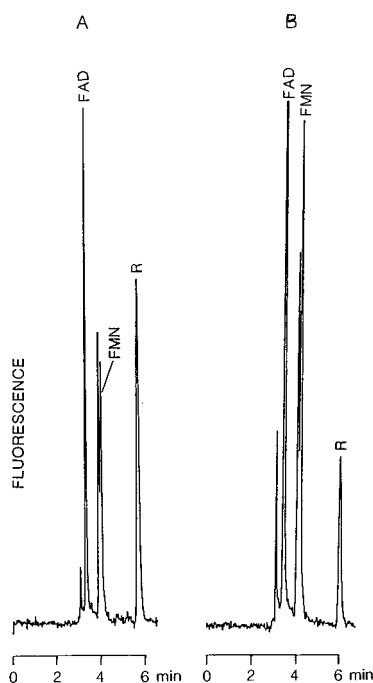


Fig. 5. Chromatograms obtained with (A) a plasma sample and (B) a blood sample with riboflavin concentrations of 50 and 20 ng/ml, respectively.

TABLE II
COLUMN-SWITCHING TIMETABLE

Time (min)	Valve operated	Event
0	Injector	The sample is injected on C1
0.1	1	TPP, TMP and PLP are eluted from C1 with buffer for separation on C2
0.9	1	C1 is washed with buffer
2.0	2	Riboflavin is eluted from C1 with 13% acetonitrile for separation on C2
5.0	2	C1 is conditioned with buffer
8.0	Injector	Next sample is injected

Fe^{3+} ions. Semicarbazide was eluted with the interstitial column volume and the polymeric column gave sufficient retention of TPP, but silica-based ODS columns were ineffective and quenching frequently occurred. Initially a simplified system was investigated where the sample was injected on the precolumn with the mobile phase for separation of the phosphates. The TEA- H_2SO_4 ion pair interfered with the subsequent separation of riboflavin, shown as peak splitting or excessive band broadening; a buffer without ion-pairing reagents had to be used for sample injection.

Attempts were made to include ascorbic acid in the same assay but the retention on the polymer column was not sufficient to separate ascorbic acid from uric acid.

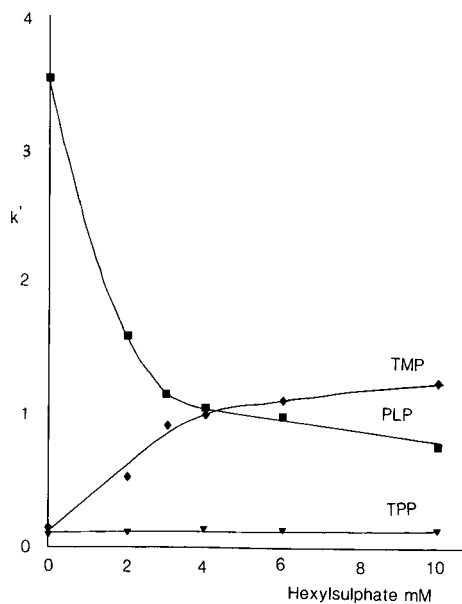


Fig. 6. Capacity factors of TPP, TMP and PLP on a polymer column as a function of hexylsulphate concentration. The mobile phase contained 10 mM triethylamine and 10 mM pyrophosphoric acid in 0.1 M phosphate buffer (pH 4) and various concentrations of hexylsulphate.

These acids have similar UV spectra and oxidation potentials and must be separated. However, precolumn separation is a very flexible technique and separations can often be tailored according to the analytical demand. The determination of ascorbic acid can, for instance, be combined with the determination of riboflavin in the system above if the polymeric column is replaced with an anion exchange-column. The same extraction method can be used if dithiothreitol is added to the TCA solution as an antioxidant.

Detection

Riboflavin was detected with high sensitivity and selectivity by its native fluorescence. The fluorescence of PLP semicarbazone gave an optimum intensity at *ca.* pH 12 (data not shown) and was not influenced by the addition of a low concentration of hexacyanoferrate(III). Hence the post-column alkalization of PLP and the alkaline oxidation of thiamine phosphates can be combined in the same reaction detector. The oxidation of TPP occurred quickly and a 3.5 m × 0.38 mm I.D. PTFE reactor was sufficient to obtain a quantitative reaction. The reactor was stitched to improve radial mixing and to reduce band broadening. The optimum wavelength for excitation was 367 and 369 nm for PLP and TPP, respectively. The optimum wavelengths for emission were 478 and 435 nm for PLP and TPP, respectively. The emission bands are wide and TPP can be detected at the emission wavelength of PLP with about a 50% decrease in sensitivity.

Accuracy and precision

The identity of the phosphates was confirmed by the disappearance of the chromatographic peaks after enzymatic hydrolysis with acid phosphatase. Further, no peaks corresponding to TPP and PLP were detected when the post- and precolumn reagents were excluded from the analysis (data not shown).

The inter-assay precision (relative standard deviation) varied from 1.2% for TPP in blood to 9.1% for riboflavin (Table II). Both plasma and blood TMP levels were close to the method detection limit of 1 ng/ml for this analyte. The sensitivity of the method was sufficient to determine TPP, PLP and riboflavin in plasma and blood at reduced levels.

CONCLUSIONS

Precolumn derivatization with semicarbazide not only dissociated PLP bound to proteins but also stabilized the analyte to avoid photochemical decomposition.

Ion-pair chromatography with TEA- H_2SO_4 on a polymer column was useful to control the selectivity for separation of TPP, TMP and PLP. These phosphates were detected with the same reaction detector after a minor compromise in emission wavelength. The use of ion-pair reagents interfered with the subsequent separation of riboflavin and therefore a separate buffer had to be used for sample injection.

Fast separations were achieved with precolumn fractionation and TPP, PLP and riboflavin were determined in plasma and blood with favourable precision within 7 min.

REFERENCES

- 1 L. J. Machlin (Editor), *Handbook of Vitamins*, Marcel Dekker, New York, 1984.
- 2 J. E. Lekelm and R. D. Reynolds (Editors), *Methods in Vitamin B-6 Nutrition, Proceedings of Workshop on Analytical Methodology and Criteria for Assessing Nutritional Status, Mt. Hood, Oregon, June 29-July 2, 1980*, Plenum Press, New York, 1981.
- 3 A. P. De Leenheer, W. E. Lambert and M. G. M. De Ruyter (Editors), *Modern Chromatographic Analysis of the Vitamins*, Marcel Dekker, New York, 1985.
- 4 L. D. Greenberg, D. F. Bohr, H. McGrath and J. F. Reinhart, *Arch. Biochem.*, 21 (1949) 237.
- 5 M. J. Woodring and C. A. Storwick, *Am. J. Clin. Nutr.*, 23 (1970) 1385.
- 6 B. Chabner and D. Livingstone, *Anal. Biochem.*, 34 (1970) 413.
- 7 J. F. Gregory and J. R. Kirk, *Am. J. Clin. Nutr.*, 32 (1979) 879.
- 8 J. Leiner, I. Simon and D. Hötzel, *Int. J. Vitam. Nutr. Res.*, 53 (1983) 166.
- 9 J. Schrijver, A. J. Speek and M. P. Schreurs, *Int. J. Vitam. Nutr. Res.*, 51 (1984) 216.
- 10 S. P. Coburn and J. D. Mahuren, *Anal. Biochem.*, 129 (1983) 310.
- 11 T. E. Heffaran, B. M. Chrisley and J. A. Driskell, *J. Chromatogr.*, 374 (1986) 155.
- 12 P. Edwards, P. K. S. Liu and G. A. Rose, *Clin. Chem.*, 35 (1989) 241.
- 13 M. Brin, *Ann. N.Y. Acad. Sci.*, 98 (1962) 528.
- 14 H. Sanemori, H. Ueki and T. Kawasaki, *Anal. Biochem.*, 107 (1980) 451.
- 15 J. Bontemps, L. Bettendorff, J. Lombet, G. Danrifosse, E. Schoffeniels, F. Nevejans, Y. Yang and M. Verzele, *Chromatographia*, 18 (1984) 424.
- 16 M. Baines, *Clin. Chim. Acta*, 153 (1985) 43.
- 17 A. M. Prentice and J. Bates, *Br. J. Nutr.*, 45 (1981) 37.
- 18 J. B. Ubbink, W. J. Serfontein and L. S. DeVilliers, *J. Chromatogr.*, 375 (1986) 399.
- 19 J. B. Ubbink, W. J. Serfontein and L. S. DeVilliers, *J. Chromatogr.*, 342 (1985) 277.
- 20 H. Y. Mohammed and H. Vening, *J. Chromatogr.*, 226 (1981) 471.
- 21 G. Jaumann and H. Engelhardt, *Chromatographia*, 20 (1985) 615.

Displacement chromatography on cyclodextrin–silicas

III. Enantiomer separations

GYULA VIGH*, GILBERTO QUINTERO and GYULA FARKAS

Chemistry Department, Texas A&M University, College Station, TX 77843-3255 (U.S.A.)

SUMMARY

The feasibility of preparative enantiomer separations by displacement chromatography on analytical-scale β -cyclodextrin–silica columns, operated in the reversed-phase mode, was demonstrated using the enantiomers of mephobarbital, hexobarbital, dansylleucine, dansylvaline and dansylphenylalanine as model solutes. The method development scheme (which relies on the determination of the elution-mode retention behavior and the adsorption isotherms of the solutes and the candidate displacers) described in Parts I and II can be used to select the appropriate displacers and the conditions leading to a successful displacement chromatographic separation. The importance of the displacer (both type and concentration) to the success of the displacement chromatographic separation is demonstrated.

INTRODUCTION

Cyclodextrins are toroidally shaped molecules that contain 6–8 glucose units (α - to γ -cyclodextrins). The interior of the cyclodextrin cavity is hydrophobic and the exterior is hydrophilic owing to the presence of secondary hydroxyl groups at the larger lip of the cavity and primary hydroxyl groups at the smaller lip of the cavity^{1–3}. Cyclodextrins can form inclusion complexes with molecules that penetrate their cavities^{4,5}. The stability of the complex depends on the tightness of the fit between the solute and the cavity and the strength of their secondary intermolecular interactions (mostly hydrogen bonds)⁶.

In liquid chromatography, cyclodextrins can be used either as mobile phase additives⁷ or as stationary phases^{3,8–12}. Cyclodextrins as mobile phase additives work well in analytical separations, but they are impractical in preparative separations, as they must be removed from the product. The cyclodextrin stationary phases are either cyclodextrin polymers^{13,14} or cyclodextrin–silicas^{10,15–21}. Currently, the hydrolytically stable cyclodextrin–silica stationary phases developed by Armstrong and co-workers^{17–19} and commercially available from Astec (Whippany, NJ, U.S.A.)²⁰ are used for most separations.

Cyclodextrins can effect the chromatographic separation of positional isomers^{21–27}, geometrical and *cis/trans* isomers^{28–33} and, owing to the presence of chiral carbon atoms, enantiomers^{34–44}.

The resolution of enantiomers by cyclodextrin stationary phases has been extensively reviewed recently^{9,10,12,37}. Chiral recognition is believed to be caused by the concerted action of inclusion complex formation between the cavity and the hydrophobic part of the solute, hydrogen bond formation between the polar functional groups of the solute in the vicinity of its chiral center and the hydroxyl groups of the cyclodextrin molecule and by the steric hindrance of substituents around the chiral center, which weaken the strength of hydrogen bonding for one of the enantiomers³⁸. Separation selectivities for the enantiomeric pairs are generally low, 1.03–1.2^{38–40}. Diastereomers occasionally show higher (2.0) separation factors³⁹.

Although there is a rich literature on the analytical-scale chromatographic application of cyclodextrin–silicas^{12–44}, papers on its preparative chromatographic use are scarce²⁰. Cyclodextrin silicas have three major drawbacks in preparative elution-mode chromatographic separations: (i) strong non-selective solute retention, (ii) low chiral selectivity and (iii) low load capacity compared with that of the other silica-based stationary phases. Therefore, the conventional elution-mode preparative separation strategy cannot be applied very well with cyclodextrin–silicas. However, some of these problems can be eliminated when cyclodextrin–silicas are used for preparative chiral separations in the displacement mode.

The old, but unique, operating principles of displacement chromatography^{45–51} can be combined with modern HPLC equipment to achieve efficient preparative separations, as demonstrated by Horváth and co-workers^{52–61}. Currently, several research groups are pursuing the theoretical and practical aspects of displacement chromatography^{52–70}.

In displacement chromatography, the sample is adsorbed on the top of the column, which is pre-equilibrated with the carrier, which is a solvent so weak that it cannot elute the sample. The sample will start to move only when it is removed from the stationary phase by the more strongly adsorbing displacer, which is fed continuously into the column at a high concentration. As the sample and displacer fronts move down the column, the components become separated according to their adsorption strengths. Eventually, in the fully developed displacement train, all components move with the velocity of the displacer front, which, in turn, depends on the adsorption isotherm and concentration of the displacer. High solute concentrations and column loads can be achieved in the displacement mode.

Although considerable information is available on the selection of the operation parameters in displacement chromatography^{52–65}, little is known about the rules of displacer selection and selectivity control. The greatest hindrance to the wider use and acceptance of displacement chromatography is the paucity of well characterized displacers and the lack of solute adsorption isotherms. Displacer selection is still done by trial and error. Most modern displacement chromatographic separations rely on a reversed-phase system to separate small polar molecules, antibiotics, oligopeptides and small proteins^{52–65}.

In Parts I⁶⁶ and II⁶⁷ we described the first displacement chromatographic separations that were realized with cyclodextrin–silicas. We combined the unique chromatographic selectivity of cyclodextrins with the preparative efficiency of displace-

ment chromatography and successfully separated several geometrical, positional⁶⁶ and *cis/trans* isomers⁶⁷. Samples as large as 60 mg could be loaded onto and separated with 4.6 mm I.D. analytical columns, operated in the reversed-phase mode. In this paper we describe the use of the same phase system for the displacement chromatographic separation of enantiomers.

EXPERIMENTAL

A computer-controlled displacement chromatograph was built for these studies, as described in Part I⁶⁶. Separations were carried out with commercially available 5- μm β -cyclodextrin-silica, Cyclobond I (Astec, Whippany, NJ, U.S.A.). The columns were slurry packed in our laboratory into 4.6 mm I.D. stainless-steel tubes of different lengths. All measurements were carried out at 30°C, maintained by thermostated water-jackets. The solute and displacer adsorption isotherms were determined by the breakthrough method, as described in Part I⁶⁶.

The barbitals and dansylamino acids were from Sigma (St. Louis, MO, U.S.A.) and the displacers from Aldrich (Milwaukee, WI, U.S.A.). All substances were used without further purification. The carrier and displacer solutions were prepared from HPLC-grade methanol and acetonitrile (Fisher, Fair Lawn, NJ, U.S.A.) and water produced by a Milli-Q unit (Millipore, Bedford, MA, U.S.A.).

The solutions were freshly prepared immediately before use by the weighing method described in Part I⁶⁶.

RESULTS

The purpose of these studies was to determine whether efficient, preparative-scale enantiomer separations are possible when cyclodextrin-silica columns are strongly overloaded and operated according to the principles of non-linear chromatography in the displacement mode. Members of two characteristic, very different substance families, barbiturates and dansylated amino acids, were used as model substances.

Preparative displacement chromatographic separation of barbiturate enantiomers

The analytical separation of the enantiomers of mephobarbital and hexobarbital was achieved with methanol-buffer eluents on Cyclobond I β -cyclodextrin-silica¹⁰. As discussed in Parts I and II^{66,67}, the first step in the development of a displacement chromatographic separation is the determination of the composition of the carrier solution. The analytical separations are often good starting points for the development of a displacement chromatographic separation.

In order to find the carrier composition that provides $k' > 5-10$ for the least retained solute^{66,67}, the $\log k'$ vs. methanol concentration relationship had to be determined. Fig. 1 shows the $\log k'$ vs. methanol concentration relationship for the mephobarbital enantiomers. As it was known from our previous work⁶⁶ that 1-naphthol is a good displacer, it was also included in the retention studies. Fig. 1 shows that the k' of (*S*)-mephobarbital exceeds 10 when the methanol concentration of the eluent becomes less than 20% (v/v). Therefore, 20% (v/v) aqueous methanol was selected as the carrier solvent.

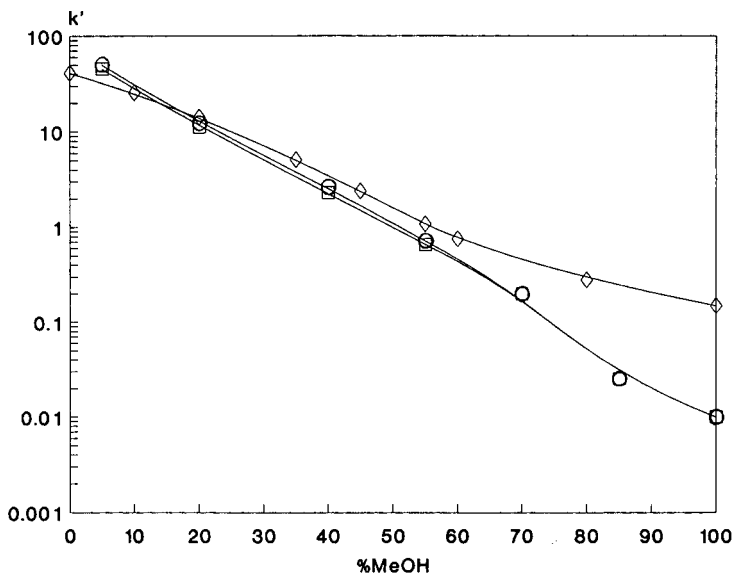


Fig. 1. Retention of the mephobarbital enantiomers and 1-naphthol on β -cyclodextrin-silica as a function of the methanol concentration of the eluent. For chromatographic conditions, see text. \diamond = 1-Naphthol; \square = (*S*)-mephobarbital; \circ = (*R*)-mephobarbital. MeOH = Methanol.

The log k' of the barbital enantiomers varies more steeply than that of 1-naphthol with methanol concentration and the retention curves cross at ca. 13% (v/v) methanol. However, in 20% (v/v) aqueous methanol, which was selected as the carrier solution, the k' of 1-naphthol (14.2) is larger than that of the more retained enantiomer, (*R*)-mephobarbital ($k' = 12.1$). Therefore, 1-naphthol was tried as a potential displacer.

The adsorption isotherms of 1-naphthol and the breakthrough volumes corresponding to each point on the isotherm were known from our previous work on the displacement chromatographic separation of positional and geometrical isomers⁶⁶. As the concentration of the displacer increases, the corresponding breakthrough volume decreases. Therefore, the highest safe displacer concentration, at which the breakthrough volume of the displacer is equal to (or greater than) the elution volume of the last-eluted (*R*)-mephobarbital, can be selected (5 mM). This value represents a conservative estimate ensuring that the displacer front will not overrun the solute, even if the concentration of the solute is very low. In reality, higher displacer concentrations are still permissible, because the partition coefficient of the solute also decreases as the sample concentration increases.

The displacement chromatogram of a 6.1 μ mol sample of racemic mephobarbital is shown in Fig. 2. The displacer was a 5 mM solution of 1-naphthol in 20% (v/v) aqueous methanol. The flow-rate of the displacer was 0.2 ml/min and the temperature was 30°C. Effluent fractions of 0.2 ml were collected during the separation and subsequently analysed in the elution mode. The analytical results are plotted in Fig. 3, yielding the reconstructed displacement chromatogram of mephobarbital. It can be seen that, although the elution-mode separation selectivity for the mephobarbital

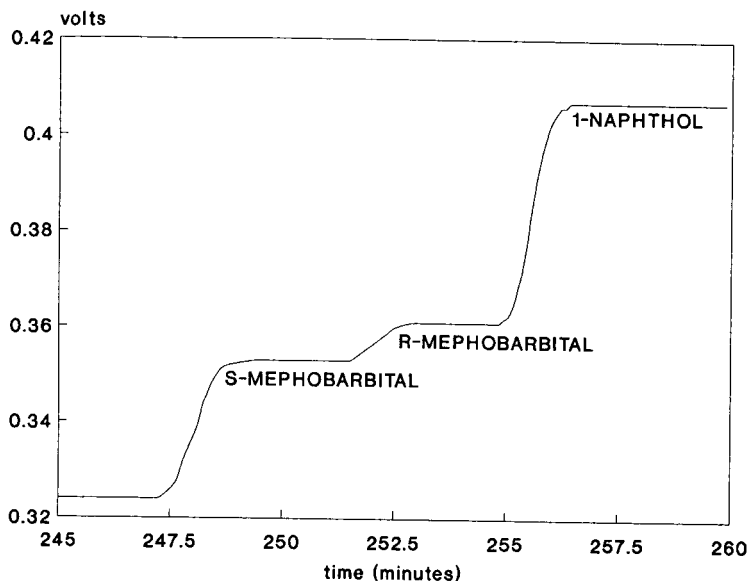


Fig. 2. Displacement chromatogram of a 6.1- μ mol racemic mephobarbital sample on two 250 \times 4.6 mm I.D. analytical β -cyclodextrin-silica columns, with a 5-mM solution of 1-naphthol in 20% (v/v) aqueous methanol as displacer; flow-rate, 0.2 ml/min; 30°C.

enantiomers is only 1.08, good separation of the two enantiomers is achieved in the preparative displacement mode.

Fig. 4 shows the $\log k'$ vs. methanol concentration relationship for the hexobarbital enantiomers and 1-naphthol. Again, sufficient retention is observed with 20%

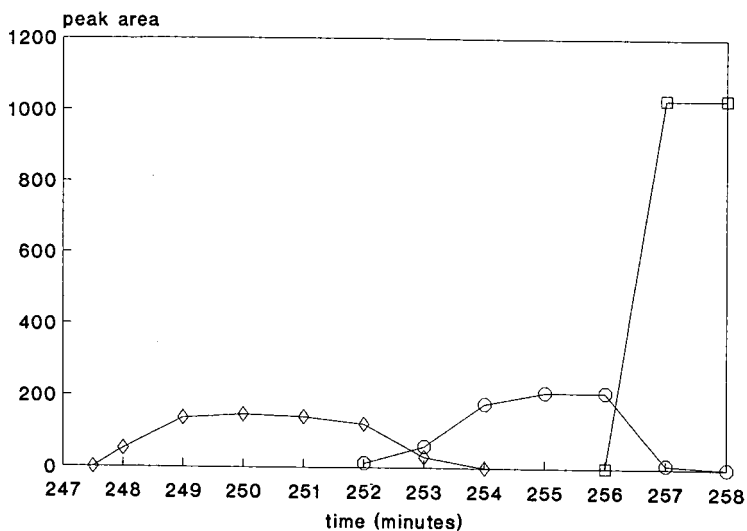


Fig. 3. Reconstructed displacement chromatogram of the separation shown in Fig. 2. Fraction size, 200 μ l. \diamond = (S)-Mephobarbital; \triangle = (R)-mephobarbital; \square = 1-naphthol. Peak area $\times 10^{-3}$ mV \cdot s.

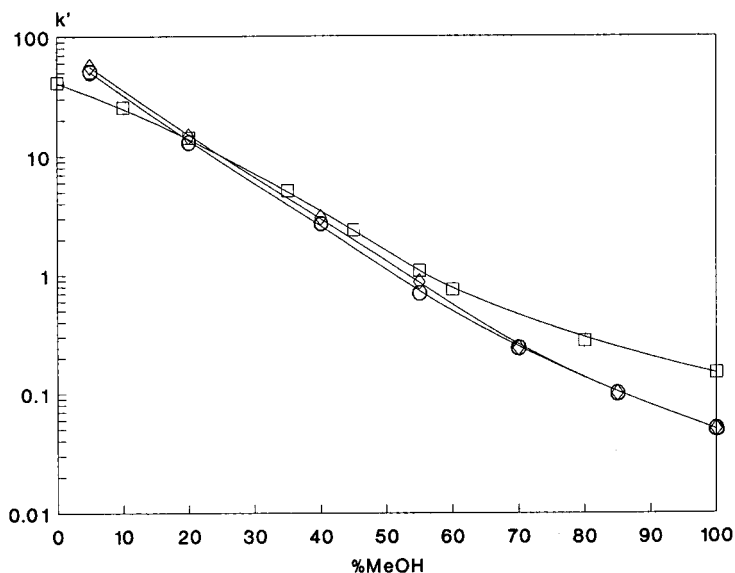


Fig. 4. Retention of the hexobarbital enantiomers and 1-naphthol on β -cyclodextrin-silica as a function of the methanol concentration of the eluent. \square = 1-Naphthol; \circ = (S)-hexobarbital; \triangle = (R)-hexobarbital.

(v/v) aqueous methanol carrier solutions. However, the hexobarbital enantiomers are more retained than the mephobarbital enantiomers, and 1-naphthol is eluted together with them by 20% (v/v) methanol. This indicates that 1-naphthol probably cannot be used as a displacer.

However, it was known from our previous work on the displacement chromatographic separation of positional isomers that cetrimide is more retained than 1-naphthol on β -cyclodextrin-silica. Cetrimide also proved to be an appropriate displacer for the separation of the naphthol isomers (see Figs. 10 and 11 in ref. 66). Therefore, a 1.5 mM cetrimide solution was prepared with the carrier solvent and used as displacer.

The displacement chromatogram of a 4- μ mol sample of racemic hexobarbital is shown in Fig. 5. The separation conditions were the same as for the mephobarbitals. Again, a clear separation of the enantiomers is obtained in the displacement mode, even though the selectivity factor for the two enantiomers in the elution mode is only 1.1.

Preparative displacement chromatographic separation of the enantiomers of dansylated amino acids

Elution-mode, analytical separations of the enantiomers of dansylated leucine, valine and phenylalanine have been carried out with β -cyclodextrin-silica and methanol-buffer eluents^{10,17,18,38}. Based on this information, a methanol concentration range leading to k' values between 5 and 20 was selected, and the capacity factors of the individual amino acid enantiomers were determined. The results are given in Table I. It can be seen that the dansylamino acids are much more strongly retained

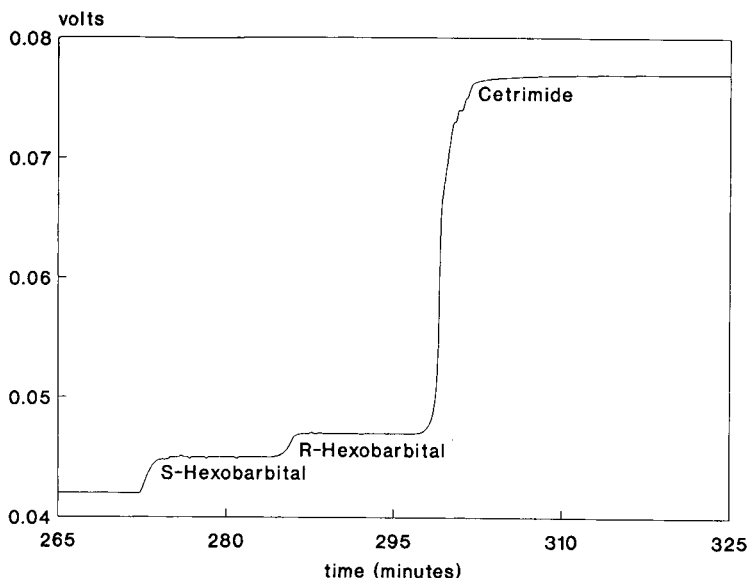


Fig. 5. Displacement chromatogram of a 4- μ mol racemic hexobarbital sample on two 250 \times 4.6 mm I.D. analytical β -cyclodextrin-silica columns, with a 1.5- M solution of cetrimide in 20% (v/v) aqueous methanol as displacer; flow-rate, 0.2 ml/min; 30°C.

than the previously studied barbiturates. The displacers described in Parts I and II^{66,67} are too weak to be used with the dansylamino acids. Therefore, a detailed search was initiated to design and synthesize a series of displacers with tailor-made retention and adsorption characteristics. These displacers consists of three main parts: an anchor group that forms an inclusion complex with the cyclodextrin cavity, a middle section that can interact via hydrogen bonding with the secondary hydroxyl groups at the larger opening of the cavity and a solubility-adjusting section that prefers the mobile phase. The results of this work will be reported in future papers^{68,69}.

TABLE I

CAPACITY FACTORS (k') AND SEPARATION SELECTIVITY FACTORS (α) OF DANSYLAMINO ACID ENANTIOMERS ON A β -CYCLODEXTRIN-SILICA COLUMN, WITH TWO METHANOL-BUFFER [0.01% (w/w) TRIETHYLAMMONIUM ACETATE, pH 4.1] ELUENTS

Solute	Enantiomer	50% (v/v) methanol		40% (v/v) methanol	
		k'	α	k'	α
Dansylleucine	D	6.57	1.05	14.61	1.07
	L	6.23		13.62	
Dansylvaline	D	6.69	1.06	14.88	1.08
	L	6.29		13.78	
Dansylphenylalanine	D	12.04	1.06	25.32	1.07
	L	11.41		23.58	

TABLE II

CAPACITY FACTORS k' OF TWO DINITROPHENYL FUNCTIONAL-GROUP-BASED DISPLACERS ON A β -CYCLODEXTRIN-SILICA COLUMN WITH TWO DIFFERENT METHANOL-BUFFER [0.01% (w/w) TRIETHYLAMMONIUM ACETATE, pH 4.1] ELUENTS

Compound	k'	
	50% (v/v) methanol	40% (v/v) methanol
2,4-Dinitrophenol	10.66	19.30
3,5-Dinitrobenzoic acid	13.27	18.67

Two of these potential displacers, both with a dinitrophenyl functional group, are more retained (Table II) than the dansylated amino acids (Table I), and have favorable solubilities in 40% (v/v) methanol-buffer solutions [0.01% (w/w) triethylammonium acetate, pH 4.1]. Both of them can be considered as potential displacers for the separation of the enantiomers of the dansylated amino acids. To test this hypothesis, their adsorption isotherms were determined in this solvent. Regular Langmuirian adsorption behavior was observed, as shown in Fig. 6.

Using the isotherms as guidelines, the displacement chromatogram of a 5.6-mg sample of racemic dansylleucine was obtained with a 10 mM solution of 2,4-dinitrophenol in the carrier solvent as displacer. The displacement chromatogram is shown in Fig. 7. The steps observed in the chromatogram have very similar heights,

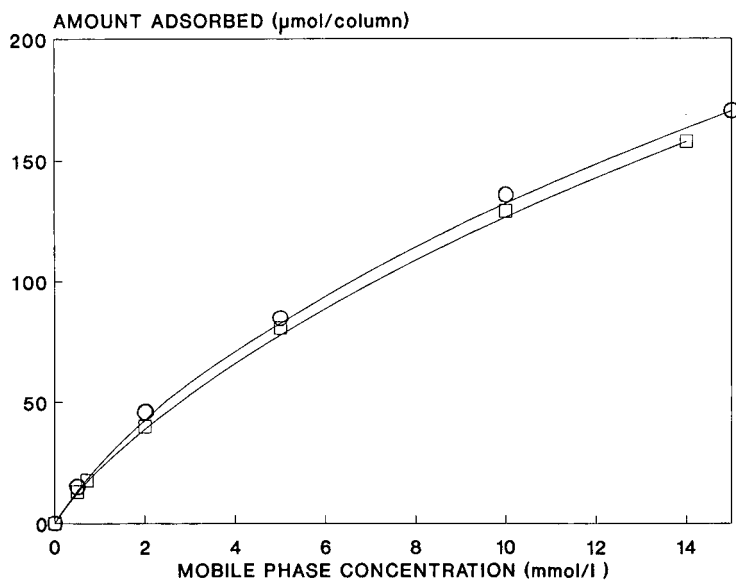


Fig. 6. Adsorption isotherms of (□) 2,4-dinitrophenol and (○) 3,5-dinitrobenzoic acid from 40% v/v methanol-buffer [0.01% (w/w) triethylammonium acetate, pH 4.1] on a β -cyclodextrin-silica column.

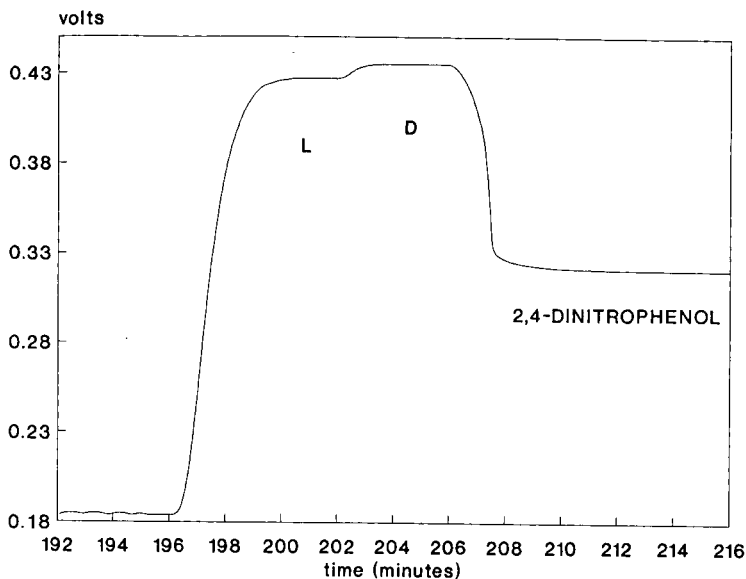


Fig. 7. Displacement chromatogram of a 5.6-mg racemic dansylleucine sample on two 250×4.6 mm I.D. analytical β -cyclodextrin-silica columns, with a 10-mM solution of 2,4-dinitrophenol in 40% (v/v) methanol-buffer [0.01% (w/w) triethylammonium acetate, pH 4.1] as displacer; flow-rate, 0.2 ml/min; 30°C.

because the adsorption isotherms of the enantiomers are very close to each other, and the equilibrium concentrations of the enantiomers in the fully developed displacement train (determined by the intersection of the operational line and the adsorption isotherms) are very similar. As their molar refractive indices are identical, the observed signals are almost the same. However, this does not mean that their separation is not complete: the quality of the separation is reflected by the ratio of the width of the pure band to the width of the transition band (information on the horizontal axis), and not by the ratio of the band heights (information of the vertical axis).

The displacement chromatogram of a 6.3-mg sample of racemic dansyl valine was obtained with a 10.5 mM solution of 2,4-dinitrophenol in the carrier solvent as displacer. The displacement chromatogram is shown in Fig. 8. As in the previous instance, the steps observed in the chromatogram have similar heights. For both amino acids good enantiomer separation was obtained in the displacement mode, even though the selectivity factors in the elution mode are as small as 1.07 and 1.08 (Table I).

As the retention of dansylphenylalanine in 40% (v/v) methanol-buffer solution is too large ($k' = 25.3$, Table I), 50% (v/v) methanol-buffer carrier solution had to be selected for the analysis. In this carrier, one of the potential displacers, 3,5-dinitrobenzoic acid, is more retained than the D-enantiomer of dansylphenylalanine and it was therefore selected as a displacer.

However, when the displacement chromatographic separation was attempted as before, analysis of the second step, the band of the dansyl-D-phenylalanine enantiomer showed that it contained a mixture of dansyl-D-phenylalanine and 3,5-

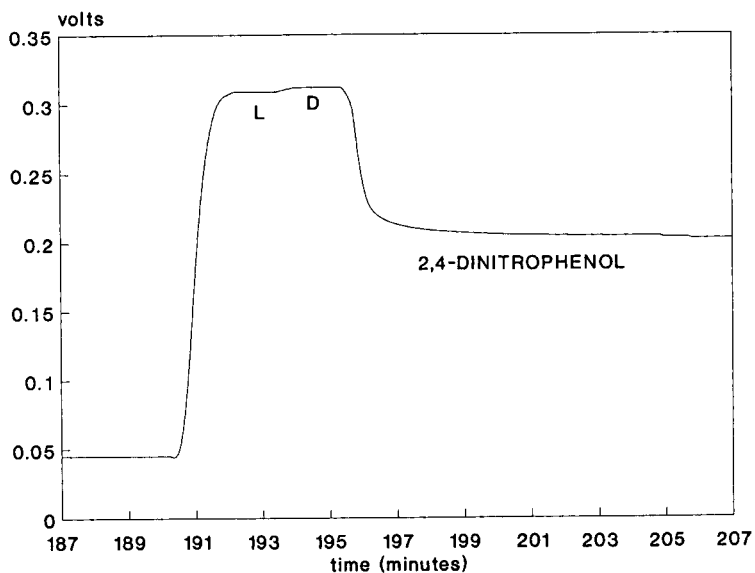


Fig. 8. Displacement chromatogram of a 6.3-mg racemic dansylvaline sample on two 250×4.6 mm I.D. analytical β -cyclodextrin-silica columns, with a 10.5-mM solution of 2,4-dinitrophenol in 40% (v/v) methanol-buffer [0.01% (w/w) triethylammonium acetate, pH 4.1] as displacer; flow-rate, 0.2 ml/min; 30°C.

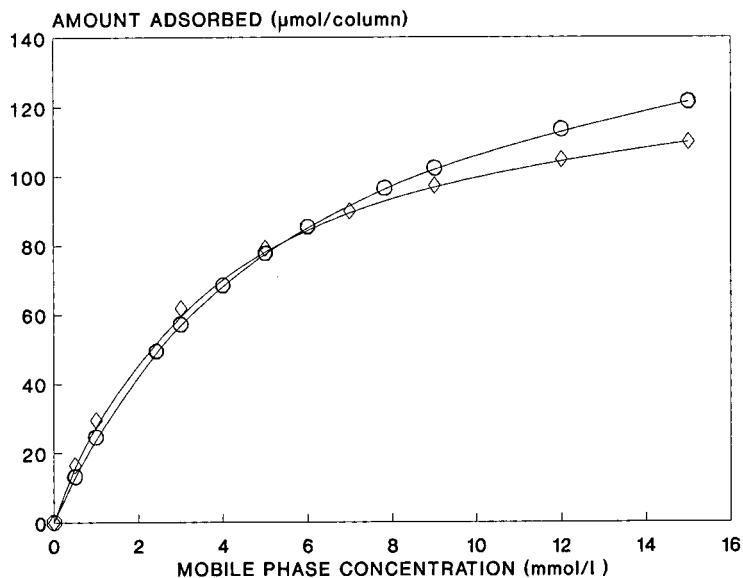


Fig. 9. Adsorption isotherms of (○) dansyl-*d*-phenylalanine and (◇) 3,5-dinitrobenzoic acid from 50% (v/v) methanol-buffer [0.01% (w/w) triethylammonium acetate, pH 4.1] on a β -cyclodextrin-silica column.

dinitrobenzoic acid. The concentration ratio of the two components remained almost constant along the entire band.

In order to find the reasons for the failed separation, the adsorption isotherms of both 3,5-dinitrobenzoic acid and dansyl-*D*-phenylalanine were determined in 50% (v/v) methanol carrier solvent. The results are shown in Fig. 9. It can be seen that dansyl-*D*-phenylalanine is more strongly adsorbed at low concentrations than is 3,5-dinitrobenzoic acid, but the two isotherms cross at higher concentrations. This means that an adsorption azeotrope⁷⁰ is formed, and separation is impossible with this displacer. This again indicates that, even though the knowledge of the elution-mode retention behaviour of the solutes and the displacers is important for the design of a displacement chromatographic separation, it is by no means sufficient in certain instances. Knowledge of the non-linear behavior of the system is indispensable for the solution of these separation problems.

CONCLUSIONS

This work has shown that the simple method development guidelines described in Parts I and II^{66,67} for the separation of positional, geometrical and *cis/trans* isomers can also be used to develop preparative, displacement chromatographic separations of enantiomers on cyclodextrin-silica stationary phases.

In most instances, the elution-mode $\log k'$ vs. organic modifier concentration, k' vs. pH and k' vs. ionic strength relationships must first be determined in order to select the composition of the carrier solution that will ensure sufficient initial sample retention for the least retained enantiomer ($5 < k' < 10$). Potential displacers can then be selected by comparing their initial breakthrough volumes and the elution-mode capacity factor of the most retained solute.

The adsorption isotherms of the selected displacer (and, preferably, of the most retained solute) must be determined when a separation has to be designed for a more complex situation. Knowledge of the adsorption isotherms takes the guesswork out of the design of the initial displacement chromatographic separation and accounts for the solubility limitations and peculiar adsorption characteristics of both the solutes and the displacer.

The first displacement chromatographic separations of a number of racemic model substances (barbiturates and amino acids) were accomplished using analytical-scale β -cyclodextrin-silica columns, methanol-buffer and acetonitrile-buffer carrier solutions and several non-chiral displacers. Further work is in progress in our laboratory to design, synthesize and characterize a number of displacers with tailor-made adsorption and solubility characteristics and to solve several isomer and enantiomer separation problems that are of current interest to the pharmaceutical industry and to the life sciences.

ACKNOWLEDGEMENTS

Financial support by the Texas Coordination Board of Higher Education TATR program (Grant Number 3376) and the Minority Access for Research Careers, National Institute of Health program (Grant Number 5F31GM11689) is acknowledged. The authors are grateful to Dr. Thomas Beesley of Astec for the β -cyclodextrin-silica stationary phase sample used.

REFERENCES

- 1 J. Szejtli, *Cyclodextrins and Their Inclusion Complexes*, Akadémiai Kiadó, Budapest, 1982.
- 2 M. L. Bender and M. Komiyama, *Cyclodextrin Chemistry*, Springer, Berlin, 1978.
- 3 J. Szejtli, B. Zsardon and T. Cserhati, in W. L. Hinze and D. W. Armstrong (Editors), *Ordered Media in Chemical Separations (ACS Symposium Series, Vol. 342)*, American Chemical Society, Washington, DC, 1987, p. 200.
- 4 K. A. Connors and D. D. Pendergast, *J. Am. Chem. Soc.*, 106 (1984) 7607.
- 5 R. E. Boehm, D. E. Martire and D. W. Armstrong, *Anal. Chem.*, 60 (1988) 522.
- 6 L. A. Spino and D. W. Armstrong, in W. L. Hinze and D. W. Armstrong (Editors), *Ordered Media in Chemical Separations (ACS Symposium Series, Vol. 342)*, American Chemical Society, Washington, DC, 1987, p. 235.
- 7 D. Sybilska, in W. L. Hinze and D. W. Armstrong (Editors), *Ordered Media in Chemical Separations (ACS Symposium Series, Vol. 342)*, American Chemical Society, Washington, DC, 1987, p. 218.
- 8 E. Smolkova-Keulemansova and L. Sojak, in W. L. Hinze and D. W. Armstrong (Editors), *Ordered Media in Chemical Separations (ACS Symposium Series, Vol. 342)*, American Chemical Society, Washington, DC, 1987, p. 247.
- 9 D. W. Armstrong, *J. Liq. Chromatogr.*, 7 (1984) 353.
- 10 T. J. Ward and D. W. Armstrong, *J. Liq. Chromatogr.*, 9 (1986) 407.
- 11 R. Dappen, H. Arm and V. R. Meyer, *J. Chromatogr.*, 373 (1986) 1.
- 12 W. H. Pirkle, in S. Ahuja (Editor), *Chromatography and Separation Chemistry: Advances and Developments (ACS Symposium Series, Vol. 297)*, American Chemical Society, Washington, DC, 1986, p. 101.
- 13 B. Zsardon, L. Decsi, M. Szilasi, F. Tudos and J. Szejtli, *J. Chromatogr.*, 270 (1983) 127.
- 14 B. Zsardon, L. Szilasi, F. Tudos and J. Szejtli, *J. Chromatogr.*, 208 (1980) 109.
- 15 Y. Kawaguchi, M. Tanaka, N. Nakae, K. Funazo and T. Shono, *Anal. Chem.*, 55 (1983) 1852.
- 16 K. Fujimura, T. Ueda and T. Ando, *Anal. Chem.*, 55 (1983) 446.
- 17 D. W. Armstrong, *U.S. Pat.*, 4 539 399, 1985.
- 18 D. W. Armstrong and W. DeMond, *J. Chromatogr. Sci.*, 22 (1984) 411.
- 19 D. W. Armstrong, A. Alak, W. DeMond, W. L. Hinze and T. E. Riehl, *J. Liq. Chromatogr.*, 8 (1985) 261.
- 20 *Cyclobond Handbook*, Astec, Whippany, NJ, 1988.
- 21 M. Tanaka, H. Ikeda and T. Shono, *J. Chromatogr.*, 398 (1987) 165.
- 22 D. W. Armstrong, W. DeMond, A. Alak, W. Hinze, T. E. Riehl and K. H. Bui, *Anal. Chem.*, 57 (1985) 234.
- 23 C. A. Chang, H. Abdel-Aziz, N. Melchor, Q. Wu, K. H. Pannell and D. W. Armstrong, *J. Chromatogr.*, 347 (1985) 51.
- 24 C. A. Chang, Q. Wu and L. Tan, *J. Chromatogr.*, 361 (1986) 199.
- 25 C. A. Chang, Q. Wu and D. W. Armstrong, *J. Chromatogr.*, 354 (1986) 454.
- 26 C. A. Chang and Q. Wu, *J. Liq. Chromatogr.*, 10 (1987) 1359.
- 27 J. Zukowski, D. Sybilska and J. Jurczak, *Anal. Chem.*, 57 (1985) 2215.
- 28 G. W. Tindall, *J. Liq. Chromatogr.*, 10 (1987) 1077.
- 29 B. G. Snider, *J. Chromatogr.*, 351 (1986) 548.
- 30 H. J. Issaq, *J. Liq. Chromatogr.*, 9 (1986) 229.
- 31 H. J. Issaq, D. Weiss, C. Ridlon, S. D. Fox and G. M. Muschik, *J. Liq. Chromatogr.*, 9 (1986) 1791.
- 32 S. L. Abidi, *J. Chromatogr.*, 362 (1986) 33.
- 33 R. D. Armstrong, T. J. Ward, N. Pattabiraman, C. Benz and D. W. Armstrong, *J. Chromatogr.*, 414 (1987) 192.
- 34 H. J. Issaq, J. H. McConnell, D. E. Weiss, D. G. Williams and J. E. Saavedra, *J. Liq. Chromatogr.*, 9 (1986) 1783.
- 35 H. J. Issaq, Glennon, D. E. Weiss, G. N. Chmurny and J. E. Saavedra, *J. Liq. Chromatogr.*, 9 (1986) 2763.
- 36 R. D. Armstrong, in W. L. Hinze and D. W. Armstrong (Editors), *Ordered Media in Chemical Separations (ACS Symposium Series, Vol. 342)*, American Chemical Society, Washington, DC, 1987, p. 273.
- 37 D. W. Armstrong, *Anal. Chem.*, 59 (1987) 84A.
- 38 W. L. Hinze, T. E. Riehl, D. W. Armstrong, W. DeMond, A. Alak and T. Ward, *Anal. Chem.*, 57 (1985) 237.

- 39 D. W. Armstrong, W. DeMond and B. P. Czech, *Anal. Chem.*, 57 (1985) 481.
- 40 D. W. Armstrong, T. J. Ward, A. Czech, B. P. Czech and R. A. Bartsch, *J. Org. Chem.*, 50 (1987) 5556.
- 41 J. S. McClanahan and J. H. Maguire, *J. Chromatogr.*, 381 (1986) 438.
- 42 J. Florance, A. Galdes, Z. Konteatis, Z. Kosarych, K. Langer and C. Martucci, *J. Chromatogr.*, 414 (1987) 313.
- 43 J. H. Maguire, *J. Chromatogr.*, 387 (1987) 453.
- 44 D. W. Armstrong, X. Yang, S. M. Han and R. A. Menges, *Anal. Chem.*, 59 (1987) 2594.
- 45 A. Tiselius, *Ark. Kemi Mineral. Geol.*, 16A (1943) 1.
- 46 G. Claesson, *Ark. Kemi Mineral. Geol.*, 24A (1946) 1.
- 47 S. M. Partridge and R. C. Brimley, *Biochem. J.*, 51 (1952) 628.
- 48 J. E. Powell and F. H. Spedding, *Chem. Eng. Symp. Ser.*, 55 (1959) 101.
- 49 F. G. Helfferich, *Ind. Eng. Chem., Fundam.*, 6 (1967) 362.
- 50 F. G. Helfferich and D. B. James, *J. Chromatogr.*, 46 (1970) 1.
- 51 F. G. Helfferich and G. Klein, *Multicomponent Chromatography — Theory of Interference*, Marcel Decker, New York, 1970.
- 52 H. Kalasz and Cs. Horváth, *J. Chromatogr.*, 215 (1981) 295.
- 53 Cs. Horváth, A. Nahum and J. H. Frenz, *J. Chromatogr.*, 218 (1981) 365.
- 54 Cs. Horváth, J. H. Frenz and Z. El Rassi, *J. Chromatogr.*, 255 (1983) 273.
- 55 Cs. Horváth and W. R. Melander, in E. Hefmann (Editor), *Chromatography, Part A, Fundamentals and Techniques (Journal of Chromatography Library, Vol. 22A)*, Elsevier, Amsterdam, 1983, p. A27.
- 56 J. Jacobson, J. H. Frenz and Cs. Horváth, *J. Chromatogr.*, 316 (1984) 53.
- 57 J. H. Frenz and Cs. Horváth, *AIChE J.*, 31 (1985) 400.
- 58 Cs. Horváth, in F. Bruner (Editor), *The Science of Chromatography (Journal of Chromatography Library, Vol. 32)*, Elsevier, Amsterdam, 1985, p. 179.
- 59 J. Jacobson, J. H. Frenz and Cs. Horváth, *Ind. Eng. Chem. Res.*, 26 (1987) 43.
- 60 S. M. Cramer, Z. El Rassi, D. M. LeMaster and Cs. Horváth, *Chromatographia*, 24 (1987) 881.
- 61 S. M. Cramer, Z. El. Rassi and Cs. Horváth, *J. Chromatogr.*, 394 (1987) 305.
- 62 G. Subramanian, M. W. Phillips and S. M. Cramer, *J. Chromatogr.*, 439 (1988) 341.
- 63 S. M. Cramer and Cs. Horváth, *Prep. Chromatogr.*, 1 (1988) 29.
- 64 M. W. Phillips, G., Subramanian and S. M. Cramer, *J. Chromatogr.*, 454 (1988) 1.
- 65 Gy. Vigh, Z. Varga-Puchony, J. Hlavay, G. Szepesi and M. Gazdag, *J. Chromatogr.*, 386 (1983) 353.
- 66 Gy. Vigh, G. Quintero and Gy. Farkas, *J. Chromatogr.*, 484 (1989) 237.
- 67 Gy. Vigh, Gy. Farkas and G. Quintero, *J. Chromatogr.*, 484 (1989) 251.
- 68 Gy. Vigh, in J. Nikelly and Cs. Horváth (Editors), *Separations in Analytical Biotechnology (ACS Symposium Series)*, American Chemical Society, Washington, DC, 1990.
- 69 G. Quintero, C. Jaszberenyi, Gy. Farkas and Gy. Vigh, in preparation.
- 70 A. Lee and Cs. Horváth, presented at the 196th National ACS Meeting, Los Angeles, CA, September 1988.

CHROMSYM. 1707

Solutions of the equilibrium and semi-equilibrium models of chromatography

SADRODDIN GOLSHAN-SHIRAZI and GEORGES GUIOCHON*

**Department of Chemistry, University of Tennessee, Knoxville, TN 37996-1600 and Division of Analytical Chemistry, Oak Ridge National Laboratory, Oak Ridge, TN (U.S.A.)*

SUMMARY

In contrast to the kinetic models, the ideal and semi-ideal models of chromatography assume the distribution of the compounds studied to be constantly at equilibrium (ideal model) or very close to equilibrium (semi-ideal model). An exact solution of the ideal model can be obtained under close form for a pure compound with any isotherm and for a binary mixture with competitive Langmuir isotherms. No exact solution of the semi-ideal model can be derived but numerical solutions are available for all isotherms. Approximate analytical solutions for this model can be obtained by assuming that the concentration of the compound studied in the mobile phase is small and, accordingly, that the equilibrium isotherm is parabolic and by neglecting some terms in the derivation. Depending on the assumptions made, the Houghton and the Haarhoff–Van der Linde equations are obtained.

These different solutions are compared. It is shown that the Haarhoff–Van der Linde equation is a much better approximation than the Houghton equation and that its range of validity depends essentially on the deviation between the true isotherm and its two-term expansion in the concentration range sampled by the band during its elution. It is usually valid for loading factors below 0.2% for an ideal column and $bC_{\text{Max}} \leq 0.05$ for real columns (the loading factor is the ratio of the sample size and the column saturation capacity, b is the second coefficient of a Langmuir isotherm and C_{Max} is the maximum concentration of the band). In practice, however, it can be used for loading factors up to 1% ($bC_{\text{Max}} \leq 0.1$ for real columns). The ideal model, in contrast, gives a valid presentation of experimental band profiles only at high sample size and column efficiencies. The reduced sample size, $m = N L_f [k'_0 / (1 + k'_0)]^2$ (N = column plate number, L_f = loading factor, k'_0 = column capacity factor), must be higher than 35. In the intermediate range, only numerical solutions can predict the band profiles accurately.

In the case of two components, the exact solution of the ideal model can be obtained under close form with competitive Langmuir isotherms. Numerical solutions can be obtained to simulate real columns. No other analytical solution, even approximate, is available. A correction made to the ideal model to account for the band-broadening effect of a finite efficiency gives good results and permits the in-

vestigation of the optimization of the experimental conditions of a separation for maximum production rate.

INTRODUCTION

Because of the importance recently acquired by preparative chromatography as a separation technique for the industrial extraction and purification of synthesis intermediates and of products in biotechnology, there is renewed interest in fundamental chromatography. In order to optimize a separation process, we need to be able to predict its results. In the case of preparative chromatography, we want an accurate prediction of the concentration signal observed at the outlet of the column as a function of the experimental parameters and of the initial and boundary conditions.

The derivation of accurate predictions requires the use of a sophisticated model. Such a model can rarely be solved exactly by an analytical solution, *i.e.*, in closed form. Approximations may be necessary or numerical solutions may be calculated. The former can be differentiated and the optimum conditions for maximum production rate under any combination of constraints regarding collected fraction purity and component recovery yield can be derived in a straightforward way. The latter have the advantage of being accurate, calculable with the required precision and available for almost any combination of the experimental parameters, but they require the selection of the proper numerical value for each parameter involved. Further, optimization is difficult to carry out using the numerical approach, as it needs repetitive calculations of chromatograms, for a long series of sets of variable experimental parameters.

Therefore, analytical solutions are highly desirable in order to investigate in detail the influence on the production rate of the column length, the size of the packing particles, the mobile phase flow velocity and composition, *i.e.*, the selectivity of the phase system, the non-linear behavior of the isotherm, the sample size and relative composition, the axial dispersion and the kinetics of radial mass transfer. Analytical solutions are so useful that we are ready to sacrifice some accuracy, make simplifying assumptions, in order to formulate a model which can be resolved into closed forms. It is important to know, however, what the importance of the error made in these simpler models is and the extent to which the profiles they predict for the concentration signal at the column exit deviate from the true profiles. The aim of this paper is to review the various analytical solutions that have been derived, assuming that the chromatographic phase system is constantly at equilibrium or very near it (*i.e.*, high column efficiency). In forthcoming papers, we shall present a similar investigation of the kinetic models of chromatography and a comparison between semi-equilibrium and kinetic models¹.

Although separation methods, and chromatography in particular, concern the extraction and purification of certain components of mixtures, the main thrust of this work will be on the prediction of the elution profile of pure compounds. There are several modes under which chromatography can be carried out, *e.g.*, isocratic, step and gradient elution, frontal analysis and displacement, but most of the theoretical effort has dealt with isocratic elution. More importantly, the difficulties with the two-component problem are such that very few papers have discussed it.

EQUILIBRIUM AND SEMI-EQUILIBRIUM MODELS

The most general approach to chromatography is a model which expresses that the mass of each component in the column is constant and relates the rate of mass transfer of each component to the local composition of the chromatographic system. The former condition is easy to write, and is called the mass balance equation. The theoretical difficulties begin with the formulation of the second set of equations, as kinetics are much more complicated than thermodynamics. Various equations, with different merits and drawbacks, have been written, which will be reviewed later¹. Because it has long been recognized that the mass transfer in the non-consolidated beds of porous particles used in chromatographic columns are usually very fast and that in most instances these columns are operated near equilibrium, a very popular and very fruitful approach is to assume, in a first step, that the mass transfer is infinitely fast and the column efficiency infinite. Then a perturbative correction is made, to take that efficiency into account. Another approach, equally fruitful, but for a different range of sample sizes, is to lump the coefficients of radial mass transfers into a coefficient of apparent axial dispersion and to consider the effect of a large concentration either as negligible (linear chromatography) or as a perturbation. Both approaches are, of course, doomed to failure when the mass transfer kinetics are very slow.

Before discussing these different approaches, we review first the basic equations of the model and the rationale for the development of the equilibrium and semi-equilibrium models (*i.e.*, the ideal and semi-ideal models).

Mass balance equation

This equation was derived by Wilson², 50 years ago. It states that the amount of a component which enters an infinitely thin slice of column in an infinitely short period of time is equal to the sum of what leaves the slice and what remains in it. It is written as

$$\frac{\partial C}{\partial t} + F \frac{\partial C_s}{\partial t} + u \frac{\partial C}{\partial z} = D \frac{\partial^2 C}{\partial z^2} \quad (1)$$

where C_s and C are the concentrations of the studied compound in the stationary and the mobile phase, respectively; z and t are the abscissa along the column (assumed to be one-dimensional) and time, respectively; u is the mobile phase velocity; F is the phase ratio, $(1 - \epsilon)/\epsilon$, where ϵ is the packing porosity, and D is the coefficient of axial dispersion, which includes the axial molecular diffusion, the packing tortuosity and the contribution of packing heterogeneity to the band dispersion.

The conditions under which this equation is a valid mass balance (non-compressible mobile phase, constant diffusion coefficient, constant partial molar volume of the solute and no sorption effect) have been discussed in previous publications and are not seriously restrictive³. An equation such as eqn. 1 should be written for each component of the system, except the mobile phase when it is pure or the weakest component of this phase^{4,5}. In practice, however, when the mobile phase is a mixed solvent and the strong components or additives of this solution are much less strongly adsorbed than the component of the sample, the mass balances of the components of the mobile phase can be neglected, provided that the isotherm of the sample components are measured by reference to the mobile phase⁴. This simplification is

valid as long as the column capacity factors of the mobile phase components at infinite dilution in the pure weak solvent are at least five times smaller than the column capacity factors of the sample components.

Kinetic equation

Eqn. 1 contains two functions of z and t , the concentrations of the studied compound in the stationary and the mobile phase. In order to solve this equation, we need a relationship between these two concentrations. Should we be able to formulate it, a kinetic equation can provide the needed intermediate.

A more detailed discussion of this problem will be presented in a forthcoming paper¹. Suffice it to say here that among the models which have been used to describe such kinetics, the three simplest are the following (in these equations, C_s is the local concentration of component in the stationary phase, q , the concentration in equilibrium with C in the mobile phase):

The Langmuir kinetics model:

$$\frac{\partial C_s}{\partial t} = k_a(q_s - C_s)C - k_d C_s \quad (2)$$

where q_s is the column saturation capacity (in the same units as C_s) and k_a and k_d are the adsorption and desorption rate constants of the compound, respectively. This equation has been used by Thomas⁶, Goldstein⁷ and later by Wade *et al.*⁸.

The linear kinetics model:

$$\frac{\partial C_s}{\partial t} = k_1 C - k_2 C_s \quad (3)$$

where k_1 and k_2 are rate constants, which has been used by Lapidus and Amundson⁹.

The linear driving force model:

$$\frac{\partial C_s}{\partial t} = k_f(q - C_s) \quad (4)$$

where q is the equilibrium value of C_s , when the mobile phase concentration is C (see discussion of the equilibrium isotherm, next section), and k_f is the lumped mass transfer coefficient. Eqn. 4 has been used by Glueckauf¹⁰, Hiester and Vermeulen¹¹ and later by Lin *et al.*¹² and Golshan-Shirazi *et al.*¹³. In linear chromatography (infinitely small sample size), this last model is a particular case of the linear kinetics model ($q = k'_0 C$, $k_f k'_0 = k_1$, $k_f = k_2$).

The properties, advantages and drawbacks of these models are discussed elsewhere, together with the characteristics of their solutions¹.

Initial and boundary conditions

All chromatographic problems can be solved by using the appropriate system of eqns. 1 and 2, 3 or 4, *i.e.*, the system composed of as many equations of either group as there are components involved in the system being studied. The solution, $C(z,t)$, the

concentration of the compound in the eluent at position z and time t , is determined, however, only when the initial and the boundary conditions are selected. The proper choice of these conditions permits the prediction of elution (constant mobile phase composition at column inlet, pulse injection), gradient elution (pulse injection, followed by pumping a mobile phase which is a ramp of strong solvent), displacement [column initially filled with a mobile phase, pulse injection, followed by the injection of a concentration plateau of a displacer (*i.e.*, a strongly retained compound) in the mobile phase], frontal analysis (injection of a concentration plateau of sample in the mobile phase, into a column filled with pure mobile phase). More complex boundary conditions can be easily derived to simulate sophisticated experiments.

In the most popular mode used in preparative chromatography, elution, the initial conditions correspond to a column filled with pure solvent:

$$C(z,0) = 0 \quad (5a)$$

and the boundary conditions correspond to a rectangular pulse injection of duration t_p and height C_0 :

$$C(0,t) = C_0 \quad 0 < t \leq t_p \quad (5b)$$

and:

$$C(0,t) = 0 \quad t_p < t \quad (5c)$$

Semi-equilibrium model in linear chromatography

In the case of a linear isotherm, Lapidus and Amundson⁹ derived an analytical solution of the system of partial differential equations combining the mass balance equation and a first-order mass transfer kinetic equation. This solution is valid only in analytical applications of chromatography, because of the limitation introduced by the assumption of a linear isotherm.

Van Deemter *et al.*¹⁴ were able to demonstrate that, when the sum of the mixing stage ($2D/u$) and the height of the mass transfer stage [$2uk'_0/(1 + k'_0)^2k_f$] is much smaller than the column length, L , the analytical solution derived by Lapidus and Amundson reduces to a Gaussian profile (k'_0 is the column capacity factor and k_f the lumped mass transfer coefficient of eqn. 4). In this case, the exact analytical solution of Lapidus and Amundson is equivalent to the solution of the simplified plate theory of Martin and Synge¹⁵. The Van Deemter equation provides the equivalence by relating the standard deviation of the Gaussian profile to which the solution of the Lapidus and Amundson equation reduces and the standard deviation of the plate model, through the value of the column plate height¹⁴:

$$H = \frac{2D}{u} + \frac{2uk'_0}{(1 + k'_0)^2k_f} \quad (6)$$

When the experimental conditions are such that the plate height increases to the point that it is no longer much smaller than the column length, the plate theory fails, and the

more general solution of Lapidus and Amundson must be used for an accurate prediction of the band profile.

Still within the framework of linear chromatography, Kucera¹⁶ derived the solution of the most general model of chromatography, with a mass balance including axial dispersion and kinetic equations including the contributions to the resistance to radial mass transfers which are due to diffusion across the boundary film between the mobile and the stagnant mobile phase, to intraparticle diffusion and to first-order reaction kinetics for the retention mechanism. This solution, however, is in closed form in the Laplace domain only, and it cannot be converted into the time domain. When the elution profile is Gaussian, comparison between the values of the second moment predicted by the general diffusion model and by the linear driving force model shows that the lumped mass transfer coefficient is related to the pore diffusion and the film mass transfer resistance by the following equation:

$$\frac{F}{k_0 k_f} = \frac{d_p}{6k_e} + \frac{d_p^2}{60\beta D_p} \quad (7)$$

where d_p is the average particle size, k_e is the external film mass transfer coefficient, F is the phase ratio, β is the inner porosity of the packing particles and D_p is the intraparticle diffusion coefficient.

Horvath and Lin¹⁷ and Huber¹⁸ derived relationships between the parameters of sophisticated mass transfer models and the column plate height. As often occurs in physical chemistry, difficulties arise when complex models have to be compared with experimental data, as the multiplication of the parameters introduced in the models in an effort to make them more exact increases arbitrarily the flexibility of the overall equation and at the same time makes the proper estimate of the various parameters more difficult and the final values less reliable.

The problem becomes much more complicated when the isotherm is not linear. There is no general analytical solution available which could compare with the solution of Lapidus and Amundson and could provide a tool for the investigation of column performance which would be as powerful and as general as the column HETP.

Semi-equilibrium model in non-linear chromatography

In his non-equilibrium theory, Giddings¹⁹ attempted to relate the band broadening due to the resistances to radial mass transfer and the experimental parameters. Central to this theoretical development is the assumption that the two phases of a chromatographic system are always close to equilibrium. This is certainly true in all modern, high-performance chromatographic techniques. The only possible exceptions are some implementations of ion-exchange chromatography and most applications of affinity chromatography, as the dissociation of the selective recognition complex is generally a slow process.

For the sake of simplicity, the concentrations in this subsection are referred to the total column volume, and not to the volumes of either mobile or stationary phases. We denote by C_m^* an equilibrium concentration and by \bar{C} an actual concentration. We can write

$$\bar{C}_m = \bar{C}_m^*(1 + \varepsilon_m) \quad (8a)$$

and

$$\bar{C}_s = \bar{C}_s^*(1 + \varepsilon_s) \quad (8b)$$

where ε_m and ε_s account for the departure from equilibrium. These quantities are small, since the system is always near equilibrium. This is because, although the concentration gradients may be large at times, they apply only over very short distances. ε_m and ε_s are related through

$$\varepsilon_m \bar{C}_m^* + \varepsilon_s \bar{C}_s^* = 0 \quad (9)$$

Now, ignoring the longitudinal, diffusional flux in the stationary phase, which is negligible, the flux of a compound, J , per unit column cross-sectional area, is

$$J = u\bar{C}_m = u\bar{C}_m^* + u\bar{C}_m^*\varepsilon_m \quad (10)$$

The second term in this equation, $\Delta J = u\bar{C}_m^*\varepsilon_m$, results from non-equilibrium. It is formally equivalent to a diffusion term, with a pseudo-diffusion coefficient \bar{D} , given by

$$D' = \frac{-\Delta J}{\partial \bar{C} / \partial z} = \frac{-u\bar{C}_m^*\varepsilon_m}{\partial \bar{C} / \partial z} \quad (11)$$

in accordance with Fick's law, where \bar{C} is the total solute concentration, hence $\bar{C}_m^* = R\bar{C}$, R being the fraction of solute in the mobile phase, *i.e.*, $1/(1 + k_0)$.

The beauty of this equation is that it shows that non-equilibrium effects, which result from lateral diffusion, can be treated as a contribution to axial dispersion. Accordingly, we can describe the chromatographic phenomenon by keeping the mass balance equation (eqn. 1), eliminate the kinetic equation from the system, replace the concentration in the stationary phase C_s in eqn. 1 by the value given by the equilibrium isotherm, $q = f(C)$, and replace the axial dispersion coefficient, D , by an apparent axial dispersion coefficient, related to the column HETP by $D_a = HL/2t_0$ (ref. 3).

Haarhoff and Van der Linde²⁰ have given a more general demonstration of this result, which is valid for a slightly overloaded column, with a parabolic isotherm. It leads to the following equation for the mass balance of a compound:

$$\frac{\partial C}{\partial t} + F \frac{\partial q}{\partial t} + u \frac{\partial C}{\partial x} = D_a \frac{\partial^2 C}{\partial z^2} \quad (12)$$

where q is the concentration of the solute in the stationary phase in equilibrium with the concentration, C , in the mobile phase, given by the isotherm equation:

$$q = f(C) \quad (13)$$

We shall discuss later the validity of this assumption and show in which range of column efficiency the semi-equilibrium model is an accurate chromatographic model¹.

Equilibrium model

If we assume that there is no axial dispersion and that the kinetics of radial mass transfer are infinitely fast, the mobile and the stationary phases are constantly at equilibrium. Then the mass balance of the compound studied (eqn. 1) becomes

$$u \frac{\partial C}{\partial z} + \left(1 + F \frac{dq}{dC} \right) \frac{\partial C}{\partial t} = 0 \quad (14)$$

Eqn. 14 was the form under which the mass balance was derived originally by Wilson², who also investigated its properties, but did not realize the possibility of the formation of shock or concentration discontinuities, which eqn. 14 can propagate as shown later by DeVault²¹ and as discussed recently by Lin *et al.*²². Thus, Wilson² concluded that the band width remains constant during the band migration, which is true only under linear conditions. Later, the problem was rediscussed by Weiss²³ and more rigorously by DeVault²¹, who explained the formation and propagation of concentration discontinuities. Glueckauf²⁴ extended the theoretical results of DeVault to the case of a sigmoidal isotherm.

The solution of the ideal model of chromatography has been intensively discussed in the past, notably by Glueckauf²⁴⁻²⁶, Amundson and co-workers^{27,28} and Guiochon and co-workers^{29,30}. Recently, an analytical solution has been formulated for the single-component problem in the case of a Langmuir isotherm³¹ and in the general case of any isotherm³². An analytical solution has also been demonstrated for a two-component mixture, when the equilibrium isotherms of the two components are given by the classical competitive Langmuir model^{33,34}. These solutions will be discussed and compared with the approximate analytical solutions and with the numerical solutions of the semi-ideal model^{3,35}.

ANALYTICAL SOLUTIONS OF THE IDEAL AND SEMI-IDEAL MODEL FOR A SINGLE COMPOUND

Four main solutions are available for the prediction of the elution profile of a pure compound on an overloaded chromatographic column. These equations are the analytical solution of the ideal model³², two approximate solutions of the semi-ideal model, suggested by Houghton³⁶ and Haarhoff and Van der Linde²⁰, and the numerical solution of the semi-ideal model³. In contrast to the ideal model solution, which neglects the kinetic effect on the band profile, the two approximate analytical solutions of the semi-ideal model consider the kinetic effect as important, and the non-linear or thermodynamic effect as a perturbation for which they account. The numerical solution of the semi-ideal model takes both thermodynamic and kinetic effects into full account.

Analytical solution of the ideal model

In a previous study³², we derived general equations which predict the elution band profile of a large size sample of a compound for which the isotherm has no inflection point in the concentration range sampled by the band. In the case of a convex

upward isotherm, the profile of the rear, diffuse part of the band is given by the following equation:

$$t = t_p + t_0 \left(1 + F \frac{dq}{dC} \right) \quad (15)$$

where F is the phase ratio. If the isotherm is convex downward, the same equation applies, but it gives the profile of the diffuse front. The profile ends (for a convex upward isotherm) at time

$$t = t_p + t_{R,0} \quad (16)$$

The retention time of the band front can be calculated by observing that, as the sample mass is constant, the area under the profile given by eqn. 15, between the retention time of the front, t_R , and the end of the profile, is equal to the sample size in chromatographic units, *i.e.*, to the product of the concentration, C_0 of the pulse injected and its width, t_p , or to the ratio of the sample size (n in moles) to the volume flow-rate, F_v . Hence, the front retention time is given by the equation

$$\left| \int_{t_R}^{t_p + t_{R,0}} C dt \right| = C_0 t_p = \frac{n}{F_v} \quad (17)$$

Alternatively, the following equations give the maximum concentration:

$$\left| q(C_{\text{Max}}) - C_{\text{Max}} \frac{\partial q}{\partial C_{C=C_{\text{Max}}}} \right| = \frac{C_0 t_p}{F t_0} = \frac{n}{F t_0 F_v} \quad (18)$$

the combination of eqns. 15 and 18 give the retention time, t_R .

Eqns. 17 and 18 can be solved in closed form for a number of classical isotherms, such as the parabolic isotherm (see below), the Langmuir isotherm³¹, the Freundlich isotherm or a two-term Langmuir isotherm³². Although it is probable that eqn. 18 can be solved for a number of other simple functional dependences, it cannot be so in the general case. Numerical solutions of eqn. 18 are easy to calculate, however.

The Langmuir isotherm is the most frequently used in liquid chromatography. It is given by

$$q = \frac{aC}{1 + bC} \quad (19)$$

In this case, eqn. 15 gives the rear profile³¹:

$$C = \frac{1}{b} \left[\sqrt{\frac{t_{R,0} - t_0}{t - t_p - t_0}} - 1 \right] \quad (20)$$

and eqn. 17 gives the retention time³¹:

$$t_R = t_p + t_0 + (t_{R,0} - t_0)(1 - \sqrt{L_f})^2 \quad (21)$$

The Houghton³⁶ and the Haarhoff-Van der Linde²⁰ solutions are derived for the parabolic isotherm obtained by a two-term expansion of the Langmuir isotherm (eqn. 19):

$$q = aC(1 - bC) \quad (22)$$

We give here, for the sake of comparison, the solutions of eqns. 15 and 17 corresponding to this isotherm. The retention time of the band front is

$$t_R = t_{R,0} + t_p - 2(t_{R,0} - t_0)\sqrt{L_f} \quad (23)$$

and the equation for the continuous, diffuse profile which is eluted after the front shock is

$$C = \frac{1}{2b} \cdot \frac{t_{R,0} + t_p - t}{(t_{R,0} - t_0)} \quad (24)$$

Combining eqns. 23 and 24 gives the maximum concentration of the band, C_{Max} :

$$C_{\text{Max}} = \sqrt{L_f}/|b| \quad (25)$$

In these equations, t_p is the band width of the injection rectangular pulse, t_0 is the hold-up time, $t_{R,0}$ is the retention time of the compound at infinite dilution, *i.e.*, $t_0(1 + k'_0)$, and L_f is the loading factor, which is defined for a Langmuir isotherm as equal to the ratio of the amount injected to the monolayer capacity:

$$L_f = \frac{bn}{\varepsilon SLk'_0} \quad (26)$$

where n is the sample size in moles, S the column cross-sectional area and L the column length. The same definition applies to the parabolic isotherm which is used here as an approximation of the Langmuir isotherm and is not expected to be valid at high concentrations.

We note in passing that this profile is identical with the asymptotic solution of the ideal model for the Langmuir isotherm, which has been reported previously³². This result is expected as the asymptotic solution depends only on the origin slope and curvature of the isotherm.

Houghton solution

Originally, Houghton derived this solution on the assumption that the mass transfer kinetics are infinitely fast, but that the axial dispersion cannot be neglected³⁶. However, in view of our previous discussion, the demonstration remains valid for mass

transfer kinetics which proceed at a finite but fast rate. The mass balance equation for the compound studied can be written as

$$u \frac{\partial C}{\partial z} + \left(1 + F \frac{dq}{dC}\right) \frac{\partial C}{\partial t} = D_a \frac{\partial C^2}{\partial z^2} \quad (27)$$

For the second-degree polynomial isotherm (eqn. 22), eqn. 27 becomes

$$\frac{\partial C}{\partial t} + \frac{\Lambda u C}{(1 + k'_0)(1 + \Lambda C)} \cdot \frac{\partial C}{\partial \xi} = \frac{D_a}{(1 + k'_0)(1 + \Lambda C)} \cdot \frac{\partial C^2}{\partial \xi^2} \quad (28)$$

with

$$\Lambda = -2b \frac{k'_0}{1 + k'_0} \quad (28a)$$

and

$$\xi = L \frac{t_{R,0} - t}{t_{R,0}} \quad (28b)$$

Eqn. 28 cannot be solved in closed form and a further simplification is necessary. Houghton proposed that the term ΛC in the denominators of the second term of the left- and right-hand sides of eqn. 28 be neglected, which gives

$$\frac{\partial C}{\partial t} + \frac{\Lambda u C}{(1 + k'_0)} \cdot \frac{\partial C}{\partial \xi} = \frac{D_a}{(1 + k'_0)} \cdot \frac{\partial C^2}{\partial \xi^2} \quad (28c)$$

It is important to note that, when this simplification is made, eqn. 28c is no longer a mass balance equation, *i.e.*, it no longer conserves mass. Using the Cole–Hopf transform, a solution of eqn. 28c can be derived. This solution, referred to later in this text as the Houghton equation, gives the elution profile of a pulse of finite width at the end of an infinitely long column³⁶. Jaulmes and co-workers^{37,38} simplified the Houghton equation for an impulse input (infinitely narrow pulse).

The Houghton solution for an infinitely narrow injection pulse can be written in dimensionless coordinates as follows, by using the values of Λ and ξ (eqns. 28a and 28b, respectively):

$$X = \left| \frac{\exp(-\tau^2/2)}{\sqrt{2\pi}[\coth m + \operatorname{erf}(\tau/\sqrt{2})]} \right| \quad (29)$$

where m is the dimensionless sample size, originally^{36,37} given by

$$m = \frac{u^2 \Lambda A}{2D_a S(1 + k'_0)} \quad (30a)$$

where A is the peak area, and which it is convenient to rewrite as

$$m = \frac{Lu}{2D_a} \left(\frac{k'_0}{1 + k'_0} \right)^2 L_t \quad (30b)$$

τ is the dimensionless time, given by

$$\tau = \frac{k'_0 L}{(1 + k'_0) \sqrt{D_a t}} \cdot \frac{t_{R,0} - t}{t_{R,0} - t_0} \quad (31)$$

and X is the dimensionless concentration, originally³⁷ given by

$$X = \left| \frac{AC}{2} \sqrt{\frac{u^2 t}{2D_a(1 + k'_0)}} \right| \quad (32a)$$

but which it is more convenient to write as

$$X = |b| C \frac{k'_0}{1 + k'_0} \sqrt{\frac{u^2 t}{2D_a(1 + k'_0)}} \quad (32b)$$

Finally, Houghton also gave the solution of the ideal model, obtained as the limit of eqn. 29 when the apparent diffusion coefficient tends towards zero. The equation of the continuous rear part of the profile is

$$C = \frac{t_{R,0}}{2|b|t} \left(\frac{t_{R,0} + t_p - t}{t_{R,0} - t_0} \right) \quad (33)$$

This equation is different from the rigorous solution of the ideal model in the case of a parabolic isotherm, given in eqn. 24, and this shows that the Houghton equation cannot be correct (see below).

Haarhoff and Van der Linde solution

Haarhoff and Van der Linde derived equations for the band profiles of both a finite size sample pulse and an impulse (injection pulse with infinitely narrow width). They used the same assumptions as Houghton but they added one more. They decided to calculate the effect of dispersion on the band at $t = t_{R,0}$, arguing that the solute concentration at column outlet is significantly different from zero only during a period of time which is of the same order of magnitude as the standard deviation of the Gaussian peak observed for an infinitely small sample size and that the column length is assumed to be infinite (in practice, much longer than the HETP). Because of this new assumption, the two solutions are significantly different.

The elution band profile is given by the same eqn. 29, but as the apparent dispersion coefficient, D_a is equal to $Hu/2$, we can replace $Lu/2D_a$ in eqn. 30b by N , so that the dimensionless sample size becomes

$$m = N \left(\frac{k'_0}{1 + k'_0} \right)^2 L_t \quad (34)$$

Similarly, in eqn. 31 we now have $D_a t = D_a t_{R,0} = H u t_{R,0}/2$, so this equation becomes

$$\tau = \sqrt{N} \frac{k'_0}{1 + k'_0} \cdot \frac{t - t_{R,0}}{t_{R,0} - t_0} \quad (35)$$

Finally, eqn. 32b can be written as

$$X = |b|C \frac{k'_0}{1 + k'_0} \sqrt{N} \quad (36)$$

The Haarhoff–Van der Linde equation is the combination of eqns. 29 and 34–36. The limit of this equation, when the column efficiency becomes infinite, is now identical with the rigorous eqn. 24. We also note for further reference that if we differentiate eqn. 29, to obtain the coordinates of the band maximum, we obtain the following result:

$$X_{\text{Max}} = \frac{|\tau_{\text{Max}}|}{2} \quad (37a)$$

Combination of eqns. 29, 35 and 37 permits the calculation of the exact retention time. Unfortunately, this cannot be solved in close form. However, combination of eqns. 35–37a gives a useful relationship:

$$k' = k'_0(1 - 2bC_{\text{Max}}) \quad (37b)$$

Comparison between the different solutions of the ideal and semi-ideal model

We have four different solutions available for predicting the elution profile of a compound at high concentration: the numerical solution^{3,35}, which can serve as a reference to compare with the solutions of the other three approaches, the Houghton and the Haarhoff–Van der Linde equations and the solution of the ideal model. We discuss first the advantages and drawback of the Houghton and Haarhoff–Van der Linde equations and compare them together. We then present a similar discussion for the analytical solution of the ideal model and compare it with the previous two solutions. Finally, we discuss the advantages and inconveniences of the numerical solution.

Haarhoff–Van der Linde and Houghton equations: influence of the first approximation, C is small. These two equations^{20,36} are very similar and both make the same two basic assumptions in order to arrive at a closed form equation for the elution band profile: the sample size is small enough and the term AC can be neglected compared to unity, and the equilibrium isotherm can be replaced with its first two-term expansion. We discuss first the range of validity of these assumptions and their consequences.

As mentioned earlier, it is assumed in the derivation of both equations that the sample size is small and the term AC can be neglected compared with unity in the denominator of two terms of eqn. 28. Houghton³⁶ suggested that, in order to satisfy this assumption, the sample size should be such that the product $|AC_{\text{Max}}|$ should not exceed 0.05. This condition is equivalent to $|bC_{\text{Max}}k'_0/(1 + k'_0)| \leq 0.025$. This threshold usually corresponds to loading factors of *ca.* 0.001 or 0.1%. The equation

obtained by simplifying eqn. 28 and dropping the two $(1 + AC)$ terms is no longer mass conservative and is inaccurate at the first order [a correct first-order approximation would replace the terms $1/(1 + AC)$ by $(1 - AC)$, not by 1].

The fact that the Houghton equation is not mass conservative can cause a larger error. In the case of an upwardly convex isotherm, A is negative and the Houghton equation will predict an increasingly large mass loss when the sample size increases, as has been reported previously³⁹. Conversely, for an upwardly concave isotherm, the Houghton equation leads to a mass gain which increases with increasing sample size. As the equation is incorrect at the first order, the mass loss or gain is proportional to the sample size at low values.

The Haarhoff–Van der Linde equation, which makes the same assumption, should suffer the same problem, but it does not because of the compensation which is introduced by calculating the axial dispersion at $t = t_{R,0}$. There is no mass loss or gain with this equation.

An exact equation for the band profile of a compound experiencing a parabolic isotherm has to be a rigorous solution of eqn. 28. There does not seem to be such a solution in closed form. An approximation has to be made, as was done by both Houghton and Haarhoff and Van der Linde. We suggest here another such approximation, which has the advantage of being more accurate than the Houghton equation and of not making the additional assumption made by Haarhoff and Van der Linde for the calculation of axial dispersion, although it results in a band profile equation which is identical with the latter.

Instead of dropping the term $1/(1 + AC)$ from eqn. 28 completely, we include it in the definition of A and D_a . Then, we replace C in these terms by the value derived from eqn. 24, *i.e.*, by the concentration obtained for an infinitely efficient column, which is $1 + AC = t/t_{R,0}$. This calculation gives an equation similar to the Houghton equation (eqn. 29). However, in eqns. 30a and 32a, D_a and A must be replaced, D_a by $D_a/(1 + AC)$, equal to $D_a t_{R,0}/t$, and A by $A/(1 + AC)$, equal to $At_{R,0}/t$. Substituting these new parameters in the Houghton equation (eqns. 29–32) gives exactly the Haarhoff–Van der Linde equation (eqns. 29 and 34–36) and constitutes a simpler and more natural procedure for deriving it. This demonstration has the further advantage of explaining why the Haarhoff–Van der Linde equation conserves mass.

Our derivation gives an approximate solution of eqn. 28 which is much closer to the exact solution of eqn. 28 than the solution of eqn. 28c, which was derived by Houghton. Because of the $(1 + AC)^{-1}$ terms, eqn. 28 cannot be solved in closed form. Replacing these terms by a close approximation (derived from the solution of the ideal model) provides a much better approximate solution than dropping the terms entirely and, especially, eliminates the mass loss encountered with the Houghton equation.

In conclusion, although it is not a rigorous solution, the Haarhoff–Van der Linde equation is a much better approximation of the band profile than the Houghton equation. It is more accurate, it conserves mass and it can be used for any sample size, as long as the equilibrium isotherm is correctly approximated by a parabolic equation. Fig. 1 shows a comparison between the profiles predicted by the two equations, for sample sizes corresponding to loading factors of 0.01–0.2%, with a column efficiency of 12 500 theoretical plates. At very low column loadings, the two equations agree exactly. Significant differences appear for a loading factor of 0.1% and they increase rapidly with increasing sample size. Also, an increasing relative mass loss is observed,

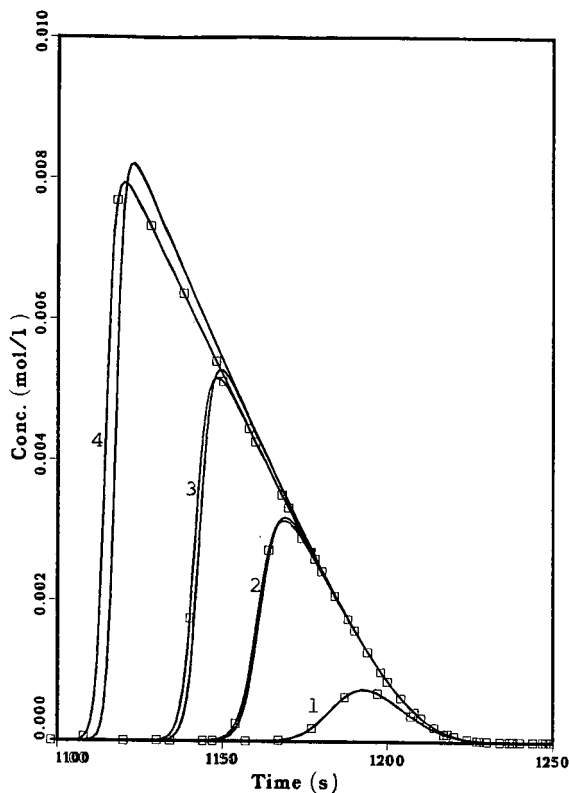


Fig. 1. Comparison between the band profiles predicted by the Houghton and Haarhoff-Van der Linde equations. Parabolic isotherm (eqn. 22), with $a = 20$, $b = 5$. Column length, 25 cm; phase ratio, 0.25; dead time, $t_0 = 200$ s; column efficiency, 12 500 theoretical plates. Loading factors: (1) 0.01%; (2) 0.05%; (3) 0.10%; (4) 0.20%. The Haarhoff-Van der Linde profiles are identified by squares. The masses lost by the Houghton profiles are (1) 0.2%, (2) 0.9%, (3) 1.5% and (4) 2.5%.

which is already 2.5% for a loading factor of 0.2%. Fig. 2 compares the band profiles obtained with the two equations, using a convex and a concave isotherm, with an equal absolute value for the second degree coefficient, b (see eqn. 22), and the same loading factor of 1% in both instances. The sign of the deviation between the two equations is reversed, and also the sign of the mass loss: with the upward convex isotherm the mass loss is 5.3% and with the downward convex isotherm the mass gain is 4.5%. It is obvious, however, that the difference has become larger than the experimental errors and one equation, the Houghton equation, has become unsuitable to account for band profiles.

Haarhoff-Van der Linde and Houghton equations: influence of the second approximation, a parabolic isotherm. The second major assumption made by Houghton³⁶ and by Haarhoff and Van der Linde²⁰ is that the isotherm is parabolic. We know that this has to be a simplification, but it is always possible to replace any isotherm by its first two-term expansion, at least in a certain concentration range. We have shown, however, that the band profile is extremely sensitive to small fluctuations of the isotherm³. This is why, in order to assess the value of our theoretical work on the

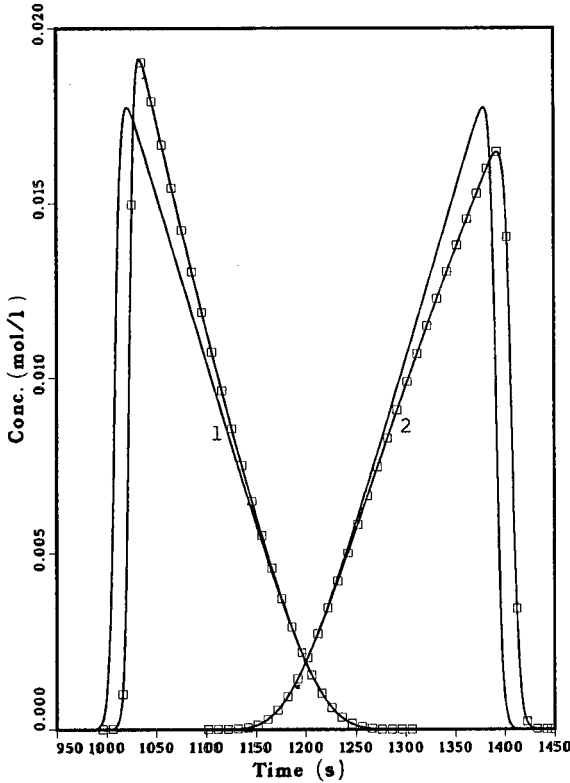


Fig. 2. Comparison between the band profiles predicted by the Houghton and Haarhoff-Van der Linde equations. Parabolic isotherms. Conditions as in Fig. 1, except loading factor, 1% in all instances. (1) Convex upward isotherm (eqn. 22, $b = 5$); (2) concave upward isotherm (eqn. 22, $b = -5$). The Houghton profiles are identified by squares. The masses lost by the Houghton profiles are (1) 5.3% and (2) -4.5%.

prediction of the band profiles of overloaded columns, we had to carry out accurate determinations of the equilibrium isotherms, and these measurements must be done on the very column on which the overloaded bands whose profiles are studied are eluted^{40,41}. Hence, we may expect the replacement of the isotherm by its first two-term expansion to have some effect on the band profile even at low concentrations.

Haarhoff and Van der Linde²⁰ have discussed this problem. They concluded that for most isotherms used in practice, their equation should give accurate band profiles, as long as the following conditions is satisfied:

$$N_{th} = 16 \left(\frac{t_{R,0}}{W_{th}} \right)^2 = \frac{4}{L_f} \left(\frac{t_{R,0}}{t_{R,0} - t_0} \right)^2 \geq 2000 \quad (38a)$$

or

$$L_f \leq 0.002 \left(\frac{1 + k'_0}{k'_0} \right)^2 \quad (38b)$$

In eqn. 38a, W_{th} is the baseline band width of the band profile predicted by the ideal model for a parabolic isotherm (see eqn. 23).

Thus, after Haarhoff and Van der Linde, their equation should give satisfactory results with any isotherm, provided that the loading factor is less than about 0.2% or, from eqn. 25, $bC_{Max} \leq 0.05$. Increasing further the loading factor results in less and less accurate band profiles, not because of the approximation made in the derivation of the analytical solution (see above) but because of the progressive deviation between the quadratic isotherm equation (eqn. 22) and the true isotherm.

A practical procedure for checking the degree of agreement between the band profiles predicted by the Haarhoff–Van der Linde equation and the true profile starts by choosing a Langmuir isotherm. The elution band profiles are calculated for samples of increasingly large size, using the numerical solution of eqn. 12. These profiles are compared with the solutions of the Haarhoff–Van der Linde equation derived using the first two-term expansion of the same Langmuir isotherm. For a Langmuir isotherm, the true thermodynamic band width is given by the equation³¹

$$W_{th} = (2\sqrt{L_f} - L_f)(t_{R,0} - t_0) \quad (39)$$

whereas with a parabolic isotherm it is

$$W_{th} = 2\sqrt{L_f}(t_{R,0} - t_0) \quad (40)$$

The first band width is the product of multiplying the latter by $1 - \sqrt{L_f}/2$, a factor which becomes really significant when the loading factor exceeds 1%. The difference between the two values of the thermodynamic band width calculated with eqns. 39 and 40, for values of the loading factor of 1 and 10%, are 5% and 18%, respectively. Obviously, however, when the column efficiency is low, the band maximum concentration is smaller than predicted by the ideal model, and the concentration range sampled by the band during its elution is correspondingly narrower. Hence, the parabolic isotherm can be used to account for the elution band profiles of larger size samples with lower efficiency columns than with higher efficiency columns, the critical condition being that bC_{Max} is less than 0.05.

Haarhoff–Van der Linde and Houghton equations: conclusion. The last assumption made by Haarhoff and Van der Linde is that the band profile becomes Gaussian when the sample size becomes infinitely small, *i.e.*, under the conditions of linear chromatography. Therefore, the model cannot be used when the mass transfer kinetics are slow and the column efficiency for small size samples is lower than about 500 theoretical plates.

In conclusion, the Haarhoff–Van der Linde equation provides an excellent representation of the elution band profiles at low column loadings, and with most HPLC columns it should be used as a convenient model for values of the loading factor not exceeding 0.2% for ideal columns ($bC_{Max} \leq 0.05$ for real columns). This equation can be used with loading factors of up to 1% for ideal columns ($bC_{Max} \leq 0.1$ for real columns), which gives an error in the band width not exceeding 5%, except, however, for the low-efficiency columns which have to be used in affinity chromatography or with some other highly specific retention mechanisms. On the other hand, we have

regretfully come to the conclusion that the use of the Houghton equation should generally be avoided.

Ideal model and the Haarhoff–Van der Linde equation. Central to the ideal model is the assumption that the column efficiency is infinite. This constitutes its major drawback when the profiles that it predicts are compared with real profiles or with those predicted by other methods, such as the Haarhoff–Van der Linde equation. Obviously, in linear chromatography the results predicted by the ideal model are unrealistic, as the elution band profile would be identical with the injection profile, since there is no band broadening. On the other hand, when the loading factor increases, especially at high column efficiency, the results of the ideal model become closer and closer to the actual band profiles. With higher and higher column efficiency, with larger and larger sample sizes, the contribution of thermodynamics, *i.e.*, of the non-linear behavior of the equilibrium isotherm to the width of the band profile, becomes more and more important. This is the contribution for which the ideal model accounts.

In fact, the effective loading factor for a real column is given by eqn. 34. It turns out that the ideal model gives a realistic representation of the true band profile whenever the effective loading factor is greater than 35. Fig. 3 shows a comparison

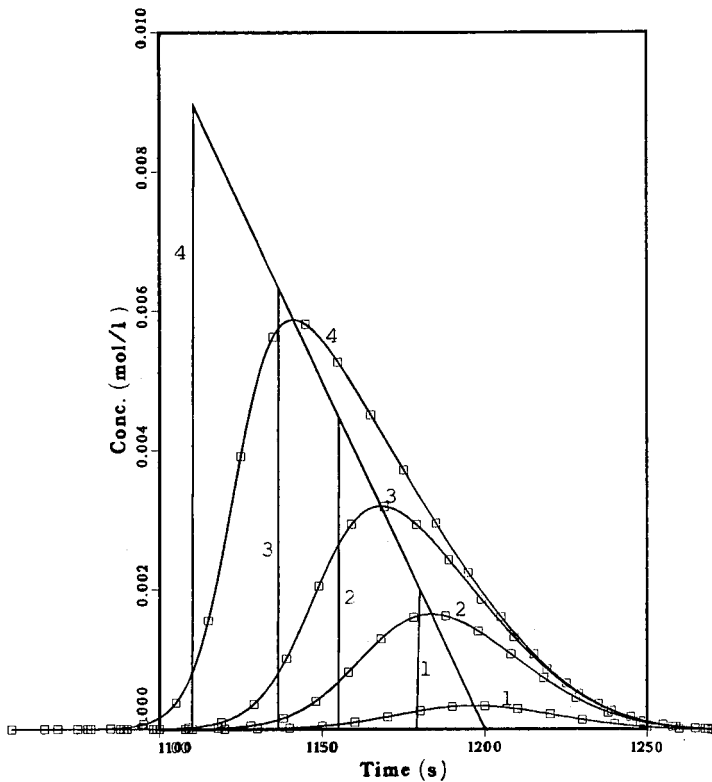


Fig. 3. Comparison between the band profiles predicted by the ideal model and the Haarhoff–Van der Linde equations. Parabolic isotherms, as for Fig. 1. Conditions as in Fig. 1, except column efficiency, 2500 plates ($m \leq 3.5$). Loading factors: 1, 0.01%; 2, 0.05%; 3, 0.1%; 4, 0.2%. The Haarhoff–Van der Linde profiles are identified by squares.

between the band profiles predicted by the ideal model and by the Haarhoff–Van der Linde equation, using in both instances a parabolic isotherm (note that the loading factor is calculated for the Langmuir isotherm having the same origin slope and curvature as the parabolic isotherm selected), for a column having 2500 theoretical plates. As expected, as the effective loading factor, m , is small (between 0.18 and 3.5), the agreement between the two models is poor, the Haarhoff–Van der Linde equation giving in this instance an excellent description of the true elution band profiles. Obviously, the ideal model cannot and should not be used in such instances.

Fig. 4, in contrast, shows a series of band profiles obtained with high column efficiencies and the same values of the loading factor as in Fig. 3. This time, the effective loading factor is $m = 35$ in all instances. The agreement between the two models is now excellent. It can only improve if the value of m exceeds 35. In Fig. 4, the retention time predicted by the ideal model is shorter by only 0.5% than the retention time predicted by the Haarhoff–Van der Linde equation; the band is 9% taller and it does not tail.

In order to assess better what in the systematic error made with the Haarhoff–Van der Linde equation comes from considering a parabolic isotherm and what is due

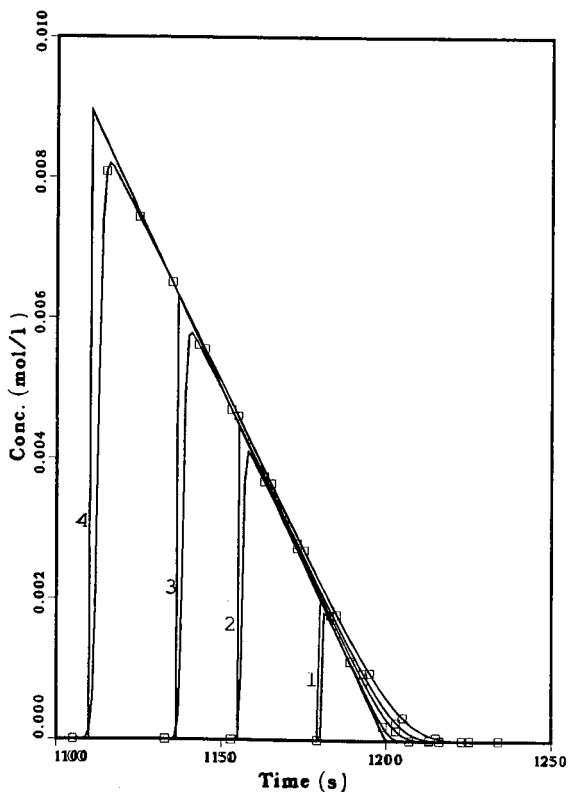


Fig. 4. Comparison between the band profiles predicted by the ideal model and the Haarhoff–Van der Linde equations. Parabolic isotherms, as for Fig. 1. Conditions as in Fig. 3, except column efficiency. Reduced sample size, $m = 35$. Loading factors and efficiency: (1) $L_t = 0.01\%$, $N = 500\ 000$; (2) $L_t = 0.02\%$, $N = 100\ 000$; (3) $L_t = 0.1\%$, $N = 50\ 000$; (4) $L_t = 0.2\%$, $N = 25\ 000$. The Haarhoff–Van der Linde profiles are identified by squares.

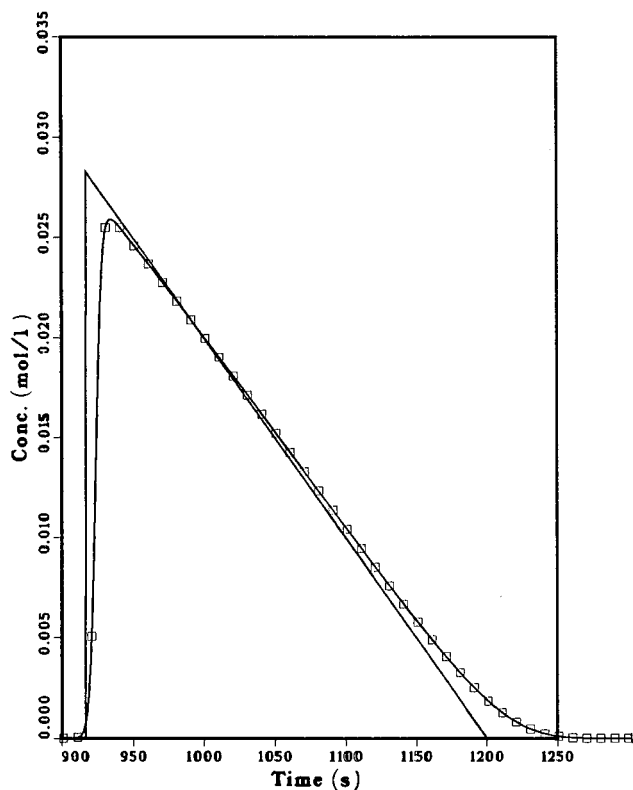


Fig. 5. Comparison between the band profiles predicted by the ideal model and the Haarhoff-Van der Linde equations. Parabolic isotherms, as for Fig. 1. Conditions as in Fig. 3, except loading factor, 2% ($m = 35$). The Haarhoff-Van der Linde profile is identified by squares.

to the assumptions made in the mathematical derivation, when considering the solute concentration C to be small, we have carried out some calculations in order to compare the band profiles predicted by the ideal model, with either a parabolic or a Langmuir isotherm, and by the Haarhoff-Van der Linde equation, using the same parabolic isotherm. The results are shown in Figs. 5 and 6.

Fig. 5 shows a comparison between the profile predicted by the two models for a parabolic isotherm, a column efficiency of 2500 theoretical plates (as for Fig. 3) and a loading factor $L_f = 2\%$. The agreement between the two profiles, which now correspond to a reduced sample size $m = 35$, is very good.

Fig. 6 shows a comparison between the profile predicted by the ideal model for a Langmuir isotherm and the profile predicted by the Haarhoff-Van der Linde equation for the corresponding isotherm. All experimental conditions are the same as in Fig. 5. The Haarhoff-Van der Linde profile is, of course, the same for both Figs. 5 and 6. The agreement between the two profiles is much less satisfactory than in Fig. 5. The retention time of the ideal model profile is the same as that of the Haarhoff-Van der Linde profile, but the latter profile begins to elute much earlier, its height is much lower and the rear part of the two profiles intersect, instead of being tangential along

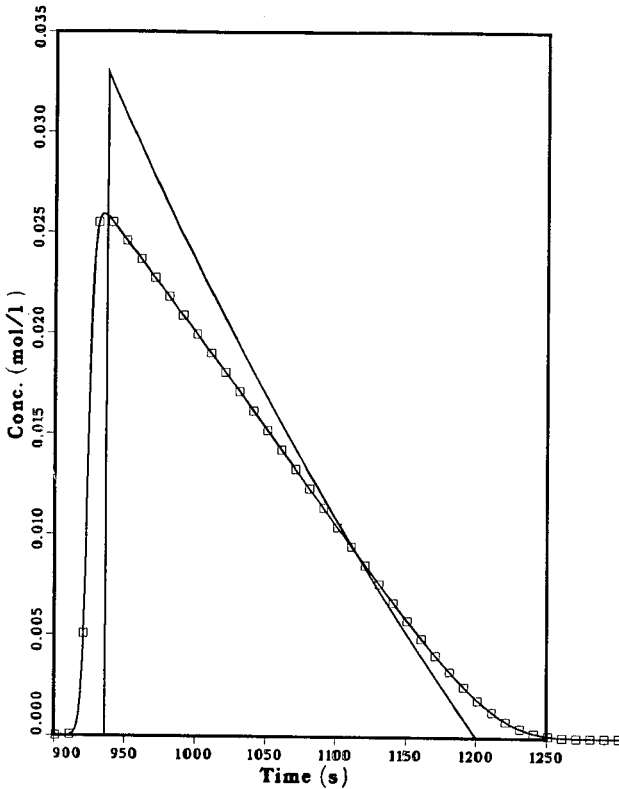


Fig. 6. Comparison between the band profiles predicted by the ideal model and the Haarhoff-Van der Linde equations. Parabolic isotherm as in Fig. 1 for the Haarhoff-Van der Linde equation, corresponding Langmuir isotherm for the ideal model. Conditions as in Fig. 5. The Haarhoff-Van der Linde profile is identified by squares.

a long arc. The comparison between Figs. 5 and 6 shows that the maximum sample size at which the Haarhoff-Van der Linde equation can be used depends very much on the extent of the deviation between the actual isotherm and its two-term expansion. The assumption of a parabolic isotherm is the major limit to the validity of the Haarhoff-Van der Linde equation at large sample sizes.

Ideal model and the Houghton equation. Although we have shown above that the Houghton equation is not as good an approximate solution as the Haarhoff-Van der Linde equation, we carried out for it a similar comparison to that in the previous section between the results of the ideal model and those of the Haarhoff-Van der Linde equation.

Fig. 7 compares the elution band profiles obtained with the ideal model and with the Houghton equation for a compound with a parabolic isotherm and a 1% loading factor in both instances, and with a column efficiency of 5000 theoretical plates for the Houghton equation. There is a poor agreement between the two profiles. The mass loss experienced is 6.75%. This confirms our earlier conclusion that the Houghton equation cannot be used to account for elution band profiles at high loading factors.

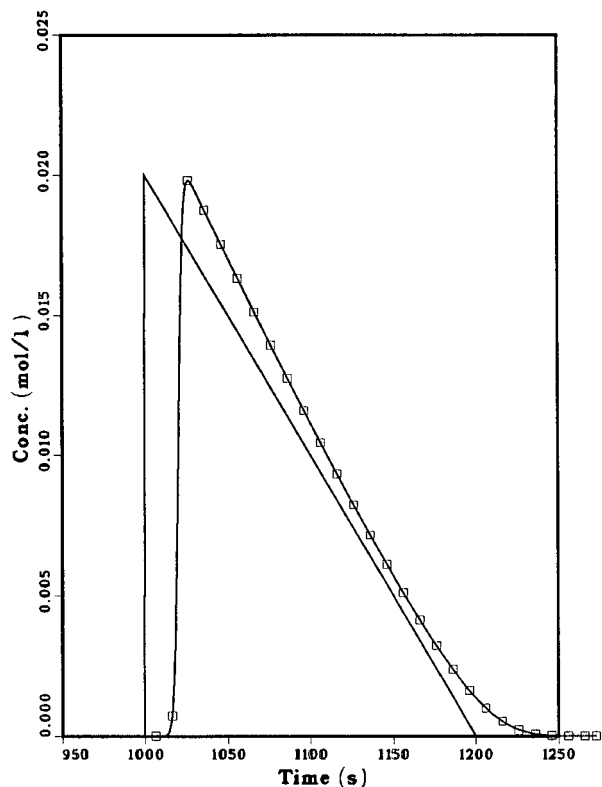


Fig. 7. Comparison between the band profiles predicted by the ideal model and the Houghton equations. Parabolic isotherms, as for Fig. 1. Conditions as in Fig. 1, except loading factor, $L_f = 1\%$, and column efficiency, 5000 plates ($m = 35$). The Houghton profile is identified by squares. The mass loss is 6.75%.

not only because of the parabolic isotherm assumption, but also because of the approximation made in the derivation of this equation and the resulting mass loss or gain. The comparison between Figs. 5 and 7 illustrates this problem.

Fig. 8 shows a comparison between the band profile predicted by the ideal model for a Langmuir isotherm and by the Houghton equation for the two-term expansion of this Langmuir isotherm. The agreement is now almost satisfactory, not because of the validity of the Houghton equation, but because of some error compensation. The loss of the AC term partially compensates for the change in the isotherm. It is certain, however, that a least-squares adjustment of the Houghton equation on experimental data will, in most instances, lead to values of the experimental parameters which have little or no physical meaning.

Haarhoff-Van der Linde equation and the dimensionless band profile plot. We have shown previously³¹ that the band profiles obtained for increasing sample sizes of a given compound under constant experimental conditions can be scaled to a dimensionless form. This result was derived from theoretical considerations regarding the band profile obtained with the ideal model, assuming a Langmuir equilibrium isotherm.

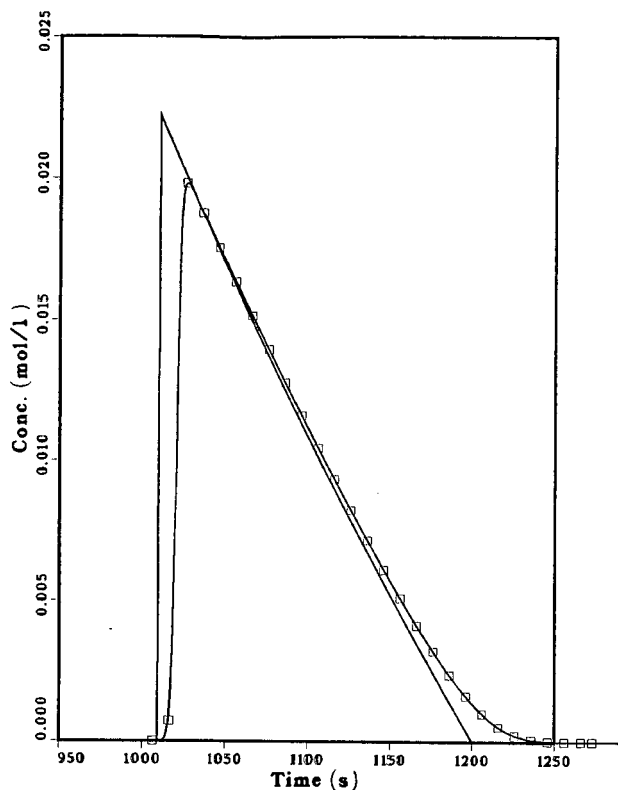


Fig. 8. Comparison between the band profiles predicted by the ideal model and the Houghton equations. Parabolic isotherm for the Houghton equation. Langmuir isotherm for the ideal model. Conditions as in Fig. 7. The Houghton profile is identified by squares.

With the ideal model, it is easy to show that a normalized dimensionless plot can be obtained by using $(t - t_0)/(t_{R,0} - t_0)$ as a reduced time coordinate and bC as a reduced concentration coordinate³¹. The profiles predicted by the Langmuir isotherm depend only on the loading factor, L_f , the ratio of the sample size to the column saturation capacity. This system of reduced parameters will be called the “ideal reduced coordinate system”. We have shown that the degree of agreement between reduced plots of data obtained with real columns in the “ideal reduced coordinate system” is good only if the different columns have the same efficiency³¹.

Similarly, eqns. 34–36 show that, for a real column with a finite efficiency and if the equilibrium isotherm is parabolic, a dimensionless plot can be obtained by using $\tau = \sqrt{Nk'_0(1 + k'_0)} [(t - t_{R,0})/(t_{R,0} - t_0)]$ (see eqn. 35) as reduced time and $X = |b|C[k'_0/(1 + k'_0)]\sqrt{N}$ (see eqn. 36) as reduced concentration. The reduced sample size, which is the only parameter on which the normalized profiles depend, is $m = N[k'_0/(1 + k'_0)]^2 L_f$ (eqn. 34). This system of reduced parameters will be called the “Haarhoff–Van der Linde reduced coordinate system”. We note that the reduced parameters depend on the column efficiency, N . We had already shown that the degree

of agreement between the solution of the ideal model and the numerical solution for a real column depends on the column efficiency and on the loading factor³¹. A correction can be derived which combines, through the variance additivity rule^{20,42}, the thermodynamic band width predicted exactly by the ideal model solution and the kinetic band width obtained from the efficiency of the band at infinite dilution^{31,43}.

This discussion provides a theoretical explanation to results which, previously, were merely qualitative. Eqn. 34, for example, explains why, and to what extent, an efficient column appears to be more overloaded by a given sample size than a less efficient column.

These results have such an important practical value that it is worthwhile investigating in detail now what their range of validity is. We note that Poppe and Kraak⁴⁴ and Eble *et al.*⁴⁵ have presented experimental results in a format that is compatible with the reduced plot just outlined (see next section).

Fig. 9 shows, in the Haarhoff–Van der Linde reduced coordinate system, a series of seven normalized band profiles corresponding to as many sets of different

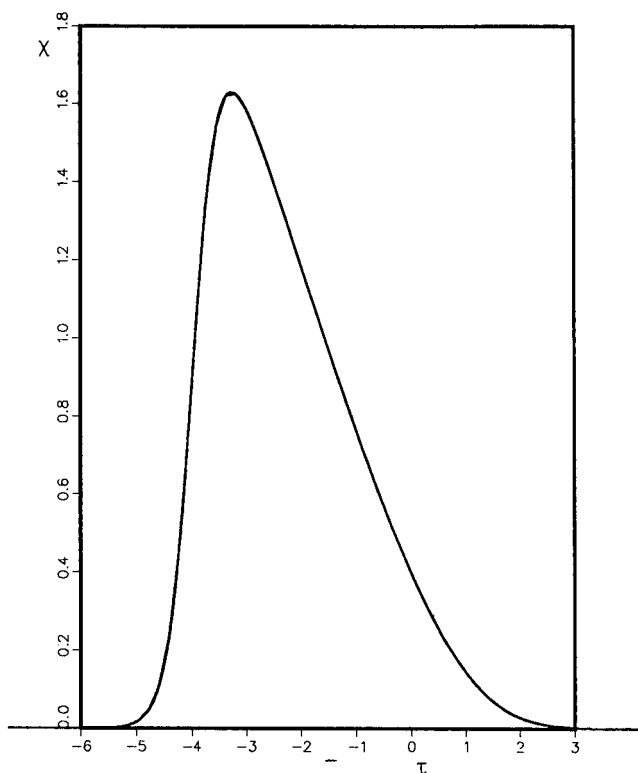


Fig. 9. Plot of seven superimposed band profiles predicted by the Haarhoff–Van der Linde equation, in the Haarhoff–Van der Linde reduced coordinate system (see text). Plot of reduced concentration (X , eqn. 36) versus reduced time (τ , eqn. 35). (1) $N = 10\,000$, $k'_0 = 1$, $b = 2$, $F_v = 1$ ml/min; (2) same as (1), except $N = 5000$; (3) same as (1), except $N = 1000$ plates; (4) same as (2), except $b = 5$; (5) same as (2), except $F_v = 5$ ml/min; (6) same as (2), except $k'_0 = 5$; (7) same as (2), except $k'_0 = 25$. The loading factor is adjusted so that all conditions correspond to the same value of $m = 5$.

experimental conditions, all of them giving the same value of the normalized loading factor, *i.e.*, the reduced sample size, m . The curves cannot be distinguished. Fig. 10 shows a series of normalized band profiles corresponding to increasing values of the reduced loading factor, from 1 to 30. The result is very similar to that reported earlier, and corresponding to Langmuir isotherms³¹. It demonstrates the principle and the practical value of the band profile reduced plot.

Figs. 11 and 12 present the converse case. They exhibit band profiles calculated with a Langmuir isotherm and plotted in the Haarhoff–Van der Linde reduced coordinate system. The four profiles presented in each figure correspond to various experimental conditions giving the same value of the reduced sample size, m , of 3.5 for Fig. 11 and 35 for Fig. 12. We have shown in Fig. 9 that when the isotherm is parabolic all band profiles corresponding to the same value of the reduced sample size give the same plot in the Haarhoff–Van der Linde reduced coordinate system. Fig. 11 shows that for a reduced sample size of 3.5 the parabolic isotherm is already a poor representation of the Langmuir isotherm. The deviation is especially large for the profile corresponding to the less efficient column, but it should be emphasized that this profile corresponds also to the largest sample size (see eqn. 34). The scatter of the different plots and their deviations from the normalized Haarhoff–Van der Linde profile (see Fig. 10) increases as expected when m is increased from 3.5 (Fig. 11) to 35

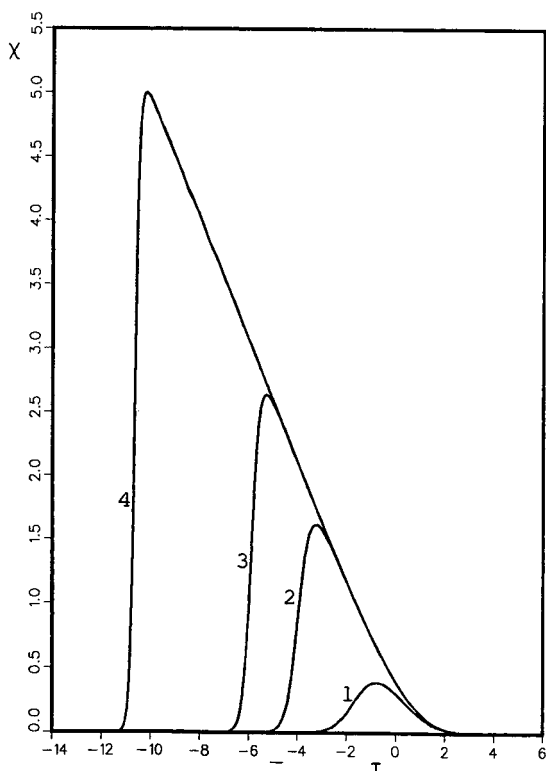


Fig. 10. Plot of band profiles predicted by the Haarhoff–Van der Linde equation, using the Haarhoff–Van der Linde reduced coordinate system (see text). Plot of reduced concentration (X , eqn. 36) versus reduced time (τ , eqn. 35). Influence of sample size. Reduced sample size, m : (1) 1; (2) 5; (3) 10; (4) 30.

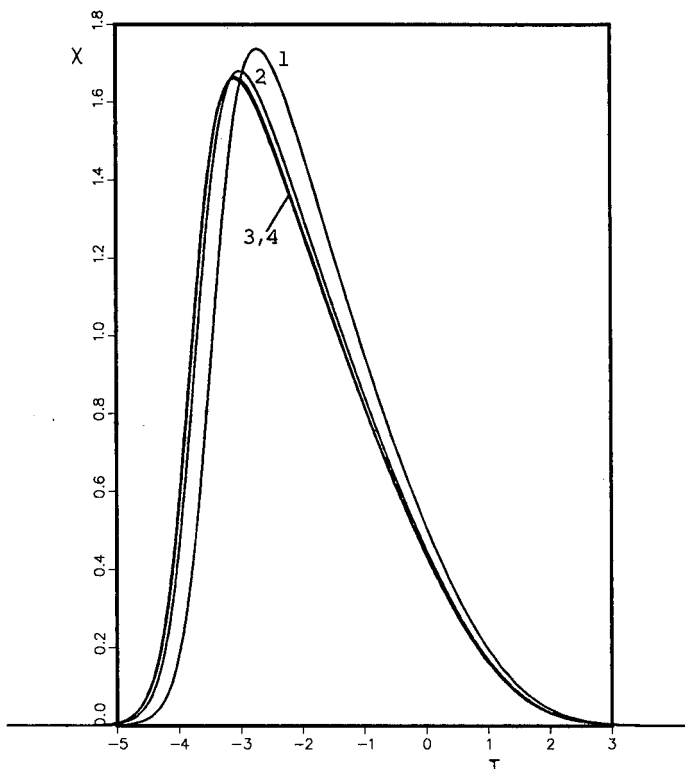


Fig. 11. Comparison between band profiles predicted by the numerical solution of the semi-ideal model, using the Langmuir isotherm, and plotted in the Haarhoff-Van der Linde reduced coordinate system (see text). Plot of reduced concentration (X , eqn. 36) versus reduced time (τ , eqn. 35). (1) $N = 1000$, $k'_0 = 1$, $b = 2$, $F_v = 1$ ml/min; (2) same as (1), except $N = 5000$; (3) same as (1), except $N = 10\,000$; (4) same as (2), except $k'_0 = 5$. The loading factors are chosen so that the reduced sample size $m = 3.5$.

(Fig. 12). These figures show that, if the isotherm is not parabolic but is Langmuirian, the Haarhoff-Van der Linde normalized plot is not applicable, and we must use the ideal reduced coordinate system, at fixed column efficiency³¹.

Fig. 13 shows a plot of two band profiles in the ideal reduced coordinate system. These bands are both solutions of the ideal model, one using a parabolic isotherm and the other a Langmuir isotherm. The two profiles are tangential at the point ($t = t_{R,0}$, $C = 0$). The band profiles are nearly identical for a loading factor of 0.2% and remain very close for a loading factor of 1%. Above the latter value, the difference between them increases rapidly. This confirms that the practical maximum limit of validity of the Haarhoff-Van der Linde equation is for a loading factor of *ca.* 1% for ideal columns ($bC_{\text{Max}} \leq 0.1$ for real columns).

EMPIRICAL SOLUTIONS

Poppe and Kraak⁴⁴ have shown that the apparent plate number of a chromatographic band, N_{app} , is related to the sample size injected by the following equation:

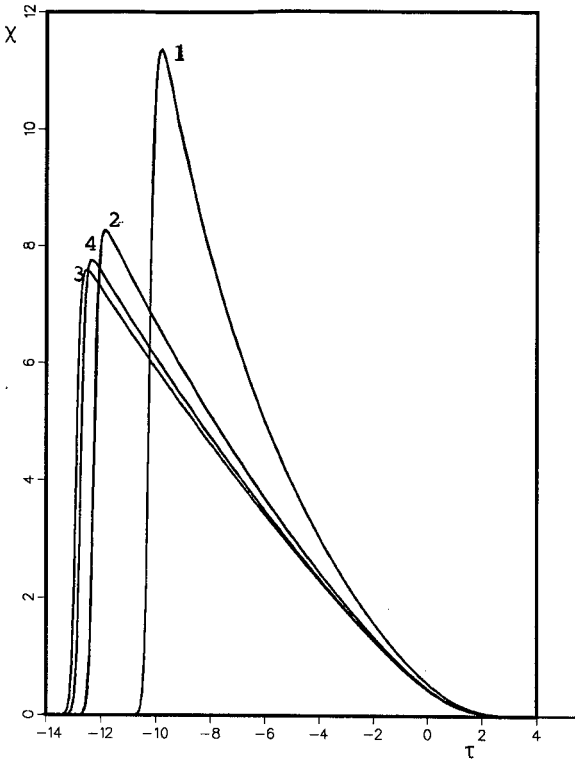


Fig. 12. Same as Fig. 11, except the loading factors are adjusted so that $m = 35$.

$$N_{\text{app}} = N f(m) \quad (41)$$

where N is the limit efficiency for a sample of infinitely small size and m has the same definition as in eqn. 34 above. A similar relationship was also given by Knox and Pyper⁴². This result has been used recently by Eble *et al.*^{45,46}. Eqn. 41 derives directly from the Haarhoff-Van der Linde equation and from the fact that the profiles can be scaled (see above, Figs. 9 and 10). In fact, Fig. 4 in ref. 20 shows the same plot of the variation of the column apparent efficiency with m as Fig. 9 in ref. 44 and Fig. 5 in ref. 45.

Similarly, Eble *et al.*⁴⁵ have suggested that the apparent column capacity factor depends on the sample size through the equation

$$k' = k'_0 g\left(\sqrt{N} \frac{k'_0}{1 + k'_0} L_t\right) \quad (42)$$

where $g(\)$ is a functional dependence. Fig. 4 in ref. 20 shows a plot of the variation of the apparent retention with m which is equivalent to Fig. 8 in ref. 44 and Fig. 6 in ref. 45. On the other hand, it results from eqn. 37 that the functional dependence of the retention time (*i.e.*, k') is

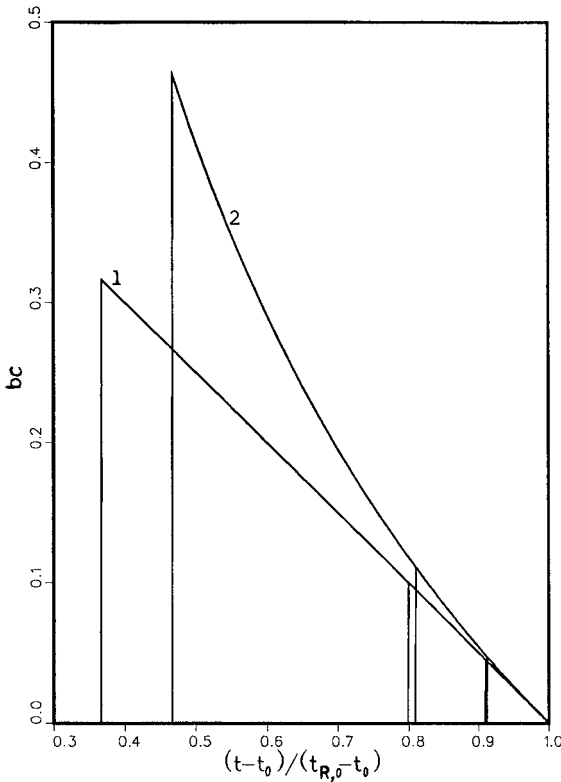


Fig. 13. Comparison between two band profiles calculated with the ideal model, using two different equilibrium isotherms. The plots are made in the ideal reduced coordinate system (see text). (1) Parabolic isotherm; (2) Langmuir isotherm.

$$\tau_{\text{Max}} = f(m) \quad (43a)$$

or

$$\sqrt{N} \frac{k'_0}{1+k'_0} \left(1 - \frac{k'}{k'_0}\right) = f \left[N \left(\frac{k'_0}{1+k'_0} \right)^2 L_f \right] \quad (43b)$$

Eqn. 42 is not equivalent to eqn. 43b and is an incorrect oversimplification.

Eqns. 41 and 43 are valid only as far as the Haarhoff–Van der Linde equation is valid, that is, as we have shown above, as long as the loading factor does not exceed ca. 1%. Accordingly, the experimental results obtained by Eble *et al.* (Figs. 6–24 in ref. 46) are a convincing verification of the Haarhoff–Van der Linde equation. As explained in the previous discussions, the deviations from a universal plot which are observed at large sample sizes are explained by the incorrect assumption made by Haarhoff and Van der Linde of a parabolic isotherm.

Semi-empirical relationships such are those derived subsequently by Eble *et al.*⁴⁵

used empirical parameters to force adjustment of experimental data on the universal plot. As the basic origin of the deviation observed, *i.e.*, the implicit assumption of a parabolic isotherm, was not understood, the approach has had only limited success.

As we have shown above, when the sample sizes used in preparative liquid chromatography correspond to values of the loading factor not exceeding 1% for ideal columns ($bC_{\text{Max}} \leq 0.1$ for real columns), the Haarhoff–Van der Linde equation and the corresponding dimensionless plot give successful predictions of the entire band profiles and of their sample size dependence. Then plots of N or k' versus complex functions of experimental parameters are of dubious practical interest as they give much less information. At higher values of the loading factors the only correct predictions can be obtained either with the solution of the ideal model, with a correction for finite efficiency^{31,43} or through the calculation of numerical solutions.

CORRECTION OF THE ANALYTICAL SOLUTION OF THE IDEAL MODEL

There is no exact solution available for eqn. 12 at high concentration. The influence of a finite column efficiency on the band profile cannot be accounted for properly. In other words, we are in a situation comparable to that at low concentrations, where the Haarhoff–Van der Linde equation assumes a simplified isotherm to account for the onset of the influence of the non-linear thermodynamic behavior on a band profile which is still essentially controlled by the kinetics of mass transfer. We would like to account for the influence of the finite column efficiency on a band profile which is essentially controlled by the non-linear behavior of the isotherm, for which the ideal model accounts perfectly.

Although there is no rigorous solution to this problem, it can be handled approximately, by using a result classical in linear chromatography and extending it to non-linear chromatography. The original idea was presented by Haarhoff and Van der Linde²⁰ and by Knox and Pyper⁴² and a more rigorous treatment was derived later³¹. We assume that the observed column height equivalent to a theoretical plate (HETP), $H_{\text{app}} = L/N_{\text{app}}$, is the sum of two independent contributions:

$$H_{\text{app}} = H + H_{\text{th}} \quad (44)$$

where H and H_{th} represent the kinetic and thermodynamic contributions to the HETP, respectively. There is no real theoretical basis to this assumption, which stems from the additivity of the independent contributions to the band variance in linear chromatography⁴⁷.

The first contribution, H , is equal to the HETP determined under linear conditions, assuming that the diffusion coefficients are independent of the solute concentration, which is valid in the concentration range used in preparative chromatography, for compounds of low or moderate molecular weight, and that the retention kinetics are fast. It accounts for the effect of the finite rate of mass transfer on the band width. The second contribution, H_{th} , results from the non-linear behavior of the isotherm and can be derived from our previous results on the ideal model, which account correctly for this effect, but for this effect only.

Eqn. 44 is equivalent to

$$N_{\text{app}} = \frac{NN_{\text{th}}}{N + N_{\text{th}}} \quad (45)$$

where N_{app} , N and N_{th} are the apparent plate number for a certain value of the loading factor, the plate number at infinite dilution for the same compound and the plate number resulting from the width of the profile as predicted by the ideal model, respectively.

This procedure has been used in the case of a Langmuir equation to calculate the band width and the apparent column efficiency³¹. It was found to give results in good agreement with those of the numerical calculations and with the experimental data previously acquired⁴³.

CONCLUSION

As we have mentioned in the previous section, the work by Eble *et al.*⁴⁶ provides a detailed verification of the validity of the Haarhoff–Van der Linde equation at low values of the column loading factor. An excellent agreement between the band profiles predicted by the ideal model and the profiles recorded for large samples of pure compounds has been reported under a variety of experimental conditions^{43,48}. The only common characteristic of these experiments was that in most cases the reduced sample size, m , was larger than 35. A correction procedure which accounts for the band broadening due to finite column efficiency kinetics has been described^{31,42}. The results were very satisfactory⁴³.

These experimental results confirm our conclusion that the use of the Houghton equation should be avoided, that the Haarhoff–Van der Linde equation gives excellent results for the prediction of band profiles at low loading factors ($L_f \leq 0.2\%$ for ideal columns or $bC_{\text{Max}} \leq 0.05$ for real columns), which become progressively less good with increasing loading factors. It should not be used with loading factors much in excess of *ca.* 1% for ideal columns ($bC_{\text{Max}} \leq 0.1$ for real columns). The ideal model give excellent results at high loading factors with values of m exceeding *ca.* 35, which, depending on the column efficiency and the retention, corresponds to values of the loading factor between 0.5% (very efficient columns, *e.g.*, $N = 10\,000$ plates and $k'_0 = 3$) and 3.3% (*e.g.*, $N = 1500$ plates and $k'_0 = 3$). In either instance, the use of the corresponding reduced coordinate system permits easy comparisons and predictions of the band profiles and of the effects of changes in the experimental conditions on these profiles and their sample size dependence.

If both analytical solutions fail, numerical solutions can be used, as discussed in the next section.

NUMERICAL SOLUTIONS OF THE SEMI-IDEAL MODEL FOR A SINGLE COMPOUND AND ANY ISOTHERM

We have shown above that the analytical solution derived by Haarhoff and Van der Linde²⁰ is valid for values of the loading factor such that $bC_{\text{Max}} \leq 0.05$. On the

other hand, we have also shown that the ideal model is valid when the reduced loading factor exceeds 35, which in most instances (*i.e.*, with columns having several thousand theoretical plates and values of k'_0 in excess of 2) corresponds to loading factor of several percent ($k'_0 = 2$, $N = 2500$ give $m = 35$ for $L_f = 3\%$). In the intermediate range of sample sizes, there is no satisfactory solution, although the band width of the profile at any fractional band height can be approximated, using the procedure suggested by Knox and Pyper⁴².

As there is no analytical solution available, we have to resort to numerical calculations. Two approaches are available: the semi-ideal model, which can be used only when the limit efficiency of the column at infinite dilution of the sample exceeds *ca.* 500 theoretical plates, and the kinetic models, which are valid in the whole range of values of the rate constants. We discuss only the former approach, as this work deals with equilibrium and semi-equilibrium models. Kinetic models are discussed in a separate paper¹.

Numerical solutions

In the semi-ideal model, the mass transfer kinetics are handled in the same way as by Van Deemter *et al.*¹⁴ and by Haarhoff and Van der Linde²⁰. The axial dispersion coefficient, D , in the mass balance equation is replaced by an apparent dispersion coefficient, $D_a = Hu/2$, which combines all the effects which, in linear chromatography, are traditionally lumped in the column HETP. The system of the mass balance equation (eqn. 1) and the kinetic equation (eqn. 4) is therefore replaced by eqn. 12. This equation is an excellent approximation of the system of partial differential equations in chromatography whenever the mass transfer kinetics are fast enough and at very low sample sizes the band profile tends towards a Gaussian profile.

The great advantage of this approach is that we do not need any detailed information regarding the mass transfer kinetics and their dependence on the solute concentration. Such information is usually difficult to collect and requires long, complicated experiments which provide only indirect determinations. With the semi-equilibrium model, we need to know the column efficiency at infinite dilution, the sample size and the equilibrium isotherm between the two phases, which is also needed with the kinetic models. The numerical solutions can accommodate any isotherm of physical significance and require no simplification.

Numerical solutions, however, do create truncation errors, because of the necessary use of finite values of space and time increments in the integration. These errors must be minimized or controlled. The classical method of finite differences lends itself to a straightforward application in the present instance. Two approaches are available. They have been discussed in detail in several previous publications^{35,49,50}, so we present here only a brief review of the numerical analysis problems.

Characteristic procedure. In this approach^{3,51}, we neglect the right-hand side of eqn. 12, *i.e.*, we write a program as if we wanted to calculate solutions of the ideal model (eqn. 14). We calculate the concentration at each point of a grid ($nh, j\tau$). We replace each differential by a finite difference, calculated for small but finite increments of the variables, space (h) and time (τ), respectively. Various finite difference schemes can be used, each introducing different truncation errors. For example, we may write³

$$\frac{C_{n+1}^j - C_n^j}{h} + \frac{1}{u} \cdot \frac{C_n^j + Fq_n^j - C_n^{j-1} - Fq_n^{j-1}}{\tau} = 0 \quad (46a)$$

which can be solved for C_{n+1}^j :

$$C_{n+1}^j = C_n^j + \frac{h}{u\tau} (C_n^j + Fq_n^j - C_n^{j-1} - Fq_n^{j-1}) \quad (46b)$$

The concentration at any point $C(n + 1, j)$ of the grid can be calculated, knowing the concentrations at the points (n, j) and $(n, j - 1)$.

This procedure creates an error, because the increments must remain finite. It can be shown that the error is equivalent to the addition of a dispersion term to the right-hand side of eqn. 14^{49,50}. Therefore, the procedure gives solutions of eqn. 12. If the space increment, h , is equal to the column HETP (*i.e.*, to H) and the time increment is equal to $2H(1 + k'_0)/u$, the truncation error in linear chromatography is exactly equal to $D_a \partial^2 C / \partial z^2$, where $D_a = Hu/2$. Therefore, the elution band profile of a column having an HETP equal to H (eqn. 12) is simulated^{49,50}.

Lax-Wendroff procedure. In this procedure, we write a program to calculate directly the solutions of eqn. 12, not those of eqn. 14, as in the previous section. The same error calculation method (*i.e.*, replacement in the finite difference equation of the value of the concentration at each point of the grid by its first three-term expansion) shows that it is possible to eliminate the excess diffusion which could arise from the truncation errors by a proper choice of the differences, *i.e.*, by using the numerical scheme described by Lax and Wendroff (see ref. 35). In linear chromatography, we obtain the following equation:

$$\frac{C_{n+1}^j - C_n^j}{\tau} + u_z \frac{C_{n+1}^j - C_{n-1}^j}{2h} = \left(\frac{\tau u_z^2}{2} + \frac{D_a}{1 + k'_0} \right) \frac{C_{n+1}^j - 2C_n^j + C_{n-1}^j}{h^2} \quad (46c)$$

where $u_z = u/(1 + k'_0)$. The extra-term, $\tau u_z^2/2$, added to the diffusion coefficient term, is introduced to compensate for the truncation error.

This procedure, however, suffers from two major drawbacks. First, the method used for the cancellation of the errors, which permits a correct simulation of the diffusion term in the right-hand side of eqn. 12, is exact only in linear chromatography, where the result is the same as the result of the calculations made using eqn. 46b. In non-linear chromatography an error appears. At moderate values of the loading factor this error is a small time shift. At higher loading factors, the error is difficult to estimate. Second, the choice of the values of the space and time increments must be made in very narrow ranges, in order to avoid numerical instabilities, resulting in unacceptable profiles. For these reasons, we prefer the former approach.

Comparison between the analytical solutions of the semi-ideal models and the numerical solutions of the semi-ideal model

We compare here the results obtained by the numerical solution of eqn. 12 and the results given by the Haarhoff-Van der Linde equation. This comparison completes

that in the previous section between the profiles predicted by this equation and by the analytical solution of the ideal model.

Fig. 14 compares the band profiles predicted by the Haarhoff-Van der Linde equation and by the numerical solution, both using a parabolic isotherm, for loading factors between 0.01 and 0.2% and a column efficiency of 2500 theoretical plates. In all four cases, the agreement between the two profiles corresponding to the same loading factor is excellent. Fig. 15 shows the same comparison, except that a Langmuir isotherm is used for the calculation of the numerical solutions, and the two-term expansion of this Langmuir isotherm for the calculations of the Haarhoff-Van der Linde equation. Although the agreement between the two profiles corresponding to a given loading factor is still very good, some significant difference begins to appear at the highest column loading. This result confirms, nevertheless, that the Haarhoff-Van der Linde equation is an excellent approximation of the band profile at low loading factors.

Fig. 16 compares the profiles predicted by the Haarhoff-Van der Linde equation and the numerical solution, both for a parabolic isotherm and for a loading factor of

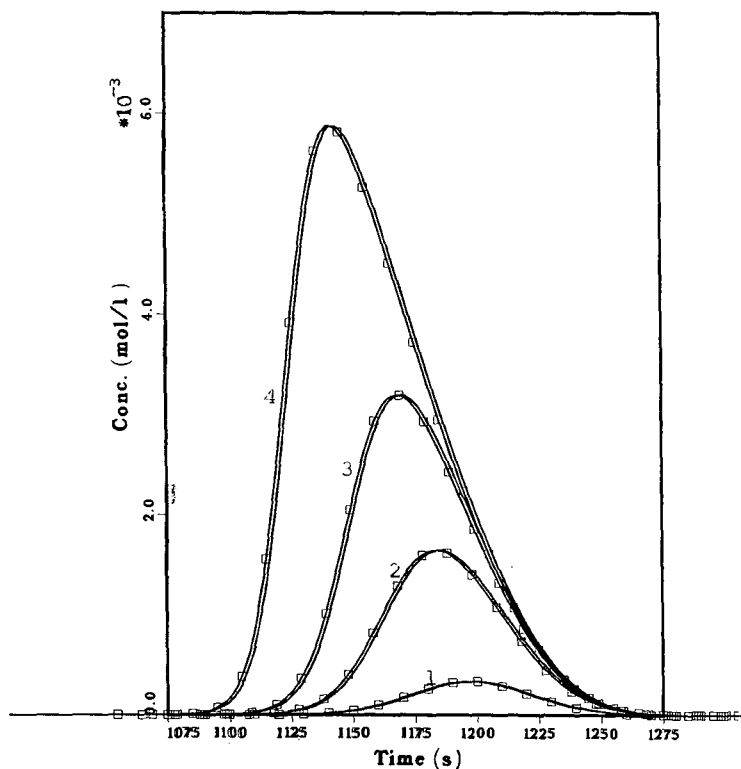


Fig. 14. Comparison between the band profiles predicted by the Haarhoff-Van der Linde equation and calculated by the numerical solution of the semi-ideal model. Parabolic isotherms, as for Fig. 1. Conditions as in Fig. 1, except column efficiency, 2500 plates. Loading factors: (1) 0.01%; (2) 0.02%; (3) 0.1%; (4) 0.2%. The Haarhoff-Van der Linde profiles are identified by squares.

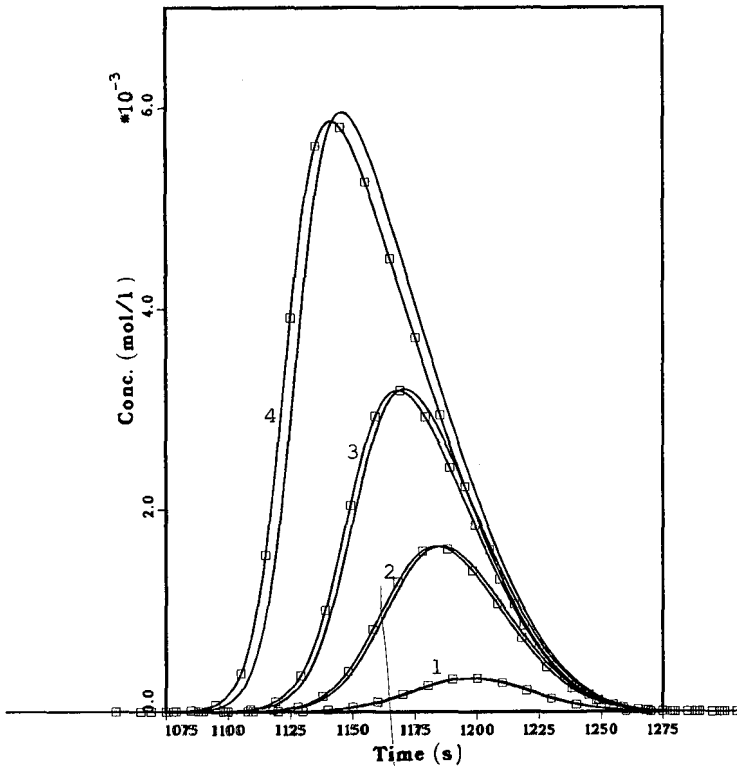


Fig. 15. Comparison between the band profiles predicted by the Haarhoff-Van der Linde equation and calculated by the numerical solution of the semi-ideal model. Parabolic isotherm as for Fig. 1 for the Haarhoff-Van der Linde equation, Langmuir isotherm for the numerical solution. Conditions as in Fig. 14. Loading factors: (1) 0.01%; (2) 0.02%; (3) 0.1%; (4) 0.2%. The Haarhoff-Van der Linde profiles are identified by squares.

0.2%, with increasing column efficiency. The agreement is excellent in all instances, from 500 to 25 000 plates. This agreement, and also the agreement observed between the experimental results and the predictions of numerical solutions at moderate and high loading factors^{40,41}, confirm the validity of our numerical algorithm, and especially the soundness of the choice of the space and time integration increments for the proper simulation of the column efficiency (see above). The progressive change in band profile when the column efficiency (*i.e.*, the mass transfer coefficient) decreases is in excellent agreement also with the prediction of the kinetic model¹². The band width, the thickness of the shock layer²² and the band retention time increase while the band height decreases with decreasing column efficiency. The semi-equilibrium models cannot predict the changes in the band profile which take place when the mass transfer coefficient decreases further and the column efficiency becomes much lower than 500 theoretical plates. This problem is discussed elsewhere¹.

Figs. 17 and 18 compare the profiles derived from the Haarhoff-Van der Linde equation and from the numerical solution, with either a parabolic or a Langmuir

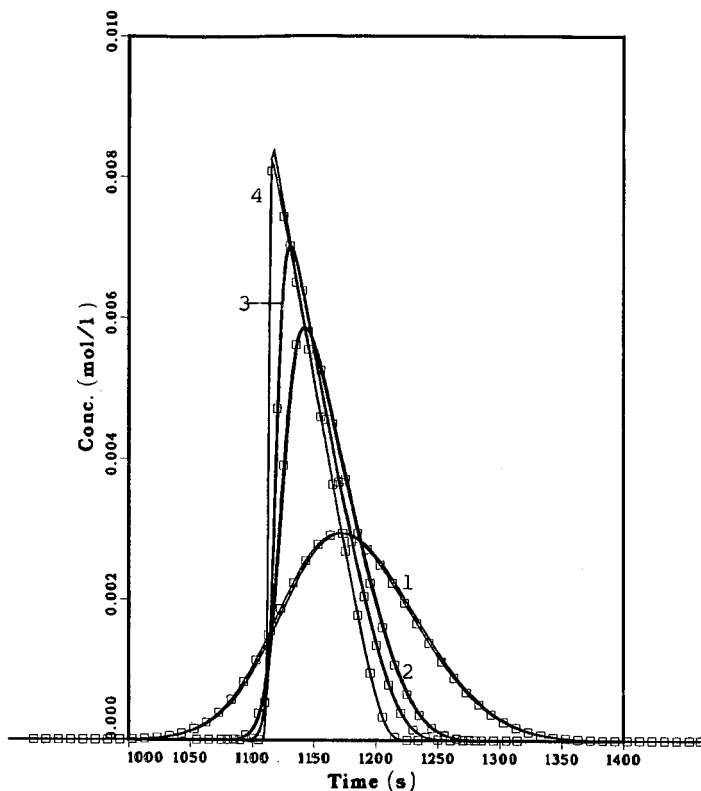


Fig. 16. Comparison between the band profiles predicted by the Haarhoff–Van der Linde equation and calculated by the numerical solution of the semi-ideal model. Parabolic isotherms, as for Fig. 1. Conditions as in Fig. 1, except loading factor, 0.2%, and variable column efficiency: (1) 500; (2) 2500; (3) 5000; (4) 25 000 plates. The Haarhoff–Van der Linde profiles are identified by squares.

isotherm, at loading factors of 1% (Fig. 17) and 5% (Fig. 18), for a 2500-plate column. In Fig. 18, the band profile derived from the Houghton equation is also shown. It is remarkable that at these high values of the loading factor the Haarhoff–Van der Linde profile is still in close agreement with the numerical solution calculated with a parabolic isotherm. This assumption, however, is unacceptable. Paradoxically, the Houghton equation, which is much less correct from a pure mathematical point of view, is in closer agreement with the correct profiles predicted by the numerical solution, in the case of a Langmuir isotherm, because of the nature of the systematic error which was introduced during its derivation (see above). Fig. 18 explains the observation reported by Wade and Carr⁵² that better fits of experimental band profiles are obtained when using the Houghton equation than with the Haarhoff–Van der Linde equation, although the former is less correct, as it does not even conserve mass.

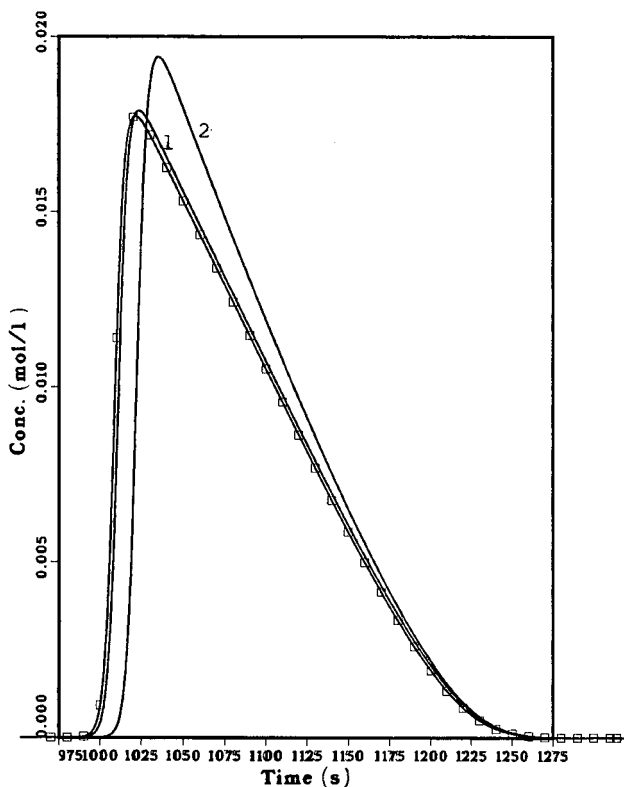


Fig. 17. Comparison between the band profiles predicted by the Haarhoff-Van der Linde equation and calculated by the numerical solution of the semi-ideal model. Influence of the isotherm. Conditions as in Figs. 7 and 8. Column efficiency, 2500 plates; loading factor, 1%. (1) Profile calculated with the numerical solution using a parabolic isotherm; (2) profile calculated by the numerical solution using a Langmuir isotherm. The Haarhoff-Van der Linde profile is identified by squares.

Comparison between the analytical solution of the ideal model and the numerical solutions of the semi-ideal model

We now compare the profile given by the analytical solution of the ideal model and the profile calculated using the numerical solution of the semi-ideal model (eqn. 12) for the same isotherm. This will permit a discussion of the validity of the ideal model and of the kinetic correction which has been described above.

Fig. 19 shows a comparison between the two profiles for a Langmuir isotherm, with loading factors between 0.5 and 20%. The reduced sample size, m (eqn. 34), varies from 7 to 280. The agreement between the two solutions corresponding to the same loading factor improves with increasing loading factor. The ideal model becomes a good approximation of the actual profile when m exceeds 35, as explained above.

Fig. 20 compares the profiles calculated by using the numerical solution of the semi-ideal model and the analytical solution of the ideal model, for different column efficiencies and loading factors, corresponding to a common value of $m = 35$. The agreement between each pair of profiles improves with increasing column efficiency,

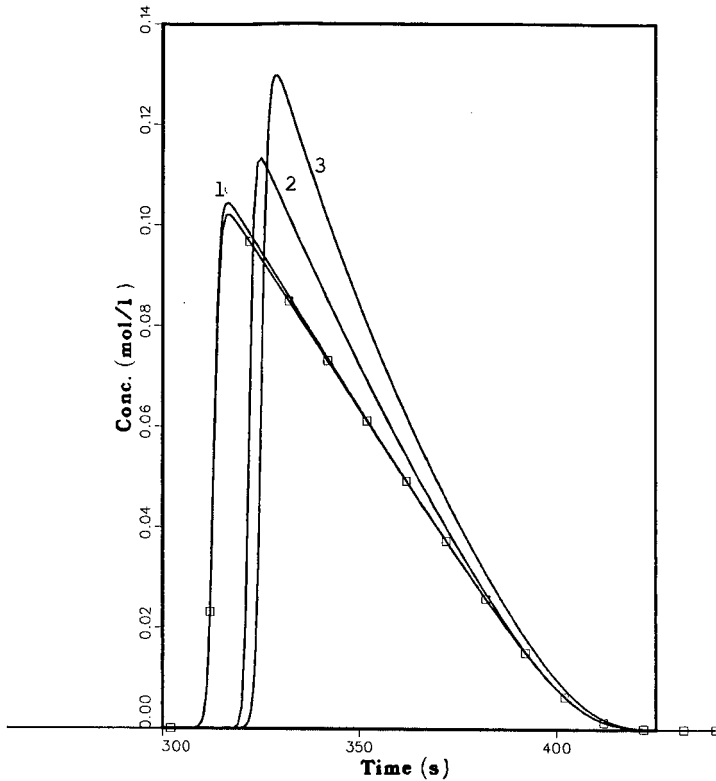


Fig. 18. Comparison between the band profiles predicted by the Haarhoff-Van der Linde and the Houghton equations and calculated by the numerical solution of the semi-ideal model. Influence of the isotherm. Conditions as in Figs. 7 and 8. Column efficiency, 2500 plates; loading factor, 5%. (1) Profile calculated with the numerical solution using a parabolic isotherm; (2) profile derived from the Houghton equation; (3) profile calculated by the numerical solution using a Langmuir isotherm. The Haarhoff-Van der Linde profile is identified by squares.

i.e., with decreasing loading factor at constant m . A similar result has been shown in Fig. 4, when comparing the Haarhoff-Van der Linde profile and the solution of the ideal model for a parabolic isotherm. It is much more apparent in the present case, however. Even at large values of the loading factor (*e.g.*, 10%), there is still a marked difference between the solutions of the ideal and semiideal model when the column efficiency is poor.

SOLUTIONS OF THE EQUILIBRIUM MODELS FOR A TWO-COMPONENT MIXTURE

The main purpose of chromatography is to separate and purify substances, not to elute single-component bands. The solution of the single-compound band profile is useful because it is the simplest non-linear chromatographic problem, so, if we cannot solve it, we cannot possibly discuss properly a multi-component problem. Further, the solution of the single-compound problem tells us how high concentration bands

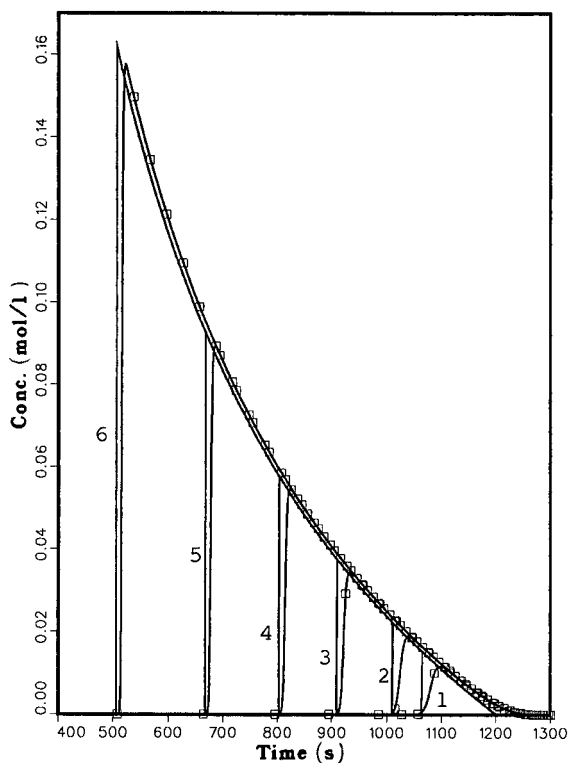


Fig. 19. Comparison between the band profiles predicted by the analytical solution of the ideal model and the numerical solution of the semi-ideal model. Influence of the loading factor at constant plate number. Conditions as in Fig. 1, except corresponding Langmuir isotherm. Column efficiency, 2000 theoretical plates. Loading factors (L_i) and reduced sample size (m): (1) 0.5%, 7; (2) 1%, 14; (3) 2.5%, 35; (4) 5%, 70; (5) 10%, 140; (6) 20%, 280.

migrate in chromatographic columns and how their profiles are affected by the non-linear behavior of the equilibrium isotherm. This solution emphasizes the main problems we are faced with when attempting to deal with the second simplest problem of non-linear chromatography, the two-component problem. There is one complicating factor, however, and it is of major importance: under non-linear conditions, the amount of one component in the stationary phase at equilibrium with a multi-component solution is a function of the concentrations of *all* the components. The solution of the two-component problem therefore requires the consideration of binary or competitive isotherms.

Semi-ideal model

It is simple and straightforward to extend to the two-component problem the formulation of the single-compound problem and to show that, provided the mass transfer kinetics are fast enough and the column efficiency exceeds a few hundred plates, the elution band profiles of each component will be solutions of the following system of partial differential equations:

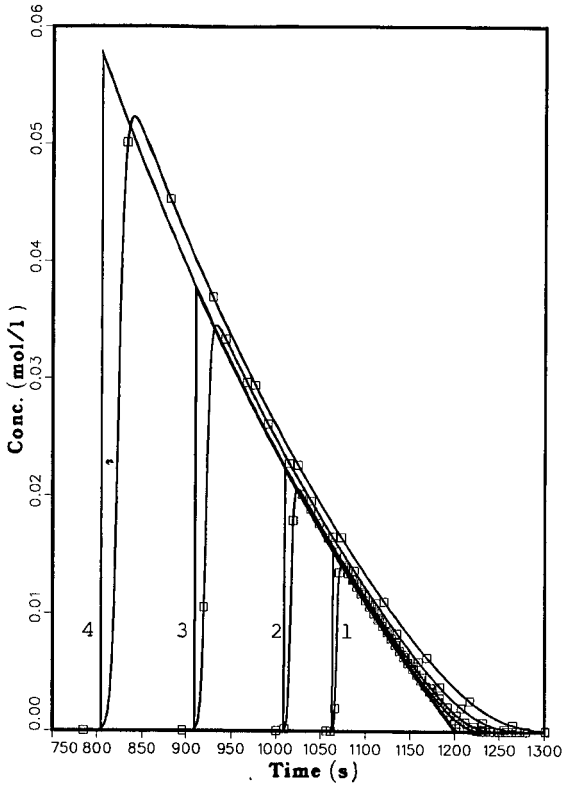


Fig. 20. Comparison between the band profiles predicted by the analytical solution of the ideal model and the numerical solution of the semi-ideal model. Influence of plate number at constant reduced sample size ($m = 35$). Conditions as in Fig. 1, except corresponding Langmuir isotherm. Column efficiencies and loading factors: (1) $N = 10\,000$, $L_f = 0.5\%$; (2) $N = 5000$, $L_f = 1\%$; (3) $N = 2000$, $L_f = 2.5\%$; (4) $N = 1000$, $L_f = 5\%$.

$$\frac{\partial C_1}{\partial t} + F \frac{\partial q_1}{\partial t} + u \frac{\partial C_1}{\partial x} = D_a \frac{\partial^2 C_1}{\partial z^2} \quad (47)$$

and

$$\frac{\partial C_2}{\partial t} + F \frac{\partial q_2}{\partial t} + u \frac{\partial C_2}{\partial x} = D_a \frac{\partial^2 C_2}{\partial z^2} \quad (48)$$

In these equations, q_1 and q_2 are given by

$$q_i = f_i(C_1, C_2) \quad i = 1, 2 \quad (49)$$

Because of the competition between the two components of the mixture for interaction with the stationary phase, the two-component problem is much more complex than the

single-compound problem. The mass balance equations of the two components, 1 and 2, are coupled by the binary isotherm equations.

Thus, neither the analytical solutions of the semi-equilibrium models (the Houghton³⁶ and Haarhoff–Van der Linde²⁰ equations) nor those of the kinetic models (Thomas⁶, Goldstein⁷ and Wade *et al.*⁸ models) can be extended to the solution of the two-component problem. The mathematical difficulties to be faced in order to solve the system of eqns. 47–49 are too formidable to be tackled with second-degree partial differential equations. The system of equations corresponding to the ideal model (*i.e.*, an infinite column efficiency, and $D_a = 0$ in eqns. 47 and 48), which is much simpler, can be solved, however (see next section). Under conditions when the ideal model does not give satisfactory results (values of m too small), a numerical solution can be obtained by extending the approach described above to the system of eqns. 47–49.

Analytical solution of the ideal model

The solution of the ideal model for two components has been discussed by Offord and Weiss⁵³ and by Glueckauf²⁶. Both obtained very important, but incomplete results. Helfferich and Klein⁵⁴ developed a theory of multi-component ideal chromatography based on the use of the concept of coherence and of the h -transform. They obtained results which are in agreement with those of the shock theory²⁸. Most of their work dealt with the application of this method to the investigation of displacement and frontal analysis. They published distance–time diagrams which describe the migration process, the dilution and the progressive separation of a pulse of a binary mixture, with competitive Langmuir isotherms.

Recently, we published an analytical solution of the two-component elution problem, in the case of binary Langmuir equilibrium isotherms, based on the use of the characteristic theory and the shock theory³³. We have also been able to derive the same equations from the previous results obtained by Helfferich and Klein, using the h -transform method³⁴. Both results are based on the use of the Langmuir competitive isotherm equation:

$$q_i = \frac{a_i C_i}{1 + b_1 C_1 + b_2 C_2} \quad (50)$$

It has not been possible yet to extend this approach to other isotherm equations, however, as was done in the case of the single compound problem³². We have also extended to the case of the two-component problem the use of the numerical algorithm derived for the solution of the semi-ideal⁵⁵ and the kinetic¹³ models of chromatography.

In the case of a single solute, with a convex upward isotherm, a concentration discontinuity or shock is formed when a rectangular sample pulse enters the column²². The continuous, simple wave solution accounts for the rear of the profile. The band top belongs to both solutions, the shock and the simple wave³¹. It turns out that its velocity as a point on the simple wave solution is higher than the shock velocity. Hence, the shock is eroded and decreases. With a two-component sample, the situation is more complex. The less strongly adsorbed component moves ahead of the more strongly

adsorbed component. Two shocks appear, one at the front of the first component band and the second at the front of a mixed band. Two simple wave solutions take place, one for the pure second component and one for the mixed band. The development of the chromatogram and the progressive separation between the two bands can be understood by using the shock theory and the simple wave theory, which describe their behavior and their interference³³.

A characteristic feature of the solution of the ideal model is the concentration plateau on the rear of the second component profile. This plateau had already been predicted by Glueckauf²⁶. It results from the fact that, in the ideal model, a velocity can be associated with each concentration. This velocity is a function of the concentration^{22,28} and, with convex upward isotherms, increases with increasing concentration. As can be expected, the theory predicts that the velocity associated with a concentration of the second component in the presence of the first component decreases with decreasing concentration of this first component, when the isotherm is a competitive Langmuir isotherm. However, theory predicts that the velocity associated with the concentration of the second component tends towards a limit when the concentration of the first component tends towards zero at the end of the mixed band. This limit velocity is higher than the velocity associated with the same concentration of the pure second component. As a result, the second component leaks out of the intermediate, mixed band at a constant concentration, hence a concentration plateau arises. The length and the concentration of this plateau depend on the feed composition; the former increases and the latter decreases with decreasing proportion of the second component in the feed.

The chromatogram includes three zones. The third zone contains the pure second component. The rear part of its profile is the same as if the second component were alone. It ends at $t_{R,2}^0 + t_p$, and begins at the concentration plateau. In the second zone the two components coexist. The first zone contains the first component, confined between the two shocks.

The analytical solution of the ideal model is relatively simple, but it appears complex because it is made of seven different points, four arcs, two concentration discontinuities and one concentration plateau (see Fig. 21). The coordinates of the seven feature points and the equations of the four arcs are given in Tables I–III, together with the definitions of the intermediate parameters used in these equations. The order of presentation of the solution emphasizes the fact that the chromatogram is anchored at its end ($t = t_{R,2}^0 + t_p$) and that the solution is progressively derived by going backwards, from the end of the chromatogram towards the front.

Finally, we emphasize here that, if the two bands are separated when they leave the column, the profile of the second one is given by the same equation which gives the profile of a pure compound, but that *the same is not true for the first component*. The first component band conserves forever the memory of its interaction with the second component.

Comparison between the analytical solution of the ideal model and the numerical solution of the semi-ideal model

Fig. 22 shows a comparison between the band profiles calculated for the two components of a binary mixture using the numerical solution and the profiles given by the equations in Tables II and III (ideal model). The coefficients of the competitive

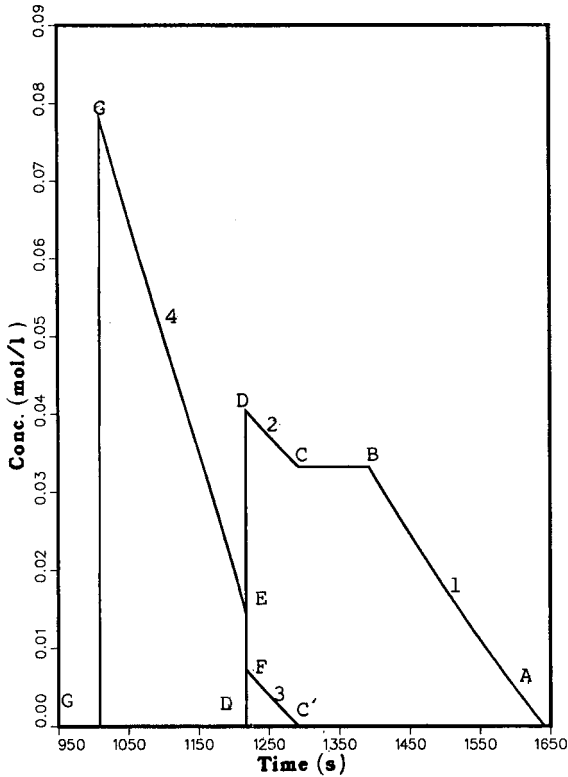


Fig. 21. Analytical solution of the ideal model for two components with competitive Langmuir isotherms. Relative composition of the mixture, 1:1. The coordinates of the points A–G and the equations of curves 1–4 are given in Table I.

Langmuir isotherms are given in the figure caption. The relative retention of the two components under linear conditions would be 1.20. The relative composition of the feed is 4:1. The column efficiency and sample size are such that the reduced sample size, m , is 120 for the first component and 30 for the second. The agreement between the two profiles is generally good, although some of the important features of the ideal model are smoothed out or totally eroded in the semi-ideal model numerical solution. For example, the second shock has totally disappeared from the rear of the first component profile, and the shock layer on the front of the second component is very thick and is also shorter than predicted. Nevertheless the broadening of the second band takes place much as predicted by the ideal model, and the result, the tag-along effect, would have been unpredictable from the mere consideration of the theory of the single compound profile. Fig. 23 compares the band profiles predicted by the ideal model under the same experimental conditions as for Fig. 22, with the numerical solution obtained under conditions where m is 24 for the first component and 6 for the second. The second component band is now nearly Gaussian and the first component band is markedly broadened and smoothed. The ideal model, which predicted correctly the

TABLE I
DEFINITIONS

Langmuir equilibrium isotherms:

$$q_i = a_i C_i / (1 + b_1 C_1 + b_2 C_2)$$

where q_i and C_i are the concentrations of component i at equilibrium in the stationary and the mobile phases, respectively

Relative retention:

$$\alpha = a_2/a_1$$

Constant γ :

$$\gamma = \frac{\alpha b_1 r_1 + b_2}{b_1 r_1 + b_2}$$

Roots of the Clairaut differential equation:

They are the roots, $r_1 > r_2$, of the following equation:

$$\alpha b_1 C_2^0 r^2 - (\alpha - 1 + \alpha b_1 C_1^0 - b_2 C_2^0) r - b_2 C_1^0 = 0$$

Loading factors:

$$L'_i = \left(1 + \frac{b_1 r_1}{b_2} \right) L_{i,2}$$

$$L_{i,2} = \frac{b_2 C_2^0 t_p}{t_{R,2}^0 - t_0} = \frac{b_2 n_2}{F_v(t_{R,2}^0 - t_0)} = \frac{b_2 n_2}{\varepsilon S L k'_{0,2}}$$

profiles at high values of the reduced sample size, m , gives a poor approximation at low values of m .

Similarly, Fig. 24 compares the band profiles obtained with the two procedures discussed, for a mixture of the same two components as for Fig. 22, but with a relative concentration of 1:4. The value of m corresponding to the sample size and the column efficiency is 30 for the first component and 120 for the second. There is excellent agreement with the profiles predicted by the two methods. The shock layers on the front of the two component profiles predicted by the numerical method are very thin, thinner than the shock layer at the rear of the first component. The plateau on the rear of the second component profile has been smoothed out by diffusion, and an inflection at the corresponding concentration is the only trace left. In Fig. 25, the corresponding values of m are only 6 and 24 for the first and second components, respectively, and as in Fig. 23 the agreement between the two profiles is poor. The interaction between the two bands is still obvious by the tail of the first component band.

Correction for the finite column efficiency

Using the analytical solution of the ideal model for two components^{3,3}, equations have been derived for the purity, the production rate and the recovery yields of these two components, as a function of the experimental parameters^{5,6}. They permit the determination of the feed injection size and the cutting times for the maximum production rate of these compounds at any degree of stated purity.

A correction based on the same principle as that used for the single-compound profile has been derived recently^{5,7}. This correction permits the investigation of the influence on the production rate of the column efficiency and of the dependence of this

TABLE II
COORDINATES OF THE CHARACTERISTIC POINTS OF THE CHROMATOGRAM IN FIG. 21

Point	Coordinates
A	$t_A = t_p + t_{R,2}^0$ $C_A = 0$
B	$t_B = t_0 + t_p + \frac{\gamma^2}{\alpha^2}(t_{R,2}^0 - t_0)$ $C_B = \frac{\alpha - 1}{b_2 + \alpha b_1 r_1}$
C	$t_C = t_p + t_0 + \frac{\gamma}{\alpha}(t_{R,1}^0 - t_0)$ $C_C = \frac{\alpha - 1}{b_2 + \alpha b_1 r_1}$
D	$t_D = t_p + t_0 + \gamma(t_{R,2}^0 - t_0)(1 - \sqrt{L'_f})^2$ $C_D = \frac{1}{b_2 + \alpha b_1 r_1} \cdot \frac{\sqrt{L'_f}}{1 - \sqrt{L'_f}}$
E	$t_E = t_D$ $C_E = \frac{[(1 - \alpha)/\alpha] + \sqrt{L'_f}}{1 - \sqrt{L'_f}}$
F	$t_F = t_D$ $C_F = \frac{r_1}{b_2 + \alpha b_1 r_1} \cdot \frac{1 - \alpha + \alpha\sqrt{L'_f}}{1 - \sqrt{L'_f}}$
G	<p>The retention time and the concentration of point G cannot be obtained in closed forms. The retention time is derived by calculating the lower boundary of the finite integral of the profiles of the first component (equations of lines 3 and 4, Table III and Fig. 21). This integral is equal to the mass injected of the first component. The concentration is then obtained by placing the retention time of the front shock in the equation of line 4. L'_f is defined in Table I.</p>

efficiency on the flow velocity. The selection of the experimental conditions permitting the maximum production rate under a certain set of constraints (purity of the products or recovery yield) becomes possible. These results are in excellent agreement with those obtained from numerical solutions of the semi-ideal model. This confirms the validity of our approach⁵⁷.

TABLE III

EQUATIONS FOR THE CONTINUOUS PROFILES ON THE CHROMATOGRAM SHOW IN FIG. 21

Line	Equation
Line 1, AB	$C_{AB} = \frac{1}{b_2} \left[\sqrt{\left(\frac{t_{R,2}^0 - t_0}{t - t_p - t_0} \right)} - 1 \right]$
Line 2, CD	$C_2 = \frac{1}{b_2 + \alpha b_1 r_1} \left[\sqrt{\gamma \cdot \frac{t_{R,2}^0 - t_0}{t - t_p - t_0}} - 1 \right]$
Line 3, CF	$C_1 = \frac{1}{b_1 + b_2/\alpha r_1} \left[\sqrt{\frac{\gamma}{\alpha} \cdot \frac{t_{R,1}^0 - t_0}{t - t_p - t_0}} - 1 \right]$
Line 4, EG	$t = t_p + t_0 + (t_{R,1}^0 - t_0) \left\{ \frac{1}{(1 + b_1 C_1)^2} - L_{f,2} \cdot \frac{\alpha - 1}{\alpha} \cdot \frac{1}{[(\alpha - 1)/\alpha + b_1 C_1]^2} \right\}$

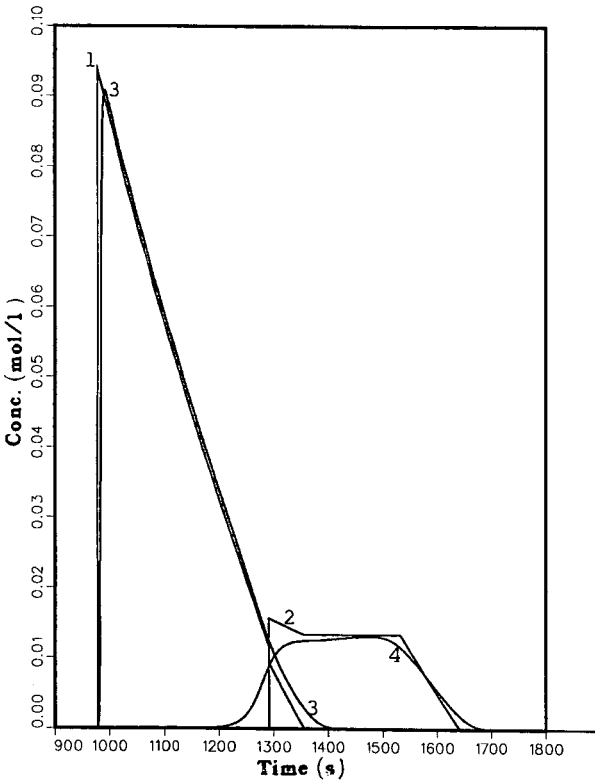


Fig. 22. Comparison between the elution band profiles of a two-component mixture calculated with the ideal model and with the numerical solution of the semi-ideal model. Langmuir competitive isotherm (eqn. 53), with $a_1 = 6$, $a_2 = 7.2$, $b_1 = 2.5$, $b_2 = 3.0$. Column length, 25 cm; dead time, $t_0 = 200$ s; column efficiency, 5000 theoretical plates; relative composition of the feed, 4:1; sample size, $L_{f,1} = 3.3\%$, $L_{f,2} = 0.83\%$. Profiles: (1) first component, ideal model; (2) second component; ideal model; (3) first component, numerical solution; (4) second component, numerical solution.

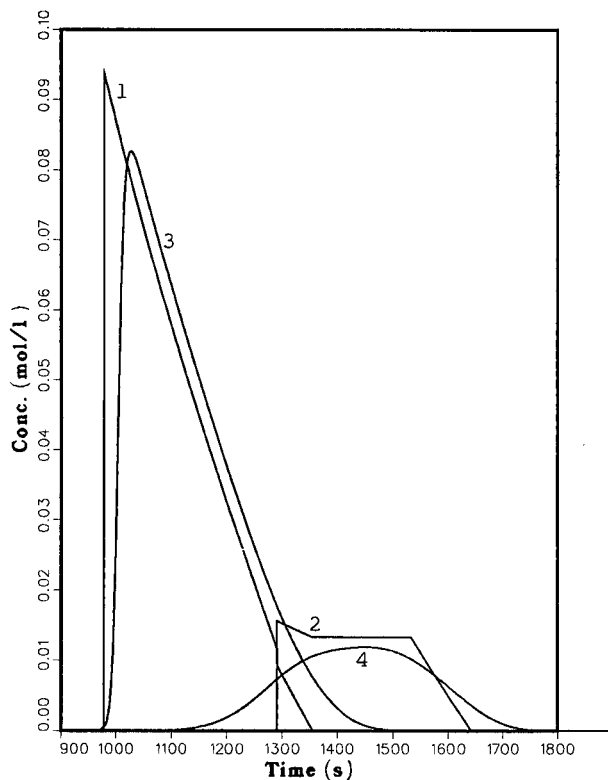


Fig. 23. Comparison between the elution band profiles of a two-component mixture calculated with the ideal model and with the numerical solution of the semi-ideal model. Conditions as in Fig. 22, except column efficiency, 1000 theoretical plates. Profiles: (1) first component, ideal model; (2) second component, ideal model; (3) first component, numerical solution; (4) second component, numerical solution.

CONCLUSION

Considerable progress have been made in the investigation of the fundamental problems of chromatography through the use of the equilibrium and semi-equilibrium models. There remain a few unsolved problems which deserve attention.

First, we still need a solution giving in closed form the equation of the elution profile of a single compound at large values of the loading factor. What we are really missing at present is an equation which would be, at high loading factors, the equivalent of the Haarhoff–Van der Linde equation at low sample sizes, an equation which would account fully for the thermodynamic effects and correct to the first order for the kinetic effects. Barring that, a practical and accurate correction of the solution of the ideal model, taking into account the smoothing effect of a finite column efficiency, would be highly valuable.

The two-component problem is much more difficult and less well understood than the single-compound problem. An extension to the case of other isotherms of the solution of the ideal model for two components which we have derived recently in the

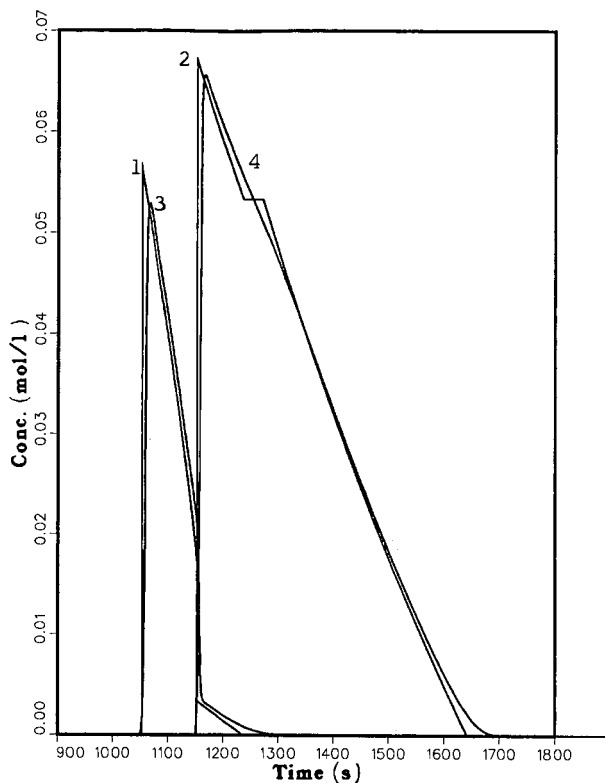


Fig. 24. Comparison between the elution band profiles of a two-component mixture calculated with the ideal model and with the numerical solution of the semi-ideal model. Conditions as in Fig. 23, except relative composition of the feed, 1:4. Profiles: (1) first component, ideal model; (2) second component, ideal model; (3) first component, numerical solution; (4) second component, numerical solution.

case of competitive Langmuir isotherms would be a further great progress. Admittedly, any progress in the understanding of the competitive behavior of the components of a mixture for adsorption (or, more generally, for interaction with the stationary phase) would be very valuable at this stage of development of non-linear chromatography. It may be that the lack of understanding of competitive isotherms is the most critical hindrance. An analytical solution of the semi-ideal model, valid at high concentrations, is needed in order to investigate in depth the various problems currently arising in connection with the optimization of the experimental conditions of preparative chromatography. At the very least, we need also a practical and accurate correction of the solution of the ideal model taking into account the effects of the finite column efficiency.

Finally, we have discussed so far only one part of the problem. The mass balance equations, the equations of the semi-ideal model, are non-linear, hyperbolic partial differential equations. They are non-linear because the coefficient of one of the partial differentials depends on the function [*i.e.*, the equilibrium isotherm, $f(C)$]. We have searched for solutions of these equations, knowing the function $f(C)$, and as we have

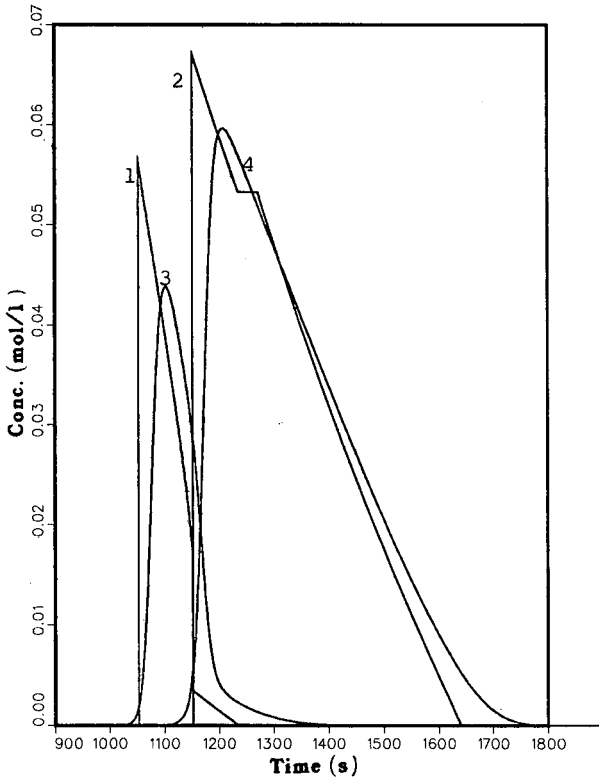


Fig. 25. Comparison between the elution band profiles of a two-component mixture calculated with the ideal model and with the numerical solution of the semi-ideal model. Conditions as in Fig. 24, except relative composition of the feed, 1:4. Sample size, $L_{r,1} = 0.83\%$, $L_{r,2} = 3.3\%$. Profiles: (1) first component, ideal model; (2) second component, ideal model; (3) first component, numerical solution; (4) second component, numerical solution.

seen it is a difficult task. Far more difficult, both from a theoretical viewpoint and in practice, is the converse problem of knowing solutions of the partial differential equation, finding access to the function in order to obtain an accurate estimate. This problem is at the forefront of mathematical research⁵⁸. In many simpler problems, direct empirical procedures have been used with some success. The principle consists in starting from a crude multi-parameter estimate of the function, calculating the corresponding solution and using various computational techniques to minimize some measure of the distance between the band profile recorded experimentally and those calculated, in order to optimize the values of the parameter. Most probably, this approach cannot be entirely satisfactory. Methods having a more sound theoretical background are needed.

SYMBOLS

- A Peak area (eqn. 30a)
 a First coefficient of the Langmuir isotherm (eqn. 19)

- b second coefficient of the Langmuir isotherm (eqn. 19)
- C Concentration of the studied compound in the mobile phase (eqn. 1)
- $C(z,t)$ Concentration of the studied compound in the mobile phase, at time t and position z (eqn. 5)
- C_{Max} Maximum concentration in a chromatographic band (eqn. 18)
- C_s Concentration of the studied compound in the stationary phase (eqn. 1)
- C_0 Concentration of the compound in the feed (injected sample) (eqn. 5)
- C_1, C_2 Concentrations of the two components of a binary mixture in the mobile phase (eqn. 47)
- \bar{C} Total concentration of the studied compound, referred to the total column volume (eqn. 11)
- \bar{C}_m Concentration of the studied compound in the mobile phase, referred to the total column volume (eqn. 8)
- \bar{C}_s Concentration of the studied compound in the stationary phase, referred to the total column volume (eqn. 8)
- \bar{C}_m^* Equilibrium concentration in the mobile phase, referred to the total column volume (eqn. 8)
- \bar{C}_s^* Equilibrium concentration in the stationary phase, referred to the total column volume (eqn. 8)
- D Coefficient of axial dispersion (eqn. 1)
- D_p Intraparticle diffusion coefficient (eqn. 7)
- D' Pseudo-diffusion coefficient (eqn. 11)
- D_a Apparent diffusion coefficient (eqn. 12)
- d_p Average particle diameter of the packing (eqn. 7)
- F Phase ratio (eqn. 1)
- V_v Volume flow-rate of mobile phase (eqn. 17)
- H Column HETP (eqn. 6)
- H_{app} Observed column HETP (eqn. 44)
- H_{th} Thermodynamic contribution to the column HETP (eqn. 44)
- h Space integration increment in the numerical calculations of elution profiles (eqn. 46)
- J Longitudinal flux of compound per unit cross-sectional area (eqn. 10)
- k_a Adsorption rate constant (eqn. 2)
- k_d Desorption rate constant (eqn. 2)
- k_f Lumped mass transfer coefficient (eqn. 4)
- k_1, k_2 Rate constants (eqn. 3)
- k'_0 Column capacity factor at infinite dilution (eqn. 6)
- k_e External film mass transfer coefficient (eqn. 7)
- L Column length (eqn. 26)
- L_f Loading factor for a compound (eqn. 11)
- L'_f Auxiliary loading factor (Table I)
- m Reduced sample size (eqn. 29)
- N Limit efficiency for an infinitely small sample size (eqn. 34)
- N_{app} Observed plate number of the column (eqn. 41)
- N_{th} Plate number observed in non-linear chromatography with an ideal column (eqn. 38a)
- n Sample size (eqn. 17)

q	Concentration of a compound in the stationary phase in equilibrium with the concentration C_m in the mobile phase (eqn. 4); also isotherm equation (eqn. 13)
q_s	Column saturation capacity (eqn. 2)
R	Fraction of a solute in the mobile phase (eqn. 11)
S	Column cross-sectional area (eqn. 26)
t	time (eqn. 1)
t_0	Column dead time (eqn. 15)
t_p	Duration of the injection of the sample (eqn. 5)
t_R	Retention time (eqn. 17)
$t_{R,0}$	Retention time at infinite dilution (eqn. 16)
u	Mobile phase velocity (eqn. 1)
W_{th}	Baseline band width of the band profile predicted by the ideal model (eqn. 38)
X	Reduced concentration in the solution of the Houghton equation (eqn. 29)
z	length (abscissa) along the column (eqn. 1)
β	Inner porosity of the packing particles (eqn. 7)
ΔJ	Contribution to the longitudinal flux of a compound due to non-equilibrium (eqn. 11)
ε	Packing porosity (eqn. 1)
$\varepsilon_m, \varepsilon_s$	Relative deviation from equilibrium (eqn. 8)
A	Reduced variable in the Houghton equation (eqn. 28)
ξ	Reduced variable in the Houghton equation (eqn. 28)
τ	Reduced time in the Houghton equation (eqn. 29); also time integration increment in the calculation of elution profiles (eqn. 46)

ACKNOWLEDGEMENTS

This work was supported in part by Grant CHE-8901382 of the National Science Foundation and by the cooperative agreement between the University of Tennessee and the Oak Ridge National Laboratory.

REFERENCES

- 1 S. Golshan-Shirazi and G. Guiochon, in preparation.
- 2 J. N. Wilson, *J. Am. Chem. Soc.*, 62 (1940) 1583.
- 3 G. Guiochon, S. Golshan-Shirazi and A. Jaulmes, *Anal. Chem.*, 60 (1988) 1856.
- 4 S. Golshan-Shirazi and G. Guiochon, *J. Chromatogr.*, 461 (1989) 1.
- 5 E. sz. Kováts, in F. Bruner (Editor), *The Science of Chromatography*, Elsevier, Amsterdam, 1985, p. 205.
- 6 H. C. Thomas, *J. Am. Chem. Soc.*, 66 (1944) 1664.
- 7 S. Goldstein, *Proc. R. Soc. London, Ser. A*, 219 (1953) 151.
- 8 J. L. Wade, A. F. Bergold and P. W. Carr, *Anal. Chem.*, 59 (1987) 1286.
- 9 L. Lapidus and N. R. Amundson, *J. Phys. Chem.*, 56 (1952) 984.
- 10 E. Glueckauf and J. I. Coates, *J. Chem. Soc.*, (1947) 1315.
- 11 N. K. Hiester and T. Vermeulen, *Chem. Eng. Prog.*, 48 (1952) 505.
- 12 B. Lin, S. Golshan-Shirazi and G. Guiochon, *J. Phys. Chem.*, 93 (1989) 3363.
- 13 S. Golshan-Shirazi, B. Lin and G. Guiochon, *J. Phys. Chem.*, 93 (1989) 6871.
- 14 J. J. Van Deemter, F. J. Zuiderweg and A. Klinkenberg, *Chem. Eng. Sci.*, 5 (1956) 271.
- 15 A. J. P. Martin and R. L. M. Synge, *Biochem. J.*, 35 (1941) 1359.
- 16 E. Kucera, *J. Chromatogr.*, 19 (1965) 237.
- 17 C. Horvath and H. J. Lin, *J. Chromatogr.*, 149 (1978) 43.
- 18 J. F. K. Huber, *Ber. Bunsenges. Phys. Chem.*, 77 (1973) 179.
- 19 J. C. Giddings, in *Dynamics of Chromatography*, Marcel Dekker, New York, 1965.

- 20 P. C. Haarhoff and H. J. Van der Linde, *Anal. Chem.*, 38 (1966) 573.
- 21 D. DeVault, *J. Am. Chem. Soc.*, 65 (1943) 532.
- 22 B. Lin, S. Golshan-Shirazi, Z. Ma and G. Guiochon, *Anal. Chem.*, 60 (1988) 2647.
- 23 J. Weiss, *J. Chem. Soc.*, (1943) 297.
- 24 E. Glueckauf, *J. Chem. Soc.*, (1947) 1302.
- 25 E. Glueckauf, *Nature (London)*, 156 (1945) 205.
- 26 E. Glueckauf, *Proc. R. Soc., London, Ser. A*, 186 (1946) 35.
- 27 H. K. Rhee, R. Aris and N. R. Amundson, *Philos. Trans. R. Soc. London, Ser. A*, 267 (1970) 419.
- 28 R. Aris and N. R. Amundson, *Mathematical Methods in Chemical Engineering*, Prentice Hall, Englewood Cliffs, NJ, 1973.
- 29 G. Guiochon and L. Jacob, *Chromatogr. Rev.*, 14 (1971) 77.
- 30 P. Valentin and G. Guiochon, *Sep. Sci.*, 10 (1975) 245.
- 31 S. Golshan-Shirazi and G. Guiochon, *Anal. Chem.*, 60 (1988) 2364.
- 32 S. Golshan-Shirazi and G. Guiochon, *J. Phys. Chem.*, 94 (1990) 495.
- 33 S. Golshan-Shirazi and G. Guiochon, *J. Phys. Chem.*, 93 (1989) 4143.
- 34 S. Golshan-Shirazi and G. Guiochon, *J. Chromatogr.*, 484 (1989) 125.
- 35 B. Lin, Z. Ma and G. Guiochon, *Sep. Sci. Technol.*, 24 (1989) 809.
- 36 G. Houghton, *J. Phys. Chem.*, 67 (1963) 84.
- 37 A. Jaulmes, C. Vidal-Madjar, A. Ladurelli and G. Guiochon, *J. Phys. Chem.*, 88 (1984) 5379.
- 38 A. Jaulmes, C. Vidal-Madjar, H. Colin and G. Guiochon, *J. Phys. Chem.*, 90 (1986) 207.
- 39 A. Jaulmes, M. J. Gonzalez, C. Vidal-Madjar and G. Guiochon, *J. Chromatogr.*, 387 (1987) 41.
- 40 S. Golshan-Shirazi, S. Ghodbane and G. Guiochon, *Anal. Chem.*, 60 (1988) 2630.
- 41 S. Golshan-Shirazi and G. Guiochon, *Anal. Chem.*, 60 (1988) 2634.
- 42 J. H. Knox and H. M. Pyper, *J. Chromatogr.*, 363 (1986) 1.
- 43 S. Golshan-Shirazi and G. Guiochon, *Anal. Chem.*, 61 (1989) 462.
- 44 H. Poppe and J. C. Kraak, *J. Chromatogr.*, 255 (1983) 395.
- 45 J. E. Eble, R. L. Grob, P. E. Antle and L. R. Snyder, *J. Chromatogr.*, 384 (1987) 25.
- 46 J. E. Eble, R. L. Grob, P. E. Antle and L. R. Snyder, *J. Chromatogr.*, 384 (1987) 45.
- 47 J. C. Giddings, in E. Heftmann (Editor), *Chromatography*, Van Nostrand Reinhold, New York, 3rd ed., 1975, p. 27.
- 48 A. M. Katti and G. Guiochon, *J. Chromatogr.*, 499 (1990) 21.
- 49 B. Lin and G. Guiochon, *Sep. Sci. Technol.*, 24 (1989) 31.
- 50 B. Lin, Z. Ma and G. Guiochon, *J. Chromatogr.*, 484 (1989) 83.
- 51 P. Rouchon, M. Schonauer, P. Valentin and G. Guiochon, *Sep. Sci.*, 22 (1987) 1793.
- 52 J. L. Wade and P. W. Carr, paper presented at PREP'89, VIth International Symposium on Preparative Chromatography, Washington, DC, May 9-11, 1989.
- 53 A. C. Offord and J. Weiss, *Nature (London)*, 155 (1945) 725.
- 54 F. Helfferich and G. Klein, *Multi-Component Chromatography. Theory of Interferences*, Marcel Dekker, New York, 1970.
- 55 G. Guiochon and S. Ghodbane, *J. Phys. Chem.*, 92 (1988) 3682.
- 56 S. Golshan-Shirazi and G. Guiochon, *Anal. Chem.*, 61 (1989) 1276.
- 57 S. Golshan-Shirazi and G. Guiochon, *Anal. Chem.*, 61 (1989) 1368.
- 58 V. G. Romanov, *Inverse Problems of Mathematical Physics*, VNU Science Press, Utrecht, 1987.

CHROMSYMP. 1771

Hydrodynamic chromatography of macromolecules on small spherical non-porous silica particles

G. STEGEMAN, R. OOSTERVINK, J. C. KRAAK* and H. POPPE

Laboratory for Analytical Chemistry, University of Amsterdam, Nieuwe Achtergracht 166, 1018 WV Amsterdam (The Netherlands)

and

K. K. UNGER

Institut für Anorganische und Analytische Chemie, Johannes Gutenberg Universität, Joh. Joachim Bercher-Weg 24, D-6500 Mainz (F.R.G.)

SUMMARY

Non-porous silica spheres with sizes in the range 1.4–2.7 μm were applied as packings for the hydrodynamic chromatography (HDC) of macromolecules. Highly efficient columns, with a reduced plate height below 2, were packed with these small particles. Up to molecular weights of 10^6 the elution behaviour of polystyrenes agreed very well with existing theoretical models. However, for larger polystyrenes the flow-rate exerted an influence on the relative peak positions. The applicability of HDC to rapid separations of soluble macromolecules and inorganic colloids was demonstrated.

INTRODUCTION

In hydrodynamic chromatography (HDC), soluble macromolecules or particles are separated on basis of their size. In a non-uniform flow profile such as occurs in a packed bed or an open capillary, large molecules are excluded from the low-velocity flow regions near the wall. As a result, large molecules experience a larger mean velocity than smaller molecules which can approach the wall more closely¹⁻⁷. Significant differences in migration rate occur only when the ratio of the solute radius to that of the flow channels (the aspect ratio), is larger than 0.01. However, when this ratio exceeds 0.3, solutes cannot migrate through the column. In practice, it appears that the working range is between the retention time for the low-molecular-weight marker, t_0 , and $0.75t_0$ for the molecules or colloids with the largest accessible size. This means that the peak capacity is dependent solely on the magnitude of peak broadening.

In the early days, HDC was performed in columns packed with non-porous particles larger than 20 μm (ref. 3), which limited its application to very large solutes. Further extension of HDC to smaller solutes was thwarted by the lack of smaller

non-porous packing particles. As open tubes were available with a wide range of diameters, capillary HDC became attractive. Open capillaries offer the additional advantages that the flow channels are well defined and good permeability allows the use of long columns. Some applications of capillary HDC for the analysis of particles with sizes in the micrometre range have been reported^{5,6}.

An interesting area of HDC is in the size range 0.001–1 μm , which includes polymers with molecular weights up to $2 \cdot 10^7$. This size range is still difficult to cover with size-exclusion chromatography (SEC). To apply capillary HDC to this group of polymers, the flow channels have to be about 1 μm or smaller to obtain a sufficiently large aspect ratio. Tijssen *et al.*⁸ managed to apply fused-silica microcapillaries with diameters down to 1 μm to the HDC of polystyrenes. However, the practical application of open tubes with such small diameters is still limited, because of the extreme requirements placed on the magnitude of the external peak broadening by injection and detection. Tijssen *et al.*⁸ solved this problem to some extent by extreme miniaturization of the injection and detection systems. However, as a result, relatively high sample concentrations had to be injected to detect the samples, which may seriously affect the migration rate of the solutes. In addition, capillary HDC does not have any (micro)preparative prospects.

Recently, non-porous spherical silica particles down to 1 μm in size became available⁹. Columns packed with these particles provide flow channels that are even smaller than those reported in capillary HDC. For example, in a column packed with 1.5- μm particles, the interstitial channels are about 0.6 μm in diameter. Still, the void volume of a packed column can be so large that common or slightly modified high-performance liquid chromatographic (HPLC) equipment can be used¹⁰. A disadvantage of packed-column HDC is that the geometry of the flow channels in a packed bed is less well defined than in open capillary tubes, which complicates the interpretation of chromatographic results in terms of the physical behaviour of molecules or colloids.

When packing particles of about 1 μm are used, HDC enters the molecular weight range traditionally covered by SEC. Although the ranges of application will probably never coincide, an overlapping area already exists between the current lower limit of HDC (weight-average molecular weight, M_w , 10^4) and the upper limit of SEC (M_w 10^6). In this range, HDC can be superior to SEC because of the extremely small band spreading, owing to the small size of the packing particles and to the absence of an intraparticle mass-transfer term. Moreover, SEC traces are more difficult to interpret, partly because HDC effects may also be present^{11,12}.

In this study, the applicability of 1.4–2.7- μm non-porous spherical silica particles as a packing for the HDC of soluble polymers and colloidal particles was investigated. The column performance and the elution behaviour of polystyrenes were studied. Some preliminary results on the HDC of colloidal silica particles are reported.

EXPERIMENTAL

Apparatus

The chromatographic set-up consisted of a constant-flow pump (Model 8500; Varian, Palo Alto, CA, U.S.A.), a pneumatically driven injection valve (Type 7413; Rheodyne, Berkeley, CA, U.S.A.) equipped with a 0.5- μl internal sample loop,

a variable-wavelength UV detector (Spectroflow 757; Kratos, Ramsey, NJ, U.S.A.) and a potentiometric recorder (Kompensograph 3; Siemens, Karlsruhe, F.R.G.). The detection cell of the UV detector was adapted by replacement of the original flow cell by a 100- μm I.D. fused-silica capillary, the protective polyimide layer of which was burned off. The amount of light that was transmitted through the quartz tube wall but did not pass through the liquid stream was minimized by means of an adjustable slit¹³. The fused-silica capillary, which had a length of about 12 cm, was coupled directly to the column outlet. The wavelength setting was 210 nm for polystyrene detection and 200 nm for colloids. Between the sample introduction part and the injection valve a precolumn filter unit was installed, containing a 0.5- μm filtering frit (Upchurch Scientific, Oak Harbor, WA, U.S.A.). Columns were made of 316 stainless steel and had dimensions of 150–250 \times 4.6 mm I.D. Column end-fittings were installed with removable frits with 0.5- μm pores (VICI, Houston, TX, U.S.A.). A dual-stage electron microscope (Model DS 130; ISI, Tokyo, Japan) was used for the determination of the packing particle size.

Materials

Analytical-reagent grade tetrahydrofuran (THF), methanol and carbon tetrachloride (Merck, Darmstadt, F.R.G.) were used without further purification. Water was deionized through a PSC filter assembly (Barnstead, Boston, MA, U.S.A.). Prior to use, the eluents were filtered by vacuum suction over a 0.5- μm filter (Type FH and VHLP; Millipore, Bedford, MA, U.S.A.).

Polystyrene (PS) standards with weight-average molecular weight (M_w) 0.5–2750 kilodalton and stated polydispersities ranging from 1.04 to 1.18 were obtained from Merck. Polystyrenes with M_w of 300–20 150 kilodalton and stated polydispersities from 1.03 to 1.30, were purchased from Macherey-Nagel (Düren, F.R.G.). The fumed silica nanospheres were obtained from Cabot (Tuscola, IL, U.S.A.).

Column preparation

The columns were packed by means of the slurry-packing technique, using methanol as both a slurry liquid and a driving liquid. A slurry was prepared by common ultrasonification of 10% (w/w) of the packing particles in methanol. Agglomerates of particles were removed by sedimentation. Prior to packing, the ultrasonic treatment was performed once more for 20 min to obtain a homogeneous suspension. During packing, a constant flow-rate of about 3 ml/min was maintained by smoothly increasing the pressure up to a final value of 700–900 bar, depending on the particle diameter and the column length. At the final pressure, the column was flushed with another 60 ml of methanol. After the pump had been switched off, the pressure was allowed to drop to zero before the column was disconnected. Finally, the column was equilibrated with the mobile phase until a stable detector baseline was obtained.

Sample preparation

The polystyrene sample solutions were prepared by carefully adding THF to the polymer up to a concentration of 0.01–0.03% (w/w). The samples were left overnight to swell and dissolve slowly. The colloid sample was prepared by suspending 14-nm silica nanospheres, 0.5% (w/w) in the mobile phase (dilute ammonia, pH 8.9). Aggregates were removed by filtration over a 0.2- μm filter (Millipore).

Chromatography

The non-porous spherical silica packing particles were prepared according to the method described by Unger and Giesche⁹. All chromatographic experiments were carried out at room temperature ($23 \pm 2^\circ\text{C}$). The reported values are the means of at least three measurements. The polystyrenes were injected together with the marker (toluene) unless peak overlap necessitated injection of the polymer and the marker separately.

THEORY

Various theoretical models have been developed to describe the migration of solutes in HDC^{8,14-19}. Most of these models include solute-wall interactions and therefore lead to complex expressions for the migration rate. Although solute-wall interactions are of importance in HDC^{18,20,21}, we assume they are absent in our experiments on the elution behaviour of polystyrenes. On that condition, a general equation is valid for the migration rate, expressed by a relative quantity τ as function of the aspect ratio λ :

$$\tau = (1 + 2\lambda - C\lambda^2)^{-1} \quad (1)$$

where $\tau = t_p/t_m$ and $\lambda = r_i/R$, t_p and t_m are the retention times of the polymer and the low-molecular-weight marker solute, respectively, r_i is the radius of the solute molecule and R is the radius of the flow channel.

For the simplest model based on a Poiseuille flow profile, the value of C would be 1. For secondary effects such as rotation, C departs from 1 and ranges between 1 and 5.3 in the different models, depending on the type of solute, *e.g.*, permeable or hard-sphere polymers⁸.

In contrast to capillary HDC, the geometry of the flow channel in a packed bed is not well defined, which makes it difficult to express λ . In order to apply the various models to packed beds, the hydraulic radius R_0 is often used. This is the radius of a capillary having the same surface-to-volume ratio as the packed bed under study. For spherical particles, the value of R_0 can be calculated from the particle size, d_p , and the bed porosity ε , according to²²

$$R_0 = \frac{d_p}{3} \cdot \frac{\varepsilon}{1 - \varepsilon} \quad (2)$$

In a packed bed the radius of the flow channel R is then replaced by R_0 .

By using eqn. 1, an expression can be derived for the resolution R_s between two solutes i and j eluting close together¹⁰:

$$R_s = \frac{t_j - t_i}{\sigma_i} = (\alpha - 1)(1 - C\lambda)\lambda\tau\sqrt{N} \quad (3)$$

where σ_i is the standard deviation of peak i , α is the ratio of the radii of solutes i and j , where $r_i > r_j$, and N is the number of theoretical plates.

RESULTS AND DISCUSSION

The main characteristics of the investigated columns are summarized in Table I. In all experiments the porosities ε of the columns were calculated from the void volume as determined by weighing the columns filled with pure solvents of different densities. The porosities calculated in this way agreed very well with those calculated from the retention times of the marker and the flow-rate settings.

The flow resistance parameters ϕ for the HDC columns in Table I are about half those usually obtained for porous particles. This results from the fact that ϕ is calculated from the migration velocity of a non-sorbed solute rather than from the velocity in interparticle space. With porous particles these two velocities differ by a factor of about 2, whereas in our case they are the same. Consequently, pressure limitations in HDC on non-porous particles are not as severe as in HPLC on porous particles.

Column efficiency

When using 1–3- μm non-porous particles in HDC, plate heights of a few micrometres can be expected¹⁰. To conserve the high column efficiency in the chromatographic system, severe demands are placed on the magnitude of the external peak broadening. For instance, the volume standard deviation σ_v for the marker solute on a 150 \times 4.6 mm I.D. column filled with 1- μm particles and having a reduced plate height of 2 would be 3.5 μl . The external contributions to zone dispersion, $\sigma_{v,\text{ext}}$, should then not exceed 1.7 μl . In our case, $\sigma_{v,\text{ext}}$ could be minimized by using both a small injection and detection cell volume and small-diameter connecting tubes. The total external contribution was measured after connecting the injection valve directly to the detector by means of a zero-dead-volume union. In the flow-rate range from 2.7 to 17 $\mu\text{l/s}$ (corresponding to a linear velocity range of 0.4–2.6 mm/s for the columns used), $\sigma_{v,\text{ext}}$ was between 0.7 and 1.3 μl . It was therefore concluded that the measured plate height would hardly be affected by extra-column band broadening.

As phase distributions are absent in HDC, existing plate-height theories^{2,3–2,5} predict that dispersion is determined exclusively by longitudinal molecular diffusion and convective mixing. At high linear velocities, molecular diffusion has a negligible influence on the overall dispersion, and a constant plate height is predicted, irrespective of the value of the molecular diffusion coefficient. The dispersion due to longitudinal molecular diffusion occurring at small linear velocities depends on the

TABLE I
COLUMN CHARACTERISTICS

Column	L (mm)	d_p (μm) ^a	ε	R_0 (μm) ^b	ϕ ^c
A	150	1.40	0.380	0.286	447
B	250	1.91	0.395	0.416	509
C	150	2.67	0.385	0.561	417

^a SEM measurements.

^b According to eqn. 2.

^c According to $\phi = Pd_p^2/(\langle v \rangle \eta L)$.

molecular weight of the polymer. Consequently, the higher the molecular weight, the smaller will be the linear velocity at which the minimum in the plate height curve is reached.

Fig. 1 shows the plate heights obtained for three solutes of different molecular weights and two particle sizes. It can be seen that the minimum of the plate height curve shifts to lower velocities for larger polymers. It appears that extremely efficient columns can be prepared with the non-porous particles used. For column C (Fig. 1a), minimum plate heights of $3.6 \mu\text{m}$ for toluene and PS 2.2 kilodalton and $3.8 \mu\text{m}$ for 336 kilodalton were found. This corresponds to a minimum reduced plate height of 1.3–1.4. The optimum plate number was thus 42 000 for the 150-mm column. Measured plate heights for column A (Fig. 1b) were even lower, in accordance with theory. The minimum value of $2.2 \mu\text{m}$ for PS 2.2 kilodalton ($N = 68\ 000$) provides a reduced plate height of 1.6, while the minimum for toluene had not been reached at the highest accessible velocity. In contrast to theoretical prediction, the curves for PS 336 kilodalton at high linear velocities do not coincide with those obtained with PS 2.2

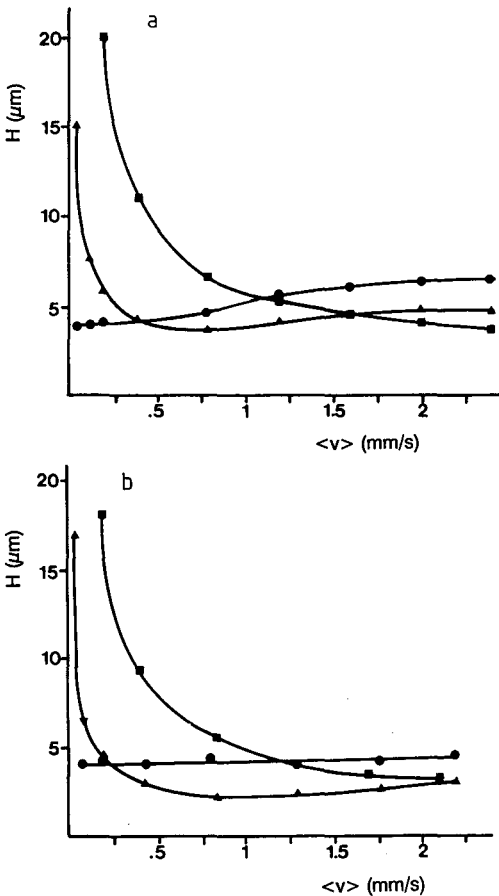


Fig. 1. Plate height, H , versus linear velocity, $\langle v \rangle$, of some standards on (a) column C and (b) column A. Solutes: \bullet , = PS 336 kilodalton; \blacktriangle = PS 2.2 kilodalton; \blacksquare = toluene.

kilodalton and toluene. The curves are almost flat and show a larger plate height value than expected. This deviation may be attributed to the polydispersity of the sample.

Knox and McLennan²⁶ investigated the effect of the polydispersity of polymer standards in SEC. They found that broadening due to polydispersity could be substantial, especially for polymers eluting in the linear part of the calibration graph. They stated that the true plate height can be calculated from the measured plate height, the polydispersity of the sample and the slope of the calibration graph. When, for example, this approach is applied to the plate height of PS 336 kilodalton on column A, using the manufacturer's data on polydispersity ($M_w/M_n = 1.03$, where M_n is the number-average molecular weight), surprisingly the corrected plate height is negative. Assuming now that the observed plate height is determined solely by the polydispersity of the sample (*i.e.*, the column has zero plate height), the upper limit of polydispersity can be calculated. The value thus obtained ($M_w/M_n < 1.01$) is considerably lower than that given by the manufacturer. At present we are not able to decide whether indeed our polymer samples are much more monodisperse, or whether on the contrary there is some experimental artefact or physical phenomenon that leads to the remarkably sharp peaks that we observed.

Elution behaviour of polystyrenes

An estimate of the radius of the dissolved polymer is needed for the application of eqn. 1. For random coil polymers several expressions exist based on the radius of gyration or the hydrodynamic radius. These expressions can be summarized by the general relationship

$$r_i = aM_w^b \quad (4)$$

Tijssen *et al.*⁸ made a strong case for the use of the so-called effective polymer radius^{27,28}, equal to 0.886 times the radius of gyration, and we followed their proposal. Substitution of the effective polystyrene radius in THF and the hydraulic radius of the packed bed (eqn. 2) in the definition of λ leads to

$$\lambda = \frac{1.23 \cdot 10^{-5} \cdot M_w^{0.588}}{R_0} \quad (5)$$

To predict the migration rate of the polymers theoretically, the parameter C in eqn. 1 remains to be established. Therefore, two theoretical models yielding different C values are discussed. In the first model, after DiMarzio and Guttman^{1,2} (DG model), the hydrodynamic behaviour is described for free-draining permeable, rotating spheres in a parabolic flow field. The DG model yields a C value of 2.70. The second model, according to Brenner and Gaydos²⁹ (BG model), is more refined and leads to $C = 4.89$. Tijssen *et al.*⁸ modified the BG model for free-draining permeable spheres and obtained $C = 5.26$. In the discussion of experimental results the two values for C , *i.e.*, 2.70 and 5.26, are used as reference points. Differences between the two migration models appear only at higher aspect ratios ($\lambda > 0.03$). Therefore, to decide which model best fits to the packed columns used in this study, it is essential to include the τ values of high-molecular-weight polymers.

Fig. 2 shows the elution of various polystyrenes on three columns filled with differently sized packing particles. Dashed lines in these figures are drawn for $C = 3.7$. The value of C does not matter too much (see Figs. 3 and 4) for the high- τ end of the figure, which will be discussed first. The drawn lines were obtained by using eqn. 1, calculating the aspect ratio with eqn. 5 and using a d_p from scanning electron microscopic (SEM) measurements. Therefore, no adjustable parameters are necessary for calibration in this part of the figure. The parameter λ , and its relation to τ , appear to be so well established that the elution can be predicted strikingly well. We may therefore conclude that the packed bed can indeed be represented in terms of an equivalent capillary model. In addition, the results indicate that the expression for the polymer radius leads to the correct description of hydrodynamic behaviour in packed beds, similarly to that observed by Tijssen *et al.*⁸ for open capillaries.

The C value of 3.7 was chosen because it was found previously¹⁰ with 2.1- μm particles to give the best fit of the experimental results. However, although the 1.4- μm data do coincide with the line for $C = 3.7$, the data for $d_p = 1.9$ and 2.7 μm deviate significantly for large molecular weights. Polymers with molecular weights larger than about $2 \cdot 10^6$ all eluted later than predicted by theory. In addition, a minimum τ value seemed to exist for columns B and C at which all polymers with molecular weights $> 2 \cdot 10^6$ coeluted. We checked whether this could be a retardation effect caused by the small frit pores. However, replacement of the 0.5- μm frit in column C by a 2.0- μm frit had no significant effect on the elution time of the large polymers. Changing the linear velocity of the eluent, on the other hand, proved to affect the elution behaviour significantly. This effect was studied in more detail for columns A and B.

The results of measurements on the flow-dependent elution behaviour are given in Table II. As can be seen, no significant velocity effect on τ is observed for $M_w < 1000$ kilodalton in the investigated velocity range. This result is in accordance with previous

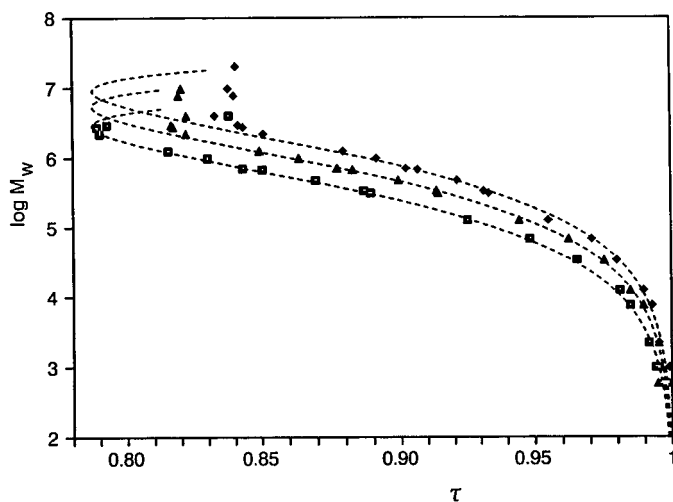


Fig. 2. Elution behaviour of PS in THF for different packing diameters: \square = 1.40 μm , column A; \blacktriangle = 1.91 μm , column B; \blacklozenge = 2.69 μm , column C. Linear velocity $\langle v \rangle \approx 0.87$ mm/s. Theoretical curves according to eqn. 1 where $C = 3.7$.

TABLE II

DEPENDENCE OF τ OF SOME HIGH- M_w POLYSTYRENES ON THE LINEAR VELOCITY $\langle v \rangle$ ON COLUMNS A AND B

Column	$M_w \cdot 10^6$	$\langle v \rangle$ (mm/s)		
		0.87	0.43	0.21
A	0.68	0.8504	0.8506	0.8503
	1.26	0.8152	0.8110	0.8107
	2.20	0.7900	0.7737	0.7722
	2.95	0.7927	0.7674	0.7583
	4.00	0.8379	0.7668	0.7436
B	0.68	0.8827	0.8827	0.8829
	1.26	0.8494	0.8452	0.8440
	2.20	0.8218	0.8105	0.8089
	2.95	0.8164	0.7993	0.7907
	4.00	0.8220	0.7872	0.7743
	9.80	0.8200	0.7878	0.7647

work¹⁰. However, for larger polystyrenes reduction of the flow-rate caused a decrease in τ . Simultaneously, peak broadening and peak tailing decreased in the chromatograms. The larger the polymer size, the more prominent these effects were. At lower velocities, the observed minimum τ values had declined and coelution of different polymers was diminished.

An explanation of the observed results might be given in terms of shear degradation of the polymers. It is well known that shear degradation increases with increasing polymer size and linear velocity^{30,31}, although quantitative predictions are difficult³². Degradation of polymers causes peaks to shift towards lower molecular weights whereas peak broadening and tailing increase, in accordance with our observations. Although shear degradation seems to be an acceptable explanation for the observed phenomena, alternative explanations might be considered. Giddings³³, for instance, considered that in packed columns retardation effects might occur for large polymers owing to collisions against the wall and trapment in crevices and apertures. These effects also depend on polymer size and flow velocity. Also, concentration^{34,35} and viscosity effects³⁶ may be of importance for these large polymers. More research has to be performed in order to explain the observed results unambiguously.

A dependence of τ on the linear velocity is not accounted for in the theoretical models. When we assume that interfering effects occur only at high velocities, we should compare the theoretical models with our low-velocity measurements. In Figs. 3 and 4, the DG model, the BG model and experimental results at different linear velocities are plotted. It can be seen that the modified BG model corresponded with the experimental results only in the low-molecular-weight range. Flow reduction even worsened the agreement. On the other hand, the DG model corresponded reasonably well up to molecular weights of about 10^6 . On flow reduction the fit of the DG model improved considerably for $M_w > 1000$ kilodalton. At the lowest flow-rate setting, the DG model almost matched the whole experimental calibration graph. Only around the

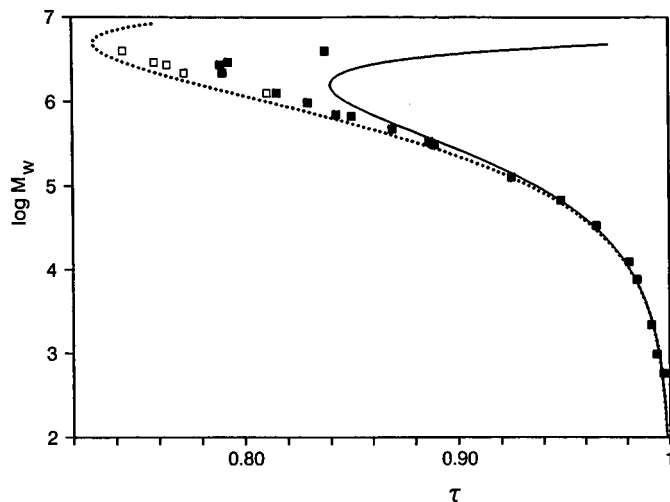


Fig. 3. Theoretical calibration graphs and experimental points for column A at different linear velocities. Theoretical: dotted line, DG model; solid line, BG model. Experimental: (■) $\langle v \rangle = 0.87$ mm/s; (□) $\langle v \rangle = 0.21$ mm/s.

backward turn of the calibration graph did the theoretical line differ from the experimental points. Whether the lowest τ values predicted by the DG model will finally be reached at even lower linear velocities is still to be determined. More research, preferably with the use of smaller packing materials, should be performed.

Both theoretical models assume infinite dilution of the polymer sample. At high solute concentrations, elution of high-molecular-weight polymers may suffer from concentration and viscosity effects. The theoretical models are then no longer valid. In

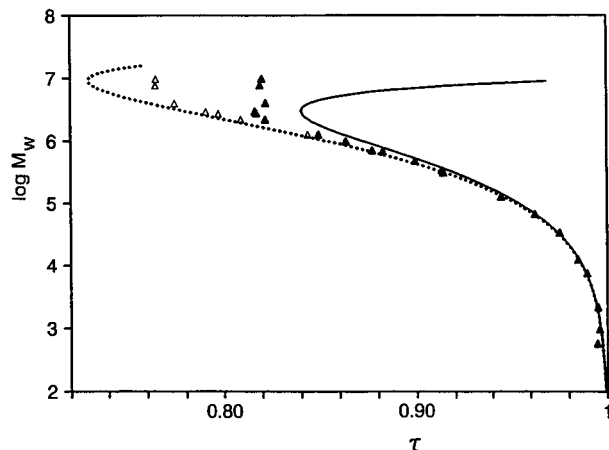


Fig. 4. Theoretical calibration graphs and experimental points for column B at different linear velocities. Theoretical: dotted line, DG model; solid line, BG model. Experimental: (▲) $\langle v \rangle = 0.87$ mm/s; (△) $\langle v \rangle = 0.21$ mm/s.

micro-capillary HDC, Tijssen *et al.*⁸ could not make an experimental distinction between the DG and BG models, because they had to use high solute concentrations (1 mg/ml) to obtain any detectable peaks. Indeed, the peaks they observed for the large polymers were triangular and elution was probably considerably affected. In our experiments, detection problems were of less importance, so more dilute samples could be used (0.1–0.3 mg/ml). We were therefore much better equipped to test the validity of the two theoretical models and the available evidence strongly indicates a preference for the DG model ($C = 2.70$).

For molecular weights up to 10^6 , the elution behaviour appeared to be independent of the flow-rate under the selected circumstances. For these samples a universal calibration graph was drawn by plotting $\log \lambda$ against τ for three columns (Fig. 5). It appears that all experimental points fall along one line with very little scatter. This illustrates that, although columns may be prepared with different-sized packing materials and with different packing pressures, hydrodynamic behaviour can be described by one universal calibration equation. The only remaining adjustable parameter in this equation is C , which at a later stage may be unequivocally determined.

Separation of polystyrene mixtures

Fig. 6 shows rapid separations of a mixture of polystyrenes on columns A (Fig. 6a) and C (Fig. 6b). Column A appears to be well suited to separate this mixture because the whole molecular weight range (τ between 0.77 and 1) is covered. On column C, R_0 is larger, resulting in smaller aspect ratios and higher τ values for all components of the polymer sample. The peaks therefore elute closer together and the resolution deteriorates (τ between 0.83 and 1).

From eqn. 3, it is clear that the resolution improves with higher plate numbers. Only for this reason may the smallest peak widths be expected for separations on

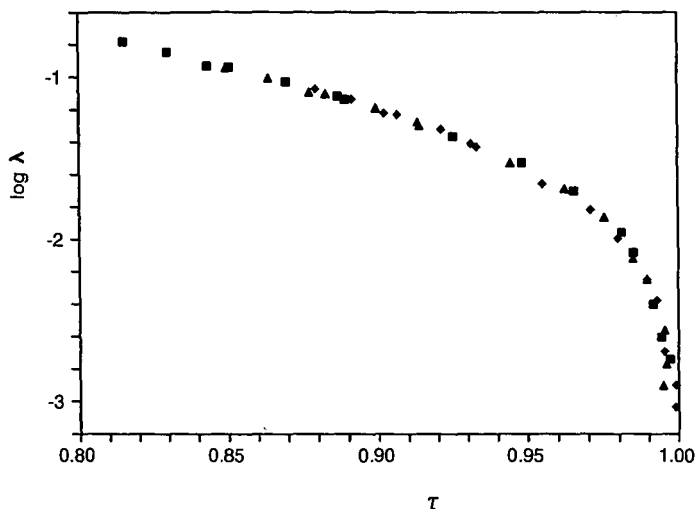


Fig. 5. Universal HDC calibration graph for polystyrenes: ■ = column A; ▲ = column B; ◆ = column C. Linear velocity range: 0.21–0.87 mm/s.

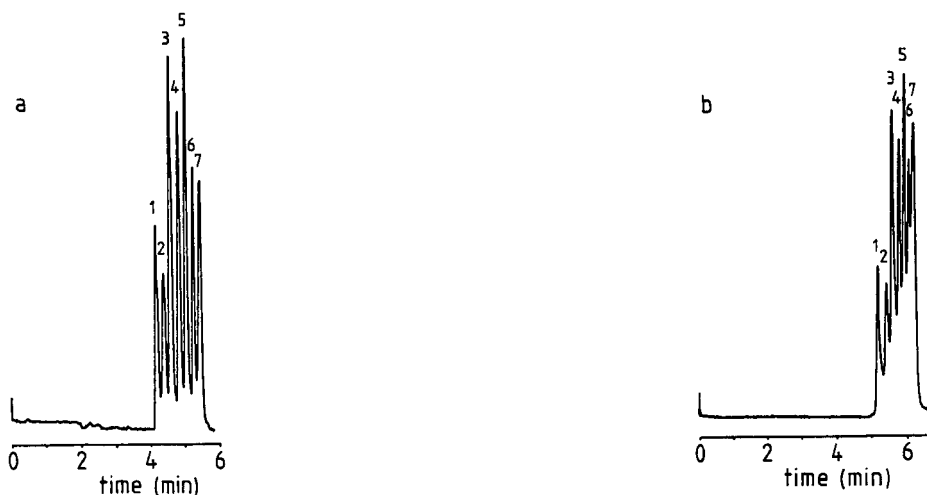


Fig. 6. HDC separation of PS standards on (a) column A and (b) column C. Sample containing: (1) 2750-; (2) 1260-; (3) 700-; (4) 310-; (5) 127-; (6) 34.5-kilodalton PS; and (7) toluene.

column A. From a previous paragraph, however, it can be concluded that this effect is largely obviated by the polydispersity of the polymer samples. To visualize the effect of polydispersity, the chromatogram shown in Fig. 6a was computer simulated (Fig. 7). Again, a zero plate height for the column was assumed and polydispersity data from the manufacturer were used. The polydispersity of toluene was artificially chosen to be 2 in order to obtain a non-zero peak width. The largest PS from the sample (2750 kilodalton) was not included in the calculations because simulating peaks that have minimum τ value (this is at the backward turn of the calibration graph) is more complicated. The theoretical calibration graph, used for simulation, was best fitted to the experimental points for $C=3.3$ at the current linear velocity.

Comparing Fig. 7 with Fig. 6a for low molecular weights reveals that in this range the contribution of polydispersity to the total band broadening is small; the experimental resolution is smaller than that predicted from the polydispersity alone. However, with increasing polymer size, the polydispersity seems more and more responsible for the observed peak widths. Surprisingly, for the highest molecular weights, the experimental resolution is even better than that in the simulated chromatogram. This again shows that the polymer fractions may be of a narrower molecular weight distribution than was suggested by the stated polydispersity data.

HDC of colloids

Some preliminary experiments were carried out to investigate the applicability of HDC to the separation of colloidal silica particles in the size range 1–100 nm. Separations in this size range have already been performed successfully by means of SEC. However, the separation efficiency in SEC for these colloids is poor because of the extremely slow mass transfer between the mobile phase and stagnant phase owing to the very small diffusion coefficients. In HDC on non-porous particles the stagnant phase is absent and a higher efficiency can be expected, provided that adsorption of the

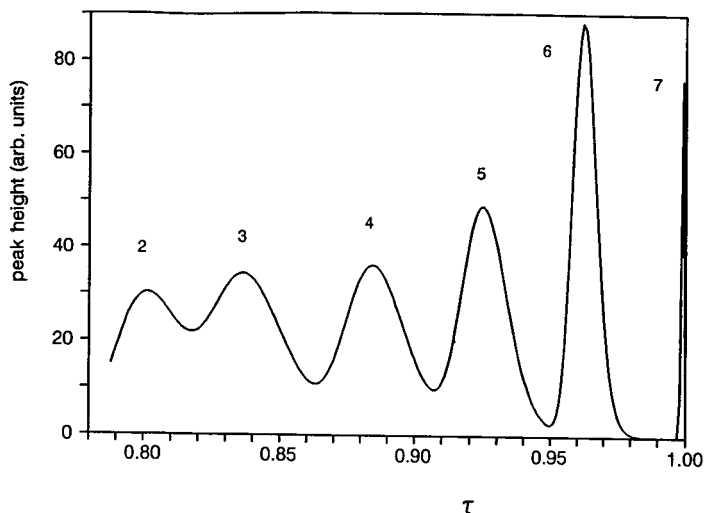


Fig. 7. Simulated chromatogram of PS on column A using eqn. 1 where $C = 3.3$. Same sample as in Fig. 6 except no 2750-kilodalton PS. Polydispersity, M_w/M_n : (2) 1.06; (3) 1.08; (4) 1.05; (5) 1.05; (6) 1.05; (7) 2.0.

colloids can be avoided. Kirkland³⁷ showed that particle-wall interactions can be kept small when the silica surface and colloidal particles repel each other. This occurs when the pH of the mobile phase is larger than 8. Under these conditions, both the surface of the packing and that of the colloidal particle bear negative charges. These repulsion effects are largest when a thick electrical double layer is present, so a low ionic strength of the mobile phase should preferably be used. Therefore, in our HDC system the aqueous phase contained about 10^{-4} M ammonia to adjust the pH to 8.9. No dissolution of the silica packing was observed during several weeks of operation.

To detect the colloidal particles by turbidity measurement (at a wavelength of 200 nm), replacement of the fused-silica detection tube by a micro-cell with a volume of $2.3 \mu\text{l}$ was required. This larger detection volume decreased the efficiency of the column by a factor of about two. Fig. 8 shows the HDC of a 14-nm nanosphere and the marker (acetone) on column A. Although the column efficiency is worse with the larger detection cell, the efficiency for both solutes is still very good (plate height *ca.* $10 \mu\text{m}$) and is much better than that obtained with SEC.

The τ value of the nanosphere is 0.83, which is significantly smaller than expected on the basis of the aspect ratio. This behaviour must be attributed to the thickness of the double layer existing on both the surface of the packing and the colloid. The presence of the double layer, whose thickness depends on the ionic strength of the mobile phase, narrows the flow channels and enlarges the radius of the colloid, so the aspect ratio increases. The influence of the double layer may have an especially large influence on the aspect ratio when extremely narrow flow channels, such as those in this study, are used. Changing the ionic strength is thus a means of manipulating the retention of colloids in HDC. This aspect is now under investigation.

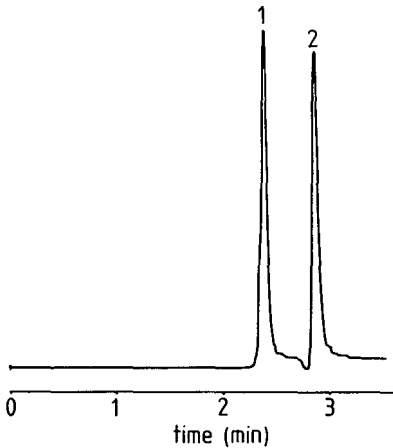


Fig. 8. HDC separation of colloidal silica particles on column A. Eluent: 10^{-4} M ammonia (pH 8.9). Sample: 1 = colloidal silica particles 14 nm; 2 = acetone (marker). $\tau_1 = 0.83$.

CONCLUSIONS

(1) Spherical non-porous particles of 1.4–2.7 μm can be efficiently packed in 150–250 \times 4.6 mm I.D. columns for HDC.

(2) Reduced plate heights below 2 can be realized when the external band spreading is kept at a level of 1 μl .

(3) Non-porous packings of 1.4–2.7 μm are suitable for the size analysis of polystyrenes by HDC in the molecular weight range 10^4 – 10^7 .

(4) The migration behaviour of polystyrenes up to M_w 10^6 agrees well with the theoretical model described by DiMarzio and Guttman^{1,2} for the investigated particle sizes.

(5) For polystyrenes with $M_w > 10^6$ the relative migration (τ) is flow dependent and indicates the occurrence of shear degradation.

(6) The application of packed-bed HDC to the analysis of inorganic colloids looks promising.

(7) The high resolving power and the large volume scale of packed-column HDC indicate that the micro-preparative use of this technique is very promising.

(8) It is worth investigating the reduction of the size of the packing particles, the influence of the nature of the solvent and the type of polymer on the elution behaviour in HDC and the applicability of HDC on small spherical porous particles in order to extend the calibration of SEC with HDC.

REFERENCES

- 1 E. A. DiMarzio and C. M. Guttman, *J. Polym. Sci.*, 7 (1969) 267.
- 2 E. A. DiMarzio and C. M. Guttman, *Macromolecules*, 3 (1970) 131, 681.
- 3 H. Small, *J. Colloid Interface Sci.*, 48 (1974) 147.
- 4 K. O. Pedersen, *Arch. Biochem. Biophys.*, *Suppl.*, 1 (1962) 157.
- 5 A. W. J. Brough, D. E. Hillman and R. W. Perry, *J. Chromatogr.*, 208 (1981) 175.

- 6 R. J. Noel, K. Gooding, F. E. Regnier, D. M. Ball, C. Orr and H. E. Mullins, *J. Chromatogr.*, 166 (1978) 373.
- 7 A. J. McHugh, *CRC Crit. Rev. Anal. Chem.*, 15 (1984) 63.
- 8 R. Tijssen, J. Bos and M. E. van Kreveland, *Anal. Chem.*, 58 (1986) 3036.
- 9 K. K. Unger and H. Giesche, *Ger. Pat.*, DE-3534 143.2 (1985).
- 10 J. C. Kraak, R. Oostervink, H. Poppe, U. Esser and K. K. Unger, *Chromatographia*, 27 (1989) 585.
- 11 S. Mori, R. S. Porter and J. F. Johnson, *Anal. Chem.*, 46 (1974) 1599.
- 12 M. G. Styring, C. J. Davidson, C. Price and C. Booth, *J. Chem. Soc., Faraday Trans. 1*, 80 (1984) 3051.
- 13 R. Tijssen, J. P. A. Bleumer and M. E. van Kreveland, *J. Chromatogr.*, 260 (1983) 297.
- 14 R. F. Stoitsits, G. W. Poehlein and J. W. Vanderhoff, *J. Colloid Interface Sci.*, 4 (1976) 549.
- 15 A. J. McHugh, C. A. Silebi, G. W. Poehlein and J. W. Vanderhoff, *J. Colloid Interface Sci.*, 4 (1976) 549.
- 16 C. A. Silebi and A. J. McHugh, *AIChE J.*, 24 (2) (1978) 204.
- 17 D. J. Nagy, C. A. Silebi and A. J. McHugh, *J. Colloid Interface Sci.*, 79 (1981) 264.
- 18 D. C. Prieve and P. M. Hoysan, *J. Colloid Interface Sci.*, 64 (1978) 201.
- 19 B. A. Buffham, *J. Colloid Interface Sci.*, 67 (1978) 154.
- 20 M. Leitzement, K. Larson and J. Dodds, *Analisis*, 12 (1984) 260.
- 21 H. Small, F. L. Saunders and J. Solc, *Adv. Colloid Interface Sci.*, 6 (1976) 237.
- 22 R. B. Bird, W. E. Stewart and E. N. Lightfoot, *Transport Phenomena*, Wiley, New York, 1960, p. 197.
- 23 J. C. Giddings, *J. Chromatogr.*, 5 (1961) 61.
- 24 J. F. K. Huber, *J. Chromatogr. Sci.*, 7 (1969) 85.
- 25 Cs. Horváth and H. Lin, *J. Chromatogr.*, 126 (1976) 401.
- 26 J. H. Knox and F. McLennan, *Chromatographia*, 10 (1977) 75.
- 27 M. E. van Kreveland and N. J. van den Hoed, *J. Chromatogr.*, 83 (1973) 111.
- 28 M. E. van Kreveland, *J. Polym. Sci., Polym. Phys. Ed.*, 13 (1975) 2253.
- 29 H. Brenner and L. J. Gaydos, *J. Colloid Interface Sci.*, 58 (1977) 312.
- 30 A. M. Basedow, K. H. Ebert and H. Hunger, *Macromol. Chem.*, 180 (1979) 411.
- 31 H. G. Müller and J. Klein, *Macromol. Chem.*, 182 (1982) 513.
- 32 J. C. Giddings, *Adv. Chromatogr.*, 20 (1982) 217.
- 33 J. C. Giddings, *Sep. Sci.*, 13 (1978) 241.
- 34 A. Rudin, *J. Polym. Sci. Part A-1*, 9 (1971) 2587.
- 35 M. Fixman and J. M. Peterson, *J. Am. Chem. Soc.*, 86 (1964) 3521.
- 36 J. C. Moore, *Sep. Sci.*, 5 (1970) 723.
- 37 J. J. Kirkland, *J. Chromatogr.*, 185 (1979) 273.

CHROMSYMP. 1703

Comparison of stationary phases for packed-column supercritical fluid chromatography

PETER J. SCHOENMAKERS*, LOUIS G. M. UUNK and HANS-GERD JANSSEN
Philips Research Laboratories, P.O. Box 80000, 5600 JA Eindhoven (The Netherlands)

SUMMARY

A study of the applicability of different stationary phases for packed-column supercritical fluid chromatography is described. The compatibility of these phases with carbon dioxide and with a number of test solutes was established qualitatively from the observed peak shapes. Retention and selectivity differences between the different columns were studied quantitatively. The stationary phases studied include chemically modified silicas, polysiloxane-coated silicas, modified and unmodified porous graphitic carbon and modified and unmodified poly(styrene-divinylbenzene) copolymers. It is concluded that differences in selectivity between different stationary phases are often due to interactions between the solute molecules and active sites on the surface. Such interactions lead to poor peak shapes and are therefore undesirable. For most of the solutes studied, with the notable exception of polyaromatics, a poly(ethylene glycol)-coated carbon phase provided the best results. Owing to the very high retentivity of unmodified carbon, this phase turned out to be very stable. The coating of different types of polymers on solid surfaces may be used to create stationary phases without residual active adsorption sites, but with considerable differences in selectivity.

INTRODUCTION

Carbon dioxide is the preferred solvent for supercritical-fluid chromatography (SFC)¹. It has a number of great advantages, including its favourable critical properties ($T_c \approx 31^\circ\text{C}$; $P_c \approx 73$ bar), favourable safety and toxicity characteristics, availability in sufficient purity at low cost and compatibility with a variety of chromatographic detectors. Unfortunately, carbon dioxide is essentially a non-polar solvent². Non-polar solutes, such as hydrocarbons, can be eluted as sharp, symmetrical peaks from many different stationary phases. Polar solutes, however, are often eluted as broad, asymmetric peaks, or are not eluted at all³⁻⁵. To improve this situation, more polar mobile phases can be used. Among the possible pure solvents, ammonia is the only realistic choice². Although ammonia has been used occasionally in SFC⁶, its routine application is likely to involve major problems. Therefore, it is

almost inevitable to use mixtures when polar mobile phases are required. The common practice is to add a small amount ($\leq 20\%$) of a polar organic solvent (a "modifier") to a non-polar mobile phase such as carbon dioxide. Although the critical temperatures of such mixtures will be higher than that of pure carbon dioxide, the values will be well within practical reach and far below the values for the pure polar solvents. Therefore, these mixtures can be used at supercritical (or near-critical) conditions, resulting in lower viscosities and higher diffusion coefficients as compared with liquids.

The addition of organic modifiers to the mobile phase will affect retention in SFC in three different ways^{7,8}: by increasing the mobile phase polarity, by increasing the mobile phase density (at constant temperature and pressure) and by deactivation of active sites on the surface. The last factor is thought to be the most important in packed-column SFC. In contrast to the first two factors, it may cause the peak shape to improve dramatically on addition of very small amounts ($< 1\%$) of modifiers, because active sites on the surface have been held responsible for causing a detrimental mixed retention mechanism in packed-column SFC⁹.

In open-tubular (capillary) SFC, the third effect of adding modifiers is much less significant than it is in packed-column SFC^{10,11}. As a consequence, a larger number of (classes of) solute molecules can be eluted from wall-coated open-tubular columns than from packed columns using pure carbon dioxide as the mobile phase. This indicates that an alternative way of dealing with polar solutes in SFC is to prepare homogeneous stationary phases without active adsorption sites.

There are some good reasons to try and avoid the use of modifiers. These include technical problems in accurately adding small amounts of modifier, column stability, instrument reliability and, especially, detection compatibility. Therefore, stationary phases for SFC are desirable which allow the elution of the largest possible variety of solutes as sharp, symmetrical peaks, using pure carbon dioxide as the mobile phase, and provide sufficient selectivity for a variety of separations. This second aspect of SFC stationary phases implies that a choice is needed between different phases that show substantial differences in selectivity. This situation is similar to that in gas chromatography (GC), but contrary to that in liquid chromatography (LC). In the latter technique, selectivity is usually varied by varying the nature and composition of the mobile phase, while keeping the stationary phase the same. If we try to use unmodified carbon dioxide as the mobile phase for SFC, we will need to achieve all variations in the selectivity by varying the stationary phase.

In this paper, we describe a study of a number of stationary phases, which were first evaluated qualitatively. Thereafter, five were selected for a quantitative evaluation. We selected a group of 25 test solutes, all of fairly low molecular weight, but with a range of different functional groups, to judge the applicability of the different phases to different classes of compounds.

EXPERIMENTAL

Columns

An octadecylsilane (ODS)-modified silica (Rosil C₁₈) was obtained from Alltech (Eke, Belgium). A poly(styrene-divinylbenzene) (PS-DVB) column (Rogel) was also obtained from Alltech. Two alkyl-modified PS-DVB (ACT-1) columns were obtained from Bêtron (Rotterdam, The Netherlands). Polysiloxane-coated silica columns were

obtained from Keystone Scientific (Bellefonte, PA, U.S.A.). A γ -aminopropyl-modified silica column was obtained from Chrompack (Middelburg, The Netherlands).

Totally porous graphitic carbon was provided by Professor J. H. Knox (University of Edinburgh, U.K.) and was packed into columns at the Technical University of Delft (The Netherlands). Columns packed with this material are commercially available from Shandon (Runcorn, U.K.). A column packed with porous carbon was coated *in situ* with poly(ethylene glycol) with an average molecular weight of 14 000 (Aldrich, Milwaukee, WI, U.S.A.), resulting in what we describe as a "carbonwax" column. Coating was performed by deposition from a concentrated solution in chloroform, followed by slow evaporation of the solvent. After coating, a very high pressure drop over the column was observed. On opening the column, a considerable amount of coated stationary phase (about 1 cm in length, *i.e.*, about 10% of the content of the column) was pressed out of the column ("toothpaste effect"). Remarkably, after reclosure an efficient and, under SFC conditions, very stable column remained. According to the supplier of commercial carbon materials (Shandon), the toothpaste problem could occur with "older" batches of carbon. In recent carbon packings the porosity has been reduced, so that the toothpaste problem will no longer occur.

Several additional chemically modified silicas⁹ have been evaluated previously, but none of these was thought to be sufficiently good (homogeneous) to be included in this study. All columns were 150 mm \times 4.6 mm I.D., except the carbon columns, which had a length of 100 mm. The instrumentation used for packed-column SFC has been described in detail elsewhere^{12,13}.

Quantitative study

The quantitative study was performed on ODS, Deltabond-C₁ and -C₈, Carbowax-modified carbon ("carbonwax") and γ -aminopropyl-modified silica columns. At a constant temperature of 50°C the pressure was adapted so that the capacity factor of *sec.*-butylbenzene relative to dichloromethane was approximately 0.5. In each instance, the pressure drop over the column was adjusted to about 10% of the inlet pressure. The resulting pressures are listed in Table I.

TABLE I

SUMMARY OF THE DIFFERENT COLUMNS USED IN THE QUANTITATIVE STUDY

All columns were used at 50°C. The inlet pressures listed are such that k (eqn. 1) for *sec.*-butylbenzene was *ca.* 0.5. $\bar{\rho}$ is the average density of carbon dioxide in the column, V_c is the volume of the empty column and V_{DM} is the retention volume of dichloromethane; ϵ_{DM} is the ratio of the two volumes.

Stationary phase	P_{in} (bar)	P_{out} (bar)	$\bar{\rho}$ (g/ml)	V_c (ml)	V_{DM} (ml)	ϵ_{DM}
ODS	142	128	0.654	2.49	1.76	0.71
Deltabond-C ₈	123	111	0.555	2.49	2.75	1.08
Deltabond-C ₁	117	106.5	0.515	2.49	3.07	1.22
Carbonwax	145	131.5	0.666	1.66	1.93	1.16
Amino	117	106.8	0.517	2.49	3.51	1.41

The test solutes used are listed in Table II. The first compound listed is dichloromethane (No. 1), which was used both as a solute and as the solvent for the other 25 test solutes (Nos. 2–26). Solute were obtained from various sources. All solutes were of such purity as to show only a single major peak in the chromatogram. Only solutes that could be observed with a UV detector were included.

Capacity factors were calculated assuming dichloromethane to be unretained, *i.e.*,

$$k_{i, \text{DM}} = \frac{t_i - t_{\text{DM}}}{t_{\text{DM}}} \quad (1)$$

where $k_{i, \text{DM}}$ is the capacity factor of solute i with respect to dichloromethane (DM), t_i is the retention time of the solute and t_{DM} that of dichloromethane. The consequences of using eqn. 1 will be considered below.

Retention of dichloromethane

The retention volume can be calculated by measuring the flow-rate leaving the system (*i.e.*, at a pressure of 1 bar) and by calculating the average density of the mobile phase in the column. The retention volumes of dichloromethane on the five different columns are given in Table I where they are compared with the volume of the empty column. The column porosity, ε , can be defined as

$$\varepsilon = V_0/V_c \quad (2)$$

where V_0 is the elution volume of an unretained component and V_c is the volume of the empty column. Reasonable values for ε for columns packed with porous particles are in the range 0.6–0.8. Assuming that dichloromethane is an unretained component, we can calculate the porosity from

$$\varepsilon_{\text{DM}} = V_{\text{DM}}/V_c \quad (3)$$

The values obtained for ε_{DM} are also listed in Table I. It appears from these values that dichloromethane does not behave as an unretained solute on all columns. It appears to be approximately unretained on the ODS column, but on both polysiloxane (Deltabond) columns, on the amino column and on the carbonwax column it is significantly retained. Moreover, the retention of a component such as dichloromethane is a strong function of the operating conditions. This is illustrated in Fig. 1, which shows the variation of the "true" capacity factor of dichloromethane *vs.* the column inlet pressure on an ODS column at 45°C. These "true" capacity factors were calculated using a column porosity of 0.578, which was obtained by the gravimetric method¹⁴. It is seen that a typical sigmoidal curve is obtained for retention *vs.* pressure in SFC, similar to what is observed for other solutes¹⁵. Clearly, even on the ODS column dichloromethane is *not* an unretained solute. At inlet pressures of *ca.* 150 bar or higher it is approximately unretained (at 45°C; see Table I), but at lower pressures its retention increases. The other columns all show much higher ε values (*i.e.*, relative retention volumes) than the ODS column, indicating that dichloromethane is more retained.

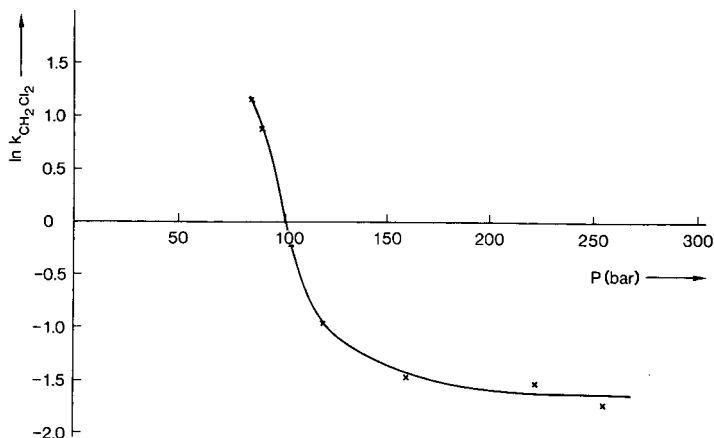


Fig. 1. Variation of the capacity factor of dichloromethane with pressure on the ODS column. Conditions: temperature, 45°C; $P_{\text{out}} = 0.9 P_{\text{in}}$.

With the unmodified carbon column, the retention is probably due to adsorption at the surface of the stationary phase. With the polysiloxane-type and poly(ethylene glycol) phases, retention is more likely to be the result of penetration of dichloromethane into the polymeric layer, where it may be retained. Both effects may play a role on PS-DVB-type columns, on which dichloromethane was also found to be significantly retained.

Despite the observation that dichloromethane is not an unretained solute, it was used as such for the present study for several reasons: it is difficult to use the gravimetric method, and for some columns, specifically the carbonwax column, it is almost impossible, because the column will change on flushing with a liquid solvent; the use of a supposedly unretained solute such as dichloromethane is a practical method for establishing a reasonable value; and provided that data on the actual retention volume of dichloromethane are available (as they are in Table I), the capacity factors presented in this paper can easily be recalculated using a different value for V_0 or ϵ by using the following equations:

$$k_i = (k_{i, \text{DM}} + 1)(V_{\text{DM}}/V_0) - 1 \quad (4)$$

or

$$k_i = (k_{i, \text{DM}} + 1)(\epsilon_{\text{DM}}/\epsilon) - 1 \quad (5)$$

The main problem is that the capacity factors reported here and in many other papers are not the real thermodynamic values, defined by

$$k = q_s/q_m \quad (6)$$

where q_s and q_m are the total amounts of solutes present in the stationary and mobile phase, respectively. In obtaining thermodynamic data from SFC experiments and, indeed, from LC experiments, considerable care must be taken to obtain correct values for V_0 .

RESULTS AND DISCUSSION

Qualitative evaluation of columns

Several of the columns were discarded from the quantitative study after an initial qualitative evaluation, in which the approximate efficiency and the peak shapes for some simple test solutes (alkylbenzenes, naphthalene and biphenyl) were considered, in addition to the column retentivity and its stability during several days or weeks of operation.

Unmodified graphitic carbon column. This column generally yielded peaks with better symmetry than, for example, the ODS column. However, this was accompanied by excessively long retention times for many solutes. For example, even at 35°C, where the densities are higher than at the temperature of 50°C used in this study, and even when the pressure was increased to 250 bar the capacity factor of *n*-butylbenzene was still above 3. Under these conditions, naphthalene could not be eluted. Because it appeared to us that the use of the unmodified carbon column in SFC would be restricted to solutes readily amenable to GC, we excluded this column from the quantitative study.

Alkyl-modified PS-DVB column. After carefully conditioning an ACT-1 column in the SFC instrument, the results were disappointing. Broad, asymmetric and even split peaks were observed. On opening the column, we found that the packed bed had collapsed and signs of flow channeling along the sides of the column were apparent even without magnification. Re-equilibration of the column with an organic solvent to allow its use in LC was not successful. Hence, the column degradation process appeared to be irreversible. A second column was purchased, installed and conditioned even more carefully, but the results were similar. Therefore, we concluded that this column packing material is not stable towards supercritical carbon dioxide, probably owing to considerable differences in the degree of swelling of the polymeric material in liquid solvents such as methanol and supercritical fluids such as carbon dioxide.

Unmodified PS-DVB column. The Rogel column showed a very high retentivity, similar to that observed with the unmodified carbon column. In both instances, the interaction with the surface appears to be stronger for aromatic solutes. After the problems we experienced with the ACT-1 columns, we also re-inspected the peak shapes obtained with the Rogel column. In the latter instance, the peaks were reasonably symmetrical, but some fronting could often be observed. Initially, we ascribed this to possible overloading of the column. Now, however, we are no longer convinced of the stability of this type of column under SFC conditions. Even though the problem is much less than it was for the ACT-1 columns, we decided not to include a PS-DVB-type column in the quantitative study.

Other columns. The remaining five columns could be used under reasonable conditions (see Table I) for a substantial portion of the test solutes and yielded reproducible retention data over longer periods of time. Therefore, these columns were included in the quantitative study.

Table II provides a summary of the peak shapes obtained for the 26 test solutes (including the solvent dichloromethane) on these five columns. In each instance pure carbon dioxide was used as the eluent. A distinction is made between sharp, symmetrical peaks (symbol +), significantly broadened and possibly asymmetrical

TABLE II

SUMMARY OF THE ELUTION CHARACTERISTICS OF VARIOUS TEST SOLUTES FROM DIFFERENT STATIONARY PHASES USING PURE CARBON DIOXIDE AS THE ELUENT

Temperature, 50°C. Pressure adapted to yield $k = 0.5$ for *sec.*-butylbenzene relative to dichloromethane. Sample concentrations, *ca.* 1 mg/ml for aromatic solutes, *ca.* 10 mg/ml for aliphatic solutes. Sample volume, 1 μ l. For identification of stationary phases see Experimental. + = Eluted as a sharp peak; ● = eluted as a broadened peak; - = eluted as a very broad, non-symmetrical peak; × = not eluted.

No.	Solute	ODS	Deltabond-C ₈	Deltabond-C ₁	Carbonwax	Amino
1	Dichloromethane	+	+	+	+	+
2	Benzene	+	+	+	+	+
3	Toluene	+	+	+	+	+
4	Ethylbenzene	+	+	+	+	+
5	<i>n</i> -Propylbenzene	+	+	+	+	+
6	<i>sec.</i> -Butylbenzene	+	+	+	+	+
7	Phenol	-	●	●	+	×
8	<i>p</i> -Nitrophenol	×	×	×	×	×
9	<i>o</i> -Nitrophenol	-	●	-	+	-
10	2,4-Dinitrophenol	×	-	×	×	×
11	Benzoic acid	×	×	×	×	×
12	Bromobenzene	+	+	+	+	+
13	Chlorobenzene	+	+	+	+	+
14	N,N-Dimethylaniline	×	×	×	+	●
15	<i>o</i> -Nitrotoluene	+	+	+	+	+
16	Benzaldehyde	-	●	●	+	×
17	Benzyl alcohol	×	×	×	+	×
18	Methyl benzoate	-	●	●	+	+
19	Nitrobenzene	+	+	+	+	+
20	Dimethyl phthalate	×	●	●	+	×
21	Naphthalene	+	+	+	●	+
22	Biphenyl	+	+	+	-	+
23	2-HEMA ^a	×	-	-	+	×
24	Diheptyl ether	+	+	+	+	+
25	2-Tridecanone	-	●	●	●	×
26	Cyclohexanone	-	-	-	● ^b	×
<i>Total score</i>						
	+	13	13	13	19	14
	●	0	6	5	3	1
	-	6	3	3	1	1
	×	7	4	5	3	10

^a 2-Hydroxyethyl methacrylate.^b Co-elutes with solvent (dichloromethane).

peaks (●) and very broad, non-symmetrical peaks (-). Components that are not eluted with a capacity factor of 30 or less are indicated by ×. The boundaries between "good", "reasonable" and "bad" peak shapes are necessarily vague. When the peak shapes are "good", the combination of the stationary phase and carbon dioxide as the mobile phase can be applied successfully for the solute concerned. This may still be the case in the "reasonable" situations, although in this instance the retentions (capacity factors) are likely to be affected by the amount of solute injected⁹. With really "bad" peak shapes or non-eluted solutes, we consider that the stationary phase cannot be

applied for these compounds with pure carbon dioxide as the mobile phase. Of course, the results in Table II represent only one set of pressure-temperature conditions for each column. However, it is our experience that the quality of the observed peaks is not a strong function of pressure and temperature. Also, because all the test solutes are of low molecular weight, very long retention times are probably the result of a particularly strong interaction.

The ODS column yields good results for 13 out of the 26 solutes, including hydrocarbons, halogenated hydrocarbons, nitro-substituted hydrocarbons and di-*n*-heptyl ether. Based on previous work³, we can add cyano-substituted hydrocarbons to this short list. The good peak shape observed for di-*n*-heptyl ether does not necessarily imply good results for other ethers. For example, in methoxy or ethoxy groups the oxygen atom may be much more accessible for interactions³. The ODS column cannot be applied to any of the other test solutes without modifying the mobile phase.

The Deltabond-C₈ and -C₁ columns yield essentially identical results in terms of peak shapes for 24 out of 26 solutes. Only for *p*-nitrophenol and 2,4-dinitrophenol does the Deltabond-C₈ column perform better. This is in contrast to the substantial improvement achieved when a silica phase is chemically reacted with long-chain silanes (such as octyl or octadecyl) compared with the use of trimethylsilyl-modified silicas⁹. Apparently, long alkyl chains connected to a polysiloxane backbone, which may shield the Si-O-Si bonds, are less beneficial than long alkyl chains connected to the silica, which may shield surface silanols.

The Deltabond columns may be used to elute some, but not all, of the phenols, esters, aldehydes and ketones. However, in all instances the observed peak shape and efficiency are substantially worse than what is achieved with, for example, hydrocarbons. In other words, there seems to be some degree of improvement relative to the ODS column, but the nature of the problem seems to remain the same. According to the supplier of the columns, the amount of stationary phase per square metre of silica surface is about three times higher than that on a typical ODS column. This would imply that only a very thin layer of polysiloxane is coated on the surface. This may cause surface silanols to play a smaller, but still significant, part in the retention mechanism. A thicker layer may result in excessively long retention times, but this problem can be avoided by starting with a parent silica with a lower specific surface area.

That a much thicker layer of a polymeric coating on a solid adsorbent is not necessarily detrimental to the column performance is demonstrated by the results obtained with the carbonwax column. The exact amount of polymer deposited on the particles is unknown, but is believed to be considerable. This column yielded very good results for 19 out of 26 solutes. Only *p*-nitrophenol, 2,4-dinitrophenol and benzoic acid could not be eluted. The polar (Carbowax) character of the stationary phase makes it useful for the elution of many polar solutes, including solutes such as *o*-nitrophenol, *N,N*-dimethylaniline, benzyl alcohol, dimethyl phthalate and 2-hydroxyethyl methacrylate, none of which could be handled successfully with any of the other columns. However, there is still evidence of the carbon character, because solutes with two aromatic rings, such as naphthalene and biphenyl, show very long retention times and asymmetric peaks, which may be indicative of a mixed retention mechanism, involving both the polymeric coating and the underlying surface. This may also be the reason for the broad peaks observed for ketones. Because the coating process has not been

optimized, the coating may not be uniform throughout the column. Therefore, it may be possible to improve the performance of this type of column.

Carbowax has been used extensively as a stationary phase in SFC, its use dating back to the early work of Sie and Rijnders¹⁶ and Rijnders¹⁷. However, the stationary phase may dissolve in the supercritical mobile phase¹⁸, leading to poor reproducibility and ageing of columns. Because of the very high retentivity of unmodified porous graphitic carbon, it may be a much better surface to retain a deposited layer of a polymeric material, without any cross-linking or chemical bonding to the surface. At least in this study, excellent stability of the carbonwax column was observed during several weeks of operation.

In our study, the γ -aminopropyl-modified silica did not perform well. Only for methyl benzoate and *N,N*-dimethylaniline did it perform better than the ODS and Deltabond columns. For all other solutes it appeared to behave similarly or worse. At first sight this seems to be in contrast with the results of Ashraf-Khorassani and Taylor⁵, who studied the applicability of a number of stationary phases for the elution of basic components and found amino-modified silicas to perform better than octadecyl-modified silicas. However, basic components were not strongly represented in our set of test solutes, so that our results do not contradict those of ref. 5. It is interesting that for the most basic solute in our test set, dimethylaniline, the carbonwax rather than the amino column yielded the best results.

Quantitative study

Table III summarizes the results of the quantitative study of the retention of our set of test compounds on the five selected columns. Values obtained from poorly shaped peaks are given in parentheses. In these cases, the capacity factor is expected to decrease with increasing amount of sample⁹ and hence the value found with one particular injection is not really meaningful. In some instances, a peak could only be observed if the sample size was increased. This was not done to enhance the detectability, but rather to reduce the retention and to sharpen the peak. When larger amounts of solutes were injected, this is indicated in the table.

There appears to be little difference in the selectivities of the stationary phases towards alkylbenzenes (methylene-group selectivity). Only for benzene do the values differ considerably, but the capacity factors are very small for this solute. As all values for benzene are larger than zero, it is (even) less suitable than dichloromethane as an "unretained" solute. The strangely high capacity factor for propylbenzene was reproducible, but could not be explained.

For biphenyl and naphthalene the carbonwax column showed large capacity factors (and poor peak shapes). The amino column also showed a relatively large retention for these solutes. For most of the other solutes, the ODS and Deltabond columns showed few differences, while the carbonwax and amino columns yielded much higher capacity factors for a number of polar solutes. These selectivity differences will be investigated in more detail in the next section.

Stationary phase selectivity

Fig. 2 shows a comparison of the capacity factors obtained on the ODS and Deltabond-C₈ columns. The logarithms of the capacity factors obtained on the different columns are plotted on the horizontal and vertical axes. If all points were to

TABLE III

CAPACITY FACTORS OF THE TEST SOLUTES ON THE FIVE DIFFERENT STATIONARY PHASES

Values obtained from distorted peaks are given in parentheses. Conditions as in Table II.

No.	Solute	ODS	Deltabond-C ₈	Deltabond-C ₁	Carbonwax	Amino
1	Dichloromethane	0 ^a	0 ^a	0 ^a	0 ^a	0 ^a
2	Benzene	0.16	0.14	0.12	0.06	0.08
3	Toluene	0.26	0.23	0.20	0.24	0.20
4	Ethylbenzene	0.32	0.32	0.30	0.34	0.30
5	<i>n</i> -Propylbenzene	0.44	0.42	0.40	0.52	0.41
6	<i>sec.</i> -Butylbenzene	0.46 ^b	0.49 ^b	0.48 ^b	0.49 ^b	0.46 ^b
7	Phenol	(3.88) ^c	(1.02)	(1.43)	6.84	—
8	<i>p</i> -Nitrophenol	—	—	—	—	—
9	<i>o</i> -Nitrophenol	(3.15) ^c	(0.70)	(0.92)	4.50	—
10	2,4-Dinitrophenol	—	(1.34)	—	—	—
11	Benzoic acid	—	—	—	—	—
12	Bromobenzene	0.56	0.52	0.49	0.94	0.57
13	Chlorobenzene	0.38	0.36	0.34	0.52	0.38
14	N,N-Dimethylaniline	(2.55) ^c	—	—	2.63	9.41
15	<i>o</i> -Nitrotoluene	0.72	0.68	0.81	3.06	4.13
16	Benzaldehyde	(2.53)	(0.74)	(0.78)	1.24	—
17	Benzyl alcohol	(19.9) ^c	—	—	2.68	—
18	Methyl benzoate	(1.85)	(0.82)	(0.83)	2.45	6.26
19	Nitrobenzene	0.71	0.62	0.78	2.46	4.46
20	Dimethyl phthalate	(7.85) ^c	(3.28)	(2.79)	6.82	—
21	Naphthalene	1.24	1.16	0.70	(9.90)	2.06
22	Biphenyl	1.59	1.58	1.40	(15.29)	3.18
23	2-HEMA ^d	—	(5.06)	(3.85) ^c	0.99	—
24	Diheptyl ether	0.82	0.78	0.71	4.33	0.58
25	2-Tridecanone	(3.17) ^c	(1.81) ^c	(1.68) ^c	(4.48) ^c	—
26	Cyclohexanone	(3.69) ^c	(1.28) ^c	(1.00)	0.08	—

^a By definition.^b Normalized value achieved by varying the pressure.^c Obtained with a 10-fold increased sample concentration.^d 2-Hydroxyethyl methacrylate.

fall on a straight line with unit slope, such as that drawn, this would indicate that there are no differences in selectivity. A straight line with a different slope indicates that the selectivity is systematically higher for all solutes on one of the phases, but that the order of elution will never change. Deviations from the straight line illustrate differences in selectivity for certain compounds and possible variations in elution order.

In Fig. 2 only four solutes, indicated by the half-black squares, deviate significantly from the straight line. For all four compounds, benzaldehyde, methyl benzoate, tridecanone and cyclohexanone, the peak shape is very bad on the ODS column. For these solutes, retention will decrease with increasing amount of sample injected, so that the points will approach the straight line. This is illustrated for two solutes in Fig. 3. The type of curves obtained in these figures has been interpreted in terms of a mixed retention mechanism⁹. In this model, the capacity factor obtained for large amounts of sample injected is thought to be due to interactions between the solute molecules and the C₁₈ chains on the surface. The rise in capacity factors observed with

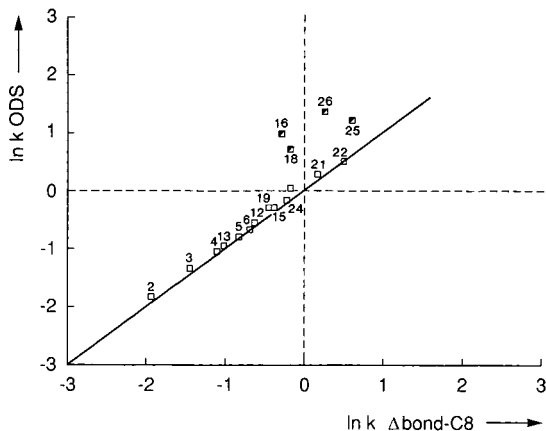


Fig. 2. Comparison of the retention of the test solutes on the ODS and Deltabond-C₈ phases (Δ bond-C₈). □ = (Reasonably) good peak shapes on both columns; ■ = bad peak shape on the column indicated on the vertical axis. For conditions see Tables I and II.

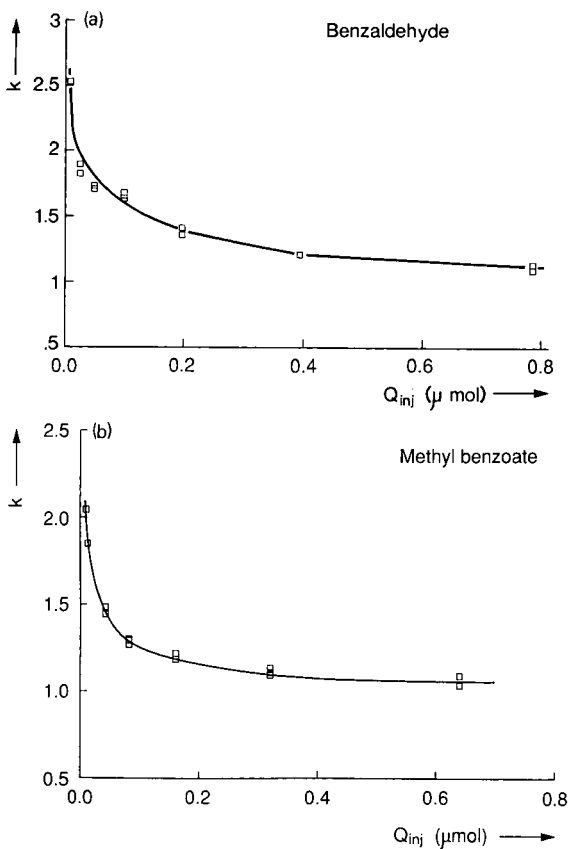


Fig. 3. Variation of the capacity factor for (a) benzaldehyde and (b) methyl benzoate on the ODS column as a function of the injected amount of solute. For conditions see Tables I and II.

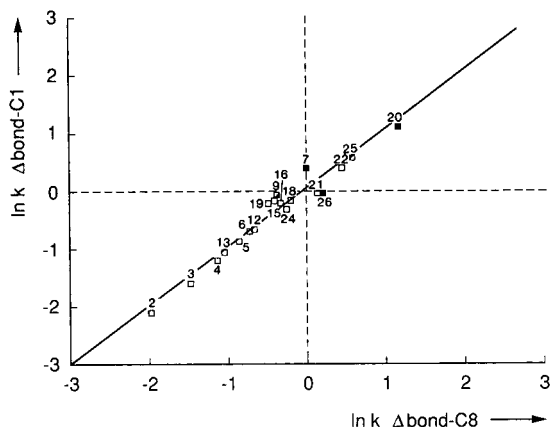


Fig. 4. Comparison of the retention of the test solutes on the Deltabond-C₁ and -C₈ phases. ◻ = Bad peak shape on the column indicated on the horizontal axis; ◼ = bad peak shapes on both columns. Other symbols and conditions as in Fig. 2.

decreasing sample size is thought to be caused by interactions between the solute molecules and residual silanols at the surface. The capacity factors obtained for large injected amounts can be seen to be approximately 1.1 for benzaldehyde, and 1.0 for methyl benzoate. These values fall very close to the straight line around which all sharp peaks are located. This suggests that any difference in selectivity observed between the ODS and Deltabond-C₈ columns are due to silanol group effects, which are undesirable, because of their detrimental influence on the peak shapes.

In Fig. 4 the retentions on the two Deltabond columns are compared. All the points are approximately situated on a straight line, so that there are hardly any selectivity differences between the two "different" phases. Considering the similar behaviour of the two columns in both qualitative (Table II) and quantitative senses (Fig. 4), one of these columns is likely to be sufficient. Also, the selectivity is identical with that of ODS columns, unless surface silanols play a role. This would cause

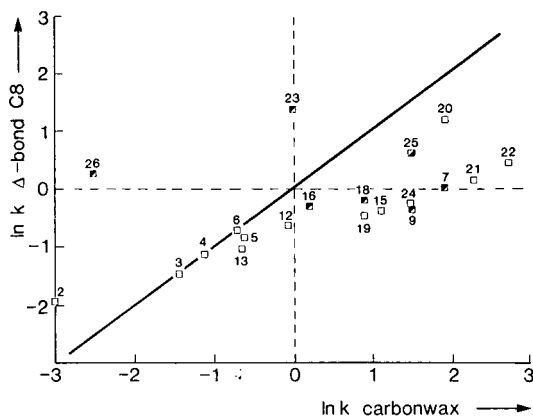


Fig. 5. Comparison of the retention of the test solutes on the carbonwax and Deltabond-C₈ phases. Symbols and conditions as in Figs. 2 and 4.

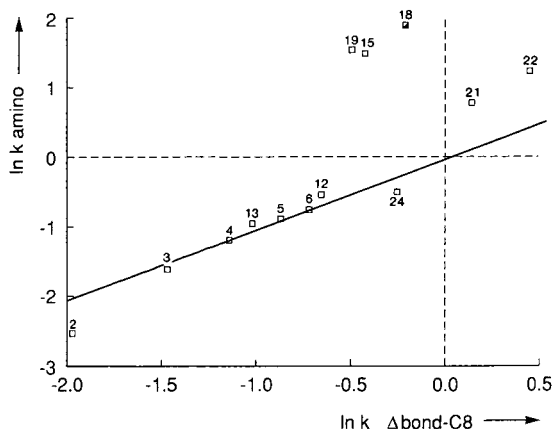


Fig. 6. Comparison of the retention of the test solutes on the amino and Deltabond-C₈ phases. Symbols and conditions as in Figs. 2 and 4.

increased retention on ODS columns (and hence selectivity differences), but also poor peak shapes and efficiencies. This will usually be too high a price to pay for an increase in selectivity.

Figs. 5 and 6 illustrate that the carbonwax and amino columns do show significant differences in selectivity for certain solutes in comparison with the non-polar phase. All solutes that can be connected by a line with a negative slope show a change in the elution order on the two different phases. It is seen that some dramatic changes are possible for these phases. In Fig. 7 the two polar phases are mutually compared.

Fig. 8 illustrates the differences in selectivity that may result from the application of different stationary phases in packed-column SFC. In this example, the selectivity for the three compounds [nitrobenzene (19), naphthalene (21) and di-*n*-heptyl ether (24)] was different on the Deltabond-C₈ (Fig. 8a) and carbonwax columns (Fig. 8b),

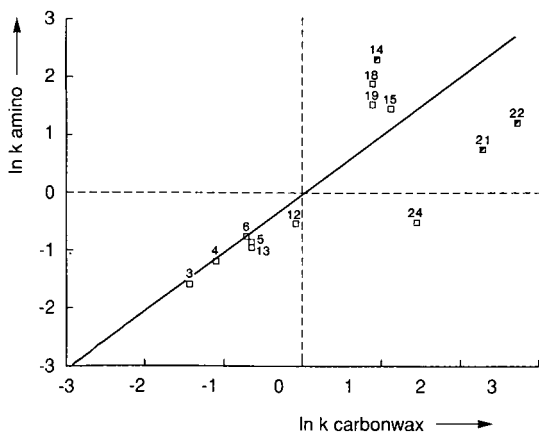


Fig. 7. Comparison of the retention of the test solutes on the carbonwax and amino phases. Symbols and conditions as in Figs. 2 and 4.

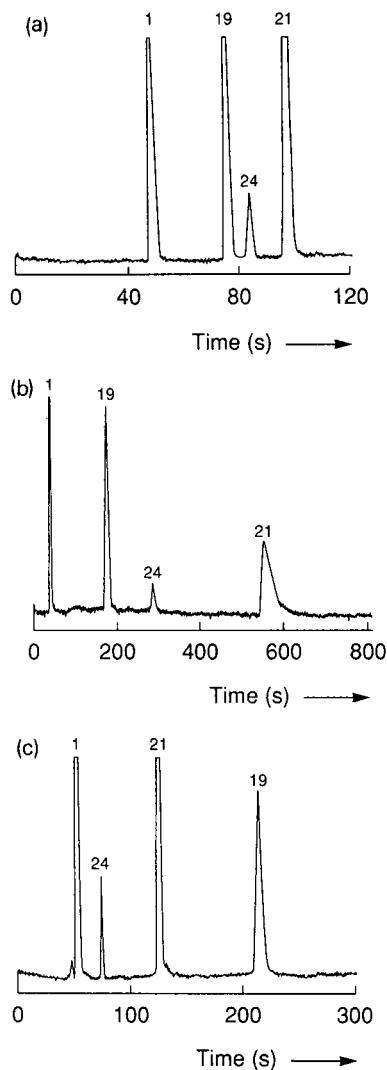


Fig. 8. Illustration of the possible differences in stationary phase selectivity in packed-column SFC. Solutes, dichloromethane (solvent, 1), nitrobenzene (19), naphthalene (21) and di-*n*-heptyl ether (24). Stationary phases: (a) Deltabond-C₈; (b) carbonwax; (c) amino. Conditions as in Fig. 2.

but the elution order was identical. On the amino column, even the elution order was different (Fig. 8c). It should be noted that only solutes that show reasonable or good peak shapes are included in this example. Fig. 8 serves to illustrate the differences in selectivity between the different columns, rather than their applicability. For the latter, Table II provides a better indication.

CONCLUSIONS

There is a requirement in SFC for stationary phases from which as many different (classes of) solutes as possible can be eluted as sharp, symmetrical peaks, using unmodified carbon dioxide as the mobile phase. Moreover, several such phases with different selectivities will be required. Octadecyl-modified silica (ODS) columns are applicable to non-polar solutes, such as hydrocarbons, but only to a very small number of polar solutes. Polysiloxane-coated silica (Deltabond) columns perform better than ODS for certain classes of solutes. However, for many polar solutes peak shapes and efficiencies still leave to be desired.

A very stable column was prepared by coating poly(ethylene glycol) on porous graphitic carbon. The resulting "carbonwax" column showed the best results for polar solutes of all columns tested. Improvements may be possible by optimizing the coating process and probably by packing the column after depositing the stationary phase on the particles.

A γ -aminopropyl-modified silica phase did not perform much better than an ODS column for our set of test solutes, in which few basic solutes were present. ODS, Deltabond-C₁ and -C₈ columns showed virtually no differences in selectivity. Significant selectivity differences were observed between these three non-polar columns and the "carbonwax" and amino columns, and between the two polar columns mutually.

The results indicate that by preparing homogeneous stationary phases, the number of solutes that can be eluted with SFC using pure carbon dioxide as the mobile phase can be greatly increased. A promising method for preparing phases is to coat relatively thick layers of a polymeric material on solid particles. To avoid excessive retention times, the specific surface area of the particles may be reduced. When coating poly(ethylene glycol) with an average molecular weight of 14 000 on porous graphitic carbon, no cross-linking or chemical bonding turned out to be necessary.

ACKNOWLEDGEMENT

Helpful suggestions by Dr. Bulvinder Kauer (Shandon) on the modification of carbon columns were appreciated.

REFERENCES

- 1 P. J. Schoenmakers and L. G. M. Uunk, *Adv. Chromatogr.*, 30 (1989) 1-80.
- 2 P. J. Schoenmakers and L. G. M. Uunk, *Eur. Chromatogr. News*, 1 (1987) 14.
- 3 P. J. Schoenmakers, F. C. C. J. G. Verhoeven and H. M. van den Bogaert, *J. Chromatogr.*, 371 (1986) 121.
- 4 T. Greibrokk, B. E. Berg, A. L. Blilie, J. Doehl, A. Farbrot and E. Lundanes, *J. Chromatogr.*, 394 (1987) 429.
- 5 M. Ashraf-Khorassani and L. T. Taylor, in C. M. White (Editor), *Modern Supercritical-Fluid Chromatography*, Hüthig, Heidelberg, 1988, pp. 115-134.
- 6 J. C. Keui, K. E. Markides and M. L. Lee, *J. High Resolut. Chromatogr. Chromatogr. Commun.*, 10 (1987) 257.
- 7 J. G. M. Janssen, P. J. Schoenmakers and C. A. Cramers, in P. Sandra (Editor), *Proceedings of the 10th International Symposium on Capillary Chromatography (Riva del Garda)*, Hüthig, Heidelberg, 1989, p. 1383.

- 8 J. G. M. Janssen, P. J. Schoenmakers and C. A. Cramers, *J. High Resolut. Chromatogr. Chromatogr. Commun.*, 12 (1989) 645.
- 9 P. J. Schoenmakers, L. G. M. Uunk and P. K. de Bokx, *J. Chromatogr.*, 459 (1988) 201.
- 10 C. R. Yonker and R. D. Smith, *J. Chromatogr.*, 361 (1986) 246.
- 11 S. M. Fields, K. E. Markides and M. L. Lee, *J. Chromatogr.*, 406 (1987) 223.
- 12 P. J. Schoenmakers and F. C. C. J. G. Verhoeven, *Trends Anal. Chem.*, 6 (1987) 10.
- 13 P. J. Schoenmakers and F. C. C. J. G. Verhoeven, *J. Chromatogr.*, 352 (1986) 315.
- 14 G. E. Berendsen, P. J. Schoenmakers, L. de Galan, G. Vigh, Z. Varga-Puchony and J. Inczedy, *J. Liq. Chromatogr.*, 3 (1981) 13.
- 15 P. J. Schoenmakers, *J. Chromatogr.*, 315 (1984) 1.
- 16 S. T. Sie and G. W. A. Rijnders, *Anal. Chim. Acta*, 38 (1967) 31.
- 17 G. W. A. Rijnders, *Chem.-Ing.-Tech.*, 49 (1970) 890.
- 18 J. J. Czubryt, M. N. Myers and J. C. Giddings, *J. Phys. Chem.*, 74 (1970) 4260.

CHROMSYM. 1731

Chiral separations of atropine and homatropine on an α_1 -acid glycoprotein-bonded stationary phase

E. ARVIDSSON* and S. O. JANSSON

Department of Analytical Chemistry, AB Hässle, S-431 83 Mölndal (Sweden)

and

G. SCHILL

Department of Analytical Pharmaceutical Chemistry, Uppsala University Biomedical Centre, P.O. Box 574, S-751 23 Uppsala (Sweden)

SUMMARY

Chiral separations of cationic compounds were studied with two structurally very similar compounds, atropine and homatropine. Retention, resolution and sensitivity were studied by isocratic and gradient elution techniques using changes in pH, temperature and concentrations of 2-propanol and anionic additives.

Anions of octanoic acid and 2-phenylbutyric acid improve the chiral separation of atropine whereas the chiral selectivity for homatropine can be suppressed. (*R*)- and (*S*)-2-phenylbutyric acid give different separation factors for atropine, which indicates a specific interaction with the solute. The antipodes of the cations are retained by different mechanisms in the presence of anionic additives, as demonstrated by experiments with factorial design, Van 't Hoff plots and the indirect detection technique.

INTRODUCTION

Enantiomeric separations are of considerable practical importance, *e.g.*, in the development of new drugs and new therapy in the biomedical field. Direct liquid chromatographic separations using chiral stationary phases have many advantages and the number of such phases is increasing. Most of them have a narrow field of application. However, phases that contain α_1 -acid glycoprotein as the chiral selector have a unique position in this respect as they are suitable for separations of charged and uncharged enantiomers with widely different structures. The wide application is due in part to the fact that the enantioselectivity can be varied and adapted to different solutes by additives to the mobile phase¹.

EnantioPac was the first commercial chiral phase containing α_1 -acid glycoprotein², but a new generation of this material, Chiral-AGP, with a particle size of 5 μm and improved chromatographic performance, has been developed³. The properties and

applications of EnantioPac have been reported in numerous papers, part of them summarized in some recent reviews^{1,4}. α_1 -Acid glycoprotein contains several chiral centres, but the mechanism for the chiral binding is so far unknown. However, some empirical conclusions on structural requirements for chiral binding have been presented¹. The separations are performed with an aqueous phase and retention and selectivity can be changed by varying the pH, uncharged, cationic and anionic additives and temperature. The effect of these changes on the chromatographic conditions is highly dependent on the structure of the solute and even small structural differences can have large effects. A drastic example is the widely different influences of charged additives on the chromatographic behaviour of methylatropine and methylhomatropine⁵

The aim of this study was to develop methods for the separation of cationic enantiomers on the Chiral-AGP phase and to optimize the systems with respect to retention, stereoselectivity and sensitivity. Atropine and homatropine were used as test samples. They have very small differences in structures (Fig. 1), atropine having one methylene group more than homatropine in a substituent at the chiral centre. However, changes in the chromatographic conditions often have different effects on their chromatographic behaviour on Chiral-AGP.

EXPERIMENTAL

Apparatus

The chromatographic system consisted of an LKB (Bromma, Sweden), Model 2150 pump, a Rheodyne 7010 injector with a 20- μ l loop and a Spectroflow 783 variable-wavelength detector (Kratos, Ramsey, NJ, U.S.A.). The column, injector and connecting tubes were thermostated using an RM6 (Messgeräte-Werk Lauda, Lauda-Königshofen, F.R.G.) or a Thermomix 1441 (Braun Melsungen, Melsungen, F.R.G.). The chromatograms were recorded on a Perkin-Elmer 56 instrument. The gradient studies were performed with two LKB Model 2150 pumps controlled by a Model 2152 HPLC controller.

Chemicals

Atropine sulphate, homatropine bromide and sodium octanoate were purchased from Merck (Darmstadt, F.R.G.), hyoscyamine, the *S*-enantiomer of atropine, from Boehringer (Mannheim, F.R.G.), (*R*)- and (*S*)-2-phenylbutyric acid from Sigma (St. Louis, MO, U.S.A.) and 4-phenylbutyric and 4-pentylbenzoic acid from Fluka (Buchs, Switzerland).

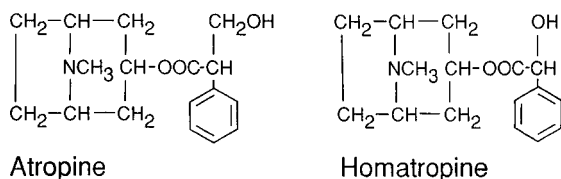


Fig. 1. Structures of atropine and homatropine.

Chromatographic conditions

The separation column was a Chiral-AGP (100 × 4.0 mm I.D.; 5 μm) from ChromTech (Stockholm, Sweden). The flow-rate used was 0.4 ml/min and the system was thermostated at 22°C if not stated otherwise. The mobile phases were phosphate buffers (ionic strength, $\mu = 0.05$) to which modifiers were added. The mobile phases for the gradient systems differed only in their content of 2-propanol and the gradient profiles were linear. The dead volume of the gradient system was 3 ml, which was taken into account by making the sample injection coincide with the gradient reaching the column inlet. The wavelength of detection was the UV absorption maximum of the solute, if not stated otherwise.

RESULTS AND DISCUSSION

Isocratic regulation of retention

pH and charged and uncharged modifiers have a large influence on retention and selectivity, as previously reported. The magnitude, however, is strongly dependent on the structure of the solute.

The effects of pH, 2-propanol and sodium octanoate on retention and selectivity were studied using a factorial design⁶. The factorial design gives information about whether a probable variable really is affecting the response, to what extent and whether the response is dependent on a combination of variables. An advantage with factorial design is that as much information as possible is achieved from a limited number of experiments. In a complete factorial design with three variables where all possible combinations at the two levels are investigated, eight (2³) experiments are made.

The compositions of the mobile phases used are summarized in Table I.

The model describing the response (retention or chiral selectivity) can be expressed as

$$y = \beta_0 + \beta_1x_1 + \beta_2x_2 + \beta_3x_3 + \beta_{12}x_1x_2 + \beta_{13}x_1x_3 + \beta_{23}x_2x_3 + \beta_{123}x_1x_2x_3 + \varepsilon \quad (1)$$

TABLE I
FACTORIAL DESIGN, REGULATION OF RETENTION

Expt. No.	x_1^a	x_2^b	x_3^c
1	-1	-1	-1
2	+1	-1	-1
3	-1	+1	-1
4	-1	-1	+1
5	+1	+1	-1
6	+1	-1	+1
7	-1	+1	+1
8	+1	+1	+1

^a x_1 = pH in the mobile phase: 6.0 (-1) or 7.5 (+1).

^b x_2 = Concentration of 2-propanol in the mobile phase: 0% (-1) or 3% (+1).

^c x_3 = Concentration of octanoate in the mobile phase: 0 mM (-1) or 4 mM (+1).

TABLE II

CALCULATED EFFECTS (β -COEFFICIENTS) OF pH (x_1), 2-PROPANOL (x_2) AND OCTANOATE (x_3) FOR ATROPINE

Parameter	β_1	β_2	β_3	β_{12}	β_{13}	β_{23}
k'_1	6.36	-5.84	-0.62	-4.44	0.09	0.52
k'_2	8.86	-8.30	1.80	-6.70	2.20	-1.54
α	0.06	-0.10	0.19	-0.04	0.04	-0.08

where β_n describes the effect of the variable x_n and β_{mn} correspondingly describes the combined effect of the variables x_m and x_n . The β -coefficients were calculated by multiplying the level of each variable with its response, adding the products and dividing the sum by the number of experiments.

The calculated effects are summarized in Table II for atropine and in Table III for homatropine. The calculated effects show for both solutes that an increased pH gives increased retention whereas the selectivity is almost unaffected. An increased content of 2-propanol in the mobile phase leads to a lower retention and selectivity. Similar effects of pH and addition of an uncharged modifier have been reported before and are probably due to increased negative charge of the protein and competition for the binding sites, respectively. The β -coefficients for octanoate show that it affects the retention less than pH and 2-propanol. The retention of the first-eluted enantiomer decreases with increasing octanoate concentration for both atropine and homatropine. For atropine the retention of the second-eluted enantiomer is increased by an increasing concentration of octanoate, giving an increased chiral separation. For homatropine the effect is the opposite, an increase in octanoate concentration decreases both k'_2 and the stereoselectivity.

The combined effects were generally smaller than the individual effects. However, the combined effect of pH and 2-propanol affects the retention negatively, less than pH and 2-propanol individually but more than octanoate.

Gradient elution

The effects of different mobile phase additives under isocratic conditions can be applied to improve the detection sensitivity using gradient elution.

The effect of the concentration of 2-propanol in the mobile phase on the retention (k') and resolution (R_s) of homatropine is demonstrated in Fig. 2. With an increase in the concentration of 2-propanol the retention and resolution decrease whereas the sensitivity increases owing to a reduction in peak width. The correspond-

TABLE III

CALCULATED EFFECTS (β -COEFFICIENTS) OF pH (x_1), 2-PROPANOL (x_2) AND OCTANOATE (x_3) FOR HOMATROPINE

Parameter	β_1	β_2	β_3	β_{12}	β_{13}	β_{23}
k'_1	4.96	-3.51	-0.10	-2.67	0.08	-4.20
k'_2	7.09	-5.40	-1.17	-4.06	-0.66	1.05
α	0.04	-0.09	-0.14	0.01	0.02	-0.005

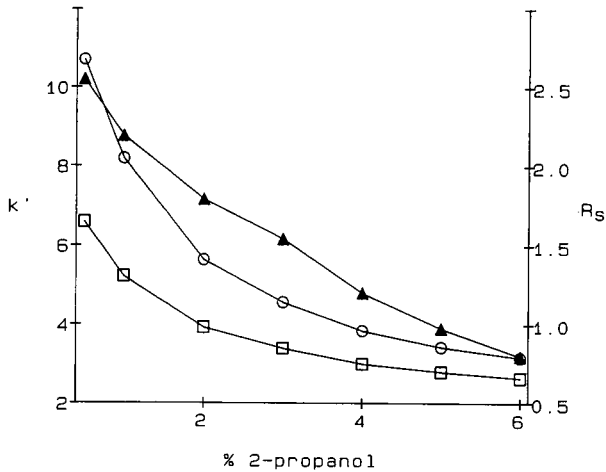


Fig. 2. Isocratic elution with 2-propanol as modifier. Solid phase: Chiral-AGP. Mobile phase: phosphate buffer (pH 7.0) + 2-propanol. Detection wavelength: 254 nm. Solute: racemate of homatropine. □ = k'_1 ; ○ = k'_2 ; ▲ = R_s .

ing effect of 2-propanol on the retention and resolution of the atropine enantiomers is demonstrated in Fig. 3. In this instance sodium octanoate was present in the mobile phase in order to obtain a sufficient stereoselectivity.

The detection sensitivity and resolution are both dependent on the steepness of the gradient in solvent gradient elution. The sensitivity increases and the resolution decreases with a steeper gradient, assuming a linear solvent strength gradient. Studies on Chiral-AGP with metoprolol showed that the decrease in retention times is balanced by the peak compression effect when the gradient is moderately steep, resulting

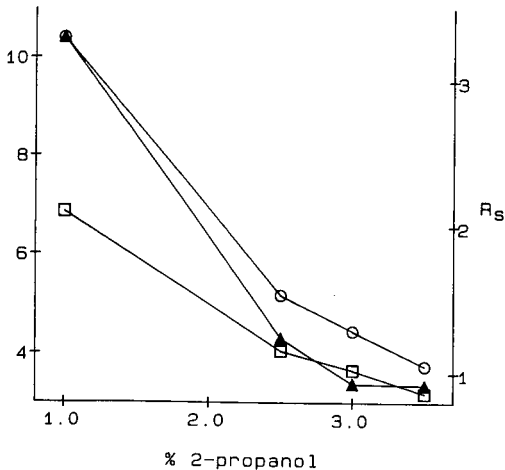


Fig. 3. Isocratic elution with 2-propanol as modifier. Solid phase: Chiral-AGP. Mobile phase: phosphate buffer (pH 7.0) + 2.5 mM octanoate and 2-propanol. Detection wavelength: 220 nm. Solute: racemate of atropine. □ = k'_1 ; ○ = k'_2 ; ▲ = R_s .

TABLE IV

OPTIMIZATION OF SENSITIVITY AND RESOLUTION USING ISOCRATIC AND GRADIENT ELUTION TECHNIQUES

Mobile phase: phosphate buffer (pH 7.0) + 2-propanol (IPA). Solute: homatropine. Detection wavelength: 254 nm.

Start IPA (%)	Δ IPA (%/min)	h_1/m^a	h_2/m^a	R_s
0.5	0	1.00	0.69	2.55
6.0	0	2.59	2.46	0.80
0.5	0.37	1.98	1.88	1.76
0.5	2.2	2.30	2.31	1.54
0.5	5.5	2.50	2.35	1.49

^a Relative sensitivity.

in almost unchanged resolution⁷. It was further observed that in a linear solvent strength gradient the sensitivity was the same for all the solutes eluted under gradient conditions, in accordance with the relationships given by Snyder *et al.*⁸.

Table IV shows gradient elution effects on homatropine. By using a steep gradient elution almost the same sensitivity is achieved as when using isocratic elution with a high concentration of 2-propanol. However, the gradient technique gives a baseline resolution ($R_s = 1.5$) whereas with isocratic elution the resolution is not complete ($R_s = 0.8$).

For atropine the gradient elution effects had to be studied with octanoate present in the mobile phase (Table V). The highest sensitivity is obtained isocratically with a high content of 2-propanol but the resolution is incomplete. A complete resolution is obtained by gradient elution but the value of the gradient technique is doubtful. It gives a certain decrease in the sensitivity and no improvement for the second enantiomer as the peak-height ratio h_2/h_1 is the same as in the isocratic run. The advantage of the propanol gradient seems to be lost when the retention is influenced by octanoate.

TABLE V

OPTIMIZATION OF SENSITIVITY AND RESOLUTION USING ISOCRATIC AND GRADIENT ELUTION TECHNIQUES

Mobile phase: phosphate buffer (pH 7.0) + 2.5 mM octanoate + 2-propanol (IPA). Solute: atropine. Detection wavelength: 220 nm.

Start IPA (%)	Δ IPA (%/min)	h_1/m^a	h_2/m^a	R_s
0.8	0	1.00	0.63	2.61
2.5	0	2.17	1.70	1.31
0.8	0.11	1.98	1.54	1.88

^a Relative sensitivity.

Effect of temperature

Temperature can also be used as a tool to regulate retention and resolution (see Table VI). The highest sensitivity is achieved using isocratic elution with a high concentration of 2-propanol and high temperature (No. 4 in Table VI). Comparison between the use of a 2-propanol gradient and isocratic elution at low temperature (Nos. 5 and 1) shows that the peak-height ratios for the two enantiomers are $h_{1,\text{grad.}}/h_{1,\text{iso.}} = 1.84$ and $h_{2,\text{grad.}}/h_{2,\text{iso.}} = 2.45$, *i.e.*, the peak heights are doubled when using a gradient. The ratio between the resolutions is only 10% lower using the gradient technique ($R_{s,\text{grad.}}/R_{s,\text{iso.}} = 0.90$). In the example given above, gradient elution is not necessary, as isocratic elution (No. 4) gives the highest sensitivity with baseline resolution. However, the gradient technique can be useful for optimizing the chromatographic systems when the resolution is lower.

The influence of temperature can be illustrated by Van 't Hoff plots, where $\ln k'$ is plotted *versus* the reciprocal of absolute temperature. A straight line indicates a single retention mechanism⁹. Plots for atropine are given in Fig. 4. Two mobile phases were used, both having the same pH and content of 2-propanol but one also containing octanoate. The octanoate has a very significant effect on the stereoselectivity and in its absence a very poor resolution is obtained.

The plots for the first-eluted enantiomer of atropine, hyoscyamine, with and without octanoate are similar, indicating that octanoate is only slightly involved in the retention of hyoscyamine. The last-eluted enantiomer has higher slope and intercept in the presence of octanoate.

The corresponding plots for homatropine are given in Fig. 5. The slope and intercept of the first-eluted enantiomer are also here of the same magnitude with and without octanoate. Addition of octanoate decreases the slope and intercept for the second-eluted enantiomer of homatropine, which means that the effect is the opposite to that obtained with atropine. This is in accordance with the results given in Tables II and III. The β -coefficients for octanoate are positive for atropine and negative for homatropine. The reason might be that the second-eluted enantiomer of atropine deviates by being retained as an ion pair with octanoate.

TABLE VI

INFLUENCE OF TEMPERATURE (*T*) AND CONCENTRATION OF 2-PROPANOL ON RESOLUTION AND SENSITIVITY

Mobile phase: phosphate buffer (pH 7.0) + 2-propanol (IPA). Solute: homatropine. Detection wavelength: 254 nm.

No.	Start IPA (%)	Δ IPA (%/min)	Temp. ($^{\circ}$ C)	h_1/m^a ($^{\circ}$ C/min)	h_2/m^a	R_s
1	0.6	—	5	1.00	0.57	3.54
2	2.5	—	5	2.26	1.38	3.01
3	0.6	—	35	2.70	1.96	2.18
4	2.5	—	35	4.79	3.79	1.49
5	0.6	0.13	5	1.84	1.38	3.17
6	0.6	0.13	35	3.29	2.76	2.08

^a Relative sensitivity.

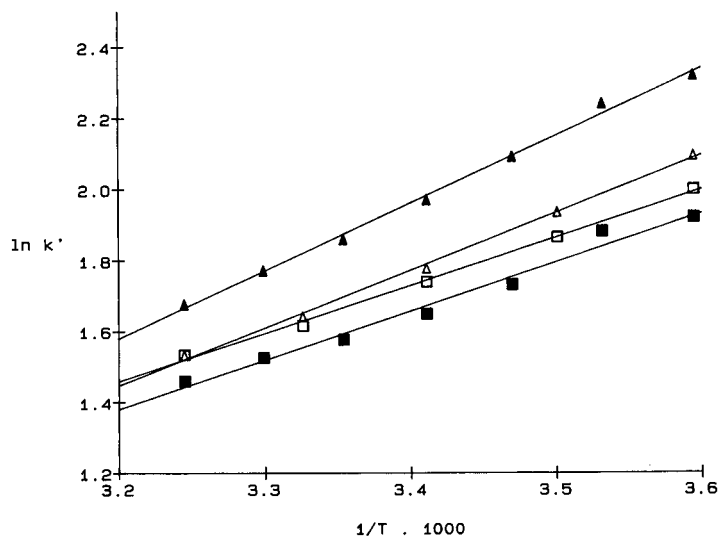


Fig. 4. Van 't Hoff plots for atropine. Mobile phase: filled symbols, phosphate buffer (pH 7.0) + 2.5 mM octanoate and 2% 2-propanol; open symbols, phosphate buffer (pH 7.0) + 2% 2-propanol. □, ■ = k'_1 ; △, ▲ = k'_2 .

Effects of anionic additives

Improvement of sensitivity. It has been shown in this and in previous studies¹⁰ that a hydrophobic anion such as octanoate is essential for the enantioselectivity of atropine on an α_1 -acid glycoprotein bonded phase. This additive can also improve the sensitivity by indirect detection effects.

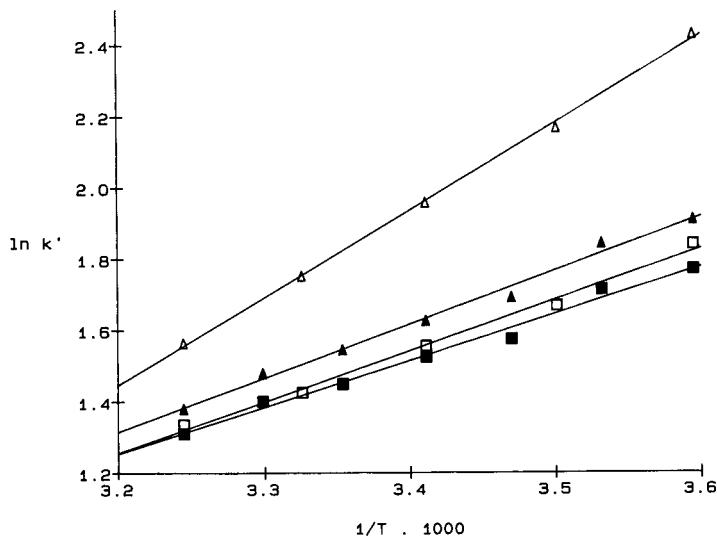


Fig. 5. Van 't Hoff plots for homatropine. Mobile phase and symbols as in Fig. 4.

Indirect detection effects appear when the mobile phase contains a detectable component (a probe) and the probe and injected solute have a common interaction. Injection of any solution differing in composition from the mobile phase, *e.g.*, a solute dissolved in the mobile phase, will disturb the established equilibria and zones with a deficit or excess of the probe will pass through the column. The resulting chromatogram will hence contain positive and negative peaks originating from injected solutes and mobile phase components (system peaks). A positive indirect response effect can improve the sensitivity for a solute with low detector response¹¹. A cationic solute, such as atropine, will in a reversed-phase system get a positive indirect response if it is more strongly retained than an anionic probe. The probe will then give rise to a negative system peak. Studies in systems with a hydrophobic adsorbent as the solid phase have shown that the indirect response depends on the retention of the solute peak relative to the system peak and on the fractional loading of the probe on the adsorbent¹¹. It should be emphasized that the expression for the relative response given in that study is valid for an adsorbing solid phase and may not be directly applied to a solid phase such as Chiral-AGP with a complex and unknown retention mechanism.

Octanoate has a fairly high molar absorptivity at low wavelengths (210–220 nm). The apparent molar absorptivities, ϵ^* , of the enantiomers of atropine calculated from the peak area¹² are given in Table VII. They are equal to that obtained for atropine in the absence of an anionic additive. Both enantiomers had similar apparent molar absorptivities. Changes in the concentration of octanoate or the organic modifier 2-propanol had no significant influence on the response. This indicates that the loading of the anionic probe on the AGP phase does not have the effect on the response that is predicted by expressions valid for a hydrophobic adsorbent¹¹. The response pattern was normal with a negative system peak appearing before the positive solute peak, indicating a common interaction between solute and probe.

Four anions with high molar absorptivity were tested for their effects on the response and the enantioselectivity on the AGP phase. 4-Pentylbenzoic acid and 4-phenylbutyric acid gave low chiral selectivity and incomplete separation of the enantiomers (Table VII). Both anions gave positive and indistinct system peaks before the solute peak, *i.e.*, no indication of a common interaction with the solute.

TABLE VII

INFLUENCE OF ANIONIC MODIFIERS ON THE DETECTION SENSITIVITY OF ATROPINE

Mobile phase: 1% 2-propanol + anionic modifier in phosphate buffer. Detection wavelength: 220 nm.

Modifier	Concentration $\times 10^4$ (M)	pH	k'_1	α	R_s	ϵ_1^{*b}	ϵ_2^{*b}
Octanoate	25	7.0	7.0	1.52	4.0	3500	3500
(S)-2-phenylbutyrate	5	6.0	2.9	3.34	3.7	4700	5800
4-Phenylbutyrate	5	6.0	2.1	1.20	0.85	—	—
4-Pentylbenzoate	5	6.0	6.0	1.06	0.3	—	—
— ^a	—	6.0	2.2	—	—	3400	—

^a Injection of (S)-atropine (hyoscyamine).

^b ϵ_1^* , ϵ_2^* = Apparent molar absorptivities of first- and second-eluted enantiomers, respectively.

(*S*)-2-Phenylbutyric acid gave high chiral selectivity and improved sensitivity (Table VII). The response pattern contained negative system peaks and positive peaks for both enantiomers (Fig. 6). The apparent molar absorptivity of both eluted enantiomers is higher than that obtained in the absence of an anionic probe. The first peak gave a smaller ϵ^* than the second peak, contrary to the response obtained in systems with an adsorbing solid phase. This might indicate that the two enantiomers have different retention mechanisms.

Influence on retention. (*S*)-2-Phenylbutyric acid gives a greater improvement in the enantioselectivity for atropine than octanoate, as shown in Table VII. The separation factor for atropine increases with increasing concentration of (*S*)-2-phenylbutyric acid (Fig. 7), mainly due to an increase in k' of the second-eluted enantiomer (Fig. 8). The k' increase might indicate binding of the solutes as an ion pair¹³ and, as the anion has a chiral centre, the diastereomeric ion pair can be bound on both a chiral and an achiral uncharged site.

The first-eluted enantiomer, which is (*S*)-atropine (hyoscyamine), is only slightly affected by an increase in the anion concentration. This might be due to binding as an ion pair combined with ionic binding to a charged site on the AGP phase, which has a negative charge in the pH range used¹⁴.

(*S*)- and (*R*)-2-phenylbutyric acid give different retentions and chiral selectivities (Table VIII), which indicates that the interaction between the enantiomers of atropine and the chiral anion has a specific character. The first-eluted enantiomer has the same retention with an *R*- and an *S*-form of the anion at pH 7.0, which supports the assumption of ionic binding to a charged site. At pH 6.0 the first-eluted enantiomer has a higher retention when (*S*)-2-phenylbutyric acid is used as an anionic additive. This might be due to the fact that the AGP phase is less strongly charged at that pH, which leads to a less strong dominance of ionic binding over ion-pair distribution.

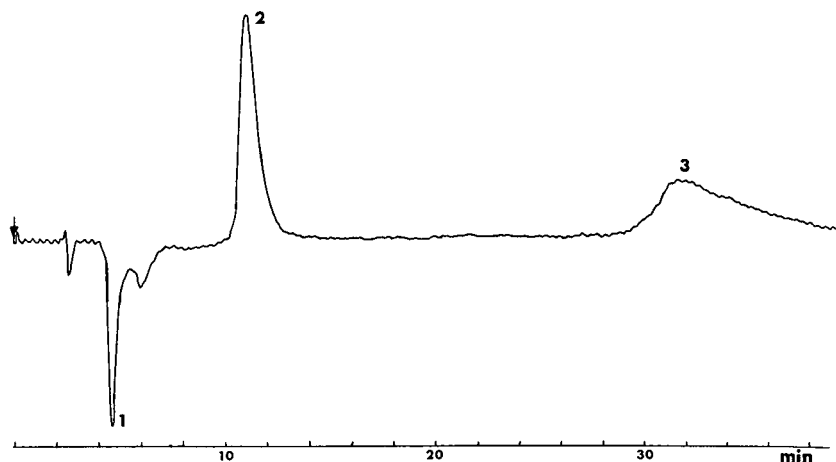


Fig. 6. Resolution of atropine enantiomers. Mobile phase: $5 \cdot 10^{-4}$ M (*S*)-2-phenylbutyric acid + 1% 2-propanol in phosphate buffer (pH 6.0). Detection wavelength: 220 nm. Peaks: 1 = system peak; 2, 3 = solute peaks.

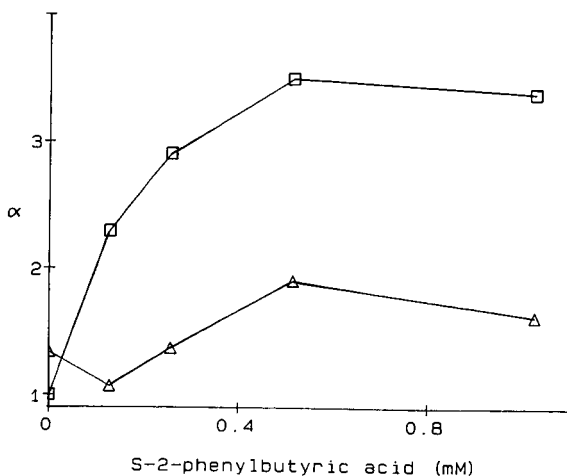


Fig. 7. Influence of (*S*)-2-phenylbutyric acid on separation factors. Mobile phase: (*S*)-2-phenylbutyric acid + 1% 2-propanol in phosphate buffer (pH 6.0). Detection wavelength: 220 nm. \square = Atropine; \triangle = homatropine.

The separation factor of homatropine also increases with increasing concentration of (*S*)-2-phenylbutyric acid (Fig. 7). The chiral selectivity is much lower and depends almost completely on an increase in k' of the last eluted enantiomer (Fig. 8).

Octanoate as an anionic additive gives a considerably smaller separation factor for atropine than (*S*)-2-phenylbutyric acid, even though it is used at higher concentration. However, the column efficiency and the peak symmetry are considerably better with octanoate and the resolution is the same as or better than that obtained with (*S*)-2-phenylbutyric acid (Table VII).

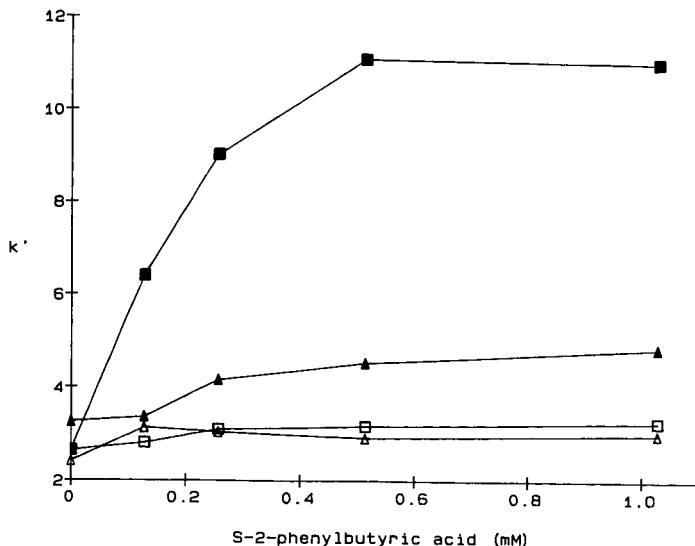


Fig. 8. Influence of (*S*)-2-phenylbutyric acid on capacity factors. Mobile phase, detection wavelength and symbols as in Fig. 7. $\triangle, \square = k'_1$; $\blacktriangle, \blacksquare = k'_2$.

TABLE VIII

EFFECT OF ANTIPODES OF 2-PHENYLBUTYRIC ACID ON CHIRAL SEPARATION OF ATROPINE

Mobile phase: $5 \cdot 10^{-4}$ M antipode of 2-phenylbutyric acid + 2-propanol in phosphate buffer. Detection wavelength: 258 nm.

Antipode of modifier	2-Propanol (%)	pH	k'_1	α	R_s
S	1	6.0	3.57	3.42	3.8
R	1	6.0	2.57	1.59	1.9
S	2	7.0	4.50	1.44	1.7
R	2	7.0	4.50	1.25	1.1

For homatropine, the retention of both enantiomers decreases with increasing concentration of octanoate. The second-eluted enantiomer is more strongly affected than the first, leading to a decrease in chiral selectivity at higher octanoate concentration.

CONCLUSION

Atropine and homatropine are structurally very similar but they show large differences in chromatographic behaviour on Chiral-AGP, particularly in the presence of anions of octanoic acid and 2-phenylbutyric acid. The anionic additives also have different influences on the antipodes of the solutes. The differences indicate binding by sites or mechanisms of different character, which in part can be due to the fact that the binding sites can be charged or uncharged. The different separation factors obtained for atropine with the enantiomers of 2-phenylbutyric acid indicate a specific steric interaction between anion and cation which might occur in the mobile phase or on the solid phase.

SYMBOLS

- h/m sensitivity (peak height/moles solute injected);
 R_s resolution [$2\Delta t_R/(W_1 + W_2)$];
 α separation factor (k'_2/k'_1);
 k' capacity factor [$(t_R - t_0)/t_0$];
 t_0 time for elution of a front peak, obtained by injecting a solution diverging from the mobile phase, e.g., water.
 t_R retention time;
 W peak width at the base, obtained by tangents

REFERENCES

- 1 J. Hermansson and G. Schill, in P. R. Brown and R. A. Hartwick (Editors), *High Performance Liquid Chromatography*, Wiley, New York, 1989, p. 337.
- 2 J. Hermansson, *J. Chromatogr.*, 298 (1984) 67.

- 3 J. Hermansson, K. Ström and R. Sandberg, *Chromatographia*, 24 (1987) 520.
- 4 J. Hermansson and G. Schill, in M. Zief and L. J. Crane (Editors), *Chromatographic Chiral Separation*, Marcel Dekker, New York, 1987, p. 245.
- 5 G. Schill, I. W. Wainer and S. A. Barkan, *J. Chromatogr.*, 365 (1986) 73.
- 6 D. L. Massart, B. G. M. Vandeginste, S. N. Deming, Y. Michotte and L. Kaufman, *Chemometrics: a Textbook (Data Handling in Science and Technology, Vol. 2)*, Elsevier, Amsterdam, 1988, p. 271.
- 7 K. Balmér, B. A. Persson and G. Schill, *J. Chromatogr.*, 477 (1989) 107.
- 8 L. R. Snyder, J. W. Dolan and J. R. Grant, *J. Chromatogr.*, 165 (1979) 3.
- 9 W. Melander, D. E. Campbell and Cs. Horváth, *J. Chromatogr.*, 158 (1978) 215.
- 10 G. Schill, I. W. Wainer and S. A. Barkan, *J. Liq. Chromatogr.*, 9 (1986) 641.
- 11 J. Crommen, G. Schill, D. Westerlund and L. Hackzell, *Chromatographia*, 24 (1987) 252.
- 12 L. Hackzell and G. Schill, *Chromatographia*, 15 (1982) 437.
- 13 A. Sokolowski and K. G. Wahlund, *J. Chromatogr.*, 189 (1980) 299.
- 14 K. Schmid, in F. W. Putnam (Editor), *The Plasma Proteins*, Academic Press, New York, 1975, p. 184.

CHROMSYMPO. 1686

Chiral chloroformates as transparent reagents for the resolution of metoprolol enantiomers by reversed-phase liquid chromatography

MARTIN AHNOFF*, SAMUEL CHEN, ANNA GREEN and INGER GRUNDEVIK
Bioanalytical Chemistry, AB Hässle, S-431 83 Mölndal (Sweden)

SUMMARY

Ten chiral chloroformates were prepared and tested as derivatizing reagents, using metoprolol and tyrosine enantiomers as model compounds. Chloroformates derived from isosorbide and isomannide monoesters gave separation factors of 1.07–2.16 for tyrosine and 1.06–1.08 for metoprolol in reversed-phase liquid chromatography. With *tert.*-butyl 3-(chloroformoxy)butyrate as derivatizing reagent a separation factor of 1.10 and a resolution of 2.0 were obtained in 12 min for (*R*)- and (*S*)-metoprolol. The reagent and its by-products did not interfere with the UV or fluorescence detection of metoprolol.

INTRODUCTION

Chloroformates have chemical properties that make them attractive as derivatizing reagents for primary and secondary amines. They have also found use in the derivatization of tertiary amines and alcohols and as coupling agents for the condensation of carboxylic acids with amines. Their reactivity with primary and secondary amines allows derivatization under mild conditions in the presence of water. Chloroformates are not harmful to common reversed-phase chromatographic columns.

So far, only two chiral chloroformate reagents have been reported as derivatizing reagents for the analytical resolution of enantiomers¹. Menthyl chloroformate has been used for gas chromatographic separations² and for the liquid chromatographic resolution of hydroxy acids³ and some secondary amines^{4,5}. 1-(9-Fluorenyl)ethyl chloroformate (FLEC) was introduced as a chiral derivatizing reagent by Einarsson *et al.*⁶, who demonstrated the simultaneous resolution of seventeen amino acids into their D- and L-forms as diastereomeric derivatives. The fluorenyl residue allowed sensitive fluorimetric detection.

The work reported here was carried out in a search for chiral chloroformate reagents suitable for the resolution of metoprolol and other β -blockers with the N-isopropylamino-2-propanol structure. These have their chiral carbon atom in

a β -position to the amino group. Ten different chloroformates (Table I) were prepared and tested, using (*S*)- and (*R,S*)-metoprolol and, for seven of the reagents, L- and DL-tyrosine as model compounds. As β -blockers can be sensitively detected by fluorescence, it was considered an advantage if the reagent itself does not contain fluorescent or UV-absorbing groups.

EXPERIMENTAL

Chemicals

Racemic 1-(cyclohexyl)ethanol, 3-hydroxytetrahydrofuran and (–)-menthyl chloroformate were obtained from Aldrich (Milwaukee, WI, U.S.A.), (*R*)-methyl 3-hydroxybutyrate and (*S*)-ethyl 3-hydroxybutyrate from Fluka (Buchs, Switzerland) and (*S*)-*tert.*-butyl 3-hydroxybutyrate from Merck (Darmstadt, F.R.G.). Isosorbide 2-mononitrate, 5-mononitrate and 2-monoacetate, isomannide mononitrate, (*R,S*)- and (*S*)-metoprolol, (*R,S*)-*N*-desisopropyl metoprolol and (*R,S*)-*N*-(2-hydroxypropyl) acetamide were obtained from the Organic Chemistry Department, AB Hässle (Möndal, Sweden). L-Tyrosine and DL-tyrosine were from Sigma (St. Louis, MO, U.S.A.).

Chromatographic equipment

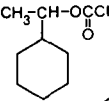
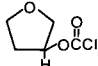
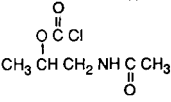
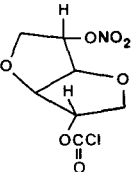
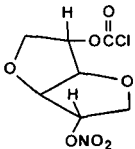
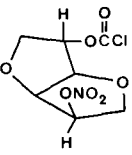
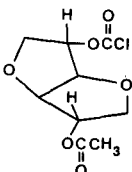
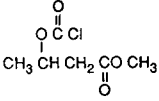
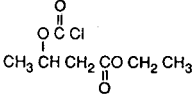
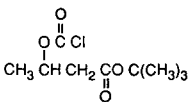
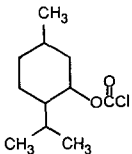
The liquid chromatograph consisted of a Model 7010 manual loop injector (Rheodyne, Berkeley, CA, U.S.A.), a pump for isocratic elution, a Model 440 UV detector (Waters Assoc., Milford, MA, U.S.A.), a Model LS4 spectrofluorimetric detector (Perkin-Elmer, Norwalk, CT, U.S.A.) and a Model 3390A integrator (Hewlett-Packard, Avondale, PA, U.S.A.). The column was 100 mm \times 4.6 mm I.D., packed with 3- μ m Microspher octadecylsilica particles (Chrompack, Middelburg, The Netherlands).

Preparation of chloroformate reagents

Chloroformates 1–10 were prepared as follows: the corresponding alcohol (0.5–5 mmol) and an equimolar amount of triethylamine were dissolved in toluene or dry diethyl ether and the solution was added to cold (0°C) toluene containing 20% (w/w) of phosgene (four-fold excess). The mixture was stirred at 0°C for 2 h, then the solid triethylammonium chloride was removed by filtration and the solvent was evaporated in a rotary evaporator.

The optical purity of the non-racemic reagents 4–7 and 10 was investigated by derivatization with (*S*)-metoprolol (optical purity > 99.8%) and racemic metoprolol, followed by liquid chromatographic separation of the diastereomers formed. With reagents 4–7, no enantiomeric impurity was detected (optical purity > 99%). Reagent 10 was 94% optically pure (see Fig. 1B), which probably reflects the optical purity of the starting material. Reagent 10 was also analysed by liquid chromatography with UV detection at 220 nm and was found to contain 10% of the parent alcohol. No characterization was carried out that required further purification of the chloroformate reagents. No decomposition of the reagents (neat or dissolved in dichloromethane) was observed after 1 week at +8°C or 1 month at –18°C.

TABLE I
STRUCTURAL FORMULAE OF CHIRAL CHLOROFORMATE REAGENTS

No.	Compound	Formula
1	<i>(R, S)</i> -1-(Cyclohexyl)ethyl chloroformate	
2	<i>(R, S)</i> -Tetrahydro-3-furanyl chloroformate	
3	<i>(R, S)</i> -N-[2-(Chloroformoxy)propyl]acetamide	
4	2-Chlorocarbonyl-L-isosorbide 5-mononitrate	
5	5-Chlorocarbonyl-L-isosorbide 2-mononitrate	
6	5-Chlorocarbonyl-L-isomannide 2-mononitrate	
7	5-Chlorocarbonyl-L-isosorbide 2-monoacetate	
8	<i>(R)</i> -Methyl 3-(chloroformoxy)butyrate	
9	<i>(S)</i> -Ethyl 3-(chloroformoxy)butyrate	
10	<i>(S)</i> - <i>tert.</i> -Butyl 3-(chloroformoxy)butyrate	
11	<i>(-)</i> -Menthyl chloroformate	

Derivatization of amines

To 20 μmol of reagents 1–10, dissolved in 0.20 ml of acetonitrile, were added 0.4 ml of 0.25 *M* borate buffer (pH 8) and 0.4 ml of a solution containing up to 0.4 μmol of the amine in 0.01 *M* hydrochloric acid. After 1–60 min at room temperature, the reaction was stopped by addition of 25 μl of 1 *M* hydrochloric acid, and the sample was then ready for injection into the chromatographic column.

Derivatization with (–)-menthyl chloroformate was performed in dichloromethane owing to the low solubility of this reagent in aqueous solutions. Solid metoprolol base (20 μmol) was added to a mixture of the reagent (200 μmol) and triethylamine (200 μmol). After reaction for 30 min at room temperature, aliquots diluted 1000-fold in the chromatographic eluent were injected.

RESULTS AND DISCUSSION

Table II lists the separation factors obtained for derivatives of metoprolol and tyrosine in reversed-phase systems. Different concentrations of the organic solvents were used, and also different solvents, as the same solvent was not optimum for all derivatives. 1-(Cyclohexyl)ethyl chloroformate resolved neither metoprolol nor tyrosine. Tetrahydro-3-furanyl chloroformate did not resolve metoprolol, but did resolve tyrosine ($\alpha = 1.16$). *N*-[2-(Chloroformoxy)propyl] acetamide resolved tyrosine ($\alpha = 1.44$), but not metoprolol.

Isosorbides and isomannides are 1,4–3,6-dianhydroglucitols with four chiral atoms and a rigid, non-planar, two-ring structure. Derived from sorbitol and mannitol, they are of high enantiomeric purity. No racemization was observed when pure (*S*)-metoprolol was derivatized. Separation factors for tyrosine ranged from 1.07

TABLE II
SEPARATION OF DIASTEREOMERIC CARBAMATES OF TYROSINE AND METOPROLOL BY REVERSED-PHASE CHROMATOGRAPHY

Column, Microspher C_{18} (3 μm) (100 mm \times 4.6 mm I.D.); mobile phase, phosphate buffer (pH 3) ($I = 0.02$) plus an organic solvent.

Reagent ^a	Tyrosine				Metoprolol			
	Mobile phase ^b	k'_1	k'_2	α	Mobile phase ^b	k'_1	k'_2	α
1	20% ACN		9.07	≤ 1.01	37% ACN		10.69	≤ 1.01
2	10% ACN	9.92	11.49	1.16	37% ACN		5.30	≤ 1.01
3	10% ACN	6.5	8.9	1.44	37% ACN		5.1	≤ 1.01
4	10% THF	12.32	21.14	1.70	30% THF	19.6	20.8	1.06
5	10% THF	9.51	10.02	1.07	30% THF	23.4	24.4	1.04
6	10% THF	8.12	17.54	2.16	30% THF	15.72	16.93	1.08
7	5% THF	6.74	10.08	1.50	20% THF	21.6	22.9	1.06
8					37% ACN	12.50	13.48	1.08
9					37% ACN	21.41	23.22	1.08
10					50% ACN	10.60	11.63	1.10
11					72% Methanol	5.68	6.38	1.12

^a See Table I.

^b ACN = Acetonitrile; THF = tetrahydrofuran.

to 2.16, showing a strong dependence on the orientation (*endo* or *exo*) of the chloroformyl group and the ester group. Separation factors for metoprolol were modest and fairly uniform. Separation factors of 1.04–1.08 were obtained when tetrahydrofuran was used as an organic modifier. Less efficient separations were achieved with mobile phases containing methanol or acetonitrile. Whereas good resolution was obtained for metoprolol ($R = 1.4$), only partial resolution was obtained for the primary amine *N*-desisopropylmetoprolol ($\alpha = 1.01$ – 1.03), the best separation being obtained with reagent 4.

The 3-(chloroformoxy)butyrates were chosen for testing as they have a simple chiral structure and contain an ester group that might be available for intramolecular hydrogen bonding of the hydroxyl of metoprolol. They gave equal or higher separation factors for metoprolol than the isosorbide and isomannide reagents. In this instance, acetonitrile gave better resolutions than tetrahydrofuran, methanol or 2-propanol. Using a 100-mm column with 7700 theoretical plates, a resolution factor (R) of 2.0 was obtained (see Fig. 1A).

The menthyl carbamate derivatives of metoprolol were resolved in a chromatographic system similar to that used by Schmitthenner *et al.*⁷ for menthyl carbamates of propranolol and flavodilol. The α -value was slightly higher than for *tert.*-butyl 3-(chloroformoxy)butyrate (reagent 10). For applications to biological extracts, the higher water solubility of reagent 10 was considered important. It allowed derivatization in an aqueous solution and injection of the reaction mixture directly into the column.

Detection properties of reagent and derivatives

The molar absorptivity of reagent 4 (1 mM in acetonitrile) at 280 nm was too low to be determined, and was calculated to be lower than $200 \text{ l mol}^{-1} \text{ cm}^{-1}$ at 254 nm. In order to detect reagents 1–11 and the corresponding alcohols in the liquid chromatographic analyses, UV detection below 240 nm had to be used. Under the conditions used for separation of metoprolol derivatives, reagents 1–10 eluted close to the front. Owing to the small disturbance from reagent blanks, sensitive detection of the metoprolol derivatives was easily obtained.

The molar absorptivity (280 nm) of metoprolol derivatives with reagent 4 appeared to be very close to that of metoprolol itself. The measured peak area of the derivatives formed was *ca.* 95% of the decrease in peak area of metoprolol. The peak area of the more retained diastereomer was slightly higher than that for the less retained (a factor 1.03), but this might be due slightly tailing peaks. The fluorescence properties were studied by coupling a UV and a fluorescence detector in series and measuring the ratio of the fluorescence signal over the UV signal for each eluted peak. The fluorescence yields of (*S*)- and (*R*)-metoprolol derivatives (reagent 4) were 90% and 95%, respectively, relative to underivatized metoprolol. Similar results were obtained when the UV and fluorescence properties of metoprolol derivatives with reagents 7 and 10 were studied.

Reaction rates and recoveries

When reagent 10 was allowed to react with metoprolol (0.4 μmol in 1.0 ml) under the conditions given under Experimental, liquid chromatography showed a 50% decrease in metoprolol concentration after 4.2 min. With reagent 4, the reaction was

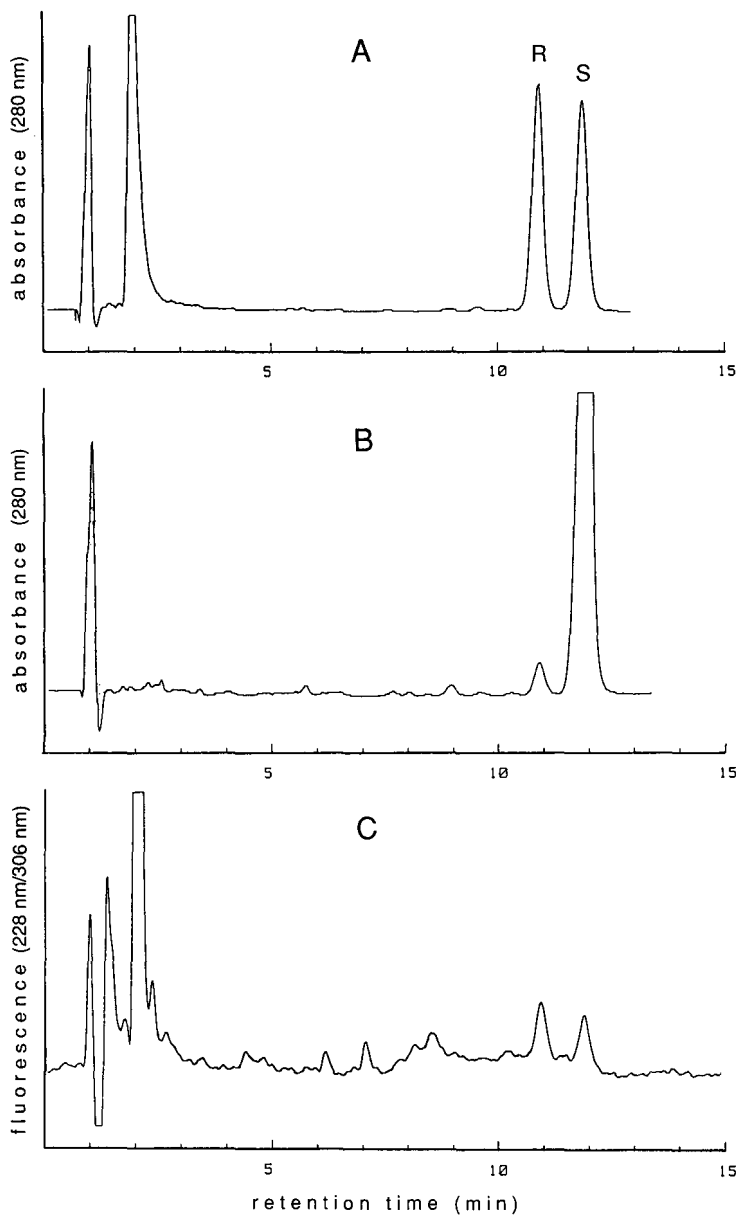


Fig. 1. Separation of (*R*)- and (*S*)-metoprolol after derivatization with *tert*-butyl 3-(chloroformoxy)-butyrate (reagent 10). (A) Metoprolol racemate. (B) 99.9% Pure (*S*)-metoprolol. The small peak is due to *ca.* 3% enantiomeric impurity of the reagent. (C) Detection of metoprolol enantiomers in human plasma after extraction and derivatization with *tert*-butyl 3-(chloroformoxy)butyrate. Concentration in plasma *ca.* 4 ng/ml (15 nmol/l) of each metoprolol enantiomer. Chromatographic conditions for A, B and C as given in Table II for reagent 10. In A and B, UV detection at 280 nm was used (0.16 a.u.f.s.); in C, fluorescence was measured at 306 nm (excitation at 228 nm).

about twice as fast. Tyrosine reacted considerably faster than metoprolol with both reagents. When the reactions between metoprolol and reagents 4 and 10 were followed by measuring the diastereomers formed, no difference in the rates of formation could be detected between the diastereomers.

The recovery of metoprolol reacted with reagent 10 (20 mM) was found to be independent of the initial metoprolol concentration (0.04–400 μ M). It was calculated to be 90–95% with no difference between the enantiomers. An accurate determination of the recovery would require the synthesis of each diastereomer with a purity close to 100%.

Determination of metoprolol enantiomers in plasma extracts

In a preliminary investigation of the potential of the reagents for bioanalytical applications, human plasma (1 ml) containing metoprolol was extracted with a 1:1 mixture of dichloromethane and diethyl ether, according to the method of Balmér *et al.*⁸. The solvent was evaporated and the residue was treated with *tert.*-butyl 3-(chloroformoxy)butyrate (reagent 10) as described above. After a 30-min reaction period, 150 μ l of the reaction mixture (1.0 ml) were separated by reversed-phase chromatography under the conditions given in Table I. Fluorescence detection (excitation at 228 or 272 nm, emission at 306 nm) showed little interference from a plasma blank, and 15 nmol/l of each enantiomer of metoprolol could be determined (Fig. 1C). Using the procedure described, α -hydroxymetoprolol, a metabolite, will also be extracted, derivatized and will be eluted in front of the metoprolol derivatives.

REFERENCES

- 1 M. Ahnoff and S. Einarsson, in W. J. Lough (Editor), *Chiral Chromatography*, Blackie, London, 1989, Ch. 4, pp. 39–80.
- 2 J. W. Westley and B. Halpern, *J. Org. Chem.*, 33 (1968) 3978.
- 3 A. R. Brash, A. T. Porter and R. L. Maas, *J. Biol. Chem.*, 260 (1985) 4210.
- 4 M. C. Arnould, B. Serkiz and J. P. Volland, *Analisis*, 8 (1980) 76.
- 5 J. I. Seeman, C. G. Chavdarian and H. V. Secor, *J. Org. Chem.*, 50 (1985) 5419.
- 6 S. Einarsson, B. Josefsson, P. Möller and D. Sanchez, *Anal. Chem.*, 59 (1987) 1191.
- 7 H. F. Schmitthenner, M. Fedorchuk and D. J. Walter, *J. Chromatogr.*, 487 (1989) 197.
- 8 K. Balmér, Y.-Y. Zhang, P.-O. Lagerström and B. A. Persson, *J. Chromatogr.*, 417 (1987) 357.

CHROMSYMP. 1682

Direct high-performance liquid chromatographic determination of the enantiomers of alfuzosin in plasma on a second-generation α_1 -acid glycoprotein chiral stationary phase

ALAIN ROUCOUSE*, MARTINE MANOHA, ALAIN DURAND and JEAN PAUL THENOT
Synthélabo Recherche (L.E.R.S.), 58 rue de la Glacière, 75013 Paris (France)

SUMMARY

A direct liquid chromatographic method was developed for the determination of the enantiomers of alfuzosin in human plasma, without derivatization, on a chiral α_1 -acid glycoprotein column. The influence of pH, of uncharged organic solvents and of a cationic modifier (tetrabutylammonium) of the mobile phase on retention and enantioselectivity was evaluated. The enantiomers and an internal standard, structurally related to alfuzosin, were extracted from plasma with dichloromethane–diethyl ether from alkaline solution, then separated with a mobile phase of 0.025 M phosphate buffer (pH 7.4) containing 0.025 M tetrabutylammonium bromide–acetonitrile (94:6, v/v). The limit of quantification for each isomer was 1 ng/ml. The method has been applied to the determination of the pharmacokinetic profile of alfuzosin enantiomers in healthy volunteers after intravenous administration of the racemate.

INTRODUCTION

Alfuzosin (XATRAL, Fig. 1), a quinazolinyl derivative, is a selective postsynaptic α_1 -adrenoceptor antagonist, recently introduced in therapeutics for the treatment of benign prostate hypertrophy. The compound is a racemate and the *R* and *S* optical isomers have similar pharmacological activity. For the determination of the pharmacokinetic behaviour of each enantiomer after administration of the racemic mixture, it was desirable to determine the two enantiomers simultaneously in plasma.

Chiral high-performance liquid chromatographic (HPLC) resolution can be achieved by indirect or direct separations^{1–4} but indirect chromatographic resolution based on the formation of diastereomers with various chiral reagents^{5–12} has proved to be difficult with alfuzosin. An improved version of a chiral column containing α_1 -acid glycoprotein (α_1 -AGP) bound to silica was described by Hermansson¹³. In this paper, we report a sensitive, stereospecific HPLC method suitable for the determination of the enantiomers of alfuzosin in plasma on this α_1 -AGP column. The effects of pH, uncharged organic solvents (acetonitrile, methanol, ethanol, 2-propa-

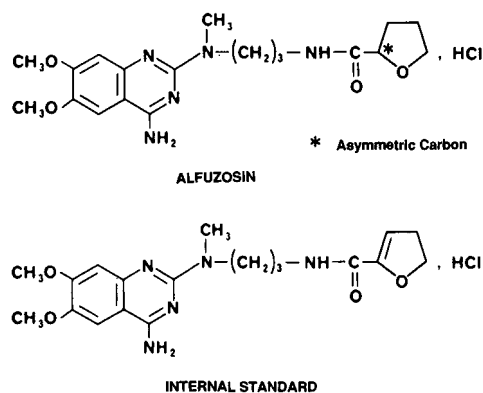


Fig. 1. Structures of alfuzosin and the internal standard.

nol) and of a cationic modifier, tetrabutylammonium, of the mobile phase on the retention and the enantioselectivity were evaluated. The assay procedure was applied to the determination of the pharmacokinetic profile of the enantiomers of alfuzosin in healthy volunteers after intravenous administration of the racemate.

EXPERIMENTAL

Materials

Racemic alfuzosin, its *R* and *S* enantiomers and an internal standard structurally related to alfuzosin (Fig. 1) were synthesized in the Chemistry Department of Synthelabo Recherche (L.E.R.S.). Anhydrous KH_2PO_4 and $\text{K}_2\text{HPO}_4 \cdot 3\text{H}_2\text{O}$ were of analytical-reagent grade from Merck (Darmstadt, F.R.G.), 1 *M* sodium hydroxide solution and 1 *M* hydrochloric acid were obtained from Prolabo (Paris, France), tetrabutylammonium bromide (TBA) from Aldrich (Strasbourg, France), HPLC-grade acetonitrile, UV-grade methanol and unstabilized diethyl ether (RPE grade) from Carlo Erba (Milan, Italy) and analytical-reagent grade dichloromethane from Prolabo. The water used for the preparation of the buffers was purified with a Milli-Q system (Millipore, Bedford, MA, U.S.A.).

Stock solutions of alfuzosin and the internal standard were prepared in methanol at a concentration of 100 ng/ μl and diluted for calibration. These solutions were stable for at least 1 month when kept at 0–5°C.

The liquid chromatograph consisted of a Beckman Model 110 B constant-flow pump (Altex, San Ramon, CA, U.S.A.) and a JASCO 820 FP spectrofluorimeter (Japan Spectroscopic, Tokyo, Japan), operated at 265 nm for excitation and 400 nm for emission. The detector was coupled to an SP 4100 integrator-calculator (Spectra-Physics, San Jose, CA, U.S.A.) for the determination of peak height.

Chromatography of alfuzosin enantiomers was performed on a commercially available (ChromTech, Norsborg, Sweden) chiral-AGP column (100 mm \times 4.0 mm I.D.). Chiral-AGP is a second-generation chiral separation column with α_1 -acid glycoprotein AGP immobilized on porous, spherical, 5- μm silica particles.

Methods

The mobile phase buffer was prepared by dissolving 0.667 g of anhydrous KH_2PO_4 , 4.587 g of $\text{K}_2\text{HPO}_4 \cdot 3\text{H}_2\text{O}$ and 8.060 g of TBA in 1 l of purified water. The standard conditions used for the determination of alfuzosin enantiomers in plasma were a flow-rate of 0.9 ml/min, ambient temperature and a mobile phase of 0.025 M K_2HPO_4 - KH_2PO_4 buffer containing 0.025 M TBA-acetonitrile (94:6, v/v) (pH 7.4).

Extraction

To 1 ml of plasma in a 15-ml screw-capped Pyrex test-tube, fitted with a PTFE screw-cap, were added 40 ng of internal standard (20 μl of a 2 ng/ μl solution in methanol), 1 ml of 0.1 M sodium hydroxide solution and 7 ml of extraction solvent (dichloromethane-diethyl ether, 3:4). The tube was shaken for 25 min on an agitator (Bioblock, Paris, France) then centrifuged at 1000 g for 5 min. The organic layer was transferred to tubes and evaporated to dryness at 30°C under a gentle stream of nitrogen. The residue was dissolved in 80 μl of the mobile phase and 20 μl were injected into the chiral-AGP column.

Quantitative yield

Five plasma samples were spiked with alfuzosin to give final concentrations of 25 ng/ml for each enantiomer and extracted according to the procedure described above, but without addition of internal standard. Exact volumes of the organic layer were sampled, and 30 ng of internal standard were added. The peak-height ratios of *R* and *S* isomers to the internal standard for the extracted samples were compared with those obtained after evaporation of solvent samples containing equivalent concentrations of alfuzosin and internal standard (unextracted samples).

Calibration and calculation

The retention times of *R* and *S* enantiomers were measured in duplicate, each isomer being injected separately. The capacity factors were calculated as $k' = (t_R - t_0)/t_0$, the separation factors, α , as k'_S/k'_R and the resolution, R_1 , as $2\Delta t_R/(W_R + W_S)$, W_R and W_S being the peak width of the *R* and *S* isomers, respectively.

The concentrations of the *R* and *S* enantiomers in unknown samples were calculated by interpolation from calibration graphs prepared as follows: to 1-ml blank plasma samples, 2, 5, 10, 20, 50 or 100 ng of alfuzosin racemate and 40 ng of internal standard were added by using appropriate volumes of diluted solutions. The samples were analysed according to the procedure. Peak-height ratios (*R* enantiomer/internal standard and *S* enantiomer/internal standard) were used to generate a least-squares regression line, weighted by 1/concentration.

For assay validation, 1-ml plasma samples were spiked with 10 or 50 ng of alfuzosin racemate (5 or 25 ng of each isomer). Two analysts performed two assay series, containing five control samples for each concentration and calibration samples (1–50 ng for each isomer), on two separate days. Accuracy, precision, linearity and sensitivity of the assay, sensitivity or limit of quantification, minimum concentration that may be evaluated with a relative standard deviation (R.S.D.) < 10% and a residue (percentage difference from theoretical value) < 15%, were measured. Furthermore, quality control samples were used in daily routine analysis.

RESULTS AND DISCUSSION

The retention times of (*R*)- and (*S*)-alfuzosin and the enantioselectivity were strongly influenced by the charged and uncharged mobile phase additives the ionic strength and the pH. When the separation of enantiomers was achieved, the *R* enantiomer was always eluted before the *S* enantiomer.

Influence of uncharged modifier

Organic solvents of different character affect the enantioselectivity differently: their adsorption changes the conformation of the α_1 -glycoprotein, and a "new" chiral phase is created by a simple adjustment of the mobile phase¹⁴. Table I summarizes the influence of different uncharged organic solvents in the mobile phase (4% methanol, ethanol, 2-propanol or acetonitrile) on the retention behaviour and the enantioselectivity. With alcohols the capacity factors decrease inversely with their hydrophobicity: the *R* and *S* enantiomers are eluted by 2-propanol ($\alpha = 1.03$) and not eluted by ethanol and methanol. The addition of alcohols reduces the retention, but these alcohols often reduce the chiral selectivity¹⁵. With 4% acetonitrile as organic solvent the capacity factors are higher than those obtained with 2-propanol, but the separation factor is better ($\alpha = 1.17$). In a series of experiments, other mobile phases with different percentage of modifiers were tested. The enantioselectivity was generally better with acetonitrile. Therefore, the resolution of alfuzosin enantiomers was optimized with acetonitrile as organic solvent.

TABLE I

INFLUENCE OF UNCHARGED MODIFIERS

Mobile phase, modifier–0.01 *M* KH₂PO₄ (pH 7.0) (4:96, v/v).

<i>Modifier</i>	k'_R	k'_S	α
2-Propanol	8.5	8.8	1.03
Acetonitrile	12.4	14.5	1.17
Methanol	Not eluted	Not eluted	–
Ethanol	Not eluted	Not eluted	–

Influence of a charged modifier (TBA) and of pH

Fig. 2 shows the effects of pH and a cationic modifier, TBA, of the mobile phase on the capacity factors (Fig. 2a) and on the resolution (Fig. 2b) of alfuzosin enantiomers with a mobile phase of 0.05 *M* buffer–acetonitrile (94:6, v/v), with 0.025 *M* TBA or without TBA.

The influence of pH is more drastic than the effect of the cationic modifier. At pH 7 the resolution is insufficient ($R = 0.8$) with or without TBA in the mobile phase. The capacity factor and the resolution improve with increase in pH. A slight change in pH affects the resolution. The latter increases from 0.8 to 1.3–1.4 when the pH increases 7.0 to 7.4. A pH of 7.4 was chosen for the separation of alfuzosin enantiomers.

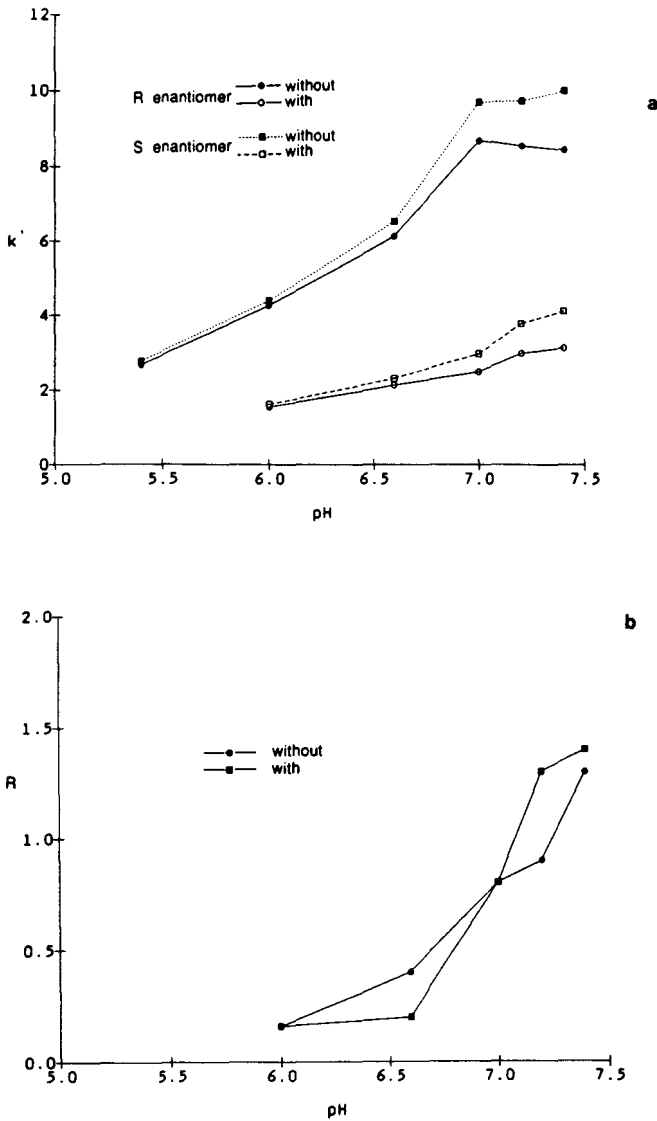


Fig. 2 Effect of pH on (a) the capacity factor (k') and (b) the resolution (R). Eluent, 0.05 M buffer-acetonitrile (94:6, v/v) with or without 0.025 M TBA.

The addition of TBA to the mobile phase enhances the resolution. In particular, it achieves enantioselectivity after 7 min ($k'_S = 4.1$ at pH 7.4). Without TBA, the capacity factors are too high. Under the same conditions at pH 7.4, k'_R decreases from 8.4 to 3.1 when TBA is added to the mobile phase, whereas the resolution is slightly improved from 1.3 to 1.4. Generally, the retention of the cationic solutes is significantly decreased by addition of a cationic modifier, but the enantioselectivity is almost unaffected¹⁴.

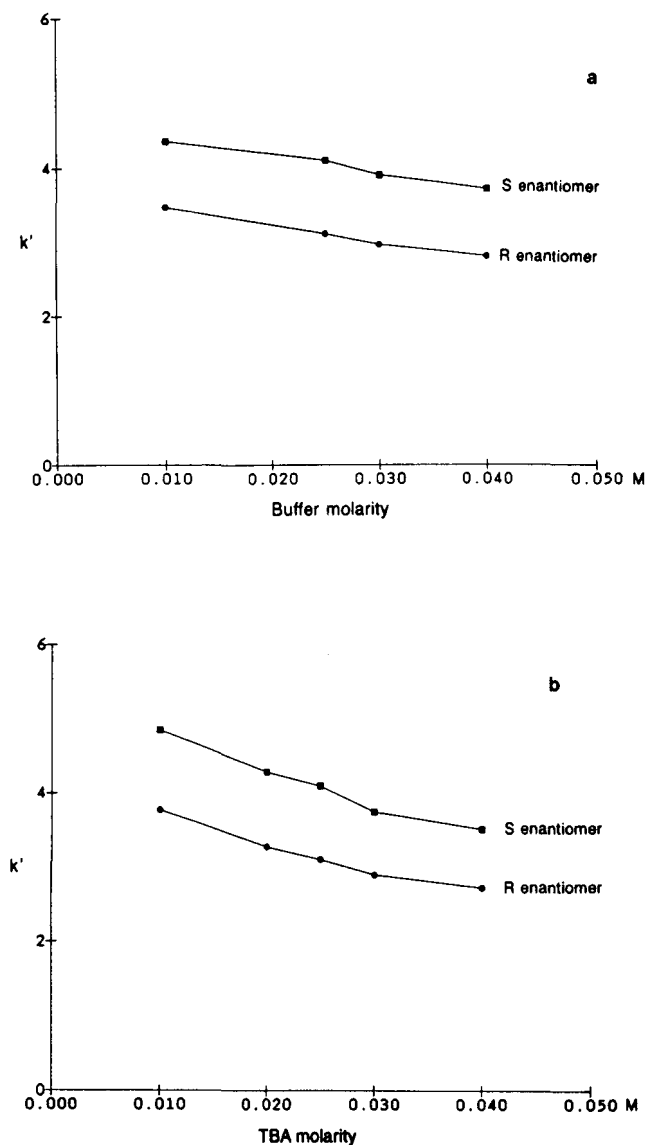


Fig. 3. (a) Effect of buffer molarity on the capacity factor (k'). TBA concentration 0.025 M. (b) Effect of TBA concentration on the capacity factor (k'). Final buffer molarity, 0.05 M. Eluent, phosphate buffer (pH 7.4) containing TBA–acetonitrile (94:6, v/v).

Influence of ionic strength

Fig. 3 illustrates the effects of buffer and TBA molarity on the capacity factors of the two isomers. The latter decreases in parallel with the buffer and TBA molarity, but these effects are not drastic; the enantioselectivity is almost unaffected. Under the analytical conditions [phosphate buffer (pH 7.4) containing 0.025 M TBA–acetonitrile (94:6; v/v)], k'_S decreases from 4.4 to 3.7 when the buffer molarity increases

from 0.01 to 0.04 *M*, the TBA molarity being constant (0.025 *M*). When the total molarity of the mobile phase is kept constant (0.05 *M*), k'_S decreases from 4.8 to 3.5 as the TBA molarity increases from 0.01 to 0.04 *M*.

The final composition of the mobile phase, established through the influence of these different parameters was 0.025 *M* KH₂PO₄-K₂HPO₄ buffer (pH 7.4) containing 0.025 *M* TBA-acetonitrile (94:6, v/v). The retention times of (*R*)- and (*S*)-alfuzosin and the internal standard were 5.32, 6.58 and 9.75 min, respectively, at a flow-rate of 0.9 ml/min. The values for the separation factor (α) and resolution were 1.35 and 1.45, respectively.

Assay validation

R and *S* enantiomer plasma control samples (5 and 25 ng/ml) were assayed four times by two analysts on two different days. The precision and accuracy of the method for these two concentrations are shown in Table II. The analytical recoveries of alfuzosin enantiomers in 20 plasma samples spiked with 5 and 25 ng/ml were identical for the two enantiomers, averaging 106% (5 ng/ml) and 105% (25 ng/ml). The R.S.D. was identical for both isomers, *ca.* 5 and 3% at 5 and 25 ng/ml, respectively.

TABLE II
SENSITIVITY LIMITS, PRECISION AND ACCURACY OF THE METHOD

Enantiomer	Sensitivity limit (ng/ml)	Accuracy and reproducibility (<i>n</i> = 20)			
		Theoretical concentration (ng/ml)	Mean observed concentration (ng/ml)	Difference from theoretical value (%)	Relative standard deviation (%)
<i>R</i>	1	5	5.28	+5.6	4.9
		25	26.12	+4.5	3.2
<i>S</i>	1	5	5.32	+6.4	5.1
		25	26.20	+4.8	2.9

Calibration graphs, weighted by the inverse of the concentration, were linear from 1 to 50 ng/ml for each isomer. The sensitivity limit, equal to the lowest point of the calibration (R.S.D. <10%; difference from the theoretical values <15%) was 1 ng/ml with fluorimetric detection. The quantitative yield of alfuzosin enantiomers in human plasma was $97.7 \pm 2.3\%$ (*n* = 5). Alfuzosin and its enantiomers were stable under our assay conditions.

The interference with the HPLC assay of other drugs that might be administered with alfuzosin in human therapy was investigated. The retention times of these compounds, listed in Table III, indicate that they would not interfere with the alfuzosin enantiomers. However, zolpidem was found to be eluted near the internal standard.

Routine analysis

The method was used in routine analysis for the determination of alfuzosin enantiomers in biological fluids, and tested by the assay of control samples (10 and 50 ng/ml of alfuzosin, *i.e.*, 5 and 25 ng/ml for each isomer) over several days. The mean

TABLE III
DRUGS TESTED FOR POSSIBLE INTERFERENCE

<i>Compound</i>	<i>Retention time (min)^a</i>	<i>Compound</i>	<i>Retention time (min)^a</i>
Metoprolol	—	Enalapril	—
Betaxolol	—	Captopril	—
Propranolol	—	Furosemide	2.0
Diazepam	—	Zolpidem	9.16
(<i>R</i>)-Alfuzosin	5.5	Piroxicam	—
(<i>S</i>)-Alfuzosin	6.8	Warfarin	—
Internal standard	10.01		

^a — Not eluted and/or not detected.

values found were 10.6 and 52.0 ng/ml ($n = 36$) with R.S.D. 4.6 and 3.0%, respectively.

Pharmacokinetic study

The method was applied to the preliminary evaluation of the pharmacokinetic profile of the *R* and *S* enantiomers in six healthy volunteers after a single intravenous dose of 5 mg of alfuzosin. Chromatograms of 1 ml of blank plasma extract and 1 ml of plasma extract, obtained from a healthy volunteer 20 min after intravenous administration, are shown Fig. 4. Blank plasma samples were free from endogenous contaminants at the retention times corresponding to alfuzosin enantiomers and the in-

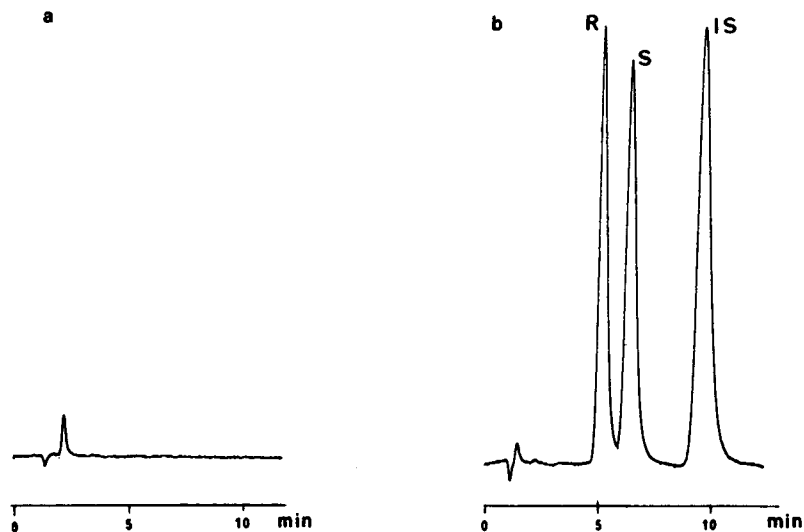


Fig. 4. Typical chromatograms of (a) blank plasma extract and (b) plasma extract obtained from a healthy volunteer, 20 min following a single intravenous administration of 5 mg of alfuzosin. Chromatographic conditions: column, 100 × 4 mm I.D., chiral-AGP, 5 μ m; mobile phase, 0.025 *M* KH_2PO_4 - K_2HPO_4 containing 0.025 *M* TBA (pH 7.4)-acetonitrile (94:6, v/v); flow-rate, 0.9 ml/min; detection, $\lambda_{\text{ex}} = 265$ nm, $\lambda_{\text{em}} = 400$ nm.

TABLE IV

MEAN PHARMACOKINETIC PARAMETERS ($n = 6$) OF *R* AND *S* ENANTIOMERS OBTAINED IN SIX HEALTHY VOLUNTEERS AFTER INTRAVENOUS ADMINISTRATION OF 5 mg OF ALFUZOSIN BY PERFUSION OVER A 30-min PERIOD

$t_{1/2}(\beta)$ = Terminal half-life; AUC = area under curve; Cl = systematic clearance; Vd = distribution volume.

	$t_{1/2}(\beta)$ (h)		AUC (ng/ml/h)		Cl (l/h/kg)		Vd (l/kg)	
	<i>R</i>	<i>S</i>	<i>R</i>	<i>S</i>	<i>R</i>	<i>S</i>	<i>R</i>	<i>S</i>
Mean	3.6	2.5	76.9	54.5	0.465	0.649	2.35	2.33
Standard error	0.3	0.1	7.7	4.3	0.027	0.037	0.10	0.12

ternal standard. The mean plasma concentration *versus* time curves for (*R*)- and (*S*)-alfuzosin after intravenous administration of the racemate shows that the pharmacokinetic profiles of the *R* and *S* enantiomers are different.

The pharmacokinetic parameters (terminal half-life, area under curve, clearance, distribution volume) were calculated with the PHARM program¹⁶ and are reported in Table IV. The *R* and *S* isomers are eliminated from the central compartment with terminal half-lives of 3.6 ± 0.6 and 2.5 ± 0.3 h, respectively. In the same way, the area under the time *versus* concentration curve for the *R* isomer was larger than that for the *S* isomer. There was no difference in the distribution volume.

CONCLUSIONS

As the amine function of alfuzosin is far from the chiral centre, the two chiral centres of diastereomers formed with chiral reagents are too far apart to allow the resolution of the diastereomers by reversed-phase chromatography¹. Direct resolution of alfuzosin enantiomers has been achieved on a new chiral AGP column. The present HPLC method is rapid, sensitive (1 ng/ml for each isomer) and was found to be suitable for the simultaneous determination of alfuzosin enantiomers in plasma after intravenous administration of the racemate (5 mg) to healthy volunteers.

The column performance decreased after the injection of 250 extracted plasma samples. As the mobile phase contained a small amount of organic solvent, no pre-column could be used to protect the column. However, the efficiency can be restored by repacking the first few millimeters of the stationary phase and then each column allows the analysis of *ca.* 500 samples.

REFERENCES

- 1 C. Pettersson, *Eur. Chromatogr. News*, 2, No 4 (1988) 16.
- 2 D. W. Armstrong, *Anal. Chem.*, 59 (1987) 84A.
- 3 A. Krstulovic, *J. Chromatogr.*, 488 (1988) 53.
- 4 D. E. Drayer, *Ther. Drug Monit.*, 10 (1988) 1.
- 5 D. Sanchez, P. Möller, S. Einarsson and B. Josefsson, *Janssen Chim. Acta*, 6 (1988) 6.
- 6 S. Einarsson, B. Josefsson, P. Möller and D. Sanchez, *Anal. Chem.*, 59 (1987) 1191.
- 7 D. Schuster, M. Woodruff Modi, D. Lalka and F. M. Gengo, *J. Chromatogr.*, 433 (1988) 318.

- 8 A. Darmon and J. P. Thénot, *J. Chromatogr.*, 374 (1986) 321.
- 9 Y. Gietl, H. Spahn and E. Mutschler, *J. Chromatogr.*, 426 (1988) 305.
- 10 J. Gal and R. C. Murphy, *J. Liq. Chromatogr.*, 7 (1984) 2307.
- 11 A. J. Sedman and J. Gal, *J. Chromatogr.*, 278 (1983) 199.
- 12 K. J. Miller, J. Gal and M. M. Ames, *J. Chromatogr.*, 307 (1984) 335.
- 13 I. Hermansson, paper presented at the *1st International Symposium on the Separation of Chiral Molecules, Paris, May 31–June 2, 1988*.
- 14 I. Hermansson, *AGP as a Chiral Selector in Chromatography, Technical Documentation*, ChromTech, Norsborg, 1989.
- 15 G. Schill, I. W. Wainer and S. A. Barkan, *J. Chromatogr.*, 365 (1986) 73.
- 16 R. Gomeni, *Comput. Biol. Med.*, 14 (1984) 25.

CHROMSYMP. 1736

Separation of the enantiomeric intermediates of some platelet-activating factor analogues on a naphthylalanine-type Pirkle column

P. L. CAMACHO, E. GEIGER and Gy. VIGH

Chemistry Department, Texas A and M University, College Station, TX 77843-3255 (U.S.A.)

and

R. WEBSTER and D. H. THOMPSON*

Department of Chemical and Biological Sciences, Oregon Graduate Institute of Science and Technology, Beaverton, OR 97006-1999 (U.S.A.)

SUMMARY

A chiral high-performance liquid-chromatographic separation method was developed for the analysis of some glycerol-based, ether-linked platelet-activating factor precursors. Using a D-naphthylalanine-type Pirkle-column and tetrahydrofuran–hexane eluents, the retention–structure relationships were determined for a large number of glycerol ether derivatives. The derivatives leading to the highest chiral selectivity factors in the analytical separations were surveyed for their applicability in large-scale isolation of chiral synthetic intermediates.

INTRODUCTION

Interest in ether-linked phospholipids has been steadily increasing over the last two decades¹, in part due to their well known platelet-activating, antihypertensive, antineoplastic and antiinflammatory properties^{2,3}. The synthetic pathways reported to date for the preparation of racemic^{4–6} or chiral ether lipids^{7–9}, however, are limited relative to the methodologies that have been developed for the synthesis of ester-linked phospholipids¹⁰. In the course of developing a new stereoselective synthesis of glycerol ether lipids from allylic alcohol precursors^{11,12}, a chiral analytical separation method was needed to monitor the stereospecificity of the reaction pathway. The method sought would also serve as the basis for the development of a preparative-scale isolation method to produce chiral materials from racemic mixtures of mono- and dialkylglycerolphosphate derivatives. If successful, this method would provide a facile, large-scale and low-cost route to these materials via nucleophilic ring-opening reactions of racemic glycidol esters¹¹ by aliphatic alcohols. An analogous route has been reported for the synthesis of chiral ether-linked phospholipids¹².

The 3,5-dinitrobenzoate (DNB) derivatives of several racemic mixtures of chiral alcohols were separated, though with low selectivity values, on naphthylalanine-type

Pirkle phases¹³. This paper reports our results of a retention–structure relationship study aimed at establishing the best analytical chiral selectivity for a set of glycerol derivatives the substituents of which allow further manipulation of the ether lipid structure.

EXPERIMENTAL

Materials

Solvents were obtained from E. M. Science (Gibbstown, NJ, U.S.A.) and were reagent grade or better. Glycidol, 1-hexadecanol, benzoyl chloride, acetyl chloride and 4-nitrobenzoyl chloride were obtained from Aldrich (Milwaukee, WI, U.S.A.). Cyclohexylcarbonyl chloride and 3-nitrobenzenesulfonyl chloride were purchased from American Tokyo Kasei (Portland, OR, U.S.A.). 3,5-Dinitrobenzoyl chloride (99.5 plus %) was supplied by Fluka (Ronkonkoma, NY, U.S.A.). Trifluoromethanesulfonic acid was obtained from 3M (St. Paul, MN, U.S.A.).

The reaction pathway used to prepare the compounds studied is shown in Fig. 1. The solutes, in most cases, were synthesized by 1% trifluoromethanesulfonic acid-catalyzed ring opening of glycidyl sulfonate or carboxylate esters¹¹ with a threefold excess of 1-hexadecanol at 65–75°C for 5 h in the absence of solvent. Alkylated glycerol silyl ethers were prepared similarly using 2% tropylium tetrafluoroborate as catalyst. The hexadecyl-derivatized material was isolated from the reaction mixture by column chromatography [25 g silica per g of crude reaction mixture; 70–230 mesh; mobile phase: hexane–ethyl acetate (3:1)], recrystallized from light

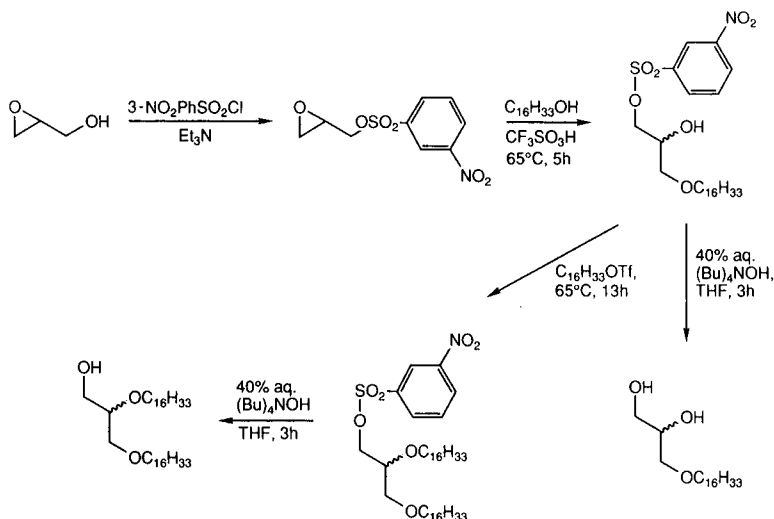


Fig. 1. Synthetic pathway for the preparation of mono- and dialkyl glycerol ethers from glycidyl 3-nitrobenzenesulfonate. Carboxylate esters were prepared in a similar fashion using the corresponding glycidyl carboxylate ester as starting material. DNB esters were prepared from the alcohol or diol precursor and DNB chloride. Ph = Phenyl; Et = ethyl; Bu = butyl; THF = tetrahydrofuran; aq. = aqueous; Tf = trifluoromethyl sulfonate.

petroleum (b.p. 37.2–57.8°C) ether, and characterized by NMR, Fourier transform (FT)-IR and mass spectrometry. Sulfonate ester cleavage was effected with a stoichiometric quantity of 40% aqueous tetrabutylammonium hydroxide in tetrahydrofuran to produce the free alcohols. DNB derivatives were prepared from these precursors in the usual manner prior to HPLC analysis¹³.

HPLC system

Separations were carried out with a custom-built liquid chromatograph assembled from a Model 2020 pump, Model 2050 variable-wavelength UV detector and Model RI 3 refractive index detector (all from Varian, Walnut Creek, CA, U.S.A.), a pneumatically controlled Model 7010 injection valve equipped with a 10- μ l sample loop (Rheodyne, Cotati, CA, U.S.A.), and a Maxima chromatographic work station (Millipore, Bedford, MA, U.S.A.).

Rexchrom 250 mm \times 4.6 mm I.D. columns, packed with 5- μ m D-naphthyl-alanine silica stationary phase (Regis, Morton Grove, IL, U.S.A.) and thermostated at 30°C [for the capacity factor (k') studies] by a circulating water bath (Science-Electronics, Dayton, OH, U.S.A.) were used to effect the chiral separations. Eluents were prepared from HPLC grade *n*-hexane and tetrahydrofuran (THF) (Fisher, Fair Lawn, NJ, U.S.A.) according to the gravimetric method¹⁴. The THF-hexane (10:90, v/v) eluent was found to give $0.5 < k' < 30$ values for all the solutes and was used throughout the experiments.

RESULTS AND DISCUSSION

The synthetic objectives of this study require that the intermediates contain a protecting group (X) that can be readily cleaved with retention of configuration at the asymmetric center while retaining favorable chiral selectivity for preparative scale separations. Chiral selectivity factors, peak resolution factors (R_s), and the k' values of the more strongly retained enantiomers (with *n*-heptane as the dead volume marker) for the materials studied are listed in Table I.

Compounds 1–9 in Table I represent leaving groups of differing overall polarity. It can be seen that solute retention increases significantly with the polarity of X (compounds 1–6). When the X groups have comparable polarities, secondary effects, such as size (compounds 2 vs. 3) may slightly alter the retention order. Comparison of the k' values of compounds 4 and 7 shows that when the two polar functional groups are in the 1,3 positions, rather than in the 1,2 positions, larger retention occurs. This agrees with a recent observation by Pirkle¹⁵, who noted that the retention of di(2,4-dinitrophenyl)- α,ω -alkyldiamines varied significantly as the length of the alkyl chain was varied, with maximum solute retention occurring when the chains contained four methylene units. They postulated that the two distant polar sites bind to two different strands of the chiral stationary phase, rather than to two sites on the same strand. This effect is believed to be operational here as well.

It also can be seen that the presence of a very polar, π -acidic functional group and the concomitant large retention alone is not sufficient to effect chiral recognition: the k' values of compounds 5 and 6 are almost identical, yet only the DNB functional group, believed to interact selectively with the naphthyl group of the stationary phase¹³, will lead to noticeable chiral recognition. Since the α value is only 1.02, even

TABLE I

CAPACITY FACTOR (k'), CHIRAL SELECTIVITY (α) AND PEAK RESOLUTION (R_s) DATA FOR THE 1-X-2-Y-3-Z-GLYCEROL DERIVATIVES

Stationary phase: D-naphthylalanine silica; eluent: THF-hexane (10:90, v/v); temperature: 30°C.

No.	X	Y	Z	k'_2 ^a	α	R_s
1	H	H	C ₁₆ H ₃₃	0.35	1	0
2	COC ₆ H ₅	H	C ₁₆ H ₃₃	0.52	1	0
3	COCH ₃	H	C ₁₆ H ₃₃	0.55	1	0
4	COC ₆ H ₄ -4-(NO ₂)	H	C ₁₆ H ₃₃	1.0	1	0
5	COC ₆ H ₃ -3,5-(NO ₂) ₂	H	C ₁₆ H ₃₃	2.08	1.02	0.5
6	SO ₂ C ₆ H ₄ -3-(NO ₂)	H	C ₁₆ H ₃₃	2.11	1	0
7	COC ₆ H ₄ -4-(NO ₂)	C ₁₆ H ₃₃	H	1.15	1	0
8	SO ₂ C ₆ H ₄ -3-(NO ₂)	C ₁₆ H ₃₃	C ₁₆ H ₃₃	0.46	1	0
9	COC ₆ H ₃ -3,5-(NO ₂) ₂	C ₁₆ H ₃₃	C ₁₆ H ₃₃	0.93	1.01	0.3
10	COC ₆ H ₁₁	COC ₆ H ₃ -3,5-(NO ₂) ₂	C ₁₆ H ₃₃	1.84	1.02	0.4
11	COCH ₃	COC ₆ H ₃ -3,5-(NO ₂) ₂	C ₁₆ H ₃₃	2.61	1.02	0.4
12	COC ₆ H ₅	COC ₆ H ₃ -3,5-(NO ₂) ₂	C ₁₆ H ₃₃	2.81	1.02	0.4
13	COC ₆ H ₄ -4-(NO ₂)	COC ₆ H ₃ -3,5-(NO ₂) ₂	C ₁₆ H ₃₃	6.85	1.05	0.9
14	SO ₂ C ₆ H ₄ -3-(NO ₂)	COC ₆ H ₃ -3,5-(NO ₂) ₂	C ₁₆ H ₃₃	16.59	1.02	0.7
15	COC ₆ H ₃ -3,5-(NO ₂) ₂	COC ₆ H ₃ -3,5-(NO ₂) ₂	C ₁₆ H ₃₃	31.38	1.06	1.3
16	COC ₆ H ₁₁	C ₁₆ H ₃₃	COC ₆ H ₃ -3,5-(NO ₂) ₂	2.36	1.01	0.3
17	COCH ₃	C ₁₆ H ₃₃	COC ₆ H ₃ -3,5-(NO ₂) ₂	3.23	1.02	0.4
18	COC ₆ H ₄ -4-(NO ₂)	C ₁₆ H ₃₃	COC ₆ H ₃ -3,5-(NO ₂) ₂	8.76	1.01	0.3

^a k'_2 = Capacity factor of the more retained enantiomer.

with the DNB group, an analytically useful separation requires the use of columns with comparatively large plate numbers (two 250-mm columns in series, operated at a flow-rate of 0.5 ml/min and temperature of 15°C). The chromatogram, which can be completed in less than 1 h represents a possible, though certainly not optimum solution of the separation problem.

Compounds 8 and 9, the dialkyl ethers, are the most desirable compounds for further synthetic work. The presence of a second hexadecyl ether group in position 2, however, greatly reduces the retention of the solutes regardless of whether the leaving group is the 3-nitrobenzenesulfonate (NBS) or the DNB group. The second hexadecyl ether group in position 2 also greatly diminishes the extent of chiral recognition offered by the DNB group. Therefore, though synthetically attractive, these solutes cannot be used to achieve the final goals of this study.

An alternative approach requires the attachment of a chiral selectivity-enhancing leaving group first, followed by epoxide ring opening (Fig. 1) and derivatization of the resulting hydroxy group in position 2 with DNB to effect chiral resolution. Chiral selectivity might be sufficiently increased by judicious choice of intermolecular interactions and synthetic utility of the leaving group. Compounds 10–15 were synthesized to test this possibility.

It can be seen in Table I that with a DNB group in position 2, retention again increases rapidly as the polarity of the leaving group is increased. Just as with the hydroxy group in position 2, the change of X from benzoate to 4-nitrobenzoate (NB) results in an almost twofold increase in retention, as does the change from NB to NBS.

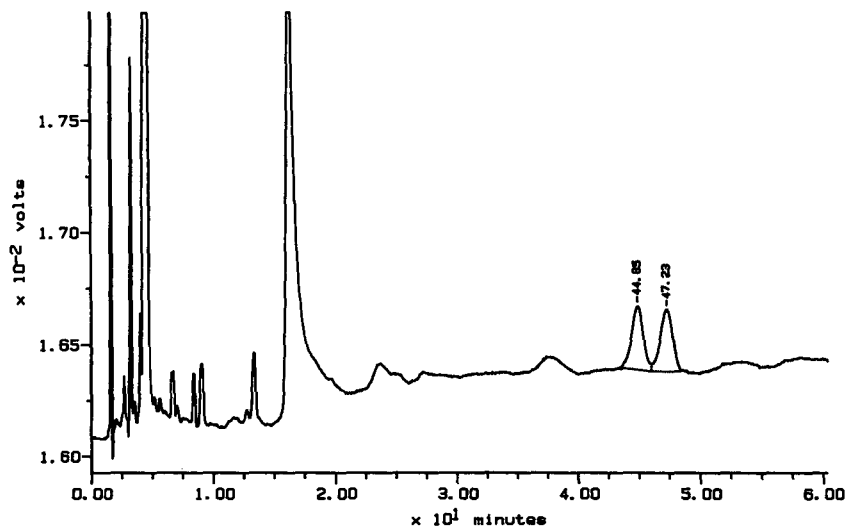


Fig. 2. Chromatogram of compound 15. Conditions: 250 mm \times 4.6 mm I.D. Rexchrom D-naphthylalanine column; THF-hexane (10:90, v/v) eluent; flow-rate: 2.0 ml/min; temperature: 30°C; detection (UV): 205 nm. Peaks at 44.85 and 47.23 min: enantiomers of compound 15.

However, unlike in the case of compounds 5 and 6, where NBS and DNB substitution lead to identical increases in retention, the addition of DNB to position 1 results in an almost twofold increase in k' (compare compounds 14 vs. 15).

The chiral selectivity values for the cyclohexylcarboxylate, acetate and benzoate derivatives (compounds 10, 11 and 12) are as low (1.02) as that of the mono-DNB derivative, compound 5, indicating that the lower polarity of these auxiliaries brings no improvement in the separation. The situation is much more favorable, however, with both the NB and the DNB functional groups: chiral selectivity increases to 1.05 and 1.06 for compounds 13 and 15, respectively. These selectivities are sufficiently large to afford baseline-baseline resolution of the enantiomers of compound 15 on a single 250-mm column, even with an eluent flow-rate as high as 2 ml/min (Fig. 2). The separation of compound 15, which can be completed in less than 1 h, promises to be slightly better for preparative work than compound 13; however, the different protecting groups of compound 13 provide greater regiochemical control of the reaction products.

When the DNB substituent is moved to position 3 and the hexadecyl ether group to position 2 (compounds 16-18), solute retention increases, presumably due to multistrand binding, as in the case of compounds 4 and 7. However, it can also be seen that multistrand binding decreases the chances of chiral resolution (which is based on sterically localized interactions), and equal or lower chiral selectivity values are obtained for each pair (compounds 10 vs. 16, 11 vs. 17 and 13 vs. 18).

CONCLUSIONS

Based on the structure-retention relationships of the glycerol ether derivatives reported here, it can be concluded that:

(i) The presence of a 3,5-dinitrobenzoate functional group is mandatory for chiral resolution.

(ii) Solute retention increases with the polarity of the second polar group in the order: hexadecyl ether < alcohol < cyclohexylcarboxylate < acetate < benzoate < 4-nitrobenzoate < 3,5-dinitrobenzoate < 3-nitrobenzenesulfonate.

(iii) Chiral selectivity is highest when the second functional group is either the 3,5-dinitrobenzoate or the 4-nitrobenzoate group.

(iv) Chiral selectivities are identical for the 1-(3,5-dinitrobenzoate)-2-X and the 1-X-2-(3,5-dinitrobenzoate) derivatives.

(v) Solute retention is larger and chiral selectivity is lower with the 3,5-dinitrobenzoate group and the second polar functional group in the 1,3 positions *versus* the 1,2 positions.

(vi) Both solute retention and chiral selectivity are greatly diminished for the dialkyl ether derivatives, even with the 3,5-dinitrobenzoate group in position 1.

Work is under way in our laboratories using compounds 5, 13 and 15 to determine their adsorption isotherms and develop viable preparative separation methods to further their synthetic utility.

ACKNOWLEDGEMENTS

Financial support by the Texas Coordinating Board of Higher Education TATR Program (Grant Number 3376) (Gy. V.) and the Medical Research Foundation of Oregon (Grant No. 19890821) (D. T.) is acknowledged. The authors are grateful to M. Huggler and M. J. Roberts of Varian for the loan of some of the equipment used in this study.

REFERENCES

- 1 W. J. Baumann, in F. Snyder (Editor), *Ether Lipids: Chemistry and Biology*, Academic Press, New York, 1972, p. 51.
- 2 L. A. Horrocks and M. Sharma, in W. Hawthorne and G. B. Ansell (Editors), *Phospholipids*, Elsevier, Amsterdam, 1982, p. 51.
- 3 F. Snyder, *Med. Res. Rev.*, 5 (1985) 107.
- 4 F. Paultauf, in H. K. Mangold and F. Paultauf (Editors), *Ether Lipids: Biochemical and Biomedical Aspects*, Academic Press, New York, 1983, p. 211.
- 5 H. Eibl, *Chem. Phys. Lipids*, 26 (1980) 405.
- 6 A. Wissner, R. E. Schaub, P. E. Sum, C. A. Kohler and B. H. Goldstein, *J. Med. Chem.*, 28 (1985) 1181.
- 7 G. Hirt and R. Barner, *Helv. Chim. Acta*, 65 (1980) 1059.
- 8 T. Aoki and C. D. Poulter, *J. Org. Chem.*, 50 (1985) 5634.
- 9 S. K. Bhatia and J. Hajdu, *Tetrahedron Lett.*, 28 (1987) 271.
- 10 R. Radhakrishnan, R. J. Robson, Y. Takagaki and H. G. Khorana, *Methods Enzymol.*, 72 (1981) 408.
- 11 C. B. Svendsen, V. C. Anderson and D. H. Thompson, *J. Org. Chem.*, submitted for publication.
- 12 P. N. Guivisdalsky and R. Bittman, *J. Am. Chem. Soc.*, 111 (1989) 3077.
- 13 W. H. Pirkle, T. C. Pochapsky, G. S. Mahler, D. E. Corey, D. S. Reno and D. M. Alessi, *J. Org. Chem.*, 51 (1986) 4991.
- 14 A. Bartha and Gy. Vigh, *J. Chromatogr.*, 260 (1983) 337.
- 15 W. H. Pirkle, personal communication, 1989.

CHROMSYMP. 1824

High-performance liquid chromatographic resolution of racemic 1,4-benzodiazepin-2-ones by means of a β -cyclodextrin silica bonded chiral stationary phase

C. BERTUCCI

Centro Studio CNR Macromolecole Stereordinate ed Otticamente Attive, Dipartimento di Chimica e Chimica Industriale, Università di Pisa, Via Risorgimento 35, 56126-Pisa (Italy)

E. DOMENICI

Scuola Normale Superiore, P.za dei Cavalieri 7, 56100-Pisa (Italy)

and

G. UCCELLO-BARRETTA and P. SALVADORI*

Centro Studio CNR Macromolecole Stereordinate ed Otticamente Attive, Dipartimento di Chimica e Chimica Industriale, Università di Pisa, Via Risorgimento 35, 56126-Pisa (Italy)

SUMMARY

A bonded β -cyclodextrin chiral stationary phase was used for the chromatographic resolution of a series of 1,4-benzodiazepin-2-ones (BDZs). This column can also be employed for the direct resolution of ionic BDZs as the hemisuccinate esters of 3-hydroxy-BDZs. Nuclear magnetic resonance spectroscopy was used to obtain preliminary information on the mechanism of chiral discrimination.

INTRODUCTION

In terms of prescribed volume, anxiolytic agents are one of the most important classes of drugs. By far the most widely used subgroup of anxiolytics are the 1,4-benzodiazepin-2-ones (BDZs)¹, several of which are chiral. Accordingly, stereochemical aspects of this group have received wide attention, in relation to both the chromatographic resolution of enantiomers²⁻⁵ and also pharmacological studies on the individual isomers⁶⁻⁹. For 3-hydroxy-BDZs (which account for the majority of the therapeutically used chiral BDZs), the pure enantiomers cannot be easily recovered because they undergo racemization in aqueous medium^{10,11}. Therefore, the relationship between their stereochemistry and pharmacological activity has been not investigated. Several studies have been reported on the enantioselective interaction of the esters of 3-hydroxy-BDZs with the receptor binding site^{12,13}.

BDZs are known to interact with cyclodextrins¹⁴. Evidence for their stereoselective complexation arises from the induced circular dichroism observed in the 1:1 complex between β -cyclodextrin and an achiral or a racemic BDZ¹⁵. This observation prompted us to use a β -cyclodextrin-based chiral stationary phase (CSP)¹⁶ for the

chromatographic resolution of several chiral members of this important class of compounds. The commercially available CSP Cyclobond I was efficient in the chromatographic resolution of several chiral BDZs, the enantiomeric separation of which, on other CSPs, has been previously reported²⁻⁵. For the first time, resolution was obtained for ionic BDZs, *i.e.*, the hemisuccinate esters of 3-hydroxy-BDZs. Simultaneous monitoring of the related hydrolysis product was also achieved. In addition, separation of the enantiomers ($\alpha = 1.1$) was observed for two BDZs (uxepam and dihydrodiazepam), which are chiral by virtue of an asymmetrically substituted C-5 carbon atom. Finally, a preliminary NMR study was carried out using an aqueous solution of β -cyclodextrin and the hemisuccinate esters of 3-hydroxy-BDZs as a model for the chromatographic system.

EXPERIMENTAL

Chromatographic separation

The chromatographic separations were carried out with a Jasco Twincle apparatus connected to a Jasco Uvidec 100 variable-wavelength UV detector. Circular dichroism (CD) detection was provided by a Jasco J-500C spectropolarimeter equipped with a high-performance liquid chromatographic (HPLC) micro-cell and a doublet of lenses to focus the light beam in the sample compartment^{3,17}. The two detectors were connected in series and both used at a fixed wavelength (254 nm). The measurements were carried out using mixtures of acetonitrile and acetate buffer (pH 4.2, 200 mM), or acetonitrile and phosphate buffer (pH 7.0, 100 mM) mixtures, at an isocratic flow-rate of 0.5 or 1 ml/min. A Cyclobond I column (25 \times 0.46 cm I.D.) from Astec (Whippany, NJ, U.S.A.) was used for all the measurements, which were performed at room temperature. The solvents were HPLC-grade chemicals and were filtered and degassed before use.

Instrumentation

¹H NMR spectra were recorded on a Varian VXR-300 spectrometer operating at 300 MHz. All measurements were carried out in ²H₂O solution at p²H 7 and at 22°C.

Mass spectra were obtained using a VG 70-70E instrument. Melting points were determined with a Reichert Thermovar apparatus, and were uncorrected.

Preparation of the compounds

Compound **1**, **2** and **3** (see Fig. 1) were obtained by Soxhlet extraction (acetone) of commercial pharmaceutical formulations. The products obtained were characterized by NMR and mass spectrometry. The data were in accordance with the expected structure¹⁸.

Compounds **4**, **5** and **10-13** were kindly provided by Prof. W. H. Pirkle (School of Chemical Sciences, University of Illinois at Urbana-Champaign, U.S.A.). Compounds **6**, **7** and **8** were prepared by acylation of **1**, **2** and **3**, respectively, with succinic anhydride in the presence of pyridine, according to the reported procedure for **6**¹⁹. The experimental conditions were changed for the recovery of the crude **6**, **7** and **8**. These compounds were extracted with chloroform from the hydrolysis mixtures and then recrystallized from ethyl acetate-hexane (1:1, v/v). Compounds **6**, **7** and **8** were

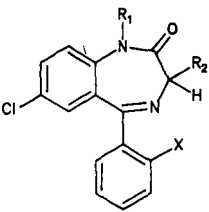
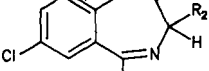
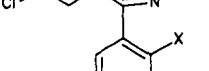
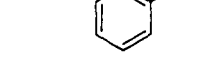


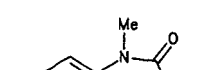
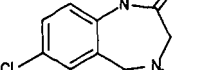
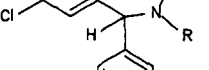
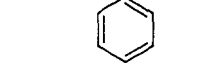
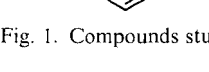
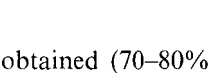
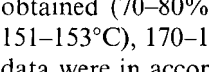
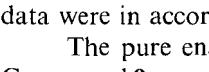
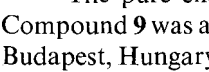
	R ₁	R ₂	X
	H	OH	H
	Me	OH	H
	H	OH	Cl
	H	OCOMe	H
	H	OCOBu ^t	H
	H	OCO(CH ₂) ₂ COOH	H
	Me	OCO(CH ₂) ₂ COOH	H
	H	OCO(CH ₂) ₂ COOH	Cl
	H	OCOMe	Cl
	H	Me	H
	Me	Me	H
	H	Pr ⁱ	H
	H	NEt ₂	H
		R	
		CONH ₂	

Fig. 1. Compounds studied. Me = Methyl; Bu^t = *tert.*-butyl; Prⁱ = isopropyl; Et = ethyl.

obtained (70–80% yield) as the crystalline powder having m.p. 152–154°C (lit.¹⁹, 151–153°C), 170–172°C and 184–186°C, respectively. NMR and mass spectrometric data were in accordance with the structure.

The pure enantiomers of **6** were kindly provided by Ravizza (Milan, Italy). Compound **9** was a gift from Dr. E. Simon-Trompler (Central Institute for Chemistry, Budapest, Hungary). Compounds **14** and **15** were kindly provided by Chemical Works Gedeon Richter (Budapest, Hungary).

RESULTS AND DISCUSSION

Chromatographic data

The results for the resolution of **1–15** on Cyclobond I are reported in Tables I and II. Fig. 2 shows the separations of **5** and **15** as representative examples. Separation factors (α) up to 1.20 (Tables I and II) were observed for most of the compounds examined. The resolution was poor for **2**, **3** and **7** (Tables I and II): a broad peak was observed using the UV detection, whereas CD detection provided evidence of partial resolution and allowed the assignment of the elution order on the basis of the CD sign at 254 nm³. No resolution at all was obtained for **8**, **9**, **11** and **12**.

Several observations can be made regarding these results. Oxazepam (**1**) and its 3-ester derivatives (**4–6**) are well resolved (Table I). A relatively high on-column load (5–10 μ g) was employed in order to monitor the CD signal and then to obtain direct stereochemical information. The efficiency of the CSP is affected by the on-column load and, under the experimental conditions adopted, resolution factors of 0.69 and

TABLE I

CHROMATOGRAPHIC RESOLUTION DATA ON CYCLOBOND I WITH ACETONITRILE-ACETATE BUFFER (pH 4.2) AS ELUENT AT 20°C

<i>Compound</i>	<i>Eluent (v/v)</i>	k'_1	α	<i>CD</i> ^a
1	15:85	2.5	1.17	—
2	10:90	5.0	1.0	—
3	10:90	4.9	1.0	—
4	10:90	4.0	1.15	—
5	15:85	10.2	1.15	—
6	15:85	4.9	1.08	—
7	15:85	6.6	1.0	—
8	15:85	7.6	1.0	—
9	15:85	2.7	1.0	—
10	10:90	6.6	1.04	—
11	10:90	8.5	1.0	—
12	10:90	13.2	1.0	—
13	10:90	2.7	1.05	—
14	10:90	3.5	1.08	+
15	10:90	6.0	1.10	+

^a Sign of the CD at 254 nm for the first-eluted enantiomer.

0.75 were obtained for **5** (Fig. 2a) and **6** (Fig. 3), respectively. However, a baseline resolution can be achieved by using a one-tenth on-column load.

Temazepam (**2**) and its hemisuccinate ester (**7**) (which differ from the oxazepam analogues in that they have a methyl group in place of the hydrogen atom at N-1), exhibit only partial chiral resolution on this CSP; separation is observed only by application of CD detection (Table I).

Lorazepam (**3**) and its 3-ester derivatives (**8** and **9**) show no chiral resolution at all on this CSP. The structure of these analytes differs from that of the corresponding oxazepam analogues in the presence of a chlorine atom at C-2' of the benzene ring linked at C-5 (Fig. 1).

TABLE II

CHROMATOGRAPHIC RESOLUTION DATA ON CYCLOBOND I WITH ACETONITRILE-PHOSPHATE BUFFER (pH 7.0) AS ELUENT AT 20°C

<i>Compound</i>	<i>Eluent (v/v)</i>	k'_1	α	<i>CD</i> ^a
1	90:10	4.0	1.20	—
5	90:10	22.5	1.14	—
6	90:10	3.6	1.10	—
	95:5	8.8	1.12	—
7	90:10	4.4	1.0	—
	95:5	12.3	1.0	—
8	90:10	4.3	1.0	—
	95:5	11.6	1.0	—
14	90:10	5.5	1.10	+
15	90:10	5.3	1.11	+

^a Sign of the CD at 254 nm for the first-eluted enantiomer.

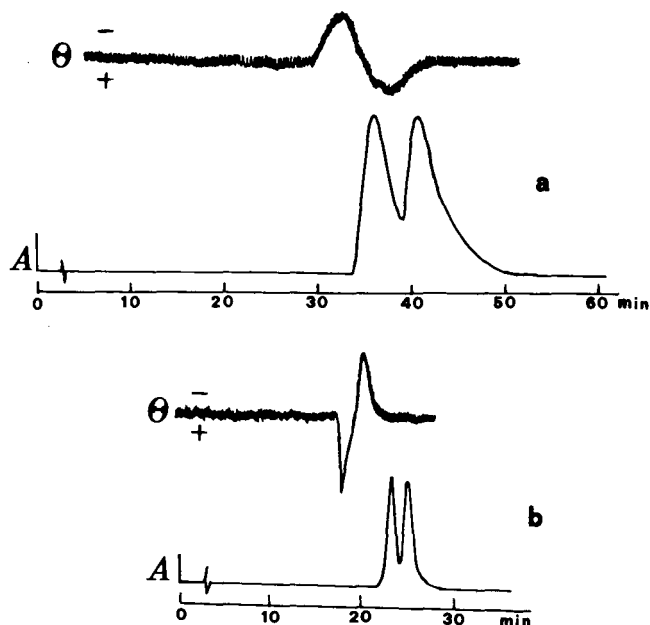


Fig. 2. Enantiomeric separation of **5** (a) (resolution, $R_s = 0.69$) and **15** (b) ($R_s = 0.75$) on Cyclobond I. UV (A) and CD (θ) detection at 254 nm. Eluent, acetonitrile-acetate buffer, pH 4.2 (15:85, v/v) (a) or (10:90, v/v) (b); 1 ml/min flow-rate.

1,4-BDZs which have the asymmetric carbon at the 5-position (dihydrodiazepam, **14** and uxezam, **15**) are resolved on the β -cyclodextrin-based CSP (Table I). The first-eluted enantiomers of **14** and **15** have a positive CD at 254 nm and correspond to (+)-(*S*)-dihydrodiazepam and (+)-(*R*)-uxepam, respectively. Interestingly, they adopt the same conformation of the seven-membered BDZ ring²⁰.

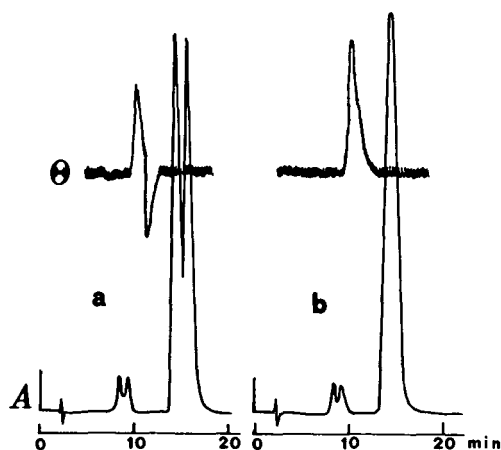
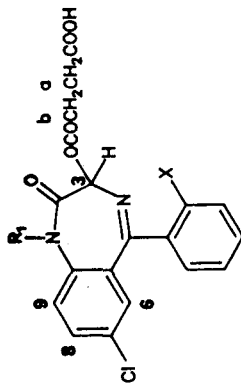


Fig. 3. Enantiomeric separation of **6** (a) ($R_s = 0.75$) and analysis of (*R*)-(-)-**6** (b) on Cyclobond I. UV (A) and CD (θ) detection at 254 nm. Eluent, acetonitrile-acetate buffer, pH 4.2 (15:85, v/v), 1 ml/min flow-rate.

TABLE III
 VARIATION OF THE ^1H NMR CHEMICAL SHIFTS OF THE TWO ENANTIOMERS OF **6**, **7** AND **8** (5 mM) INDUCED BY INTERACTION WITH β -CYCLODEXTRIN (10 mM), $^2\text{H}_2\text{O}$ SOLUTION, PHOSPHATE BUFFER, p²H 7.0



6: R₁ = H; X = H
7: R₁ = CH₃; X = H
8: R₁ = H; X = Cl

Proton	6 ^a		7		8	
	$\Delta\delta(+)$	$ \delta(+)-\delta(-) $	$\Delta\delta(-)$	$ \delta(+)-\delta(-) $	$\Delta\delta(+)$, $\Delta\delta(-)^b$	$ \delta(+)-\delta(-) $
a	-0.014	0.011	-0.003	0	+0.003, +0.003	0
b	+0.053	0.005	+0.024, +0.033	0.009	+0.021, +0.021	0
3	-0.013	0	-0.031, -0.023	0.008	N.d., N.d.	0
6	-0.109	0.009	-0.083, -0.073	0.010	-0.048, -0.062	0.014
8	+0.065	0.030	+0.033, +0.043	0.010	+0.042, -0.035	0.007
9	+0.088	0.036	N.d., N.d.	0.012	+0.048, +0.056	0.008
CH ₃			+0.030, +0.042			

^a $\Delta\delta(+)$ = $\delta(\text{complexed}) - \delta(\text{free})$ for the (+)-enantiomer; $\Delta\delta(-)$ = $\delta(\text{complexed}) - \delta(\text{free})$ for the (-)-enantiomer; $|\delta(+)-\delta(-)|$ = absolute value of the chemical shift difference of the two enantiomers in the complexed form.

^b For **7** and **8** only the racemates were available; therefore, it was not possible to distinguish the shifts due to (+)- or (-)-enantiomers.

This CSP allows the analysis of ionic BDZs, *i.e.*, the hemisuccinate esters of 3-hydroxy-1,4-benzodiazepin-2-ones (**6–8**) without derivatization of the carboxyl group.

This column appears to be particularly useful for the analysis of the 3-ester derivatives, because it allows the possibility of simultaneously monitoring the presence of their hydrolysis products. This method may be used to monitor the possible occurrence of hydrolysis during receptor binding studies²¹. Significant differences have been observed in the receptor affinity values of the esters of **1**, depending on the preparation of the synaptosomal membrane, *i.e.*, depending on the presence of brain esterases²². As shown in Fig. 3, simultaneous measurement of the chemical and optical purity of **6** is possible²¹. The resolution can be improved by injecting smaller amounts of sample²¹, although under these conditions CD detection became impracticable. In Fig. 3a the chromatographic analysis of racemic **6** is reported and the resolution peaks of the hydrolysis product, *i.e.*, **1**, is present at a shorter retention time. Interestingly, we can observe the racemization of **1**; in Fig. 3b, the chromatographic analysis of (*R*)-(–)-**6** is reported, and again two peaks are observable at shorter retention times, owing to the presence of racemic **1**.

NMR analysis

To elucidate the nature of the interaction between the substrate and the chromatographic support, we carried out an investigation by ¹H NMR spectroscopy of the complexes formed between the BDZ hemisuccinate esters, **6–8** and β -cyclodextrin, a system which can be assumed to be a free solution model of the CSP.

¹H NMR spectra (Table III) of the three BDZs were recorded in ²H₂O solution at p²H 7 (phosphate buffer, 22°C) in the free state and in the presence of a 2-fold molar excess of β -cyclodextrin. Spectral analysis led to the following observations.

Variations of the chemical shifts of proton nuclei of **6–8** are caused by interaction with the cyclodextrin. This observation provides evidence for the formation of inclusion complexes between cyclodextrin and benzodiazepine derivatives. The changes in the chemical shifts are different for the two complexed enantiomers. With **6**, for which the two pure enantiomers were available, the (+)-enantiomer showed a larger complexation shift than the (–)-isomer. This indicates that the former is more tightly complexed within the cyclodextrin cavity than is the latter. This result agrees with the data for elution order, (+)-**6** being the more retained antipode on the β -cyclodextrin column. Both the actual molecular location of the protons which differentiate in the diastereoisomeric pair and the magnitude of the diastereoisomeric shift observed are different for **6**, **7** and **8** (Table III).

It is the aromatic protons of **6–8** that are the most affected by interaction with β -cyclodextrin, the diastereoisomeric shift being larger for these protons than for those bonded to the alkyl chain. On this basis, it is reasonable to postulate that the three hemisuccinate esters enter the cyclodextrin torus by means of the hydrophobic aromatic nuclei. The magnitude of the above effects follows the trend **6** > **7** > **8**. Therefore, **6** (both enantiomers) forms more stable inclusion complexes with β -cyclodextrin than does **7** or **8**, at least under these experimental conditions.

The mode of interaction between the polar groups of the cyclodextrin and those of the BDZs are probably different in all three instances. On interaction of racemic **6** with β -cyclodextrin, duplication of the alkyl chain protons is observed, whereas the

proton H-3 bonded to the chiral centre does not differentiate. It therefore appears that the carboxyl group of **6** is probably involved in a electrostatic interaction with external OH groups of the β -cyclodextrin molecule. With **7** no relevant differences are found in the chemical shifts of alkyl chain protons, whereas the H-3 and N-methyl resonances duplicate in the two complexed enantiomers. With **8**, duplication of resonances is not observed for alkyl chain protons or the H-3 proton.

CONCLUSIONS

The β -cyclodextrin-based CSP was efficient in the chromatographic resolution of a series of 1,4-benzodiazepin-2-ones. This method is particularly useful for ionic BDZs (*i.e.*, the hemisuccinate esters of 3-hydroxy-BDZs), which can be analysed without derivatization of the carboxyl group. This method also provided a means of assessing the degree of hydrolysis that may occur when esters are used in *in vitro* pharmacological studies.

On the basis of the chromatographic data for the hemisuccinate esters of the 3-hydroxy-BDZs and of the NMR data for the soluble model, the chiral discrimination of β -cyclodextrin appears to be related to the interaction of the aromatic moiety of the substrate with the hydrophobic cavity of the oligosaccharide and of the hemisuccinic chain with the hydrophilic residues outside the cavity.

ADDITIONAL NOTE

A successful optical resolution of 3-hydroxy-BDZs was reported using β -cyclodextrin as a mobile phase additive²³. In the same paper, partially successful attempts were made to resolve the enantiomers of 3-hydroxy-BDZs on a β -cyclodextrin-based CSP.

ACKNOWLEDGEMENT

This work was partially supported by the Progetto Finalizzato Chimica Fine e Secondaria 2, CNR, Italy.

REFERENCES

- 1 C. Hallstrom and M. Lader, *J. Psych. Treatment Evaluation*, 4 (1982) 293.
- 2 W. H. Pirkle and A. Tsiouras, *J. Chromatogr.*, 291 (1984) 291.
- 3 C. Bertucci, C. Rosini, D. Pini and P. Salvadori, *J. Pharm. Biomed. Anal.*, 5 (1987) 171.
- 4 S. Allenmark, *J. Liq. Chromatogr.*, 9 (1986) 425.
- 5 G. Blaschke, *J. Liq. Chromatogr.*, 9 (1986) 359.
- 6 M. Simonyi, *Med. Res. Rev.*, 4 (1984) 359.
- 7 H. Möhler and T. Okada, *Science (Washington, D.C.)*, 198 (1977) 848.
- 8 I. Kovacs, G. Maksay, Zs. Tegye, J. Visy, I. Fitos, M. Kajtar, M. Simonyi and L. Ötvös, *Stud. Org. Chem. (Bio-Org. Heterocycl.)*, 18 (1984) 239.
- 9 G. Blaschke, H. Kley and W. E. Müller, *Arzneim.-Forsch./Drug Res.*, 36 (1986) 893.
- 10 G. Blaschke, *Angew. Chem., Int. Ed. Engl.*, 19 (1980) 13.
- 11 A. Corbella, P. Gariboldi, G. Jommi, A. Forgiione, F. Marcucci, P. Martelli, E. Mussini and F. Mauri, *J. Chem. Soc., Chem. Commun.*, (1973) 721.
- 12 J. L. Waddington and F. Owen, *Neuropharmacology*, 17 (1978) 215.
- 13 W. E. Müller, U. Schlafer and U. Wollert, *Neurosci. Lett.*, 9 (1978) 239.

- 14 F. M. Andersen and H. Bundgaard, *Arch. Pharm., Chem. Sci. Ed.*, 10 (1982) 80.
- 15 S. M. Han, N. Purdie and K. A. Swallows, *Anal. Chim. Acta*, 197 (1978) 57.
- 16 T. J. Ward and D. W. Armstrong, *J. Liq. Chromatogr.*, 9 (1986) 407.
- 17 P. Salvadori, C. Rosini and C. Bertucci, *J. Org. Chem.*, 49 (1984) 5050.
- 18 H. Schütz, *Benzodiazepines —A Handbook— Basic Data, Analytical Methods, Pharmacokinetics and Comprehensive Literature*, Springer, Berlin, 1982.
- 19 M. Babbini, F. De Marchi, N. Montanaro, P. Strocchi and M. V. Torrielli, *Arzneim.-Forsch.*, 19 (1969) 1931.
- 20 J. Angyan, G. Banhegyi, M. Kajtar and A. I. Kiss, *Magy. Kem. Lapja*, 35 (1980) 307.
- 21 P. Salvadori, C. Bertucci, E. Domenici and G. Giannaccini, *J. Pharm. Biomed. Anal.*, in press.
- 22 G. Maksay, J. Kardos, M. Simonyi, Zs. Tegyei and L. Ötvös, *Arzneim.-Forsch./Drug Res.*, 31 (1981) 979.
- 23 A. F. Fell, T. A. G. Noctor, J. E. Mama and B. J. Clark, *J. Chromatogr.*, 434 (1988) 377.

Direct high-performance liquid chromatographic separation of (+)- and (-)-medetomidine hydrochloride with an α_1 -acid glycoprotein chiral column

G. ÖRN*, K. LAHTONEN and H. JALONEN

Farmos Group Ltd., Pharmaceutical Division, Research Centre, P.O. Box 425, 20101 Turku (Finland)

SUMMARY

The aim of this work was to find a fast and reliable separation method for the two enantiomers of the new animal drug medetomidine hydrochloride. Several attempts had earlier been made with commercially available chiral columns but with unsatisfactory results. A direct, fast and reproducible separation method using a commercially available α_1 -acid glycoprotein column, Chiral-AGP, was developed for the complete separation of the two enantiomers. The chiral stationary phase was immobilized on porous spherical silica particles ($5 \mu\text{m}$), which enables high-performance liquid chromatography to be operated in the reversed-phase mode. The column showed good stability during several months of frequent use. The separation was performed with various mixtures of an organic modifier (1-propanol, 2-propanol, methanol, ethanol and acetonitrile) and phosphate buffer as the mobile phase. The effect of changing the mobile phase solvent ratio, temperature, flow-rate, buffer concentration and buffer pH on the capacity factors, selectivity and resolution was studied. The chromatographic conditions chosen for the separation permitted the rapid separation of the two enantiomers within 8 min.

INTRODUCTION

Medetomidine hydrochloride (Recommended International Nonproprietary Name, Rec. INN), (\pm)-4-[1-(2,3-dimethylphenyl)ethyl]-1*H*-imidazole hydrochloride (DOMITOR®; Farmos Group) (Fig. 1), a white, crystalline compound¹, is an α_2 -agonist which has potent sedative and analgaesic effects²⁻⁶ and is used to facilitate

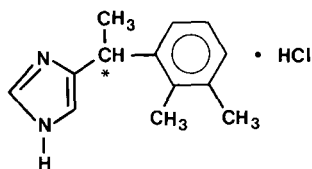


Fig. 1. Molecular structure of medetomidine hydrochloride.

minor surgical and diagnostic procedures in dogs and cats. Intensive pharmacological studies with both enantiomers have been carried out in recent years and the results have shown that only the (+)-form, dexmedetomidine hydrochloride (Rec. INN), is pharmacologically active^{7,8}. For future purposes, *e.g.*, to determine the purity of one enantiomer, it was necessary to develop a rapid and reliable direct method for the separation of these enantiomers.

It is possible to separate the two enantiomers by forming carbamate derivatives with ethyl chloroformate and to separate them by high-performance liquid chromatography (HPLC) using a Bakerbond Chiral Phase DNBPBPG covalent column (J. T. Baker, Phillipsburgh, NJ, U.S.A.)⁹. This very sensitive method has some drawbacks, however. The reaction time between medetomidine hydrochloride and ethyl chloroformate is fairly long (2–3 h) and the reaction also produces minor side-products, although these do not significantly interfere with the analysis.

A direct and a faster means of separating the two enantiomers of medetomidine hydrochloride was needed, and we decided to investigate the use of different chiral HPLC columns. First the “brush-type” column materials were studied^{10–13}. In these commercial columns, N-(3,5-dinitrobenzoyl)leucine and D-phenylglycine are covalently bound to a spherical silica gel (5 μm) (Bakerbond Chiral Phase DNBLeu covalent, J. T. Baker, and Hi-Chrom reversible Pirkle leucine and L-phenylglycine covalent columns, Regis Chemical, Morton Grove, IL, U.S.A.). It turned out, however, that the interactions of the two enantiomers of medetomidine hydrochloride with the “brush-type” phases were similar and resolution was therefore not observed.

Experiments with commercially available cavity columns based on α -, β - and γ -cyclodextrin bound to a spherical silica gel (5 μm)^{14,15} were performed (Cyclobond I, II and III, Advanced Separation Technologies, Whippany, NJ, U.S.A.). Resolution, based on the different strengths of the inclusion complexes of the enantiomers, was not achieved, however.

After these attempts, our interest turned to protein columns, which are known to be suitable for the separation of enantiomers of several drug substances. The separation mechanism of these protein columns is based on bioaffinity with different interactions. First a commercially available column based on bovine serum albumin covalently bonded to a silica gel^{16,17} (Resolvosil BSA-7, Macherey-Nagel, Düren, F.R.G.) was tried. Soon it turned out that a protein-type column could provide a solution to our problem. A promising qualitative separation between the two enantiomers of medetomidine hydrochloride was observed with this BSA column, but the separation was not sufficient for quantitative work (Fig. 2a).

Finally another commercially available protein column was chosen. This column was based on 10- μm diethylaminoethylsilica gel onto which α_1 -acid glycoprotein has been immobilized by ionic binding and cross-linking^{18–29} (EnantioPak cartridge, LKB, Stockholm, Sweden). With this column a good quantitative separation method for the two enantiomers was developed (Fig. 2b). Subsequently a second-generation α_1 -AGP column (Chiral-AGP, ChromTech, Norsborg, Sweden) was tested. In this column the protein is immobilized on 5- μm silica particles by both cross-linking and covalent binding. A suitable separation method was developed with this column (Fig. 2c) and is discussed in this paper. A better resolution and improved column stability were observed compared with the columns mentioned above.

EXPERIMENTAL

Chemicals and materials

Analytical-reagent grade chemicals were used unless indicated otherwise.

2-Propanol was obtained from J. T. Baker (Deventer, The Netherlands), 1-propanol, KH_2PO_4 and $\text{Na}_2\text{HPO}_4 \cdot 2\text{H}_2\text{O}$ from Merck (Darmstadt F.R.G.), acetonitrile and methanol of HPLC grade from Mallinckrodt (Paris, KY, U.S.A.) and ethanol from Alko (Rajamäki, Finland).

The water used was deionized, ultrafiltered, reverse osmosis water, prepared in-house.

The phosphate buffers used were prepared according to Sörensen.

The HVLP 0.45- μm filters used for mobile phase filtration were obtained from Millipore (Molsheim, France).

Apparatus

Chromatographic data were obtained using a Hewlett-Packard 1090 M liquid chromatographic system equipped with a built-in diode-array detector (HP 79880A), automatic sampling system (HP 79847A), variable-volume injector (HP 79846A), binary solvent-delivery system (HP 79835A) and analytical workstation (HP 79994A). The system was additionally equipped with a built-in oven and was connected to an HP ThinkJet printer and a HP ColorPro graphics plotter.

A Chiral-AGP (particle size 5 μm) column (10 cm \times 4 mm I.D.) was used.

Chromatographic procedure

Racemic (\pm)-medetomidine hydrochloride and its pure enantiomers were dissolved in water at concentrations of 0.03 mg/ml. The volume injected was 20 μl and the detection wavelength was 220 nm. Different mobile phase compositions (mixtures of different organic modifiers and phosphate buffer) and parameters (mobile phase solvent ratio, temperature, flow-rate, buffer concentration and buffer pH) were changed in turn and the effects on the capacity factors (k'), selectivity (α) and resolution (R_s) were calculated from the recorded chromatograms using the equations

$$\begin{aligned} k' &= t/t_a - 1 \\ \alpha &= (t_2 - t_a)/(t_1 - t_a) \\ R_s &= 2(t_2 - t_1)/(W_1 + W_2) \approx (t_2 - t_1)/[W_{1(h/2)} + W_{2(h/2)}] \end{aligned}$$

where t = retention time; t_a = retention time of non-retarded component (methanol); W = width of peak; $W_{n/2}$ = width of peak at half height; 1 and 2 = 1st and 2nd eluted component.

RESULTS AND DISCUSSION

The results are presented in Tables I–V. It can be seen that a rapid and complete separation of the two enantiomers can be achieved by using the Chiral-AGP column based on α_1 -acid glycoprotein as a chiral stationary phase.

The results show that changing the temperature, flow-rate or buffer concentration does not have a very significant effect on the selectivity or resolution. Changing

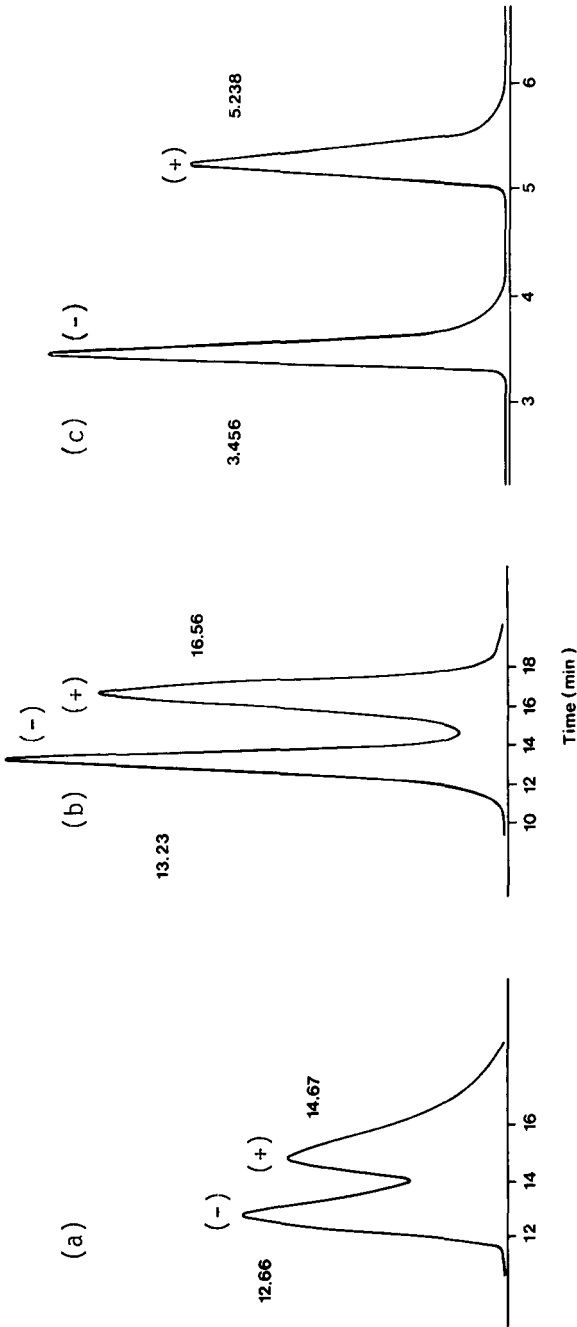


Fig. 2. Separation of the two enantiomers of medetomidine hydrochloride by using different protein-type chiral columns. (a) Resolvosil BSA-7. Mobile phase, 2-propanol-0.005 M phosphate buffer of pH 8.0 (2:98); flow-rate, 0.5 ml/min; temperature, ambient. (b) EnantioPak cartridge. Mobile phase, 2-propanol-0.005 M phosphate buffer of pH 6.5 (8:92); flow-rate, 0.3 ml/min; temperature, ambient. (c) Chiral-AGP. Mobile phase, acetonitrile-0.03 M phosphate buffer of pH 7.0 (17.5:82.5); flow-rate, 1.0 ml/min; temperature, ambient.

TABLE I

EFFECT OF MOBILE PHASE SOLVENT RATIO WHEN USING 2-PROPANOL AS ORGANIC MODIFIER ON CAPACITY FACTOR (k'), SELECTIVITY (α) AND RESOLUTION (R_s)

Mobile phase, 2-propanol-0.03 M phosphate buffer of pH 7.0; flow-rate, 1.0 ml/min; temperature, ambient.

2-Propanol-buffer (v/v)	k'^a	α	R_s
8:92	11.8	1.69	3.21
9:91	10.3	1.63	2.96
10:90	9.3	1.59	2.76
11:89	8.2	1.53	2.54

^a Capacity factor of the second-eluted (+)-enantiomer.

TABLE II

EFFECT OF TEMPERATURE ON CAPACITY FACTOR (k'), SELECTIVITY (α) AND RESOLUTION (R_s)

Mobile phase, 2-propanol-0.03 M phosphate buffer of pH 7.0 (10:90); flow-rate, 1.0 ml/min.

Temperature (°C)	k'^a	α	R_s
Ambient (28)	9.1	1.52	2.54
30	7.7	1.48	2.43
35	6.4	1.43	2.26
40	5.4	1.39	2.08

^a Capacity factor of the second-eluted (+)-enantiomer.

TABLE III

EFFECT OF FLOW-RATE ON CAPACITY FACTOR (k'), SELECTIVITY (α) AND RESOLUTION (R_s)

Mobile phase, 2-propanol-0.03 M phosphate buffer of pH 7.0 (10:90); temperature, ambient.

Flow-rate (ml/min)	k'^a	α	R_s
0.6	9.2	1.53	2.79
0.7	9.2	1.53	2.74
0.8	9.2	1.53	2.65
0.9	9.2	1.53	2.59
1.0	9.1	1.52	2.54

^a Capacity factor of the second-eluted (+)-enantiomer.

TABLE IV

EFFECT OF BUFFER CONCENTRATION ON CAPACITY FACTOR (k'), SELECTIVITY (α) AND RESOLUTION (R_s)

Mobile phase, 2-propanol-phosphate buffer of pH 6.0 (5:95); flow-rate, 1.0 ml/min; temperature, ambient.

Buffer concentration (M)	k'^a	α	R_s
0.005	13.3	1.17	1.29
0.01	10.7	1.22	1.40
0.02	8.2	1.25	1.43
0.03	7.9	1.29	1.59
0.05	6.8	1.31	1.67

^a Capacity factor of the second-eluted (+)-enantiomer.

TABLE V

EFFECT OF BUFFER pH ON CAPACITY FACTOR (k'), SELECTIVITY (α) AND RESOLUTION (R_s)Mobile phase, 2-propanol-0.03 M phosphate buffer (8:92); flow-rate, 1.0 ml/min; temperature, ambient.

pH	k'^a	α	R_s
5.5	4.5	1.10	0.67
6.0	6.4	1.17	1.03
6.5	9.4	1.37	2.05
7.0	12.1	1.63	3.04
7.5	13.3	1.84	3.61

^a Capacity factor of the second-eluted (+)-enantiomer.

the buffer pH, on the other hand, has a strong effect on all parameters. The higher the pH of the buffer, the better is the resolution of the two enantiomers. As the use of pH values higher than 7.5 for longer periods may decrease the column lifetime, owing to decomposition of the silica, a pH of 7.0 was chosen for routine analysis.

A phosphate buffer concentration of 0.03 M was selected as suitable buffer concentrations are 0.01–0.035 M and buffer concentrations above 0.03 M do not seem to have a significant positive effect on the capacity factor.

A flow-rate of 1.0 ml/min was chosen as higher flow-rates permit much faster separations, and this outweighs the fact that higher flow-rates give a slightly lower resolution.

Ambient temperature was used for analysis, as higher temperatures had a slight adverse effect on resolution.

When choosing the mobile phase solvent ratio for the analysis it was important to obtain a baseline separation of the two enantiomers without too long analysis times. In this instance 2-propanol-0.03 M phosphate buffer of pH 7.0 (11:89) gave a baseline resolution, but the ratio 10:90 was chosen for analysis to ensure a baseline separation even if the column performance declined.

The above chromatographic conditions selected for the separation of the two enantiomers of medetomidine hydrochloride permits a baseline resolution within 8 min.

TABLE VI

EFFECT OF MOBILE PHASE SOLVENT RATIO WHEN USING ACETONITRILE AS ORGANIC MODIFIER ON CAPACITY FACTOR (k'), SELECTIVITY (α) AND RESOLUTION (R_s)

Mobile phase, acetonitrile-0.03 M phosphate buffer of pH 7.0; flow-rate, 1.0 ml/min; temperature, ambient.

Acetonitrile-buffer (v/v)	k'^a	α	R_s
12.5:87.5	14.8	1.93	3.49
15.0:85.0	9.9	1.77	3.12
17.5:82.5	8.0	1.71	2.83
20.0:80.0	5.1	1.57	2.35
22.5:77.5	3.5	1.48	1.88

^a Capacity factor of the second-eluted (+)-enantiomer.

So far the experimental part of this work had been carried out using 2-propanol as organic modifier. Other organic modifiers were also tested. 1-Propanol, methanol and ethanol separated the two enantiomers but not as well as 2-propanol. With acetonitrile, however, a better separation was achieved. The effects of changing the mobile phase solvent ratio when using acetonitrile as organic modifier on the capacity factors, selectivity and resolution are shown in Table VI. The results show that a better and faster resolution is achieved when using acetonitrile instead of 2-propanol as organic modifier. Acetonitrile-0.03 M phosphate buffer (17.5:82.5) permits a baseline separation.

The conditions chosen for analysis not only permit a baseline separation of the (-)- and (+)-enantiomers (with retention times of *ca.* 3.5 and 5.2 min, respectively),

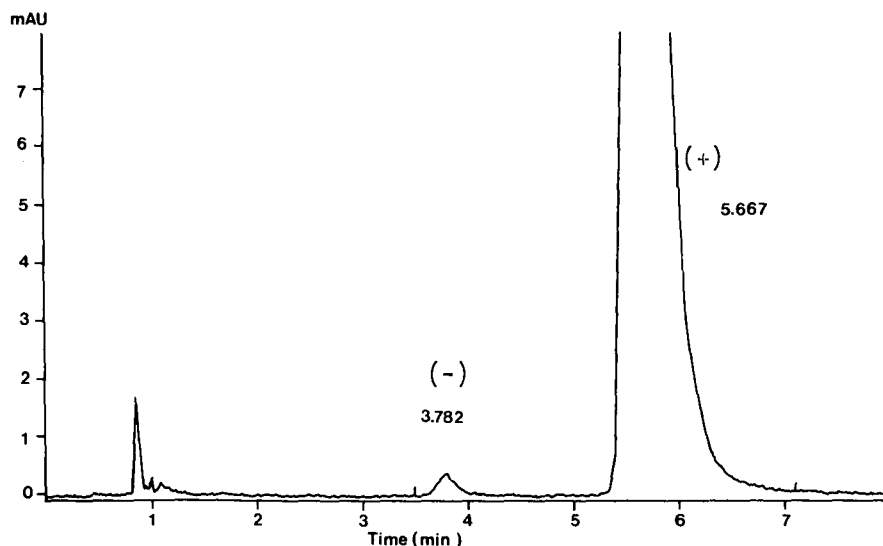


Fig. 3. Chromatogram of 0.5% (-)-medetomidine hydrochloride in (+)-medetomidine hydrochloride. Mobile phase, acetonitrile-0.03 M phosphate buffer of pH 7.0 (17.5:82.5); flow-rate, 1.0 ml/min; and temperature, ambient.

TABLE VII

STABILITY OF THE COLUMN BY COMPARING CAPACITY FACTOR (k'), SELECTIVITY (α) AND RESOLUTION (R_s)

Mobile phase, 2-propanol-0.005 *M* phosphate buffer of pH 6.0 (5:95); flow-rate, 1.0 ml/min; temperature, ambient. The filling of the column was done after the second check-point.

Time (months)	k' ^a	α	R_s
0.5	10.5	1.42	3.22
1.5	7.7	1.34	1.78
4.0	8.6	1.31	1.42
4.0 ^b	10.3	1.39	1.72

^a Capacity factor of the second-eluted (+)-enantiomer.

^b Selectivity and resolution when the capacity factor is adjusted to the initial value (approximately) by changing the mobile phase solvent ratio to 4:96.

but as the peak shape is sharp and symmetrical it is also possible to determine very small amounts of (-)-medetomidine hydrochloride when present as an impurity in (+)-medetomidine hydrochloride, as shown in Fig. 3.

The Chiral-AGP column also showed satisfactory stability. During analysis the performance of the column and the symmetry of the peaks declined. The "shoulder" problem was solved by filling the empty space formed at the inlet end of the column with new sorbent, which restored the peak symmetry. The frequent and diverse use of the column inevitably had a slight negative effect on the column performance. However, by slightly changing the chromatographic parameters, *e.g.*, mobile phase solvent ratio or buffer pH, it is easy to maintain a rapid and complete separation of the two enantiomers even with a slightly deteriorated column.

The stability of the column (selectivity and resolution) can be seen in Table VII. The selectivity and resolution decrease the longer the column has been in use, which is due to a slight deterioration of the column. The capacity factor was higher at the 4-month check-point compared with the previous check-point, which is probably due to the filling of the column.

When the capacity factor of the second-eluted (+)-enantiomer after a 4-month interval is adjusted to approximately the same value as that at the initial check-point by changing the mobile phase composition, it can be seen how much worse the resolving ability of the column has actually become. It should be noted, however, that although the selectivity and resolution have decreased after 4 months of use, the performance of the column is still sufficient to perform a rapid baseline separation of the two enantiomers of medetomidine hydrochloride.

CONCLUSION

The separation of the two enantiomers of medetomidine hydrochloride turned out to be a difficult chromatographic problem. Only protein-type chiral columns showed a sufficient separation capacity. The Chiral-AGP column was found to be very suitable for the separation of the two enantiomers. With this column and the optimized

conditions [mobile phase acetonitrile–0.03 M phosphate buffer of pH 7.0 (17.5:82.5), flow-rate 1.0 ml/min and ambient temperature], it is possible to achieve a complete baseline separation of (+)- and (–)-medetomidine hydrochloride within 8 min. The narrow and symmetrical form of the peaks also makes it possible to determine small amounts of one enantiomer as an impurity in the other.

ACKNOWLEDGEMENTS

We thank Mrs. Pirjo Eemilä, Mrs. Leena Koski and Mrs. Pirkko Tanskanen for their capable technical assistance.

REFERENCES

- 1 E. Laine, R. Rajala, K. Lahtonen and J. Savolainen, *Acta Pharm. Fenn.*, 95 (1986) 119.
- 2 R. Virtanen, in A. S. J. P. A. M. van Miert (Editor), *Proceedings of the 3rd Congress of the European Association for Veterinary Pharmacology and Toxicology, 25–29 August, 1985, Ghent, E.A.V.P.T., Utrecht, 1985*, p. 39.
- 3 R. Virtanen, *Acta Vet. Scand.*, 82 (1986) 35.
- 4 M. Scheinin, A. Kallio, M. Koulu, J. Viikari and H. Scheinin, *Br. J. Clin. Pharmacol.*, 24 (1987) 443.
- 5 R. Virtanen, J.-M. Savola, V. Saano and L. Nyman, *Eur. J. Pharmacol.*, 150 (1988) 9.
- 6 E. MacDonald, H. Scheinin and M. Scheinin, *Eur. J. Pharmacol.*, 158 (1988) 119.
- 7 R. Virtanen, T. Viitamaa and L. Nyman, in *Abstracts of the XVIth Collegium Internationale Neuro-Psychopharmacologicum Congress, 15–19 August, 1988, Munich*, Suppl. to Vol. 96, 1988, Abstract No. 34.01.28, p. 371.
- 8 R. Lammintausta, O. Vainio, R. Virtanen and T. Vähä-Vahe (Editors), *Acta Vet. Scand., Suppl.*, 85 (1989) 1.
- 9 J. Savolainen, personal communication.
- 10 F. Mikes, G. Boshart and E. Gil-Av, *J. Chromatogr.*, 122 (1976) 205.
- 11 W. H. Pirkle, J. M. Feiss, J. L. Schreiner and B. C. Hamper, *J. Am. Chem. Soc.*, 103 (1981) 3964.
- 12 W. H. Pirkle, C. J. Welch and M. H. Hyun, *J. Org. Chem.*, 48 (1983) 5022.
- 13 I. W. Wainer and T. D. Doyle, *Liq. Chromatogr. Mag.*, 2 (1984) 88.
- 14 D. W. Armstrong, T. J. Ward, R. D. Armstrong and T. E. Beesley, *Science (Washington, D.C.)*, 232 (1986) 1132.
- 15 D. W. Armstrong and W. Li, *Chromatography*, March (1987) 43.
- 16 S. Allenmark and B. Bomgren, in P. G. D. Dean, W. S. Johnson and F. A. Middle (Editors), *Affinity Chromatography—A Practical Approach*, IRL Press, Oxford, 1985, p. 108.
- 17 S. Allenmark, B. Bomgren and S. Andersson, *Prep. Biochem.*, 14 (1984) 139.
- 18 J. Hermansson, *J. Chromatogr.*, 269 (1983) 71.
- 19 J. Hermansson, *J. Chromatogr.*, 298 (1984) 67.
- 20 J. Hermansson, M. Eriksson and O. Nyquist, *J. Chromatogr.*, 336 (1984) 321.
- 21 J. Hermansson, *J. Chromatogr.*, 316 (1984) 537.
- 22 J. L. G. Nilsson, J. Hermansson, U. Hacksell and S. Sundell, *Acta Pharm. Suec.*, 21 (1984) 309.
- 23 J. Hermansson, *J. Chromatogr.*, 325 (1985) 379.
- 24 J. Hermansson and M. Eriksson, *J. Liq. Chromatogr.*, 9 (1986) 621.
- 25 G. Schill, I. Wainer and S. Barkan, *J. Liq. Chromatogr.*, 9 (1986) 641.
- 26 G. Schill, I. Wainer and S. Barkan, *J. Chromatogr.*, 365 (1986) 73.
- 27 J. Hermansson and G. Schill, in M. Zief and L. Crane (Editors), *Chromatographic Chiral Separations*, Marcel Dekker, New York, 1987, p. 245.
- 28 J. Hermansson and G. Schill, in P. A. Brown and R. A. Hartwick (Editors), *High Performance Liquid Chromatography*, Wiley-Interscience, New York, 1988, p. 337.
- 29 J. Hermansson, K. Ström and R. Sandberg, *Chromatographia*, 24 (1987) 520.

Author Index

- Aguilar, M. I., see Hodder, A. N. 17
- Ahnoff, M.
- , Chen, S., Green, A. and Grundevik, I.
Chiral chloroformates as transparent reagents for the resolution of metoprolol enantiomers by reversed-phase liquid chromatography 593
- Albert, K., see Pfeleiderer, B. 343
- Arvidsson, E.
- , Jansson, S. O. and Schill, G.
Chiral separations of atropine and homatropine on an α_1 -acid glycoprotein-bonded stationary phase 579
- Ascah, T. L.
- and Feibush, B.
Novel, highly deactivated reversed-phase for basic compounds 357
- Bartha, A.
- , Vigh, Gy. and Ståhlberg, J.
Extension of the electrostatic retention model of reversed-phase ion-pair chromatography to include the simultaneous effects of the organic modifier and the pairing ion 85
- Bayer, E., see Pfeleiderer, B. 343
- Belliardo, F.
- , Chiantore, O., Berek, D., Novák, I. and Lucarelli, C.
Development and use of carbon adsorbents in the liquid chromatographic separation of isomers 371
- Berek, D., see Belliardo, F. 371
- Bertucci, C.
- , Domenici, E., Uccello-Barretta, G. and Salvadori, P.
High-performance liquid chromatographic resolution of racemic 1,4-benzodiazepin-2-ones by means of a β -cyclodextrin silica bonded stationary phase 617
- Boppana, V. K.
- and Rhodes, G. R.
High-performance liquid chromatographic determination of guanidino compounds by automated pre-column fluorescence derivatization 279
- Bristow, P.A.
- Towards a chromatographic quantitor 265
- Camacho, P. L.
- , Geiger, E., Vigh, Gy., Webster, R. and Thompson, D. H.
Separation of the enantiomeric intermediates of some platelet-activating factor analogues on naphthylalanine-type Pirkle column 611
- Chen, S., see Ahnoff, M. 593
- Cheung, A. P.
- and Kenney, D.
Partition coefficients and capacity factors of some nucleoside analogues 119
- Chiantore, O., see Belliardo, F. 371
- Clark, B. J., see Marr, J. G. D. 289
- Cserhádi, T., see Valkó, K. 35
- Czok, M.
- and Guiochon, G.
Aligned fiber columns for size-exclusion chromatography 303
- Davankov, V. A., see Kurganov, A. 391
- Dohi, T., see Sakuma, I. 223
- Domenici, E., see Bertucci, C. 617
- Dominguez, E., see Marko-Varga, G. 423
- Driessche, N. Vanden, see Maris, F. 211
- Duijsters, P. P. E., see Tock, P. P. H. 185
- Durand, A., see Rouchouse, A. 601
- Edlund, P. O., see Johansen, K. 471
- Elteková, S. A.
- Retention times and heats of adsorption of aromatic compounds on carbon adsorbents 335
- Engelsma, M.
- , Kok, W. Th. and Smit, H. C.
Selective determination of trace levels of phenol in river water using electrochemical concentration modulation correlation chromatography 201
- Eray, B., see Kurganov, A. 391
- Eriksson, B.-M., see Gustafsson, S. 75
- Farkas, Gy., see Vigh, Gy. 481
- Feibush, B., see Ascah, T. L. 357
- Fell, A. F., see Marr, J. G. D. 289
- Fellegvári, I., see Valkó, K. 35
- Fornstedt, T.
- , Westerlund, D. and Sokolowski, A.
Studies on system peaks in ion-pair adsorption chromatography. III. Regulation of system peak gradient retention for obtaining analyte peak compression 61
- Frank, H., see Welsch, T. 97
- Fujimoto, C., see Jinno, K. 443
- Fukui, Y., see Sakuma, I. 223
- Geiger, E., see Camacho, P. L. 611
- Golshan-Shirazi, S.
- and Guiochon, G.
Solutions of the equilibrium and semi-equilibrium models of chromatography 495
- Gorton, L., see Marko-Varga, G. 423
- Green, A., see Ahnoff, M. 593
- Grundevik, I., see Ahnoff, M. 593

- Guiochon, G., see Czok, M. 303
 —, see Golshan-Shirazi, S. 495
 Gustafsson, S.
 —, Eriksson, B.-M. and Nilsson, I.
 Multiple peak formation in reversed-phase liquid chromatography of ramipril and ramiprilate 75
 Hann-Hägerdal, B., see Marko-Varga, G. 423
 Hara, S., see Uchida, T. 327
 Hayashida, M.
 —, Nihira, M., Watanabe, T. and Jinno, K.
 Application of a computer-assisted high-performance liquid chromatographic multi-wavelength ultraviolet detection system to simultaneous toxicological drug analyses 133
 Hearn, M. T. W., see Hodder, A. N. 17
 Hindriks, R., see Maris, F. 211
 Hirata, N., see Noguchi, K. 145
 Hodder, A. N.
 —, Aguilar, M. I. and Hearn, M. T. W.
 High-performance liquid chromatography of amino acids, peptides and proteins, XCVII. The influence of the gradient elution mode and displacer salt type on the retention properties of closely related protein variants separated by high-performance anion-exchange chromatography 17
 Ishikawa, T., see Yamakawa, Y. 319
 Izu, H., see Uchida, T. 327
 Jalonen, H., see Örn, G. 627
 Janssen, H.-G., see Schoenmakers, P. J. 563
 Jansson, S. O., see Arvidsson, E. 579
 Jinno, K.
 — and Fujimoto, C.
 Coupling of microcolumn high-performance liquid chromatography with Fourier transform infrared spectrometry 443
 —, see Hayashida, M. 133
 Johansen, K.
 — and Edlund, P. O.
 Determination of water-soluble vitamins in blood and plasma by coupled-column liquid chromatography 471
 Kaliszan, R.
 — and Ośmiałowski, K.
 Correlation between chemical structure of non-congeneric solutes and their retention on polybutadiene-coated alumina 3
 Kasai, M., see Noguchi, K. 145
 —, Uchida, T. 327
 Kenney, D., see Cheung, A. P. 119
 Keresztes, P., see Papp, E. 157
 Kikuta, C., see Mascher, H. 417
 Kok, W. Th., see Engelsma, M. 201
 Kraak, J. C., see Stegeman, G. 547
 —, see Tock, P. P. H. 185
 Kurganov, A.
 —, Kuzmenko, O., Davankov, V. A., Eray, B., Unger, K. K. and Trüding, U.
 Effect of polystyrene coating on pore, structural and chromatographic properties of silica packings 391
 Kuzmenko, O., see Kurganov, A. 391
 Lahtonen, K., see Örn, G. 627
 Lee, H. K., see Li, S. F. Y. 245
 Li, S. F. Y.
 —, Lee, H. K. and Ong, C. P.
 Optimization of mobile phase composition for high-performance liquid chromatographic separation by means of the overlapping resolution mapping scheme 245
 Lucarelli, C., see Belliardo, F. 371
 Lundahl, P., see Yang, Q. 379
 Lunte, C. E., see Scott, D. O. 461
 Lynch, R. J., see Schoenmakers, P. J. 169
 Manoha, M., see Rouchouse, A., 601
 Maris, F.
 —, Hindriks, R., Vink, J., Peeters, A., Vanden Driessche, N. and Massart, L.
 Validation of an expert system for the selection of initial high-performance liquid chromatographic conditions for the analysis of basic drugs 211
 Marko-Varga, G.
 —, Dominguez, E., Hahn-Hägerdal, B. and Gorton, L.
 Selective post-column liquid chromatographic determination of sugars in spent sulphite liquor with two enzymatic electrochemical detectors in parallel 423
 Marr, J. G. D.
 —, Seaton, G. G. R., Clark, B. J. and Fell, A. F.
 Multiple absorbance ratio correlation—a new approach for assessing peak purity in liquid chromatography 289
 Mascher, H.
 — and Kikuta, C.
 Determination of amoxicillin in plasma by high-performance liquid chromatography with fluorescence detection after on-line oxidation 417
 Massart, L., see Maris, F. 211
 Miyasaka, K., see Yamakawa, Y. 319
 Nihira, M., see Hayashida, M. 133
 Nilsson, I., see Gustafsson, S. 75
 Nilsson, L. B.
 Regulation of peak compression effects for substituted benzamides in reversed-phase liquid chromatography 253

- Noguchi, K., see Uchida, T. 327
- , Yanagihara, Y., Kasai, M. and Hirata, N.
Chromatographic characteristics of nucleic acid components on vinyl alcohol copolymer gel columns 145
- Novák, I., see Belliardo, F. 371
- Örn, G.
—, Lahtonen, K. and Jalonen, H.
Direct high-performance liquid chromatographic separation of (+)- and (-)-medetomidine hydrochloride with an α_1 -acid glycoprotein chiral column 627
- Ohkubo, A., see Sakuma, I. 223
- Ohtani, T., see Uchida, T. 327
- Okuyama, T., see Yamakawa, Y. 319
- Ong, C. P., see Li, S. F. Y. 245
- Oostervink, R., see Stegeman, G. 547
- Ośmiałowski, K., see Kaliszan, R. 3
- Papp, E.
— and Keresztes, P.
Retention behaviour of mono- and dicarboxylic acids, carbohydrates and alcohols in ion-exclusion chromatography 157
- Peeters, A., see Maris, F. 211
- , see Schoenmakers, P. J. 169
- Pfeffer, W. D.
— and Yeung, E. S.
Indirect fluorometric detection in open-tubular capillary column chromatography 401
- Pfleiderer, B.
—, Albert, K. and Bayer, E.
Investigations by ^{29}Si cross-polarization magic angle spinning NMR spectroscopy of reaction pathways of silica gel polyfunctional modification 343
- Poppe, H.
Secondary equilibria and their interaction with chromatographic transport 45
- , see Stegeman, G. 547
- , see Tock, P. P. H. 185
- Quintero, G., see Vigh, Gy. 481
- Rhodes, G. R., see Boppana, V. K. 279
- Rouchouse, A.
—, Manoha, M., Durand, A., Thenot, J. P.
Direct high-performance liquid chromatographic determination of the enantiomers of alfuzosin in plasma on a second-generation α_1 -acid glycoprotein chiral stationary phase 601
- Sági, J., see Valkó, K. 35
- Sakuma, I.
—, Takai, N., Dohi, T., Fukui, Y. and Ohkubo, A.
Resolution of unresolved peaks containing unknown components by high-performance liquid chromatography with multi-wavelength detection 223
- Salvadori, P., see Betucci, C. 617
- Schill, G., see Arvidsson, E. 579
- Schoenmakers, P. J.
—, Peeters, A. and Lynch, R. J.
Optimization of chromatographic methods by a combination of optimization software and expert systems 169
- , Uunk, L. G. M. and Janssen, H.-G.
Comparison of stationary phases for packed-column supercritical fluid chromatography 563
- Scott, D. O.
—, Sorensen, L. R. and Lunte, C. E.
In vivo microdialysis sampling coupled to liquid chromatography for the study of acetaminophen metabolism 461
- Seaton, G. G. R., see Marr, J. G. D. 289
- Siwek, A.
— and Śliwiok, J.
Reversed-phase high-performance liquid chromatography in the investigation of the hydrophobicity of selected ketones 109
- Śliwiok, J., see Siwek, A. 109
- Smit, H. C., see Engelsma, M. 201
- Sokolowski, A., see Fornstedt, T. 61
- Sorensen, L. R., see Scott, D. O. 461
- Ståhlberg, J., see Bartha, A. 85
- Stegeman, G.
—, Oostervink, R., Kraak, J. C., Poppe, H. and Unger, K. K.
Hydrodynamic chromatography of macromolecules on small spherical non-porous silica particles 547
- Szemző, A., see Valkó, K. 35
- Takagi, T.
Application of low-angle laser light scattering detection in the field of biochemistry. Review of recent progress 409
- Takai, N., see Sakuma, I. 223
- Thenot, J. P., see Rouchouse, A. 601
- Thompson, D. H., see Camacho, P. L. 611
- Tock, P. P. H.
—, Duijsters, P. P. E., Kraak, J. C. and Poppe, H.
Theoretical optimization of open-tubular columns for liquid chromatography with respect to mass loadability 185
- Trüdinger, U., see Kurganov, A. 391
- Ucello-Barretta, G., see Bertucci, C. 617
- Uchida, T.
—, Ohtani, T., Kasai, M., Yanagihara, Y., Noguchi, K., Izu, H. and Hara, S.
Peptide behaviour and analysis on a chemically stable C_{18} -bonded vinyl alcohol copolymer column with alkaline and acidic eluents 327
- Unger, K. K., see Kurganov, A. 391
- , see Stegeman, G. 547

- Uunk, L. G. M., see Schoenmakers, P. J. 563
- Valkó, K.
—, Cserhádi, T., Fellegvári, I., Sági, J. and Szemző, A.
Application of chromatographic retention data in an investigation of a quantitative structure-nucleotide incorporation rate relationship 35
- Vanden Driessche, N., see Maris, F. 211
- Vigh, Gy., see Bartha, A. 85
—, see Camacho, P. L. 611
—, Quintero, G. and Farkas, Gy.
Displacement chromatography on cyclodextrin-silicas. III. Enantiomer separations 481
—, see Welsch, T. 97
- Vink, J., see Maris, F. 211
- Wallstén, M., see Yang, Q. 379
- Watanabe, T., see Hayashida, M. 133
- Webster, R., see Camacho, P. L. 611
- Welsch, T.
—, Frank, H. and Vigh, Gy.
Silanol effects in reversed-phase liquid chromatography 97
- Westerlund, D., see Fornstedt, T. 61
- Yamada, Y., see Yamakawa, Y. 319
- Yamakawa, Y.
—, Miyasaka, K., Ishikawa, T., Yamada, Y. and Okuyama, T.
High-performance liquid chromatography of transfer ribonucleic acids on spherical hydroxyapatite beads 319
- Yanagihara, Y., see Noguchi, K. 145
—, see Uchida, T. 327
- Yang, Q.
—, Wallstén, M. and Lundahl, P.
Lipid-vesicle-surface chromatography 379
- Yeung, E. S., see Pfeffer, W. D. 401

PUBLICATION SCHEDULE FOR 1990

Journal of Chromatography and Journal of Chromatography, Biomedical Applications

MONTH	J	F	M	A	M	J	The publication schedule for further issues will be published later
Journal of Chromatography	498/1 498/2 499	500 502/1	502/2 503/1 503/2 504/1	504/2 505/1	505/2 506 507 508/1	508/2 509/1 509/2 510	
Cumulative Indexes, Vols. 451-500		501					
Bibliography Section		524/1		524/2		524/3	
Biomedical Applications	525/1	525/2	526/1	526/2 527/1	527/2	528/1 528/2	

INFORMATION FOR AUTHORS

(Detailed *Instructions to Authors* were published in Vol. 478, pp. 453-456. A free reprint can be obtained by application to the publisher, Elsevier Science Publishers B.V., P.O. Box 330, 1000 AH Amsterdam, The Netherlands.)

Types of Contributions. The following types of papers are published in the *Journal of Chromatography* and the section on *Biomedical Applications*: Regular research papers (Full-length papers), Notes, Review articles and Letters to the Editor. Notes are usually descriptions of short investigations and reflect the same quality of research as Full-length papers, but should preferably not exceed six printed pages. Letters to the Editor can comment on (parts of) previously published articles, or they can report minor technical improvements of previously published procedures; they should preferably not exceed two printed pages. For review articles, see inside front cover under Submission of Papers.

Submission. Every paper must be accompanied by a letter from the senior author, stating that he is submitting the paper for publication in the *Journal of Chromatography*. Please do not send a letter signed by the director of the institute or the professor unless he is one of the authors.

Manuscripts. Manuscripts should be typed in double spacing on consecutively numbered pages of uniform size. The manuscript should be preceded by a sheet of manuscript paper carrying the title of the paper and the name and full postal address of the person to whom the proofs are to be sent. Authors of papers in French or German are requested to supply an English translation of the title of the paper. As a rule, papers should be divided into sections, headed by a caption (*e.g.*, Summary, Introduction, Experimental, Results, Discussion, etc.). All illustrations, photographs, tables, etc., should be on separate sheets.

Introduction. Every paper must have a concise introduction mentioning what has been done before on the topic described, and stating clearly what is new in the paper now submitted.

Summary. Full-length papers and Review articles should have a summary of 50-100 words which clearly and briefly indicates what is new, different and significant. In the case of French or German articles an additional summary in English, headed by an English translation of the title, should also be provided. (Notes and Letters to the Editor are published without a summary.)

Illustrations. The figures should be submitted in a form suitable for reproduction, drawn in Indian ink on drawing or tracing paper. Each illustration should have a legend, all the *legends* being typed (with double spacing) together on a *separate sheet*. If structures are given in the text, the original drawings should be supplied. Coloured illustrations are reproduced at the author's expense, the cost being determined by the number of pages and by the number of colours needed. The written permission of the author and publisher must be obtained for the use of any figure already published. Its source must be indicated in the legend.

References. References should be numbered in the order in which they are cited in the text, and listed in numerical sequence on a separate sheet at the end of the article. Please check a recent issue for the layout of the reference list. Abbreviations for the titles of journals should follow the system used by *Chemical Abstracts*. Articles not yet published should be given as "in press" (journal should be specified), "submitted for publication" (journal should be specified), "in preparation" or "personal communication".

Dispatch. Before sending the manuscript to the Editor please check that the envelope contains three copies of the paper complete with references, legends and figures. One of the sets of figures must be the originals suitable for direct reproduction. Please also ensure that permission to publish has been obtained from your institute.

Proofs. One set of proofs will be sent to the author to be carefully checked for printer's errors. Corrections must be restricted to instances in which the proof is at variance with the manuscript. "Extra corrections" will be inserted at the author's expense.

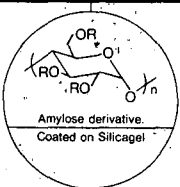
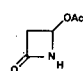
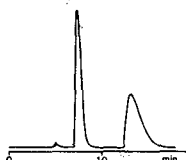
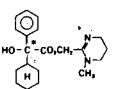
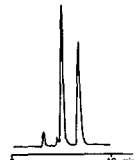
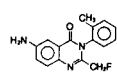
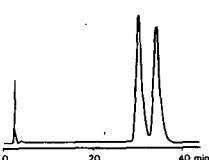
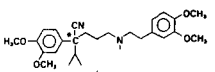
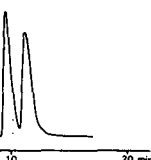
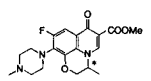
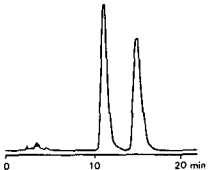
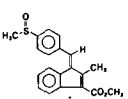
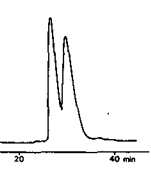
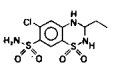
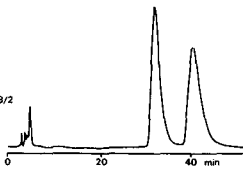
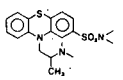
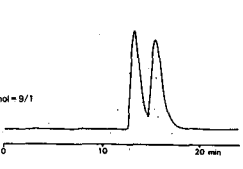
Reprints. Fifty reprints of Full-length papers, Notes and Letters to the Editor will be supplied free of charge. Additional reprints can be ordered by the authors. An order form containing price quotations will be sent to the authors together with the proofs of their article.

Advertisements. Advertisement rates are available from the publisher on request. The Editors of the journal accept no responsibility for the contents of the advertisements.

For Superior Chiral Separation

The finest from DAICEL.....

Why look beyond DAICEL? We have developed the finest CHIRALCEL, CHIRALPAK and CROWNSPAK with up to 17 types of HPLC columns, all providing superior resolution of racemic compounds.

NEW CHIRALPAK AS		NEW CHIRALPAK AD	
<p>•CHIRALPAK AS</p> $R: -C(=O)-N(H)-C^*(CH_3)-C_6H_4$ <p>*: S*</p> <p>for β-Lactam antibiotics</p>	 <p>Amylose derivative Coated on Silicagel</p>	<p>•CHIRALPAK AD</p> $R: -C(=O)-N(H)-C_6H_3(CH_3)_2$	
<p>4-Acetoxy-2-azetidine</p>  <p>Eluent : Hexane/Ethanol = 8/2 Flow rate : 1.0ml/min Temperature : r.t. Detection : UV254nm</p> 	<p>Oxyphenyclimine</p>  <p>Eluent : Hexane/2-Propanol = 8/1 Flow rate : 1.0ml/min Temperature : r.t. Detection : UV254nm</p> 		
<p>Afloqualone</p>  <p>Eluent : Hexane/EtOH = 95/5 Flow rate : 1.3ml/min Temperature : 60°C Detection : UV254nm</p> 	<p>Verapamil</p>  <p>Eluent : Hexane/2-Propanol = 9/1 Flow rate : 1.0ml/min Temperature : r.t. Detection : UV254 nm</p> 		
<p>Ofloxacin methyl ester</p>  <p>Eluent : Hexane/EtOH = 8/2 Flow rate : 1.2ml/min Temperature : 40°C Detection : UV254 nm</p> 	<p>Sulindac methyl ester</p>  <p>Eluent : Hexane/2-Propanol = 9/1 Flow rate : 1.0ml/min Temperature : r.t. Detection : UV254 nm</p> 		
<p>Ethiazide</p>  <p>Eluent : Hexane/Ethanol = 8/2 Flow rate : 1.0ml/min Temperature : 40°C Detection : UV254 nm</p> 	<p>Dimethothiazine</p>  <p>Eluent : Hexane/2-Propanol = 9/1 Flow rate : 1.0ml/min Temperature : r.t. Detection : UV254 nm</p> 		

■ Separation Service

- A pure enantiomer separation in the amount of 100g~10kg is now available.
- Please contact us for additional information regarding the manner of use and application of our chiral columns and how to procure our separation service.



DAICEL CHEMICAL INDUSTRIES, LTD.

8-1, Kasumigaseki 3-chome, Chiyoda-ku, Tokyo 100, Japan Phone: 03 (507) 3151 FAX: 03 (507) 3193

DAICEL (U.S.A.), INC.

Fort Lee Executive Park
Two Executive Drive, Fort Lee,
New Jersey 07024
Phone: (201) 461-4466
FAX: (201) 461-2776

DAICEL (U.S.A.), INC.

23456 Hawthorne Blvd.
Bldg. 5, Suite 130
Torrance, CA 90505
Phone: (213) 791-2030
FAX: (213) 791-2031

DAICEL (EUROPA) GmbH

Oststr. 22
4000 Düsseldorf 1, F.R. Germany
Phone: (211) 369848
Telex: (41) 8588042 DCEL D
FAX: (211) 364429

DAICEL CHEMICAL (ASIA) PTE. LTD.

65 Chulia Street #40-07
OCBC Centre, Singapore 0104
Phone: 5332511
FAX: 5326454